Cover Picture

Joseph G. Cordaro, Daniel Stein, Heinz Rüegger, and Hansjörg Grützmacher*

The quest for cyaphide, the phosphorus equivalent of cyanide, has been a challenge for many years. In their Communication on page 6159 ff., H. Grützmacher and co-workers describe their approach to prepare the first stable terminal cyaphide complex [RuH(CP)(dppe)$_2$] (dppe = bis(1,2-diphenylphosphinoethane)). In an initial silyl-protected complex, the Ru center was P-coordinated by the C≡P ligand. Removal of the silyl group yielded the C-coordinated Ru complex, whose structure is shown on the cover picture.

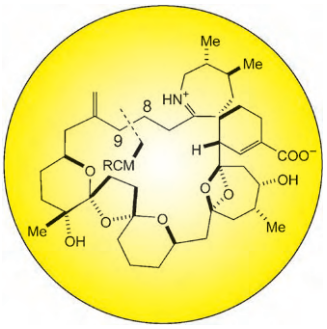

Macrocyclization
One of the decisive steps in the synthesis of many natural products is a macrocyclization by ring-closing matathesis. J. Pérez-Castells and A. Gradillas describe in their Minireview on page 6086 ff. the conditions that are advantageous for this reaction.

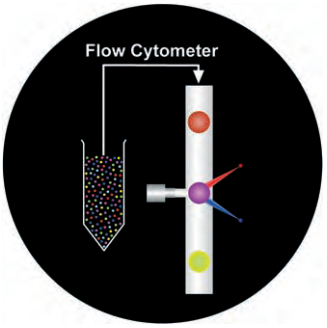

Multiplex Analysis
Though not well known, suspension systems of coded microspheres are potentially far better suited for multiplex analysis than the established planar-array techniques. R. Wilson and co-workers describe this new approach and its advantages in their Review on p. 6104 ff.

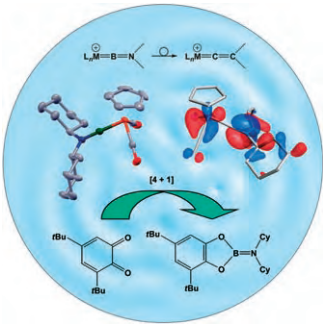

B–N Vinylidene Analogue
In their Communication on page 6118 ff., S. Aldridge, C. Jones, and co-workers present a cationic terminal amino borylene complex that displays delocalized Fe-B-N bonding and undergoes [4+1] cycloaddition with an *ortho*-benzoquinone.

Contents

VIP *The following Communications have been judged by at least two referees to be "very important papers" and will be published online at www.angewandte.org soon:*

*F. P. Seebeck, A. Guainazzi, C. Amoreira, K. K. Baldridge, D. Hilvert**
Stereoselectivity and Expanded Substrate Scope of an Engineered PLP-Dependent Aldolase

U. Klar, B. Buchmann, W. Schwede, W. Skuballa, J. Hoffmann, R. Lichtner*
Total Synthesis and Antitumor Activity of ZK-EPO: The First Fully Synthetic Epothilone in Clinical Development

D. Stacchiola, S. K. J. Weissenrieder, H. Kuhlenbeck, S. Shaikhutdinov, H.-J. Freund, M. Sierka, T. K. Todorova, J. Sauer*
Synthesis and Structure of an Ultrathin Aluminosilicate Film

*M. C. Wood, D. C. Leitch, C. S. Yeung, J. A. Kozak, L. L. Schafer**
Chiral, Neutral Zirconium Amidate Complexes for the Asymmetric Hydroamination of Alkenes

*J. M. Wiseman, D. R. Ifa, Q. Song, R. G. Cooks**
Tissue Imaging at Atmospheric Pressure Using Desorption Electrospray Ionization (DESI) Mass Spectrometry

*N. Pour, L. Itzhaki, B. Hoz, E. Altus, H. Basch, S. Hoz**
Auxetics at the Molecular Level: A Negative Poisson's Ratio in Molecular Rods

News

Organic Chemistry: A.-M. Caminade and S. Quideau honored ____ **6078**

Books

Supercritical Carbon Dioxide in Polymer Reaction Engineering	Maartje F. Kemmere, Thierry Meyer	*reviewed by M. Pagliaro*	**6079**
Bio-Based Polymers and Composites	Richard P. Wool, Xiuzhi Susan Sun	*reviewed by J. E. Mark*	**6079**
Mechanical Properties of Polymers Based on Nanostructure and Morphology	Georg H. Michler, Francisco J. Balta'-Calleja	*reviewed by J. E. Mark*	**6080**

Highlights

Alkane Metathesis

J.-M. Basset, C. Copéret,* D. Soulivong, M. Taoufik, J. Thivolle-Cazat **6082 – 6085**

From Olefin to Alkane Metathesis: A Historical Point of View

Is two better than one? The recent discovery of a homogeneous catalytic system for alkane metathesis is analyzed and compared to other existing systems. The new catalytic system is a combination of two catalysts that carry out dehydrogenation/hydrogenation and olefin metathesis (see scheme).

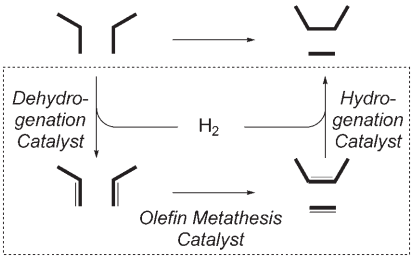

Minireviews

Macrocycles

A. Gradillas, J. Pérez-Castells* ____ **6086 – 6101**

Macrocyclization by Ring-Closing Metathesis in the Total Synthesis of Natural Products: Reaction Conditions and Limitations

Closing the circle: The formation of macrocycles by ring-closing metathesis (RCM) has for a long time been a key step in the synthesis of natural products that contain large rings. Which reaction conditions are preferable for a macro-RCM? An overview of the current research is given to help when planning future key macrocyclization steps in the synthesis of natural macrocycles.

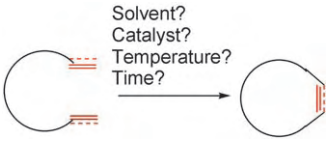

InterScience

© 2006 Wiley-VCH Verlag GmbH & Co. KGaA, Weinheim

Reviews

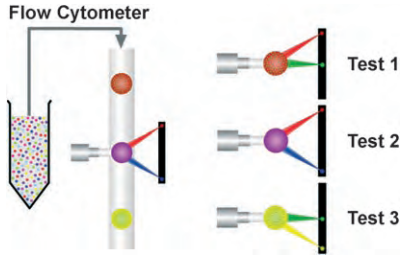

Faster, smaller, more sensitive: Since the decoding of the human genome a defining trait has been the quest to obtain more and more molecular information from smaller and smaller samples. Latex microspheres encoded with fluorescent dyes allow dozens of molecules to be detected in the same sample at the same time, but the race is now on to develop new types of encoded particle that can extract even more information.

Coded Microparticles

R. Wilson,* A. R. Cossins, D. G. Spiller ——— **6104 – 6117**

Encoded Microcarriers For High-Throughput Multiplexed Detection

Communications

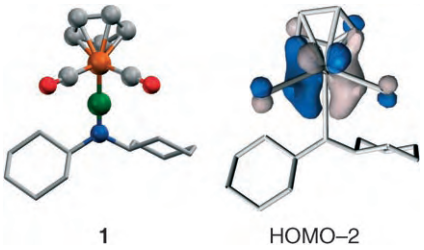

Charge changes everything: The cationic terminal aminoborylene complex $[CpFe(CO)_2(BNCy_2)]^+[BAr^F{}_4]^-$ (**1**, Cy = cyclohexyl, Ar^F = 3,5-$(CF_3)_2C_6H_3$; Fe orange, B green, N blue, O red, C gray) was structurally characterized. DFT studies (see HOMO−2) indicate delocalized π bonding along the linear Fe-B-N framework and significant Fe–B and B–N multiple-bond character.

Borylene Complexes

S. Aldridge,* C. Jones,* T. Gans-Eichler, A. Stasch, D. L. Kays (née Coombs), N. D. Coombs, D. J. Willock **6118 – 6122**

Cationic Terminal Borylene Complexes: Structure/Bonding Analysis and [4+1] Cycloaddition Reactivity of a BN Vinylidene Analogue

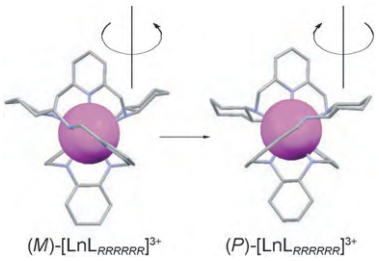

Giving lanthanides a new twist: The chiral nonaaza macrocycle L wraps tightly around lanthanide(III) ions in a helical fashion (see picture). The all-*R* enantiomer of the macrocycle, L_{RRRRRR}, forms kinetically controlled complexation products of *M* helicity (100% *de*), which undergo inversion to the *P* diastereomer (90% *de*). Both products have been isolated in enantiopure form and structurally characterized.

Helical Structures

J. Gregoliński, J. Lisowski* **6122 – 6126**

Helicity Inversion in Lanthanide(III) Complexes with Chiral Nonaaza Macrocyclic Ligands

For the USA and Canada:
ANGEWANDTE CHEMIE International Edition (ISSN 1433-7851) is published weekly by Wiley-VCH PO Box 191161, D 69451 Weinheim, Germany. Air freight and mailing in the USA by Publications Expediting Inc. 200 Meacham Ave., Elmont, NY 11003. Periodicals postage paid at Jamaica NY 11431. US POSTMASTER: send address changes to *Angewandte Chemie*, Wiley-VCH, 111 River Street, Hoboken, NJ 07030. Annual subscription price for institutions: US$ 5685/5168 (valid for print and electronic / print or electronic delivery); for individuals who are personal members of a national chemical society prices are available on request. Postage and handling charges included. All prices are subject to local VAT/sales tax.

© 2006 Wiley-VCH Verlag GmbH & Co. KGaA, Weinheim

The best in chemistry –

for more than a hundred years

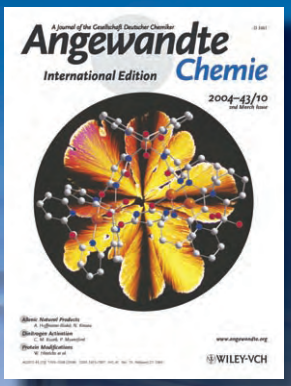

A Journal of the Gesellschaft Deutscher Chemiker

Angewandte
International Edition **Chemie**

www.angewandte.org

1888: ***The beginning of a success story***

Constant Innovations

1962: *First issue of the International Edition*
1976: *Graphical abstracts*
1979: *Cover pictures*
1988: *Centenary of Angewandte*
1989: *Routine use of color*
1991: *New section: Highlights*
1992: *Computerized editorial tracking system*
1995: *Internet service for readers*
1998: *Regular press service; full-text online*
2000: *New section: Essays; EarlyView: Communications available online ahead of the printed version*
2001: *New section: Minireviews*
2002: *Online submission of manuscripts*
2003: *Weekly publication; new section: News; new layout*
2004: *Backfiles (1962-1997); ManuscriptXpress: Online system for authors and referees*

Angewandte's advisors...

Richard R. Ernst
ETH Zürich

» I support ***Angewandte Chemie*** *because it is a first rank international journal of European origin. More than many other renowned journals, it implements a pioneering spirit, being ready for innovating its form and contents. Its bilingual mode of appearance is another plus. I am looking forward to an equally prosperous future for* ***Angewandte Chemie.*** *«*

Angewandte Chemie International Edition *is a journal of the German Chemical Society (GDCh)*

GDCh

WILEY InterScience® DISCOVER SOMETHING GREAT

WILEY-VCH

1821404_gu

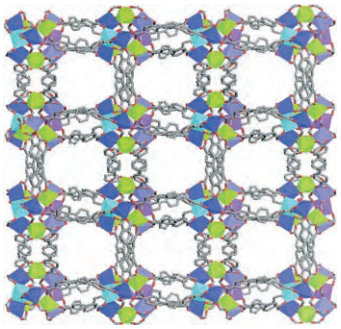

Flexible ligands afford large pores: A novel metal–organic framework constructed from cadmium carboxylate cluster secondary building units and formic acid bridging molecules is reported (see picture). This highly porous material displays rare body-centered cubic topology, as well as good sorption characteristics and optoelectronic properties.

Porous Materials

Q. R. Fang, G. S. Zhu,* Z. Jin, M. Xue, X. Wei, D. J. Wang, S. L. Qiu* ——— **6126 – 6130**

A Multifunctional Metal–Organic Open Framework with a bcu Topology Constructed from Undecanuclear Clusters

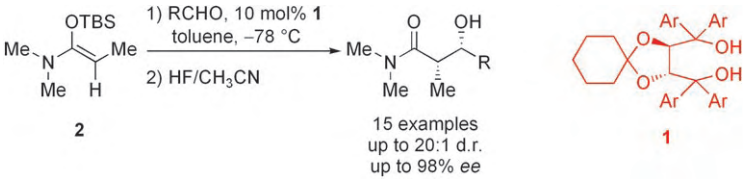

Enzyme lite: Like a minimalist enzyme, a simple chiral alcohol of the taddol family, **1**, catalyzes Mukaiyama aldol reactions between silyl enolates of amides and aldehydes to afford products with high diastereo- and enantioselectivities (see scheme; TBS = *tert*-butyldimethylsilyl).

Asymmetric Catalysis

J. D. McGilvra, A. K. Unni, K. Modi, V. H. Rawal* ——— **6130 – 6133**

Highly Diastereo- and Enantioselective Mukaiyama Aldol Reactions Catalyzed by Hydrogen Bonding

Running in reverse: A set of enzymes selected according to their RNA-dependent DNA polymerase activity from a library of more than 10^7 mutant enzymes has been characterized. The product was specifically bound to catalytically active proteins displayed on filamentous bacteriophage. The selected variants have a catalytic efficiency for reverse transcription that is two orders of magnitude higher.

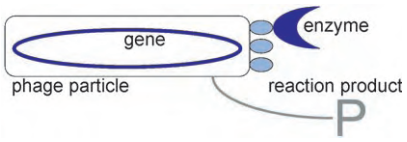

Directed Evolution

S. Vichier-Guerre, S. Ferris, N. Auberger, K. Mahiddine, J.-L. Jestin* ——— **6133 – 6137**

A Population of Thermostable Reverse Transcriptases Evolved from *Thermus aquaticus* DNA Polymerase I by Phage Display

It takes two to transfer: A synthetic Cu^I metalloprotein undergoes bimolecular photoinduced electron transfer in the inverted Marcus regime. The buried $Cu^I_4S_4(N/O)_4$ cofactor (purple) has a high reorganization energy and experiences weak electronic coupling to electron acceptors (Q) in the bulk solvent. This lowers k_{ET} below the diffusion limit and allows observation of inverted Marcus behavior.

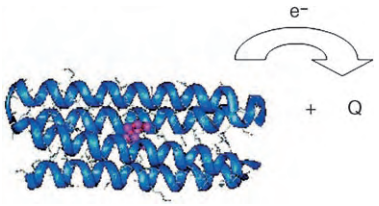

Photoinduced Electron Transfer

J. Hong, O. A. Kharenko, J. Fan, F. Xie, A. K. Petros, B. R. Gibney, M. Y. Ogawa* ——— **6137 – 6140**

Evidence That a Miniature Cu^I Metalloprotein Undergoes Collisional Electron Transfer in the Inverted Marcus Region

© 2006 Wiley-VCH Verlag GmbH & Co. KGaA, Weinheim

Contents

Living Polymerization

M. B. Harney, Y. Zhang, L. R. Sita* ——— 6140 – 6144

Bimolecular Control over Polypropene Stereochemical Microstructure in a Well-Defined Two-State System and a New Fundamental Form: Stereogradient Polypropene

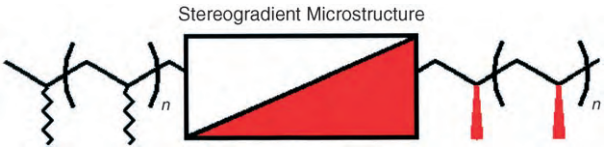

A new slant on polypropene: By taking advantage of the living nature of propene polymerization in a well-defined two-state system, an unlimited variety of polypropene microstructures, including a new stereogradient structure, can be prepared with stereochemical microstructural homogeneity.

DNA Recognition

N. Griesang, K. Gießler, T. Lommel, C. Richert* ——— 6144 – 6148

Four-Color, Enzyme-Free Interrogation of DNA Sequences with Chemically Activated, 3′-Fluorophore-Labeled Nucleotides

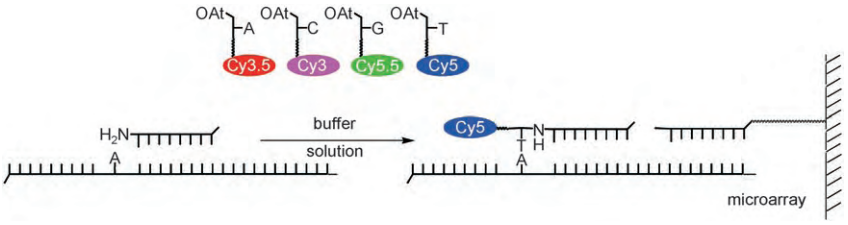

Color reveals base: The enzymatic template-directed elongation of primers with fluorophore-labeled nucleoside triphosphates is the most frequently used reaction for determining DNA sequences. Primer extension followed by optical read out can now be achieved without enzymes.

Bifunctional Metal Complexes

M. Kang, A. Chouai, H. T. Chifotides, K. R. Dunbar* ——— 6148 – 6151

2D NMR Spectroscopic Evidence for Unprecedented Interactions of *cis*-[Rh_2(dap)(μ-O_2CCH_3)$_2$(η^1-O_2CCH_3)-(CH_3OH)](O_2CCH_3) with a DNA Oligonucleotide: Combination of Intercalative and Coordinative Binding

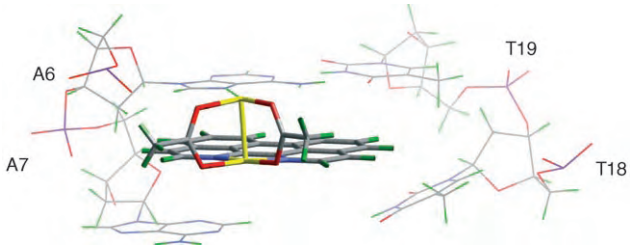

Slip it in: The dual capability of intercalation and coordination binding of dirhodium complexes was observed in the reaction of the title complex with d(CTCTCAACTTCC). A major adduct with the 1,12-diazaperylene (dap) group intercalated between the A6 and A7 residues was produced. Additionally, the Rh atom that is not bound to the dap group forms a coordinative bond to the N7 site of A6.

Polymeric Sensors

M. Sebastian, M. Hissler, C. Fave, J. Rault-Berthelot, C. Odin, R. Réau* ——— 6152 – 6155

Phosphole-Modified Poly(thiophene)s: Unique Postfunctionalizable Conjugated Polymers That Sense Elemental Chalcogenides

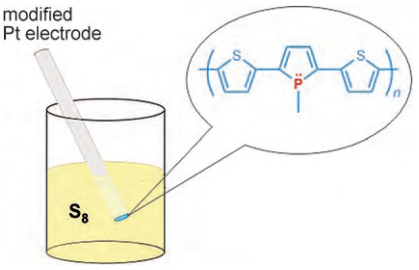

Bulk response: Following the development of conjugated polymers that sense ions or neutral molecules, the first π-conjugated polymer which is capable of detecting elemental chalcogens is presented. Individual reactions at the phosphole moieties (see picture) result in macroscopic responses of the bulk polymer.

© 2006 Wiley-VCH Verlag GmbH & Co. KGaA, Weinheim

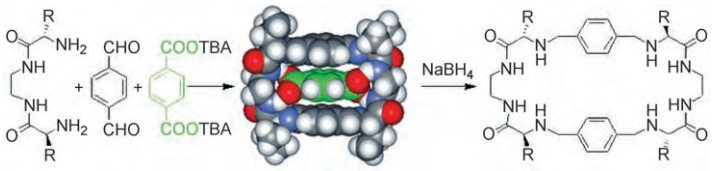

A very welcome guest: The terephthalate anion efficiently templates the selective assembly of a tetraimino dianion host–guest complex, which can be reduced to the final [2+2] pseudopeptidic macrocycle (see scheme; O red, blue N).

Macrocyclic Systems

M. Bru, I. Alfonso,* M. I. Burguete, S. V. Luis* ——— **6155 – 6159**

Anion-Templated Syntheses of Pseudopeptidic Macrocycles

Cyaphide attained: A high-yielding synthesis for the first stable terminal cyaphide complex [RuH(CP)(dppe)$_2$] (dppe = bis(1,2-diphenylphosphinoethane); see structure: P orange, Ru silver, C gray, H white) was developed from the silyl-substituted phosphaalkyne complex [RuH(dppe)$_2$(Ph$_3$SiC≡P)]OTf (OTf = $CF_3SO_3^-$) and sodium phenoxide.

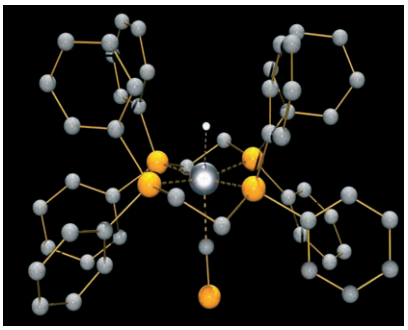

C≡P Ligands

J. G. Cordaro, D. Stein, H. Rüegger, H. Grützmacher* ——— **6159 – 6162**

Making the True "CP" Ligand

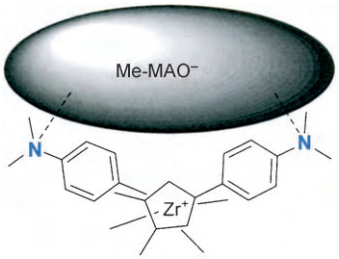

Unbridged yet isospecific metallocene polypropylene catalytic systems can be generated in situ during the MAO-assisted activation step (see picture; MAO = methyl aluminum oxane), as demonstrated with a dimethylaminophenyl-substituted zirconocene that has a racemic, C_2-symmetric structure in the solid state and produces highly isotactic polypropylene.

Polymerization Catalysts

S. K. Kim, H. K. Kim, M. H. Lee, S. W. Yoon, Y. Do* ——— **6163 – 6166**

Endowing Aspecific, Unbridged-Metallocene Propylene-Polymerization Catalysts with Isospecificity: The Unprecedented Role of MAO

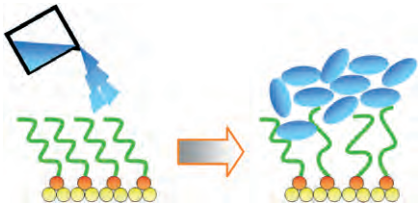

Reversible switching between order and disorder in a 1-nonanethiol self-assembled monolayer (SAM) is easily accomplished by alternately exposing the monolayer to liquid ethanol then to a helium stream (see picture). Upon removing the liquid phase, the development of crystalline order in the monolayer takes place over a time scale of hours, which implies the sequential crystallization of individual thiol domains.

Self-Assembled Monolayers

M. J. Capitán,* J. Álvarez, J. J. Calvente, R. Andreu ——— **6166 – 6169**

Onset of Crystalline Order in 1-Nonanethiol Monolayers Deposited from Solution

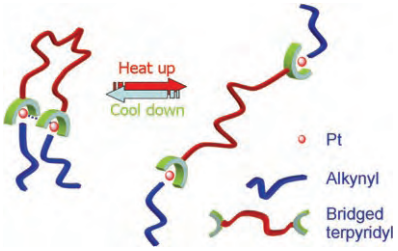

Sticking together: Dinuclear platinum(II) terpyridyl complexes display a high tendency towards intramolecular self-association, in which the two Pt terpy units "stick together". The driving force is provided by metal–metal and π–π interactions which can be controlled by temperature modulation.

Coordination Chemistry

V. W.-W. Yam,* K. H.-Y. Chan, K. M.-C. Wong, B. W.-K. Chu **6169 – 6173**

Luminescent Dinuclear Platinum(II) Terpyridine Complexes with a Flexible Bridge and "Sticky Ends"

© 2006 Wiley-VCH Verlag GmbH & Co. KGaA, Weinheim

Contents

Micelles

Y. J. Jun, U. S. Toti, H. Y. Kim, J. Y. Yu, B. Jeong, M. J. Jun, Y. S. Sohn* ——— **6173 – 6176**

Thermoresponsive Micelles from Oligopeptide-Grafted Cyclotriphosphazenes

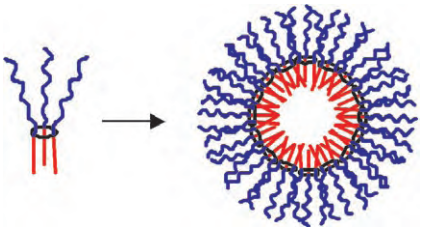

Hard graft: Amphiphilic cyclic phosphazene trimers grafted with hydrophobic oligopeptide (red) and hydrophilic methoxypolyethylene glycol (blue) show a variety of thermoresponsive properties including lower critical solution temperatures near body temperature. They form strong micelles in aqueous solution at an appropriate hydrophobic-to-hydrophilic balance.

Prebiotic Chemistry

C. Anastasi, M. A. Crowe, M. W. Powner, J. D. Sutherland* ——— **6176 – 6179**

Direct Assembly of Nucleoside Precursors from Two- and Three-Carbon Units

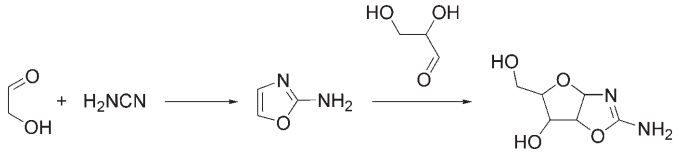

Sweetness and life: Pentose aminooxazolines—intermediates in potentially prebiotic nucleoside synthesis—can be produced in water from a reaction that bypasses the corresponding sugar. 2-Aminooxazole, a condensation product of glycolaldehyde and cyanamide, reacts with glyceraldehyde under mild conditions in a remarkable process that is essentially quantitative, and is highly stereoselective for ribose and arabinose aminooxazolines.

Thioglycoside Hydrolysis

V. L. Y. Yip, S. G. Withers* — **6179 – 6182**

Family 4 Glycosidases Carry Out Efficient Hydrolysis of Thioglycosides by an α,β-Elimination Mechanism

Thioglycosides are widely used as competitive inhibitors of glycosidases. The first glycosidase capable of hydrolyzing unactivated thioglycosides—BglT, a 6-phospho-β-glucosidase from glucosidase family 4—has been found. The efficient cleavage of the thioglycosidic linkage is a consequence of the α,β-elimination mechanism used by GH4 enzymes, in contrast to the nucleophilic displacement mechanisms of "classical" glycosidases.

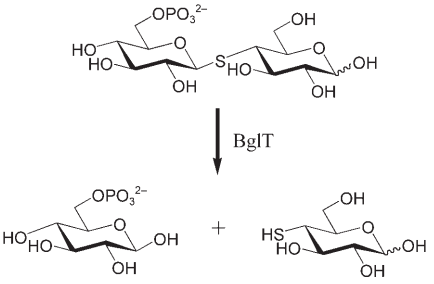

Radicals in Synthesis

J. Y. Lee, Y.-T. Hong, S. Kim* **6182 – 6186**

Radical Alkylation of Bis(silyloxy)enamine Derivatives of Organic Nitro Compounds

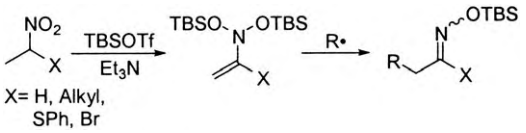

Alkylation β to a nitro group by radical chemistry is made possible by initial conversion of the organic nitro compound into a bis(silyloxy)enamine (see scheme; TBSOTf = *tert*-butyldimethylsilyl trifluoromethanesulfonate). An advantage of the method is the simultaneous conversion of the nitro group into a synthetically useful oxime ether group.

© 2006 Wiley-VCH Verlag GmbH & Co. KGaA, Weinheim

Deuces wild: From catalysis through materials science to biology, N-heterocyclic carbenes (NHCs) can truly be regarded as a wild card of ligands. A new series of "two-faced" (Janus-type) ligands composed of two linearly opposed NHCs fused to an arene linker has been synthesized and can be used to prepare discrete bimetallic complexes.

Carbene Ligands

D. M. Khramov, A. J. Boydston, C. W. Bielawski* ——— **6186 – 6189**

Synthesis and Study of Janus Bis(carbene)s and Their Transition-Metal Complexes

High-transparency optical limiters: A series of solution-processable white metallopolyynes are shown to be excellent optical power limiters (see picture) with optimized optical transparency/nonlinearity trade-off. They exhibit an optical-limiting performance superior to those of the common reverse saturable absorption dyes, such as C_{60} and metal phthalocyanine complexes.

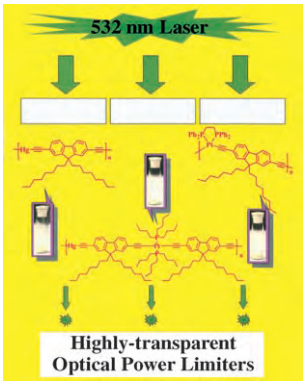

Metallopolyynes

G.-J. Zhou, W.-Y. Wong,* Z. Lin, C. Ye ——— **6189 – 6193**

White Metallopolyynes for Optical Limiting/Transparency Trade-off Optimization

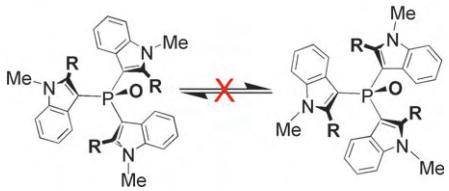

Fixing the propeller: There is general consensus that phosphine oxides and phosphines carrying three identical aryl groups are operationally achiral compounds. Herein it is shown that suitably tailored triarylphosphine oxides give rise to configurationally stable residual enantiomers, which were isolated in an enantiopure state.

Chirality

T. Benincori, G. Celentano, T. Pilati, A. Ponti, S. Rizzo, F. Sannicolò* ——— **6193 – 6196**

Configurationally Stable Molecular Propellers: First Resolution of Residual Enantiomers

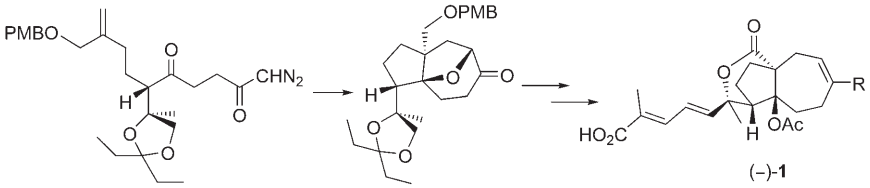

The antiangiogenic and cytotoxic natural product pseudolaric acid A ((−)-**1**) has been obtained by a 26-step synthetic route. This enantioselective synthesis employed an intramolecular carbene cyclization cycloaddition cascade reaction as the key step to construct the carbocyclic framework. PMB = *para*-methoxybenzyl.

Total Synthesis

Z. Geng, B. Chen, P. Chiu* **6197 – 6201**

Total Synthesis of Pseudolaric Acid A

© 2006 Wiley-VCH Verlag GmbH & Co. KGaA, Weinheim

Contents

Surface Organometallic Chemistry

F. Blanc, C. Copéret,* J. Thivolle-Cazat, J.-M. Basset* ——— **6201 – 6203**

Alkane Metathesis Catalyzed by a Well-Defined Silica-Supported Mo Imido Alkylidene Complex: [(≡SiO)Mo(=NAr)(=CH*t*Bu)(CH_2*t*Bu)]

A two-functions-in-one catalyst precursor allows an olefin metathesis catalyst to be turned into an alkane metathesis catalyst. A silica-supported alkyl alkylidene molybdenum complex containing an ancillary imido ligand is a highly active olefin metathesis catalyst and also acts as a catalyst precursor for alkane metathesis. This system involves a single metal with dual properties and shows that ancillary ligands are compatible with alkane metathesis reactions.

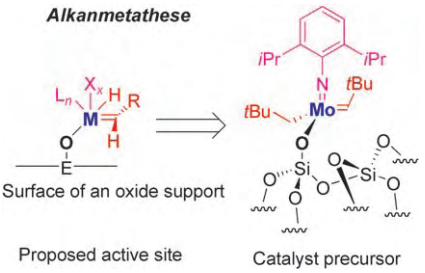

Asymmetric Catalysis

I. Lyothier, C. Defieber, E. M. Carreira* ——— **6204 – 6207**

Iridium-Catalyzed Enantioselective Synthesis of Allylic Alcohols: Silanolates as Hydroxide Equivalents

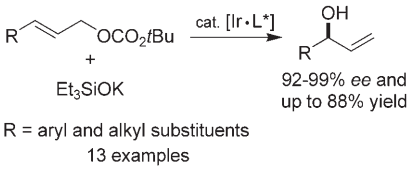

Masked hydroxide: A highly regio- and enantioselective Ir-catalyzed allylic etherification of acyclic, achiral allylic carbonates can be achieved by using potassium silanolates as nucleophiles. The use of these hydroxide equivalents allows access to valuable chiral allylic alcohols.

Solid-Phase Chemistry

L. Liu, M. Yan* ——— **6207 – 6210**

A General Approach to the Covalent Immobilization of Single Polymers

Stuck fast: The covalent immobilization of polymeric single molecules is achieved by the photochemically induced C–H/N–H insertion reaction of perfluorophenylazides (see picture). When the concentration of the surface azido groups is decreased, isolated polymeric single molecules are observed. This technique is especially suited for materials that do not possess functional groups and are difficult to be immobilized by other means.

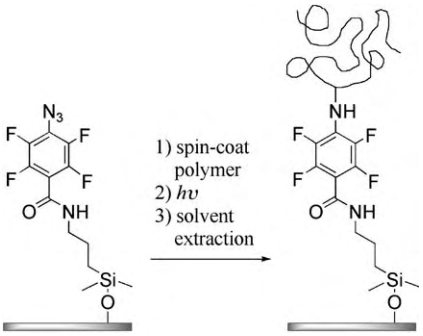

U–U Multiple Bonds

G. La Macchia, M. Brynda, L. Gagliardi* ——— **6210 – 6213**

Quantum Chemical Calculations Predict the Diphenyl Diuranium Compound [PhUUPh] To Have a Stable ^1A_g Ground State

Nice to see U_2! The [PhUUPh] molecule (see picture; U pink, C gray, H white) has been studied by multiconfigurational quantum chemical methods. It was found that a quintuple bond is formed between the two uranium atoms with a U–U bond length of 2.29 Å. The phenyl ligand was used to mimic a bulky terphenyl ligand, which could be a promising candidate for the stabilization of multiply bonded uranium compounds.

© 2006 Wiley-VCH Verlag GmbH & Co. KGaA, Weinheim

Light-driven metallo-organic catalysis: Intramolecular photoelectron transfer in the heterodinuclear complex **1** facilitates the photocatalytic production of hydrogen and the selective hydrogenation of tolane to give *cis*-stilbene. All three well-coordinated parts of the supramolecular system are essential: the $(tbbpy)_2Ru$ fragment as a photoactive unit, the redox-active bridging ligand as an electron relay and storage site, and the palladium as a catalytically active center.

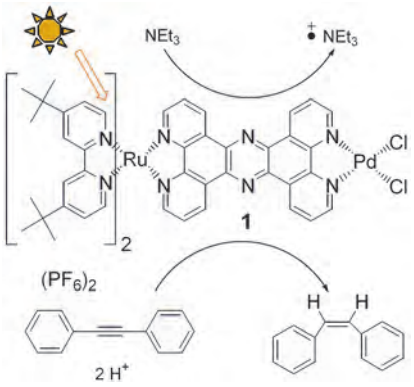

Photocatalysis

S. Rau,* B. Schäfer, D. Gleich, E. Anders, M. Rudolph, M. Friedrich, H. Görls, W. Henry, J. G. Vos ——— **6215 – 6218**

A Supramolecular Photocatalyst for the Production of Hydrogen and the Selective Hydrogenation of Tolane

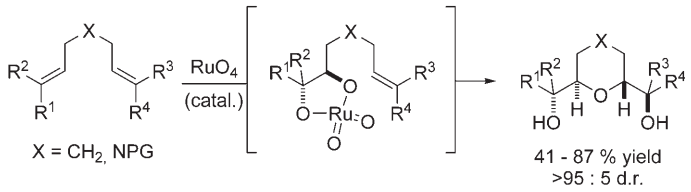

Widely applicable: Substituted tetrahydropyran products can be obtained in good to high yields and excellent diastereoselectivity by oxidative cyclization of 1,6-dienes (see scheme, PG = protecting group). In situ generated ruthenium tetroxide (1–5 mol %) serves as a catalyst and sodium periodate on wet silica serves as a terminal oxidant. The conversion of a cyclization product into a synthetically useful δ-lactone building block is also presented.

Heterocyclic Synthesis

S. Roth, C. B. W. Stark* ——— **6218 – 6221**

Efficient Oxidative Cyclization of 1,6-Dienes: A Highly Diastereoselective Entry to Substituted Tetrahydropyrans

Six packs: Hydrogen-bonded pyrogallol[4]arene hexameric nanocapsules self-assemble into spheres (A; see picture), tubules, and combinations of both (B) on the sub-micron scale. These assemblies were characterized by using dynamic light scattering, scanning electron microscopy, transmission electron microscopy (see inset), and atomic force microscopy techniques.

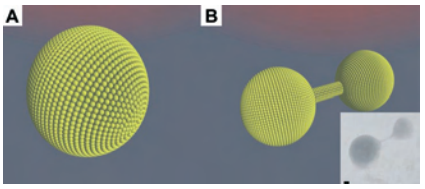

Supramolecular Chemistry

M. W. Heaven, G. W. V. Cave, R. M. McKinlay, J. Antesberger, S. J. Dalgarno, P. K. Thallapally, J. L. Atwood* ——— **6221 – 6224**

Hydrogen-Bonded Hexamers Self-Assemble as Spherical and Tubular Superstructures on the Sub-Micron Scale

The issues for September 2006 appeared online on the following dates
Issue 33: August 11. · Issue 34: August 12. · Issue 35: September 1. · Issue 36: September 5

© 2006 Wiley-VCH Verlag GmbH & Co. KGaA, Weinheim

Sources

Product and Company Directory

You can start the entry for your company in "Sources" in any issue of *Angewandte Chemie*.

If you would like more information, please do not hesitate to contact us.

Wiley-VCH Verlag – Advertising Department
Tel.: 0 62 01 - 60 65 65
Fax: 0 62 01 - 60 65 50
E-Mail: MSchulz@wiley-vch.de

Service

Keywords ____ 6226

Authors ____ 6227

Angewandte's Sister Journals ____ 6225

Preview ____ 6229

Novartis Chemistry Lectureship

Novartis Pharma AG is pleased to announce the following Novartis Chemistry Lecturers for 2006 – 2007

Eiichi Nakamura
University of Tokyo, Tokyo, Japan

Samir Z. Zard
CNRS-Ecole Polytechnique, Palaiseau, France

Brian K. Shoichet
University of California, San Francisco, USA

Erik J. Sorensen
Princeton University, Princeton, USA

Andrew D. Hamilton
Yale University, New Haven, USA

James C. Anderson
University of Nottingham, Nottingham, UK

F. Dean Toste
University of California, Berkeley, USA

Mark Bradley
University of Edinburgh, Edinburgh, UK

Viresh H. Rawal
University of Chicago, Chicago, USA

The Novartis Chemistry Lectureship is awarded to scientists in recognition of outstanding contributions to organic and computational chemistry, including applications to biology.

NOVARTIS

© 2006 Wiley-VCH Verlag GmbH & Co. KGaA, Weinheim

SFC Prize for Organic Chemistry to A.-M. Caminade

The Société Française de Chimie (SFC, French Chemical Society) has awarded Anne-Marie Caminade (Laboratoire de Chimie de Coordination, LCC, Toulouse, France) with the Prize of the Organic Chemistry Division. Her research is focused on the chemistry of phosphorus, particularly with low coordination numbers, metallic hydrides, macrocycles and cryptands, as well as dendrimers and highly branched polymers. She is considered a pioneer in the area of phosphorus-containing dendrimers, which nowadays can be efficiently synthesized and have many applications in the fields of catalysis, materials, and medicine, among others. One such application involves a process that allows the mass production of human natural killer (NK) cells from a simple blood sample. Her recent Minireview on phosphorus-containing dendrons was highlighted on the cover of the *European Journal of Inorganic Chemistry*.[1a] Also, her group reported in *Angewandte Chemie* on the development of water-soluble dendrimers for in vivo imaging.[1b]

A.-M. Caminade

Caminade completed her PhD in 1984 at the Université Paul Sabatier in Toulouse under the guidance of M. Koenig. She then joined H. Mimoun at the Institut Français du Pétrole and completed a second PhD in 1988 at the LCC (J.-P. Majoral). Subsequently, she worked as an A. von Humboldt fellow in the group of M. Veith at the Universität des Saarlandes (Saarbrücken, Germany) before taking a position at the LCC in Toulouse. She is presently co-director of the Molecular, Macromolecular, and Supramolecular Heterochemistry Group at the LCC.

S. Quideau receives Acros-SFC Prize

The Acros-SFC Prize is also awarded by the Organic Chemistry Division of the SFC, and this year it goes to Stéphane Quideau (Université de Bordeaux I). Quideau studied chemistry at the Université Catholique d'Angers and the Université de Nantes, and completed his PhD in 1990 at the University of Wisconsin–Madison under the guidance of J. Ralph on the oxidative coupling of *p*-hydroxycinnamic acid derivatives to lignins. He then joined K. Feldmann at the University of Pennsylvania, where he carried out postdoctoral studies on the chemistry of ellagitannins. In 1997 he accepted a position as an assistant professor at Texas Tech University in Lubbock, and a year later he moved back to France as a professor at Bordeaux. In 1999 he was appointed a co-director of the Institute of Natural Products; In 2003 he accepted a position as group leader at the European Institute of Chemistry and Biology at Pessac in Bordeaux. His research group is affiliated with the CNRS Laboratory of Organic and Organometallic Chemistry.

S. Quideau

Quideau is a member of the University Institute of France.

The research interests of Quideau's group lie in the area of structure elucidation, synthesis, and biomechanistic study of biologically active natural products. In particular, they are interested in the oxidation of phenols, the asymmetric dearomatization of aromatic alcohols, and the heterocyclization reactions of *ortho*-quinols for the construction of nitrogen polycycles, which have been applied to the synthesis of lycorine and its analogues. He has developed new methods for C–C bond formation through oxidative nucleophilic substitutions mediated by hypervalent iodine(III) and recently described the regioselective hypervalent-iodine(III)-mediated dearomatizing phenylation of phenol derivatives through direct ligand coupling in *Angewandte Chemie*.[2a] Another achievement was the development of SIBX—a stable form of the powerful oxidizing agent iodoxybenzoic acid (IBX). As an inhabitant of Bordeaux, Quideau is no stranger to wine: he recently discussed the chemistry of wine polyphenolic *C*-glycosidic ellagitannins, which are found in wine as a result of the ageing process in oak barrels and which target human topoisomerase II, in *Chemistry—A European Journal*.[2b]

[1] a) A.-M. Caminade, A. Maraval, J.-P. Majoral, *Eur. J. Inorg. Chem.* **2006**, 887; b) T. R. Krishna, M. Parent, M. H. V. Werts, L. Moreaux, S. Gmouh, S. Charpak, A.-M. Caminade, J.-P. Majoral, M. Blanchard-Desce, *Angew. Chem.* **2006**, *118*, 4761; *Angew. Chem. Int. Ed.* **2006**, *45*, 4645.

[2] a) A. Ozanne-Beaudenon, S. Quideau, *Angew. Chem.* **2005**, *117*, 7227; *Angew. Chem. Int. Ed.* **2005**, *44*, 7065; b) S. Quideau, M. Jourdes, D. Lefeuvre, D. Montaudon, C. Saucier, Y. Glories, P. Pardon, P. Pourquie, *Chem. Eur. J.* **2005**, *11*, 6503.

DOI: 10.1002/anie.200603237

WILEY InterScience DISCOVER SOMETHING GREAT
© 2006 Wiley-VCH Verlag GmbH & Co. KGaA, Weinheim

Alkane Metathesis

DOI: 10.1002/anie.200602155

From Olefin to Alkane Metathesis: A Historical Point of View**

Jean-Marie Basset, Christophe Copéret, Daravong Soulivong, Mostafa Taoufik, and Jean Thivolle-Cazat*

Keywords:
alkane metathesis · dehydrogenation · heterogeneous catalysis · homogeneous catalysis · olefin metathesis

Alkane conversion has been a major focus of petrochemical research for the past century,[1–3] and in fact the discovery of olefin metathesis on supported MoO_3 or WO_3 systems by Banks and Bailey was the result of the investigation of the reactivity of alkane and olefin mixtures on such types of catalysts.[4,5] Under these conditions, only olefins were transformed, which led to the development of very important industrial processes such as the Lummus ABB process, which converts ethylene into propylene through cross-metathesis with 2-butenes on W-based catalysts.[6] This discovery was rapidly turned into an alkane conversion process first by Banks (Philipps) and then by Hughes (Chevron)[7,8] by combining heterogeneous dehydrogenation/hydrogenation and olefin metathesis catalysts, which allows a given alkane to be converted into its lower and higher homologues. This reaction [Eq. (2)], like olefin metathesis [Eq. (1)], is thermoneutral (Figure 1), but requires the intermediate formation of olefins from alkanes [Eq. (3)], which

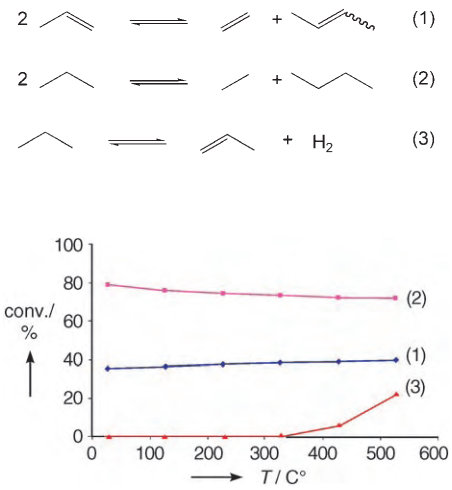

Figure 1. Thermodynamic data (conversion as a function of temperature) of the chemical processes olefin metathesis [Eq. (1)], alkane metathesis [Eq. (2)], and alkane dehydrogenation [Eq. (3)].

is highly disfavored. Therefore, high temperatures are required for high concentration of olefins (Figure 1). For example, in the Chevron process, which relies on a mixture of Pt/Al_2O_3 (dehydrogenation/hydrogenation) and WO_3/SiO_2 (metathesis), high temperatures and high pressures are necessary, typically 400 °C and 60 bar (Figure 2).[9]

In 1997, within a research program targeted at the activation of C–H bonds by supported transition-metal catalysts, J.-M. Basset et al. reported the conversion of alkanes at low temperatures and pressures, typically 150 °C and 1 bar, into their lower and higher homologues. The catalyst was a silica-supported tantalum hydride,[10] and the reaction was named alkane metathesis by analogy with olefin metathesis (Scheme 1 a). An important research effort in collaboration with BP Chemicals and BP has yielded numerous catalytic systems based on Group 5 and Group 6 hydride and alkyl systems,[11–13] and currently the best system is a W hydride supported on alumina (turnover number (TON) = 120 after 120 h under ca. 0.8 bar of propane; Scheme 1 b).[13] Notably, the catalytic systems based on hydrides give better results under pressure and can be regenerated by treatment under H_2.

Recent kinetic and mechanistic studies in our laboratories[12,14] have shown that the key carbon–carbon bond-breaking and bond-making steps correspond to those of olefin metathesis, that is, a [2+2] cycloreversion and a cycloaddition step.[15,16] The transformation of the alkane into an olefin and carbenic propagating species involves additional key elementary steps. It has been proposed that an alkyl species is formed by C–H activation of alkanes, which, by a subsequent β-H or α-H transfer step, yields the olefin or a hydridocarbene intermediate, the necessary propagating center for olefin metathesis (Scheme 1 c). The corresponding reverse step yields the alkane metathesis product. Notably, and in contrast to the Chevron process, alkane metathesis is carried out on a dual catalyst based on a single metal having all the necessary properties (C–H activation, dehydro-

[*] Dr. J.-M. Basset, Dr. C. Copéret, Dr. D. Soulivong, Dr. M. Taoufik, Dr. J. Thivolle-Cazat
LCOMS UMR 9986
CPE Lyon
43 Bd du 11 Novembre 1918, 69616
Villeurbanne Cedex (France)
Fax: (+33) 4-7243-1795
E-mail: coperet@cpe.fr

[**] We are indebted to the CNRS, the Ministère délégué à l'Enseignement supérieur et à la Recherche, the Région Rhônes-Alpes, and CPE Lyon for financial support. We would also like to thank our industrial partners INEOS and BP for continuous support, and more specifically S. Chakka, B. M. Maunders, S. Spitzmesser, and G. J. Sunley. Finally, we thank the graduate students and postdoctoral fellows who carry out research in the LCOMS.

InterScience
© 2006 Wiley-VCH Verlag GmbH & Co. KGaA, Weinheim

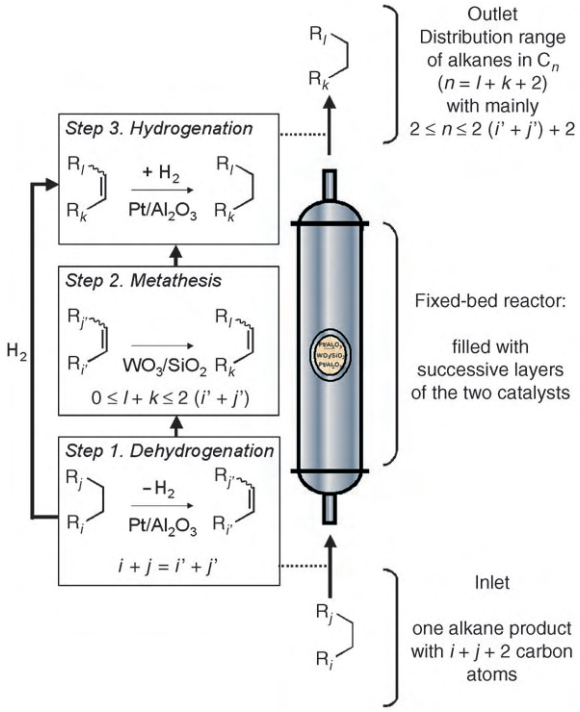

Figure 2. Schematic view of the homologation processes taking place within a fixed-bed reactor.

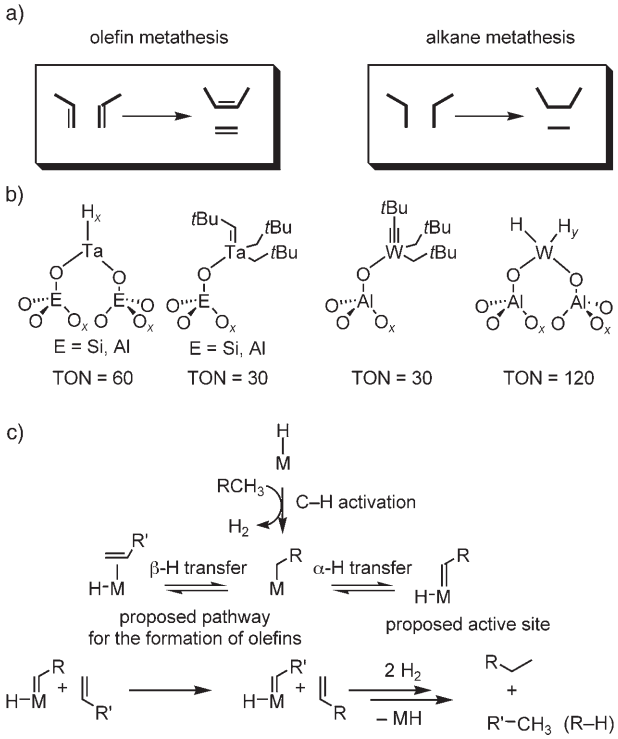

Scheme 1. a) Analogy between olefin and alkane metathesis. b) Examples of alkane metathesis catalysts developed by J.-M. Basset et al. (TON data for experiments performed under the same reaction conditions, $p = 0.8$ bar, $T = 150\,°C$. The subscripts x and y symbolize the number of O and H atoms ($x = 1$ for E = Si, $1 < x < 3$ for E = Al; $1 < y < 3$). c) Proposed reaction pathway with supported hydride catalysts.

genation, metathesis, and hydrogenation), and moreover, these catalytic systems can be used to incorporate methane into higher homologues.[17] Finally, these systems are selective towards C_{n-1} and C_{n+1} homologues, because the major pathway involves the cross-metathesis of the terminal olefin ($R' = C_{n-2}$, Scheme 1c) and the alkylidene species resulting from the activation of the terminal C–H bond of the alkane ($R = C_{n-1}$, Scheme 1c)

After nearly 30 years without external reports, Chevron has published new patents on their system,[18,19] and just recently a collaborative effort of the groups of Brookhart, Goldman, and Chevron has provided a homogeneous catalytic system related to the original Chevron process,[20] but based on a combination of homogeneous catalysts, the Kaska Ir complexes **1**[21–23] as dehydrogenation/hydrogenation catalysts, and the Mo imido olefin metathesis catalyst **2** of Schrock[24,25] (Figure 3a). In the presence of **1a** ($L = C_2H_4$) and **2**, hexane is converted into a mixture of C_2–C_{14} alkane products (0.75–2.05 M, Figure 3b), which corresponds to a TON of about 49–128 based on **2**.

It is noteworthy that the reaction takes place at such a low temperature because the amount of olefin must be

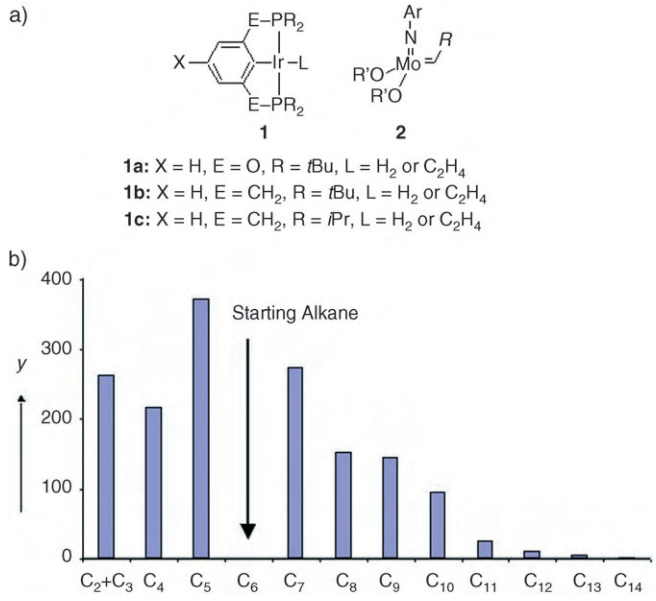

Figure 3. a) Homogeneous catalytic precursors; in **2**: Ar = 2,6-*i*$Pr_2C_6H_3$, R = CMe_2Ph, R′ = $C(CH_3)(CF_3)_2$. b) Product distribution y (expressed in mmol L^{-1}) for hexane metathesis (7.6 M) with **1a** ($L = C_2H_4$; 10 mM) and **2** (16 mM) after 4 days of reaction at 125 °C (data extracted from reference [20]).

© 2006 Wiley-VCH Verlag GmbH & Co. KGaA, Weinheim

very low, which shows that both catalysts must be quite efficient. The Ir catalyst precursors can be **1a**, **1b**, or **1c**, but in each case, it is necessary to add an activator, 3,3-dimethyl-1-butene (2 equiv), a well-known H_2 scavenger,[26,27] to the dihydrogen derivative. The catalytic system slowly deactivates with time, and this is mainly a result of the slow decomposition of **2**. In fact, adding an extra amount of **2** allows the alkane mixture to be further converted. Notably, the Grubbs-type Ru catalysts[28] are not efficient for this system because they are not compatible with complexes **1** (decomposition).

The product distribution (all linear alkanes from C_2–C_{14}) clearly indicates that the reaction corresponds to successive steps of dehydrogenation, olefin metathesis, and hydrogenation. Notably, the products do not arise from the selective metathesis of 1-hexene, the kinetic product of the Ir-based system,[29] which would give only the C_2 and C_{10} homologues, but from the cross-metathesis of all hexene isomers. Moreover, the formation of alkanes of carbon number greater than 10 in small amounts is evidence for successive reactions such as the cross-metathesis of hexane (as hexenes) with higher homologues. It is also noteworthy that the distribution of the products is consistent with their formation through nearly a statistical metathesis of an equilibrated mixture of hexene isomers (internal olefins in greater amount than terminal ones leading to homologues of shorter chain lengths compared to those derived from the metathesis of terminal olefins). This is a major difference compared with the systems based on catalysts prepared through surface organometallic chemistry which give mainly the C_{n-1} and C_{n+1} homologues (see above). Finally, the absence of formation of methane with the homogenous catalytic system shows that the methylidene propagating species (and probably other alkylidene species) does not react with H_2 through hydrogenolysis, and that alkanes are solely formed by hydrogenation of olefins at the Ir center.

Moreover, one initiation product, 2-methyl-2-phenylbutane, which probably results from the cross-metathesis of the neophylidene Mo complex **2** and 1-hexene and subsequent hydrogenation, has been detected. More information on **2** through spectroscopy studies have so far been hindered by the presence of many propagating species and deactivation. On the other hand, it was possible to observe the resting states of the Ir systems by monitoring the reaction mixture by NMR: depending on whether **1a** or **1b** is used, it is either the olefin or the dihydrogen complex, respectively. This type of study will probably allow further improvement of the catalytic system based on a structure–reactivity relationship.

Finally, owing to the instability of **2**, the combination of the Ir homogeneous catalyst with a heterogeneous olefin metathesis catalyst, Re_2O_7 on alumina, has also been investigated. Starting from decane, a distribution of alkane products is also obtained: a TON of 180/Ir has been achieved after three hours, after nine days of reaction this value increases to about 400/Ir. It is noteworthy that the authors have chosen Re-based catalysts because they are usually more susceptible to deactivation at higher temperatures than the analogous Mo or W-based systems. The latter systems, however, require higher temperatures, which could be detrimental to the Ir catalysts.

The groups of Brookhart and Goldman have reported the first approach to a homogeneous alkane metathesis catalytic system based on the Chevron technology that is the combination of two catalysts: a dehydrogenation/hydrogenation catalyst and an olefin metathesis catalyst. A first attempt to combine the Ir dehydrogenation catalyst with a more robust heterogeneous olefin metathesis catalyst, Re_2O_7/Al_2O_3, has yielded promising results, and the use of spectroscopic studies has already given some insight about the fate of the homogeneous catalysts, which should lead to the development of better catalytic systems. Thus, new rapid advances in the field of alkane conversions are expected, and significant developments can be anticipated.[30] There are still several challenges ahead such as finding stable—easily regenerated—catalysts and achieving a selective transformation of alkanes into a minimum number of homologues.

Published online: August 29, 2006

[1] R. H. Crabtree, *J. Chem. Soc. Dalton Trans.* **2001**, 2437.
[2] J. A. Labinger, J. E. Bercaw, *Nature* **2002**, *417*, 507.
[3] G. A. Olah, A. Molnar, *Hydrocarbon Chemistry*, 2nd ed., Wiley Interscience, New York, **2003**.
[4] R. L. Banks, G. C. Bailey, *Ind. Eng. Chem. Prod. Res. Dev.* **1964**, *3*, 170.
[5] L. F. Heckelsberg, R. L. Banks, G. C. Bailey, *Ind. Eng. Chem. Prod. Res. Dev.* **1969**, *8*, 259.
[6] J. C. Mol, *J. Mol. Catal. A* **2004**, *213*, 39.
[7] L. F. Heckelsberg, R. L. Banks (Phillips Petroleum Co.), US3445541, **1969**.
[8] T. R. Hughes (Chevron Research Co.), US3773845, **1971**.
[9] R. L. Burnett, T. R. Hughes, *J. Catal.* **1973**, *31*, 55.
[10] V. Vidal, A. Theolier, J. Thivolle-Cazat, J.-M. Basset, *Science* **1997**, *276*, 99.
[11] C. Copéret, O. Maury, J. Thivolle-Cazat, J.-M. Basset, *Angew. Chem.* **2001**, *113*, 2393; *Angew. Chem. Int. Ed.* **2001**, *40*, 2331.
[12] E. Le Roux, M. Chabanas, A. Baudouin, A. de Mallmann, C. Copéret, E. A. Quadrelli, J. Thivolle-Cazat, J.-M. Basset, W. Lukens, A. Lesage, L. Emsley, G. J. Sunley, *J. Am. Chem. Soc.* **2004**, *126*, 13391.
[13] E. Le Roux, M. Taoufik, C. Copéret, A. de Mallmann, J. Thivolle-Cazat, J.-M. Basset, B. M. Maunders, G. J. Sunley, *Angew. Chem.* **2005**, *117*, 6913; *Angew. Chem. Int. Ed.* **2005**, *44*, 6755.
[14] J. M. Basset, C. Copéret, L. Lefort, B. M. Maunders, O. Maury, E. Le Roux, G. Saggio, S. Soignier, D. Soulivong, G. J. Sunley, M. Taoufik, J. Thivolle-Cazat, *J. Am. Chem. Soc.* **2005**, *127*, 8604.
[15] J. L. Herisson, Y. Chauvin, *Makromol. Chem.* **1971**, *141*, 161.
[16] X. Solans-Monfort, E. Clot, C. Copéret, O. Eisenstein, *J. Am. Chem. Soc.* **2005**, *127*, 14015.
[17] D. Soulivong, C. Copéret, J. Thivolle-Cazat, J.-M. Basset, B. M. Maunders, R. B. A. Pardy, G. J. Sunley, *Angew. Chem.* **2004**, *116*, 5480; *Angew. Chem. Int. Ed.* **2004**, *43*, 5366.
[18] D. O'Rear, D. H. Mohr, C.-Y. Chen, P. J. White (Chevron USA Inc., USA), WO200116059, **2001**.
[19] C.-Y. Chen, D. J. O'Rear, S. R. Brundage (Chevron USA Inc., USA), WO2002000578, **2002**.
[20] A. S. Goldman, A. H. Roy, Z. Huang, R. Ahuja, W. Schinski, M. Brookhart, *Science* **2006**, *312*, 257.
[21] M. Gupta, C. Hagen, R. J. Flesher, W. C. Kaska, C. M. Jensen, *Chem. Commun.* **1996**, 2083.
[22] M. Gupta, C. Hagen, W. C. Kaska, R. E. Cramer, C. M. Jensen, *J. Am. Chem. Soc.* **1997**, *119*, 840.

 © 2006 Wiley-VCH Verlag GmbH & Co. KGaA, Weinheim

[23] C. M. Jensen, *Chem. Commun.* **1999**, 2443.
[24] R. R. Schrock, *Chem. Rev.* **2002**, *102*, 145.
[25] R. R. Schrock, *J. Mol. Catal. A* **2004**, *213*, 21.
[26] D. Baudry, M. Ephritikhine, H. Felkin, *J. Chem. Soc. Chem. Commun.* **1982**, 606.
[27] D. Baudry, M. Ephritikhine, H. Felkin, R. Holmes-Smith, *J. Chem. Soc. Chem. Commun.* **1983**, 788.
[28] T. M. Trnka, R. H. Grubbs, *Acc. Chem. Res.* **2001**, *34*, 18.
[29] F. Liu, E. B. Pak, B. Singh, C. M. Jensen, A. S. Goldman, *J. Am. Chem. Soc.* **1999**, *121*, 4086.
[30] F. Blanc, C. Copéret, J. Thivolle-Cazat, J.-M. Basset, *Angew. Chem.* **2006**, *118*, 6347; *Angew. Chem. Int. Ed.* **2006**, *45*, 6201.

Wiley-VCH BOOK SHOP

Maintaining your Expertise in Organic Chemistry

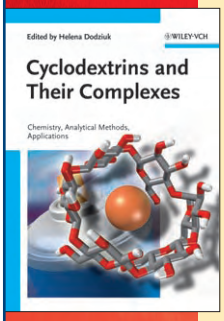

H. Dodziuk (ed.)
Cyclodextrins and Their Complexes
Chemistry, Analytical Methods, Applications
Cyclodextrins present a fascinating and multifunctional substance class: they play a major role in pharmaceutical industry, in analytical science and in supramolecular chemistry.
507 pp, cl, € 149.00
ISBN-10: 3-527-31280-3
ISBN-13: 978-3-527-31280-1

A. Gossauer
Struktur und Reaktivität der Biomoleküle
Eine Einführung in die Organische Chemie
Das Lehrbuch behandelt den für den Grundkurs in organischer Chemie obligatorischen Stoff. Die Darstellung erfolgt allerdings aus einer neuen Perspektive.
approx. 700 pp, pr, approx. € 98.00
ISBN-10: 3-906390-29-2
ISBN-13: 978-3-906390-29-1

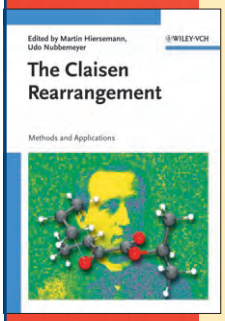

M. Hiersemann / U. Nubbemeyer (eds.)
The Claisen Rearrangement
Methods and Applications
The first comprehensive coverage of all facets of this elegant reaction type, helping every organic chemist to find the best solution for any claisen rearrangement problem.
608 pp, cl, € 155.00
ISBN-10: 3-527-30825-3
ISBN-13: 978-3-527-30825-5

A. Loupy (ed.)
Microwaves in Organic Synthesis
approx. 952 pp, cl,
Prepublication price approx. € 249.00
valid until December 2006
thereafter ca. € 299.00
ISBN-10: 3-527-31452-0
ISBN-13: 978-3-527-31452-2

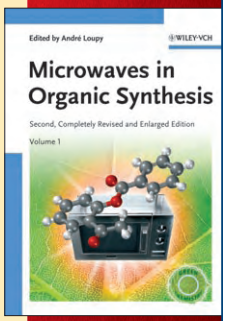

You can order online via **http://www.wiley-vch.de**
Wiley-VCH Verlag GmbH & Co. KGaA · POB 10 11 61 · D-69451 Weinheim, Germany
Phone: 49 (0) 6201/606-400 · **Fax:** 49 (0) 6201/606-184 · **E-Mail:** service@wiley-vch.de

WILEY-VCH

BS_0605_C_OC1_4C_1-2h_gu

© 2006 Wiley-VCH Verlag GmbH & Co. KGaA, Weinheim

DOI: 10.1002/anie.200600641

Macrocycles

Macrocyclization by Ring-Closing Metathesis in the Total Synthesis of Natural Products: Reaction Conditions and Limitations

*Ana Gradillas and Javier Pérez-Castells**

Keywords:
bioactivity · macrocycles · metathesis · natural products · synthesis design

The construction of macrocycles by ring-closing metathesis (RCM) is often used as the key step in the synthesis of natural products containing large rings. This reaction is attractive because of its high functional group compatibility and the possibility for further transformations. The finding of suitable reaction conditions is critical for the success of the synthesis. In this Minireview we summarize the efforts of many research groups to develop efficient RCM reactions on their way towards the total synthesis of natural macrocyclic products. Their findings should help in future synthesis to reduce the time-consuming phase of the optimization of the reaction conditions.

1. Introduction

The metathesis reaction has attracted a great deal of attention for a long time.[1] Ring-closing metathesis (RCM) of alkenes allows the synthesis of cycles from 5- or 6-membered rings to macrocycles. The reaction with alkynes, ring-closing alkyne metathesis (RCAM), is also useful for the construction of large rings. Successful metathesis reactions involving metal carbenes has been achieved by the development of stable and easy to handle catalysts.

Almost one third of current drugs are natural products, or their derivatives, or mimics. Macrocycles are particularly common in antitumoral, antibiotic, and antifungal compounds. Total synthesis is crucial for confirming the structure of the drugs and to open up the possibility of developing derivatives that modulate the biological activity or the pharmacokinetic properties. Synthetic efforts towards macrocycles are often expensive undertakings and unpractical. The macrocyclization, usually the key step, is not unproblematic since there is competition between the desired intramolecular reaction and intermolecular processes that give polymers. Some classic synthetic strategies used are macrolactonizations, macrolactamizations, and macroaldolizations. Organometallic reactions have joined these strategies in recent years and metathesis is becoming the most popular way to construct large rings. RCM has the advantage of being compatible with a wide range of functional groups and gives rise to double bonds which can be transformed into other functional groups and which are generally not affected in further stages of the synthesis. The disadvantage is the control over the stereochemistry of the double bond formed and the finding of appropriate reaction conditions to maximize the yields and minimize the formation of by-products.

This Minireview focuses on the total synthesis of natural macrocycles through the use of diene and the diyne metathesis reactions.[2] We aim to summarize the reaction conditions used in the synthesis of natural and bioactive macrocycles to help those who are planning future syntheses. The choice of the catalyst, solvent, temperature, concentration, and reaction time is crucial in these transformations. We have organized the information by families of natural products so that the reaction conditions used with compounds with structural similarities can be compared.

[*] Dr. A. Gradillas, Prof. J. Pérez-Castells
Departamento de Química
Facultad de Farmacia
Universidad San Pablo-CEU
Urb. Montepríncipe, 28668 Boadilla del Monte, Madrid (Spain)
Fax: (+34) 91-351-0475
E-mail: jpercas@ceu.es

2. Reaction Conditions for RCM

There are numerous parameters that influence metathesis reactions, and so there are no general conditions that can be given that will guarantee the success of the process.[3]

WILEY InterScience DISCOVER SOMETHING GREAT

© 2006 Wiley-VCH Verlag GmbH & Co. KGaA, Weinheim

The catalysts **A**–**E** and **G** represent three generations of ruthenium complexes, while **F** is the molybdenum Schrock catalyst. Of these, catalyst **A** is the cheapest, but it is thermally

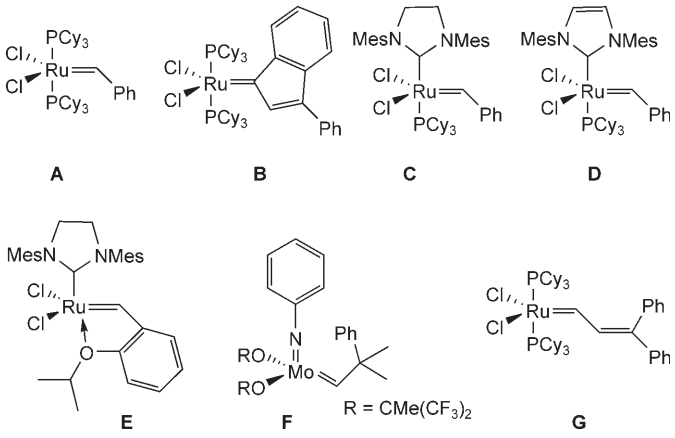

unstable and, in general, fails to react with substituted olefins. Some derivatives of this first generation complex, such as **B**, improve the kinetics of the initial reaction.[4] The second-generation catalysts **C** and **D** are reported to give better results with substituted olefins, as does the Hoveyda–Grubbs catalyst **E**. Modification of **E** by substitution in the aromatic ring has given rise to a new family of "third generation" catalysts.[5] In general, complexes **C**–**E** are prepared in a straightforward manner from the commercially available catalyst **A**. The molybdenum species **F** is highly reactive but sensitive to water, oxygen, and to several functional groups.

The mechanism of the RCM reaction is well established: it begins with the dissociative loss of a phosphine group and the formation of a $14e^-$ intermediate (Scheme 1). The formation

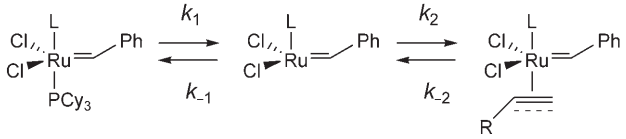

Scheme 1. Initial steps of RCM.

of this unusual unsaturated complex was demonstrated through kinetic studies.[6] The increase in the activity of the second-generation catalysts is not a result of an increase in the rate of the phosphine dissociation but to a better ratio between the rate constant k_2 for the coordination of the olefin and the rate constant k_{-1} for the recoordination of phosphine. In the next step a ruthenacyclobutane is formed, which gives rise to a new carbene. The reaction of this new species with another unsaturated bond gives the final product and a methylene carbene, which is thought to be a less-stable intermediate in many metathesis reactions.[7] There are some studies that suggest a different pathway for the different generations of catalysts, and there are still unclear aspects of the enyne reaction.[8]

Thermal stability plays a critical role in the lifetime of the species and the turnover number (TON).[3] Thus, **C** is stable for one hour at 100 °C in [D_8]toluene, while **A** decomposes by up to 75 % under the same conditions. The stability of **C** arises from the stability gained from the incorporation of the N-heterocyclic carbene (NHC) ligand. **E** is also thermally stable and survives chromatography on silica gel, thus enabling it to be purified, recovered, and reused after the reaction. Grubbs and co-workers have shown the reaction is favored in nonpolar solvents, and in most studies toluene or dichloromethane are preferred.[6]

The presence of heteroatoms in the substrates leads to a variety of results.[9] Nitrogen is generally not tolerated unless nonbasic functional groups such as tosylamides are used. Certain metathesis reactions of amine-containing compounds were carried out with one equivalent of *p*-toluenesulfonic acid to prevent coordination of the electron pair on the nitrogen atom to the catalysts.[10] Oxygen appears to be beneficial for the metathesis in some studies,[11] while in other cases no influence is observed. In the majority of cases, however, oxygen has a negative influence on the reaction.[12,13] The thermal stability of the final product also influences the metathesis reaction.[14]

Ring-closing alkyne metathesis (RCAM) has recently been reviewed by Fürstner and Davies,[15] and so here we will only summarize RCAM reaction conditions in Tables to complete the overview. Common RCAM initiators include compounds **H** and **I**.

Javier Pérez-Castells was born in Madrid, Spain, in 1967. He received his BSc in Chemistry at the Universidad Complutense de Madrid in 1990, and completed his PhD in Organic Chemistry there in 1994 under the supervision of Prof. Miguel A. Sierra and Prof. Benito Alcaide. Since 1995 he has been assistant professor at the Universidad San Pablo-CEU, where he works on metal-catalyzed cyclization reactions.

Ana Gradillas worked in the research group of Prof. J. V. Sinisterra in 1989 during her undergraduate studies in the Pharmacy Faculty of Complutense University of Madrid. She obtained her PhD in 1995 with Prof. E. F. Llama and Prof. C. Pérez-del Campo at Complutense University. During 1996 she worked with Dr. J. Vulfson at the Institute of Food Research (Reading, UK). In 1997 she joined San Pablo-CEU University (Madrid), where she also has had a teaching position. Her research interests include the synthesis of compounds for antitumor drugs.

© 2006 Wiley-VCH Verlag GmbH & Co. KGaA, Weinheim

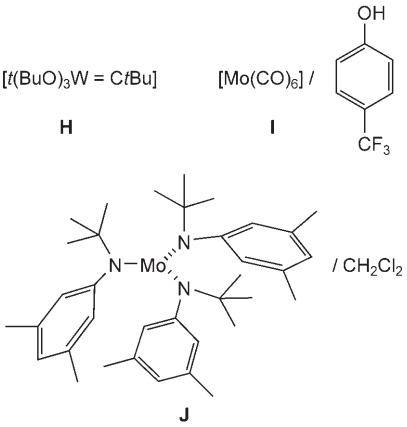

3. Macrocyclic Lactones

Macrocyclic structures that have one or more ester linkages are generally referred to as macrolides or macrocyclic ring lactones. Macrolides are very important target molecules in synthetic studies because of their biological and medicinal activity.

3.1. Resorcinylic Macrolides

The macrolides **1**–**8** from the resorcinylic family were synthesized by using a RCM reaction for the construction of the macrocycle. Several total synthesis of radicicol (**1**) have been accomplished by using RCM to construct the macrocyclic ring.[16] Danishefsky and co-workers have optimized the temperature and concentration conditions for the RCM used for the synthesis of cycloproparadicicol (**19**, Scheme 2a).[17] RCM of **9**, which bears an epoxide at the C7′/C8′ position and an OTBS group, occurred under mild conditions (0.2 mM, CH_2Cl_2, 42 °C) to give the monomeric macrocyclic product **12**. However, when similar conditions were applied to the cyclopropyl precursor **15**, the majority of the isolated products were dimeric 28-membered macrocycles. However, performing the reaction at 110 °C in toluene and quenching after a short period of time resulted in clean conversion of **15** into the primary cyclization product **17**.

Fürstner et al. developed an RCM-based approach to zeranol (**2**, Scheme 2b).[18] The poor reactivity of diene **20** resulted in them deprotecting the ketone prior to ring closure. The same authors[18] synthesized (*R*)-(+)-lasiodiplodin (**4**, Scheme 2c). Complex **A** was totally ineffective for the construction of the macrocycle of (*S*)-(−)-zearalenone (**3**); however, complex **D** proved to be an effective catalyst (Scheme 2d).[18]

The syntheses of *trans*- and *cis*-resorcylides **5** and **6** were the first examples of RCM cyclizations of enolizable enones. Thus, *trans*-alkene **28** was isolated as a sole isomer and in relatively high yield by subjecting diene **27** to the modified protocol developed by Danishefsky and co-workers for the synthesis of radicicol (Scheme 3).[19] The cyclization of diene **29** was rather problematic and only the combination of extremely high dilution, elevated temperature (0.5 mM, CH_2Cl_2, reflux), and low catalyst loading enabled the *cis*-resorcylide to be isolated in reasonable yield, along with the head-to-tail, 24-membered macrocyclic dimer.[20]

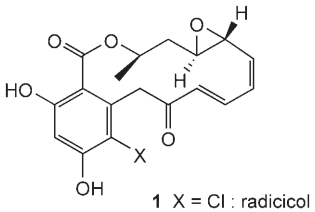

1 X = Cl : radicicol
X = H : monocillin I

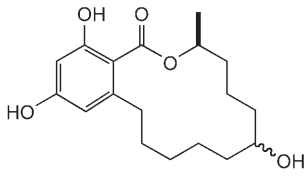

2
zeranol

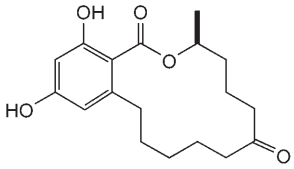

3
zearalenone

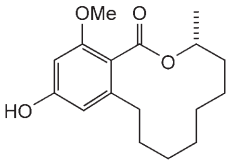

4
lasiodiplodin

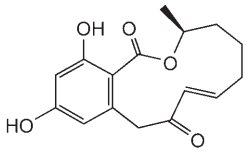

5
trans-resorcylide

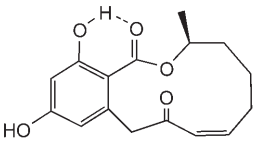

6
cis-resorcylide

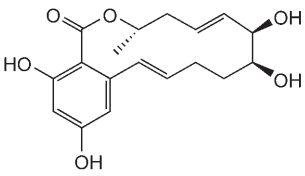

7
aigialomycin D

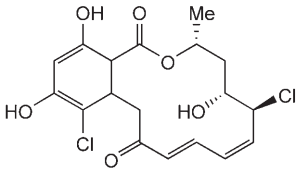

8
pochonin C

The same authors designed a new and highly efficient synthetic route—the "ynolide" methodology—which provided an efficient route to cycloproparadicicol (**19**)[21] and to other resorcinylic macrolides such as aigialomycin D (**7**).[22] The synthesis involved a cobalt-complexation-promoted RCM to generate the ynolide **32** in excellent yield, followed by a Diels–Alder reaction using a disiloxydiene to elaborate the benzenic system (Scheme 4). The complexation of the ethynyl linkage to cobalt avoids competitive enyne metathesis reactions and brings C-7′ and C-8′ into proximity, thus favoring RCM.

Polyene RCM has been used for the synthesis of pochocin C (**8**).[23] Thus, treatment of intermediate **33** with catalyst **C** in toluene at 120 °C led to **34** as an inseparable mixture of *cis* and *trans* olefins (1:1). The thioether group was then removed to obtain **35**. The selectivity of the elimination reaction suggested that carrying out the metathesis on diene **36** should lead to the desired *trans*,*cis*-diene. Indeed oxidation/elimination of thioether **33** prior to RCM at 120 °C led exclusively to **37** in 10 minutes (Scheme 5). Table 1 summarizes the studies on the RCM reaction conditions used for the macrolide syntheses described in this section.

© 2006 Wiley-VCH Verlag GmbH & Co. KGaA, Weinheim

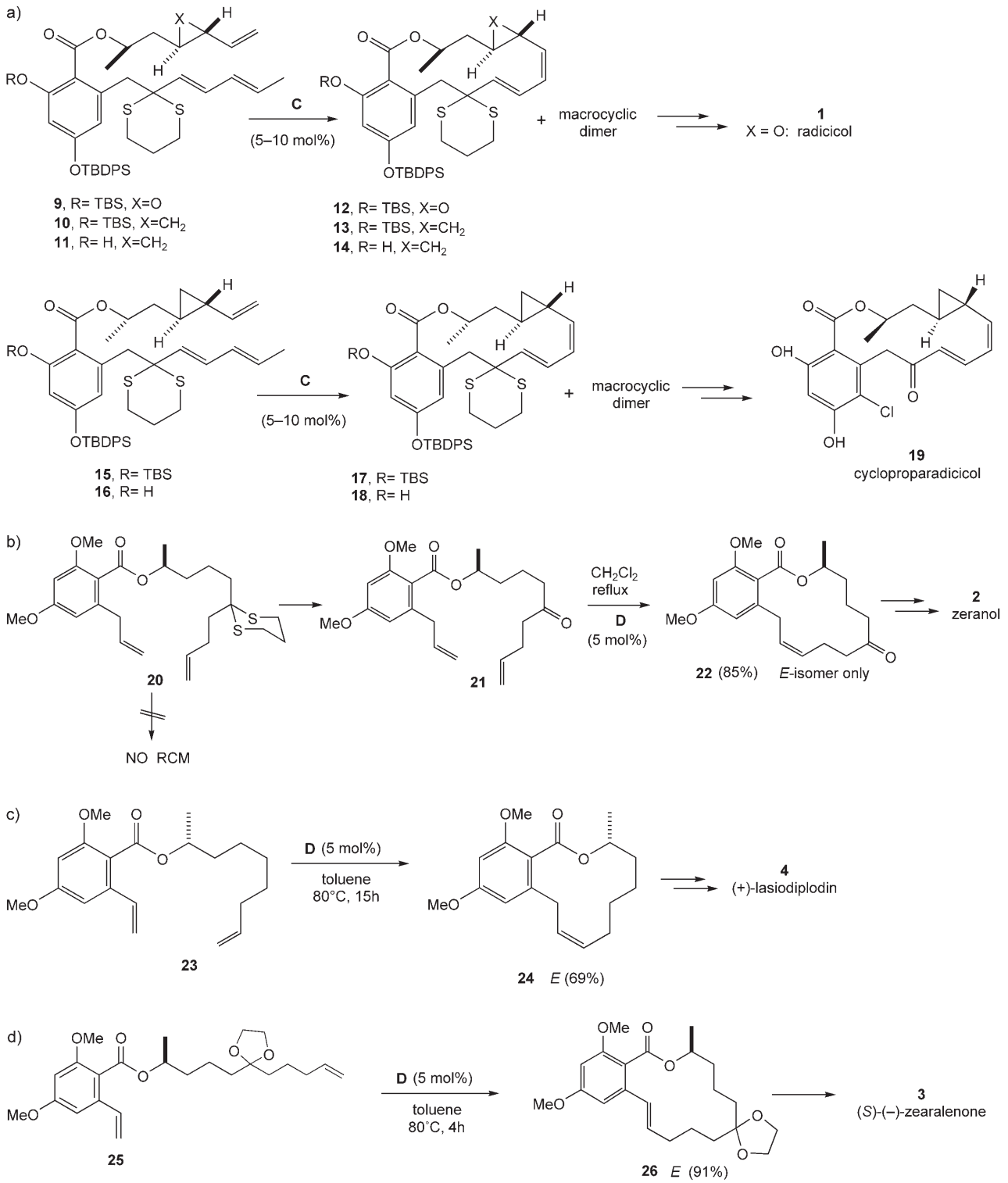

Scheme 2. Synthesis of a) macrocycle **1** (top) and **19** (bottom) by RCM, b) zeranol, c) (*R*)-(+)-lasiodiplodin, and d) (*S*)-(−)-zearalenone.

3.2. Salicylate Macrolides

A family closely related to resorcinylic macrolides are the salicylate enamide macrolides, which include salicylihalamides A and B (**38**) and oximidines I–III, (**39**–**41**).[24] The complex structures of these natural products combined with their novel mode of biological action have stimulated a number of synthesis programs.

The three general approaches proposed for salicylihalamide A and B are the Mitsunobu/RCM strategy as well as

 © 2006 Wiley-VCH Verlag GmbH & Co. KGaA, Weinheim

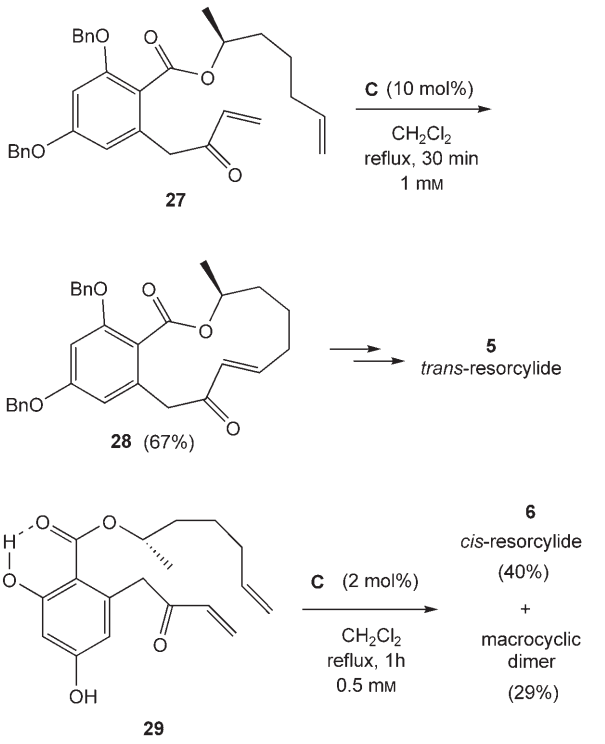

Scheme 3. Synthesis of *trans*- and *cis*-resorcylides.

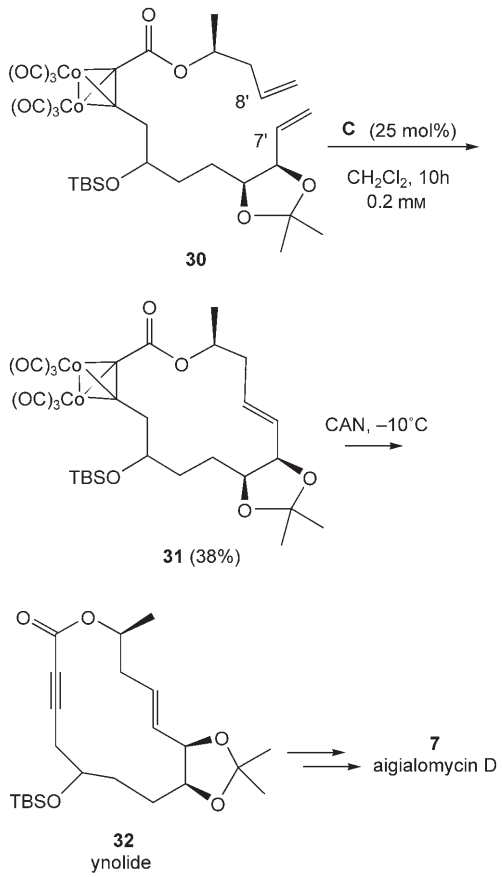

Scheme 4. Synthesis of macrolactone **31** by RCM.

the Suzuki and Stille cross-coupling approaches.[25] The careful study of the influence of remote substituents in RCM precursors, such as **42**, and of the catalyst activity on the stereochemistry have led to the conditions indicated in Scheme 6 and Table 2.[26]

Oximidine II and III were constructed by using a relay RCM strategy to facilitate the crucial macrocyclization reaction (Scheme 7).[26] A well-defined substrate possessing two differently functionalized RCM alkene partners was found to be required for the RCM-RCM process. A faster addition of the substrate resulted in reduced decomposition of the product and both catalysts **E** and **C**. The production of oligomers was minimized at a higher temperature.[24]

Table 1: Reaction conditions used for the synthesis of resorcinylic macrolides.[a]

Conditions	Catalyst, yield	Compd	Ref.
toluene, 110 °C, 10 min, 0.2 mM	**C** (5–10 mol %), 60 %	**12**	[17]
CH_2Cl_2, Δ*T*	**D** (5 mol %), 85 % (*E*)	**22**	[18]
toluene, 80 °C, 15 h	**D** (6 mol %), 69 % (*E*)	**24**	[18]
toluene, 80 °C, 4 h	**D** (5 mol %), 91 % (*E*)	**26**	[18]
CH_2Cl_2, Δ*T*, 30 min, 1 mM	**C** (10 mol %), 67 %	**28**	[20]
CH_2Cl_2, Δ*T*, 1 h, 0.5 mM	**C** (2 mol %), 40 %	**6**	[20]
CH_2Cl_2, Δ*T*, 10 h.	**C** (25 mol %), 38 %	**31**	[22]
toluene, 120 °C, 10 min, 2 mM	**C** (5 mol %), 87 %	**37**	[23]

[a] The best conditions leading to the desired macrocycle are shown.

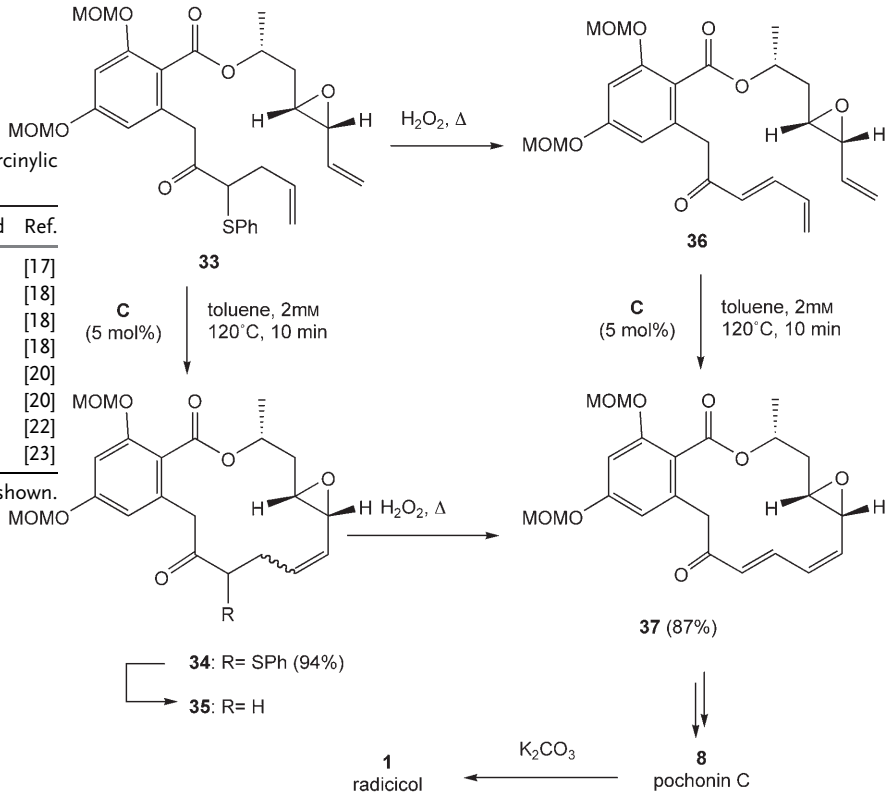

Scheme 5. Synthesis of pochonin C by RCM.

© 2006 Wiley-VCH Verlag GmbH & Co. KGaA, Weinheim

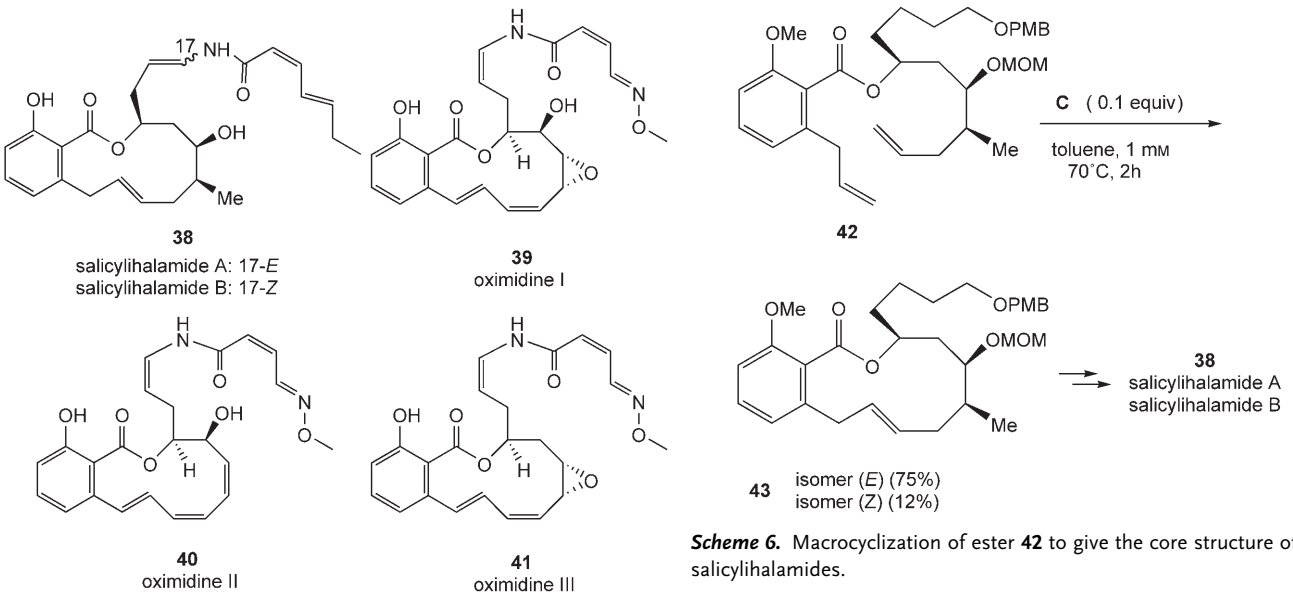

Scheme 6. Macrocyclization of ester **42** to give the core structure of salicylihalamides.

Table 2: Reaction conditions for the macrocyclization by RCM in the total synthesis of salicylate macrolides.

Conditions	Catalyst, yield	Compd	Ref.
toluene, 70°C, 2 h, 1 mM	**C** (10 mol%), 75% (*E*)	**43**	[25]
CH_2Cl_2, ΔT, 70 min, 2 mM	**C** (5 mol%), 48%	**45**	[26]
$(ClCH_2)_2$, 50°C, addition time 30 min, 2.0 mM	**E** (10 mol%), 71%	**47**	[24]

3.3. Antibiotic Macrolides

Numerous biologically active macrocycles are antibiotics, which have been isolated from various microorganisms. The wide variety of antibiotic macrolide structures is illustrated by compounds **48**–**54**. Table 3 summarizes the reaction conditions that resulted in macrocyclization.

3.4. Macrocyclic Musk

Muscone (**55**) and civetone (**56**) are two of the most important classical sources of musk odors for perfumes. Both

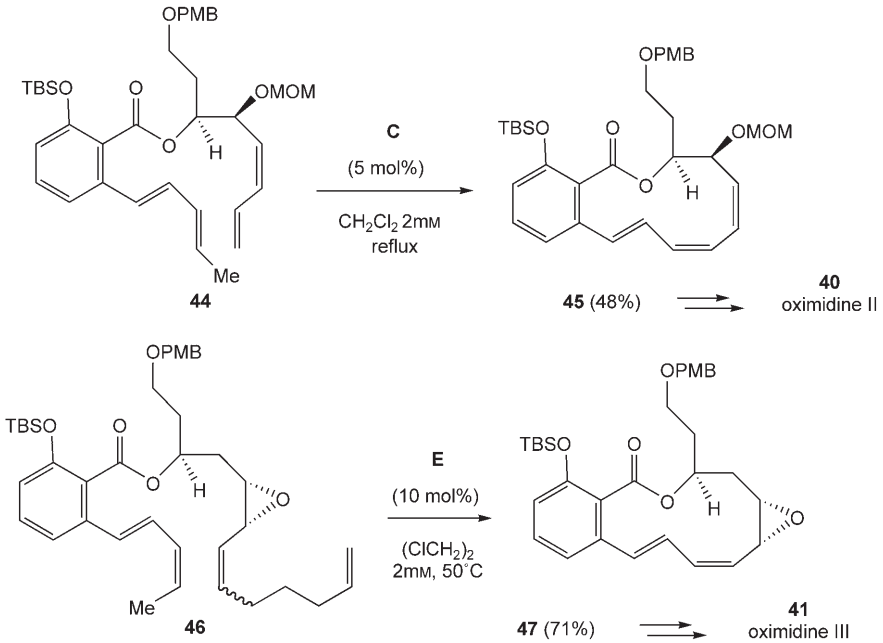

Scheme 7. Application of relay RCM for the synthesis of oximidines.

 © 2006 Wiley-VCH Verlag GmbH & Co. KGaA, Weinheim

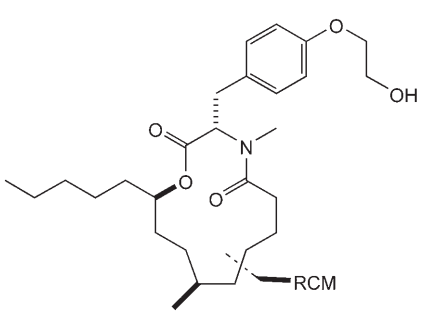

48
PF1163B

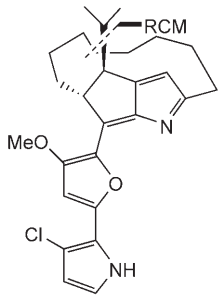

49
roseophilin

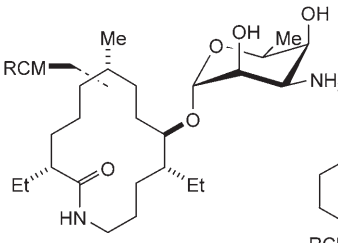

50
Sch38516 (fluvirucin B1)

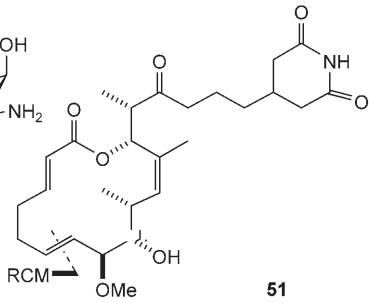

51
(+)-migrastatin

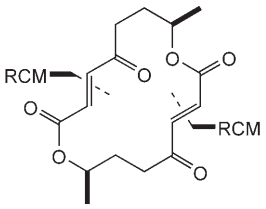

52
(–)-pyrenophorin

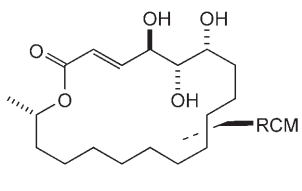

53
(+)-aspicilin

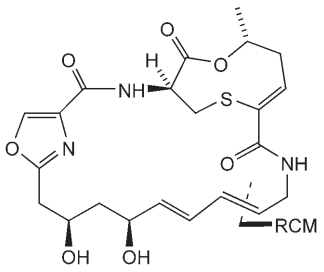

54
(–)-griseoviridin

of these chemicals are nowadays produced synthetically by RCM under the conditions shown in Table 4.

Other relatively simple macrolides include exaltolide (**57**), which was the first macrolactone to be prepared by RCM, recifeiolide (**58**), and muscopyridine (**59**). Other olfactory molecules such as yuzu lactone (**60**) and ambretolide (**61**) were obtained stereoselectively by RCAM followed by Lindlar hydrogenation or an equivalent semireduction.

Table 3: Examples of macrolide antibiotics synthesized by RCM.[a]

Conditions	Catalyst, yield	Compd	Ref.
$(ClCH_2)_2$, 82 °C, 6 h, 2 mM	**C** (12 mol %), 60 % *E*/*Z* mixture	**48**	[27]
CH_2Cl_2, 40 °C, 30–72 h, 0.25–0.5 mM	**A** (20–30 mol %), 88–91 % *E*/*Z* mixture	**49**	[28]
C_6H_6, 60 °C	**C** (20 mol %), 90 %	**50**	[29]
toluene, ΔT, 0.5 mM	**C** (20 mol %), 50 %	**51**	[30]
CH_2Cl_2, ΔT	**C** (5 mol %), 46 %	**52**	[31]
CH_2Cl_2, RT, 1.5 mM	**A** (5 mol %), 83 % (*Z*)	**53**	[32]
toluene, 100 °C, 1 mM	**A** (30 mol %), 37–42 % (*E*)	**54**	[33]

[a] The best conditions leading to the desired macrocycle are shown.

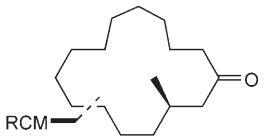

55
(–)-muscone

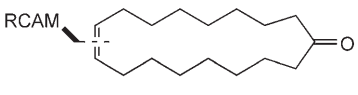

56
civetone

Table 4: Conditions for RCM to give simple musk macrolides.

Conditions	Catalyst, yield	Compd	Ref.
$(ClCH_2)_2$, 50 °C	**A** (7 mol %), 56 %	**55**	[34]
toluene, 80 °C	**H** (10 mol %, 65 %	**56**	[35]
CH_2Cl_2, 40 °C	**G** (4 mol %), 79 %	**57**	[36]
CH_2Cl_2, 40 °C	**G** (3 mol %), 80 %	**58**	[37]
CH_2Cl_2, ΔT, 14 h, 6 mM	**B** (10 mol %), 57 %	**59**	[38]
CH_2Cl_2, 40 °C	**I** (5 mol %), 62 %	**60**	[39]
CH_2Cl_2, 40 °C	**I** (5 mol %), 69 %	**61**	[39]

[a] The best conditions leading to the desired macrocycle are shown.

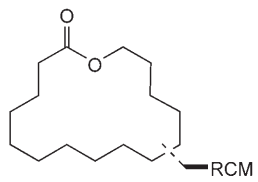

57
exaltolide

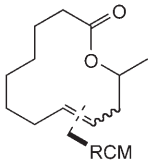

58
recifeiolide

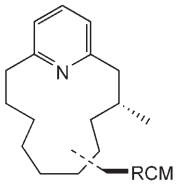

59
(+)-muscopyridine

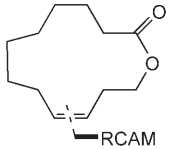

60
yuzu lactone

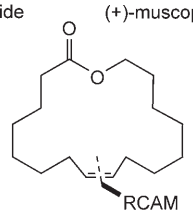

61
ambretolide

3.5. Other Macrolides

Other pharmacologically active macrolides have highly substituted structures, as can be seen from the examples **62**–**65** (macrolides containing an 11- and a 14-membered lactone

© 2006 Wiley-VCH Verlag GmbH & Co. KGaA, Weinheim

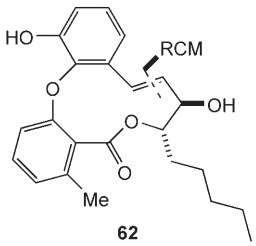

62
(+)-aspercylide C

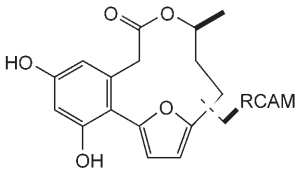

63
citreofuran

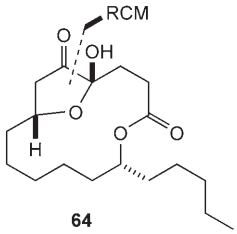

64
(–)-gloeosporone

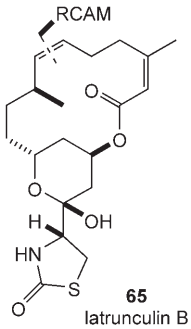

65
latrunculin B

ring), **68**–**70** (macrolides containing a 16-membered lactone ring), and **71**–**75** (macrolides containing an 18- and a 20-membered lactone ring). The reaction conditions used for the RCM key macrocyclization steps are summarized in Table 5.

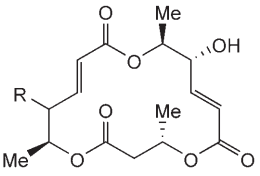

68 R = COH; macrosphelide A
R = C=O; macrosphelide B

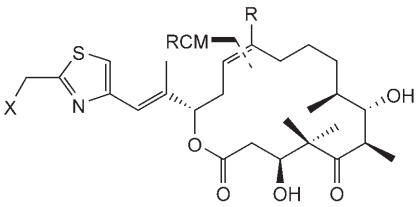

69a EpoC (X=R=H)
69b EpoD (X=H, R=Me)

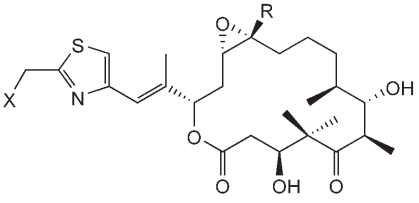

70a EpoA (X=R=H)
EpoB (X=H, R=Me)
70b EpoE (X=OH, R=H)
EpoF (X=OH, R=Me)

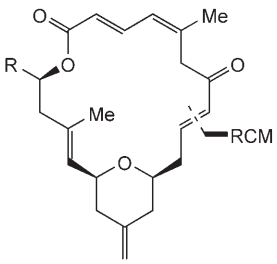

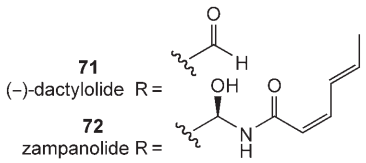

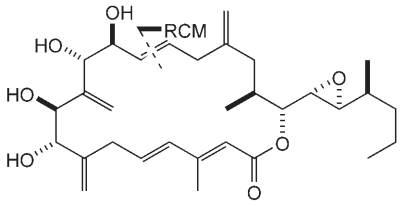

73
amphidinolide A

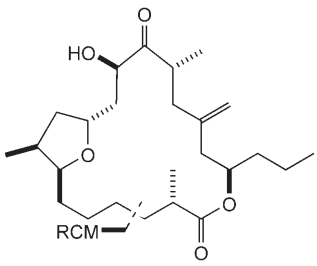

74
amphidinolide T3

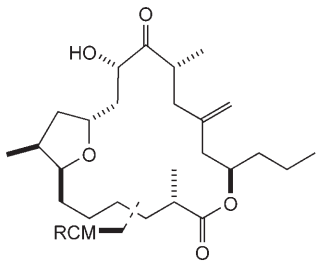

75
amphidinolide T4

Table 5: Macrolides containing a 11- to 20-membered lactone ring.

Conditions	Catalyst, yield	Compd	Ref.
toluene, Δ*T*, 4 h, 2 mM	**D** (20 mol%), 69% (*E*/*Z*=5:1)	**62**	[40]
toluene, 85 °C, 1 h, 8.5 mM	**I** (10 mol%), 78%	**63**	[41]
CH_2Cl_2, 40 °C	**A** (3 mol%) $Ti(OiPr)_4$ (30 mol%), 80%	**64**	[36]
CH_2Cl_2/toluene	**J** (10 mol%), 70%	**65**	[42]
CH_2Cl_2/toluene, 80 °C	**J** (10 mol%), 70%	**81**	[48]
CH_2Cl_2, RT	**C** (10 mol%), 77%	**68**	[43]
CH_2Cl_2/toluene, 80 °C	**J** (10 mol%), 80%	**69a**	[2]
toluene, 110 °C, 10–20 min, 3 mM	**C** (30 mol%), 70%	**69b**	[2]
CH_2Cl_2, 40 °C, 8–48 h, 3 mM	**C** (30 mol%), 89% (*E*:*Z*=1:1)	**70a**	[2]
C_6H_6, 60 °C	**C** (50 mol%), 77% (*E*)	**71**, **72**	[44]
CH_2Cl_2, Δ*T*, 24 h	**C** (50 mol%), 35%	**73**	[45]
toluene, 110 °C	**C** (20 mol%), 82% (*E*:*Z*=2:1)	**74**	[46]
CH_2Cl_2, ΔT, 24 h	**B** (50% mol), 86% (*E*:*Z*=6:1)	**75**	[47]

[a] The best conditions leading to the desired macrocycle are shown.

The scope of RCM has been fully illustrated by the synthesis of epothilones (Epo A–F; **69**–**70**) and has been reviewed recently.[2] The total synthesis of (+)-aspercylide C (**62**), was

 © 2006 Wiley-VCH Verlag GmbH & Co. KGaA, Weinheim

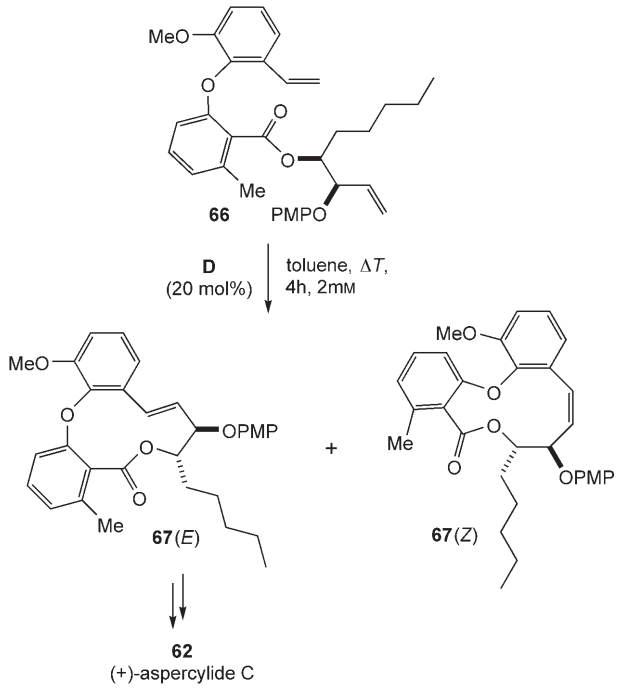

Scheme 8. Kinetically controlled RCM reaction to form **67**.

reported recently.[40] The key step was a kinetically controlled RCM reaction to form an 11-membered cycle (Scheme 8).

Ring-closing alkyne metathesis was used as the key step in the formation of the macrolide latrunculin B (**65**). A concise and efficient synthesis of another congener, latrunculin A (**81**), was recently achieved (Scheme 9).[48] Compound **76** underwent enyne-yne metathesis to give the desired product **77** in the presence of catalytic amounts of **J**, activated in situ with CH_2Cl_2. The inability to cleave the remaining *N*-PMB group prevented formation of **81**. Conversion of **76** into the Teoc derivative **79** allowed the crucial enyne-yne metathesis to form the highly strained 16-membered cyclic product **80** in 70% yield.

4. Macrocyclic Glycolipids

The performance and excellent application profile of RCM and RCAM are illustrated by the total synthesis of various resin glycosides and sugar-based macrodiolides such as tricolorins A and G, woodrosin I, and sophorolipid. The synthesis of these amphiphilic natural products has led to advances in carbohydrate chemistry (Table 6).[15]

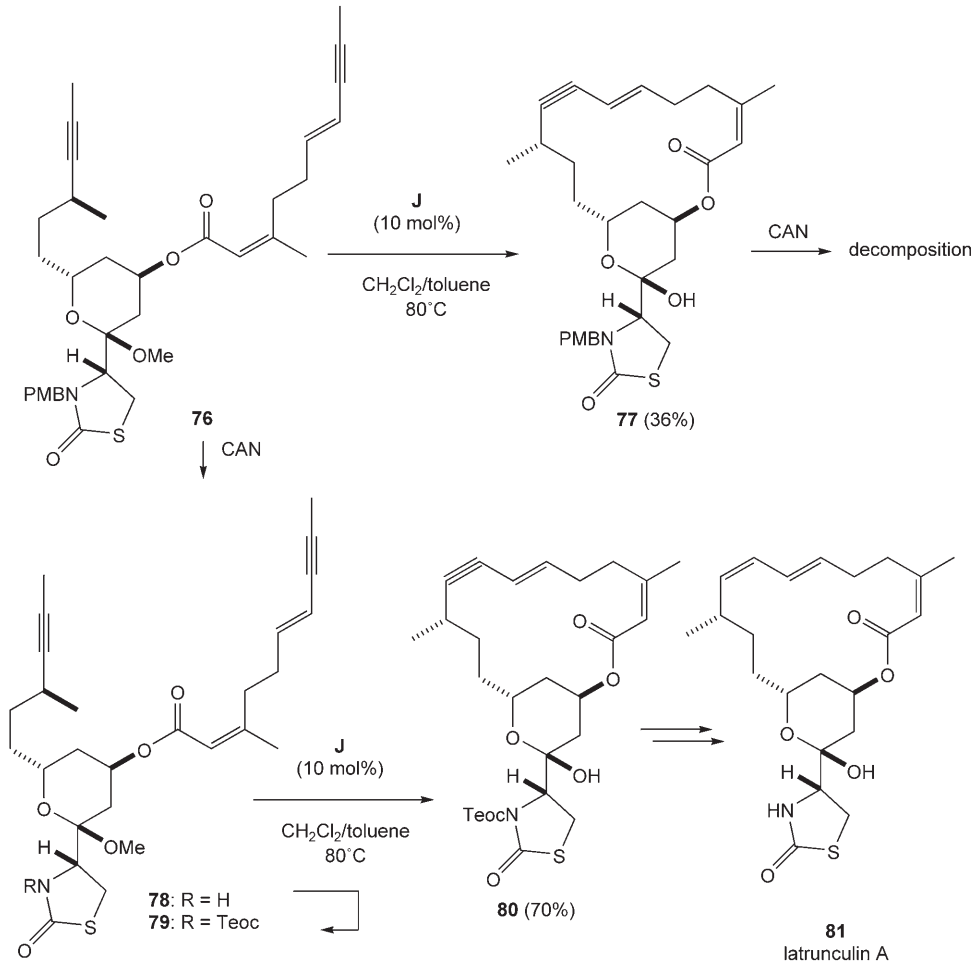

Scheme 9. Ring-closing enyne-yne metathesis in the total synthesis of latrunculin A.

© 2006 Wiley-VCH Verlag GmbH & Co. KGaA, Weinheim

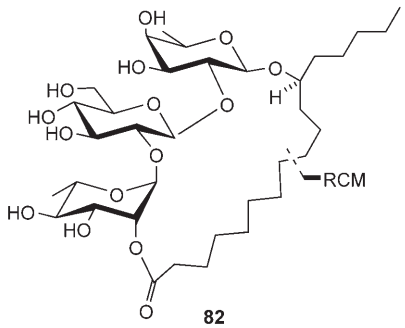

82
tricolorin G

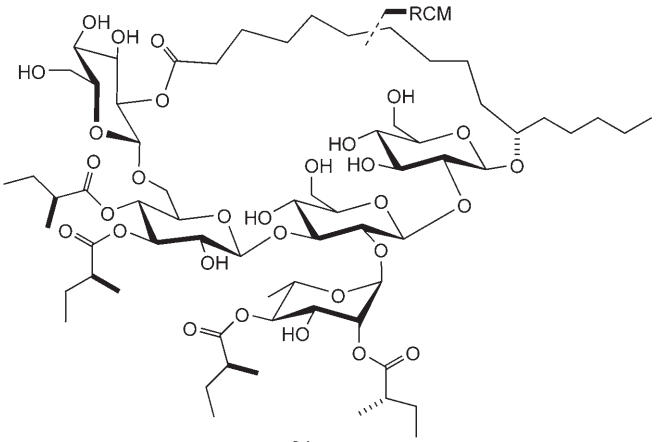

84
woodrosin I

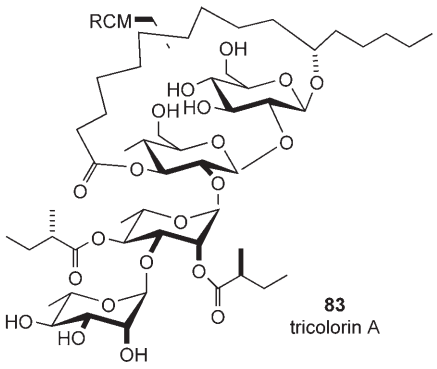

83
tricolorin A

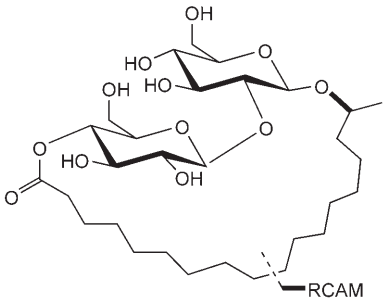

85
sophorolipid

Table 6: RCAM in the total synthesis of resin glycosides and the sophorolipid lactone.

Conditions	Catalyst, yield	Compd	Ref.
CH_2Cl_2, ΔT, 22 h	**G** (10 mol%), 93%	**82**	[49]
CH_2Cl_2, ΔT, 24 h	**G** (10 mol%), 90%	**83**	[50]
CH_2Cl_2, 40°C	**B** (10 mol%), 94%	**84**	[51]
toluene/CH_2Cl_2, 80°C	**J** (10 mol%), 78%	**85**	[52]

5. Macrocyclic Lactams

5.1. Amsamycin Macrolides

Four new members of the ansamycin family, cytotrienins A–D (**89**), have been described recently.[53] They have stimulated the asymmetric synthesis of the fully elaborated macrocyclic core **87**. The synthetic route reported included the use of a RCM reaction as a way to efficiently install the (*E*,*E*,*E*)-triene and simultaneously construct the macrocyclic lactam, by using the bis(1,3-diene) **86** as the triene precursor (Scheme 10). Reaction of **86** with catalyst **C** unexpectedly gave diene **88** in 47% yield. To overcome this problem and initiate the RCM at one of the terminal olefins, **86** was exposed to the less reactive catalyst **A** in refluxing dichloromethane, which afforded the expected (*E*,*E*,*E*)-triene **87** with excellent selectivity and yield.

6. Terpenoids

Only a few natural terpenic compounds bearing large cycles have also been obtained by using RCM.

6.1. Diterpenoids

Several strategies exist for the construction of macrocyclic diterpene tonantzitlolone (**95**) by RCM.[54] The formation of the double bond between C-1 and C-2 was unsuccessful, probably because of steric congestion created by the three allylic methyl groups present in the starting material. Thus, the position of macrocyclization was shifted to the less congested site at C-4 and C-5. Indeed, desilylation of **90**, and subsequent RCM of **91** using catalyst **C** yielded the macrocyclic *Z*-configured diene **92** which unfortunately could not be transformed into the final compound. Therefore, **90** was transformed into **93** which provided the macrocycle **94** with high *E* selectivity. Subsequent reactions led to the desired tonantzitlolone (Scheme 11).

The highly strained and congested 11-membered ring of coleophomones B–C (**96–97**) was constructed by using an impressive olefin metathesis reaction to build the bond between C-16 and C-17 (Table 7).[55]

 © 2006 Wiley-VCH Verlag GmbH & Co. KGaA, Weinheim

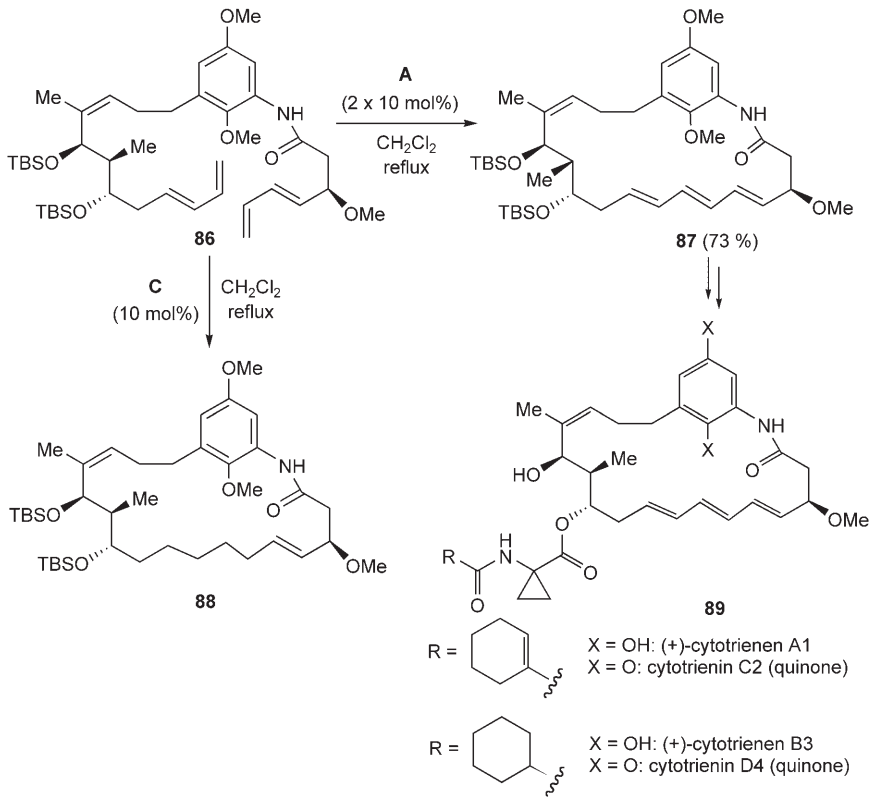

Scheme 10. Synthesis of the macrocyclic core of cytotrienins.

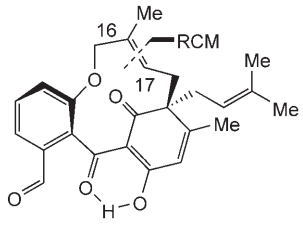

96
coleophomone B
D16,17-*E*-macrocycle

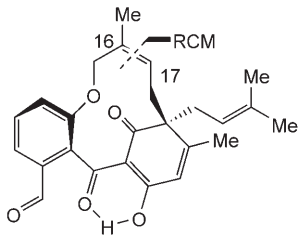

97
coleophomone C
D16,17-*Z*-macrocycle

7. Depsipeptides

Cyclodepsipeptides are cyclic peptides with a wide range of biological activities that are characterized by the occurrence of at least one ester linkage. The total synthesis of spongidepsin (**100**) was accomplished by a ring-closing metathesis as the key step (Scheme 12).[56] Exposure of **98** to catalyst **C** in refluxing toluene yielded the four possible macrocyclic 5*E*/*Z*, 7*R*/*S* diastereomers in a combined yield of 80%. The two *E* alkenes (**99a–b**) were obtained in a 1:1 ratio and predominated over the *Z* isomers (>10:1). The two C7 epimers **99a–b** could be separated by flash column chromatography.

8. Macrocyclic Alkaloids

The rich variety of biological activities associated with both plant-derived and animal-derived alkaloids has stimulated many research groups to synthesize their core structures. Prototype alkaloids with spermidine-like tails are (−)-isooncinotine (**101**) and motuporamine C (**102**).

As described in Section 2, the presence of nitrogen atoms is normally not tolerated in RCM substrates. To avoid chelation of the catalyst with the N atoms in the synthesis of **101**, precursor **103** was protonated, and the bond between C-15 and C-16 was selected to close the macrocycle as a result of its remote relative situation from the carbonyl group of the amide. The resulting 22-membered cycloalkene was hydrogenated directly without isolation of **104** (Scheme 13).[57]

The synthesis of cryptophycin-24 (arenastatin A, **106**) was achieved by using a RCM of **105**. The reaction proceeded in high yield with exclusive formation of the *E* isomer, despite the presence of the chemically reactive styrene epoxide moiety (Scheme 14).[58] In the total synthesis of pinnatoxin A (**110**), the bulky silyl protecting groups in **107** had to be removed, as they prevented RCM. Therefore, macro-RCM reaction of **108** gave **109**, from which pinnatoxin A was synthesized (Scheme 15).[59] Some other recent applications of RCM to the synthesis of other alkaloids, including **111**, a

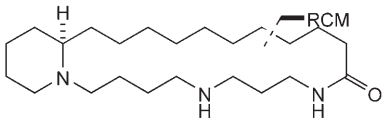

101
(−)-isooncinotine

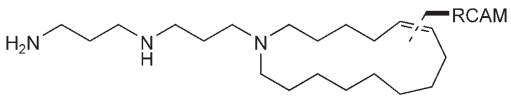

102
motuporamine C

Table 7: Synthesis of coleophomones B and C by stereoselective RCM.

Conditions	Catalyst, yield	Compd	Ref.
CH_2Cl_2, 40 °C, 3 h	**C** (10 mol%), 86%	**96**	[55]
CH_2Cl_2, 40 °C, 1–5 h	**C** (10 mol%), 80%	**97**	[55]

© 2006 Wiley-VCH Verlag GmbH & Co. KGaA, Weinheim

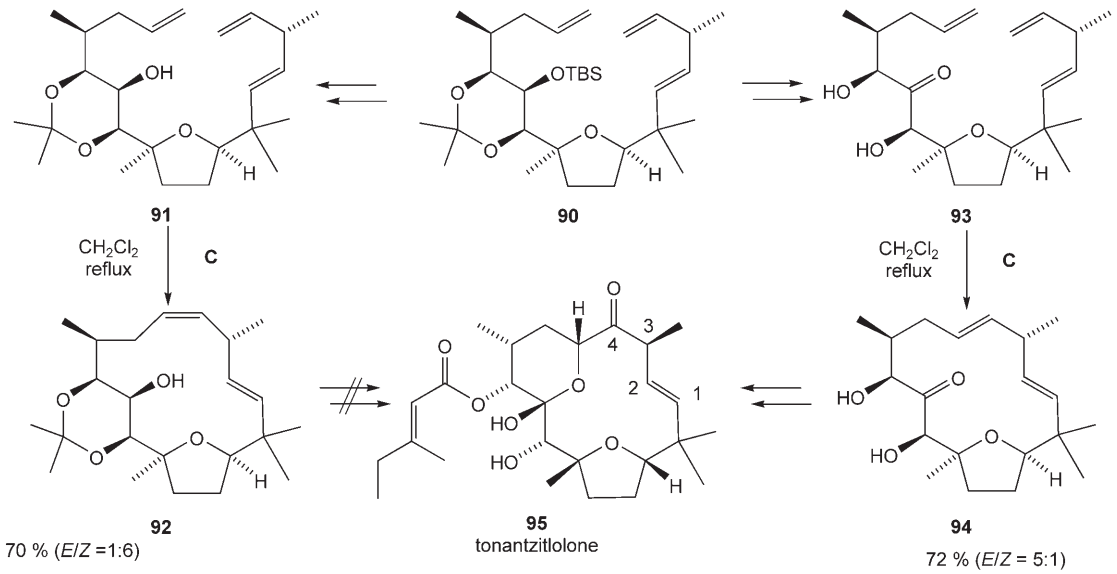

Scheme 11. Two strategies to construct **95** by RCM.

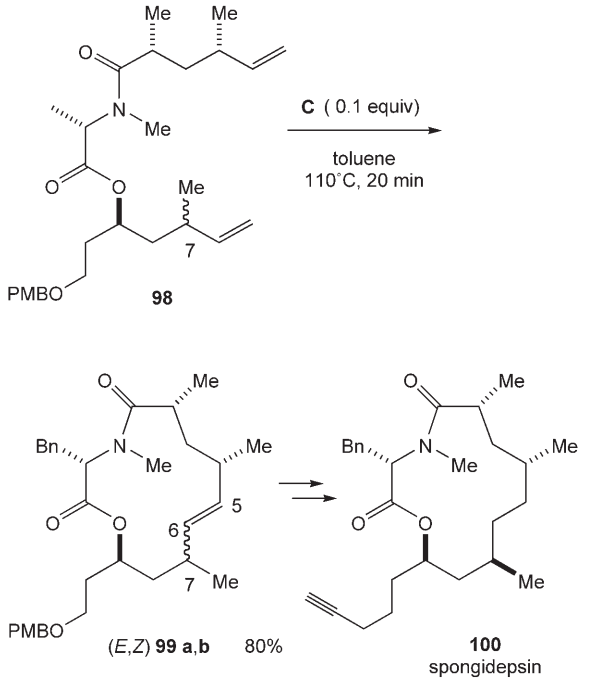

Scheme 12. RCM as a key step in the total synthesis of **100**.

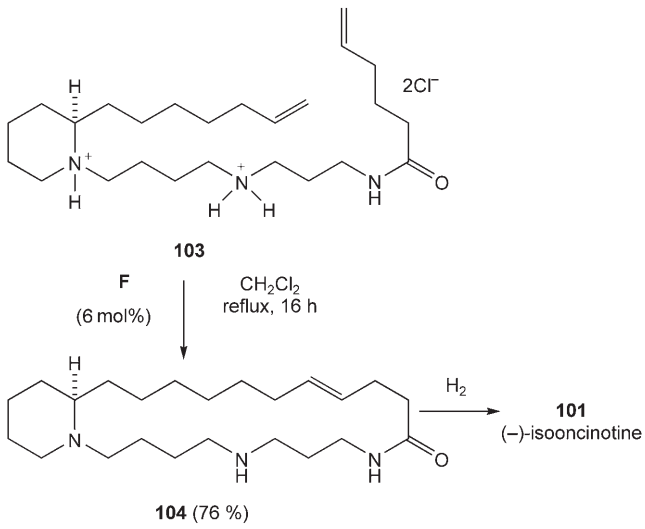

Scheme 13. RCM in the synthesis of **101**.

defensive insect alkaloid, and **113**, a manzamine from a family of marine alkaloids, are also summarized in Table 8.

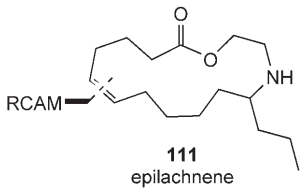

Table 8: Conditions for the RCM to give alkaloids.

Conditions	Catalyst, yield	Compd	Ref.
CH_2Cl_2, ΔT, 16 h	**B** (6 mol%), 76%	**101**	[57]
PhCl, ΔT	**H** (10 mol%), 68%	**102**	[60]
CH_2Cl_2, ΔT, 6 h	**A** (10 mol%), 70%	**106**	[58]
CH_2Cl_2, ΔT	**A** (0.1 equiv), 75%	**110**	[59]
CH_2Cl_2, ΔT	**I** or **J** (5 mol%), 70%	**111**	[61]
CH_2Cl_2, 50°C, 24 h, 0.5 mM	**A** (15 mol%), 26% (Z/E=41:59)	**112**	[62]
CH_2Cl_2, ΔT	**A** (13 mol%), 67%	**113**	[63]
CH_2Cl_2, ΔT, 3 h, 5 mM	**A** (13 mol%), 76% (Z/E=8:1)	**114**	[63]
CH_2Cl_2, ΔT, 5 h, 0.4 mM	**C** (10 mol%), 49%	**115**	[64]

[a] The best conditions leading to the desired macrocycle are shown.

 © 2006 Wiley-VCH Verlag GmbH & Co. KGaA, Weinheim

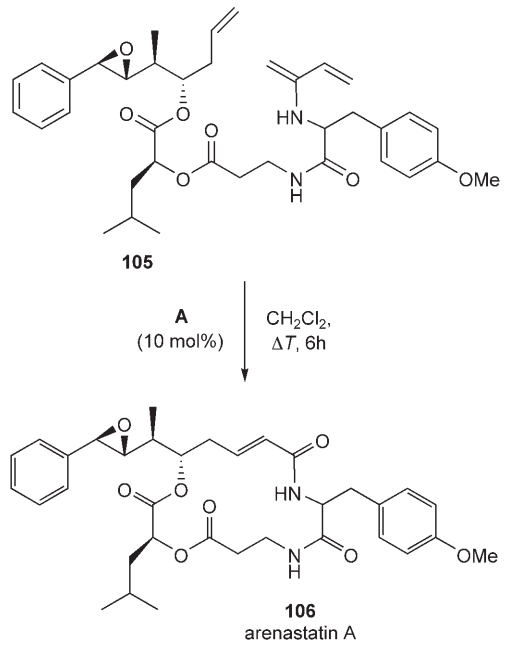

Scheme 14. RCM in the total synthesis of the cyclopeptide alkaloid arenastatin A.

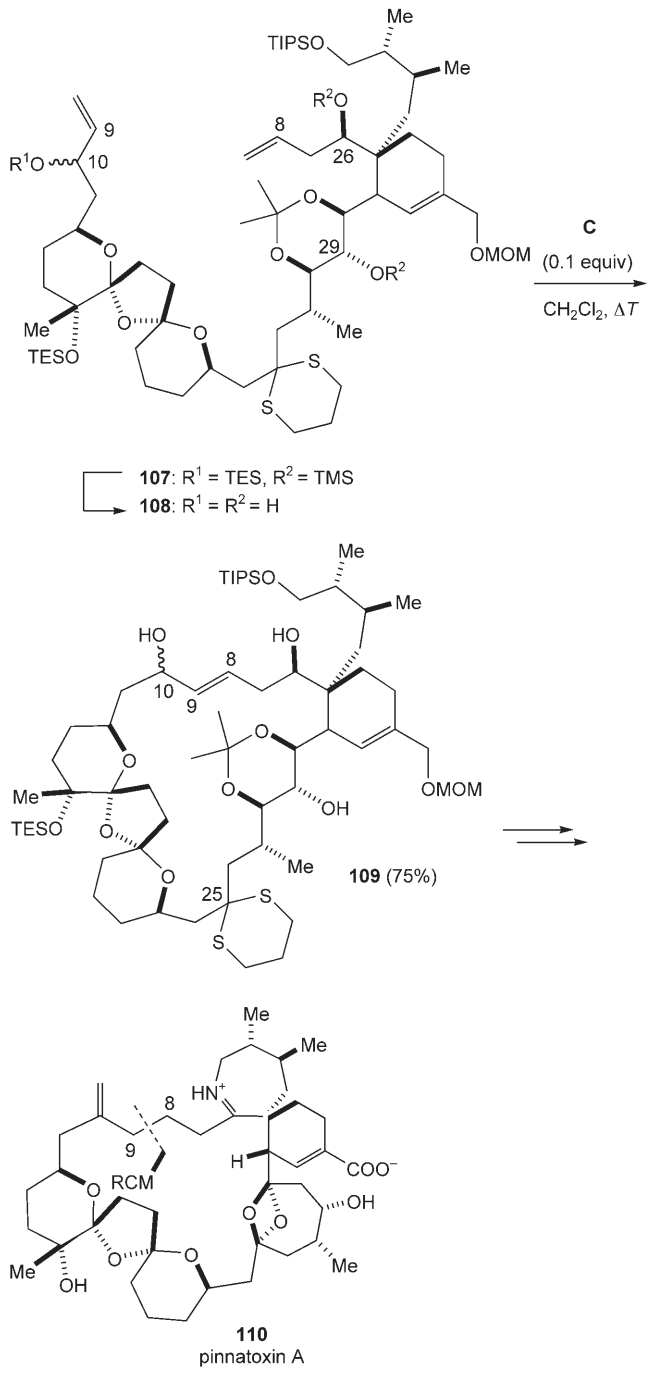

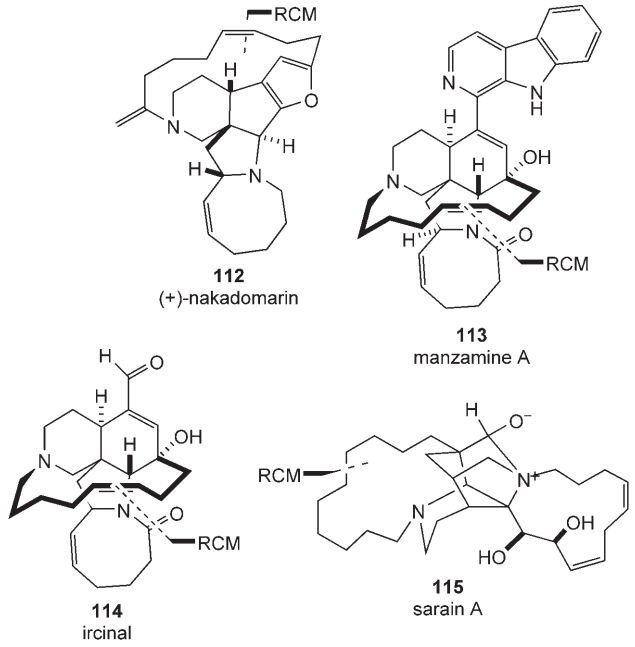

Scheme 15. RCM in the total synthesis of the cyclopeptide alkaloid arenastatin A.

9. Cyclophanes

Some naturally occurring cyclophanes (**116**, **117** (R = H, cylindrocyclophane F; R = OH, cylindrocyclophane A and **118**) have been synthesized by using RCM reactions (Table 9). In the case of (−)-longithorone, an enyne RCM was used for the construction of a macrocyclic diene, which gave rise to ring C after a Diels–Alder cycloaddition.[65]

Table 9: Conditions for RCM to give cyclophanes.

Conditions	Catalyst, yield	Compd	Ref.
$H_2C{=}CH_2$, CH_2Cl_2, 45 °C, 40 h, 3 mM	**A** (30–40 mol%), 31–47%	**116**	[65]
C_6H_6, 40 °C, 1 h	**C** (34 mol%), 50%	**117**	[66]
C_6H_5Cl, 135 °C, 6 h	**I** (10 mol%), 76%	**118**	[67]

© 2006 Wiley-VCH Verlag GmbH & Co. KGaA, Weinheim

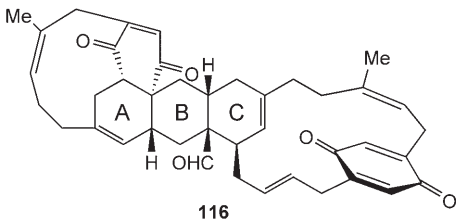

116
(–)-longithorone A

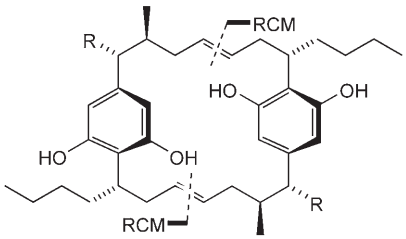

117
cylindrocyclophanes

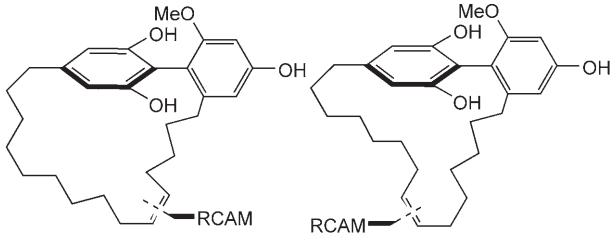

118
turrianes

10. Prostaglandins

The RCAM strategy has also been applied to the synthesis of the marine natural product prostaglandin E2-1,15-lactone (Table 10).

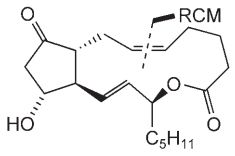

119
PGE_2-1,15-lactone

Table 10: Prostaglandin synthesis based on RCAM.

Conditions	Catalyst, yield	Compd	Ref.
toluene, 80 °C	**J** (7.5 mol %), 68–73 %	**119**	[68]

11. Outlook

Some criteria in the selection of reaction conditions for a macrocycle construction by RCM are quite straightforward. These are solvent selection (toluene, CH_2Cl_2, $(ClCH_2)_2$) and the reaction temperature (from RT to refluxing toluene).

There is no clear rule that indicates the best catalyst to use. Subtle variations in the substrate structure and in the type of final product may lead to different results with each type of carbene complex. In particular, the substitution pattern, the steric demand of the substrate, the ring size to be formed, and the presence of coordinating heteroatoms have an important influence on the results. The yield and the *E*/*Z* ratio of the product may be influenced by all these factors as well as by secondary isomerization reactions mediated by the metathesis complexes.[69] The catalyst loading varies from case to case (from 1 to 25 %) and is highly dependent on the species used. Other important aspects are concentration (0.25 to 8 mM) and the addition time, which is sometimes done slowly. Long reaction times are sometimes recorded when working at low temperatures as most catalytic species are not thermally stable. When planning a new synthesis, it is worth testing different catalysts, temperatures, and concentrations with additional fine tuning of the loading and addition rate.

Abbreviations

Bn	benzyl
CAN	calcium ammonium nitrate
Cy	cyclohexyl
L	ligand
Mes	2,4,6-trimethylphenyl
MOM	methoxymethyl
PMB	4-methoxybenzyl
PMP	4-methoxyphenyl
RCAM	ring-closing alkyne metathesis
RCM	ring-closing metathesis
TBDPS	*tert*-butyldiphenylsilyl
TBS	*tert*-butyldimethylsilyl
Teoc	(2,2,2-trichloroethoxy)carbonyl
TES	triethylsilyl
TIPS	triisopropylsilyl
TMS	trimethylsilyl

Received: February 17, 2006
Published online: August 21, 2006

[1] Recent reviews: a) A. Giessert, S. T. Diver, *Chem. Rev.* **2004**, *104*, 1317–1382; b) B. Schmidt, *Eur. J. Org. Chem.* **2004**, 1865–1880; c) A. H. Hoveyda, D. G. Gillingham, J. J. Van Veldhuizen, O. Kataoka, S. B. Garber, J. S. Kingsbury, J. P. Harrity, A. *Org. Biomol. Chem.* **2004**, *2*, 8–23; d) R. H. Grubbs, *Tetrahedron* **2004**, *60*, 7117–7140; e) J. Prunet, *Angew. Chem.* **2003**, *115*, 2932–2936; *Angew. Chem. Int. Ed.* **2003**, *42*, 2826–2830; corrigendum: J. Prunet, *Angew. Chem.* **2003**, *115*, 3444; *Angew. Chem. Int. Ed.* **2003**, *42*, 3322; f) "Ene-yne Metathesis" M. Mori, *Handbook of Metathesis*, *Vol. 2* (Ed.: R. H. Grubbs), Wiley-VCH, Weinheim, **2003**, p. 176; g) C. S. Poulsen, R. Madsen, *Synthesis* **2003**, 1–18; h) T. M. Trnka, R. H. Grubbs, *Acc. Chem. Res.* **2001**, *34*, 18–29; i) A. Fürstner, *Angew. Chem.* **2000**, *112*, 3140–3172; *Angew. Chem. Int. Ed.* **2000**, *39*, 3012–3043; j) M. E. Maier, *Angew. Chem.* **2000**, *112*, 2153–2157; *Angew. Chem. Int. Ed.* **2000**, *39*, 2073–2077; k) L. Yet, *Chem. Rev.* **2000**, *100*, 2963–3007; l) M. L. Randall, M. L. Snapper, *Strem Chem.* **1998**, *17*, 1–9; m) S. K. Armstrong, *J. Chem. Soc. Perkin Trans. 1*

 © 2006 Wiley-VCH Verlag GmbH & Co. KGaA, Weinheim

1998, 371 – 388; n) R. H. Grubbs, S. Chang, *Tetrahedron* **1998**, *54*, 4413 – 4450.

[2] The synthesis of heterocycles and the total syntheses of some natural macrocycles have been reviewed recently: a) J. Mulzer, E. Öhler, *Top. Organomet. Chem.* **2004**, *13*, 269 – 366; b) K. C. Nicolaou, P. G. Bulger, D. Sarlah, *Angew. Chem.* **2005**, *117*, 4564 – 4601; *Angew. Chem. Int. Ed.* **2005**, *44*, 4490 – 4527; c) A. Deiters, S. F. Martin, *Chem. Rev.* **2004**, *104*, 2199 – 2238.

[3] S. Y. Hong, M. W. Day, R. H. Grubbs, *J. Am. Chem. Soc.* **2004**, *126*, 7414 – 7415.

[4] Synthesis of **C** and **D**: a) M. Scholl, S. Ding, C. W. Lee, R. H. Grubbs, *Org. Lett.* **1999**, *1*, 953 – 956; b) T. M. Trnka, J. P. Morgan, M. S. Sanford, T. E. Wilhelm, M. Scholl, T.-L. Choi, S. Ding, M. W. Day, R. H. Grubbs, *J. Am. Chem. Soc.* **2003**, *125*, 2546 – 2558.

[5] Synthesis of **E**: J. S. Kingsbury, J. P. A. Harrity, P. J. Bonitatebus, Jr., A. H. Hoveyda, *J. Am. Chem. Soc.* **1999**, *121*, 791 – 799; see also: a) H. Wakamatsu, S. Blechert, *Angew. Chem.* **2002**, *114*, 794 – 796; *Angew. Chem. Int. Ed.* **2002**, *41*, 794 – 796; b) S. B. Garber, J. S. Kingsbury, B. L. Gray, A. H. Hoveyda, *J. Am. Chem. Soc.* **2000**, *122*, 8168 – 8179; c) J. J. Van Veldhuizen, S. B. Garber, J. S. Kingbury, A. H. Hoveyda, *J. Am. Chem. Soc.* **2002**, *124*, 4954 – 4955; for substituted Hoveyda–Grubbs carbenes see: d) R. Bujok, M. Bieniek, M. Masnyk, A. Michrowska, A. Sarosiek, H. Stepowska, D. Arlt, K. Grela, *J. Org. Chem.* **2004**, *69*, 6894 – 6896; e) A. Michrowska, R. Bujok, S. Harutyunyan, V. Sashuk, G. Dolgonos, K. Grela, *J. Am. Chem. Soc.* **2004**, *126*, 9318 – 9325; f) A. M. Dunne, S. Mix, S. Blechert, *Tetrahedron Lett.* **2003**, *44*, 2733 – 2736; g) M. Zaja, S. J. Connon, A. M. Dunne, M. Rivard, N. Buschmann, J. Jiricek, S. Blechert, *Tetrahedron* **2003**, *59*, 6545 – 6558.

[6] a) M. S. Sanford, J. A. Love, R. H. Grubbs, *J. Am. Chem. Soc.* **2001**, *123*, 6543 – 6554; b) M. S. Sanford, M. Ulman, R. H. Grubbs, *J. Am. Chem. Soc.* **2001**, *123*, 749 – 750; c) O. M. Aagaard, R. J. Meier, F. Buda, *J. Am. Chem. Soc.* **1998**, *120*, 7174 – 7182.

[7] a) T. Kitamura, Y. Sato, M. Mori, *Chem. Commun.* **2001**, 1258 – 1259; b) T. R. Hoye, S. M. Donaldson, T. J. Vos, *Org. Lett.* **1999**, *1*, 277 – 280.

[8] For studies with density functional theory, see: S. F. Vyboishchikov, M. Bühl, W. Thiel, *Chem. Eur. J.* **2002**, *8*, 3962 – 3975.

[9] a) B. Kang, D.-H. Kim, Y. Do, S. Chang, *Org. Lett.* **2003**, *5*, 3041 – 3043; b) F. Dolhem, C. Lièvre, G. Demailly, *Eur. J. Org. Chem.* **2003**, 2336 – 2342; c) C. S. Poulsen, R. Madsen, *J. Org. Chem.* **2002**, *67*, 4441; d) N. Saito, Y. Sato, M. Mori, *Org. Lett.* **2002**, *4*, 803 – 805; e) M. Mori, N. Sakakibara, A. Kinoshita, *J. Org. Chem.* **1998**, *63*, 6082 – 6083; f) T. M. Trunka, M. W. Day, R. H. Grubbs, *Organometallics* **2001**, *20*, 3845 – 3847.

[10] D. L. Wright, J. P. Schulte, M. A. Page, *Org. Lett.* **2000**, *2*, 1847 – 1850.

[11] a) R. J. Davoille, D. T. Rutherford, S. D. R. Christie, *Tetrahedron Lett.* **2000**, *41*, 1255 – 1259; b) S. Krikstolaityte, K. Hammer, K. Undheim, *Tetrahedron Lett.* **1998**, *39*, 7595 – 7598; c) T. R. Hoye, H. Zhao, *Org. Lett.* **1999**, *1*, 1123 – 1125.

[12] a) M. K. Gurjar, P. Yakambram, *Tetrahedron Lett.* **2001**, *42*, 3633 – 3636; b) L. A. Paquette, I. Efremov, *J. Am. Chem. Soc.* **2001**, *123*, 4492 – 4501.

[13] a) C. S. Poulsen, R. Madsen, *J. Org. Chem.* **2002**, *67*, 4441 – 4449; b) T. K. Maishal, D. K. Sinha-Mahapatra, K. Paranjape, A. Sarkar, *Tetrahedron Lett.* **2002**, *43*, 2263 – 2267.

[14] a) R. Garcia-Fandiño, E. M. Cadesido, E. Sobarzo-Sánchez, L. Castedo, J. R. Granja, *Org. Lett.* **2004**, *6*, 193 – 196; b) K. Yamamoto, K. Biswas, C. Gaul, S. J. Danishefsky, *Tetrahedron Lett.* **2003**, *44*, 3297 – 3299; c) A. Fürstner, L. Ackermann, B. Gabor, R. Goddard, C. W. Lehmann, R. Mynott, F. Stelzer, R. Thiel, *Chem. Eur. J.* **2001**, *7*, 3236 – 3253.

[15] A. Fürstner, P. W. Davies, *Chem. Commun.* **2005**, 2307 – 2320.

[16] X. Geng, Z.-Q. Yang, S. J. Danishefsky, *Synlett* **2004**, 1325 – 1333.

[17] K. Yamamoto, K. Biswas, C. Gaul, S. J. Danishefsky, *Tetrahedron Lett.* **2003**, *44*, 3297 – 3299.

[18] A. Fürstner, G. Seidel, N. Kindler, *Tetrahedron* **1999**, *55*, 8215 – 8230.

[19] R. M. Garbaccio, S. J. Stachel, D. K. Baeschlin, S. J. Danishefsky, *J. Am. Chem. Soc.* **2001**, *123*, 10903 – 10908.

[20] E. A. Couladouros, A. P. Mihou, E. A. Bouzas, *Org. Lett.* **2004**, *6*, 977 – 980.

[21] Z.-Q. Yang, X. Geng, D. Solit, C. A. Pratilas, N. Rosen, S. J. Danishefsky, *J. Am. Chem. Soc.* **2004**, *126*, 7881 – 7889.

[22] X. Geng, S. J. Danishefsky, *Org. Lett.* **2004**, *6*, 413 – 416.

[23] S. Barluenga, P. López, E. Moulin, N. Winssinger, *Angew. Chem.* **2004**, *116*, 3549 – 3552; *Angew. Chem. Int. Ed.* **2004**, *43*, 3467 – 3470.

[24] X. Wang, E. J. Bowman, B. J. Bowman, J. A. Porco, *Angew. Chem.* **2004**, *116*, 3685 – 3689; *Angew. Chem. Int. Ed.* **2004**, *43*, 3601 – 3605.

[25] C. Herb, A. Bayer, M. E. Maier, *Chem. Eur. J.* **2004**, *10*, 5649 – 5660.

[26] L. Yet, *Chem. Rev.* **2003**, *103*, 4283 – 4306.

[27] F. Bouazza, B. Renoux, C. Bachmann, J.-P. Gesson, *Org. Lett.* **2003**, *5*, 4049 – 4052.

[28] a) D. L. Boger, J. Hong, *J. Am. Chem. Soc.* **2001**, *123*, 8515 – 8519; b) P. E. Harrington, M. A. Tius, *J. Am. Chem. Soc.* **2001**, *123*, 8509 – 8514.

[29] J. H. Humphrey, Y. Liao, A. Ali, T. Rein, Y.-Y. Wong, H.-J. Chen, A. K. Courtney, S. F. Martin, *J. Am. Chem. Soc.* **2002**, *124*, 8584 – 8592.

[30] C. Gaul, J. T. Njardarson, S. J. Danishefsky, *J. Am. Chem. Soc.* **2003**, *125*, 6042 – 6043.

[31] C. W. Lee, R. H. Grubbs, *J. Org. Chem.* **2001**, *66*, 7155 – 7158.

[32] D. J. Dixon, A. C. Foster, S. V. Ley, *Org. Lett.* **2000**, *2*, 123 – 125.

[33] C. A. Dvorak, W. D. Schmitz, D. J. Poon, D. C. Pryde, J. P. Lawson, R. A. Amos, A. I. Meyers, *Angew. Chem.* **2000**, *112*, 1730 – 1732; *Angew. Chem. Int. Ed.* **2000**, *39*, 1664 – 1666.

[34] J. Louie, C. W. Bielawski, R. H. Grubbs, *J. Am. Chem. Soc.* **2001**, *123*, 11312 – 11313.

[35] A. Fürstner, G. Seidel, *J. Organomet. Chem.* **2000**, *606*, 75 – 78.

[36] A. Fürstner, K. Langemann, *J. Am. Chem. Soc.* **1997**, *119*, 9130 – 9136.

[37] A. Fürstner, K. Langemann, *Synthesis* **1997**, 792 – 803.

[38] A. Fürstner, A. Leitner, *Angew. Chem.* **2003**, *115*, 320 – 323; *Angew. Chem. Int. Ed.* **2003**, *42*, 308 – 311.

[39] A. Fürstner, O. Guth, A. Rumbo, G. Seidel, *J. Am. Chem. Soc.* **1999**, *121*, 11108 – 11113.

[40] A. Fürstner, C. Müller, *Chem. Commun.* **2005**, 5583 – 5585.

[41] A. Fürstner, A.-S. Castanet, K. Radkowski, C. W. Lehmann, *J. Org. Chem.* **2003**, *68*, 1521 – 1528.

[42] A. Fürstner, D. De Souza, L. Parra-Rapado, J. T. Jensen, *Angew. Chem.* **2003**, *115*, 5516 – 5518; *Angew. Chem. Int. Ed.* **2003**, *42*, 5358 – 5360.

[43] Y. Matsuya, T. Kawaguchi, H. Nemoto, *Org. Lett.* **2003**, *5*, 2939 – 2941.

[44] T. R. Hoye, M. Hu, *J. Am. Chem. Soc.* **2003**, *125*, 9576 – 9577.

[45] a) E. R. Malecka, Jr., L. R. Terrell, F. Geng, J. S. Ward III, *Org. Lett.* **2002**, *4*, 2841 – 2844; b) B. Trost, J. Chisholm, S. Wrobleski, M. Jung, *J. Am. Chem. Soc.* **2002**, *124*, 12420 – 12421; c) H. W. Lam, G. Pattenden, *Angew. Chem.* **2002**, *114*, 526 – 529; *Angew. Chem. Int. Ed.* **2002**, *41*, 508 – 511.

[46] C. Aïssa, R. Riveiros, J. Ragot, A. Fürstner, *J. Am. Chem. Soc.* **2003**, *125*, 15512 – 15520.

[47] A. Fürstner, C. Aissa, R. Riveiros, J. Ragot, *Angew. Chem.* **2002**, *114*, 4958 – 4960; *Angew. Chem. Int. Ed.* **2002**, *41*, 4763 – 4766.

[48] A. Fürstner, L. Turet, *Angew. Chem.* **2005**, *117*, 3528 – 3532; *Angew. Chem. Int. Ed.* **2005**, *44*, 3462 – 3466.

[49] A. Fürstner, T. Müller, *J. Am. Chem. Soc.* **1999**, *121*, 7814 – 7821.

© 2006 Wiley-VCH Verlag GmbH & Co. KGaA, Weinheim

[50] A. Fürstner, T. Müller, *J. Org. Chem.* **1998**, *63*, 424 – 425.
[51] a) A. Fürstner, F. Jeanjean, P. Razon, *Angew. Chem.* **2002**, *114*, 2203 – 2206; *Angew. Chem. Int. Ed.* **2002**, *41*, 2097 – 2101; b) A. Fürstner, F. Jeanjean, P. Razon, C. Wirtz, R. Mynott, *Chem. Eur. J.* **2003**, *9*, 320 – 326.
[52] A. Fürstner, K. Radkowski, J. Grabowski, C. Wirtz, R. Mynott, *J. Org. Chem.* **2000**, *65*, 8758 – 8762.
[53] G. Evano, J. V. Schaus, J. S. Panek, *Org. Lett.* **2004**, *6*, 525 – 528.
[54] C. Jasper, R. Wittenberg, M. Quitschalle, J. Jakupovic, A. Kirschning, *Org. Lett.* **2005**, *7*, 479 – 482.
[55] K. C. Nicolaou, T. Montagnon, G. Vassilikogiannkabis, C. J. N. Mathison, *J. Am. Chem. Soc.* **2005**, *127*, 8872 – 8888.
[56] J. Chen, C. J. Forsyth, *Angew. Chem.* **2004**, *116*, 2200 – 2204; *Angew. Chem. Int. Ed.* **2004**, *43*, 2148 – 2152.
[57] B. Scheiper, F. Glorius, A. Leitner, A. Fürstner, *Proc. Natl. Acad. Sci. USA* **2004**, *101*, 11960 – 11965.
[58] N. K. Tripathy, G. I. Georg, *Tetrahedron Lett.* **2004**, *45*, 5309 – 5311.
[59] S. Sakamoto, H. Sakazaki, K. Hagiwara, K. Kamada, K. Ishii, T. Noda, M. Inoue, M. Hirama, *Angew. Chem.* **2004**, *116*, 2200 – 2204; *Angew. Chem. Int. Ed.* **2004**, *43*, 6505 – 6510.
[60] a) W. P. D. Goldring, L. Weiler, *Org. Lett.* **1999**, *1*, 1471 – 1473; b) A. Fürstner, A. Rumbo, *J. Org. Chem.* **2000**, *65*, 2608 – 2611.
[61] A. Fürstner, O. Guth, A. Rumbo, G. Seidel, *J. Am. Chem. Soc.* **1999**, *121*, 11108 – 11113.
[62] T. Nagata, M. Nakagawa, A. Nishida, *J. Am. Chem. Soc.* **2003**, *125*, 7484 – 7485.
[63] S. F. Martin, J. M. Humphrey, A. Ali, M. C. Hillier, *J. Am. Chem. Soc.* **1999**, *121*, 866 – 867.
[64] a) O. Irie, K. Samizu, J. R. Henry, S. M. Weinreb, *J. Org. Chem.* **1999**, *64*, 587 – 595; b) M. J. Sung, H. I. Lee, H. B. Lee, J. K. Cha, *J. Org. Chem.* **2003**, *68*, 2205 – 2208.
[65] M. E. Layton, C. A. Morales, M. D. Shair, *J. Am. Chem. Soc.* **2002**, *124*, 773 – 775.
[66] A. B. Smith III, C. M. Adams, S. A. Kozmin, D. V. Paone, *J. Am. Chem. Soc.* **2001**, *123*, 5925 – 5937.
[67] A. Fürstner, F. Stelzer, A. Rumbo, H. Krause, *Chem. Eur. J.* **2002**, *8*, 1856 – 1871.
[68] A. Fürstner, K. Grela, C. Mathes, C. W. Lehmann, *J. Am. Chem. Soc.* **2000**, *122*, 11799 – 11805.
[69] See: C. W. Lee, R. H. Grubbs, *Org. Lett.* **2000**, *2*, 2145 – 2147, and Ref. [1b].

For all customers in Europe!

We, TCI Europe, deliver all our products directly from BELGIUM.

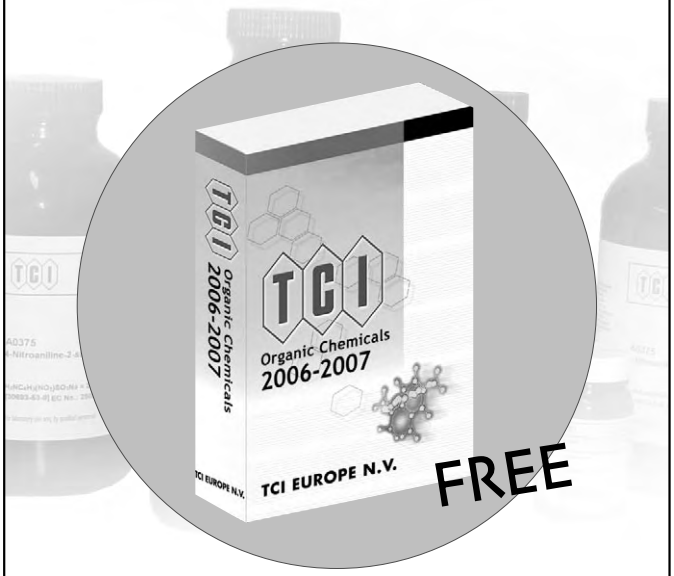

TCI EURO CATALOGUE 2006 - 2007

- ✔ 18 000 organic chemicals
- ✔ 1000 new products
- ✔ more physical properties
- ✔ more chemical structures

... and, LOWER PRICES for many items!

Ask your free copy today!

Visit us!

CPhI Worldwide 2006 : 5A39
3-5 October 2006, Paris

TCI EUROPE N.V.
00 800 46 73 86 67 • +32 (0)3 735 07 00
Fax +32 (0)3 735 07 01
sales@tcieurope.be • www.tcieurope.be
<Head Office>
TOKYO CHEMICAL INDUSTRY CO., LTD.
www.tokyokasei.co.jp

DOI: 10.1002/anie.200600288

Coded Microparticles

Encoded Microcarriers For High-Throughput Multiplexed Detection

Robert Wilson, Andrew R. Cossins, and David G. Spiller*

Keywords:
barcodes · combinatorial chemistry · microspheres · nanoparticles · suspension array

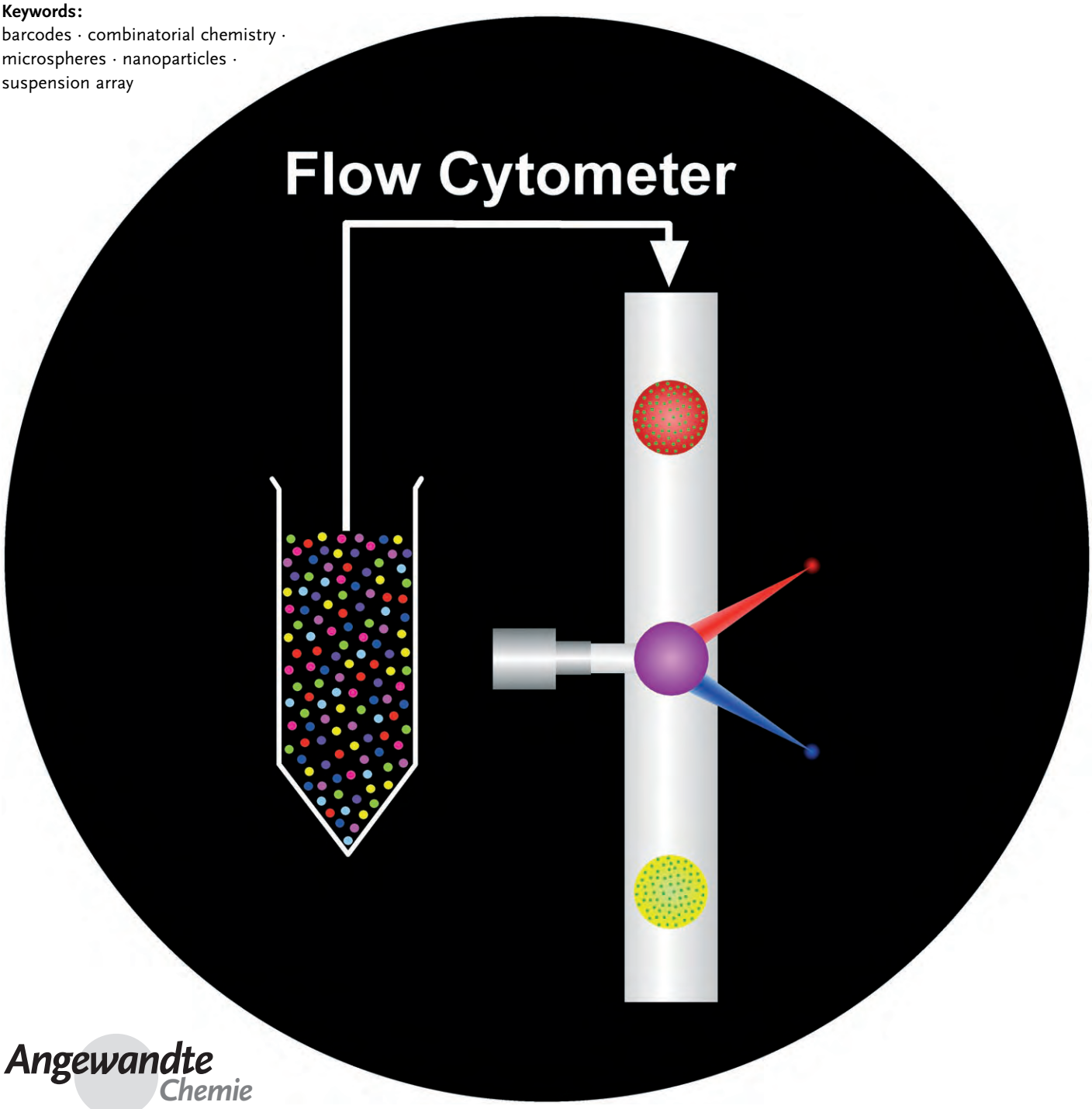

© 2006 Wiley-VCH Verlag GmbH & Co. KGaA, Weinheim

Since the decoding of the human genome, the quest to obtain more and more molecular information from smaller and smaller samples is intensifying. Today the burden of this challenge is being borne by planar arrays, but the quality of the data provided by this approach is limited by variations in performance between different arrays. Suspension arrays of encoded microspheres provide higher quality data, but the amount of molecular information that can be acquired with them is limited by the number of codes that can be distinguished in the same sample. New methods of preparing encoded particles promise to alleviate this problem, but in the face of a growing number of new technologies it is sometimes difficult to decide which, if any, will succeed. Herein we appraise these new forms of encoded particle critically, and ask if they can deliver the necessary multiplexing power and whether they will perform well in multiplexed assays.

From the Contents

1. Introduction	6105
2. The Problem	6106
3. Optical Encoding	6106
4. Chemical Encoding	6110
5. Graphical Encoding	6110
6. Electronic Encoding	6112
7. Physical Encoding	6112
8. Reading the Code	6113
9. Two-Dimensional Arrays of Optically Encoded Microspheres	6114
10. Future Prospects of Suspension Arrays	6114

1. Introduction

Following the completion of the first draft of the Human Genome project in 2001 there has been a huge increase in the amount of biomolecular information that must be accessed for research, and increasingly for clinical purposes. Perhaps the most popular approach to addressing and separately quantifying the many thousands of entities available in this "post-genomic" era is provided by planar-array technologies, which involve depositing two-dimensional grids of probe molecules (antibodies, oligonucleotides, drug candidates etc) onto flat solid supports, each array location acting as a probe for a known target molecule. Although arrays are having a major impact on high-density screening, the quality of the results and the speed at which they can be obtained are severely limited by the properties of the planar surface. By contrast, the current range of automated immunoassay systems allows rapid detection of small and large molecules over a wide range of concentrations, using competitive and non-competitive formats. To achieve this detection they take advantage of the latest developments in separation technology to resolve bound and unbound antigens. Many of these systems use latex microspheres as the solid phase because they allow fast binding kinetics and facilitate the separation step.[1] Herein we ask whether micrometer-sized particles have the potential to confer the same benefits on genomics, proteomics, and drug discovery.

Microspheres have significant advantages over planar arrays in terms of the way they are produced and used. Regardless of whether planar arrays are produced by photolithography or robotic spotting, there is a relatively low upper limit to the number of arrays that can be produced at the same time. Probe molecules must be attached to each spot of a planar array individually, whereas they can be conjugated to millions of microspheres at the same time, with a degree of reproducibility that is impossible to reproduce in microarray production. Many of the problems that afflict planar arrays stem from the fact that all probe molecules must be attached to the array under the same conditions using the same surface chemistry, which may not be suitable for all of them. By contrast, individual probe molecules can be attached to separate batches of microspheres by a variety of proven chemistries under conditions that are optimum for each probe.

Planar arrays are often inflexible because they impose a predetermined panel of tests on the user, but when microspheres are used the panel can easily be changed by adding or subtracting microspheres with different probes. The rates of hybridization and binding on planar arrays are limited by diffusion to the surface, but the kinetics of binding to microspheres can be accelerated by efficient mixing. The sensitivity of planar arrays is limited by variations in feature properties between arrays and even within the same array,[2] a problem that is minimized when microspheres are used. Microspheres facilitate the separation and washing steps, and may even allow these to be eliminated altogether. They are inexpensive to produce in large numbers and allow minute sample volumes to be interrogated. The use of many microspheres for each target molecule in the same assay permits rigorous statistical scrutiny of the data and leads to high quality results. The main advantage of planar arrays is that

[*] Dr. R. Wilson
Department of Chemistry
Liverpool University
Liverpool L69 7ZD (UK)
Fax: (+44) 151-794-3588
E-mail: r.wilson@liv.ac.uk
Prof. A. R. Cossins, Dr. D. G. Spiller
School of Biological Sciences
Liverpool University
Liverpool L69 7ZD (UK)

© 2006 Wiley-VCH Verlag GmbH & Co. KGaA, Weinheim

they allow thousands of individual tests to be performed in parallel, but during the last few years the possibility of using suspension arrays of encoded microcarriers has emerged as an alternative.[3–7]

In this Review we divide encoded microcarriers into different groups depending on how they are encoded. Where appropriate, we also describe how they are manufactured, because this also will help to determine whether they are suitable for high-throughput applications. We then describe the different platforms that can be used to decode encoded microcarriers. Finally we review the properties that have contributed to the success of traditional microspheres and discuss the future prospects of encoded microcarriers in the context of these properties. The term multiplex has become imprecise in recent years; herein it refers to multiple assays performed on the same undivided volume of sample at the same time.

2. The Problem

When two-dimensional arrays (Figure 1 A) are used to perform multiplexed assays the identity of each probe molecule is known from its location in the grid. This method of identification is known as positional encoding. The benefits of using microspheres stem from their freedom to move in three dimensions, but this rules out positional encoding. Instead each microsphere must contain some form of code that identifies the probe molecules attached to it (Figure 1 B). Provided the probes can be identified, the target molecules bound to them can be identified in the same way as molecules bound to two-dimensional arrays. Encoded microcarriers can also be used as reaction supports in combinatorial methods that generate diverse product libraries by combining individual building blocks in a relatively small number of reaction steps. The type of code used in multiplexed assays is fixed and remains unchanged during the assay, but in combinatorial chemistry it is sometimes advantageous to use an active encoding method. In a split-and-mix synthesis individual carriers take independent pathways through a series of reaction vessels. At the end of the synthesis each carrier has a product attached to it, but identifying this product can be time consuming and technically challenging. By actively encoding the carriers at each step in the synthesis it is possible to record the reaction history and thereby identify the products attached to them without further analysis. Specific examples of fixed and active encoding methods are described below.

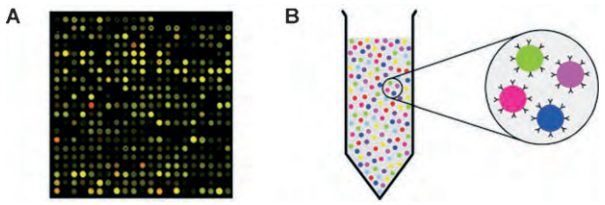

Figure 1. A) A conventional microarray consists of a two-dimensional grid of recognition molecules (antibodies, peptides, oligonucleotides etc.). The identity of the recognition molecules at each spot in the array is known from its location in the grid. B) A suspension array is composed of recognition molecules attached to encoded particles (in this image the particles are encoded with different colors). The identity of the recognition molecules attached to each particle is revealed by reading the particle code.

3. Optical Encoding

3.1. Optical Encoding with Organic Dyes

Most of the suspension arrays described in the literature are composed of polymer microspheres internally doped with one or more fluorescent dyes. Polystyrene microspheres become swollen when suspended in an organic solvent, allowing the dye molecules diffuse into them, but when the microspheres are transferred to an aqueous solution they shrink and the dye molecules become entrapped. By trapping dyes with different emission spectra at different concentrations (and thus intensities), microspheres with unique spectral codes are obtained. The number of codes depends on the number of dyes and intensities according to the formula: $C = N^{m-1}$ (where C = the number of codes, N = the number of intensity levels and m = the number of colors), but in practice other factors limit the number of spectrally distinct codes that can be generated. The dyes must be compatible in the swelling solvent and the doping process must be reproducible; this becomes more difficult as the numbers and concentrations of the dyes increase. Small differences in the diameter and composition of the microspheres are reported to affect the doping process. If the dyes have different excitation wavelengths then multiple excitation lasers are required, which increases the cost of the decoding instrument, and when the spectra overlap radiative and/or nonradiative energy transfer may complicate the code. For multiplexed detection a reporter dye is required and the region of the spectrum that is occupied by its emission profile is not available for encoding. Luminex Corp (Austin, TX) supplies microspheres that are encoded with organic dyes as part of their xMAP liquid array technology.[8,9] They encode 5.5-μm microspheres with two dyes at ten different concentrations to produce up to 100 different sets of microspheres (Figure 2 A). Each set is matched to a different probe molecule that confers specificity on the microspheres in multiplexed assays (Figure 2 B). Although the level of multiplexing that has been achieved with this platform is considerably lower than some of the more inflated predictions about suspension arrays it has been successfully used for a wide range of multiplexed assays, including human cytokines,[10] human immunodeficiency virus (HIV) and hepatitis B seroconversion,[11] single nucleotide polymorphisms (SNPs),[12] thyroid levels,[13] kinase testing,[14] cystic fibrosis screening,[15] allergy testing,[16] infectious disease diagnosis,[17] and the detection of biological warfare agents.[18] Becton Dickinson Biosciences (San Diego, CA) have developed a related system based on 7.5-μm microspheres doped with one fluorescent dye at different concentrations.[19,20] Their BD Cytometric Array system is designed to run on FACScan and FACalibur flow cytometers, but it is

 © 2006 Wiley-VCH Verlag GmbH & Co. KGaA, Weinheim

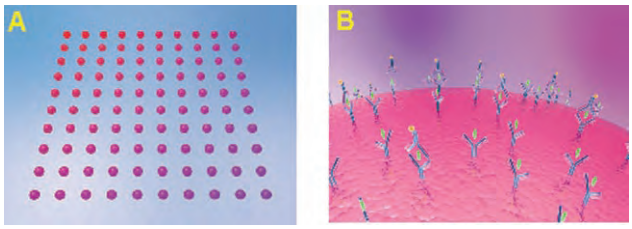

Figure 2. A) Suspension array composed of 100 sets of optically encoded microspheres. In this image one microsphere from each set has been organized into a two dimensional grid to emphasize the similarities and differences between suspension and planar arrays. Each set of microspheres in a suspension array is equivalent to one probe molecule in a planar array. Reading the code, rather than determining the position, reveals the identity of the probe molecules attached to the microspheres. B) Each set of microspheres in a suspension array has a different probe molecule attached to its surface. This schematic image shows one frame in the progress of an immunoassay on the surface of a single microsphere. The target molecules (green) have already bound to the probe molecules (capture antibodies) attached to the surface of the microsphere, and are in the process of being sandwiched between them and detector antibodies conjugated to an orange fluorescent label. (Courtesy of Luminex Corp.)

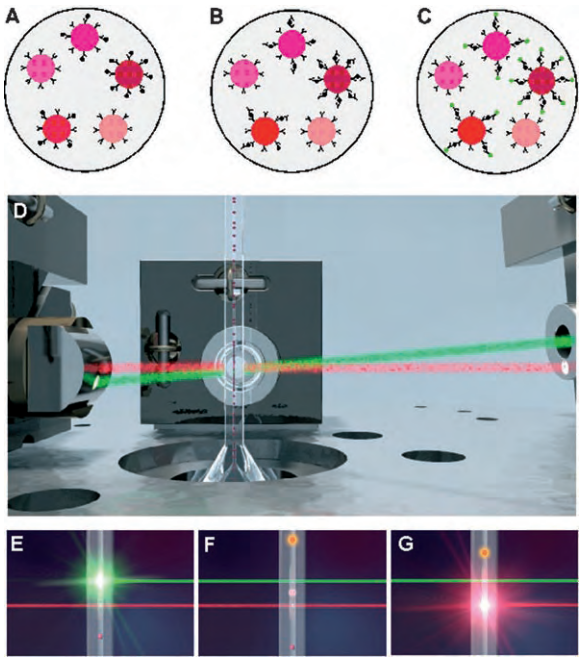

Figure 3. This series of images shows how multiplexed assays are carried out with a suspension array. They are based on the work of Kellar and Douglas who used the Luminex technology to perform multiplexed immunoassays for eight different cytokines.[10] A) The suspension array, composed of encoded microspheres conjugated to capture antibodies, is mixed with a sample containing different cytokines. B) The cytokines are sandwiched between the capture antibodies and the corresponding biotinylated detector antibodies. C) Bound detector antibodies are labeled with fluorescent reporter molecules. D) A stream of individual microspheres flows through the sensing points of a cytometer. E–G) Images of a single encoded microsphere with bound reporter molecules as it flows past E) a green laser that excites the reporters and G) a red laser that excites the code. (Courtesy of Luminex Corp.)

compatible with any cytometer that is equipped with a 488 nm laser, and capable of distinguishing emissions at 576 and 670 nm. The company markets a large number of multiplexed immunoassays, but the maximum level multiplexing in these is less than ten.

3.2. Multiplexing with an Encoded Suspension Array

To illustrate how multiplexed assays are carried out with a suspension array one specific example will be described (Figure 3). Although some of the encoded particles described in this Review are substantially different from the fluorescent polymer microspheres used in this example, they must be compatible with similar experimental methods if they are to be of practical use. Kellar and Douglass[10] used the Luminex platform to carry out multiplexed immunoassays for eight different (8-plex) cytokines in serum. Figure 3 A: Different sets of microspheres, each coated with a different capture antibody and each having a different code, were suspended in the wells of a multiwell filter bottom plate with the sample; each well contained approximately 2000 microspheres from each set After incubating the microspheres with the sample on a plate shaker the wells were washed (vacuum-aspirated) to remove unbound cytokines and then incubated with biotinylated reporter antibodies (Figure 3B) and fluorescent streptavidin conjugates (Figure 3C). After further washing and fixing, the contents of the wells were aspirated into a Luminex 100 cytometer where individual microspheres were interrogated sequentially as they passed the two lasers (Figure 3D). At least 100 replicates from each set of microspheres were interrogated per well. The time required to complete the multiplexed assay was less than the time required to carry out one single analyte ELISA (enzyme-linked immunosorbent assay) but the reproducibility and specificity were comparable, and the range of concentrations over which cytokines could be detected was greater. Enhanced sensitivity and/or increased concentration range compared with ELISA has also been observed by other researchers.[19,21] Before the multiplexed assay was ready for routine use a period of assay development was necessary. Problems that are more likely to be encountered during multiplexed assay development are cross-reactivity and non-specific binding. These problems tend to become more pronounced as the level of multiplexing is increased. Potential users should always bear in mind that multiplexing is not only about developing platforms with the necessary encoding power, but also about accommodating multiple probe molecules in the same assay.

3.3. Optical Encoding with Photoluminescent Nanoparticles

Semiconductor quantum dots (QDs)[22,23] are photoluminescent nanoparticles that have dimensions smaller than the exciton Bohr radius of the corresponding bulk material. For spherical CdS nanoparticles this limit is reached when the particles have a diameter of less than 10 nm. The effect of quantum confinement gives rise to unique optical and

 © 2006 Wiley-VCH Verlag GmbH & Co. KGaA, Weinheim

electronic properties that are different from those of the component atoms or the bulk solids composed of them. These include narrow, QD-size-tunable emission spectra (20–30 nm full width at half maximum; FWHW), and the possibility of exciting all colors at the same wavelength. Their narrow emission spectra allow 10–12 different colors to be resolved in the visible region (400–800 nm) with acceptable spectral overlap. ODs are also brighter and more resistant to photobleaching than fluorescent dyes. These properties make QDs ideal for encoding. They can be incorporated into microspheres during synthesis[24,25] or entrapped by solvent swelling methods similar to those used for fluorescent dyes.[26–28] In theory, six colors at six different intensities would yield around 40 000 different codes, but in practice overlap between the different intensities is a major limitation. It is still necessary to use a reporter for multiplexed assays and this region of the spectrum is not available for encoding. Recently, Gao and Nie increased the porosity of commercial microspheres in an organic solvent and then infused hydrophobic QDs into the pores. By this method they encoded microspheres with different ratios of two colors of QD to give a total of eleven different codes, and demonstrated that these could be resolved at high speed with a flow cytometer.[28]

Quantum Dot Corp has developed a very simple method for encoding suspension arrays (Figure 4). Hydrophobic trioctylphosphine (TOP)/trioctyphosphine oxide (TOPO) QDs are directly adsorbed onto the surface of oligonucleotide-functionalized microspheres.[29] Two colors at three intensities gave nine different spectral codes that were used to identify up to ten different single nucleotide polymorphisms (SNPs). Decoding and detection were carried out in a flow-cytometer, but Quantum Dot Corp have suggested that the future of high-throughput highly multiplexed quantitative assays will be based on imaging systems, such as the Mosaic Q1000 that they have developed in collaboration with Matsushita/Panasonic (see Section 8.2).

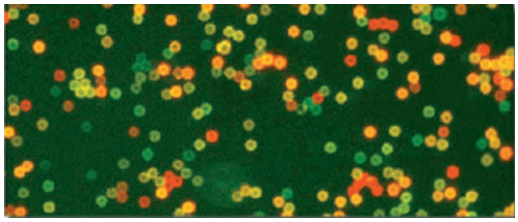

Figure 4. Microspheres encoded with different colors and ratios of semiconductor quantum dots (QDs). QDs are photoluminescent nanoparticles that have several advantages over fluorescent dyes: all colors can be excited at the same wavelength, the emission spectra can be tuned, and the narrow emission profiles allow more colors to be resolved within the same window of the electromagnetic spectrum. They are brighter than most fluorescent dyes and less prone to photobleaching. (Courtesy of Quantum Dot Corp.)

3.4. Microspheres That Record Their History

Microspheres can also be encoded by depositing fluorescent dyes or nanoparticles onto their external surface. Existing methods for encoding split-and-mix libraries are often based on the covalent attachment of detectable chemical tags to the support microspheres at each step in the synthesis. This process is known as chemical encoding. Examples of chemical tags are fluorescent dyes,[30] nucleic acids,[31] secondary amines[32] and haloaromatics molecules.[33] Unfortunately many of these encoding chemistries can interfere with compound synthesis, and the decoding methods are generally expensive, laborious, and not very amenable to automation. Gallop and colleagues[31] synthesized a library of approximately one million heptapeptide sequences on 10-μm beads and encoded them with oligonucleotides. Every time a new amino acid was added to the peptide sequence two more bases were added to the encoding oligonucleotides. The library was screened with labeled antibodies, and microspheres that displayed a high level of fluorescence were selected with a flow cytometer and sorted into polymerase chain reaction (PCR) tubes. Oligonucleotides attached to individual microspheres were amplified by PCR and sequenced to reveal the identity of peptides with high affinities for the antibodies. The method is only practical if the number of hits is low because of the logistics of sorting individual microspheres into separate PCR tubes. It is also time consuming because oligonucleotides attached to each bead must be amplified and then sequenced.

Peptides can be encoded with oligonucleotides because the chemistries for synthesizing both of them are compatible, but other polymers may not be so amenable. Trau and colleagues devised a much simpler method of active encoding for tracking the path of microspheres through a combinatorial split-and mix synthesis.[34–37] The compounds are synthesized on large ($\approx$100-μm diameter) support microspheres and encoded with smaller (0.2–5.0-μm diameter) encoding microspheres doped with fluorescent dyes. At each step in the synthesis the support microspheres are mixed with the encoding microspheres that code for that reaction step. The encoding microspheres are coated with polyelectrolytes to enhance their adsorption onto the support microspheres. Between 50 and 400 encoding microspheres are adsorbed at each step, and at the end of the synthesis the code reveals the reaction history of individual support microspheres. The power of this approach lies in the efficient use of relatively few fluorescent dyes to record a large amount of information on the microspheres, but it would be necessary to determine the location of the encoding microspheres on the support microspheres as well as their spectral code in order to harness this. In a practical demonstration, Trau and colleagues adsorbed different combinations of twenty different encoding microspheres onto support microspheres at each step in the combinatorial synthesis of 100-member tripeptide library.[35] After three steps the support microspheres were encoded with different colors and ratios of encoding microspheres, which allowed the products attached to them to be identified without further analysis. Bear in mind, however, that even if the necessary encoding power does become available it will not on its own lead to a revolution in the way in which combinatorial libraries are screened. The methods that are used to synthesize the individual components of these libraries on solid supports may produce artifacts that generate false positives during the screening process. This problem

 © 2006 Wiley-VCH Verlag GmbH & Co. KGaA, Weinheim

becomes more prominent as the size of the library increases. Even standard peptide chemistry does not yield pure products, and the results of more general synthetic processes may be even less satisfactory.

3.5. Microspheres with a Nanoscale Architecture

Van Blaaderen and Vrij prepared microspheres with the fluorescent dye fluoresceinisothiocyanate (FITC) located in concentric shells surrounding a silica core,[38] and more recently Trau and colleagues have prepared similar microspheres with up to six different fluorescent-dye shells alternating with nonfluorescent silica spacer shells (see physical encoding, Section 7).[39] When dye molecules with overlapping excitation and emission spectra are located in close proximity the emission spectra may be complicated by resonance energy transfer. It has been suggested that for encoded microspheres this increase in complexity represents an increase in the information content, but an alternative view is that it simply makes the code more difficult to decipher. Resonance energy transfer decreases according to the inverse of the sixth power of the intermolecular distance between the dyes and therefore locating them in separate shells can prevent it. The microspheres prepared by Van Blaaderen and Vrij became less stable as the number of shells increased, but there are other methods of locating dyes in separate shells. Caruso and colleagues encoded microspheres with concentric shells of up to three fluorescent dyes using layer-by-layer (LBL) chemistry.[40] This approach involved the sequential deposition of oppositely charged polymers (polyelectrolytes) onto microspheres; the dyes were covalently attached to one of the polymers. In the final step antibodies were adsorbed onto the surface and then the microspheres were used as labels in solid-phase immunoassays. The same group used LBL chemistry to assemble semiconductor QDs[41] and lanthanum phosphate nanoparticles (LPNPs) onto microspheres.[42] LPNPs are similar in size to QDs, but their photoluminescence depends on their bulk properties rather than size-dependent band-gap transitions. They have high quantum yields and are resistant to photobleaching. Their emission wavelength can be adjusted by doping with different rare-earth elements and more than one color can be excited at the same wavelength. Caruso and colleagues assembled mixed layers of two different colors onto microspheres and proposed that they could be used as labels in biorecognition assays.

3.6. Time Resolved Reading of Optical Codes

It has already been pointed out that resonance energy transfer can lead to loss of coding information when the excitation spectrum of a luminescent dye (the acceptor) overlaps the emission spectrum of another luminescent dye (the donor). However, if two dyes have overlapping spectra and different luminescence decay times, changing the ratio of the acceptor and donor can modulate the decay times of both dyes. This change in decay time can be used to encode microspheres and nanoparticles, an approach that was first investigated by Keij and Steinkamp using Luminex microspheres doped with different ratios of orange and red dyes.[43] They reported that 13 out of 20 spectrally different microspheres could be resolved by measuring total emission intensity and average luminescence lifetime, but Luminex microspheres are not ideal for this. A better way would be to dope microspheres with different ratios of two dyes that have similar spectra, but substantially different luminescence lifetimes. Kürner et al. synthesized nanoparticles that contained a ruthenium complex as the donor and cyanine dyes as acceptors.[44] As the relative concentration of the acceptor was increased, the luminescence lifetimes of the donor decreased and those of the acceptors increased. Using this variation it was possible to resolve a series of encoded nanoparticles doped with the metal complex and four different cyanine dyes, by measuring emission wavelength and fluorescence lifetime of the acceptors. An advantage of this variation is that all the colors of the cyanine dye could be excited at the same wavelength. Suspension arrays encoded in this way should become more attractive now that CompuCyte Corp (Cambridge, MA) have begun marketing laser-scanning cytometers that can measure fluorescence decay times.

3.7. Other Methods of Optical Encoding

Although encoding microspheres with luminescent dyes or nanoparticles is the most popular method for producing encoded suspension arrays, a growing number of alternatives are being explored. Fenniri and colleagues synthesized resins which have 24 unique IR and Raman codes by polymerizing styrene and alkyl styrene monomers.[45] These resins had a similar chemistry to the supports used in solid-phase synthesis, and therefore they could be used to encode combinatorial libraries.

Raman spectroscopy has traditionally been regarded as more useful for structural analysis than for ultra-sensitive detection, but the signal intensity may increase by many orders of magnitude when: 1) a molecule is in close proximity to a fractally rough metal surface, such as colloidal silver, and 2) the wavelength of the incident light is resonant with the molecule and the plasmon of the metal. Unfortunately surface-enhanced resonant Raman spectra (SERRS) are prone to interference from anything that disrupts the close association between the molecules and the metal. Doering and Nie overcame this problem by embedding dye molecules in a silica shell surrounding a gold nanoparticle core. Raman spectra were enhanced by factors of 10^{13}–10^{14} [46] and it was suggested that multiple dyes could be used for encoding. However, He and colleagues have pointed out that decoding the Raman spectrum of a plurality of dyes may be difficult owing to spectral overlap.[5]

Mirkin and colleagues have also demonstrated that Raman spectroscopy can be used for multiplexed detection.[47] They conjugated dye-labeled oligonucleotides to gold nanoparticles and used them as labels in microbead assays. Each set of gold nanoparticles was conjugated to a different oligonucleotide sequence and encoded with a unique combi-

 © 2006 Wiley-VCH Verlag GmbH & Co. KGaA, Weinheim

nation of fluorescent dyes. In multiplexed assays the target sequences were sandwiched between capture oligonucleotides conjugated to 300-μm silica microspheres and the encoded gold nanoparticles. The Raman spectra of the bound labels were enhanced by gold-nanoparticle-catalyzed deposition of silver onto the microspheres. Oxonica plc (Kidlington, UK) are developing a related approach based on benzotriazole dyes and silver nanoparticles encapsulated in polymer microspheres. These microspheres could be used as sensitive labels, but the possibility of using them as carriers in multiplexed assays is also being investigated.

Photonic crystals with well-resolved optical features can be produced by electrochemically etching silicon. Sailor and colleagues produced square stacks of silicon on a silicon substrate photolithographically and then converted them into photonic crystals by applying a periodic electrochemical etch.[48] The stacks were released from the substrate by applying a current pulse and then converted into particles by mechanical agitation or ultrasonic fracture. These particles have very sharp reflectivity lines (ca. 11 nm FWHM) in the visible or infrared region of the spectrum. The position of these lines can be tuned to a given wavelength by altering the etching conditions and one particle can reflect more than one line. In theory, thousands of codes could be generated, but this would require fine control over the etching conditions that may not be possible in practice. The particles have been used to distinguish between albumins from two different species in a simple multiplexed immunoassay.

Elastic scattering from microspheres can be amplified by coating them with metal nanoparticles. Siiman and colleagues encoded microspheres with gold or silver nanoparticles and then conjugated them to antibodies specific for different subpopulations of white blood cells.[49] In whole blood, multiple microspheres bind to individual cells, which can then be simultaneously identified and counted in a flow cytometer.

4. Chemical Encoding

A method that harnesses the high capacity of nucleic acids for information storage to encode combinatorial libraries has already been described in a previous section. Mirkin and colleagues have used nucleic acid codes for multiplexed biomolecular assays. Their biobarcodes are nano- or microparticles conjugated to recognition molecules (antibodies, oligonucleotides, etc.) and encoded with DNA oligonucleotides. Target molecules are sandwiched between capture probe molecules conjugated to magnetic microspheres and the biobarcodes (Figure 5). The magnetic microspheres and biobarcodes bound to them are separated from the solution magnetically and washed, and then the encoding oligonucleotides are released and detected. This approach has achieved high sensitivity in immunoassays for single analytes,[50] but it can also be used for multiplexed detection if the encoding oligonucleotides are resolved with a planar array.[51] Biobarcodes can be produced in large batches and they should perform well in biomolecular assays, but decoding with a planar array is complicated and time consuming compared

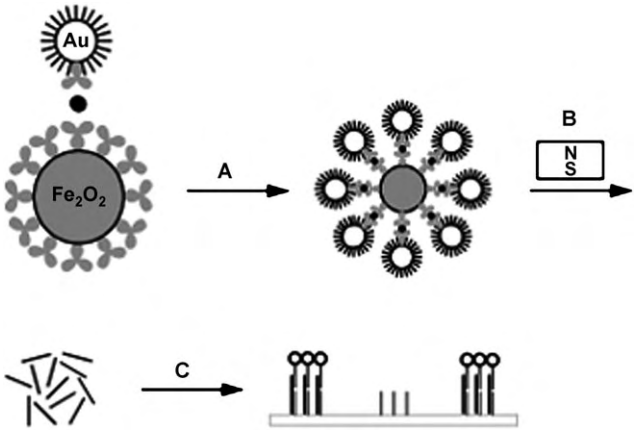

Figure 5. Biocodes are nano- or microparticles conjugated to recognition molecules and encoded with oligonucleotides. A) Sandwich immunoassays are carried out with the biocodes (Au) and magnetic microspheres (Fe_2O_3). B) The magnetic microspheres and biocodes bound to them are separated and washed, and then the encoding oligonucleotides are released. C) The released oligonucleotides are resolved with a universal planar array. The identities and concentrations of the target molecules in the original sample can be determined from the locations and spot densities of the oligonucleotides hybridized to the array.

with the high-throughput detection in a flow cytometer. The number of codes that could be resolved is similar to the number of zip-codes that can be distinguished with a universal array.[52] If gold nanoparticles are used as reporters the arrays can be silver stained and imaged with inexpensive equipment, but the vagaries of silver staining suggest that results obtained in this way would only be qualitative.

5. Graphical Encoding

The decoding methods described in Section 3 rely on resolving a complex optical signal into its individual components. Decoding a graphical code relies on deciphering a two-dimensional pattern. Supermarket barcodes and the text on this page are examples of graphical codes. Rare-earth ions in glass hosts have narrow emission spectra (ca. 10–20 nm FWHM) in the visible region. Multiple colors can be excited at the same UV wavelength and they are resistant to photobleaching. Microbarcodes (Figure 6 A) are made by fusing glass blocks doped with rare-earth ions in a predetermined series and drawing out the product into a ribbon fiber with a cross-section of 20×100 μm.[53] The ribbon is cut into 20-μm sections at a rate of 5 mm s^{-1}. At this rate it would take about one month to produce the same number of microbarcodes as there are microspheres in one milliliter of a commercial microsphere product. The number of codes is given by the formula where $C = N^s/2$ where C is the number of codes, N is the number of colors and s is the number of stripes; at least four colors can be resolved from each other and fluorescent reporter molecules. Microbarcodes have a relative density of 2.5 (that is, 2.5-times the density of water). They are chemically robust and can be functionalized for attachment of probe molecules using silane attachment chemistries. A

 © 2006 Wiley-VCH Verlag GmbH & Co. KGaA, Weinheim

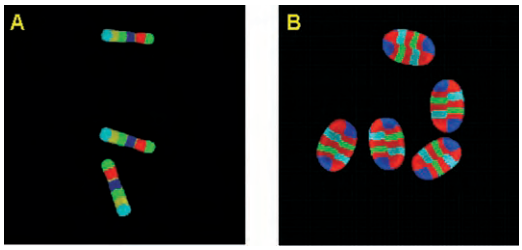

Figure 6. A,B) Microbarcodes are glass rods encoded with bands of photoluminescent rare-earth ions. All the colors in the microbarcode can be excited at the same wavelength and the material from which they are made is robust and amenable to a wide range of surface chemistries, but they are about ten times as large as traditional microspheres and two-and-a-half times as dense. At reported rates of production it would take about one month to produce the same number of microbarcodes as there are microspheres in a single milliliter of commercial product. (Courtesy of Corning, Inc.)

multiplexed assay that discriminated between human and microbial DNA has been demonstrated, and more recently microbarcodes with the potential for higher levels of coding have been made (Figure 6B).

A second method of graphical encoding is the use of striped metal nanorods (nanobarcodes), which are prepared by sequential electrochemical deposition of metals, such as gold and silver, in mesoporous aluminum templates.[54–57] The number of rods produced per square centimeter of template is equivalent to the number of microspheres in 10 mL of a commercial microsphere solution; it only takes a few hours to produce these. The stripes have micrometer dimensions and can be distinguished because of the different reflectivity of the metals. When gold and silver nanorods are illuminated at 405 nm the silver stripes are bright and the gold stripes are dark (Figure 7A). The formula for the total number of codes is the same as for microbarcodes (see above). The minimum stripe length that can be resolved is probably around 500 nm (but see ref. [57] for a discussion) and therefore 5-μm rods made of two metals would have a maximum of 10 stripes, which corresponds to 528 codes. Increasing the length of the rods or the number of metals (Pt, Pd, Ni, Co, Cu) would increase the number of codes, but some metals cannot be resolved by reflectance and not all metals are as easy to functionalize with probe molecules as gold and silver. The rods can be decoded with a light-microscope and pattern-recognition software[56] and bound target molecules are reported with a fluorescent dye. Gold and silver have relative densities of 19.3 and 10.5, respectively, and therefore vigorous mixing is required to maintain rods made of these metals in suspension, but under these conditions the rods may bend, or break at the junction between two metals. It has been suggested that making large numbers of different nanorods would be impractical because only one code can be generated per template, but there is no reason why multiple rods could not be manufactured in parallel electroplating baths. Striped metal nanorods (Nanoplex Technologies, Inc., CA) have been used in a multiplexed immunoassay for two analytes,[54] and may also be useful as covert taggants that distinguish authentic from counterfeit products.[57]

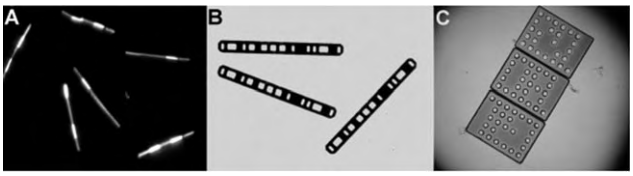

Figure 7. A selection of graphical codes. A) Striped metal nanorods (nanobarcodes) imaged with illumination at 405 nm. Each metal nanorod in the image consists of alternating stripes of gold and silver. The apparent difference in diameter between the highly reflective silver and the less reflective gold in this image is due to differences in brightness and not a real difference in diameter. Metal nanorods can be produced in production-line quantities suitable for suspension arrays and they have dimensions that are similar to traditional microspheres. They are much denser, however, which suggests that vigorous mixing would be required to maintain them in suspension during biomolecular assays. This mixing could damage fragile biological molecules in solution and/or lead to bending or breakage of the nanorods themselves (courtesy of Nanoplex Technologies). B) Aluminum rods encoded with a pattern of holes imaged with a light microscope. The rods are larger than traditional microspheres, but they are only about 2.5-times as dense and therefore require less vigorous mixing during biomolecular assays than rods made of gold and silver. SmartBead Technologies is currently the only commercial organization to offer a multiplexing platform based on graphical encoding (courtesy of SmartBead Technologies Ltd). C) ImageCodes are polymer wafers encoded with a pattern of holes. They are about 10-times as large as traditional microspheres, but their density is similar and their size could probably be reduced. The L-shaped pattern of holes along the perimeter is used for orientation purposes during decoding and the inner pattern of holes is used to identify individual wafers.

SmartBead Technologies Ltd (Cambridge, UK) has developed a graphical system based on encoded aluminum rods that are manufactured using standard semiconductor microfabrication techniques.[58] Approximately two million rods are produced per three-inch wafer. This would be enough rods to carry out approximately 1000 assays. The relative density of aluminum is 2.7 and the rods have dimensions of $100 \times 10 \times 1$ μm. The code consists of a pattern of holes as shown in Figure 6B. In theory, millions of different codes are possible. Probe molecules are attached to the rods using proprietary surface chemistry and bound target molecules are reported with fluorescent dyes. Multiplexed assays are carried out in 96-well filter plates with a fully automated liquid handling and imaging system. SmartBead's UltraPlex platform has been launched into the autoimmune diagnostics market and is aimed at high-volume customers, such as hospitals. The company is not planning to make the platform available to users who wish to develop similar multiplexed assays in-house, but it can be licensed for non-competing applications. De Smedt and colleagues avoided the relatively high density of metal carriers by photobleaching patterns into fluorescent polymer microspheres with a confocal scanning microscope.[59] Some of their codes were composed of a series of bars and spaces just like a macroscopic barcode, but the encoding process is extremely slow and decoding depends on precise orientation of the microspheres with respect to the decoder.

3D Molecular Sciences Ltd (Cambridge, UK) developed a system of polymer particles encoded with a pattern of holes.[60]

 © 2006 Wiley-VCH Verlag GmbH & Co. KGaA, Weinheim

These ImageCodes (Figure 7C) were made by optically burning a pattern into wafers of negative photoresist with UV light and a mask. They had dimensions of $500 \times 300 \times 25$ μm, but the relative density was similar to traditional microspheres. Target molecules were reported with a fluorescent dye. It was suggested that several thousand particles could be decoded at the same time using pattern-recognition software.

6. Electronic Encoding

The use of radio-frequency devices for encoding combinatorial libraries was first reported by two different groups at about the same time.[61,62] In one of these reports each $8 \times 1 \times 1$ mm semiconductor device was enclosed in a chemically inert porous container along with polymer microspheres that were used as reaction supports.[62] The containers were split into separate groups and then each group was encoded with a radio-frequency signal that corresponded to the building block that was about to be added to the microspheres. After adding the building block the groups were pooled so that common reactions, such as washing, drying and deprotection could be performed. Then the pool was split into groups and encoded in preparation for the next building block. At the end of the synthesis the compounds attached to the microspheres were identified with specially designed radio-frequency memory-retrieving equipment. The memory capacity of radio-frequency devices is so high that other relevant information, such as the reaction conditions can also be stored. They are chemically inert and coding is non-invasive, but they are not suitable for multiplexed assays because of their size.

Recently PharmaSeq, Inc. (Princeton, NJ) have developed a much smaller 64 bit read-only memory device (microtransponder) that has dimensions of $250 \times 250 \times 100$ μm.[63] Each transponder comprises an integrated circuit connected to a photovoltaic cell and an antenna (Figure 8). The transponders are decoded in a capillary as they flow past a laser that simultaneously excites fluorescent reporter molecules and prompts the transmission of a radio-frequency code. The number of codes that are possible with this type of device is around 2^{40}, but the dimensions are large compared with a typical microsphere.

7. Physical Encoding

Physical characteristics, such as size and refractive index, are usually the properties of entire particles and therefore do not offer much scope for multiplexing. The Copalis system developed by DiaSorin (Saluggia, Italy) was based on particle size.[64] Their dedicated flow cytometer was able to discriminate approximately 0.1-μm differences in bead diameter on the basis of low-angle light scattering. Multiplexed assays for three analytes were carried out with four different microspheres (1.1, 1.4, 1.7, and 1.9 μm diameter). The three largest microspheres were coated with different capture antigens and the smallest microspheres were used as a reference. When the sample contained the corresponding antibodies, the microspheres formed aggregates that were detected in the flow cytometer.

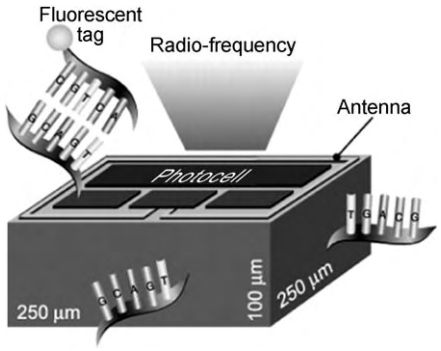

Figure 8. Microtransponders are microscopic read-only memory devices. When a laser is shone on the device it simultaneously excites fluorescent reporters on its surface and triggers the transmission of a 40-bit radio frequency code. The potential number of codes that could be produced by this approach far exceeds the number that could be generated by any other method described herein, and large numbers of transponders could be produced by methods that are already in use in the semiconductor industry. The principal barrier preventing their widespread use in biomolecular assays is their size, which is about 25-times that of traditional microspheres, but this approach should benefit from future advances in micro- and nanofabrication and may eventually supersede the alternatives. (Courtesy of Pharmaseq, Inc.)

3D Molecular Sciences proposed a method based on optically readable polymer particles encoded with different shapes (FloCodes)[60] It was suggested that these particles could be decoded in a customized flow cytometer that simultaneously measures the fluorescence of reporter molecules and the pattern of scattered light as it passes the detector, but no information about the level of multiplexing that could be achieved was ever provided.

Although individual physical properties offer limited scope for multiplexing they can be combined with each other, and with other encoding strategies. Modern flow cytometers can decode particles on the basis of size and refractive index as well as photoluminescence. Trau and colleagues have prepared microspheres encoded with up to six fluorescent dyes located in separate shells alternating with nonfluorescent spacer shells round a silica core.[39] Microspheres prepared in this way display a diverse range of optical signatures derived from a combination of fluorescence wavelength and intensity, size and refractive index, but only those with a unique optical signatures are suitable for combinatorial chemistry. These are obtained by passing the microspheres through a flow cytometer programmed to reject duplicates. To synthesize a library of oligonucleotides this population of optically distinguishable microspheres would then be split into four portions that would each be treated with a different nucleotide base. Each portion would then be passed through the flow cytometer to record the optical signature of the microspheres that had been treated with a given base. The microspheres would then be mixed and divided into four new portions before repeating the process of reaction and recording until oligonucleotides of the desired length had been synthesized.

 © 2006 Wiley-VCH Verlag GmbH & Co. KGaA, Weinheim

8. Reading the Code

8.1. In a Flow Cytometer

Flow cytometers[9,65] are instruments that measure the fluorescence of cells or particles in suspension as they flow past a sensing point. Therefore they can be used to decode suspension arrays composed of photoluminescent microspheres and detect fluorescent reporter molecules bound to their surface. They consist of a light source, fluidics, collection optics, detection hardware, and computing power to convert the signals into data. In most flow cytometers the light source is a laser that emits coherent light at a specified wavelength that is focused on the sensing point. The fluidics system is designed to deliver single particles to the sensing point with an accuracy of ± 1 μm. This accuracy is achieved by injecting the sample into the center of an enclosed channel through which a column of liquid (the sheath fluid) is flowing. Particles in the sample are hydrodynamically focused into the center of the column. For a given excitation source the scattered light and fluorescence are collected by two lenses (one opposite the light source and one at right angles) and resolved by a series of beam splitters and filters. This set up allows photoluminescence at multiple wavelengths, and physical characteristics, such as particle size and shape, to be determined. The laser is focused on a very small volume of solution surrounding the particle. This approach reduces the background signal and even allows separation-free assays to be carried out. Detectors are usually photomultiplier tubes (PMTs) that can detect as few as 100 reporter molecules per particle. Top-of-the-line instruments are equipped with multiple excitation lasers and detectors that can detect scattering and up to 18 colors from thousands of particles per second. Most flow cytometers are also equipped with a downstream sorting system that allows specific particles to be selected for further processing.

Luminex originally designed their encoded microspheres to be used with a Becton–Dickinson benchtop cytometer equipped with a 488-nm argon laser (FlowMetrix System). The disadvantage of this system was the need to compensate for the overlap in fluorescence between the reporter dye and the microspheres. Subsequently Luminex developed their own benchtop Model 100 instrument that incorporates a green (532 nm) frequency-doubled YAG laser to excite R-phycoerythrin reporter molecules that emit at 580 nm, and a 635 nm diode laser to excite the dyes in the microspheres. These emit at 658 and 712 nm and have no spectral overlap with the phycoerythrin. Fluorescence and sideways scatter are detected by avalanche photodiodes. The Model 100 is unique among commercial flow cytometers because it incorporates high-speed digital pulse processing and fluidics that are optimized for 5.5-μm diameter microspheres. The cytometer is interfaced with a Gilson 215 Multiprobe fluidics system that performs multiplexed assays on encoded microspheres in 96- or 384-well filter plates. The contents of each well are then aspirated into the cytometer and each bead is interrogated individually as they pass the two laser beams (see Figure 3). The software provides a full statistical report on the microspheres and calculates the mean reporter intensity for each code. The main disadvantages of using flow cytometers for multiplexed assays is that they are bulky and expensive, but recently Partec GmbH (Münster, Germany) have introduced a portable flow cytometer powered by a car battery or solar panels, and ongoing developments in microfluidics should lead to further reductions in size and cost.

Another important development is the combination of flow cytometry with imaging hardware. ImageStream 100 (Amnis Corp, Seattle, USA) is like a flow cytometer, but the traditional detectors have been replaced by a sensitive CCD camera that acquires up to six independent images (brightfield, darkfield, and four colors) at a rate of 100 particles per second (Figure 9). This instrument overcomes some of the problems that are encountered when particles are imaged on a planar surface and it could be used to read graphical codes.

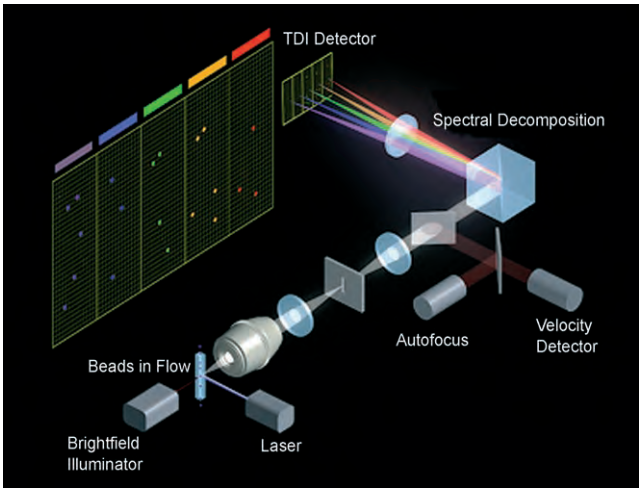

Figure 9. The ImageStream 100 is the first commercial instrument that combines the fluidics of a flow cytometer with a method that allows individual cells and particles to be imaged as they pass the detector. It could be used to read graphical codes and detect fluorescent reporter molecules bound to their surface. The detectors found in traditional flow cytometers have been replaced by a sensitive CCD camera that acquires up to six independent images (brightfield, darkfield, and up to four colors) of the particles as they pass the detector, at a rate of about 100 particles per second. (Courtesy of Amnis Corp.)

8.2 Reading The Code with an Imaging System

Optically encoded microspheres can also be decoded with an imaging system. An example is the Mosaic Q1000 imaging and data analysis platform that has been developed by Quantum Dot Corp and Matushita/Panasonic. It consists of an inverted epifluorescence microscope equipped with a 405-nm excitation laser and CCD camera. Multiplexed assays are carried out in multiwell plates using QD encoded microspheres and magnetic-separation technology to facilitate washing and separation. Decoding and detection take place within the wells of the plate. Multicolor images of the microspheres are acquired with the microscope and decoded by image-recognition software that assigns numerical values to individual pixels depending on their intensity. CCD

© 2006 Wiley-VCH Verlag GmbH & Co. KGaA, Weinheim

cameras are much less sensitive than the detectors used in flow cytometers and therefore it can be difficult to detect low numbers of reporter molecules. One solution to this problem is to use a laser scanning cytometer.[66,67] In these instruments one or more lasers are scanned over the imaging surface. Emitted light is detected with wavelength-specific photomultiplier tubes. These instruments are less dependent on focus than fluorescence microscopes. For microspheres that are optically encoded imaging is an alternative to flow cytometry, but for most graphically encoded particles it is indispensable. However, this method is also more complicated because the orientation of the particles must be determined before they can be decoded, and slower because of the limited number of particles that can be imaged at one time. Regardless of how complicated the decoding process is the propensity of microspheres to move about as a result of convection currents and/or to aggregate can interfere with the decoding process. If there are slight variations in the height of the imaging surface some particles will be out of focus and multiple images may be required to accommodate this. Many of these problems were encountered by Coleman and colleagues when they attempted to image Luminex microspheres on a planar surface.[2] Most graphical methods still use photoluminescence to detect reporter molecules and this increases the cost of the imaging platform compared with systems based on photoluminescence alone. At present some of these problems are difficult to overcome, but the technology required is similar to that being developed for biometric recognition and related applications. Billions of dollars are being invested in this area and there should be significant advances during the next few years.

9. Two-Dimensional Arrays of Optically Encoded Microspheres

Microarrays of oligonucleotides can be prepared by light-directed combinatorial synthesis (Affymetrix, Inc, Santa Clara, USA)[68] or high-speed robotic printing.[69] Illumina, Inc (San Diego, USA) have developed an alternative method in which oligonucleotide-functionalized microspheres are randomly assembled in an array of microwells etched into the tips of optical fibers.[70–72] Images cannot be transmitted through conventional optical fibers because spatial resolution is lost. Imaging optical fibers are manufactured by melting bundles of large optical fibers and drawing them out into a thread that has the same organization as the original bundle, but is much reduced in diameter. Typically this thread is composed of 50 000 individual fibers with diameters of around 5 μm. Each individual fiber carries its own signal, from which images can be constructed pixel by pixel if the thread is interfaced with an imaging system, such as a microscope and CCD camera. Individual fibers are composed of two different types of glass. This difference allows the core of the fiber to be selectively etched away with buffered hydrofluoric acid. By controlling the etching conditions it is possible to form microwells with known dimensions. When an ethanolic solution of oligonucleotide-functionalized microspheres is pipetted onto an etched fiber in the thread they spontaneously assemble into the wells. After wiping away excess microspheres the array of oligonucleotides that remains is many times denser than a robotically spotted array. The array has overall dimensions of around 1.4 mm, which allows it to be used with very small sample volumes. The main problem is that the location of the oligonucleotides-functionalized microspheres is random and therefore the array must be decoded before it can be used. In an early version of the decoding process the microspheres were optically encoded, but this approach appears to have been inefficient owing to variations in bead quality.[70,71] More recently the company have adopted a decoding method based on the sequential hybridization of fluorescent oligonucleotides to the array.[73] This method is time consuming and requires large numbers of synthetic oligonucleotides, but once the array has been decoded it can be reused many times. Random assemblies of optically encoded microspheres functionalized with recognition molecules on a planar surface are still used as microarrays in the BeadChip platform (BioArray Solutions Ltd., USA).[74] The microspheres are decoded at the same time as target molecules bound to them are detected.

10. Future Prospects of Suspension Arrays

At the beginning of this Review it was pointed out that the aim of using an encoded suspension array is to harness the advantages of microspheres for multiplexed assays. Many of the advantages that microspheres have over planar arrays stem from the way in which they are manufactured. High-volume manufacturing methods allow a degree of reproducibility to be attained that is impossible to reproduce in planar-array production. The first question to ask when evaluating any suspension-array technology, therefore, is would it be possible to manufacture the individual encoded particles reproducibly in large numbers? If the answer is no then the particles are unlikely to suitable for multiplexed detection.

Microspheres and target molecules interact with near solution-phase kinetics. This property also facilitates separation and washing steps. To interact efficiently with the sample, the microspheres must be maintained in suspension. The time taken for a range of different microspheres to settle out is shown in Table 1.

Large and/or dense particles that take only seconds or minutes to settle require vigorous mixing to maintain them in suspension, but this may damage the probe and target molecules, and even the particles themselves. When evaluating any suspension-array technology, ask about the kinetics. Microsphere-conjugates reach equilibrium with their target molecules in less than 30 min and particles in a suspension array should do the same.

Miniaturization has been a driver in assay development for many years. The goal is to obtain increasing amounts of molecular information from ever decreasing volumes of sample. Multiplexed assays with the Luminex platform are usually performed in 384-well filter plates. In a 100-plex assay it would be necessary to add a total of about 20 000 microspheres to each well. The working volume of the well is about

 © 2006 Wiley-VCH Verlag GmbH & Co. KGaA, Weinheim

Table 1: Physical parameters for various microparticles

Diameter [μm]	Material	Settling time[a]	20000 Microspheres[b] [μL]	Pelleting time
0.1	polystyrene	1 year	0.00000002	4 h
1	polystyrene	4 days	0.00002	144 s
10	polystyrene	1 h	0.02	< 1 s
100	polystyrene	1 min	20	–
1000	polystyrene	0.5 s	20000	–
10	gold	10 s	–	–
10	aluminum	2 min	–	–
10	silica	3 min	–	–

[a] Approximate settling out time of a suspension through a distance of 1 cm under the influence of gravity. [b] Approximate volume requirement of 20000 microspheres.

20 μL. Table 1 shows how the minimum volume occupied by 20000 microspheres increases as the diameter of the microspheres increases. Microspheres with a diameter of 10 μm only occupy 0.1 % of the working volume, but microspheres with a diameter of 100 μm occupy a volume equivalent to the entire working volume of the well. Even if the number of 100-μm microspheres is decreased by an order of magnitude they will still occupy 10 % of the working volume. Under these conditions the microspheres would be unable to interact efficiently with the sample.

The data considered so far suggests that the ideal particle for microsphere-based assays would be made from a low-density material and have the smallest dimensions that are compatible with its role as a carrier of capture probe molecules. In practice the density must be slightly greater than water to ensure that the microspheres do not simply float on the surface of the solution, and a minimum size is imposed by the requirements of the separation and washing steps that are part of most microsphere assays. The ideal separation process should be fast, efficient, and take place under mild conditions that do not result in any loss of microspheres. The main methods in use are centrifugal precipitation, filtration, and magnetic separation. Table 1 compares the effect of diameter on the time required to pellet microspheres with a centrifuge at 10000 g (the pelleting time can be decreased by increasing the speed of the centrifuge, but this can lead to irreversible aggregation of the microspheres). Very small particles are difficult to pellet. If filtration is used the filter should retain all of the microspheres, but allow fast and efficient removal of molecules in solution. To achieve this the microspheres must be significantly larger than reporter molecules, such as antibodies, which have a hydrodynamic volume equivalent to a 10-nm diameter particle. Magnetic separation depends on the attraction between paramagnetic nanoparticles and a magnet. Individual paramagnetic nanoparticles require high-gradient separators for fast separation, but commercial magnetic microspheres can be separated in a few minutes using an inexpensive magnetic separator because each bead is large enough to contain many nanoparticles. The lower size limit of magnetic microspheres is determined by the minimum volume that can accommodate enough paramagnetic nanoparticles to allow a fast separation.

The sum of all the above considerations leads to the conclusion that microspheres for multiplexed assays should be made from a material that is slightly denser than water and have dimensions of around a micrometer so that they can interact efficiently with small sample volumes, but can be separated from the sample and washed under relatively mild conditions. A review of suppliers' data sheets shows that in fact most of the microspheres designed for use in biomolecular assays are made from materials such as polystyrene (relative density: 1.05) and have diameters in the range 0.3–10 μm. To perform well in multiplexed assays, encoded particles should retain the properties of traditional microspheres, but they must also be large enough to host some form of code. Some coded particles, such as those supplied by Luminex (5.5-μm diameter polystyrene), do retain these properties, but many others appear to be either too large and/or too dense to perform well in multiplexed assays. There is also the problem of production. Microspheres can be produced in large batches and conjugated to capture molecules with high degree of batch-to-batch reproducibility. To compete with them, alternative microcarriers must offer similar advantages, but the problem of reproducibly manufacturing large batches has usually been overlooked, and in most cases it is difficult to envisage how it would be carried out. In the foreseeable future suspension arrays are likely to be based on optically encoded latex microspheres. The remaining challenge is to find ways of increasing the number of encoded microspheres that can be resolved under high-throughput conditions.

The number of unique optical codes that can be generated with photoluminescent dyes or nanoparticles is given by the equation $C = N^{m-1}$ (see Section 3 "Optical Encoding"). This relationship indicates that five colors at six intensities would yield nearly 8000 unique codes, but in practice nothing like this number of codes has ever been demonstrated. Major problems with this approach are reproducibly manufacturing microspheres with multiple colors and intensities, and the expense of a decoding platform that could distinguish subtle differences in intensity on a time scale that is compatible with high-throughput detection.

A more realistic approach would be based on colors alone. Each color would represent one digit in a binary code. The total number of codes is given by the formula 2^n where n is the number of colors. Twelve colors would yield 4000 codes. This number would compete with some microarrays, but remaining problems include finding enough encoding elements and the logistics of manufacturing so many different encoded microspheres in large amounts. A more likely scenario is that suspension arrays will be used to study subsets of target molecules that have previously been identified with two-dimensional arrays, because microspheres are more flexible, less expensive, and provide higher quality quantitative results. The level of multiplexing that would satisfy many of these applications is in the order of a few hundreds rather than many thousands. This target can probably be achieved and it is anticipated that suspension arrays that offer this level of multiplexing will emerge in the next few years.

Received: January 23, 2006
Published online: August 29, 2006

 © 2006 Wiley-VCH Verlag GmbH & Co. KGaA, Weinheim

[1] M. B. Meza, *Drug Discovery Today* **2000**, 1 (HTS Suppl.), 38 – 41.
[2] R. S. Rao, S. R. Visuri, M. T. McBride, J. S. Albala, D. L. Mathews, M. A. Coleman, *J. Proteome Res.* **2004**, *3*, 736 – 742.
[3] M. C. O. Probst, G. Rothe, G. Schmitz, *J. Lab. Med.* **2003**, *27*, 182 – 187.
[4] K. Braeckmans, S. C. De Smedt, M. Leblans, R. Pauwels, J. Demeester, *Nat. Rev. Drug Discovery* **2002**, *1*, 447 – 456.
[5] N. H. Finkel, X. H. Lou, C. Y. Wang, L. He, *Anal. Chem.* **2004**, *76*, 353 A – 359 A.
[6] P. Fortina, L. J. Kricka, S. Surrey, P. Grodzinski, *Trends Biotechnol.* **2005**, *23*, 168 – 173.
[7] K. Braeckmans, *Mod. Drug Discovery* **2003**, *6*, 28 – 32.
[8] D. A. A. Vignali, *J. Immunol. Methods* **2000**, *243*, 243 – 255.
[9] K. L. Kellar, M. A. Iannone, *Exp. Hematol.* **2002**, *30*, 1227 – 1237.
[10] K. L. Kellar, J. P. Douglass, *J. Immunol. Methods* **2003**, *279*, 277 – 285.
[11] Z. Lukacs, A. Dietrich, R. Ganschow, A. Kohlschutter, R. Kruithof, *Clin. Chem. Lab. Med.* **2005**, *43*, 141 – 145.
[12] J. D. Hurley, L. J. Engle, J. T. Davis, A. M. Welsh, J. E. Landers, *Nucleic Acids Res.* **2004**, *32*, e186.
[13] R. Bellisario, R. J. Colinas, K. A. Pass, *Clin. Chem.* **2000**, *46*, 1422 – 1424.
[14] Y. Luo, *Curr. Opin. Mol. Ther.* **2005**, *7*, 251 – 255.
[15] L. Edelmann, G. Hashmi, Y. H. Song, Y. Han, R. Kornreich, R. J. Desnick, *Genet. Med.* **2004**, *6*, 431 – 438.
[16] G. S. Whitehead, J. K. L. Walker, K. G. Berman, W. M. Foster, D. A. Schwartz, *Am. J. Physiol. Lung Cell. Mol. Physiol.* **2003**, *285*, L32 – L42.
[17] X. Yan, W. Zhong, A. Tang, E. G. Schielke, W. Hang, J. P. Nolan, *Anal. Chem.* **2005**, *77*, 7673 – 7678.
[18] M. T. McBride, S. Gammon, M. Pitesky, T. W. O'Brien, T. Smith, J. Aldrich, R. G. Langlois, B. Colston, K. S. Venkateswaran, *Anal. Chem.* **2003**, *75*, 1924 – 1930.
[19] E. Morgan, R. Varro, H. Sepulveda, J. A. Ember, J. Apgar, J. Wilson, L. Lowe, R. Chen, L. Shivraj, A. Agadir, R. Campos, D. Ernst, A. Gaur, *Clin. Immunol.* **2004**, *110*, 252 – 266.
[20] A. Tarnok, J. Hambsch, R. Chen, R. Varro, *Clin. Chem.* **2003**, *49*, 1000 – 1002.
[21] J. Dasso, J. Lee, H. Bach, R. G. Mage, *J. Immunol. Methods* **2002**, *263*, 23 – 33.
[22] A. J. Sutherland, *Curr. Opin. Solid State Mater. Sci.* **2002**, *6*, 365 – 370.
[23] W. C. W. Chan, D. J. Maxwell, X. H. Gao, R. E. Bailey, M. Y. Han, S. M. Nie, *Curr. Opin. Biotechnol.* **2002**, *13*, 40 – 46.
[24] P. O'Brien, S. S. Cummins, D. Darcy, A. Dearden, O Masala, N. L. Pickett, S. Ryley, A. J. Sutherland, *Chem. Commun.* **2003**, 2532 – 2533.
[25] Y. Li, E. C. Y. Liu, N. Pickett, P. J. Skabara, S. S. Cummins, S. Ryley, A. J. Sutherland, P. O'Brien, *J. Mater. Chem.* **2005**, *15*, 1238 – 1243.
[26] X. H. Gao, W. C. W. Chan, S. M. Nie, *J. Biomed. Opt.* **2002**, *7*, 532 – 537.
[27] M. Y. Han, X. H. Gao, J. Z. Su, S. Nie, *Nat. Biotechnol.* **2001**, *19*, 631 – 635.
[28] X. H. Gao, S. M. Nie, *Anal. Chem.* **2004**, *76*, 2406 – 2410.
[29] H. X. Xu, M. Y. Sha, E. Y. Wong, J. Uphoff, Y. H. Xu, J. A. Treadway, A. Truong, E. O'Brien, S. Asquith, M. Stubbins, N. K. Spurr, E. H. Lai, W. Mahoney, *Nucleic Acids Res.* **2003**, *31*, e43.
[30] B. J. Egner, S. Rana, H. Smith, N. Bouloc, J. G. Frey, W. S. Brocklesby, M. Bradley, *Chem. Commun.* **1997**, 735 – 736.
[31] M. C. Needels, D. G. Jones, E. H. Tate, G. L. Heinkel, L. M. Kochersperger, M. M. Dower, R. W. Barrett, M. A. Gallop, *Proc. Natl. Acad. Sci. USA* **1993**, *90*, 10700 – 10704.
[32] Z. J. Ni, D. Maclean, C. P. Holmes, M. M. Murphy, B. Ruhland, J. W. Jacobs, E. M. Gordon, M. A. Gallop, *J. Med. Chem.* **1996**, *39*, 1601 – 1608.
[33] M. H. J. Ohlmeyer, R. N. Swanson, L. W. Dillard, J. C. Reader, G. Asoline, R. Kobayashi, M. Wigler, W. C. Still, *Proc. Natl. Acad. Sci. USA* **1993**, *90*, 10922 – 10926.
[34] L. Grøndahl, B. J. Battersby, D. Bryant, M. Trau, *Langmuir* **2000**, *16*, 9709 – 9715.
[35] B. J. Battersby, D. Bryant, W. Meutermans, D. Mathews, M. L. Smythe, M. Trau, *J. Am. Chem. Soc.* **2000**, *122*, 2138 – 2139.
[36] M. Trau, B. J. Battersby, *Adv. Mater.* **2001**, *13*, 975 – 979.
[37] B. J. Battersby, G. A. Lawrie, M. Trau, *Drug Discovery Today* **2001**, *6* (HTS Suppl.), S19 – S26.
[38] A. Van Blaaderen, A. Vrij, *Langmuir* **1992**, *8*, 2921 – 2931.
[39] G. A. Lawrie, B. J. Battersby, M. Trau, *Adv. Funct. Mater.* **2003**, *13*, 887 – 896.
[40] W. Yang, D. Trau, R. Renneberg, N. T. Yu, F. J. Caruso, *J. Colloid Interface Sci.* **2001**, *234*, 356 – 362.
[41] D. Y. Wang, A. L. Rogach, F. Caruso, *Nano Lett.* **2002**, *2*, 857 – 861.
[42] P. Schuetz, F. Caruso, *Chem. Mater.* **2002**, *14*, 4509 – 4516.
[43] J. F. Keij, J. A. Steinkamp, *Cytometry* **1998**, *33*, 318 – 323.
[44] J. M. Kürner, I. Klimant, C. Krause, E. Pringsheim, O. S. Wolfbeis, *Anal. Biochem.* **2001**, 297, 32 – 41.
[45] H. Fenniri, L. H. Ding, A. E. Ribbe, Y. Zyrianov, *J. Am. Chem. Soc.* **2001**, *123*, 8151 – 8152.
[46] W. E. Doering, S. M. Nie, *Anal. Chem.* **2003**, *75*, 6171 – 6176.
[47] R. Jin, Y. C. Cao, C. S. Thaxton, C. A. Mirkin, *Small* **2006**, *2*, 375 – 380.
[48] F. Cunin, T. A. Schmedake, J. R. Link, Y. Y. Li, J. Koh, S. N. Bhatia, M. J. Sailor, *Nat. Mater.* **2002**, *1*, 39 – 41.
[49] O. Siiman, K. Gordon, A. Burshteyn, J. A. Maples, J. K. Whitesell, *Cytometry* **2000**, *41*, 298 – 307.
[50] J.-M. Nam, C. S. Thaxton, C. A. Mirkin, *Science* **2003**, *301*, 1884 – 1886.
[51] B.-K. Oh, J.-M. Nam, S. W. Lee, C. A. Mirkin, *Small* **2006**, *2*, 103 – 108.
[52] N. P. Gerry, N. E. Witowski, J. Day, R. P. Hammer, G. Barany, F. Barany, *J. Mol. Biol.* **1999**, *292*, 251 – 262.
[53] M. J. Dejneka, A. Streltsov, S. Pal, A. G. Frutos, K. Yost, P. K. Yuen, U. Muller, J. Lahiri, *Proc. Natl. Acad. Sci. USA* **2003**, *100*, 389 – 393.
[54] S. R. Nicewarner-Peña, R. G. Freeman, B. D. Reiss, L. He, D. J. Peña, I. D. Walton, R. Cromer, C. D. Keating, M. J. Natan, *Science* **2001**, *294*, 137 – 141.
[55] B. D. Reiss, R. G. Freeman, I. D. Walton, S. M. Norton, P. C. Smith, W. G. Stonas, C. D. Keating, M. J. Natan, *J. Electroanal. Chem.* **2002**, *522*, 95 – 103.
[56] I. D. Walton, S. M. Norton, A. Balasingham, L. He, D. F. Oviso, D. Gupta, P. A. Raju, M. J. Natan, R. G. Freeman, *Anal. Chem.* **2002**, *74*, 2240 – 2247.
[57] C. D. Keating, M. J. Natan, *Adv. Mater.* **2003**, *15*, 451 – 454.
[58] A. Dames, J. England, E. Colby, WO Patent 00/16893, **2000**.
[59] K. Braeckmans, S. C. De Smedt, C. Roelant, M. Leblans, R. Pauwels, J. Demeester, *Nat. Mater.* **2003**, *2*, 169 – 173.
[60] M. Evans, C. Sewter, E. Hill, *Assay Drug Dev. Technol.* **2003**, *1*, 199 – 207.
[61] E. J. Moran, S. Sarshar, J. F. Cargill, M. M. Shahbaz, A. Lio, A. M. M. Mjalli, R. W. Armstrong, *J. Am. Chem. Soc.* **1995**, *117*, 10787 – 10788.
[62] K. C. Nicolaou, X. Y. Xiao, Z. Parandoosh, A. Senyei, M. P. Nova, *Angew. Chem* **1995**, *107*, 2476 – 2479; *Angew. Chem. Int. Ed. Engl.* **1995**, *34*, 2289 – 2291.
[63] W. Mandecki, M. G. Pappas, N. Kogan, Z. Y. Wang, B. Zamlynny, *ACS Symp. Ser.* **2002**, *815*, 57 – 69.
[64] M. J. Benecky, D. R. Post, S. M. Schmitt, M. S. Kochar, *Clin. Chem.* **1997**, *43*, 1764 – 1770.

 © 2006 Wiley-VCH Verlag GmbH & Co. KGaA, Weinheim

[65] L. Bonetta, *Nat. Methods* **2005**, *2*, 785 – 794.
[66] L. Reeve, D. A. Rew, *Eur. J. Surg. Oncol.* **1997**, *23*, 98 – 108.
[67] G. Woltmann, A. J. Wardlaw, D. A. Rew, *Cytometry* **1998**, *33*, 362 – 365.
[68] S. P. A. Fodor, *Science* **1997**, *277*, 393 – 395.
[69] R. P. Auburn, D. P. Kreil, L. A. Meadows, B. Fischer, S. S. Matilla, S. Russell, *Trends Biotechnol.* **2005**, *23*, 374 – 379.
[70] J. A. Ferguson, F. J. Steemers, D. R. Walt, *Anal. Chem.* **2000**, *72*, 5618 – 5624.
[71] D. R. Walt, *Science* **2000**, *287*, 451 – 452.
[72] D. R. Walt, *Curr. Opin. Chem. Biol.* **2002**, *6*, 689 – 695.
[73] K. L. Gunderson, M. S. Graige, F. Garcia, B. G. Kermani, C. F. Zhao, D. P. Che, T. Dickinson, E. Wickam, J. Bierle, D. Doucet, M. Milewski, R. Yang, C. Siegmund, J. Haas, L. X. Zhou, A. Oliphant, J. B. Fan, M. S. Chee, *Genome Res.* **2004**, *14*, 870 – 877.
[74] G. Hashmi, T. Shariff, M. Seul, P. Vissavjjhala, K. Hue-Roye, C. Lomas-Francis, A. Chaudhuri, M. E. Reid, *Transfusion* **2005**, *45*, 680 – 688.

© 2006 Wiley-VCH Verlag GmbH & Co. KGaA, Weinheim

Borylene Complexes

DOI: 10.1002/anie.200602162

Cationic Terminal Borylene Complexes: Structure/Bonding Analysis and [4+1] Cycloaddition Reactivity of a BN Vinylidene Analogue**

Simon Aldridge, Cameron Jones,* Timo Gans-Eichler, Andreas Stasch, Deborah L. Kays (née Coombs), Natalie D. Coombs, and David J. Willock*

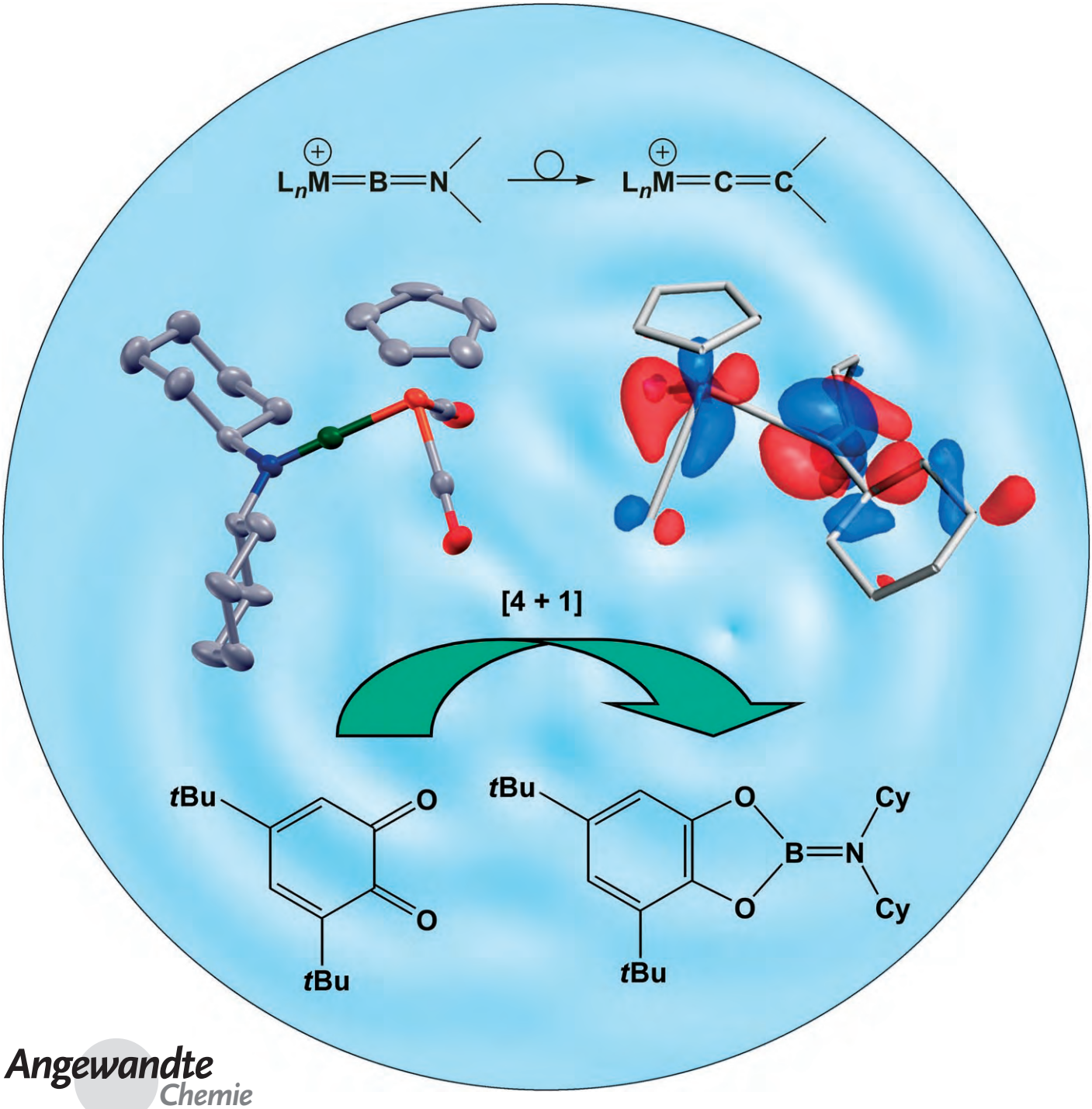

InterScience

© 2006 Wiley-VCH Verlag GmbH & Co. KGaA, Weinheim

The predominant routes to transition-metal borylene complexes $[(L_nM)_mBX]$ ($m = 1, 2, 3$), namely salt elimination and photolytic transfer chemistries, have been instrumental in accessing two-coordinate systems containing M–B double bonds.[1] Such compounds have excited interest not only from a desire to relate fundamental issues of geometric and electronic structure to patterns of chemical reactivity, but also as a result of obvious parallels in the classical organometallic chemistry of carbonyl, carbene, and vinylidene ligands.[2] Utilizing these synthetic approaches, four structurally authenticated species of the type $[L_nM{=}BX]$ have been reported to date.[3,4] Mirroring chemistry reported for unsaturated Group 14 ligand systems,[5] we have sought to exploit halide abstraction chemistry to access *cationic* diyl systems, $[L_nM(EX)]^+$ (E = Group 13 element), not only to broaden the range of available synthetic routes, but also to assess the influence of overall charge on the chemistry of these complexes.[6–8] This strategy has, to date, given access to the only structurally characterized example of a cationic two-coordinate borylene complex, namely $[Cp^*Fe(CO)_2(BC_6H_2Me_3\text{-}2,4,6)]^+[BAr^F{}_4]^-$ ($Ar^F = C_6H_3(CF_3)_2\text{-}3,5$).[6]

Given the widespread interest in transition-metal carbene and vinylidene species, for example in metathesis chemistry, and the numerous examples of systems of the type $[(\eta^5\text{-}C_5R_5)ML_n(CCR_2)]^+$,[9] we have sought to extend the halide abstraction methodology to the synthesis of the isoelectronic BN complexes $[(\eta^5\text{-}C_5R_5)ML_n(BNR_2)]^+$. Such cationic terminal aminoborylenes would not only offer insight into the CC/BN analogy, but also by comparison with neutral amino borylene and cationic aryl borylene compounds[3a,b,d,6] allow for systematic investigation of structure/bonding and reactivity on the basis of net charge and borylene substituent. As a result of these efforts, we report herein the synthesis of $[CpFe(CO)_2(BNCy_2)]^+[BAr^F{}_4]^-$ and an investigation of its structural and reaction chemistry.

The reaction of $[CpFe(CO)_2\{B(NCy_2)Cl\}]$ (**1**) with $Na[BAr^F{}_4]$ proceeds as outlined in Scheme 1 and leads to the isolation of $[CpFe(CO)_2(BNCy_2)]^+[BAr^F{}_4]^-$ (**2**) in 80% yield. In contrast to the analogous (diisopropylamino)borylene complex, which is an oil,[8] **2** is a crystalline solid which was characterized by standard spectroscopic and analytical techniques, and by X-ray diffraction. Revealingly, ^{11}B NMR and IR data for **2** and $[CpFe(CO)_2(BNiPr_2)]^+[BAr^F{}_4]^-$ are essentially identical ($\delta = 93.1$ and 93.5 ppm; $\tilde{\nu}(CO) = 2071$, 2028 and 2070, 2028 cm^{-1}, respectively) and fall within the ranges expected for a cationic aminoborylene complex.[8] In the case of $[CpFe(CO)_2(BNiPr_2)]^+[BAr^F{}_4]^-$ the presence of an Fe=B bond was inferred from spectroscopic, computational, and reactivity data;[8] in the case of **2** this double bond can be demonstrated explicitly by X-ray crystallography. Compound **2** therefore represents only the second structurally characterized cationic terminal borylene complex,[6] and the first such system featuring a heteroatom donor at boron. As such, it provides a unique basis for discussion of structure and bonding, both as a function of net charge (compare with the neutral analogues $[L_nM(BNR_2)]$)[3a,b,d] and borylene substituent (compare with $[Cp^*Fe(CO)_2(BC_6H_2Me_3\text{-}2,4,6)]^+$).[6] As a further aid to understanding the bonding situation in **2** we have also synthesized and structurally characterized the 4-picoline adduct $[CpFe(CO)_2\{B(NCy_2)(4\text{-pic})\}][BAr^F{}_4]^-$ (**4**) (see the Supporting Information for details), thus allowing for the first time direct structural comparison of otherwise identical two-coordinate and base-stabilized borylenes.

The structure of **2** (Figure 1) features the linear M-B-X framework common to other base-free terminal borylene complexes (∢Fe-B-N 178.8(5)°),[3,6] with that for **4** (131.6(3)°) showing the expected narrowing upon base coordination.[10] The M–B bond length for **2** (1.859(6) Å) is much shorter than those found for *neutral* aminoborylene complexes (for example, 1.959(6) and 1.996(6) Å for $[CpV(CO)_3\{BN(SiMe_3)_2\}]$ and $[(OC)_5Cr\{BN(SiMe_3)_2\}]$, respectively),[3b,d] with this trend reflecting the expected changes in bond length as a function of metal fragment (compare the mean M–CO bond lengths of 1.816, 1.91, and 1.915 Å for $[CpFe(CO)_3]^+$, $[CpV(CO)_4]$ and $[Cr(CO)_6]$, respectively).[11] The Fe–B bond length in **2** is, however, significantly longer than that found in $[Cp^*Fe(CO)_2(BC_6H_2Me_3\text{-}2,4,6)]^+[BAr^F{}_4]^-$ (1.788 Å (mean)),[6] despite the reduced bulk of the cyclopentadienyl ligand. At a simplistic level this trend can be ascribed to the reduced π acidity of the boron center in the presence of the π donor amino substituent.[3b,c] Consistent with this, the B–N bond length in **2** is indicative of significant multiple-bond character (1.324(6) vs. 1.332 Å (mean) for $[R(R')N{=}B{=}NR(R')]^+$; R = *t*Bu, R′ = CH_2Ph).[12] Moreover,

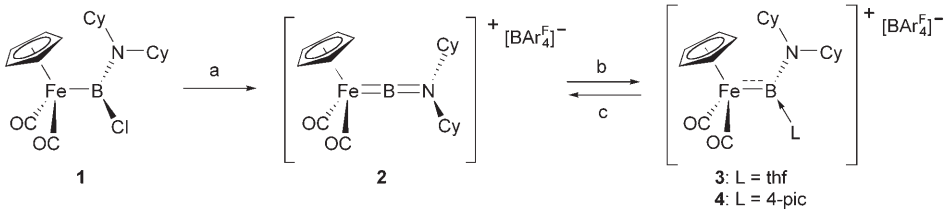

Scheme 1. Synthesis and simple Lewis acid/base chemistry of **2**. Reaction conditions: a) $Na[BAr^F{}_4]$ (1.1 equiv), CH_2Cl_2, −78 to 20 °C, 6 h, 80%; b) Lewis base L (1000 equiv for **3**, 5 equiv for **4**), CH_2Cl_2, 20 °C, 1 h, 52% yield of isolated product (for **4**); c) for **3**: continuous vacuum (ca. 0.1 Torr for 60 min), quantitative by ^{11}B NMR. Cy = cyclohexyl; 4-pic = 4-picoline.

[*] Dr. S. Aldridge, Prof. C. Jones, Dr. T. Gans-Eichler, Dr. A. Stasch, Dr. D. L. Kays (née Coombs), N. D. Coombs, Dr. D. J. Willock
Centre for Fundamental and Applied Main Group Chemistry
School of Chemistry
Cardiff University
Main Building
Park Place, Cardiff, CF10 3AT (UK)
Fax: (+44) 2920-874-030
E-mail: AldridgeS@cardiff.ac.uk
jonesca6@cardiff.ac.uk

[**] We thank the EPSRC for funding and for access to the National Mass Spectrometry facility.

Supporting information for this article is available on the WWW under http://www.angewandte.org or from the author.

 © 2006 Wiley-VCH Verlag GmbH & Co. KGaA, Weinheim

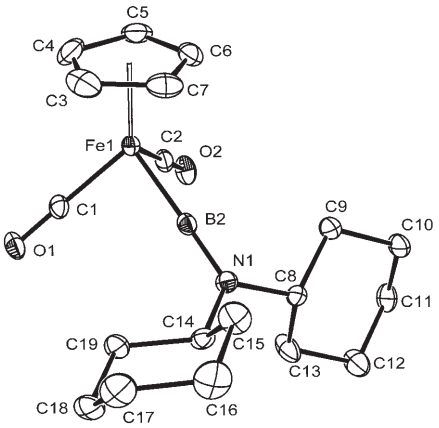

Figure 1. Structure of the cationic component of **2**·CH_2Cl_2 (ellipsoids at 50% probability; H atoms, anion, and CH_2Cl_2 molecule omitted for clarity). Relevant bond lengths [Å] and angles [°]: Fe1-B2 1.859(6), Fe1-C1 1.786(5), Fe1-Cp(centroid) 1.722(6), B2-N1 1.324(7); Fe1-B2-N1 178.8(5), B2-N1-C8 122.0(4), B2-N1-C14 121.6(4), C8-N1-C14 116.4(4); angle between least-squares planes defined by Cp(centroid)-Fe1-B2-N1 and B2-N1-C8-C14 83.3.

the shortening of both Fe–B and B–N bonds in **2** in comparison with three-coordinate systems **1** (Fe–B 2.053(3), B–N 1.396(4) Å) and **4** (Fe–B 2.049(4), B–N 1.391(5) Å) is also consistent with increased Fe–B and B–N π bonding. Indeed, the shortening of the Fe–B bond (9.4% with respect to **1**) is similar to that observed between $[Cp^*Fe(CO)_2(BC_6H_2Me_3\text{-}2,4,6)]^+$ and $[Cp^*Fe(CO)_2\{B(C_6H_2Me_3\text{-}2,4,6)Cl\}]$ (9.7%),[6] and comparable to that between archetypal alkyl and carbene systems (for example, 12.6% between $[CpFe(CO)_2(CCl_2)]^+$ and $[CpFe(CO)_2(n\text{-}C_5H_{11})]$),[13] implying a geometric basis for the presence of Fe=E bonds (E = B or C) in all three cases.

The validity of an Fe=B=N vinylidene-like bonding model for **2** was further examined by using DFT methods.[6c] Agreement between calculated (BLYP/TZP) and crystallographically determined geometric parameters is very good (see the Supporting Information), and relevant molecular orbitals are depicted in Figure 2. In addition to the HOMO−2 (−9.64 eV), which shows Fe–B π-bonding character utilizing the Fe $3d_{yz}$ and B $2p_y$ orbitals (with the LUMO + 2 (−5.25 eV) having corresponding π* character), two orbitals can be identified (the HOMO−1 (−9.48 eV) and the HOMO (−9.18 eV)) which have B–N π character. The HOMO features an isolated B–N π component which has an antibonding phase relationship with the $3d_{xz}$ orbital of the iron center. The HOMO−1, by contrast, features a component which is delocalized along the entire Fe-B-N framework in the xz plane, thus providing additional Fe–B π overlap perpendicular to the HOMO−2 by utilizing the $3d_{xz}$ orbital. Partitioning of the bonding density for the Fe–B linkage in **2** yields a σ:π breakdown of 70:29,[6c] thus indicating a smaller π component than for the "isolated" Fe=B system in $[Cp^*Fe(CO)_2(BC_6H_2Me_3\text{-}2,4,6)]^+$ (38%), but a similar breakdown for the Fe–C linkage in the isoelectronic vinylidene complex $[CpFe(CO)_2(CCiPr_2)]^+$ (67:33).[*] Thus, in addition to geometric arguments, quantum chemical data argue in favor of a bonding situation analogous to classical cationic Group 8 vinylidene complexes $[CpML_2(=C=CR_2)]^+$.

Certain patterns of reactivity that were elucidated for **2** are also reminiscent of classical Group 8 vinylidenes, namely, addition chemistry at the α position towards C, N, and O nucleophiles.[9] Thus, 4-picoline readily coordinates at the boron center, and the weaker donor tetrahydrofuran can be shown by NMR measurements to coordinate *reversibly*. Such reactivity is consistent with significantly greater electrophilicity than typically displayed by *neutral* aminoborylenes.[14] Similar chemistry can also be exploited towards the formation of B–C bonds. Thus, reaction of **2** with triphenylphosphonium cyclopentadienide leads to the formation of $[CpFe(CO)_2\{B(NCy_2)(C_5H_4PPh_3)\}]^+[BAr^F{}_4]^-$ (**5**; Scheme 2 and Figure 3), which features a rare example of structurally authenticated σ coordination of the ylid cyclopentadienide ring,[15] in this case through the sterically less-encumbered C3 position. The crystallographically characterized product is also consistent with an additional *net* 1,3-hydrogen migration, such that C3 is trigonal planar (sum of angles: 359.0°) and there is a methylene group in the 5-position. Spectroscopic data for single crystals redissolved in CD_2Cl_2 imply the presence of a second species, which is thought to be an alternative isomer featuring the methylene group in the 4-position. The existence in solution of disubstituted cyclopentadienes of the type

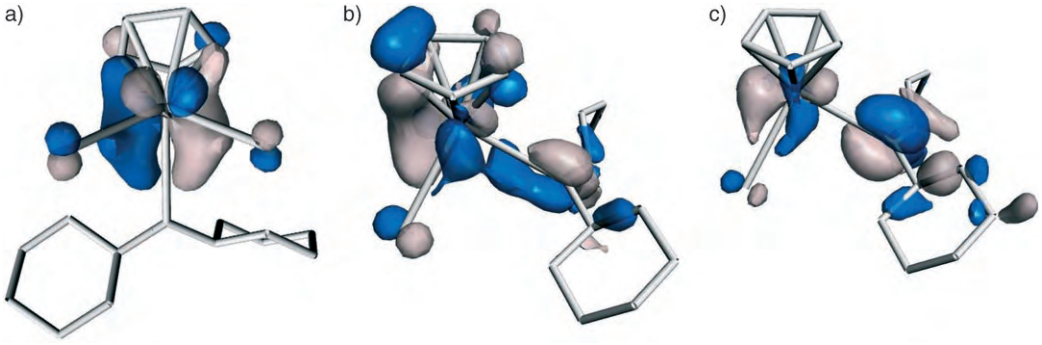

Figure 2. HOMO−2 (a), HOMO−1 (b), and HOMO (c) calculated by DFT (BLYP/TZP) for the cation $[CpFe(CO)_2(BNCy_2)]^+$ showing, respectively, Fe–B π-, Fe-B-N π-, and B–N π-bonding character. The *z*-axis is taken to be aligned with the Fe–B bond.

[*] *i*Pr groups were employed for the vinylidene complex $[CpFe(CO)_2(CCiPr_2)]^+$, as the corresponding Cy system failed to adequately meet all convergence criteria. For comparison, the σ:π breakdown for the strictly isoelectronic bis(isopropylamino)borylene complex $[CpFe(CO)_2(BNiPr_2)]^+$ is calculated to be 70:30.

 © 2006 Wiley-VCH Verlag GmbH & Co. KGaA, Weinheim

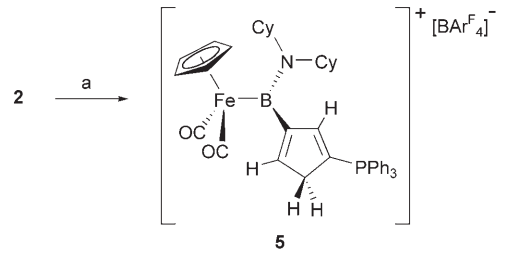

Scheme 2. Reaction of **2** with triphenylphosphonium cyclopentadienide, $Ph_3PC_5H_4$. Reaction conditions: a) $Ph_3PC_5H_4$ (1.0 equiv), CH_2Cl_2, 20 °C, 1 h, 54 %.

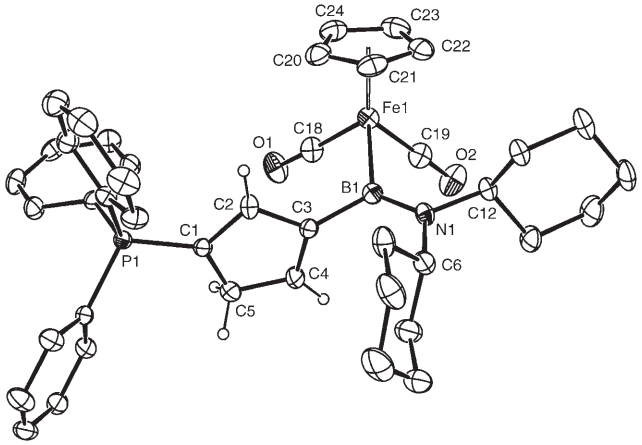

Figure 3. Structure of the cationic component of **5** (ellipsoids at 50 % probability; H atoms, except those attached to C2, C4, and C5, and anion omitted for clarity). Relevant bond lengths [Å] and angles [°]: Fe1-B1 2.102(5), Fe1-C18 1.748(5), Fe1-Cp(centroid) 1.733(5), B1-N1 1.405(6), B1-C3 1.583(6), C1-C2 1.411(6), C2-C3 1.487(6), C3-C4 1.354(6), C4-C5 1.473(6), C1-P1 1.756(4); Fe1-B1-N1 126.7(3), Fe1-B1-C3 111.3(3), N1-B1-C3 122.0(4), B1-C3-C2 127.8(4), B1-C3-C4 125.0(4), C2-C3-C4 106.2(4).

1,3-$(Ph_3P)(X)C_5H_4$ as a mixture of isomers has previously been demonstrated.[16]

Divergent patterns of reactivity for **2** compared to other borylene systems can also be illustrated by its reaction with 3,5-di-*tert*-butyl-*ortho*-benzoquinone (Scheme 3). Although trapping of subvalent Group 14 compounds by quinone reagents has previously been demonstrated,[17,18] examples of borylene cycloaddition reactions are extremely rare.[19] Thus, the formation of **6** represents, to our knowledge, the first example of a net [4+1] cycloaddition reaction for a borylene complex.

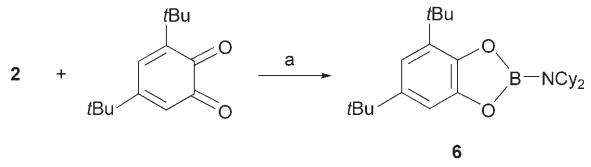

Scheme 3. [4+1] Cycloaddition chemistry of **2** with 3,5-di-*tert*-butyl-*ortho*-benzoquinone. Reaction conditions: a) 3,5-di-*tert*-butyl-*ortho*-benzoquinone (1.0 equiv), CH_2Cl_2, 20 °C, 1 h, 81 % yield of isolated product.

In conclusion, we have reported the synthesis and structural characterization of the cationic terminal borylene complex $[CpFe(CO)_2(BNCy_2)]^+[BAr^F{}_4]^-$ (**2**), the first such system containing a π-donor substituent at boron. In addition, structural characterization of the picoline adduct $[CpFe(CO)_2\{B(NCy_2)(4\text{-pic})\}]^+[BAr^F{}_4]^-$ (**4**) allows, for the first time, comparative analysis of structural parameters for otherwise identical base-stabilized and base-free complexes. DFT and crystallographic studies are consistent with delocalized π bonding along the linear Fe-B-N framework in **2**, which incorporates significant Fe–B and B–N multiple-bond character. Compound **2** therefore represents a BN analogue of classical Group 8 cationic vinylidene systems $[(\eta^5\text{-}C_5R_5)ML_2(=C=CR_2)]^+$. In addition to reactivity characteristic of such vinylidene compounds, for example, nucleophilic addition at the α center (boron), the reactivity of **2** is also marked by the first reported example of borylene [4+1] cycloaddition. Further studies aimed at exploration of trends in structure and reactivity (including cycloaddition) for borylene systems as a function of the metal and ligand set will be reported in due course.

Experimental Section

Included here are the preparative and characterization data for compound **2**; data for **1**, **4**, **5**, and **6** are included in the Supporting Information.

2: A mixture of **1** (0.410 g, 1.02 mmol) and $Na[BAr^F{}_4]$ (1.1 equivalents) in CH_2Cl_2 (30 mL) was warmed from −78 to 20 °C. After stirring for a further 6 h the reaction was judged to be complete by ^{11}B NMR spectroscopy. Filtration of the mixture, concentration of the filtrate to about 5 mL, layering with hexanes (ca. 10 mL), and storage at −30 °C led to the formation of **2** as colorless crystals suitable for X-ray diffraction. Yield of isolated product: 1.00 g, 80 %; ^1H NMR (400 MHz, CD_2Cl_2): $\delta = 1.17$–2.13 (m, 20H, CH_2 of Cy), 2.87 (m, 2H, CH of Cy), 5.24 (s, 5H, Cp), 7.49 (s, 4H, *para*-CH of $BAr^F{}_4^-$), 7.64 ppm (s, 8H, *ortho*-CH of $BAr^F{}_4^-$); ^{13}C NMR (76 MHz, CD_2Cl_2): $\delta = 24.1$, 25.0, 35.5 (CH_2 of Cy), 58.6 (CH of Cy), 86.3 (Cp), 116.7 (*para*-CH of $BAr^F{}_4^-$), 123.8 (q, $^1J_{CF} = 272$ Hz, CF_3 of $BAr^F{}_4^-$), 128.0 (q, $^2J_{CF} = 31$ Hz, *meta*-C of $BAr^F{}_4^-$), 134.0 (*ortho*-CH of $BAr^F{}_4^-$), 161.0 (q, $^1J_{CB} = 50$ Hz, *ipso*-C of $BAr^F{}_4^-$), 204.8 ppm (CO); ^{11}B NMR (96 MHz, CD_2Cl_2): $\delta = -7.6$ ($BAr^F{}_4^-$), 93.1 ppm (br, frequency width at half maximum ca. 850 Hz, borylene); ^{19}F NMR (283 MHz, CD_2Cl_2): $\delta = -62.7$ ppm (CF_3); IR (CD_2Cl_2): $\tilde{\nu}$(CO) = 2071, 2028 cm^{-1}. Elemental analysis (%) calcd for **2**·CH_2Cl_2 ($C_{52}H_{41}B_2Cl_2F_{24}FeNO_2$): C 47.45, H 3.14, N 1.06; found: C 47.59, H 3.13, N 1.08; m.p. 108 °C.

Crystallographic data for **2**·CH_2Cl_2: $C_{52}H_{41}B_2Cl_2F_{24}FeNO_2$, $M_r = 1316.2$, triclinic, $P\bar{1}$, $a = 12.917(3)$, $b = 13.749(3)$, $c = 17.471(4)$ Å, $\alpha = 88.53(3)$, $\beta = 79.89(3)$, $\gamma = 74.41(3)$°, $V = 2941.5(10)$ Å^3, $Z = 2$, $\rho_{calcd} = 1.486$ Mg m^{-3}, $T = 150(2)$ K, $\lambda = 0.71073$ Å. 19823 reflections collected, 10666 independent (R(int) = 0.0313), which were used in all calculations. $R_1 = 0.0883$, $wR_2 = 0.2492$ for observed unique reflections ($F^2 > 2\sigma(F^2)$) and $R_1 = 0.1096$, $wR_2 = 0.2668$ for all unique reflections. Max. and min. residual electron densities 1.44 and −1.25 e Å^{-3} (both near Cl2). CCDC 609044 contains the supplementary crystallographic data for this paper. These data can be obtained free of charge via www.ccdc.cam.ac.uk/conts/retrieving.html.

Received: May 31, 2006
Published online: July 25, 2006

 © 2006 Wiley-VCH Verlag GmbH & Co. KGaA, Weinheim

Keywords: boron · borylene ligands · cycloaddition · density functional calculations · iron

[1] For recent reviews of borylene chemistry, see: a) H. Braunschweig, M. Colling, *Eur. J. Inorg. Chem.* **2003**, 393 – 403; b) S. Aldridge, D. L. Coombs, *Coord. Chem. Rev.* **2004**, *248*, 535 – 559; c) H. Braunschweig, *Adv. Organomet. Chem.* **2004**, *51*, 163 – 192; d) H. Braunschweig, D. Rais, *Heteroat. Chem.* **2005**, *16*, 566 – 571; e) H. Braunschweig, C. Kollann, D. Rais, *Angew. Chem.*, DOI: 10.1002/ange.200600506; *Angew. Chem. Int. Ed.*, DOI: 10.1002/anie.200600506.

[2] See, for example: W. A. Nugent, J. M. Mayer, *Metal Ligand Multiple Bonds*, Wiley Interscience, New York, **1988**.

[3] a) H. Braunschweig, C. Kollann, U. Englert, *Angew. Chem.* **1998**, *110*, 3355 – 3357; *Angew. Chem. Int. Ed.* **1998**, *37*, 3179 – 3180; ; b) H. Braunschweig, M. Colling, C. Kollann, H. G. Stammler, B. Neumann, *Angew. Chem.* **2001**, *113*, 2359 – 2361; *Angew. Chem. Int. Ed.* **2001**, *40*, 2298 – 2300; ; c) H. Braunschweig, M. Colling, C. Kollann, K. Merz, K. Radacki, *Angew. Chem.* **2001**, *113*, 4327 – 4329; *Angew. Chem. Int. Ed.* **2001**, *40*, 4198 – 4200; ; d) H. Braunschweig, M. Colling, C. Hu, K. Radacki, *Angew. Chem.* **2003**, *115*, 215 – 218; *Angew. Chem. Int. Ed.* **2003**, *42*, 205 – 208.

[4] For examples of charge-neutral terminal borylene complexes featuring coordination numbers at boron of greater than two, see: a) A. H. Cowley, V. Lomeli, A. Voight, *J. Am. Chem. Soc.* **1998**, *120*, 6401 – 6402; b) G. J. Irvine, C. E. F. Rickard, W. R. Roper, A. Williamson, L. J. Wright, *Angew. Chem.* **2000**, *112*, 978 – 980; *Angew. Chem. Int. Ed.* **2000**, *39*, 948 – 950; ; c) C. E. F. Rickard, W. R. Roper, A. Williamson, L. J. Wright, *Organometallics* **2002**, *21*, 4862 – 4872; d) H. Braunschweig, D. Rais, K. Uttinger, *Angew. Chem.* **2005**, *117*, 3829 – 3832; *Angew. Chem. Int. Ed.* **2005**, *44*, 3763 – 3766.

[5] See, for example: G. P. Mitchell, T. D. Tilley, *J. Am. Chem. Soc.* **1997**, *119*, 11236 – 11243.

[6] a) D. L. Coombs, S. Aldridge, C. Jones, D. J. Willock, *J. Am. Chem. Soc.* **2003**, *125*, 6356 – 6357; b) D. L. Coombs, S. Aldridge, A. Rossin, C. Jones, D. J. Willock, *Organometallics* **2004**, *23*, 2911 – 2926; c) S. Aldridge, A. Rossin, D. L. Coombs, D. J. Willock, *Dalton Trans.* **2004**, 2649 – 2654.

[7] a) N. R. Bunn, S. Aldridge, D. L. Coombs, A. Rossin, D. J. Willock, C. Jones, L.-L. Ooi, *Chem. Commun.* **2004**, 1732 – 1733; b) N. R. Bunn, S. Aldridge, D. L. Kays, N. D. Coombs, A. Rossin, D. J. Willock, C. Jones, L.-L. Ooi, *Organometallics* **2005**, *24*, 5891 – 5900.

[8] D. L. Kays, J. K. Day, L.-L. Ooi, S. Aldridge, *Angew. Chem.* **2005**, *117*, 7623 – 7626; *Angew. Chem. Int. Ed.* **2005**, *44*, 7457 – 7460.

[9] For reviews on transition-metal vinylidene chemistry, see, for example: a) M. I. Bruce, *Chem. Rev.* **1991**, *91*, 197 – 257; b) C. Bruneau, P. H. Dixneuf, *Acc. Chem. Res.* **1999**, *32*, 311 – 323; c) H. Katayama, F. Ozawa, *Coord. Chem. Rev.* **2004**, *248*, 1703 – 1715; d) H. Werner, *Coord. Chem. Rev.* **2004**, *248*, 1693 – 1702.

[10] For related examples of cationic base-stabilized terminal borylene complexes, see: a) H. Braunschweig, K. Radacki, D. Rais, D. Scheschkewitz, *Angew. Chem.* **2005**, *117*, 5796 – 5799; *Angew. Chem. Int. Ed.* **2005**, *44*, 5651 – 5654; b) D. L. Kays, J. K. Day, S. Aldridge, R. W. Harrington, W. Clegg, *Angew. Chem.* **2006**, *118*, 3593 – 3596; *Angew. Chem. Int. Ed.* **2006**, *45*, 3513 – 3516.

[11] a) J. B. Wilford, A. Whitla, H. M. Powell, *J. Organomet. Chem.* **1967**, *8*, 491 – 494; b) M. E. Gress, R. A. Jacobson, *Inorg. Chem.* **1973**, *12*, 1746 – 1749; c) B. Rees, A. Mitschler, *J. Am. Chem. Soc.* **1976**, *98*, 7918 – 7924.

[12] P. Kolle, H Nöth, *Chem. Ber.* **1986**, *119*, 313 – 324.

[13] a) A. M. Crespi, D. F. Shriver, *Organometallics* **1985**, *4*, 1830 – 1835; b) R. O. Hill, C. F. Marais, J. R. Moss, K. J. Naidoo, *J. Organomet. Chem.* **1999**, *587*, 28 – 37.

[14] H. Braunschweig, personal communication.

[15] a) N. C. Baenziger, R. M. Flynn, D. C. Swenson, N. L. Holy, *Acta Crystallogr. Sect. B* **1978**, *34*, 2300 – 2301; b) R. M. G. Roberts, *Tetrahedron* **1980**, *36*, 3295 – 3300; c) A. J. Deeming, N. I. Powell, C. Whittaker, *J. Chem. Soc. Dalton Trans.* **1991**, 1875 – 1880.

[16] F. F. Pérez-Pla, S. Housseini, J. Palou, . C. D. Hall, *Int. J. Chem. Kinet.* **1997**, *29*, 561 – 574.

[17] See, for example: C. Laurent, S. Mazières, H. Lavayssière, P. Mazerolles, G. Doussse, *J. Organomet. Chem.* **1993**, *452*, 41 – 45.

[18] For an example of related reactivity of a gallium(I) diyl compound towards an α,β-unsaturated reagent, see: N. J. Hardman, R. J. Wright, A. D. Phillips, P. P. Power, *J. Am. Chem. Soc.* **2003**, *125*, 2667 – 2679.

[19] H. Braunschweig, T. Herbst, D. Rais, F. Seeler, *Angew. Chem.* **2005**, *117*, 7627 – 7629; *Angew. Chem. Int. Ed.* **2005**, *44*, 7461 – 7463.

 © 2006 Wiley-VCH Verlag GmbH & Co. KGaA, Weinheim

Helical Structures

DOI: 10.1002/anie.200602464

Helicity Inversion in Lanthanide(III) Complexes with Chiral Nonaaza Macrocyclic Ligands**

*Janusz Gregoliński and Jerzy Lisowski**

Controlling the chirality of metal complexes or supramolecular assemblies continues to be a challenging and fascinating area of research.[1] The chirality of these systems may be related, for example, to the spatial disposition of chelating ligands around a metal ion,[1a] to the formation of double or triple helices,[2] to the helical twist of a macrocyclic ligand,[3] or to the rotation of the side arms of a macrocyclic ligand.[4] In favorable cases, these chiral compounds can be separated into enantiopure forms.[2c,5] Alternatively, the enantiopure supramolecular assemblies and metal complexes can be obtained by diastereoselective synthesis from nonracemic chiral organic building blocks, which may determine the chirality of the assembly or complex (for example, the handedness of a helical structure). Generally, this strategy is successful when one of the possible diastereoisomers is thermodynamically favored.[6] In the case of DNA, however, diastereoisomeric structures of opposite helicity can be obtained from sugar

[*] J. Gregoliński, Prof. J. Lisowski
Department of Chemistry
University of Wrocław
F. Joliot-Curie 14, 50 383 Wrocław (Poland)
Fax: (+48) 713-282-348
E-mail: jurekl@wchuwr.chem.uni.wroc.pl

[**] This work was supported by MNiSW grant 1 T09A 143 30. We thank Prof. T. Lis for help with the determination of the X-ray crystal structures.

Supporting information for this article is available on the WWW under http://www.angewandte.org or from the author.

WILEY InterScience DISCOVER SOMETHING GREAT
© 2006 Wiley-VCH Verlag GmbH & Co. KGaA, Weinheim

building blocks of the same chirality. Furthermore, the normal right-handed helix of the B form of DNA can be inverted (for example, by increasing the salt concentration) to the left-handed helix of the Z form.[7] Similar controlled helicity inversion is very rare for artificial systems.[8] Herein, we report a unique example of helicity inversion between the kinetic and thermodynamic complexation products of a macrocyclic ligand, as well as the isolation of both products in enantiopure form. We describe diastereoisomeric lanthanide(III) (Ln^{III}) complexes with the nonaaza macrocycle L (Scheme 1), which have the same configuration at all stereogenic carbon atoms, yet opposite helicity (Scheme 2).

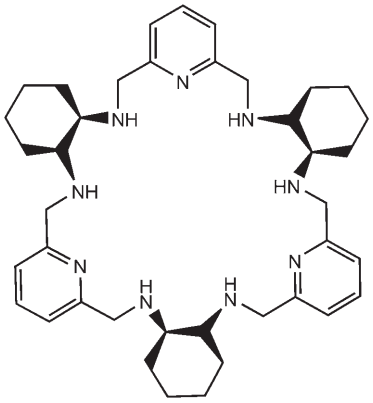

Scheme 1. The L_{RRRRRR} macrocycle.

Depending on the reaction conditions, the condensation of 2,6-diformylpyridine and *trans*-1,2-diaminocyclohexane leads to various 2+2, 3+3, and 4+4 macrocyclic Schiff bases, which can be easily converted into the corresponding macrocyclic amines.[9] While the 2+2 macrocycles form complexes with transition-metal and Ln^{III} ions,[3] the coordination properties of the chiral 3+3 macrocyclic amine L have not yet been explored, with the exception of the electrospray ionization mass spectrometry (ESI MS) characterization of a dinuclear $[Cd_2L]^{6+}$ complex generated in solution.[9b] The chiral ligand L can be obtained in the enantiopure forms L_{RRRRRR} and L_{SSSSSS}, which correspond to all-*R* or all-*S* configurations of the diaminocyclohexane carbon atoms, respectively.[9b,c]

The addition of Ln^{III} nitrate or chloride salts to solutions of the free L_{RRRRRR} macrocycle results in smooth complex formation, as indicated by ^{1}H NMR spectroscopy. Depending on the metal/ligand ratio and the reaction conditions, the complexes formed can be isolated as enantiopure nitrate salts ((*M*)-$[EuL_{RRRRRR}](NO_3)_3\cdot CHCl_3\cdot 2H_2O$, (*M*)-$[TbL_{RRRRRR}](NO_3)_3$sdot;$0.5\,CHCl_3\cdot 1.5\,H_2O$, and (*M*)-$[YbL_{RRRRRR}](NO_3)_3\cdot CHCl_3\cdot H_2O$) or as derivatives containing an additional complex $[Ln(NO_3)_5]^{2-}$ counterion ((*M*)-$[EuL_{RRRRRR}]_2[Eu(NO_3)_5](NO_3)_4\cdot 2H_2O$ and (*M*)-$[YbL_{RRRRRR}]_2[Yb(NO_3)_5](NO_3)_4\cdot 4H_2O$; see Supporting Information for experimental details and characterization of the compounds). For a given Ln^{III} ion, both types of derivatives, as well as the species generated in solution, give rise to very similar NMR spectra, indicating that, in each case, the same type of $[LnL]^{3+}$ complex is present. The presence of this type of cationic complex is also supported by the ESI mass spectra (see Supporting Information). The ^{1}H NMR spectra of the $[LnL]^{3+}$ complexes consist of 29 lines, most of which are well resolved for the paramagnetic Eu^{III}, Tb^{III}, and Yb^{III} derivatives (see Supporting Information). In the case of the $[EuL]^{3+}$ complex, the combination of correlation spectroscopy (COSY), total correlation spectroscopy (TOCSY), nuclear Overhauser effect spectroscopy (NOESY), rotational Overhauser effect spectroscopy (ROESY), and heteronuclear multiple quantum correlation (HMQC) data allowed a complete assignment of all resonances (see Supporting Information). The TOCSY spectrum of (*M*)-$[EuL_{RRRRRR}](NO_3)_3\cdot CHCl_3\cdot 2H_2O$ clearly indicates that the only symmetry element of the complex is a C_2 axis that passes through one of the pyridine rings and bisects the opposite cyclohexane ring.

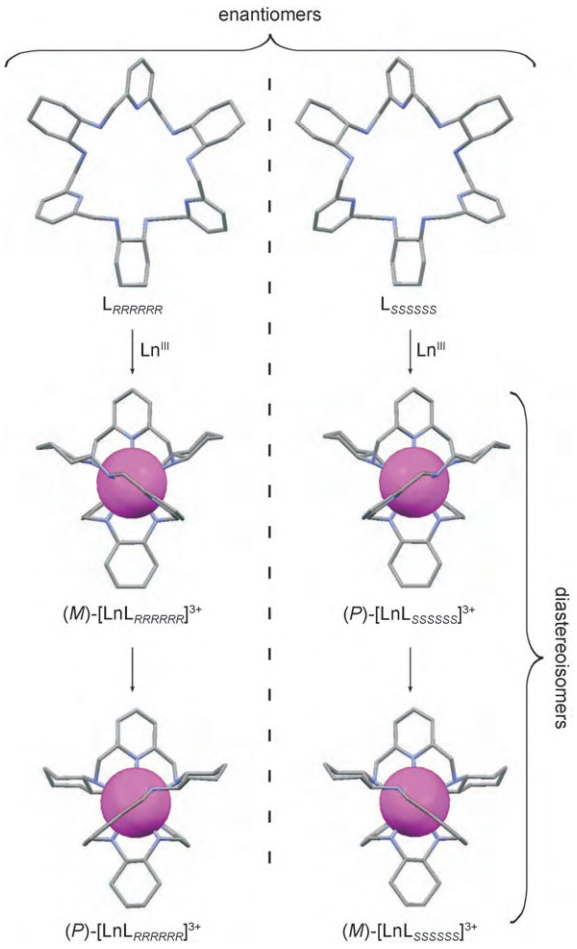

Scheme 2. Preparation and transformation of the $[LnL]^{3+}$ diastereoisomers. The conformations of the free ligand L (based on the molecular structure of the protonated form $H_6L_{RRRRRR}{}^{6+}$[9b]) and the complex cations $[LnL]^{3+}$ (based on the molecular structures of (*M*)-$[YbL_{RRRRRR}]^{3+}$ and (*P*)-$[YbL_{RRRRRR}]^{3+}$) are shown. Yb pink, C gray, N blue; H omitted.

The X-ray crystal structure of (*M*)-$[EuL_{RRRRRR}]_2[Eu(NO_3)_5](NO_3)_4\cdot 2H_2O$ reveals that the nonaaza macrocyclic $[EuL_{RRRRRR}]^{3+}$ complex adopts a new type of geometry (Figure 1).[10] Because the cavity radius of the "open" form of the ligand (2.55 Å)[9b] is far too large to accommodate a

 © 2006 Wiley-VCH Verlag GmbH & Co. KGaA, Weinheim

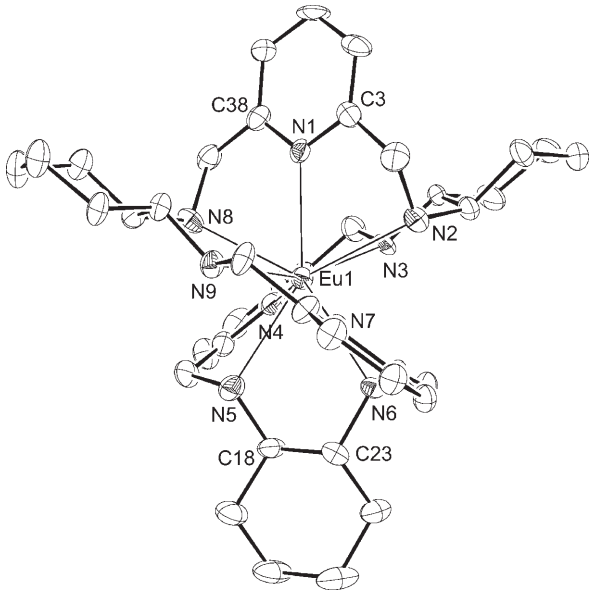

Figure 1. Molecular structure of the (*M*)-$[EuL_{RRRRRR}]^{3+}$ complex cation; H omitted.

single Eu^{III} ion, the ligand wraps around the cation in a helical fashion, leading to the generation of a new element of chirality: a left-handed *M* double helix (Figure 1). The helical twist of the macrocycle is determined by the mutual orientation of the pyridine and cyclohexane rings positioned on the (noncrystallographic) C_2 axis. For the (*M*)-$[EuL_{RRRRRR}]^{3+}$ molecule shown in Figure 1, the helical twist, which corresponds to the improper torsion angle C3-C38-C18-C23, is −186.8°; for the second independent molecule in the crystal structure, the twist is −185.5°. These values are among the largest reported for macrocyclic complexes and are much larger than those observed for Ln^{III} complexes with related 2+2 macrocycles.[3] In accord with the spin systems observed in the TOCSY spectrum, the pyridine and cyclohexane rings positioned on the (noncrystallographic) C_2 axis are different from the remaining pairs of pyridine and cyclohexane rings, which are each related by (noncrystallographic) C_2 symmetry. All nine nitrogen atoms of the macrocycle [27]trieneN$_9$ core coordinate to the metal ion, which is the first example of this type of coordination for a nonaaza macrocycle. The donor atoms of L satisfy the coordination sphere of the Eu^{III} ion; unlike most of the known macrocyclic Ln^{III} complexes, no other ligand, such as a counteranion or solvent molecule, is coordinated to the metal ion. The helical twist of the macrocycle imposes the *S*,*S* chirality at the nitrogen atoms attached to the unique axial cyclohexane ring and the *R*,*S* chirality at the nitrogen atoms attached to the two nearly equivalent cyclohexane rings. The structure of the (*M*)-$[EuL_{RRRRRR}]^{3+}$ complex is completely different from that of the Eu^{III} complex of an analogous 3+3 macrocycle derived from 2,6-diformylphenol.[11].

The X-ray crystal structure of (*M*)-$[YbL_{RRRRRR}]$-$(NO_3)_3 \cdot 2.33\,CH_3CN \cdot 2\,H_2O$ reveals the presence of a similar complex cation (Figure 2; Scheme 2).[12] The helical twists of the macrocycles in the two independent (*M*)-$[YbL_{RRRRRR}]^{3+}$

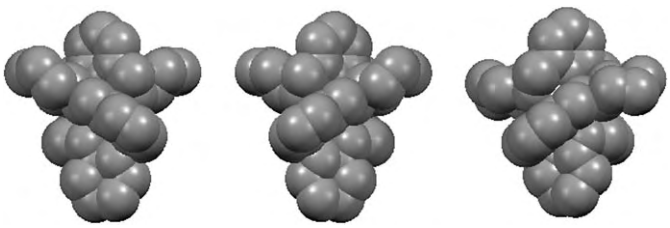

Figure 2. Molecular structures of the (*M*)-$[YbL_{RRRRRR}]^{3+}$ (left) and (*P*)-$[YbL_{RRRRRR}]^{3+}$ (right) complex cations. The mirror image of (*M*)-$[YbL_{RRRRRR}]^{3+}$, that is, (*P*)-$[YbL_{SSSSSS}]^{3+}$ (middle) is presented for comparison.

molecules are −192.5° and −193.8°, which are even greater than those of the (*M*)-$[EuL_{RRRRRR}]^{3+}$ complex. This difference reflects the tighter wrapping of the macrocycle around the smaller Yb^{III} ion.

The ^{1}H NMR spectra of the (*M*)-$[LnL_{RRRRRR}]^{3+}$ complexes reflect their relatively high stability in solution. For instance, the ^{1}H NMR spectrum of a water solution of (*M*)-$[EuL_{RRRRRR}]^{3+}$ shows only traces of a new complex after 3 weeks. The (*M*)-$[YbL_{RRRRRR}]^{3+}$ complex is somewhat less stable. In water, it gradually converts into a new paramagnetic complex (see Supporting Information). After heating at 238 K for 339 h, equilibrium is reached, with 95% conversion into the new form. The process can also be observed by circular dichroism (CD) spectroscopy, which reveals profound differences between the two forms (Figure 3).

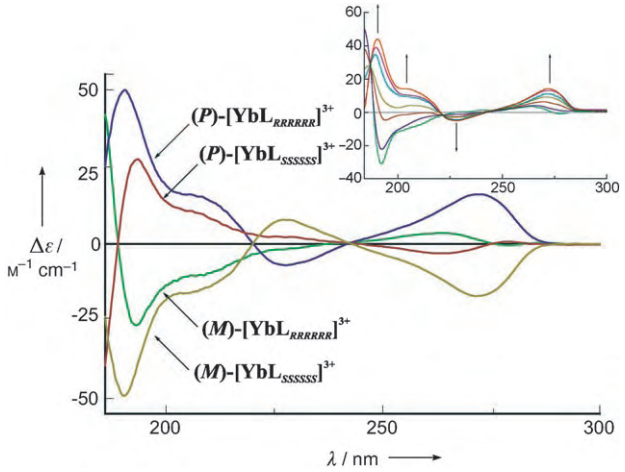

Figure 3. CD spectra of the $[YbL]^{3+}$ diastereoisomers. Inset: CD spectra recorded during the conversion of the starting (*M*)-$[YbL_{RRRRRR}]^{3+}$ complex cation into (*P*)-$[YbL_{RRRRRR}]^{3+}$, after heating in water solution at 238 K for 0, 5, 29, 50, 74, 171, and 339 h; arrows indicate changes on increasing heating time.

The new enantiopure complex (*P*)-$[YbL_{RRRRRR}]^{3+}$ can be isolated from solutions of enantiopure (*M*)-$[YbL_{RRRRRR}]^{3+}$ upon long standing; however, synthesis of the (*P*)-$[YbL_{RRRRRR}]^{3+}$ complex from the free ligand, using modified reaction conditions, is more practical (see Supporting Information).[13] Although the NMR spectra of the new form clearly differ from those of (*M*)-$[YbL_{RRRRRR}]^{3+}$, the ESI mass

 © 2006 Wiley-VCH Verlag GmbH & Co. KGaA, Weinheim

spectrum of (*P*)-$[YbL_{RRRRRR}]^{3+}$ contains the same signals as that of the starting complex, indicating the formation of an isomeric complex (see Supporting Information). The ^{1}H NMR spectrum of (*P*)-$[YbL_{RRRRRR}]^{3+}$ consists of 29 signals, which indicates that the new form also has C_2 symmetry. Note that ^{1}H NMR spectra of paramagnetic Yb^{III} complexes with macrocyclic ligands are very sensitive to any structural changes.[3a,14] In contrast, the UV/Vis spectra of both forms are nearly identical (see Supporting Information), reflecting the similar chemical character of the isomers.

The formation of the isomeric complex was confirmed by the X-ray crystal structure of (*P*)-$[YbL_{RRRRRR}](NO_3)_3{\cdot}2\,CH_3CN{\cdot}0.5\,H_2O$, which reveals the presence of the *P*-helical complex cation (*P*)-$[YbL_{RRRRRR}]^{3+}$ (Figure 2; Scheme 2).[15] In this cation, the twist of the macrocycle +255.6°, even greater than that of the starting *M* form. More importantly, the direction of the twist is opposite (see Supporting Information), which imposes a different chirality at the donor nitrogen atoms; the two nitrogen atoms attached to the unique cyclohexane ring positioned on the (non-crystallographic) C_2 symmetry axis have an *R* configuration, while the four remaining amine nitrogen atoms have an *S* configuration.

We have also synthesized the Yb^{III} complex of the all-*S* form of the ligand L, (*P*)-$[YbL_{SSSSSS}](NO_3)_3{\cdot}CHCl_3{\cdot}H_2O$, and its inversion product, (*M*)-$[YbL_{SSSSSS}](NO_3)_3{\cdot}0.5\,CH_3CN{\cdot}4\,H_2O$. As expected, the NMR spectra of the two complexes of each enantiomeric pair ((*M*)-$[YbL_{RRRRRR}]^{3+}$/(*P*)-$[YbL_{SSSSSS}]^{3+}$ and (*P*)-$[YbL_{RRRRRR}]^{3+}$/(*M*)-$[YbL_{SSSSSS}]^{3+}$) are identical, but their CD spectra are mirror images of one another (Figure 3; Scheme 2). Although the CD spectra of all four stereoisomers differ, the spectrum of (*P*)-$[YbL_{RRRRRR}]^{3+}$ somewhat resembles that of the (*P*)-$[YbL_{SSSSSS}]^{3+}$ diastereoisomer and is very different from that of the parent diastereoisomer (*M*)-$[YbL_{RRRRRR}]^{3+}$ (as is also true for the other pair of diastereoisomers). This observation is in accord with the fact that the overall shape of the (*P*)-$[YbL_{RRRRRR}]^{3+}$ complex is similar to that of the (*P*)-$[YbL_{SSSSSS}]^{3+}$ diastereoisomer (Figure 2; Scheme 2) and reflects that the *P*/*M* helicity has a stronger influence on the CD spectra of the complexes (for example, by an exciton-coupling mechanism) than does the *R*/*S* configuration at the cyclohexane fragments.

The conversion of (*M*)-$[YbL_{RRRRRR}]^{3+}$ into the (*P*)-$[YbL_{RRRRRR}]^{3+}$ isomer was rather unexpected. In principle, either the stability of two diastereoisomers derived from the same enantiopure form of a ligand are comparable, and a mixture of both forms is obtained, or one diastereoisomer exhibits a higher thermodynamic stability, leading to diastereoselection. In the present case, the less stable (*M*)-$[YbL_{RRRRRR}]^{3+}$ isomer is a kinetic product of the complexation of the free ligand (100% *de*), and the (*P*)-$[YbL_{RRRRRR}]^{3+}$ isomer is a thermodynamic product (90% *de*). Luckily, the conversion rate of the *M* form into the more stable *P* form is slow enough to allow the isolation and characterization of both enantiomers. The helicity-inversion process is dependent on the size of the Ln^{III} ion. Inversion is also observed for solutions of the $[TbL]^{3+}$ complex, while only traces of the inverted isomer are observed for $[EuL]^{3+}$.

In conclusion, we have demonstrated the formation of enantiopure complexes of opposite helicity with the same configuration at all stereogenic carbon centers from one enantiomer of a chiral ligand. The NMR, CD, ESI MS, and X-ray crystal-structure data confirm the isolation of the four enantiopure stereoisomers (*M*)-$[YbL_{RRRRRR}]^{3+}$, (*P*)-$[YbL_{RRRRRR}]^{3+}$, (*P*)-$[YbL_{SSSSSS}]^{3+}$, and (*M*)-$[YbL_{SSSSSS}]^{3+}$ and show that the kinetic complexation product slowly converts into the thermodynamic product of opposite helicity. Thus, helicity inversion corresponding to the conversion of the enantiopure complex (*M*)-$[YbL_{RRRRRR}]^{3+}$ into (*P*)-$[YbL_{RRRRRR}]^{3+}$ can be realized on a preparative scale. Note that the helicity inversion described herein differs from the inversion observed during the racemization of enantiopure helical structures and also from the inversion of helicity observed in polymeric systems,[16] as we observe a clear conversion of well-defined molecular compounds into their diastereoisomers. The properties of the complexes described are currently under investigation, in view of the many applications of enantiopure chiral lanthanide complexes, including macrocyclic derivatives, as enantioselective catalysts and spectroscopic probes.

Received: June 19, 2006
Published online: August 21, 2006

Keywords: chirality · diastereoselectivity · helical structures · lanthanides · macrocyclic ligands

[1] a) U. Knof, A. von Zelewsky, *Angew. Chem.* **1999**, *111*, 312; *Angew. Chem. Int. Ed.* **1999**, *38*, 302; b) M. A. Mateos-Timoneda, M. Crego-Calama, D. N. Reinhoudt, *Chem. Soc. Rev.* **2004**, *33*, 363.

[2] Selected examples: a) R. M. Yeh, K. N. Raymond, *Inorg. Chem.* **2006**, *45*, 1130; b) O. Mamula, M. Lama, S. G. Telfer, A. Nakamura, R. Kuroda, H. Stoeckli-Evans, R. Scopelitti, *Angew. Chem.* **2005**, *117*, 2583; *Angew. Chem. Int. Ed.* **2005**, *44*, 2527; c) M. Cantuel, G. Bernardinelli, G. Muller, J. P. Riehl, C. Piguet, *Inorg. Chem.* **2004**, *43*, 1840; d) P. K. Bowyer, V. C. Cook, N. Gharib-Naseri, P. A. Gugger, A. D. Rae, G. F. Swiegers, A. C. Willis, J. Zank, S. B. Wild, *Proc. Natl. Acad. Sci. USA* **2002**, *99*, 4877; e) B. Hasenknopf, J.-M. Lehn, N. Boumediene, E. Leize, A. Van Dorsselaer, *Angew. Chem.* **1998**, *110*, 3458; *Angew. Chem. Int. Ed.* **1998**, *37*, 3265; f) M. Albrecht, *Chem. Rev.* **2001**, *101*, 3457.

[3] a) J. Lisowski, S. Ripoli, L. Di Bari, *Inorg. Chem.* **2004**, *43*, 1388; b) J. Lisowski, J. Mazurek, *Polyhedron* **2002**, *21*, 811; c) S. W. A. Bligh, N. Choi, E. G. Evagorou, M. McPartlin, K. N. White, *J. Chem. Soc. Dalton Trans.* **2001**, 3169; d) L. H. Bryant, Jr., A. Lachgar, S. C. Jackels, *Inorg. Chem.* **1995**, *34*, 4230; e) A. Lachgar, K. S. Coates, S. C. Jackels, *Inorg. Chem.* **1994**, *33*, 2219; f) S. W. A. Bligh, N. Choi, E. G. Evagorou, W.-S. Li, M. McPartlin, *Chem. Commun.* **1994**, 2399; g) D. E. Fenton, R. W. Matthews, M. McPartlin, B. P. Murphy, I. J. Scowen, P. A. Tasker, *J. Chem. Soc. Chem. Commun.* **1994**, 1391; h) T. Tsubomura, K. Yasaku, T. Sato, M. Morita, *Inorg. Chem.* **1992**, *31*, 447; i) W. Radecka-Paryzek, V. Patroniak, J. Lisowski, *Coord. Chem. Rev.* **2005**, *249*, 2156; j) P. A. Vigato, S. Tamburini, *Coord. Chem. Rev.* **2004**, *248*; k) A. Werner, M. Michels, L. Zander, J. Lex, E. Vogel, *Angew. Chem.* **1999**, *111*, 3666; *Angew. Chem. Int. Ed.* **1999**, *38*, 3650; l) J. L. Sessler, S. J. Weghorn, V. Lynch, M.-R. Johnson,

 © 2006 Wiley-VCH Verlag GmbH & Co. KGaA, Weinheim

Angew. Chem. **1994**, *106*, 1572; *Angew. Chem. Int. Ed. Engl.* **1994**, *33*, 1509.

[4] a) D. Parker, *Chem. Soc. Rev.* **2004**, *33*, 156; b) L. Di Bari, G. Pescitelli, A. D. Sherry, M. Woods, *Inorg. Chem.* **2005**, *44*, 8391; c) M. Woods, Z. Kovacs, S. Zhang, A. D. Sherry, *Angew. Chem.* **2003**, *115*, 6069; *Angew. Chem. Int. Ed.* **2003**, *42*, 5889; d) R. S. Dickins, J. A. K. Howard, C. W. Lehmann, J. Moloney, D. Parker, R. D. Peacock, *Angew. Chem.* **1997**, *109*, 541; *Angew. Chem. Int. Ed. Engl.* **1997**, *36*, 521; e) R. S. Dickins, S. Aime, A. S. Batsanov, A. Beeby, M. Botta, J. I. Bruce, J. A. K. Howard, C. S. Love, D. Parker, R. D. Peacock, H. Puschmann, *J. Am. Chem. Soc.* **2002**, *124*, 12697.

[5] L. Burai, E. Toth, A. Sour, A. E. Merbach, *Inorg. Chem.* **2005**, *44*, 3561.

[6] For instance, the important magnetic resonance imaging (MRI) contrast-enhancing agent GdDOTA and related Ln^{III} complexes of 1,4,7,10-tetraazacyclododecane-1,4,7,10-tetraacetic acid (DOTA) can exist as four stereoisomers, the enantiomeric pairs Λ(δδδδ)/Δ(λλλλ) and Δ(λλλλ)/Λ(δδδδ), where Δ/Λ denote chirality related to the coordination around the Ln^{III} ion and the rotation of the coordinated side arms, while δ/λ denote chirality related to the conformation of the cyclene macrocycle. These complexes, which lack stereogenic carbon atoms, exist either as a mixture of all four stereoisomers, or as a mixture of just one of the two enantiomeric pairs. In contrast, the introduction of additional chiral centers into the system, as carbon atoms of defined *R* or *S* configuration, results in the preferential formation of only one of the four possible stereoisomers.[4]

[7] P. Belmont, J.-F. Constant, M. Demeunynck, *Chem. Soc. Rev.* **2001**, *30*, 70.

[8] a) M. Hutin, J. Nitschke, *Chem. Commun.* **2006**, 1724; b) H. Miyake, H. Sugimoto, H. Tamiaki, H. Tsukube, *Chem. Commun.* **2005**, 4291; c) H. Miyake, K. Yoshida, H. Sugimoto, H. Tsukube, *J. Am. Chem. Soc.* **2004**, *126*, 6524; d) M. K. J. ter Viel, R. A. van Delden, A. Meetsma, B. L. Feringa, *J. Am. Chem. Soc.* **2003**, *125*, 15076; e) V. V. Borovkov, G. A. Hembury, Y. Inoue, *Angew. Chem.* **2003**, *115*, 5468; *Angew. Chem. Int. Ed.* **2003**, *42*, 5310; f) P. Biscarini, R. Kuroda, *Inorg. Chim. Acta* **1988**, *154*, 209.

[9] a) J. Gregoliński, J. Lisowski, T. Lis, *Org. Biomol. Chem.* **2005**, *3*, 3161; b) A. González-Álvarez, I. Alfonso, F. López-Oritz, Á. Aguirre, S. García-Granda, V. Gotor, *Eur. J. Org. Chem.* **2004**, 1117; c) N. Kuhnert, G. M. Rossignolo, A. Lopez-Periago, *Org. Biomol. Chem.* **2003**, *1*, 1157; d) A. González-Álvarez, I. Alfonso, V. Gotor, *Chem. Commun.* **2006**, 2224.

[10] Crystal data for (*M*)-$[EuL_{RRRRRR}]_2[Eu(NO_3)_5](NO_3)_4{\cdot}2H_2O$, orthorhombic, $P2_12_12_1$, $Z=4$, $a=15.092(5)$, $b=20.099(6)$, $c=30.470(10)$ Å, $V=9243(5)$ Å^3, $\mu(Cu_{K\alpha})=15.172$ mm^{-1}, $T=100$ K, 21952 measured reflections, 18115 unique ($R_{int}=0.1208$), 1232 parameters, $R_1=0.0808$, $wR=0.1307$ (all data); see Supporting Information for additional data and experimental details. CCDC-611055 ((*M*)-$[EuL_{RRRRRR}]_2[Eu(NO_3)_5](NO_3)_4{\cdot}2H_2O$), CCDC-611056 ((*M*)-$[YbL_{RRRRRR}](NO_3)_3{\cdot}2.33CH_3CN{\cdot}2H_2O$), CCDC-611057 ((*P*)-$[YbL_{RRRRRR}](NO_3)_3{\cdot}2CH_3CN{\cdot}0.5H_2O$) contain the supplementary crystallographic data for this paper. These data can be obtained free of charge from The Cambridge Crystallographic Data Centre via www.ccdc.cam.ac.uk/data_request/cif.

[11] M. Paluch, J. Lisowski, T. Lis, *Dalton Trans.* **2006**, 381.

[12] Crystal data for (*M*)-$[YbL_{RRRRRR}](NO_3)_3{\cdot}2.33CH_3CN{\cdot}2H_2O$: orthorhombic, $C222_1$, $Z=4$, $a=15.897(3)$, $b=20.029(4)$, $c=48.300(10)$ Å, $V=15379(5)$ Å^3, $\mu(Mo_{K\alpha})=1.895$ mm^{-1}, $T=100$ K, 31187 measured reflections, 24569 unique ($R_{int}=0.0663$), 913 parameters, $R_1=0.0802$, $wR=0.1067$ (all data); see Supporting Information for additional data and experimental details.

[13] The formation of (*P*)-$[YbL_{RRRRRR}]^{3+}$ is accelerated by the slightly basic conditions arising from the presence of excess free L, by longer reaction times, or by higher temperatures.

[14] a) J. Lisowski, J. L. Sessler, V. Lynch, T. D. Mody, *J. Am. Chem. Soc.* **1995**, *117*, 2273; b) V. Patroniak, M. Kubicki, A. Mondry, J. Lisowski, W. Radecka-Paryzek, *Dalton Trans.* **2004**, 3295.

[15] Crystal data for (*P*)-$[YbL_{RRRRRR}](NO_3)_3{\cdot}2CH_3CN{\cdot}0.5H_2O$: trigonal, $P3_221$, $Z=3$, $a=15.157(3)$, $c=39.340(10)$ Å, $V=7827(3)$ Å^3, $\mu(Mo_{K\alpha})=1.896$ mm^{-1}, $T=100$ K, 24278 measured reflections, 12520 unique ($R_{int}=0.0963$), 622 parameters, $R_1=0.0941$, $wR=0.1156$ (all data); see Supporting Information for additional data and experimental details.

[16] a) A. Ajayaghosh, R. Varghese, S. J. George, C. Vijayakumar, *Angew. Chem.* **2006**, *118*, 1159; *Angew. Chem. Int. Ed.* **2006**, *45*, 1141; b) A. Lohr, M. Lysetska, F. Würthner, *Angew. Chem.* **2005**, *117*, 5199; *Angew. Chem. Int. Ed.* **2005**, *44*, 5071; c) H.-Z. Tang, B. M. Novak, J. He, P. L. Polavarapu, *Angew. Chem.* **2005**, *117*, 7464; *Angew. Chem. Int. Ed.* **2005**, *44*, 7298.

 © 2006 Wiley-VCH Verlag GmbH & Co. KGaA, Weinheim

Porous Materials

DOI: 10.1002/anie.200601668

A Multifunctional Metal–Organic Open Framework with a bcu Topology Constructed from Undecanuclear Clusters**

Qian-Rong Fang, Guang-Shan Zhu, Zhao Jin, Ming Xue, Xiao Wei, De-Jun Wang, and Shi-Lun Qiu**

The synthesis and characterization of metal–organic frameworks (MOFs) have attracted much attention, owing to their enormous variety of interesting structural topologies and wide potential applications as functional materials.[1] Recently, the design of MOFs with excellent properties that combine porosity with magnetism, luminescence, or opto-

[*] Dr. Q. R. Fang, Prof. G. S. Zhu, Z. Jin, Dr. M. Xue, Prof. S. L. Qiu
State Key Laboratory of Inorganic Synthesis & Preparative Chemistry
Jilin University
Changchun 130012 (P.R. China)
Fax: (+86) 431-516-8331
E-mail: zhugs@mail.jlu.edu.cn
sqiu@mail.jlu.edu.cn

Dr. X. Wei, Prof. D. J. Wang
College of Chemistry
Jilin University
Changchun 130023 (P.R. China)

[**] This work was supported by the National Natural Science Foundation of China (grant nos. 20371020 and 20531030) and the Graduate Innovation Lab of Jilin University. We are very grateful for the help provided by Ankersmid Company, Netherlands. bcu = body-centered cubic.

Supporting Information for this article is available on the WWW under http://www.angewandte.org or from the author.

WILEY InterScience DISCOVER SOMETHING GREAT
© 2006 Wiley-VCH Verlag GmbH & Co. KGaA, Weinheim

electronic effects has become one of the major challenges in the pursuit of multifunctional materials.[2–4] Yaghi and co-workers, for example, have reported the synthesis of $[Tb_2(bdc)_3]\cdot 4H_2O$, which has an extended structure (pore volume: 0.099 $cm^3 g^{-1}$), from terbium nitrate and 1,4-benzenedicarboxylic acid (H_2bdc) in the presence of triethylamine, and have investigated its luminescence lifetime.[2a] As for the study of multifunctional materials that are both porous and magnetic, Riou, Férey, and co-workers have synthesized the hybrid organic–inorganic solid $[V(OH)(bdc)]\cdot x H_2bdc$ ($x \approx 0.75$), which has very large pores (BET surface area: 930(30) $m^2 g^{-1}$) and good magnetic characteristics (antiferromagnetic below 95 K), by using rigid organic linkers containing delocalized π electrons to connect chains of corner-sharing vanadium-centered octahedra.[3a] Our group has successfully prepared the novel 3D noninterpenetrating MOF $[Zn_7O_2(bda)_5(H_2O)_2]\cdot 5DMF\cdot 4EtOH\cdot 6H_2O$ (H_2bda = 1,4-benzenediacrylic acid; DMF = dimethylformamide), which is constructed from heptanuclear zinc carboxylate secondary building units (SBUs) and contains an intersecting channel system with a spacing of approximately 17.3 Å. This compound exhibits excellent adsorption, H_2 storage, and photoelectronic properties.[4]

Our strategy for preparing novel multifunctional structures is to construct metal carboxylate SBUs. The construction of metal carboxylate cluster SBUs has been demonstrated to be an effective and powerful synthetic method to produce a new generation of highly porous MOFs.[5,6] Interestingly, Powell and co-workers have pioneered studies on aluminum–ligand units with Al_{15} cluster aggregates containing the flexible ligand hpdta ($H_5hpdta = HOCH_2[CH_2N(CH_2COOH)_2]_2$), such as $[Al_{15}(\mu_3\text{-}O)_4(\mu_3\text{-}OH)_6(\mu\text{-}OH)_{14}(hpdta)_4]^{3-}$.[7] However, although many MOFs built from different transition-metal carboxylate cluster SBUs have been synthesized, they usually consist of di-, tri-, or tetranuclear metal carboxylate clusters, in which a water molecule plays an important role as a bridging ligand.[8] The number of metal centers held together by the bridging water molecule is limited by its weak coordination ability. To overcome this difficulty, our strategy is to substitute the bridging water molecule with formic acid (HCOOH), which has a strong coordination ability, to construct stable metal carboxylate cluster SBUs. As an example of our design principle, we describe herein the synthesis and structure, as well as the sorption and optoelectronic properties of the large-pore open-framework complex $[Cd_{11}(\mu_4\text{-}HCOO^-)_6(bpdc)_9]\cdot 9DMF\cdot 6H_2O$ (**1**; H_2bpdc = 4,4′-biphenyldicarboxylic acid), which is constructed from undecanuclear clusters. To our knowledge, this MOF has the largest transition-metal carboxylate cluster SBUs reported to date.

Polymer **1** was synthesized under mild conditions by carefully adjusting the relative quantities of the rigid (bpdc) and flexible (HCOOH) ligands. X-ray crystallography revealed that **1** crystallizes in the trigonal system (space group *R*3*c* (no. 161)).[9] All of the cadmium atoms in the structure of **1** have octahedral coordination environments. As shown in Figure 1a, the Cd^{II}-centered octahedra are linked together by 18 carboxylate groups from bpdc anions, which bind in a didentate or a chelating/bridging didentate fashion,

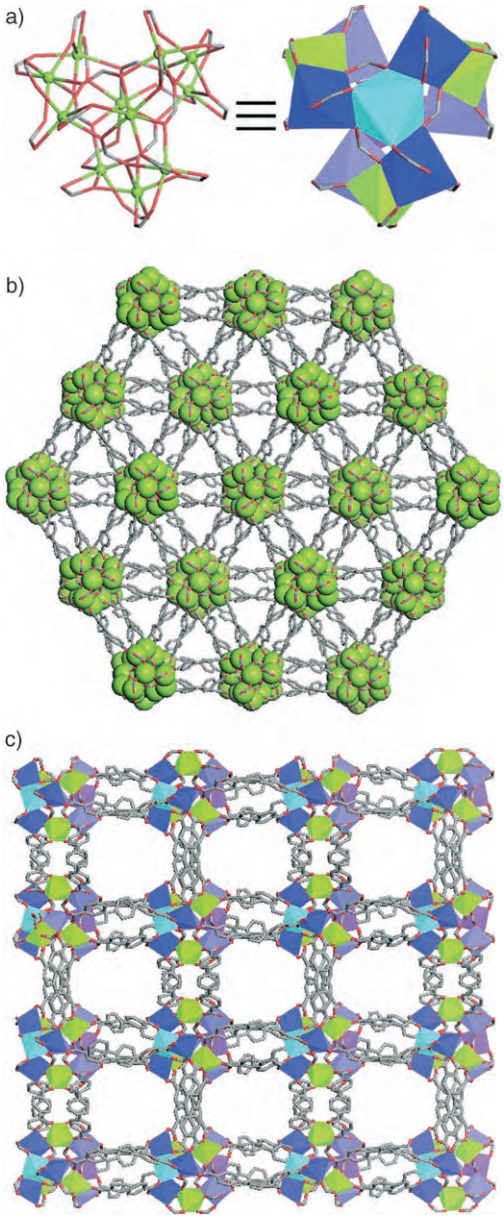

Figure 1. a) Ball-and-stick (left) and polyhedral (right) representations of the $\{Cd_{11}(\mu_4\text{-}HCOO^-)_6(CO_2)_{18}\}$ SBU of **1**, which has dimensions of approximately 10.5 × 11.5 × 12.8 $Å^3$. b) View of the 3D framework of **1** along the [001] direction. c) View of the 3D framework of **1** along the [$\bar{1}$11] direction, showing large channels with dimensions of approximately 9.7 × 12.2 $Å^2$. Cd green, O red, C gray; CdO_6 octahedra; H atoms omitted for clarity

and six μ_4-$HCOO^-$ moieties to build up a nanosized undecanuclear $\{Cd_{11}(\mu_4\text{-}HCOO^-)_6(CO_2)_{18}\}$ cluster with C_3 symmetry and dimensions of approximately 10.5 × 11.5 × 12.8 $Å^3$ (measured between opposite atoms along the three directions). These undecametallic clusters, which behave as SBUs, are interconnected through the biphenyl groups of bpdc molecules to generate an extended 3D framework (Figure 1b). Figure 1c shows the rectangular channels of 9.7 × 12.2 $Å^2$ (measured between opposite atoms) in **1**, which run along the [$\bar{1}$11] and [211] directions, and are filled with guest H_2O and DMF molecules, as established by elemental,

 © 2006 Wiley-VCH Verlag GmbH & Co. KGaA, Weinheim

inductively coupled plasma (ICP), and thermogravimetric (TG) analysis (see Supporting Information).

A better insight into the structure of **1** can be obtained by the standard procedure of reducing multidimensional structures to simple node-and-linker reference nets known as the topological approach.[11] As shown in Figure 2a, each unde-

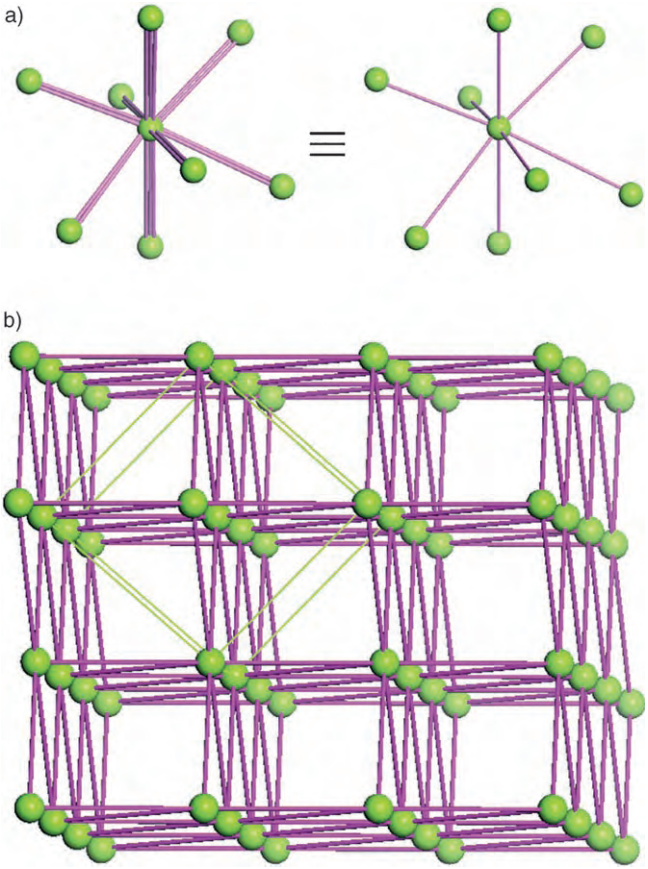

Figure 2. a) Left: each SBU (green circle) of **1** is connected to eight adjacent SBUs through eighteen biphenyl groups (pink lines) of bpdc molecules; right: the SBU represented as an eight-connected node. b) Schematic representation of the bcu topology of the eight-connected framework of **1**; the bcu unit cell is indicated by green lines.

canuclear SBU in **1** is connected to adjacent SBUs through three biphenyl groups of bpdc molecules along the [001] direction and through two biphenyl groups along three other directions. Therefore, each SBU of **1** can be defined as an eight-connected node. As bpdc only acts as a bridging ligand, there is no need to consider it in the topological analysis. On the basis of this simplification, the structure of **1** can be described as an eight-connected 3D network with the Schläfli symbol ($4^{24}\cdot6^4$), which corresponds to a body-centered cubic (bcu) topology that is rare for MOFs (Figure 2b).[12]

Adsorption isotherms for **1** were measured at room temperature (293 K). As shown in Figure 3, type I behavior, which is characteristic of solids with micropores, is observed for the H_2O, CH_3OH, and C_2H_5OH adsorption isotherms in the range $P/P_0 = 0$–0.7. These results indicate that the incoming guests can move freely into the channels and that

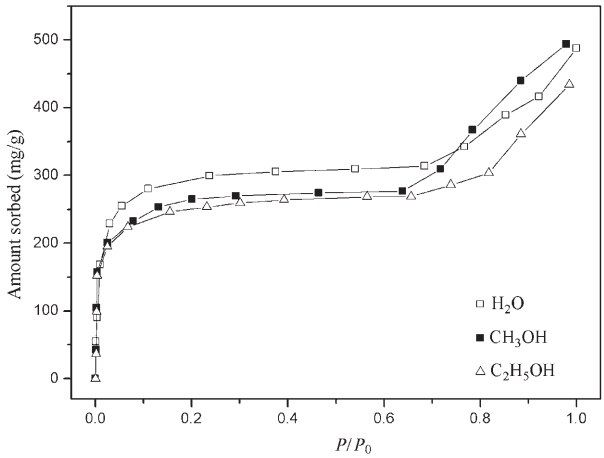

Figure 3. H_2O, CH_3OH, and C_2H_5OH adsorption isotherms for **1** at 293 K.

the framework maintains its rigidity and porosity throughout the analyses. The second increase in the adsorption isotherms above $P/P_0 = 0.7$ can be attributed to adsorption on the external crystallite surface.[13] At the first saturation, the amounts of H_2O, CH_3OH, and C_2H_5OH adsorbed by **1** are 314, 277, and 269 $mg\,g^{-1}$, respectively, equivalent to the adsorption of approximately 468 molecules of H_2O, 234 molecules of CH_3OH, and 162 molecules of C_2H_5OH per unit cell. The pore volume for **1** is, therefore, approximately 0.35 $cm^3\,g^{-1}$. Detailed sorption data for **1** are presented in Table 1.

Table 1: Sorption data for **1**.

Guest	Adsorption amount [$mg\,g^{-1}$]	Guests per asymmetric unit	Guests per unit cell	Pore volume [$cm^3\,g^{-1}$]
H_2O	314	26	468	0.31
CH_3OH	277	13	234	0.35
C_2H_5OH	269	9	162	0.34

Encouraged by the single-crystal X-ray diffraction results, which reveal the presence of undecanuclear cadmium clusters in the framework, photovoltage (PV) transients were recorded for **1** at atmospheric pressure and room temperature (293 K).[14] As is well known, PV transients can be used to characterize semiconductor materials, and a PV signal will arise whenever light-induced excess charge carriers are separated in space.[15] Figure 4 shows the PV transients for **1** at different intensities of the exciting laser pulse (355 nm). The transient PV signals of **1** clearly exhibit a time lag caused by the slow and independent diffusion of excess electrons and holes. Although the intensities of the exciting laser pulses are different (0.05, 0.10, 0.20, and 0.30 mJ), the times of their PV maxima are similar ($t \approx 0.013$ s). These maxima are related to the separation of charge at the **1**/indium tin oxide (ITO) interface, and the gradient of excess electron and hole concentrations is caused by the nonhomogeneous absorption of light with photons with $h\nu$ larger than the optical bandgap

 © 2006 Wiley-VCH Verlag GmbH & Co. KGaA, Weinheim

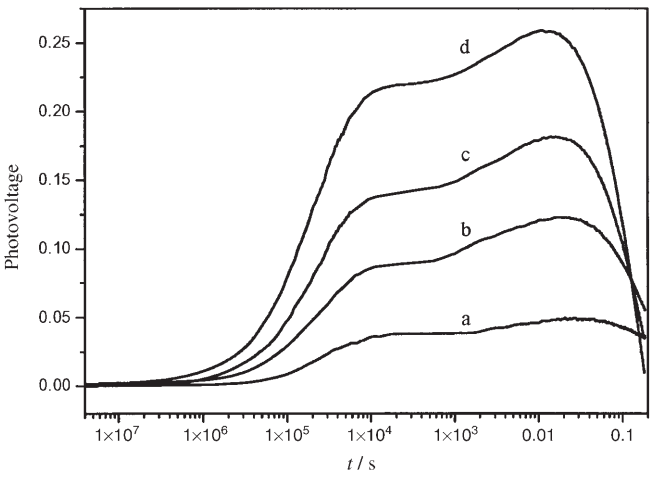

Figure 4. PV transients for **1** upon illumination by a 355-nm pulse laser at intensities of a) 0.05, b) 0.10, c) 0.20, and d) 0.30 mJ.

(E_g). Additionally, the PV transient signals are positive, which means that the photoexcited electrons move faster than holes towards the **1**/ITO interface. The maxima of the transients are linearly enhanced when the intensity of the pulse is increased from 0.05 to 0.30 mJ. This observation implies that **1** possesses the characteristics of a diffusion PV transient, but not of a Dember PV transient, which is similar to the case for nanosized metal oxide semiconductors.[16]

In summary, we have successfully synthesized the large-pore, open-framework complex $[Cd_{11}(\mu_4\text{-}HCOO^-)_6(bpdc)_9]\cdot 9DMF\cdot 6H_2O$ (**1**), which contains the largest known Cd^{II}–carboxylate cluster SBU and has a rare bcu topology, by rationally utilizing a flexible organic acid (HCOOH) as a strong bridging ligand. Polymer **1** shows good sorption and optoelectronic properties. Other novel architectures with unusual topologies and metal carboxylate cluster SBUs should be obtainable by following a similar synthetic strategy. We believe that such MOFs with large clusters and channels will further facilitate the exploration of new types of multifunctional materials with interesting properties, including the combination of porosity and magnetic, luminescence, or optoelectronic properties.

Experimental Section

1: A mixture of $Cd(NO_3)_2\cdot 4H_2O$ (0.03 g, 0.1 mmol), H_2bpdc (0.01 g, 0.05 mmol), HCOOH (0.02 mL), and DMF (15.0 mL) was stirred in air for 4 h, and then a DMF solution (0.5 mL) of 2-propanolamine (0.05 mL) was slowly diffused into the mixture over 7 d at 60 °C. The resulting colorless, block-shaped single crystals of **1** were collected in 32 % yield based on cadmium. The complex is insoluble in common organic solvents such as acetone, methanol, ethanol, dichloromethane, acetonitrile, chloroform, and DMF. Elemental and ICP analysis (%) calcd for $C_{159}H_{153}Cd_{11}N_9O_{63}$ (4434.5): C 43.07, H 3.48, Cd 27.88, N 2.84; found: C 43.11, H 3.52, Cd 27.94, N 2.78. FT-IR (KBr): $\tilde{\nu}$ = 3433 (m), 3067 (w), 2928 (w), 1931 (w), 1659 (s), 1593 (s), 1504 (s), 1394 (s), 1267 (w), 1180 (m), 1105 (m), 1063 (w), 1007 (m), 860 (m), 771 (s), 677 (m), 526 cm^{-1} (w).

Received: April 27, 2006
Published online: July 27, 2006

Keywords: cadmium · carboxylate ligands · clusters · materials science · supramolecular chemistry

[1] a) N. W. Ockwig, O. Delgado-Friederichs, M. O'Keeffe, O. M. Yaghi, *Acc. Chem. Res.* **2005**, *38*, 176; b) B. Moulton, M. J. Zaworotko, *Chem. Rev.* **2001**, *101*, 1629; c) S. R. Batten, R. Robson, *Angew. Chem.* **1998**, *110*, 1558; *Angew. Chem. Int. Ed.* **1998**, *37*, 1460; d) G. Férey, C. Mellot-Draznieks, C. Serre, F. Millange, *Acc. Chem. Res.* **2005**, *38*, 217; e) X. Zhao, B. Xiao, A. J. Fletcher, K. M. Thomas, D. Bradshaw, M. J. Rosseinsky, *Science* **2004**, *306*, 1012; f) S. Kitagawa, R. Kitaura, S. Noro, *Angew. Chem.* **2004**, *116*, 2388; *Angew. Chem. Int. Ed.* **2004**, *43*, 2334; g) A. Erxleben, *Coord. Chem. Rev.* **2003**, *246*, 203; h) C. Janiak, *Dalton Trans.* **2003**, 2781; i) Q. R. Fang, G. S. Zhu, M. Xue, J. Y. Sun, Y. Wei, S. L. Qiu, R. R. Xu, *Angew. Chem.* **2005**, *117*, 3913; *Angew. Chem. Int. Ed.* **2005**, *44*, 3845.

[2] a) T. M. Reineke, M. Eddaoudi, M. Fehr, D. Kelley, O. M. Yaghi, *J. Am. Chem. Soc.* **1999**, *121*, 1651; b) Q. R. Fang, G. S. Zhu, M. Xue, J. Y. Sun, F. X. Sun, S. L. Qiu, *Inorg. Chem.* **2006**, *45*, 3582.

[3] a) K. Barthelet, J. Marrot, D. Riou, G. Férey, *Angew. Chem.* **2002**, *114*, 291; *Angew. Chem. Int. Ed.* **2002**, *41*, 281; b) K. Barthelet, K. Adil, F. Millange, C. Serre, D. Riou, G. Férey, *J. Mater. Chem.* **2003**, *12*, 2208; c) K. Barthelet, D. Riou, G. Férey, *Chem. Commu.* **2002**, 1492; d) K. Barthelet, D. Riou, M. Nogues, G. Férey, *Inorg. Chem.* **2003**, *42*, 1739.

[4] Q. R. Fang, G. S. Zhu, M. Xue, Q. L. Zhang, J. Y. Sun, X. D. Guo, S. L. Qiu, S. T. Xu, P. Wang, D. J. Wang, Y. Wei, *Chem. Eur. J.* **2006**, *12*, 3754.

[5] a) M. Eddaoudi, D. B. Moler, H. Li, B. Chen, T. M. Reineke, M. O'Keeffe, O. M. Yaghi, *Acc. Chem. Res.* **2001**, *34*, 319; b) S. S. Y. Chui, S. M. F. Lo, J. P. H. Charmant, A. G. Orpen, I. D. Williams, *Science* **1999**, *283*, 1148; c) L. Pan, H. M. Liu, X. G. Lei, X. Y. Huang, D. H. Olson, N. J. Turro, J. Li, *Angew. Chem.* **2003**, *115*, 560; *Angew. Chem. Int. Ed.* **2003**, *42*, 542.

[6] a) Q. R. Fang, G. S. Zhu, M. Xue, J. Y. Sun, G. Tian, G. Wu, S. L. Qiu, *Dalton Trans.* **2004**, 2202; b) Q. R. Fang, G. S. Zhu, X. Shi, G. Wu, G. Tian, R. W. Wang, S. L. Qiu, *J. Solid State Chem.* **2004**, *177*, 1060; c) Q. R. Fang, X. Shi, G. Wu, G. Tian, G. S. Zhu, R. W. Wang, S. L. Qiu, *J. Solid State Chem.* **2003**, *176*, 1.

[7] W. Schmitt, E. Baissa, A. Mandel, C. E. Anson, A. K. Powell, *Angew. Chem.* **2001**, *113*, 3689; *Angew. Chem. Int. Ed.* **2001**, *40*, 3578.

[8] a) H. L. Li, M. Eddaoudi, M. O'Keeffe, O. M. Yaghi, *Nature* **1999**, *402*, 276; b) J. Kim, B. Chen, T. M. Reineke, H. Li, M. Eddaoudi, D. B. Moler, M. O'Keeffe, O. M. Yaghi, *J. Am. Chem. Soc.* **2001**, *123*, 8239; c) J. S. Seo, D. Whang, H. Lee, S. I. Jun, J. Oh, Y. J. Jeon, K. Kim, *Nature* **2000**, *404*, 982; d) G. Férey, C. Mellot-Draznieks, C. Serre, F. Millange, J. Dutour, S. Surblé, I. Margiolaki, *Science* **2005**, *309*, 2040; e) B. Kesanli, Y. Cui, M. R. Smith, E. W. Bittner, B. C. Bockrath, W. B. Lin, *Angew. Chem.* **2005**, *117*, 74; *Angew. Chem. Int. Ed.* **2005**, *44*, 72.

[9] A colorless block-shaped crystal of **1** was selected for X-ray structural analysis, and intensity data were collected on a Bruker SMART CCD diffractometer at 298 K. Crystal data: $0.40\times 0.40\times 0.38$ mm^3, trigonal, space group $R3c$, a = 31.936(5), c = 42.607(9) Å, V = 37634(11) $Å^3$, Z = 6, λ = 0.71073 Å, ρ_{calcd} = 0.971 $g\,cm^{-3}$, $\mu(Mo_{K\alpha})$ = 0.958 mm^{-1}, $F(000)$ = 10692. 65660 reflections were collected in the range $0.88 < \theta < 25.00$, of which 12567 were unique. The structure was solved and refined by full-matrix least-squares on F^2 (SHELXL-97).[10] Non-hydro-

 © 2006 Wiley-VCH Verlag GmbH & Co. KGaA, Weinheim

gen atoms were refined anisotropically. Hydrogen atoms were fixed at calculated positions and refined by using a riding model. The final $R1$ and $wR2$ values for 11332 independent reflections with $[I > 2\sigma(I)]$ were 0.0642 and 0.1770, respectively. CCDC-603457 contains the supplementary crystallographic data for this paper. These data can be obtained free of charge from The Cambridge Crystallographic Data Centre via www.ccdc.cam.ac.uk/data_request/cif.

[10] G. M. Sheldrick, SHELX-97, Program for Structure Refinement, University of Göttingen, Germany, **1997**.

[11] a) A. F. Wells, *Further Studies of Three-Dimensional Nets*, American Crystallographic Association, New York (distributed by Polycrystal Book Service, Pittsburgh, PA), **1979**; b) A. F. Wells, *Three-Dimensional Nets and Polyhedra*, Wiley, New York, **1977**; c) A. J. Blake, N. R. Champness, P. Hubberstey, W. S. Li, M. A. Withersby, M. Schröder, *Coord. Chem. Rev.* **1999**, *183*, 117; d) O. D. Friedrichs, M. O'Keeffe, O. M. Yaghi, *Acta Crystallogr. Sect. A* **2003**, *59*, 22; e) C. Qin, X. L. Wang, E. B. Wang, Z. M. Su, *Inorg. Chem.* **2005**, *44*, 7122.

[12] a) D. L. Long, A. J. Blake, N. R. Champness, C. Wilson, M. Schröder, *Angew. Chem.* **2001**, *113*, 2509; *Angew. Chem. Int. Ed.* **2001**, *40*, 2443; b) D. L. Long, R. J. Hill, A. J. Blake, N. R. Champness, P. Hubberstey, D. M. Proserpio, C. Wilson, M. Schröder, *Angew. Chem.* **2004**, *116*, 1887; *Angew. Chem. Int. Ed.* **2004**, *43*, 1851; c) R. J. Hill, D. L. Long, P. Hubberstey, M. Schröder, N. R. Champness, *J. Solid State Chem.* **2005**, *178*, 2414; d) T. T. Luo, H. L. Tsai, S. L. Yang, Y. H. Liu, R. D. Yadav, C. C. Su, C. H. Ueng, L. G. Lin, K. L. Lu, *Angew. Chem.* **2005**, *117*, 6217; *Angew. Chem. Int. Ed.* **2005**, *44*, 6063; e) J. Lu, W. T. A. Harrison, A. J. Jacobson, *Angew. Chem.* **1995**, *107*, 2759; *Angew. Chem. Int. Ed. Engl.* **1995**, *34*, 2557; f) J. U. Schutze, R. Eckhardt, R. D. Fischer, D. C. Apperley, N. A. Davies, R. K. Harris, *J. Organomet. Chem.* **1997**, *534*, 187.

[13] M. Eddaoudi, H. L. Li, O. M. Yaghi, *J. Am. Chem. Soc.* **2000**, *122*, 1391.

[14] Q. L. Zhang, D. J. Wang, X. Wei, T. F. Xie, Z. H. Li, Y. H. Lin, M. Yang, *Thin Solid Films* **2005**, *491*, 242.

[15] V. Duzhko, V. Yu. Timoshenko, F. Koch, T. Dittrich, *Phys. Rev. B* **2001**, *64*, 075204.

[16] T. Dittrich, V. Duzhko, F. Koch, V. Kytin, J. Rappich, *Phys. Rev. B* **2001**, *65*, 155319.

 © 2006 Wiley-VCH Verlag GmbH & Co. KGaA, Weinheim

Asymmetric Catalysis

DOI: 10.1002/anie.200601638

Highly Diastereo- and Enantioselective Mukaiyama Aldol Reactions Catalyzed by Hydrogen Bonding**

*Jeff D. McGilvra, Aditya K. Unni, Kriti Modi, and Viresh H. Rawal**

Although still in its infancy, the area of asymmetric catalysis promoted by hydrogen bonds has seen explosive growth in the past few years.[1–5] Reports from several research groups have demonstrated that many asymmetric reactions that had previously been the domain of metal-based Lewis acids, can now be catalyzed by organic compounds capable of donating a hydrogen bond. However, unlike traditional Lewis acids, which catalyze a diverse range of reactions with useful levels of enantioselectivity (>90% *ee*), hydrogen-bond catalysts have been shown to be efficacious for relatively few reactions, such as the Diels–Alder, aza-Henry, Mannich, Michael, Morita–Baylis–Hillman, and Strecker reactions.[2–4] In connection with our interest in hydrogen-bond-promoted reactions, we have examined the application of this mode of catalysis to the Mukaiyama aldol.

The Mukaiyama aldol reaction has proven to be one of the most powerful transformations for the controlled assembly of β-hydroxycarbonyl units, a structural motif found in numerous natural products.[6] The reaction involves the C–C bond coupling of two fragments, with the formation of up to two new stereogenic centers. Much effort has been directed to asymmetric catalysis of this reaction, and the vast majority of the successes have been recorded with metal-based chiral Lewis acids.[7] Among the few metal-free methods that have been developed, the most successful have involved the use of chiral phosphoramides as Lewis bases.[8] Despite its central importance in the synthesis of complex molecules, there is, to date, only a single report of the Mukaiyama aldol reaction catalyzed by hydrogen bonding (3 examples, 30–56% *ee*).[5,9] We now report that simple, chiral hydrogen-bond donors are effective as metal-free catalysts for the promotion of highly diastereo- and enantioselective Mukaiyama aldol reactions.

Among the many permutations of Mukaiyama aldol reactions, we focused our efforts on the reaction of silylated enolates of amides, since the presence of the enamine unit was

[*] J. D. McGilvra, A. K. Unni, K. Modi, Prof. V. H. Rawal
Department of Chemistry
The University of Chicago
Chicago, IL 60637 (USA)
Fax: (+1) 773-702-0805
E-mail: vrawal@uchicago.edu

[**] This work was supported by the NSF and the NIH. Dr. Ian Steele is acknowledged for determination of the X-ray crystal structure shown in Figure 1.

Supporting information for this article is available on the WWW under http://www.angewandte.org or from the author.

WILEY InterScience DISCOVER SOMETHING GREAT
© 2006 Wiley-VCH Verlag GmbH & Co. KGaA, Weinheim

expected to render these compounds highly nucleophilic. Indeed, Myers and Widdowson have reported that such *O*-silyl-*N*,*O*-ketene acetals react with aldehydes at ambient temperature to yield the expected aldol products as a mixture of diastereomers.[10] We began our investigation with the expectation that if the reaction were carried out in the presence of a chiral hydrogen-bond donor, then the two prochiral faces of the aldehyde could be differentiated on complexation, and enantiomerically enriched aldol products would be formed. Previous work from our research group has shown that simple diols of the taddol family are highly effective catalysts for enantioselective reactions (taddol = α,α,α′,α′-tetraaryl-2,2-dimethyl-1,3-dioxolane-4,5-dimethanol).[2a,b,d] In initial trials, *O*-silyl-*N*,*O*-acetal **2** was treated with benzaldehyde in the presence of 10 mol% of commercially available tetra-1-naphthyl-taddol (**1a**) at −40°C in toluene. The reaction proceeded rapidly at this temperature, with complete consumption of **2** within 4 h, to give the aldol adducts in 83% yield, as a 6:1 mixture of *syn* and *anti* diastereomers, with *ee* values of 90 and 77%, respectively (Scheme 1). Crude β-hydroxyamide product **3a** was isolated after stirring the reaction mixture in the presence of HF (1–2 h), with no observed erosion in the diastereomeric ratio.

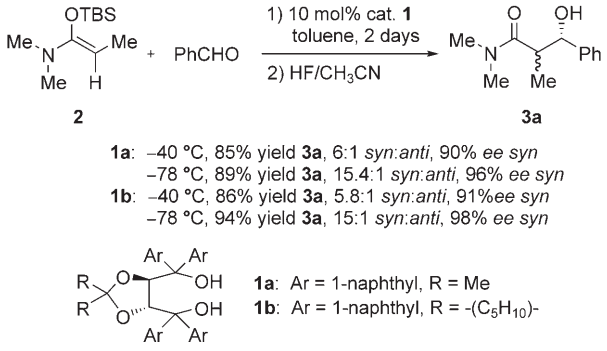

Scheme 1. Initial discovery of taddol-catalyzed aldol reaction of **2.** **1a**: tetra-1-naphthyl-taddol, **1b**: cyclohexylidene-taddol, TBS = *tert*-butyldimethylsilyl.

Through a brief study, where nearly a dozen readily prepared taddol catalysts were screened, it was determined that the cyclohexylidene-taddol derivative **1b** gave the best combination of diastereo- and enantioselectivity for the aldol reaction of **2** with benzaldehyde. Catalysts bearing various alkyl- and alkoxy-substituted phenyl rings gave products with diminished d.r. and *ee* values. The selectivities increased significantly when the reaction was carried out at −78°C. Optimal conditions for the reaction of **2** with benzaldehyde were realized using 10 mol% of **1b** and 2 equivalents of benzaldehyde in toluene at −78°C for 2 days, which gave **3a** in 94% yield with a 15:1 *syn*:*anti* ratio and 98% *ee* for the major diastereomer (84% *ee* minor diastereomer).

The scope of the Mukaiyama aldol reaction of **2** with a range of aldehydes was examined under optimized conditions using taddol **1b** as the catalyst (Table 1). Examination of the results shows that the aldol products are generally formed in good yields with high to excellent diastereo- and enantioselectivities. For the sake of consistency, most of the reactions were performed for 2 days, although comparable results were obtained with shorter reaction times: quenching the reactions after 16 and 20 h gave the expected products in good yield and high selectivity (Table 1, entries 2 and 5). The reaction of **2** with *para*-substituted aromatic aldehydes possessing either electron-withdrawing or weakly electron-donating functionalities in the presence of **1b** gave superior results (Table 1, entries 3–6). Substrates containing a strong electron-donating group *para* to the aldehyde were found to be less reactive. For example, the reaction of *p*-anisaldehyde proceeded sluggishly at −78°C. At higher temperature (−40°C), the reaction progressed to afford **3i** in modest yield (47%), but with lower d.r. and *ee* values (Table 1, entry 10). *Meta* substitution is tolerated well and affords products in reasonable diastereoselectivity and with high *ee* values (Table 1, entries 7, 8 and 11). Substrates with a substituent *ortho* to the aldehyde, such as *o*-anisaldehyde and 1-naphthaldehyde (Table 1, entries 12 and 13), gave diminished diastereoselectivity, although still with high enantioselectivity. Heteroaromatic aldehydes are also good Mukaiyama aldol partners, as demonstrated by the reaction of 2-thiophenecarboxaldehyde (Table 1, entry 15). Although we have not fully explored the taddol-catalyzed aldol reactions of aliphatic aldehydes, a preliminary study

Table 1: Asymmetric Mukaiyama aldol reaction catalyzed by a taddol derivative.[a]

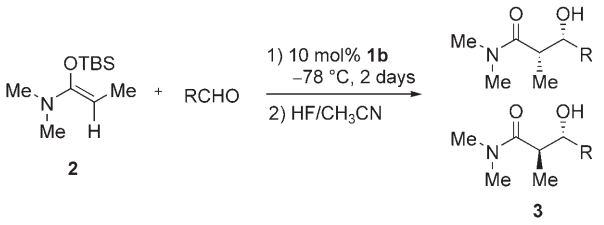

Entry	Product	R	Yield [%][b]	d.r.[c]	*ee syn* [%](*anti*)[d]
1	**3a**[e]	Ph	94	15:1	98 (84)
2	**3a**[f]	Ph	88	14:1	98
3	**3b**	4-(NO_2)-C_6H_4	93	13:1	94 (82)
4	**3c**	4-Cl-C_6H_4	86	20:1	97
5[g]	**3d**	4-(CF_3)-C_6H_4	84	>25:1	96
6	**3e**	4-(CH_3)-C_6H_4	77	16:1	97
7	**3f**	3-(CH_3)-C_6H_4	77	9:1	96 (73)
8	**3g**	3-Br-C_6H_4	84	9:1	95 (67)
9	**3h**	3,4-$(Cl)_2$-C_6H_3	71	9:1	94 (58)
10	**3i**	4-(MeO)-C_6H_4[h]	47	5:1	87 (72)
11	**3j**	3-(MeO)-C_6H_4	81	13:1	97
12	**3k**	2-(MeO)-C_6H_4	50	8:1	91 (58)
13	**3l**	1-naphthyl	80	2:1	90 (86)
14	**3m**	2-naphthyl	50	10:1	97
15	**3n**	2-thiophene	88	10:1	95 (48)
16	**3o**	*n*-propyl	47	9:1	91

[a] Reactions were performed using 1 equiv ketene acetal **2**, 2 equiv aldehyde, and 0.1 equiv catalyst **1b** in 0.5 mL of toluene for 2 days in an argon atmosphere. Following workup with 5 mmol aq HF, the products were isolated by flash column chromatography on silica gel. [b] Yield of isolated product. [c] Determined by ^{1}H NMR analysis of the crude reaction mixture prior to separation by column chromatography. [d] Determined by chiral HPLC analysis. [e] 1*S*,2*S* absolute configuration.[11] [f] Reaction time was 16 h. [g] Reaction time was 20 h. [h] Reaction run at −40°C for 2 days.

 © 2006 Wiley-VCH Verlag GmbH & Co. KGaA, Weinheim

with butyraldehyde showed that the reaction proceeded with good diastereoselectivity and high enantioselectivity (Table 1, entry 16).

To render the above method more broadly applicable to the synthesis of complex molecules, we examined methods for the transformation of the amide functionality into an aldehyde group. Provided this conversion could be accomplished without eroding the high diastereo- and enantioselectivities, then the outcome would correspond to the products of crossed-aldol reactions of aldehydes. After a brief examination of aluminum-based reducing agents,[12] we directed out attention to the use of Schwartz's reagent. Georg and co-workers showed previously the direct reduction of achiral *N,N*-dialkylamides to the corresponding aldehydes using this reagent.[13] Subjecting amide **4a** to the conditions reported by Georg and co-workers produced the desired aldehyde product, but with considerable diminution in the diastereomeric ratio. This erosion in diastereoselectivity can be understood by considering the suggested mechanism for the reduction, wherein the proposed iminium intermediate can isomerize to an enamine, with loss of stereochemistry at the carbon atom α to the carbonyl group. Consistent with this rationale is the observation that the diastereoselectivity decreases with longer reaction times. Examination of the reaction parameters showed that the reduction proceeded rapidly in CH_2Cl_2 and gave the desired aldol product in high yield. Under optimized conditions (using three equivalents of Schwartz's reagent in CH_2Cl_2) the amide aldol products **4** were converted into the corresponding chiral aldehydes **5** in high yields with limited or no epimerization of the α stereocenter (Scheme 2).

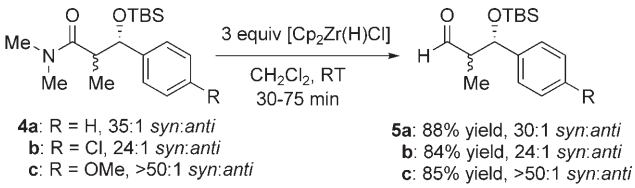

4a: R = H, 35:1 *syn:anti*
b: R = Cl, 24:1 *syn:anti*
c: R = OMe, >50:1 *syn:anti*

5a: 88% yield, 30:1 *syn:anti*
b: 84% yield, 24:1 *syn:anti*
c: 85% yield, >50:1 *syn:anti*

Scheme 2. Reduction of chiral amides to aldehydes under mild conditions. Cp = cyclopentadienyl

The high enantioselectivity observed in the above reactions implies the intermediacy of a highly ordered transition state, generated by hydrogen bonding between the chiral diol and the aldehyde. In our study of taddol-catalyzed Diels–Alder reactions, we presented a hypothesis based on the X-ray structures of uncomplexed taddols to rationalize the observed enantioselectivities.[2b,14a] We have now succeeded in obtaining the first crystal structure of a complex between a taddol (racemic **1a**) and an aldehyde (Figure 1).[14b] The X-ray structure clearly supports some of the basic tenets of our hypothesis by showing the presence of an intramolecular hydrogen bond between the two hydroxy groups of the catalyst and an intermolecular hydrogen bond to the carbonyl oxygen atom of *p*-anisaldehyde. This complex is consistent with the suggested mode of activation of the carbonyl group through a single-point hydrogen bond to a preorganized

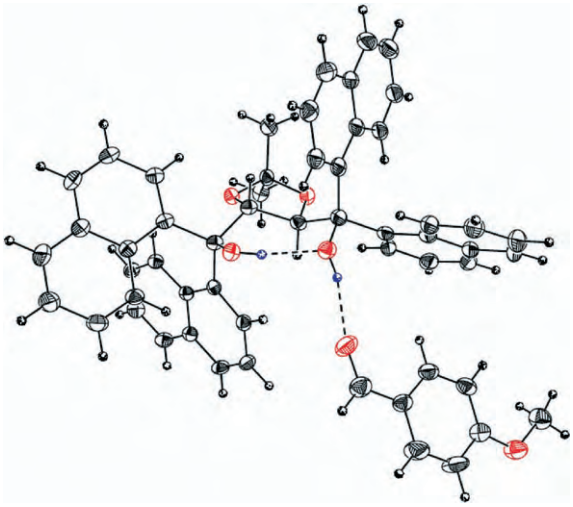

Figure 1. X-ray structure of the complex formed between the catalyst *rac*-**1a** and *p*-anisaldehyde. Red = oxygen atom, blue = hydrogen atom involved in hydrogen bonding.

catalyst. Since hydrogen bonding is a subset of the Lewis acid type of interaction, the present mode of activation represents a form of Lewis acid assisted Lewis acid catalysis.[1c]

In this report, we have described the catalysis of highly diastereo- and enantioselective Mukaiyama aldol reactions of *O*-silyl-*N,O*-ketene acetals mediated solely through activation by hydrogen bonding. The catalyzed reaction was effective for a range of aldehydes, and gave products in synthetically useful yields and selectivities. The mild conversion of the amide aldol products into the corresponding aldehydes using Schwartz's reagent, with little or no erosion in diastereoselectivity, renders this reaction useful for further synthetic applications. The crystal structure of the taddol–aldehyde complex clearly shows coordination of the aldehyde carbonyl group through a single-point hydrogen-bonding interaction. This mode of activation is likely critical for the Mukaiyama aldol reaction presented here as well as for the cycloaddition reactions that we reported previously. [2]

A desired characteristic of any highly useful catalyst is the capacity to effect a broad range of reactions. The results presented herein when taken in conjunction with our previous studies shows that taddol may well be considered a "privileged" scaffold for asymmetric catalysis mediated by hydrogen bonding.[15,16] Further investigation of taddol ligands as chiral hydrogen-bond donors should provide exciting new developments in asymmetric catalysis.

Received: April 25, 2006
Revised: June 28, 2006
Published online: August 14, 2006

Keywords: asymmetric catalysis · enantioselectivity · hydrogen bonds · Mukaiyama aldol · organocatalysis

[1] For reviews, see: a) P. M. Pihko, *Angew. Chem.* **2004**, *116*, 2110–2113; *Angew. Chem. Int. Ed.* **2004**, *43*, 2062–2064; b) P. I. Dalko,

 © 2006 Wiley-VCH Verlag GmbH & Co. KGaA, Weinheim

L. Moisan, *Angew. Chem.* **2004**, *116*, 5248 – 5286; *Angew. Chem. Int. Ed.* **2004**, *43*, 5138 – 5175; c) H. Yamamoto, K. Futatsugi, *Angew. Chem.* **2005**, *117*, 1958 – 1977; *Angew. Chem. Int. Ed.* **2005**, *44*, 1924 – 1942; d) M. S. Taylor, E. N. Jacobsen, *Angew. Chem.* **2006**, *118*, 1550 – 1573; *Angew. Chem. Int. Ed.* **2006**, *45*, 1520 – 1543; e) for examples of antibody- and enzyme-catalyzed reactions, see: T. D. Machajewski, C.-H. Wong, *Angew. Chem.* **2000**, *112*, 1406 – 1430; *Angew. Chem. Int. Ed.* **2000**, *39*, 1352 – 1374.

[2] For earlier work from our research group on asymmetric reactions of carbonyl electrophiles catalyzed by hydrogen bonding, see: a) Y. Huang, A. K. Unni, A. N. Thadani, V. H. Rawal, *Nature* **2003**, *424*, 146; b) A. N. Thadani, A. R. Stankovic, V. H. Rawal, *Proc. Natl. Acad. Sci. USA* **2004**, *101*, 5846 – 5850; c) A. K. Unni, N. Takenaka, H. Yamamoto, V. H. Rawal, *J. Am. Chem. Soc.* **2005**, *127*, 1336 – 1337; d) V. B. Gondi, M. Gravel, V. H. Rawal, *Org. Lett.* **2005**, *7*, 5657 – 5660.

[3] For other examples of highly enantioselective asymmetric reactions of carbonyl electrophiles catalyzed by hydrogen bonding, see: a) N. T. McDougal, S. E. Schaus, *J. Am. Chem. Soc.* **2003**, *125*, 12094 – 12095; b) N. Momiyama, H. Yamamoto, *J. Am. Chem. Soc.* **2005**, *127*, 1080 – 1081; c) Y. Hoashi, T. Okino, Y. Takemoto, *Angew. Chem.* **2005**, *117*, 4100 – 4103; *Angew. Chem. Int. Ed.* **2005**, *44*, 4032 – 4035; d) S. Rajaram, M. S. Sigman, *Org. Lett.* **2005**, *7*, 5473 – 5475; e) T. Tonoi, K. Mikami, *Tetrahedron Lett.* **2005**, *46*, 6355 – 6358; f) H. Du, D. Zhao, K. Ding, *Chem. Eur. J.* **2004**, *10*, 5964 – 5970.

[4] For examples of asymmetric reactions of imines catalyzed by hydrogen bonding, see: a) M. S. Sigman, P. Vachal, E. N. Jacobsen, *Angew. Chem.* 2000, 112, 1336 – 1338; *Angew. Chem. Int. Ed.* **2000**, *39*, 1279 – 1281; b) A. G. Wenzel, E. N. Jacobsen, *J. Am. Chem. Soc.* **2002**, *124*, 12964 – 12965; c) T. Akiyama, J. Itoh, K. Yokota, K. Fuchibe, *Angew. Chem.* **2004**, *116*, 1592 – 1594; *Angew. Chem. Int. Ed.* **2004**, *43*, 1566 – 1568; d) B. M. Nugent, R. A. Yoder, J. N. Johnston, *J. Am. Chem. Soc.* **2004**, *126*, 3418 – 3419; e) D. Uraguchi, M. Terada, *J. Am. Chem. Soc.* **2004**, *126*, 5356 – 5357.

[5] W. Zhuang, T. B. Poulsen, K. A. Jørgensen, *Org. Biomol. Chem.* **2005**, *3*, 3284 – 3289.

[6] a) M. T. Davies-Coleman, M. J. Garson, *Nat. Prod. Rep.* **1998**, *15*, 477 – 493; b) I. Paterson, C. J. Cowden, D. J. Wallace in *Modern Carbonyl Chemistry* (Ed.: J. Otera), Wiley-VCH, Weinheim, **2000**, pp. 249 – 297.

[7] a) S. G. Nelson, *Tetrahedron: Asymmetry* **1998**, *9*, 357 – 389; b) E. M. Carreira in *Comprehensive Asymmetric Catalysis, Vol. 3* (Eds.: E. N. Jacobsen, A. Pfaltz, H. Yamamoto), Springer, Berlin, **1999**, pp. 997 – 1065; c) E. M. Carreira in *Modern Carbonyl Chemistry* (Ed.: J. Otera), Wiley-VCH, Weinheim, **2000**, pp. 227 – 248; d) K. Ishihara, H. Yamamoto in *Modern Aldol Reactions, Vol. 2* (Ed.: R. Mahrwald), Wiley-VCH, Weinheim, **2004**, pp. 25 – 68; e) C. Palomo, M. Oiarbide, J. M. Garcia, *Chem. Soc. Rev.* **2004**, *33*, 65 – 75.

[8] For examples of aldol reactions catalyzed by Lewis basic phosphoramides, see: a) S. E. Denmark, R. A. Stavenger, *Acc. Chem. Res.* **2000**, *33*, 432 – 440; b) S. E. Denmark, S. M. Pham, *Org. Lett.* **2001**, *3*, 2201 – 2204; c) S. E. Denmark, J. R. Heemstra, Jr., G. L. Beutner, *Angew. Chem.* **2005**, *117*, 4760 – 4777; *Angew. Chem. Int. Ed.* **2005**, *44*, 4682 – 4698.

[9] For a vinylogous Mukaiyama aldol (VMA) reaction promoted by hydrogen bonding, see Ref. [2d].

[10] A. G. Myers, K. L. Widdowson, *J. Am. Chem. Soc.* **1990**, *112*, 9672 – 9674.

[11] The absolute configuration of **3a** was determined by chemical correlation ($LiEt_3BH$ then TBAF) to (1S,2R)-1-phenyl-2-methylpropane-1,3-diol. For preparation of the diol, see: S. G. Davies, A. A. Mortlock, *Tetrahedron: Asymmetry* **1991**, *2*, 1001 – 1004.

[12] For examples of reduction of chiral amides to aldehydes, see: a) D. A. Evans, M. DiMare, *J. Am. Chem. Soc.* **1986**, *108*, 2476 – 2478; b) J. C. Barrish, H. L. Lee, E. G. Baggiolini, M. R. Uskoković, *J. Org. Chem.* **1987**, *52*, 1372 – 1375; c) A. Hinman, J. Du Bois, *J. Am. Chem. Soc.* **2003**, *125*, 11510 – 11511.

[13] J. M. White, A. R. Tunoori, G. I. Georg, *J. Am. Chem. Soc.* **2000**, *122*, 11995 – 11996.

[14] Several taddol-ketone complexes have been reported, see:a) K. Tanaka, F. Toda, *Chem. Rev.* **2001**, *100*, 1025 – 1074; b) Crystal Data for **1a**-anisaldehyde: $C_{63}H_{54}O_8$, $M_r = 939.06$, clear crystal, $a = 19.792(5)$, $b = 13.665(3)$, $c = 17.750(4)°$, $V = 4800.5(19)$ Å^3, $T = 100(2)$ K, space group $P21/c$, $Z = 4$, $\rho_{calcd} = 1.299$ g cm^{-3}, $\mu = 0.71073$ mm^{-1}. CCDC-604557 contains the supplementary crystallographic data for this paper. These data can be obtained free of charge from The Cambridge Crystallographic Data Centre under www.ccdc.cam.ac.uk/data_request/cif.

[15] T. P. Yoon, E. N. Jacobsen, *Science* **2003**, *299*, 1691 – 1693.

[16] Taddol has already been established as a "privileged" ligand for metal-catalyzed asymmetric reactions. See: D. Seebach, A. K. Beck, A. Heckel, *Angew. Chem.* **2001**, *113*, 96 – 142; *Angew. Chem. Int. Ed.* **2001**, *40*, 92 – 138.

 © 2006 Wiley-VCH Verlag GmbH & Co. KGaA, Weinheim

Directed Evolution

DOI: 10.1002/anie.200601217

A Population of Thermostable Reverse Transcriptases Evolved from *Thermus aquaticus* DNA Polymerase I by Phage Display**

*Sophie Vichier-Guerre, Stéphane Ferris, Nicolas Auberger, Karim Mahiddine, and Jean-Luc Jestin**

Nucleic acid replicases are unique catalysts as they do not only catalyze conversion of substrates into products, but also amplify the substrate. For DNA polymerase to be an active enzyme that catalyses phosphodiester bond formation, magnesium dications are necessary. Substitution by manganese

[*] Dr. S. Vichier-Guerre, S. Ferris, N. Auberger, K. Mahiddine, Dr. J.-L. Jestin
Unité de Chimie Organique URA 2128 CNRS
Département de Biologie Structurale et Chimie
Institut Pasteur
28 rue du Dr. Roux, 75724 Paris 15 (France)
Fax: (+33) 145-688-404
E-mail: jjestin@pasteur.fr

[**] We thank F. Bahrami, M. Delarue, P. A. Kaminski, and S. Wain-Hobson for critical comments on the manuscript, T. Huynh-Dinh and P. E. Bost for advice, and C. Gouyette, O. Helynck, and V. Huteau for technical help. This work was supported by the Ministère de la Recherche (ACI blanche), the CNRS (Programme Physique et Chimie du Vivant), and the Pasteur–Weizmann Foundation.

Supporting information for this article is available on the WWW under http://www.angewandte.org or from the author.

© 2006 Wiley-VCH Verlag GmbH & Co. KGaA, Weinheim

dications or addition of manganese ions to magnesium cations is known to broaden the enzyme substrate specificity: DNA polymerases then incorporate ribonucleotides or dideoxynucleotides.[1] Enlarged enzyme specificity has also been reported for template DNA analogues, such as RNA, threose nucleic acids (TNA), and hexitol nucleic acids (HNA).[2] Reverse transcription by *Thermus aquaticus* DNA polymerase I depends on the presence of manganese ions,[3] which are known to alter fidelity. Furthermore, site-directed mutagenesis has been used for the study of polymerase mutants and for the design of DNA polymerase variants with improved incorporation of deoxynucleotide analogues.[4] So far, directed DNA polymerase evolution experiments focused largely on the alteration of nucleotide triphosphate specificity.[5] To gain an insight into the amino acid side chains that can be mutated to change the template specificity of DNA polymerases, a directed-evolution experiment of the Stoffel fragment of *Thermus aquaticus* DNA polymerase I towards thermostable reverse transcriptases (RTs) was carried out. The process started from a large library of polymerase variants displayed on the surface of filamentous bacteriophages (*Inovirus*).

For the construction of library I (6×10^6 clones), mutations within the polymerase domain including the conserved motifs A, B, and C were introduced by polymerase chain reaction (PCR) mutagenesis in the presence of manganese ions.[6,7] To construct library II, the oligonucleotides assembled by PCR were degenerate at positions corresponding to eleven amino acids (483, 486, 539, 545, 547, 548, 570, 575, 578, 736, and 739) in *T. aquaticus* DNA polymerase I. The amino acids with homologous positions in T7 DNA polymerase are known to interact with the template strand.[8] A bias towards the hydrophilic and neutral amino acids, namely glutamine, asparagine, serine, and threonine, was introduced. A library of about 1.1×10^7 mutant polymerases displayed on phage resulted from the combination of libraries I and II.

For the isolation of rare thermostable RTs that are active in the presence of magnesium ions only as dications, we adapted an in vitro selection that we had previously established for the isolation of DNA-dependent DNA polymerases and their genes according to their catalytic activity.[9] Briefly, the selection consists of substrate coupling to phage proteins and the isolation of labeled reaction products by affinity chromatography (Figure 1). High enrichment factors of more than 10^3 were found and were similar to those measured for selections in vitro of proteins according to their affinity for an antigen.[10] It was further shown that the selection for DNA-dependent DNA polymerase activity allows the isolation of very rare polymerases on-phage even among a 10^8-fold excess of an other phage.[11] This method to enrich populations of proteins into catalysts was then considered to be efficient enough for use in a directed-enzyme-evolution experiment. DNA primers modified at their 5′ end by a maleimidyl group were coupled to the phage polymerase mutant library, hybridised to a template RNA, and reacted with deoxynucleotide triphosphates whose uridine was labeled by a biotin group. Selection of active polymerases and their genes was then performed by affinity chromatography for biotin. Cycles of phage–polymerase selection for RT activity, of amplification of the corresponding genes, and of phage preparation were iterated (Figure 2). The increasing activity of the phage population with the cycles showed that the in vitro selection of polymerases is also a selection of proteins according to their catalytic turnover: the higher the catalytic turnover, the higher the number of products bound to the phage, and the higher the avidity of the phage particle for the solid phase used for affinity chromatography. Between cycles five and six, the RT activity of the population of phage polymerase variants did not improve significantly (Figure 2); we therefore decided to stop the directed-enzyme-evolution experiment after the sixth cycle.

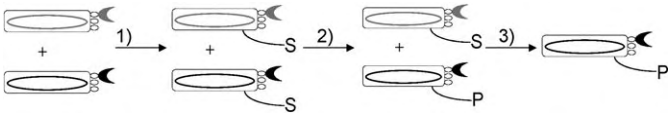

Figure 1. Principle for the isolation of active enzymes and their genes by phage display. Active and inactive enzymes are represented as black and gray, respectively. Each variant enzyme is expressed on the surface of a phage particle that contains the corresponding gene that can be amplified and sequenced to characterize the displayed enzyme. The in vitro selection of catalysts consists of three steps: 1) the cross-linking of substrate (S) to the phage particle; 2) the intramolecular conversion of the substrate into product (P); and 3) the affinity chromatography for the product. Selection cycles are iterated to reduce the background of the selection and thereby to enrich the population of the mutant enzymes into catalysts.

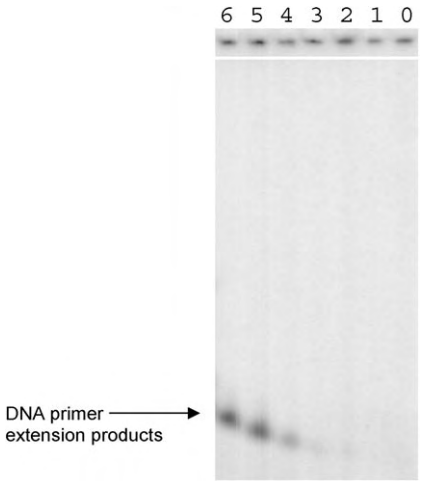

Figure 2. RT activity of the selected phage-variant populations. Column 0 highlights the RT activity of the initial library of more than 10^7 variants (not detectable). Column 6 shows the RT activity of the polyclonal phage–polymerase population after the sixth selection cycle. RT activity was detected by using a DNA-primer extension assay: DNA primer 13 hybridized to RNA template 12 was extended with radioactively labeled α^{32}P-deoxythymidine triphosphate (dTTP) by 10^8 phage–polymerases; electrophoresis of the products on a 20% polyacrylamide gel was followed by detection of the extended primers by using a Phosphorimager screen (see the Supporting Information).

To characterize the selected population of catalysts after the sixth selection cycle, 116 polymerase variants were isolated and sequenced. Twenty eight variants were reported

 © 2006 Wiley-VCH Verlag GmbH & Co. KGaA, Weinheim

Table 1: Variants and their mutations associated with the catalytic activity shift from DNA- to RNA-dependent DNA polymerization.

Mutations[a]	Variant	Abundance[b]	Phage RT activity[c]
L552H, T509S, M779K	**1**	1	0.3
L552P, A661T, A800V, **E820K**	**2**	2	0.2
A608V	**3**	1	0.1
A608V, I553F, **F749S**	**4**	2	0.4
A608T, E520G, **W827R**	**5**	1	1.4
S612N, **P816S**	**6**	6	0.5
S612N, N483Q, S486Q, T539N, Y545Q, D547T, P548Q, A570Q, D578Q, A597T W604R, V730L, R736Q, S739N, **M747R**	**7**	3	1.0
Y696N	**8**	1	0.2
Y696C	**9**	2	0.3
Y696C, K767E	**10**	1	0.3
Y696C, E530G, A803V	**11**	1	0.4
M747R	**12**	3	1.0
M747K	**13**	1	1.3
M747K, E742K	**14**	1	5.5
M747K, Q698L, **P816L**	**15**	1	0.7
m747K, V586I, I638F, G776E	**16**	11	1.8
F749Y, A568V	**17**	4	0.4
F749Y, P550Q, R556S, V740E, V819A	**18**	3	0.7
F749Y, F482L, T664A, P770T, M775T	**19**	1	0.3
M761V	**20**	4	0.5
M761T, D547G, I584V	**21**	34	1
E820K, I599N, L780P	**22**	1	0.2
W827R	**23**	7	0.7
W827R, H480R	**24**	1	0.4
W827R, A517V, T664S, F769S	**25**	2	0.7
D551G, V783I	**26**	1	0.3
Q534R, A764T	**27**	1	0.5
R651Q	**28**	1	0.2

[a] Mutations are indicated by their amino acid position within *T. aquaticus* DNA-polymerase I and are noted in bold if the mutated position occurred at least twice in distinct variants. [b] The abundance of each variant within a sample of the selected population after the sixth selection cycle is indicated. [c] The RT activity of the phage–polymerase variants is given as quantities of products formed relative to those of the most abundant variant that is, **21**. This activity assay made use of RNA template 31 (X = A) hybridized to DNA primer 32 that was extended by radioactively labeled α^{32}P-dTTP. Reaction products were separated by electrophoresis on a 20% polyacrylamide gel for detection of extended primers on a Phosphorimager screen prior to quantification using the Imagequant software.

with their population-sample abundances and relative RT activity (Table 1). The most abundant clone after the sixth cycle (variant **21**) represented about one third of the clones in the population sample. Among the 27 other distinct variants, 15 were represented by a single clone, thereby highlighting the diversity of the selected population. Variant **7** was the only variant derived from library II, which was obtained by PCR assembly of degenerate oligonucleotides: 10 non-neutral mutations occurred at targeted amino acid positions and five mutations were introduced during the PCR assembly and amplification. The other 27 variants with RT activity had, on average, 2.4 mutations. The mutations E742K, M747K, and E820K could be structurally interpreted in terms of salt-bridge formation with negatively charged template phosphodiester groups located close to the amino acids 742 and 747 or with the nucleotide's triphosphate group close to amino acid 820 (Figure 3). Interestingly, amino acids 608 and 612, which were mutated in several variants, surround in a beta strand the aspartate 610 known to bind a magnesium ion at the polymerase active site (compare 2KTQ and 1LV5 structures in the protein databank (PDB))[12] The Stoffel fragment, the most-abundant polymerase **21**, and two of the most-active variants **5** and **14** were then expressed in *E. coli* and purified by two affinity-chromatography steps for kinetic characterization (Table 2). For the reverse-transcription reaction, the most-abundant polymerase **21** had an almost tenfold improved catalytic efficiency as measured by the k_{cat}/K_m ratio when compared with the Stoffel fragment. Variant **5** had rate constants k_{cat} of about two orders of magnitude larger than those of the Stoffel fragment. Remarkably, variants **5** and **14** had catalytic efficiencies for DNA-dependent DNA polymerization that were similar or higher than those of the wild-type Stoffel fragment even though no selection for the wild-type activity was applied during the experimental evolution. Our directed-polymerase-evolution experiment yielded variants endowed with two catalytic activities, namely RNA-dependent DNA polymerization (EC 2.7.7.49), and DNA-dependent DNA polymerization (EC 2.7.7.7). To further estimate the fidelity during reverse transcription, the variants **5**, **14**, and **21** were then used to copy a part of messenger RNA (mRNA) into complementary DNA (cDNA) prior to subcloning for sequencing of reverse transcription products. The sequences showed that selected variants could polymerize more than 300 nucleotides and were not limited to the addition of single nucleotides at the 3′ end of DNA primers. The substitution rates per base for RNA-dependent DNA polymerization of the most active variants, **5** (1.5×10^{-3}) and **14** (2.2×10^{-3}), were found to be similar or lower than that of avian myeloblastosis virus (AMV) RT (2.2×10^{-3}), which was used as a standard. Interestingly, the most abundant variant **21** (2.3×10^{-4}) had a fidelity which was about 10-times higher than that of AMV RT.

Enzymes generally evolved to have finely tuned substrate specificities. This directed-enzyme-evolution experiment allowed the identification of mutations associated with a broadened template specificity for DNA polymerase. The catalytic efficiency of a selected variant was improved by about two orders of magnitude for reverse transcription when compared with the Stoffel fragment of Taq DNA polymerase. Some of these engineered and thermostable DNA polymerases, which can copy RNA as well as DNA with high

 © 2006 Wiley-VCH Verlag GmbH & Co. KGaA, Weinheim

Table 2: Kinetic parameters of the DNA- and RNA-dependent DNA polymerization reactions.[a]

		DNA.DNAP				RNA.DNAP			
		Stoffel fragment	Variant **21**	Variant **5**	Variant **14**	Stoffel fragment	Variant **21**	Variant **5**	Variant **14**
k_{cat} [s^{-1}]	dATP	$9.6\ (0.6)\times10^{-2}$	$2.8\ (0.2)\times10^{-2}$	$6.5\ (0.3)\times10^{-1}$	$2.0\ (0.1)\times10^{-1}$	$1.7\ (0.1)\times10^{-2}$	$7.5\ (0.7)\times10^{-2}$	3.3 (0.2)	1.4 (0.1)
	dCTP	$1.3\ (0.6)\times10^{-1}$	$1.7\ (0.2)\times10^{-2}$	$3.1\ (0.3)\times10^{-1}$	$2.8\ (0.2)\times10^{-1}$	$6.0\ (0.4)\times10^{-2}$	$9.3\ (1.0)\times10^{-2}$	2.2 (0.2)	$8.5\ (1.0)\times10^{-1}$
	dTTP	$1.2\ (0.1)\times10^{-1}$	$1.2\ (0.1)\times10^{-2}$	$2.8\ (0.1)\times10^{-1}$	$1.8\ (0.1)\times10^{-1}$	$1.0\ (0.1)\times10^{-2}$	$8.5\ (0.6)\times10^{-2}$	2.6 (0.6)	$9.7\ (1.6)\times10^{-1}$
K_m [μM]	dATP	3.0 (1.0)	45 (16)	5.7 (1.1)	2.7 (0.4)	60 (15)	33 (7)	292 (48)	86 (20)
	dCTP	6.1 (1.2)	33 (22)	8.5 (2.7)	3.4 (1.0)	177 (31)	31 (6)	344 (61)	72 (37)
	dTTP	5.2 (1.9)	22 (10)	7.9 (1.6)	10 (2)	77 (34)	63 (7)	240 (83)	250 (112)
k_{cat}/K_m [$L\,mol^{-1}\,s^{-1}$]	dATP	3.1×10^4	6.1×10^2	1.1×10^5	7.4×10^4	2.9×10^2	2.2×10^3	1.1×10^4	1.6×10^4
	dCTP	2.3×10^4	5.3×10^2	3.6×10^4	8.2×10^4	3.4×10^2	3.0×10^3	6.4×10^3	1.2×10^4
	dTTP	2.3×10^4	5.6×10^2	3.6×10^4	1.8×10^4	1.5×10^2	1.3×10^3	1.1×10^4	3.9×10^3

[a] Reactions performed at 37°C for the three polymerase variants **5**, **14** and **21** and for the Stoffel fragment of *T. aquaticus* DNA-polymerase I. The polymerases were overexpressed in *E. coli* and purified by two-step affinity chromatography. The single-turnover kinetic experiments at the steady state made use of 5′ ^{32}P labeled DNA primer 32 and of the template RNA 31 (X = A, U or G) or of the template DNA 30 (X = A, T or G). The labeled substrates and products were separated, detected, and quantified as indicated in Table 1. DNAP = DNA polymerization.

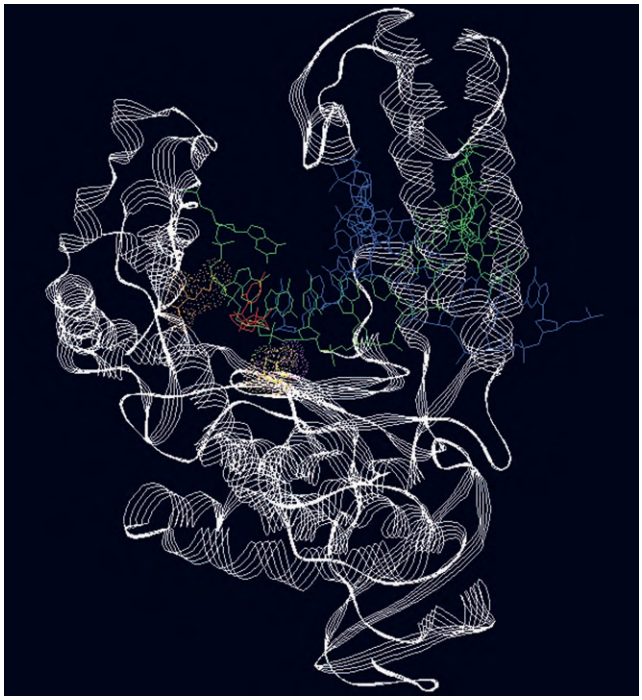

Figure 3. Structure of the Stoffel fragment of *Thermus aquaticus* DNA polymerase I (2KTQ) plotted by using Swiss PdbViewer. The polymerase (white) is in a complex with dideoxycytidine triphosphate (red) and a DNA template (green) that is hybridized to a DNA primer (blue). The amino acids M747 (orange), E820 (yellow) and D610 (purple) are highlighted.

fidelity, may find applications in the field of diagnostics for the detection of rare RNAs by reverse transcription-PCR.

Received: March 28, 2006
Revised: May 29, 2006
Published online: July 12, 2006

Keywords: directed evolution · DNA structures · enzyme catalysis · enzymes · selection

[1] a) J. H. Van de Sande, P. C. Loewen, H. G. Khorana, *J. Biol. Chem.* **1972**, *247*, 6140–6148; b) S. Tabor, C. C. Richardson, *Proc. Natl. Acad. Sci. USA* **1989**, *86*, 4076–4080; c) S. Tabor, C. C. Richardson, *Proc. Natl. Acad. Sci. USA* **1995**, *92*, 6339–6343.

[2] a) J. C. Chaput, J. K. Ichida, J. W. Szostak, *J. Am. Chem. Soc.* **2003**, *125*, 856–857; b) S. Pochet, P. A. Kaminski, A. Van Aerschot, P. Herdewijn, P. Marliere, *C. R. Biol.* **2003**, *326*, 1175–1184; c) H. Shandilya, K. Griffiths, E. K. Flynn, M. Astatke, P. J. Shih, J. E. Lee, G. F. Gerard, M. D. Gibbs, P. L. Bergquist, *Extremophiles* **2004**, *8*, 243–251.

[3] V. I. Grabko, L. G. Chistyakova, V. N. Lyapustin, V. G. Korobko, A. I. Miroshnikov, *FEBS Lett.* **1996**, *387*, 189–192.

[4] a) R. Sousa, R. Padilla, *EMBO J.* **1995**, *14*, 4609–4621; b) D. T. Minnick, M. Astatke, C. M. Joyce, T. A. Kunkel, *J. Biol. Chem.* **1996**, *271*, 24954–24961; c) A. Tosaka, M. Ogawa, S. Yoshida, M. Suzuki, *J. Biol. Chem.* **2001**, *276*, 27562–27567; d) M. Astatke, K. Ng, N. D. Grindley, C. M. Joyce, *Proc. Natl. Acad. Sci. USA* **1998**, *95*, 3402–3407; e) M. Ogawa, A. Tosaka, Y. Ito, S. Yoshida, M. Suzuki, *Mut. Res. DNA Repair* **2001**, *485*, 197–207; f) Y. Li, V. Mitaxov, G. Waksman, *Proc. Natl. Acad. Sci. USA* **1999**, *96*, 9491–9496.

[5] a) S. Brakmann, *ChemBioChem* **2001**, *2*, 212–219; b) A. Shinkai, P. H. Patel, L. A. Loeb, *J. Biol. Chem.* **2001**, *276*, 18836–18842; c) G. Xia, L. Chen, T. Sera, M. Fa, P. G. Schultz, F. E. Romesberg, *Proc. Natl. Acad. Sci. USA* **2002**, *99*, 6597–6602; d) M. Fa, A. Radeghieri, A. A. Henry, F. E. Romesberg, *J. Am. Chem. Soc.* **2004**, *126*, 1748–1754; e) F. J. Ghadessy, N. Ramsay, F. Boudsocq, D. Loakes, A. Brown, S. Iwai, A. Vaisman, R. Woodgate, P. Holliger, *Nat. Biotechnol.* **2004**, *22*, 755–759; f) J. Chelliserrykattil, A. D. Ellington, *Nat. Biotechnol.* **2004**, *22*, 1155–1160; g) S. Brakmann, *Cell. Mol. Life Sci.* **2005**, *62*, 2634–2646; h) R. C. Holmberg, A. A. Henry, F. E. Romesberg, *Biomol. Eng.* **2005**, *22*, 39–49; i) D. Summerer, N. Z. Rudinger, I. Detmer, A. Marx, *Angew. Chem.* **2005**, *117*, 4791–4794; *Angew. Chem. Int. Ed.* **2005**, *44*, 4712–4715.

[6] M. Fromant, S. Blanquet, P. Plateau, *Anal. Biochem.* **1995**, *224*, 347–353.

[7] R. C. Cadwell, G. F. Joyce, *PCR Methods Appl.* **1994**, *3*, 136–140.

[8] S. Doublié, S. Tabor, A. M. Long, C. C. Richardson, T. Ellenberger, *Nature* **1998**, *391*, 251–258.

[9] J. L. Jestin, P. Kristensen, G. Winter, *Angew. Chem.* **1999**, *111*, 1196–1200; *Angew. Chem. Int. Ed.* **1999**, *38*, 1124–1127.

 © 2006 Wiley-VCH Verlag GmbH & Co. KGaA, Weinheim

[10] a) E. Orsi, J. L. Jestin, *C. R. Chim.* **2003**, *6*, 501 – 506; b) J. D. Marks, H. R. Hoogenboom, A. D. Griffiths, G. Winter, *J. Biol. Chem.* **1992**, *267*, 16007 – 16010.
[11] S. Vichier-Guerre, J. L. Jestin, *Biocatal. Biotransform.* **2003**, *21*, 75 – 78.
[12] a) Y. Li, S. Korolev, G. Waksman, *EMBO J.* **1998**, *17*, 7514 – 7525; b) S. J. Johnson, J. S. Taylor, L. S. Beese, *Proc. Natl. Acad. Sci. USA* **2003**, *100*, 3895 – 3900.
[13] F. C. Lawyer, S. Stoffel, R. K. Saiki, K. Myambo, R. Drummond, D. H. Gelfand, *J. Biol. Chem.* **1989**, *264*, 6427 – 6437.
[14] H. Strobel, D. Ladant, J. L. Jestin, *Mol. Biotechnol.* **2003**, *24*, 1 – 9.
[15] P. Kristensen, G. Winter, *Folding Des.* **1998**, *3*, 321 – 328.
[16] S. Creighton, L. B. Bloom, M. F. Goodman, *Methods Enzymol.* **1995**, *262*, 232 – 256.

 © 2006 Wiley-VCH Verlag GmbH & Co. KGaA, Weinheim

Photoinduced Electron Transfer

DOI: 10.1002/anie.200601517

Evidence That a Miniature Cu^I Metalloprotein Undergoes Collisional Electron Transfer in the Inverted Marcus Region**

*Jing Hong, Olesya A. Kharenko, Jiufeng Fan, Fei Xie, Amy K. Petros, Brian R. Gibney, and Michael Y. Ogawa**

The field of protein design seeks to develop synthetic proteins with chemical functions that can be tailored and distinct from those found in natural systems.[1] Much work has thus been directed towards the "bottom-up" design of new proteins that can perform unique chemical tasks[2] and the "top-down" re-engineering of native proteins to enable them to perform new chemical functions.[3] This communication builds on recent work from our group[4–6] to provide evidence that the introduction of a luminescent Cu^I cluster into the hydrophobic interior of a synthetic protein allows collisional photoinduced electron-transfer (ET) reactions to occur in the inverted Marcus region. Whereas the observation of decreasing ET rates with increasing driving force has long been observed in unimolecular,[7] or otherwise diffusionally restricted donor/acceptor systems,[8,9] such behavior has rarely been seen when the donor and acceptor complexes are allowed to diffuse freely in solution.[10,11]

Our group recently reported[5,6] the metal-binding properties of the 32-residue polypeptide C16C19-GGY whose sequence is based on the $(IEALEGK)_n$ heptad repeat previously shown to self-assemble into α-helical coiled coils.[12,13] However, the third heptad repeat of C16C19-GGY was modified by substituting cysteine residues at positions 16 and 19 of the sequence to construct a potential metal-binding site within the hydrophobic core of the coiled coil. It was noted that these apparently simple substitutions were structurally invasive, as the apopeptide exists as a disordered random coil. However, the addition of Cu^I resulted in the self-assembly of a four-stranded coiled coil that encapsulates a cyclic $Cu^I_4S_4(N/O)_4$ cofactor in which each Cu^I atom is trigonally coordinated to two bridging cysteine residues and a terminal nitrogen or oxygen ligand (Figure 1).[5]

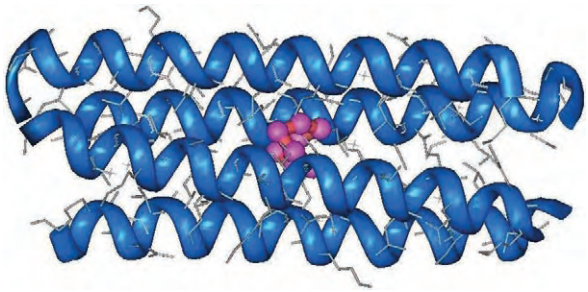

Figure 1. Proposed model of the Cu^I adduct of C16C19-GGY. The metalloprotein exists as a four-stranded helical bundle that contains a cyclic $Cu^I_4S_4(N/O)_4$ cofactor.

The work described herein exploits the fact that Cu^I/C16C19-GGY in aqueous solution displays intense room-temperature luminescence[5] similar to that of multinuclear Cu^I thiolate clusters in both small molecule systems[14] and native metalloproteins.[15] The decay of this emission can be accurately fit to a sum of two single exponential functions [Eq. (1)]

$$I(t) = A_S \exp(\tau_S^{-1} t) + A_L \exp(\tau_L^{-1} t) \quad (1)$$

in which A_S, τ_S, A_L, τ_L are the amplitudes and emission lifetimes of the shorter and longer emission components, respectively (inset, Figure 2). The origin of these two lifetime components is not known and is currently under investigation.

In the absence of quencher, a nonlinear least-squares fit of the data to Equation (1) yields values of $\tau_S = 1.02 \pm 0.01$ μs, $\tau_L = 7.75 \pm 0.02$ μs, and $A_S/A_L = 1.0$. The addition of $[Ru(NH_3)_6]^{3+}$ shortens the emission lifetime of the metalloprotein (inset, Figure 2). Importantly, the emission decay remains biexponential in the presence of this and other quenchers (Table 1), and the data can be fit to Equation (1) to yield

[*] J. Hong, O. A. Kharenko, J. Fan, F. Xie, Prof. M. Y. Ogawa
Department of Chemistry and
Center for Photochemical Sciences
Bowling Green State University
Bowling Green, OH 43403 (USA)
Fax: (+1) 419-372-9809
E-mail: mogawa@bgsu.edu
A. K. Petros, Prof. B. R. Gibney
Department of Chemistry
Columbia University
New York, NY 10027 (USA)

[**] This work was partially supported by NSF grant no. CHE-0455441 (M.Y.O.), ACS-PRF grant no. 34901-AC (M.Y.O.), and AHA grant no. 0455900T (B.R.G.). A.K.P. is an NSF-GK-12 fellow (NSF-DGE-02-31875). We thank Prof. M. A. J. Rodgers for helpful discussions and Prof. F. Castellano for use of the laser facilities.

 © 2006 Wiley-VCH Verlag GmbH & Co. KGaA, Weinheim

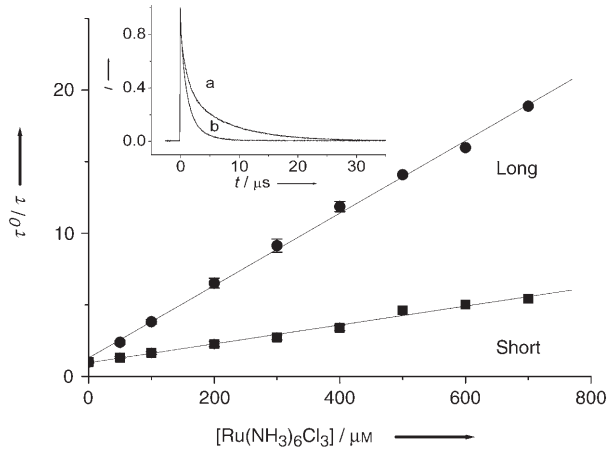

Figure 2. Stern–Volmer plot for the emission quenching of ca. 25 μM Cu^{I}/C16C19-GGY by $[Ru(NH_3)_6]^{3+}$ in 0.2 M acetate buffer (pH 5.5) at 25 °C. Error bars are standard deviations from the mean of triplicate data points and are mostly within the symbols. Inset: Emission lifetime traces of the Cu^{I} adduct of C16C19-GGY taken in the absence (a) and presence (b) of 0.1 mM $[Ru(NH_3)_6]^{3+}$. Solid lines are fits of the data to Equation (1) as described in the text.

Table 1: Electron-transfer driving forces and observed bimolecular quenching constants.

Quencher[a]	$E(Q/Q^-)$[b] [mV vs. NHE]	ΔG [eV]	k_q(short) [10^9 M^{-1}s^{-1}]	k_q(long) [10^9 M^{-1}s^{-1}]
$[RuA_5Cl]^{2+}$	−40	−1.66	3.27 ± 0.14	2.53 ± 0.09
$[RuA_6]^{3+}$	60	−1.76	5.86 ± 0.21	3.47 ± 0.05
$[RuA_5(lut)]^{3+}$	255	−1.95	4.43 ± 0.06	2.44 ± 0.08
$[RuA_5(py)]^{3+}$	300	−2.00	2.46 ± 0.07	1.36 ± 0.05
$[RuA_5(nic)]^{3+}$	353	−2.05	3.46 ± 0.04	1.96 ± 0.06
$[RuA_5(dmpd)]^{3+}$	392	−2.09	1.71 ± 0.21	0.96 ± 0.08

[a] A = NH_3; lut = 3,5-lutidine; py = pyridine; nic = nicotinamide; dmpd = dimethyl 3,5-pyridine dicarboxylate. [b] Determined by cyclic voltammetry in 0.2 M acetate buffer (pH 5.4).

values of $A_S/A_L = 1.0$ under all conditions studied. Thus, the two lifetimes of Cu^{I}/C16C19-GGY were analyzed separately according to the Stern–Volmer equation [Eq. (2)], in which τ^0

$$\tau^0/\tau = 1 + k_q\,\tau^0[Q] \qquad (2)$$

and τ are the emission lifetimes of the short or long emission component measured in the absence or presence of the quencher (Q), respectively, and k_q is the rate constant for the bimolecular quenching reaction. Figure 2 shows that the data for the quenching of both the short and long emission components of Cu^{I}/C16C19-GGY follow linear Stern–Volmer behavior with unity intercepts. Thus, the emission quenching arises from a purely collisional mechanism, and no evidence is seen for a ground-state protein–quencher complex. Analysis of the data obtained for $[Ru(NH_3)_6]^{3+}$ as quencher yields values of $k_q(\text{short}) = (5.86 \pm 0.21) \times 10^9\,\text{M}^{-1}\text{s}^{-1}$ and $k_q(\text{long}) = (3.47 \pm 0.05) \times 10^9\,\text{M}^{-1}\text{s}^{-1}$.

Linear Stern–Volmer behavior is also observed when the different members of a related series of ruthenium(III) ammine complexes ($[Ru(NH_3)_5L]^{n+}$; Table 1) are used to quench the emission of the Cu^{I} protein. Significantly, when L = pyridine or 3,5-lutidine, the emission quenching is accompanied by an increased transient absorption at 400 nm corresponding to the MLCT bands of the reduced $[Ru(NH_3)_5L]^{2+}$ species (inset, Figure 3). The results thus indicate that the emission of Cu^{I}/C16C19-GGY is quenched through a bimolecular electron-transfer reaction.

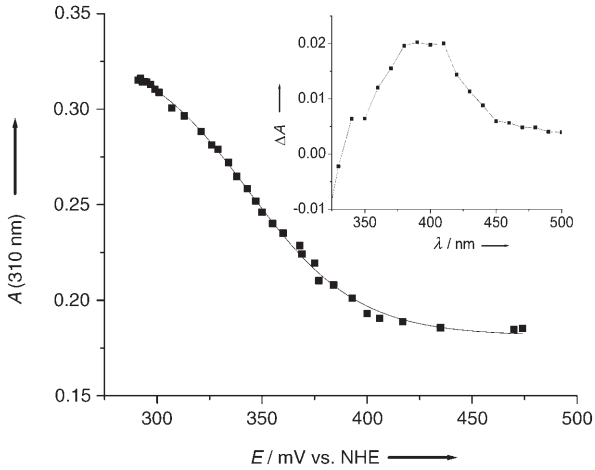

Figure 3. Redox potentiometry of Cu^{I}/C16C19-GGY performed in 0.2 M acetate buffer (pH 5.5) under anaerobic conditions at 25 °C. Inset: Transient absorption spectrum of a solution of Cu^{I}/C16C19-GGY (83 μM) and $[RuA_5(lut)]^{3+}$ (330 μM) measured 20 μs after the laser flash.

The one-electron reduction potential of the Cu^{I}/C16C19-GGY metalloprotein was determined by solution redox potentiometry[16] using $K_2[IrCl_6]$ as an oxidant. Figure 3 plots the absorbance at 310 nm versus the measured solution potential and shows a fit to the Nernst equation ($n = 1$) which yields a single midpoint potential of 343 ± 15 mV versus the normal hydrogen electrode (NHE). Similar results were obtained when the metalloprotein oxidation was monitored by the loss of emission at 600 nm (not shown).

The free-energy change (ΔG) for electron transfer from the Cu^{I}/C16C19-GGY photoexcited donor to the aqueous ruthenium ammine quenchers is calculated by Equation (3)[17], in which $E(Cu^{II}/Cu^{I})$ is the reduction potential of

$$\Delta G = E(Cu^{II}/Cu^{I}) - E(Q/Q^-) - E_{0\text{-}0} \qquad (3)$$

the metalloprotein, $E(Q/Q^-)$ is the reduction potential of the quencher, and $E_{0\text{-}0} = 2.04$ eV (610 nm) is the energy of the excited state as determined by the emission spectrum of Cu^{I}/C16C19-GGY at 77 K measured in 50 % v/v glycerol in 0.1 M acetate buffer (pH 5.4). Table 1 lists the ΔG values and observed bimolecular quenching constants for the reactions studied. Overall, the values of k_q exhibit a greater than threefold decrease with increasingly negative values of ΔG.

Marcus theory[18] describes how the rates of electron-transfer reactions are controlled by the interplay between the thermodynamic driving force ($-\Delta G^0$) and reorganization energy (λ) for the reaction. Equation (4) predicts that

 © 2006 Wiley-VCH Verlag GmbH & Co. KGaA, Weinheim

$$k_{ET} = \sqrt{\frac{4\pi^3}{h^2 \lambda R T}} H_{DA}^2(r) \exp\left\{-\frac{(\Delta G^0 + \lambda)^2}{4\lambda R T}\right\} \quad (4)$$

electron-transfer rates should increase with increasing driving force, reach a maximum value determined by the magnitude of the electronic coupling matrix element (H_{DA}) when $-\Delta G = \lambda$, and then decrease with further increases in driving force as the system enters the Marcus inverted region.

Although numerous examples of inverted Marcus behavior exist for unimolecular ET reactions,[7] there are only a few reports of such behavior for forward charge-separation reactions involving a collisional mechanism.[10,11] Bimolecular ET processes typically occur in a series of steps [Eqs. (5)–(7)]

$$D + A \underset{k_{-d}}{\overset{k_{+d}}{\rightleftharpoons}} [DA] \quad (5)$$

$$[DA] \xrightarrow{k_{ET}} [D^+A^-] \quad (6)$$

$$[D^+A^-] \underset{k'_{+d}}{\overset{k'_{-d}}{\rightleftharpoons}} D^+ + A^- \quad (7)$$

consisting of 1) the formation of a diffusional encounter complex [Eq. (5)]; 2) a unimolecular electron-transfer event within this complex [Eq. (6)]; and 3) the subsequent dissociation of the successor complex [Eq. (7)]. Under the steady-state approximation, Equation (8) is obtained for the

$$k_{obs} = k_q = \frac{k_{+d} k_{ET}}{k_{-d} + k_{ET}} \quad (8)$$

observed second-order rate constant for electron transfer. Thus, in cases of relatively slow electron-transfer reactions ($k_{-d} \gg k_{ET}$), the expression simplifies to $k_{obs} = K_{eq} k_{ET}$, in which $K_{eq} = k_{+d}/k_{-d}$ is the equilibrium constant for the formation of the diffusional encounter complex. However, at higher driving forces, the magnitude of k_{ET} will increase according to Equation (4), and when $k_{ET} \gg k_{-d}$, the reaction will become diffusion-controlled ($k_{obs} = k_d$). Under these conditions, the values of k_{obs} will remain invariant with increases in driving force, thus prohibiting the observation of inverted Marcus behavior. Such is typically the case for bimolecular ET reactions occurring at high driving force.

The observed free-energy dependence of k_q(short) and k_q(long) can be interpreted in terms of inverted Marcus behavior given the reasonable assumptions that the values of K_{eq} remain relatively constant throughout this series of reactions and that the related ruthenium quenchers bind to the Cu^I protein in a similar manner. Figure 4 shows how the values of k_q(short) and k_q(long) decrease with increasing driving force. Fits of the data to Equation (4) yield values of $\lambda = 1.7 \pm 0.1$ eV and $H_{DA} = 4.8 \pm 0.4$ cm^{-1} for the short component, and $\lambda = 1.7 \pm 0.1$ eV and $H_{DA} = 3.9 \pm 0.4$ cm^{-1} for the long component. The source of the scatter in the data is not presently known but, in light of the previous assumptions, might reflect small differences in either the K_{eq} values or relative binding sites of the different acceptors.[19]

Whereas interpretation of H_{DA} is problematic because the equilibrium constant is unknown, further insights into the redox properties of the Cu^I metalloprotein can be obtained by a cross-relation[18] analysis of the λ values obtained above. Assuming $\lambda_{11} = 1.2$ eV for the ruthenium pentaammine acceptors,[20] a value of $\lambda_{22} = 2.2$ eV is obtained for Cu^I/C16C19-GGY which is very similar to that reported for $[Cu(phen)_2]^{2+/+}$ ($\lambda = 2.4$ eV).[21] These results suggest that one-electron oxidation causes a significant conformational change of the $Cu^I_4S_4(N/O)_4$ cluster.

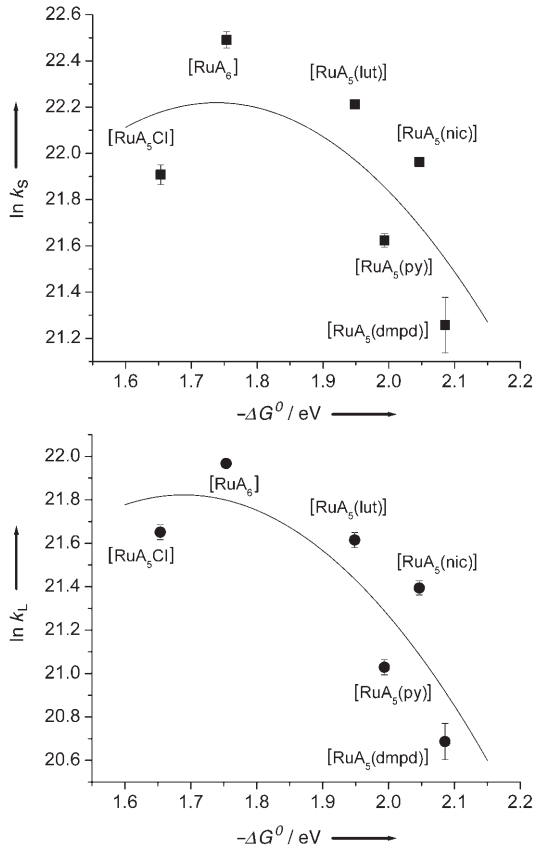

Figure 4. Free-energy plot of k_{obs} values for the short (top) and long (bottom) components to the emission lifetime. Error bars represent the deviation from the mean of triplicate experiments. The solid lines are fits of the data to Equation (4).

In summary, evidence is presented to indicate that the miniature Cu^I/C16C19-GGY metalloprotein undergoes collisional photoinduced electron transfer to a variety of ruthenium(III) acceptors in solution. Inverted Marcus behavior is observed as the buried $Cu^I_4S_4(N/O)_4$ cofactor has a very high reorganization energy and experiences weak electronic coupling to the aqueous acceptors. This latter effect might be due to the positioning of the cofactor within the hydrophobic core of the protein which prohibits close approach between the donor and acceptor to lower the value of H_{DA}.

Experimental Section

The peptide C16C19-GGY and its Cu^I derivative were prepared as previously described.[5,12] Emission-lifetime measurements[22] were performed on argon-saturated solutions containing 100 μM $[Cu(CH_3CN)_4]^+$, 100 μM C16C19-GGY, and 0–700 μM $[Ru(NH_3)_5L]^{n+}$ (L = Cl, NH_3, 3,5-lutidine, nicotinamide, pyridine, and dimethyl 3,5-pyridinedicarboxylate) dissolved in 0.2 M acetate buffer (pH 5.4). The concentration of the C16C19-GGY stock solutions (ca. 200 μM in 0.2 M acetate buffer) were determined by UV/Vis spectroscopy by

 © 2006 Wiley-VCH Verlag GmbH & Co. KGaA, Weinheim

using a value of $\varepsilon_{275} = 1450\,\text{M}^{-1}\text{cm}^{-1}$. These solutions were freshly prepared and stored under argon before each experiment. The concentrations (0.01–0.05 M) of the stock solutions of the $[Ru(NH_3)_5L]^{3+}$ (L = 3,5-lutidine, nicotinamide, pyridine, and dimethyl 3,5-pyridinedicarboxylate) quenchers were obtained by reducing the sample with excess ascorbic acid and measuring the absorption of their MLCT bands. The concentrations (0.01–0.05 M) of the stock solution of the $[Ru(NH_3)_5L]^{n+}$ (L = Cl and NH_3) quenchers were measured directly by UV/Vis spectroscopy. The $[Cu(CH_3CN)_4]PF_6$ stock solution (0.01 M) in acetonitrile was prepared anaerobically by syringe techniques. In the presence of metallopeptide, the concentration of the higher-potential quenchers was corrected for ground-state reduction as determined by measuring the MLCT absorption bands.

Received: April 17, 2006
Published online: August 22, 2006

Keywords: copper · electron transfer · Marcus theory · protein design · ruthenium

[1] J. D. Bloom, M. M. Meyer, P. Meinhold, C. R. Otey, D. MacMillan, F. H. Arnold, *Curr. Opin. Struct. Biol.* **2005**, *15*, 447.
[2] J. Kaplan, W. F. DeGrado, *Proc. Natl. Acad. Sci. USA* **2004**, *101*, 11566.
[3] K. Hult, P. Berglund, *Curr. Opin. Biotechnol.* **2003**, *14*, 395.
[4] J. Hong, O. A. Kharenko, M. Y. Ogawa, *Inorg. Chem.* **2006**, in press.
[5] O. A. Kharenko, D. C. Kennedy, B. Demeler, M. J. Maroney, M. Y. Ogawa, *J. Am. Chem. Soc.* **2005**, *127*, 7678.
[6] O. A. Kharenko, M. Y. Ogawa, *J. Inorg. Biochem.* **2004**, *98*, 1971.
[7] G. L. Closs, L. T. Calcaterra, N. J. Green, K. W. Penfield, J. R. Miller, *J. Phys. Chem.* **1986**, *90*, 3673.
[8] T. M. McCleskey, J. R. Winkler, H. B. Gray, *J. Am. Chem. Soc.* **1992**, *114*, 6935.
[9] I. R. Gould, S. Farid, *Acc. Chem. Res.* **1996**, *29*, 522.
[10] C. Turro, J. M. Zaleski, Y. M. Karabatsos, D. G. Nocera, *J. Am. Chem. Soc.* **1996**, *118*, 6060.
[11] S. Fukuzumi, K. Ohkubo, H. Imahori, D. M. Guldi, *Chem. Eur. J.* **2003**, *9*, 1585.
[12] A. Y. Kornilova, J. F. Wishart, W. Z. Xiao, R. C. Lasey, A. Fedorova, Y. K. Shin, M. Y. Ogawa, *J. Am. Chem. Soc.* **2000**, *122*, 7999.
[13] M. V. Tsurkan, M. Y. Ogawa, *Chem. Commun.* **2004**, 2092.
[14] P. C. Ford, E. Cariati, J. Bourassa, *Chem. Rev.* **1999**, *99*, 3625.
[15] D. L. Pountney, I. Schauwecker, J. Zarn, M. Vasak, *Biochemistry* **1994**, *33*, 9699.
[16] P. L. Dutton, *Methods Enzymol.* **1978**, *54*, 411.
[17] D. Rehm, A. Weller, *Isr. J. Chem.* **1970**, *8*, 259.
[18] R. A. Marcus, N. Sutin, *Biochim. Biophys. Acta* **1985**, *811*, 265.
[19] A. G. Mauk, R. A. Scott, H. B. Gray, *J. Am. Chem. Soc.* **1980**, *102*, 4360.
[20] G. M. Brown, N. Sutin, *J. Am. Chem. Soc.* **1979**, *101*, 883.
[21] H. B. Gray, B. G. Malmstrom, R. J. P. Williams, *J. Biol. Inorg. Chem.* **2000**, *5*, 551.
[22] D. S. Tyson, F. N. Castellano, *J. Phys. Chem. A* **1999**, *103*, 10955.

 © 2006 Wiley-VCH Verlag GmbH & Co. KGaA, Weinheim

Living Polymerization

DOI: 10.1002/anie.200601616

Bimolecular Control over Polypropene Stereochemical Microstructure in a Well-Defined Two-State System and a New Fundamental Form: Stereogradient Polypropene**

*Matthew B. Harney, Yonghui Zhang, and Lawrence R. Sita**

The recent development of transition-metal complexes that can function as catalysts for the stereoselective Ziegler–Natta polymerization of propene has provided a wealth of new polypropene-based materials through extensive manipulations of the ligand environment about the metal center.[1] The currently practiced "one catalyst–one material" strategy, however, has significant disadvantages and practical limitations for fine-tuning physical properties of the polypropene material through minor adjustments about a given microstructure, or for accessing a completely different microstructure altogether. Thus, not only is it a labor-intensive synthetic undertaking to prepare a large variety of catalyst structural variants that may, or may not, yield a desired microstructure but even after several decades of effort the "rational design" of new catalysts that can produce a specific polypropene microstructure is still out of reach; and even more so for non-metallocene-based systems.[2]

Dynamic unimolecular processes that are competitive with propagation, such as site isomerization in structurally constrained C_1-symmetric *ansa*-bridged metallocenes,[3] conformational flexibility in unconstrained "oscillating" metallocenes,[4] and "chain-end epimerization"[5] or ligand-sphere rearrangements in non-metallocenes,[6] can give rise to polypropene materials that display promising technologically desirable properties as the result of varying degrees and patterns of stereoerror incorporation, such as in the case of elastomeric polypropene.[3–6] Owing to the intrinsically low energy barriers associated with these unimolecular processes, however, to date, the only means available by which to exert some level of external control in order to access, to a significant degree, a wider range of microstructures for a given catalyst has been to capitalize on the bimolecular nature of propagation (olefin complexation) by varying propene pressure, and hence the rate of propagation (v_p) versus that of

[*] M. B. Harney, Y. Zhang, Prof. L. R. Sita
Department of Chemistry and Biochemistry
University of Maryland
College Park, MD 20742 (USA)
Fax: (+1) 301-314-9121
E-mail: lsita@umd.edu

[**] Funding for this work was provided by the NSF (CHE-0092493). We thank the ACS Division of Organic Chemistry for a graduate fellowship (to M.B.H.) sponsored by the Proctor and Gamble Company.

Supporting information for this article is available on the WWW under http://www.angewandte.org or from the author.

WILEY InterScience DISCOVER SOMETHING GREAT
© 2006 Wiley-VCH Verlag GmbH & Co. KGaA, Weinheim

the unimolecular process.[3g] Herein, we now provide a different strategy by which to break the "one catalyst–one material" strategy by documenting control over a dynamic bimolecular process within a well-defined two-state system composed of active (configurationally stable) and dormant (configurationally unstable) centers that interconvert through methyl group exchange. Importantly, as the evolution of microstructure in this system is a function of the frequency with which the growing polymer chain resides in the dormant state, we demonstrate that it is possible to exert an unprecedented level of control in accessing virtually an unlimited number of discrete polypropene microstructures that range from being highly isotactic to atactic as the result of predictable degrees of incorporation of stereoerrors of a known type. By taking advantage of the living nature of propene polymerization in this system, we further demonstrate the ability to overlay both temporal and bimolecular control as a means by which to prepare a fundamental new form, stereogradient polypropene, for which unequivocal proof of stereochemical microstructural homogeneity is presented.

We previously documented that upon full "activation" of the preinitiator, (η^5-C_5Me_5)$ZrMe_2$[N(Et)C(Me)N(*t*Bu)] (**1**), through methyl group protonolysis using a stoichiometric amount of the borate, [$PhNHMe_2$][$B(C_6F_5)_4$] (**2**), the living Ziegler–Natta polymerization of propene and higher α-olefins, such as 1-hexene, is highly isotactic ($mmmm = 0.71$, $\sigma = 0.94$) for the former and isospecific ($\sigma = 1.0$) for the latter.[7,8] At substoichiometric levels of activation (i.e. $[\mathbf{1}]_0/[\mathbf{2}]_0 > 1.0$), propagation still occurs in living fashion, but it now proceeds through the degenerative methyl group transfer process shown in Scheme 1 in which all metal centers, both

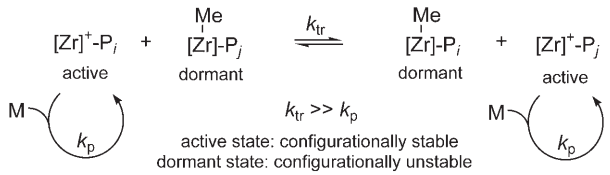

Scheme 1. Living degenerative-transfer Ziegler–Natta polymerization of α-olefins. P_i and P_j refer to growing polymer chains.

active and dormant, appear to propagate simultaneously due to the rate of methyl group transfer being much faster than that of propagation, $v_{tr} \gg v_p$.[9,10] These relative rates also ensure that the number-average degree of polymerization (X_n) is a function of only the initial concentration of the preinitiator, not the amount of borate activator employed (i.e. $X_n \approx [M]_0/[\mathbf{1}]_0$), and that the polypropene materials display narrow polydispersities ($D = M_w/M_n$) as $D \approx 1 + (k_p/k_{tr})$ and $k_{tr} \gg k_p$.[11] However, as a result of a dormant state that is configurationally unstable with respect to metal-centered epimerization, which proceeds with a rate that must be faster than both methyl group transfer and propagation (i.e. $v_{epi} > v_{tr} \gg v_p$), an atactic microstructure is produced at 50% activation (i.e. $[\mathbf{1}]_0/[\mathbf{2}]_0 = 2.0$).[8,9,12]

A more detailed analysis of stereoerror incorporation that occurs during propagation at substoichiometric levels of activation of **1** by **2** is presented in Scheme 2. Here it can be

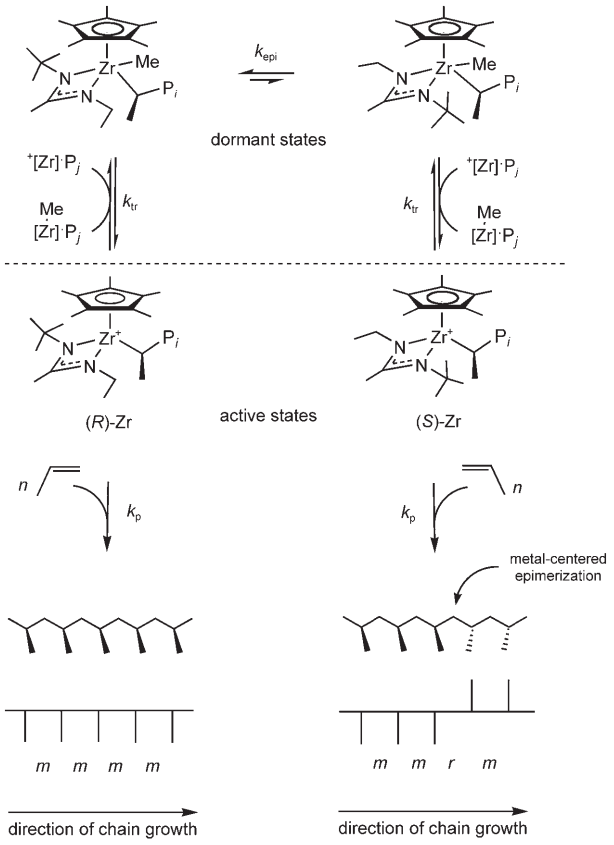

Scheme 2. Mechanism of stereoerror incorporation that occurs under living degenerative-transfer conditions. P_i and P_j refer to growing polymer chains, and *m* and *r* denote *meso* and racemic (*rac*) stereochemical relationships, respectively, between adjacent stereocenters of the polymer backbone.[13] Depicted relative and absolute configurational relationships for the metal centers and the polymer chains are for illustrative purposes only.

seen that because monomer enchainment is highly stereoselective for the cationic active sites, the occurrence of an isolated *mmrm* pentad stereoerror[13] is directly traceable to the growing polymer chain having resided in the dormant state, where metal-centered epimerization occurs to provide one of two different diastereomeric propagating centers with equal probability upon exiting back to the active state (see the processes occurring above the dashed line in Scheme 2). Accordingly, by directly manipulating the bimolecular rate of group transfer (v_{tr}) relative to the rate of propagation (v_p), which is pseudo-first order in the presence of a large excess of monomer, and by simply changing either the absolute concentration of all the metal-containing species in solution or the concentration of transferable methyl groups using different levels of substoichiometric activation, it should be possible to influence the frequency of attaining the dormant state, and thereby, the stereochemical microstructure of the growing polymer chain. Gratifyingly, in practice, this proved

 © 2006 Wiley-VCH Verlag GmbH & Co. KGaA, Weinheim

to be the case as observed by the series of ^{13}C NMR spectra for the methyl region of the polypropene materials shown in Figure 1 in which the highly isotactic microstructure obtained

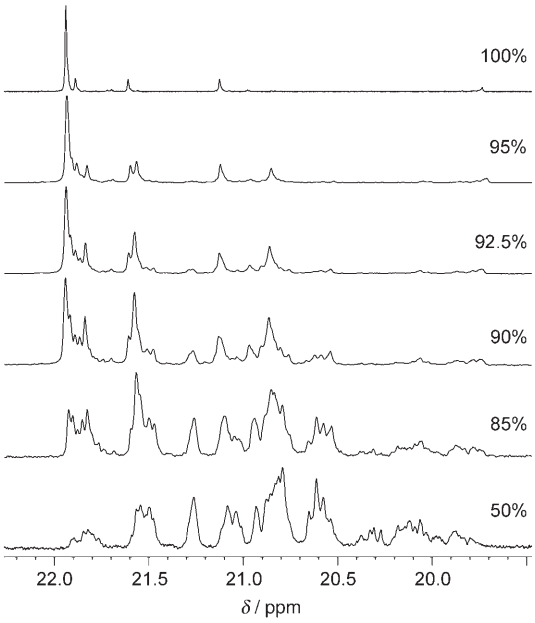

Figure 1. $^{13}C\{^1H\}$ NMR (125 MHz, 1,1,2,2-$C_2D_4Cl_2$, 70 °C) spectra of the methyl region of polypropene obtained as a function of % activation of **1** by **2**. Note that the spectra are shown with increasing arbitrary *y* scaling (top to bottom) for the sake of clarity (polymerization conditions: 34.5 kPa propene, −10 °C, C_6H_5Cl, $[\mathbf{1}]_0 = 2.5$ mM).

at 100 % activation is transformed to an atactic one by simply decreasing the level of activation. In Figure 2, the % *mm* stereochemical triad content is plotted as a function of % activation and better illustrates the rate and nonlinear fashion in which this transformation occurs. Furthermore, a

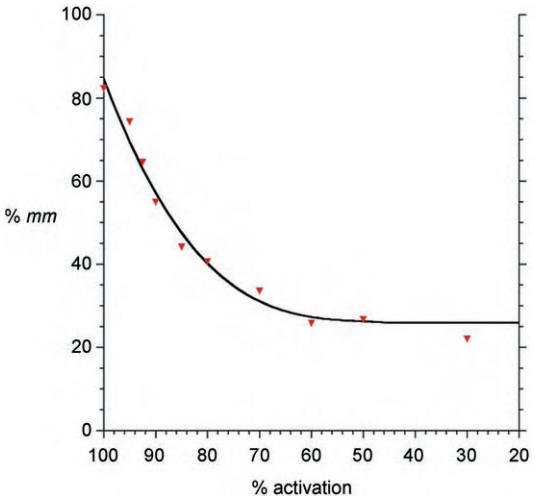

Figure 2. % *mm* (at the triad level of ^{13}C NMR stereoerror analysis) of the ^{13}C NMR spectra of Figure 1 and other polypropene materials obtained as a function of % activation under the same polymerization conditions.

preliminary stereochemical analysis of these spectra at the heptad and higher level of analysis (Figure 3) is consistent with the expected decrease in isotactic sequence length with a

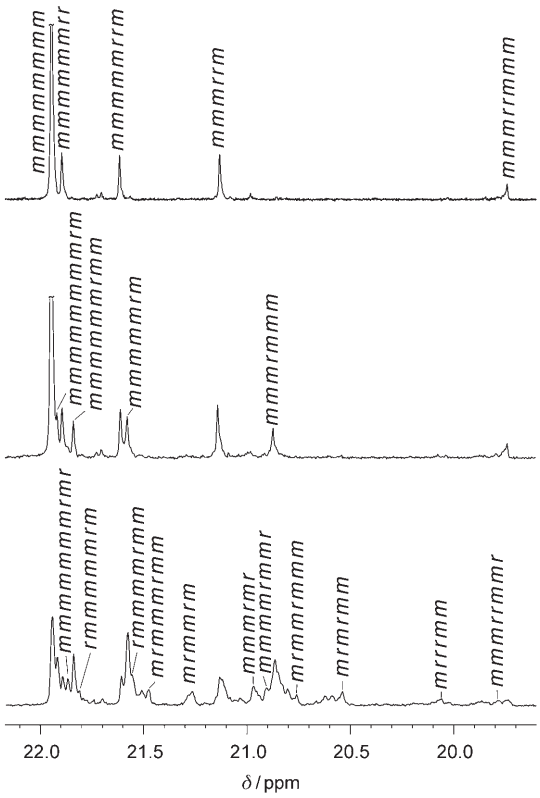

Figure 3. ^{13}C NMR spectra from Figure 1 showing partial heptad and higher level stereoerror assignments for the methyl region of polypropene obtained as a function of % activation of **1** (top to bottom: 100, 95, and 90 %). Note that at 100 % activation the nature of the stereoerrors are consistent with exclusive enantiomorphic site control of propagation.[1b]

decrease in % activation due to an increasing incorporation of isolated *mr* triad stereoerrors that arise as the result of epimerization of the propagating center according to Scheme 2. Confirmation of this mechanism of stereoerror incorporation is of significant importance in that, until now, it has only been possible to introduce varying amounts of *rr* triad stereoerrors as a means of controlling polypropene isotacticity by manipulating the degree of stereoselectivity for propene enantioface complexation and subsequent insertion.[1d] While propagation by a "chain-end control" mechanism that is dictated by the growing polymer chain can give rise to the type of isolated *mr* pentad stereoerror observed here,[1b] no clear means exist by which one could conceivably manipulate, over a wide range, the degree of chain-end control through modification of the ligand sphere of the catalyst. Accordingly, our demonstrated approach to introduce varying levels of *mr* triad stereoerrors in simple fashion by using only a single catalyst is not only unique but the range of new polypropene materials that are now obtainable by this process may exhibit technologically desirable physical properties. Finally, although not presented here, in preliminary

 © 2006 Wiley-VCH Verlag GmbH & Co. KGaA, Weinheim

investigations we have been able to demonstrate that for a given level of % activation, another level of bimolecular control (i.e. "fine-tuning") about a particular microstructure can be achieved by simply varying solvent volume, and hence, the absolute concentrations of the active and dormant species. As expected, isotacticity increases as the concentrations of these species decrease.

In addition to providing an unprecedented level of control over *mr* stereoerror incorporation, the present bimolecular control of stereochemical microstructure can be used to prepare a new fundamental form, stereogradient polypropene, by simply varying the concentration of the dormant species as a function of time. Importantly, this stereogradient polypropene can only be produced by using a living system, as chain-transfer that occurs in nonliving systems would produce stereochemical heterogeneity within the final isolated material. As a proof of concept, after an initial 30 min period of atactic chain growth at 60% activation, a programmable syringe pump was used to steadily increase the level of activation to a final 100% by introducing an additional 0.5 equiv of the borate **2** as a function of time (see Figure 4A). To unequivocally establish both the stereogradient nature and the stereochemical homogeneity of the final material, pre-initiator **1**, with ^{13}C(99%)-labeled methyl groups, was used to place a ^{13}C-labeled methyl end group at the beginning of polymer chain growth. Aliquots were then taken as a function of time, and ^{13}C NMR spectra were obtained for the isolated materials, a selection of which are shown in Figure 4B. By using the ^{13}C-labeled methyl end group resonances that appear between $\delta = 22.5$–23.0 ppm (not shown) as an internal reference, difference ^{13}C NMR spectra were produced (Figure 4C) which confirmed that chain growth steadily changes from being completely atactic to being highly isotactic as a function of time. Importantly, with additional aliquots and difference spectra it was possible to demonstrate that the % *mmmm* content of the material closely tracks the ramp profile for addition of **2** (see red shading in Figure 4A). Thus, by programming different ramp profiles, together with reversing the direction of the ramp through addition of a recently reported reagent that can be used to selectively methylate cationic propagating centers so as to increase the concentration of dormant states (i.e. to essentially "lower" the level of activation),[8] an infinite variety of new stereogradient polypropene materials can be envisioned and prepared.

In summary, by taking advantage of the bimolecular nature of degenerative-transfer living Ziegler–Natta polymerization, we have demonstrated that an intrinsic configurational instability of the dormant state can be harnessed to produce an unlimited variety of new polypropene materials from a single catalyst. The strategy presented here should also be readily transferable to other catalyst systems (e.g. those that are syndioselective at 100% activation), thereby expanding even further the range, and possibly the future, of polypropene-based commercial products.

Received: April 24, 2006
Published online: August 21, 2006

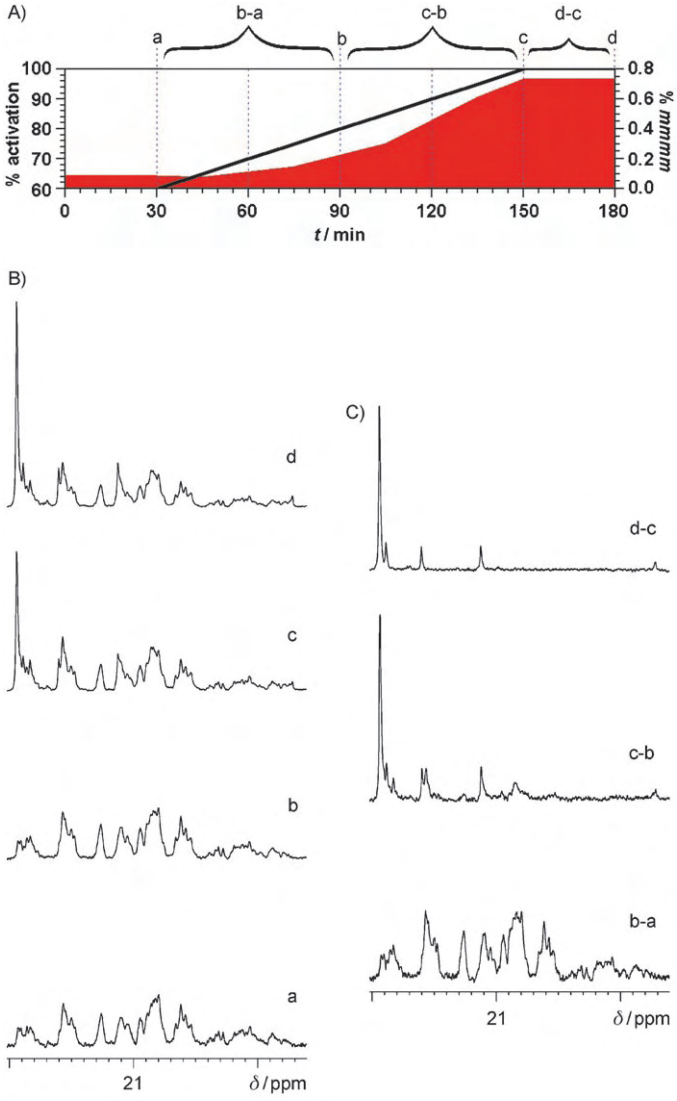

Figure 4. A) Ramp profile (black line) for addition of 0.5 equiv of **2** to change the level of activation from 60% to 100% and % *mmmm* content as a function of time (red shading) as determined from: B) ^{13}C NMR (125 MHz, 1,1,2,2-$C_2D_4Cl_2$, 70°C) spectra (for the methyl region of polypropene) of aliquots taken as a function of time, and C) their difference spectra using the resonances (not shown) of a ^{13}C(99%)-labeled methyl end group as an internal reference.

Keywords: block copolymers · polymerization · polypropene · thermoplastic elastomers · Ziegler–Natta polymerization

[1] a) H. H. Brintzinger, D. Fischer, R. Müllhaupt, B. Rieger, R. M. Waymouth, *Angew. Chem.* **1995**, *107*, 1255; *Angew. Chem. Int. Ed. Engl.* **1995**, *34*, 1143; b) L. Resconi, L. Cavallo, A. Fait, F. Piemontesi, *Chem. Rev.* **2000**, *100*, 1253; c) G. Müller, B. Rieger, *Prog. Polym. Sci.* **2002**, *27*, 815; d) C. De Rosa, F. Auriemma, A. Di Capua, L. Resconi, S. Guidotti, I. Camurati, I. E. Nifant'ev, I. P. Lashevtsev, *J. Am. Chem. Soc.* **2004**, *126*, 17040.

[2] See, for example: G. Talarico, V. Busico, L. Cavallo, *J. Am. Chem. Soc.* **2003**, *125*, 7172.

[3] a) D. T. Mallin, M. D. Rausch, Y. G. Lin, S. Dong, J. C. W. Chien, *J. Am. Chem. Soc.* **1990**, *112*, 2030; b) J. C. W. Chien, G. H. Llinas, M. D. Rausch, G.-Y. Lin, H. H. Winter, *J. Am. Chem. Soc.*

 © 2006 Wiley-VCH Verlag GmbH & Co. KGaA, Weinheim

1991, *113*, 8570; c) W. J. Gauthier, J. F. Corrigan, N. J. Taylor, S. Collins, *Macromolecules* **1995**, *28*, 3771; d) W. J. Gauthier, S. Collins, *Macromolecules* **1995**, *28*, 3779; e) A. M. Bravakis, L. E. Bailey, M. Pigeon, S. Collins, *Macromolecules* **1998**, *31*, 1000; f) U. Dietrich, M. Hackmann, R. Bernhard, M. Klinga, M. Leskelä, *J. Am. Chem. Soc.* **1999**, *121*, 4348; g) E. J. Thomas, C. W. J. Chien, M. D. Rausch, *Macromolecules* **2000**, *33*, 1546.

[4] a) G. W. Coates, R. M. Waymouth, *Science* **1995**, *267*, 217; b) S. Lin, R. M. Waymouth, *Acc. Chem. Res.* **2002**, *35*, 765.

[5] V. Volkis, E. Nelkenbaum, A. Lisovskii, G. Hasson, R. Semiat, M. Kapon, M. Botoshansky, Y. Eishen, M. S. Eisen, *J. Am. Chem. Soc.* **2003**, *125*, 2179.

[6] E. Smolensky, M. Kapon, J. D. Woollins, M. S. Eisen, *Organometallics* **2005**, *24*, 3255.

[7] K. C. Jayaratne, L. R. Sita, *J. Am. Chem. Soc.* **2000**, *122*, 958.

[8] M. B. Harney, Y. Zhang, L. R. Sita, *Angew. Chem.* **2006**, *118*, 2460; *Angew. Chem. Int. Ed.* **2006**, *45*, 2400.

[9] Y. Zhang, R. J. Keaton, L. R. Sita, *J. Am. Chem. Soc.* **2003**, *125*, 9062.

[10] Y. Zhang, L. R. Sita, *J. Am. Chem. Soc.* **2004**, *126*, 7776.

[11] A. H. E. Müller, R. Zhuang, D. Yan, G. Litvinenko, *Macromolecules* **1995**, *28*, 4326.

[12] If the rate of propagation for propene is equal or greater in magnitude to the rate of methyl group exchange between active and dormant sites, or the rate of epimerization of the dormant site, that is, $v_p \geq v_{tr}$, v_{epi}, or if $v_{tr} \geq v_{epi}$, then an atactic microstructure will not be formed under degenerative-transfer conditions.

[13] For reviews of the use of ^{13}C NMR spectroscopy for stereochemical microstructural analysis of polypropene, see Ref. [1b] and V. Busico, R. Cipullo, *Prog. Polym. Sci.* **2001**, *26*, 443.

 © 2006 Wiley-VCH Verlag GmbH & Co. KGaA, Weinheim

DNA Recognition

DOI: 10.1002/anie.200600804

Four-Color, Enzyme-Free Interrogation of DNA Sequences with Chemically Activated, 3′-Fluorophore-Labeled Nucleotides**

*Niels Griesang, Kerstin Gießler, Tanja Lommel, and Clemens Richert**

The technology for interrogating nucleic acid sequences affects the progress of genetics, medical diagnostics, and biotechnology. A recent review on DNA sequencing technologies states: "Current sequencing technologies are too expensive, labor intensive, and time consuming for broad application in human sequence variation studies".[1] The vision of the "$1000 human genome" calls for significant improvements over existing sequencing and genotyping techniques.[2] The benchmark method for interrogating DNA is Sanger sequencing[3] with fluorophore-labeled dideoxynucleoside triphosphates[4] and capillary electrophoresis, monitored by a charge-coupled-device (CCD) camera. It involves enzymes and substrates that are costly. Furthermore, it produces an oligonucleotide for every position to be interrogated in reactions that must be run in individual vessels. An entirely chemical approach to sequencing by synthesis promises a less-expensive access to sequence information, particularly if one was to perform a nonenzymatic primer extension in a microarray format.

To the best of our knowledge, no enzyme-free protocol for sequencing by stepwise primer extension currently exists. Nonenzymatic primer extension has been previously demonstrated, however. Studies focused on prebiotic chemistry have shown that RNA strands complementary to a template can be formed in the absence of enzymes.[5] A number of chemically activated nucleic acids have been shown to undergo chemical primer extension,[6] and a number of related reactions have been shown to occur in a templated fashion.[7] A chemical primer-extension method for nonenzymatic genotyping of single-nucleotide polymorphisms was recently reported.[8] This method employs azaoxybenzotriazolides of 2′-deoxynucleotides (OAt-dNMPs) as activated monomers and short "helper oligonucleotides" to achieve primer conversion within hours,[9] but requires mass spectrometry as a read-out technique.

Herein we report that OAt-dNMP-driven primer extensions can be carried out with fluorophore-labeled monomers. The labeled nucleotides allow for optical read out.[10] The focus of this study was on genotyping, that is, the extension of primers by a single nucleotide. Syntheses for all four dNMPs, each labeled with a different dye, are reported together with a protocol for their activation. We also report the first activated monomers in which the fluorophore is attached through a photolabile linker.[10c] This allows it to be removed after the optical read out through irradiation with UV light.

Our first efforts to prepare activated, fluorophore-labeled mononucleotides for sequence determination led to an imidazolide of thymidine 5′-monophosphate with a directly linked carboxyfluorescein moiety in a lengthy, solution-phase synthesis.[11] This imidazolide showed low reactivity in primer-extension assays, prompting us to use azaoxybenzotriazolides[8] for the current study. The current nucleotides (**1a**, **c**, **g**, **t**, Scheme 1) also feature a hexaethyleneglycol linker to minimize steric interference from the dyes. The fluorophores were appended to the 3′-position to prevent undesired multiple extension reactions. The ability to decorate the 3′-position with a substituent is one of the advantages of chemical primer extension. The active sites of polymerases, on the other hand, put an α helix on the base pair between the incoming dNTP and the templating nucleotide[12] leaving little space for substituents or protecting groups at the 3′-position,

[*] Dr. N. Griesang, Dipl.-Chem. K. Gießler, T. Lommel, Prof. C. Richert
Institut für Organische Chemie
Universität Karlsruhe (TH)
76131 Karlsruhe (Germany)
Fax: (+49) 721-608-4825
E-mail: cr@rrg.uka.de
Homepage: http://chip.chemie.uni-karlsruhe.de

[**] The authors thank U. Plutowski, C. Ahlborn, and S. Vogel for helpful discussions. This work was supported by the DFG (grant No. 1063/1-3) and the Fonds der Chemischen Industrie.

Supporting information for this article is available on the WWW under http://www.angewandte.org or from the author.

 InterScience DISCOVER SOMETHING GREAT © 2006 Wiley-VCH Verlag GmbH & Co. KGaA, Weinheim

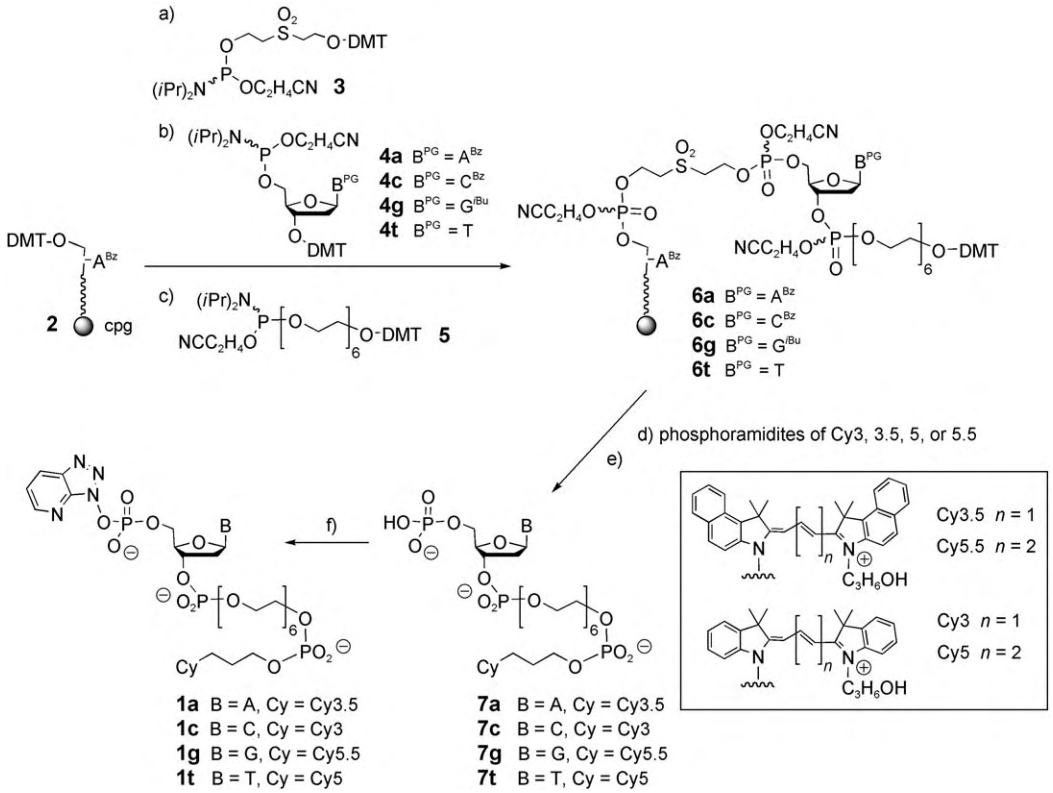

Scheme 1. Synthesis of labeled active esters of mononucleotides **1a**, **c**, **g**, **t**. Conditions: a) Coupling cycle with **3**, b) coupling cycle with **4a**, **c**, **g**, **t**, c) coupling cycle with **5**, d) coupling cycle with phosphoramidites of cyanine dyes, e) NH_4OH, f) HOAt, EDC·HCl; pH 5. Bz = benzoyl, PG = protecting group.

which is the most obvious position for labeling and (reversibly) blocking extensions.[13]

The synthesis of active esters **1a**, **c**, **g**, **t** (Scheme 1) started from controlled pore glass (cpg) loaded with a deoxynucleoside presenting a dimethoxytrityl(DMT)-protected hydroxy group.[14] Four phosphoramidite coupling cycles, including oxidation, capping, and detritylation, were run on a 2-μmol scale on a DNA synthesizer using phosphorylating reagent **3**,[15] 5′-phosphoramidites **4a**, **c**, **g**, **t**,[16,17] hexaethyleneglycol linker reagent **5**,[18] and the phosphoramidite of one of the four fluorophores chosen (Cy3, 3.5, 5, or 5.5). Nucleotides **7a**, **c**, **g**, **t** were obtained in 17–56% overall yields and were characterized by NMR spectroscopy, MS, and UV/Vis spectroscopy. The normalized fluorescence spectra are shown in Figure 1.

Each of the labeled nucleotides were converted into its active ester (**1a**, **c**, **g**, **t**). Best results were obtained with aqueous buffers containing *N*′-(3-dimethylaminopropyl)-*N*-ethylcarbodiimide hydrochloride (EDC)[19] and hydroxyazabenzotriazole.[8] Compounds **1a**, **c**, **g**, **t** are (necessarily) labile and evidence for their formation was obtained by MALDI MS (see the Supporting Information). Solutions of **1a**, **c**, **g**, **t**, when diluted, were directly used for primer extension.

Primer **8**, featuring a 3′-amino-2′,3′-dideoxynucleotide at the 3′-terminus, was employed for assays (Scheme 2), as amines are known to be reactive toward chemically activated nucleotides and nucleic acids.[20] Assays used equimolar mixtures of OAt-esters **1a**, **c**, **g**, **t** (3.6 mM each), a buffer

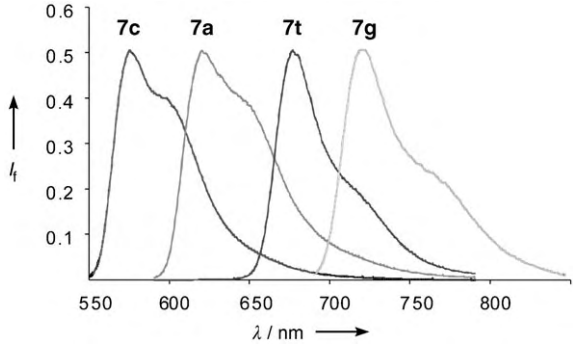

Figure 1. Fluorescence spectra of **7a**, **c**, **g**, **t**. Conditions: **7a** (0.39 μM in water), excitation wavelength: 585 nm; **7c** (0.31 μM in water) excitation wavelength: 545 nm; **7g** (0.23 μM in water) excitation wavelength: 680 nm; **7t** (0.18 μM in water), excitation wavelength: 643 nm. I_f = fluorescence intensity.

containing 2-[4-(2-hydroxyethyl)-1-piperazinyl]ethanesulfonic acid (HEPES; 0.2 M), NaCl (0.4 M), and $MgCl_2$ (0.08 M) at pH 8.9, and were performed at room temperature. Four templates (**9a**, **c**, **g**, **t**), displaying any of the four nucleobases at the site to be interrogated, were reacted with OAt-dNMPs in the presence of downstream-binding helper oligonucleotide **10**, which helped to retain nucleotides at the reaction site.[8,9] First, activated nucleotides without fluorophore labels were reacted to establish the kinetics of primer extension for the sequence motif chosen under conditions identical to those used earlier.[8] Half-life times for primer conversion between

 © 2006 Wiley-VCH Verlag GmbH & Co. KGaA, Weinheim

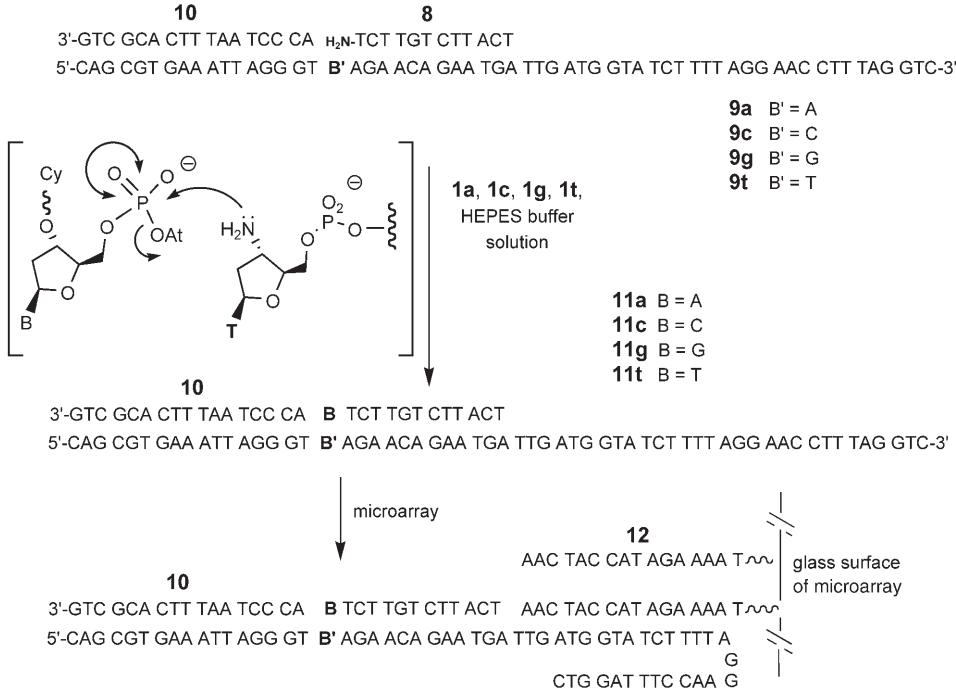

Scheme 2. Determining nucleotides in DNA templates through non-enzymatic primer extension with fluorophore-labeled, activated nucleotides **1a**, **c**, **g**, **t**. Oligodeoxynucleotide **10** serves as a "helper oligonucleotide",[8] generating additional stacking surfaces for the activated nucleotide. The nucleobase in the template (B′) can be determined through fluorescence (Figure 3).

0.13 and 2.5 h and sequence-selective reactions were measured (see the Supporting Information). Next, 90 pmol of each template was reacted with an equimolar mixture of fluorescent nucleotides **1a**, **c**, **g**, **t** (3.6 mM), and the formation of extended, fluorophore-labeled primers **11a**, **c**, **g**, **t** was measured.

MALDI mass spectra confirmed that in each case the correct nucleotide was incorporated opposite the templating base with high fidelity (Figure 2). The same result was obtained when the oligonucleotides were bound on microarrays[21] featuring capture oligonucleotides (**12**) on spots of their surface. After incubation and washing, scans of the microarray surface with four different filter settings and appropriate corrections for the relative fluorescence intensities of the cyanine dyes allowed for unambiguous base calls for each of the templates (Figure 3). (The filter settings and correction factors had been established separately in calibration experiments with Cy-labeled oligonucleotides; see the Supporting Information.) Furthermore, primer extension with the unrelated template sequence 5′-GGAATCACACGTGCG-3′ and labeled monomers **1a**, **c**, **g**, **t** again showed high selectivity (see the Supporting Information).

Finally, we performed exploratory assays to determine the potential for reading more than one nucleotide in the target strands. For this, **13** was prepared, whose cyanine fluorophore is linked to the 3′-amino-2′,3′-dideoxynucleotide through a photolabile linker[10c] (Scheme 3, see also the Supporting Information). Thymidines, such as **13**, are the most difficult cases for chemical primer extension, as their nucleobase

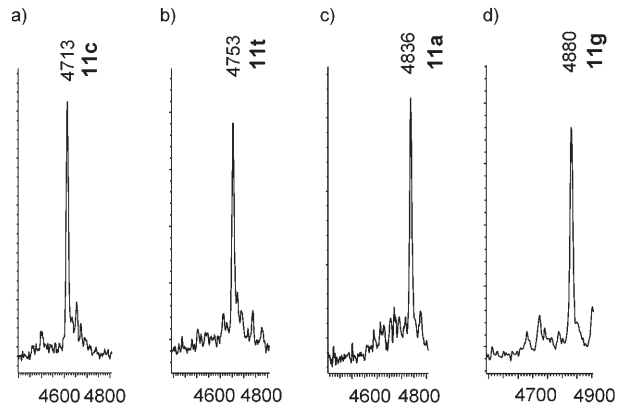

Figure 2. MALDI-TOF spectra of products of primer extension with labeled nucleotides **1a**, **c**, **g**, **t** at a 36 μM concentration of oligonucleotides, after 14 h at room temperature; a) template **9g**, b) template **9a**, c) template **9t**, d) template **9c**.

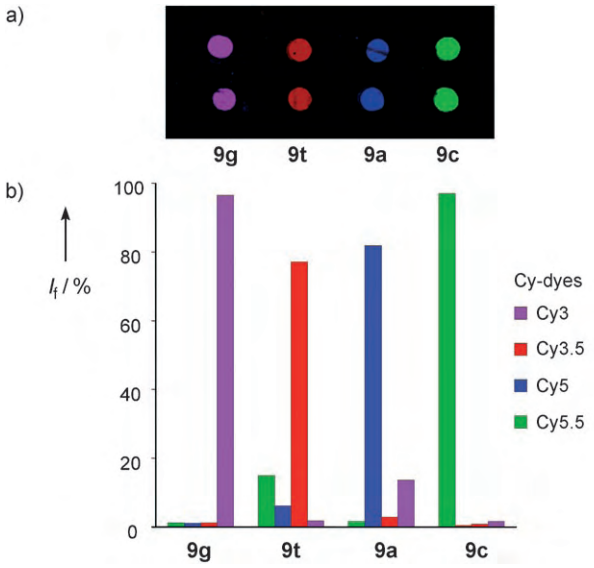

Figure 3. Scans of a microarray with the capture oligonucleotide **12** after hybridization with products from primer extensions with templates **9a**, **9c**, **9g**, or **9t**. a) Overlay of false-color fluorescence images, generated with the settings for each of the fluorophores (Cy3/3.5/5/5.5) using filters, correction factors, and exposure times established in calibration experiments (see the Supporting Information). Products were analyzed in duplicate (two spots vertically above each other). b) Integration of the fluorescence signal obtained in every channel for each pair of spots; the small bars accompanying those for the correct signals are believed to result from mismatch incorporation.

© 2006 Wiley-VCH Verlag GmbH & Co. KGaA, Weinheim

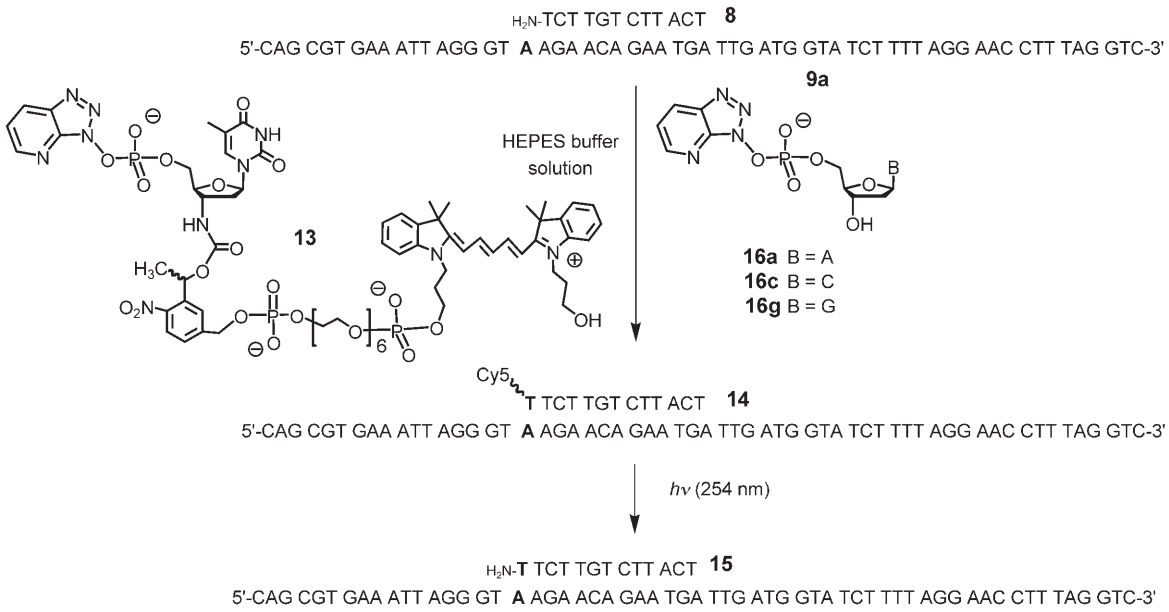

Scheme 3. Enzyme-free primer extension with **13**, whose fluorophore is linked through a photolabile linker. In a competitive reaction with equimolar amounts of **16a**, **c**, **g** and **13** (3.6 mM/18 mM), the residue of **13** is appended to primer **8** to give extended primer **14**. The adenosine base in template **9a** was successfully identified through a fluorescence scan on a microarray (not shown). Subsequent irradiation of **14**:**9a** with UV light cleaves the photolabile linker, removing the Cy5 label and producing the amino-terminal primer **15**, which is suitable for a subsequent primer-extension reaction. Compare Figure 4 for mass spectra.

forms only two hydrogen bonds and the binding site at the template offers little stacking surface for the pyrimidine. Even for the unlabeled OAt-dNMPs, primer extension is, therefore, an order of magnitude slower than for the strongly base pairing nucleotides (see the Supporting Information). Despite the odds, which were worsened by the lack of a helper oligonucleotide in the "multiple-extension case," **13** reacted selectively with primer **8** to give **14** in the presence of competitor nucleotides **16a**, **c**, **g** (Scheme 3), as seen in MALDI-TOF mass spectra (Figure 4) and fluorescence images of a microarray read-out experiment. When the oligonucleotide complex containing **14** was irradiated with UV light (254 nm) from a simple, hand-held lamp for 5 min, the linker with the fluorophore was removed, generating the extended primer **15**, which was suitable for a subsequent interrogation of the next position in the template (Figure 4). An exploratory assay with the deoxycytidine analogue of **13** showed that a dual primer extension is feasible (see the Supporting Information). We are in the process of optimizing conditions to ensure full primer conversion, even for weakly base-pairing nucleotides, and developing a capping scheme that ensures blocking of failure strands.

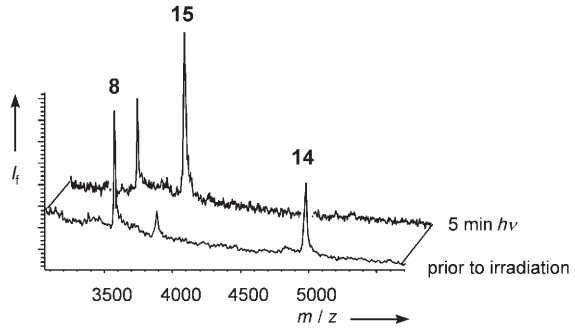

Figure 4. MALDI-TOF mass spectra of samples drawn from the reaction shown in Scheme 3. Assay conditions: template (**9a**; 36 μM) and primer (**8**); HEPES buffer solution (0.2 M), NaCl (0.4 M), and $MgCl_2$ (0.08 M), pH 8.9, 26 h, RT. Please note that longer sequences give smaller signals as a consequence of lower desorption/ionization efficiencies.

Together, these results suggest that chemical primer extension with inexpensive, fluorescent substrates is suitable for determining nucleotides in DNA sequences, including read-out in a parallel fashion through microarrays. In favorable cases, the colors of the fluorophores may be detected with the naked eye, providing a simplified form of the current assays (Scheme 2) that might serve as a "lacmus test" for detecting single-nucleotide polymorphisms. The more-sophisticated form involving microarrays and a chip scanner might prove an inexpensive alternative to current genotyping systems. Modifications in the helper[22] and primer,[23] as well as adjustments in the nucleotide concentration and activation chemistry might eventually lead to assays that go to completion in minutes, rather than in hours. Though far from competitive at the moment, assay formats involving removable fluorophores might thus become suitable for reading short stretches of DNA. Photolabile linkers have the advantage of enabling the use of light to control when the next nucleotide is admitted. Unlike most chemical deprotection agents, light does not induce the dissociation of primer–template duplexes. We are currently working on syntheses for nucleotides containing all four nucleobases (A/C/G/T) with photolably linked fluorophores. Independent of

 © 2006 Wiley-VCH Verlag GmbH & Co. KGaA, Weinheim

further technical advances, the current results again demonstrate that nucleic acids in themselves have a strong propensity to undergo spontaneous replication reaction sequence selectively.

Received: March 1, 2006
Published online: August 22, 2006

Keywords: DNA recognition · DNA replication · oligonucleotides · primer extension · single-nucleotide polymorphism

[1] M. L. Metzker, *Genome Res.* **2005**, *15*, 1767 – 1776.
[2] a) J. Shendure, R. D. Mitra, C. Varma, G. M. Church, *Nat. Rev. Genet.* **2004**, *5*, 335 – 344; b) C. H. Arnaud, *Chem. Eng. News* **2005**, *83*(51), 60 – 61.
[3] F. Sanger, G. M. Air, B. G. Barrell, N. L. Brown, A. R. Coulson, J. C. Fiddes, C. A. Hutchison III, P. M. Slocombe, M. Smith, *Nature* **1977**, *265*, 687 – 695.
[4] B. B. Rosenblum, L. G. Lee, S. L. Spurgeon, S. H. Khan, S. M. Menchen, C. R. Heiner, S. M. Chen, *Nucleic Acids Res.* **1997**, *25*, 4500 – 4504.
[5] I. A. Kozlov, L. E. Orgel, *Mol. Biol.* **2000**, *34*, 781 – 789.
[6] Selected references: a) I. A. Kozlov, S. Pitsch, L. E. Orgel, *Proc. Natl. Acad. Sci. USA* **1998**, *95*, 13448 – 13452; b) M. Koppitz, P. E. Nielsen, L. E. Orgel, *J. Am. Chem. Soc.* **1998**, *120*, 4563 – 4569; c) C. Hartel, M. W. Göbel, *Helv. Chim. Acta* **2000**, *83*, 2541 – 2549; d) J. C. Chaput, C. Switzer, *J. Am. Chem. Soc.* **2000**, *122*, 12866 – 12867; e) I. A. Kozlov, M. Zielinski, B. Allart, L. Kerremans, A. Van Aerschot, R. Busson, P. Herdewijn, L. E. Orgel, *Chem. Eur. J.* **2000**, *6*, 151 – 155; f) X. Wu, G. Delgado, R. Krishnamurthy, A. Eschenmoser, *Org. Lett.* **2002**, *4*, 1283 – 1286; g) S. Ficht, A. Mattes, O. Seitz, *J. Am. Chem. Soc.* **2004**, *126*, 9970 – 9981.
[7] X. Li, D. R. Liu, *Angew. Chem.* **2004**, *116*, 4956 – 4979; *Angew. Chem. Int. Ed.* **2004**, *43*, 4848 – 4870.
[8] P. Hagenbuch, E. Kervio, A. Hochgesand, U. Plutowski, C. Richert, *Angew. Chem.* **2005**, *117*, 6746 – 6750; *Angew. Chem. Int. Ed.* **2005**, *44*, 6588 – 6592.
[9] Compare also: S. R. Vogel, C. Deck, C. Richert, *Chem. Commun.* **2005**, 4922 – 4924.
[10] For selected recently developed sequencing methods that employ parallel optical read-outs, see, for example: a) J. Shendure, G. J. Porreca, N. B. Reppas, X. Lin, J. P. McCutheon, A. M. Rosenbaum, M. D. Wang, K. Zhang, R. D. Mitra, G. M. Church, *Science* **2005**, *309*, 1728 – 1732; b) M. Margulies, M. Egholm, W. E. Altman, S. Attiya, J. S. Bader, L. A. Bemben, J. Berka, M. S. Braverman, Y.-J. Chen, Z. Chen, S. B. Dewell, L. Du, J. M. Fierro, X. V. Gomes, B. C. Godwin, W. He, S. Helgesen, C. H. Ho, G. P. Irzyk, S. C. Jando, M. L. I. Alenquer, T. P. Jarvie, K. B. Jirage, J.-B. Kim, J. R. Knight, J. R. Lanza, J. H. Leamon, S. M. Lefkowitz, M. Lei, J. Li, K. L. Lohman, H. Lu, V. B. Makhijani, K. E. McDade, M. P. McKenna, E. W. Myers, E. Nickerson, J. R. Nobile, R. Plant, B. P. Puc, M. T. Ronan, G. T. Roth, G. J. Sarkis, J. F. Simons, J. W. Simpson, M. Srinivasan, K. R. Tartaro, A. Tomasz, K. A. Vogt, G. A. Volkmer, S. H. Wang, Y. Wang, M. P. Weiner, P. Yu, R. F. Begley, J. M. Rothberg, *Nature* **2005**, *437*, 376 – 377; c) T. S. Seo, X. Bai, D. H. Kim, Q. Meng, S. Shi, H. Ruparel, Z. Li, N. J. Turro, J. Ju, *Proc. Natl. Acad. Sci. USA* **2005**, *102*, 5926 – 5931.
[11] N. Griesang, E. Kervio, C. Richert, *Synthesis* **2005**, 2327 – 2334.
[12] S. Doublie, S. Tabor, A. M. Long, C. C. Richardson, T. Ellenberger, *Nature* **1998**, *391*, 251 – 258.
[13] H. Ruparel, L. Bi, Z. Li, X. Bai, D. H. Kim, N. J. Turro, J. Ju, *Proc. Natl. Acad. Sci. USA* **2005**, *102*, 5932 – 5937.
[14] The nucleoside-loaded cpg was chosen as an inexpensive source of a DMT-protected, alcohol-displaying support for automated DNA synthesis, even though the deoxynucleoside loaded onto the support was, in itself, not required. The first nucleoside does serve as a useful internal standard for HPLC analyses of crudes, however.
[15] T. Horn, M. S. Urdea, *Tetrahedron Lett.* **1986**, *27*, 4705 – 4708.
[16] E. Uhlmann, J. Engels, *Tetrahedron Lett.* **1986**, *27*, 1023 – 1026.
[17] W. H. Connors, S. Narayanan, O. P. Kryatova, C. Richert, *Org. Lett.* **2003**, *5*, 247 – 250.
[18] S. Altmann, A. M. Labhardt, D. Bur, C. Lehmann, W. Bannwarth, M. Billeter, K. Wüthrich, W. Leupin, *Nucleic Acids Res.* **1995**, *23*, 4827 – 4835.
[19] K. J. Prabahar, T. D. Cole, J. P. Ferris, *J. Am. Chem. Soc.* **1994**, *116*, 10914 – 10920.
[20] a) R. Lohrmann, L. E. Orgel, *Nature* **1976**, *261*, 342 – 344; b) W. S. Zielinski, L. E. Orgel, *Nucleic Acids Res.* **1987**, *15*, 1699 – 1715; c) W. S. Zielinski, L. E. Orgel, *Nature* **1987**, *327*, 346 – 347; d) A. Kanavarioti, M. W. Stronach, R. J. Ketner, T. B. Hurley, *J. Org. Chem.* **1995**, *60*, 632 – 637; e) A. Luther, R. Brandsch, G. von Kiedrowski, *Nature* **1998**, *396*, 245 – 248.
[21] The microarrays were prepared as described in: K. L. Dombi, N. Griesang, C. Richert, *Synthesis* **2002**, 816 – 824, with the modifications mentioned in: Z. Dogan, R. Paulini, J. A. Rojas Stütz, S. Narayanan, C. Richert, *J. Am. Chem. Soc.* **2004**, *126*, 4762 – 4763.
[22] J. A. Rojas Stütz, C. Richert, *Chem. Eur. J.*, **2006**, *12*, 2472 – 2481.
[23] P. Baumhof, N. Griesang, M. Bächle, C. Richert, *J. Org. Chem.* **2006**, *71*, 1060 – 1067.

 © 2006 Wiley-VCH Verlag GmbH & Co. KGaA, Weinheim

Bifunctional Metal Complexes

DOI: 10.1002/anie.200600938

2D NMR Spectroscopic Evidence for Unprecedented Interactions of *cis*-$[Rh_2(dap)(\mu\text{-}O_2CCH_3)_2(\eta^1\text{-}O_2CCH_3)(CH_3OH)](O_2CCH_3)$ with a DNA Oligonucleotide: Combination of Intercalative and Coordinative Binding **

*Mijeong Kang, Abdellatif Chouai, Helen T. Chifotides, and Kim R. Dunbar**

Coordination binding to nucleic acid bases[1,2] and intercalation between DNA bases[3–5] are two major interactions that metal complexes establish with DNA. These binding modes

[*] M. Kang, Dr. A. Chouai, Dr. H. T. Chifotides, Prof. Dr. K. R. Dunbar
Department of Chemistry
Texas A&M University
College Station, TX 77842 (USA)
Fax: (+1) 979-845-7177
E-mail: dunbar@mail.chem.tamu.edu

[**] K.R.D. is grateful to the Robert A. Welch Foundation for support of this research. dap = 1,12-diazaperylene.

Supporting information for this article is available on the WWW under http://www.angewandte.org or from the author.

WILEY InterScience DISCOVER SOMETHING GREAT
© 2006 Wiley-VCH Verlag GmbH & Co. KGaA, Weinheim

cause changes in the DNA structure that can affect cellular processes and may result in cytotoxicity and cell death. Most metal complexes, including the well-known anticancer drug cisplatin,[1] are mononuclear complexes that coordinatively bind to DNA purines. There are, however, a few cases of inorganic or organometallic antitumor agents that incorporate more than one metal unit, for example, by introducing a hydrocarbon chain or polypeptide unit to form a multifunctional complex with improved binding affinity to DNA. Examples of systems under study are polynuclear platinum complexes,[6–12] compounds with one or more intercalative binding units,[3,13,14] and metal complexes with bifunctional coordinative and intercalative binding units.[8–12,15–20] There are also reports of intercalative and coordinatively bound organometallic ruthenium(II) anticancer complexes that possess both an intercalating arene group and a labile chloride ligand.[21–23]

Among the many metal complexes that are known to exhibit antitumor activity are dirhodium compounds that establish coordinative interactions with DNA[24,25] with a preference for the N7 sites of adenine and guanine.[25,26] Recently, an entirely new class of dirhodium(II) carboxylate complexes with intercalating groups has been developed jointly by Dunbar, Turro, and co-workers as potential agents for photochemotherapy.[27] Of specific interest to the present study are complexes that contain a chelating intercalating ligand on one of the two Rh atoms and two *cis* labile ligands on the second Rh center, a situation that poises the compounds to act as dual intercalative/coordinative binding agents for DNA.

To date, most studies on metal complexes that show combined coordinative and intercalative interactions with DNA have made use of UV/Vis and CD spectroscopies as well as thermostability measurements to probe these interactions. To our knowledge, however, there are no NMR spectroscopic investigations of such adducts to probe the precise mode of binding to DNA oligonucleotides. Herein, we report a 2D NMR spectroscopic investigation of a new dirhodium complex binding to a DNA 12 mer by combined intercalative and coordinative interactions.

The compound *cis*-[Rh_2(dap)(μ-O_2CCH_3)$_2$(η^1-O_2CCH_3)-(CH_3OH)](O_2CCH_3) (**1**; dap = 1,12-diazaperylene),[28] as shown in Scheme 1, was selected for the present study owing to the fact that it contains the intercalating dap ligand on one Rh atom and a labile, monodentate acetate group on the other Rh center. Compound **1** was incubated with d(CTCTCAACTTCC) (AA12 mer) in a 1:1 ratio in water at 37 °C (see the Supporting Information). The major dirhodium–DNA adduct was isolated by combined reverse-phase and anion-exchange HPLC chromatography.

The complementary strand d(GGAAGTTGAGAG) (TT12 mer) was added to the isolated single-stranded dirhodium adduct (see the Supporting Information) and the major dirhodium double-stranded (ds) DNA adduct Rh_2(dap)-(O_2CCH_3)$_2$–AA12 mer_ds was investigated by 2D NMR spectroscopy, which revealed several interesting features. First, the DQF-COSY spectrum of the major adduct shows noticeable changes in the chemical shifts of the protons of residues C5 and C8 of the dirhodium adduct as compared to the DQF-COSY spectrum of the unmodified AA12 mer_ds (see the Supporting Information). Second, overall upfield shifts were observed for the resonances of the ligand protons upon metal binding. The most significant shifts were observed for the LH9 and LH10 protons ($\approx$1 ppm), which are located on the opposite side of the dangling acetate group in **1**. Finally, it was possible to complete the NOESY "walk" with the cross-peaks of the aromatic protons of the bases to the H1′ protons of the sugar rings for the metalated double-stranded DNA. The connections between the A6 and A7, and the T18 and T19 residues, however, were not clear, which is an indication of disruption of this base step (see the Supporting Information). The absence of the respective H2 and H8 proton correlations of the A6 and A7 residues in other regions of the NOESY spectrum, which normally give very strong NOESY cross-peaks in double-stranded B-DNA (Figure 1), also corroborates disruption of this base step.

The previous observations imply that the distance between the A6–T19 and the A7–T18 base step is longer than that in normal B-DNA due to the insertion of the dap group between these bases. The latter is fully supported by the prevalent NOE cross-peaks of the H2 and H8 protons of A6 and A7 residues to the dap protons (Figure 2). If the dirhodium compound was merely coordinatively bound to either the A6 or A7 residues, the dap ligand would be located on either the major- or minor-groove of DNA. In this case, the NOE correlation peaks of the dap protons would be

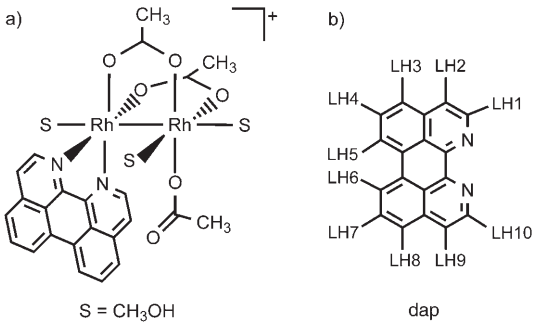

Scheme 1. Structures of a) *cis*-[Rh_2(dap)(μ-O_2CCH_3)$_2$(η^1-O_2CCH_3)-(CH_3OH)](O_2CCH_3) and b) numbering scheme for the dap ligand.

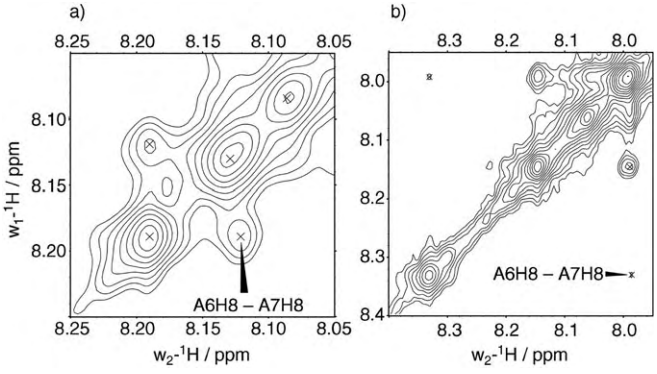

Figure 1. Comparison of the sizes of the NOE correlation peaks between A6H8 and A7H8 in double-stranded DNA oligonucleotides. a) Unmodified AA12 mer_ds, b) Rh_2(dap)(O_2CCH_3)$_2$–AA12 mer_ds.

 © 2006 Wiley-VCH Verlag GmbH & Co. KGaA, Weinheim

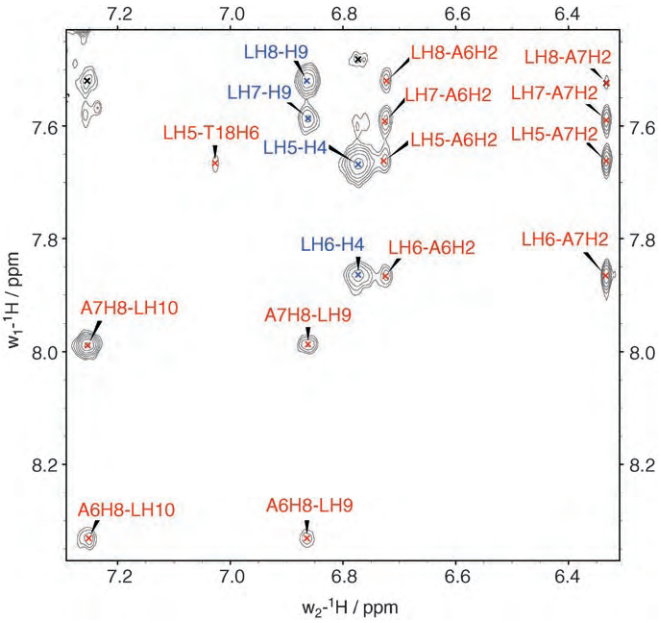

Figure 2. Expansion of the NOESY spectrum of $Rh_2(dap)(O_2CCH_3)_2$–AA12 mer_ds in D_2O at 15 °C. The blue labels indicate the NOE cross-peaks between dap protons and the red labels between the aromatic protons of the AA12 mer and the dap protons.

observable with either the H8 or H2 protons, but not with both, because the H2 and H8 protons are located on opposite sides of the double-stranded DNA. As NOE cross-peaks are observed for both H2 and H8 with the dap protons (Figure 2), the NOESY data provide solid evidence for the intercalation of the dap ligand between the A6 and A7 residues.

Apart from the intercalation between DNA bases in $Rh_2(dap)(O_2CCH_3)_2$–AA12 mer_ds, the NMR spectroscopic data support coordinative binding of the adenine residue A6 to the dirhodium unit. The assignment of the N7 atom of residue A6 as the binding site of the dirhodium complex, instead of the N7 atom of residue A7, is mainly due to the downfield chemical shift of the H8 proton of A6 ($\Delta\delta =$ 0.14 ppm) in contrast to the upfield shift ($\Delta\delta = -0.12$ ppm) of the H8 proton of the A7 residue. The downfield shift of A6H8 is rather small when compared with the dirhodium adduct from the reaction of $Rh_2(O_2CCH_3)_4$ with the same AA12 mer ($\Delta\delta = 0.55$ ppm)[29] in which the dirhodium unit binds to the N7 atom of the A6 residue. In the present case, however, the change in chemical shift for A6H8 reflects both the downfield shift induced by the coordinative binding of the metal on the protons near the metal-binding site (inductive effect)[30] and the upfield shift induced by the intercalation effect on the protons located above or below the intercalator, due to the ring current of the aromatic group.[31] On the other hand, pure upfield shifts due to intercalation are evident for the H2 protons of the A6 and A7 residues of the dirhodium adduct when compared to the AA12mer_ds ($\Delta\delta = -0.51$ and -1.24 ppm, respectively), as well as for the LH9 and LH10 protons with upfield shifts of ≈ 1 ppm as compared to **1** (see the Supporting Information). As compared to the LH9 and LH10 protons, however, the upfield shifts of protons LH1 and LH2 are relatively small ($\Delta\delta = -0.13$ to -0.19 ppm; see the Supporting Information). This may be due to the fact that the dap ligand intercalates more towards the AA12 mer rather than the complementary strand owing to coordination bonding to the N7 site of residue A6. Based on the watergate-NOESY data of the dirhodium–DNA adduct at different temperatures, the coordinative binding and intercalation appear to disrupt the structure more severely at the downstream end of the DNA oligonucleotide duplex, for example, residues A7, C8, and T18. The intensity of the NOE cross-peak of the A7H2–T18N3H pair is much weaker than that of A6H2–T19N3H, and the former nearly disappears when the temperature is raised from 7 °C to 15 °C (see the Supporting Information).

The aforementioned 2D NMR data corroborate coordinative binding and intercalation of **1** in the AA12 mer_ds as proposed in Figure 3. The combined effects of coordinative

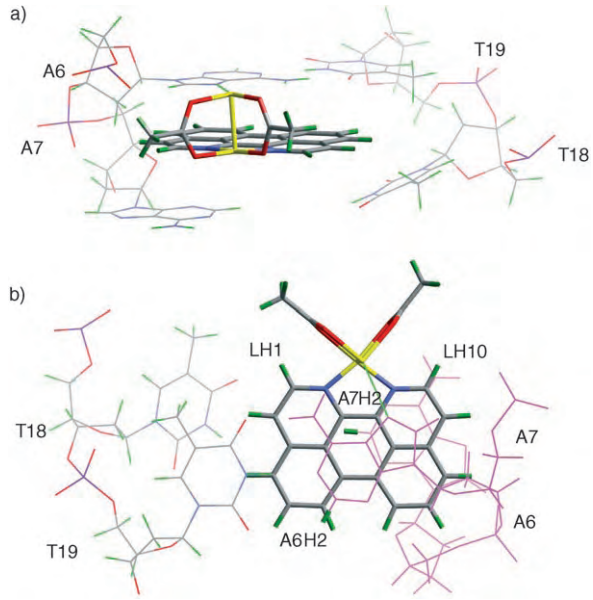

Figure 3. Proposed binding model for $Rh_2(dap)(O_2CCH_3)_2$–AA12 mer_ds with a combination of intercalative and coordinative binding. a) Side view and b) top view along the DNA axis of the oligonucleotide duplex.

and intercalative binding on the physical properties of the AA12 mer are also evident from the changes in the T_m (melting temperature) value of $Rh_2(dap)(O_2CCH_3)_2$–AA12 mer_ds ($\Delta T_m = -6.0$ °C; see the Supporting Information) as compared to the dirhodium adduct ($Rh_2(O_2CCH_3)_3$–AA12 mer_ds), which involves only coordination binding at the same site ($\Delta T_m = -22.9$ °C),[29] to cisplatin coordination binding ($\Delta T_m = -13.5$ °C),[32] or to metallointercalators ($\Delta T_m = 16$ °C).[33] Thus, in the present dirhodium–DNA adduct, the effects of coordination binding appear to dominate over the effects of intercalation for both the chemical shift of A6H8 and T_m value changes.

Owing to the octahedral coordination environment of both Rh atoms, the equatorial coordination binding to the N7 atom of the A6 residue renders the dap group capable of stacking with the adenine bases without causing any bending

 © 2006 Wiley-VCH Verlag GmbH & Co. KGaA, Weinheim

of the aromatic groups, as observed in the case of a rhenium(II) biphenyl compound.[21,22] Furthermore, this dual binding of the dirhodium complex lends stability to the metal–DNA adduct.

In conclusion, we have shown that the dirhodium dap complex has the dual capability of intercalative and coordinative binding, which is an exciting new direction for designing dirhodium compounds that bind tightly and specifically to DNA. Future studies on this type of dirhodium compounds[34] with double-stranded DNA are in progress and the results will be reported in due course.

Received: March 9, 2006
Published online: August 22, 2006

Keywords: bifunctional metal complexes · coordination modes · dirhodium compounds · intercalation · NMR spectroscopy

[1] a) E. R. Jamieson, S. J. Lippard, *Chem. Rev.* **1999**, *99*, 2467 – 2498; b) Z. Guo, P. J. Sadler, *Angew. Chem.* **1999**, *111*, 1512 – 1531; *Angew. Chem. Int. Ed.* **1999**, *38*, 1512 – 1531; c) B. A. J. Jansen, J. M. Pérez, A. Pizarro, C. Alonso, J. Reedijk, C. N. Navarro-Ranniger, *J. Inorg. Biochem.* **2001**, *85*, 229 – 235; d) S. O. Ano, F. P. Intini, G. Natile, L. G. Marzilli, *J. Am. Chem. Soc.* **1997**, *119*, 8570 – 8571.

[2] a) K. R. Barnes, S. J. Lippard, *Met. Ions Biol. Syst.* **2004**, *42*, 143 – 177; b) M. Carlone, L. G. Marzilli, G. Natile, *Eur. J. Inorg. Chem.* **2005**, 1264 – 1273; c) Y. Liu, J. Vinje, C. Pacifico, G. Natile, E. Sletten, *J. Am. Chem. Soc.* **2002**, *124*, 12854 – 12862; d) V. Beljanski, J. M. Villanueva, P. W. Doetsch, G. Natile, L. G. Marzilli, *J. Am. Chem. Soc.* **2005**, *127*, 15833 – 15842; e) K. M. Williams, T. Scarcia, G. Natile, L. G. Marzilli, *Inorg. Chem.* **2001**, *40*, 445 – 454.

[3] a) K. E. Erkkila, D. T. Odom, J. K. Barton, *Chem. Rev.* **1999**, *99*, 2777 – 2795; b) C. R. Brodie, J. G. Collins, J. R. Aldrich-Wright, *Dalton Trans.* **2004**, 1145 – 1152.

[4] U. Schatzschneider, J. K. Barton, *J. Am. Chem. Soc.* **2004**, *126*, 8630 – 8631.

[5] W. Lu, D. A. Vicic, J. K. Barton, *Inorg. Chem.* **2005**, *44*, 7970 – 7980.

[6] a) Y. Qu, N. J. Scarsdale, M.-C. Tran, N. Farrell, *J. Biol. Inorg. Chem.* **2003**, *8*, 19 – 28; b) Y. Qu, N. Farrell, *Inorg. Chem.* **1995**, *34*, 3573 – 3576.

[7] N. Farrell, Y. Qu, U. Bierbach, M. Valsecchi, E. Menta, *Cisplatin* **1999**, 479 – 496.

[8] N. Farrell, *Platinum-Based Drugs in Cancer Therapy* **2000**, pp. 321–338.

[9] N. J. Wheate, J. G. Collins, *Coord. Chem. Rev.* **2003**, *241*, 133 – 145.

[10] M. Kloster, H. Kostrhunova, R. Zaludova, J. Malina, J. Kasparkova, V. Brabec, N. Farrell, *Biochemistry* **2004**, *43*, 7776 – 7786.

[11] V. Brabec, J. Kasparkova, *Drug Resist. Updates* **2005**, *8*, 131 – 146.

[12] A. Harris, Y. Qu, N. Farrell, *Inorg. Chem.* **2005**, *44*, 1196 – 1198.

[13] B. Önfelt, P. Lincoln, B. Nordén, *J. Am. Chem. Soc.* **1999**, *121*, 10846 – 10847.

[14] L. M. Wilhelmsson, F. Westerlund, P. Lincoln, B. Nordén, *J. Am. Chem. Soc.* **2002**, *124*, 12092 – 12093.

[15] B. E. Bowler, K. J. Ahmed, W. I. Sundquist, L. S. Hollis, E. E. Whang, S. J. Lippard, *J. Am. Chem. Soc.* **1989**, *111*, 1299 – 1306.

[16] M. Milkevitch, H. Storrie, E. Brauns, K. J. Brewer, B. W. Shirley, *Inorg. Chem.* **1997**, *36*, 4534 – 4538.

[17] L. C. Perrin, P. D. Prenzler, C. Cullinane, D. R. Phillips, W. A. Denny, W. D. McFadyen, *J. Inorg. Biochem.* **2000**, *81*, 111 – 117.

[18] M. D. Temple, W. D. McFadyen, R. J. Holmes, W. A. Denny, V. Murray, *Biochemistry* **2000**, *39*, 5593 – 5599.

[19] H. Baruah, C. S. Day, M. W. Wright, U. Bierbach, *J. Am. Chem. Soc.* **2004**, *126*, 4492 – 4493.

[20] S. Gençaslan, W. S. Sheldrick, *Eur. J. Inorg. Chem.* **2005**, 3840 – 3849.

[21] H. Chen, J. A. Parkinson, S. Parsons, R. A. Coxall, R. O. Gould, P. J. Sadler, *J. Am. Chem. Soc.* **2002**, *124*, 3064 – 3082.

[22] H. Chen, J. A. Parkinson, R. E. Morris, P. J. Sadler, *J. Am. Chem. Soc.* **2003**, *125*, 173 – 186.

[23] Y. K. Yan, M. Melchart, A. Habtemariam, P. J. Sadler, *Chem. Commun.* **2005**, 4764 – 4776.

[24] S. U. Dunham, H. T. Chifotides, S. Mikulski, A. E. Burr, K. R. Dunbar, *Biochemistry* **2005**, *44*, 996 – 1003.

[25] a) H. T. Chifotides, K. R. Dunbar, *Acc. Chem. Res.* **2005**, *38*, 146 – 156; b) H. T. Chifotides, K. M. Koshlap, L. M. Pérez, K. R. Dunbar, *J. Am. Chem. Soc.* **2003**, *125*, 10703 – 10713; c) H. T. Chifotides, K. M. Koshlap, L. M. Pérez, K. R. Dunbar, *J. Am. Chem. Soc.* **2003**, *125*, 10714 – 10724.

[26] J. L. Bear, H. B. Gray, Jr., L. Rainen, I. M. Chang, R. Howard, G. Serio, A. P. Kimball, *Cancer Chemother. Rep. Part 1* **1975**, *59*, 611 – 620.

[27] A. M. Angeles-Boza, P. M. Bradley, P. K. L. Fu, S. E. Wicke, J. Bacsa, K. R. Dunbar, C. Turro, *Inorg. Chem.* **2004**, *43*, 8510 – 8519.

[28] a) A. Chouai, S. E. Wicke, C. Turro, J. Bacsa, K. R. Dunbar, D. Wang, R. P. Thummel, *Inorg. Chem.* **2005**, *44*, 5996 – 6003; b) O. Schmelz, A. Mews, T. Basche, A. Herrmann, K. Müllen, *Langmuir* **2001**, *17*, 2861 – 2865.

[29] M. Kang, Ph.D. Thesis, Texas A&M University (USA), **2005**.

[30] S. U. Dunham, S. U. Dunham, C. J. Turner, S. J. Lippard, *J. Am. Chem. Soc.* **1998**, *120*, 5395 – 5406.

[31] R. M. Silverstein, G. C. Bassler, T. C. Morrill *Spectrometric Identification of Organic Compounds*, 5th ed., Wiley, New York, **1991**.

[32] B. I. Kankia, D. W. Kupke, L. A. Marky, *J. Phys. Chem. B* **2001**, *105*, 11402 – 11405.

[33] C. M. Dupureur, J. K. Barton, *Inorg. Chem.* **1997**, *36*, 33 – 43.

[34] H. T. Chifotides, K. R. Dunbar "Rhodium Compounds" (Chapter 12) *Mutiple Bonds Between Metal Atoms* (Eds.: F. A. Cotton, C. Murillo, R. A. Walton), Springer-Science and Business Media, New York, **2005**, 465 – 589.

 © 2006 Wiley-VCH Verlag GmbH & Co. KGaA, Weinheim

Polymeric Sensors

DOI: 10.1002/anie.200601844

Phosphole-Modified Poly(thiophene)s: Unique Postfunctionalizable Conjugated Polymers That Sense Elemental Chalcogenides**

*Manuel Sebastian, Muriel Hissler, Claire Fave, Joëlle Rault-Berthelot, Christophe Odin, and Régis Réau**

Dedicated to Professor Ulrich Zenneck on the occasion of his 60th birthday

A fruitful strategy for diversifying the properties and expanding the functions of classical π-conjugated polymers such as poly(thiophene)s involves the incorporation of reactive heteroatoms into the conjugated chain.[1] This approach has been intensively investigated with Lewis acidic boron groups[2] which can, for example, bind anions or nucleophiles to afford sensor properties in the polymeric materials.[2e,f] In contrast, very few conjugated polymers incorporating Lewis basic σ^3,λ^3-phosphorus moieties are known[3] although the versatile reactivity of the P centers (nucleophilicity, coordination ability, etc.)[4] should allow a variety of postfunctionalizations. Herein, we describe the synthesis of the first poly(thiophene) modified by its P analogue, namely the σ^3,λ^3-phosphole ring. We show that the P centers are strongly electronically coupled with the conjugated π system and that they are recognition sites acting in a cooperative fashion, a property which is highly desirable for the design of efficient chemosensors.[5a–c] Moreover, the presence of the σ^3,λ^3-P moieties allows for the detection of elemental chalcogens, which are important oligoelements,[6] and thereby provides an unprecedented sensor property for organic conducting polymers.

σ^3,λ^3-Phospholes are a unique building block for the engineering of molecular π-conjugated systems[7] owing to the presence of reactive phosphorus centers which offer a direct access to novel derivatives with different electronic properties.[8] For example, the facile complexation of the bis-(thienyl)-σ^3,λ^3-phosphole **1** with [(tht)AuCl] yields the σ^4 Au^I complex **2**[8c] (Scheme 1), which displays a red-shifted λ_{max} wave and lower oxidation potential than **1**. The challenge was thus to extend this unique *molecular* approach to

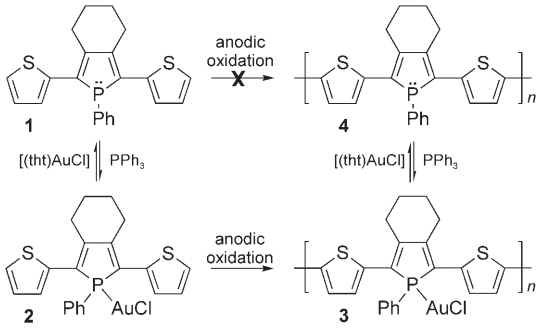

Scheme 1. Synthesis of polymers **3** and **4**; tht = tetrahydrothiophene.

polymers by synthesizing the σ^3,λ^3-phosphole-modified poly-(thiophene) **4** (Scheme 1). Unfortunately, a direct access to **4** (**1**→**4**) is not viable because the σ^3-phosphole ring of **1** does not tolerate oxidative electropolymerization of thiophene units, probably as a result of reactions of the nucleophilic P atom either with radical cations or protons formed during the chain-growth process. In order to avoid these lone-pair interferences, we investigated a synthetic P-protection/electropolymerization/P-deprotection strategy since electropolymerization has been successfully applied for some thienyl-capped σ^4-phosphole monomers.[8a,b] Quite surprisingly, the reaction of **1** with BH_3, a common protecting group for σ^3-P atoms,[4] affords an unstable adduct. Therefore, the readily accessible, P-protected σ^4 Au^I complex **2** was submitted to anodic electropolymerization (**2**→**3**, Scheme 1) which was either performed by potentiostatic oxidation or by cyclic voltammetry (CV) on a Pt electrode. Upon repeated cycling between −0.5 V and 1.25 V in CH_2Cl_2, one observes the regular growth of a new reversible wave (0.5 V vs. ferrocene/ferrocenium (Fc/Fc^+)) and the increase of the main oxidation wave of **2** at 0.8 V versus Fc/Fc^+.[9] These data show the formation of an electroactive polymer film **3** (Scheme 1) since no shift to more positive potentials and no decrease of intensity were observed after 10 sweeps. The material which was dedoped at 0.0 V exhibits a reversible redox process at 0.5 V, and upon recurrent sweeps, the p-doping process of **3** appears to be stable and reversible between −0.5 and 0.85 V.[9]

Dedoped polymer **3** is an insoluble material, and its solid-state UV/Vis spectrum[9] is notably red-shifted compared to that of monomer **2** ($\Delta\lambda_{max} = 175$ nm, $\Delta\lambda_{onset} = 290$ nm). The elemental composition of film **3**, determined by energy-dispersive X-ray analysis (EDX),[9] is the same as the monomer **2** within experimental error. Solid-state, high-resolution ^{31}P NMR spectroscopy gives a clue to establishing the intimate structure of the insoluble polymer **3**. Its magic angle spinning (MAS) ^{31}P NMR spectrum (Figure 1) shows a main broad singlet at $\delta = 45$ ppm, which is a chemical shift characteristic of Au^I phosphole moieties (**2**: $\delta = 39$ ppm), and a minor signal at $\delta = 16$ ppm, which is probably the result of a small amount of P-decomplexed subunits (< 10 %). Material

[*] Dr. M. Sebastian, Dr. M. Hissler, Dr. C. Fave, Dr. J. Rault-Berthelot, Prof. Dr. R. Réau
Sciences Chimiques de Rennes
CNRS UMR 6226 Université de Rennes 1
Campus de Beaulieu, 35042 Rennes Cedex (France)
Fax: (+33) 2-2323-6939
E-mail: regis.reau@univ-rennes1.fr
Dr. C. Odin
Groupe Matière Condensée et Matériaux
CNRS UMR 6626 Université de Rennes 1
Campus de Beaulieu, 35042 Rennes Cedex (France)

[**] We thank the Ministère de la Recherche, the Institut Universitaire de France, the CNRS, and the Deutsche Forschungsgemeinschaft.
Supporting information for this article is available on the WWW under http://www.angewandte.org or from the author.

InterScience
© 2006 Wiley-VCH Verlag GmbH & Co. KGaA, Weinheim

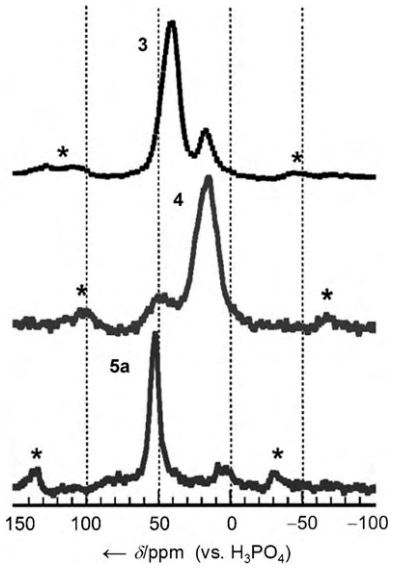

Figure 1. ^{31}P MAS NMR spectra (at 10 kHz spinning) of polymers **3**, **4**, and **5a** (an asterisk (*) indicates the rotation bands).

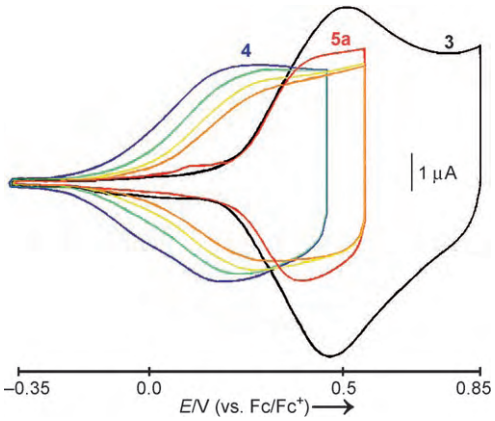

Figure 2. Cyclic voltammograms of polymers **3** (black), **4** (blue), **5a** (red), and **6a**$_1$ (green, $t = 2^1/_2$ min), **6a**$_2$ (yellow, $t = 5$ min), **6a**$_3$ (orange, $t = 10$ min); t = contact time of **4** with a 0.3 M S_8 solution.

3 is one of the very rare poly(thiophene)s featuring metal centers intimately connected to the extended π-conjugated system.[10] It is noteworthy that **3** is not air- or moisture-sensitive; it can be stored for months in air without any modification of its physical properties.

The final step towards target polymer **4** (Scheme 1) required the deprotection of the P atoms of **3** by release of the Au^I fragments. At the molecular level, the addition of an excess of triphenylphosphine to a CH_2Cl_2 solution of complex **2** instantly affords the free phosphole **1** and [(PPh_3)AuCl]. Hence, a Pt electrode coated with polymer **3** was immersed in a CH_2Cl_2 solution of PPh_3 (0.1 M) for one minute and then washed with pure CH_2Cl_2. This treatment resulted in a mass loss of polymer **3** (monitored by microgravimetric quartz-crystal microbalance analysis[9]) corresponding to the release of more than 90% of the {AuCl} protecting groups. EDX analysis[9] of the novel material **4** indicated a low gold content (Au/P < 0.1), and its ^{31}P MAS NMR spectrum (Figure 1) consists of a major resonance at $\delta = 15$ ppm, which is characteristic of σ^3,λ^3-phosphole fragments (**1**: $\delta = 13$ ppm), along with a small peak centered at $\delta = 45$ ppm (non-deprotected P centers). These results show that the metalated conjugated polymer **3** exhibits the same coordination behavior as the molecular complex **2** and that more than 90% of the P moieties of the insoluble material **3** are accessible for chemical reactions. Furthermore, they illustrate the analytical power of ^{31}P MAS NMR spectroscopy in characterizing chemical modifications of phosphole-containing poly(thiophene)s. Indeed, molecular P chemistry (ligand exchange, NMR spectroscopic analysis, etc.) can be simply extended to P-containing conductive materials. The easily synthesized σ^3,λ^3-phosphole-modified poly(thiophene) **4** is not air- or moisture-sensitive and can therefore be handled without special care. On going from **3** to **4** (Scheme 1), a significant negative shift of the oxidation current offset ($\Delta E_{pa} = 260$ mV, Figure 2) and a blue shift of the UV/Vis band[9] associated with π–π* transitions ($\Delta\lambda_{onset} = 41$ nm) were recorded. These modifications of the electrochemical and optical properties, which parallel those observed at the molecular level (that is, **1** has a lower oxidation potential and higher optical HOMO–LUMO gap than **2**),[8c] clearly indicate a close electronic coupling of the P moieties with the π-conjugated system of the polymer backbones. It is likely that, as observed for molecular phosphole-based systems, the intimate coupling of the P moieties with the π-conjugated pathway involves hyperconjugation effects.[8f]

The postfunctionalization of **4** through P modifications was then investigated since conjugated polymers that can covalently attach molecules and translate this chemical information into an observable optical/electrochemical response are very attractive sensor materials.[5] Hence, we tried to duplicate the reactivity pattern of molecular σ^3,λ^3-phosphole **1** with the solid polymeric material **4**. At first, deposited **4** was treated with [(tht)AuCl] to re-form polymer **3** (Scheme 1), a chemical modification which was easily monitored by CV (Figure 2). Hence, owing to the presence of the reactive phosphole moieties, polymer **4** fulfils the prerequisite of sensor materials. This result prompted us to investigate the reactivity of polymer **4** towards elemental sulfur and selenium since chalcogens are well-known to oxidize σ^3,λ^3-P centers at the molecular level.[4] The detection of these chalcogens is of special interest because they are essential oligoelements and also because their sensing is particularly challenging as a result of their chemical and binding inertia under mild reaction conditions.

Polymer **4**, deposited on a Pt electrode, was submerged in a toluene solution of S_8 (0.3 M) for 20 minutes and was then rinsed with pure toluene. The formation of σ^4-thiophosphole polymer **5a** (Scheme 2) is supported by its SEM–EDX analysis,[9] which revealed an S/P ratio of about 3:1, and its ^{31}P MAS NMR spectrum (Figure 1), which shows a signal at $\delta = 52$ ppm, is consistent with the proposed structure.[8b] These results prove that almost all of the σ^3,λ^3-P centers of **4** have been transformed into sulfurized σ^4,λ^5-P centers. The responses accompanying the transformation **4**→**5a** are: 1) a large positive shift of the oxidation current offset ($\Delta E_{pa} =$

 © 2006 Wiley-VCH Verlag GmbH & Co. KGaA, Weinheim

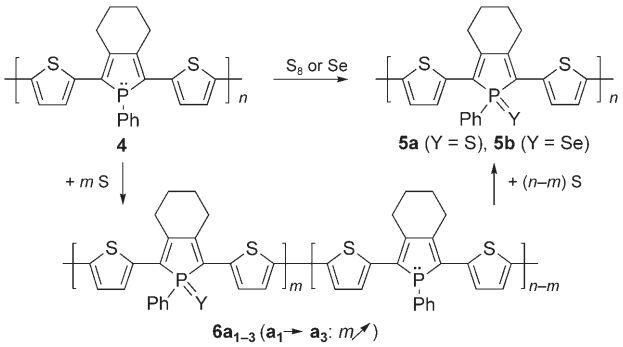

Scheme 2. Chemical modification of polymer **4** with S_8 or Se yielding **5a**,**b** and **6a**$_{1-3}$.

230 mV, Figure 2) and 2) a bathochromic shift of the UV/Vis band ($\Delta\lambda_{onset} = 38$ nm).[9] Hence, this quantitative chemical transformation of the P centers (P→P=S) induces significant modifications of the conjugated polymer properties. Note that **4** can display a real-time response to elemental sulfur (1 minute) upon addition of a small amount of NEt_3 (acting as an S_8 activator) to the toluene solution. In the same way, material **4** also reacts with a suspension of selenium (gray or red) in CH_2Cl_2 to yield **5b** (Scheme 2). This reaction is rather slow because of the poor solubility of selenium, and is accompanied by a significant anodic shift (about 110 mV after 5 hours). Indeed, phosphole-modified polythiophene **4** is the first conjugated polymer which can detect elemental chalcogens. The ability of σ^3-P centers to react with elemental sulphur and selenium is trivial in molecular phosphorus chemistry. However, transposed to the field of conjugated polymers, this reaction is the key to affording unprecedented sensing properties since these chemical postmodifications result in easily measurable macroscopic responses.

Intriguingly, when a Pt electrode that is modified with the polymer **4** is submerged in a solution of S_8 (0.3 M) for just 2.5 minutes, a 60-mV positive offset shifting of the oxidation wave of the resulting material **6a$_1$** is observed (CV in green, Figure 2). It is important to recall that the complete transformation **4**→**5a** (Scheme 2) requires 20 minutes. Further similar sequential exposures of **6a$_1$** to the S_8 solution resulted in a gradual shift of the oxidation peak (**6a$_1$**→**6a$_2$**→**6a$_3$**, Figure 2) until a signal similar to that of **5a** was recorded. Having fully characterized the final adduct **5a**, it is obvious that increasing the contact time involves a progressive sulfurization of the σ^3,λ^3-P centers of **4** (m(**6a$_1$**) < m(**6a$_2$**) < m(**6a$_3$**), Scheme 2).[11] Despite the fact that **6a$_{1-3}$** feature both σ^3- and σ^4-P centers, cyclovoltammetric measurements show just one collective response (Figure 2). Hence, the modification of a collective system response (shift in E_{pa}) upon gradual binding of the σ^3,λ^3-P sites of polymer **4** shows that these recognition sites act in a cooperative fashion. This behavior, which is also observed upon treating **4** with [(tht)AuCl],[9] is an essential prerequisite for the design of sensors that show signal amplification.[5a,b]

In conclusion, these results show that molecular P chemistry (coordination chemistry, P derivatization, NMR analysis, etc.) can be extended to conjugated polymers, and they illustrate the specific properties that directly result from the incorporation of σ^3,λ^3-phosphole moieties into the conjugated backbone. Owing to its intimate coupling with the π system, the P moiety has the capacity to influence the overall properties of the conductive material in a cooperative way. Moreover, its versatile reactivity allows for the detection of elemental chalcogens, thus representing a novel development in the field of molecular recognition by conjugated polymers. The optimization of this P-based material, in terms of selectivity, reversibility, and sensitivity, to obtain an applicable chemosensor is under active investigation.

Received: May 10, 2006
Published online: August 14, 2006

Keywords: chalcogens · cyclic voltammetry · electropolymerization · phosphorus heterocycles · sensors

[1] a) K. Müllen, G. Wegner, *Electronic Materials: The Oligomer Approach*, Wiley-VCH, Weinheim, **1998**; b) D. Fichou, *Handbook of Oligo- and Polythiophenes*, Wiley, New York, **1999**.

[2] a) Z. Yuan, J. C. Collings, N. J. Taylor, T. B. Marder, C. Jardin, J.-F. Halet, *J. Solid State Chem.* **2000**, *154*, 5–12; b) C. D. Entwistle, T. B. Marder, *Chem. Mater.* **2004**, *16*, 4574–4585; c) R. J.-P. Corriu, T. Deforth, W. E. Douglas, G. Guerrero, W. S. Siebert, *Chem. Commun.* **1998**, 963–964; d) N. Matsumi, K. Naka, Y. Chujo, *J. Am. Chem. Soc.* **1998**, *120*, 10776–10777; e) S. Yamaguchi, S. Akiyama, K. Tamao, *J. Am. Chem. Soc.* **2001**, *123*, 11372–11375; f) A. Sundararaman, M. Victor, R. Varughese, F. Jäkle, *J. Am. Chem. Soc.* **2005**, *127*, 13748–13749.

[3] a) S. S. H. Mao, T. D. Tilley, *Macromolecules* **1997**, *30*, 5566–5569; b) B. L. Lucht, N. O. St. Onge, *Chem. Commun.* **2000**, 2097–2098; c) Y. Morisaki, Y. Aiki, Y. Chujo, *Macromolecules* **2003**, *36*, 2594–2597; d) Z. Jin, B. L. Lucht, *J. Am. Chem. Soc.* **2005**, *127*, 5586–5595.

[4] a) F. Mathey, *Phosphorus-Carbon Heterocyclic Chemistry: The Rise of a New Domain*, Elsevier Science, Oxford, **2001**; b) F. Mathey, J. F. Nixon, K. B. Dillon, *Phosphorus: The Carbon Copy*, Wiley-VCH, Weinheim, **1997**.

[5] a) T. M. Swager, *Acc. Chem. Res.* **1998**, *31*, 201–207; b) D. T. McQuade, A. Pullen, T. M. Swager, *Chem. Rev.* **2000**, *100*, 2537–2574; c) A. Rose, Z. Zhu, C. F. Madigan, T. M. Swager, V. Bulovic, *Nature* **2005**, *434*, 876–879; d) M. Leclerc, *Adv. Mater.* **1999**, *11*, 1491–1498.

[6] a) *The Biological Chemistry of the Elements*; (Eds.: J. J. R. Fraústo da Silva, R. J. P. Williams, Oxford University Press, Oxford, **2001**; b) M. P. Rayman, *Lancet* **2000**, *356*, 233–241; c) J. Chen, M. J. Berry, *J. Neurochem.* **2003**, *86*, 1–12.

[7] a) O. M. Bevierre, F. Mercier, L. Richard, F. Mathey, *Angew. Chem.* **1990**, *102*, 672–675; *Angew. Chem. Int. Ed. Engl.* **1990**, *29*, 655–657; b) E. Deschamps, L. Richard, F. Mathey, *Heteroat. Chem.* **1991**, *2*, 377–383; c) O. M. Bevierre, F. Mercier, F. Mathey, S. Jutand, C. Amatore, *New J. Chem.* **1991**, *15*, 545; d) T. Baumgartner, T. Neumann, B. Wirges, *Angew. Chem.* **2004**, *116*, 6323–6328; *Angew. Chem. Int. Ed.* **2004**, *43*, 6197–6201; e) T. Baumgartner, W. Bergmans, T. Kárpáti, T. Neumann, M. Nieger, L. Nyulászi, *Chem. Eur. J.* **2005**, *11*, 4687–4699; f) T. Baumgartner, W. Wilk, *Org. Lett.* **2006**, *8*, 503–506.

[8] a) C. Hay, C. Fischmeister, M. Hissler, L. Toupet, R. Réau, *Angew. Chem.* **2000**, *112*, 1882–1885; *Angew. Chem. Int. Ed.* **2000**, *39*, 1812–1815; b) C. Hay, M. Hissler, C. Fischmeister, J. Rault-Berthelot, L. Toupet, L. Nyulászi, R. Réau, *Chem. Eur. J.* **2001**, *7*, 4222–4236; c) C. Fave, T.-Y. Cho, M. Hissler, C.-W. Chen, T.-Y. Luh, C.-C. Wu, R. Réau, *J. Am. Chem. Soc.* **2003**,

 © 2006 Wiley-VCH Verlag GmbH & Co. KGaA, Weinheim

125, 9254 – 9255; d) C. Fave, M. Hissler, T. Kárpáti, J. Rault-Berthelot, V. Deborde, L. Toupet, L. Nyulászi, R. Réau, *J. Am. Chem. Soc.* **2004**, *126*, 6058 – 6063; e) H.-C. Su, O. Fadhel, C.-J. Yang, T.-Y. Cho, C. Fave, M. Hissler, C.-C. Wu, R. Réau, *J. Am. Chem. Soc.* **2006**, *128*, 983 – 995; f) L. Nyulászi, O. Hollóczki, C. Lescop, M. Hissler, R. Réau, *Org. Biomol. Chem.* **2006**, *4*, 996 – 998; g) J. Casado, R. Réau, J.-T. Lopez-Navarrete, *Chem. Eur. J.* **2005**, *11*, 3759 – 3767.

[9] See the Supporting Information.

[10] a) O. Clot, M. O. Wolf, B. Patrick, *J. Am. Chem. Soc.* **2000**, *122*, 10456 – 10457; b) D. Weinberger, T. Higgins, C. Mirkin, L. Liable-Sands, A. L. Rheingold, *Angew. Chem.* **1999**, *111*, 2748 – 2750; *Angew. Chem. Int. Ed.* **1999**, *38*, 2565 – 2568; c) O. Clot, M. O. Wolf, B. Patrick, *J. Am. Chem. Soc.* **2001**, *123*, 9963 – 9973; for reviews, see: d) M. O. Wolf, *Adv. Mater.* **2001**, *13*, 545 – 553; e) B. J. Holliday, T. M. Swager, *Chem. Commun.* **2005**, 23 – 36.

[11] The exact degree of sulfurization in $\mathbf{6a_{1-3}}$ cannot be determined because: 1) of the impossibility to obtain sufficient sample quantities for ^{31}P MAS NMR spectroscopy at each step (ca. 50 mg), 2) the mass alterations were not significant for microgravimetric quartz-crystal microbalance analysis, and 3) the random distribution of the sulfurized σ^4,λ^5-P moieties in $\mathbf{6a_{1-3}}$ prevents a reliable determination by SEM–EDX analysis.

 © 2006 Wiley-VCH Verlag GmbH & Co. KGaA, Weinheim

Macrocyclic Systems

DOI: 10.1002/anie.200602206

Anion-Templated Syntheses of Pseudopeptidic Macrocycles**

Miriam Bru, Ignacio Alfonso, M. Isabel Burguete, and Santiago V. Luis**

The design of molecular systems with programmable properties is a major challenge in modern chemistry. Among these properties, a key issue is the development of new procedures for the preparation of complex molecules based on the efficient programmed assembly of the corresponding structural components.[1] Supramolecular approaches to this problem have been developed over recent decades,[2] and templated synthesis, mainly based on cationic templates, is a well-known process.[3] However, anion templation is still in its infancy, as it is restricted to inorganic spherical species in most cases.[4] Recently, we synthesized and studied new pseudopeptidic macrocycles[5] with interesting properties as organogelators,[6] molecular receptors,[7] chemosensors,[8] or molecular devices.[9] During this ongoing research, we envisioned the preparation of larger structures to increase the size and complexity of the substrates within the molecular recognition event. To achieve this goal, reductive amination between the corresponding bisamidoamine **1** and dialdehyde **2** seemed to be a reasonable option (Scheme 1). Unfortunately, we found that a well-defined configurational preorganization is mandatory for the formation of the desired [2+2] tetraimino intermediate.[10] In the absence of such preorganization, the reaction always led to a complex mixture of oligomers.

In the light of those results, we applied a rational approach to overcome this problem. According to the well-established binding modes between anions and NH amide groups,[11] we screened several anions as templates for the desired process in silico.[12] Starting from the modeled structure for the [2+2] tetraimino intermediate, we studied the possible noncovalent complexes between the proposed macrocycle and different anions. Monte Carlo analyses rendered terephthalate (**3**) the best candidate, as it shows an excellent structural complementarity with the macrocycle (Figure 1). According to the computer-generated structure, this dianion would present four hydrogen bonds between the carboxylate groups and the amide hydrogen atoms of the bisamide moieties and a π-stacking interaction with the aromatic rings of the macrocycle.

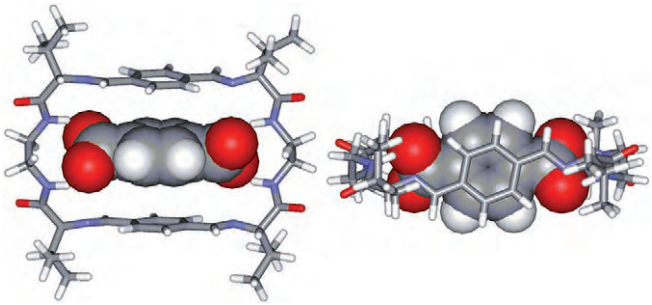

Figure 1. Top and side views of the optimized geometry for the proposed supramolecular complex between the tetraimino macrocycle (stick representation) and terephthalate dianion (space-filling representation). O red, N violet, C gray, H white.

The ^{1}H NMR spectrum of the crude product from the reaction between **1a** and **2** ([D_4]methanol, room temperature, 3 h) showed a complicated group of signals (Figure 2a). An observation of the aldehyde ($\delta = 9.9$–$\delta = 10.2$ ppm) and α-methoxyamine ($\delta \approx 5.6$ ppm) protons clearly demonstrates the existence of open-chain derivatives. The presence of different anions (as tetrabutylammonium (TBA) salts) had minor effects on the ^{1}H NMR spectra (see Figure 2b for chloride ions). However, when the terephthalate dianion (**3**) was used, the spectrum after 3 hours showed an almost quantitative conversion to a major (> 90 %) imino compound

[*] M. Bru, Dr. I. Alfonso, Dr. M. I. Burguete, Dr. S. V. Luis
Departamento de Química Inorgánica y Orgánica, UAMOA, Universidad Jaume I/CSIC
Avd. Sos Baynat s/n, 12071 Castellón (Spain)
Fax: (+34) 964-728-214
E-mail: ialfonso@qio.uji.es
luiss@qio.uji.es

[**] Financial support from the Spanish Ministerio de Educacion y Ciencia (BQU2003-09215-C03-02) Bancaixa-UJI (P/IB2004-38), and Generalitat Valenciana (GRUPOS 04/031) is gratefully acknowledged. I.A. and M.B. thank MEC for financial support (Ramón y Cajal and FPU Programs, respectively).

Supporting information for this article is available on the WWW under http://www.angewandte.org or from the author.

 © 2006 Wiley-VCH Verlag GmbH & Co. KGaA, Weinheim

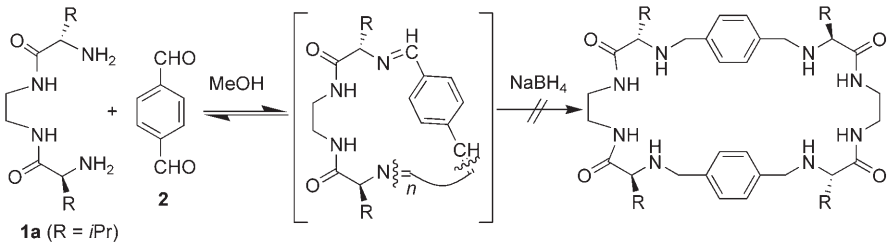

Scheme 1. Proposed reductive amination macrocyclization reaction. Bn = benzyl.

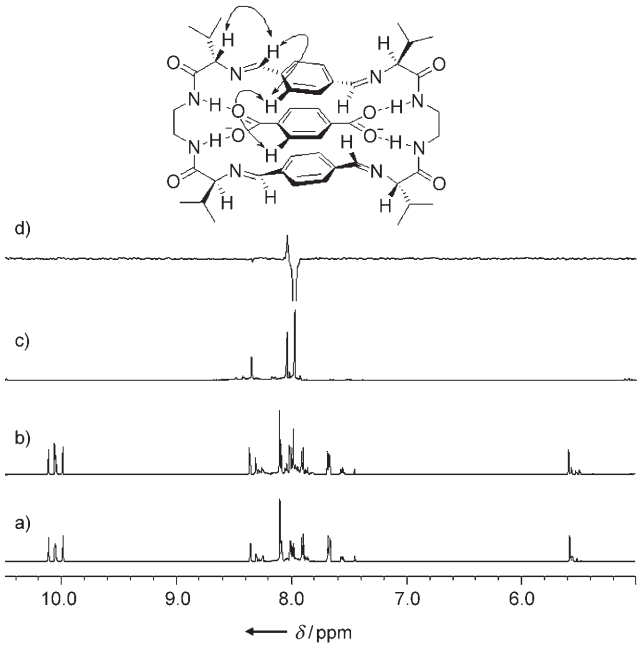

Figure 2. Partial ^{1}H NMR spectra (500 MHz, 303 K, CD_3OD) of a mixture of **1a** and **2** (a) and in the presence of either TBACl (b) or **3**-$(TBA)_2$ (c). d) A 1D ROESY trace upon irradiation of the template signal. Key ROE effects are also shown with double-headed arrows.

with a remarkable D_2 symmetry (Figure 2c). The supramolecular species thus formed was completely characterized by a full set of NMR experiments, thus showing a good agreement with the proposed structure. The macrocycle shows only one imine methyne signal at $\delta = 8.24$ ppm and one single aromatic peak at $\delta = 7.99$ ppm. Besides, the ^{13}C NMR chemical shift for the inimo C=N atom ($\delta =$ 162.7 ppm) suggests a conjugated aromatic diimine moiety. The high symmetry of the spectra implies an *S–trans* configuration of the diimino moieties. The imino proton signal showed a strong rotating-frame nuclear overhauser effect (ROE) effect with the $C_\alpha H$ proton of the pseudopeptidic moiety. This finding supports the connectivity between both substructures, and a *syn* disposition between these hydrogen atoms in the major species (Figure 2), which is in good agreement with the computed geometry. By following the gradual increase of the imine signal, we observed that the formation of the imine bond in the presence of **3**-$(TBA)_2$ was approximately sixfold faster than in the absence of the template. These data suggest that the template also catalyzes the imine condensation.[13] The proposed inclusion of the anion within the macrocyclic polyimine was also demonstrated by different techniques. For example, intermolecular 1D ROESY enhancement was observed between the *ortho* protons of the aromatic imine and the *ortho* protons from the template (see Figure 2d), thus supporting a proximity between both nuclei (3.6–3.8 Å in the computed structure). Moreover, pulsed-field gradient spin-echo (PGSE) NMR[14] experiments showed that signals from the macrocyclic imine and the anion diffuse at the same rate, thus supporting that they form part of the same supramolecular entity. Quantitative analysis rendered a self-diffusion coefficient $D = 5.9 \pm 0.1 \times 10^{-10}\ m^2 s^{-1}$, which is much smaller than that of the free solvated template ($6.4 \pm 0.1 \times 10^{-10}\ m^2 s^{-1}$). Accordingly, the diffusion volume of the supramolecular complex was estimated to be 950 Å^3, whereas the computed volume of the minimized structure was 907 Å^3.[12] This finding represents a very good agreement considering the number of approximations assumed.[15]

Definitive proof for the existence of the proposed supramolecular structure was obtained by ESI-TOF mass spectra (negative detection mode) of the reaction mixture, which showed two major peaks at *m*/*z* 438.2 and 877.5, which correspond to the dianionic and sodiated monoanionic complexes, respectively. Full isotopic analyses also confirmed these assignments (Figure 3).

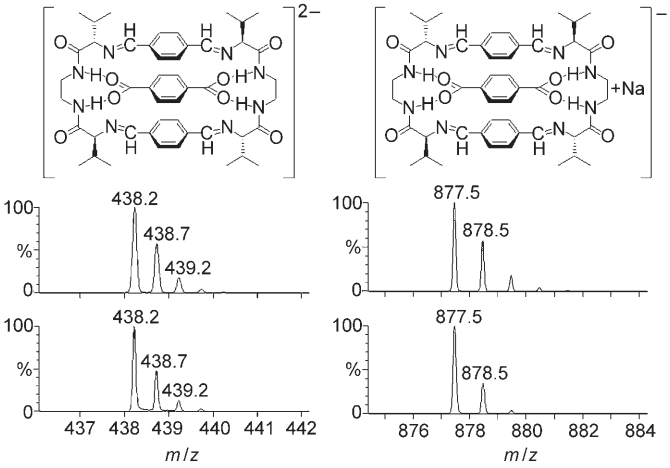

Figure 3. Experimental (lower trace) and simulated (upper trace) ESI-TOF mass spectra for the dianionic (left) and the sodiated monoanionic (right) supramolecular complexes.

For the formation of a highly ordered complex as shown in Figure 1, the spatial disposition of aromatic chromophores must be well defined. This effect can be also accurately studied by circular dichroism (CD) spectroscopy. Thus, CD spectra were acquired for the crude condensation reactions in the presence and absence of **3**. A more pronounced cotton effect was found in the presence of the template (Figure 4), thus suggesting a more organized system. Moreover, the

 © 2006 Wiley-VCH Verlag GmbH & Co. KGaA, Weinheim

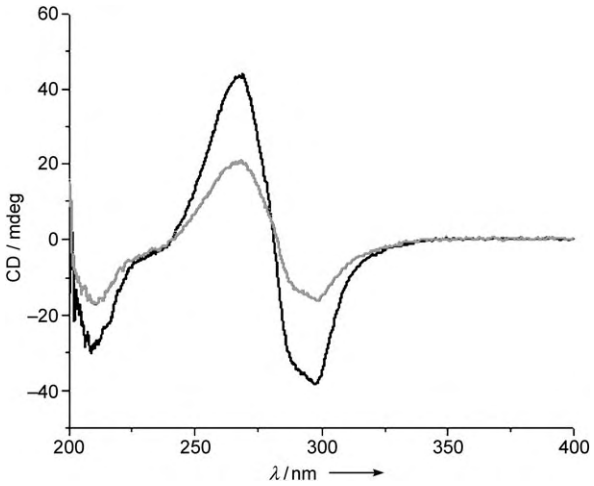

Figure 4. CD traces of a mixture of **1a** and **2** (MeOH, 3 h, 0.04 M, final concentration = 25 μM) in the absence (gray) and presence (black) of 0.5 equivalents of **3**-$(TBA)_2$.

observed negative sign also reflects the relative disposition of the chromophores in the computed geometry.[16]

In such a supramolecular species, the anion must induce a structural organization to adapt the macrocyclic imine group to the molecular shape and charge density of the template. To understand that process, we studied the effect of the template in the hypothetical intermediate previous to the formation of the last C=N bond, which would lead to the final macrocycle. Monte Carlo simulations of the corresponding open-chain tris(imino)aminoaldehyde precursor were carried out, both in the absence and presence of **3** (Figure 5).[12] Binding with **3**

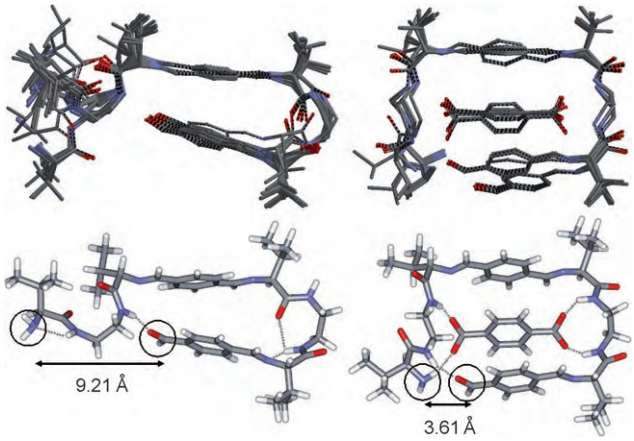

Figure 5. Superimposed structures within a energy gap of 2 kcal mol^{-1} (upper view) and global minima (lower view) for the hypothetical aminoaldehyde intermediate in the absence (left) and presence (right) of the template (hydrogen bonds indicated as gray dotted lines).

increases the rigidity of the intermediate (lower number of accessible local minima) and approximates the extremes of the molecule with the correct geometry for the nucleophilic attack of the amine on the aldehyde carbonyl functionality (see the distances between the encircled groups in Figure 5).

Moreover, the hydrogen-bonding pattern involving terephthalate also suggests that **3** could act as a proton shuttle, thereby explaining the observed acceleration of the templated cyclization process by general acid–base catalysis.

We also wondered if the template-induced molecular organization would be operative in the presence of different configurations of the chiral centers of the open-chain precursors. As control experiments, we carried out the templated condensation reaction using either (*R*,*R*)-**1a** or (*S*,*S*)-**1b** (Figure 6a,b, respectively) in separate experiments,

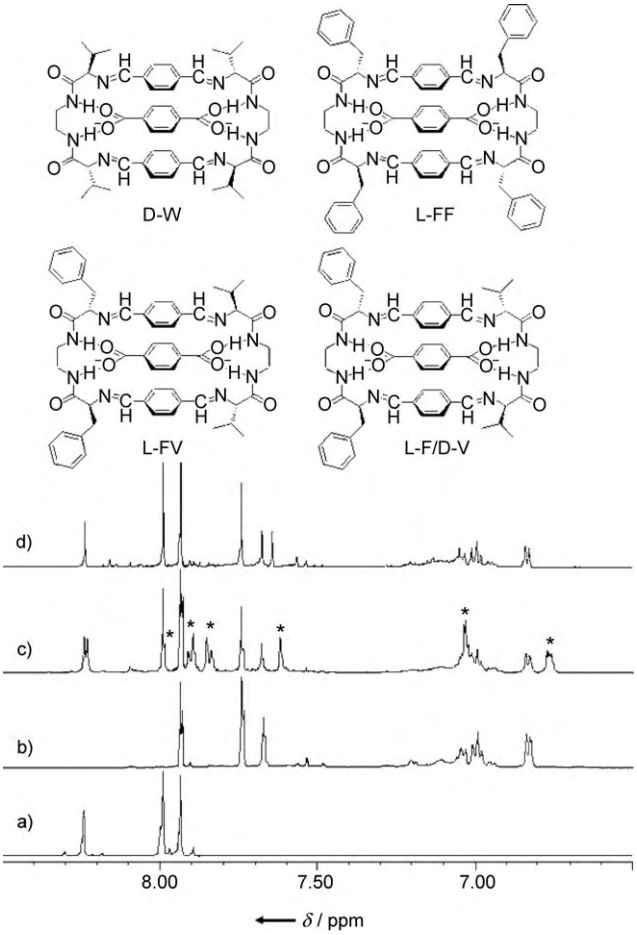

Figure 6. Partial ^{1}H NMR spectra (500 MHz, 303 K, CD_3OD) for a) D-VV, b) L-FF, c) L-FF + L-FV + L-VV (1:2:1 molar ratio), and d) L-FF + D-V. Signals corresponding to mixed nonsymmetrical L-FV are marked with an asterisk in (c).

thereby allowing the assignment of the corresponding signals for D-VV and L-FF complexes (see Figure 6 for the assumed terminology). Moreover, the spectrum obtained by mixing **2**, **3**-$(TBA)_2$, (*S*,*S*)-**1a**, and (*S*,*S*)-**1b** (2:1:1:1 molar ratio) showed the statistical formation of pure and mixed macrocycles (L-FF/L-FV/L-VV complexes in a 1:2:1 molar ratio; Figure 6c), thus supporting that there are no detectable side-chain effects on the macrocyclization. Strikingly, when mixing equivalent amounts of **2** and the corresponding (*R*,*R*)-**1a** and (*S*,*S*)-**1b** bisamidoamines in the presence of the template, no mixed macrocycle was detected by NMR spectroscopic analysis

 © 2006 Wiley-VCH Verlag GmbH & Co. KGaA, Weinheim

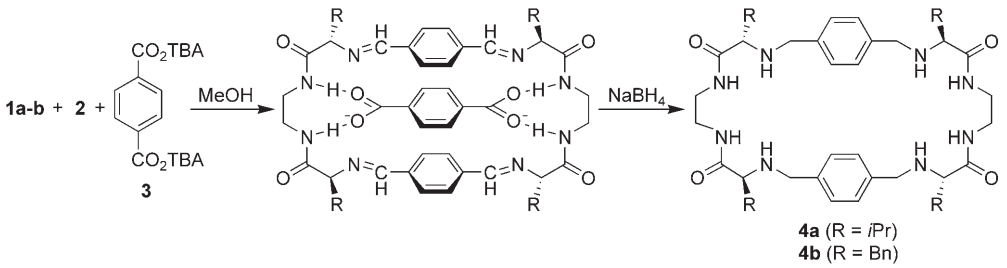

Scheme 2. Anion-templated syntheses of pseudopeptidic macrocycles.

(Figure 6d), thus implying that entities bearing the same side chain (and concomitantly, the same configuration) were exclusively formed. These results showed that anion templation induces a highly stereoselective molecular self-recognition, as only homochiral macrocycles were formed within the detection limit of ^{1}H NMR spectroscopy.[17]

Although the dynamic nature of the supramolecular complexes and imine-bond formation equilibria can make the isolation of these complexes difficult,[18] reduction of the corresponding C=N bonds in situ allowed us to obtain macrocycles **4a**,**b** in 60–65% overall yield from **1a**,**b** after chromatographic purification (Scheme 2) in a one-pot two-step process with synthetic utility. Besides, preliminary studies with systems derived from open-chain derivatives related to **1a**,**b**, but bearing larger aliphatic spacers, also confirm the trends described herein.

In summary, we have reported an unprecedented anion-templated reaction designed for the syntheses of new macrocycles. The formation of the intermediate supramolecular complex has been studied by different experimental and theoretical approaches and shows a perfect structural host–guest complementarity. This molecular organization is even expressed through a remarkable homochiral self-recognition. Further investigations on different templates and synthetic applications of this methodology are underway and will be published in due course.

Received: June 2, 2006
Published online: August 14, 2006

Keywords: anions · host–guest systems · macrocycles · reductive amination · templated synthesis

[1] J.-M. Lehn, *Supramolecular Chemistry: Concepts and Perspectives*, Weinheim, VCH, **1995**.

[2] a) S. J. Rowan, S. J. Cantrill, G. R. L. Cousin, J. K. M. Sanders, J. F. Stoddart, *Angew. Chem.* **2002**, *114*, 938–993; *Angew. Chem. Int. Ed.* **2002**, *41*, 898–952; b) R. L. E. Furlan, S. Otto, J. K. M. Sanders, *Proc. Natl. Acad. Sci. USA* **2002**, *8*, 4801–4804; c) J.-M. Lehn, A. V. Eliseev, *Science* **2001**, *291*, 2331–2332; d) B. Klekota, B. L. Miller, *Trends Biotechnol.* **1999**, *17*, 205–209; e) J.-M. Lehn, *Chem. Eur. J.* **1999**, *5*, 2455–2463; f) R. Hoss, F. Vögtle, *Angew. Chem.* **1994**, *106*, 389–398; *Angew. Chem. Int. Ed. Engl.* **1994**, *33*, 375–384.

[3] For selected papers, see: a) S. Rucareanu, A. Schuwey, A. Gosseauer, *J. Am. Chem. Soc.* **2006**, *128*, 3396–3413; b) Z. R. Laughrey, B. C. Gibb, *Top. Curr. Chem.* **2005**, *249*, 67–125; c) M. Crego-Calama, D. N. Reinhoudt, M. G. J. ten Cate, *Top. Curr. Chem.* **2005**, *249*, 285–316; d) C. A. Schalley, T. Weilandt, J. Bruggemann, F. Vögtle, *Top. Curr. Chem.* **2004**, *248*, 141–200; e) D. H. Busch, N. A. Stephensen, *Coord. Chem. Rev.* **1990**, *100*, 119–154; f) R. Cacciapaglia, L. Mandolini, *Chem. Soc. Rev.* **1993**, *22*, 221–231; g) N. V. Gerbeleu, V. B. Arion, J. Burgess, *Template Synthesis of Macrocyclic Compounds*, Wiley-VCH, Weinheim, **1999**; h) *Templated Organic Synthesis* (Ed.: F. Diederich, P. J. Stang), Wiley-VCH, Weinheim, **2000**; i) T. J. Hubin, D. H. Busch, *Coord. Chem. Rev.* **2000**, *200*, 5–52; j) S. Anderson, H. L. Anderson, J. K. M. Sanders, *Acc. Chem. Res.* **1993**, *26*, 469–475.

[4] a) P. D. Beer, M. R. Sambrook, D. Curiel, *Chem. Commun.* **2006**, 2105–2117; b) D. Meshcheryakov, V. Böhmer, M. Bolte, V. Hubscher-Bruder, F. Arnaud-Neu, H. Herschbach, A. Van Dorsselaer, I. Thondorf, W. Mögelin, *Angew. Chem.* **2006**, *118*, 1679–1682; *Angew. Chem. Int. Ed.* **2006**, *45*, 1648–1652; c) E. A. Katayev, G. Dan Pantos, M. D. Reshetova, V. N. Khrustalev, V. M. Lynch, Y. A. Ustynyuk, J. L. Sessler, *Angew. Chem.* **2005**, *117*, 7552–7556; *Angew. Chem. Int. Ed.* **2005**, *44*, 7386–7390; d) C. S. Campos-Fernández, B. L. Schottel, H. T. Chifotides, J. K. Bera, J. Bacsa, J. M. Koomen, D. H. Russell, K. R. Dunbar, *J. Am. Chem. Soc.* **2005**, *127*, 12909–12923; e) M. R. Sambrook, P. D. Beer, J. A. Wisner, R. L. Paul, A. R. Cowley, F. Szemes, M. G. B. Drew, *J. Am. Chem. Soc.* **2005**, *127*, 2292–2302; f) M. R. Sambrook, P. D. Beer, J. A. Wisner, R. L. Paul, A. R. Cowley, *J. Am. Chem. Soc.* **2004**, *126*, 15364–15365; g) P. Diaz, D. M. P. Mingos, R. Vilar, A. J. P. White, D. J. Williams, *Inorg. Chem.* **2004**, *43*, 7597–7604; h) R. Vilar, *Angew. Chem.* **2003**, *115*, 1498–1516; *Angew. Chem. Int. Ed.* **2003**, *42*, 1460–1477; i) C. Reuter, W. Wienand, G. M. Hübner, C. Seel, F. Vögtle, *Chem. Eur. J.* **1999**, *5*, 2692–2697.

[5] For some recent examples, see: a) S. E. Gibson, C. Lecci, *Angew. Chem.* **2006**, *118*, 1392–1405; *Angew. Chem. Int. Ed.* **2006**, *45*, 1364–1377; b) L. A. Wessjohann, B. Voigt, D. G. Rivera, *Angew. Chem.* **2005**, *117*, 4863–4868; *Angew. Chem. Int. Ed.* **2005**, *44*, 4785–4790; c) J. Becerril, M. Bolte, M. I. Burguete, F. Galindo, E. García-España, S. V. Luis, J. F. Miravet, *J. Am. Chem. Soc.* **2003**, *125*, 6677–6686.

[6] a) J. Becerril, B. Escuder, J. F. Miravet, R. Gavara, S. V. Luis, *Eur. J. Org. Chem.* **2005**, 481–485; b) J. Becerril, M. I. Burguete, B. Escuder, F. Galindo, R. Gavara, J. F. Miravet, S. V. Luis, G. Peris, *Chem. Eur. J.* **2004**, *10*, 3879–3890.

[7] I. Alfonso, M. I. Burguete, S. V. Luis, J. F. Miravet, P. Seliger, E. Tomal, *Org. Biomol. Chem.* **2006**, *4*, 853–859.

[8] a) F. Galindo, M. I. Burguete, L. Vigara, S. V. Luis, D. A. Russell, N. Kabir, J. Gavrilovic, *Angew. Chem.* **2005**, *117*, 6662–6666; *Angew. Chem. Int. Ed.* **2005**, *44*, 6504–6508; b) F. Galindo, J. Becerril, M. I. Burguete, S. V. Luis, L. Vigara, *Tetrahedron Lett.* **2004**, *45*, 1659–1662.

[9] I. Alfonso, M. I. Burguete, S. V. Luis, *J. Org. Chem.* **2006**, *71*, 2242–2250.

[10] M. Bru, I. Alfonso, M. I. Burguete, S. V. Luis, *Tetrahedron Lett.* **2005**, *46*, 7781–7785.

[11] a) A. Bianchi, K. Bowman-James, E. García-España, *Supramolecular Chemistry of Anions*, VCH, Weinheim, **1997**; b) M. J. Chimielewski, J. Jurczak, *Chem. Eur. J.* **2005**, *11*, 6080–6090; c) S. O. Kang, D. VenderVelde, D. Powell, K. Bowman-James, *J. Am. Chem. Soc.* **2004**, *126*, 12272–12273; d) C. R. Body, S. J. Loeb, *Coord. Chem. Rev.* **2003**, *240*, 77–99; e) P. D. Beer, E. J. Hayes, *Coord. Chem. Rev.* **2003**, *240*, 167–189.

 © 2006 Wiley-VCH Verlag GmbH & Co. KGaA, Weinheim

[12] Monte Carlo conformational searches with MMFF force-field minimizations and estimation of molecular volumes were performed with the Spartan 04 package.
[13] S. Ramos, E. Alcalde, G. Doddi, P. Mencarelli, L. Pérez-García, *J. Org. Chem.* **2002**, *67*, 8463 – 8568.
[14] For recent reviews, see: a) P. S. Pregosin, P. G. A. Kumar, I. Fernández, *Chem. Rev.* **2005**, *105*, 2977 – 2998; b) Y. Cohen, L. Avram, L. Frish, *Angew. Chem.* **2005**, *117*, 524 – 560; *Angew. Chem. Int. Ed.* **2005**, *44*, 520 – 554.
[15] The experimental molecular volume was calculated by approximating the shape of the molecule to a sphere ($V = 4/3\pi r^3$) of a radius equal to the hydrodynamic radius r_H, which was estimated using the Stokes–Einstein equation: $D = k_b T/6\pi\eta r_H$ where k_b is the Boltzmann constant and η is the viscosity of pure solvent. All these approximations could render a quantitative difference between the theoretical and experimental value of molecular volume. Additionally, one referee nicely drew our attention to the fact that the counterions and solvation shell were not considered for the molecular modeling structure. These factors also would increase the experimentally obtained volume relative to the theoretical one.
[16] N. Berova, K. Nakanishi, R. W. Woody, *Circular Dichroism. Principles and Applications*, New York, Wiley-VCH, **2000**.
[17] ESI mass-spectrometric experiments showed similar trends, although in this case a small amount of the mixed nonsymmetrical L-F/D-V complex was also detected, which can be a consequence of the very different conditions for the measurements and could destabilize the supramolecular complex in the mass spectrometer.
[18] Until now many attempts to obtain crystals suitable for X-ray diffraction analysis have been unsuccessful, probably as a result of the dynamic nature of the supramolecular complexes.

 © 2006 Wiley-VCH Verlag GmbH & Co. KGaA, Weinheim

C≡P Ligands

DOI: 10.1002/anie.200602499

Making the True "CP" Ligand**

*Joseph G. Cordaro, Daniel Stein, Heinz Rüegger, and Hansjörg Grützmacher**

The quest for cyaphide, the phosphorus equivalent of cyanide, has been a continuous struggle for many years. Potential applications arising from the use of C≡P as a bridging ligand between two metals, the incorporation of C≡P into coordination polymers and new materials, and the basic synthetic challenges of making C≡P have provided inspiration for decades. While phosphaalkynes (R−C≡P) have been known for some time,[1–3] the terminal M−C≡P has only been reported as a transient species.[4,5] Other C-functionalized X−C≡P compounds (X = R_3Si,[6] R_2N,[7,8] RO,[8] F,[9] Cl,[10]), anionic species $[X-C\equiv P]^-$ (X = R_3B,[11] RN,[8] O,[12] S[13]), and the cationic phosphonio phosphaalkyne $[R_3P-C\equiv P]^+$,[14] have been synthesized, but the vast majority of reports deal with *tert*-butyl,[15] adamantyl,[16] 2,4,6-trimethylphenyl[17] and 2,4,6-tri-*tert*-butylphenyl[18] phosphaalkynes. Recently, we devised a very simple method for accessing the kinetically stable crystalline triphenylmethyl (trityl)-substituted phosphaalkyne, $Ph_3CC\equiv P$ (**1**), which allowed for the economical metal-promoted synthesis of phosphorus heterocycles. However, our ultimate goal and incentive for synthesizing the trityl-substituted phosphaalkyne was to find an adequate leaving group that would lead us to cyaphide.[19]

Treatment of **1** or its complexes $[MH(dppe)_2(Ph_3C-C\equiv P)]OTf$ (M = Fe or Ru; dppe = bis(1,2-diphenylphosphinoethane); OTf = trifluoromethanesulfonate) with nucleophiles (Nu) did not furnish the desired cyaphide, $C\equiv P^-$, or its complexes [Eq. (1); electrophile (E) = C].

$$Ph_3E-C\equiv P + Nu^- \rightarrow Ph_3E-Nu + C\equiv P^- \quad (1)$$

Therefore, we reasoned that silicon would be more susceptible to nucleophilic attack (E = Si) and applied an analogous synthetic procedure to access the higher homologue $Ph_3SiC\equiv P$ (**3**).

Conversion of Ph_3SiCH_2Cl into the Grignard reagent followed by treatment with PCl_3 produced the silyl-substituted alkyl phosphonous dichloride, $Ph_3SiCH_2PCl_2$ (**2**), in over 87% yield (Scheme 1). Employing 2.2 equiv of DABCO (1,8-diazabicyclo[2.2.2]octane) effected the dehydrohalogenation reaction, and **2** was fully transformed into the triphenylsilyl-substituted phosphaalkyne **3**. The reaction occurred at ambient temperature and in multiple solvents in less than one hour. (In contrast, the reaction of DABCO with $Ph_3CCH_2PCl_2$ to furnish $Ph_3CC\equiv P$ required a 10-fold excess of base, elevated temperatures, and proceeded best in acetonitrile.[19])

While DABCO alone was effective for the conversion of **2** into **3**, we saw rapid decomposition of this new phosphaalkyne, which was dependent on the solvent. Qualitatively, the rate of decomposition of **3** followed the order $Et_2O \approx$ toluene < THF ≪ CH_3CN. Suspecting that DABCO-HCl was acting as a soluble source of chloride anion in the more polar solvents that then attacked silicon to produce Ph_3SiCl and the CP anion, which is seemingly unstable under the reaction conditions, we added AgOTf to the reaction mixture. When a solution of **2** in toluene was pretreated with 2.2 equiv of AgOTf for 5 min followed by addition of 2.2 equiv of DABCO, complete conversion into **3** was observed in less than one hour. Filtration through diatomaceous earth to remove insoluble salts furnished indeed a clean solution of **3**, which only slowly decomposed. In the ^{31}P NMR spectrum of **3**, a deshielded signal at $\delta = 111$ ppm was observed. The α-

[*] Dr. J. G. Cordaro, Dr. D. Stein, Dr. H. Rüegger, Prof. Dr. H. Grützmacher
Laboratorium für Anorganische Chemie
Departement Chemie und Angewandte Biowissenschaften
ETH Zürich
8093 Zürich (Switzerland)
Fax: (+41) 44-633-1418
E-mail: gruetzmacher@inorg.chem.ethz.ch

[**] We thank the ETH Zürich for financial support and Theo Zweifel for helpful suggestions.

Supporting information for this article is available on the WWW under http://www.angewandte.org or from the author.

 © 2006 Wiley-VCH Verlag GmbH & Co. KGaA, Weinheim

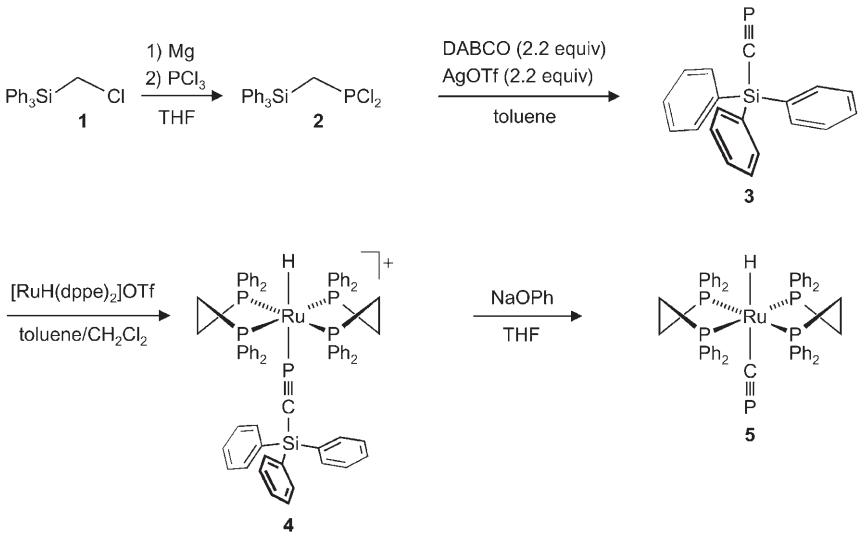

Scheme 1. Synthesis of ruthenium cyaphide complex **5** from the silyl-substituted phosphaalkyne **3** (see text for details).

carbon atom, which gives a signal at $\delta = 193.3$ ppm (d, $J_{C\text{-}P} = 16.4$ Hz) in the ^{13}C NMR spectrum, was also shifted significantly downfield compared to other phosphaalkynes.[20]

Attempts to isolate **3** were unfortunately unsuccessful. If a solution of **3** was concentrated, a red precipitate formed which gave no detectable ^{31}P NMR signal upon redissolving in more polar solvents. However, the lifetime of **3** in toluene or diethyl ether ($t_{1/2} \approx 1$ day at 23 °C) was sufficiently long so that ^{31}P and ^{13}C NMR data could be acquired and, more importantly, coordination of **3** to $[RuH(dppe)_2]OTf$ was successful. Addition of a solution of **3** in toluene to 0.5 equiv of $[RuH(dppe)_2]OTf$ in CH_2Cl_2 resulted in a color change from dark red to yellow-orange. After workup, the colorless η^1-coordinated complex $[RuH(dppe)_2(Ph_3SiC{\equiv}P)]OTf$ (**4**) was isolated in over 80% yield as the only product. In the $^{31}P\{^1H\}$ NMR spectrum, coordination of **3** to the ruthenium cation was confirmed by the downfield-shifted signal at $\delta = 143.8$ ppm for the phosphaalkyne, which appeared as a quintet ($^2J_{P\text{-}P} = 27.8$ Hz) as a result of coupling with the four equivalent phosphorus atoms of the dppe ligands. The dppe ligands were seen as a doublet at $\delta = 60.1$ ppm. A doublet of quintets in the ^1H NMR spectrum at $\delta = -8.13$ ppm (*trans*-$^2J_{H\text{-}P} = 122.1$ Hz, *cis*-$^2J_{H\text{-}P} = 17.0$ Hz) for the ruthenium hydride was most diagnostic for the formation of **4**. The signal for the α-carbon atom of the coordinated phosphaalkyne was observed at $\delta = 175.1$ ppm in the ^{13}C NMR spectrum with a significantly larger C–P coupling constant of $J_{C\text{-}P} = 71.4$ Hz as compared to **3**.

The molecular structure of **4** is presented in Figure 1.[21] The X-ray data for **4** are the only available data for any silyl-substituted phosphaalkyne. The P–C bond length (1.530 Å) for **4** is not significantly different when compared to those in the free phosphaalkyne $Ph_3CC{\equiv}P$ (**1**; 1.538 Å) and its iron complex $[Fe(dppe)_2H(Ph_3CC{\equiv}P)]OTf$ (1.535 Å). The deviation from linearity seen in the P-C-Si angle (165.5°) is likewise not unusual and certainly has steric origins.[22]

When **4** was treated with fluoride, no clean reaction occurred. The observation of signals with large P–F couplings in the ^{31}P NMR spectrum of the reaction mixture indicated that phosphorus was attacked by fluoride. Reactions with alkoxides and hydroxide similarly resulted in nucleophilic attack at phosphorus, as indicated by the ^{31}P NMR chemical shifts. However, when **4** was treated with a slight excess of sodium phenoxide (NaOPh) in THF, the immediate formation of an intermediate was observed[23] which was then converted into a new product **5** after 14 h. Product **5** showed a broad signal in the ^{31}P NMR spectrum at $\delta = 165$ ppm, which was weakly coupled to another broad signal at $\delta = 65.2$ ppm. In the ^1H NMR spectrum, the hydride appeared as a sextet at $\delta = -11.22$ ppm with $J_{P\text{-}H} \approx 20$ Hz. A ^{31}P-^1H HMQC (heteronuclear multiple-quantum correlation) experiment revealed cross-peaks between the hydride and both phosphorus signals. In a selective $^1H\{^{31}P\}$ NMR experiment, the

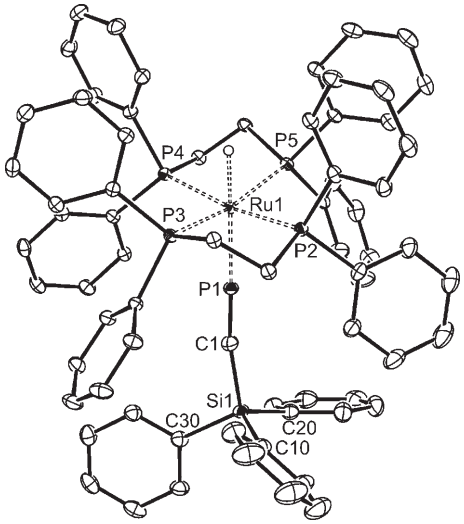

Figure 1. Molecular structure of **4**. The anion and hydrogen atoms are omitted for clarity. Thermal ellipsoids are drawn at 30% probability. Selected bond lengths [Å] and angles [°]: P1–C1 1.530(3), C1–Si1 1.825(3), Ru1–P1 2.2485(8), Ru1–P2 2.3811(7), Ru1–P3 2.3721(7), Ru1–P4 2.3559(7), Ru1–P5 2.3694(7); P1-C1-Si1 165.5(2), C10-Si1-C20 114.4(2), C20-Si1-C30 109.0(2), C10-Si1-C30 110.2(2), P1-Ru1-P2 94.79(3), P1-Ru1-P3 94.12(3), P1-Ru1-P4 94.06(3), P1-Ru1-P5 98.34(3), P2-Ru1-P3 82.96(3), P3-Ru1-P4 97.50(3), P4-Ru1-P5 82.63(3), P5-Ru1-P2 95.00(3).

^{31}P NMR signal at $\delta = 165$ ppm coupled with the hydride to form a doublet with $J_{P\text{-}H} = 19.5$ Hz, while the signal at $\delta = 65.2$ ppm coupled with the hydride to give a quintet with $J_{P\text{-}H} = 20.5$ Hz. Finally, a ^{13}C-^1H HMQC experiment with phosphorus decoupling centered at $\delta = 65$ ppm, detected a cross-peak for a quaternary carbon atom at $\delta = 287.1$ ppm in the ^{13}C dimension, which correlated with the hydride. Coupling between the phosphorus and carbon centers corresponded to $^1J_{C\text{-}P} \approx 90$ Hz. These spectroscopic data are fully consistent

 © 2006 Wiley-VCH Verlag GmbH & Co. KGaA, Weinheim

with a {RuH(dppe)$_2$} fragment carrying a CP ligand *trans* to the hydride.

Crystals suitable for X-ray analysis were grown from a THF solution layered with hexane. The results confirm the NMR data and demonstrate the first structurally characterized metal cyaphide complex [RuH(CP)(dppe)$_2$] (**5**; Figure 2). As expected, the CP ligand has rotated from

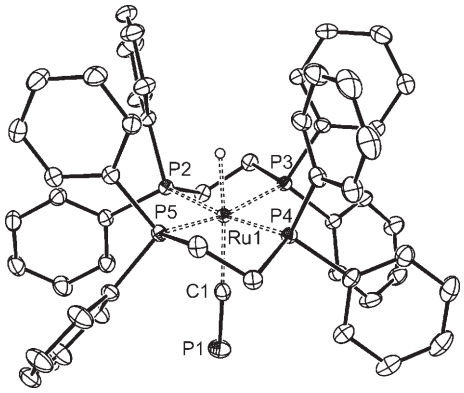

Figure 2. Molecular structure of **5**. Hydrogen atoms are omitted for clarity. Thermal ellipsoids are drawn at 30% probability. Selected bond lengths [Å] and angles [°]: P1–C1 1.573(2), Ru1–C1 2.057(2), Ru1–P2 2.3342(5), Ru1–P3 2.3315(5), Ru1–P4 2.3222(5), Ru1–P5 2.3396(4); Ru1-C1-P1 177.9(1), C1-Ru1-P2 92.48(5), C1-Ru1-P3 96.86(5), C1-Ru1-P4 93.74(5), C1-Ru1-P5 94.30(5), P2-Ru1-P3 82.63(2), P3-Ru1-P4 94.60(2), P4-Ru1-P5 83.31(2), P5-Ru1-P2 98.25(2).

being P-coordinated in the starting complex **4** to C-coordinated in the product **5**. With a CP bond length of 1.573(2) Å, **5** displays the longest reported uncoordinated C–P triple bond, possibly arising from the ability of ruthenium to backbond to the π^* orbitals of the CP fragment.

An intense band at 1229 cm^{-1} seen in both the Raman and IR spectra was assigned to the CP stretching frequency by comparison with the calculated value of 1336 cm^{-1} (DFT B3LYP/6-31G* for P,C,H; LANL2DZ for Ru). The CP stretching frequency for alkyl-substituted phosphaalkynes is typically found at higher energy (> 1500 cm^{-1}), while Willner reported a value of 1468 cm^{-1} for $[(CF_3)_3B(CP)]^-$.[11] In the solid state, **5** was only moderately air-sensitive. Crystals of **5** were extremely kinetically insoluble in [D$_8$]THF. Although **5** was more soluble in CD_2Cl_2, a slow reaction was observed that yielded a product identified as [RuHCl(dppe)$_2$] by NMR spectroscopy.

In conclusion, we have reported a rational synthesis to access the first "true" M-CP complex. Using the triphenylsilyl-substituted phosphaalkyne **3**, which functioned with Ph_3Si as a protecting group for the CP anion, we were able to effectively deliver cyaphide to ruthenium upon deprotection of the silyl group with phenoxide. We hope that our method for synthesizing $Ph_3Si{-}C{\equiv}P$ will be generally applicable and potentially lead to novel M-CP-M complexes.

Experimental Section

All manipulations were performed under an inert atmosphere of argon using standard Schlenk techniques. NaOPh was synthesized from PhOH and Na in THF. The isolated salt was dried under vacuum at 200 °C. Selected analytical data are given below (see Supporting Information for more details).

$Ph_3SiCH_2PCl_2$ (**2**): A 250-mL Schlenk flask equipped with a stir bar was charged with freshly ground Mg turnings (10 g, 0.411 mol) and THF (50 mL). Meanwhile, Ph_3SiCH_2Cl[24] (13.0 g, 0.042 mol) was dissolved in THF (50 mL) in a separate Schlenk flask. The alkyl chloride was slowly added to the Mg turnings in 10 mL portions over 1 h, at which time the Grignard reaction was initiated. An additional 50 mL of THF was used to rinse the remaining alkyl chloride into the reaction mixture. The Grignard reagent was mixed for 3 h and then transferred via cannula to a solution of PCl_3 (11 mL, 0.126 mol) in THF (100 mL) cooled to −78 °C. The mixture was stirred and allowed to warm to room temperature over 18 h. After removal of the volatile materials, the gray solid was extracted with toluene (ca. 200 mL) and filtered through diatomaceous earth on a medium-pore fitted glass filter frit. The volatile materials were removed under reduced pressure to furnish a white solid. Crystallization from THF/hexane at −30 °C afforded analytically pure material (13.8 g, 87.6%); m.p.: 96–97 °C; ^{1}H NMR (300 MHz, C_6D_6, 23 °C): $\delta = 2.60$ ppm (d, $^2J_{H\text{-}P} = 14.3$ Hz, 2H); $^{13}C\{^1H\}$ NMR (75.5 MHz, C_6D_6, 23 °C): $\delta = 32.52$ ppm (d, $J_{C\text{-}P} = 64.6$ Hz); $^{31}P\{^1H\}$ NMR (121.5 MHz, C_6D_6, 23 °C): $\delta = 199.7$ ppm.

$Ph_3SiC{\equiv}P$ (**3**): A 20-mL scintillation vial equipped with a stir bar was charged with $Ph_3SiCH_2PCl_2$ (**2**; 0.375 g, 1.00 mmol), AgOTf (0.564 g, 2.20 mmol), and toluene (18 mL). The suspension was protected from light and vigorously stirred. After 5 min, DABCO (0.248 g, 2.20 mmol) was added to the vial and stirring was continued. After an additional 60 min, the mixture was filtered through a pad of diatomaceous earth on a medium-pore fitted glass filter frit eluting with toluene (ca. 10 mL). The resulting yellow solution was used immediately. $^{13}C\{^1H\}$ NMR (75.5 MHz, Et_2O, 23 °C): $\delta = 193.3$ ppm (d, $^1J_{C\text{-}P} = 16.4$ Hz); $^{31}P\{^1H\}$ NMR (121.5 MHz, Et_2O, 23 °C): $\delta = 111.3$ ppm.

[RuH(dppe)$_2$($Ph_3SiC{\equiv}P$)]OTf (**4**): A 250-mL Schlenk flask equipped with a stir bar was charged with [RuH(dppe)$_2$]OTf[25] (0.524 g, 0.500 mmol) and CH_2Cl_2 (80 mL). The silyl-substituted phosphaalkyne **3** (1.0 mmol, 2 equiv) synthesized above was added via cannula transfer, resulting in a color change from red to light orange. After 1 h, the solution was concentrated to approximately 40 mL under reduced pressure which resulted in copious amounts of white precipitate. The suspension was mixed for 2 h then allowed to settle. The mother liquor was removed via cannula filtration, and the faint yellow solid was washed with diethyl ether (3 × 10 mL). Excess solvent was removed under reduced pressure to furnish a white solid (0.576 g, 84.5%). Analytically pure material was obtained through crystallization from THF/toluene; m.p.: 185 °C (dec.); ^{1}H NMR (300 MHz, [D$_8$]THF, 23 °C): $\delta = -8.13$ ppm (dqnt, *trans*-$^2J_{P\text{-}H} = 122.1$ Hz, *cis*-$^2J_{P\text{-}H} = 17.0$ Hz, 1H); $^{13}C\{^1H\}$ NMR (75.5 MHz, [D$_8$]THF, 23 °C): $\delta = 175.1$ ppm (d, $^1J_{C\text{-}P} = 71.4$ Hz); ^{19}F NMR (188 MHz, [D$_8$]THF, 23 °C): $\delta = -78.4$ ppm; $^{31}P\{^1H\}$ NMR (121.5 MHz, [D$_8$]THF, 23 °C): $\delta = 143.8$ ppm (qnt, $^2J_{P\text{-}P} = 27.8$ Hz, 1P), 60.1 ppm (d, $^2J_{P\text{-}P} = 27.3$ Hz, 4P).

[RuH(dppe)$_2$(C≡P)] (**5**): A 20-mL vial equipped with a stir bar was charged with **4** (0.270 g, 0.20 mmol) and THF (18 mL). The solid dissolved after stirring for 5 min. The solution was then cooled to −30 °C, and NaOPh (0.032 g, 0.276 mmol) in THF (2 mL) was added. The solution was warmed to 23 °C over 30 min. After mixing for 14 h, the yellow-orange solution was filtered through a pad of silica gel, eluting with THF (5 mL). After removal of the volatile materials, the solid was washed with CH_3CN (2 × 10 mL) then redissolved in THF (ca. 15 mL) and filtered through diatomaceous earth in a Pasteur filter pipette. Excess solvent was removed under reduced pressure to furnish a yellow solid (0.135 g, 71.8%). This product was > 95% pure

 © 2006 Wiley-VCH Verlag GmbH & Co. KGaA, Weinheim

by NMR spectroscopy. Crystallization from THF/hexane furnished analytically pure material, which was also suitable for X-ray analysis (0.60 g, 31.9%); m.p. > 198 °C (decomp); ^{1}H NMR (300 MHz, [D$_8$]THF, 23 °C): $\delta = -11.22$ ppm (dqnt, *cis*-$^2J_{H\text{-}P} = 20.7$ Hz, *trans*-$^3J_{H\text{-}P} = 20.4$ Hz, 1H); ^{13}C{^{1}H} NMR (75.5 MHz, [D$_8$]THF, 23 °C): $\delta =$ 287.1 ppm (m); ^{31}P{^{1}H} NMR (121.5 MHz, [D$_8$]THF, 23 °C): $\delta =$ 165.0 (br, 1P), 65.2 ppm (br, 4P); Raman: $\tilde{\nu} = 1885$ (w, Ru-H), 1228 (vs, C≡P).

Received: June 21, 2006
Published online: August 28, 2006

Keywords: cyaphides · phosphaalkynes · P ligands · ruthenium · silanes

[1] T. E. Gier, *J. Am. Chem. Soc.* **1961**, *83*, 1769.
[2] M. Regitz, P. Binger, *Angew. Chem.* **1988**, *100*, 1541; *Angew. Chem. Int. Ed. Engl.* **1988**, *27*, 1484.
[3] F. Mathey, *Angew. Chem.* **2003**, *115*, 1616; *Angew. Chem. Int. Ed.* **2003**, *42*, 1578.
[4] H. Jun, R. J. Angelici, *Organometallics* **1994**, *13*, 2454.
[5] H. Jun, V. G. Young, R. J. Angelici, *J. Am. Chem. Soc.* **1992**, *114*, 10064.
[6] R. Appel, A. Westerhaus, *Tetrahedron Lett.* **1981**, *22*, 2159.
[7] R. Appel, M. Poppe, *Angew. Chem.* **1989**, *101*, 70; *Angew. Chem. Int. Ed. Engl.* **1989**, *28*, 53.
[8] G. Becker, H. Brombach, S. T. Horner, E. Niecke, W. Schwarz, R. Streubel, E. U. Würthwein, *Inorg. Chem.* **2005**, *44*, 3080, and references therein.
[9] H. W. Kroto, J. F. Nixon, N. P. C. Simmons, *J. Mol. Spectrosc.* **1980**, *82*, 185.
[10] J. C. Guillemin, T. Janati, P. Guenot, P. Savignac, J. M. Denis, *Angew. Chem.* **1991**, *103*, 191; *Angew. Chem. Int. Ed. Engl.* **1991**, *30*, 196.
[11] M. Finze, E. Bernhardt, H. Willner, C. W. Lehmann, *Angew. Chem.* **2004**, *116*, 4254; *Angew. Chem. Int. Ed.* **2004**, *43*, 4160.
[12] G. Becker, G. Heckmann, K. Hübler, W. Schwarz, *Z. Anorg. Allg. Chem.* **1995**, *621*, 34.
[13] G. Becker, K. Hübler, *Z. Anorg. Allg. Chem.* **1994**, *620*, 405.
[14] U. Fleischer, H. Grützmacher, U. Krüger, *J. Chem. Soc. Chem. Commun.* **1991**, 302.
[15] G. Becker, G. Gresser, W. Uhl, *Z. Naturforsch. B* **1981**, *36*, 16.
[16] T. Allspach, M. Regitz, G. Becker, W. Becker, *Synthesis* **1986**, 31.
[17] A. Mack, E. Pierron, T. Allspach, U. Bergsträsser, M. Regitz, *Synthesis* **1998**, 1305.
[18] G. Markl, H. Sejpka, *Tetrahedron Lett.* **1986**, *27*, 171.
[19] J. G. Cordaro, D. Stein, H. Grützmacher, *J. Am. Chem. Soc.* **2006**, *118*, in press.
[20] M. Regitz, *Chem. Rev.* **1990**, *90*, 191.
[21] Structural data for **4**: Colorless, air-sensitive single crystals of **4** used for X-ray analysis had the composition [RuH(dppe)$_2$-(Ph$_3$SiC≡P)](BF$_4$)$_{0.94}$(Cl)$_{0.06}$ and were obtained from the reaction starting from [RuH(dppe)$_2$]BF$_4$ rather than the OTf salt and recrystallized from CH_2Cl_2 layered with hexane at 23 °C; $C_{72}H_{66}B_{0.94}Cl_{0.06}F_{3.76}P_5RuSi$; tetragonal; space group $I4(1)/a$; $a = 40.152(2)$, $b = 40.152(2)$, $c = 16.203(1)$ Å; $V = 26121(3)$ Å^3; $Z = 16$; $\rho_{calcd} = 1.393$ Mg m^{-3}; crystal dimensions $0.46 \times 0.25 \times 0.14$ mm^3; Bruker SMART Apex diffractometer with CCD area detector; $Mo_{K\alpha}$ radiation (0.71073 Å), 150 K, $2\Theta_{max} = 56.66°$; 95351 reflections, 16245 independent ($R_{int} = 0.0607$); direct methods; empirical absorption correction SADABS (v2.03); refinement against full matrix (versus F^2) with SHELXTL (v6.12) and SHELXL-97; 787 parameters, 3 restraints (BF$_4$/Cl, Ru-H), $R1 = 0.0487$ and w$R2$(all data) = 0.1321, max/min residual electron density: 1.140/−1.329 e Å^{-3}. All non-hydrogen atoms were refined anisotropically. The contribution of the hydrogen atoms, in their calculated positions, was included in the refinement using a riding model. The dichloromethane molecule in the crystal lattice is slightly disordered. Structural data for **5**: Pale yellow, air-sensitive single crystals were obtained from a THF/hexane solution of **5** at room temperature; $C_{53}H_{49}P_5Ru$; monoclinic; space group $P2(1)/n$; $a = 10.8585(6)$, $b = 24.019(1)$, $c = 17.5981(9)$ Å; $V = 4481.3(4)$ Å^3; $Z = 4$; $\rho_{calcd} = 1.396$ Mg m^{-3}; crystal dimensions $0.30 \times 0.26 \times 0.26$ mm^3; Bruker SMART Apex diffractometer with CCD area detector; $Mo_{K\alpha}$ radiation (0.71073 Å), 200 K, $2\Theta_{max} = 56.68°$; 33735 reflections, 11153 independent ($R_{int} = 0.0258$); direct methods; refinement against full matrix (versus F^2) with SHELXTL (v6.12) and SHELXL-97; 536 parameters, 1 restraint (Ru-H), $R1 = 0.0323$ and w$R2$(all data) = 0.0888, max/min residual electron density 0.862/−0.251 e Å^{-3}. All non-hydrogen atoms were refined anisotropically. The contribution of the hydrogen atoms, in their calculated positions, was included in the refinement using a riding model. CCDC 611173 (**4**) and 611174 (**5**) contain the supplementary crystallographic data for this paper. These data can be obtained free of charge from The Cambridge Crystallographic Data Centre via www.ccdc.cam.ac.uk/data_request/cif.
[22] For related complexes with silylalkynyl ligands, see: a) K. Venkatesan, T. Fox, H. W. Schmalle, H. Berke, *Organometallics* **2005**, *24*, 2834; b) B. Siggelkow, M. B. Meder, C. H. Galka, L. H. Gade, *Eur. J. Inorg. Chem.* **2004**, 3424.
[23] An intermediate species was observed by ^{31}P NMR spectroscopy at $\delta = +310$ ppm suggesting reversible attack at P before irreversible attack at Si (J. G. Cordaro, D. Stein, A. Ehlers, H. Grützmacher, unpublished results).
[24] J. J. Eisch, C. C. S. Chiu, *Heteroat. Chem.* **1994**, *5*, 265.
[25] [RuH(dppe)$_2$]OTf was made through anion metathesis of [RuH(dppe)$_2$]BF$_4$ in THF using KOTf (1.2 mol equiv) followed by filtration through Celite to remove the precipitated KBF$_4$; for [RuH(dppe)$_2$]BF$_4$, see: S. P. Nolan, T. R. Belderrain, R. H. Grubbs, *Organometallics* **1997**, *16*, 5569.

 © 2006 Wiley-VCH Verlag GmbH & Co. KGaA, Weinheim

Polymerization Catalysts

DOI: 10.1002/anie.200600666

Endowing Aspecific, Unbridged-Metallocene Propylene-Polymerization Catalysts with Isospecificity: The Unprecedented Role of MAO**

*Seong Kyun Kim, Hwa Kyu Kim, Min Hyung Lee, Seung Woong Yoon, and Youngkyu Do**

The relationship between the nature of catalyst systems and the resulting polymer has been well established in single-site olefin-polymerization systems and now provides the opportunity to tailor the polymer's properties.[1–4] In particular, chiral *ansa*-metallocene catalysts, which follow an enantiomorphic site-control mechanism, have been intensively investigated to obtain stereochemical control of propylene polymerization by varying the ligand structure.[5–7] Unbridged-metallocene-based systems, on the other hand, have received little attention owing to their aspecific nature[8,9] in spite of their ability to produce iso-rich[10,11] or isotactic–atactic block polypropylene[12,13] when containing rotationally hindered ligands. As unbridged metallocenes are far easier to synthesize than *ansa*-metallocenes, we have been investigating isospecific, unbridged-metallocene catalytic systems that can be generated in situ during the activation step. To this end, we have designed "class I" unbridged metallocenes, a new class analogous to the known aspecific, unbridged metallocenes of "class II".[8,9] The Lewis basic sites E in class I complexes are found to interact with [Me-MAO]$^-$ to generate rigid, *rac*-like cationic active species, thereby endowing aspecific, unbridged-metallocene precatalysts with isospecificity. Herein, we report a novel example of a sterically unhindered, unbridged zirconocene system that is able to produce highly isotactic polypropylene through the unprecedented role of methyl aluminum oxane (MAO).

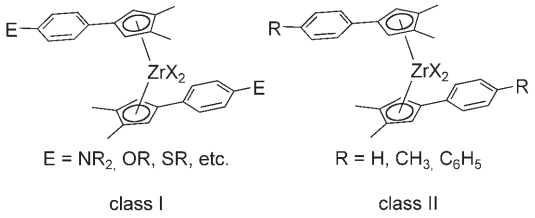

The amine-functionalized, unbridged zirconocenes [{1-(*p*-$Me_2NC_6H_4$)-3,4-$Me_2C_5H_2$}$_2$$ZrX_2$] [(AP)$_2$$ZrX_2$; X = Cl (**2**), X = Me (**3**)] were obtained from newly synthesized ligand **1** as outlined in Scheme 1. The molecular structure of **2** has C_2 symmetry in the solid state (Figure 1). The polymerization

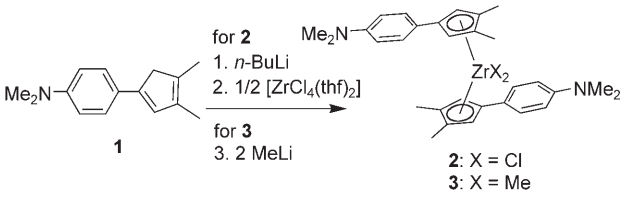

Scheme 1. Synthetic routes to zirconocenes **2** and **3**.

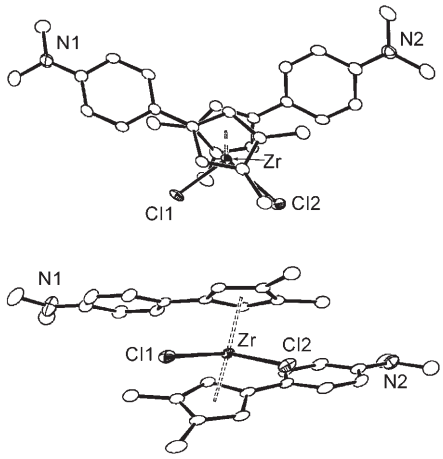

Figure 1. Molecular structure of **2**. Top: top view; bottom: side view.

of propylene with **2**/MAO ([Al]/[Zr] = 1000) was performed at various temperatures (T_p = 0, 25, 50, and 70 °C; Table 1, entries 1–4, respectively). The **2**/MAO system shows lower catalytic activity but produces higher molecular weight polypropylenes than the well-known isospecific catalyst *rac*-[Et(Ind)$_2$$ZrCl_2$] (EBIZr)/MAO (entry 9) under identical reaction conditions. The differential scanning calorimetry (DSC) and gel permeation chromatography (GPC) traces indicate that all the crude polypropylenes from the **2**/MAO system show multiple melting transitions (T_m) and broad molecular-weight distributions (M_w/M_n) of between 4.5 and 11 (Figure 2).

The crude polypropylenes were fractionated by stepwise solvent extraction[14] into three portions for further analysis, 1) diethyl ether soluble, 2) diethyl ether insoluble and *n*-heptane soluble, and 3) diethyl ether insoluble and *n*-heptane insoluble. The *mmmm* methyl pentad values in Table 2 suggest that these portions correspond to atactic-like, mod-

[*] Dr. S. K. Kim, H. K. Kim, Dr. M. H. Lee, S. W. Yoon, Prof. Dr. Y. Do
Department of Chemistry
School of Molecular Science BK-21
Center for Molecular Design and Synthesis
and
Polyolefin Materials Research Center
Korea Advanced Institute of Science and Technology
Daejeon, 305-701 (Republic of Korea)
Fax: (+82) 42-869-2810
E-mail: ykdo@kaist.ac.kr
Homepage: http://xray.kaist.ac.kr/

[**] The authors are grateful for financial support from CMDS, POMRC, the BK-21 project, and the Honam Petrochemical Co. S.K.K. thanks Mr. H. S. Shin for performing the NMR spectroscopy experiments. MAO = methyl aluminum oxane.

Supporting Information for this article is available on the WWW under http://www.angewandte.org or from the author.

 © 2006 Wiley-VCH Verlag GmbH & Co. KGaA, Weinheim

Table 1: Propylene polymerization data.[a]

Entry	Cat.	Cocat.	T_p [°C]	Yield [g]	Act.[b]	M_w [$\times 10^{-3}$]	M_w/M_n
1	**2**	MAO	0	1.02	102	227	4.56
2	**2**	MAO	25	6.24	624	166	10.7
3	**2**	MAO	50	7.25	725	32.0	9.50
4	**2**	MAO	70	3.41	341	10.1	5.27
5	**3**	MAO	25	6.38	638	168	11.4
6[c]	**3**	borate/TIBA	25	6.95	695	15.2	2.10
7[c]	**3**	borate/TOA	25	2.37	237	16.6	2.10
8[d]	BPZr	MAO	0	2.83	566	58.9	1.87
9[e]	EBIZr	MAO	25	12.4	5930	19.1	2.13
10[f]	**3**	MAO	25	1.02	204	126	12.4
11[f]	**3**	MAO/borate	25	2.18	435	13.3	2.66
12[f]	**3**	borate/MAO	25	1.22	244	22.4	2.00

[a] Polymerization conditions: P(propylene) = 1 bar, [Zr] = 5.0 μmol, [Al]/[Zr] = 1000, solvent = 50 mL of toluene, t_p = 120 min; Entry numbers 1–9 correspond to those in Table 2. [b] Activity, in units of (kg of PP)/[(mol of Zr) h bar]. [c] borate = $[Ph_3C][B(C_6F_5)_4]$; TIBA = triisobutylaluminum; TOA = trioctylaluminum; [B]/[Zr] = 1, [Al]/[Zr] = 200. [d] t_p = 60 min; BPZr = [{1-(*p*-$C_6H_5C_6H_4$)-3,4-$Me_2C_5H_2$}$_2$$ZrCl_2$]. [e] t_p = 25 min; EBIZr = *rac*-[$Et(Ind)_2ZrCl_2$]. [f] t_p = 60 min; [Al]/[Zr] = 200, [B]/[Zr] = 1.

erately isotactic, and highly isotactic polypropylenes, respectively. The amount of *n*-heptane insoluble polypropylene decreases as the polymerization temperature increases, while that of the diethyl ether soluble portion increases. The *n*-heptane insoluble portions have remarkably high *mmmm* values of around 86% (Figure 3A) and a T_m of 151°C (Table 2, entry 2). The class II complex [{1-(*p*-$C_6H_5C_6H_4$)-3,4-$Me_2C_5H_2$}$_2$$ZrCl_2$] (BPZr)[9] gives atactic polypropylene even at 0°C (entry 8). These results clearly demonstrate that the unbridged zirconocene **2**/MAO system is capable of producing highly isotactic polypropylene and also that the simple functionalization of class II to class I metallocenes should be an effective route for endowing

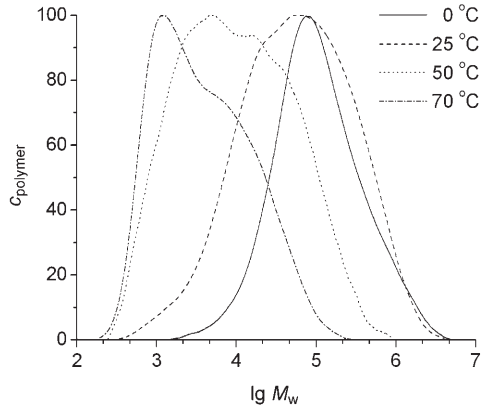

Figure 2. Molecular-weight distribution of the polymers obtained with **2**/MAO.

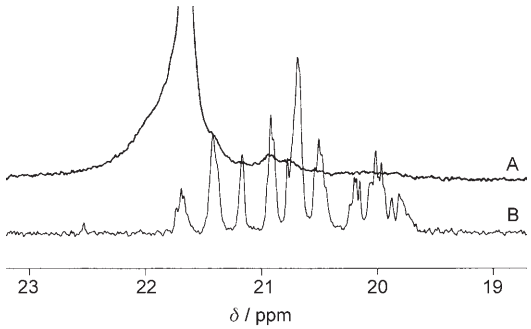

Figure 3. Methyl region of the ^{13}C NMR spectra of polypropylenes obtained from the *n*-heptane insoluble portion from: A) the reaction with **2**/MAO given as entry 2 of Table 1 and Table 2 and B) for the crude polymer obtained from the reaction with **3**/borate/TIBA given as entry 6 of Table 1 and Table 2.

Table 2: Detailed analysis of each extracted portion of the polymer samples.[a]

Entry[b]	Extraction portion	Wt%	T_m [°C]	M_w [$\times 10^{-3}$]	M_w/M_n	*mmmm* [%]
1	EE-sol	13	–	n/d[c]	n/d[c]	14
	EE-insol/C7-sol	21	151.1	85.8	2.45	55
	C7-insol	66	155.7	337	3.44	85
2	EE-sol	20	–	27.2	5.23	19
	EE-insol/C7-sol	21	131.8	68.4	4.20	53
	C7-insol	59	151.3	273	4.26	86
3	EE-sol	50	–	10.7	4.66	17
	EE-insol/C7-sol	32	146.4	39.4	3.80	67
	C7-insol	18	148.3	113	2.59	86
4	EE-sol	64	–	5.3	3.35	19
	EE-insol/C7-sol	22	127.3	17.8	2.59	53
	C7-insol	14	140.6	48.1	2.18	86
5	EE-sol	21	n/d[c]	n/d[c]	n/d[c]	n/d[c]
	EE-insol/C7-sol	44	n/d[c]	n/d[c]	n/d[c]	n/d[c]
	C7-insol	35	n/d[c]	n/d[c]	n/d[c]	n/d[c]
6	EE-sol	100	–	15.2	2.10	5.4
7	EE-sol	100	–	16.6	2.10	3.2
8	EE-sol	100	–	58.9	1.87	n/d[c]
9	EE-insol/C7-sol	97	129	19.1	2.13	76

[a] EE = diethyl ether, C7 = *n*-heptane; See Supporting Information for detailed analysis. [b] Entry numbers correspond to those in Table 1. [c] Not determined.

aspecific, unbridged-metallocene precatalysts with isospecificity.

The use of **3**, the dimethyl analogue of **2**, provides clues to the nature of the isospecific catalytic species in the **2**/MAO system. When **3** is activated with $[Ph_3C][B(C_6F_5)_4]$ in the presence of TIBA or TOA ([Al]/[Zr] = 200),[15] for example, the resulting catalytic systems give completely diethyl ether soluble, atactic polypropylenes (Figure 3B; see also Tables 1 and 2 entries 6 and 7), while **3**/MAO affords polypropylene whose tacticity distribution is similar to that obtained with **2**/MAO (see Tables 1 and 2, entry 5). Therefore, the involvement of MAO appears to be essential in achieving isospecificity in propylene polymerization. Furthermore, when the activation of **3** is effected by initial treatment with MAO and subsequent treatment with $[Ph_3C][B(C_6F_5)_4]$ (see Table 1, entry 11), the resulting catalytic species gives completely atactic, diethyl ether solu-

 © 2006 Wiley-VCH Verlag GmbH & Co. KGaA, Weinheim

ble polypropylene whose M_w/M_n value of 2.66 reflects its single-site catalytic nature. ^{1}H NMR spectroscopy experiments revealed that the addition of $[Ph_3C][B(C_6F_5)_4]$ to **3**/MAO causes the formation of Ph_3CMe, as judged by the appearance of a signal at $\delta = 1.96$ ppm,[16] while the treatment of neutral MAO with $[Ph_3C][B(C_6F_5)_4]$ at room temperature does not produce Ph_3CMe. Since $[Me\text{-}MAO]^-$ is the generally assumed counteranion formed in metallocene/MAO systems,[17] the formation of Ph_3CMe can be understood in terms of Me^- abstraction by $[Ph_3C]^+$ from $[Me\text{-}MAO]^-$.[18] Therefore, the treatment of **3**/MAO with $[Ph_3C][B(C_6F_5)_4]$ causes the transformation of the isospecific $[(AP)_2ZrMe]^+$-$[Me\text{-}MAO]^-$ in **3**/MAO to aspecific $[(AP)_2ZrMe]^+[B(C_6F_5)_4]^-$ and neutral MAO. This observation, and the additional finding that the catalytic system generated by treating **3** initially with $[Ph_3C][B(C_6F_5)_4]$ ([B]/[Zr] = 1) and then with MAO (Al/Zr = 200) (see Table , entry 12) also gives completely atactic polypropylene, implies that the influence of MAO on the isospecificity occurs due to $[Me\text{-}MAO]^-$ rather than neutral MAO.

Variable-temperature ^{1}H NMR spectroscopy studies of **3** and **3**/MAO (Al/Zr = 200) solutions in [D$_8$]toluene (Figure 4)[16] provide further evidence for the nature of the

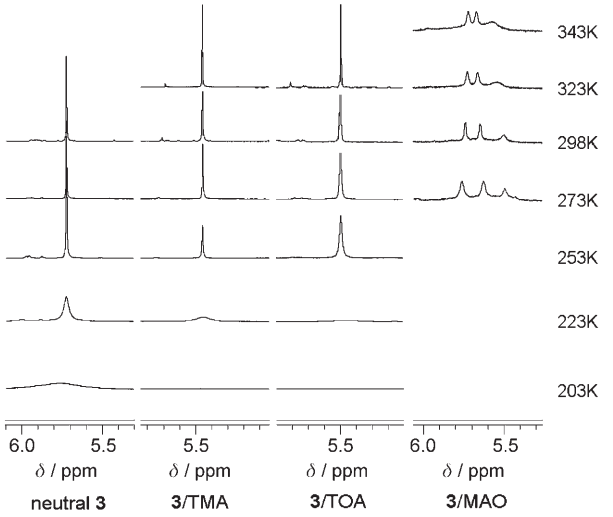

Figure 4. Cyclopentadienyl (Cp) proton region of the variable-temperature NMR (VT-NMR) spectra of **3**, **3**/TMA, **3**/TOA(Al/Zr=3), and **3**/MAO(Al/Zr=200). TMA = trimethylaluminum.

isospecific catalytic species. The singlet appearance of the two magnetically different Cp protons of **3** at temperatures as low as 203 K suggests that the ligand in **3** rotates rapidly in solution. Waymouth-type neutral precatalysts undergo very rapid ligand rotation in solution,[19] and the bulky precatalyst bis(2-(3,5-di-*tert*-butylphenyl)indenyl)dimethylzirconium rotates at a rate of 94 700 s^{-1} even at 196 K, as measured by the longitudinal relaxation time.[20] Therefore, the ligand rotation rate of compound **3** should be at least of the order of 10^4 s^{-1} at the low-temperature limit.

The addition of MAO to **3** causes the appearance of one set of two Cp proton signals, with equal intensities, at around $\delta = 5.7$ ppm and an upfield shift of the Me_2N signal,[21] thus indicating the presence of an active species in which the ligand rotation is restricted on the NMR timescale, up to 343 K, and the formation of Al···N interactions, respectively. Although coalescence was not observed up to 343 K, the ligand rotation rate of the active species in **3**/MAO can be calculated as 122 s^{-1} at the coalescence temperature by taking 273 K as the no-exchange limit;[22] it is therefore slower than 122 s^{-1} at the polymerization temperatures.

The position of the upfield-shifted Me_2N signal shows a large temperature dependency such that at the higher temperature limit the chemical-shift value approaches that of neutral **3**. Therefore, the Al···N Lewis acid–base interaction is stable at the low-temperature limit but is likely to be cleaved at the higher temperature limit, thereby leading to a thermal equilibrium between the species with and without this interaction. **3**/TMA and **3**/TOA (Al/Zr = 3) systems also show an upfield shift of the Me_2N signal but only one Cp proton signal. Thus, trialkylaluminum is capable of forming an Al···N interaction but is not able to prevent the ligand rotation.

Overall, the above observations support the formation of a *rac*-like ion-pair of the type $[(AP)_2ZrP]^+[Me\text{-}MAO]^-$ (**IS**) as the isospecific catalytic species (Scheme 2). The simultaneous presence of the cation–anion pairing and interactions between the Lewis acid sites in $[Me\text{-}MAO]^-$ and the nitrogen atoms of the amine-functionalized, unbridged-zirconocene cation in **IS** is effective in preventing the ligands from rotating rapidly, which leads to the prevalence of a racemic, C_2-symmetric-like active species in solution. The fact that the hydrodynamic diameter (25 Å)[23] of $[Me\text{-}MAO]^-$ is larger than the separation (ca. 15 Å) between two nitrogen atoms in **2** is also in favor of such interactions. The broad molecular-weight distribution as well as the presence of polymer fractions with different tacticities associated with **2**/MAO imply that **IS** is in thermal equilibrium with the other species shown in the upper part of Scheme 2. A similar temperature-dependent Al···N interaction has been employed in alkylamine-functionalized zirconocene/MAO to modulate the molecular-weight distribution of polyethylene.[24] Clearly,

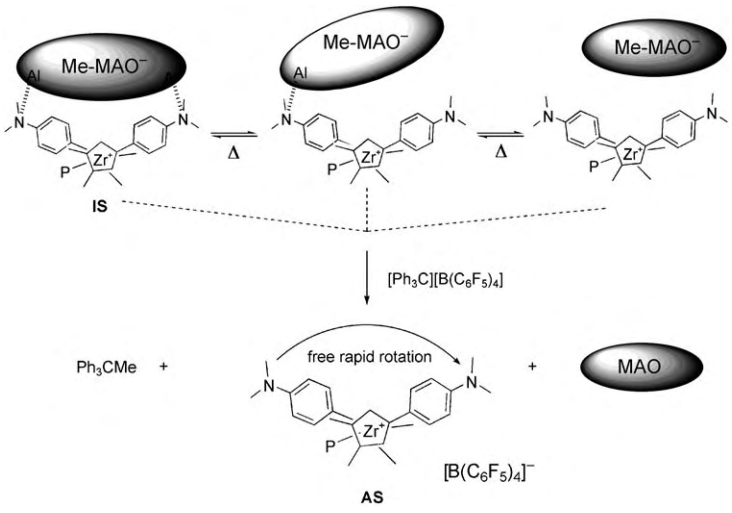

Scheme 2. Suggested thermal equilibrium of possible active species upon MAO activation (top) and generation of the aspecific active species **AS** by the addition of $[Ph_3C][B(C_6F_5)_4]$ to the **3**/MAO system (bottom).

 © 2006 Wiley-VCH Verlag GmbH & Co. KGaA, Weinheim

MAO, in the form of [Me-MAO]$^-$, acts as an in situ *ansa*-bridge and plays the unprecedented role of endowing aspecific class I unbridged-metallocene precatalysts with isospecificity, although cocatalysts are also known to affect the stereoselectivity of unbridged-metallocene catalysts to some extent.[25–27]

In conclusion, we have devised a novel synthetic strategy for the synthesis of isospecific, unbridged-metallocene catalytic systems for propylene polymerization. The class I unbridged metallocene with E = NEt_2, OMe, SMe, etc. behaves similarly and efforts are continuing to establish the scope of the synthetic strategy.[28]

Received: February 20, 2006
Revised: June 9, 2006
Published online: August 22, 2006

Keywords: isotactic polypropylene · Lewis acids · metallocenes · polymerization · zirconium

[1] Special issue on *Frontiers in Metal-Catalyzed Polymerization* (Ed.: J. A. Gladysz): *Chem. Rev.* **2000**, *100*, 1167.
[2] V. C. Gibson, S. K. Spitzmesser, *Chem. Rev.* **2003**, *103*, 283.
[3] W. Kaminsky, *Adv. Catal.* **2001**, *46*, 89.
[4] H. H. Brintzinger, D. Fischer, R. Mülhaupt, B. Rieger, R. M. Waymouth, *Angew. Chem.* **1995**, *107*, 1255; *Angew. Chem. Int. Ed. Engl.* **1995**, *34*, 1143.
[5] L. Resconi, L. Cavallo, A. Fait, F. Piemontesi, *Chem. Rev.* **2000**, *100*, 1253.
[6] J. A. Ewen, M. J. Elder, R. L. Jones, A. L. Rheingold, L. M. Liable-Sands, R. D. Sommer, *J. Am. Chem. Soc.* **2001**, *123*, 4763.
[7] S. A. Miller, J. E. Bercaw, *Organometallics* **2004**, *23*, 1777.
[8] J. L. Maciejewski Petoff, M. D. Bruce, R. M. Waymouth, A. Masood, T. K. Lal, R. W. Quan, S. J. Behrend, *Organometallics* **2004**, *23*, 1777.
[9] M. H. Lee, Y. Do, *J. Organomet. Chem.* **2005**, *690*, 1240.
[10] G. Erker, R. Nolte, R. Aul, S. Wilker, C. Krüger, R. Noe, *J. Am. Chem. Soc.* **1991**, *113*, 7594.
[11] A. Razavi, *J. Am. Chem. Soc.* **1993**, *115*, 7529.
[12] G. Coates, R. M. Waymouth, *Science* **1995**, *267*, 217.
[13] S. Lin, R. M. Waymouth, *Acc. Chem. Res.* **2002**, *35*, 765.
[14] A. Lehtinen, R. Paukkeri, *Macromol. Chem. Phys.* **1994**, *195*, 1539.
[15] The use of additional AlR_3 is required since the treatment of **3** with $[Ph_3C][B(C_6F_5)_4]$ did not afford active species. A similar phenomenon is also reported in ref. [24].
[16] See Supporting Information for more details.
[17] E. Y.-X. Chen, T. J. Marks, *Chem. Rev.* **2000**, *100*, 1391.
[18] The formation of Ph_3CMe from $[Ph_3C]^+$ by the abstraction of Me^- from the anionic dinuclear alumoxane has been reported: S. J. Obrey, S. G. Bott, A. R. Barron, *Organometallics* **2001**, *20*, 5162.
[19] M. D. Bruce, G. W. Coates, E. Hauptman, R. M. Waymouth, J. W. Ziller, *J. Am. Chem. Soc.* **1997**, *119*, 11174.
[20] G. M. Wilmes, M. B. France, S. R. Lynch, R. M. Waymouth, *Organometallics* **2004**, *23*, 2405.
[21] The intensity of the upfield peak at $\delta = 5.5$ ppm is dependent on the [Al]/[Zr] ratio. This peak disappears at ratios higher than 200. Its origin is considered to be due to a **3**···TMA species since a mixture of **3** and TMA gives a Cp signal at the same position.
[22] A [D_8]toluene solution of **3**/MAO at 273 K is extremely viscous and no proton signal was seen at the lower temperatures. Thus, 273 K was taken as the no-exchange limit. In addition, owing to the possible influence of viscosity on the line width at 273 K, the line-shape-analysis expression $(k = \pi((W_{1/2})_e - (W_{1/2})_o)$ where $W_{1/2}$, e, and o stand for the peak-width at half height, with exchange, and no exchange, respectively, for the rates in the slow-exchange regime below the coalescence point cannot be used. Thus, the rotation rate at the coalescence point was calculated and taken as a comparison value: $k = \pi\Delta\nu_0/2^{1/2} = \pi(2307–2252\ \text{Hz})/2^{1/2} = 122\ s^{-1}$.
[23] D. E. Babushkin, H. H. Brintzinger, *J. Am. Chem. Soc.* **2002**, *124*, 12869.
[24] C. Müller, D. Lilge, M. O. Kristen, P. Jutzi, *Angew. Chem.* **2000**, *112*, 800; *Angew. Chem. Int. Ed.* **2000**, *39*, 789.
[25] G. M. Wilmes, J. L. Polse, R. H. Waymouth, *Macromolecules* **2002**, *35*, 6766.
[26] V. Busico, V. V. A. Castelli, P. Aprea, R. Cipullo, A. Segre, G. Talarico, M. Vacatello, *J. Am. Chem. Soc.* **2003**, *125*, 5451.
[27] A. Macchioni, *Chem. Rev.* **2005**, *105*, 2039.
[28] CCDC 299059 contains the supplementary crystallographic data for this paper. These data can be obtained free of charge from The Cambridge Crystallographic Data Centre via www.ccdc.cam.ac.uk/data_request/cif.

 © 2006 Wiley-VCH Verlag GmbH & Co. KGaA, Weinheim

Self-Assembled Monolayers

DOI: 10.1002/anie.200600926

Onset of Crystalline Order in 1-Nonanethiol Monolayers Deposited from Solution**

María José Capitán, Jesús Álvarez, Juan José Calvente, and Rafael Andreu*

A plethora of applications of thiol self-assembled monolayers (SAMs) have been developed during the last two decades.[1] A unique combination of factors, such as ease of preparation,

[*] Dr. M. J. Capitán
Instituto de Estructura de la Materia
and
U.A. Nanoestructuras Autoensambladas en Superficies
CSIC
c/Serrano 119. 28006 Madrid (Spain)
Fax: (+34) 914-973-048
E-mail: capitan@iem.cfmac.csic.es
Dr. J. Álvarez
Dpto. Física de la Materia Condensada
CIII and U.A. N.A.S.
Universidad Autónoma de Madrid
Ctra. Colmenar Viejo km 15.5. 28049 Madrid (Spain)
Dr. J. J. Calvente, Dr. R. Andreu
Dpto. Química-Física. Facultad de Química
Universidad de Sevilla
c/Prof. García González s/n 41012 Sevilla (Spain)

[**] The authors thank Dr. O. Seeck for his fruitful help at the W1.1 beamline in Hasylab. We acknowledge the financial support of MCYT, Spain, grant nos. MAT2004-2007, CTQ 2005-01184, CAM, Spain, grant no. 07N/0023/2002, and the EC under the FP6 "Structuring the European Research Area" Programme Contract RII3-CT-2004-506008

WILEY InterScience DISCOVER SOMETHING GREAT
© 2006 Wiley-VCH Verlag GmbH & Co. KGaA, Weinheim

mechanical robustness, transferability, and a broad choice of commercially available metallic substrates and thiols, has prompted their use in a variety of scientific areas such as molecular electronics,[2] corrosion protection,[3] nanolithography,[4] electrochemical sensing,[5] and cellular adhesion.[6] Moreover, there seems to be a wide acceptance that these systems exhibit a high degree of structural order, particularly in the prototypical case of alkanethiol ($HS-(CH_2)_n-CH_3$) SAMs deposited on Au(111). This assumption is well supported from X-ray and helium diffraction,[7] IR,[8] and STM[9] studies carried out under either ultrahigh vacuum (UHV) or ambient conditions, but it turns out to be more controversial when the organic monolayer is in contact with a liquid phase. A number of in situ STM and AFM studies of alkanethiol monolayers[10] (with $2 \le n \le 17$) have visualized ordered domains in the presence of a variety of solvents, which include water, ethanol, 2-butanol, and heptane. In all cases, these domains reproduce the $(\sqrt{3}\times\sqrt{3})$R30° overlayer structure that is observed in the absence of solvent, and some of them display also the characteristic c(4×2) superlattice (Figure 1).[10d–f] However, in situ vibrational spectra of these

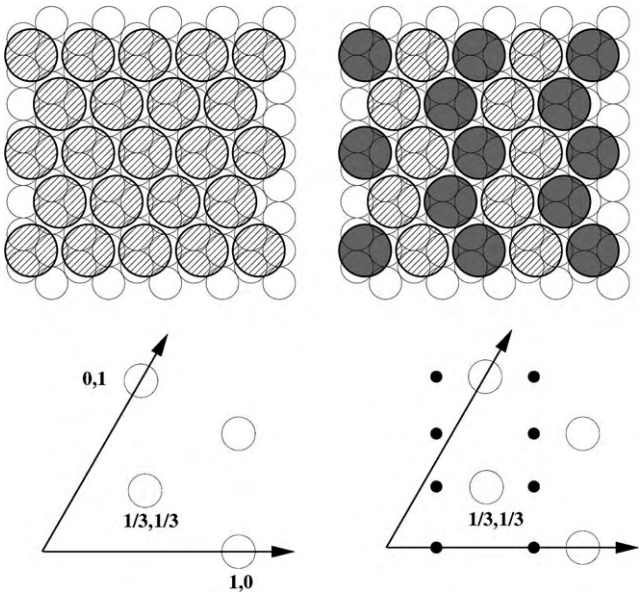

Figure 1. Real-space (top) and reciprocal-space (bottom) representations of the $(\sqrt{3}\times\sqrt{3})$R30° structure (left) and of its c(4×2) superlattice (right), which describe a typical packing of alkanethiol SAMs deposited on Au(111). Small and large circles in the real-space representations correspond to gold atoms and alkanethiol chains, respectively.

monolayers indicate the presence of some conformational disorder near the alkyl chain terminus.[11] There is also a conspicuous lack of reported diffraction results that support the persistence of crystalline order when the monolayer is in contact with a liquid phase.[12] Herein, we report the time evolution of the diffraction peaks associated with the appearance of the $(\sqrt{3}\times\sqrt{3})$R30° structure in a 1-nonanethiol SAM deposited on Au(111) from an ethanolic thiol solution. The presence of a liquid phase is shown to disrupt the monolayer structure, and crystallographic order is seen to develop only when the contacting solution is removed.

1-Nonanethiol monolayers were deposited on Au(111) by thiol adsorption from an ethanolic solution. No diffraction peaks were observed at the 1/3,1/3,1 reciprocal-space position during the deposition ($\approx$2 h) and rinsing ($\approx$10 min) stages. When ethanol was replaced by a continuous flow of helium ($\approx$30 mL min^{-1}), a diffraction peak, characteristic of the $(\sqrt{3}\times\sqrt{3})$R30° overlayer structure, developed over a long time period ($\approx$10 h; see Figure 2a and solid triangles in Figure 3 for the time evolution of the Bragg peak). It should be noted that no diffraction peak was detected if the sample was kept in contact with the solution for up to 20 h. It was verified that the

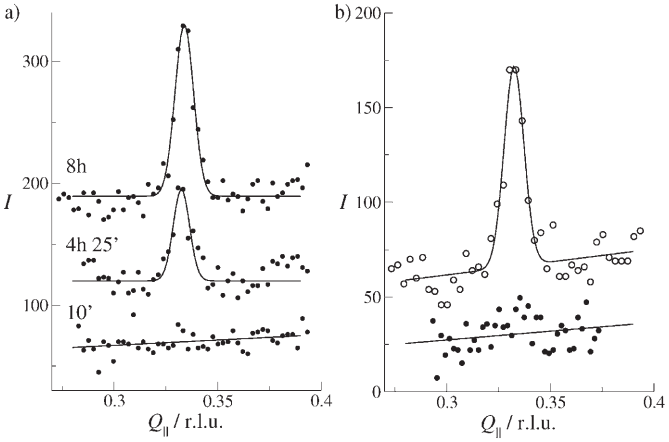

Figure 2. Time evolution of intensity of the 1/3,1/3,1 Bragg peak as a function of the in-plane momentum transfer (r.l.u. = reciprocal lattice units) a) after replacing ethanol by a continuous flow of helium, and b) after the previously ordered 1-nonanethiol monolayer (○) is put into contact with liquid ethanol for 30 min (●). Plots have been shifted vertically for clarity. The time elapsed since the liquid phase was removed from the thin-layer cell is indicated on each plot.

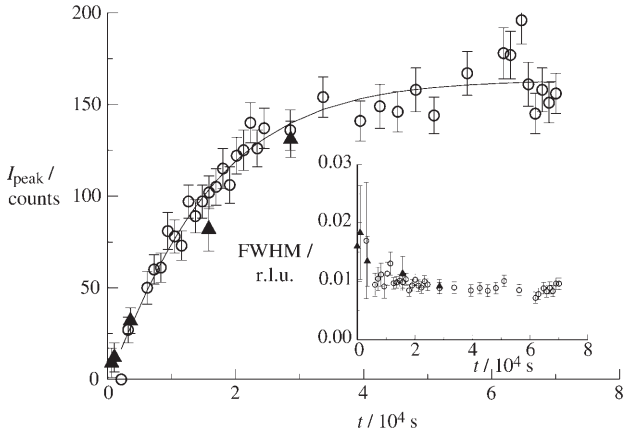

Figure 3. Background-subtracted peak intensity of the 1/3,1/3,1 in-plane Bragg peak as a function of the time elapsed since the solution was removed. Triangles (▲) are data obtained just after monolayer formation, and circles (○) were recorded after the already-ordered monolayer was put into contact with ethanol for 30 min (some of these peaks are shown in Figure 2). The solid line is the best fit of Equation (1) to the data. The inset shows the corresponding FWHM values of the peak.

 © 2006 Wiley-VCH Verlag GmbH & Co. KGaA, Weinheim

background signal in both Au(111) crystal truncation rods (CTRs) and thiol structure rods remained constant during the measurements, thereby ruling out the possibility that the development of the diffraction peak could be due to a decrease in the solvent background.

To assess whether the observed ordering process was initiated after removal of the liquid phase, rather than after completion of a full monolayer coverage in the presence of ethanol, the already ordered monolayer was subjected to a wetting/drying cycle by successive injection of ethanol and helium. As shown in Figure 2b, contact with the liquid phase destroys completely the crystalline order in the SAM, whereas the previous ordering sequence is regained upon flushing again the cell with helium (see circles in Figure 3). The good agreement between the two sets of data in Figure 3 indicates the absence of significant X-ray induced damage in the monolayer, which is likely to be precluded by the continuous flow of helium over the sample.[13]

After the kinetic runs were completed, the final thiol structure was inspected by recording a complete set of in-plane and out-of-plane X-ray scans (see Experimental Section). The intensity ratios of the measured Bragg rods are identical to those reported by Fenter et al. for decanethiol SAMs,[14] which indicates that the 1-nonanethiol monolayers presented herein also display the c(4×2) superstructure.

The time evolution of the ordering process illustrated in Figure 3 can be reproduced by Equation (1),[15] in which θ is

$$\theta(t) = \frac{I(t)}{I_{t\to\infty}} = 1-\exp(-k\,t^n) \qquad (1)$$

the surface coverage of ordered domains, I is the intensity of the diffraction peak, and k and n are kinetic parameters whose physical meaning is analysed below. The best fit to the data in Figure 3 is obtained for $k = 2.2\times10^{-5}\ s^{-1}$ and $n = 1.1$. According to the Kolmogorov–Avrami theory,[15] n is related to the effective dimensionality of the growing domains. A value of n close to 1 may arise in either a) a constant rate of nucleation, combined with ordered domains of homogeneous size whose number increases with time, or b) an instantaneous (delta-shaped) nucleation rate, combined with a domain growth along one dimension only.[15] It is possible to discriminate between these two alternatives by considering the time evolution of the full width at half maximum (FWHM) values of the diffraction peaks, which are a measure of the average domain size ($l = 2\pi$/FWHM).[16] As shown in the inset of Figure 3, peak widths remain constant during the ordering process, thus providing a time-independent average mosaic size of 50 nm. This behavior is consistent with our first hypothesis only, and it provides a straightforward visualization of the ordering process as a sequence of sudden crystallization events that affect individual domains independently. The invariance of the average domain size with respect to repetitive wetting/drying cycles suggests that domain boundaries remain undisturbed by exposing the monolayer to a liquid phase and that their pattern is determined after completion of a full monolayer adsorption from solution. The kinetic parameter k defines the time scale of monolayer crystallization. Additional experiments carried out in a controlled atmosphere chamber indicate that full removal of the solvent molecules from the monolayer appears to be a rate-limiting prerequisite for the onset of the ordering process. The presence of a limited number of intercalated solvent molecules in the disordered monolayer is supported by the electrochemical quartz balance and ellipsometric measurements reported by Blanchard and Karpovich.[17]

Our results provide for the first time evidence of the dynamic structure of alkanethiol SAMs in contact with a liquid phase. The observation of crystalline order found with X-ray diffraction after hours without solvent is coherent with other SAMs X-ray diffraction experiments developed under UHV.[14] We have verified that the obtained crystalline order for the thiol SAMs in such conditions extends in both in-plane and out-of-plane directions. Though the X-ray diffraction is more sensitive to atoms with a higher atomic number (Z), the fact that 1-nonanethiol monolayers contain nine carbon atoms per sulphur atom means the overall scattering power of the monolayer is governed by the carbon moiety. The structural study of the data obtained from the ordered SAM shows that the rod intensity value measured at the surface for the normal momentum transfer $L = 1$ is mainly governed by the total chain structure factor.[14] Thus, the observed ordering process can be unambiguously associated with a rearrangement of the whole alkyl chains. Furthermore, in situ IR experiments have also provided evidence of solvent-induced disorder in these monolayers, although it was apparently confined to the outermost methyl groups.[11] Our results show that in the presence of a liquid phase, even if the thiol heads can be periodically arranged on the gold substrate, the alkyl chains, which contribute most of the monolayer scattering power at the recorded L position, do not display long-range order, particularly along the surface normal where the scanning probe techniques are silent.

We have shown in this work how reversible switching between crystalline order and disorder in a 1-nonanethiol monolayer can be accomplished by alternately exposing the monolayer to ethanol or to a helium stream. Analysis of the time-dependent X-ray measurements has provided a detailed description of the surface crystallization process.

Experimental Section

Ethanol and 1-nonanethiol were obtained from Aldrich and used without further purification. Au(111) single crystals were purchased from MaTeck (Germany), as 10 mm diameter disks. They were first anodically electropolished and then annealed in a hydrogen flame. The electropolishing/annealing cycle was repeated until a sharp diffraction pattern, characteristic of a clean flat gold surface, was obtained. The Au(111) single crystals were then mounted in a thin-layer flow cell with a polyethylene window. The gold surface was flushed with a deoxygenated solution of 1-nonanethiol (10 mM) in ethanol for 2 h. Electrochemical desorption experiments confirmed that a fully grown thiol monolayer is produced under these conditions.[18] After completion of the adsorption stage, samples were washed with pure ethanol and kept under a helium stream during the measurements. Diffraction experiments were performed at the W1.1 beamline of the HASYLAB synchrotron at DESY with a wavelength of 0.1397 nm. The angle of incidence of the X-ray beam was fixed at 2°. Two sets of data were collected to characterize the 1-nonanethiol SAM structure: 1) in-plane data having an L index

 © 2006 Wiley-VCH Verlag GmbH & Co. KGaA, Weinheim

(i.e., the ordinal Miller index of the surface-normal momentum transfer in reciprocal lattice units, r.l.u.) close to 1, which was shown in preliminary experiments to be very sensitive to the arrangement of the carbon atoms in the monolayer. L is related to the perpendicular momentum transfer ($Q_\perp$ with $Q_\perp = L \times c^*$, where L is the ordinal Miller index of the perpendicular momentum transfer and $c^* = 2\pi/c = 0.8891$ Å^{-1} is the inverse lattice parameter of the Au(111) substrate); 2) out-of-plane data corresponding to different rods. The sample holder was in thermal contact with an electrical resistance to control its temperature at 30 ± 2 °C.

Received: March 9, 2006
Published online: August 14, 2006

Keywords: crystal growth · kinetic resolution · monolayers · self-assembly · X-ray diffraction

[1] a) J. C. Love, L. A. Estroff, J. K. Kriebel, R. G. Nuzzo, G. M. Whitesides, *Chem. Rev.* **2005**, *105*, 1103; b) D. Witt, R. Klajn, P. Barski, B. A. Grzybowski, *Curr. Org. Chem.* **2004**, *8*, 1763; c) F. Schreiber, *Prog. Surf. Sci.* **2000**, *65*, 151.

[2] a) M. A. Reed, C. Zhou, C. J. Muller, T. P. Burgin, J. M. Tour, *Science* **1997**, *278*, 252; b) A. Salomon, D. Cahen, S. Lindsay, J. Tomfohr, V. B. Engelkes, C. D. Frisbie, *Adv. Mater.* **2003**, *15*, 1881; c) Y. Xiao, F. Patolsky, E. Katz, J. H. Hainfeld, I. Willner, *Science* **2003**, *299*, 1877.

[3] a) J. Scherer, M. R. Vogt, O. M. Magnussen, R. J. Behm, *Langmuir* **1997**, *13*, 7045; b) C. Whelan, M. Kinsella, L. Carbonell, H. Ho, K. Maex, *Microelectron. Eng.* **2003**, *70*, 551.

[4] a) Y. N. Xia, G. M. Whitesides, *Angew. Chem.* **1998**, *110*, 568; *Angew. Chem. Int. Ed.* **1998**, *37*, 550; b) S. Kraemer, R. R. Fuierer, C. B. Gorman, *Chem. Rev.* **2003**, *103*, 4367; c) D. S. Ginger, H. Zhang, C. A. Mirkin, *Angew. Chem.* **2004**, *116*, 30; *Angew. Chem. Int. Ed.* **2004**, *43*, 30.

[5] a) I. Turyan, D. Mandler, *Anal. Chem.* **1997**, *69*, 894; b) J. J. Gooding, F. Mearns, W. Yang, J. Liu, *Electroanalysis* **2003**, *15*, 81.

[6] a) Y. Y. Luk, M. Kato, M. Mrksich, *Langmuir* **2000**, *16*, 9604; b) R. G. Chapman, E. Ostuni, S. Takayama, R. E. Holmlin, L. Yan, G. M. Whitesides, *J. Am. Chem. Soc.* **2000**, *122*, 8303.

[7] a) C. E. D. Chidsey, G. Y. Liu, P. Rowntree, G. Scoles, *J. Chem. Phys.* **1989**, *91*, 4421; b) L. Strong, G. M. Whitesides, *Langmuir* **1988**, *4*, 546; c) C. E. D. Chidsey, D. N. Loiacano, *Langmuir* **1990**, *6*, 682; d) P. Fenter, A. Eberhardt, K. S. Liang, P. Eisenberger, *J. Chem. Phys.* **1997**, *106*, 1600.

[8] a) R. G. Nuzzo, L. H. Dubois, D. L. Allara, *J. Am. Chem. Soc.* **1990**, *112*, 558; b) R. G. Nuzzo, E. M. Korenic, L. H. Dubois, *J. Chem. Phys.* **1990**, *93*, 767.

[9] a) G. E. Poirier, M. Tarlov, *Langmuir* **1994**, *10*, 2853; b) G. E. Poirier, E. D. Pylant, *Science* **1996**, *272*, 1145.

[10] a) J. Pan, N. Tao, S. M. Lindsay, *Langmuir* **1993**, *9*, 1556; b) R. Yamada, K. Uosaki, *Langmuir* **1998**, *14*, 855; c) G. Nelles, H. Schönherr, M. Jaschke, H. Wolf, M. Schaub, J. Küther, W. Tremel, E. Bamberg, H. Ringsdorf, H. Butt, *Langmuir* **1998**, *14*, 808; d) F. T. Arce, M. E. Vela, R. C. Salvarezza, A. J. Arvia, *Electrochim. Acta* **1998**, *44*, 1053; e) M. E. Vela, H. Martin, C. Vericat, G. Andreasen, A. H. Creus, R. C. Salvarezza, *J. Phys. Chem. B* **2000**, *104*, 11878; f) E. Paradis, P. Rowntree, *J. Electroanal. Chem.* **2003**, *550*, 175.

[11] a) S. M. Stole, M. D. Porter, *Langmuir* **1990**, *6*, 1199; b) T. H. Ong, R. N. Ward, P. B. Davies, C. D. Bain, *J. Am. Chem. Soc.* **1992**, *114*, 6243; c) M. R. Anderson, M. Gatin, *Langmuir* **1994**, *10*, 1638; d) M. R. Anderson, M. N. Evaniak, M. Zhang, *Langmuir* **1996**, *12*, 2327.

[12] a) SAM deposited on Au(111) and in contact with an aqueous solution: J. Li, K. S. Liang, G. Scoles, A. Ulman, *Langmuir* **1995**, *11*, 4418; b) SAM deposited on liquid mercury and in contact with an inert atmosphere: B. M. Ocko, H. Kraack, P. S. Pershan, E. Sloutskin, L. Tamam, M. Deutsch, *Phys. Rev. Lett.* **2005**, *94*, 017802.

[13] P. Fenter, F. Schreiber, L. Berman, G. Scoles, P. Eisenberger, M. J. Bedzyk, *Surf. Sci.* **1998**, *412*/413, 213.

[14] P. Fenter, A. Eberhardt, P. Eisenberger, *Science* **1994**, *266*, 1216.

[15] a) Y-L. Loo, R. A. Register, A. J. Ryan, *Phys. Rev. Lett.* **2000**, *84*, 4120; b) A. N. Kolmogorov, *Izv. Akad. Nauk SSSR Ser. Mater.* **1937**, *3*, 355; c) M. Avrami, *J. Chem. Phys.* **1941**, *9*, 177; d) G. Reiter, G. Castelein, J.-U. Sommer, A. Röttele, T. Thurn-Albrecht, *Phys. Rev. Lett.* **2001**, *87*, 226101.

[16] a) B. E. Barren, *X-Ray Diffraction*, Addison-Wesley, Reading, MA, **1969**; b) E. Vlieg, J. F. van der Veen, S. J. Gyurman, C. Norris, J. E. MacDonald, *Surf. Sci.* **1980**, *210*, 301.

[17] D. S. Karpovich, G. J. Blanchard, *Langmuir* **1997**, *13*, 4031.

[18] J. J. Calvente, Z. Kovacova, M. D. Sanchez, R. Andreu, W. R. Fawcett, *Langmuir* **1996**, *12*, 5696.

 © 2006 Wiley-VCH Verlag GmbH & Co. KGaA, Weinheim

Coordination Chemistry

DOI: 10.1002/anie.200600962

Luminescent Dinuclear Platinum(II) Terpyridine Complexes with a Flexible Bridge and "Sticky Ends"**

Vivian Wing-Wah Yam, Kenneth Hoi-Yiu Chan, Keith Man-Chung Wong, and Ben Wai-Kin Chu*

Luminescent square-planar d^8 platinum(II) complexes have attracted much attention because of their intriguing photophysical and spectroscopic properties.[1–8] In particular, platinum(II) derivatives with terpyridyl ligands and their analogues have been widely studied for their luminescence behavior.[3–7] Owing to their planar coordination geometry, which permits easy access to important frontier orbitals of the metal center, d^8–d^8 metal–metal interactions as well as π–π interactions between chromophores of the polypyridyl plat-

[*] Prof. Dr. V. W.-W. Yam, K. H.-Y. Chan, Dr. K. M.-C. Wong, Dr. B. W.-K. Chu
Centre for Carbon-Rich Molecular and Nano-Scale Metal-Based Materials Research and
Department of Chemistry
The University of Hong Kong
Pokfulam Road, Hong Kong (P.R. China)
Fax: (852) 2857-1586
E-mail: wwyam@hku.hk

[**] V.W.-W.Y. acknowledges support from the University Development Fund of The University of Hong Kong. This work has been supported by a Central Allocation Vote (CAV) Grant from the Research Grants Council of Hong Kong Special Administrative Region, China (Project No. HKU 2/05C). K.H.-Y.C. acknowledges the receipt of a postgraduate studentship, administered by The University of Hong Kong.

Supporting information for this article is available on the WWW under http://www.angewandte.org or from the author.

 © 2006 Wiley-VCH Verlag GmbH & Co. KGaA, Weinheim

inum(II) complexes lead to extensive polymorphism of these complexes in the solid state.[5a,c,7,8]

Recently, we showed that mononuclear alkynyl platinum(II) terpyridyl complexes could show interesting intermolecular aggregation and oligomerization phenomena in the solution state with drastic color changes and luminescence enhancement caused by polymer-induced or solvent-induced self-assembly of the metal complexes.[5] Tunable solution-state intermolecular Pt···Pt interactions and π–π stacking were suggested to be responsible for these remarkable spectroscopic changes upon variations in the solvent composition, counteranion, and pH value of the polyelectrolyte. However, the related intramolecular association or self-assembly of this class of complexes in solution were not extensively explored.[3b–d]

In this context, we prepared a series of dinuclear alkynyl platinum(II) terpyridyl complexes in which the two platinum(II) units are linked through a flexible bridge (Scheme 1)

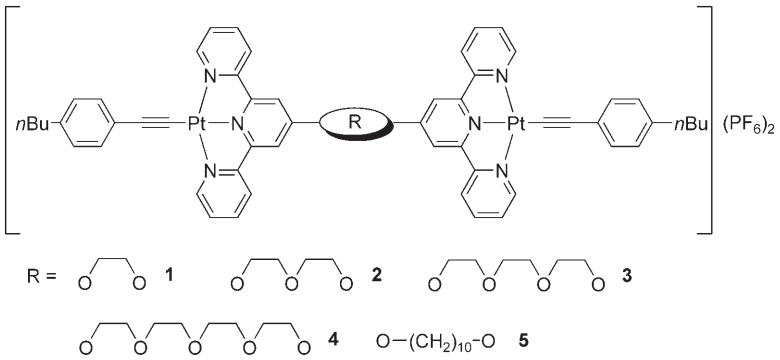

Scheme 1. Structure of the dinuclear alkynyl platinum(II) terpyridyl complexes **1**–**5**.

and studied their solution-state intramolecular aggregation properties. The two platinum(II) terpyridyl moieties of the molecule showed a high tendency towards intramolecular association. The effect of temperature on the aggregation and deaggregation properties of these dinuclear platinum(II) complexes was investigated by ^{1}H NMR, electronic absorption, and emission spectroscopy. The present work demonstrates the versatility of the platinum(II) terpyridyl chromophore as reporters of intramolecular association and the ability of metal–metal and π–π interactions in providing the driving force for intramolecular aggregation or "molecular sticking" that can be controlled by temperature modulation.

The dinuclear chloroplatinum(II) precursor complexes were synthesized according to a modified literature synthesis for $[Pt(tpy)Cl]^+$ (tpy = 2,2′:6′,2″-terpyridyl)[7a,9] by the reaction of the corresponding bridged terpyridyl ligands with $K_2[PtCl_4]$ in a 1:2 molar ratio. Reaction of the newly synthesized dinuclear chloroplatinum(II) precursors and 4-*n*-butylphenylacetylene in the presence of a base and a catalytic amount of copper(I) iodide, followed by a metathesis reaction in saturated methanolic ammonium hexafluorophosphate solution gave the dinuclear platinum(II) complexes [(4-*n*Bu-C_6H_4C≡C)Pt(tpy–R–tpy)Pt(C≡C-C_6H_4-*n*Bu-4)]$(PF_6)_2$ (R = OCH_2CH_2O **1**; $O(CH_2CH_2O)_2$ **2**; $O(CH_2CH_2O)_3$ **3**; $O(CH_2CH_2O)_4$ **4**; $O(CH_2)_{10}O$ **5**) in moderate yield. All the complexes gave satisfactory elemental analyses and were characterized by ^{1}H NMR spectroscopy, IR spectroscopy, and FAB mass spectrometry.

The ^{1}H NMR spectra of **1** and **2** in [D_6]DMSO at 25 °C showed sharp signals with chemical shifts and splitting patterns consistent with their chemical formulation. In contrast, broad signals that were relatively upfield-shifted and poorly resolved were observed for **3**–**5** under the same conditions. Attempts to record the ^{1}H NMR spectra of dilute solutions of **3**–**5** by reducing the concentration from 10^{-3} to 10^{-5} M to minimize intermolecular interactions did not yield any improvement in the bandwidth and the resolution of the NMR signals. However, increasing the solution temperature dramatically improved the resolution of the ^{1}H NMR signals of **3**–**5**, and the signals became sharpened. At 90 °C, the signals were well resolved with a downfield shift of the signals corresponding to the terpyridyl protons. The ^{1}H NMR spectra of **4** in [D_6]DMSO at different temperatures are shown in Figure 1. The upfield shift and broadening of the proton resonances of **3**–**5** at lower temperature are independent of concentration and suggest the presence of molecular interactions or self-assembly processes, probably intramolecular in nature.

Similar line broadening and upfield shifts were also observed in planar aromatic metal complexes[10] and were ascribed to self-assembly. It is likely that complexes **1** and **2**, which have short bridging ligands, do not undergo self-association or aggregation at room temperature, as revealed by their NMR spectra. In contrast, complexes **3**–**5** with longer flexible bridges could readily self-associate and aggregate in solution, with complexes **4** and **5** occurring more readily than the shorter chain **3**, as reflected in their variable-temperature NMR spectra. As a result, intramolecular aggregation is predominant in solution at room temperature for **3**–**5**, whereas deaggregation takes place when the samples are heated (Figure 2). Self-assembly of two platinum(II) terpyridyl units in a molecule

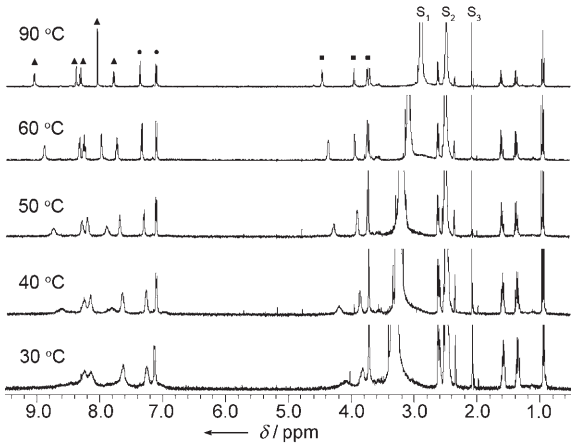

Figure 1. Variable-temperature ^{1}H NMR spectra of **4** in [D_6]DMSO. Proton signals correspond to the terpyridyl moiety (▲), the phenyl ring (●), and the oligo(oxyethylene) group (■). S_1, S_2, and S_3 represent the H_2O, DMSO, and acetonitrile signals, respectively.

 © 2006 Wiley-VCH Verlag GmbH & Co. KGaA, Weinheim

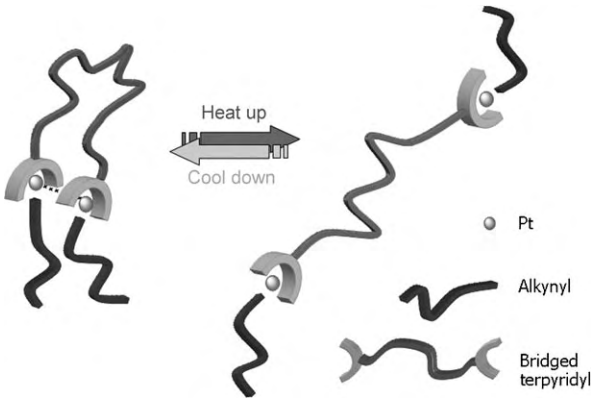

Figure 2. Aggregation and deaggregation of the platinum(II) complexes by temperature modulation.

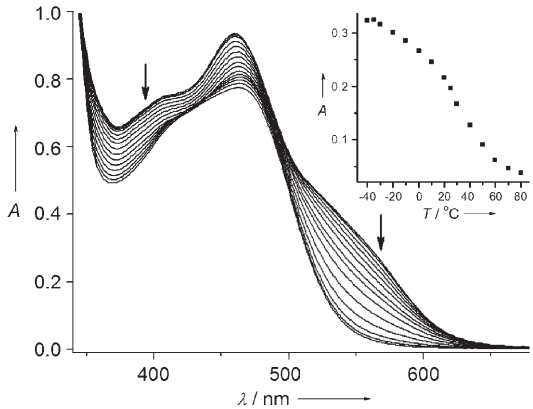

Figure 3. UV/Vis spectra of **4** with increasing temperature from −40 to 80 °C. Inset: Absorbance at 555 nm against temperature.

gave rise to intramolecular Pt···Pt and π–π stacking interactions that accounted for the NMR signal broadening and upfield shift. The length of the bridge was shown to play an important role in governing the occurrence and the extent of intramolecular aggregation.

Dissolution of **1**–**5** in acetonitrile gave yellow-to-orange solutions with similar UV/Vis absorption patterns at 25 °C that consisted of intense absorption bands at 280–350 nm and a low-energy absorption at 400–480 nm. With reference to previous spectroscopic work on alkynyl platinum(II) terpyridyl complexes,[4a,c,d,5] the higher-energy absorption bands are assigned as intraligand (IL) [π→π*] transitions of the terpyridyl and alkynyl ligands, whereas the low-energy absorption is assigned as a metal-to-ligand charge-transfer (MLCT) [dπ(Pt)→π*(tpy)] transition mixed with an alkynyl-to-terpyridine ligand-to-ligand charge-transfer (LLCT) [π(C≡C)→π*(tpy)] transition.

Electronic absorption spectra of the complexes in acetonitrile were measured in the temperature range between −40 and 80 °C. In general, temperature effects on the spectral changes of **1** and **2** were negligible when compared with those of **3**–**5**. At low temperature (−40 °C), a prominent absorption shoulder at about 550 nm appears in **3**–**5**, which is in a region typical of metal-metal-to-ligand charge-transfer (MMLCT) transitions.[5] The absorbance of this shoulder decreased with increasing temperature of the sample solutions and approached zero upon heating to 80 °C. Solutions of **4** and **5** change color from orange to yellow upon heating. The absorption spectra of **4** are shown in Figure 3 with an inset showing the absorbance changes at 555 nm as a function of temperature. It is believed that the newly formed absorption shoulder originates from the MMLCT transition as a result of intramolecular association within the complexes brought about by the Pt···Pt and π–π interactions between the platinum(II) terpyridyl moieties. The sigmoid curve in the inset of Figure 3 reflects the degree of aggregation and indicates complete aggregation at low temperature and almost complete deaggregation at elevated temperature. The electronic spectra agree well with the proton NMR studies, which suggest that **3**–**5** form aggregates at room temperature and at lower temperature, whereas **1** and **2** do not, even when they are cooled down to the freezing point of the solvent.

With reference to the analogous DNA hairpin studies,[11] the equilibrium absorbance spectra were analyzed in terms of a two-state van't Hoff model.[12] The melting temperatures T_m for **4** and **5** are 299 and 287 K, respectively. The enthalpy changes $\Delta H°$ for the deaggregation process (Figure 2) of **4** and **5** were determined to be $+37\ kJ\,mol^{-1}$ ($+8.8\ kcal\,mol^{-1}$) and $+35\ kJ\,mol^{-1}$ ($+8.5\ kcal\,mol^{-1}$), respectively, and the entropy changes $\Delta S°$ were found to be $+124\ J\,mol^{-1}\,K^{-1}$ ($+29.6\ cal\,mol^{-1}\,K^{-1}$) and $+123\ J\,mol^{-1}\,K^{-1}$ ($+29.5\ cal\,mol^{-1}\,K^{-1}$), respectively.

In acetonitrile at 25 °C, all complexes except **2** are emissive upon excitation at $\lambda > 400$ nm. Complex **1** exhibits an emission band at 658 nm, which was assigned to an excited state of predominantly ^{3}MLCT character, whereas the emission maxima of **3**–**5** are significantly red-shifted to about 830 nm. This substantial red shift, together with the self-association revealed from ^{1}H NMR and UV/Vis absorption studies, suggested that the emission is of ^{3}MMLCT origin, similar to that found for other alkynyl platinum(II) terpyridyl systems.[5] The change in the emission origin from the short-chain complex **1** to the longer-chain complexes **3**–**5** clearly demonstrates the difference in their solution-state intramolecular self-association behavior. In line with the NMR and absorption studies, no obvious intramolecular self-association of **1** at room temperature is evident, whereas effective intramolecular Pt···Pt and π–π interactions do exist in **3**–**5** under the same conditions.

Solutions of **3**–**5** in acetonitrile were then subjected to variable-temperature emission experiments in the temperature range from 5 to 75 °C. The complexes were excited at the isosbestic points of the UV/Vis spectra. As the temperature was increased, a gradual decrease in intensity of the ^{3}MMLCT emission band at 830 nm was observed with a mild and concomitant growth of an emission band at about 600–650 nm. The variable-temperature emission spectra of **5** are shown in Figure 4. Although nonradiative decay of the excited molecules would become more efficient at high temperature, the major reason for the diminishment of the ^{3}MMLCT emission band is the deaggregation of the "sticky"

 © 2006 Wiley-VCH Verlag GmbH & Co. KGaA, Weinheim

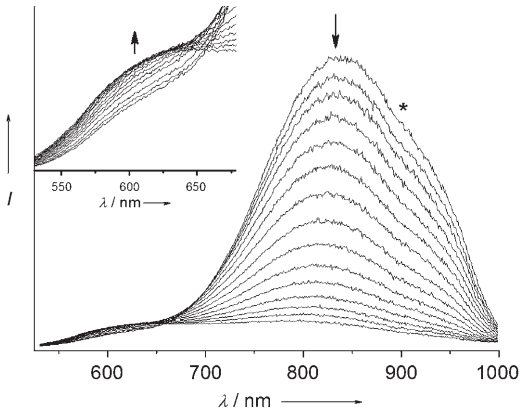

Figure 4. Corrected emission spectral changes of **5** upon an increase in temperature from 5 to 75 °C. Inset: Expansion of emission spectra in the 530–680 nm region. (λ_{ex} = 405 nm, * denotes an instrumental artifact.)

Pt(tpy) units, as the slight increase in the intensity of the ^{3}MLCT band eliminates the possible influence of the contribution from the nonradiative decay in this case.

In conclusion, we have demonstrated the first examples of dinuclear platinum(II) complexes that show a high tendency towards spontaneous solution-state intramolecular self-association by using ^{1}H NMR, UV/Vis absorption, and emission spectroscopy. The self-assembly of these systems was found to be dependent on bridge length and temperature. One may visualize such controllable aggregation and deaggregation properties in this class of molecules as synthetic organometallic analogues of DNA hairpin mimics with sticky ends. The present work demonstrates the versatility of Pt···Pt and π–π interactions in providing the driving force for molecular self-association and assembly.

Experimental Section

Dinuclear chloroplatinum(II) precursor complexes **P1**–**P5** with triflate ($CF_3SO_3^-$) as the counteranion were synthesized by a modified literature method for the synthesis of $[Pt(tpy)Cl]^+$.[7a,9] Complexes **1**–**5** were synthesized by a modification of the Cu^I-catalyzed reaction for alkynyl platinum(II) complexes.[13] The corresponding dinuclear chloroplatinum(II) precursor was dissolved in degassed *N*,*N*-dimethylformamide containing triethylamine, and 4-*n*-butylphenylacetylene and a catalytic amount of copper(I) iodide were added. The reaction mixture was stirred overnight at room temperature, after which diethyl ether was added and stirred for 10 min. The precipitate that formed was isolated by filtration and washed with diethyl ether. A saturated methanolic solution of ammonium hexafluorophosphate was added to a solution of this precipitate in methanol. The PF_6^- salt of the product complex was isolated by filtration, washed with methanol, and dried. Subsequent recrystallization of the complexes was accomplished by diffusion of diethyl ether vapor into solutions of the complexes in acetonitrile.

The characterization data for a representative complex (detailed characterization data for **P1**–**P5**, **1**–**3**, and **5** are given in the Supporting Information): **4**: Yield: 144 mg (82 %). ^{1}H NMR (500 MHz, [D$_6$]DMSO, 363 K): δ = 9.05 (d, J = 5.6 Hz, 4H, terpyridyl H), 8.39 (d, J = 8.0 Hz, 4H, terpyridyl H), 8.31 (t, J = 8.0 Hz, 4H, terpyridyl H), 8.04 (s, 4H, terpyridyl H), 7.79 (d, J = 5.6 Hz, 4H, terpyridyl H), 7.36 (d, J = 8.0 Hz, 4H, -C_6H_4-), 7.11 (t, J = 8.0 Hz, 4H, -C_6H_4-), 4.47 (t, J = 4.6 Hz, 4H, OCH_2CH_2O), 3.96 (t, J = 4.6 Hz, 4H, OCH_2CH_2O), 3.76–3.69 (m, 8H, OCH_2CH_2O), 2.63 (t, J = 7.4 Hz, 4H, -*n*Bu), 1.61 (q, J = 7.4 Hz, 4H, -*n*Bu), 1.39 (s, J = 7.4 Hz, 4H, -*n*Bu), 0.95 ppm (t, J = 7.4 Hz, 6H, -*n*Bu); IR (nujol): $\tilde{\nu}$ = 2118(w) ν(C≡C), 842(s) cm^{-1} ν(P-F); positive-ion FAB-MS: *m*/*z* 1506 $[M-PF_6]^+$; elemental analysis calcd (%) for $C_{62}H_{62}F_{12}N_6O_5P_2Pt_2$: C 45.10, H 3.78, N 5.09; found: C 45.34, H 3.54, N 4.99.

Received: March 11, 2006
Revised: July 4, 2006
Published online: August 17, 2006

Keywords: aggregation · deaggregation · luminescence · N ligands · platinum

[1] a) J. W. Schindler, R. C. Fukuda, A. W. Adamson, *J. Am. Chem. Soc.* **1982**, *104*, 3596; b) V. M. Miskowski, V. H. Houlding, C. M. Che, Y. Wang, *Inorg. Chem.* **1993**, *32*, 2518; c) H. K. Yip, H. M. Lin, Y. Wang, C. M. Che, *Inorg. Chem.* **1993**, *32*, 3402.

[2] a) D. M. Roundhill, H. B. Gray, C. M. Che, *Acc. Chem. Res.* **1989**, *22*, 55; b) V. M. Miskowski, V. H. Houlding, *Inorg. Chem.* **1989**, *28*, 1529; c) V. H. Houlding, V. M. Miskowski, *Coord. Chem. Rev.* **1991**, *111*, 145; d) M. G. Hill, J. A. Bailey, V. M. Miskowski, H. B. Gray, *Inorg. Chem.* **1996**, *35*, 4585; e) B. Ma, J. Li, P. I. Djurovich, M. Yousufuddin, R. Bau, M. E. Thompson, *J. Am. Chem. Soc.* **2005**, *127*, 28.

[3] a) K. W. Jennette, J. T. Gill, J. A. Sadownick, S. J. Lippard, *J. Am. Chem. Soc.* **1976**, *98*, 6159; b) H. K. Yip, C. M. Che, Z. Y. Zhou, T. C. W. Mak, *J. Chem. Soc. Chem. Commun.* **1992**, 1369; c) H. K. Yip, L. K. Cheng, K. K. Cheung, C. M. Che, *J. Chem. Soc. Dalton Trans.* **1993**, 2933; d) J. A. Bally, V. M. Miskowski, H. B. Gray, *Inorg. Chem.* **1993**, *32*, 369.

[4] a) V. W. W. Yam, R. P. L. Tang, K. M. C. Wong, K. K. Cheung, *Organometallics* **2001**, *20*, 4476; b) V. W. W. Yam, R. P. L. Tang, K. M. C. Wong, X. X. Lu, K. K. Cheung, N. Zhu, *Chem. Eur. J.* **2002**, *8*, 4066; c) V. W. W. Yam, K. M. C. Wong, N. Zhu, *Angew. Chem.* **2003**, *115*, 1438; *Angew. Chem. Int. Ed.* **2003**, *42*, 1400; d) K. M. C. Wong, W. S. Tang, B. W. K. Chu, N. Zhu, V. W. W. Yam, *Organometallics* **2004**, *23*, 3459.

[5] a) V. W. W. Yam, K. M. C. Wong, N. Zhu, *J. Am. Chem. Soc.* **2002**, *124*, 6506; b) C. Yu, K. M. C. Wong, K. H. Y. Chan, V. W. W. Yam, *Angew. Chem.* **2005**, *117*, 801; *Angew. Chem. Int. Ed.* **2005**, *44*, 791; c) V. W. W. Yam, K. H. Y. Chan, K. M. C. Wong, N. Zhu, *Chem. Eur. J.* **2005**, *11*, 4535.

[6] a) T. K. Aldridge, E. M. Stacy, D. R. McMillin, *Inorg. Chem.* **1994**, *33*, 722; b) J. F. Michalec, S. A. Bejune, D. R. McMillin, *Inorg. Chem.* **2000**, *39*, 2708; c) D. R. McMillin, J. J. Moore, *Coord. Chem. Rev.* **2002**, *229*, 113.

[7] a) J. A. Bailey, M. G. Hill, R. E. Marsh, V. M. Miskowski, W. P. Schaefer, H. B. Gray, *Inorg. Chem.* **1995**, *34*, 4591; b) R. Büchner, J. S. Field, R. J. Haines, C. T. Cunningham, D. R. McMillin, *Inorg. Chem.* **1997**, *36*, 3952; c) R. Büchner, C. T. Cunningham, J. S. Field, R. J. Haines, D. R. McMillin, G. C. Summerton, *J. Chem. Soc. Dalton Trans.* **1999**, 711; d) T. J. Wadas, Q. M. Wang, Y. J. Kim, C. Flaschenreim, T. N. Blanton, R. Eisenberg, *J. Am. Chem. Soc.* **2004**, *126*, 16841.

[8] a) R. S. Osborn, D. Rogers, *J. Chem. Soc. Dalton Trans.* **1974**, 1002; b) W. B. Connick, R. E. Marsh, W. P. Schaefer, H. B. Gray, *Inorg. Chem.* **1997**, *36*, 913; c) R. H. Herber, M. Croft, M. J. Coyer, B. Bilash, A. Sahiner, *Inorg. Chem.* **1994**, *33*, 2422; d) W. B. Connick, L. M. Henling, R. E. Marsh, H. B. Gray, *Inorg. Chem.* **1996**, *35*, 6261.

[9] a) G. T. Morgan, F. H. Burstall, *J. Chem. Soc.* **1934**, 1498; b) M. Howe-Grant, S. Lippard, *Inorg. Synth.* **1980**, *20*, 101.

[10] a) A. Gourdon, J. P. Launay, *Inorg. Chem.* **1998**, *37*, 5336; b) X. F. Wang, Y. Z. Shen, Y. Pan, Y. Q. Liang, *Langmuir* **2001**,

 © 2006 Wiley-VCH Verlag GmbH & Co. KGaA, Weinheim

17, 3162; c) S. H. Toma, M. Uemi, S. Nikolaou, D. M. Tomazela, M. N. Eberlin, H. E. Toma, *Inorg. Chem.* **2004**, *43*, 3521.

[11] Y. Q. Shen, S. V. Kuznetsov, A. Ansari, *J. Phys. Chem. B* **2001**, *105*, 12202.

[12] For analysis of the equilibrium absorbance measurements, a two-state transition $A(T)=\theta(T)[A_U(T)-A_L(T)]+A_L(T)$ was used in which A_U and A_L represent upper and lower baselines, and $\theta(T)$ is a van't Hoff function [Eq. (1)] with straight lines for the asymptotes.

$$\theta(T)=1/\{1+\exp[-\Delta H/R(1/T-1/T_m)]\} \qquad (1)$$

Here ΔH is the enthalpy change for the deaggregation process and is assumed to be temperature independent, T_m is the melting temperature of the molecule, and the upper and lower baselines were parameterized as straight lines with independently varying slopes.

[13] a) K. Sonogashira, S. Takahashi, N. Hagihara, *Macromolecules* **1997**, *10*, 879; b) S. Takahashi, M. Kariya, T. Yakate, K. Sonogashira and N. Hagihara, *Macromolecules* **1978**, *11*, 1063; c) V. W. W. Yam, C. H. Tao, L. Zhang, K. M. C. Wong, K. K. Cheung, *Organometallics* **2001**, *20*, 453.

 © 2006 Wiley-VCH Verlag GmbH & Co. KGaA, Weinheim

Micelles

DOI: 10.1002/anie.200601108

Thermoresponsive Micelles from Oligopeptide-Grafted Cyclotriphosphazenes**

*Yong Joo Jun, Udaya S. Toti, Hye Young Kim, Ji Young Yu, Byeongmoon Jeong, Moo Jin Jun, and Youn Soo Sohn**

Polymeric micelles have attracted much attention because of scientific interest and their high potential utility in the biomedical field as drug carriers, surfactants, and surface modifiers.[1] Amphiphilic di- or triblock copolymers consisting of both hydrophilic and hydrophobic segments in an appropriate ratio are known to form micelles by self-assembly in aqueous solution.[2] The hydrophobic blocks of the copolymer form the core of the micelle, while the hydrophilic blocks form the corona or outer shell. A variety of drugs including genes, proteins, and hydrophobic drugs can be incorporated into the hydrophobic core of the micelle. Polyethylene glycol (PEG) is most widely used as the hydrophilic block, but many low-molecular-weight hydrophobic polymers, such as poly (propylene oxide) and poly(lactic acid), are employed as a hydrophobic block.[3] Nearly all the micelle-forming polymers reported so far are amphiphilic grafted or block copolymers with a linear backbone, but to our knowledge, no micellar polymer with a cyclic backbone has been reported.

We have synthesized amphiphilic cyclotriphosphazenes grafted with equimolar amounts of oligopeptide and methoxypolyethylene glycol (MPEG), which form strong micelles by self-assembly in aqueous solution. Herein, we report the synthesis and properties of these micellar cyclic trimers.

The amphiphilic trimers were prepared by two-step nucleophilic substitution reactions according to Scheme 1. We have shown in our previous work that nucleophilic substitution of hexachlorocyclotriphosphazene (**I**) with the sodium salt of MPEG at low temperature ($T < -60\,^{\circ}C$) gives rise to the half-substituted intermediate (**II**) with *cis* nongeminal conformation as a major product.[4] Further substitution of the intermediate with an oligopeptide ethyl ester (H_2NR') produced a final amphiphilic product (**III**), which was purified twice by precipitation at the lower critical solution temperature (LCST) in aqueous solution. The LCST is the temperature at which the polymer solution undergoes phase transition from a soluble to an insoluble state. All final products showed a clean and sharp singlet peak of ^{31}P NMR resonance at $\delta = 22$ ppm, thus confirming the *cis* nongeminal conformation of the side groups of the trimers. Three hydrophobic oligopeptides are oriented in one direction opposite to that of three hydrophilic MPEG groups with respect to the phosphazene ring (see Scheme 1). The trimeric products were obtained as a yellow viscoelastic liquid in 30–60% yields. Various trimeric derivatives with a different hydrophobic-to-hydrophilic balance were prepared using different combinations of the hydrophilic and hydrophobic groups; the products are listed in Table 1.

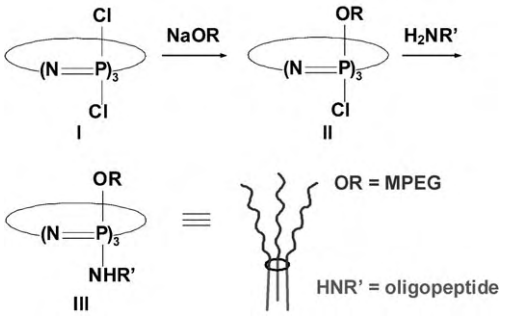

Scheme 1. Synthetic route to micellar cyclotriphosphazenes.

[*] Dr. U. S. Toti, H. Y. Kim, J. Y. Yu, B. Jeong, Prof. Y. S. Sohn
Department of Chemistry, Division of Nano Science
Ewha Womans University
Daehyun-Dong 11-1, Seodaemun-Ku, Seoul 120-750 (Korea)
Fax: (+82) 2-3277-3419
E-mail: yssohn@ewha.ac.kr
Y. J. Jun, Prof. M. J. Jun
Department of Chemistry
Yonsei University
Shinchon 134, Seoul 120-749 (Korea)

[**] This work was supported by the SRC program of the Korea Science and Engineering Foundation through the Center for Intelligent Nano-Bio Materials at Ewha Womans University (Grant R11-2005-008-01002-0) and by a Korean Research Foundation Grant (KRF-2004-005-C00090).

Supporting information for this article is available on the WWW under http://www.angewandte.org or from the author.

 © 2006 Wiley-VCH Verlag GmbH & Co. KGaA, Weinheim

Table 1: Characteristic properties of cyclic trimers.

Trimer	Compound	LCST [°C][a]	DLS [nm][b]	PDI[c]
1	$[NP(MTEG)GlyPheGlyEt)]_3$	34.0	2.2	1.0
2	$[NP(MPEG350)(GlyPheLeuEt)]_3$	37.0	12.3[d]	0.31
3	$[NP(MPEG350)(GlyPheLeuAspEt_2)]_3$	27.0	13.9	0.25
4	$[NP(MPEG350)(GlyPheLeuGluEt_2)]_3$	24.0	13.3	0.44
5	$[NP(MPEG550)(GlyPheLeuAspEt_2)]_3$	60.0	3.7 (94%)[e] 13.8 (6%)	0.21

[a] The lower critical solution temperature in pure water. [b] Dynamic light scattering measurements at 25 °C of 0.5 % aqueous solutions filtered with a 0.45-μm syringe filter. [c] The polydispersity index represents S/d_h, where S is the standard error in hydrodynamic diameter d_h. [d] Measured at 30 °C. [e] 94 % monomer (see text for details).

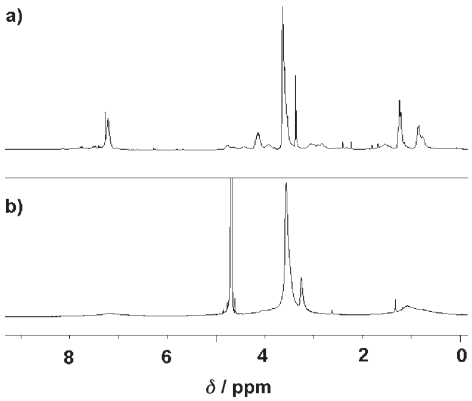

Figure 1. ^1H NMR spectra of trimer **3** in a) $CDCl_3$ and b) D_2O.

The trimers were fully characterized by multinuclear (^1H,^{31}P) NMR spectroscopy, elemental analysis, and MALDI mass spectrometry.[5a] In particular, the MALDI mass spectrum of monodisperse trimer **1** clearly shows the major parent peak at m/z 1697.7 (**1**·Na^+), which confirms the exact trimer composition. All the trimers are immediately soluble and show thermoresponsive properties with an LCST in water. Especially, except for trimer **5**, all trimers exhibit an LCST below body temperature, which is very useful for biomedical applications. The local tolerance tests for trimer **3** showed excellent biocompatibility, the results of which will be published separately. It is known that the LCST of amphiphilic copolymers is determined by their hydrophobic-to-hydrophilic balance.[6] Comparison of the LCSTs of trimers **2**–**4** that bear the same hydrophilic PEG350 indicates that their LCSTs decrease as the chain length of the oligopeptides increases.

Among the trimers listed in Table 1, trimer **1** bearing the shortest tetraethylene glycol and tripeptide side groups demonstrated remarkably different behaviors from those of the other trimers in aqueous solution. Trimer **1** showed exactly the same proton NMR spectral pattern with good resolution in both $CDCl_3$ and D_2O at 20 °C, which indicates that there is not considerable molecular aggregation in aqueous solution. However, trimer **3** showed broadened resonances of all the oligopeptide protons in aqueous solution while there was no significant change in the MPEG proton peaks at $\delta = 3.5$–3.7 ppm (see Figure 1), which is strong evidence for micelle formation in aqueous solution.

Therefore, dynamic light scattering (DLS) measurements were performed for all the trimers with a Melvern Zetasizer Nano ZS instrument, and their mean particle diameters are listed in Table 1 along with their polydispersity index (PDI) values. Interestingly, trimer **1** bearing the tetraethylene glycol with the least hydrophilicity ($\log P = -0.92$; $P = [\text{solute}]_{n\text{-octanol}}/[\text{solute}]_{\text{water}}$), calculated by a reported method,[7] and the least hydrophobic tripeptide GlyPheGlyEt ($\log P = -0.63$) does not form a micelle, but exists as a monomer in solution, as its mean diameter of 2.2 nm is almost equivalent to its unimolecular size. On the other hand, trimer **2** bearing the more hydrophilic PEG350 ($\log P = -1.42$) and a more hydrophobic tripeptide GlyPheLeuEt ($\log P = 1.11$) clearly indicates micelle formation relative to trimer **1**, with a mean diameter of 12.3 nm like that of trimers **3** and **4**, which bear larger hydrophobic tetrapeptides. The size distributions of trimers **1** and **3** (see Figure 2) are relatively narrow. Trimer **5** bearing the most hydrophilic PEG550 ($\log P = -2.24$) and the same hydrophobic tetrapeptide as trimer **3** showed a bimodal size distribution with the monomer in the majority (94 %), probably because of its high hydrophilicity. It is known that if the hydrophilicity is too high compared with the hydrophobicity in a diblock copolymer, then the copolymer exists as a monomer in water.[3a]

To examine the temperature-dependent behavior of the present trimers, the sizes of representative trimers **1**–**3** were measured as their solution temperature was increased from 20 °C to their LCST. Trimer **1** showed a constant unimolecular size of 2.2 nm up to 28 °C, near its LCST (34 °C), but beyond this temperature it started to associate to microparticles. The micellar structure of trimer **3** remained at constant size up to its LCST (27 °C), but the micelles rapidly aggregated to larger particles to precipitate beyond its LCST. Most interesting is

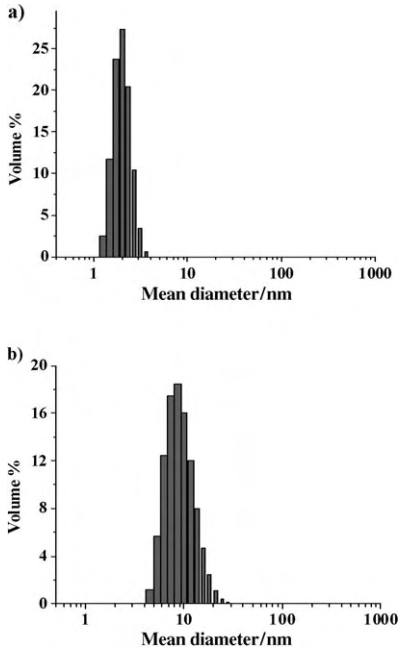

Figure 2. Size distribution by volume of trimers a) **1** and b) **3**.

 © 2006 Wiley-VCH Verlag GmbH & Co. KGaA, Weinheim

the finding that trimer **2** exhibited not only an LCST at 37 °C but also an upper critical solution temperature (UCST) at 27 °C in aqueous solution. As shown in Figure 3, the micellar structure of trimer **2** is maintained between its UCST and LCST. This is the reason why the DLS measurement for trimer **2** was performed at 30 °C. The particle size of trimer **2** below its UCST was measured as approximately 150–200 nm. All other trimers showed only an LCST without a UCST.

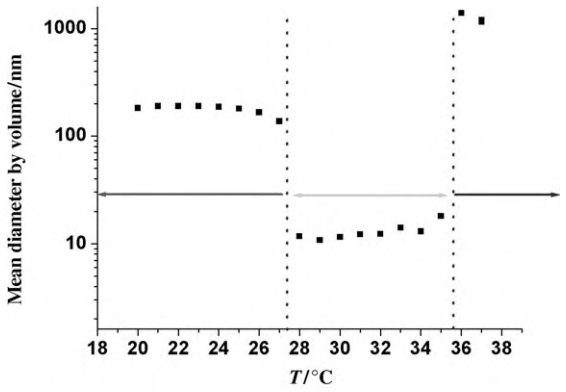

Figure 3. Temperature-dependent sizes of trimer **2**.

The LCST is frequently observed for amphiphilic copolymers, but the UCST is rarely observed. Furthermore, only a few copolymers were reported to show both an LCST and a UCST in aqueous solution.[8] The phase transition from a soluble to an insoluble state at the LCST is known to be a consequence of weakening of the hydrogen bonding between the hydrophilic part of the copolymer and the solvent water molecules.[9] The phase transition at the UCST is known to be associated with unfavorable intermolecular interactions between the polymer and solvent molecules in the low-temperature region.[10] Therefore, it seems that the UCST of trimer **2** is related to the remarkably high hydrophobicity of its grafted oligopeptide, GlyPheLeuEt ($\log P = 1.11$), relative to the other oligopeptides, GlyPheLeuAspEt$_2$ ($\log P = 0.32$) and GlyPheLeuGluEt$_2$ ($\log P = 0.57$). Such a variety of thermoresponsive properties of the trimers depending on their hydrophobic-to-hydrophilic balance can be ascribed to their unique molecular structure. The *cis* nongeminal conformation of the hydrophilic and hydrophobic side groups, in particular, may enhance effectively the intermolecular hydrophobic interaction to form micelles by self-assembly.

The morphology of the present trimeric micelles is not very clear, but from the ^{1}H NMR spectra (Figure 1), which show the near-disappearance of the oligopeptide protons of the trimer in aqueous solution, the larger hydrodynamic volume of MPEG relative to that of the oligopeptides, and the narrow size distribution of micelles we propose a spherical form of self-assembled micelles (see Figure 4). The core of the micelle seems to contain some solvent water trapped during the process of micelle formation,[2a] which is not surprising because the tetrapeptides ($\log P = 2.1$–3.7) employed are still considerably water soluble, although they are very hydrophobic compared with MPEGs.

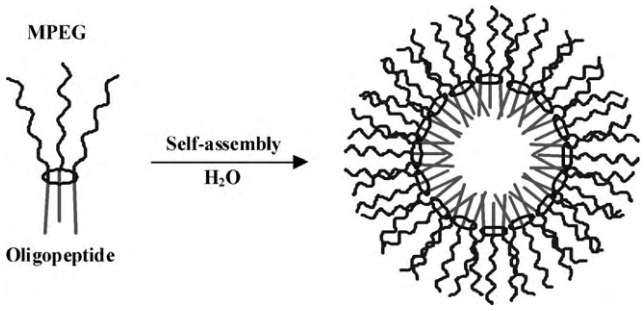

Figure 4. Micelle formation by self-assembly from trimers.

The stability of polymeric micelles is very important for biomedical applications. In particular, the critical micelle concentration (CMC) of polymers is an important measure for applications in injectable drug delivery because the micelles should remain undestroyed even after dilution by injection. Therefore, various known methods were attempted to measure the CMC of the present trimers. However, optical methods could not be used for our trimers because they showed strong absorption in the UV/Vis region and also fluorescence in the UV region. We employed the surface tension method to measure the CMC of trimer **3**,[11] which gave rise to a value of 0.11 mg L^{-1}.[5b] This value, which was further confirmed by the DLS method, is very low relative to those of known linear block copolymers, for example, 1.2 mg L^{-1} for PCL$_{21}$-*b*-PEO$_{44}$[2a] (PCL = polycaprolactone, PEO = poly(ethylene oxide)). Such a high thermodynamic stability of the trimeric micelles seems to be a result of the unique molecular structure of our trimers, as mentioned above.

In summary, new oligopeptide-grafted cyclotriphosphazenes were synthesized that show unique thermoresponsive properties depending on the hydrophobic-to-hydrophilic balance of the side groups. Strong micellar trimers could be prepared by designing appropriate hydrophobic oligopeptides that match the hydrophilicity of PEG350.

Experimental Section

All the synthetic reactions were performed under an argon atmosphere with thoroughly dried chemicals and solvents. ^{1}H and ^{31}P NMR spectra were measured with a Varian Unity INOVA-500 spectrometer operating at 500 MHz and using tetramethylsilane (TMS) and phosphoric acid, respectively, as external standards. The LCST at which trimers in aqueous solution (0.5 wt %) undergo phase transition from sol to precipitate was measured by UV/Vis spectroscopy. The MALDI-TOF mass spectrum of trimer **1** was measured with a Voyager-DE STR spectrometer. DLS measurements for the trimers in aqueous solution (0.1 %) were performed with a Melvern Zetasizer Nano ZS instrument. The CMC was measured by the Wilhelmy plate method using a Kruss K-12 surface tension apparatus equipped with a processor to acquire the data automatically.

1: Methoxytetraethylene glycol (MTEG) with a molecular weight of 208.25 (2.16 g, 10.3 mmol) was treated with sodium metal (0.24 g, 10.4 mmol) in dried THF for 24 h under an argon atmosphere to obtain the sodium salt of MTEG. The unreacted sodium was removed by filtration, the filtrate was slowly added over 30 min to a solution of hexachlorocyclotriphosphazene (1.00 g, 2.88 mmol) in dried THF in a separate reaction vessel cooled in a dry ice–acetone bath (−78 °C),

 © 2006 Wiley-VCH Verlag GmbH & Co. KGaA, Weinheim

and the reaction solution was stirred for 30 min. After the dry ice–acetone bath was removed, the reaction was allowed to continue for a further 8 h at room temperature. A solution (100 mL) of triethylamine (2.61 g, 25.80 mmol) and a tripeptide (GlyPheGly(Et); 3.98 g, 12.9 mmol) in THF was added, and the reaction mixture was stirred at 50 °C for 12 h. The mixture was filtered to remove the solid by-products (NEt_3·HCl and NaCl) and the filtrate was concentrated under reduced pressure. The concentrate was dissolved in THF and an excess amount of diethyl ether or hexane was added to induce precipitation. This process was repeated twice. The resultant product was dissolved in a small amount of distilled water (20 mL) for dialysis for 24 h using the dialysis membrane (MWCO: 1000) in distilled water and then freeze dried to obtain the trimer **1**, $[NP(MTEG)(GlyPheGlyEt)]_3$. The product was further purified by reprecipitation from aqueous solution (10%) at its LCST. Other trimeric derivatives were prepared by the same procedure using different PEGs and oligopeptides. Yield: 31.5%; elemental analysis (%) calcd for $C_{72}H_{117}N_{12}O_{27}P_3 \cdot 3H_2O$: C 50.00, H 7.17, N 9.72; found: C 50.33, H 7.10, N 9.86; ^{1}H NMR (250 MHz, D_2O, 25 °C): $\delta = 1.18$ (t, 3H; Gly-OCH$_2$CH_3), 3.05 (m, 2H; Phe-CH_2), 3.27 (s; MTEG-OCH_3), 3.4–3.6 (b, 16H; TetEG-OCH_2CH_2), 3.7–3.8 (d, 2H; Gly-CH_2), 4.05 (q, 2H; Gly-CH_2CH$_3$), 4.69 (m, 1H; Phe-CH), 7.14 ppm (m, 5H; Phe-arom); ^{31}P NMR (500 MHz, D_2O, 25 °C): $\delta = 22.4$ ppm; LCST: 34 °C. Characterization data for trimers **2**–**5** are also available.[5c]

Received: March 21, 2006
Revised: June 30, 2006
Published online: August 14, 2006

Keywords: amphiphiles · drug delivery · micelles · oligopeptides · phosphazenes

[1] a) K. Yu, A. Eisenberg, *Macromolecules* **1996**, *29*, 6359–6361; b) K. Kataoka, A. Harada, Y. Nagasaki, *Adv. Drug Delivery Rev.* **2001**, *47*, 113–131; c) H. Otsuka, Y. Nagasaki, K. Kataoka, *Adv. Drug Delivery Rev.* **2003**, *55*, 403–419; d) H. R. Allcock, E. S. Powell, Y. Chang, *Macromolecules* **2004**, *37*, 7163–7167.
[2] a) C. Allen, D. Maysinger, A. Eisenberg, *Colloids Surf. B* **1999**, *16*, 3–27; b) A. Rösler, G. W. M. Vandermeulen, H.-A. Klok, *Adv. Drug Delivery Rev.* **2001**, *53*, 95–108; c) J. X. Zhang, L. Y. Qiu, K. J. Zhu, Y. Jin, *Macromol. Rapid Commun.* **2004**, *25*, 1563–1567.
[3] a) V. P. Torchilin, *J. Controlled Release* **2001**, 137–172; b) A. Lavasanifar, J. Samuel, G. S. Kwon, *Adv. Drug Delivery Rev.* **2002**, *54*, 169–190.
[4] S. B. Lee, S.-C. Song, J.-I. Jin, Y. S. Sohn, *J. Am. Chem. Soc.* **2000**, *122*, 8315–8316.
[5] Supporting Information: a) MALDI mass spectrum of trimer **1**; b) the result of CMC measurement of trimer **3**; c) characterization data for trimers **2**–**5**.
[6] Y. S. Sohn, J. I. Kim, R. Song, B. Jeong, *Polymer* **2004**, *45*, 3081–3084.
[7] V. N. Viswanadhan, A. K. Ghose, G. R. Revankar, R. K. Robins, *J. Chem. Inf. Comput. Sci.* **1989**, *29*, 163–172.
[8] a) J. Virtanen, M. Arotcarena, B. Heise, S. Ishaya, A. Laschewsky, H. Tenhu, *Langmuir* **2002**, *18*, 5360–5365; b) G. Bokias, G. Staikos, I. Iliopoulos, *Polymer* **2000**, *41*, 7399–7405.
[9] S.-C. Song, S. B. Lee, J.-I. Jin, Y. S. Sohn, *Macromolecules* **1999**, *32*, 2188–2193.
[10] F. Wang, S. Saeki, T. Yamaguchi, *Polymer* **1999**, *40*, 2779–2785.
[11] P. Taboada, D. Attwood, J. M. Ruso, M. García, F. Sarmiento, V. Mosqueral, *J. Colloid Interface Sci.* **1999**, *220*, 288–292.

 © 2006 Wiley-VCH Verlag GmbH & Co. KGaA, Weinheim

Prebiotic Chemistry

DOI: 10.1002/anie.200601267

Direct Assembly of Nucleoside Precursors from Two- and Three-Carbon Units**

*Carole Anastasi, Michael A. Crowe, Matthew W. Powner, and John D. Sutherland**

The efficient synthesis of ribose, the sugar component of RNA, has long been a major goal of research aimed at investigating the origin of life. In strongly alkaline solution, glycolaldehyde and formaldehyde participate in the formose reaction—a series of aldol reactions and rearrangements—giving a range of sugars, including tetroses, pentoses, and hexoses.[1] However, aldose–ketose equilibration[2] and lack of stereocontrol in the formose reaction result in the yield of ribose being extremely low (< 1 %).[3] In an elegant series of experiments, Eschenmoser and co-workers showed that the alkaline reaction of glycolaldehyde phosphate and formaldehyde produced a much narrower range of products, with ribose-2,4-diphosphate predominating (10–20 %).[4] However, the high pH value required for this process in solution and the phosphorylation pattern of the products do not support its intermediacy in the production of RNA, since RNA is base-labile and contains 5′→3′ phosphate diester linkages. More recently, amino acids have been shown to catalyze the synthesis of sugars in water,[5] with Darbre and co-workers showing that the zinc–proline complex catalyzes the aldolization of glycolaldehyde and glyceraldehyde to give ribose (19 %),[5c] but as a component of a complex mixture containing tetroses, the other pentoses, and aldo- and ketohexoses.

The instability of ribose ($t_{1/2} < 3$ h, pH ≈ 10, 55 °C) is another concern,[6,7] and one which prompted Benner and co-workers to consider complexation of the sugar with borate as a means of achieving stabilization.[8] It was shown that pentoses could be synthesized from glycolaldehyde and glyceraldehyde in the presence of borate, and that, once formed, the pentoses were significantly stabilized by complexation. However, this reaction again requires a high pH value and displays no selectivity for ribose over the other pentoses. Furthermore, although the complexation with borate is stabilizing, it is also likely to slow, or prevent,

[*] Dr. C. Anastasi, M. A. Crowe, M. W. Powner, Prof. Dr. J. D. Sutherland
School of Chemistry
The University of Manchester
Oxford Road, Manchester M13 9PL (UK)
Fax: (+44) 161-275-4939
E-mail: john.sutherland@manchester.ac.uk

[**] This work was carried out as part of the EU COST action D27 "Prebiotic Chemistry and Early Evolution", and was funded by the Engineering and Physical Sciences Research Council through the provision of a postdoctoral fellowship to C.A. and studentships to M.W.P. and M.A.C. We thank Dr. A. Parkes and Dr. M. Helliwell for preliminary experiments.

Supporting information for this article is available on the WWW under http://www.angewandte.org or from the author.

WILEY InterScience DISCOVER SOMETHING GREAT
© 2006 Wiley-VCH Verlag GmbH & Co. KGaA, Weinheim

elaboration of the ribose into ribonucleosides by addition of a nucleobase. Direct addition of a nucleobase to the free sugar is extremely inefficient with purines and is not possible with pyrimidines, but a stepwise assembly of pyrimidine nucleobases on a sugar scaffold has been demonstrated.[9–11] An ideal situation would therefore be one in which ribose could be stabilized as a derivative that could also function as an intermediate en route to a ribonucleoside, and in this regard the reaction of ribose with cyanamide has been investigated. Ribose, the other pentose sugars, and the tetroses all form aminooxazoline derivatives with cyanamide (Scheme 1 and

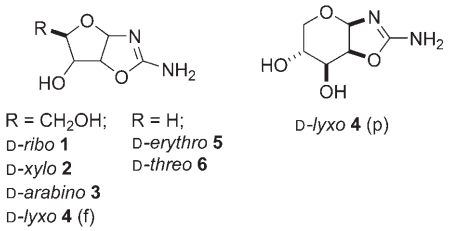

Scheme 1. Tetrose and pentose aminooxazolines. The D-tetroses, D-ribose, D-arabinose, and D-xylose all form furanose aminooxazolines.[7,9,12,13] D-Lyxose aminooxazoline displays anomalous behavior and exists in equilibrium between furanose (f) and pyranose (p) forms (**4**(p)/**4**(f), ca. 5:1).[13]

see the Supporting Information).[9,12,13] Springsteen and Joyce have shown that the D-ribose aminooxazoline derivative **1** degrades 70-fold more slowly than the free sugar ($t_{1/2}>$ 1 week, pH ≈ 10, 55 °C),[7] and therefore it seems reasonable to assume that **2**–**6** will also be more stable than their parent sugars. Additionally, these aminooxazolines react with cyanoacetylene to give cytidine nucleosides;[9,11–13] for example, **1** gives α-D-cytidine **7** (Scheme 2). However, RNA is composed of β-D-ribonucleotides, so stereochemical inversion at the anomeric center of **7** is subsequently required. Photoanomerization of **7** to β-D-cytidine **8** is a relatively inefficient reaction,[9] so we explored an alternative pathway involving **9**, the 3′-phosphate derivative of the arabinose aminooxazoline

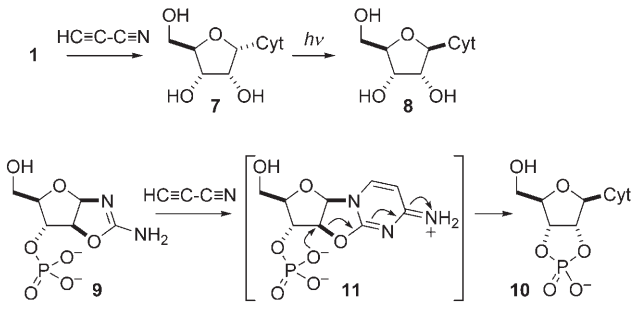

Scheme 2. Conversion of aminooxazolines into cytidine nucleosides. Reaction of **1** with cyanoacetylene, followed by irradiation, gives β-D-cytidine **8**. Reaction of **9** (the 3′-phosphate of **3**) with cyanoacetylene gives the activated ribonucleotide **10** by intramolecular nucleophilic substitution of the intermediate **11**. These conversions establish **1** and **3** as being more advanced RNA precursors than free ribose. Cyt = cytosine.

3.[11] Reaction of **9** with cyanoacetylene gave the activated ribonucleotide **10** via the anhydronucleotide **11** (Scheme 2).[10] Their stability and subsequent conversion into nucleosides, therefore, suggest a central role for the aminooxazolines **1** and **3** in the prebiotic synthesis of RNA. Since **1** and **3** have only ever been synthesized from their parent pentose sugars, it has been necessary to invoke a somewhat unlikely assembly sequence in which the pentoses are exposed to cyanamide after their generation, but before their degradation.[7,14] To get round this problem, we wondered if it might be possible to bypass the free pentoses and assemble **1** and **3** directly from C_2 and C_3 units. It is known that reaction of cyanamide with glycolaldehyde gives 2-aminooxazole **12**,[16] and we recognized that if this compound contained a sufficiently nucleophilic C atom to react with an α-hydroxyaldehyde[17] the resultant intermediate might cyclize to an aminooxazoline (Scheme 3). Accordingly, we

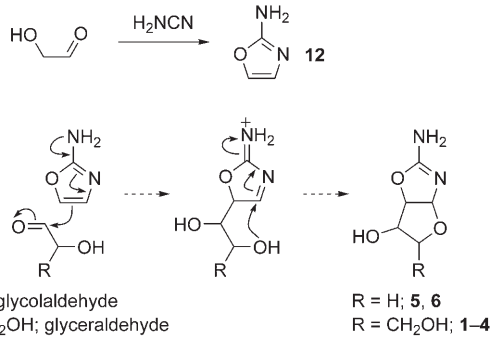

Scheme 3. Synthesis of 2-aminooxazole **12** from prebiotic starting materials and the potential involvement of **12** in tetrose and pentose aminooxazoline formation.

investigated the reaction of **12** with α-hydroxyaldehydes, deciding, for the sake of analytical simplicity, to first study the potential $C_2 + C_2$ assembly of **5** and/or **6**. A neutral, aqueous solution of **12** and glycolaldehyde in a 1:1 stoichiometry was incubated at 40 °C for 12 h before being lyophilized. The resulting residue was dissolved in D_2O and analyzed by ^{1}H NMR spectroscopy (500 MHz, see the Supporting Information). This showed conversion of the starting materials into a mixture of *rac*-**5** and *rac*-**6** in approximately 90 % yield (*rac*-**5**/*rac*-**6** 46:43). The reaction was extremely clean and the high yield of C_4 products, uncontaminated by C_6 products, suggests that glycolaldehyde homoaldolization and subsequent addition of **12** to the resultant free tetroses do not occur. We next investigated the reaction of **12** with *rac*-glyceraldehyde hoping to uncover an efficient $C_2 + C_3$ route to *rac*-**1** and/or *rac*-**3**. On the basis of the reaction of **12** and glycolaldehyde, we also expected to see a slight selectivity for the *erythro* products in the reaction with glyceraldehyde, but it was not clear whether there would be any facial selectivity in the glyceraldehyde component. Under the same mild conditions, the reaction again proceeded extremely cleanly, with the products *rac*-**1** to *rac*-**4** obtained in approximately 95 % overall yield, as determined by ^{1}H NMR analysis, with *rac*-**1** and *rac*-**3** predominant (*rac*-**1**/*rac*-**3**/*rac*-**4**/*rac*-**2** 44:30:13:8)

 © 2006 Wiley-VCH Verlag GmbH & Co. KGaA, Weinheim

(Figure 1 and see the Supporting Information).[19] The high yield of the *ribo* and *arabino* stereoisomers is remarkable given the outcome of previous $C_2 + C_3$ aldolization routes to pentoses (see the Supporting Information). We think that the stereochemical preference for *rac*-**1** and *rac*-**3** is due to control of facial selectivity of the *rac*-glyceraldehyde component through formation of a hydrogen-bonded chelate, along with the obligatory *Z* geometry and low facial selectivity of the nucleophilic C=C bond of **12** (see the Supporting Information).

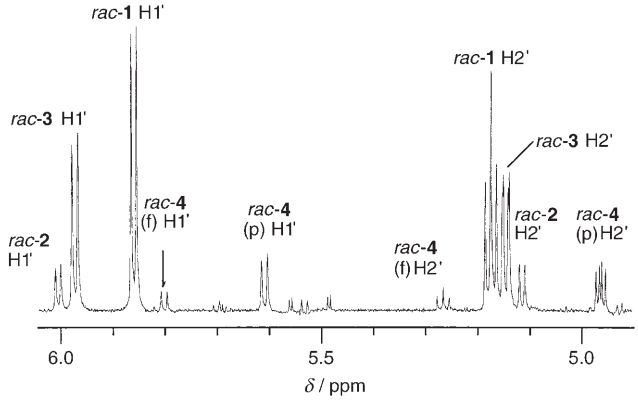

Figure 1. Stereoselectivity in the reaction of **12** with *rac*-glyceraldehyde. Partial ^{1}H NMR spectrum (500 MHz, D_2O) of the crude products from the reaction of **12** with *rac*-glyceraldehyde showing the predominance of *rac*-**1** and *rac*-**3**.

It was noted in their initial synthesis that compound **3** is more soluble than **1** in water ,[9] and it was found that **1** is the least soluble of all the pentose aminooxazolines **1**–**4**, thus permitting its isolation from mixtures by direct crystallization.[7] Since *rac*-**1** and *rac*-**3** are both produced in high yield in our reaction, and since it is not clear which is the more important ribonucleoside precursor, we sought a means of separating them that is prebiotically plausible. We realized that crystallization of *rac*-**1** from the crude products of the reaction of **12** and *rac*-glyceraldehyde would not only furnish a pure sample of *rac*-**1**, but would also change the composition of the supernatant such that *rac*-**3** might now be the predominant solute. To test this idea, we carried out a reaction between **12** and *rac*-glyceraldehyde using the same 1:1 stoichiometry as before, but at higher concentrations. After incubation of the reaction at 40 °C for 12 h, it was cooled to 4 °C whereupon crystals formed. The crystals were separated from the supernatant and both were examined by ^{1}H NMR spectroscopy. As expected, the crystals proved to be pure *rac*-**1**, and from weighing these crystals, it was determined that approximately half the total amount of *rac*-**1** expected from the reaction had crystallized. Thus, the amount of *rac*-**1** in the supernatant was correspondingly reduced and the major product in the supernatant was now *rac*-**3** (*rac*-**3**/*rac*-**1**/*rac*-**4**/*rac*-**2** 28:25:11:9). In this way, starting from a solution containing only **12** and *rac*-glyceraldehyde, *rac*-**1** can be produced in pure form as a solid, and *rac*-**3** as the predominant species in solution, simply by the warming and cooling that might have occurred during a day/night cycle on early Earth.

Ideally, crystalline enantiopure **1**, rather than *rac*-**1**, should be produced by this approach, and on the face of it, this would require the starting glyceraldehyde to be enantiopure. However, the incomplete crystallization of *rac*-**1** from solution suggested that it might be possible to obtain enantiopure **1** from scalemic (sca-) glyceraldehyde if enantiopure and racemic **1** had different solubilities. The space group of both the enantiopure and racemic **1** is $P2_12_12_1$, and the racemic material has been shown to form enantiomorphously twinned crystals.[7,12] Hexahelicene crystals belong to the same space group and racemic (and near-racemic) material also forms enantiomorphously twinned crystals, but above a threshold *ee* value, enantiopure crystals may be formed.[20] We considered that **1** might show similar behavior, in which case the formation of crystalline enantiopure **1** from sca-glyceraldehyde might be possible. To test this supposition, we prepared solutions of D-, L- and sca-**1** with a range of *ee* values, and allowed partial crystallization to take place. Crystals from each sample were then dissolved in a phosphate buffer at pH 4.5, and the optical rotation of the resultant solutions determined. To our delight, enantiopure **1** crystallizes from solutions of *rac*-**1** with $\geq 60\,\%$ *ee* (Figure 2). We

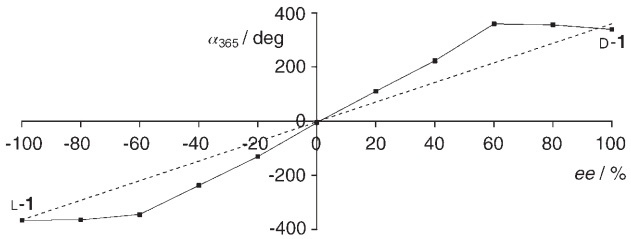

Figure 2. Asymmetric amplification in the crystallization of **1** from solutions of scalemic material. Crystals obtained from solutions of **1** with varying *ee* values (abscissa) were re-dissolved in a pH 4.5 buffer, and optical rotations (α) were measured (ordinate). The dotted line indicates the rotation that would have been expected if the crystals had the same *ee* value as the starting solutions.

then carried out a reaction between 2-aminooxazole **12** and D-glyceraldehyde with 60 % *ee* and obtained crystals of optically pure D-**1**. This amplification of optical asymmetry during the formation of a nucleoside precursor has potential relevance to the origin of biomolecular homochirality.

Since **12** is also formed from glycolaldehyde and cyanamide under mild conditions, we are now investigating the chemistry of glycolaldehyde, glyceraldehyde, and cyanamide mixtures with a view to establishing conditions for the direct synthesis of *rac*-**1** to *rac*-**6**. We are also investigating the stereochemical consequences of carrying out reactions of **12** with *rac*-glyceraldehyde in the presence of chiral additives.

Received: March 31, 2006
Revised: May 31, 2006
Published online: August 17, 2006

 © 2006 Wiley-VCH Verlag GmbH & Co. KGaA, Weinheim

Keywords: carbohydrates · nucleobases · nucleosides · prebiotic chemistry · ribose

[1] T. Mizuno, A. H. Weiss, *Adv. Carbohydr. Chem. Biochem.* **1974**, *29*, 173.
[2] J. C. Speck, Jr., *Adv. Carbohydr. Chem. Biochem.* **1958**, *13*, 63.
[3] R. Shapiro, *Origins Life Evol. Biospheres* **1988**, *18*, 71.
[4] D. Müller, S. Pitsch, A. Kittaka, E. Wagner, C. E. Wintner, A. Eschenmoser, *Helv. Chim. Acta* **1990**, *73*, 1410.
[5] a) S. Pizzarello, A. L. Weber, *Science* **2004**, *303*, 1151; b) A. Córdova, I. Ibrahem, J. Casas, H. Sundén, M. Engqvist, E. Reyes, *Chem. Eur. J.* **2005**, *11*, 4772; c) J. Kofoed, J.-L. Reymond, T. Darbre, *Org. Biomol. Chem.* **2005**, *3*, 1850.
[6] R. Larralde, M. P. Robertson, S. L. Miller, *Proc. Natl. Acad. Sci. USA* **1995**, *92*, 8158.
[7] G. Springsteen, G. F. Joyce, *J. Am. Chem. Soc.* **2004**, *126*, 9578.
[8] A. Ricardo, M. A. Carrigan, A. N. Olcott, S. A. Benner, *Science* **2004**, *303*, 196.
[9] R. A. Sanchez, L. E. Orgel, *J. Mol. Biol.* **1970**, *47*, 531.
[10] C. M. Tapiero, J. Nagyvary, *Nature* **1971**, *231*, 42.
[11] A.-A. Ingar, R. W. A. Luke, B. R. Hayter, J. D. Sutherland, *ChemBioChem* **2003**, *4*, 504.
[12] V. Borsenberger, M. A. Crowe, J. Lehbauer, J. Raftery, M. Helliwell, K. Bhutia, T. Cox, J. D. Sutherland, *Chem. Biodiversity* **2004**, *1*, 203.
[13] N. Saewan, M. A. Crowe, M. Helliwell, J. Raftery, K. Chantrapromma, J. D. Sutherland, *Chem. Biodiversity* **2005**, *2*, 66.
[14] The temporal or spatial separation of the oxygenous chemistry (required for sugar synthesis) from the nitrogenous chemistry (required for nucleobase assembly) has previously been assumed, because of the "drastically enhanced chemical complications" expected for a scenario without that separation.[15]
[15] K.-U. Schöning, P. Scholz, S. Guntha, X. Wu, R. Krishnamurthy, A. Eschenmoser, *Science* **2000**, *290*, 1347.
[16] A. F. Cockerill, A. Deacon, R. G. Harrison, D. J. Osborne, D. M. Prime, W. J. Ross, A. Todd, J. P. Verge, *Synthesis* **1976**, 591.
[17] By way of partial precedent, 2-amino-4-methyloxazole has been shown to react as a C-based nucleophile with 4-methoxybenzaldehyde in hot toluene.[18] However, in this case the intermediate lacks a suitably positioned hydroxy group and so cannot cyclize to an aminooxazoline. Instead, the intermediate re-aromatizes giving 2-amino-5-[1-hydroxy-1-(4-methoxyphenyl)methyl]-4-methyloxazole.
[18] H. R. Khan, G. Crank, *Tetrahedron Lett.* **1987**, *28*, 3381.
[19] The identity of the products was confirmed by spiking with authentic samples of **1**–**4** (for example, see the Supporting Information).
[20] B. S. Green, M. Knossow, *Science* **1981**, *214*, 795.

 © 2006 Wiley-VCH Verlag GmbH & Co. KGaA, Weinheim

Thioglycoside Hydrolysis

DOI: 10.1002/anie.200601421

Family 4 Glycosidases Carry Out Efficient Hydrolysis of Thioglycosides by an α,β-Elimination Mechanism**

*Vivian L. Y. Yip and Stephen G. Withers**

Considerable efforts have been extended towards the development of glycosidase inhibitors, both as stable substrate analogues for structural and mechanistic studies and for potential therapeutic and industrial applications.[1,2] Amongst those developed, thioglycosides, in which the glycosidic oxygen has been replaced by a sulfur atom, have proved to be stable analogues of the ground-state substrate and have been employed in a number of insightful structural studies.[3,4][*] Glycosidases are known to effect hydrolysis by acid/base-catalyzed mechanisms involving oxocarbenium-ion-like transition states.[5–7] Consequently, the resistance of the thioglycosidic bond to cleavage has been ascribed to the lower proton affinity of sulfur over that of oxygen, resulting in inefficient general acid catalysis to the departing aglycone.[8–10]

[*] V. L. Y. Yip, Prof. S. G. Withers
Department of Chemistry
University of British Columbia
2036 Main Mall, Vancouver, BC V6T 1Z1 (Canada)
Fax: (+1) 604-822-8869
E-mail: withers@chem.ubc.ca

[**] We thank Dr. Gideon Davies for providing the BglT plasmid, Dr. John Thompson for providing the kinase BglK, Dr. J. Müllegger for providing the thioglycoligase Abg E170Q, and Dr. Hongming Chen for providing *p*-nitrophenyl 4-deoxy-4-thio-D-glucoside. We also thank the Natural Sciences and Engineering Research Council of Canada for financial support. V.L.Y.Y. is funded by graduate fellowships from the Natural Sciences and Engineering Research Council of Canada and the Michael Smith Foundation for Health Research.

Supporting information for this article is available on the WWW under http://www.angewandte.org or from the author.

[*] The one exception is a specialized group of *S*-glycosidases of plant origin, called the myrosinases (E.C. 3.2.3.1), which specifically hydrolyze glucosinolate substrates, anionic 1-thio-β-glucosides. By sequence aligment, the myrosinases are associated with the family 1 glycosidases, which catalyze the hydrolysis of β-*O*-glycosides with retention of the substrate anomeric configuration. While the majority of family 1 glycosidases contain a conserved glutamate as the catalytic nucleophile, in the myrosinases the glutamic acid that serves as the acid/base catalyst is replaced by a glutamine residue. It has been proposed that the myrosinases are able to catalyze the cleavage of glucosinolate, because the substrates contain inherently good leaving groups and thus do not require general acid assistance for leaving-group departure.[25] A bound ascorbate anion appears to function as the general base catalyst for hydrolysis of the glycosyl–enzyme intermediate. A similar explanation is given for the GH84 human *O*-GlcNAcase, which is proposed to catalyze the hydrolysis of activated thioglycosides via a very dissociative transition state and without general acid catalysis to protonate the thiolate leaving group.[21]

© 2006 Wiley-VCH Verlag GmbH & Co. KGaA, Weinheim

The enzymes that have evolved to cleave carbon–sulfur linkages generally appear to use an anionic elimination mechanism. Excellent examples include cysteine Cβ-Sγ lyases,[11] β-cystathionase,[12] *S*-(β-aminoethyl)-cysteine,[13] *S*-alkylcysteine lyase,[14,15] *S*-adenosyl homocysteine hydrolase (AdoHCyase),[16] and the more recently uncovered ribosyl homocysteinase.[17] Most significantly, AdoHCyase[16] utilizes an NAD^+ cofactor to oxidize the ribose C3 hydroxy group of *S*-adenosyl homocysteine, thereby lowering the pK_a of the C4 proton and facilitating deprotonation and hence α,β-elimination of the thiol. The Michael acceptor then undergoes 1,4 nucleophilic attack by a water molecule, followed by reduction of the C3 ketone by the "on-board" NADH, yielding adenosine and homocysteine and returning the enzyme to its initial catalytic state.

We recently unveiled a completely new mechanism of enzymatic glycoside hydrolysis analogous to that of AdoHCyase and also involving anionic transition states. The glycosidases that employ this mechanism are found within glycoside hydrolase family 4 (GH4), which also use an "on-board" NAD^+. In this case, the cofactor is used to transiently oxidize the C3 hydroxy group, as shown in Scheme 1.[18] Key features of the mechanism include oxidation of the C3 hydroxy group, formation of an enediolate intermediate stabilized by a bound Mn^{2+} cofactor, addition of water to the Michael acceptor so formed, and finally reduction of the ketone.

The similarities of the elimination mechanisms of AdoHCyase and glycosidases from family 4 raised the question as to whether GH4 enzymes, in contrast to all other glycosidases, can efficiently hydrolyze thioglycosidic bonds. Not only is this of fundamental mechanistic interest, but also it is highly relevant to the design of specific glycosidase inhibitors as potential therapeutics. Preliminary results[19] had indicated that thioglycosides might, in general, function as substrates since *p*-nitrophenyl 6-phospho-β-D-thioglucoside (*S*-pNPG6P) was shown to be hydrolyzed with kinetic parameters that are very similar to those of its oxygen-containing counterpart, *p*-nitrophenyl 6-phospho-β-D-glucoside (*O*-pNPG6P).[19] However, the use of an activated aryl leaving group could be misleading in this case as previous studies with a "normal" family 1 β-glucosidase, Abg,[20] and a GH84 human *O*-GlcNAcase[21] have shown that activated aryl thioglycosides could indeed be cleaved reasonably efficiently. To properly test whether family 4 enzymes can cleave thioglycosides, it was necessary to study the hydrolysis of non-activated thiodisaccharide substrates. Accordingly, we set out to synthesize and test thioglycoside analogues of the natural substrate for the *Thermotoga maritima* BglT, a 6-phospho-β-glucosidase from GH4 for which a three-dimensional structure and a number of mechanistic studies are available. To simplify assays, as well as synthetic routes, we elected to synthesize the *p*-nitrophenyl glycoside of thiocellobiose, as well as its oxygen-linked counterpart.

p-Nitrophenyl 4-deoxy-4-thio-6′-phospho-β-D-cellobioside (*S*-pNPC6′P) was synthesized according to the chemoenzymatic route shown in Scheme 2 starting with *p*-nitrophenyl 4-deoxy-4-thio-β-D-glucoside. The key step involved an enzymatic coupling using the thioglycoligase technology recently developed in our group to produce the thiodisac-

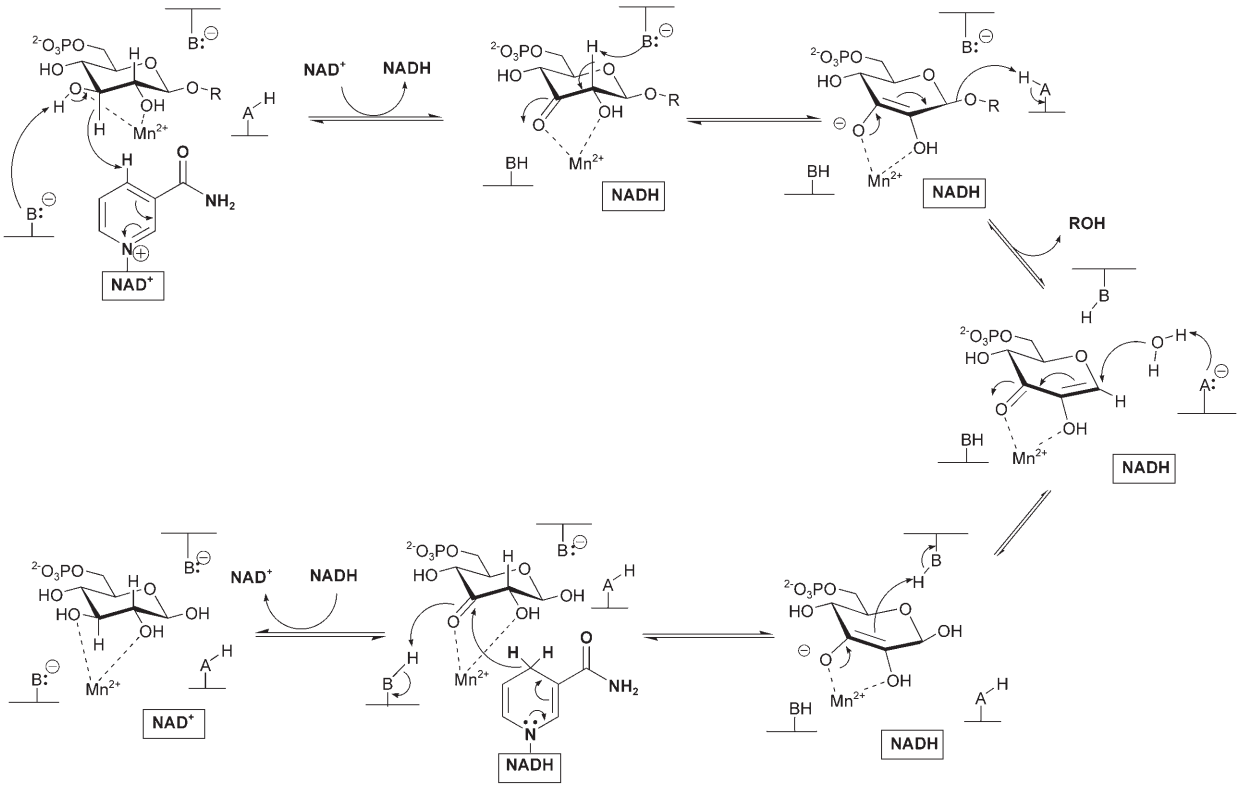

Scheme 1. Proposed mechanism of BglT, a 6-phospho-β-glucosidase from GH4.

 © 2006 Wiley-VCH Verlag GmbH & Co. KGaA, Weinheim

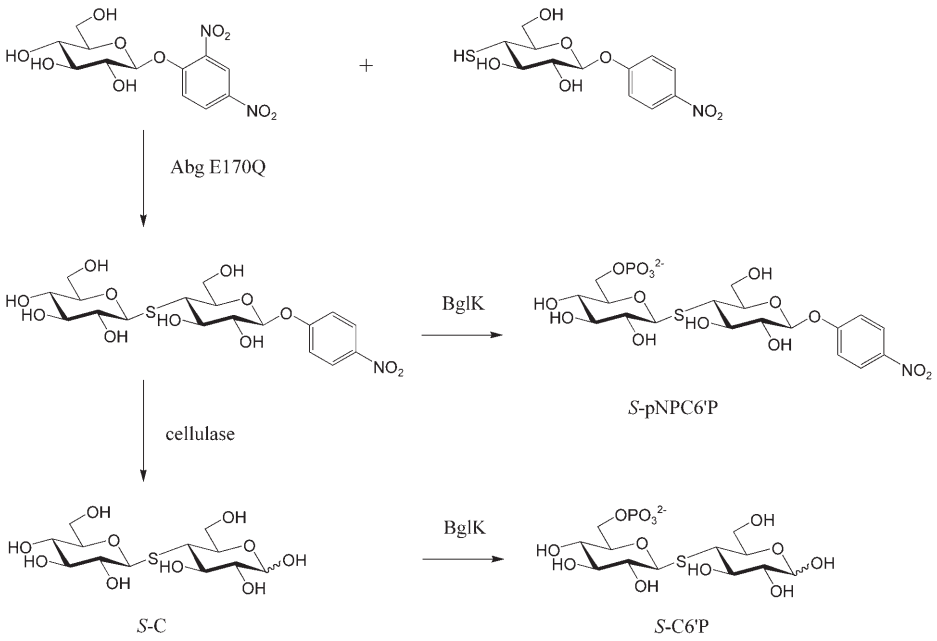

Scheme 2. Synthesis of *S*-pNPC6′P and *S*-C6′P.

charide *p*-nitrophenyl 4-deoxy-4-thio-β-D-cellobioside (*S*-pNPC).[22] The free disaccharide, 4-deoxy-4-thio-D-cellobiose (*S*-C; Scheme 2), was prepared from *S*-pNPC by removal of the *p*-nitrophenyl group at C1 using the cellulase Onozuka R-10 from *Trichoderma viride*. The disaccharide products *S*-pNPC and *S*-C were then selectively phosphorylated at O6′ using the kinase BglK from *Klebsiella pneumoniae* that is associated with the phosphoenolpyruvate-dependent sugar: phosphotransferase system (PEP:PTS) used by many bacterial species for the simultaneous phosphorylation and translocation of carbohydrates into the cell.[23] The oxygen analogues, *p*-nitrophenyl 6′-phospho-β-D-cellobioside (*O*-pNPC6′P) and D-cellobiose 6′-phosphate (*O*-C6′P), were synthesized analogously from the *p*-nitrophenyl β-D-cellobioside and D-cellobiose, respectively, using the same kinase (Scheme 3).

Kinetic parameters for all substrates were determined using a coupled assay system, in which the formation of the glucose 6-phosphate product was coupled to the reduction of NADP through inclusion of the enzyme glucose 6-phosphate dehydrogenase. A second, coupled assay system was also employed in which the *p*-nitrophenyl β-D-glucoside released from *O*-pNPC6′P was hydrolyzed by an added β-glucosidase. However, since *p*-nitrophenyl 4-deoxy-4-thio-β-D-glucoside is not a substrate for Abg, this coupled assay could not be used for *S*-pNPC6′P.

The kinetic parameters for the hydrolysis of the disaccharide substrates are shown in Table 1 along with K_i values for each disaccharide as an inhibitor of *O*-pNPG6P hydrolysis. The kinetic parameters for the disaccharide substrates are similar; the k_{cat} and K_M values for *S*-pNPC6′P are larger than those for *O*-pNPC6′P, resulting in similar k_{cat}/K_M values. Meanwhile, the k_{cat} and K_M values for *O*-C6′P are both slightly larger than those for *S*-C6′P, resulting in similar k_{cat}/K_M values. The similarities of the K_M and K_i values in each case confirms that the reaction is indeed occurring through the same active site. Furthermore, product analyses by NMR spectroscopy and mass spectrometry showed that the expected products (glucose 6-phosphate and 4-deoxy-4-thioglucose) are indeed formed when *S*-C6′P is reacted with BglT. In addition, deuterium incorporation from the solvent into the glucose 6-phosphate product strongly suggests that BglT utilizes the same mechanism in the hydrolysis of thiodisaccharides as that of *O*-glycosidic linkages. Overall, there is no significant difference between the rates of hydrolysis of *O*- and *S*-glycosidic linkages as catalyzed by BglT. Hence, we have shown that BglT is the first glycosidase capable of efficiently cleaving unactivated thioglycosides.

These findings clearly indicate a fundamental difference in the BglT mechanism compared to that of most glycosidases,

Table 1: Summary of kinetic parameters for the hydrolysis of *O*- and *S*-glucosides by BglT.

Substrate	k_{cat} [s^{-1}]	K_M [μM]	k_{cat}/K_M [s^{-1} mM^{-1}]	K_i [μM]
O-pNPG6P[a]	1.9	41	46	–
S-pNPG6P[a]	1.6	41	39	–
O-pNPC6′P	0.017	1.0	17	1.0
S-pNPC6′P	0.072	8.0	9.0	5.0
O-C6′P[b]	0.61	69	8.8	70
S-C6′P	0.53	37	14	33

[a] Data obtained from Ref. [19]. [b] Data obtained from Ref. [24].

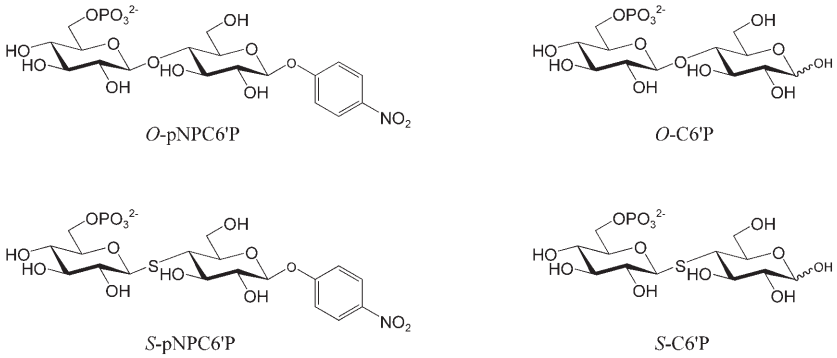

Scheme 3. Disaccharide substrates for BglT.

 © 2006 Wiley-VCH Verlag GmbH & Co. KGaA, Weinheim

which cannot cleave unactivated thioglycosides. The efficient hydrolysis of thiodisaccharides therefore provides further supporting evidence for the novel glycosidase mechanism proposed for family 4 enzymes. Cleavage of such thioglycosides at rates comparable to those of their oxygen counterparts is quite reasonable for the anionic mechanism proposed but not for reactions via oxocarbenium-ion-like transition states. The majority of glycosidases do not hydrolyze thioglycosidic linkages, and those that have been reported to possess thioglycosidase activity only react with thioglycosides containing highly activated leaving groups, as clearly demonstrated by the Brønsted plot determined for thioglycoside hydrolysis in the case of *O*-GlcNAcase.[21] The cleavage of the thioglycosidic linkages by *O*-GlcNAcase does not rely on general acid catalysis, and there is substantial development of negative charge on the sulfur atom at the transition state.[21] Since the cleavage of the glycosidic linkage is not rate-limiting for BglT,[24] it is reasonable that substitution of the glycosidic oxygen with a sulfur atom does not significantly affect the overall rate.

On the basis of these results, it is clear that thioglycosides should not be employed in any inhibition strategies for family 4 enzymes whether this be for structural or mechanistic studies or as part of any biological control strategy. Indeed, the ability to cleave a thiodisaccharide could be a useful diagnostic of whether a new glycosidase belongs to family 4. Finally, these findings raise the question of whether *O*-C6′P is in fact the natural substrate for BglT, or whether this enzyme has evolved to cleave some other, as yet undiscovered, substrate. The locations of the genes encoding many GH4 enzymes within the PEP:PTS operon argues strongly that the disaccharide 6-phosphates are the natural substrates and that the facile cleavage of thioglycosides is just a circumstantial consequence of the mechanism utilized by the enzyme. However, the uncanny similarities between the mechanisms utilized by GH4 enzymes and by AdoHCyase suggests that other possibilities should be kept in mind.

Received: April 10, 2006
Revised: June 20, 2006
Published online: August 17, 2006

Keywords: elimination · enzyme catalysis · glycoside hydrolase · thioether cleavage · thioglycosides

[1] Z. J. Witczak, *Curr. Med. Chem.* **1999**, *6*, 165.
[2] N. Asano, *Glycobiology* **2003**, *13*, 93R.
[3] D. Mandelman, A. Belaich, J. P. Belaich, N. Aghajari, H. Driguez, R. Haser, *J. Bacteriol.* **2003**, *185*, 4127.
[4] G. Sulzenbacher, H. Driguez, B. Henrissat, M. Schulein, G. J. Davies, *Biochemistry* **1996**, *35*, 15280.
[5] M. L. Sinnott, *Chem. Rev.* **1990**, *90*, 1171.
[6] D. L. Zechel, S. G. Withers, *Acc. Chem. Res.* **2000**, *33*, 11.
[7] D. E. Koshland, *Biol. Rev.* **1953**, *28*, 416.
[8] J. L. Jensen, W. P. Jencks, *J. Am. Chem. Soc.* **1979**, *101*, 1476.
[9] J. P. Ferraz, E. H. Cordes, *J. Am. Chem. Soc.* **1980**, *102*, 1488.
[10] T. H. Fife, T. J. Przystas, *J. Am. Chem. Soc.* **1980**, *102*, 292.
[11] M. Bertoldi, B. Cellini, T. Clausen, C. B. Voltattorni, *Biochemistry* **2002**, *41*, 9153.
[12] C. R. Gentry-Weeks, J. Spokes, J. Thompson, *J. Biol. Chem.* **1995**, *270*, 7695.
[13] I. Rossol, A. Puhler, *J. Bacteriol.* **1992**, *174*, 2968.
[14] H. Kamitani, N. Esaki, H. Tanaka, K. Soda, *Agric. Biol. Chem.* **1990**, *54*, 2069.
[15] C.-H. Tai, P. F. Cook, *Acc. Chem. Res.* **2001**, *34*, 49.
[16] J. L. Palmer, R. H. Abeles, *J. Biol. Chem.* **1979**, *254*, 1217.
[17] D. Pei, J. Zhu, *Curr. Opin. Chem. Biol.* **2004**, *8*, 492.
[18] V. L. Y. Yip, A. Varrot, G. J. Davies, S. S. Rajan, X. J. Yang, J. Thompson, W. F. Anderson, S. G. Withers, *J. Am. Chem. Soc.* **2004**, *126*, 8354.
[19] A. Varrot, V. L. Y. Yip, Y. Li, S. S. Rajan, X. Yang, W. F. Anderson, J. Thompson, S. G. Withers, G. J. Davies, *J. Mol. Biol.* **2005**, *346*, 423.
[20] A. G. Day, *Purification and Preliminary Characterization of* β-*Glucosidase from Alcaligenes faecalis (ATCC 21400)*, MSc Thesis, **1985**.
[21] M. S. Macauley, K. A. Stubbs, D. J. Vocadlo, *J. Am. Chem. Soc.* **2005**, *127*, 17202.
[22] J. Mullegger, M. Jahn, H. Chen, R. A. J. Warren, S. G. Withers, *Protein Eng. Des. Sel.* **2005**, *18*, 33.
[23] N. D. Meadow, D. K. Fox, S. Roseman, *Annu. Rev. Biochem.* **1990**, *59*, 497.
[24] V. L. Y. Yip, S. G. Withers, *Biochemistry* **2006**, *45*, 571.
[25] W. P. Burmeister, S. Cottaz, H. Driguez, R. Iori, S. Palmieri, B. Henrissat, *Structure* **1997**, *5*, 663.

 © 2006 Wiley-VCH Verlag GmbH & Co. KGaA, Weinheim

Radicals in Synthesis

DOI: 10.1002/anie.200601461

Radical Alkylation of Bis(silyloxy)enamine Derivatives of Organic Nitro Compounds**

*Jin Young Lee, Young-Taek Hong, and Sunggak Kim**

Organic nitro compounds are valuable intermediates in organic synthesis that undergo a variety of carbon–carbon bond-forming reactions. The alkylation of primary and secondary alkyl nitro compounds proceeds via dianion species to yield α- and β-alkylated nitro compounds, respectively.[1] The conjugate addition and nitroaldol reaction of organic nitro compounds have also found wide application in synthesis.[2] Despite the great synthetic importance of the nitro

[*] J. Y. Lee, Y.-T. Hong, Prof. Dr. S. Kim
Center for Molecular Design & Synthesis and
Department of Chemistry
School of Molecular Science
Korea Advanced Institute of Science and Technology
Daejeon 305-701 (Korea)
Fax: (+82) 42-869-8370
E-mail: skim@kaist.ac.kr

[**] We thank the CMDS and BK21 programs for financial support.

Supporting information for this article is available on the WWW under http://www.angewandte.org or from the author.

WILEY InterScience DISCOVER SOMETHING GREAT
© 2006 Wiley-VCH Verlag GmbH & Co. KGaA, Weinheim

group, radical-mediated reactions of this functional group have not been well studied. Previously reported chain processes via radical anion intermediates nicely complement standard enolate alkylations, as they give good results with tertiary alkyl and aryl halides.[3,4] The nitroalkylation of alkyl iodides via silyl nitronates[5] has also been described, as well as the previously known reduction of tertiary nitro groups with Bu_3SnH/2,2′-azobisisobutyronitrile (AIBN).[6]

Our approach for the radical alkylation of organic nitro compounds is outlined in Scheme 1. It involves the addition of an alkyl radical to a bis(silyloxy)enamine **3** and subsequent homolytic cleavage of one N–O bond to yield an oxime ether **6**. Thus, this approach would enable alkylation at the β position to the nitro group together with the conversion of the nitro group into the synthetically important oxime ether group. We began our study with 2-nitropropane (**1b**). The treatment of **1b** with *tert*-butyldimethylsilyl trifluoromethanesulfonate (TBSOTf; 2.0 equiv) and triethylamine (2.2 equiv) afforded the bis(silyloxy)enamine **3b** via **2**.[7] Since **3b** underwent rearrangement into **4b** when passed through a column of silica gel,[7c] the remaining reactions were carried out with the crude product after an aqueous workup. Irradiation of a solution of **3b**, iodomethyl phenyl sulfone, and hexamethylditin in benzene at 300 nm for 9 h afforded

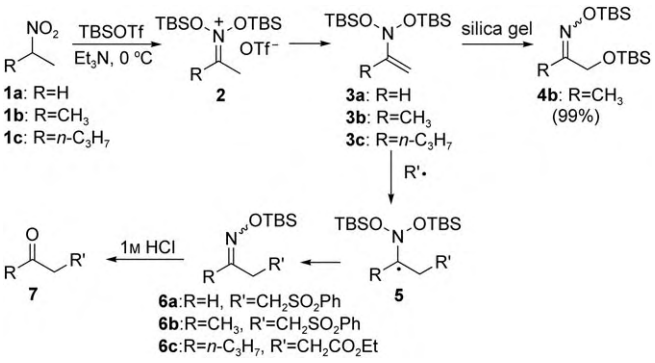

Scheme 1. Radical alkylation of the organic nitro compound **1**.

the oxime ether **6b** in 71 % yield. The hydrolysis of **6b** with 1M HCl then gave the ketone **7b** in 91 % yield. Furthermore, the oxime ether group can be converted into an amino[8] or nitro group.[9] When **1c** was treated with TBSOTf and triethylamine under similar conditions, the deprotonation of **2c** by triethylamine occurred at the less-substituted carbon atom, thereby yielding **3c** in a regioselective manner.

Our experimental results are summarized in Table 1. The radical reaction of the conjugated bis(silyloxy)enamine **3e**,

Table 1: Radical alkylation of organic nitro compounds.[a]

Nitro compound		Enamine		Oxime ether		Yield [%]	Carbonyl compound		Yield [%]
		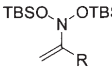							
1a	R = H	**3a**	R = H	**6a**	R = H R′ = CH_2SO_2Ph	85	**7a**	R = H R′ = CH_2SO_2Ph	86
1b	R = CH_3	**3b**	R = CH_3	**6b**	R = CH_3 R′ = CH_2SO_2Ph	71	**7b**	R = CH_3 R′ = CH_2SO_2Ph	91
1c	R = *n*-C_3H_7	**3c**	R = *n*-C_3H_7	**6c**	R = *n*-C_3H_7 R′ = CH_2CO_2Et	70	**7c**	R = *n*-C_3H_7 R′ = CH_2CO_2Et	85
1d	R = Ph	**3d**	R = Ph	**6d**	R = Ph R′ = CH_2CO_2Et	82	**7d**	R = Ph R′ = CH_2CO_2Et	93
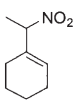		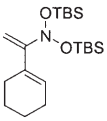		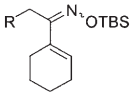			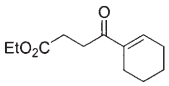		
1e		**3e**		**6e**	R = CH_2SO_2Ph	79	**7e**		85
				6f	R = CH_2CO_2Et	72			
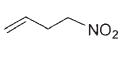		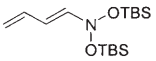		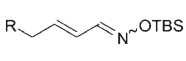			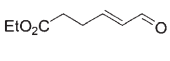		
1f		**3f**		**6g**	R = CH_2CO_2Et	65	**7f**		93
				6h	R = CH_2SO_2Ph	62			
		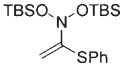		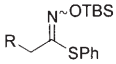			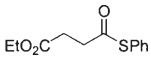		
1g		**3g**		**6i**	R = CH_2CO_2Et	76	**7g**		73
				6j	R = CH_2SO_2Ph	79			
		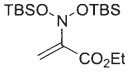		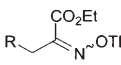					
1h		**3h**		**6k**	R = CH_2CO_2Et	70	**7h**		88

[a] Reaction conditions: $(Me_3Sn)_2$ (1 equiv), benzene, 300 nm.

 © 2006 Wiley-VCH Verlag GmbH & Co. KGaA, Weinheim

derived from the allylic nitro compound **1e**, with iodomethyl phenyl sulfone gave the conjugated oxime ether **6e** in 79% yield. When a benzene solution of ethyl iodoacetate and the conjugated enamine **3f**, derived from 4-nitro-1-butene (**1f**), was subjected to the standard reaction conditions, **7f** was isolated after acidic hydrolysis of the oxime ether **6g**. The successful synthesis of **7f** indicates that the procedure is useful for the preparation of γ-alkylated enals from γ,δ-unsaturated nitro compounds.

This method can be further extended to other α-substituted nitro compounds to yield several types of synthetically useful carbonyl derivatives. For example, the radical reaction of **3g** under the same conditions, followed by acidic hydrolysis, afforded the thiol ester **7g** in good yield. Furthermore, the radical reaction of **3h** afforded the oxime ester **6k**, which underwent acidic hydrolysis to give the synthetically important α-ketoester **7h**.

Oxime ether **10** was obtained by radical alkylation of the bromo-substituted enamine **9** under similar conditions. The acidic hydrolysis of **10** in methanolic HCl at reflux gave the corresponding methyl ester **11** in 93% yield, whereas the radical reaction of **10** with Bu_3SnH/AIBN in refluxing benzene provided the nitrile **12** in 84% yield. Furthermore, **10** underwent 1,3-dipolar cycloaddition upon treatment with potassium fluoride in *N*,*N*-dimethylformamide (DMF) in the presence of polarophiles via the nitrile oxide **13** generated in situ. An acrylic ester, a vinyl sulfone, and phenylacetylene underwent smooth 1,3-dipolar cycloadditions with **13** to give the corresponding isoxazolines **14a** and **14b**, and isoxazole **14c** (Scheme 2).[10]

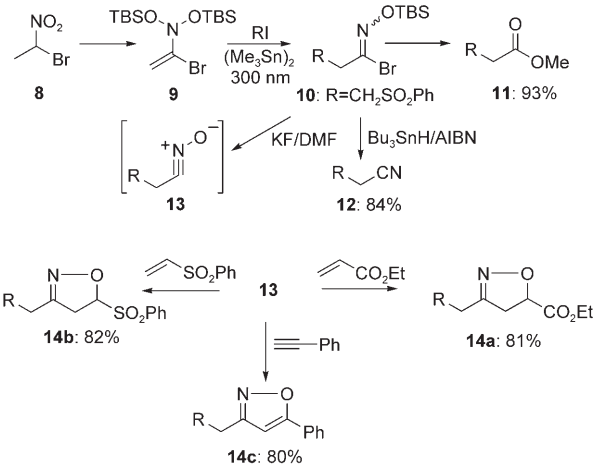

Scheme 2. Radical alkylation of **9** followed by 1,3-dipolar cycloaddition.

Isoxazole derivatives can also be prepared by the radical alkylation of **15**. The radical reaction of **16** with phenyl sulfonyl bromide under similar conditions afforded the oxime ether **17** in 50% yield. When **17** was subjected to hydrolysis in HCl/MeOH at reflux for 1 h, the isoxazole **19** was obtained in 79% yield.[11] Similarly, the use of ethyl iodoacetate as an alkylating agent provided the isoxazole **21** after transesterification of **20** under acidic conditions (Scheme 3).

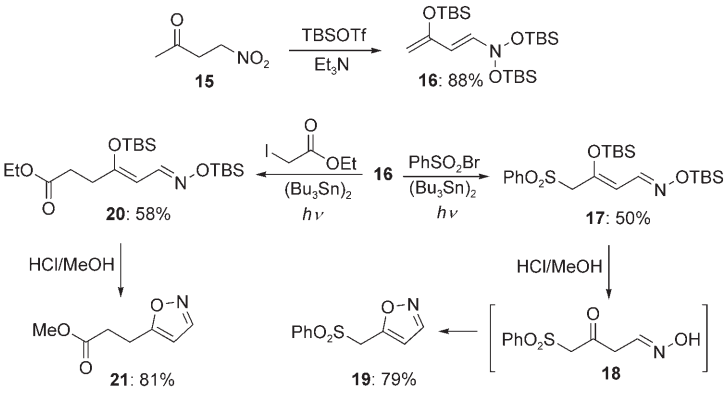

Scheme 3. Synthesis of isoxazoles by radical reactions of **16**.

Tin-based reagents are not always convenient because of the inherent toxicity of organotin derivatives and the difficulties often encountered in removing tin residues from the product.[12] For a tin-free approach,[13] we implemented the findings of our previous studies on the radical rearrangement of silyloxy radicals into the corresponding silyl radicals.[14] Thus, the treatment of **1d** with *tert*-butyldiphenylsilyl chloride (TBDPSCl) and triethylamine in the presence of silver triflate in dichloromethane afforded the bis-(silyloxy)enamine **22** in 92% yield. When the radical reaction was carried out with **22** and ethyl iodoacetate in the presence of 2,2′-azobis(4-methoxy-2,4-dimethylvaleronitrile) (V-70) as the initiator in dichloromethane at 30 °C for 9 h, the oxime ether **23** was isolated in 83% yield (Scheme 4). To determine the efficiency and the scope of the present method, additional experiments were carried out with **22** and several different alkyl halides. As shown in Table 2, alkyl iodides with an electron-withdrawing substituent at the α position underwent clean radical alkylation reactions under tin-free conditions.

In conclusion, we have developed a novel radical alkylation reaction of organic nitro derivatives via bis-(silyloxy)enamines. The method enables not only alkylation

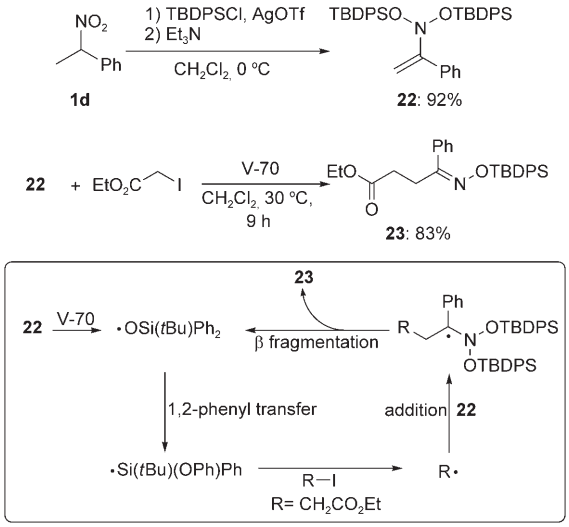

Scheme 4. Tin-free radical alkylation of **1d** via **22**.

 © 2006 Wiley-VCH Verlag GmbH & Co. KGaA, Weinheim

Table 2: Tin-free radical alkylation of the organic nitro compound **1d**.[a]

Entry	Substrate	Product	Yield [%]
1	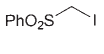	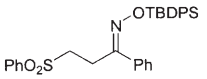	61
2	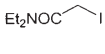	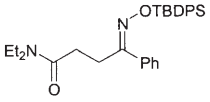	63
3	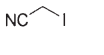	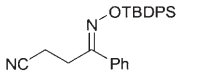	68
4	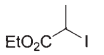	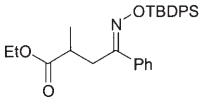	72
5	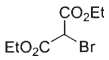	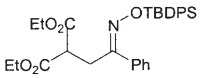	75

[a] Reaction conditions: V-70, CH_2Cl_2, 30 °C, 9 h.

β to the nitro group, but also the conversion of the nitro group into an oxime ether functionality. Furthermore, the radical alkylation can be carried out under tin-free conditions.

Experimental Section

Typical procedure A: A solution of iodomethyl phenyl sulfone (56 mg, 0.2 mmol), **3b** (95 mg, 0.3 mmol), and hexamethylditin (65 mg, 0.2 mmol) in benzene (1 mL; 0.2 M in iodide) was purged with nitrogen for 10 min and then irradiated in a photochemical reactor at 300 nm for 9 h. The solvent was then evaporated under reduced pressure, and the residue was purified by column chromatography on silica gel with EtOAc/hexane (1:5) as the eluent to give **6b** (49 mg, 71%, *E*/*Z* 5:1 (ratio calculated from the ^{1}H NMR spectrum)). ^{1}H NMR ($CDCl_3$, 400 MHz): δ(*E* isomer) = 0.04 (s, 6H), 0.79 (s, 9H), 1.85 (s, 3H), 2.61–2.66 (m, 2H), 3.22–3.26 (m, 2H), 7.53–7.57 (m, 2H), 7.62–7.64 (m, 1H), 7.87–7.90 ppm (m, 2H); δ(*Z* isomer) = 0.07 (s, 6H), 0.86 (s, 9H), 1.80 (s, 3H), 2.52–2.57 (m, 2H), 3.30–3.35 (m, 2H), 7.53–7.57 (m, 2H), 7.62–7.64 (m, 1H), 7.87–7.90 ppm (m, 2H); ^{13}C NMR ($CDCl_3$, 100 MHz): δ(*E* isomer) = −5.3 (2C), 17.8, 20.2, 23.5, 25.9 (3C), 51.7, 128.1, 129.3, 133.8, 138.6, 157.4 ppm; IR (polymer): $\tilde{\nu}$ = 784, 839, 938, 1155, 1253, 1309, 1654, 2859, 2933 cm^{-1}; HRMS: calcd for $C_{16}H_{27}NO_3SSi$ [M^+]: 341.1481; found: 341.1430.

Typical procedure B (tin-free conditions): A solution of ethyl iodoacetate (45 mg, 0.2 mmol), **22** (188 mg, 0.3 mmol), and V-70 (12 mg, 0.04 mmol) in dichloromethane (1 mL; 0.2 M in iodide) was purged with nitrogen for 10 min and then stirred at 30 °C under nitrogen for 9 h. The solvent was then evaporated under reduced pressure, and the residue was purified by column chromatography on silica gel with EtOAc/hexane (1:20) as the eluent to give **23** (82 mg, 83%, *E*/*Z* 3.3:1 (ratio calculated from the ^{1}H NMR spectrum)). ^{1}H NMR ($CDCl_3$, 400 MHz): δ(*E* isomer) = 1.14 (s, 9H), 1.21 (t, *J* = 7.1 Hz, 3H), 2.66–2.70 (m, 2H), 3.23–3.27 (m, 2H), 4.11 (q, *J* = 7.1 Hz, 2H), 7.31–7.40 (m, 10H), 7.61–7.62 (m, 2H), 7.71–7.73 ppm (m, 3H); δ(*Z* isomer) = 1.00 (s, 9H), 1.21 (t, *J* = 7.1 Hz, 3H), 2.50–2.54 (m, 2H), 2.84–2.88 (m, 2H), 3.91 (q, *J* = 7.1 Hz, 2H), 7.31–7.40 (m, 10H), 7.61–7.62 (m, 2H), 7.71–7.73 ppm (m, 3H); ^{13}C NMR ($CDCl_3$, 100 MHz): δ(*E* isomer) = 14.1, 19.4, 22.2, 27.2 (3C), 31.0, 60.6, 126.4, 127.4, 127.5 (2C), 127.9, 128.4, 129.3, 129.6, 133.7, 135.1, 135.5 (2C), 161.5, 172.6 ppm; IR (polymer): $\tilde{\nu}$ = 704, 744, 1114, 1528, 1566, 1690, 1732, 2859, 2934 cm^{-1}; HRMS: calcd for $C_{28}H_{33}NO_3Si$ [M^+]: 459.2230; found: 459.2231.

Received: April 13, 2006
Revised: May 23, 2006
Published online: August 14, 2006

Keywords: alkylation · ketones · nitro compounds · radicals · synthetic methods

[1] a) G. Rosini in *Comprehensive Organic Synthesis*, *Vol. 2* (Ed.: B. M. Trost), Pergamon Press, Oxford, **1991**, pp. 321–340; b) N. Ono, *The Nitro Group in Organic Synthesis*, Wiley, New York, **2001**, pp. 126–140; c) M. Eyer, D. Seebach, *J. Am. Chem. Soc.* **1985**, *107*, 3601–3606.

[2] a) N. Halland, R. G. Hazell, K. A. Jørgensen, *J. Org. Chem.* **2002**, *67*, 8331–8338; b) R. Ballini, L. Barboni, G. Giarlo, *J. Org. Chem.* **2003**, *68*, 9173–9176; c) T. Ooi, S. Fujioka, K. Maruoka, *J. Am. Chem. Soc.* **2004**, *126*, 11790–11791.

[3] a) N. Kornblum, R. E. Michel, R. C. Kerber, *J. Am. Chem. Soc.* **1966**, *88*, 5660–5662; b) G. A. Russell, W. C. Danen, *J. Am. Chem. Soc.* **1966**, *88*, 5663–5665; c) N. Kornblum, W. J. Kelly, M. M. Kestner, *J. Org. Chem.* **1985**, *50*, 4720–4724.

[4] a) K. Narasaka, K. Iwakura, T. Okauchi, *Chem. Lett.* **1991**, 423–426; b) B. Barlaam, J. Boivin, S. Z. Zard, *Tetrahedron Lett.* **1993**, *34*, 1023–1026; c) J.-T. Liu, Y.-J. Jang, Y.-K. Shih, S.-R. Hu, C.-M. Chu, C.-F. Yao, *J. Org. Chem.* **2001**, *66*, 6021–6028; d) G. Ouvry, B. Quiclet-Sire, S. Z. Zard, *Org. Lett.* **2003**, *5*, 2907–2909.

[5] S. Kim, J.-Y. Yoon, C. J. Lim, *Synlett* **2000**, 1151–1153.

[6] a) N. Ono, H. Miyake, A. Kamimura, I. Hamamoto, R. Tamura, A. Kaji, *Tetrahedron* **1985**, *41*, 4013–4023; b) D. D. Tanner, D. J. Harrison, J. Chen, A. Kharrat, D. D. M. Wayner, D. Griller, D. J. McPhee, *J. Org. Chem.* **1990**, *55*, 3321–3325; c) J. Tormo, D. S. Hays, G. C. Fu, *J. Org. Chem.* **1998**, *63*, 5296–5297.

[7] a) A. D. Dilman, I. M. Lyapkalo, S. L. Ioffe, Y. A. Strelenko, V. A. Tartakovsky, *J. Org. Chem.* **2000**, *65*, 8826–8829; b) A. D. Dilman, I. M. Lyapkalo, S. L. Ioffe, H. Mayr, *J. Org. Chem.* **2001**, *66*, 3196–3200; c) A. A. Tishkov, A. D. Dilman, V. I. Faustov, A. A. Birukov, K. S. Lysenko, P. A. Belyakov, S. L. Ioffe, Y. A. Strelenko, M. Y. Antipin, *J. Am. Chem. Soc.* **2002**, *124*, 11358–11367.

[8] a) Y. Sakito, Y. Yoneyoshi, G. Suzukamo, *Tetrahedron Lett.* **1988**, *29*, 223–224; b) S. Itsuno, T. Matsumoto, D. Sato, T. Inoue, *J. Org. Chem.* **2000**, *65*, 5879–5881.

[9] a) W. D. Emmons, A. S. Pagano, *J. Am. Chem. Soc.* **1955**, *77*, 4557–4559; b) M. W. Barnes, *J. Org. Chem.* **1976**, *41*, 733–735; c) G. A. Olah, P. Ramaiah, C. S. Lee, G. K. S. Prakash, *Synlett* **1992**, 337–339.

[10] a) P. A. Wade, H. R. Hinney, *Tetrahedron Lett.* **1979**, 139–142; b) M. H. Seo, Y. Y. Lee, Y. M. Goo, *Synth. Commun.* **1994**, *24*, 1433–1439.

[11] a) N. J. Doorenbos, L. Milewich, D. P. Hollis, *J. Org. Chem.* **1967**, *32*, 718–721; b) M. E. Lloris, M. Moreno-Mafias, *Tetrahedron Lett.* **1993**, *34*, 7119–7122.

[12] a) P. A. Baguley, J. C. Walton, *Angew. Chem.* **1998**, *110*, 3272–3283; *Angew. Chem. Int. Ed.* **1998**, *37*, 3072–3082; b) A. Studer, S. Amrein, *Synthesis* **2002**, 835–849.

[13] For our previous studies on tin-free radical reactions, see: a) S. Kim, H.-J. Song, T.-L. Choi, J.-Y. Yoon, *Angew. Chem.* **2001**, *113*, 2592–2594; *Angew. Chem. Int. Ed.* **2001**, *40*, 2524–2526; b) S. Kim, C. J. Lim, *Angew. Chem.* **2002**, *114*, 3399–3401; *Angew. Chem. Int. Ed.* **2002**, *41*, 3265–3267; c) S. Kim, C. J. Lim, *Bull. Korean Chem. Soc.* **2003**, *24*, 1219–1222; d) S. Kim, S. Kim, N. Otsuka, I. Ryu, *Angew. Chem.* **2005**, *117*, 6339–6342; *Angew. Chem. Int. Ed.* **2005**, *44*, 6183–6186.

 © 2006 Wiley-VCH Verlag GmbH & Co. KGaA, Weinheim

[14] a) S. Kim, C. J. Lim, C. Song, W.-J. Chung, *J. Am. Chem. Soc.* **2002**, *124*, 14306 – 14307; b) S. Kim, C. J. Lim, *Angew. Chem.* **2004**, *116*, 5492 – 5494; *Angew. Chem. Int. Ed.* **2004**, *43*, 5378 – 5380; c) A. K. Shubber, R. L. Dannley, *J. Org. Chem.* **1971**, *36*, 3784 – 3787; d) R. L. Dannley, G. Jalics, *J. Org. Chem.* **1965**, *30*, 3848 – 3851.

 © 2006 Wiley-VCH Verlag GmbH & Co. KGaA, Weinheim

Carbene Ligands

DOI: 10.1002/anie.200601583

Synthesis and Study of Janus Bis(carbene)s and Their Transition-Metal Complexes**

*Dimitri M. Khramov, Andrew J. Boydston, and Christopher W. Bielawski**

The construction of new organic–inorganic hybrid materials with interesting structural features and technologically useful functions is a vibrant area of research with considerable potential.[1] The key to growth in this field is the development of new, tunable molecular scaffolds that can bridge transition metals. Ideal linkers should be readily accessible, exhibit high affinities toward a broad range of transition metals, and possess modular features amenable for precisely manipulating their inherent physical and electronic characteristics. Stable N-heterocyclic carbenes (NHCs),[2] and in particular imidazolylidenes,[3] fulfill these requirements. These carbenes have been found to form robust complexes with nearly every transition metal[2,4] and both the basic *N*-heterocyclic nucleus, and its substituents on the N atoms can be acutely modified.[5] As a result, an impressive amount of attention has been devoted toward optimizing and understanding the interaction of carbenes with various transition metals to form monometallic complexes.[2–6] However, comparatively less attention has been directed toward the development of discrete, multitopic carbenes that are poised to bind multiple transition metals.[7,8] Herein, we report the synthesis and characterization of benzobis(imidazolylidene)s, a new class of Janus[9] bis(carbene)s, composed of two linearly opposed imidazolylidenes annulated to a common arene backbone. Their utility in preparing new organometallic materials is also demonstrated.

Requisite benzobis(imidazolium) salts **1** possessing a range of substituents on N were synthesized by Pd-catalyzed aryl amination of 1,2,4,5-tetrabromobenzene followed by formylative cyclization or by reductive cyclization of the respective 2,5-diamino-1,4-benzoquinonediimine, according to our previously reported procedures.[10] Independent treatment of **1a–c** with 2.2 equivalents of lithium diisopropylamide (LDA) in THF at RT caused precipitation of products **2a** and **2b**, which were subsequently isolated by filtration in yields of 83 and 99%, respectively (Scheme 1). While **2a** and **2b** were

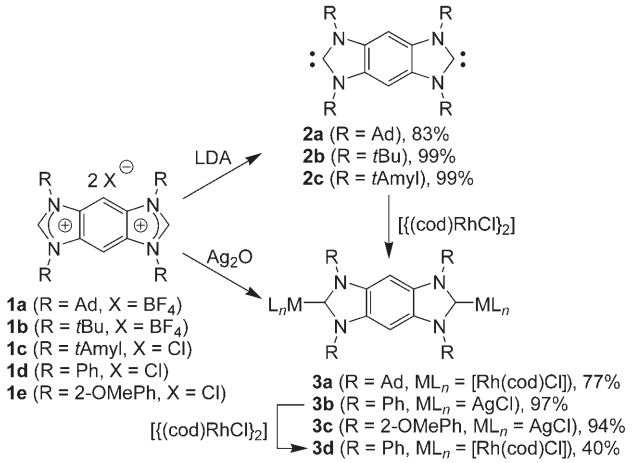

Scheme 1. Synthesis of benzobis(imidazolylidene)s and their related transition-metal complexes. Ad = adamantyl, cod = cycloocta-1,5-diene.

only slightly soluble in common organic solvents (for example, THF, toluene, and benzene), a highly soluble derivative featuring *N-tert*-amyl groups (**2c**) was obtained in 99% yield, after LiCl had been precipitated with excess toluene and removed by filtration.[11]

The ^{13}C NMR spectra of products **2a–c** in C_6D_6 all exhibited a single, diagnostic signal between $\delta = 227$–231 ppm, indicative of highly symmetric structures (Scheme 1) and consistent with other known annulated imidazolylidenes.[12] A crystal of **2a** was obtained by vapor diffusion of pentane into a saturated toluene/THF solution (1:1 v/v) and analyzed using X-ray diffraction.[13] An ORTEP view of the molecular structure is shown in Figure 1, with selected bond lengths and angles listed in the caption. Notably, the N-C-N bond angle was found to be 104.8(2)°,[14] which is similar to that found in saturated imidazolylidenes[15] and benzimidazolylidenes.[12a] This promising result strongly suggested that the reactivity and affinity of each carbene "face" of the Janus ligand toward transition metals should be similar to that of their monotopic analogues.

Addition of an equimolar amount of [{(cod)RhCl}$_2$] to a THF solution of **2a** at RT resulted in the precipitation of the Rh complex **3a** as a yellow solid, which was isolated in 77% yield. Analysis of this complex by NMR spectroscopy

[*] D. M. Khramov, A. J. Boydston, Prof. C. W. Bielawski
Department of Chemistry & Biochemistry
The University of Texas at Austin
Austin, TX 78712 (USA)
Fax: (+1) 512-471-8696
E-mail: bielawski@cm.utexas.edu

[**] We are grateful to the U.S. Army Research Office (W911NF-05-1-0430) and The University of Texas at Austin for their generous support of this research. A.J.B. thanks The University of Texas at Austin for a University Continuing Fellowship. J. W. Kamplain is acknowledged for his assistance.

Supporting information for this article is available on the WWW under http://www.angewandte.org or from the author.

InterScience © 2006 Wiley-VCH Verlag GmbH & Co. KGaA, Weinheim

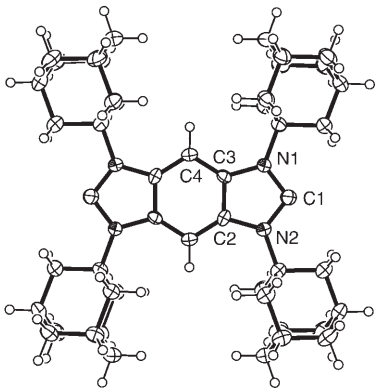

Figure 1. ORTEP view of **2a** (ellipsoids at the 50% probability level). Selected bond lengths [Å] and angles [°]: C1-N1 1.369(3), C1-N2 1.368(3), N1-C3 1.411(3), N2-C2 1.408(3), C2-C3 1.402(3), C3-C4 1.388(3); N1-C1-N2 104.8(2).

confirmed that the stoichiometry between the Rh centers and bis(carbene) nucleus was 2:1. A single ^{13}C NMR resonance appeared at $\delta = 198$ ppm, and two distinct sets of olefinic ^{1}H NMR signals were observed at 3.0 ppm (*cis* to the carbene) and 5.0 ppm (*trans* to the carbene), which was suggestive of a square planar geometry for each of the metal centers.[16] The structure of **3a** was confirmed by X-ray diffraction analysis after a suitable crystal was obtained by slow cooling of a hot $CHCl_3$ solution (Figure 2). Although key bond lengths were

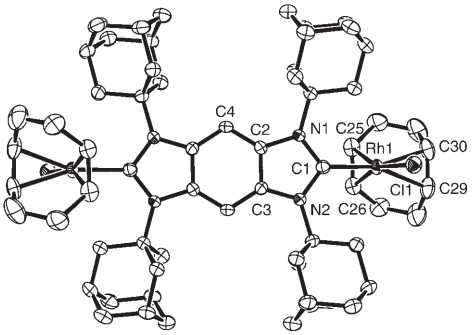

Figure 2. ORTEP view of **3a** (ellipsoids at the 50% probability level). Selected bond lengths [Å] and angles [°]: Rh1-C1 2.073(3), Rh1-C25 2.125(3), Rh1-C26 2.131(3), Rh1-C29 2.184(3), Rh1-C30 2.197(3), C1-N1 1.387(4), C1-N2 1.406(4), N1-C2 1.406(4), N2-C3 1.395(4), C2-C3 1.401(4), C2-C4 1.397(4); N1-C1-N2 105.7(2). Hydrogen atoms have been removed for clarity.

in accord with known NHC–Rh complexes,[16] a notable exception were the positions of the Rh atoms, which were displaced perpendicularly from the plane of the benzobis(imidazolylidene) by 0.75 Å. This unusual structural feature was attributed to the substantial steric bulk of the *N*-adamantyl groups balanced by the high affinity of imidazolylidenes for Rh^{I}.[17]

In cases where the free bis(carbene)s were not isolable (**1d–e**),[18] an alternative method of forming metal complexes was desired. Attention shifted toward the versatile Ag-mediated carbene-transfer protocol developed by Wang and Lin,[19] for accessing organometallic complexes.[20] Bis(azolium) salts **1d** and **1e** were respectively treated with 1 equivalent of Ag_2O in CH_2Cl_2 (23 °C) and CH_3CN (40 °C) (Scheme 1). Following filtration of the inorganic salts that precipitated during the reaction, concentration of the resulting solutions afforded products **3b** and **3c** in excellent yields (97 and 94%, respectively). Crystals of **3c** were obtained by slow diffusion of hexanes into a saturated CH_2Cl_2 solution and analyzed using X-ray diffraction. As shown in Figure 3, the

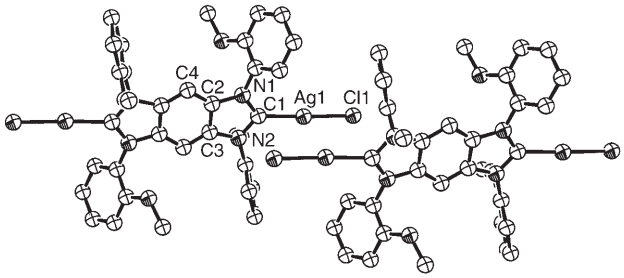

Figure 3. ORTEP view of **3c** (ellipsoids at the 50% probability level). Selected bond lengths [Å] and angles [°]: Ag1-C1 2.072(11), Ag1-Cl1 2.236(3), C1-N1 1.352(12), C1-N2 1.360(11), N1-C2 1.409(11), N2-C3 1.409(12), C2-C3 1.411(12), C2-C4 1.353(13), Ag···Ag 3.3054(15); N1-C1-N2 106.4(9). Hydrogen atoms have been removed for clarity.

structure is essentially linear along its main axis with a C1-Ag1-Cl1 bond angle of 176°; the *N*-aryl substituents are rotated out of the plane of the benzobis(imidazolylidene) with an average dihedral angle of 69°. Interestingly, in the solid state, the complexes arranged themselves in infinite rows that appeared to be governed by intermolecular argentophilic interactions.[20]

Treatment of bimetallic Ag complex **3b** with an equimolar amount of $[\{(cod)RhCl\}_2]$ in CH_2Cl_2 at 50 °C for 24 h afforded the bimetallic Rh complex **3d** as an orange-brown powder in 40% yield (Scheme 2).[21] Although solution and solid-state[22] structural analyses indicated that **3d** and **3a** are superficially similar, a key difference is that the Rh atoms were now coplanar with the benzobis(imidazolylidene). Considering that the *N*-phenyl groups were rotated by an average of 63° relative to this same plane (minimizing any electronic contributions), and both complexes showed a similar *trans* effect (average Rh–olefin separation in **3a**: 2.20 Å, in **3d**: 2.19 Å), the size of the substituents on the N atoms appeared to dominate structural features about the metal centers.

Finally, we focused on the synthesis of bis(azolium) **4**, a desymmetrized precursor that was envisioned to provide a Janus bis(carbene) with differential characteristics at each carbene "face". The dissimilar environments of the 1,3-dimethyl- and 1,3-di-*tert*-butylimidazolium fragments were manifested in the ^{1}H NMR spectrum ([D_6]DMSO) of **4**, which exhibits signals at $\delta = 9.9$ and 9.0 ppm, respectively. Deprotonation of **4** using 2.1 equivalents of NaH (and catalytic KO*t*Bu) in toluene at 120 °C resulted in selective dimerization to afford enetetraamine **5**, which was subsequently isolated in 94% yield (Scheme 2). Crystals suitable for X-ray analysis were obtained by slow cooling of a saturated toluene solution

 © 2006 Wiley-VCH Verlag GmbH & Co. KGaA, Weinheim

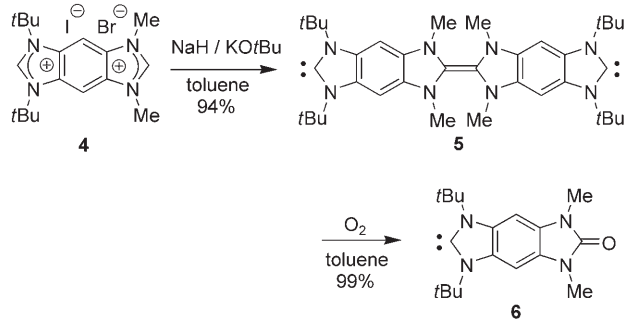

Scheme 2. Selective dimerization and oxidation of a desymmetrized Janus bis(carbene) precursor.

of **5**, and an ORTEP view of the structure of this compound is shown in Figure 4. Key bond lengths and angles of the benzimidazolylidene fragments were consistent with those of

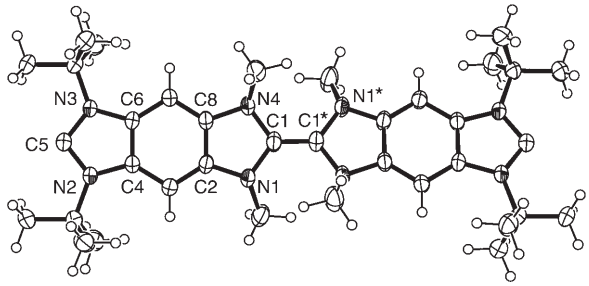

Figure 4. ORTEP view of **5** (ellipsoids at the 50% probability level). Selected bond lengths [Å] and angles [°]: C5-N3 1.366(3), C5-N2 1.371(3), N3-C6 1.406(2), N2-C4 1.404(3), C4-C6 1.397(3), C1-N1 1.426(3), C1-N4 1.424(3), N4-C8 1.416(3), N1-C2 1.408(2), C2-C8 1.399(3), C1-C1* 1.349(4); C1-N4-C18 117.79(18), N2-C5-N3 104.00(17), N1-C1-N4 108.48(16).

2b,[13] and the torsion angle about the enetetraamine was 15.2°, consistent with that of the dimer of 1,3-dimethylbenzimidazolylidene.[16a] The structure of **5** in solution was confirmed by treatment with O_2, which rapidly and selectively oxidized the enetetramine moiety to afford urea **6** (Scheme 2).[23]

In summary, we report the first Janus bis(carbene)s with facially opposed imidazolylidenes annulated to a common arene core. Synthetic routes employed to obtain these compounds were modular and high yielding, and permitted access to derivatives with *N*-alkyl or *N*-aryl substituents, as well as a desymmetrized variant. The promise of the Janus bis(carbene) ligands was borne out through synthesis of a variety of new homobimetallic complexes; efforts toward heterobimetallic complexes are currently underway.

Received: April 21, 2006
Revised: June 29, 2006
Published online: August 14, 2006

Keywords: azolium salts · carbene ligands · heterometallic complexes · organic–inorganic hybrid composites · transition metals

[1] a) P. Baxter, J.-M. Lehn, A. DeCian, J. Fischer, *Angew. Chem.* **1993**, *105*, 92; *Angew. Chem. Int. Ed. Engl.* **1993**, *32*, 69; b) S. Leininger, B. Olenyuk, P. J. Stang, *Chem. Rev.* **2000**, *100*, 853; c) F. A. Cotton, C. Lin, C. A. Murillo, *Acc. Chem. Res.* **2001**, *34*, 759; d) M. F. Lappert, *J. Organomet. Chem.* **2005**, *690*, 5467.

[2] For excellent reviews, see: a) W. A. Herrmann, K. Köcher, *Angew. Chem.* **1997**, *109*, 2256; *Angew. Chem. Int. Ed. Engl.* **1997**, *36*, 2162; b) A. J. Arduengo III, *Acc. Chem. Res.* **1999**, *32*, 913; c) D. Bourissou, O. Guerret, F. P. Gabbaï, G. Bertrand, *Chem. Rev.* **2000**, *100*, 39.

[3] a) A. J. Arduengo III, R. L. Harlow, M. Kline, *J. Am. Chem. Soc.* **1991**, *113*, 361; b) A. J. Arduengo III, F. Davidson, H. V. R. Dias, J. R. Goerlich, D. Khasnis, W. J. Marshall, T. K. Prakasha, *J. Am. Chem. Soc.* **1997**, *119*, 12742.

[4] a) M. F. Lappert, *J. Organomet. Chem.* **1988**, *358*, 185; b) W. A. Herrmann, *Angew. Chem.* **2002**, *114*, 1342; *Angew. Chem. Int. Ed.* **2002**, *41*, 1290; c) F. E. Hahn, *Angew. Chem.* **2006**, *118*, 1374; *Angew. Chem. Int. Ed.* **2006**, *45*, 1348.

[5] For representative examples, see:a) D. Enders, K. Breuer, G. Raabe, J. Runsink, J. H. Teles, J.-P. Melder, K. Ebel, S. Brode, *Angew. Chem.* **1995**, *107*, 1119; *Angew. Chem. Int. Ed. Engl.* **1995**, *34*, 1021; b) R. W. Alder, P. R. Allen, M. Murray, A. G. Orpen, *Angew. Chem.* **1996**, *108*, 1211; *Angew. Chem. Int. Ed. Engl.* **1996**, *35*, 1121; c) A. J. Arduengo III, J. R. Goerlich, W. J. Marshall, *Liebigs Ann.* **1997**, 365; d) R. Weiss, S. Reichel, M. Handke, F. Hampel, *Angew. Chem.* **1998**, *110*, 352; *Angew. Chem. Int. Ed.* **1998**, *37*, 344; e) C. Burstein, C. W. Lehmann, F. Glorius, *Tetrahedron* **2005**, *61*, 6207; f) C. Präsang, B. Donnadieu, G. Bertrand, *J. Am. Chem. Soc.* **2005**, *127*, 10182; g) A. J. Arduengo III, D. Tapu, W. J. Marshall, *J. Am. Chem. Soc.* **2005**, *127*, 16400.

[6] For theoretical treatments of NHC–metal interactions, see: a) C. Boehme, G. Frenking, *Organometallics* **1998**, *17*, 5801; b) D. S. McGuinness, N. Saendig, B. F. Yates, K. J. Cavell, *J. Am. Chem. Soc.* **2001**, *123*, 4029; c) D. V. Deubel, *Organometallics* **2002**, *21*, 4303; d) C. D. Abernethy, G. M. Codd, M. D. Spicer, M. K. Taylor, *J. Am. Chem. Soc.* **2003**, *125*, 1128; e) A. T. Termaten, M. Schakel, A. W. Ehlers, M. Lutz, A. L. Spek, K. Lammertsma, *Chem. Eur. J.* **2003**, *9*, 3577; f) X. Hu, I. Castro-Rodriguez, K. Olsen, K. Meyer, *Organometallics* **2004**, *23*, 755.

[7] For representative examples of bimetallic complexes formed between transition metals and (nonrigid) bis(carbene)s connected through saturated linkers, see: a) W. A. Herrmann, M. Elison, J. Fischer, C. Köcher, G. R. J. Artus, *Chem. Eur. J.* **1996**, *2*, 772; b) R. S. Simons, P. Custer, C. A. Tessier, W. J. Youngs, *Organometallics* **2003**, *22*, 1979; c) E. Peris, R. H. Crabtree, *Coord. Chem. Rev.* **2004**, *248*, 2239; d) F. E. Hahn, M. C. Jahnke, V. Gomez-Benitez, D. Morales-Morales, T. Pape, *Organometallics* **2005**, *24*, 6458.

[8] For other examples of bis(carbene) architectures, see:a) O. Guerret, S. Solé, H. Gornitzka, M. Teichert, G. Trinquier, G. Bertrand, *J. Am. Chem. Soc.* **1997**, *119*, 6668; b) W. Li, PhD thesis, University of Alabama, Tuscaloosa (USA), **2004**; c) B. Gehrhus, P. B. Hitchcock, M. F. Lappert, *Z. Anorg. Allg. Chem.* **2005**, *631*, 1383; d) A. J. Boydston, K. A. Williams, C. W. Bielawski, *J. Am. Chem. Soc.* **2005**, *127*, 12496.

[9] Janus ligands are named after the Roman god *Janus Geminus*, who is represented in Roman art as two-faced. The god has one face looking forward which is fused to another looking backward. For other examples of Janus-type molecules, see: a) S. J. Cristol, D. C. Lewis, *J. Am. Chem. Soc.* **1967**, *89*, 1476; b) A.

 © 2006 Wiley-VCH Verlag GmbH & Co. KGaA, Weinheim

Marsh, E. G. Nolen, K. M. Gardinier, J.-M. Lehn, *Tetrahedron Lett.* **1994**, *35*, 397.
[10] a) D. M. Khramov, A. J. Boydston, C. W. Bielawski, *Org. Lett.* **2006**, *8*, 1831; b) A. J. Boydston, D. M. Khramov, C. W. Bielawski, *Tetrahedron Lett.* **2006**, *47*, 5123.
[11] Addition of 1.0 equivalent of base to benzobis(imidazolium) salts **1** afforded polymeric materials,[24] see: A. J. Arduengo III, S. F. Gamper, M. Tamm, J. C. Calabrese, F. Davidson, H. A. Craig, *J. Am. Chem. Soc.* **1995**, *117*, 572.
[12] a) F. E. Hahn, L. Wittenbecher, R. Boese, D. Bläser, *Chem. Eur. J.* **1999**, *5*, 1931; b) F. M. Rivas, U. Riaz, A. Giessert, J. A. Smulik, S. T. Diver, *Org. Lett.* **2001**, *3*, 2673; c) S. Saravanakumar, A. I. Oprea, M. K. Kindermann, J. Heinicke, *Chem. Eur. J.* **2006**, *12*, 3143; d) F. E. Hahn, L. Wittenbecher, D. Le Van, R. Fröhlich, *Angew. Chem.* **2000**, *112*, 551; *Angew. Chem. Int. Ed.* **2000**, *39*, 541.
[13] The crystal structure of **2b** was also determined and found to be similar to that of **2a**.[24]
[14] For comparison, X-ray structures were determined for the bis(azolium) salts **1a**[24] and **1e**.[10b]
[15] a) A. J. Arduengo III, J. R. Goerlich, W. J. Marshall, *J. Am. Chem. Soc.* **1995**, *117*, 11027; b) M. K. Denk, A. Thadani, K. Hatano, A. J. Lough, *Angew. Chem.* **1997**, *109*, 2719; *Angew. Chem. Int. Ed. Engl.* **1997**, *36*, 2607; c) F. E. Hahn, M. Paas, D. Le Van, T. Lügger, *Angew. Chem.* **2003**, *115*, 5402; *Angew. Chem. Int. Ed.* **2003**, *42*, 5243.
[16] a) E. Çetinkaya, P. B. Hitchcock, H. Küçükbay, M. F. Lappert, S. J. Al-Juaid, *J. Organomet. Chem.* **1994**, *481*, 89; b) F. E. Hahn, T. von Fehren, L. Wittenbecher, R. Fröhlich, *Z. Naturforsch.* **2004**, *59b*, 544.
[17] These structural characteristics are consistent with [(cod)RhCl(1,3-diadamantylbenzimidazolylidene)].[24]
[18] Attempts to deprotonate **1d** and **1e** resulted in dark red solutions of polymeric materials, see: J. W. Kamplain, C. W. Bielawski, *Chem. Commun.* **2006**, 1727.
[19] H. M. J. Wang, I. J. B. Lin, *Organometallics* **1998**, *17*, 972.
[20] For an excellent review of Ag–NHC complexes, see: J. C. Garrison, W. J. Youngs, *Chem. Rev.* **2005**, *105*, 3978.
[21] Deprotonation of **1d** followed by addition of $[\{(cod)RhCl\}_2]$ also afforded complex **3d**, although in lower yields (34%).
[22] The X-ray crystal structure of **3d** was determined (structure not shown). Crystals were obtained by slow diffusion of hexanes into a saturated CH_2Cl_2 solution of **3d**.[24]
[23] For other examples of oxidizing NHC dimers with O_2, see: a) H. E. Winberg, J. E. Carnahan, D. D. Coffman, *J. Am. Chem. Soc.* **1965**, *87*, 2055; b) Z. Shi, R. P. Thummel, *J. Org. Chem.* **1995**, *60*, 5935.
[24] See the Supporting Information for additional details.

 © 2006 Wiley-VCH Verlag GmbH & Co. KGaA, Weinheim

Metallopolyynes

DOI: 10.1002/anie.200601651

White Metallopolyynes for Optical Limiting/Transparency Trade-off Optimization**

Gui-Jiang Zhou, Wai-Yeung Wong, Zhenyang Lin, and Cheng Ye*

With the rapid development of laser technology in the photonic era, the damage of human eyes, optical sensors, and sensitive optical components caused by exposure to sudden intense laser pulses has driven many researchers to become involved in the search for effective optical limiters that possess high solubility, fast response speeds, good linear transparency, and high linear transmission.[1] Optical limiters are materials that protect sensitive electro-optical sensors against intrusive, possibly damaging, frequency-agile pulsed laser irradiation.[2] Currently, the materials employed for optical-power limiting (OPL) are largely small molecules such as fullerenes (C_{60}),[3] phthalocyanines,[2b,4] porphyrins,[5] diacetylenes,[6] nanotubes,[7] and organometallic compounds.[8] Among these, metallophthalocyanines and metalloporphyrins are the most effective optical limiters as the heavy metal effect magnifies the OPL response by enhancement of the intersystem crossing (ISC) from S_1 to T_1 states.[9] However, their poor solubility and the technical difficulties associated with fabricating OPL devices have hindered their practical applications so far. The deep colors of fullerenes, phthalocyanines, and porphyrins also hamper their use in practical devices for the protection of human eyes because there are unavoidable absorption bands in the visible wavelength region.[2a,10] While it is known that a bathochromic shift of the ground-state absorption maximum (λ_{max}) generally leads to an increase in the third-order optical nonlinearity,[11] previously reported excellent optical limiters have not yet achieved nonlinearity/transparency trade-off optimization. Recent work has shown that some conjugated organic

[*] Dr. G.-J. Zhou, Dr. W.-Y. Wong
Department of Chemistry
Hong Kong Baptist University
Waterloo Road, Kowloon Tong, Hong Kong (P.R. China)
Fax: (+852) 3411-7348
E-mail: rwywong@hkbu.edu.hk
Dr. Z. Lin
Department of Chemistry
The Hong Kong University of Science and Technology
Clearwater Bay, Hong Kong (P.R. China)
Prof. C. Ye
Centre for Molecular Science, Institute of Chemistry
Chinese Academy of Sciences
Beijing 100080 (P.R. China)

[**] This work was supported by a CERG grant from the Research Grants Council of the Hong Kong SAR, P.R. China (project no. HKBU 2022/03P) and Hong Kong Baptist University.

Supporting Information for this article is available on the WWW under http://www.angewandte.org or from the author.

© 2006 Wiley-VCH Verlag GmbH & Co. KGaA, Weinheim

polyynes are good OPL materials with a performance close to that of C_{60}; however, their λ_{max} values still go beyond 400 nm.[12] Although small-molecule platinum acetylides[13] and their dendritic structures[13e,14] have been shown to be good chromophores for OPL, less attention has been paid to the corresponding metallopolyynes,[13g] and related studies in mercury-derived arylene–ethynylene copolymers remain unexplored. Here, we report the unprecedented examples of some solution-processable white homo- and heterometallic polyynes that reveal superior OPL/transparency trade-offs.

The synthesis of the metal polyynes and their well-defined model compounds is shown in Scheme 1 (the use of long octyl chains can increase the solubility of metallopolymers). Interestingly, **Pt-Hg-P** is the first rigid-rod heteronuclear Pt^{II}/Hg^{II} σ-alkynyl polymer and is soluble in organic solvents. All compounds were isolated as stable white/off-white solids in high purity. The model compounds were investigated by comparing their electronic and structural properties with the parent polymers and studying the effect of chain length in the OPL phenomenon. The high decomposition temperatures of the samples (366–406 °C) indicate their good thermal stability. The rigid-rod nature of the polymer is best illustrated by the X-ray structure of **Pt-Hg-T** (see Supporting Information),[15] which also provides valuable structural information for the computational studies. While there is a transparency window at 532 nm for all the materials, the OPL response was measured as a 92% transmitting solution at this wavelength using the Z-scan method. From Figure 1a and 1b, it is clear that all of them show excellent OPLs at a high linear transmittance of 92%; these values are superior to current state-of-the-art materials such as C_{60}, Zn^{II}-tetrakis(4-phenyl)-porphyrin (Zn-TPP), and Cu^{II}-tetrakis(*tert*-butyl)phthalocyanine (CuPc-*t*Bu_4). We also found that the mercury atom plays a key role in this enhanced OPL performance.

Based on the five-level reverse saturable absorption (RSA) mechanism,[16] the system can be reduced to a three-level one by assuming that there is no saturation, diffusion, or recombination during the laser pulse. Thus, we can neglect all the excitations higher than the first singlet excitation (S_1) provided that the ISC rate is fast (compared with the laser pulse duration) and all of the initial excitations are populated in the first triplet state (T_1). Excitation of the T_1 state leads to the nonlinear absorption, and the strong energy absorption that is accompanied by a $T_1 \rightarrow T_n$ transition serves as a major contributor to the nanosecond OPL behavior.

Owing to the short lifetime of the S_1 state (< 10 ns), the triplet state plays a pivotal role in the nonlinear optical process, therefore photoluminescence (PL) spectra were

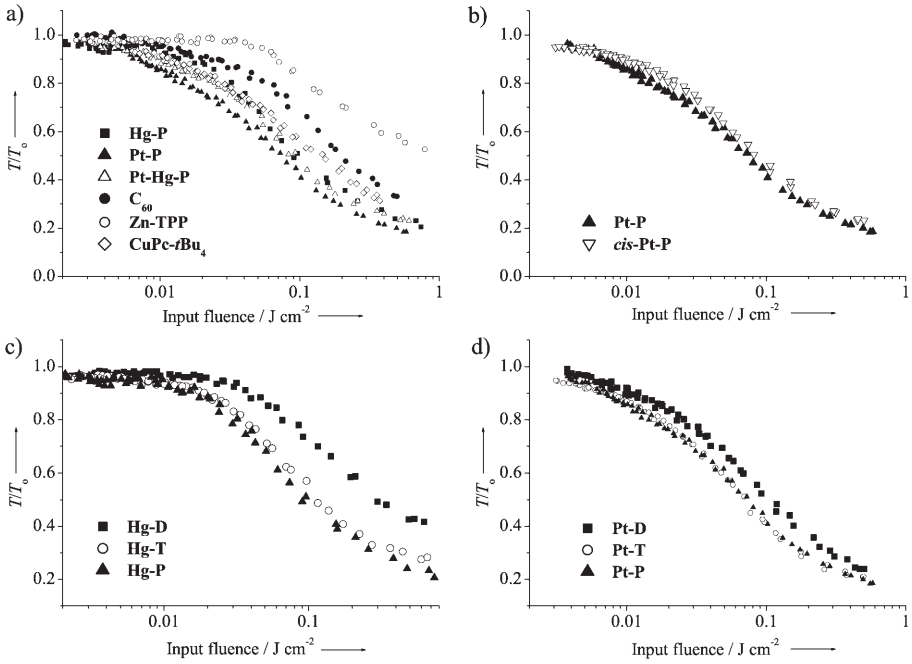

Figure 1. Normalized transmittance (T/T_o) of metal polyynes and their model complexes at the same linear transmittance (T_o = 92%) versus incident fluence (T_o = 86% for C_{60}, Zn-TPP, and CuPc-*t*Bu_4).

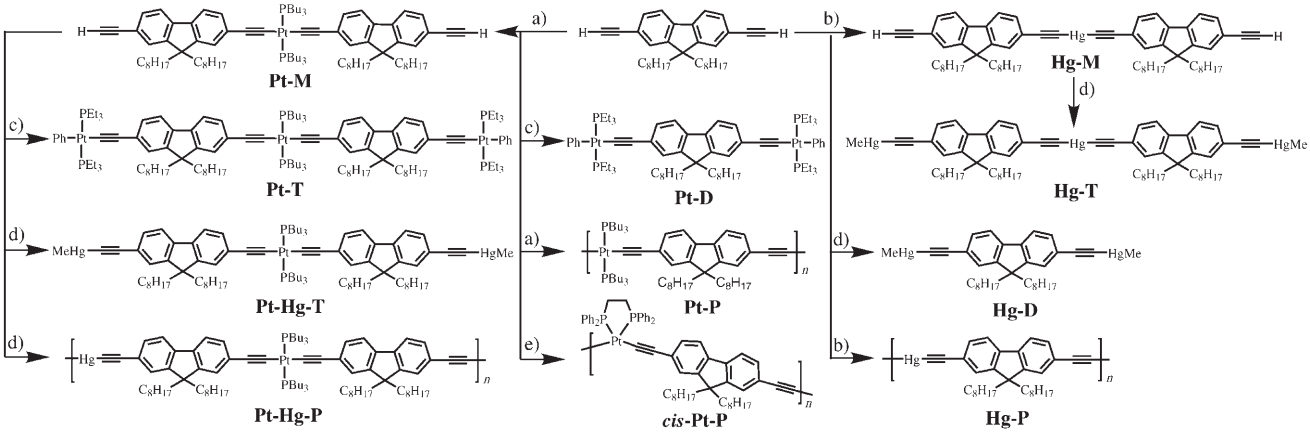

Scheme 1. Synthesis of the metal polyynes and model complexes. a) *trans*-[$PtCl_2(PBu_3)_2$], CuI, *i*Pr_2NH; b) $HgCl_2$, NaOMe; c) *trans*-[PtPh(Cl)-(PBu_3)$_2$], CuI, *i*Pr_2NH; d) MeHgCl, NaOMe; e) [$PtCl_2$(dppe)], CuI, *i*Pr_2NH. dppe = 1,2-bis(diphenylphosphanyl)ethane.

 © 2006 Wiley-VCH Verlag GmbH & Co. KGaA, Weinheim

measured for the singlet and triplet states (Figure 2). These PL spectra show an intense triplet emission at 77 K, which is attributed to the strong spin–orbit coupling between the ligand π and the metal d orbitals in the polyynes.[13c,d] To confirm this, molecular orbital calculations on **Pt-M**, **Hg-M**, and **Pt-Hg-T** as models for **Pt-P**, **Hg-P**, and **Pt-Hg-P**, respectively, were carried out at the B3LYP level of density functional theory based on their experimental geometries. In general, the HOMO and LUMO are mainly confined to the π and π* orbitals of the conjugated organic ligands, although mixing of the metal d_π orbitals with the ligand π orbitals in the HOMOs can also be seen. The contribution of the d_π orbitals of Pt^{II} in both **Pt-M** and **Pt-Hg-T** and Hg^{II} in **Hg-M** to the HOMOs of their corresponding complexes is 13.2%, 10.2%, and 0.5%, respectively, according to the Mulliken population analysis (see Supporting Information). It is known that spin–orbit coupling increases with the extent of metal–ligand orbital mixing, therefore **Pt-P** and **Pt-Hg-T**, which show a stronger spin–orbit coupling effect, have a more effective ISC that gives rise to a larger OPL response according to the RSA mechanism. These theoretical results were confirmed experimentally by the observation of weak triplet emission at room temperature in **Pt-P** and **Pt-Hg-P**, which is almost absent in **Hg-P**, and their slightly stronger OPL compared with that of **Hg-P**. In spite of this, the OPL performance of **Hg-P** is still attractive, and indicates that the OPL effect is not only induced by the triplet absorption. To look for a possible mechanism, we can see from the DFT results that the contribution from the d_π orbitals of Hg^{II} to the HOMO of **Hg-M** is only 0.5%, while the metal p_π orbitals contribute 19.6% to its LUMO. This reveals that the $S_0 \rightarrow S_1$ electronic transition of **Hg-P** due to $\pi(C{\equiv}CR) \rightarrow \pi^*(C{\equiv}CR)$ orbitals also possesses charge-transfer (CT) character.[9b] Its OPL effects may be enhanced by the strong absorption of CT states, which is known to be beneficial to OPL in other organometallic systems.[13b]

We have recognized the salient problem of how to increase the optical transparency range while maintaining the OPL response of the polymers constant. In order to improve the transparency window of **Pt-P** further, it is highly desirable to reduce its dragged absorption tail behind 400 nm by reducing the π-conjugation. Normally, if the π-conjugation is reduced the optical nonlinearity, and hence the OPL effect, will be lessened.[17] However, from Figure 1c and 1d it is evident that the conjugation factor will become less important as the chain length is increased up to the trimer, and **Hg-T** (or **Pt-T**) shows almost the same OPL as that of **Hg-P** (or **Pt-P**). As the order of π-delocalization through the metal chromophore is $Pt^{II} > Hg^{II}$, we expect that coupling of Hg^{II} to the backbone of **Pt-P** breaks the π-conjugation to some extent but favorably optimizes the transparency/nonlinearity trade-off. As mentioned earlier, intramolecular CT states exist between the Hg ion and the conjugated ligand that would also contribute to the OPL action of **Pt-Hg-P**. So, copolymerization of **Pt-M** with Hg^{II} ion in the polyyne backbone will shorten the conjugation length of the ligands and result in a higher energy triplet state accompanied by an increase in the triplet quantum yield (Φ_P), in accordance with the energy-gap law for the triplet states in metal polyynes.[18] This is also reflected by the lower singlet quantum yield (Φ_F) of **Pt-Hg-P** compared with that of **Pt-P** (see Supporting Information). Pertaining to the RSA mechanism, we note that the contribution of an increased Φ_P of **Pt-Hg-P** to OPL can compensate for the loss in OPL due to interruption of the conjugation by Hg, hence **Pt-Hg-P** still shows a similar OPL to that of **Pt-P** (Figure 1a). In addition, **Pt-Hg-P** has an improved transparency window for optimizing the properties of OPL materials of this kind ($\lambda_{max} = 386$ nm for **Pt-Hg-P** vs. 399 nm for **Pt-P**, with the former being whiter than the latter). By following the same approach to increase Φ_P through such a conjugation-breaking strategy, *cis*-**Pt-P** was designed and synthesized.[19] By changing from a *trans*- to a *cis*-configured Pt^{II} unit, the conjugation chain in *cis*-**Pt-P** remains disturbed ($\lambda_{max} = 364$ nm). What is remarkable here is that *cis*-**Pt-P** shows almost the same OPL as **Pt-P** (Figure 1b), thus indicating that the negative effect on OPL caused by conjugation-interruption can be overcome effectively by the positive contribution of increased Φ_P. This is supported by the much stronger triplet emission at 298 K (Figure 2a) and much lower Φ_F for *cis*-**Pt-P** compared with that of **Pt-P**.

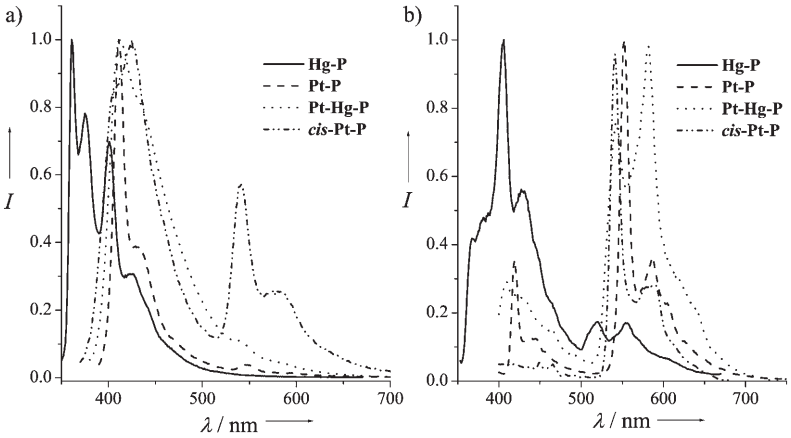

Figure 2. PL spectra for the metal polyynes in CH_2Cl_2 at a) 298 K and b) 77 K.

Comparing the UV/Vis spectra of the polyynes and common optical-limiting materials currently in use (Figure 3), the merits of our polyynes as RSA optical limiters for protecting eyes and optical sensors are obvious. They are all white powders with very good transparencies in the visible region, and *cis*-**Pt-P** in particular has a high triplet yield, all of which makes these metallopolyynes excellent for OPL applications. Some of the best ever materials, including CuPc-*t*Bu_4, Zn-TPP, and C_{60}, are all deeply colored with strong visible absorption bands, therefore their poor optical transparencies will make them less competitive with our metallopolyynes as optical limiters for the protection of human eyes.

The performance of excited-state absorbers can be quantitatively characterized by the Figure of Merit factor

 © 2006 Wiley-VCH Verlag GmbH & Co. KGaA, Weinheim

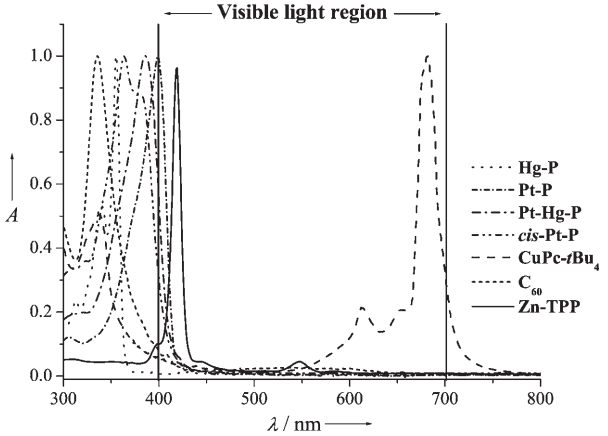

Figure 3. Comparison of the optical transparency of our metal polyynes with some good optical limiters.

σ_{eff}/σ_o, where σ_{eff} and σ_o are the effective excited-state and ground-state absorption cross-sections, respectively. From Table 1, it is clear that our metallopolymers are efficient

Table 1: Comparison of the optical limiting parameters of metal polyynes with some state-of-the-art materials.

Compound	F_{th} [J cm^{-2}][a]	T_o [%][b]	L [mm][c]	σ_{eff}/σ_o[d]
[{tri(*n*-hexyl)siloxy}InPc][4a]	0.070	84	10	16[4a]
[{tri(*n*-hexyl)siloxy}AlPc][4a]	0.26	84	10	10[4a]
[{tri(*n*-hexyl)siloxy}GaPc][4a]	0.12	84	10	14[4a]
PbPc(β-CP)$_4$[20a]	0.070	62	[e]	[e]
CuPc-*t*Bu$_4$[20b]	0.10	[e]	[e]	[e]
CuPc-*t*Bu$_4$	0.13	86	1	6.20
C_{60}[20c]	0.18	55	2	[e]
C_{60}	0.19	84	1	3.89
Hg-P	0.11	92	1	20.81
Pt-P	0.070	92	1	19.07
Pt-Hg-P	0.083	92	1	18.32
cis-**Pt-P**	0.080	92	1	18.62

[a] Optical-limiting threshold, F_{th}, defined as the input light fluence at which the output light fluence is 50% of that predicted by linear transmittance. [b] T_o is the linear transmittance. [c] Sample thickness. [d] $\sigma_{eff}/\sigma_o = \ln T_{sat}/\ln T_o$, where σ_{eff} is the effective excited-state absorption cross-section, σ_o is the ground-state absorption cross-section, and T_{sat} is the transmittance at the saturation fluence. [d] Not reported.

OPLs with very impressive σ_{eff}/σ_o values (18.3–20.8), which exceed by a factor of about five that of C_{60}, a benchmark optical limiter. These figures are also remarkably higher than those of various popular metal phthalocyanines. Moreover, *cis*-**Pt-P**, **Pt-P**, and **Pt-Hg-P** manifest very low optical-limiting thresholds in the narrow range of 0.07–0.11 J cm^{-2} at 92% linear transmittance; these characteristics approach those necessary for a practical device. These thresholds are comparable to those of the best InPc and PbPc dyes (T_o = 84%) currently in use (Table 1).

In conclusion, we have reported the first study of a series of soluble and tractable metallopolyynes with substantial OPL responses that perform better than some state-of-the-art optical limiters. Importantly, we can greatly improve the transparency window of the polyynes in the visible regime, whilst maintaining their OPL performance, by interrupting π-conjugation by copolymerizing with Hg and tuning the Pt geometry. These results are an encouraging milestone in the progress towards commercially viable optical-limiting polymers with optimized transparency/OPL trade-offs.

Experimental Section

Pt-Hg-T: **Pt-M** (0.100 g, 0.068 mmol) and MeHgCl (0.043 g, 0.169 mmol) were mixed in MeOH/CH_2Cl_2 (40 mL, 1:40, v/v) to form a clear solution. A basic NaOMe solution (1.0 mL, 0.2 mmol L^{-1} in MeOH) was added to the mixture at room temperature. After stirring the mixture overnight at room temperature, it was filtered and the filtrate was allowed to evaporate slowly to form pale-yellow crystals of **Pt-Hg-T**. These were collected and recrystallized from a CH_2Cl_2/MeOH (3:1, v/v) solution (yield: 0.085 g, 66%).

cis-**Pt-P**: 2,7-Diethynyl-9,9-dioctylfluorene (0.055 g, 0.126 mmol), [$PtCl_2$(dppe)] (0.083 g, 0.126 mmol), and CuI (3 mg) were mixed in NEt_3/CH_2Cl_2 (40 mL, 1:10, v/v) at room temperature. After stirring overnight at room temperature, the reaction mixture was filtered through a short pad of silica gel. The filtrate was concentrated and the solution was poured into MeOH (50 mL). The polymer powder was collected, washed with hexane, and dried under vacuum (yield: 0.097 g, 75%).

Pt-Hg-P: **Pt-M** (0.150 g, 0.102 mmol) and $HgCl_2$ (0.028 g, 0.102 mmol) were dissolved in MeOH/CH_2Cl_2 (40 mL, 1:50, v/v) at room temperature. A basic NaOMe solution (1.2 mL, 0.2 mmol L^{-1} in MeOH) was added. After stirring the reaction mixture overnight at room temperature, it was filtered through a short pad of silica gel to remove the insoluble solid. The solvent was removed under reduced pressure. The residue was dissolved in a minimum volume of CH_2Cl_2 (6 mL) and the solution poured into MeOH (50 mL). The white precipitate was collected by filtration and washed with hexane to afford the copolymer (yield: 0.125 g, 73%). All the spectroscopic data can be found in the Supporting Information.

Received: April 26, 2006
Revised: June 21, 2006
Published online: August 17, 2006

Keywords: alkynes · mercury · platinum · polymers · polyynes

[1] C. W. Spangler, *J. Mater. Chem.* **1999**, *9*, 2013–2020, and references therein.
[2] a) T. J. Mckay, J. Staromlynska, P. Wilson, J. Davy, *J. Appl. Phys.* **1999**, *85*, 1337–1341; b) J. W. Perry, K. Mansour, I.-Y. S. Lee, X.-L. Wu, P. V. Bedworth, C.-T. Chen, D. Ng, S. R. Marder, P. Miles, T. Wada, M. Tian, H. Sasabe, *Science* **1996**, *273*, 1533–1536.
[3] a) L. W. Tutt, A. Kost, *Nature* **1992**, *356*, 225–226; b) M. Cha, N. S. Sariciftci, A. J. Heeger, J. C. Hummelen, F. Wudl, *Appl. Phys. Lett.* **1995**, *67*, 3850–3852.
[4] a) J. W. Perry, K. Mansour, S. R. Marder, K. J. Perry, D. Alvarez, Jr., I. Choong, *Opt. Lett.* **1994**, *19*, 625–627; b) J. S. Shirk, R. G. S. Pong, F. J. Bartoli, A. W. Snow, *Appl. Phys. Lett.* **1993**, *63*, 1880–1882; c) T. H. Wie, D. J. Hagan, M. J. Sence, E. W. van Stryland, J. W. Perry, D. R. Coulter, *Appl. Phys. B* **1992**, *54*, 46–51.
[5] a) W. Blau, H. Byrne, W. M. Dennis, J. M. Kelly, *Opt. Commun.* **1985**, *56*, 25–29; b) K. McEwan, K. Lewis, G.-Y. Yang, L.-L. Chng, Y.-W. Lee, W.-P. Lau, K.-S. Lai, *Adv. Funct. Mater.* **2003**, *13*, 863–867.
[6] P. Zhu, C. Yu, J. Liu, Y. Song, C. Li, *Proc. SPIE-Int. Soc. Opt. Eng.* **1996**, *2879*, 289–294.
[7] B. Z. Tang, H. Y. Xu, *Macromolecules* **1999**, *32*, 2569–2576.
[8] a) M. Pittman, P. Plaza, M. M. Martin, Y. H. Meyer, *Opt. Commun.* **1998**, *158*, 201–212; b) G. R. Allan, D. R. Labergerie,

 © 2006 Wiley-VCH Verlag GmbH & Co. KGaA, Weinheim

S. J. Rychnovsky, T. F. Boggess, A. L. Smirl, L. Tutt, *J. Phys. Chem.* **1992**, *96*, 6313 – 6317; c) S. Shi, W. Ji, X. Q. Xin, *J. Phys. Chem.* **1995**, *99*, 894 – 898.

[9] a) J. E. Rogers, B. C. Hall, D. C. Hufnagle, J. E. Slagle, A. P. Ault, D. G. McLean, P. A. Fleitz, T. M. Cooper, *J. Chem. Phys.* **2005**, *122*, 214708-1–214708-8; b) J. E. Rogers, T. M. Cooper, P. A. Fleitz, D. J. Glass, D. G. McLean, *J. Phys. Chem. A* **2002**, *106*, 10108 – 10115; c) T. M. Cooper, B. C. Hall, D. G. McLean, J. E. Rogers, A. R. Burke, K. Turnbull, A. Weisner, A. Fratini, Y. Liu, K. S. Schanze, *J. Phys. Chem. A* **2005**, *109*, 999 – 1007; d) A. Krivokapic, H. L. Anderson, G. Bourhill, R. Ives, S. Clark, K. J. McEwan, *Adv. Mater.* **2001**, *13*, 652 – 656; e) J. S. Shirk, R. G. S. Pong, S. R. Flom, H. Heckmann, M. Hanack, *J. Phys. Chem. A* **2000**, *104*, 1438 – 1449; f) R. B. Martin, H. P. Li, L. R. Gu, S. Kumar, C. M. Sanders, Y. P. Sun, *Opt. Mater.* **2005**, *27*, 1340 – 1345.

[10] J. W. Perry, K. Mansour, S. R. Marder, C. T. Chen, P. Miles, M. E. Kenney, G. Kwag, *Mater. Res. Soc. Symp. Proc.* **1995**, *374*, 257 – 265.

[11] L. T. Cheng, W. Tam, S. H. Stevenson, G. R. Meredith, G. Rikken, S. R. Marder, *J. Phys. Chem.* **1991**, *95*, 10631 – 10643.

[12] G. J. Zhou, S. Zhang, P. J. Wu, C. Ye, *Chem. Phys. Lett.* **2002**, *363*, 610 – 614.

[13] a) P. Nguyen, G. Lesley, T. B. Marder, I. Ledoux, J. Zyss, *Chem. Mater.* **1997**, *9*, 406 – 408; b) F. Guo, W. Sun, Y. Liu, K. Schanze, *Inorg. Chem.* **2005**, *44*, 4055 – 4065; c) J. Staromlynska, T. J. McKay, J. A. Bolger, J. R. Davy, *J. Opt. Soc. Am. B* **1998**, *15*, 1731 – 1735; d) T. J. McKay, J. A. Bolger, J. Staromlynska, J. R. Davy, *J. Chem. Phys.* **1998**, *108*, 5537 – 5541; e) C. E. Powell, M. G. Humphrey, *Coord. Chem. Rev.* **2004**, *248*, 725 – 756; f) I. R. Whittall, M. G. Humphrey, M. Samoc, B. Luther-Davies, *Angew. Chem.* **1997**, *109*, 386 – 388; *Angew. Chem. Int. Ed. Engl.* **1997**, *36*, 370 – 371; g) I. Manners, *Synthetic Metal-Containing Polymers*, Wiley-VCH, Weinheim, **2004**.

[14] R. Vestberg, R. Westlund, A. Eriksson, C. Lopes, M. Carlsson, B. Eliasson, E. Glimsdal, M. Lindgren, E. Malmström, *Macromolecules* **2006**, *39*, 2238 – 2246.

[15] CCDC-605324 contains the supplementary crystallographic data for this paper. These data can be obtained free of charge from The Cambridge Crystallographic Data Centre via www.ccdc.cam.ac.uk/data_request/cif.

[16] G. L. Wood, M. J. Miller, A. G. Mott, *Opt. Lett.* **1995**, *20*, 973 – 975.

[17] N. J. Long, *Angew. Chem.* **1995**, *107*, 37-56; *Angew. Chem. Int. Ed. Engl.* **1995**, *34*, 21 – 38.

[18] J. S. Wilson, N. Chawdhury, M. R. A. Al-Mandhary, M. Younus, M. S. Khan, P. R. Raithby, A. Köhler, R. H. Friend, *J. Am. Chem. Soc.* **2001**, *123*, 9412 – 9417.

[19] a) N. J. Long, C. K. Wong, A. J. P. White, *Organometallics* **2006**, *25*, 2525 – 2532; b) R. Saha, M. Abdul Qaium, D. Debnath, M. Younus, N. Chawdhury, N. Sultana, G. K. Kociok-Köhn, L. L. Ooi, P. R. Raithby, M. Kijima, *Dalton Trans.* **2005**, 2760 – 2765.

[20] a) J. S. Shirk, R. G. S. Pong, S. R. Flom, F. J. Bartoli, M. E. Boyle, A. W. Snow, *Pure Appl. Opt.* **1996**, *5*, 701 – 707; b) P. W. Zhu, P. Wang, W. F. Qiu, Y. Q. Liu, C. Ye, G. Y. Fang, Y. L. Song, *Appl. Phys. Lett.* **2001**, *78*, 1319 – 1321; c) Y. P. Sun, J. E. Riggs, B. Liu, *Chem. Mater.* **1997**, *9*, 1268 – 1274.

 © 2006 Wiley-VCH Verlag GmbH & Co. KGaA, Weinheim

Chirality

DOI: 10.1002/anie.200601869

Configurationally Stable Molecular Propellers: First Resolution of Residual Enantiomers**

*Tiziana Benincori, Giuseppe Celentano, Tullio Pilati, Alessandro Ponti, Simona Rizzo, and Francesco Sannicolò**

There is general consensus that three-bladed propeller-shaped molecules are operationally achiral because of the easy reversal of helicity at room temperature. A few attempts to control the specific configuration of the propeller were based on the introduction of chiral substituents.[1–3] We supposed that molecular propellers bearing identical blades devoid of any rigid stereogenic element could be obtained as configurationally stable enantiomers by exploiting residual stereoisomerism,[4–8] a phenomenon discovered by Mislow and up until now considered just as an academic facet of stereochemistry. Strict correlation of the ring torsional motion is a necessary condition for the existence of residual stereoisomerism.[4] We considered that this requirement is well satisfied in tris(2-alkyl-1-methyl-3-indolyl)phosphine oxides **1**, which are readily prepared in good yield from 2-alkyl-1-methylindoles (Scheme 1). The motional correlation is enhanced by increasing the size of the *ortho* group from methyl to ethyl and isopropyl (**1a**–**c**).

There are eight predictable chiral stereoisomers for **1**, which form four enantiomeric pairs[9] (Scheme 2). We used a sequence of four descriptors to describe each stereoisomer,

[*] Prof. F. Sannicolò
Dipartimento di Chimica Organica e Industriale
Università di Milano and CIMaINa—Centro Interdisciplinare Materiali e Interfacce Nanostrutturati
via Venezian 21 and via Celoria 16, 20133 Milano (Italy)
Fax: (+39) 02-5031-4139
E-mail: staclaus@unimi.it

Dr. T. Pilati, Dr. A. Ponti, Dr. S. Rizzo
Istituto di Scienze e Tecnologie Molecolari—CNR
via Golgi 19, 20133 Milano (Italy)

Prof. T. Benincori
Dipartimento di Scienze Chimiche ed Ambientali
Università dell'Insubria
via Valleggio 11, 22100 Como (Italy)

G. Celentano
Istituto di Chimica Organica "A. Marchesini"
Università di Milano
via Golgi 19, 20133 Milano (Italy)

[**] We thank Prof. M. Pierini (University of Rome "La Sapienza") for a preliminary HPLC simulation, Prof. M. Gullotti (University of Milan) for CD spectra, and Jasco Europe Srl for technical assistance in HPLC experiments with a circular dichroism detector. T.B. is grateful to the Dipartimento di Chimica Organica e Industriale of the Università di Milano for hospitality. Financial support from project FIRB2003-RBNE033 KMIA is acknowledged.

Supporting information for this article is available on the WWW under http://www.angewandte.org or from the author.

© 2006 Wiley-VCH Verlag GmbH & Co. KGaA, Weinheim

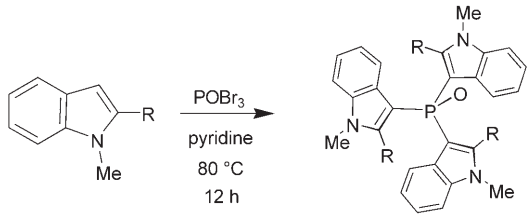

1a R = Me
1b R = Et
1c R = *i*Pr

Scheme 1. The preparation of tris(2-alkyl-1-methyl-3-indolyl)phosphine oxides **1**.

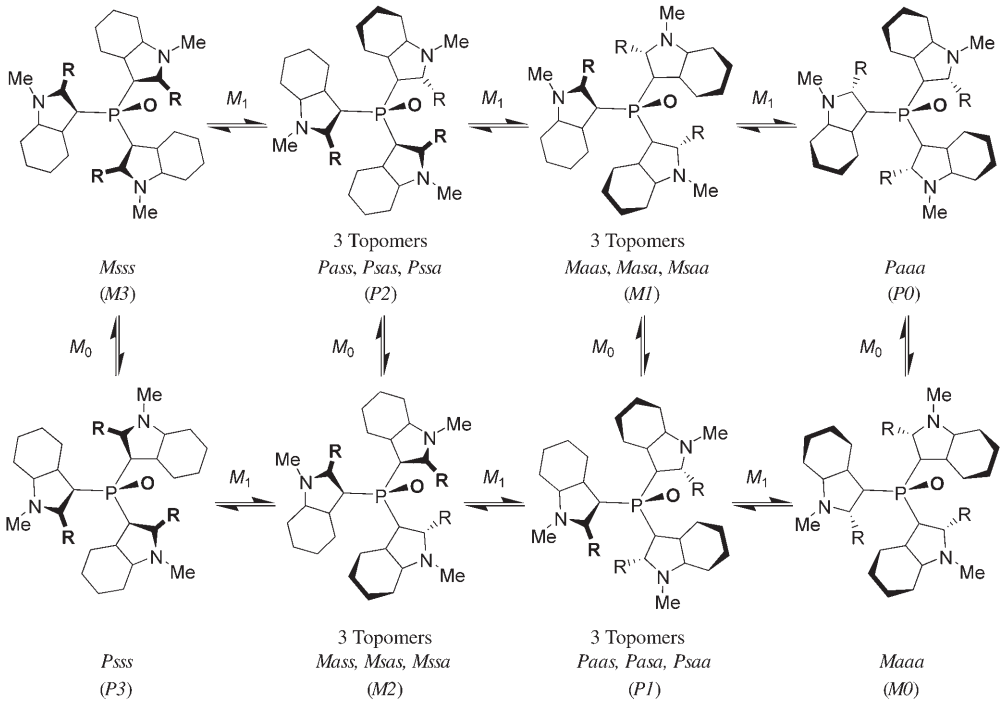

Scheme 2. The eight possible stereoisomers of **1** and their interconversion processes. Each row, which comprises four stereoisomers, represents the residual enantiomers. The double bonds of the indole structures are omitted for clarity.

the first one refers to the helicity (*P*, *M*) and the three others describe the orientation of the priority (CIP rules) edge of each ring with respect to the P=O bond. We used indices *s* (contraction of *syn*) and *a* (contraction of *anti*) according to the usual rules for simple rotors. Given the identity of the aryl rings, one can also use a simpler notation *Xn* (in brackets in Scheme 2), *X* is the helicity and *n* is the number of rings with index *s*. There are four stereomerization mechanisms M_k, characterized by the number ($k = 0, 1, 2, 3$) of rings undergoing edge interchange with respect to the reference plane (the plane defined by the three carbon atoms bound to the phosphorus atom). The other rings "flip", that is, they pass through a plane perpendicular to the reference plane. All four isomerizations involve helicity reversal.[9] The M_1 mechanism,[6,7,10–13] which involves one edge interchange and two ring flips is, without known exception, the threshold stereomerization mechanism.[11] It does not allow free interconversion inside the full set of eight isomers, but only within two closed subsets of four isomers each, namely {*M3*, *P2*, *M1*, *P0*} and {*P3*, *M2*, *P1*, *M0*}. As the stereoisomers belonging to one subset are enantiomers of those present in the other one, the two subsets of isomers are residual enantiomers. The M_0 mechanism only inverts the helicity and therefore converts any stereoisomer into its enantiomer; M_2 also converts stereoisomers from different subsets, whereas M_3 converts stereoisomers within a single subset.

Before undertaking the difficult task of the resolution of **1**, we resorted to DFT-B3LYP calculations to check whether the residual enantiomers of **1** could be stable enough to be separated. The main computational results are reported in Table 1 and Table 2. The most stable isomers are *X3* ($X = M, P$) in all cases. The *X3* isomers largely predominate with a molar fraction larger than 98% at 298 K, small amounts of *X2* isomers can be present with a molar fraction of less than 2%, and the *X1* and *X0* isomers are virtually absent. The activation barriers involved in the M_1 mechanism are low enough that the M_1 isomerizations should be fast even at room temperature. The barriers of the M_0 mechanism are higher than 100 kJ mol^{-1}. M_0 stereomerization is slower than M_1 as all three indole moieties are parallel to the P=O bond and steric strain is larger in its transition states. The antipodes of **1a** should be not configurationally stable enough at room temperature to be isolated in a pure state (enantiomerization half-life, $t_{1/2} \cong 2$ days), whereas **1b** ($t_{1/2} \cong 1$ month) and **1c** ($t_{1/2} \cong 10^4$ years) are increasingly stable. The transition

Table 1: Computed relative energies and Boltzmann population of the stereoisomers of tris(2-alkyl-1-methyl-3-indolyl)phosphine-oxides **1a**–**c**.[a]

Isomer	**1a**		**1b**		**1c**	
	ΔE [kJ mol^{-1}]	Population [%]	ΔE [kJ mol^{-1}]	Population [%]	ΔE [kJ mol^{-1}]	Population [%]
X3	0	98.6	0	99.4	0	97.8
X2	13	1.4	15	0.6	12	2.2
X1	27	0.0	39	0.0	27	0.0
X0	39	0.0	58	0.0	37	0.0

[a] DFT B3LYP/3-21G* calculations with thermal correction within the harmonic approximation; relative energies ΔE and percentage Boltzmann population are given.

 © 2006 Wiley-VCH Verlag GmbH & Co. KGaA, Weinheim

Table 2: Computed activation parameters for the *M3*⇌*P2* and *M3*⇌*P3* stereomerizations by the M_1 and M_0 mechanisms, respectively, in **1a–c**.[a]

Process	Parameter	1a	1b	1c
M3⇌*P2* via M_1	$\Delta E^{\neq}$ [kJ mol^{-1}]	33	38	36
	$\Delta H^{\neq}$ [kJ mol^{-1}]	29	34	33
	$\Delta S^{\neq}$ [J K^{-1} mol^{-1}]	−30	−54	−26
	$\Delta G^{\neq}_{25^\circ C}$ [kJ mol^{-1}]	38	51	40
M3⇌*P3* via M_0	$\Delta E^{\neq}$ [kJ mol^{-1}]	98	104	122
	$\Delta H^{\neq}$ [kJ mol^{-1}]	95	100	130
	$\Delta S^{\neq}$ [J K^{-1} mol^{-1}]	−33	−36	−47
	$\Delta G^{\neq}_{25^\circ C}$ [kJ mol^{-1}]	105	111	144
	$t_{1/2}$ (25 °C)	≈2 days	≈1 month	≈10^4 years

[a] DFT B3LYP/3-21G* calculations with thermal correction within the harmonic approximation: Activation enthalpy ($\Delta H^{\neq}$), entropy ($\Delta S^{\neq}$), free energy at 25 °C ($\Delta G^{\neq}_{25^\circ C}$), and enantiomerization half-life at 25 °C ($t_{1/2}$(25 °C)).

states for the M_2 and M_3 mechanisms could not be located as a result of the huge steric overcrowding between edge exchanging rings. Hence, the picture that arises from the computational results is that 1) *M3* and *P3* are the major isomers in all cases; 2) M_1 isomerizations within each residual enantiomer are fast at room temperature in all cases; 3) the rate of the M_0 isomerization, and thus the configurational stability of residual antipodes, is very sensitive to the size of the *ortho* alkyl substituent and small enough that the more sterically crowded terms are configurationally stable.

In agreement with the calculations, only *X3* isomers were observed by X-ray diffraction (XRD) studies in the crystals of **1a–c** (see Figure 1a and the Supporting Information). Also ^{1}H and ^{13}C NMR spectroscopic analysis revealed the presence of a single C_3-symmetric enantiomeric pair in solution down to −90 °C.

Resolution by chiral HPLC with a circular dichroism (CD) detector provided the experimental proof that **1a** is a residual racemate. The first eluted enantiomer shows negative ellipticity at $\lambda = 230$ nm and positive ellipticity at $\lambda = 280$ nm. The opposite behavior is obviously exhibited by its residual antipode (Figure 1b). These experiments are direct evidence of the first successful resolution of a residual racemate. Variable-temperature (VT; 0–70 °C) HPLC experiments with UV detection demonstrated, however, the interconversion between the residual enantiomers (Figure 1c). A small plateau is observed at 0 °C and the peaks coalesce at 70 °C. The dynamic HPLC profiles have been accurately fitted by exploiting the stochastic theory of chromatography.[14,15] This approach provided the M_0 enantiomerization activation parameters for **1a** (Table 3), which is not configurationally stable at room temperature, in satisfactory agreement with the calculations.

Table 3: Experimental activation parameters for the *M3*⇌*P3* stereomerization by the M_0 mechanism in **1a–c**.[a]

Parameter	1a[b]	1b[c]	1c[c]
$\Delta H^{\neq}$ [kJ mol^{-1}]	77 ± 3	102.5 ± 0.1	127 ± 4
$\Delta S^{\neq}$ [J K^{-1} mol^{-1}]	−87 ± 10	−86.5 ± 0.1	−93 ± 3
$\Delta G^{\neq}_{25^\circ C}$ [kJ mol^{-1}]	103 ± 4	128.2 ± 0.1	155 ± 4
$t_{1/2}$(25 °C)	≈7 h	≈20 years	≈10^6 years

[a] Activation enthalpy ($\Delta H^{\neq}$), entropy ($\Delta S^{\neq}$), free energy at 25 °C ($\Delta G^{\neq}_{25^\circ C}$), and enantiomerization half-life at 25 °C ($t_{1/2}$(25 °C)). [b] Dynamic HPLC analysis. [c] Dynamic ^{1}H NMR spectroscopic analysis.

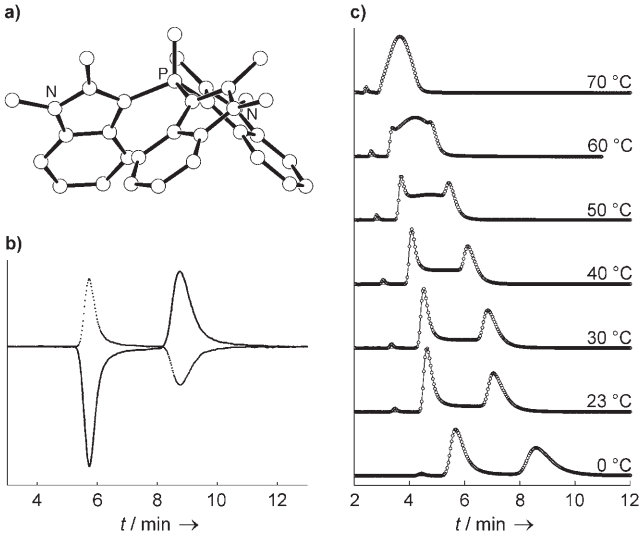

Figure 1. a) XRD structure of tris(1,2-dimethyl-3-indolyl)phosphine oxide (**1a**) at 90 K (hydrogen atoms are omitted; the N atom on the indole (front right) is eclipsing the N atom on the indole ring behind it). b) Chiral HPLC with CD detection of **1a** at room temperature (solid line: detection at 230 nm; dotted line: detection at 280 nm). c) VT dynamic HPLC of **1a** (open circles: experimental; solid line: optimized).

Also in the case of **1b**, chiral HPLC proved very efficient in resolving the racemate (Figure 2a), but the enantiomerization plateau is not observed in this case, so **1b** has a larger configurational stability than **1a**. The methylene protons in **1b** are diastereotopic as long as the enantiomerization by the M_0 mechanism is slow, otherwise they are enantiotopic. Hence, they are effective probes for dynamic ^{1}H NMR experiments[16] (Figure 2b). The shape variation of their complex multiplet near $\delta = 3$ ppm with increasing temperature allowed us to estimate the M_0 barrier parameters that are reported in Table 1.[17] The enantiomerization half-life time is about 20 years at room temperature, therefore **1b** is the racemate of configurationally stable residual enantiomers.

Following the same line of reasoning and exploiting the diastereotopism of the isopropylic methyl groups, the M_0 barrier parameters could be estimated for **1c** as well (Figure 2e and Table 1). In agreement with our calculations, **1c** is the racemate of extremely stable residual enantiomers: the M_0 barrier is estimated to be much larger than that of **1b** and the half-life time of **1c** is estimated to be about 10^6 years. As expected, chiral HPLC experiments carried out on **1c** do not show any evidence of enantiomerization up to 60 °C. In this case, we have been able to obtain some milligrams of almost enantiopure residual antipodes of **1c** by semipreparative HPLC (Figure 2c). The first eluted enantiomer is dextrorotatory (589 nm, CH_2Cl_2) and has been isolated in

 © 2006 Wiley-VCH Verlag GmbH & Co. KGaA, Weinheim

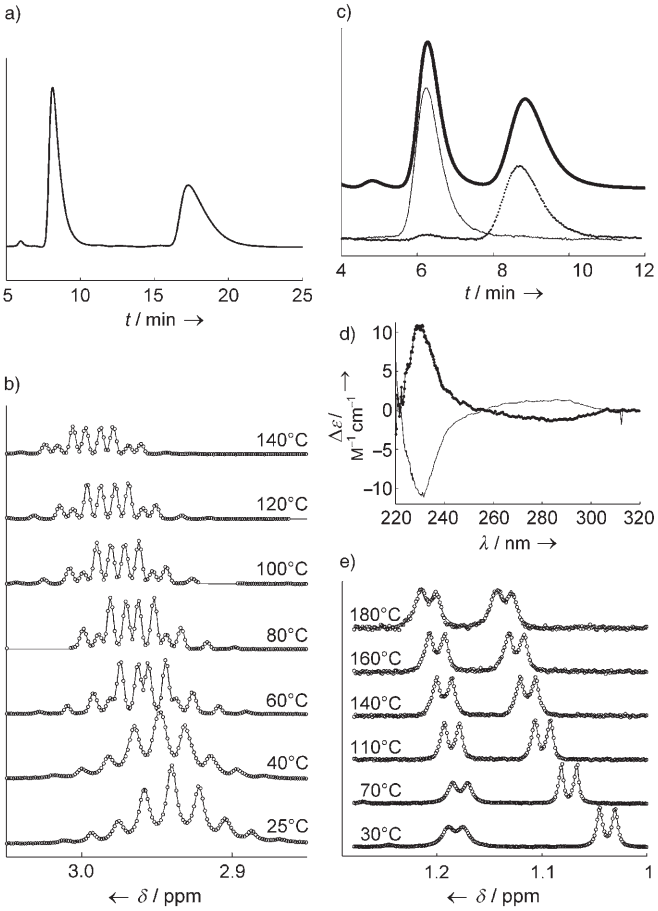

Figure 2. a) Chiral HPLC with UV detection of **1b** at 23 °C. b) VT ^{1}H NMR ([D$_6$]DMSO) spectra of the methylene protons of **1b** (open circles: experimental; solid line: optimized). c) Control of the enantiomeric purity of the residual enantiomers of **1c** obtained from semipreparative chiral HPLC resolution (thick line: residual racemate; thin line: dextrorotatory residual enantiomer; dotted line: levorotatory residual enantiomer (see text)). d) CD spectra (CH_2Cl_2) of the residual enantiomers of **1c** (solid line: dextrorotatory residual enantiomer; dotted line: levorotatory residual enantiomer). e) VT ^{1}H NMR ([D$_6$]DMSO) spectra of the isopropylic methyl protons of **1c** (open circles: experimental; solid line: optimized).

very high enantiomeric purity (e.r. $> 99.5\,\%$). The enantiomeric ratio of the second eluted enantiomer was 95 %. Their CD spectra ($c = 5 \times 10^{-4}$ M, CH_2Cl_2) are identical in shape and opposite in sign (Figure 2d). These experiments are direct evidence of the successful isolation of residual enantiomers.

We have thus demonstrated that configurationally stable residual enantiomers can be rationally designed and easily synthesized.

As triarylphosphine oxides can be transformed into the corresponding phosphines, we performed preliminary computations of the M_0 barrier of tris(2-alkyl-1-methyl-3-indolyl)phosphines. This barrier is 15–30 kJ mol^{-1} lower than that for the corresponding oxides, thus suggesting that at least the most crowded term is configurationally stable, although enantiomerization by pyramidal inversion was not assessed. Therefore, it seems that a novel class of chiral phosphines could be available to synthetic organic chemists. The transition-metal complexes of these phosphines could represent a new series of asymmetric homogeneous catalysts for stereoselective reactions.[18]

Received: May 11, 2006
Published online: August 23, 2006

Keywords: chirality · dynamic NMR spectroscopy · liquid chromatography · phosphine oxides · residual enantiomerism

[1] M. R. Whitnall, K. K. Hii, M. Thornton-Pett, T. P. Kee, *J. Organomet. Chem.* **1997**, *529*, 35 – 50.
[2] M. T. Powell, A. M. Porte, K. Burgess, *Chem. Commun.* **1998**, 2161 – 2162.
[3] R. Dorta, L. Shimon, D. Milstein, *J. Organomet. Chem.* **2004**, *689*, 751 – 758.
[4] K. Mislow, *Acc. Chem. Res.* **1976**, *9*, 26 – 33.
[5] P. Finocchiaro, D. Gust, K. Mislow, *J. Am. Chem. Soc.* **1973**, *95*, 8172 – 8173.
[6] P. Finocchiaro, D. Gust, K. Mislow, *J. Am. Chem. Soc.* **1974**, *96*, 3198 – 3205.
[7] P. Finocchiaro, D. Gust, K. Mislow, *J. Am. Chem. Soc.* **1974**, *96*, 3205 – 3213.
[8] C. A. Johnson, A. Guenzi, K. Mislow, *J. Am. Chem. Soc.* **1981**, *103*, 6240 – 6242.
[9] D. Gust, K. Mislow, *J. Am. Chem. Soc.* **1973**, *95*, 1535 – 1547.
[10] J. D. Andose, K. Mislow, *J. Am. Chem. Soc.* **1974**, *96*, 2168 – 2176.
[11] J. P. Hummel, D. Gust, K. Mislow, *J. Am. Chem. Soc.* **1974**, *96*, 3679 – 3681.
[12] J. F. Blount, P. Finocchiaro, D. Gust, K. Mislow, *J. Am. Chem. Soc.* **1973**, *95*, 7019 – 7036.
[13] P. Finocchiaro, D. Gust, K. Mislow, *J. Am. Chem. Soc.* **1974**, *96*, 2176 – 2182.
[14] R. A. Keller, J. C. Giddings, *J. Chromatogr.* **1960**, *3*, 205 – 220.
[15] O. Trapp, G. Schoetz, V. Schurig, *Chirality* **2001**, *13*, 403 – 414.
[16] A. D. Bain, *Prog. Nucl. Magn. Reson. Spectrosc.* **2003**, *43*, 63 – 103.
[17] ^{1}H DNMR spectroscopy yields an estimate of the activation barrier, rather than an accurate measure, for the following reasons: 1) the whole dynamical range could not be observed and 2) the thermal variation of the chemical shift, as a result of changing solvent–solute interactions, may contribute to the lineshape variation with temperature.
[18] The authors' contributions are as follows: F.S. conceived the project and designed the synthesis; T.B. and S.R. carried out all experimental work, including semipreparative HPLC experiments; G.C. carried out analytical HPLC experiments; T.P. determined the X-ray structures; A.P. designed and carried out the DFT calculations and the analysis of the dynamic HPLC and NMR data; and A.P. and F.S. wrote the Communication.

 © 2006 Wiley-VCH Verlag GmbH & Co. KGaA, Weinheim

Total Synthesis

DOI: 10.1002/anie.200602056

Total Synthesis of Pseudolaric Acid A**

*Zhe Geng, Bin Chen, and Pauline Chiu**

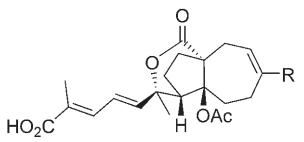

Scheme 1. Pseudolaric acid A (**1**), R = Me; pseudolaric acid B (**2**), R = CO_2Me

The pseudolaric acids A and B, first isolated in 1965, are the main biologically active constituents of *tujinpi*, a traditional Chinese medicinal herb in use since the 17th century for the treatment of dermatological fungal infections.[1] This medicinal preparation is harvested from the root bark of the tree *Pseudolarix kaempferi* Gordon (Pinaceae). The antifertile, antifungal, and cytotoxic properties of the pseudolaric acids have been recognized for quite some time.[2] However, the past few years have seen a resurgence of interest in these natural products for several reasons. The pseudolaric acids were identified as a new class of peroxisome proliferator-activated receptor (PPAR) agonists.[3] Additionally, pseudolaric acid B was found to activate c-Jun N-terminal kinase and caspase-3 in HeLa cells.[4] Studies recently disclosed the antiangiogenic effects of both pseudolaric acid A and B.[5,6] Our own studies revealed that pseudolaric acids A and B inhibit tubulin polymerization in vitro.[7] The resultant antimitotic activity and disruption of normal microtubule assembly appears to be their mode of anticancer action. Notably, pseudolaric acid B is able to circumvent the action of the P-glycoprotein (Pgp) efflux pump, which is responsible for the acquired resistance to many tubulin-binding agents, which allows pseudolaric acid B to maintain its activity, even on some multidrug-resistant cancers. We have further demonstrated the in vivo antitumor effects of pseudolaric acid B towards a liver cancer resistant to taxol in a murine xenograft model.

Structurally, the pseudolaric acids are novel diterpenoids with a highly oxygenated perhydroazulene skeletal framework (Scheme 1). The *trans* arrangement of the lactone and acetoxy group at the fused-ring junction is an unusual arrangement in natural perhydroazulenes, but is a representative structural feature of this family of compounds. The central δ-lactone is characterized by contiguous quaternary or tertiary stereocenters at all four tetrahedral carbon atoms. All of these structural elements congested within a relatively small space constitute the synthetic challenge at hand. The biological activity and molecular architecture of the pseudolaric acids have already attracted a number of synthetic efforts.[8–11] Herein, we describe our studies on pseudolaric acid A, which culminated in the first total synthesis of this natural product.[12]

Our retrosynthetic strategy towards pseudolaric acid A (**1**) is illustrated in Scheme 2, in which cleavage of the lactone functionality and a Wittig-type disconnection at C13–C14

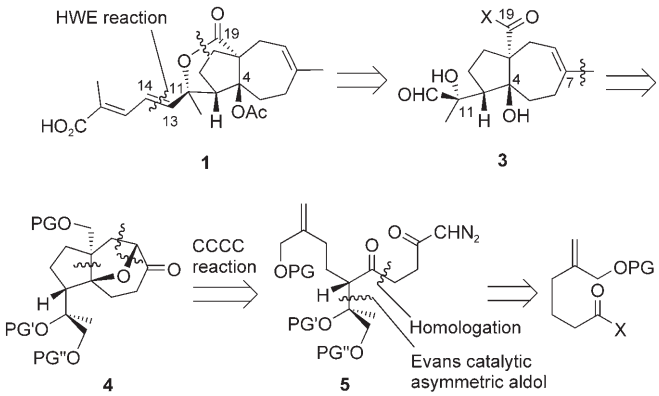

Scheme 2. Retrosynthetic analysis of pseudolaric acid A. HWE = Horner–Wadsworth–Emmons; CCCC = carbene cyclization cycloaddition cascade; PG, PG′, PG″ = protecting groups.

yields the stereochemically loaded aldehyde **3**. Redox interconversions at C11 and C19, and a crucial reductive cleavage reveal key oxatricyclic intermediate **4** as the precursor. In this way, the tertiary hydroxy acetate/hydroxy group at C4 is protected from dehydration and other side reactions in the form of the oxygen bridge. This oxatricyclic intermediate **4** could be obtained through an intramolecular carbene cyclization cycloaddition cascade (CCCC) reaction of acyclic diazoketone **5**.[13–15] This reaction would be the key step in the construction of the stereochemically defined perhydroazulene platform in the present synthetic strategy.[16] Diazoketone **5** could be constructed from three carbon fragments, as shown. The stereochemically defined southern portion of diazoketone **5** could be obtained from an Evans catalytic

[*] Z. Geng, B. Chen, Prof. Dr. P. Chiu
Department of Chemistry and
Open Laboratory of Chemical Biology
Institute of Molecular Technology for Drug Discovery and Synthesis
The University of Hong Kong
Pokfulam Road, Hong Kong (P.R. China)
Fax: (+852) 2857-1586
E-mail: pchiu@hku.hk
Homepage: http://chem.hku.hk/~chemhome/staff/pchiu/pchiu.htm

[**] The work was supported by the Research Grants Council of Hong Kong SAR, P.R. China (Project No. HKU 7017/04P), the Areas of Excellence Scheme (Project No. AoE/P-10/01) administered by the University Grants Committee (HKSAR), and The University of Hong Kong. B.C. acknowledges the award of a postgraduate student exchange scholarship from the University of Hong Kong. We thank Prof. G. W. Qin of the Shanghai Institute of Materia Medica for a sample of pseudolaric acid A, and W.-T. Ma and Prof. Z. Cai (HKBU) for obtaining high-resolution mass spectra.

Supporting information for this article is available on the WWW under http://www.angewandte.org or from the author.

 © 2006 Wiley-VCH Verlag GmbH & Co. KGaA, Weinheim

asymmetric aldol reaction,[17] another key reaction in this total synthesis.

Following this retrosynthetic analysis, and based on results from model studies,[12] we began the synthesis with commercially available allyl dichloride **6**. Reaction of **6** with sodium *p*-methoxybenzyl alcoholate produced a mixture of substitution products, the major one being 3-chloro-2-benzyloxymethylpropene (**7**; Scheme 3). Coupling **7** with the zinc homoenolate derived from methyl 3-iodopropionate smoothly afforded homologated ester **8**,[18] which was subsequently converted into thioester **10** via acid **9**.

The Evans catalytic asymmetric aldol reaction was employed to introduce the initial stereochemical elements in the molecule.[17] Thus, **10** was converted into its silyl enol ether and treated with methyl pyruvate under catalysis by the [Cu{(S,S)-*t*Bu-box}][OTf]$_2$ complex (Scheme 3). Substrate **10** is one of the more demanding cases for this reaction, because of the longer alkyl chain, which leads to a more hindered enol ether derivative. The use of the trimethylsilyl enol ether of **10** gave capricious results in the aldol reaction, but the use of the triethylsilyl enol ether led to consistent yields of aldol **11**, albeit at a noticeably slower reaction rate. The use of dichloromethane as the solvent was also critical, since the conversion rate was low in the more common solvent THF. The increased reaction rate in dichloromethane is indicative of a change in the rate-determining step from copper catalyst decomplexation to aldol condensation. In this manner, aldol diastereomer **11** bearing vicinal tertiary stereocenters was synthesized in a yield of 76% and with an *ee* value of 88%.[19] Protection of the newly generated tertiary alcohol was achieved using TBSOTf to give **12**.

Direct homologation of thioester **12** was surprisingly difficult. Nucleophilic addition to the thioester functionality was hampered by branching at the β carbon atom, and further complicated by the competitive reactivity of the proximate carbomethoxy functional group. Although the more reactive aldehyde derivative **13** could be obtained from thioester **12** through a Fukuyama reduction,[20] homologation of this substrate also failed. Under more forcing conditions, side products arose, apparently from reaction of both the ester and the aldehyde.[21] To circumvent these problems, the interfering ester functionality was removed by reduction. Direct treatment of **11** with LAH resulted in a significant portion of the hydroxyketone undergoing a retroaldol reaction. Therefore, the protected aldol **12** was subjected to exhaustive reduction instead. This reaction resulted in migration of the TBS group and led to isolation of a mixture of diols. However, after desilylation a single triol **14** was obtained as the sole product in good yield. Treatment of triol **14** with 3,3-dimethoxypentane resulted in the exclusive formation of desired dioxolane **15**, in which the alcohol derived from the thioester remained available for further elaboration.[22] Alcohol **15** was converted into aldehyde **16** by a Dess–Martin oxidation.

Homologation was then attempted on aldehyde **16**. Although aldehyde **16** has steric hindrance comparable to that in substrate **13,** but lacks the electrophilic group at the β position, it could be smoothly converted into diol **17** in 90% yield, using the variant of the Grignard reagent ClMgO-

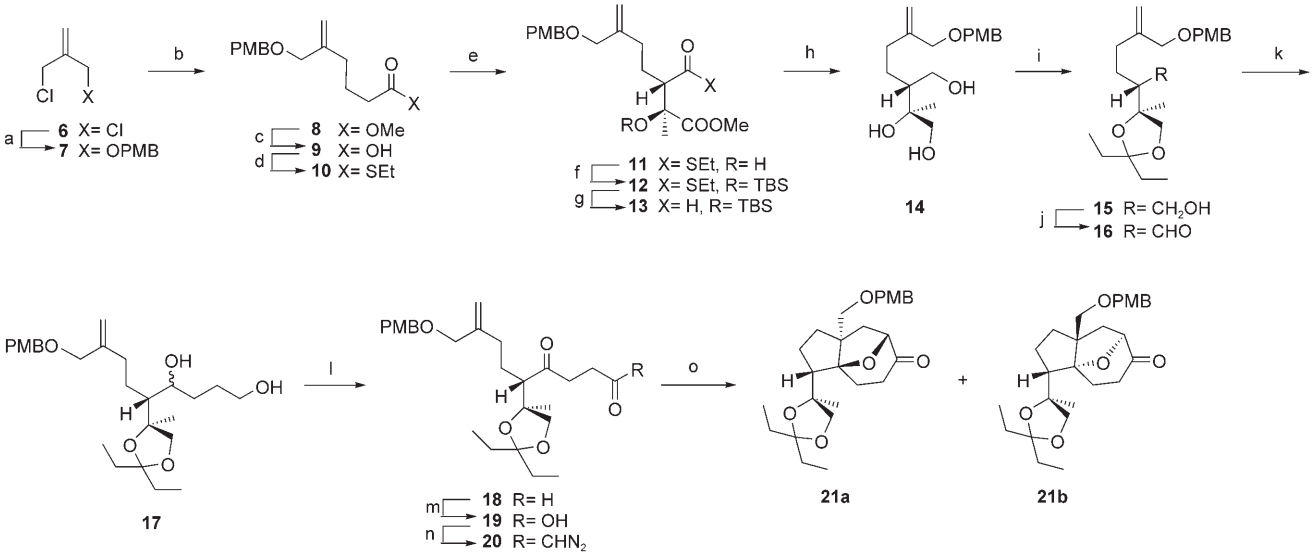

Scheme 3. Reagents and conditions: a) NaH, PMBOH, THF, reflux, 61%; b) $ICH_2CH_2CO_2Me$, Zn(Cu), CuCN, DMA, THF, 60°C, 12 h, 91%; c) 20% NaOH, MeOH, RT, 4 h, 96%; d) EtSH, DCC, DMAP, CH_2Cl_2, 3 h, 97%; e) 1. LDA, TESCl, THF, −78°C-RT; 2. [Cu{(*S*,*S*)-*t*Bu-box}][OTf]$_2$, methyl pyruvate, CH_2Cl_2, −78°C, 76%, 88% *ee*; f) TBSOTf, 2,6-lutidine, CH_2Cl_2, RT, 97%; g) Et_3SiH, Pd/C, CH_2Cl_2, 81%; h) 1. LAH, THF, 0°C, 4 h; 2. TBAF, THF, RT, 2 h; i) 3,3-dimethoxypentane, PTSA, RT, 1 h, 66% from **12**; j) Dess–Martin periodinane, CH_2Cl_2, RT, 88%; k) $ClMgO(CH_2)_3MgCl$, THF, 0°C, 90%; l) Swern oxidation, 90%; m) $NaClO_2$, NaH_2PO_4, *t*BuOH, 2-methyl-2-butene, RT, 96%; n) 1. *i*BuOCOCl, Et_3N, THF/Et_2O, −20→0°C, 0.5 h; 2. CH_2N_2, Et_2O, 0°C–RT, 3 h, 71%; o) 3% [Rh_2{(*S*)-bptv}$_4$], $PhCF_3$, −40°C, 82% yield (50% **21a**, 32% **21b**). PMB = *p*-methoxybenzyl, DMA = *N*,*N*-dimethylacetamide, DCC = *N*,*N*′-dicyclohexylcarbodiimide, DMAP = 4-dimethylaminopyridine, LDA = lithium diisopropylamide, TES = triethylsilyl, box = bis(oxazoline), Tf = trifluoromethanesulfonyl, TBS = *tert*-butyldimethylsilyl, LAH = lithium aluminum hydride, TBAF = tetra-*n*-butylammonium fluoride, PTSA = *p*-toluenesulfonic acid, bptv = α-(*tert*-butyl)-1,3-dihydro-1,3-dioxo-2*H*-benz[*f*]isoindole-2-acetato.

 © 2006 Wiley-VCH Verlag GmbH & Co. KGaA, Weinheim

$(CH_2)_3MgCl$ reported by Normant et al.[23] Oxidation of both alcohols was accomplished under Swern conditions, followed by Lindgren oxidation to cleanly yield ketoacid **19**. Activation with isobutylchloroformate and treatment with diazomethane by using standard methods[24] afforded diazoketone **20**.

With chiral diazoketone **20** in hand, the carbene cyclization cycloaddition cascade reaction was studied.[14,15] This transformation would complete the stereochemical configuration of the molecule, as well as assemble the polycyclic carboskeleton of pseudolaric acid A from acyclic precursor **20** in one step. We have studied various model substrates in the context of this reaction.[12] With achiral dirhodium catalysts, the CCCC reaction of **20** was found to favor the formation of undesired diastereomer **21b**. For example, the CCCC reaction of **20** catalyzed by $[Rh_2(OAc)_4]$ at 0°C in CH_2Cl_2 generated a 61% yield of a 1:3 mixture of **21a**/**21b**. The preference for this mode of cycloaddition arose from the unfavorable interactions between the sterically demanding dioxolane and the PMB ether, which would be *syn* on the same face of the ring, in the transition state of the intramolecular cyclcoaddition leading to **21a** . We have examined various factors in this reaction, including catalysts, solvents, and temperature, and after optimization found that 3% of the chiral catalyst, developed by Hashimoto and co-workers, $[Rh_2\{(S)\text{-bptv}\}_4]$ in benzotrifluoride at −40°C, afforded the desired isomer **21a** as the major product.[25] Under these conditions, a 82% yield of the CCCC cycloadducts **21a** and **21b** was obtained in a ratio of 1.6:1, which translates to a 50% yield of the desired diastereomer **21a** to carry forward in the total synthesis. Thus, the remaining two stereocenters and the carbocyclic skeleton in pseudolaric acid A were efficiently constructed.

Our synthetic strategy was to mask the acetate group in pseudolaric acid A as an oxygen bridge to prevent dehydration or elimination side reactions, as observed in previous approaches. However, the oxabicyclic nucleus turned out to be quite robust and did not yield easily to reaction. Exploratory experiments on **21a** demonstrated that the construction of the final ring was difficult, if not impossible, in the presence of the bridging oxygen atom, because of rigidification of the carbobicyclic ring system. Thus, cleavage of the oxygen bridge in **21a** proved to be another challenge. This crucial transformation was finally achieved through a reductive elimination protocol (Scheme 4).[26] Ketone **21a** was treated with MeMgCl to give alcohol **22** as a single diastereomer. The diastereoselective *syn* approach of the nucleophile with respect to the oxygen bridge is well established. Conversion of the tertiary alcohol into the diastereomeric chlorides **23** was achieved using thionyl chloride. Both diastereomers of **23** underwent reductive elimination with sodium in refluxing diethyl ether with concomitant opening of the oxygen bridge to reveal perhydroazulene **24** in 78% yield over two steps from **21a**. At this stage, the central nucleus in pseudolaric acid A bearing all of the required stereocenters in their correct absolute configurations had been constructed.

With the ring-opened compound **24** in hand, the final functionalizations were accomplished as follows. Oxidative removal of the PMB group in **24** yielded the deprotected alcohol **25**, which was further oxidized to the aldehyde.

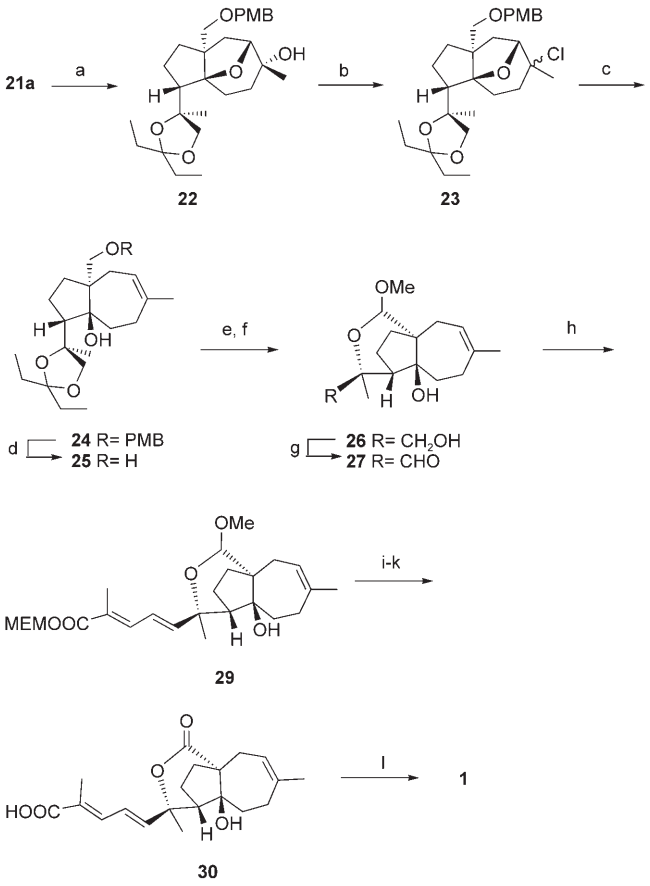

Scheme 4. Reagents and conditions: a) MeMgCl, THF, 0°C, 96%; b) $SOCl_2$, DMPU, 0°C–RT; c) Na, Et_2O, reflux, 78% over 2 steps from **22**; d) DDQ, CH_2Cl_2/H_2O, RT, 86%; e) Dess–Martin periodinane, CH_2Cl_2, RT, 91%; f) MeOH, CSA, RT, 95%; g) Dess–Martin periodinane, CH_2Cl_2, RT, 93%; h) (*E*)-$(EtO)_2POCH_2CH{=}C(CH_3)CO_2MEM$ **28**, *n*BuLi, THF, 83%; i) 60% AcOH, 60°C, 1 h; j) Dess–Martin periodinane, CH_2Cl_2; k) 3 N HCl/THF, RT, 66% over 3 steps from **29**; l) AcCl, DMAP, 80%. DMPU = 1,3-dimethylhexahydro-2-pyrimidinone, DDQ = 2,3-dichloro-5,6-dicyano-1,4-benzoquinone, CSA = camphorsulfonic acid, MEM = 2-(methoxyethoxy)methyl.

Subsequent treatment with camphorsulfonic acid in methanol to deprotect the diol also induced spontaneous acetalization, engaging only the tertiary alcohol, to give the mixed acetal **26** in excellent yield as a single diastereomer. With this transformation we had achieved the construction of the final ring in pseudolaric acid A, opportunely leaving the primary alcohol free for oxidation to aldehyde **27** by Dess–Martin periodinane, in preparation for the Wittig homologation. In the event, the Horner–Emmons reagent **28**, the methoxymethyl diethylphosphonate of (*E*)-2-methylbut-2-enoate, reacted with aldehyde **27** under basic conditions to yield compound **29**.[10a] As expected, only the (*E*,*E*)-diene **29** was obtained. Hydrolysis of the mixed acetal and oxidation gave the lactone functionality, and acid-induced deprotection of the MEM group afforded acid **30**. Finally, acetylation of the hindered tertiary alcohol at C4 afforded pseudolaric acid A (**1**). The spectroscopic data of pseudolaric acid A obtained from this synthesis was in accordance with the natural product;[27] for example, the optical rotation of the synthetic

 © 2006 Wiley-VCH Verlag GmbH & Co. KGaA, Weinheim

material is $[\alpha]_D^{20} = -37.1°$, and that of natural pseudolaric acid is $[\alpha]_D^{20} = -39.6°$.[28] Pseudolaric acid B (**2**) has been documented to be available from **1** by chemical transformations.[29]

In conclusion, we have accomplished the synthesis of pseudolaric acid A. The highlights of this synthetic route are the Evans catalytic asymmetric aldol reaction to establish the absolute stereochemistry of the first two tertiary carbon stereocenters, the carbene cyclization cycloaddition cascade reaction to install the remainder of the stereochemical elements and the polycyclic framework, as well as a reductive elimination protocol to unmask the oxatricyclic structure to reveal the perhydroazulene nucleus and facilitate cyclization to construct the final lactone ring. The present synthetic approach is amenable for the preparation of analogues and derivatives of pseudolaric acids that will be useful to the evaluation of the biological potential of these kinds of compounds.

Received: May 23, 2006
Published online: August 14, 2006

Keywords: antitumor agents · carbenoids · domino reactions · natural products · total synthesis

[1] a) B. N. Zhou in *Phytochemistry of Plants Used in Traditional Medicine* (Eds.: K. Hostettmann, A. Marston, M. Maillard, M. Hamburger), Clarendon Press, Oxford, **1995**, pp. 313–334; b) J. X. Yao, X. Y. Lin, *Acta Chim. Sin. (Engl. Ed.)* **1982**, *40*, 385–389; c) B. N. Zhou, B. P. Ying, G. Q. Song, Z. X. Chen, J. Han, Y. F. Yan, *Planta Med.* **1983**, *47*, 35–38; d) B. P. Ying, R. S. Xu, J. F. Mi, J. Han, *Acta Chim. Sin.* **1988**, *46*, 85–86; e) Z. Li, L. Han, D. J. Pan, C. Q. Hu, Q. L. Wu, S. S. Yang, *Acta Chim. Sin. (Engl. Ed.)* **1982**, *40*, 447–451.

[2] a) M. O. Hamburger, H. L. Shieh, B. N. Zhou, J. M. Pezzuto, G. A. Cordell, *Magn. Reson. Chem.* **1989**, *27*, 1025; b) W. C. Wang, Z. P. Gu, A. Koo, W. S. Chen, *Acta Pharmacol. Sin.* **1991**, *12*, 423–425; c) E. Li, A. M. Clark, C. D. Hufford, *J. Nat. Prod.* **1995**, *58*, 57–67; d) D. J. Pan, Z. L. Li, C. Q. Hu, K. Chen, J. J. Chang, K. H. Lee, *Planta Med.* **1990**;56: 383–385; e) W. C. Wang, R. F. Lu, S. X. Zhao, Y. Z. Zhu, *Acta Pharmacol. Sin.* **1982**, *3*, 188–192.

[3] M. S. Jardat, D. J. Noonan, B. Wu, M. A. Avery, D. R. Feller, *Planta Med.* **2002**, *8*, 667–671.

[4] X. Gong, M. Wang, Zhen, W. S. Tashiro, S. Onodera, T. Ikejima, *Exp. Mol. Med.* **2004**, *36*, 551–556.

[5] a) M. H. Li, Z. H. Miao, W. F. Tan, J. M. Yue, C. Zhang, L. P. Lin, X. W. Zhang, J. Ding, *Clin. Cancer Res.* **2004**, *10*, 8266–8274; b) W. Tan, X. Zhong, M. Li, J. Yue, Y. Chen, L. Lin, J. Ding, *Eur. J. Pharmacol.* **2004**, *499*, 219–228; c) J. Ding, Y. Zhen, Y. Tong, J. Yue, D. Xiao, *Jpn. J. Cancer Chemother.* **2002**, *29*(Suppl.I), 59–66; d) Y. G. Tong, X. W. Zhang, M. Y. Geng, J. M. Yue, X. L. Xin, F. Tian, X. Shen, L. J. Tong, M. H. Li, C. Zhang, W. H. Li, L. P. Lin, J. Ding, *Mol. Pharm.* **2006**, *69*, 1226–1233.

[6] "Preparation of pseudolaric acid B derivatives and pharmaceutical activities": J. Yue, S. Yang, J. Ding, D. Xiao, S. Yuan, Y. Wu, Y. Tong, L. Dong, PCT Int. Appl. **2003**, p. 29.

[7] V. K. W. Wong, P. Chiu, S. S. M. Chung, L. M. C. Chow, Y. Z. Zhao, B. B. Yang, B. C. B. Ko, *Clin. Cancer Res.* **2005**, *11*, 6002–6011.

[8] B. C. Pan, H. Y. Chang, G. L. Cai, Y. S. Guo, *Pure Appl. Chem.* **1989**, *61*, 389–392.

[9] R. I. Higuchi, PhD Thesis, Stanford University (USA), **1995**.

[10] a) B. Wu, J. M. Karle, E. B. Watkins, M. A. Avery, *Tetrahedron Lett.* **2002**, *43*, 4095–4098; b) J. D. Bonk, PhD Thesis, University of Mississippi (USA), **1997**.

[11] a) Y. Hu, L. Ou, D. Bai, *Tetrahedron Lett.* **1999**, *40*, 545–548; b) L. Ou, Y. Hu, G. Song, D. Bai, *Tetrahedron* **1999**, *55*, 13999–14004.

[12] a) P. Chiu, B. Chen, K. F. Cheng, *Org. Lett.* **2001**, *3*, 1721–1724; b) B. Chen, R. Y. Y. Ko, M. S. M. Yuen, K. F. Cheng, P. Chiu, *J. Org. Chem.* **2003**, *68*, 4195–4205; c) P. Chiu, *Pure Appl. Chem.* **2005**, *77*, 1183–1189; d) P. Chiu, B. Chen, K. F. Cheng, *Tetrahedron Lett.* **1998**, *39*, 9229–9232.

[13] Reviews on cascade or domino reactions: a) L. F. Tietze, *Chem. Rev.* **1996**, *96*, 115–136; b) L. F. Tietze, U. Beifuss, *Angew. Chem.* **1993**, *105*, 137–170; *Angew. Chem. Int. Ed. Engl.* **1993**, *32*, 131–163; c) J. D. Winkler, *Chem. Rev.* **1996**, *96*, 167–176; d) P. J. Parsons, C. S. Penkett, A. J. Shell, *Chem. Rev.* **1996**, *96*, 195–206.

[14] Reviews on the carbene cyclization cycloaddition cascade reaction: a) G. Mehta, S. Muthusamy, *Tetrahedron* **2002**, *58*, 9477–9504; b) A. Padwa, *J. Organomet. Chem.* **2005**, *690*, 5533–5540; c) M. P. Doyle, M. A. Mckervey, T. Ye, *Modern Catalytic Methods for Organic Synthesis with Diazo Compounds*, Wiley, New York, **1998**, chap. 7, pp. 397–416; d) A. Padwa, *Chem. Commun.* **1998**, 1417–1424; e) A. Padwa, *Top. Curr. Chem.* **1997**, *189*, 121–158; f) A. Padwa, M. D. Weingarten, *Chem. Rev.* **1996**, *96*, 223–269; g) A. Padwa, S. F. Hornbuckle, *Chem. Rev.* **1991**, *91*, 263–309.

[15] Recent applications of the carbene cyclization cycloaddition cascade reaction in synthesis: a) X. Zhang, R. Y. Y. Ko, S. Li, R. Miao, P. Chiu, *Synlett* **2006**, 1197–1200; b) S. Shin, A. K. Gupta, C. Y. Rhim, C. H. Oh, *Chem. Commun.* **2005**, 4429–4431; c) A. Padwa, J. Boonsombat, P. Rashatasakhon, J. Willis, *Org. Lett.* **2005**, *7*, 3725–3727; d) T. Graening, V. Bette, J. Neudörfl, J. Lex, H.-G. Schmalz, *Org. Lett.* **2005**, *7*, 4317–4320; e) D. M. Hodgson, F. Le Strat, *Chem. Commun.* **2004**, 822; f) S. Muthusamy, C. Gunanathan, E. Suresh, *Tetrahedron* **2004**, *60*, 7885–7897; g) S. Nakamura, Y. Hirata, T. Kurosaki, M. Anada, O. Kataoka, S. Kitagaki, S. Hashimoto, *Angew. Chem.* **2003**, *115*, 5509–5513; *Angew. Chem. Int. Ed.* **2003**, *42*, 5351–5355.

[16] Other strategies toward bicyclo[5.3.0]undecane systems: a) C. H. Heathcock, S. L. Graham, M. C. Pirrung, F. Plavac, C. T. White in *The Total Synthesis of Natural Products Vol. 5* (Ed.: J. ApSimon), Wiley, New York, **1982**; b) P. A. Wender, C. D. Jesudason, H. Nakahira, N. Tamura, A. L. Tebbe, Y. Ueno, *J. Am. Chem. Soc.* **1997**, *119*, 12976–12977; c) M. Harmata, V. R. Fletcher, R. J. Claassen II, *J. Am. Chem. Soc.* **1991**, *113*, 9861–9862; d) H. M. L. Davies, N. J. S. Huby, W. R. Cantrell, J. L. Olive, *J. Am. Chem. Soc.* **1993**, *115*, 9468–9479; e) G. Majetich, J. S. Song, A. J. Leigh, S. M. Condon, *J. Org. Chem.* **1993**, *58*, 1030–1037; f) B. M. Trost, R. I. Higuchi, *J. Am. Chem. Soc.* **1996**, *118*, 10094–10105.

[17] a) D. A. Evans, M. C. Kozlowski, J. A. Murry, C. S. Burgey, K. R Campos, . B. T. Connell, R. J. Staples, *J. Am. Chem. Soc.* **1999**, *121*, 669–685; b) D. A. Evans, C. S. Burgey, M. C. Kozlowski, S. W. Tregay, *J. Am. Chem. Soc.* **1999**, *121*, 686–699.

[18] H. Ochiai, Y. Tamaru, K. Tsubaki, Z. Yoshida, *J. Org. Chem.* **1987**, *52*, 4418–4420.

[19] A minor aldol diastereomer was also obtained in 7% yield, along with about 10% of recovered starting material.

[20] a) H. Tokuyama, S. Yokoshima, S. C. Lin, L. Li, T. Fukuyama, *Synthesis* **2002**, 1121–1123; b) T. Fukuyama, S. C. Lin, L. Li, *J. Am. Chem. Soc.* **1990**, *112*, 7050–7051.

[21] One side product obtained was from the addition of the newly generated alkoxide to the ester, hence the reactivity of the ester functional group proved to be a problem.

 © 2006 Wiley-VCH Verlag GmbH & Co. KGaA, Weinheim

[22] a) C. R. Schmid, P. A. Bradley, *Synthesis* **1992**, 587–590; b) S. Hanessian, S. Sahoo, M. Botta, *Tetrahedron Lett.* **1987**, *28*, 1147–1150.
[23] J. F. Normant, G. Cahiez, A. Alexakis, *Tetrahedron Lett.* **1978**, *19*, 3013–3014.
[24] T. Ye, M. A. McKervey, *Tetrahedron* **1992**, *48*, 8007–8022.
[25] S. Kitagaki, M. Anada, O. Kataoka, K. Matsuno, C. Umeda, N. Watanabe, S. I. Hashimoto, *J. Am. Chem. Soc.* **1999**, *121*, 1417–1418.
[26] S. M. Bromidge, P. G. Sammes, L. J. Street, *J. Chem. Soc. Perkin Trans. 1* **1985**, 1725–1730.
[27] Natural pseudolaric acid A was obtained courtesy of Prof. G. W. Qin of the Shanghai Institute of Materia Medica.
[28] According to the optical rotation, the synthetic material has an *ee* value of 94% . From the initial 88% *ee* obtained in Evans asymmetric aldol reaction, some enantiomeric enrichment has occurred, apparently in the chiral $[Rh_2\{(S)\text{-bptv}\}_4]$-induced CCCC reaction.
[29] Z. Li, L. Han, D. J. Pan, C. Q. Hu, Q. L. Wu, S. S. Yang, *Acta Chim. Sin. (Engl. Ed.)* **1982**, *40*, 757–761.

 © 2006 Wiley-VCH Verlag GmbH & Co. KGaA, Weinheim

Surface Organometallic Chemistry

DOI: 10.1002/anie.200602171

Alkane Metathesis Catalyzed by a Well-Defined Silica-Supported Mo Imido Alkylidene Complex: [(≡SiO)Mo(=NAr)(=CH*t*Bu)(CH_2*t*Bu)]**

Frédéric Blanc, Christophe Copéret, Jean Thivolle-Cazat, and Jean-Marie Basset**

The conversion of alkanes at low temperatures has gained interest over the past few years because more efficient routes to chemicals are necessary to optimize oil resources.[1,2] Within this context, we reported in 1997, the reaction of alkane metathesis, which catalytically transforms a given alkane into its lower and higher homologues using a silica-supported tantalum hydride[3] prepared by surface organometallic chemistry (SOMC). Based on kinetic and structure–reactivity relationship studies, we have shown that π-bond metathesis (interaction of an olefin and a carbene) was the key carbon–carbon bond-cleavage and formation process and that alkylidene hydrides are critical intermediates (Scheme 1).[4–7] Other systems have been reported[8,9] that

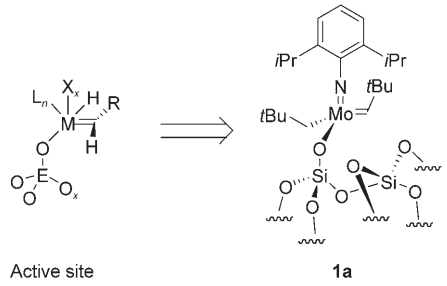

Scheme 1. Proposed active sites in alkane metathesis and possible catalyst precursor **1a**.

are based on a combination of dehydrogenation/hydrogenation and olefin metathesis catalysts, with the most recent example[9] using a mixture of homogenous catalysts.[10–13] The best catalysts prepared by SOMC[14] are based on very simple monoatomic systems: hydrides, alkyl alkylidenes, or alkyl alkylidynes of Group 5 or 6 metals supported on oxides. Although introducing ligands that play a key role in controlling the reactivity and the selectivity of catalysts has been a long-term goal, all ancillary ligands introduced so far (alkylidyne, pentamethylcyclopentadiene (Cp*), Cl) have been detrimental to catalyst performances.[5] Herein, we report that a well-defined silica-supported alkyl alkylidene/Mo complex containing an imido ligand (**1a**)[15] is a good catalyst precursor for alkane metathesis (Scheme 1).[5,6]

When propane (540 equiv) is brought into contact with **1a** at 150 °C in a batch reactor, it is converted into mainly ethane (56.1 %), butane (35.3 %), and small quantities of methane (0.1 %), isobutane (2.7 %), and pentanes (5.9 %). These selectivities are constant over time (see the Supporting Information), and noteworthy the selectivity in methane, probably produced by hydrogenolysis,[16] is low as already observed for other Group 6 supported systems.[7,17] Moreover, the turnover frequency is constant for 40 h (ca. 1 TON h^{-1}; TON = turnover number), and then there is a reproducible decrease of conversion (Table 1 and Figure 1). Note that this well-defined catalyst precursor achieves about the same TON (55) in 120 h as the original tantalum hydride catalyst supported on silica (TON = 60) despite the presence of ancillary ligands.

Besides propane metathesis products, 2,2-dimethylpropane (*t*BuCH_2–H; 0.82 equiv), 2,2-dimethylbutane (*t*BuCH_2–Me; 0.34 equiv), and 2,2-dimethylpentane (*t*BuCH_2–Et; 0.10 equiv) are formed within 120 h (Table 2), whereas no *t*BuCH_2–Pr is detected (< 0.01 % if any). Firstly, 2,2-dimethylpropane is probably formed by exchange of the neopentyl by a propyl ligand, either directly through σ-bond metathesis or in two steps through C–H activation on the neopentylidene unit followed by a decomposition of the penta-coordinated complex through an α-H abstraction to regenerate an alkylidene alkyl/Mo center (**1b**, R = Et, R′ = *t*Bu;

[*] F. Blanc, Dr. C. Copéret, Dr. J. Thivolle-Cazat, Dr. J.-M. Basset
Laboratoire de Chimie Organométallique de Surface
UMR 9986 CNRS–ESCPE Lyon
43 bd du 11 Novembre 1918, 69616 Villeurbanne Cedex (France)
Fax: (+33) 472431795
E-mail: coperet@cpe.fr
basset@cpe.fr

[**] F.B. is grateful to the French Ministry of Education, Research, and Technology (MENRT) for a predoctoral fellowship. We thank R. R. Schrock and A. Sinha for providing a sample of [Mo(=NAr)(=CH*t*Bu)(CH_2*t*Bu)$_2$]. We are also indebted to the CNRS and ESCPE Lyon for financial support.

Supporting information for this article is available on the WWW under http://www.angewandte.org or from the author.

 © 2006 Wiley-VCH Verlag GmbH & Co. KGaA, Weinheim

Table 1: TONs and selectivities in the metathesis of various alkanes catalyzed by **1a** in a batch reactor after 120 h.

Alkane	TON[a]	Alkane selectivity[b]						
		C_1	C_2	C_3	C_4[c]	C_5[c]	C_6[d]	C_7[d]
ethane	2 (0.4)	35.9	n.a.[e]	62.0	1.5/0.8	n.o.[f]	n.o.	n.o.
propane	55 (9.9)	0.1	56.1	n.a.	35.3/2.7	5.2/0.7	0.6	< 0.1
butane	90 (17.7)	< 0.1	11.1	56.5	n.a./0.5	21.7/0.4	7.7	2.0
isobutane	3 (0.7)	1.0	35.9	17.1	7.0/n.a.	16.4/n.o	22.8	n.o.

[a] TON is expressed in mol of alkane transformed per mol of Mo. The values in parentheses are conversions. [b] The selectivities are defined as the amount of product *i* over the total amount of products (they do not significantly change with time and conversion). [c] Linear/branched alkanes. [d] Selectivity for the sum of all isomers. [e] n.a. = not applicable. [f] n.o. = not observed (< 0.01 % if any).

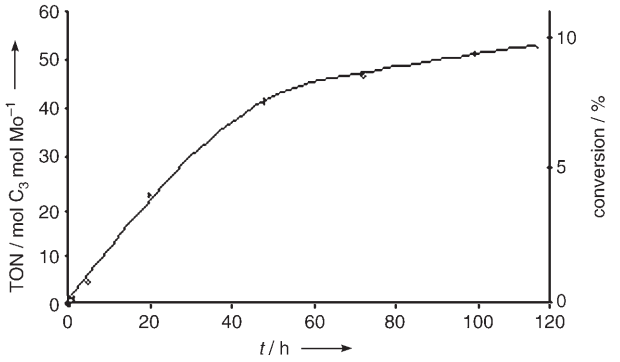

Figure 1. Turnovers obtained (expressed in mol of propane converted per mol of Mo) during the metathesis of propane catalyzed by **1a** in a batch reactor.

Scheme 2). Secondly, 2,2-dimethylbutane and 2,2-dimethylpentane are probably obtained through cross-metathesis of the neopentylidene ligand attached to the Mo center and a propene moiety, which results from β-H transfer on the propyl chain in **1b**, followed by metathesis and subsequent similar reverse steps (insertion of the olefin into a metal hydride and exchange of the ligand by successive C–H activation on the carbene ligand and α-H abstraction). Note that the alkane cross-metathesis products are obtained in a 3.4:1 ratio, which is very close to the ratio of olefin cross-metathesis products 3,3-dimethylbutene and (*E*)-4,4-dimethyl-2-pentene, obtained during the metathesis of propene on **1a** (that is, 2.7:1), and this is consistent with the proposed elementary steps, and especially with olefin metathesis being the key carbon–carbon bond-formation step.[15]

The selectivity of initiation products can therefore be understood on the basis of the model developed for olefin metathesis, which is based on the minimization of steric interactions in the metalla-cyclobutane intermediates (or in their formation);[18] that is, by the relative position of the substituents: typically substituents in the [1,3]-positions of the metalla-cyclobutane intermediate generate less steric hindrance than in the [1,2]-positions (Scheme 2). This model is also consistent with the observed product selectivity and explains the greater selectivity of butane relative to that of pentane when starting from **1c** (R = R′ = Et) and when the cross-metathesis of the resulting propagating alkylidene hydride intermediate **2b** (X = H, R = Et) and propene is involved. Lower alkane homologues are formed using the same elementary steps, that is, by exchanging ligands through C–H activation on carbene intermediates and extrusion processes (α-H abstraction). Although this mechanism is based on a single-site mechanism, it is also possible to involve two sites, one that generates the olefin and the other that carries out the metathesis.

Table 2: Cross-metathesis products in the metathesis of various alkanes catalyzed by **1** in a batch reactor after 120 h.[a]

Alkane	tBuCH$_2$H	tBuCH$_2$Me	tBuCH$_2$Et	tBuCH$_2$Pr	tBuCH$_2$$i$Pr
ethane	1.01	0.35	n.o.[b]	n.o.	n.o.
propane	0.82	0.34	0.10	n.o.	n.o.
butane	0.88	0.10	0.14	0.05	n.o.
isobutane	0.83	0.20	0.04	n.o.	n.o.

[a] The values given are equivalents of alkanes per Mo. [b] n.o. = not observed (< 0.01 % if any).

Butane is also converted efficiently into its lower and higher homologues (TON = 90 in 120 h) and its cross-meta-

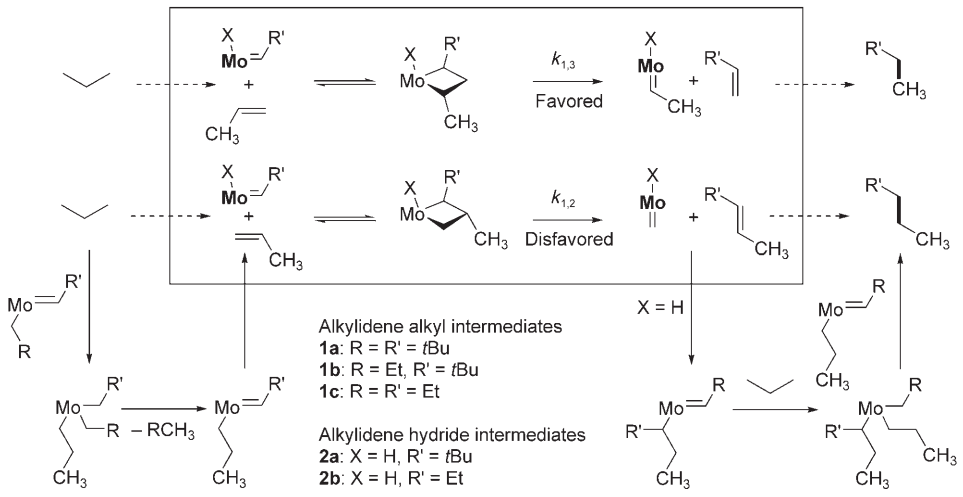

Scheme 2. Metathesis of propane catalyzed by **1**.

 © 2006 Wiley-VCH Verlag GmbH & Co. KGaA, Weinheim

thesis products (Table 1 and Table 2), whereas ethane is not. This finding is in contrast to that observed for Ta-based catalysts, for which an equimolar mixture of methane and propane is obtained from ethane; however, it consistent with the absence of methane in the metathesis of other alkanes (propane and butane). Finally, **1a** does not catalyze the metathesis of 2-methylpropane, a branched alkane, under the same reaction conditions, despite the presence of a reasonable amount of one of the initiation products. Therefore, the propagation step is probably hindered by the olefin-metathesis step, which would require a disfavored [2+2] cycloaddition between a disubstituted carbene and a disubstituted olefin.

In conclusion, the well-defined Mo/imido surface complex **1a** belongs to a new type of silica-supported catalyst precursor for the metathesis of linear alkanes at moderate temperatures (150 °C). The product selectivity clearly shows that the products are formed by π-bond metathesis as a key carbon–carbon bond-breaking and -forming step. Nonetheless, this system involves a single metal with dual properties in contrast to the Goldman–Brookhart system, which relies on mixing two catalysts. More importantly, this result shows for the first time that ancillary ligands, an imido group in this case, can be used. Further development of alkane metathesis catalysts through the investigation of structure–reactivity relationships are currently underway.

Experimental Section

General procedure: All experiments were carried out under dry oxygen-free Ar using either high-vacuum lines (1.34 Pa) or glovebox techniques. [(≡SiO)Mo(=NAr)(=CH*t*Bu)(CH_2*t*Bu)] (**1a**) was obtained according to a previously reported procedure:[15] [Mo(=NAr)(=CH*t*Bu)(CH_2*t*Bu)$_2$][19] (Ar = 2,6-diisopropylphenyl) was impregnated on silica that had been partially dehydroxylated at 700 °C. The alkanes were dried and deoxygenated before use by passing them through a mixture of freshly regenerated molecular sieves (3 Å) and R-3-15 catalysts (BASF).

Procedure for the metathesis reaction of alkanes in a batch reactor: A mixture of catalyst precursor **1a** (13.5 μmol) and dry alkane (540–580 Torr, 500–540 equiv) were heated at 150 °C in batch reactor of known volume (220 mL). Aliquots were drawn and analyzed by gas chromatography over time (HP5890 apparatus, KCl/Al_2O_3 on a fused-silica column, 50 m × 0.32 mm) and the products identified by GC–mass-spectrometric analysis. The selectivities S_i are defined as the amount of product *i* over the total amount of products.

Received: May 31, 2006
Published online: August 17, 2006

Keywords: alkanes · alkylidene ligands · imido ligands · metathesis · molybdenum

[1] J. A. Labinger, J. E. Bercaw, *Nature* **2002**, *417*, 507–514.
[2] G. A. Olah, A. Molnar, *Hydrocarbon Chemistry*, 2nd ed., **2003**.
[3] V. Vidal, A. Théolier, J. Thivolle-Cazat, J.-M. Basset, *Science* **1997**, *276*, 99–102.
[4] C. Copéret, O. Maury, J. Thivolle-Cazat, J.-M. Basset, *Angew. Chem.* **2001**, *113*, 2393–2296; *Angew. Chem. Int. Ed.* **2001**, *40*, 2331–2234.
[5] E. Le Roux, M. Chabanas, A. Baudouin, A. de Mallmann, C. Copéret, E. A. Quadrelli, J. Thivolle-Cazat, J.-M. Basset, W. Lukens, A. Lesage, L. Emsley, G. J. Sunley, *J. Am. Chem. Soc.* **2004**, *126*, 13391–13399.
[6] J. M. Basset, C. Copéret, L. Lefort, B. M. Maunders, O. Maury, E. Le Roux, G. Saggio, S. Soignier, D. Soulivong, G. J. Sunley, M. Taoufik, J. Thivolle-Cazat, *J. Am. Chem. Soc.* **2005**, *127*, 8604–8605.
[7] E. Le Roux, M. Taoufik, C. Copéret, A. de Mallmann, J. Thivolle-Cazat, J.-M. Basset, B. M. Maunders, G. J. Sunley, *Angew. Chem.* **2005**, *117*, 6913–6916; *Angew. Chem. Int. Ed.* **2005**, *44*, 6755–6758.
[8] R. L. Burnett, T. R. Hughes, *J. Catal.* **1973**, *31*, 55–64.
[9] A. S. Goldman, A. H. Roy, Z. Huang, R. Ahuja, W. Schinski, M. Brookhart, *Science* **2006**, *312*, 257–261.
[10] M. Gupta, C. Hagen, R. J. Flesher, W. C. Kaska, C. M. Jensen, *Chem. Commun.* **1996**, 2687–2688.
[11] C. M. Jensen, *Chem. Commun.* **1999**, 2443–2449.
[12] R. R. Schrock, *Chem. Rev.* **2002**, *102*, 145–179.
[13] R. R. Schrock, *J. Mol. Catal. A* **2004**, *213*, 21–30.
[14] C. Copéret, M. Chabanas, R. Petroff Saint-Arroman, J.-M. Basset, *Angew. Chem.* **2003**, *115*, 164–191; *Angew. Chem. Int. Ed.* **2003**, *42*, 156–181.
[15] F. Blanc, C. Copéret, J. Thivolle-Cazat, J.-M. Basset, A. Lesage, L. Emsley, A. Sinha, R. R. Schrock, *Angew. Chem.* **2006**, *118*, 1238–1242; *Angew. Chem. Int. Ed.* **2006**, *45*, 1216–1220.
[16] M. Chabanas, V. Vidal, C. Copéret, J. Thivolle-Cazat, J.-M. Basset, *Angew. Chem.* **2000**, *112*, 2038–2041; *Angew. Chem. Int. Ed.* **2000**, *39*, 1962–1965.
[17] M. Taoufik, E. Le Roux, C. Copéret, J. Thivolle-Cazat, J.-M. Basset, B. Maunders, G. J. Sunley, *Top. Catal.* **2006**, in press.
[18] J. L. Bilhou, J. M. Basset, R. Mutin, W. F. Graydon, *J. Am. Chem. Soc.* **1977**, *99*, 4083–4090.
[19] A. Sinha, R. R. Schrock, *Organometallics* **2004**, *23*, 1643–1645.

 © 2006 Wiley-VCH Verlag GmbH & Co. KGaA, Weinheim

Asymmetric Catalysis

DOI: 10.1002/anie.200602408

Iridium-Catalyzed Enantioselective Synthesis of Allylic Alcohols: Silanolates as Hydroxide Equivalents**

*Isabelle Lyothier, Christian Defieber, and Erick M. Carreira**

The development of efficient processes that give rapid and easy access to optically active building blocks is of great importance, particularly for the synthesis of complex molecules. The metal-catalyzed asymmetric allylic substitution reaction, which involves the addition of a range of diverse nucleophiles to an allylmetal intermediate, is one of the most studied processes.[1] The use of Ir complexes in this transformation provides access to products that are complementary to those obtained from Pd catalysis.[2,3] The types of nucleophiles that have been employed in Ir-catalyzed processes have included enolates derived from malonates, but recently other nucleophiles such as amines, phenols, and alkoxides have been used.[4–6] Omitted from this list is the use of hydroxide, or its equivalent, to give the corresponding product with a free alcohol. Herein, we describe the first example of an iridium-catalyzed enantioselective allylation involving the use of silanolates as nucleophiles, which allows convenient access to chiral allylic alcohols, useful building blocks in asymmetric synthesis [Eq. (1)]. The isolated products are formed in useful yields and 92–99% *ee*.

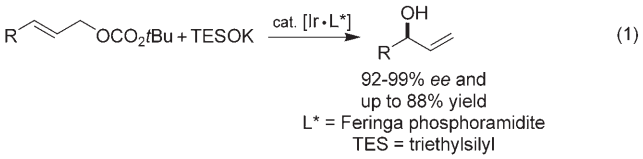

(1)

Over the last few years, iridium catalysis of asymmetric allylic substitution reactions has been the subject of considerable attention, because it allows access to chiral allylic products.[2,4–6] Its use offers a simple, complementary advantage over other methods, since it gives chiral, branched substitution products **4** from achiral, linear allylic derivatives **1**, whereas catalysis of the substitution reaction using palladium favors the linear, achiral adduct **3** from the same starting materials (Scheme 1). This reaction has led to excellent results using C, N, and O nucleophiles reported by the research groups of Hartwig,[4] Helmchen,[5] and Alexakis.[6]

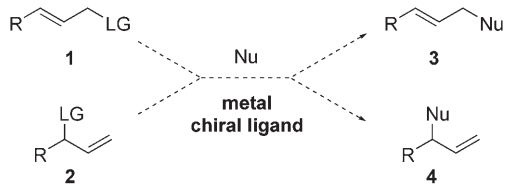

Scheme 1. Transition-metal-catalyzed allylic substitution. LG = leaving group, Nu = nucleophile.

We have documented the use of chiral dienes as ligands in an Ir-catalyzed kinetic resolution of branched allylic carbonates using phenol as a nucleophile.[7] We have been searching to further expand the scope of nucleophiles that can be employed, with particular attention on the development of a process that employs water, or its equivalent, to give rise directly to allylic alcohols. This process became important to us for two reasons: a) the Ir-catalyzed allylic displacement reaction to give the secondary alcohol directly has not been reported to the best of our knowledge,[8] despite the fact that b) the resulting allylic alcohol adducts are amenable to further elaboration.[9] The methods reported to date that could in principle give rise to the free benzylic/allylic alcohols from an allylation process involve the use of the copper salt of benzyl alcohol.[4e,10] However, the chemoselective removal of the *O*-benzyl ether protecting group (**I**, Figure 1) from the products is difficult because of the presence of the C=C bond (**II**, Figure 1) as well as the potential for undesired hydrogenolytic cleavage of the benzylic/allylic C–O bond that defines the stereogenic center (**III**, Figure 1).

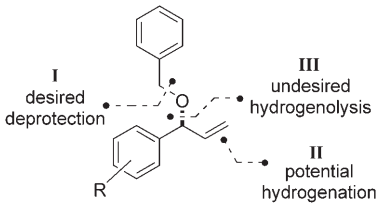

Figure 1. Potential selectivity problems during deprotection.

At the outset of our investigations we employed *tert*-butyl cinnamyl carbonate as a test substrate and examined its reaction with water in the presence of the catalyst derived from Feringa's phosphoramidite ligand[11] and iridium(I).[12] Despite repeated attempts at this reaction, no secondary alcohol was observed. We then screened a number of substrates equivalent to hydroxide, with specific interest in silanols, which appeared to be a particularly attractive class of nucleophiles.[13,14] Silanols can be considered as water surro-

[*] Dr. I. Lyothier, C. Defieber, Prof. Dr. E. M. Carreira
Laboratorium für Organische Chemie
ETH Zürich, HCI H335
8093 Zürich (Switzerland)
Fax: (+41) 44-632-1328
E-mail: carreira@org.chem.ethz.ch

[**] This research was supported by a Swiss National Science Foundation Grant and ETH Zürich. I.L. is grateful to the Roche Research Foundation and the Novartis Foundation for postdoctoral fellowships.

Supporting information for this article is available on the WWW under http://www.angewandte.org or from the author.

InterScience
© 2006 Wiley-VCH Verlag GmbH & Co. KGaA, Weinheim

gates, because cleavage of the silyl ether is known to proceed under a variety of mild conditions.[15] Unfortunately, neither commercially available TMSOK nor TESOH led to the formation of any adducts (Table 1, entries 1 and 2). However, when using the corresponding potassium salt of the latter (TESOK) a promising result was obtained: the secondary silyl ether was formed in 39% yield and 96% *ee* (entry 3).[16] The

Table 1: Investigations into the Ir-catalyzed allylic etherification.

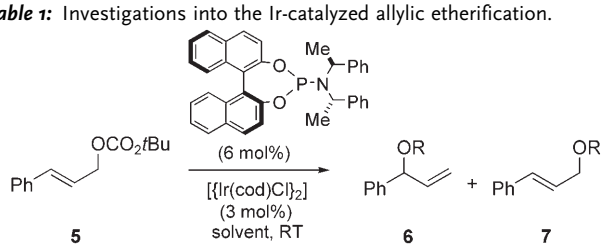

5 **6** **7**

Entry	Nucleophile	Solvent	Ratio **6**:**7**[a]	Yield [%][b]	*ee* [%][c]
1	TESOH	THF	–	–	–
2	TMSOK	THF	–	–	–
3	TESOK	THF	3:1	39	96
4	TESOK	1,4-dioxane	4:1	n.d.	n.d.
5	TESOK	CH_2Cl_2	99:1	90	97
6	TMSOK	CH_2Cl_2	n.d.	30[d]	94
7	TBSOK	CH_2Cl_2	97:3	79	98
8	TIPSOK	CH_2Cl_2	86:14	64	99

[a] Determined by ^{1}H NMR spectroscopy of the unpurified reaction mixtures. [b] Yield of the silyl ether after purification by chromatography. [c] The *ee* value was determined by HPLC on a chiral stationary phase (after deprotection using TBAF in THF). [d] The reaction was slow and did not reach completion. TMS = trimethylsilyl, TBS = *tert*-butyldimethylsilyl, TIPS = triisopropylsilyl, cod = cycloocta-l,5-diene, TBAF = tetra-*n*-butylammonium fluoride, n.d. = not determined.

modest yield was attributed to the poor regioselectivity (**6**/**7** 3:1). A range of different leaving groups were screened with the aim of optimizing the process, but all to no avail. Cinnamyl acetate led only to the formation of the undesired linear product **7**, and cinnamyl carbonates with small alkyl groups underwent alcoholate exchange in competition with etherification.

Gratifyingly, subsequent screening of reaction conditions showed that excellent results arose from changing the reaction solvent to CH_2Cl_2 (Table 1, entry 5). It is interesting that the Ir-catalyzed enantioselective allylations to date have been largely conducted in THF.[4–6] The pronounced solvent effect we observe may be relevant in other processes.[17]

In the context of our preliminary investigations, we noted that various silanolates could be utilized, including TBSOK and TIPSOK (Table 1, entries 7 and 8), with the products formed in 98 and 99% *ee*, respectively. Although the triisopropylsilanolate gave somewhat lower regioselectivity (**6**/**7** 86:14), the *tert*-butyldimethylsilanolate gave the ether **6** in high regioselectivity (**6**/**7** 97:3). The fact that both unhindered, labile (TES) as well as hindered, robust (TBS and TIPS) silyl ethers can be generated is significant. This conveniently permits access to free, optically active secondary alcohols (when using TES) as well as stable silyl ethers (TBS, TIPS) that can be carried through multistep reaction sequences.

Once the standard conditions were identified, our efforts focused on examining the range of substrates that would be tolerated (Table 2). Various electron-poor (Table 2, entries 2–

Table 2: Enantiomerically enriched allylic alcohols from achiral allylic carbonates.

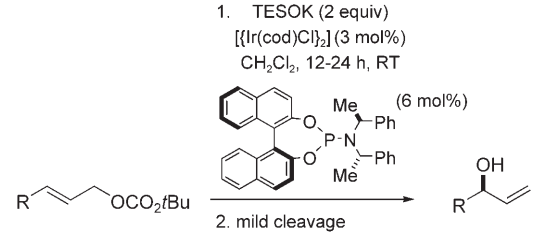

Entry	Substrate	Product	Yield [%][a]	*ee* [%][e]
1	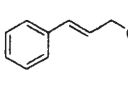	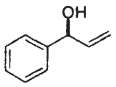	88[b]	97
2	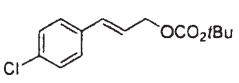	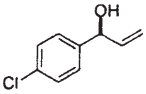	74[b]	98
3	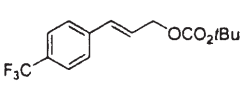	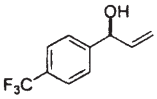	78[b]	98
4	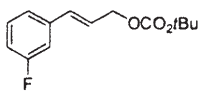	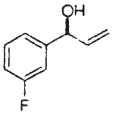	64[c]	98
5	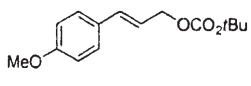	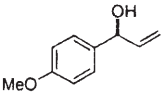	75[b]	95
6	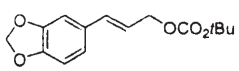	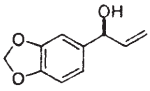	72[b]	92
7	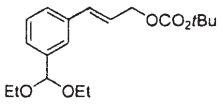	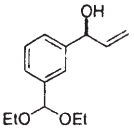	70[c]	98
8	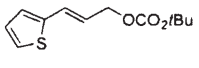	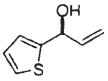	62[b]	99
9	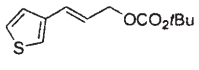	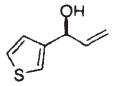	67[c]	98
10	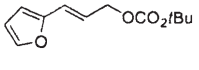	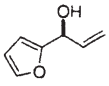	50[c]	97
11	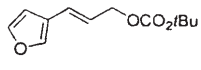	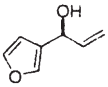	60[c]	99
12	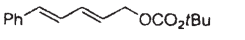	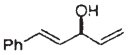	65[b]	97
13	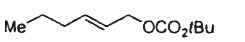	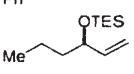	65[d]	95

[a] Yield after purification by chromatography; the regioselectivity was found to be >99:1 in favor of the branched product. [b] Silyl ether cleavage was carried out by using 30% aq NaOH in MeOH. [c] Cleavage of the silyl ether was carried out using TBAF. [d] Isolated as the silyl ether because of volatility problems of the corresponding alcohol. [e] The *ee* value was determined by HPLC or GC on chiral stationary phases; the absolute configuration was established as (*S*) for entry 1.

 © 2006 Wiley-VCH Verlag GmbH & Co. KGaA, Weinheim

4) and electron-rich (Table 2, entries 5 and 6) aryl-substituted allylic carbonates can be used as the starting materials for the transformation. The subsequent cleavage of the silyl ether proceeds uneventfully to yield chiral alcohols in 64–88% yield and with 92–98% *ee*. Notably, the cleavage is conveniently carried out using TBAF in THF. However, a simple deprotection of the crude material with 30% aqueous NaOH in MeOH also allows straightforward access to chiral allylic alcohols. The process tolerates substrates with additional functional groups (for acetals, compare Table 2, entries 6 and 7) without showing any deleterious impact on the yield or enantioselectivity. Furthermore, the reaction can be carried out with heterocyclic-substituted allylic carbonates. Thus, thiophene- (Table 2, entries 8 and 9) and furan-substituted allylic alcohols (Table 2, entries 10 and 11) can be obtained in good yields and excellent enantioselectivities (97–99% *ee*). The reaction of a dienyl carbonate proceeds to give products with high regio- and enantioselectivity (Table 2, entry 12). The method is also tolerant of alkyl-substituted allylic carbonates (Table 2, entry 13).[18]

In conclusion, we have reported the first highly regio- and enantioselective Ir-catalyzed allylic etherification of a wide range of achiral allylic carbonates substituted with aryl and alkyl groups, by using potassium silanolates as the nucleophiles. Subsequent cleavage of the silyl ether of the TES adducts gives rapid and reliable access to chiral allylic alcohols in high yields and enantioselectivities. Stable silyl ethers (TBS, TIPS), which can be carried through multistep reaction sequences, can also be formed in excellent yields and enantioselectivities. The fact that optically active allylic alcohols are easily accessed with this methodology opens up new avenues for the synthesis of complex molecules by Ir catalysis. Additionally, the use of silanolates may be of interest in other carbon–oxygen bond-forming reactions. Further exploration of this methodology and its application in synthesis is underway, and will be reported in due course.

Experimental Section

Representative procedure: A Schlenk flask under argon was charged with $[\{Ir(cod)Cl\}_2]$ (10.1 mg, 15 μmol, 3 mol%) and (*S*)-(+)-(3,5-dioxa-4-phosphacyclohepta[2,1-a;3,4-a′]dinaphthalen-4-yl)bis[(1*S*)-1-phenylethyl]amine (Feringa phosphoramidite) (16.2 mg, 30 μmol, 6 mol%). THF (0.5 mL) and *n*-propylamine (0.5 mL) were added, and the reaction mixture was stirred at 50°C for 30 min. The solution was allowed to cool to RT and the volatiles were removed under high vacuum (30 min). A solution of potassium silanolate (1.00 mmol, 2 equiv) in CH_2Cl_2 (2 mL) was added, followed by *tert*-butyl carbonate (0.50 mmol, 1 equiv) in CH_2Cl_2 (2 mL), and the reaction mixture was stirred at RT. After completion of the reaction (usually 14 h), as determined by TLC, the crude mixture was partitioned between H_2O (20 mL) and CH_2Cl_2 (20 mL). The aqueous layer was then extracted with CH_2Cl_2 (3 × 15 mL). The combined organic layers dried (Na_2SO_4) and concentrated under reduced pressure to afford the crude silyl ether. The ratio of regioisomers was determined by ^1H NMR analysis of the unpurified sample. The mixture was then dissolved in THF (5 mL), cooled to 0°C, and treated with TBAF (1M in THF, 1 mL, 2 equiv). The reaction mixture was stirred for 2 h, then partitioned between H_2O (50 mL) and CH_2Cl_2 (20 mL). The aqueous layer was then extracted with CH_2Cl_2 (3 × 15 mL). The combined organic layers were dried (Na_2SO_4) and concentrated under reduced pressure to afford the crude allylic alcohol. Purification of the residue by flash column chromatography on silica gel afforded the desired product.

Received: June 15, 2006
Published online: August 17, 2006

Keywords: alcohols · allylic compounds · asymmetric catalysis · iridium · nucleophilic substitution

[1] a) B. M. Trost, C. Lee in *Catalytic Asymmetric Synthesis*, 2nd ed. (Ed.: I. Ojima), Wiley, New York, **2000**, p. 593; b) A. Pfaltz, M. Lautens in *Comprehensive Asymmetric Catalysis I–III* (Eds.: E. N. Jacobsen, A. Pfaltz, H. Yamamoto), Springer, Berlin, **1999**, p. 833; c) B. M. Trost, M. Crawley, *Chem. Rev.* **2003**, *103*, 2921; d) for recent examples, see: O. Pàmies, M. Diéguez, C. Claver, *J. Am. Chem. Soc.* **2005**, *127*, 3646.

[2] a) R. Takeuchi, *Synlett* **2002**, 1954; b) H. Miyabe, Y. Takemoto, *Synlett* **2005**, 1641; c) for a recent example of racemic allylic etherification, see: J. P. Roberts, C. Lee, *Org. Lett.* **2005**, *7*, 2679.

[3] For industrial applications, metal prices may also be an important factor: $205 iridium, $290 palladium, $3400 rhodium ($ per oz, January 2006); http://www.platinum.matthey.com.

[4] a) T. Ohmura, J. F. Hartwig, *J. Am. Chem. Soc.* **2002**, *124*, 15164; b) F. Lopez, T. Ohmura, J. F. Hartwig, *J. Am. Chem. Soc.* **2003**, *125*, 3426; c) C. A. Kiener, C. Shu, C. Incarvito, J. F. Hartwig, *J. Am. Chem. Soc.* **2003**, *125*, 14272; d) A. Leitner, C. Shu, J. F. Hartwig, *Proc. Natl. Acad. Sci. USA* **2004**, *101*, 5830; e) C. Shu, J. F. Hartwig, *Angew. Chem.* **2004**, *116*, 4898; *Angew. Chem. Int. Ed.* **2004**, *43*, 4794; f) C. Shu, A. Leitner, J. F. Hartwig, *Angew. Chem.* **2004**, *116*, 4901; *Angew. Chem. Int. Ed.* **2004**, *43*, 4797; g) A. Leitner, C. Shu, J. F. Hartwig, *Org. Lett.* **2005**, *7*, 1093; h) A. Leitner, S. Shekhar, M. J. Pouy, J. F. Hartwig, *J. Am. Chem. Soc.* **2005**, *127*, 15506.

[5] a) J. P. Janssen, G. Helmchen, *Tetrahedron Lett.* **1997**, *38*, 8025; b) B. Bartels, G. Helmchen, *Chem. Commun.* **1999**, 741; c) B. Bartels, C. Garcia-Yebra, F. Rominger, G. Helmchen, *Eur. J. Inorg. Chem.* **2002**, 2569; d) B. Bartels, C. Garcia-Yebra, G. Helmchen, *Eur. J. Org. Chem.* **2003**, 1097; e) G. Lipowsky, N. Miller, G. Helmchen, *Angew. Chem.* **2004**, *116*, 4695; *Angew. Chem. Int. Ed.* **2004**, *43*, 4595; f) S. Streiff, C. Welter, M. Schelwies, G. Lipowsky, N. Miller, G. Helmchen, *Chem. Commun.* **2005**, 2957; g) C. Welter, A. Dahnz, B. Brunner, S. Streiff, P. Dübon, G. Helmchen, *Org. Lett.* **2005**, *7*, 1239; h) M. Schelwies, P. Dübon, G. Helmchen, *Angew. Chem.* **2006**, *118*, 2526; *Angew. Chem. Int. Ed.* **2006**, *45*, 2466; i) A. Dahnz, G. Helmchen, *Synlett* **2006**, 697.

[6] a) K. Tissot-Croset, D. Polet, A. Alexakis, *Angew. Chem.* **2004**, *116*, 2480; *Angew. Chem. Int. Ed.* **2004**, *43*, 2426; b) A. Alexakis, D. Polet, *Org. Lett.* **2004**, *6*, 3529; c) D. Polet, A. Alexakis, *Org. Lett.* **2005**, *7*, 1621; d) D. Polet, A. Alexakis, K. Tissot-Croset, C. Corminboeuf, K. Ditrich, *Chem. Eur. J.* **2006**, *12*, 3596.

[7] C. Fischer, C. Defieber, T. Suzuki, E. M. Carreira, *J. Am. Chem. Soc.* **2004**, *126*, 1628.

[8] For an Ir-catalyzed enantioselective etherification using hydroxylamines as nucleophiles, see: a) H. Miyabe, A. Matsumara, K. Moriyama, Y. Takemoto, *Org. Lett.* **2004**, *6*, 4631; b) H. Miyabe, K. Yoshida, M. Yamauchi, Y. Takemoto, *J. Org. Chem.* **2005**, *70*, 2148; c) for Pd-catalyzed deracemization of allylic carbonates in water for a limited set of substrates, see: H.-J. Gais, T. Jagusch, N. Spalthoff, F. Gerhards, M. Frank, G. Raabe, *Chem. Eur. J.* **2003**, *9*, 4202; d) B. J. Lüssem, H.-J. Gais, *J. Am. Chem. Soc.* **2003**, *125*, 6066; e) H.-J. Gais, O. Bondarev, R. Hetzer, *Tetrahedron Lett.* **2005**, *46*, 6279.

[9] For alternative synthesis of chiral allylic alcohols, see: a) Y. Gao, J. M. Klunder, R. M. Hanson, H. Masamune, S. Y. Ko, K. B.

 © 2006 Wiley-VCH Verlag GmbH & Co. KGaA, Weinheim

Sharpless, *J. Am. Chem. Soc.* **1987**, *109*, 5765; b) K. Burgess, L. D. Jennings, *J. Am. Chem. Soc.* **1990**, *112*, 7434; c) S. F. Kirsch, L. E. Overman, *J. Am. Chem. Soc.* **2005**, *127*, 2866; d) D. Tomita, R. Wada, M. Kania, M. Shibasaki, *J. Am. Chem. Soc.* **2005**, *127*, 4138.

[10] For enantiospecific Rh-catalyzed allylic etherification using copper alkoxides, see: a) P. A. Evans, D. K. Leahy, *J. Am. Chem. Soc.* **2002**, *124*, 7882; b) P. A. Evans, D. K. Leahy, L. M. Slieker, *Tetrahedron: Asymmetry* **2003**, *14*, 3613.

[11] When referring to Feringa's phosphoramidite, we mean (*S*)-(+)-(3,5-dioxa-4-phosphacyclohepta[2,1-a;3,4-a′]dinaphthalen-4-yl) bis[(1*S*)-1-phenylethyl]amine, which is part of the commercially available DSM monophos ligand kit; see also: a) B. L. Feringa, *Acc. Chem. Res.* **2000**, *33*, 346; b) L. A. Arnold, R. Imbos, A. Mandoli, A. H. M. De Vries, R. Naasz, B. L. Feringa, *Tetrahedron* **2000**, *56*, 2865; c) A. Alexakis, S. Rosset, J. Allamand, S. March, J. Guillen, C. Benhaim, *Synlett* **2001**, 1375.

[12] We use the same type of catalyst activation as described in reference [4g]. For details, see the Supporting Information.

[13] For a single example using Ph_3SiOH as the nucleophile in a Pd-catalyzed opening of a vinyl epoxide, see: a) B. M. Trost, N. Ito, P. D. Greenspan, *Tetrahedron Lett.* **1993**, *34*, 1421; b) for applications of this methodology, see: B. M. Trost, P. D. Greenspan, H. Geissler, J. H. Kim, N. Greeves, *Angew. Chem.* **1994**, *106*, 2296; *Angew. Chem. Int. Ed. Engl.* **1994**, *33*, 2182.

[14] Silanols are considerably more acidic than their corresponding alcohols. In DMSO, H_2O: $pK_a = 31.2$, *t*BuOH: $pK_a = 32.2$, TIPSOH: $pK_a = 24.4$, see: J. A. Soderquist, J. Vaquer, M. J. Diaz, A. M. Rane, F. G. Bordwell, S. Zhang, *Tetrahedron Lett.* **1996**, *37*, 2561.

[15] a) M. Lalonde, T. H. Chan, *Synthesis* **1985**, 817; b) T. D. Nelson, R. D. Crouch, *Synthesis* **1996**, 1031.

[16] The reaction only proceeded with low conversion when using TESOLi or TESONa (17% and 44%, respectively). This might be partially attributed to the low solubility of these reactants in CH_2Cl_2.

[17] An increase of regioselectivity in a Pd-catalyzed allylic etherification was observed when changing to more polar solvents, with CH_3CN being optimal: B. M. Trost, F. D. Toste, *J. Am. Chem. Soc.* **1999**, *121*, 4545.

[18] Our current investigations show that α-branched aliphatic allylic carbonates display diminished reactivity.

 © 2006 Wiley-VCH Verlag GmbH & Co. KGaA, Weinheim

Solid-Phase Chemistry

DOI: 10.1002/anie.200602097

A General Approach to the Covalent Immobilization of Single Polymers**

*Li Liu and Mingdi Yan**

Nano- and molecular-scale materials and devices have demonstrated great potential for unique properties and functions that are unattainable at macroscopic scales.[1] Studies of single molecules and their interactions and reactions at the single-molecule level provide new perspectives on important fundamental issues in physics, chemistry, and biology.[2] Often it is desirable to anchor the molecules on suitable substrates to facilitate the study and application of single molecules under various conditions for physical measurement and chemical processing. Two common approaches to single-polymer immobilization are electrostatic adsorption and chemical grafting. The first method involves the deposition of a very dilute polymer solution on a substrate followed by evaporation of the solvent. A key requirement is that the polymer and the substrate possess opposite charges under the experimental conditions for the electrostatic interactions to occur.[3–5] The second method involves chemically grafting the polymer to the substrate. In this case, the polymer is derivatized with a functional group that is subsequently conjugated to the substrates. Examples include Cl-terminated poly(dimethylsiloxane) on silicon,[6] disulfide-modified polystyrene on gold,[7] and polysilanyllithium on a brominated quartz surface.[8] Relative to noncovalent and electrostatic interactions, covalent immobilization offers more stable and robust attachments that can withstand harsh experimental conditions. Herein, we report a general approach to the covalent immobilization of single polymer molecules. This method does not require chemical derivatization of the polymer and is applicable to a variety of materials, including those that do not possess reactive functional groups.

The immobilization chemistry is based on the photochemically or thermally initiated C–H/N–H insertion reactions of perfluorophenylazides (PFPAs).[9–11] The presence of fluorine atoms markedly increases the insertion reaction yield relative to their non-fluorinated counterparts.[12] In the example shown in Scheme 1, a glass or silicon wafer is first treated with PFPA–silane, thus attaching azido groups to the

[*] Dr. L. Liu, Prof. M. Yan
Department of Chemistry
Portland State University
Portland, OR 97207 (USA)
Fax: (+1) 503-725-9525
E-mail: yanm@pdx.edu

[**] The authors acknowledge the financial support from an NIH AREA award 1R15 GM066279-01A2.

Supporting information for this article is available on the WWW under http://www.angewandte.org or from the author.

© 2006 Wiley-VCH Verlag GmbH & Co. KGaA, Weinheim

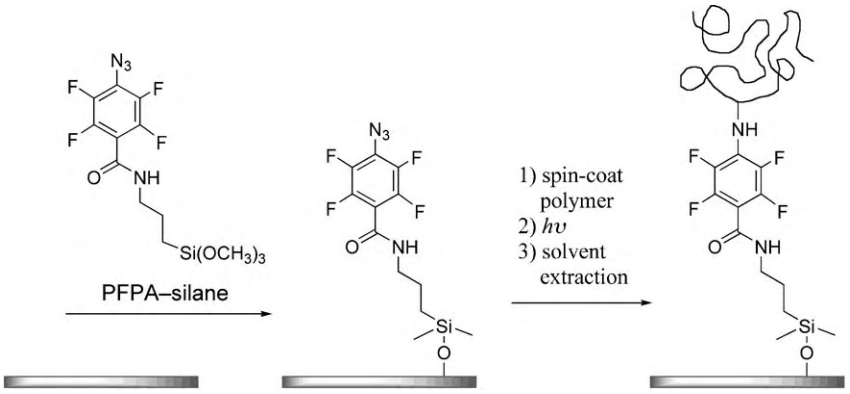

Scheme 1. Covalent immobilization of polymers on silicon oxide using PFPA–silane as the photo-cross-linker.

surface. The polymer is then coated and the azido groups activated to form covalent linkages to the polymer. We found that this immobilization method is highly reproducible and tolerant of defects. Uniform polymer films were obtained from wafers treated with PFPA–silane at concentrations of a few micromoles, or when more than 100 times of a non-photoactive silane was added,[13] which is because in principle, only one attachment point is necessary to tether the entire polymer chain to the surface. We therefore hypothesize that as the density of the surface azido groups continues to decrease, the immobilized polymer will no longer be uniform. The thickness of the polymer film will decrease and eventually the surface will be populated by isolated single polymer molecules. The density of the surface azido groups can be controlled by the concentration of PFPA–silane or by treating the surface with a mixture of PFPA–silane and a non-photoactive silane.[13]

Herein, we report the covalent immobilization of single polymer molecules using dilute PFPA–silane solutions. Comprehensive studies were conducted on polystyrene, a polymer that does not possess any functional groups. In the experiment, cleaned silicon wafers were treated with solutions of PFPA–silane in toluene, the concentrations of which ranged from 5×10^{-1} to 5×10^{-5} mg mL^{-1}. The wafers were then spin-coated with polystyrene. Irradiation followed by removal of the unbound polymer with toluene yielded covalently attached polymers. The thickness and water-contact angles of the resulting films are shown in Figure 1.

As the concentration of PFPA–silane decreased, the immobilized polymer became thinner (Figure 1a). At the PFPA–silane concentration of 5×10^{-3} mg mL^{-1}, the contact angle decreased to approximately 57°, thus indicating the collapse of the film (Figure 1b). Further dilution resulted in lower contact angles and no film was detected by ellipsometry. When the immobilization was carried out on wafers treated with PFPA–silane at 5×10^{-5} mg mL^{-1}, isolated single polystyrene molecules were observed (Figure 2a).

To confirm that the particles were indeed polymer single molecules, polystyrene of various molecular weights was used. The size of a polymer is directly related to its molecular weight: the higher the molecular weight, the larger the radius of gyration (R_g) and thus the size of the molecule. Indeed, we observed that the size of the particles, that is, the immobilized single polymer molecules, increased with the molecular weight of the polymer (Figure 2).

We found that the higher the molecular weight, the lower the concentration of PFPA–silane was needed to obtain single-molecule immobilization (see Figure 2). This finding is consistent with the immobilization chemistry shown in Scheme 1. As the molecular weight and thus size of the polymer increases, less surface azido groups are needed to attach the polymer. The concentration of PFPA–silane was therefore lowered to observe isolated single molecules.

Atomic force microscopy (AFM) revealed that

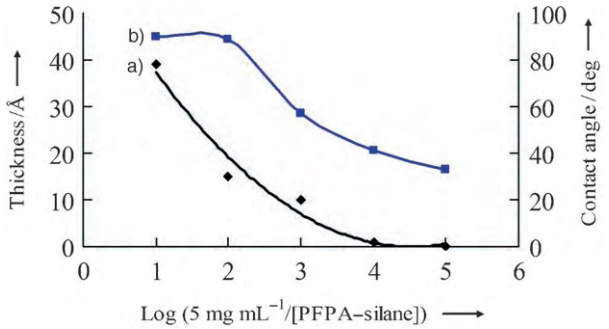

Figure 1. a) Thickness, measured by ellipsometry, and b) water contact angle of the immobilized polymer as a function of PFPA–silane concentration. The contact angle of the unfunctionalized silicon wafer was measured to be approximately 17°.

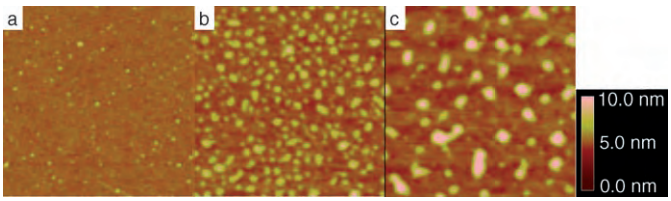

Figure 2. Single polystyrene molecules covalently immobilized on silicon wafers. Monodisperse polystyrene used: a) $M_w = 223\,200$, b) 570 000, and c) 1 877 000 g mol^{-1}. The wafers were treated with PFPA–silane at concentrations of a) 5×10^{-5}, b) 1×10^{-5}, c) 5×10^{-6} mg mL^{-1}, respectively. The scan area is 1×1 μm^2 for all three images.

the immobilized polystyrene adopted a cone shape (Figure 3). The volume of a single polystyrene molecule V can thus be calculated according to Equation (1), where H is the height and D is the diameter of the molecule measured by AFM. Results showed that the measured values (V) are in good agreement with those calculated from the molecular weights of the polymer (V_{calcd}; Table 1).[4]

$$V = {}^1\!/_3 H\pi\left(\frac{D}{2}\right)^2 \qquad (1)$$

 © 2006 Wiley-VCH Verlag GmbH & Co. KGaA, Weinheim

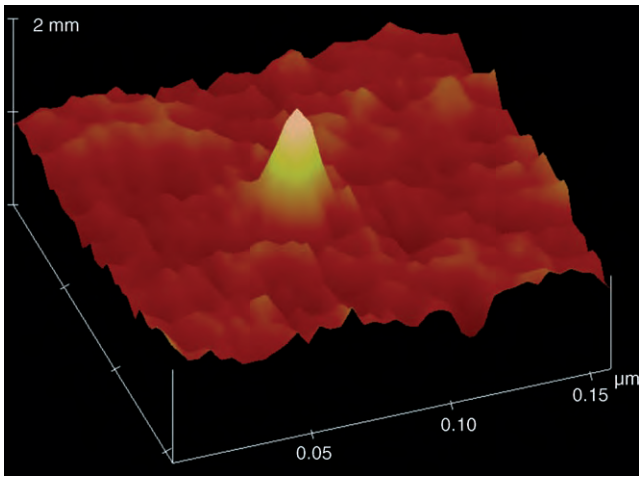

Figure 3. AFM topographic image enlarged from Figure 2a.

Table 1: Measured and calculated sizes of single molecules.

M_w	D [nm]	H [nm]	V [nm^3]	V_{calcd} [nm^3]
223 200	32 ± 6[a]	1.6 ± 0.6[a]	429	370
570 000	50 ± 7[b]	1.9 ± 0.5[b]	1243	947
1 877 000	69 ± 14[c]	2.7 ± 1.2[c]	3364	3118

The D and H values were measured and averaged from [a] 112, [b] 85, and [c] 51 particles from the corresponding images in Figure 2, excluding obvious large aggregates.

The versatility of the method was tested with poly(2-ethyl-oxazoline) (PEOX), a hydrophilic polymer that also lacks reactive functional groups. Following a similar procedure, single molecules of PEOX were successfully immobilized (Figure 4). A much higher concentration of PFPA–silane was needed for PEOX (5×10^{-1} mg mL^{-1}) than for polystyrene (10^{-5} mg mL^{-1}, $M_w = 570\,000$). This difference can be attributed to the difference in the immobilization efficiency of the two polymers, which is in part governed by the local concentration of the polymer in proximity to the azide-functionalized surface.[14] Evaluation of 62 particles from the AFM image yielded the average particle volume of 1764 nm^3 ($D = (53 \pm 8)$ nm, $H = (2.4 \pm 1.1)$ nm), whereas the calculated molecular volume is 830 nm^3 based on the average molecular weight of the sample ($M_w = 500\,000$). Unlike polystyrene samples, which are monodisperse, the PEOX obtained from Aldrich is polydisperse (molecular weight distribution is unknown); a polydisperse polymer is more heterogeneous than its monodisperse counterpart with respect to molecular weight. When a polymer containing various sized molecules is coated on a surface with a limited amount of azido groups, larger molecules, that is, polymers of higher molecule weight, are more likely than smaller molecules to be attached. The molecular volume of the immobilized polymer is thus larger than the theoretical value that is calculated from the average molecular weight of the original sample. This preferential immobilization of larger sized polymers was also observed for polystyrene (Table 1), although the deviations were smaller than PEOX as a result of the monodisperse nature of the polystyrene samples.

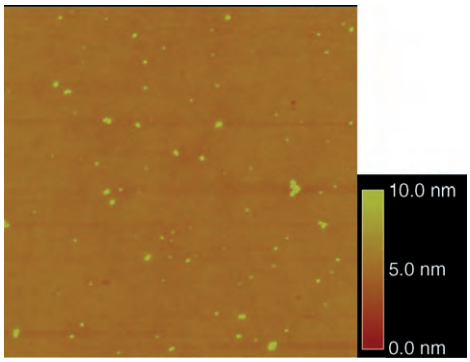

Figure 4. AFM topographic image of immobilized PEOX ($M_w = 500\,000$ g mol^{-1}) on a silicon wafer treated with 5×10^{-1} mg mL^{-1} of PFPA–silane in toluene. The scan area is 3×3 μm^2.

Extended single polymer chains were occasionally observed as shown in Figure 5. The curvilinear length was measured to be 430 nm. This value falls in the range of 95–953 nm, as calculated from the molecular-weight distribution of the polystyrene sample.[15–16]

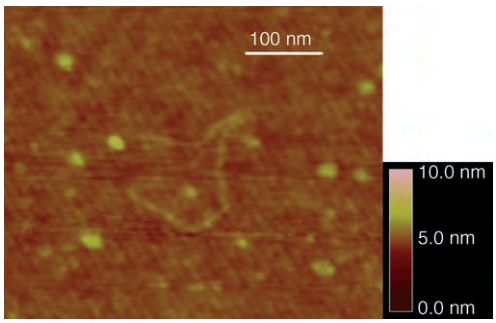

Figure 5. An extended polystyrene molecule ($M_w = 223\,200$ g mol^{-1}).

In summary, a simple and general method has been developed for the covalent immobilization of single polymer molecules on silicon wafers. Because the immobilization is based on C–H/N–H insertion reactions, it is versatile and especially suited for molecules that do not possess functional groups and are difficult to be immobilized by other means. Single-polymer immobilization was also achieved by treating the wafer surface with a mixture of PFPA–silane and a non-photoactive silane. Studies are underway to investigate the nature of the attachment, including the polymer attachment point and orientation.

Received: May 25, 2006
Published online: August 14, 2006

Keywords: immobilization · photochemistry · polymers · scanning probe microscopy · single-molecule studies

[1] a) T.-H. Lee, J. I. Gonzalez, J. Zheng, R. M. Dickson, *Acc. Chem. Res.* **2005**, *38*, 534–541; b) L. Venkataraman, J. E. Klare, I. W.

 © 2006 Wiley-VCH Verlag GmbH & Co. KGaA, Weinheim

Tam, C. Nuckolls, M. S. Hybertsen, M. L. Steigerwald, *Nano Lett.* **2006**, *6*, 458 – 462.
[2] a) S. A. Rosenberg, M. E. Quinlan, J. N. Forkey, Y. E. Goldman, *Acc. Chem. Res.* **2005**, *38*, 583 – 593; b) F. L. H. Brown, *Acc. Chem. Res.* **2006**, *39*, 363 – 373; c) X. Michalet, S. Weiss, M. Jager, *Chem. Rev.* **2006**, *106*, 1785 – 1813.
[3] M. Radmacher, M. Fritz, H. G. Hansma, P. K. Hansma, *Science* **1994**, *265*, 1577 – 1579.
[4] G. Gorodyska, A. Kiriy, S. Minko, C. Tsitsilianis, M. Stamm, *Nano Lett.* **2003**, *3*, 365 – 368.
[5] V. Bocharova, A. Kiriy, M. Stamm, F. Stoffelbach, R. Jérôme, C. Detrembleur, *Small* **2006**, *2*, 910 – 916.
[6] S. Al-Maawali, J. Bemis, B. Akhremitchev, R. Leecharoen, B. Janesko, G. Walker, *J. Phys. Chem. B* **2001**, *105*, 3965 – 3971.
[7] S. Al-Maawali, J. Bemis, B. Akhremitchev, H. Liu, G. Walker, *J. Adhes.* **2005**, *81*, 999 – 1016.
[8] K. Furukawa, *Acc. Chem. Res.* **2003**, *36*, 102 – 110.
[9] M. Bartlett, M. Yan, *Adv. Mater.* **2001**, *13*, 1449 – 1451.
[10] M. Yan, M. Bartlett, *Nano Lett.* **2002**, *2*, 275 – 278.
[11] M. Yan, J. Ren, *Chem. Mater.* **2004**, *16*, 1627 – 1632.
[12] W. T. Borden, N. P. Gritsan, C. M. Hadad, W. L. Karney, C. R. Kemnitz, M. S. Platz, *Acc. Chem. Res.* **2000**, *33*, 765 – 771.
[13] L. Liu, M. Yan, unpublished results.
[14] M. Yan, J. Ren, *J. Mater. Chem.* **2005**, *15*, 523 – 527.
[15] J. Kumaki, Y. Nishikawa, T. Hashimoto, *J. Am. Chem. Soc.* **1996**, *118*, 3321 – 3322.
[16] J. Kumaki, T. Hashimoto, *J. Am. Chem. Soc.* **2003**, *125*, 4907 – 4917.

 © 2006 Wiley-VCH Verlag GmbH & Co. KGaA, Weinheim

U–U Multiple Bonds

DOI: 10.1002/anie.200602280

Quantum Chemical Calculations Predict the Diphenyl Diuranium Compound [PhUUPh] To Have a Stable ^1A_g Ground State**

*Giovanni La Macchia, Marcin Brynda, and Laura Gagliardi**

Use of sterically hindered ligands to maintain the integrity of normally unstable chemical entities is a widespread technique in modern synthetic chemistry. Bulky aryl and alkyl substituents have been designed to stabilize sensitive compounds, such as main-group-element dimers with multiple bonds,[1] including the alkyne analogues of heavier Group 14 elements.[2,3] This methodology was recently employed in the generation of a new stable low-valent chromium dimer that, according to experimental and theoretical evidence, exhibited a Cr–Cr quintuple bond.[4,5] The synthesis and characterization of this crystalline compound, [Ar′CrCrAr′] (Ar′ = C_6H_3-2,6(C_6H_3-2,6-*i*Pr_2)$_2$), has renewed interest in metal-metal multiple bonding. A subsequent computational study[5] on a simplified model for [Ar′CrCrAr′], [PhCrCrPh], predicted a fivefold bonding picture with filled bonding orbitals ($\sigma^2\pi^4\delta^4$) as the predominant electronic configuration in the singlet ground state.

In contrast to the multiple bonding between early transition metals, like, for example, the quadruple bond in $K_2[Re_2Cl_8]\cdot 2H_2O$,[6] only rare examples of direct M–M interactions are known in actinide chemistry. The only known bonds of such type occur in the hydride $[H_2UUH_2]$[7] or in the U_2 species, experimentally trapped in argon matrices,[8] which we have previously described through high-level calculations.[9] In the U_2 dimer,[9] two uranium atoms bind to form a quintuple bond, thus suggesting that this U_2 unit could form the framework for the development of more diverse diuranium chemistry. The U_2^{2+} cation[10] was also found to be metastable, exhibiting a large number of low-lying electronic states with a short bond length of about 2.30 Å, compared to 2.43 Å in the neutral U_2 molecule.

The natural tendency of a uranium atom to be preferentially complexed by a ligand, rather than to explicitly form a direct U–U bond, has to date precluded the isolation of stable uranium species exhibiting direct metal–metal bonding. From the experimental point of view, the synthesis of multiply bonded uranium compounds poses many challenges. Although the uranium ionic radius is not exceedingly large, the presence of many electrons combined with the preference for certain coordination modes with common ligands make the task of stabilizing the hypothetical U–U bond difficult. With the relatively low first ionization energies of 584 ($M\rightarrow M^+$) and 1420 kJ mol^{-1} ($M^+\rightarrow M^{2+}$) and the ground-state electron configuration corresponding to $[Rn]5f^36d^17s^2$, uranium seems nevertheless to be a promising candidate to form multiply bonded species in actinide chemistry. Despite the fact that this most common actinide exhibits a large range of oxidation states (the most common is U^{+6}, but less common oxidation states such as U^{+2}, U^{+3}, U^{+4}, and U^{+5} are also known), monovalent uranium ions have not yet been formally identified.[11]

Light atoms that are present in various organic ligands are known to bind tightly to uranium ions.[12–15] Furthermore, hexa- or tetrafluoro complexes with U^{6+} and U^{4+} are easily formed,[16] and tetravalent uranium is also stable in hydroxides, hydrated fluorides, and phosphates.[17] Hexavalent uranium is the most stable oxidation state, and the most commonly occurring uranium oxide is U_3O_8. Experimental studies taking advantage of the complex behavior of the f orbitals of uranium result in new variations of the already known moieties described above. For example, recent reports of uranium rings containing bimetallic nitride linkages[15] or of

[*] G. La Macchia, Prof. L. Gagliardi
Département de chimie physique
Université de Genève
30, Quai Ernest Ansermet, 1211 Genève (Switzerland)
Fax: (+41) 22-379-6518
E-mail: laura.gagliardi@chiphy.unige.ch
Dr. M. Brynda
Department of Chemistry
University of California
Davis One Shields Avenue, Davis, CA 95616 (USA)

[**] G.L.M. and L.G. thank the Swiss National Foundation (grant no. 200021-111645/1). The authors thank P. P. Power and B. O. Roos for stimulating discussions.

Supporting information for this article is available on the WWW under http://www.angewandte.org or from the author.

 InterScience © 2006 Wiley-VCH Verlag GmbH & Co. KGaA, Weinheim

an ammonium salt of uranium polyazide, $[U(N_3)_7]^{3-}$,[14] show that more can be done in this quickly expanding field.

To obtain direct metal–metal bonds, at least two conditions must be fulfilled. A proper supporting ligand has to be prepared, and one has to control the oxidation state of the dimeric metal moiety. To maximize the bonding interactions between metal centers, the number of orbitals engaged in metal–ligand bonding should be reduced, and each metal center should have a maximum number of valence electrons to fill the remaining bonding orbitals. These criteria can be achieved if the metal is in a low oxidation state and bound to a monodentate ligand. The ligand, in turn, must be sufficiently bulky as to stabilize the metal center and prevent further reaction. In the case of uranium, however, the tendency for the higher oxidation states would suggest that if a multiple bond is to be formed between uranium atoms, such a species would rather bear several ligands on each multivalent U center. We have recently studied computationally such multiply bonded molecules (U_2Cl_6, $[U_2Cl_8]^{2-}$).[18] On the other hand, there is no evidence against formation of a lower oxidation state for uranium, and experimental evidence exists for the formation of several uranium hydrides (UH, UH_2, UH_3, U_2H_2, UH_4, U_2H_4), thus implying that a continuous range of oxidation states is available.[7]

Although U–O, U–N, and U–C bonds with σ character form easily,[19] several studies indicate that such bonds might already possess a multiple character.[15,20–24] This property is mainly a result of the presence of the 5f and 6d orbitals that can directly participate in the bonding. It is therefore difficult to predict to what extent the bonding between two uranium atoms will be characterized by a higher bond order.

Based on several experimental reports of compounds in which the uranium center is bound to a carbon atom, we have considered the possibility that a {CUUC} core containing two U^{1+} ions could be incorporated between two sterically hindered ligands. Herein, we present the results of a theoretical study of a simplified model for such a hypothetical molecule, namely [PhUUPh]. We have chosen to mimic the bulky terphenyl ligands, which could be potentially promising candidates for the stabilization of multiply bonded uranium compounds, by using the simplest phenyl moiety. We demonstrate that [PhUUPh] could be a stable chemical entity with a singlet ground state.

The complete active space (CAS) self-consistent field (SCF) method[25] was used to generate molecular orbitals and reference functions for subsequent multiconfigurational second-order perturbation theory calculations of the dynamic correlation energy (CASPT2). Additional density functional theory (DFT) calculations were also performed.

The structures of two isomers were initially optimized using DFT, namely the bent-planar [PhUUPh] isomer **A** and the linear isomer **B** (Figure 1). Starting from a *trans*-bent-planar structure, the geometry optimization for isomer **A** predicted a rhombic structure (a bis(μ-phenyl) structure) belonging to the D_{2h} point group and analogous to the experimentally known species U_2H_2.[7] Linear structure **B** also belongs to the D_{2h} point group.

CASPT2 geometry optimizations for several electronic states of various spin multiplicities were performed on

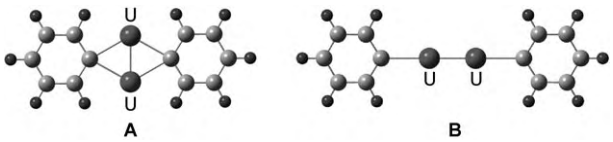

Figure 1. The bent-planar [PhUUPh] isomer (**A**) and the linear [PhUUPh] isomer (**B**).

selected structural parameters, namely the U–U and U–C bond lengths, while the geometry of the phenyl fragment was kept fixed. The most relevant CASPT2 structural parameters for the lowest electronic states of the isomers **A** and **B**, together with the relative CASPT2 energies, are reported in Table 1. The ground state of [PhUUPh] is a ^1A_g singlet with a

Table 1: Most significant CASPT2 structural parameters and relative energies for the lowest electronic states of isomer **A** and **B** of [PhUUPh].

Isomer	State	*d*(U–U) [Å]	*d*(U–C) [Å]	U-C-U [°]	C-U-C [°]	Δ*E* [kcal mol^{-1}][1]
A	^1A_g	2.286	2.315	59.2	120.8	0 (−2.46378)[a]
A	^3A_g	2.263	2.325	58.3	121.8	+0.76
A	$^5B_{3g}$	2.537	2.371	64.7	115.3	+4.97
A	$^5B_{3u}$	2.390	2.341	61.4	118.6	+7.00
A	$^3B_{3g}$	2.324	2.368	58.8	121.2	+7.00
A	$^1B_{3g}$	2.349	2.373	59.3	120.7	+7.14
B	$^5B_{2u}$	2.304	2.395		180	+19.67
B	$^3B_{3g}$	2.223	2.430		180	+22.16
B	^3A_g	2.221	2.430		180	+22.69
B	$^1B_{3g}$	2.255	2.416		180	+27.62

[a] For the ^1A_g ground state the total CASPT2 energy is reported in parentheses (Hartree). The other total energies and the full structure of ^1A_g are reported in the Supporting Information.

bis(μ-phenyl) structure (**A**, Figure 1) and an electronic configuration $\sigma^2\sigma^2\pi^4\delta^2$, thus corresponding to a formal U–U quintuple bond. This configuration has a total weight of 49% in the CASSCF wave function. The following occupation numbers are obtained from the CASSCF calculation: σ_g (1.88), σ_u^* (0.06), σ_g (1.65), σ_u^* (0.35), π_u (3.50), π_g^* (0.47), δ_g (1.62), δ_u^* (0.36), thus yielding an effective bond order of 3.7 between the two uranium atoms.

It is interesting to compare the electronic configurations of the formal U_2^{2+} moiety in [PhUUPh] and the bare metastable U_2^{2+} cation.[10] The U_2^{2+} cation has a singlet ground state with a total orbital angular momentum quantum number (Λ) equal to 10, corresponding to a ^1N_g state. The $^1\Sigma_g^+$ state lies 279 cm^{-1} above the ground state and is degenerate with a triplet state. The ground state of U_2^{2+} has an electronic configuration $\sigma^2\pi^4\delta_g^1\delta_u^1\varphi_u^1\varphi_g^1$, thus corresponding to a triple bond between the two U atoms and four fully localized electrons. In [PhUUPh], the electronic configuration is different, mainly because the molecular environment decreases the coulomb repulsion between the two U^{1+} centers, thus making the U–U bond stronger than in U_2^{2+}. The corresponding U–U bond length (2.29 Å) is also slightly shorter than in U_2^{2+} (2.30 Å). A single bond is present between the U and C atoms. The molecular orbitals that form

 © 2006 Wiley-VCH Verlag GmbH & Co. KGaA, Weinheim

the chemical bonds between the U–U and U–C atoms are represented in Figure 2.

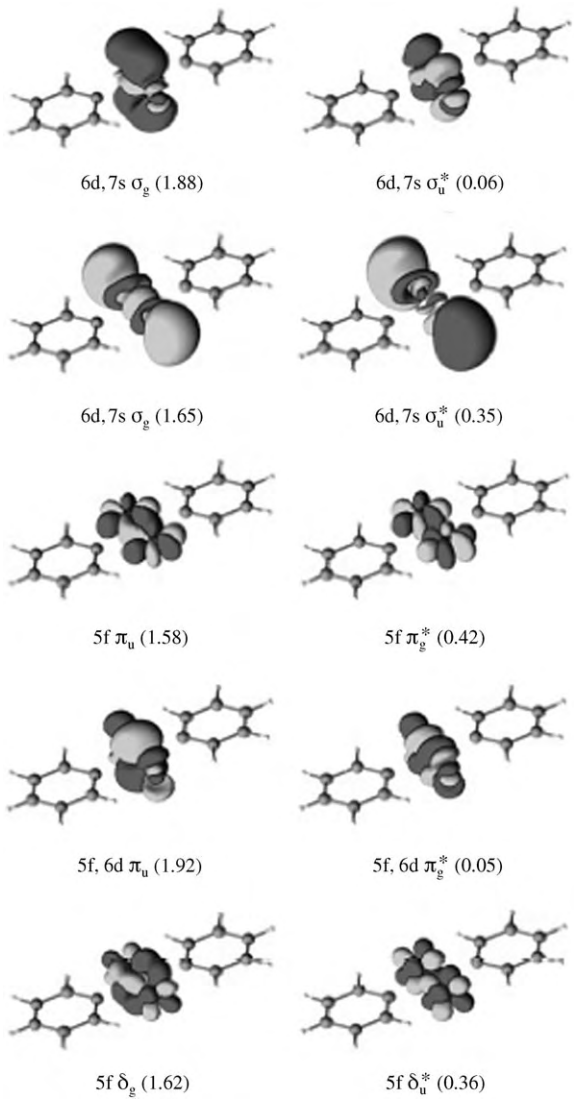

Figure 2. Active molecular orbitals of the bent-planar isomer ^1A_g.

Inspection of Table 1 shows that the lowest triplet state, ^3A_g, is almost degenerate with the ground state (0.76 kcal mol^{-1} higher). Several triplet and quintet states lie 5–7 kcal mol^{-1} above the ground state. The lowest electronic states of the linear structure lie about 20 kcal mol^{-1} above the ground state of the bis(μ-phenyl) structure.

Since the ^1A_g and the ^3A_g states are close in energy, they may interact through the spin–orbit coupling operator. To evaluate the impact of such an interaction, the spin–orbit coupling between several singlet and triplet states was computed at the ground-state (^1A_g) geometry. First, the ordering of the electronic states is not affected by the inclusion of spin–orbit coupling. Analogous computation with the geometry of the ^3A_g state yields the singlet as the lowest state. The only difference concerns the energy difference ΔE_{S1-S2} between the two lowest spin states (^1A_g and ^3A_g), which is reduced to 0.3 kcal mol^{-1}.

To assess the strength of the U–U bond in [PhUUPh], its bonding energy was computed as the difference between the energy of [PhUUPh] and those of the two unbound [PhU] fragments. The ground state of [PhU] (with the U, C1, and C2 atoms collinear) was found to be a quartet ($^4B_2$) in C_{2v} symmetry. The CASPT2 Ph–U bond length is 2.38 Å. [PhUUPh] is lower in energy than two [PhU] fragments by about 60 kcal mol^{-1}, with the inclusion of a basis-set superposition error correction.

The question that one would like to answer is how to make [PhUUPh] and similar species experimentally. [PhUUPh] could in principle be formed in a matrix—analogous to the already detected diuranium polyhydride species[7]—by laser ablation of uranium and co-deposition with biphenyl in an inert matrix. The phenyl ligand might however be too large to be made in a matrix, and species such as [CH_3UUCH_3] may be more feasible.

Experimental Section

The calculations were performed using the software MOLCAS 6.2.[26] All electron basis sets of atomic natural-orbital type, developed for relativistic calculations with the Douglas–Kroll–Hess Hamiltonian,[27] were employed for all atoms. For uranium, a primitive set 26s23p17d13f5g3h was contracted to 8s7p5d3f1g. For carbon, the primitive set 14s9p4d3f2g was contracted to 3s2p1d. For hydrogen, the primitive set 8s4p3d1f was contracted to 2s1p.

The starting geometries were obtained from DFT geometry optimizations by using the B3LYP exchange correlation functional with the same basis set as described above. The C_{2h} symmetry constraint was imposed during the geometry optimization.

Subsequent multiconfigurational wave function calculations, followed by second-order perturbation theory, were performed using the CASSCF/CASPT2[28] method available in MOLCAS 6.2.

The active space was formed by 14 molecular orbitals (MOs), which are linear combinations of uranium 7s, 6d, 5f, and carbon (bonded to the U atoms) 2p orbitals. Ten active electrons were distributed in the 14 MOs.

In the subsequent CASPT2 calculations the orbitals up to and including the U 5d orbital were kept frozen. Selected bond lengths (U–U, U–C) were reoptimized at the CASPT2 level of theory.

Spin–orbit effects were taken into account by using the RASSCF state interaction method (RASSI),[29] which allows CASSCF wave functions for different electronic states to interact under the influence of a spin–orbit Hamiltonian.

The CASSCF/CASPT2/RASSI methods and the basis sets used here have been successful in a number of studies on dimetal compounds.[30,31]

The effective bond order between the two U atoms in [PhUUPh] was calculated as the sum of the occupation numbers of the bonding orbitals minus the sum of the occupation numbers of the antibonding orbitals, divided by two.

Received: June 7, 2006
Published online: August 14, 2006

Keywords: density functional calculations · metal–metal interactions · multiple bonds · structure elucidation · uranium

[1] P. P. Power, *Inorg. Chim. Acta* **1992**, *198–200*, 443–447.
[2] L. Pu, A. D. Phillips, A. F. Richards, M. Stender, R. S. Simons, M. M. Olmstead, P. P. Power, *J. Am. Chem. Soc.* **2003**, *125*, 11626–11636.

 © 2006 Wiley-VCH Verlag GmbH & Co. KGaA, Weinheim

[3] M. Stender, A. D. Phillips, R. J. Wright, P. P. Power, *Angew. Chem.* **2002**, *114*, 1863 – 1865; *Angew. Chem. Int. Ed.* **2002**, *41*, 1785 – 1787.
[4] T. Nguyen, A. D. Sutton, M. Brynda, J. C. Fettinger, G. J. Long, P. P. Power, *Science* **2005**, *310*, 844 – 847.
[5] M. Brynda, L. Gagliardi, P.-O. Widmark, P. P. Power, B. O. Roos, *Angew. Chem.* **2006**, *118*, 3888 – 3891; *Angew. Chem. Int. Ed.* **2006**, *45*, 3804 – 3807.
[6] F. A. Cotton, N. F. Curtis, C. B. Harris, B. F. G. Johnson, S. J. Lippard, J. T. Mague, W. R. Robinson, J. S. Wood, *Science* **1964**, *145*, 1305 – 1307.
[7] P. F. Souter, G. P. Kushto, L. Andrews, M. Neurock, *J. Am. Chem. Soc.* **1997**, *119*, 1682 – 1687.
[8] L. N. Gorokhov, A. M. Emelyanov, Y. S. Khodeev, *Teplofiz. Vys. Temp.* **1974**, *12*, 1307 – 1309.
[9] L. Gagliardi, B. O. Roos, *Nature* **2005**, *433*, 848 – 851.
[10] L. Gagliardi, P. Pyykkö, B. O. Roos, *Phys. Chem. Chem. Phys.* **2005**, *7*, 2415 – 2417.
[11] W. J. Evans, S. A. Kozimor, *Coord. Chem. Rev.* **2006**, *250*, 911 – 935.
[12] T. Arliguie, C. Lescop, L. Ventelon, P. C. Leverd, P. Thuery, M. Nierlich, M. Ephritikhine, *Organometallics* **2001**, *20*, 3698 – 3703.
[13] M. Brynda, T. A. Wesolowski, K. Wojciechowski, *J. Phys. Chem. A* **2004**, *108*, 5091 – 5099.
[14] M.-J. Crawford, A. Ellern, P. Mayer, *Angew. Chem.* **2005**, *117*, 8086 – 8090; *Angew. Chem. Int. Ed.* **2005**, *44*, 7874 – 7878.
[15] W. J. Evans, S. A. Kozimor, J. W. Ziller, *Science* **2005**, *309*, 1835 – 1838.
[16] A. W. Savage, Jr., J. C. Browne, *J. Am. Chem. Soc.* **1960**, *82*, 4817 – 4821.
[17] V. Vallet, Z. Szabo, I. Grenthe, *Dalton Trans.* **2004**, 3799 – 3807.
[18] B. O. Roos, L. Gagliardi, *Inorg. Chem.* **2006**, *45*, 803 – 807.
[19] J. T. Lyon, L. Andrews, *Inorg. Chem.* **2006**, *45*, 1847 – 1852.
[20] K. A. N. S. Ariyaratne, R. E. Cramer, J. W. Gilje, *Organometallics* **2002**, *21*, 5799 – 5802.
[21] R. E. Cramer, J. H. Jeong, J. W. Gilje, *Organometallics* **1987**, *6*, 2010 – 2012.
[22] R. E. Cramer, R. B. Maynard, J. C. Paw, J. W. Gilje, *J. Am. Chem. Soc.* **1981**, *103*, 3589 – 3590.
[23] M. Straka, M. Patzschke, P. Pyykkö, *Theor. Chem. Acc.* **2003**, *109*, 332 – 340.
[24] K. Tatsumi, A. Nakamura, *Appl. Quantum Chem. Proc. Nobel Laureate Symp.* **1986**, 299 – 311.
[25] B. O. Roos in *Advances in Chemical Physics, Ab Initio Methods in Quantum Chemistry, Vol. II* (Eds.: K. P. Lawley), Wiley, Chichester, **1987**, chap. 69, p. 399.
[26] G. Karlström, R. Lindh, P.-Å. Malmqvist, B. O. Roos, U. Ryde, V. Veryazov, P.-O. Widmark, M. Cossi, B. Schimmelpfennig, P. Neogrady, L. Seijo, *Comput. Mater. Sci.* **2003**, *28*, 222 – 239.
[27] B. A. Hess, *Phys. Rev. A* **1986**, *33*, 3742 – 3748.
[28] K. Andersson, P.-Å. Malmqvist, B. O. Roos, A. J. Sadlej, K. Wolinski, *J. Phys. Chem.* **1990**, *94*, 5483 – 5488.
[29] B. O. Roos, P.-Å. Malmqvist, *Phys. Chem. Chem. Phys.* **2004**, *6*, 2919 – 2927.
[30] L. Gagliardi, B. O. Roos, *Inorg. Chem.* **2003**, *42*, 1599 – 1603.
[31] F. Ferrante, L. Gagliardi, B. E. Bursten, A. P. Sattelberger, *Inorg. Chem.* **2005**, *44*, 8476 – 8480.

 © 2006 Wiley-VCH Verlag GmbH & Co. KGaA, Weinheim

Photocatalysis

DOI: 10.1002/anie.200600543

A Supramolecular Photocatalyst for the Production of Hydrogen and the Selective Hydrogenation of Tolane**

Sven Rau, Bernhard Schäfer, Dieter Gleich, Ernst Anders, Manfred Rudolph, Manfred Friedrich, Helmar Görls, William Henry, and Johannes G. Vos*

The central processes in natural photosynthesis are light-driven electron transfer from the special-pair chromophore to the primary acceptor, and the subsequent charge separation to enable the reduction of substrates. The transfer of these design principles to artificial systems has led to the development of catalytic multicomponent systems for the photocatalytic reduction of CO_2[1] and for the production of hydrogen.[2] In these systems, photoredox-active metal complexes and separate redox catalysts are used to facilitate directed photoinduced electron transfer. For example, Grätzel et al. showed that heterogeneous photocatalyst systems can be used for the generation of hydrogen,[3] and Currao et al. reported the photochemical[4] splitting of water with a system consisting of a photoactive silver/silver chloride anode and a silicon solar cell acting as a cathode. However, in these heterogeneous systems, the electron-transfer processes depend on many interfacial parameters that are difficult to influence. Homogeneous systems, consisting of a photoactive Ru or Ir complex and an electron relay of Co or Pd complexes,[5] which generate H_2 in intermolecular reactions, have also been described. Their effectiveness is limited by the instability of the reduced photocatalysts.

In an *intra*molecular photocatalyst it should be easier to control a vectorial photoelectron transfer by precise tuning of the physical properties and orientation of the molecular components. If it were also possible to slow down charge-recombination processes, efficient photocatalytic systems may become feasible. With complex **1**, we report the first supramolecular photocatalyst meeting these requirements.[6] Under mild conditions (25 °C, irradiation at 470 nm) and in homogeneous solution, this compound catalyzes the generation of hydrogen and the selective hydrogenation from tolane to *cis*-stilbene without added H_2.

The heterodinuclear Ru–Pd complex used as photocatalyst consists of the following three components (see Scheme 1, compound **1**):

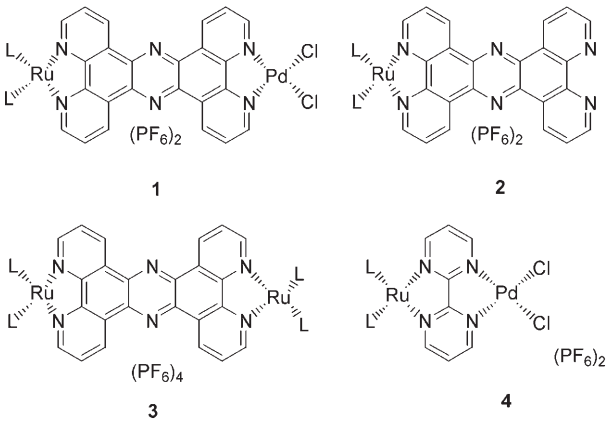

Scheme 1. Structures of complexes **1**–**4**; L = 4,4′-di-*tert*-butyl-2,2′-bipyridine.

- a photoactive ruthenium(II) fragment acting as a light absorber,[7]
- a $PdCl_2$ unit which, when coordinated at the other end of the assembly, acts as a catalytic center,
- a bridging unit (tetrapyridophenazine, tpphz) connecting the two metal centers through a conjugated reducible π-electron system.[8]

Compounds **1**–**4** (Scheme 1) were isolated in high yields and have been fully characterized.

In the first step of the photocatalytic process the ruthenium moiety was excited using 470-nm light. To facilitate efficient electron transfer to the Pd center, the electron donor triethylamine (TEA) was utilized to re-reduce the photochemically formed Ru^{III} center.[9] The results obtained in this study are summarized in Table 1. We observed no catalytic development of hydrogen in the dark (run 6) and found that the heterodinuclear complex **1** is the only effective photocatalyst (runs 1–5, Table 1). The Pd-free complex **2** and the binuclear Ru complex **3** are poor photocatalysts and form only very small amounts of H_2 (TON = 0.56, runs 9 and 10, Table 1). The replacement of the tpphz bridging ligand by bipyrimidine in complex **4** also resulted in a loss of catalytic activity (run 11, Table 1). These results show that the presence all three components in **1** is essential for the catalytic process. With **1**, turnover numbers of 56 mol hydrogen per mol catalyst can be achieved.

Table 1 also demonstrates that the amount of photocatalytically formed hydrogen depends strongly on the TEA concentration and the exposure time (runs 1–5, Table 1), and

[*] Dr. S. Rau, Dr. B. Schäfer, Dr. M. Rudolph, Dr. M. Friedrich, Dr. H. Görls
IAAC FSU Jena
Lessingstrasse 8, 07743 Jena (Germany)
Fax: (+49) 364-194-8102
E-mail: sven.rau@uni-jena.de
Dr. D. Gleich, Prof. Dr. E. Anders
IOMC FSU Jena
Humboldtstrasse 10, 07743 Jena (Germany)
W. Henry, Prof. Dr. J. G. Vos
National Centre for Sensor Research
School of Chemical Sciences, Dublin City University
Dublin 9 (Ireland)

[**] We thank Prof. D. Walther (Jena) for support and inspiration, and also the referees for their helpful comments. This work was supported financially by the DFG (SFB 436) and Enterprise Ireland SC20030074.

Supporting information for this article is available on the WWW under http://www.angewandte.org or from the author.

 © 2006 Wiley-VCH Verlag GmbH & Co. KGaA, Weinheim

Table 1: Examination of the photocatalytic development of hydrogen and hydrogenation of tolane in presence of TEA at 25 °C.[a]

Run	Cat.	c_{tolane} [mol L^{-1}]	c_{TEA} [mol L^{-1}]	c_{TBACl} [mol L^{-1}]	$t_{irrad.}$ (470 nm) [min]	TON for H_2[b]	TON for stilbene[c]	TOF
1	**1**	–	0.00086	0	120	0.15	–	65
2	**1**	–	0.0086	0	120	1.45	–	628
3	**1**	–	0.086	0	120	2.25	–	975
4	**1**	–	0.86	0	120	3.6	–	1560
5	**1**	–	2.08	0	1750	56.4	–	1676
6[d]	**1**	–	2.04	0	0	0	–	0
7	**1**	–	0	0	360	0	–	0
8	**1**	–	0.16	0.16	150	0.04	–	1.4
9	**2**	–	2.08	0	1550	0.56	–	1.9
10	**3**	–	2.08	0	1550	0.56	–	1.9
11	**4**	–	2.08	0	1550	0	–	0
12	**1**	0.026	3.6	0	6960	0	63	471
13	**2**	0.026	3.6	0	6960	0	0	0
14[e]	**1**	0.026	3.6	0	0	0	0	0
15[e]	**1**	0.026	0	0	0	0	485	4203[e]

[a] Reaction conditions: $c_{complex} = 5.2 \times 10^{-5}$ mol L^{-1}, solvent: acetonitrile; TBACl = tetrabutylammonium chloride, TON [mol product mol^{-1} catalyst], TOF [nmol product min^{-1}]. [b] Turnover number determined by GC analysis of the products in the N_2 carrier gas. [c] Determined by GC or GC–MS analysis of the products. [d] Sample without irradiation after 360 min. [e] Sample without irradiation after 6000 min.

that chloride ions inhibit the reaction (run 8, Table 1). A detailed analysis of hydrogen formation as a function of reaction time shows that the amount of H_2 produced increases steadily and levels off after 1200 min. After about 1800 min no more hydrogen is produced.[10] Initially the rate of hydrogen formation increases with increasing TEA concentration (runs 1–4, Table 1), but at a TEA concentration of 0.86 mol L^{-1}, the rate becomes relatively independent (ca. 1600 nmol min^{-1} in runs 4 and 5, Table 1).

Under the same conditions, complex **1** can also catalyze the selective reduction of tolane to *cis*-stilbene. Again, turnover numbers of more than 50 are achieved without additional formation of H_2 (run 12, Table 1). The exclusive generation of the *cis* isomer as well as the inactivity of the palladium-free compound **2** (run 13, Table 1) indicate that the alkyne reduction occurs at the palladium center. Since **1** is inert without irradiation (run 14, Table 1), the tolane reduction observed ("without hydrogen") is also photocatalytic in nature. Also without irradiation and without TEA, **1** can reduce tolane to *cis*-stilbene if hydrogen is added (run 15, Table 1). This confirms that the palladium moiety acts as the catalytic center.

To obtain further information on the role of the palladium and the bridge in the photocatalytic reduction process, photophysical, electrochemical, (Table 2), EPR, and NMR studies as well as theoretical investigations were carried out. It is generally accepted that for tpphz complexes the electronic coupling between the bipyridine M-coordination sphere and the central phenazine ring is weak and that the ^{3}MLCT state, which is located on the phenazine component, to the ligand may reduce an adjacent metal center.[8] Our photo-EPR examinations show that upon irradiation of **1**–**3** at 436 nm in CH_3CN/TEA mixtures, an EPR signal is detected that can be assigned to a pyrazine-based radical anion. This becomes evident by a comparison with electrochemically generated data reported by Kaim et al.[11] Cyclovoltammetry measurements for **1** indicate that the first reduction is

Table 2: Photophysical and electrochemical data for compounds **1**–**3**.

Cmpd	$\lambda_{max,abs.}$ [nm][a]	$\lambda_{max,em.}$ [nm][a]	τ_{aer} [ns][b]	E_{red} [V][c]
1	445	650[d]	27	−0.59, −0.78,[e] −1.05, −1.24, −1.39
2	445	638	154	−0.61, −1.08, −1.30, −1.48, −1.76
3	445	652[d]	27/130	−0.33, −1.05, −1.24, −1.48

[a] 293 K, CH_3CN. [b] τ_{aer} is the lifetime of the excited state in air-saturated solvent. [c] In CH_3CN versus Ag/AgCl ($Fc/Fc^+ = 0.83$ V). [d] Very weak. [e] Peak potential of irreversible Pd reduction; E_{ox}(Ru)-[**1**,**2**,**3**] = 1.6 V.

phenazine based (−0.59 V), while an irreversible reduction of the Pd^{II} is observed at −0.78 V. The bipyridine ligands are reduced at more negative potentials (between −1.05 and −1.39 V).

In addition, ^{1}H NMR measurements indicate that the signals of protons adjacent to the Pd center are almost unchanged upon irradiation, moving slightly from 9.20 to 9.26 ppm. This indicates that palladium remains coordinated during irradiation. Further evidence for this conclusion can be drawn from the attempted photoreaction between **1**/triethylamine and cyclohexene. Cyclohexene is not hydrogenated under these conditions. The presence of colloidal palladium would be expected to result in the catalytic formation of cyclohexane.[12]

For additional information on the location of the excited state and the radical anion formed in the photoreduced complex **1**, we examined simplified models (**M1** and **M2**), without *tert*-butyl groups at the bipyridine ligands, by means of DFT methods using the X-ray data obtained for **2** and **3** (Figure 1).[12] A comparison of the structural parameters of the DFT-optimized structure of **M2** with those obtained in the solid state for **2** show very good agreement.[10] The coordination of the {$PdCl_2$} fragment (**M1**) does not lead to large

 © 2006 Wiley-VCH Verlag GmbH & Co. KGaA, Weinheim

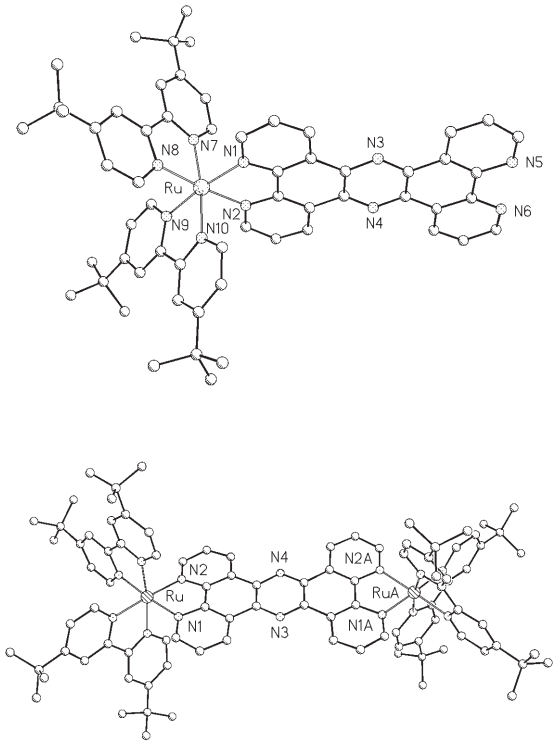

Figure 1. Solid-state structures of **2** (top) and **3** (bottom).

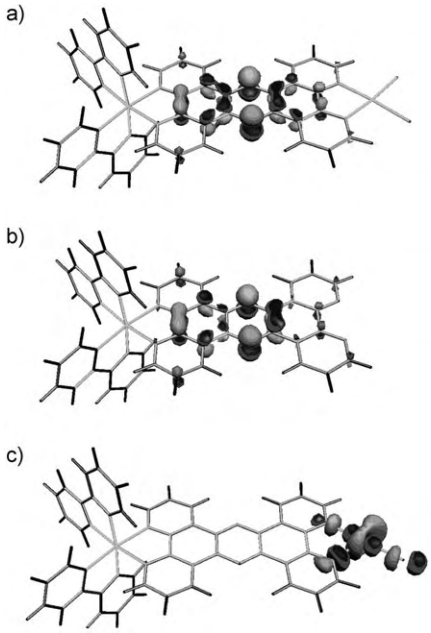

Figure 2. SOMOs of a) **M1**, b) **M2**, and c) the model after chloride dissociation (**M1D**).

changes in the structural parameters. As expected, in both compounds the HOMO is centered on the ruthenium center, while the LUMO is located on the pyrazine ring. The reduced state of **M1** and **M2** was simulated by a decrease of the total charge by one. In both model systems the SOMO is situated on the pyrazine ring and corresponds to the LUMO in the initial complexes; this is in excellent agreement with the EPR and emission spectra (Figure 2a,b).

Since chloride ions inhibit hydrogen generation with **1**, a chloride ion was removed from the palladium center in the reduced model complex **M1**, and the structure was optimized once more (**M1D**). This optimized structure indicates not only the relocation of the SOMO to the Pd center (Figure 2c[13]), but also the regeneration of the photoredox-active {Ru^{II}–tpphz} fragment, which can once again enter into a photocatalytic cycle with TEA.

The experimental and theoretical results suggest that in both catalytic processes **1** transfers two electrons to the substrates during the catalytic cycle. At this stage no detailed mechanistic data are available, but a likely reaction pathway may include the following steps: a twofold photoreduction of **1** by Et_3N according to Equation (1) (see reference [9]), and the subsequent reduction of the protons at the Pd center according to Equation (2). In the presence of tolane the photoreduced catalyst can reduce the alkyne as described by Equation (3).

$$2\,Et_3N + \mathbf{1} \xrightarrow{(h\nu)} (\mathbf{1} + 2\,e^-) + 2\,H^+ + \text{oxidation products of } Et_3N \quad (1)$$

$$2\,H^+ + (\mathbf{1} + 2\,e^-) \rightarrow H_2 + \mathbf{1} \quad (2)$$

$$2\,H^+ + (\mathbf{1} + 2\,e^-) + \text{Ph-C}\equiv\text{C-Ph} \rightarrow \textit{cis}\text{-Ph-CH=CH-Ph} + \mathbf{1} \quad (3)$$

At present, we assume that after the first photoelectron-transfer step and the generation of the Ru^{III}–phenazine$^{(-)}$–Pd^{II} radical, Ru^{III} is reduced to Ru^{II} by TEA. After the chloride loss from the Pd^{II} center, electron transfer from phenazine$^{(-)}$ to the Pd^{II} center takes place yielding a Pd^{I} moiety. When this sequence of steps is repeated, two electrons are stored in the molecule. These electrons are then utilized to reduce two protons[9] originating from oxidized TEA. Alternatively, the deprotonated, photooxidixed triethylamine can also transfer another electron to the singly reduced catalyst.[14] At present we are not able to differentiate between these two possibilities. In the presence of tolane, a fast photo-induced reduction of the substrate is observed. In both catalytic systems, the Pd center is therefore acting both as an electron storage site and as a catalytic center.

The supramolecular assembly presented here opens up various possibilities for increasing the catalytic efficiency. For example, the HOMO/LUMO difference in the bridging-ligand/metal fragment can be adjusted by derivatization of the bridge, by introduction of other metals at the periphery, or by variation of the coordinated anions. Moreover, attachment of these oligonuclear metal complexes to TiO_2 surfaces could influence not only the direction but also the kinetics of the photoinduced electron transfer. These investigations will also facilitate a more detailed insight into the reaction cycle and may as well lead to new photocatalytic reactions with other substrates.

Received: February 9, 2006
Revised: April 26, 2006
Published online: August 17, 2006

 © 2006 Wiley-VCH Verlag GmbH & Co. KGaA, Weinheim

Keywords: homogeneous catalysis · hydrogen · palladium · ruthenium · supramolecular chemistry

[1] J. Hawecker, J.-M. Lehn, R. Ziessel, *J. Chem. Soc. Chem. Commun.* **1983**, 536.
[2] J.-M. Lehn, J.-P. Sauvage, *Nouv. J. Chim* **1977**, *1*, 449.
[3] K. Kalyanasundaram, J. Kiwi, M. Grätzel, *Helv. Chim. Acta* **1978**, *61*, 2720.
[4] A. Currao, V. R. Reddy, M. K. van Veen, R. E. I. Schropp, G. Calzaferri, *Photochem. Photobiol. Sci.* **2004**, *3*, 1017, and references therein.
[5] J. I. Goldsmith, W. R. Hudson, M. S. Lowry, T. H. Anderson, S. Bernhard, *J. Am. Chem. Soc.* **2005**, *127*, 7502 – 7510; J. R. Fisher, D. J. Cole-Hamilton, *J. Chem. Soc. Dalton Trans.* **1984**, 809 – 813.
[6] After submission of this manuscript a publication by Sakai et al. appeared (online publishing date: March 28, 2006) describings a heterodinuclear ruthenium–platinum photocatalyst capable of producing H_2 with a TON of 2.4: H. Ozawa, M. Haga, K. Sakai, *J. Am. Chem. Soc.* **2006**, *128*, 4926 – 4927.
[7] B. Dietzek, W. Kiefer, J. Blumhoff, L. Böttcher, S. Rau, D. Walther, U. Uhlemann, M. Schmitt, J. Popp, *Chem. Eur. J.* **2006**, *12*, 5105.
[8] C. Chiorboli, M. A. J. Rodgers, F. Scandola, *J. Am. Chem. Soc.* **2003**, *125*, 483 – 491.
[9] R. Konduri, H. Ye, F. M. MacDonnell, S. Serroni, S. Campagna, K. Rajeshwar, *Angew. Chem.* **2002**, *114*, 3317; *Angew. Chem. Int. Ed.* **2002**, *41*, 3185 – 3187.
[10] See the Supporting Information.
[11] J. Fees, W. Kaim, M. Moscherosch, W. Matheis, J. Klíma, M. Krejčík, S. Záliš, *Inorg. Chem.* **1993**, 32, 166 – 174.
[12] M. W. van Laren, C. J. Elsevier *Angew. Chem.* **1999**, 111, 3926 – 3928; *Angew. Chem. Int. Ed.* **1999**, *38*, 3715 – 3717.
[13] The following references can be found in the background information. All calculations (Gaussian03)[Za] were carried out without symmetry restrictions with the hybrid functional B3LYP.[Zb] Ru and Pd were described by means of quasi-relativistic effective nuclear potentials ("small core").[Zc] Level I: standard basis set 6-311G(d,p) (implemented in Gaussian03) for H, C, N and Cl;[Zd] level II: 6-311G(d,p) basis set, solvent acetonitrile (CPCM model[Ze]). References [Za–Ze] are given in the Supporting Information.
[14] We thank one of the referees for pointing out this important mechanistic alternative.

 © 2006 Wiley-VCH Verlag GmbH & Co. KGaA, Weinheim

Heterocyclic Synthesis

DOI: 10.1002/anie.200504572

Efficient Oxidative Cyclization of 1,6-Dienes: A Highly Diastereoselective Entry to Substituted Tetrahydropyrans**

*Stefanie Roth and Christian B. W. Stark**

The oxidative cyclization[1] of 1,5-dienes represents a unique method for the preparation of 2,5-disubstituted tetrahydrofurans (Scheme 1).[2] For this nonclassical approach to these herterocycles stoichiometric amounts of permanganate[3] or

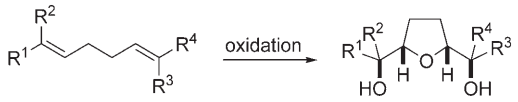

Scheme 1. Oxidative cyclization of 1,5-dienes.

catalytic amounts of osmium[4] or ruthenium tetroxide[5,6] have been used. This methodology has been known for some time and recent investigations have led to high-yielding procedures as well as some synthetic applications.[7]

Whereas the oxidative cyclization of 1,5-dienes thus appears to be a firmly established process, the corresponding oxidative cyclization of homologous 1,6-dienes has rarely been studied[8] and never achieved satisfactorily. In view of the relevance of tetrahydropyrans[2] as substructures in many classes of natural products, we decided to investigate this transformation in detail. Herein, we report the first general method for the oxidative cyclization of 1,6-dienes which provides access to diastereomerically pure tetrahydropyrans (THPs).

On the basis of our previous investigations in the area of oxidative cyclizations,[6] we employed ruthenium tetroxide as a catalyst and sodium periodate on wet silica[9] as the terminal oxidant. Initial experiments on 1,6-diene **1** (Table 1, entry 1), chosen as a model substrate, yielded the desired cyclization product only as a minor component among a range of other products, including stereoisomers, dihydroxylation, and C–C-bond cleavage products. Pleasingly, systematic optimization

[*] Dipl.-Chem. S. Roth, Jr.-Prof. Dr. C. B. W. Stark
Institut für Chemie und Biochemie
Freie Universität Berlin
Takustrasse 3, 14195 Berlin (Germany)
Fax: (+49) 30-838-55367
E-mail: stark@chemie.fu-berlin.de

[**] We thank the Deutsche Forschungsgemeinschaft (STA-634/1-1), the Fonds der Chemischen Industrie, and the Ernst-Schering-Stiftung (fellowship to S.R.) for financial support of this work. We are also grateful to Professor H.-U. Reissig for helpful discussions and generous support.

Supporting information for this article (detailed experimental procedures and representative spectroscopic data) is available on the WWW under http://www.angewandte.org or from the author.

WILEY InterScience DISCOVER SOMETHING GREAT
© 2006 Wiley-VCH Verlag GmbH & Co. KGaA, Weinheim

Table 1: Oxidative cyclization of 1,6-dienes.[a]

Entry	Substrate		Product		Yield [%][b]	d.r.[c]
1	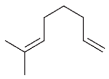	**1**	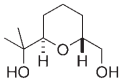	**2**	85[d]	>95:5
2	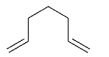	**3**	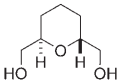	**4**	53[e]	>95:5
3	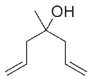	**5**	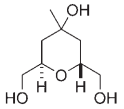	**6**	70	>95:5
4	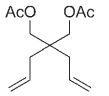	**7**	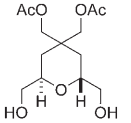	**8**	65[e]	>95:5
5	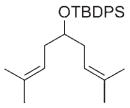	**9**	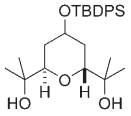	**10**	58	>95:5
6	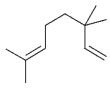	**11**	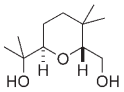	**12**	48	>95:5
7	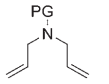	**13**[g]	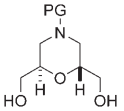	**14**	60[d,e]	>95:5
8		**15**[g]		**16**	87[d,e]	>95:5
9	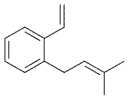	**17**	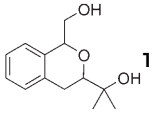	**18**	41	60:40
10	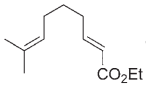	**19**	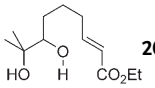	**20**	52(72)[f]	–

[a] Reaction conditions: 5 mol% $RuCl_3$, 4 equiv $NaIO_4$ on wet silica, EtOAc/MeCN (1:1), 0°C, 10 min. [b] Yields of isolated cyclization product after column chromatography. [c] Ratio determined by ^1H NMR spectroscopy or gas chromatography of crude reaction mixtures. [d] 1 mol% ruthenium catalyst was used. [e] A reductive work up was carried out to convert small amounts of aldehyde side product into the same diol main product (see the Supporting Information). [f] The yield in parenthesis refers to the sum of the yields of the diol and tetrol product. [g] **13**: PG = Bz (benzoyl), **15**: PG = $p$$NO_2$Bz.

of reaction parameters (solvent, temperature, concentration, and precatalyst) enabled the formation of these unwanted products to be almost completely suppressed. Both a polar solvent mixture (MeCN/EtOAc) and a dilute reaction solution (0.03 M) proved crucial for achieving good results. Under optimized reaction conditions using 5 mol% ruthenium trichloride as a precatalyst (for the in situ generation of ruthenium tetroxide) the cyclization product **2** was obtained in high yield (85%) and, more importantly, as a single diastereoisomer.

Gratifyingly, this protocol was applicable to a range of 1,6-dienes (Table 1). The cyclization product was formed rapidly (usually within 10 min at 0°C) and with high selectivity, irrespective of the starting material. Terminal alkenes, which are commonly known to result in diminished yields in the case of 1,5-dienes,[3] afforded the heterocyclic products in good yields. Even a chiral morpholine derivative was accessible in excellent yield (87%) starting from simple protected diallylamine (Table 1, entry 8). Since a solid-supported terminal oxidant[10] is used, the work-up procedure is extremely simple and requires only filtration after deactivation of the catalyst (see the Supporting Information). Thus, even hydrophilic diol and triol products can be isolated without difficulty.

In contrast to the oxidative cyclization of 1,5-dienes,[5,6] α,β-unsaturated esters did not undergo cyclization, and only dihydroxylation products[11] were observed (Table 1, entry 10). Neither the diol nor the tetrol could be forced to undergo cyclization, even when stirred for extended reaction times or under forcing reaction conditions.[12] From all the 1,6-diene substrates investigated in this study, such electron-deficient alkenes represent the only class of substrates that did not undergo oxidative cyclization.

The diastereoselectivity of the cyclization was generally high, and the 2,6-*cis*-THP could usually not be detected in the crude reaction mixtures (NMR or GC). Only isochromane (**18**) was obtained as a mixture of isomers (60:40; Table 1, entry 9) presumably because of the almost planar linkage between the two reacting double bonds. The relative stereochemistry of THP products was established by spectroscopic means and was confirmed by comparison with authentic samples (for compounds **2** and **4**).[13] Interestingly, in all cases the contra-thermodynamic 2,6-*trans*-substituted THP derivatives were formed.[14] It is also worth noting that most cyclization products depicted in Table 1 are either C_2- or pseudo-C_2-symmetric (with a chiral chirotopic C atom) and methods for the desymmetrization of these compounds are conceivable.[15]

Mechanistically we presume a similar pathway[16] as was first suggested by Baldwin et al.[16a] for the related permanganate-promoted oxidative cyclization of 1,5-dienes. Thus, after conversion of the precatalyst into ruthenium tetroxide a [3+2] cycloaddition[17] to one of the double bonds occurs (Scheme 2). This step is followed by a second intramolecular [3+2] cycloaddition to the adjacent olefin. At this crucial stage the stereochemistry across the THP system is set. Finally, hydrolysis of the intermediate ruthenate ester **B** (Scheme 2) liberates the product and a low-valent ruthenium species which in turn is oxidatively converted into the active ruthenium(VIII) catalyst.

We next investigated the stereoselectivity of the process using starting materials containing a stereogenic center within the C_3 bridge. Thus, the two chiral and nonracemic substrates **21** and **23** (Scheme 3) were submitted to the optimized oxidation conditions. Disappointingly, no influence on the stereochemical course of the reaction was detectable, irrespective of the position of the stereogenic center (Scheme 3). In both cases the cyclization products were obtained as a 1:1 mixture of diastereoisomers. The lack of any stereochemical induction is most likely a result of the fact that the initial [3+2] cycloaddition occurs at the double bond remote from the branched stereogenic center.[4c] Although the diastereo-

 © 2006 Wiley-VCH Verlag GmbH & Co. KGaA, Weinheim

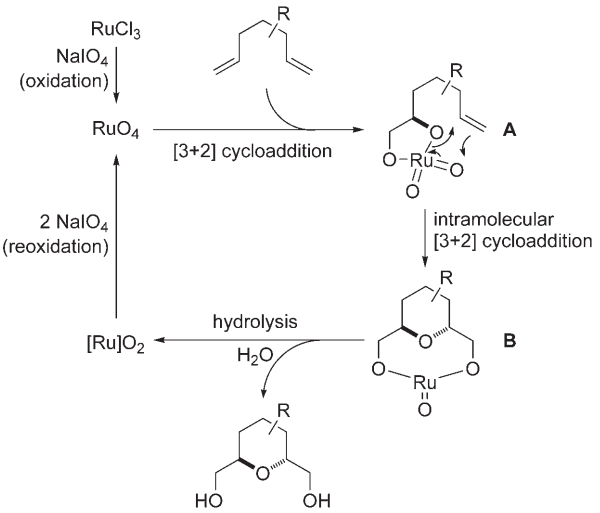

Scheme 2. Proposed mechanism for the oxidative cyclization of 1,6-dienes.

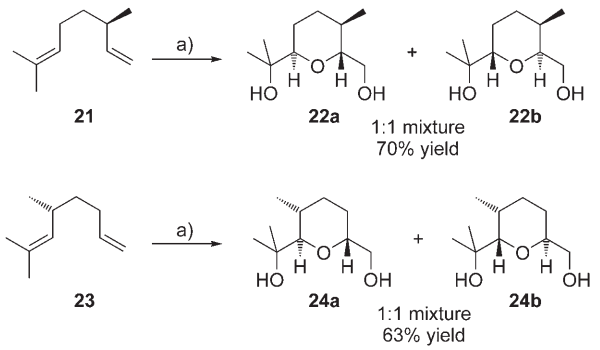

Scheme 3. Oxidative cyclization of chiral 1,6-dienes: a) 5 mol% $RuCl_3$, 4 equiv $NaIO_4$ on wet silica, EtOAc/MeCN (1:1), 0°C, 10 min, reductive work up.

selectivity of this transformation is not satifactory it should be noted that enantiomerically pure products with two new stereogenic centers are accessible after separation.

We next sought to extend the scope of this new oxidative cyclization by seeking conditions to convert the 2,6-bis(hydroxymethyl)tetrahydropyrans into δ-lactones. The primary hydroxy function of the cyclization product **2** (which could be prepared on a gram scale) was first protected (Scheme 4). Conditions for the oxidative cleavage of the tertiary hydroxy methyl group were then investigated. Pyridinium chlorochromate (PCC)[18] proved to be the most efficient reagent for this purpose, and the oxidative cleavage to δ-lactone **26** proceeded smoothly (70% yield). Fluoride-induced deprotection provided the free alcohol **27** in an overall yield of 47% (over 4 steps) starting from commercially available diene **1**. This δ-lactone has previously been used as a key intermediate in natural product synthesis.[19]

In summary, the first general and efficient procedure for the oxidative cyclization of 1,6-dienes has been presented. The cyclization products were obtained in good to high yields and excellent diastereoselectivity. 1–5 mol% ruthenium tetroxide is sufficient to accomplish complete conversion of the starting diene within minutes. The scope of this novel cyclization method has been extended by the conversion of the initial cyclization product into a synthetically useful δ-lactone. Further investigations into the mechanism and the development of an asymmetric variant of this type of oxidation reaction are currently underway.

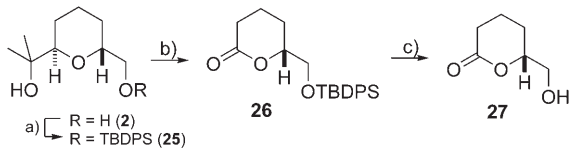

Scheme 4. Synthesis of 6-hydroxymethyl-δ-valerolactone (**27**): a) TBDPSCl, imidazole, CH_2Cl_2, 89%; b) PCC, 4-Å MS, CH_2Cl_2, 50°C, 70%; c) TBAF, THF, 0°C, 88%. TBDPSCl = *tert*-butyldiphenylsilyl chloride, PCC = pyridinium chlorochromate, MS = molecular sieves, TBAF = tetrabutyl ammoniumfluoride.

Received: December 22, 2005
Revised: June 1, 2006
Published online: July 24, 2006

Keywords: cyclization · heterocycles · oxidation · ruthenium tetroxide · tetrahydropyrans

[1] For a review on the related oxidative cyclization of bis-homoallylic alcohols, see: J. Hartung, M. Greb, *J. Organomet. Chem.* **2002**, *661*, 67–84.
[2] a) T. L. B. Boivin, *Tetrahedron* **1987**, *43*, 3309–3362; b) U. Koert, *Synthesis* **1995**, 115–132; c) M. C. Elliott, E. Williams, *J. Chem. Soc. Perkin Trans. 1* **2001**, 2303–2340, and references therein.
[3] a) E. Klein, W. Rojahn, *Tetrahedron* **1965**, *21*, 2353–2358; b) R. C. D. Brown, J. F. Keily, *Angew. Chem.* **2001**, *113*, 4628–4630; *Angew. Chem. Int. Ed.* **2001**, *40*, 4496–4498; c) R. C. D. Brown, C. J. Bataille, R. M. Hughes, A. Kenney, T. J. Luker, *J. Org. Chem.* **2002**, *67*, 8079–8085.
[4] a) M. de Champdoré, M. Lasalvia, V. Piccialli, *Tetrahedron Lett.* **1998**, *39*, 9781–9784; b) T. J. Donohoe, J. J. G. Winter, M. Helliwell, G. Stemp, *Tetrahedron Lett.* **2001**, *42*, 971–974; c) T. J. Donohoe, S. Butterworth, *Angew. Chem.* **2003**, *115*, 978–981; *Angew. Chem. Int. Ed.* **2003**, *42*, 948–951.
[5] a) P. H. J. Carlsen, T. Katsuki, V. S. Martin, K. B. Sharpless, *J. Org. Chem.* **1981**, *46*, 3936–3938; b) L. Albarella, D. Musumeci, D. Sica, *Eur. J. Org. Chem.* **2001**, 997–1003; c) V. Piccialli, N. Cavallo, *Tetrahedron Lett.* **2001**, *42*, 4695–4699; a review on ruthenium tetroxide mediated reactions can be found in B. Plietker, *Synthesis* **2005**, 2453–2472.
[6] S. Roth, S. Göhler, H. Cheng, C. B. W. Stark, *Eur. J. Org. Chem.* **2005**, 4109–4118.
[7] a) D. M. Walba, C. A. Przybyla, C. B. Walker, Jr., *J. Am. Chem. Soc.* **1990**, *112*, 5624–5625; b) P. J. Kocieński, R. C. D. Brown, A. Pommier, M. Proctor, B. Schmidt, *J. Chem. Soc. Perkin Trans. 1* **1998**, 9–40; c) A. R. L. Cecil, R. C. D. Brown, *Org. Lett.* **2002**, *4*, 3715–3718.
[8] a) V. Piccialli, *Tetrahedron Lett.* **2000**, *41*, 3731–3733; b) A. R. L. Cecil, R. C. D. Brown, *Tetrahedron Lett.* **2004**, *45*, 7269–7271.
[9] Y.-L. Zhong, T. K. M. Shing, *J. Org. Chem.* **1997**, *62*, 2622–2624; see also Ref. [6].
[10] a) S. V. Ley, I. R. Baxendale, R. N. Bream, P. S. Jackson, A. G. Leach, D. A. Longbottom, M. Nesi, J. S. Scott, R. I. Storer, S. J.

 © 2006 Wiley-VCH Verlag GmbH & Co. KGaA, Weinheim

Taylor, *J. Chem. Soc. Perkin Trans. 1* **2000**, 3815 – 4195; b) A. Kirschning, H. Monenschein, R. Wittenberg, *Angew. Chem.* **2001**, *113*, 670 – 701; *Angew. Chem. Int. Ed.* **2001**, *40*, 650 – 679.
[11] a) T. K. M. Shing, V. M. F. Tai, E. K. W. Tam, *Angew. Chem.* **1994**, *106*, 2408 – 2409; *Angew. Chem. Int. Ed. Engl.* **1994**, *33*, 2312 – 2313; b) B. Plietker, *J. Org. Chem.* **2003**, *68*, 7123 – 7125; c) B. Plietker, *Eur. J. Org. Chem.* **2005**, 1919 – 1929.
[12] At extended reaction times the amount of tetrol product increased and no cyclization product could be detected. We believe that both the diol and the tetrol are derived form a competing dihydroxylation reaction and not intermediates en route to the cyclization product.
[13] For an investigation of the relative stereochemistry for compounds **2** and **4**, see Ref. [8a]; a comparison with the independently prepared *cis* isomer of compound **4** is also most instructive, see: A. C. Cope, A. Fournier, Jr., *J. Am. Chem. Soc.* **1957**, *79*, 3896 – 3899.
[14] *Trans*-substituted THPs were also obtained in the related oxidative cyclization of tris-homoallylic alcohols, see: F. E. McDonald, A. D. Singhi, *Tetrahedron Lett.* **1997**, *38*, 7683 – 7686.
[15] C. S. Poss, S. L. Schreiber, *Acc. Chem. Res.* **1994**, *27*, 9 – 17.
[16] a) J. E. Baldwin, M. J. Crossley, E.-M. M. Lehtonen, *J. Chem. Soc. Chem. Commun.* **1979**, 918 – 920; b) S. Wolfe, C. F. Ingold, *J. Am. Chem. Soc.* **1981**, *103*, 940 – 941.
[17] D. V. Deubel, G. Frenking, *Acc. Chem. Res.* **2003**, *36*, 645 – 651.
[18] S. Baskaran, S. Chandrasekaran, *Tetrahedron Lett.* **1990**, *31*, 2775 – 2778.
[19] a) E. J. Corey, S. G. Pyne, W. G. Su, *Tetrahedron Lett.* **1983**, *24*, 4883 – 4886; b) P. Coutrot, C. Grison, C. Bômont, *Tetrahedron Lett.* **1994**, *35*, 8381 – 8384.

 © 2006 Wiley-VCH Verlag GmbH & Co. KGaA, Weinheim

Supramolecular Chemistry

DOI: 10.1002/anie.200600671

Hydrogen-Bonded Hexamers Self-Assemble as Spherical and Tubular Superstructures on the Sub-Micron Scale**

*Michael W. Heaven, Gareth W. V. Cave, Robert M. McKinlay, Jochen Antesberger, Scott J. Dalgarno, Praveen K. Thallapally, and Jerry L. Atwood**

In the advancing fields of supramolecular chemistry and nanotechnology, the ability to manipulate and control supra- and supermolecular self-assembly is a prerequisite. Within the realms of supramolecular chemistry at least, these recently developed abilities have been exploited in the design of complementary molecules that form interesting spherical or capsular architectures that are, as is often the case in nature, of high symmetry.[1–3] These supramolecular assemblies have potential in drug delivery, selective catalysis, or cell mimicry. In terms of nanotechnology and supermolecular self-assembly, related examples include complex interlocking capsules that can envelop unstable materials,[4] enhance reaction rates,[5] or provide transportation through otherwise unfriendly environments.[6] Covalent and noncovalent tubular architectures show ever increasing promise for application[7,8] and complex combinations of phospholipid containers and nanotubes have been used to form microscopic networks that allow the passage of molecular material through interlinking tubules.[9] Biological examples of the interaction between "spheres" and "tubules" include the cell-to-cell communication through nanotubular cytonemes (as probed with fluorescently labeled wheat germ agglutinin)[10] and the synergic action between amphiphysin and dynamin in clathrin-mediated endocytosis.[11]

Herein we describe the supermolecular self-assembly of a nanometer-scale supramolecular architecture into sub-micron spheres and tubules, or combinations thereof. By using

[*] M. W. Heaven, Dr. G. W. V. Cave, R. M. McKinlay, J. Antesberger, Dr. S. J. Dalgarno, Dr. P. K. Thallapally, Prof. J. L. Atwood
Department of Chemistry
University of Missouri-Columbia
601 South College Avenue, Columbia, MO 65211 (USA)
Fax: (+1) 573-882-2754
E-mail: atwoodj@missouri.edu

Dr. G. W. V. Cave
School of Biomedical and Natural Sciences
Nottingham Trent University
Clifton Lane, Nottingham, NG11 8NS (UK)

[**] We acknowledge the NSF for financial support of this work. We thank the University of Missouri Structural Biology Core for technical assistance and use of the light scattering instrument, and the Electron Microscopy Core for the use of the TEM and SEM facilities.

Supporting information for this article is available on the WWW under http://www.angewandte.org or from the author.

© 2006 Wiley-VCH Verlag GmbH & Co. KGaA, Weinheim

various electron or force microscopy techniques these superstructures are shown to link and/or bud from one another. The tecton in question ($\mathbf{1}_6$ or $\mathbf{3}_6{\cdot}Ga_{12}$, Figure 1), a near spheroidal hexameric nanocapsule based on pyrogallol[4]arene (Pg or **1**, **2**, and **3**, general structure shown in Figure 1), is held together

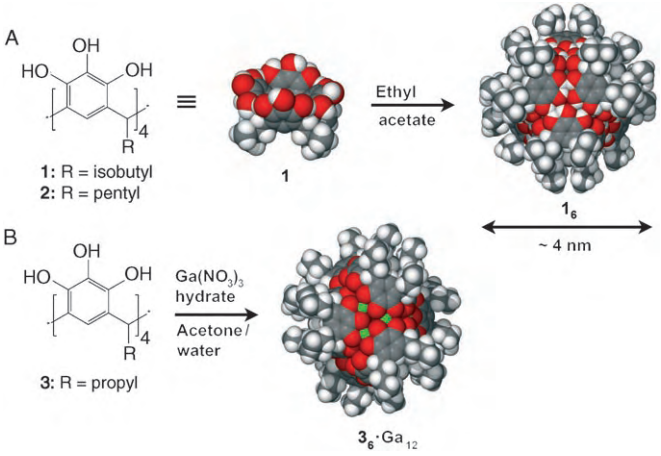

Figure 1. The formation of hydrogen-bonded and metal-coordinated pyrogallol[4]arene hexameric capsules. A) Crystallization from an appropriate solvent (ethyl acetate, for example) results in the formation of hydrogen-bonded hexamers with radiating alkyl chains. The average diameter of a single hexamer in the solid state is approximately 4 nm.[13] B) Reaction of gallium nitrate hydrate in a water/acetone mixture of **3** results in the formation of metal-coordinated capsules within which metal centers replace hydrogen atoms of the pyrogallol[4]arene hydroxo groups; gray C, white H, red O, green Ga; ethyl acetate and water molecules removed for clarity.[23]

by 72 hydrogen bonds, and has lipophilic alkyl chains of varying length that radiate from the spheroid shell to different extents depending on the precursor selected.[12–14] For particular carbon-chain lengths, the hydrogen-bonded "seams" or "faces" of the spheroid can become exposed (in the solid state at least) and it is proposed that these combined factors may play a crucial role in superstructure stabilization on the submicron level.

Pyrogallol[4]arenes crystallize in either bilayer or hexameric nanocapsule motifs depending on the crystallization solvent employed.[12–14] The stability of these hexamers in either polar or nonpolar media has been demonstrated in a number of solution-phase studies.[15–17] Indeed, this stability has been recently utilized in the spectroscopic study of capsule-bound fluorescent probe molecules with a view to reporting on the interior order of the assembly.[14] To date however, little is known of the aggregation and supermolecular assembly of these solution-stable entities. Using dynamic light scattering (DLS) techniques, large supermolecular aggregates were observed for different Pg hexamers under dilute conditions (typical concentration ca. 10^{-3} M).[18] The diameters of the aggregates were found to be in the range of 80–120 nm. Sonication of these solutions resulted in the formation of species of roughly 4 nm size, indicative of individual Pg hexamers (Figure 1 A). Over a number of hours, the larger aggregates re-formed and could be detected by subsequent DLS studies. This aggregation phenomenon was not however observed in the aqueous phase, and only discrete hexamers were detected using DLS. Given the stability and recurring nature of the aggregates in solvents other than water, we employed transmission electron microscopy (TEM), scanning electron microscopy (SEM), and atomic force microscopy (AFM) techniques to examine the particles, the results of which were to some extent unexpected.

Upon evaporation of an approximately 10^{-4} M acetone solution of the Pg hexamer ($\mathbf{1}_6$, where R = isobutyl, Figure 1 A) under ambient conditions, large aggregates were observed by TEM (Figure 2 A). The aggregates were found to be spherical, of uniform shape, and to be of wide-ranging diameters (92 ± 42 nm) when formed from acetone solutions. In addition, spherical aggregates were, on occasion, found to be linked by interesting tubular architectures (Figure 2 B). The rate of evaporation was found to play a role in aggregate formation, as when solvents of a higher boiling point were employed, the number of observed aggregates was reduced, and also led to alternative crystal growth as observed by TEM studies.[19]

At similar concentrations in acetonitrile (ca. 10^{-4} M), or upon moving to higher concentrations in chloroform (ca. 10^{-2} M), the spherical aggregates could be stacked upon one another rather than coalescing (Figure 2 C,D). Notably, TEM studies of an aqueous solution of $\mathbf{1}_6$ repeatedly showed amorphous material rather than spherical aggregates. Ethyl acetate was also found to be a poor solvent for aggregate formation, presumably owing to the high boiling point[20] and that a number of Pg hexamers are readily crystallized from this solvent.[13]

For a direct hexamer and bilayer comparison using TEM, $\mathbf{1}_6$ was recrystallized in the bilayer motif from acetone, a solvent known to retain the supramolecular assembly motif whether hexamer or bilayer (note: ethyl acetate exclusively forms hexamers). The bilayer arrangement, when observed using TEM, showed only a limited number of the sub-micron spherical aggregates and a large mass of amorphous material (see Supporting Information). The fact that some spherical aggregates were observed implied that bilayer to hexamer conversion was occurring over time, a phenomenon that was elucidated by X-ray powder diffraction (see Supporting Information) and further TEM studies.[20]

With respect to the sphere-connecting tubular architectures, these were most readily observed when samples were prepared from chloroform or methylene chloride solutions (although formation was also observed in acetonitrile or acetone on occasion, Figure 2 B). In general, these tubular connectors were of smaller diameter than the spherical aggregates (which were often found at the tubule ends) and were found to exist in both smooth and rugged morphologies (Figure 2 E–J). The smoother tubes were more prevalent and were most commonly formed with lengths approaching one micrometer (Figure 2 E–I). The rugged tubes were most commonly formed from chloroform solutions, and were found to be of greater diameter and shorter in length than the smooth analogues (lengths approaching 400 nm, Figure 2 J). Examination of the smooth and rugged tubes using TEM and SEM, respectively, showed hemispheric swellings

 © 2006 Wiley-VCH Verlag GmbH & Co. KGaA, Weinheim

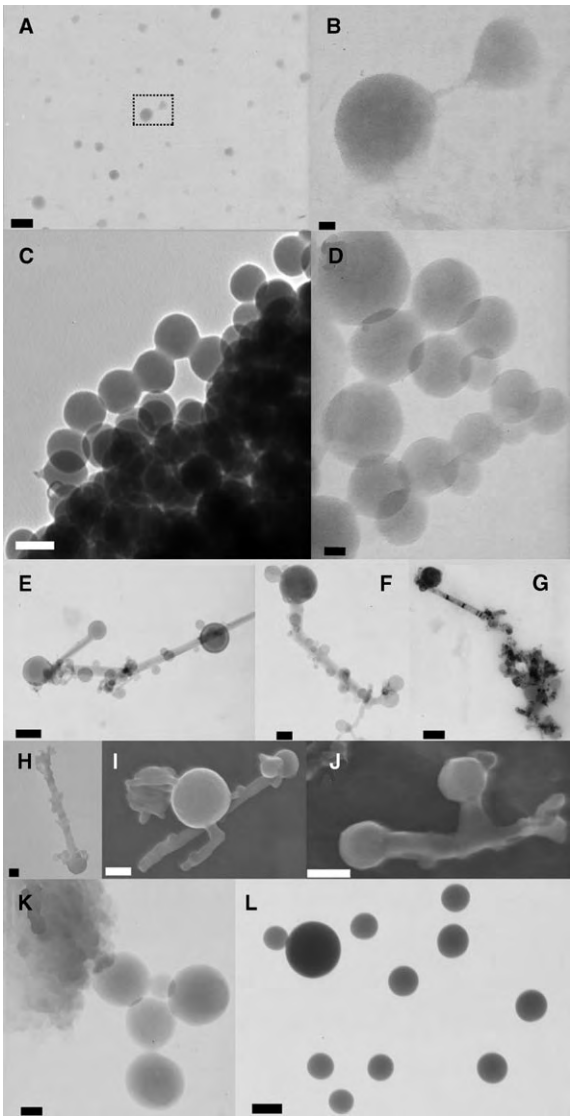

Figure 2. TEM and SEM images of aggregates formed from pyrogallol[4]arene hexamers. A) TEM of spherical aggregates formed from an acetone solution of $\mathbf{1}_6$ (R = isobutyl, Figure 1 A). B) Expansion of marked area in (A) showing a tubular connection between two spheres. C) TEM of a chloroform solution of $\mathbf{1}_6$ showing aggregate layering. D) TEM of spherical aggregates formed from an acetonitrile solution of $\mathbf{1}_6$. E,F) TEM of spheres and tubes formed from a chloroform solution of $\mathbf{1}_6$. G) TEM of a network of spheres and tubes formed from a methylene chloride solution of $\mathbf{1}_6$. H–J) SEM of spheres and tubes formed from a chloroform solution of $\mathbf{1}_6$. K,L) TEM of metal-coordinated capsules $\mathbf{3}_6$·Ga_{12} (R = propyl, Figure 1 B) formed from an acetone solution (Scale bars. A,G: 200 nm; B,D: 20 nm; C,E,H–J: 100 nm; F,K,L: 50 nm).

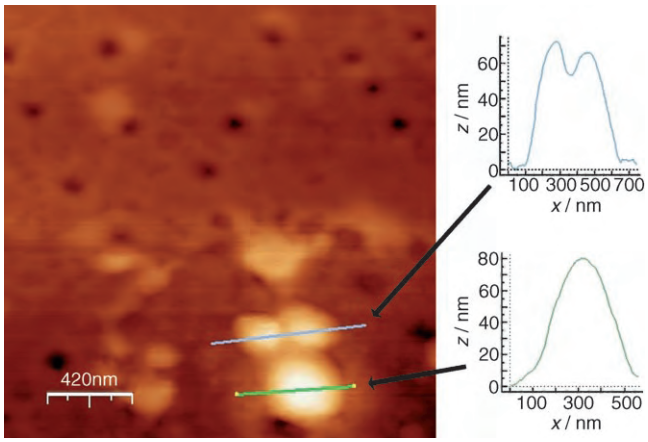

Figure 3. AFM image of hexamer $\mathbf{2}_6$ (R = pentyl, Figure 1 A) in acetone showing height measurements of spheroidal aggregates.

that appeared to be spherical aggregates budding from the tubular architectures (Figure 2 E,F,H–J). These budding aggregates are spread randomly across the length of the tubes and are of comparable diameter.

AFM corroborated the electron microscopy findings with regard to both structure and spatial height of the spherical superstructures. Examination of the aggregates using contact mode AFM showed spherical regions with heights in the 60–80 nm range (aggregates formed from $\mathbf{2}_6$, Figure 1 A, Figure 3 and Supporting Information). This result correlates well with the aggregate diameters found in both DLS and TEM studies.

To determine whether the sub-micron aggregates were composed of pyrogallol[4]arene based layers or hexamers, metal-coordinated capsules (hexamers that are incapable of disassembly in the solvent systems employed) were studied using TEM (gallium-coordinated hexamer $\mathbf{3}_6$·Ga_{12}, Figure 1 B).[21] Spherical aggregates that are of comparable dimensions to those of the hydrogen-bonded hexamers were observed by TEM, although the images were significantly darker, presumably owing to the high content of gallium in the resultant superstructures (Figure 2 K,L). This evidence indicates that the spherical aggregates are indeed composed of many discrete hexamer building blocks, and are not a bilayer related motif. This conclusion is further supported by the studies of Coleman et al. in which *p*-acylcalix[4]arene was manipulated into solid lipid nanoparticles (SLNs).[22] In those studies, the formation of large objects of 250 nm in diameter was observed although these flattened slightly during the drying process. From their studies, Coleman et al. deduced that the objects were matricial. Liposomal systems cannot survive under such conditions (they collapse), and therefore we conclude that the objects observed in the current studies are also matricial, made up of many neighboring hexamers rather than a bilayer based motif (Figure 4).

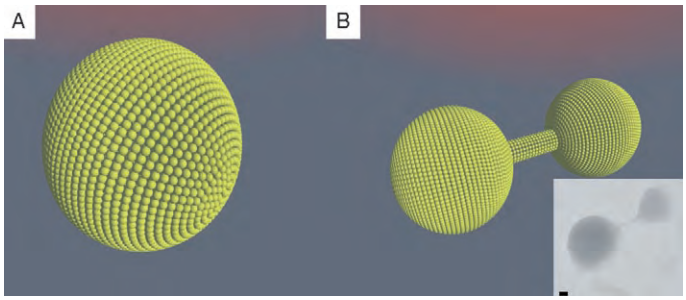

Figure 4. Theoretical representation of hexamers assembling as A) spherical and B) tubular superstructures. Inset: Negative of Figure 2 B, which is modeled in (B) (Scale bar: 20 nm).

 © 2006 Wiley-VCH Verlag GmbH & Co. KGaA, Weinheim

Unlike almost all examples of artificial molecular-based vesicle systems, the supramolecular system herein is unique in that the self-assembly of the hexamer takes place prior to the formation of larger aggregates. Solvent properties are very important in the formation of these large structures, and an abundance of water appears to hinder aggregate formation, thereby suggesting that hexamer-to-hexamer interactions may be disturbed under such conditions. Although the specific interhexamer interactions are unknown to date, the aggregation phenomenon is general for a number of pyrogallol[4]arenes.[23] The large aggregates may either be stabilized by a large number of van der Waals interactions between neighboring alkyl chains, or by face-to-face hexamer interactions between hydrophilic regions of the discrete supramolecular assemblies, as is observed in the solid state.[13] The ability to attach a range of functionalities to the alkyl chains of the nanospheroids, coupled with the ability to modify the interior of the hexamers with a range of guest molecules will undoubtedly prove useful in the future study and application of these spherical and tubular sub-micron assemblies.

Received: February 20, 2006
Revised: May 16, 2006
Published online: July 25, 2006

Keywords: calixarenes · electron microscopy · materials science · self-assembly · supramolecular chemistry

[1] J. L. Atwood, J. E. D. Davies, D. D. MacNicol, F. Vögtle, *Comprehensive Supramolecular Chemistry*, *Vol. 1–11*, Elsevier Science, Oxford, **1996**.
[2] C. Li, X. Zhang, Z. Cao, *Science* **2005**, *309*, 909 – 911.
[3] R. Zandi, D. Reguera, R. F. Bruinsma, W. M. Gelbart, J. Rudnick, *Proc. Natl. Acad. Sci. USA* **2004**, *101*, 15556 – 15560.
[4] J. L. Dye, *Science* **1990**, *247*, 663 – 668.
[5] A. Koçer, M. Walko, W. Meijberg, B. L. Feringa, *Science* **2005**, *309*, 755 – 758.
[6] M. Antonietti, S. Förster, *Adv. Mater.* **2003**, *15*, 1323 – 1333.
[7] R. H. Baughman, A. A. Zakhidov, W. A. de Heer, *Science* **2002**, *297*, 787 – 792.
[8] S. Fernandez-Lopez, H.-S. Kim, E. C. Choi, M. Delgado, J. R. Granja, A. Khasanov, K. Kraehenbuehl, G. Long, D. A. Weinberger, K. M. Wilcoxen, M. R. Ghadiri, *Nature* **2001**, *412*, 452 – 456.
[9] A. Karlsson, R. Karlsson, M. Karlsson, A.-S. Cans, A. Strömberg, F. Ryttsén, O. Orwar, *Nature* **2001**, *409*, 150 – 152.
[10] A. Rustom, R. Saffrich, I. Markovic, P. Walther, H.-H. Gerdes, *Science* **2004**, *303*, 1007 – 1010.
[11] K. Takei, V. I. Slepnev, V. Haucke, P. D. Camilli, *Nat. Cell Biol.* **1999**, *1*, 33 – 39.
[12] T. Gerkensmeier, W. Iwanek, C. Agena, R. Frölich, S. Kotila, C. Näther, J. Mattay, *Eur. J. Org. Chem.* **1999**, *1999*, 2257 – 2262.
[13] G. W. V. Cave, J. Antesberger, L. J. Barbour, R. M. McKinlay, J. L. Atwood, *Angew. Chem.* **2004**, *116*, 5375 – 5378; *Angew. Chem. Int. Ed.* **2004**, *43*, 5263 – 5266.
[14] S. J. Dalgarno, S. A. Tucker, D. B. Bassil, J. L. Atwood, *Science* **2005**, *309*, 2037 – 2039.
[15] L. C. Palmer, J. Rebek, Jr., *Org. Lett.* ***2005***, *7*, 787 – 792.
[16] J. Rebek, Jr., *Angew. Chem.* **2005**, *44*, 2068 – 2078; *Angew. Chem. Int. Ed.* **2005**, *44*, 2068 – 2078.
[17] Y. Cohen, L. Avram, L. Frish, *Angew. Chem.* **2005**, *117*, 524 – 560; *Angew. Chem. Int. Ed.* **2005**, *44*, 520 – 554.
[18] The Pg hexamers were crystallized from ethyl acetate over a period of 12–48 h, except for $\mathbf{3}_6{\cdot}Ga_{12}$ (crystallized from acetone/water). The crystals were weighed and the appropriate solvent added to make stock solutions of desired molarity. All samples were stored in glass vials and were analyzed within 12 h of the crystals being dissolved, except when long-term viability was being assessed. See Supporting Information for analytical techniques involved.
[19] This was typically observed when high-boiling-point solvents were employed in sample preparation. Single-crystal growth was observed by TEM when ethyl acetate or a water/acetone mixture was used, although small amounts of microcrystalline material was also found on occasion for other solvents.
[20] An acetone solution of re-dissolved bilayer crystals of the Pg hexamer $\mathbf{1}_6$ was found to revert to the corresponding hexamer when allowed to stand overnight, as indicated by subsequent X-ray powder diffraction and TEM studies. TEM studies on the solution showed the formation of approximately 80-nm spherical aggregates. The remaining solution was evaporated at room temperature and the solid residue examined using X-ray powder diffraction, which showed reflections indicative of hexamer formation.
[21] R. M. McKinlay, P. K. Thallapally, G. W. V. Cave, J. L. Atwood, *Angew. Chem.* **2005**, *117*, 5879 – 5882; *Angew. Chem. Int. Ed.* **2005**, *44*, 5733 – 5736.
[22] P. Shahgaldian, E. Da Silva, A. W. Coleman, B. Rather, M. J. Zawarotko, *Int. J. Pharm.* **2003**, *253*, 23 – 28, and references therein.
[23] Information regarding the assembly and examination of aggregates based on other pyrogallol[4]arene hexamers can be found in the Supporting Information.

 © 2006 Wiley-VCH Verlag GmbH & Co. KGaA, Weinheim

Cover Picture

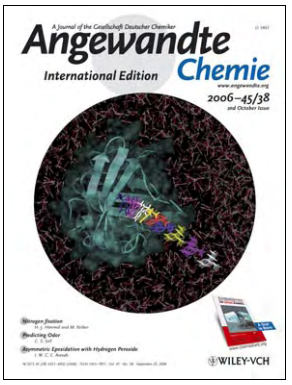

Natalia Shimokhina, Agnieszka Bronowska, and Steve W. Homans*

Ligand–protein interactions are associated with the desolvation of a ligand as it enters the protein-binding pocket (see cover picture). Homans and co-workers describe in their Communication on page 6374 ff. an estimate of the thermodynamic cost associated with this desolvation process. These data permit a complete breakdown of the binding thermodynamics into contributions from the ligand, protein, and solvent for the interaction of a small-molecule ligand with the mouse major urinary protein.

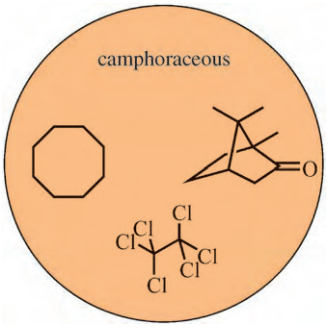

Structure and Smell

In his Minireview on page 6254 ff., C. S. Sell discusses why prediction of the odor character, intensity, and threshold for a given molecule from its structure will remain a statistical exercise despite our increased understanding of the mechanism of olfaction.

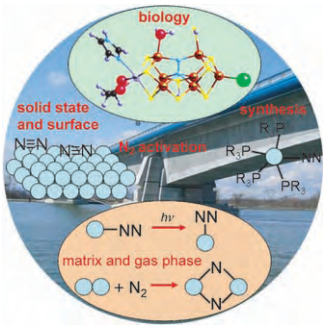

Dinitrogen Activation

The fundamental interaction of metal atoms with dinitrogen is considered in the Review by H.-J. Himmel and M. Reiher on page 6264 ff. DFT calculations show the extent of N_2 activation in these complexes.

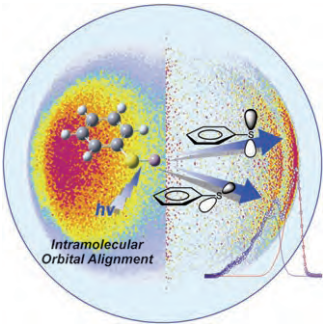

Chemical Dynamics

In their Communication on page 6290 ff., S. K. Kim and co-workers report how photodissociation of [D_1]thiophenol produces two distinct phenylthiyl radicals in which the reactive singly occupied molecular orbital is oriented either parallel or perpendicular to the molecular plane.

Contents

VIP *The following Communications have been judged by at least two referees to be "very important papers" and will be published online at www.angewandte.org soon:*

*F. P. Seebeck, A. Guainazzi, C. Amoreira, K. K. Baldridge, D. Hilvert**
Stereoselectivity and Expanded Substrate Scope of an Engineered PLP-Dependent Aldolase

U. Klar, B. Buchmann, W. Schwede, W. Skuballa, J. Hoffmann, R. B. Lichtner*
Total Synthesis and Antitumor Activity of ZK-EPO: The First Fully Synthetic Epothilone in Clinical Development

D. Stacchiola, S. K. J. Weissenrieder, H. Kuhlenbeck, S. Shaikhutdinov, H.-J. Freund, M. Sierka, T. K. Todorova, J. Sauer*
Synthesis and Structure of an Ultrathin Aluminosilicate Film

*M. C. Wood, D. C. Leitch, C. S. Yeung, J. A. Kozak, L. L. Schafer**
Chiral, Neutral Zirconium Amidate Complexes for the Asymmetric Hydroamination of Alkenes

*J. M. Wiseman, D. R. Ifa, Q. Song, R. G. Cooks**
Tissue Imaging at Atmospheric Pressure Using Desorption Electrospray Ionization (DESI) Mass Spectrometry

*N. Pour, L. Itzhaki, B. Hoz, E. Altus, H. Basch, S. Hoz**
Auxetics at the Molecular Level: A Negative Poisson's Ratio in Molecular Rods

News

Supramolecular Chemistry: Diederich honored ____ **6246**

Organic Chemistry: Seebach awarded ____ **6246**

Self-Assembly: Nitschke receives prize ____ **6246**

Books

Electroorganic Reduction Synthesis — Sigeru Torii — *reviewed by H. J. Schäfer* ____ **6247**

Anticancer Agents from Natural Products — Gordon Cragg, David Kingston, David Newman — *reviewed by K.-H. Altmann* ____ **6248**

Highlights

Asymmetric Epoxidations

I. W. C. E. Arends* ____ **6250 – 6252**

Metal-Catalyzed Asymmetric Epoxidations of Terminal Olefins Using Hydrogen Peroxide as the Oxidant

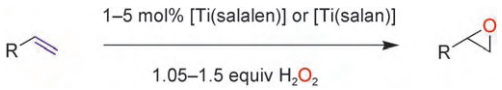

The state of the art in asymmetric epoxidation catalysis using the green H_2O_2 as oxidant has been drastically improved. Chiral [Ti(salalen)] and simple chiral [Ti(salan)] catalysts are reported to be surprisingly active chiral catalysts for styrene and 1-octene, thereby leading to high yields and enantioselectivities.

Minireviews

Structure–Odor Relationships

C. S. Sell* ____ **6254 – 6261**

On the Unpredictability of Odor

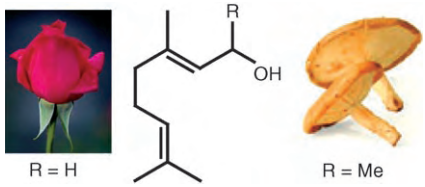

..., but how does it smell? Organic chemists have long been fascinated by the relationship between the structure of a molecule and its odor. Structure–odor models abound, but so do exceptions to the general rules. Our knowledge of the mechanism of olfaction has increased significantly over recent years; however, we are still far from consistently accurate and precise predictions of odor properties of molecules from their structures.

WILEY InterScience DISCOVER SOMETHING GREAT
© 2006 Wiley-VCH Verlag GmbH & Co. KGaA, Weinheim

Reviews

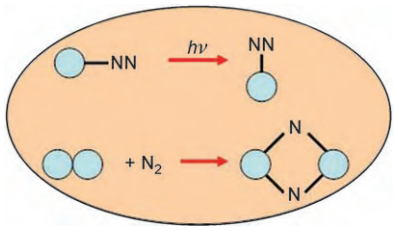

Building bridges between diverse research fields—biological, biomimetic, and heterogeneous dinitrogen fixation—sheds light on the key questions of dinitrogen activation. The focus of this Review is on the bonding of N_2 in the simplest model systems: metal atoms and their dimers (see scheme).

Nitrogen Fixation

H.-J. Himmel,* M. Reiher* _ **6264 – 6288**

Intrinsic Dinitrogen Activation at Bare Metal Atoms

Communications

In-plane or out-of-plane: Two low-energy states of the phenylthiyl radical were observed in the photodissociation of [D_1]thiophenol. The relative orientation of the singly occupied molecular orbital (SOMO) distinguishes the two species, namely $\tilde{X}(B_1)$ and $\tilde{A}(B_2)$. This orbital is largely localized on the sulfur atom and exhibits atomic-orbital-like alignment with respect to the molecular plane (see picture).

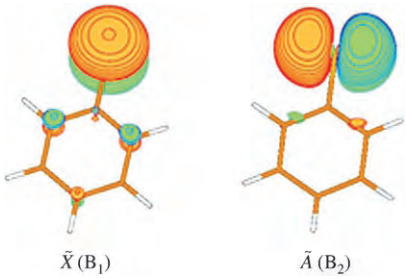

Chemical Dynamics

J. S. Lim, I. S. Lim, K.-S. Lee, D.-S. Ahn, Y. S. Lee,* S. K. Kim* _____ **6290 – 6293**

Intramolecular Orbital Alignment Observed in the Photodissociation of [D_1]Thiophenol

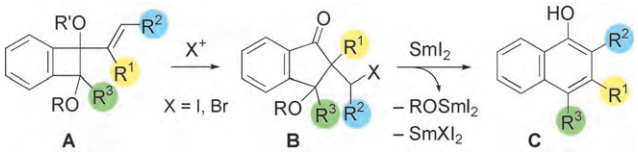

Twice expanded: Substituted naphthols were prepared in a novel synthetic route starting from alkenyl benzocyclobutenol derivatives. The conversion includes two successive ring-enlargement processes (**A**→**B**→**C**; see scheme). The halonium ion (X^+) induces expansion of the four-membered ring to a five-membered ring, and SmI_2 promotes the expansion of the five-membered ring to the six-membered ring with concomitant elimination of $ROSmI_2$.

Polyaromatic Compounds

T. Hamura, T. Suzuki, T. Matsumoto, K. Suzuki* _____ **6294 – 6296**

Tandem Ring Expansion of Alkenyl Benzocyclobutenol Derivatives into Substituted Naphthols

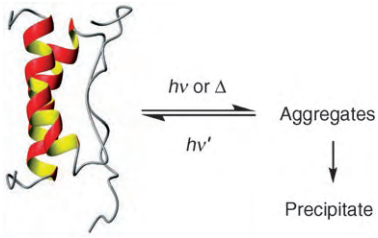

Flip a switch: A peptide capable of adopting different conformations is constructed upon insertion of an azobenzene linker into the polypeptide backbone. A simple transformation (irradiation or heating) can be used to switch from one form to the other.

Conformational Switch

S. Jurt, A. Aemissegger, P. Güntert, O. Zerbe,* D. Hilvert* _____ **6297 – 6300**

A Photoswitchable Miniprotein Based on the Sequence of Avian Pancreatic Polypeptide

For the USA and Canada:
ANGEWANDTE CHEMIE International Edition (ISSN 1433-7851) is published weekly by Wiley-VCH PO Box 191161, D 69451 Weinheim, Germany. Air freight and mailing in the USA by Publications Expediting Inc. 200 Meacham Ave., Elmont, NY 11003. Periodicals postage paid at Jamaica NY 11431. US POSTMASTER: send address changes to *Angewandte Chemie*, Wiley-VCH, 111 River Street, Hoboken, NJ 07030. Annual subscription price for institutions: US$ 5685/5168 (valid for print and electronic / print or electronic delivery); for individuals who are personal members of a national chemical society prices are available on request. Postage and handling charges included. All prices are subject to local VAT/sales tax.

© 2006 Wiley-VCH Verlag GmbH & Co. KGaA, Weinheim

The best in chemistry – for more than a hundred years

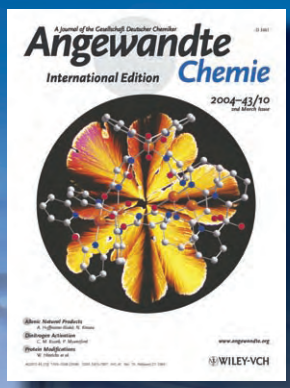

A Journal of the Gesellschaft Deutscher Chemiker

Angewandte International Edition **Chemie**

www.angewandte.org

1888: ***The beginning of a success story***

Constant Innovations

1962: *First issue of the International Edition*
1976: *Graphical abstracts*
1979: *Cover pictures*
1988: *Centenary of Angewandte*
1989: *Routine use of color*
1991: *New section: Highlights*
1992: *Computerized editorial tracking system*
1995: *Internet service for readers*
1998: *Regular press service; full-text online*
2000: *New section: Essays; EarlyView: Communications available online ahead of the printed version*
2001: *New section: Minireviews*
2002: *Online submission of manuscripts*
2003: *Weekly publication; new section: News; new layout*
2004: *Backfiles (1962-1997); ManuscriptXpress: Online system for authors and referees*

Angewandte's advisors...

Horst Kessler
Institut für Organische und Biochemie, Technische Universität München

» If you want to be recognized send your best papers to ***Angewandte Chemie****. The journal is scientifically of top quality; the layout makes the articles easy to read and contributes to the overall impact. An important step forward was the coverage in Medline making the life sciences community aware of the journal's content. Now the field of bioorganic chemistry is also becoming stronger in* ***Angewandte Chemie****. «*

Angewandte Chemie International Edition *is a journal of the German Chemical Society (GDCh)*

GDCh

WILEY InterScience® DISCOVER SOMETHING GREAT

WILEY-VCH

1831404_gw

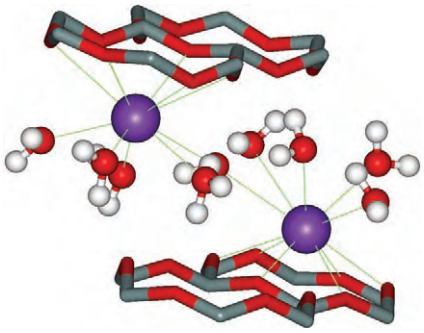

Caged: Potassium ions are trapped in coordination cages composed of surface hexagons and water molecules in a smectite interlayer (see picture; blue K, red O, white H). This microstructure leads to a striking stability of the single-layer K-smectite hydrate and inhibits further swelling of the clay.

Clay Swelling

X.-D. Liu, X.-C. Lu* ——— **6300 – 6303**

A Thermodynamic Understanding of Clay-Swelling Inhibition by Potassium Ions

---

Transparent Si nanosheets with a thickness of 0.37 nm are produced by chemically exfoliating calcium disilicide with propylamine hydrochloride (PA·HCl; see picture, Ca white, Si red). The nanosheets have a two-dimensional silicon backbone and are an order of magnitude thinner than previously reported silicon nanostructures.

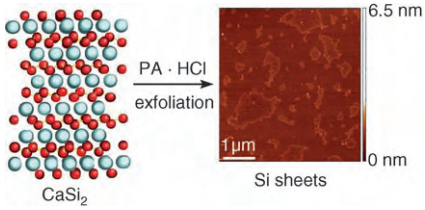

Layered Compounds

H. Nakano,* T. Mitsuoka, M. Harada, K. Horibuchi, H. Nozaki, N. Takahashi, T. Nonaka, Y. Seno, H. Nakamura ——— **6303 – 6306**

Soft Synthesis of Single-Crystal Silicon Monolayer Sheets

The pipes, the pipes are calling: Organic parallelogram-shaped pipes of micrometer dimensions have been obtained by simply allowing drops of a solution of low-molecular-weight compounds to evaporate. This unique structure is formed by self-templated crystal growth during the evaporation. The mechanism of formation involves two polymorphic crystal forms in dynamic nonequilibrium conditions.

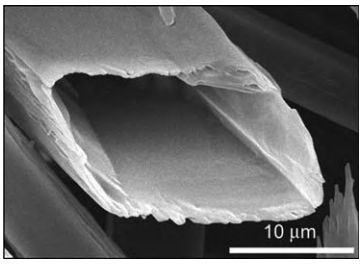

Supramolecular Chemistry

M. Seo, G. Seo, S. Y. Kim* _ **6306 – 6310**

Molecular Self-Assembly of Macroporous Parallelogrammatic Pipes

---

Parallel chains of Co^{II} dimers are interlinked by *trans*-1,2-cyclohexanedicarboxylate ligands in a laminated coordination polymer (see picture; C gray, Co tourquise, O red), which exhibits single-chain-magnet behavior due to strong Ising-like intrachain ferromagnetic interaction that can not easily be reversed by the relatively weak interchain antiferromagnetic interaction.

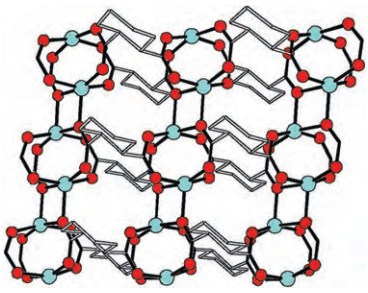

Low-Dimensional Magnet

Y.-Z. Zheng, M.-L. Tong, W.-X. Zhang, X.-M. Chen* ——— **6310 – 6314**

Assembling Magnetic Nanowires into Networks: A Layered Co^{II} Carboxylate Coordination Polymer Exhibiting Single-Chain-Magnet Behavior

© 2006 Wiley-VCH Verlag GmbH & Co. KGaA, Weinheim

Contents

Conductive Polymers

J. Huber, S. Mecking* ——— **6314 – 6317**

Processing of Polyacetylene from Aqueous Nanoparticle Dispersions

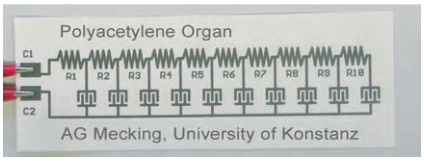

Printed circuits: Aqueous polyacetylene dispersions were prepared by catalytic polymerization of acetylene in an aqueous emulsion with a cationic palladium catalyst with a bulky diphosphine ligand. Facile processing is demonstrated by ink-jet printing of the conductive-polymer dispersions to produce a functioning electronic device (see picture).

Photoisomerization

N. S. S. Kumar, S. Varghese, G. Narayan, S. Das* ——— **6317 – 6321**

Hierarchical Self-Assembly of Donor–Acceptor-Substituted Butadiene Amphiphiles into Photoresponsive Vesicles and Gels

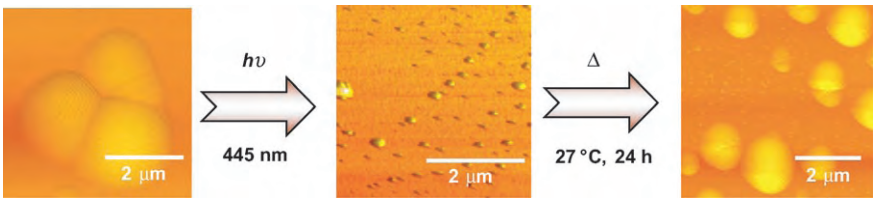

It all gels well: Amphiphilic donor–acceptor-substituted butadienes undergo spontaneous concentration-dependent self-assembly into highly fluorescent vesicles and gels. The vesicles and gels exhibit light-induced destruction and self-repair as a result of the photochromic nature of the butadiene chromophore.

Biotechnology

L. L. Parker, J. W. Kurutz, S. B. H. Kent, S. J. Kron* ——— **6322 – 6325**

Control of the Yeast Cell Cycle with a Photocleavable α-Factor Analogue

Under arrest: Photodegradation of a synthetic yeast α-factor analogue releases yeast from mating-factor-induced arrest into the cell cycle. This peptide has sufficient activity to arrest cells in G1 at reasonable doses and it can be specifically degraded through exposure to UV light at a wavelength that is "safe" for most cells. FITC-A = absorption of a fluorescein isothiocyanate analogue.

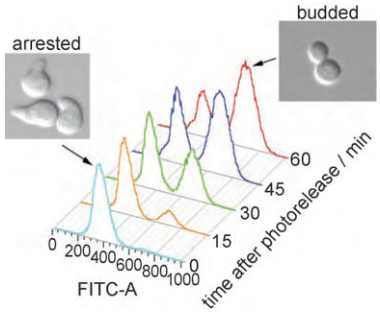

Nanoelectronics

Y. Jin,* D. Cahen, N. Friedman, M. Sheves ——— **6325 – 6328**

Gold-Nanoparticle-Enhanced Current Transport through Nanometer-Scale Insulating Layers

Coupling of noble-metal nanoparticles (NPs) into electronics might lead to interesting new avenues in nanoelectronics. It was found that currents through metal//organic (or inorganic) insulator/Au NP monolayer//metal planar junctions (2) are orders of magnitude higher than what is obtained without the NP monolayer (1).

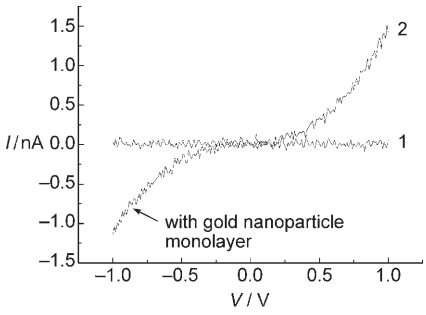

© 2006 Wiley-VCH Verlag GmbH & Co. KGaA, Weinheim

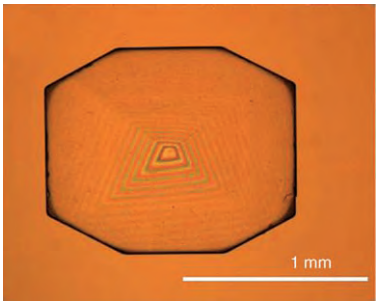

Special *k*: Pure silica zeolites (PSZs) have been shown experimentally to display a remarkably higher elastic modulus than amorphous porous silicas at any given porosity or dielectric constant (k) value as a result of their crystalline structure. The combined experimental and theoretical findings suggest that PSZs have the necessary properties for use as the next generation of low-k insulators.

Pure Silica Zeolites

Z. Li, M. C. Johnson, M. Sun, E. T. Ryan, D. J. Earl, W. Maichen, J. I. Martin, S. Li, C. M. Lew, J. Wang, M. W. Deem, M. E. Davis, Y. S. Yan* ____ **6329 – 6332**

Mechanical and Dielectric Properties of Pure-Silica-Zeolite Low-k Materials

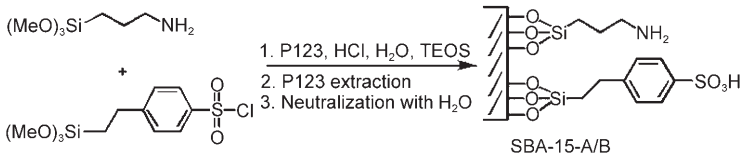

Dual functions: The simultaneous immobilization of primary amines and sulfonic acids on mesoporous silica SBA-15 (SBA-15-A/B; see scheme) creates a heterogeneous catalyst that exhibits cooperative catalytic behavior in the aldol condensation reaction. The respective chemical reactivities of the acid and base groups are maintained, whereas homogeneous analogues are neutralized in solution. TEOS = tetraethoxysilane.

Acid–Base Catalysis

R. K. Zeidan, S.-J. Hwang, M. E. Davis* ____ **6332 – 6335**

Multifunctional Heterogeneous Catalysts: SBA-15-Containing Primary Amines and Sulfonic Acids

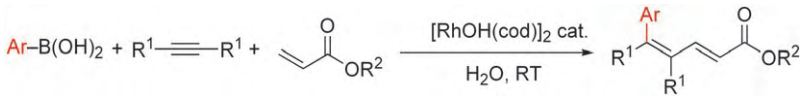

Only in water: A fully intermolecular rhodium-catalyzed domino coupling reaction, in which aryl boronic acids react with alkynes and acrylates to afford substituted 1,3-dienes, can only be successfully carried out in water. The reaction predominantly provides 1,4-addition products in aqueous THF and Heck-type addition products in a homogenized system with sodium decyl sulfate. cod = 1,5-cyclooctadiene.

Heterogenous Catalysis

T. Kurahashi, H. Shinokubo,* A. Osuka ____ **6336 – 6338**

Intermolecular Rhodium-Catalyzed Carbometalation/Heck-Type Reaction in Water

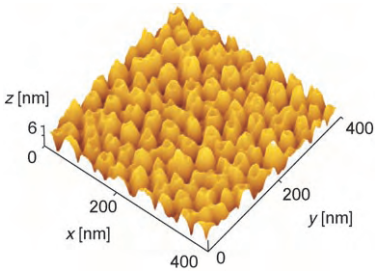

Small capsules: Nanoscale silica capsules can be synthesized by the oxidation of nanoscale bubbles in the poly(dimethylsiloxane) domains of poly(styrene-*b*-dimethylsiloxane). These nanobubbles are introduced by a process involving supercritical carbon dioxide. The nanocapsules are opened up after dry etching (see AFM image).

Silica Nanostructures

L. Li, H. Yokoyama* ____ **6338 – 6341**

Nanoscale Silica Capsules Ordered on a Substrate: Oxidation of Nanocellular Thin Films of Poly(styrene-*b*-dimethylsiloxane)

© 2006 Wiley-VCH Verlag GmbH & Co. KGaA, Weinheim

Contents

Gas-Phase N_2 Complexes

S. G. Francis, S. L. Matthews, O. K. Poleshchuk, N. R. Walker, A. C. Legon* ——— **6341 – 6343**

N_2–Cu–F: A Complex of Dinitrogen and Cuprous Fluoride Characterized by Rotational Spectroscopy

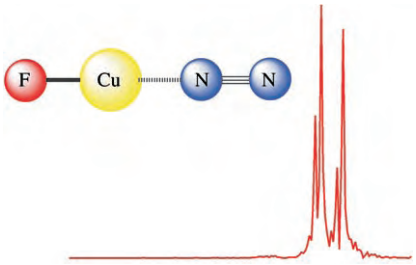

Dinitrogen bound: A compound formed by dinitrogen with cuprous fluoride has been synthesized by laser ablation of a copper rod in the presence of a source of F atoms and N_2. The rotational spectrum of $^{15}N_2$–Cu–F has been assigned, and the rotational, centrifugal, and nuclear hyperfine coupling constants have been determined. These constants and electronic structure calculations give conclusions about the nature of this novel molecule.

Template Synthesis

E. Kassianidis, D. Philp* ——— **6344 – 6348**

Design and Implementation of a Highly Selective Minimal Self-Replicating System

Self-direction: A rationally designed self-complementary template (see picture) is capable of replication, thereby amplifying itself from a reaction mixture to the exclusion of its diastereomer. This approach allows a highly selective amplification by focusing on templates that display a high level of complementarity to transition states.

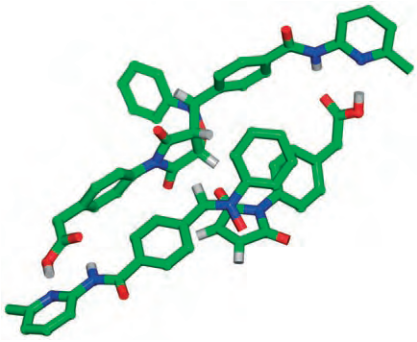

Supported Oligosaccharides

H. Tanaka, T. Ishida, N. Matoba, H. Tsukamoto, H. Yamada, T. Takahashi* ——— **6349 – 6352**

Efficient Polymer-Assisted Strategy for the Deprotection of Protected Oligosaccharides

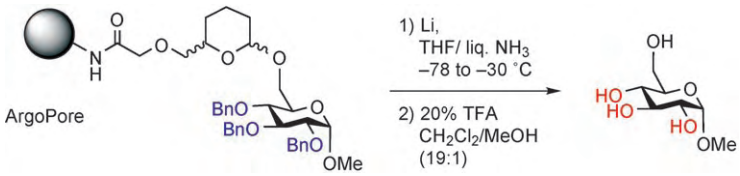

New strategies in sugar synthesis: A prelinker containing a dihydropyranyl moiety and an activated ester can be attached to a sugar, which is then loaded onto an amino-modified support by amidation. Standard protecting-group manipulations are possible. Final cleavage of the linker under mildly acidic conditions provides the fully deprotected oligosaccharides. TFA = trifluoroacetic acid.

Selective Protein Recognition

S. J. Koch, C. Renner, X. Xie, T. Schrader* ——— **6352 – 6355**

Tuning Linear Copolymers into Protein-Specific Hosts

Being picky: A new concept for selective protein recognition by artificial receptor molecules involves statistical copolymerization of simple binding monomers in defined stoichiometric ratios. As an example of its efficiency, an arginine-rich lysozyme is recognized by a bisphosphonate-rich copolymer with a remarkable K_d value of 25 nM, 100-times superior to that of cytochrome c, which is comparable in size and isoelectric point.

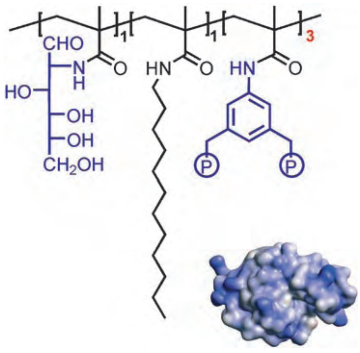

© 2006 Wiley-VCH Verlag GmbH & Co. KGaA, Weinheim

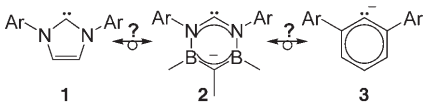

NB! The anionic ligand **2** was synthesized through deprotonation of a planar, formally zwitterionic diazadiborine precursor, isolated as a lithium salt, and structurally characterized. According to experimental evidence and theoretical calculations, **2** can be considered as an intermediate between two classical classes of ligands: N-heterocyclic carbenes **1** and terphenyls **3**.

Ligand Design

T. D. Forster, K. E. Krahulic, H. M. Tuononen, R. McDonald, M. Parvez, R. Roesler* ——— **6356 – 6359**

A σ-Donor with a Planar Six-π-Electron $B_2N_2C_2$ Framework: Anionic N-Heterocyclic Carbene or Heterocyclic Terphenyl Anion?

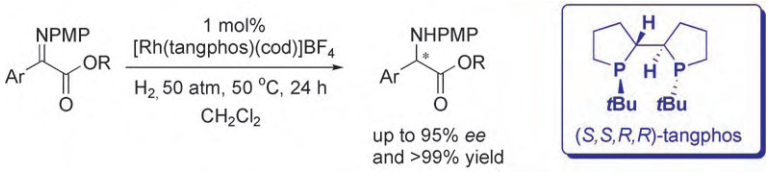

A highly enantioselective synthesis of aryl glycine derivatives from asymmetric hydrogenation was achieved by subjecting *N*-PMP-protected α-aryl imino esters to hydrogenation under Rh–bisphosphine catalysis (see scheme; PMP = *para*-methoxyphenyl, cod = cycloocta-1,5-diene). The PMP group could be easily removed for the preparation of enantiomerically pure aryl glycine derivatives.

Asymmetric Catalysis

G. Shang, Q. Yang, X. Zhang* ——— **6360 – 6362**

Rh-Catalyzed Asymmetric Hydrogenation of α-Aryl Imino Esters: An Efficient Enantioselective Synthesis of Aryl Glycine Derivatives

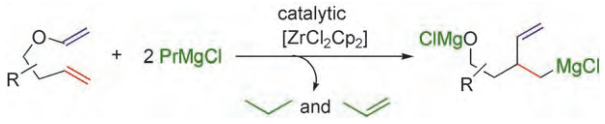

A straightforward approach: An unprecedented zirconocene-catalyzed isomerization–magnesation reaction of readily available alkene-substituted enol ethers allows the direct synthesis of functionalized Grignard reagents. Cp = cyclopentadienyl.

Rearrangement

J. Barluenga,* L. Álvarez-Rodrigo, F. Rodríguez, F. J. Fañanás ——— **6362 – 6365**

Zirconocene-Catalyzed Reactions of Alkenyl-Substituted Enol Ethers

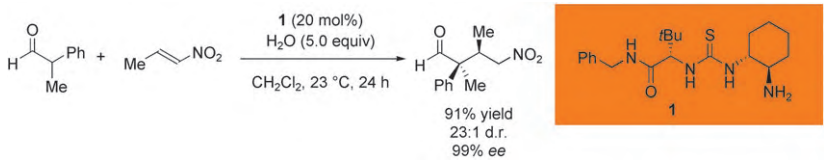

Dual activation: The bifunctional primary amine thiourea catalyst **1** promotes the highly enantioselective direct conjugate addition of α-branched aldehydes to nitroalkenes (see scheme). Cooperative activation of both the nucleophile and electrophile allows the use of mild reaction conditions and provides access to a wide variety of adducts with vicinal quaternary and tertiary stereogenic centers (> 90% *ee*).

Organocatalysis

M. P. Lalonde, Y. Chen, E. N. Jacobsen* ——— **6366 – 6370**

A Chiral Primary Amine Thiourea Catalyst for the Highly Enantioselective Direct Conjugate Addition of α,α-Disubstituted Aldehydes to Nitroalkenes

© 2006 Wiley-VCH Verlag GmbH & Co. KGaA, Weinheim

Contents

Si–Si Multiple Bonds

R. Tanaka, T. Iwamoto,*
M. Kira* ——— **6371 – 6373**

Fused Tricyclic Disilenes with Highly Strained Si–Si Double Bonds: Addition of a Si–Si Single Bond to a Si–Si Double Bond

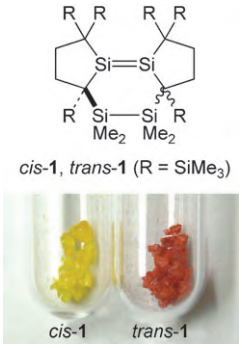

Internal fusion: The stable fused tricyclic tetraalkyl disilenes *cis*-**1** and *trans*-**1** were synthesized as yellow and red-purple crystals, respectively (see picture). X-ray analysis has shown that the geometry around the Si=Si bond in *trans*-**1** is unusually distorted, but is rather normal in *cis*-**1**. Disilene *trans*-**1** isomerizes stereospecifically to a tetracyclic isomer by unprecedented addition of a Si–Si single bond to a Si–Si double bond.

Protein Binding

N. Shimokhina, A. Bronowska,
S. W. Homans* ——— **6374 – 6376**

Contribution of Ligand Desolvation to Binding Thermodynamics in a Ligand–Protein Interaction

Solvation is free: The affinities within biomolecular associates are governed by a complex interplay between structure and dynamics of the interacting species and solvent water. The contribution of ligand desolvation in the binding of small ligands to the major urinary protein has been examined to give a complete breakdown of binding thermodynamics in this system.

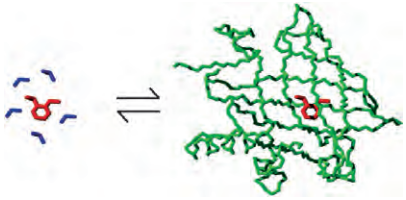

Natural Product Synthesis

J. O. Bunte, A. N. Cuzzupe, A. M. Daly,
M. A. Rizzacasa* ——— **6376 – 6380**

Formal Total Synthesis of (+)-Zaragozic Acid C through an Ireland–Claisen Rearrangement

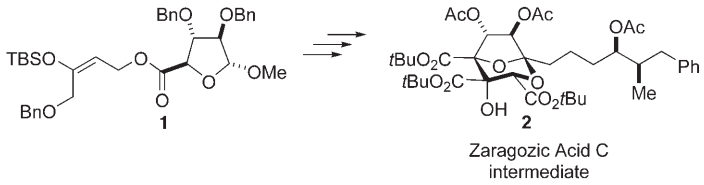

A simple rearrangement: A formal total synthesis of zaragozic acid C (**1**) was achieved by the synthesis of intermediate **2**. The key step involves an Ireland–Claisen rearrangement of an allylic ester to generate a carbon–carbon bond and two asymmetric centers simultaneously.

Drug Polymorphism

C. Näther,* I. Jeß ——— **6381 – 6383**

New News about an Old Drug: Investigations on the Polymorphism of Triamcinolone Acetonide

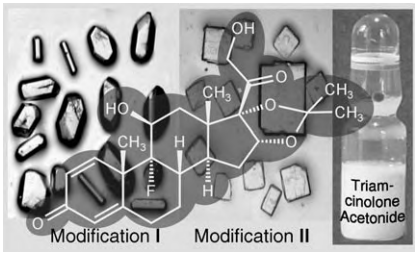

Even a very old drug holds some surprises when its polymorphism is investigated in detail. The commercially available form of triamcinolone acetonide (modification **I**) is a hydrate that contains a small amount of water, which is responsible for its stability. The removal of water results in a transformation into the previously unknown modification **II**. This finding may have a large impact on the production of the dosage form.

© 2006 Wiley-VCH Verlag GmbH & Co. KGaA, Weinheim

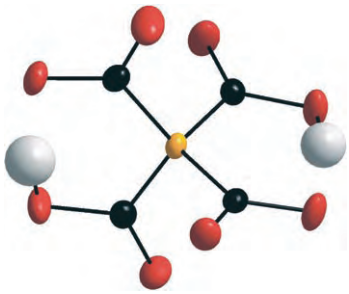

Series clincher: The synthesis of salts of the $[B(CO_2H)_4]^-$ ion and the $[B(CNCH_3)_4]^{3+}$ ion starting from $[nBu_4N][B(CN)_4]$ are described. Thus, the series including $[B(CN)_4]^-$, $[B(CO_2H)_4]^-$, and $[B(CF_3)_4]^-$ has now been completed. The figure shows the $[B(CO_2)_2(CO_2H)_2]^{3-}$ ion in $[Co(NH_3)_6][B(CO_2)_2(CO_2H)_2]\cdot 2H_2O$ (O red, C black, B yellow, H white).

Carboxyborates

E. Bernhardt,* D. J. Brauer, M. Finze, H. Willner* ——— **6383 – 6386**

$[B(CO_2H)_4]^-$ and $[B(CNCH_3)_4]^{3+}$: Homoleptic Boron Complexes Containing Carboxy and Methylisocyanide Ligands

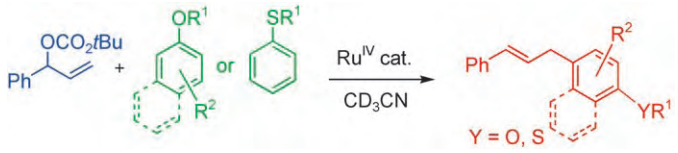

Unexpected linkage: The use of dicationic Ru^{IV} complexes in the Friedel–Crafts-type allylation of aromatic alcohols leads unexpectedly to the formation of a new C–C bond and not to the phenolation product (see scheme). NMR spectroscopy, diffusion data, DFT calculations, and X-ray diffraction analysis provide new insights with respect to the mechanism of this reaction.

Allylations

I. Fernández, R. Hermatschweiler, F. Breher, P. S. Pregosin,* L. F. Veiros, M. J. Calhorda ——— **6386 – 6391**

High-Yield Ruthenium-Catalyzed Friedel–Crafts-Type Allylation Reactions Using Dicationic Ru^{IV} Catalysts

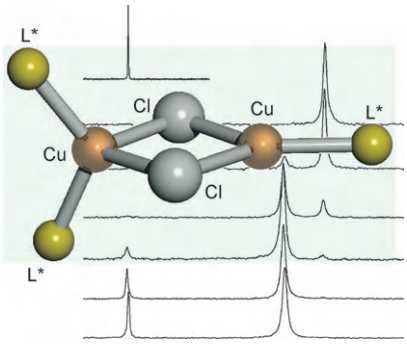

1+1 is more than 2: A binuclear copper phosphoramidite precatalyst with mixed trigonal/tetrahedral coordination environments (see picture) is proposed based on NMR spectroscopy, mass spectrometry, and elemental analysis. The precatalyst represents a new structural motif for stereoselective copper catalysts and explains ligand acceleration and salt sensitivity in highly enantioselective 1,4-additions to enones.

Copper Catalysts

H. Zhang, R. M. Gschwind* **6391 – 6394**

Structure Identification of Precatalytic Copper Phosphoramidite Complexes in Solution

Looking for outstanding employees?

Do you need another expert for your excellent team?
... Chemists, PhD Students, Managers, Professors, Sales Representatives...

Place an advert in the printed version and have it made available online for 1 month, free of charge!

Angewandte Chemie International Edition
Advertising Sales Department: Marion Schulz
Phone: 0 62 01 - 60 65 65
Fax: 0 62 01 - 60 65 50
E-Mail: MSchulz@wiley-vch.de

Service

Keywords ——— *6398*

Authors ——— *6399*

Angewandte's Sister Journals ——— *6396 – 6397*

Vacancies ——— *6395*

Preview ——— *6401*

© 2006 Wiley-VCH Verlag GmbH & Co. KGaA, Weinheim

Contents

Corrigenda

Gold–Organic–Inorganic High-Surface-Area Materials as Precursors of Highly Active Catalysts

G. Budroni, A. Corma* ____ **3328–3321**

Angew. Chem. Int. Ed. **2006**, *45*

DOI 10.1002/anie.200600552

In Table 1 of this Communication, data for three catalysts used for comparison purposes were calculated erroneously. Thus, for the catalysts MCM-41, MCM-48, and SBA-15 (last three entries in Table 1), specific rates of 0.62, 0.35, and 0.47 $mol_{CO}\,g_{Au}^{-1}\,h^{-1}$, respectively, are obtained at $T = 80\,^{\circ}C$ and a contact time of 23 $g_{cat}\,h\,mol_{CO}^{-1}$. These catalysts are at least 3.3 times less active than the presented gold nanoparticle catalyst at a reaction temperature of 80 °C.

Conductance and Stochastic Switching of Ligand-Supported Linear Chains of Metal Atoms

I-W. P. Chen, M.-D. Fu, W.-H. Tseng, J.-Y. Yu, S.-H. Wu, C.-J. Ku, C.-h. Chen,* S.-M. Peng* ____ **5814–5818**

Angew. Chem. Int. Ed. **2006**, *45*

DOI 10.1002/anie.200600800

In the list of addresses for the authors of this Communication, the country should read as Republic of China. The editors apologize for the error in the print version of their article.

Ligand-Selective Aqueous Synthesis of One-Dimensional CdTe Nanostructures

H. Zhang, D. Wang,* H. Möhwald ____ **748–751**

Angew. Chem. Int. Ed. **2006**, *45*

DOI 10.1002/anie.200502751

In Scheme 1 of this Communication, the molecular structure of L-cysteine (LCS) was incorrectly represented and should be as depicted here. The molecular structure of LCS is a combination of those of 2-mercaptoethylamine (MA) and 3-mercaptopropionic acid (MPA); however, LCS strongly facilitated the formation of CdTe nanorods whereas MA and MPA did not. This difference may arise from the strong chelation of Cd ions by the cooperation of the neighboring NH_2 and COOH groups of LCS.

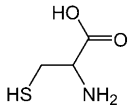

 © 2006 Wiley-VCH Verlag GmbH & Co. KGaA, Weinheim

Awarded...

F. Diederich receives A. W. von Hofmann Medal

During the opening ceremony of the First European Chemistry Congress (ECC) in Budapest (Hungary), the German Chemical Society (Gesellschaft Deutscher Chemiker, GDCh) presented the native Luxembourger François Diederich (ETH Zürich, Switzerland) with the August Wilhelm von Hofmann Medal. The medal, which commemorates von Hofmann (1818–1892), who in his long career served as President of the Chemical Society in London and later became the founding president of what was to become the GDCh,[1] is awarded to foreign chemists and German scientists (non-chemists). Diederich presented a lecture on the Principles of Supramolecular Chemistry in Drug Discovery Research. Besides the areas of molecular recognition in chemistry and biology, supramolecular nanochemistry, the chemistry of synthetic fullerenes, and novel materials from carbon-rich acetylene derivatives,[2a] Diederich's research group is also interested in medicinal chemistry and recently discussed antimalarial drugs in *Angewandte Chemie*.[2b]

F. Diederich

Diederich completed his PhD in 1979 at the University of Heidelberg (Germany) with H. A. Staab. He carried out postdoctoral research at the University of California in Los Angeles (UCLA; USA) and at the Max Planck Institute for Medicinal Research in Heidelberg. After completing his habilitation in 1985 he returned to UCLA, and in 1992 he joined the ETH Zürich. Diederich serves on the advisory board of *Chemistry – A European Journal* and has been the chairman of the editorial board of *Angewandte Chemie* since 2004.

D. Seebach gives EuCheMS Lecture

The European Association for Chemical and Molecular Sciences (EuCheMS) Lecture was given by Dieter Seebach (ETH Zürich) at the ECC in Budapest on the topic of Structural and Biological Investigations of Peptides Consisting of Homologated Proteinogenic Amino Acids. Seebach, a former member of the editorial board of *Angewandte Chemie*, completed his PhD at the University of Karlsruhe (Germany) with R. Criegee, then undertook postdoctoral research with E. J. Corey at Harvard University (USA). In 1971 he became professor in Giessen (Germany), and then in 1977 at the ETH Zürich. His research is broadly concerned with the development of methodology in organic chemistry. One of his current projects focuses on β-peptides, and he recently discussed their role in passive transfer through the lipid bilayer in *ChemBioChem*.[3a] Over a period of almost 30 years, *Angewandte Chemie* has published 11 Reviews by Seebach on a wide range of topics, including umpolung, Ti and Zr nucleophiles, asymmetric synthesis, and his legendary view on the future of organic synthesis.[3b]

D. Seebach

European Young Chemist Award to J. R. Nitschke

The European Young Chemist Awards, which are presented to chemists under 34 years of age, were presented for the first time at the ECC, Budapest. The Gold Medal went to Jonathan R. Nitschke (University of Geneva, Switzerland), who presented a lecture on Construction, Substitution, and Sorting Using Subcomponent Self-Assembly. Nitschke completed his PhD in 2001 at the University of California, Berkeley (USA), and then joined J.-M. Lehn (Chemistry Nobel Prize 1987) at the Université Louis Pasteur, Strasbourg (France), as a postdoctoral researcher. Since 2003, he has been an independent junior researcher (Maître-assistant) at the University of Geneva. His research revolves around helicates; he recently reported in *Chemistry – A European Journal* on dynamic topological control on subcomponent self-assembly to give helicates, macrocycles, or catenanes[4a] and on a dynamic Cu_3 double helicate.[4b]

J. R. Nitschke

Runner-up prizes (Silver Medals) went to Javier García Martínez (University of Alicante, Spain; Circular Porosity Induced by Membrane Phospholipids) and Leroy Cronin (University of Glasgow, UK; Supramolecular Self-Assembly of Polyoxometalate Clusters towards Functional Nanosystems[5]). Elisabete Barros de Carvalho (University of Porto (Portugal); Interaction of Salivary Proteins with Grape Seed Procyanidins) and Irina Koval (University of Leiden (The Netherlands); Copper Complexes as Biomimetic Models of Catechol Oxidase) received special mention from the jury.

[1] C. Meinel, *Angew. Chem.* **1992**, *104*, 1293; *Angew. Chem. Int. Ed. Engl.* **1992**, *31*, 1265.

[2] a) M. Kivala, F. Mitzel, C. Boudon, J.-P. Gisselbrecht, P. Seiler, M. Gross, F. Diederich, *Chem. Asian J.* **2006**, *1*, 479; b) F. Hof, A. Schütz, C. Fäh, S. Meyer, D. Bur, J. Liu, D. E. Goldberg, F. Diederich, *Angew. Chem.* **2006**, *118*, 2193; *Angew. Chem. Int. Ed.* **2006**, *45*, 2138.

[3] a) B. Geueke, K. Namoto, I. Agarkova, J.-C. Perriard, H.-P. E. Kohler, D. Seebach, *ChemBioChem* **2005**, *6*, 982; b) D. Seebach, *Angew. Chem.* **1990**, *102*, 1363; *Angew. Chem. Int. Ed. Engl.* **1990**, *29*, 1320.

[4] a) M. Hutin, C. A. Schalley, G. Bernardinelli, J. R. Nitschke, *Chem. Eur. J.* **2006**, *12*, 4096; b) M. Hutin, R. Frantz, J. R. Nitschke, *Chem. Eur. J.* **2006**, *12*, 4077.

[5] D.-L. Long, P. Kögerler, L. J. Farrugia, L. Cronin, *Chem. Asian J.* **2006**, *1*, 352.

DOI: 10.1002/anie.200603096

WILEY InterScience DISCOVER SOMETHING GREAT

© 2006 Wiley-VCH Verlag GmbH & Co. KGaA, Weinheim

Asymmetric Epoxidations

DOI: 10.1002/anie.200602044

Metal-Catalyzed Asymmetric Epoxidations of Terminal Olefins Using Hydrogen Peroxide as the Oxidant

*Isabel W. C. E. Arends**

Keywords:
asymmetric synthesis · epoxidation · hydrogen peroxide · ligand design · metal catalysis

Asymmetric epoxidation of alkenes has the potential of creating two chiral centers in one step and is therefore a pivotal reaction in drug synthesis (Scheme 1). State-of-the-art oxidation

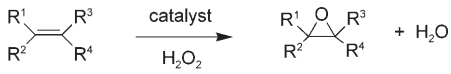

R = H or alkyl

Scheme 1. Asymmetric epoxidations using H_2O_2 as oxidant.

technologies should be characterized by high atom economy and selectivity, broad substrate scope, use of environmentally benign oxidation reagents, and sufficient catalyst stability and productivity. Moreover, for industrial applications, systems which are simple and easy to work up are important. In terms of atom efficiency, after oxygen, aqueous hydrogen peroxide would be the oxidant of choice since it produces water as the sole by-product and can therefore be classified as the ultimate green oxidant. Furthermore, oxidation with aqueous hydrogen peroxide is cheap, safe, and easy to operate.[1]

Many research efforts have been dedicated to the development of chiral metal catalysts that can perform asymmetric epoxidation. Most well-known is probably the Sharpless method, based on titanium tartrate complexes, for epoxidizing allylic alcohols.[2] The Jacobsen–Katsuki method uses Mn(salen) complexes and provides an efficient method for unfunctionalized and particularly *cis* olefins.[3,4] However, these methods require the use of alkyl hydroperoxides, hypochlorite, or other non-atom-efficient reagents as the oxidant. For electron-deficient olefins the Julia–Colonna method, which uses aqueous H_2O_2 as the oxidant and polypeptides as the catalyst, is available and can be applied on an industrial scale.[5] But in general, there is still a significant number of alkenes that cannot be converted to epoxides with stereochemical control. In particular, the asymmetric oxidation of terminal nonactivated olefins remains an area to be developed. The challenge, therefore, is to develop catalysts which can perform asymmetric epoxidations with a wider scope by using H_2O_2 as oxidant.

The main obstacle when using hydrogen peroxide is the high activity of many later and first-row transition metals in the decomposition thereof, the so-called catalase reaction. For example, Ru and Mn complexes will decompose H_2O_2 rapidly. Furthermore, complexes of early transition metals, for example, Ti, Mo, and V complexes, are often hampered by their instability in the presence of hydrogen peroxide and/or water. Therefore, until recently, results obtained in the asymmetric epoxidation with H_2O_2 and chiral metal catalysts (notably Mn and Ru) have been rather disappointing.[6]

An alternative methodology has been developed by Shi and others[7,8] using chiral ketone-derived organocatalysts. The sugar-derived system developed by Shi is able to epoxidize trisubstituted *trans* alkenes and certain *cis* alkenes with good to excellent stereocontrol.[7] In most cases potassium peroxomonosulfate ($KHSO_5$), commonly denoted as oxone, is used as the oxidant. Moreover, hydrogen peroxide can be used as the oxidant in the presence of acetonitrile (the so-called Payne reagent).[9] In this case acetonitrile not only serves as a solvent but also as a reagent to react with H_2O_2 to form the peroxyimidic acid; an example is given in Table 1. This technology has been scaled up for industrial purposes, but the major disadvantage is that it requires up to 15 mol% of catalyst and is not selective for terminal olefins.

Another noteworthy development is the use of cell-free monooxygenases as biocatalysts. Recently flavin-dependent styrene monooxygenases were coupled to a formate-driven regeneration system, whereby the major obstacle of providing the reducing equivalents was overcome.[10] Volumetric product formation rates of around $1\,g_L^{-1}h^{-1}$ were reported.[10b] Various styrene derivatives were converted into the essentially optically pure (*S*)-epoxides.

The recent reports of Katsuki and Beller in which Ti-[11,12] and Ru-based[13] complexes were used for asymmetric epoxidation with H_2O_2, have however changed the state of the art in the area of metal-catalyzed asymmetric epoxidations. Especially for titanium in combination with reduced salen-type ligands, excellent stereochemical control was achieved for terminal olefins using hydrogen peroxide as the oxidant.[11,12] Also with ruthenium, which is notorious for its catalase activity, excellent yields and enantioselectivities were obtained for *cis* and activated olefins.[13] In Ta-

[*] Dr. I. W. C. E. Arends
Department of Biotechnology
Delft University of Technology
Julianalaan 136
2628 Delft (The Netherlands)
Fax: (+31) 15-278-1415
E-mail: i.w.c.e.arends@tudelft.nl

InterScience
© 2006 Wiley-VCH Verlag GmbH & Co. KGaA, Weinheim

Table 1: Comparison of metal catalysts for the asymmetric epoxidation of alkenes using aqueous H_2O_2.

Substrate	Cat.	Cat. loading [mol%]	Equivalents 30% aqueous H_2O_2	Yield [%] Epoxide	*ee* [%] Epoxide	Ref.
	1[a]	1	1.05	90	93	[11]
	2[b]	5	1.5	47	82	[12]
	3[c,d]	5	3	85	59	[13a]
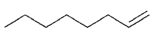	**1**[a]	1	1.05	70	82	[11]
	2[b]	5	1.5	25	55	[12]
	1[a]	1	1.05	99	99	[11]
	2[b]	5	1.5	87	96	[12]
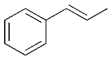	**3**[c]	5	3	95	72	[13a]
	4[e]	15	4	93	92	[9]

[a] Room temperature, 12–48 h, CH_2Cl_2 as solvent. [b] 25 °C, 6–24 h, CH_2Cl_2 as solvent. [c] Room temperature, 12 h, 2-methylbutan-2-ol as solvent. [d] Acetic acid (20 mol%) was added. [e] 0 °C, 12 h, CH_3CN/2.0 M K_2CO_3 in 4×10^{-4} M EDTA.

ble 1 an overview is given of the performance of titanium and ruthenium complexes as catalysts with hydrogen peroxide. The structures of the complexes are given in Scheme 2.

For titanium, only 1 mol% of catalyst **1** and 1.05 equivalents of H_2O_2 are required to obtain high yields and selectivities. 1,2-Dihydronaphthalene is an activated *cis* olefin, which obviously gives the best results (yield and enantioselectivity of over 98%) using little or no excess of hydrogen peroxide. However, also for simple styrene, 93% *ee* can be achieved by using the chiral titanium complex **1**. What is most striking is the result obtained for 1-octene. For this simple nonactivated olefin a reasonable 82% *ee* could be attained. Catalyst **1** is a chiral di-μ-oxo titanium half-reduced salen complex. It was prepared in 60% yield using an in situ Meerwein–Ponndorf–Verley reduction. This complex adopts a homochiral (*aR*,*S*,*Δ*,*aR*,*S*,*Δ*) configuration, and it maintains its dimeric structure in methanol for over 24 hours. This finding is exceptional because the corresponding salen complex, which is completely ineffective as an epoxidation catalyst with aqueous H_2O_2, immediately dissociates into the monomeric [Ti(salen)] species in methanol. For catalyst **1** in the presence of hydrogen peroxide, the active species in solution is most likely a monomeric peroxotitanium species. It is speculated that this peroxotitanium species is activated by an intramolecular hydrogen bond with the amine proton as indicated in Scheme 3.

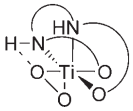

Scheme 3. Putative peroxotitanium species activated by hydrogen bonding.

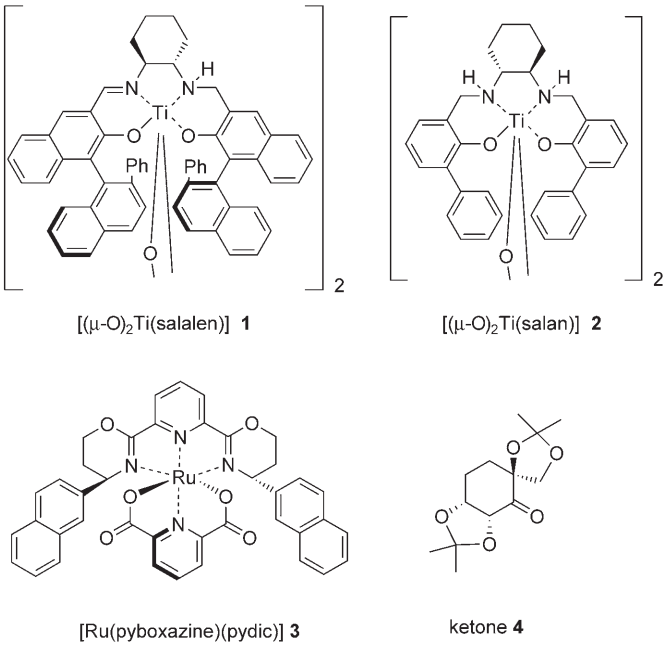

Scheme 2. State-of-the-art catalysts for asymmetric epoxidation using H_2O_2.

However, catalyst **1** has an elaborate structure, and its synthesis is rather specific for this particular ligand. For catalysis, construction of a more flexible and easy-to-synthesize ligand is important. Therefore, a range of the more accessible [Ti(salan)] complexes were tested as well.[12] Catalyst **2** (Scheme 2) is less robust (5 mol% instead of 1 mol% of catalyst is required) and selective than catalyst **1**. However, its ease of synthesis and tunability offer a large advantage. Moreover, catalyst **2** can be conveniently synthesized in situ from $Ti(OiPr)_4$ and the salan ligand with almost comparable enantioselectivities.[13] Results in Table 1 for catalysts **1** and **2** were obtained using dichloromethane as the solvent. However, results with titanium catalyst **1** in toluene or ethyl acetate gave equally good results.[11]

Many research groups have studied ruthenium for asymmetric oxidations owing to its rich complexation chemistry. In most cases, non-atom-efficient oxidants were used.[14,15] Recently, Beller and co-workers introduced a new approach towards optimizing activity and selectivity in Ru-catalyzed asymmetric epoxidations. The Ru catalyst **3** was the best in a whole series of [Ru(pybox)] and [Ru(pyboxazine)] complexes, which all contained pyridinedicarboxylate (pydic) as the second ligand.[13] The strategy that was followed by the group of Beller was to study

 © 2006 Wiley-VCH Verlag GmbH & Co. KGaA, Weinheim

ruthenium complexes with a combination of two meridional ligands, which provided the ability to tune both the activity and the asymmetric induction of the catalyst separately. The original catalyst [Ru(pybox)(pydic)] was reported by Nishiyama et al. for the epoxidation of *trans*-stilbene in the presence of $PhI(OAc)_2$ as the oxidant.[16] The pydic ligand turned out to be essential to suppress the catalase activity of ruthenium, and still in this case three equivalents of H_2O_2 were required. The enantioselectivity could then be optimized by screening a range of pybox and pyboxazine ligands. The latter could be synthesized easily from β-amino acid derivatives. The best results with complex **3** were obtained with *trans*-disubstituted styrene and reached up to 84% *ee* (not shown).[13b] Furthermore, although the results for ruthenium complex **3** were obtained using 5 mol% of catalyst, the authors reported that a similar level of efficiency could be reached with 0.5 mol% of catalyst.[13a]

It was suggested that the corresponding ruthenium dioxo complex is the active catalyst.[13] Electrospray ionization mass spectrometry of the reaction mixture showed molecular ions corresponding to both mono-oxo and dioxo complexes. However, the mono-oxo complex turned out to be quite stable and not active in oxygen transfer. Regarding the origin of the enantioselectivity, it is believed that π–π interactions between the ligand and the substrate are the dominating factor for the asymmetric induction. The ruthenium system is therefore also extremely promising because it provides numerous handles for optimizing the enantioselectivity in epoxidation reactions with H_2O_2. At this point it is not clear whether it will also be able to perform the asymmetric epoxidation of nonactivated olefins.

In conclusion, the state of the art in asymmetric epoxidation catalysts using aqueous hydrogen peroxide as the oxidant is represented by [Ti(salalen)] and [Ti(salan)] complexes. For the first time, asymmetric catalytic epoxidation for a nonactivated terminal olefin has been demonstrated. However, the Ti catalysts are closely rivaled by chiral pyridine dicarboxylate Ru complexes. Obviously, for industrial applications, higher turnover frequencies and higher chiral inductions for terminal olefins are required. Therefore, these systems are still prone to improvement, but the major disadvantages in terms of greenness have been overcome.

Published online: September 4, 2006

[1] I. W. C. E. Arends, R. A. Sheldon, *Top. Catal.* **2002**, *19*, 133 – 141.

[2] R. A. Johnson, K. B. Sharpless in *Catalytic Aymmetric Synthesis* (Ed.: I. Ojima), VCH, New York, **1993**, chap. 4.1.

[3] E. N. Jacobsen in *Catalytic Aymmetric Synthesis* (Ed.: I. Ojima), VCH, New York, **1993**, chap. 4.2.

[4] T. Katsuki, *Adv. Synth. Catal.* **2002**, *344*, 131 – 147.

[5] For a review, see: D. R. Kelly, S. M. Roberts, *Biopolymers* **2006**, *84*, 74 – 89.

[6] Selected examples for asymmetric epoxidations of styrene with H_2O_2: a) R. M. Stoop, A. Mezzetti, *Green Chem.* **1999**, *1*, 39 – 41; b) C. Bolm, D. Kadereit, M. Valacchi, *Synlett* **1997**, 687 – 688; c) C. Bolm, N. Meyer, G. Raabe, T. Weyhermüller, E. Bothe, *Chem. Commun.* **2000**, 2435 – 2436; d) R. I. Kureshy, N. H. Khan, S. H. R. Abdi, S. T. Patel, R. V. Jasra, *Tetrahedron: Asymmetry* **2001**, *12*, 433 – 437.

[7] Y. Shi, *Acc. Chem. Res.* **2004**, *37*, 488 – 496.

[8] D. Yang, *Acc. Chem. Res.* **2004**, *37*, 497 – 505.

[9] L. Shu, Y. Shi, *Tetrahedron* **2001**, *57*, 5213 – 5218.

[10] a) F. Hollmann, P.-C. Lin, B. Witholt, A. Schmid, *J. Am. Chem. Soc.* **2003**, *125*, 8209 – 8217; b) K. Hofstetter, J. Lutz, I. Lang, B. Witholt, A. Schmid, *Angew. Chem.* **2004**, *116*, 2215 – 2218; *Angew. Chem. Int. Ed.* **2004**, *43*, 2163 – 2166.

[11] K. Matsumoto, Y. Sawada, B. Saito, K. Sakai, T. Katsuki, *Angew. Chem.* **2005**, *117*, 4676 – 4678; *Angew. Chem. Int. Ed.* **2005**, *44*, 4935 – 4939.

[12] Y. Sawada, K. Matsumoto, S. Kondo, H. Watanabe, T. Ozawa, K. Suzuki, B. Saito, T. Katsuki, *Angew. Chem.* **2006**, *118*, 3558 – 3560; *Angew. Chem. Int. Ed.* **2006**, *45*, 3478 – 3480.

[13] a) M. K. Tse, C. Döbler, S. Bhor, M. Klawonn, W. Mägerlein, H. Hugl, M. Beller, *Angew. Chem.* **2004**, *116*, 5367 – 5372; *Angew. Chem. Int. Ed.* **2004**, *43*, 5255 – 5260; b) M. K. Tse, S. Bhor, M. Klawonn, G. Anilkumar, H. Jiao, A. Spannenberg, C. Döbler, W. Mägerlein, H. Hugl, M. Beller, *Chem. Eur. J.* **2006**, *12*, 1875 – 1888.

[14] G. A. Barf, R. A. Sheldon, *J. Mol. Catal. A* **1995**, *102*, 23 – 39.

[15] Ruthenium in Organic Synthesis (Ed.: S.-I. Murahashi), Wiley-VCH, Weinheim, **2004**.

[16] H. Nishiyama, T. Shimada, H. Itoh, H. Sugiyama, Y. Motoyama, *Chem. Commun.* **1997**, 1863 – 1864.

 © 2006 Wiley-VCH Verlag GmbH & Co. KGaA, Weinheim

DOI: 10.1002/anie.200600782

Structure–Odor Relationships

On the Unpredictability of Odor

*C. S. Sell**

Keywords:
fragrances · olfaction · receptors · structure–activity relationships

The relationship between molecular structure and odor has fascinated and puzzled chemists for more than a century. Despite a great deal of research on structure–odor relationships, prediction of the odor of a novel molecule remains a statistical exercise and models only provide a probability of the character, threshold, and intensity. Surprises are still commonplace, and serendipity continues to be an important factor in the discovery of novel fragrant molecules. Recent advances in our understanding of the mechanism of olfaction provide an explanation for this and suggest that our ability to predict odor properties of molecules will not improve significantly in the near future.

1. Introduction

The search to correlate the molecular structure and the odor character of a chemical compound has a long recorded history. In ancient Greece, the proponents of Democritus' atomic theory proposed that the atoms of sweet-smelling substances had smooth surfaces whereas those of acidic materials had sharp points that pricked and irritated the nose. Since the development of synthetic organic chemistry in the 19th century, chemists have sought a clearer understanding of the relationship between molecular structure and the odor of a molecule, largely with the intention to design novel molecules with desirable odor properties.

However, this search for understanding has proved to be a very difficult task. There are many puzzling observations that often have no simple or obvious explanation. For example, on one hand, quite different molecules can have similar odors, whereas, on the other hand, similar molecules can have dissimilar odors. Thus, despite the significant differences in their structures, muscone (**1**),[1] musk ketone (**2**),[2] Traseolide (**3**),[3] and Helvetolide (**4**)[4] all have similar musk odors (Figure 1), whereas the two very similar structures **5** and **6** have very different organoleptic properties: **5** has an intense urinous character while **6** is odorless.[5]

Sometimes, the functional group present in an odorant is all-important. For example, the ester group is often associated with a fruity character.[6] Thus, both Fruitate (**7**)[7] and Manzanate (**8**)[8] have distinctly fruity odors despite the differences in size and structural complexity between them (Figure 2). However, in other cases, the functional group seems unimportant: for example, structures **9**–**12** all have camphoraceous odors.[9]

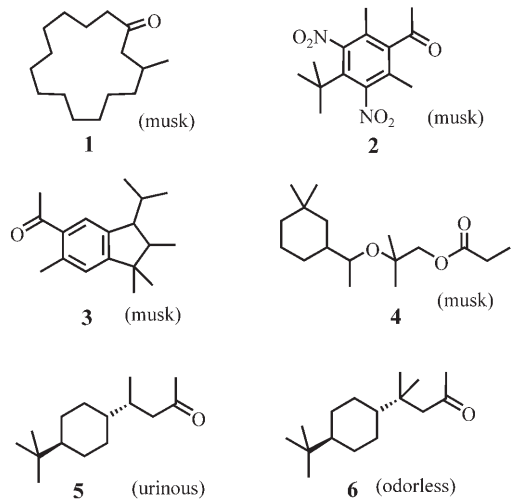

Figure 1. Different molecules, similar odors; and vice versa.

In many instances factors such as these can be brought together in triads, where the odd molecule out in structural terms is *not* the odd one out in odor. For example, of the structures **13**–**15** the last, **15**, is the odd one out in chemical terms as it is an alicyclic alcohol, whereas the other two, namely **13** and **14**, are both cinnamaldehyde derivatives (Figure 3). However, in terms of odor, it is α-methylcinna-

[*] Dr. C. S. Sell
Quest International
Willesborough Road
Ashford, Kent, TN24 0LT (UK)
Fax: (+44) 1233-644-738
E-mail: charles.sell@questintl.com

InterScience
© 2006 Wiley-VCH Verlag GmbH & Co. KGaA, Weinheim

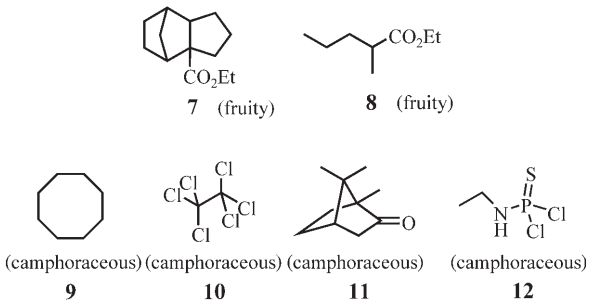

Figure 2. Role of the functional group.

maldehyde (**14**) which is the odd one out as it has a cinnamon odor[10] whereas Lilial (**13**, also known as Lily Aldehyde and Lilestralis)[11] and Florosa or Florol (**15**)[8] both have muguet (lily-of-the-valley) odors. As stated above, the ester group is usually associated with fruity scents, but *tert*-amyl acetate (**17**) has an odor which is much closer to that of camphor (**11**) than to the fruity, banana–pear scent of its isomer, *n*-amyl acetate (**16**; Figure 3).[6]

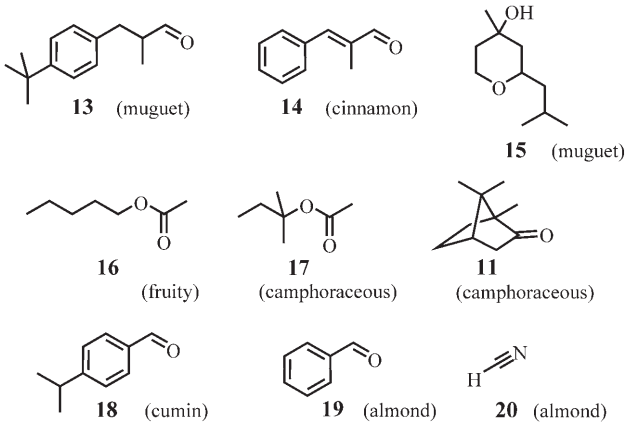

Figure 3. Triads of molecules in which the odd one out structurally is not necessarily the odd one out in odor.

Perhaps the most bizarre and best known of these triads is that involving structures **18**–**20**. Cuminaldehyde (**18**),[12] as its name suggests, smells of cumin, whereas benzaldehyde (**19**)[13] and hydrogen cyanide (**20**)[14] both smell of almond. Some theories have been proposed to account for the similarity in odor between **19** and **20**, for example, by invoking oligomerization of HCN in the receptor binding site.[15] However, the explanation is surely more likely to lie in higher-order neuroprocessing.[16]

Charles S. Sell completed his BSc and MSc (James Grimshaw) degrees at Queen's University (Belfast) and then took up a scholarship at the Australian National University, where he completed his PhD in the group of Arthur Birch in 1974. After postdoctoral fellowships with Albert Eschenmoser (ETH Zürich) and Bernard Golding (University of Warwick), he joined Quest International. His interests since then have involved both discovery and process research in fragrance and flavor chemistry. His main research interests are terpenoid chemistry and the mechanism of olfaction.

2. Structure–Odor Models

Over the last century, many theories have been proposed relating to the primary events in olfaction and to relationships between molecular structure and odor. The review by Rossiter[17] gives an excellent summary of these theories. However, the prediction of odor remains a statistical exercise. For example, Chastrette and De Sainte Laumer developed a model based on a neural network for the prediction of the musk odor of nitrobenzene derivatives.[18] Their model gave results that were correct in 77% of test materials. Similarly, Bersuker et al. developed a model for musk activity based on an electron-topological approach.[19] Their results were impressive, yet 15 of their set of 362 materials were incorrectly predicted.

Most structure–odor models are concerned with the character of the odor. However, the commercially important parameters of detection threshold, recognition threshold, and superthreshold intensity of odorants have received much less attention, partly because of the difficulty[20] and cost of measurement of these parameters and/or because such models are even more difficult to construct. Nevertheless, detection threshold models are beginning to appear and examples include studies by Kraft on materials with marine[21] and musk[22] odor characters.

In his review of the subject, Weyerstahl concluded: "*Despite numerous excellent studies during the last 30 years the area of structure–odour relationships remains rather confusing.*"[23]

3. The Effect of Structural Modifications

One phenomenon that seriously disrupts attempts to correlate odor properties with molecular structure is that a given structural modification can induce a dramatic change in odor properties in one situation whilst having little or no effect in another. The following list of examples serves to illustrate that this is a general phenomenon that is applicable across a wide range of structural modifications and not just a few isolated instances.

The majority of odorants contain only one strongly polar function in the molecular structure. It is generally believed that this polar group will form a hydrogen bond or some other dipolar attachment to a polar site on an olfactory receptor, with the remainder of the molecule occupying a hydrophobic space in the receptor. Such polar groups have therefore come to be known as osmophoric groups or osmophores,[22] and they are used in structure–activity relationships (SARs) as a molecular reference point.[21,22] (Occasionally, a second, usually weaker, electron donor or acceptor is also involved.) Structures **21**–**24** all contain a cyclohexane ring with an osmophoric group at one end and either an isopropyl or *tert*-

 © 2006 Wiley-VCH Verlag GmbH & Co. KGaA, Weinheim

butyl group at the other (Figure 4). In dihydrocryptyl acetate (**21**) and *p*-*tert*-butylcyclohexyl acetate (**22**), the osmophore is an acetate and there is little effect on the odor upon changing an isopropyl group for a *tert*-butyl substituent; Arctander

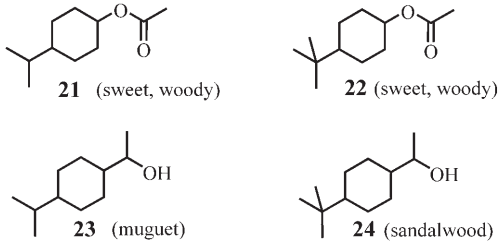

Figure 4. Role of the osmophore.

describes both as being predominantly sweet and woody in character.[24,25] However, when the osmophore is the secondary alcohol group of structures **23** and **24**, a similar small structural change has a major effect on the odor, taking it from muguet to sandalwood.[26]

Similarly, substitution of the *tert*-butyl group of **22** by an isobutyl group to give **25** changes the odor from sweet and woody to a harsh raspberry character,[27] whereas the same exchange has little effect on the muguet character of Lilial (**13**), whose isobutyl analogue Silvial (**26**) has a similar muguet odor (Figure 5).[28]

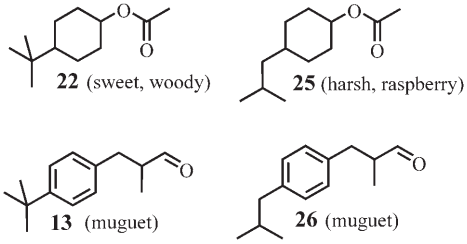

Figure 5. Role of the hydrophobic residue.

Analogous examples also exist in the case of geometric isomers. For instance, in the case of Rossitol, the odor is muguet/citrus whether the alcohol function lies *trans* (**27**) or *cis* (**28**) to the isobutyl group. However, in the analogues in which the isobutyl group has been replaced by a cyclohexyl substituent, the *trans* isomer **29** has a strong, specifically muguet odor whereas that of the *cis* isomer **30** is much weaker, woody, and only generally floral (Figure 6).[29]

The same pattern applies to geometric isomers of double bonds. (*Z*)-4-Heptenal (**31**) has a creamy, buttery odor,[30] whereas the *E* isomer **32** has an aggressive, green and putty-like odor.[31] However, in the case of 2-tetradecenal, both isomers **33** and **34** have fresh, orange odors (although that of **33** is more mandarin-like; Figure 7).[23]

Positional isomers around rings are also subject to this phenomenon. The odor of the *meta* isomer **35** of Lilial (**13**) is reported to be stronger than that of the *para* isomer,[26] whereas the odors of both *m*- and *p*-Cyclamen Aldehydes

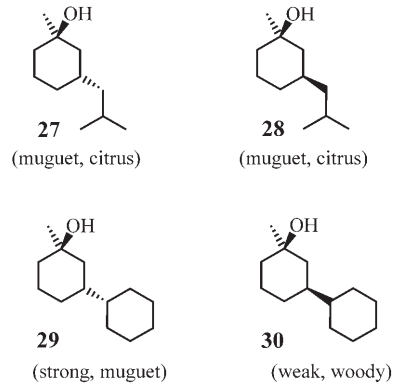

Figure 6. Odors of geometric isomers in rings.

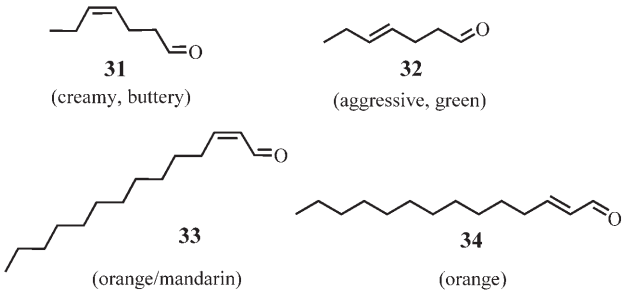

Figure 7. Odors of geometric isomers in olefins.

(**36** and **37**, respectively) are similar in character and intensity (Figure 8).[32] With the dihydrocinnamaldehydes **13** and **35**–**37**, the intensity of the odor varies but the character of all four remains similar. However, in the case of the acylcyclohexenes **38** and **39**, the shift from *meta* to *para* substitution results in a change in odor character from the green and fatty notes of **38** to the fruity odor of **39** (Figure 8).[33]

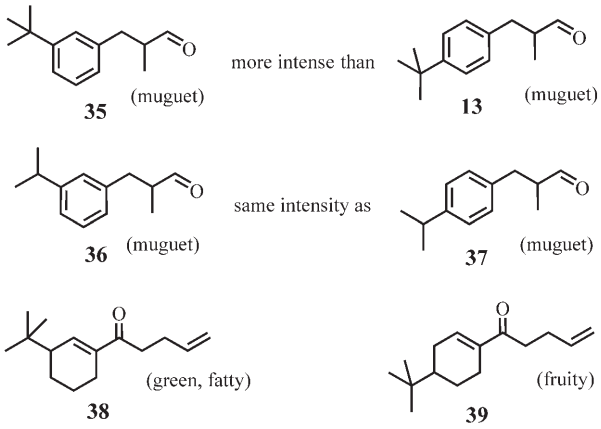

Figure 8. Effect of positional isomers on odor.

The presence or absence of a double bond also provides examples. Linalool (**40**)[34] and dihydrolinalool (**41**)[35] have similar refreshing floral, woody, and citrus odors. However, a similar saturation of a double bond with concomitant

© 2006 Wiley-VCH Verlag GmbH & Co. KGaA, Weinheim

conversion from an allylic alcohol into a saturated alcohol changes the odor from the intense, earthy mushroom character of **42**[11] to the sweet, warm, herbaceous, and nutty scent of **43** (Figure 9).[36]

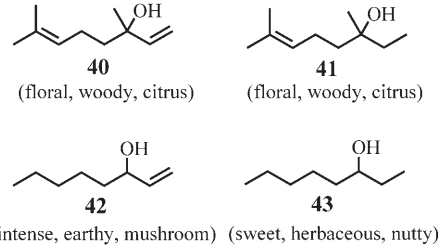

Figure 9. Effect of saturation of a double bond.

The conversion of a primary alcohol into a secondary alcohol by the addition of a methyl group also gives unpredictable results. Geraniol (**44**) is well known for its rosy odor,[37] whereas the higher homologue **45** has an intense fungal odor.[38] On the other hand, a similar transformation from Sandal Mysore Core (Santacore; **46**) to **47**, the dehydro analogue of Sandalore, has only a relatively small effect on the central sandalwood character (Figure 10).[11,39,40]

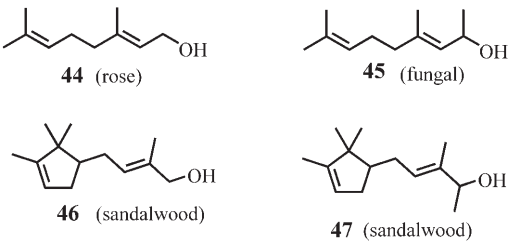

Figure 10. Effect of conversion from primary into secondary alcohols.

As stated above, functional groups are usually important in determining odor character, however, sometimes the exchange of one function for another has little or no effect. In the next three examples, a ketone group is exchanged for the acetate of the corresponding alcohol with three different levels of effect. On going from acetophenone (**48**) to styrallyl acetate (**49**), the odor shifts from sweet hawthorn-like[41] to dry, fruity, and green.[11] On moving from Patchone (**50**) to *p*-*tert*-butylcyclohexyl acetate (**51**), the degree of change is somewhat less as the odors of both materials have woody characters; that of patchone is very much on the camphoraceous and minty side of wood,[42] whereas the odor of **51** has a sweet, almost fruity character (Figure 11).[25] At the other end of this spectrum, polywood ketone (**52**) and Polywood (**53**) have similar woody, ambergris odors.[23]

Substitutions by a fragment with similar stereoelectronic properties is a common practice in fragrance ingredient discovery, just as it is in drug discovery. For example, when following up on a lead from nature, the isobutenyl group of terpenoid compounds is often substituted by a benzene ring.[43] Thus, citronellol (**54**) served as a lead for Mefrosol (also known as Phenoxanol; **55**) and the odors of both

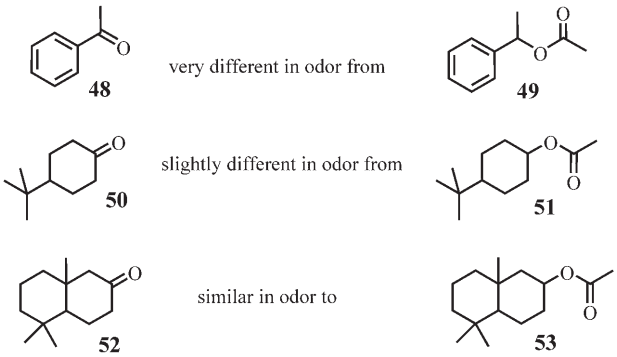

Figure 11. Effect of changing a ketone to an acetate.

compounds have a rosy character.[11] However, the green, pungent, herbaceous character of 2-methylhept-2-ene-6-one (**56**)[44] is not replicated by the sweet, floral character of benzylacetone (**57**; Figure 12).[11]

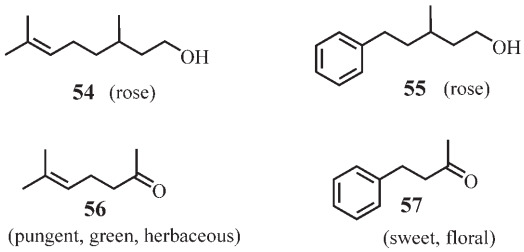

Figure 12. Effect of substitution a fragment with similar stereoelectronic properties.

Another standard substitution is that of a cyclopropane ring for a double bond. The alcohol **46** and ketone **58** both have sandalwood-like odors. Cyclopropanation of both double bonds of **46** produces Javanol (**59**), which is considered to be the strongest sandalwood-scented material known, and both "intermediate" monocyclopropanated species also have predominantly sandalwood characters (Figure 13).[45] However, cyclopropanation of one of the double bonds of **58** to give **60** leads to complete loss of the sandalwood-like odor.[33]

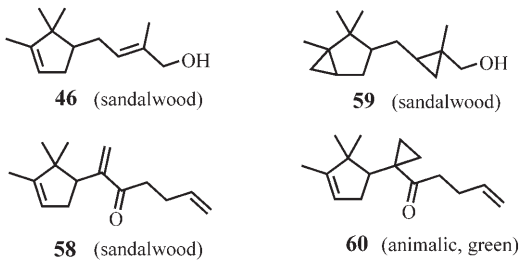

Figure 13. Effect of a cyclopropyl substituent.

Chirality also provides us with many examples of the unpredictability of the effect of changes in molecular structure on the odor of the molecule.[46] In the case of Lilial (**13**) one enantiomer is odorless,[47] whereas the odors of both

 © 2006 Wiley-VCH Verlag GmbH & Co. KGaA, Weinheim

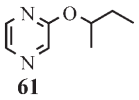
61

enantiomers of the pyrazine **61** are identical in character and threshold.[48] The pair of ethers **62** and **63** have identical thresholds of detection but different odor characters (Table 1).[49] The odors of the musks (−)-**1** and (+)-**1** have the same character, but the threshold of (−)-**1** is 0.43 ng L^{-1} whereas that of its enantiomer (+)-**1** is over twenty times higher at 9.5 ng L^{-1}.[50] The odors of the enantiomers of dihydro-α-ionone, **64** and **65**, differ in both character and threshold.[51]

Table 1: Effect of chirality on the odor of a molecule.

Compound	Odor	Threshold [ng L^{-1}]	Compound	Odor	Threshold [ng L^{-1}]
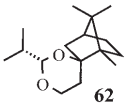 62	woody, pineapple	40	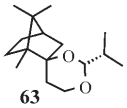 63	woody, rose	40
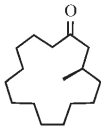 (−)-1	musk	0.43	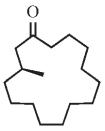 (+)-1	musk	9.5
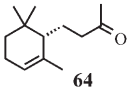 64	orris	100	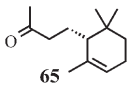 65	violet	31

Subsequent developments based on the discoveries of Buck and Axel have enabled molecular biologists to extract the genes involved and to incorporate them into cells in culture and therefore to profile the sensitivity of individual receptor types. One interesting outcome of this discovery is that we now know that olfactory receptors are expressed in sites other than the nose and that they serve quite different functions in these other sites. An example of such work was published by Spehr et al.,[58] who showed that the human receptor hOR17-4 (which is found in sperm as well as in the nose) responds to compounds **13**, **37**, and **66**–**73**, but not to compounds **19** and **74**–**82** (Figure 14). The strongest response is observed with Bourgeonal (**70**), although this compound is not the natural substrate of the receptor in either the nose or in sperm. To the discovery chemist, this observation points towards a binding site that requires an aldehyde as a hydrogen-bond acceptor and a shape based around that of an alkyl-substituted dihydrocinnamaldehyde. This information can now be used to build a model that could be of use in designing new molecules which could potentially serve as ligands for hOR17-4. One important observation here is that the results confirm that there is not a simple correlation between receptor activity and odor. For example, phenylacetaldehyde (**66**) fires the receptor but its intense green odor[59] is a far cry from the muguet character of Lilial,[11] which is another agonist.

4. Recent Advances in Understanding Odor Perception

In the 15 years since Weyerstahl's review,[23] our ability to predict the odor of a molecule from its molecular structure has not changed much. What has changed, however, is our understanding of why such predictions are so difficult.

The major breakthrough came in 1991 when Buck and Axel identified the gene family that encodes for the olfactory receptor proteins.[52] The proteins belong to the family of seven transmembrane G-protein-coupled receptors (GPCRs) and constitute the largest family in the genome. Eight years later, Buck and co-workers[53] showed that each of the receptors was broadly tuned, in that it responds to a range of odorant molecules and that, conversely, each odorant molecule triggers a range of receptor types. This report confirmed the hypothesis proposed by Polak that the sense of smell works on a combinatorial basis.[54] Buck and Axel received the Nobel Prize in Physiology or Medicine in 2004 for their work,[55] and their accounts were published recently.[56,57] One might expect that such huge advances in our understanding of the initial stages of odor perception would help us to predict the odor of molecules, but they do not. On the contrary, the breadth of receptor tuning and the large number of receptors involved actually explain why it is so difficult and why it will remain so for a very considerable time to come.

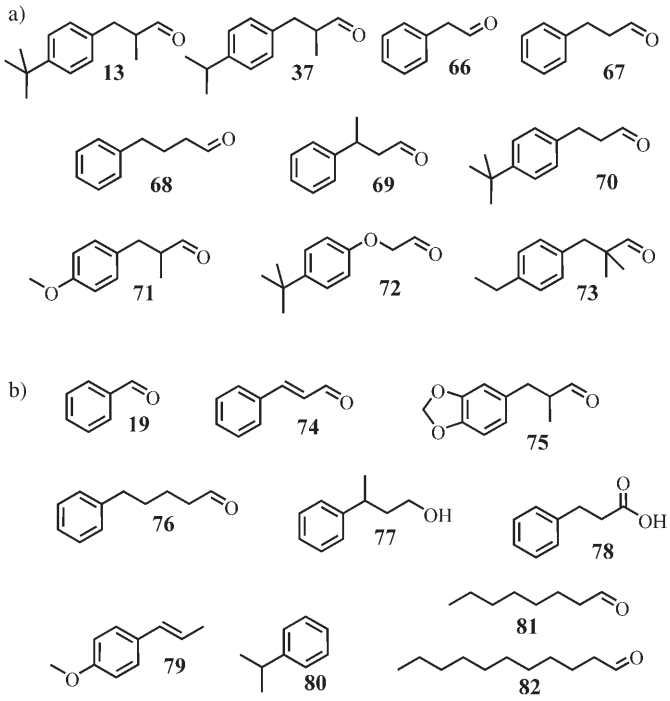

Figure 14. Agonists (a) and non-agonists (b) for hOR-17.

© 2006 Wiley-VCH Verlag GmbH & Co. KGaA, Weinheim

Araneda et al.[60] studied the receptive range of the rat olfactory receptor ORI7. Whereas Spehr et al. carried out direct measurements on the receptor cells, Araneda et al. assessed activity indirectly by measuring activity in the olfactory bulb at the glomerulus which corresponds with receptor neurons that possess ORI7. They found that this receptor responds to certain aliphatic aldehydes. From the degree of binding to 90 different test materials, they were able to establish that the binding site seems to recognize only aldehydes. There seems to be a strong steric restriction close to the aldehyde-binding point but much less strict steric requirements further away from it until a limit is reached at a chain length of 11 carbon atoms. Thus, as with hOR17-4, we can now construct a model to aid in molecular design, in this case with an aldehyde-docking area and a hydrophobic pocket with a specific overall length, and which is slightly broader at the end distant from the aldehyde.

The results described above with ORI7 and hOR17-4 point towards reasonably selective binding sites, whereas those from other receptors are much less clear-cut. For instance, Sanz et al.[61] investigated the specificity of two olfactory receptors, human class I OR52D1 and human class II OR1G1, with rather different results (Table 2). OR1G1 responds strongly to 2-ethylhexan-1-ol (**83**) and to 1-nonanol (**84**) but only weakly to 1-heptanol (**85**) and various isomeric octanols. It reveals a moderate response to decanoic acid (**86**) but no response to octanoic acid (**87**) and only a weak one to nonanoic acid (**88**). In the aldehyde series, its strongest response is to nonanal (**89**). With octanal (**81**) and decanal (**90**) it elicits only weak responses, whereas with benzaldehyde (**19**) and Lyral (**91**) it responds moderately. Of 16 esters tested, OR1G1 responds strongly only to ethyl isobutyrate (**92**); its response to the isomeric ethyl butyrate (**93**) is only weak and that to butyl butyrate (**94**) is almost zero. Strong responses were also observed to molecules as diverse as methyl thiobutanoate (**95**), benzothiazole (**96**), and γ-undecalactone (**97**). Thus OR1G1 seems to be quite selective *within* a class of substrates (for example, alcohols or acids) but not selective *between* classes, as it responds to alcohols, aldehydes, acids, esters, lactones, and a variety of heterocyclic systems. On the other hand, receptor OR52D1 generally responded more weakly to the materials in the same test set of 100 but with a different and equally puzzling pattern. It is difficult to see how one might design a model for a typical substrate for either of these receptors.

Research based on Buck and Axel's work has revealed the primary sequences of all of the human olfactory receptor proteins and now allows us to determine which are expressed in any individual. However, these proteins are proving difficult to work with experimentally and none have yet been

Table 2: Response of OR1G1 receptor to various odorant substrates.

Response			
strong	moderate	weak	none
83, **84**	**86**	**85**, **88**	**87**
89	**19**, **91**	**81**, **90**	
92, **95**, **96**, **97**		**93**	**94**

© 2006 Wiley-VCH Verlag GmbH & Co. KGaA, Weinheim

isolated in pure form. Model studies are based on extrapolation from the structure of bovine rhodopsin, which is the only GPCR for which an X-ray crystal structure exists. There are a number of assumptions in this extrapolation that must be borne in mind. Rhodopsin is an unusual GPCR in several ways, most significantly in that it requires a cofactor, 11-(*Z*)-retinal. There is also an assumption about conservation of tertiary structure from the crystalline environment to the membrane environment in which it is active. The putative binding sites in olfactory receptors are based on the binding site of 11-(*Z*)-retinal in rhodopsin rather than on in vivo experimental evidence. Spehr et al.[58] showed that activation of hOR-17 by Bourgeonal (**70**) is inhibited by undecanal (**82**), a non-agonist, and this result might suggest allosteric interactions and hence multiple binding sites. The role of odor-binding proteins (OBPs) in the olfactory mucosa is not understood and it is not known for certain whether or not they play an active role in olfaction or serve merely to remove excess odorant. However, work such as that of Spehr et al.[58] shows that, in the case of sperm or HEK cells, the receptor can be fired without the presence of an OBP.

Nonetheless, some excellent work is being done on building models of putative receptor sites and correlating these with in vivo activity. The work of Goddard and co-workers[62–64] serves as an illustration. Such work nicely complements the substrate-modeling approach of traditional SAR models.

Traditional SAR and binding-site models are essentially static in nature. A recent paper by Lai et al.[65] suggests that this might not be the best approach. Like Araneda et al.,[60] they looked at rat ORI7 receptors. Lai et al. generated a computer model of the receptor and fitted models of potential ligands into the putative binding site. They then set the whole assembly into normal motion and observed whether or not the ligand remained in the binding pocket. Molecules **81** and **98–102** remained in the binding site, whereas **103** and **104** moved out of the pocket once vibratory motion started (Figure 15). This model correlates with experiment as **81** and **98–102** are all activators in vivo whereas **103** and **104** are not. These results suggest that dynamics should be considered in addition to the traditional static stereoelectronic space-fitting approach. Prediction of new structures would be more difficult using a dynamic model and its use as an in silico screen prior to in vivo evaluation would seem more likely.

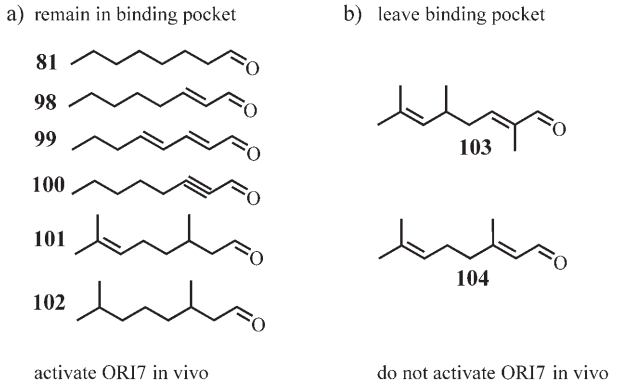

Figure 15. Results of dynamic modeling of ORI7.

5. Summary and Outlook

From all of the above examples, it is clear that even when the structure of an olfactory receptor is known it is far from certain that one could predict how well any novel potential ligand would bind to it. Facing an array of 350–400 receptors, the task would be even more difficult as a subtle change in structure might affect the binding of any one of the receptors which even a close analogue activates. In other words, the chances of correctly predicting the total pattern of receptor signaling for an odorant molecule are hundreds of times less than doing so for a pharmaceutical target. Furthermore, there are many levels of neurotransmission between the receptors and the cortex, where the signals from the receptor array are eventually interpreted as the phenomenon that we refer to as odor. At each level there are gates with opportunities for interaction between signals from different receptors and the possibility for either reduction or enhancement of individual signal components. All of this would have to be understood in order to know how the initial signal pattern would come together in the higher brain. A subtle change in signal intensity from one receptor type could have a disproportionately large effect on the overall interpretation in terms of odor character, threshold, and/or perceived intensity.

It would therefore seem that consistently accurate prediction of odors will not be possible for a very considerable time and not until a great amount of further research has been completed, the cost of which could not be borne by the flavor and fragrance industry.

In his review, Weyerstahl[23] outlined the objectives of structure–odor correlations as being 1) prediction of odors, 2) rational design of odorants, and 3) understanding the mechanism of olfaction. Since then, advances in the biosciences have greatly increased our understanding of the mechanism of olfaction but in a way that does not bode well for Weyerstahl's other two objectives. It would appear that our SAR tools will be refined and improved, although, for the foreseeable future, the prediction of odor will remain only statistical probabilities rather than certainties. There will be plenty of room for surprises and serendipity.

I would like to thank my colleagues Richard Butcher, Dr. Karen Jenner, Dr. Keith Perring, and Dr. Anton van der Weerdt for their help in preparing the manuscript.

Received: February 28, 2006

[1] S. Arctander, *Perfume and Flavor Chemicals*, S. Arctander, Montclair, New Jersey, **1969**, Monograph 2276.
[2] S. Arctander, *Perfume and Flavor Chemicals*, S. Arctander, Montclair, New Jersey, **1969**, Monograph 2279.
[3] P. C. Traas, H. Renes, H. Boelens (Naarden International), US 4,352,748, **1982**.
[4] A. Boix Camps, *Perfum. Flavor.* **2004**, *29*, 42–65.
[5] G. Ohloff, W. Giersch, W. Thommen, B. Willhalm, *Helv. Chim. Acta* **1983**, *66*, 1343–1354.
[6] C. S. Sell, *Seifen Öle Fette Wachse* **1986**, 112 (8), 267–270.
[7] T. Asada, Y. Ataka, J. Etsuno, H. Takase (Kao Corporation), JP 09151164, **1997**.

© 2006 Wiley-VCH Verlag GmbH & Co. KGaA, Weinheim

[8] A. Boix Camps, *Perfum. Flavor.* **1999**, *24*, 17 – 47.
[9] J. E. Amoore in *Molecular Basis of Odour*, Charles C. Thomas, Illinois, **1970**, Library of Congress Card No. 70–97521.
[10] P. Z. Bedoukian, *Perfumery Synthetics and Isolates*, D. van Nostrand, New York, **1951**, p. 43.
[11] H. Surburg, J. Panten, *Common Fragrance and Flavor Materials*, 5th ed., Wiley-VCH, Weinheim, **2006**.
[12] S. Arctander, *Perfume and Flavor Chemicals*, S. Arctander, Montclair, New Jersey, **1969**, Monograph 753.
[13] S. Arctander, *Perfume and Flavor Chemicals*, S. Arctander, Montclair, New Jersey, **1969**, Monograph 268.
[14] S. Arctander, *Perfume and Flavor Materials of Natural Origin*, S. Arctander, Elizabeth, New Jersey, **1960**.
[15] M. H. Klouwen, *Perfum. Essent. Oil Rec.* **1959**, 27 – 33.
[16] C. S. Sell, *Chem. Br.* **1997**, *3*, 39 – 42.
[17] K. J. Rossiter, *Chem. Rev.* **1996**, *96*, 3201 – 3240.
[18] M. Chastrette, J. Y. De Saint Laumer, *Eur. J. Med. Chem.* **1991**, *26*, 829 – 833.
[19] I. B. Bersuker, A. S. Dimoglo, M. Yu. Gorbachov, P. F. Vlad, M. Pesaro, *New J. Chem.* **1991**, *15*, 307 – 320.
[20] "The Measuring of Odour": N. Neuner-Jehle, F. Etzweiler in *Perfumes: Art, Science and Technology* (Eds.: P. M. Müller, D. Lamparsky), Elsevier, London, **1991**, pp. 153 – 212.
[21] P. Kraft, W. Eichenberger, *Eur. J. Org. Chem.* **2003**, 3735 – 3743.
[22] P. Kraft in *Chemistry and Technology of Flavors and Fragrances* (Ed.: D. J. Rowe), CRC, Boca Raton, **2005**, pp. 143 – 168.
[23] P. Weyerstahl, *J. Prakt. Chem.* **1994**, *336*, 95 – 109.
[24] S. Arctander, *Perfume and Flavor Chemicals*, S. Arctander, Montclair, New Jersey, **1969**, Monograph 2693.
[25] S Arctander, *Perfume and Flavor Chemicals*, S. Arctander, Montclair, New Jersey, **1969**, Monograph 440.
[26] "Synthesis of New Floral Fragrances Supported by Molecular Modelling": R. Pelzer, U. Harder, H. Krempel, H. Sommer, H. Surburg, P. Höver in *Recent Developments in Flavour and Fragrance Chemistry, Proceedings 3rd International H&R Symposium* (Eds.: R. Hopp, K. Mori), VCH, Weinheim, **1993**, pp. 29 – 67.
[27] S. Arctander, *Perfume and Flavor Chemicals*, S. Arctander, Montclair, New Jersey, **1969**, Monograph 437.
[28] A. Boix Camps, *Perfum. Flavor.* **2004**, *29*, 54 – 80.
[29] K. J. Rossiter (Quest International), US 6,313,087, **2001**.
[30] P. Haverkamp-Begemann, J. C. Koster, *Nature* **1964**, *202*, 552 – 553.
[31] S. K. Mukerji, H. L. Sharma, *Tetrahedron Lett.* **1966**, *7*, 2479 – 2481.
[32] W. Berends, L. M. van der Linde, *Perfum. Essent. Oil Rec.* **1967**, (June), 372 – 378.
[33] J. A. Bajgrowicz, K. Berg-Schultz, G. Brunner, *Bioorg. Med. Chem.* **2003**, *11*, 2931 – 2946.
[34] S. Arctander, *Perfume and Flavor Chemicals*, S. Arctander, Montclair, New Jersey, **1969**, Monograph 1803.
[35] S. Arctander, *Perfume and Flavor Chemicals*, S. Arctander, Montclair, New Jersey, **1969**, Monograph 160.
[36] S. Arctander, *Perfume and Flavor Chemicals*, S. Arctander, Montclair, New Jersey, **1969**, Monograph 2402.
[37] S. Arctander, *Perfume and Flavor Chemicals*, S. Arctander, Montclair, New Jersey, **1969**, Monograph 1426.
[38] W. Czeslaw, A. Zabra, *Perfum. Flavor.* **1983**, *8*, 39 – 47.
[39] R. E. Naipawer, W. M. Easter (Givaudan), US 4,052,341, **1977**.
[40] R. E. Naipawer (Givaudan), EP 203,528, **1986**.
[41] S. Arctander, *Perfume and Flavor Chemicals*, S. Arctander, Montclair, New Jersey, **1969**, Monograph 24.
[42] S. Arctander, *Perfume and Flavor Chemicals*, S. Arctander, Montclair, New Jersey, **1969**, Monograph 436.
[43] W. Sturm, *Parfuem. Kosmet.* **1974**, *55*, 351 – 355.
[44] S. Arctander, *Perfume and Flavor Chemicals*, S. Arctander, Montclair, New Jersey, **1969**, Monograph 2043.
[45] J. A. Bajgrowicz, I. Frank, G. Fráter, M Hennig, *Helv. Chim. Acta* **1998**, *81*, 1349 – 1358.
[46] C. S. Sell, *Chem. Biodiversity* **2004**, *1*, 1899 – 1920.
[47] D. Bartschat, S. Börner, A. Mosandl, J. W. Bats, *Z. Lebensm.-Unters.-Forsch. A* **1997**, *205*, 76 – 79.
[48] M. Masuda, S. Mihara, *Agric. Biol. Chem* **1989**, *53*, 3367 – 3368.
[49] J. A. Bajgrowicz, I. Frank, *Tetrahedron: Asymmetry* **2001**, *12*, 2049 – 2057.
[50] C. Fehr, J. Galindo, O. Etter, *Eur. J. Org. Chem.* **2004**, 1953 – 1957.
[51] E. Brenna, C. Fuganti, S. Serra, P. Kraft, *Eur. J. Org. Chem.* **2002**, 967 – 978.
[52] L. Buck, R. Axel, *Cell* **1991**, *65*, 175 – 187.
[53] B. Malnic, J. Hirono, T. Sato, L. B. Buck, *Cell* **1999**, *96*, 713 – 723.
[54] E. H. Polak, *J. Theor. Biol.* **1973**, *40*, 469 – 484.
[55] http://nobelprize.org/nobel prizes/medicine/.
[56] R. Axel, *Angew. Chem.* **2005**, *117*, 6264 – 6282; *Angew. Chem. Int. Ed.* **2005**, *44*, 6111 – 6127.
[57] L. B. Buck, *Angew. Chem.* **2005**, *117*, 6283 – 6296; *Angew. Chem. Int. Ed.* **2005**, *44*, 6128 – 6140.
[58] M. Spehr, G. Gisselmann, A. Poplawski, J. A. Riffell, C. H. Wetzel, R. K. Zimmer, H. Hatt, *Science* **2003**, *299*, 2054 – 2058.
[59] S. Arctander, *Perfume and Flavor Chemicals*, S. Arctander, Montclair, New Jersey, **1969**, Monograph 2470.
[60] R. C. Araneda, A. D. Kini, S. Firestein, *Nat. Neurosci.* **2000**, *3*, 1248 – 1255.
[61] G. Sanz, C. Schlegel, J.-C. Pernollet, L. Briand, *Chem. Senses* **2005**, *30*, 69 – 80.
[62] P. Hummel, N. Vaidehi, W. B. Floriano, S. E. Hall, W. A. Goddard III, *Protein Sci.* **2005**, *14*, 703 – 710.
[63] S. E. Hall, W. B. Floriano, N. Vaidehi, W. A. Goddard III, *Chem. Senses* **2004**, *29*, 595 – 616.
[64] W. B. Floriano, N. Vaidehi, W. A. Goddard III, *Chem. Senses* **2004**, *29*, 269 – 290.
[65] P. C. Lai, M. S. Singer, C. J. Crasto, *Chem. Senses* **2005**, *30*, 781 – 792.

© 2006 Wiley-VCH Verlag GmbH & Co. KGaA, Weinheim

H.-J. Himmel and M. Reiher

DOI: 10.1002/anie.200502892

Dinitrogen Activation

Intrinsic Dinitrogen Activation at Bare Metal Atoms

Hans-Jörg Himmel and Markus Reiher**

Keywords:
density functional calculations · gas-phase reactions · matrix isolation · nitrogen fixation · reaction mechanisms

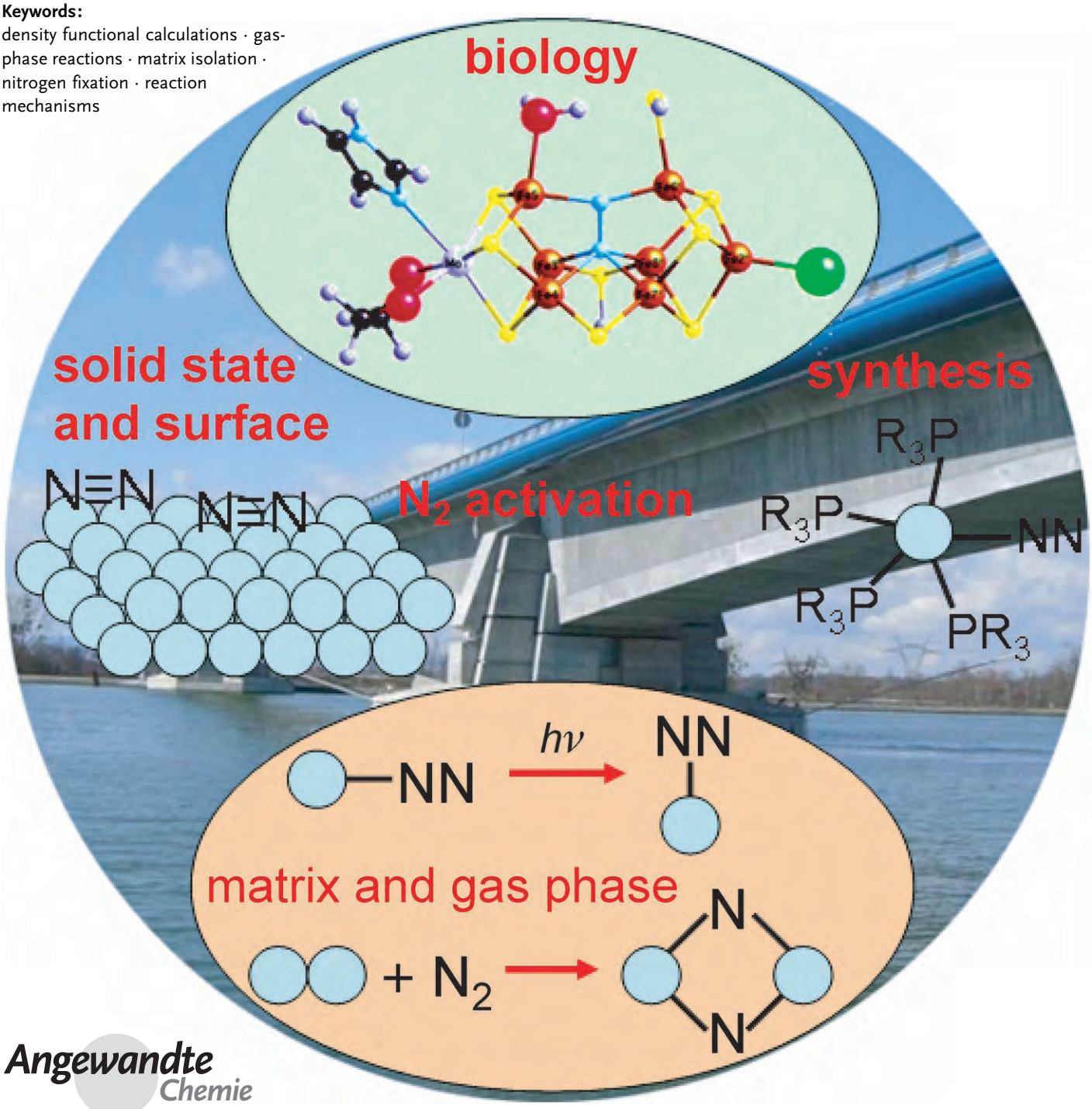

© 2006 Wiley-VCH Verlag GmbH & Co. KGaA, Weinheim

There is ongoing interest in metal complexes which bind dinitrogen and facilitate either its reduction or oxidation under mild conditions. In nature, the enzyme nitrogenase catalyzes this process, and dinitrogen fixation occurs under mild and ambient conditions at a metal–sulfur cluster in the center of the MoFe protein, but the mechanism of this process remains largely unknown. In the last few years, new important discoveries have been made in this field. In this review are discussed recent findings on the interaction of N_2 with metal atoms and metal-atom dimers from all groups of the periodic table as provided by gas-phase as well as matrix-isolation experiments. Intrinsic dinitrogen activation at such bare metal atoms is then related to corresponding processes at complexes, clusters, and surfaces.

From the Contents

1. Introduction 6265
2. Binding Modes 6267
3. Catalytic Dinitrogen Reduction under Mild Conditions 6267
4. Valence-Saturated Dinitrogen Complexes 6268
5. Dinitrogen Fixation at Bare Metal Atoms 6270
6. General Discussion and Analysis 6279
7. Conclusions and Future Perspectives 6284

1. Introduction

Activation of small molecules and in particular of dinitrogen remains a fundamental challenge to synthetic as well as theoretical chemistry. With a D_0 value of 941.7 kJ mol^{-1}, the N–N bond in N_2 is one of the strongest bonds (see Table 1). Impressive progress has been achieved in the field of dinitrogen fixation and activation in the last few years. However, this progress is often made accidentally rather than by rigorously planned approaches. Rationalization and theoretical understanding of dinitrogen activation is then provided only a posteriori once the experimental results are known. Since the discovery of the first dinitrogen complex $[Ru(NH_3)_5(N_2)]^{2+}$ in 1965,[1] a large number of dinitrogen complexes have been synthesized.[2] To obtain detailed information about the bonding properties and activation modes (and especially the differences in properties compared with corresponding isoelectronic CO complexes), N_2 complexes with metal atoms have been studied intensively in the past. In 1971, Turner and Burdett reported the first observation of nickel dinitrogen complexes $[Ni(N_2)_4]$ ($n = 1$–4) by using the matrix-isolation technique.[3] The discovery of dinitrogen complexes of the elements Cr and Pt followed only one year later.[4]

Table 1: Some properties of noncoordinated N_2.

electronic ground state	$^1\Sigma_g^+$
bond length r_e	109.768 pm
harmonic frequency ν(N–N)	2358.57 cm^{-1}
anharmonicity constant $\omega_e x_e$	14.324 cm^{-1}
valence force constant f	2239 N m^{-1}
dissociation energy D_0	941.7 kJ mol^{-1}
melting point	−210 °C
boiling point	−195.8 °C

Modern research in the field of dinitrogen activation is concentrated on the following four areas (Figure 1).

a) Evaluation of dinitrogen fixation and reduction in biological systems: High-resolution diffraction data of the metal cluster core inside nitrogenase have led to new biomimetic models for dinitrogen activation.
b) Solid-state and surface science: There is a great demand for new systems for catalytic dinitrogen reduction or oxidation under mild conditions at surfaces. Moreover, the

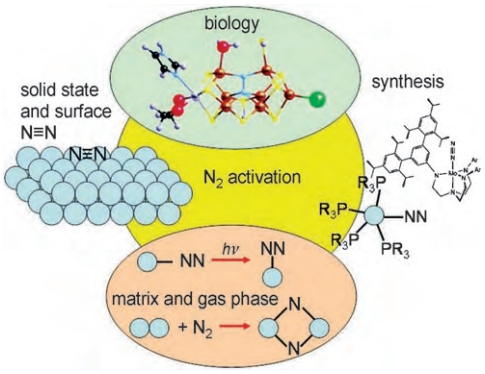

Figure 1. Research on N_2 activation by metals is concentrated on 1) evaluation of the mechanisms for activation in biological systems, 2) surface and solid-state chemistry, 3) synthesis of metal complexes, and 4) matrix and gas phase studies. The model of the center of nitrogenase in one of the steps leading to N_2 reduction is taken from reference [16h].

[*] Prof. Dr. H.-J. Himmel
Anorganisch-Chemisches Institut
Ruprecht-Karls-Universität Heidelberg
Im Neuenheimer Feld 270, 69120 Heidelberg (Germany)
Fax: (+49) 6221-54-5707
E-mail: hans-jorg.himmel@aci.uni-heidelberg.de
Prof. Dr. M. Reiher
Laboratorium für Physikalische Chemie
ETH Zürich, Hönggerberg
Wolfgang-Pauli-Strasse 10, 8093 Zürich (Switzerland)
Fax: (+41) 44-63-31594
E-mail: markus.reiher@phys.chem.ethz.ch

© 2006 Wiley-VCH Verlag GmbH & Co. KGaA, Weinheim

preparation of many industrially important nitrides is carried out in an N_2 atmosphere.

c) Synthesis of metal complexes in solution and reduction or oxidation of the N_2 ligand: Although several systems are now known, there is still a need to find and understand systems for reduction or oxidation under mild conditions, especially if these reactions are to be performed catalytically.

d) Matrix-isolation and gas-phase studies: These studies give important insight into the (generic and intrinsic) bonding properties and mechanisms of dinitrogen activation.

Unfortunately, the interaction between these four fields, which is essential for a more complete understanding of dinitrogen activation, is not always as good as it should be. Often, such interactions are restricted to a plain comparison of mechanisms at, for example, metal surfaces and FeMoco,[5,6] although general and transferable knowledge and concepts would be helpful. One of the intentions of this article is therefore to identify overlaps between the fields. For instance, the metal atom must effectively transfer electron density to the N_2 molecule to populate the π^* MOs of the molecule (if one argues from the standpoint of qualitative MO theory). Therefore, in the case of metal complexes in solution, phosphine coligands are often needed to build up the electron density on the metal center. However, some phosphines such as PF_3 can also act as competing π acceptors, and therefore it might be of even more importance to achieve a low formal oxidation state of the metal. For activation at surfaces, alkali or alkali earth metal atoms are often added. Hence an effective reagent needs to be electron-rich, such that preferably more than one valence electron occupies (or has easy access to) a high-energy orbital that furthermore has the right symmetry and energy to interact effectively with the π^* orbital of N_2. Table 2 summarizes some important differences between bare-metal-atom and ligand-bearing complexes of N_2.

In this review, structures and properties of dinitrogen complexes of bare main-group and transition elements will be discussed in detail. Although these systems seem simple at first glance, it will become evident that they are often difficult to characterize and that several electronic states with different structures exhibit very similar energies. These difficulties are less pronounced in transition-metal complexes with saturated valencies. Nonetheless dinitrogen activation by bare metal atoms may allow us to extract general conclusions for larger complexes and clusters with various (often mutually incompatible) ligand spheres. We will see that dinitrogen complexes of main-group elements, being generally only weakly bound, lend themselves predominantly to studies in the gas phase, while similar complexes of transition metals are more appropriately studied in matrix-isolation experiments. Electronic spectroscopy in the gas phase is often complicated for transition-metal complexes because of the high density of electronic states which precludes the resolution of vibrational or rotational structure (see, for example, the complex $[CrN_2]^+$ discussed in Section 5.2.4). It should be pointed out that the scope of this article makes it impossible to summarize all the work that has been carried out in this field. The discussion is thus limited to a relatively small number of selected but representative systems.

Table 2: Qualitative description of differences between the reactions $M + N_2$ and $L_nM + N_2$ (L = neutral ligand).

$M + N_2$	$L_nM + N_2$
• M often has electrons in the valence s orbital (for example, Ti: $3d^24s^2$). Therefore there is a significant degree of σ repulsion and a reduced possibility for π back-donation. Photoactivation might enhance the reactivity.	• Electron configuration on the metal changes. The s orbitals are unoccupied, thus leading to less σ repulsion and more possibility for π back-donation.
• N_2 activation should increase with higher number of electrons in valence d orbitals. However, the orbital energies decrease from left to right in the periodic table.	• Electron-donating ligands increase the electron density on the metal and therefore the possibility for π back-donation.
• No ligand–ligand repulsion.	• Steric effects and ligand–ligand interactions might play a significant role. Ligand reactivity in general is an important issue.

Hans-Jörg Himmel obtained his Ph.D. in Bochum under the supervision of Prof. C. Wöll at the Institute of Physical Chemistry. From 1998 to 2000 he worked with Prof. T. Downs at the University of Oxford (D.Phil. 2000). He then moved to the University of Karlsruhe, Germany, and completed his habilitation in the group of Prof. H. Schnöckel in April 2004. In October 2005 he returned to Oxford as a Lecturer at Queen's College. Meanwhile he has moved to the University of Heidelberg, Germany, to become Full Professor in Inorganic Chemistry starting from October 2006. He was awarded the ADUC prize in 2003.

Markus Reiher is Associate Professor for Theoretical Chemistry at the Laboratory for Physical Chemistry at ETH Zürich. He earned his Ph.D. in theoretical chemistry from the University of Bielefeld with Prof. J. Hinze in 1998 and completed his habilitation at the University of Erlangen-Nürnberg with Professor Dr. B. A. Hess in 2002. He was a Privatdozent at the University of Bonn (2003–2005) and then accepted a position as Professor for Physical Chemistry at the University of Jena in April 2005. His awards include the ADUC prize (2003), the Emmy Noether Habilitation Award of the University of Erlangen-Nürnberg, and the Dozentenstipendium of the Fonds der Chemischen Industrie.

 © 2006 Wiley-VCH Verlag GmbH & Co. KGaA, Weinheim

2. Binding Modes

Before we start with a summary of some of the most important findings in the fields of complexes synthesized in solution and generated with the help of the matrix-isolation techniques, some comments should be made on the possible N_2 binding modes. In mononuclear complexes, the N_2 unit is generally end-on bonded. However, the energy difference to an excited state featuring side-on coordinated N_2 can be small (Scheme 1).

Matrix-isolation experiments and quantum chemical calculations confirmed that for some systems it is possible to photolytically induce a change in the coordination mode from end-on to side-on. Just to give one recent example, the end-on bonded, matrix-isolated complex [OTiNN] undergoes, when photolyzed with light of wavelength $400 < \lambda < 580$ nm, photoconversion into the side-on bonded complex $[OTi(N_2)]$.[7] More examples will be mentioned below in Section 5.2,

Scheme 1. Possible binding modes in mononuclear N_2 complexes (no differentiation is made between single, double, and triple bonds).

which deals with $[MN_2]$ species. Meanwhile the first *crystallographic* evidence for a mononuclear, side-on bonded complex has been reported.[8] On irradiation of $[Os(NH_3)_5(N_2)](PF_6)_2$ with light of wavelength $330 < \lambda < 460$ nm at 100 K, the N_2 ligand changes from the end-on to the side-on binding mode, which is, according to density functional theory (DFT) calculations, about 0.8 eV higher in energy.

End-on to side-on conversion can also be achieved by thermal means. Thus a side-on bonded N_2 ligand has been proposed as the intermediate of the end-to-end rotation of the coordinated η^1-N_2 ligand in $[Cp^*Re(CO)_2(N_2)]$.[9] The only experimentally verified example of a species which is side-on bonded in its *electronic ground state* is $[LiN_2]$, which seems to form a C_{2v}-symmetric ion pair (see discussion in Section 6.2). Binuclear complexes can bear either a bridging μ,η^1,η^1-N_2 ligand or a side-on bonded μ,η^2,η^2-N_2 unit (either planar or nonplanar). Moreover, there are some rare examples of μ,η^1,η^2 coordination (Scheme 2). We will discuss possible models for understanding some of these binding modes later in this review.

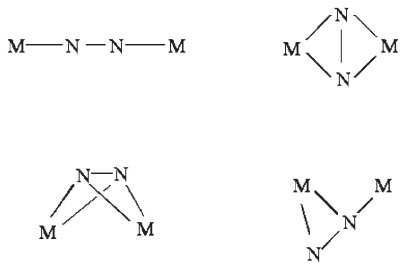

Scheme 2. Possible binding modes in binuclear N_2 complexes (no differentiation is made between single, double, and triple bonds).

It should be pointed out already here that all attempts to understand the bonding by use of simple molecular orbital (MO) models (modified Dewar–Chatt–Duncanson models)[10] were only partially successful, although they were helpful for understanding some structural details. For example, the conformation of the two terminal N_2 units in the binuclear zirconium complex $[\{(\eta^5\text{-}C_5Me_5)_2Zr(\eta^1\text{-}N_2)\}_2(\mu_2,\eta^1,\eta^1\text{-}N_2)]$[11] can easily be explained by interactions of the π orbitals of the bridging N_2 ligand with suitable orbitals of the zirconocene fragments. However, it will be shown below that for other cases the qualitative MO picture fails (Section 6).

There are also some examples that involve more than two metal atoms (Scheme 3). In the titanium complex $[\{(C_{10}H_8)Cp_2Ti_2\}\{(C_5H_4)Cp_3Ti_2\}(\mu_3\text{-}N_2)]$, the N_2 unit has an N–N bond length of 130(1) pm and exists as a μ_3-η^1,η^1,η^2 ligand.[12] In $[(LAu)_6(N_2)](BF_4)_2$ (L = PPh_2iPr, for example) an N_2 bridge connects two Au_3 clusters.[13]

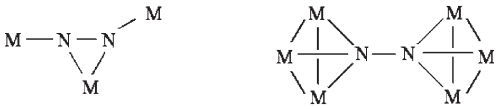

Scheme 3. Possible binding modes in N_2 complexes involving more than two metal atoms (no differentiation is made between single, double, and triple bonds).

3. Catalytic Dinitrogen Reduction under Mild Conditions

Before we turn to the discussion of dinitrogen fixation by bare metal atoms comprising all groups of the periodic table, we shall briefly review the present state of *catalytic* dinitrogen reduction. The achievement of this reaction under ambient conditions by using mild reductants and acids represents the most ambitious challenge and ultimate goal of research in dinitrogen fixation. Despite intense investigation, the mechanism of biological N_2 fixation remains still largely unknown. It is catalyzed by the enzyme nitrogenase, which consists of a two-component metalloprotein, the Fe protein and the MoFe protein. A recent crystallographic analysis with a high resolution of 1.16 Å has shown new details of the active center of the MoFe protein, that is, of the FeMo cofactor.[14] The data indicate the presence of a central atom X (which can be N, O, or C)[15] which is surrounded by six Fe atoms in a trigonal-prismatic arrangement, with average Fe–X distances of (200 ± 5) pm. The Fe atoms are bound to S atoms with N-Fe-S bond angles of $(102 \pm 2)°$. Thus the coordination number is four for each of the Fe atoms (previously a coordination number of three was assumed). The six Fe atoms are joined through bridging sulfides to two metal atoms (either Mo, V, or Fe).

Because of the size and complexity of the FeMo cofactor only quantum chemical calculations that are based on DFT are feasible. Consequently, several groups have published such investigations, but a consensus on the mechanism has not been reached.[16] This dilemma is a result of the limited accuracy of contemporary DFT methods. While most of the

© 2006 Wiley-VCH Verlag GmbH & Co. KGaA, Weinheim

recent calculations assume that N_2 is bound by one or more Fe atoms, the Mo atom cannot be ruled out as a potential binding site. Also the subsequent reduction steps are still a matter of debate.

All quantum chemical calculations are also necessarily based on model assumptions and simplifications with respect to the geometric structure, spin, and charge states of the active center. For this reason, studies on small generic systems like dinitrogen complexes of bare metal atoms provide a valuable link to assess the accuracy of the quantum chemical methods (see also a very brief survey on the pros and cons of these theoretical methods in the appendix).

Despite these difficulties interesting findings on possibly important elementary reaction steps were obtained for many different FeMoco models. For example, in one of the earlier efforts, a model cluster of the overall formula $[(HS)(H_2S)Fe\text{-}S\text{-}Fe(SH)(SH_2)]$ was studied.[17] The binding energy of N_2 to this cluster amounts to not more than 3.8 kJ mol^{-1}, and the N_2 ligand is end-on coordinated to only one of the two Fe atoms according to B3LYP/6311 + G(2d,2p) calculations. However, addition of a hydrogen atom to the bridging sulfur atom leads to a $[(HS)(H_2S)Fe\text{-}SH\text{-}Fe(SH)(SH_2)]$ complex and reduces the $Fe_2^{II,II}$ system to $Fe_2^{I,II}$, and the N_2 ligand thus coordinates to both Fe atoms. As a consequence, the binding energy increases to 133 kJ mol^{-1}. The subsequent addition of H atoms to the bridging N_2 unit has been analyzed and found to be exothermic.

The first synthetic complex that could catalytically reduce dinitrogen under mild conditions and thus perform the job of nitrogenase was published only recently. Yandulov and Schrock reported the molybdenum trisamidoamine complex **1** as a catalyst for the reduction of dinitrogen to ammonia at room temperature and a pressure of one atmosphere.[18] Here the bulky ligands prevent the formation of what would presumably be a relatively stable and unreactive bimetallic complex containing a Mo–N=N–Mo unit. Schrock and collaborators have also characterized several potential intermediates.

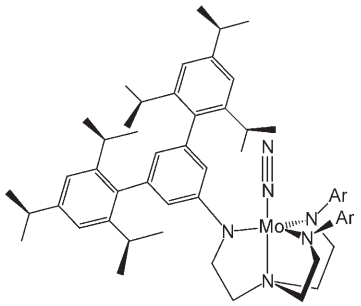

1
Ar=3,5-(2,4,6-*i*Pr$_3$C$_6$H$_2$)$_2$C$_6$H$_3$

Several factors make it difficult to understand the dinitrogen reduction at FeMoco. First, theoretical predictions based on very similar quantum chemical techniques disagree in important points on the potential biological mechanism. Moreover, experimental data are not available with sufficient space and time resolution. Thus, it is advisable to understand dinitrogen fixation for smaller complexes with various metal atoms—and for bare metal atoms in the limiting case. Consequently, Schrock's trisamidoamine molybdenum complex was the focus of theoretical studies. Essential steps of the reduction process at Schrock's complex have been studied with DFT methods for simplified models[19] as well as for the experimentally known system.[20] Interestingly, it was found that the simplified models do not reproduce all reaction energies of essential steps (compare the supporting information of reference [20b]).

4. Valence-Saturated Dinitrogen Complexes

A number of transition-metal complexes have been synthesized in the last four decades and analyzed with respect to their capacity to bind dinitrogen.[21] These complexes can be grouped according to the degree of dinitrogen activation.[22] According to the Dewar–Chatt–Duncanson model,[10] the metal should have a large number of electrons in the valence d orbitals which can contribute to the π back-bonding. On the other hand, the energy of the d orbitals generally decreases from left to right in the periodic table. This decrease could lead to a reduced interaction between the orbitals at the N_2 ligand and a late transition metal. Generally, complexes of transition metals in the middle of one period are more efficient in dinitrogen activation than those of very early or late transition metals. Presumably, the balance between the two opposing effects (electron density at the metal and orbital energy of the valence d orbital) is best achieved for these metals. Thus, according to DFT calculations, the binding energy decreases for model complexes in the series $[V(N_2)_2(PH_3)_4]^- > [Cr(N_2)_2(PH_3)_4] > [Mn(H)(N_2)(PH_3)_4] > [Fe(N_2)(PH_3)_4] > [FeCl(N_2)(PH_3)_4]$.[23] However, there can be exceptions in the case of anionic complexes, such as *trans*-$[Na(thf)][V(N_2)_2(dppe)_2]$ (dppe = $Ph_2PCH_2CH_2PPh_2$),[24] in which there is a significant degree of interaction between the N_2 unit and the counterion. Thus, polymers with linear V–N≡N···Na units arranged in chains are formed in the solid state. These complexes are surprisingly labile and lose N_2 under slightly reduced pressure. About 25% of the coordinated N_2 can be converted to NH_4^+ (plus a small amount of hydrazine) with an appropriate acid.

There are already numerous reviews on valence-saturated dinitrogen complexes,[2,25] and here we shall only mention some selected examples of dinitrogen activation by metal complexes for the purposes of comparison and to highlight the interactions between the above-mentioned fields and the interest in specific metals.

4.1. Main-Group Elements

Of the main-group elements, Li is exceptional in that it slowly reacts with N_2 already at room temperature, leading finally to the nitride Li_3N. However, this reaction is hardly an activation of the N_2 molecule in the desired sense, since the

 © 2006 Wiley-VCH Verlag GmbH & Co. KGaA, Weinheim

reaction is facilitated by the extraordinarily strong reducing power of Li and the large lattice energy of the ionic product Li_3N. As such, the N atoms in the product are strongly bound and are thus not accessible for further reactions. That some chemistry is nevertheless possible has recently been shown by the discovery that Li_3N can be used for hydrogen storage, and the equilibrium in Equation (1) was suggested.[26]

$$Li_3N + 2\,H_2 \rightleftharpoons Li_2NH + LiH + H_2 \rightleftharpoons LiNH_2 + 2\,LiH \qquad (1)$$

Elemental Li is used in several systems to activate dinitrogen. For example, it has been found that in a solution of TiX_4 (X = Cl, O*i*Pr) in THF, when stirred with an excess of Me_3SiCl and Li for 24 hours in dry air and subsequently hydrolyzed with 10% aqueous HCl and neutralized with a K_2CO_3 solution, PhCOCl is converted into $PhCONH_2$ in high yields.[27] The authors suggest that an intermediate complex of the form $[TiX_m\{N(SiMe_3)_n\}_p]$ binds the amide that is formed after cleavage of the N_2 bond by the Li metal. A very rare example of a species featuring a Li_2 dication that contains a side-on bonded N_2 unit (with a very short bond length of 106(1) pm) is $[Cp_2Zr(\mu\text{-}PPh)]_2[\{(thf)_3Li\}_2(\mu\text{-}N_2)]$.[28] The question then arises: to what extent is a single Li atom or small Li cluster able to activate N_2?

4.2. Transition Elements

Recently, a series of titanium sandwich complexes with activated dinitrogen ligands have been structurally characterized.[29] Two N_2 units bind to the Ti^{II} center in complexes of the form $[(C_5Me_4R)_2Ti]$ (R = CMe_3, $SiMe_3$, $CHMe_2$, or CH_3). The temperature up to which these complexes are stable increases as a function of R in the order $CMe_3 < SiMe_3 < CHMe_2 < CH_3$. The N–N stretching modes for all of these complexes were detected at similar wave numbers (R = CMe_3: 2090 and 1982 cm^{-1}, R = $SiMe_3$: 2098 and 2002 cm^{-1}, R = $CHMe_2$: 2090 and 1986 cm^{-1}).

There are also several examples of binuclear complexes with a bridging N_2 unit. Reduction of $[\{(Me_2N)C(N\textit{i}Pr)_2\}_2TiCl_2]$, which can be prepared from $[Ti(NMe_2)_2Cl_2]$ and *i*PrNCN*i*Pr in diethyl ether, with Mg powder in THF in an atmosphere of dinitrogen yielded the dinuclear complex $[\{[Me_2NC(N\textit{i}Pr)_2]_2Ti\}_2(\mu_2\text{-}\eta^1,\eta^1\text{-}N_2)]$.[30] Dinuclear complexes with two bridging (and side-on bonded) N_2 units are also known. One such complex is the anion of the salt $[Li(tmeda)_2]^+[\{[(Me_3Si)_2N]_2Ti\}_2(\mu_2\text{-}\eta^2,\eta^2\text{-}N_2)_2]^-$, which can be obtained in the form of paramagnetic, deep-purple/black crystals as one of the products of the reaction of *trans*-$[(tmeda)_2TiCl_2]$ with $(Me_3Si)_2NLi$ and N_2.[31] The Ti–N and N–N bond lengths were measured to be 223.6/229.0 and 137.9(2.1) pm, respectively.

Similarly to the situation for the pair Fe/Ru, complexes of the second-row element Zr might be even more interesting for N_2 activation than Ti. Zirconium complexes are in fact known to bind dinitrogen molecules to give complexes with substantially weakened N–N bonds. An example is the dinuclear Zr complex $[(p_2n_2)Zr(\mu\text{-}\eta^2\text{:}\eta^2\text{-}N_2)Zr(p_2n_2)]$ (p_2n_2 = $PhP(CH_2SiMe_2NSiMe_2CH_2)_2PPh$), which reacts with dihydrogen at pressures of 1–4 bar to give $[(p_2n_2)Zr(\mu\text{-}\eta^2\text{-}N_2H)(\mu\text{-}H)Zr(p_2n_2)]$.[32] The bonding properties within the planar Zr_2N_2 core of this dinitrogen complex (with an N–N bond length of 143 pm) have been analyzed in detail by applying resonance Raman, IR, and UV/Vis spectroscopies.[33] Recently, the complex $[\{(\eta^5\text{-}C_5Me_4H)_2Zr\}_2(\mu\text{-}\eta^2,\eta^2\text{-}N_2)]$ (**2**) was synthesized by reduction of $[(\eta^5\text{-}C_5Me_4H)_2ZrCl_2]$[34] with sodium amalgam under one atmosphere of N_2.[35] This complex was shown to react immediately at 22 °C with H_2 to give the complex $[\{(\eta^5\text{-}C_5Me_4H)_2ZrH\}_2\{\mu_2\text{-}\eta^2,\eta^2\text{-}N_2H_2\}]$ (**3**).[35,36] It will be proposed in Section 5.2.2 that small ligand-free Ti clusters might be very efficient in weakening the bond in N_2. The dimer Ti_2 reacts with N_2 to give a $[Ti_2N_2]$ molecule which features two nitrido bridges. These findings pose the question of whether the Group 4 metal atoms can activate N_2 to some extent.

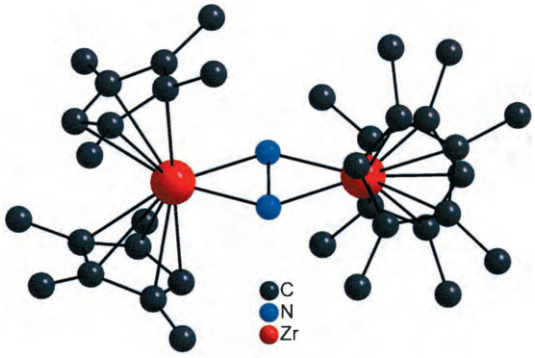

2

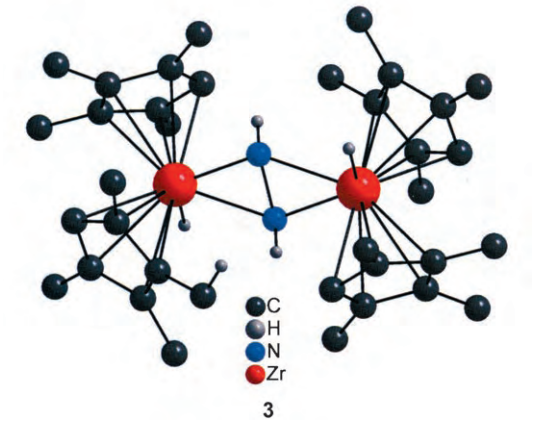

3

Several vanadium complexes of N_2 have been reported in the literature ($[Na(thf)][V(N_2)_2(dppe)_2]$ was mentioned previously). Dinuclear complexes of V^{II} and V^{III} have also been shown to bind dinitrogen. Examples include tetracoordinated vanadium atoms (for example, $[Na(diglyme)_2]^+[Mes_3V\text{-}N_2\text{-}VMes_3(\mu\text{-}Na)]^-$ with V^{II} centers or $[Na(diglyme)_2]^+[Mes_3V\text{-}N_2\text{-}VMes_3]^-$ with V^{II} and V^{III}; Mes = 2,4,6-$(CH_3)_3C_6H_2$; diglyme = $CH_3OCH_2CH_2OCH_2CH_2OCH_3$) and hexacoordinated vanadium atoms (for example, $[\{[o\text{-}(Me_2NCH_2)C_6H_4]_2V(py)\}_2(\mu\text{-}N_2)]$ with V^{II} atoms; py = pyridine).[37] The binding in model tetra- and hexacoordinated

© 2006 Wiley-VCH Verlag GmbH & Co. KGaA, Weinheim

dinuclear V^{II} and V^{III} complexes has been analyzed by quantum chemical calculations (of the simple Hartree–Fock (HF) type but also within the configuration interaction (CI) model).[38] The dinuclear vanadium complex [{RN-$(CH_2CH_2NR)_2V(\mu\text{-Cl})\}_2$] ($R = SiMe_3$) is capable of cleaving the N_2 bond to form a bisnitrido complex [{RN-$(CH_2CH_2NR)_2V(\mu\text{-N})\}_2$].[39] The Ta^{IV} tetrahydride [{(npn)Ta}$_2(\mu\text{-H})_4$](npn=PhP$(CH_2SiMe_2NPh)_2$) has been shown to react with N_2 with loss of H_2 to give the dinitrogen complex [{(npn)Ta$(\mu\text{-H})\}_2(\mu\text{-}\eta^1{:}\eta^2\text{-}N_2)$].[40] In this complex, the N_2 ligand adopts a side-on and end-on dinuclear binding mode (compare Scheme 2).

Several Mo and W complexes are well-known to bind dinitrogen.[41] One of the first molybdenum N_2 complexes to be discovered was *trans*-[Mo$(N_2)_2$(dppe)$_2$].[42] H_2 was found to displace the ligating N_2 in complexes of this kind.[43] The ligating N_2 can be transformed into NH_3 or hydrazine by treatment with inorganic acids such as H_2SO_4 and HCl (if no bidentate phosphine ligand is present). In more recent research, it has been shown that *cis*-[W$(N_2)_2$(PMe$_2$Ph)$_4$] reacts with [RuCl$(\mu\text{-H}_2)$(dppe)$_2$]X (X = PF_6, BF_4, OTf, BPh_4), which is in equilibrium with [RuCl(dppe)$_2$]X and H_2, to give NH_3, [Ru(H)Cl(dppe)$_2$], and other products.[44] With the triamidoamine molybdenum complex **1**, the first synthetic complex was found for the catalytic reduction of N_2 to NH_3 under mild conditions. This is remarkable since the mononuclear Mo complex is able to accommodate the π-accepting dinitrogen ligand as well as the σ-donating ammonia ligand. These results have again raised the question of whether only the Mo atom (instead of the seven Fe atoms) in nitrogenase is involved in N_2 binding.[45]

The N_2 ligands in Fe^{II} complexes have been shown to be relatively weakly bound. The Fe–N_2 bond in [FeCl(N_2)-(depe)$_2$]BPh_4 (depe = 1,2-bis(diethylphosphanyl)ethane) is thermally labile at 300 K.[46] UV/Vis irradiation also leads to the release of N_2. The ΔG^0 value for complex formation was calculated to amount to not more than 20 kJ mol^{-1}.[47] Interestingly, the complex formation represents a spin-forbidden reaction, since [FeCl(depe)$_2$]$^+$ exhibits a triplet and [FeCl(N_2)(depe)$_2$]$^+$ a singlet electronic ground state.[48] This change in spin multiplicity appears to be a general feature of iron complexes as it has also been observed for thiolate and thioether complexes of iron.[49]

Since binding of dinitrogen is more difficult for iron than for its higher homologue ruthenium, mono- and dinuclear ruthenium N_2 complexes have also been the focus of current research.[50] Ruthenium N_2 complexes generally have more strongly bound N_2 ligands than their Fe homologues. Consequently, dinitrogen often binds only to the Ru center and not to the Fe center in a sphere of sulfur ligands, as present in the biological system. Coordination of dinitrogen is often the crucial step, and most of these Sellmann-type complexes can also bind N_2H_2 and N_2H_4. This finding is important since the N_2 ligand in a biological complex is likely to be reduced by coupled 2 H$^+$/2 e$^-$ reduction steps via diazene and hydrazine species to ammonia.[51]

Despite the comparatively unsuccessful attempts on dinitrogen fixation and activation on well-defined Fe complexes, N_2 adsorption on various Fe surfaces has been studied in depth, and there are not many heterogeneous catalytic reactions that are understood as well as the Haber–Bosch process. Hence it has been shown that dissociation of dinitrogen is the rate-limiting step in the industrial production of NH_3 over alkali-promoted Fe catalysts. The adsorption of N_2 on an Fe(111) surface has been studied, for example, by IR measurements, and a band at 1550 cm^{-1} was assigned to π-bonded N_2 units which are likely to be intermediates in the catalytic dissociation of N_2.[52] Side-on bonding of dinitrogen to Fe surfaces has been modelled, for example, by multi-configuration self-consistent field CASSCF calculations.[53] In a more recent study, the role of defects in N_2 dissociation on Fe(110) and Fe/Ru(0001) surfaces has been analyzed.[54] Not surprisingly, it emerges that defects are of importance for the dissociation to take place. Apparently, the fixation of dinitrogen at an Fe surface is stronger than fixation by a single iron atom in a chelate ligand environment. Questions arise about the extent to which the binding energy of end-on coordinated dinitrogen to Fe complexes can be increased and in the end about whether dinitrogen chemistry can better be facilitated by di- or multinuclear Fe complexes.

As already mentioned, a dinitrogen ligand bridges two gold clusters in the compound [(LAu)$_6(N_2)$][BF_4]$_2$ (for example, with L = Ph$_2$*i*Pr; Scheme 3).[13] The N–N bond length in this complex measures 147.5(1.4) pm and is thus close to the value expected for a N–N single bond (in hydrazine, the N–N bond length amounts to 145 pm). The complex can be reduced to obtain NH_3 or mixtures of NH_3 and N_2H_4.

The fact that complexes of actinides have also to be considered is impressively highlighted by the Th complex [{[2-*t*Bu-4-Me$C_6H_2O)_2CH_2$]$_2$Th(dme)}(μ-Cl){K(dme)$_2$}] (dme = dimethoxyethane), which has been shown to react with $KC_{10}H_8$ and dinitrogen to give the complex [{(2-*t*Bu-4-Me$C_6H_2O)_2CH_2\}_2$Th(dme)(NH_2)]$^-$.[55] The first example of an f-element complex in which a formally neutral N_2 ligand is bound end-on is the monometallic uranium complex [$(C_5Me_5)_3U(\eta^1\text{-}N_2)$].[56] However, for the sake of brevity this review does not consider actinides in any further detail.

5. Dinitrogen Fixation at Bare Metal Atoms

In order to present an overview of dinitrogen coordination and activation by generic metal fragments of all groups of the periodic table the discussion should highlight general principles as observed in experimental and theoretical data, which can then be extrapolated to more involved cases with complicated ligand structures and environments. An attempt is made to compare results obtained for different dinitrogen complexes. Although many complexes have also been investigated with quantum chemical methods, most results are hardly comparable because of the various degrees of approximations and methods employed (compare also the comments given in the appendix). Thus, the individual results can be affected by limitations and incapabilities of the quantum chemical methods employed. For this reason, we discuss the theoretical studies from the literature in light of DFT (B3LYP/TZVPP) calculations especially carried out for this

 © 2006 Wiley-VCH Verlag GmbH & Co. KGaA, Weinheim

review in order to provide a homogeneous theoretical basis for the comparisons made.

Since intrinsic mechanisms of dinitrogen coordination and activation are established for most simple model compounds, namely the N_2 complexes of bare metal atoms, we shall collect and review experimental as well as supporting theoretical data on these systems in the following sections. This will allow us to present a very detailed homogeneous overview on dinitrogen activation by elements of the whole periodic table and in microscopic detail. The wealth of unique data is presented in Sections 5.1 and 5.2, and in Tables 2 and 3 are collected some essential results.

5.1. Examples of N_2 Complexes of Bare Main-Group Atoms

5.1.1. Hydrogen

The HN_2 species can be regarded as the ultimate unactivated $[MN_2]$ reference complex owing to the simple electronic structure of the H atom. According to quantum chemical calculations, the dissociation reaction of HN_2, with a bent structure and $^2A'$ symmetry, is unstable with respect to dissociation into H atoms and N_2.[57] The energy of HN_2 (including zero-point vibrational-energy (ZPVE) corrections) is about 35 kJ mol^{-1} higher than the total energy of H atoms and N_2. However, dissociation is opposed by a small but

Table 3: Some important findings for neutral main-group and transition-metal dinitrogen complexes [MNN] from experimental studies or quantum chemical calculations.

M	Important findings	Ref.	M	Important findings	Ref.
H	Calculated to exhibit an end-on, but bent structure with a $^2A'$ electronic ground state. Unstable towards decomposition into N_2 and H.	[57]	Sc	$^4\Sigma^-$ electronic ground state according to quantum chemical calculations. Observed in matrix experiments.	[95]
Li	Experimental data suggest side-on bonded structure with almost purely ionic bonding.	[63]	Ti	$^5\Delta$ electronic ground state according to calculations. Weakly bound complex observed in matrix experiments only after photoactivation of the Ti atoms.	[98]
Na	Calculated to be linear ($^2\Sigma^+$ electronic ground state). The side-on bonded complex is, however, very similar in energy.	[55]	V	$^6\Sigma^+$ electronic ground state according to calculations.	[109]
Al	Experimentally derived Al–N_2 bond energy of 5.6 kJ mol^{-1}.	[76]	Cr	Bent structure with a $^5A'$ electronic ground state according to calculations.	[109]
Ga	Ga–N_2 bond energy of about 19 kJ mol^{-1} derived from experimental (resonance Raman) and theoretical data.	[77]	Mn	$^6\Pi$ electronic ground state according to calculations.	[109]
In	Zero-field ionization-threshold measurements available, experimentally determined In–N_2 bond energy of 18.2 kJ mol^{-1}.	[82]	Fe	$^3\Sigma^-$ electronic ground state. Observed in matrix-isolation studies. $^5\Sigma$ state calculated to be slightly higher in energy.	[118]
C	Experimental EPR data suggest $^3\Sigma^-$ electronic ground state. The N–N and the C–N bonds both are double bonds. CNN is less stable than NCN.	[83, 84]	Co	$^2\Delta$ electronic ground state. Observed in matrix-isolation studies.	[121]
Si	Calculated to be an end-on bonded, linear complex. EPR data suggest a $^3\Sigma^-$ electronic ground state.	[89–91]	Ni	Linear, end-on bonded complex with a $^1\Sigma^+$ electronic ground state. The force constant f(N–N) = 1800 N m^{-1} was determined from experimental matrix-isolation data.	[128]
			Pd	Linear, end-on bonded complex with $^1\Sigma^+$ electronic ground state. In Ar matrices, the presence of small quantities of the molecule in the $^3\Sigma^+$ state was suggested on the basis of the experimentally derived absorption spectra.	[137, 138]
			Pt	$^1\Sigma^+$ electronic ground state calculated.	[138]
			Cu	Calculated to be bent ($^2A'$ electronic ground state).	[142]
			Hg	Information about two excited electronic states derived from LIF spectra. Emission spectra of the $[HgN_2]^*$ exciplex reported for the matrix-isolated molecule.	[143, 144]

© 2006 Wiley-VCH Verlag GmbH & Co. KGaA, Weinheim

significant barrier. The lack of a signal for HN_2 in experiments in which a beam of HN_2^+ was neutralized by electron transfer from an alkali metal indicates that the molecule has a lifetime shorter than 0.5 μs.[58] In calculations analyzing the one-dimensional tunneling effects, the lifetime of the lowest vibrational level was estimated to lie between 8.8×10^{-11} and 5.8×10^{-9} s.[59] In contrast to neutral HN_2, the cation HN_2^+ is stable. Interest in this species has been spurred by its identification (through microwave emission lines in the radioastronomical spectrum) as one of the constituents of the interstellar media.[60] Details of the geometry and vibrational properties of this linear molecule have been explored experimentally by high-resolution IR laser spectroscopy.[61] The experimental N–N bond length is 109.3 pm and the H–N bond length is 103.4 pm. In its electronic ground state, the molecule can be described approximately as H^+ plus the ground $^1\Sigma_g^+$ state of N_2, thus resulting in a $^1\Sigma^+$ potential-energy surface. Hence, this species is in a sense more important as the generic molecule produced after protonation of (activated) N_2 rather than as an activation of N_2 by H^+. Fundamentals of HN_2^+, which can be described as the H–N_2 and the HN–N stretching modes, were observed at 3234 and 2258 cm^{-1}.[62] The bending mode has been calculated to occur at 690 cm^{-1}.

5.1.2. Group 1

Studies of the reaction of thermally evaporated, neutral Li atoms with N_2 in N_2 matrices have given evidence for the formation of $[LiN_2]$ and $[Li_2N_4]$, the latter containing two equivalent N_2 units.[63] The data suggest a more or less ionic $[Li^+N_2^-]$ formulation for the 1:1 complex. It was also found that small quantities of C_2H_4 catalyze the formation of $[LiN_2]$ in an Ar matrix.[64] The experimental data indicate side-on binding of N_2^- to Li^+. On the evidence of quantum chemical calculations, Li^+ forms a linear complex with neutral N_2.[65] The D_e value of this complex amounts to about 53 kJ mol^{-1}. From total-cross-section measurements of Li^+ ions scattered by N_2, a value of about 31 kJ mol^{-1} was estimated for the well depth of the spherically symmetric component of $[LiN_2]^+$.[66]

Recently, the neutral $[NaN_2]$ species was studied theoretically within the CCSD(T)-coupled cluster model.[67] According to these calculations, the binding energy amounts to not more than 0.3 kJ mol^{-1}. The complex is believed to exhibit a linear minimum-energy structure, although a saddle point for a T-shaped structure is only 0.09 kJ mol^{-1} higher in energy. There is also experimental evidence for an interaction between Na atoms and N_2. The optical excitation of the collision pair $[NaN_2]$ has been measured,[68] and the data revealed differences of electronic structures between the $[NaN_2]$ and $[Na(C_2H_2)]$ collision complexes. The cationic complex $[NaN_2]^+$ has been studied experimentally by several groups.[69] The heat of association of one N_2 unit with Na^+ was estimated to be −33.5 kJ mol^{-1}. Addition of a second N_2 unit is accompanied by a significantly smaller enthalpy change of −22.2 kJ mol^{-1}. According to CCSD(T) calculations, the dissociation energy of $[NaN_2]^+$ amounts to 33.1 kJ mol^{-1},[70] a value in excellent agreement with the experimental one. This shows that, as anticipated, the interaction with N_2 is much stronger for the Na^+ cation than for the neutral Na atom, as a positively charged metal atom can better polarize the N_2 molecule than a neutral one. Also, the bond between Na^+ and N_2 is weaker than that between Na^+ and NH_3, for which a reaction enthalpy of −121.8 kJ mol^{-1} was determined.[71] CCSD(T) calculations on the complex between K^+ and N_2 yield a linear minimum-energy structure.[72,73] The dissociation energy D_0 (dissociation into K^+ and N_2) was estimated to be 18.4 kJ mol^{-1}. The interaction energy thus decreases with increasing nuclear charge within Group 1.

5.1.3. Group 2

The interactions of Mg^+ and Ca^+ with N_2 have been studied in the gas phase through mass-selected photodissociation spectroscopy.[74,75] The fragmentation energy (used here as an estimate for D_0) for $[CaN_2]^+$ in one of its excited electronic states ($^2\Pi_{1/2}$) was estimated to be 77.6 kJ mol^{-1} on the basis of a LeRoy–Bernstein analysis of the observed vibrational progression. This excited state corresponds to Ca^+ in the ^{2}P state. The energy required to excite $[CaN_2]^+$ from its $^2\Sigma^+$ electronic ground state into the $^2\Pi_{1/2}$ state (0→0 transition) was determined to be 244.5 kJ mol^{-1}. Using the energy for relaxation of Ca^+ from the ^{2}P excited state into its ^{2}S electronic ground state (301.3 kJ mol^{-1}), one obtains through an energetic cycle a dissociation energy of about 21 kJ mol^{-1} for $[CaN_2]^+$ in its electronic ground state. This value is of comparable size like the dissociation energy of $[KN_2]^+$. According to quantum chemical calculations relying on MP3 perturbation theory, Be^{2+}, Mg^{2+}, and Ca^{2+} form linear N_2 complexes with binding energies of 373, 168, and 83 kJ mol^{-1}, respectively.[73] Thus, as anticipated, the metal–N_2 interaction is stronger in N_2 complexes of the dications M^{2+} than in those of the monocations M^+, as a result of the higher electrostatic interactions. With increasing nuclear charge, the interaction energy decreases approximately exponentially for the dications, whereas the decrease follows a roughly linear relationship for the monocations.

5.1.4. Group 13

Threshold photoionization studies of the $[AlN_2]$ complex in the gas phase yield a bond energy of about 5.6 kJ mol^{-1} for the complex in its electronic ground state.[76] The experiments also show that, as anticipated, the interaction in the $[AlN_2]^+$ cation is stronger than in the neutral complex.

In the case of Ga, the interaction with N_2 has been studied in our group by using the matrix-isolation technique.[77] Figure 2 shows Raman spectra obtained for an N_2 matrix containing Ga atoms. For comparison, the spectrum of a pure N_2 matrix is also shown. The most intense scattering in both spectra is associated with the ν(N–N) mode of unperturbed N_2. However, the spectrum measured for the matrix containing Ga atoms gives evidence for an additional, slightly red-shifted signal assignable to a weakly bound complex $[GaN_2]$. Raman spectra that were recorded at different laser energies show that a strong resonance effect is operative. From the intensity profile, the electronic absorption responsible for the resonance effect can be estimated to be centered at about

 © 2006 Wiley-VCH Verlag GmbH & Co. KGaA, Weinheim

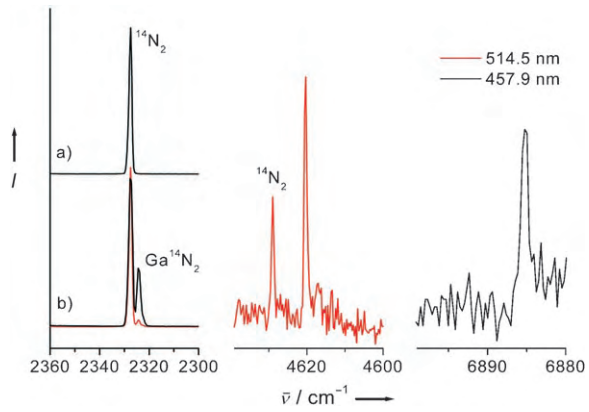

Figure 2. Raman spectra of a) a pure N_2 matrix and b) Ga vapor isolated in an N_2 matrix. The Raman spectra were recorded at different laser energies (456 and 514 nm).

410 nm. This value is in good agreement with the wavelength of a broad absorption detected in the UV/Vis spectra. Figure 2 shows three sections of the Raman spectrum of $[GaN_2]$ that contains signals attributable to overtones of the N–N stretching fundamental. The measured wave numbers for these overtones can be used to estimate the bond energy. The Ga–N_2 dissociation energy can be divided into two contributions (see Figure 3). During fragmentation the Ga–

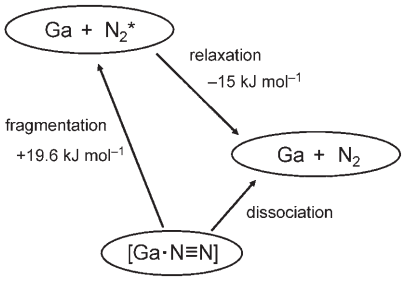

Figure 3. Illustration of the relationship between the dissociation energy and the fragmentation and relaxation energies in the case of $[GaN_2]$.

N_2 bond is cleaved and two separated Ga and N_2 fragments are formed. Then follow electronic and structural relaxation of these fragments. The experimental data give information about the change in the N–N bond energy upon complexation. This energy change is a good approximation for the relaxation energy (to which the electronic contribution should be minimal). The analysis results in a value of about 14.5 kJ mol^{-1}. CCSD(T) calculations that were performed by other groups suggest a dissociation energy of about 4.6 kJ mol^{-1}.[78] With these values, a fragmentation energy (or bond energy) of about 19 kJ mol^{-1} results. In the case of the $[GaN_2]$ complex, therefore, most of the bond energy is consumed by the necessary slight elongation of the N–N distance of the N_2 molecule. Hence our results showed that the magnitude of the relaxation energy can be much higher than the dissociation energy. It follows that the contribution of relaxation to the bond energy should not be neglected.

Studies of the complex in the gas phase have also been carried out using laser-induced fluorescence spectroscopy, and the fragmentation energy (which leads to an electronically excited state of Ga) in one of the detected excited states of the complex has been estimated to be 15.2 kJ mol^{-1}.[79] As anticipated, the interaction of Ga atoms with N_2 is much weaker than with NH_3.[80,81] This difference can be understood qualitatively by comparison of the dipole moments and polarizabilities of N_2 and NH_3. The R2PI method has been used to study experimentally the $[InN_2]^+$ and $[InN_2]$ complexes.[82] As anticipated, the results indicate that the bonding in $[InN_2]^+$ is much stronger than in $[InN_2]$. The (zero-field) ionization threshold of $[InN_2]$ was determined to be 43372 cm^{-1} (about 518.7 kJ mol^{-1}). Using two dye lasers in the R2PI experiments, two electronic transitions were measured near 33400 and 35600 cm^{-1}, both showing vibrational progressions. The harmonic wave numbers of the corresponding fundamentals in both excited states are found to be 76.7 and 87.7 cm^{-1}. On the assumption that these progressions can be assigned to ν(In–N_2) vibrations, the fragmentation energies of the states can be estimated from a Birge–Sponer extrapolation to be 11.9 and 9.9 kJ mol^{-1}. The spectra also gave evidence for hot bands which can be used to obtain information about the fragmentation energy in the ground state of the $[InN_2]$ complex. On the basis of all the available experimental data, the harmonic wave number of the ν(In–N_2) fundamental and the fragmentation energy (intrinsic bond energy) in the ground state can be estimated to be 100.2 cm^{-1} and 18.2 kJ mol^{-1}, respectively. Thus, the interaction between In and N_2 is comparable with that between Ga and N_2. In the case of $[InN_2]^+$, a much higher fragmentation energy of 57.6 kJ mol^{-1} is obtained.[82]

5.1.5. Group 14

CNN can be generated by photolysis of NCN_3 in fluorohydrocarbon matrices. EPR data[83] reveal a linear geometry and a $^3\Sigma^-$ electronic ground state. According to laser-induced fluorescence measurements ($^3\Pi \rightarrow {}^3\Sigma^-$), the symmetric and antisymmetric C–N stretching modes occur at 1235 and 1419 cm^{-1}, respectively, and the bending mode at 396 cm^{-1}.[84] A force constant of 860 N m^{-1} is thereby derived for both N–N and C–N stretching, together with a force constant of 30 N m^{-1} for C-N-N bending. These values argue for the presence of C–N and N–N double bonds in the molecule (contrary to an earlier report[85]). According to full-valence CASSCF calculations, the N–N and C–N bond lengths come out to be 121.3 and 124.1 pm, respectively.[86] The rotational–vibrational energy-level structure of CNN in its $^3\Sigma^-$ electronic ground state has recently been calculated to assist an experimental analysis.[87] CNN is less stable than NCN (also linear). Excited singlet states of CNN ($^1\Delta$ and $^1\Sigma^+$) have been located at excitation energies from the $^3\Sigma^-$ ground state of (81.7 ± 1.4) and (127.9 ± 1.4) kJ mol^{-1}, respectively.[88]

According to EPR, IR, and UV/Vis studies,[89,90] as well as quantum chemical calculations,[91] SiNN is, like CNN, a linear

 © 2006 Wiley-VCH Verlag GmbH & Co. KGaA, Weinheim

molecule with a $^3\Sigma^-$ electronic ground state. The calculated dissociation energy amounts to about 68 kJ mol^{-1}. The lowest singlet electronic state has an energy 66 kJ mol^{-1} higher than the triplet ground state. A side-on bonded complex (with a $^1A_1$ electronic ground state) is about 56 kJ mol^{-1} higher in energy according to a B3LYP estimate. In the matrix experiments, this species has been generated upon photolysis from the end-on bonded complex or from the bis(dinitrogen) complex $Si(NN)_2$.[90] $Si(NN)_2$ exhibits a $^1A_1$ electronic ground state (such that the Si atom is electronically excited) with C_{2v} symmetry. The Si-N-N bond angles, at 167.7°, are significantly less than 180°, a phenomenon which has also been reported for bis(carbonyl) complexes of other main-group elements, for example, $[Ga(CO)_2]$.[92] These angles may simply reflect the optimum overlap between the vacant np valence orbital of the metal coincident with the twofold axis of the molecule and the n,π orbitals of the CO ligands. The π-type bonding resulting from overlap of orbitals perpendicular to the molecular plane is not affected greatly. Alternative explanations for carbonyl compounds which are discussed in this context are:[93] 1) repulsion between the σ orbital of CO and the valence s orbital at the metal center; 2) a long-range attraction between the two C atoms; and 3) coulombic repulsion between the O atoms which carry a small but significant negative charge and are otherwise brought unusually close together by the narrow C-M-C angle. The isotopic data measured for matrix-isolated $Si(NN)_2$ indicate a matrix-induced distortion from C_{2v} symmetry. Species with the overall formula Si_2N_2 have also been detected in matrix experiments. Linear Si=NN=Si with a $^1\Sigma_g^+$ electronic ground state defines the energy-minimum form. Photolysis at $\lambda = 254$ nm brings about conversion into linear Si=N–Si≡N ($^1\Sigma^+$ electronic state) and the four-membered ring species $Si(\mu\text{-}N)_2Si$ ($^1A_1$ electronic state). For these compounds B3LYP calculations find energy minima which are 109 and 84 kJ mol^{-1} higher than that of the $^1\Sigma_g^+$ electronic ground state. NNSiSiNN (C_{2h} symmetry, ^1A_g electronic ground state) has also been observed in the matrix experiments. Photolysis in the wavelength range $280 \le \lambda \le 420$ nm leads to loss of N_2 and formation of Si=N–N=Si.

Reaction of Ge atoms, produced by laser-ablation with N_2, in an N_2 matrix yielded linear GeNNGe ($D_{\infty h}$ symmetry and $^1\Sigma_g$ electronic ground state).[94] Unfortunately, this interesting molecule has so far only been characterized with IR, but not with Raman spectroscopy. Therefore, only one of its vibrational modes has been detected. The authors suggest that this species is formed directly from Ge_2 with N_2.

5.2. N_2 Complexes of Bare Transition-Metal Atoms

5.2.1. Group 3

The end-on bonded [ScNN] complex was first identified in matrix-isolation experiments in which laser-ablated Sc atoms were isolated together with N_2 in Ar matrices.[95] According to DFT calculations (BP86), this linear complex exhibits a $^4\Sigma^-$ electronic ground state. The calculations also indicate that a side-on bonded complex $[Sc(N_2)]$ with C_{2v} symmetry and a $^4B_1$ electronic ground state might lie only slightly higher in energy (11 kJ mol^{-1}). Our own calculations are in agreement with these calculations (the energy difference comes out to be even slightly smaller). The IR spectra of the matrices do indeed suggest the presence of this molecule, which in an N_2 matrix coordinates additional N_2 molecules in an end-on fashion. On the basis of the isotopic data and comparison with the results of DFT calculations, an additional absorption was assigned to D_{2d}-symmetric $[Sc(N_2)_2]$, which contains two side-on bonded N_2 units and exhibits a $^4B_1$ electronic ground state. According to the BP86 calculations, this species has an energy 24 kJ mol^{-1} higher than that of end-on bonded $[Sc(NN)_2]$ ($^4\Sigma_g^-$ electronic ground state). The formation of these side-on bonded complexes is made possible only by the presence of electronically excited metal atoms that are generated by the laser-ablation process. It should also be pointed out that the results of DFT calculations on this kind of molecule have to be considered with caution. For example, it will be shown in the case of the $[Ti_2N_2]$ molecule that DFT calculations produce the wrong electronic ground state. For the sake of completeness, we note that N_2 complexes to ScO and ScO^+ have also been studied in matrix-isolation experiments.[96]

5.2.2. Group 4

Ti atoms in their electronic ground state do not react with N_2, presumably because of significant σ repulsion. Ti atoms have $3d^24s^2$ (^3F) ground states and $3d^34s^1$ (^5F) excited (metastable) states that are 77.2 kJ mol^{-1} higher in energy. It has been shown in the case of the CO complex of Ti that the $3d^34s^1$ configuration is more reactive as there is less σ repulsion and a greater possibility for π back-donation.[97] After photolytic activation, Ti atoms form a weakly bound N_2 complex.[98] According to preliminary DFT (BP86) calculations, the end-on coordinated complex exhibits a $^5\Delta$ electronic ground state. Side-on bonded complexes with $^3A_2$ and $^5B_1$ electronic states are 14 and 65 kJ mol^{-1} higher in energy. Experiments with laser-ablated Ti atoms gave also evidence for a cyclic $[Ti(N_2)]$ species, presumably with a $^1A_1$ electronic state. The energy is 66 kJ mol^{-1} higher than that calculated for the linear [TiNN] complex. Finally, the spectra indicate the presence of a [NTiN] species in which there is no direct interaction between the N atoms. DFT (BP86) calculations found a $^3B_2$ electronic state for this species. This molecule, destabilized by 236 kJ mol^{-1} relative to the linear [TiNN] complex, is formed only when highly excited Ti atoms and even N atoms, as produced in the laser-ablation process, are present. In our laboratory we have compared the reactivities of Ti atoms and Ti_2 dimers towards N_2. Previous experiments had led us to study in depth the Ti_2 dimer by using a combination of experimental results and quantum chemical calculations.[99,100] With resonance Raman spectroscopy, it proved possible to detect a series of overtones of the vibrational fundamental of the dimer (Figure 4), which can be used to estimate a dissociation energy to about 120 kJ mol^{-1}.[101] Quantum chemical multireference CI calculations argue for a somewhat higher value (about 150 kJ mol^{-1}).[100] The calculations also predict a $^3\Delta_g$ electronic ground state. Absorption spectroscopy was then employed to obtain information about electronically excited states. Four

 © 2006 Wiley-VCH Verlag GmbH & Co. KGaA, Weinheim

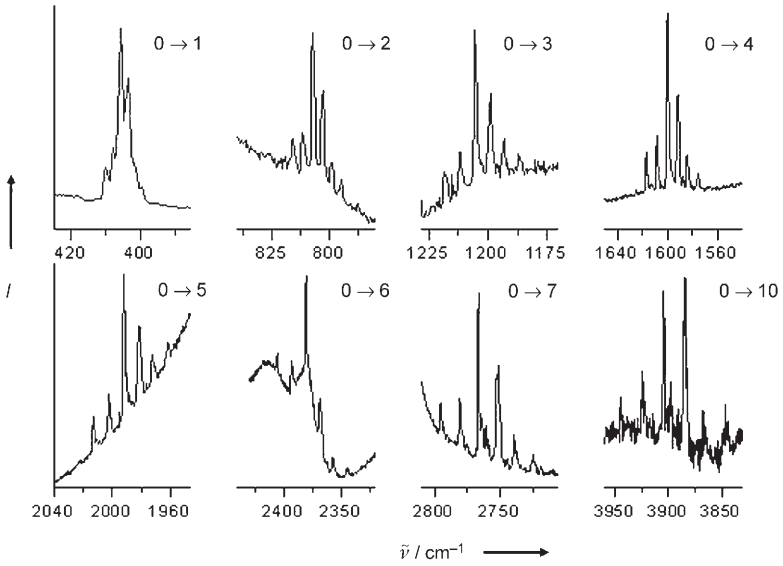

Figure 4. Resonance Raman spectrum of Ti_2 (isolated in an Ar matrix) showing the ν(Ti–Ti) fundamental and a series of overtones.

electronically excited states—$1^3\Pi_u$, $1^3\Phi_u$, $2^3\Pi_u$, and $2^3\Phi_u$—were characterized. The excitation energies are no larger than 0.41, 0.43, 0.73, and 0.94 eV, respectively. Excitations into several vibronic states of these electronic states were observed (Figure 5), thus allowing the determination of not

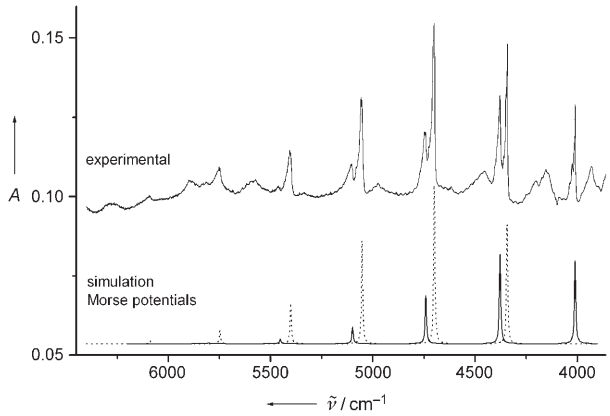

Figure 5. Absorption spectra of a Ti_2-doped Ne matrix in the region 8000–4000 cm^{-1}. Bands resulting from excitation into different vibrational levels of the $1^3\Pi_u$ and $1^3\Phi_u$ electronic states are shown.

only harmonic frequencies and force constants, but also, through a Franck–Condon analysis, the bond lengths relative to that in the electronic ground state (195.4 pm according to our calculations). The experiments indicate elongations of the Ti–Ti bond by (9 ± 2), (10 ± 2), (13 ± 2), and (13 ± 4) pm in the $1^3\Pi_u$, $1^3\Phi_u$, $2^3\Pi_u$, and $2^3\Phi_u$ excited states, respectively.[100]

Before we discuss the results of the matrix reaction between Ti_2 and N_2, we will first summarize briefly the results obtained for solid Ti metal. Solid Ti has been shown to react exothermally with dinitrogen. The standard enthalpy of formation of solid TiN is very high (−675 kJ mol^{-1}). However, the reaction takes place only at very high temperatures, which indicates the presence of a massive activation barrier. In the course of this reaction, the hcp lattice of Ti remains intact for low dinitrogen dosages, and the N atoms are dispersed in this lattice. The strong N–N triple bond is thus completely cleaved. For increased concentrations of dinitrogen, a distorted NaCl structure is finally adopted. Solid TiN is an interesting material which is used in industry for hard coatings and as diffusion barrier layers in silicon semiconductors on account of its slow diffusion rates and high conductivity.[102] In summary, a single Ti atom in its electronic ground state does not react with N_2, and solid Ti metal reacts only at very high temperatures.

In light of these facts, it comes as a surprise that our matrix experiments demonstrated quite clearly that Ti_2 reacts spontaneously with N_2.[103] In the course of this reaction, the N–N triple bond is completely cleaved with the formation of a four-membered, planar $[Ti_2N_2]$ ring compound. The experiments have been repeated with different dinitrogen isotopomers. The measured vibrational spectra do not only indicate the presence of two equivalent N atoms, but also allow an estimate for the N-Ti-N bond angle (about 90°) and the Ti–N bond length (about 175 pm).

Quantum chemical (multireference CISD + Q) calculations clearly show that $[Ti_2N_2]$ exhibits a ^1A_g electronic ground state (in disagreement with earlier DFT results using the BP86 functional which suggested a $^3B_{1u}$ state).[98] In Figure 6 the

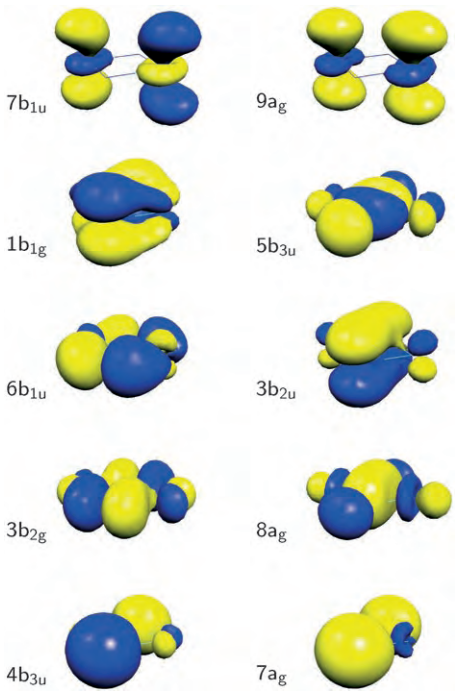

Figure 6. Isodensity surfaces of the valence orbitals of the ^1A_g ground state of $[Ti_2N_2]$.

 © 2006 Wiley-VCH Verlag GmbH & Co. KGaA, Weinheim

isodensity surfaces of the valence orbitals of this ^1A_g ground state are plotted. The two energetically highest orbitals (containing 1.5 and 0.5 electrons) are the bonding and antibonding combinations of Ti d orbitals. Next in order of decreasing energy are six N(p)–Ti(d) bonding orbitals (about 1.95 electrons per orbital). Finally, there are two orbitals comprising essentially the nitrogen lone pairs. A bond order of 1.5 per Ti–N bond is obtained from the six approximately doubly occupied Ti–N bonding orbitals. The $^7B_{2u}$ state of $[Ti_2N_2]$ has also been studied by CASSCF calculations.[104] The N–N and Ti–Ti bond lengths in this electronic state are 126 and 413 pm, respectively. In this state, therefore, there is still a bond between the two N atoms. The calculations argue for significant coulombic contributions (Ti^+ cations and N_2^{2-} anions). However, this state has a significantly higher energy than the singlet electronic ground state. In Figure 7 the

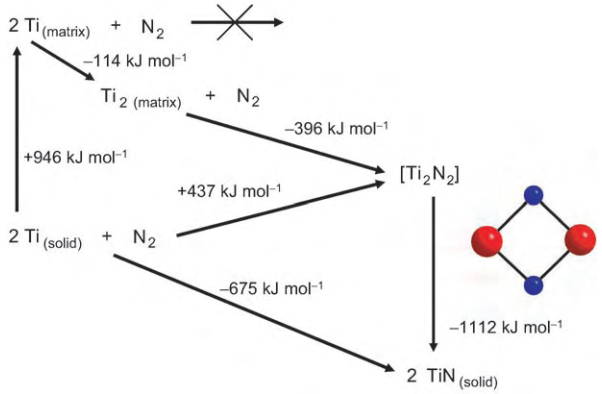

Figure 7. Enthalpy changes for reactions leading finally to solid TiN.

reaction enthalpies for the various processes leading finally to solid TiN are summarized. The standard enthalpy of formation of $[Ti_2N_2]$ was obtained with the help of isodesmic reactions and quantum chemical calculations.[103]

Clusters with the overall formula $[TiN]_n$ (n up to 126) were obtained in the gas phase through the reaction between laser-ablated Ti atoms and NH_3,[105] and the ions that were generated by multiphoton ionization with the third harmonic of a Nd:YAG laser (355 nm) were subsequently analyzed in a TOF mass spectrometer. Cubic structures are suggested for these clusters. The structures and binding energies of neutral $[TiN]_n$ clusters have been calculated.[106] For $[Ti_4N_4]$, a somewhat distorted heterocubane structure is suggested. The reaction of TiO with N_2 was shown to yield the end-on bonded complex [OTiNN], which can be converted to the side-on bonded complex upon irradiation with visible light.[107] Matrix-isolation studies of the interaction of laser-ablated Zr and Hf atoms with dinitrogen[98] indicate the formation of both η^1- and η^2-coordinated complexes. According to BP86 calculations, cyclic $[Zr(N_2)]$ exhibits a $^1A_1$ electronic ground state. The degree of dinitrogen activation in the complexes increases in the order Ti < Zr < Hf, a trend which has been rationalized by the increasing size of the valence nd orbitals. A bis(η^2:η^2-dinitrogen) complex of Zr, presumably with a $^5B_{3g}$ electronic ground state, has also been observed in these experiments. There is, furthermore, some indication that bent [NZrN] and [NHfN] species are generated as a consequence of the laser-ablation process. Finally, the data suggest the formation of the four-membered [Zr(μ-N)$_2$Zr] ring compound (^1A_g electronic ground state) which features no direct N–N interaction. Several other complexes with various numbers of N_2 ligands appeared also to be formed.

5.2.3. Group 5

The interaction of vanadium atoms with N_2 in pure N_2 matrices was analyzed with the aid of matrix-isolation experiments and by using IR,[108,109] ESR,[110] and UV/Vis[111] spectroscopy. These experiments give evidence for the complex $[V(N_2)_6]$. The EPR spectra that were measured for $[V(N_2)_6]$ and also $[Nb(N_2)_6]$ in solid N_2 indicate a tetragonal axial elongation as a consequence of a Jahn–Teller effect, so that they exhibit not O_h but only D_{4h} symmetry (in disagreement with earlier reports,[112] but in agreement with the geometry of the corresponding vanadium hexacarbonyl[113]). The molecules adopt a $^2B_{2g}$ electronic ground state.

The reactions of laser-ablated V atoms with N_2 in Ar or other noble-gas matrices appear to give a series of further complexes incorporating a smaller number of N_2 ligands.[109] According to DFT calculations, the linear complex [VNN] has a $^6\Sigma^+$ electronic ground state. The side-on coordinated $[V(N_2)]$ complex was also observed in the matrix. DFT calculations (BPL functional) suggest a $^6A_1$ electronic state of this species with an energy about 50 kJ mol^{-1} higher than that of the end-on bonded complex. Our B3LYP/TZVPP results (see Section 6) are in agreement to these calculations, although the energy difference is smaller (33 kJ mol^{-1}). The energy of a $^4B_2$ electronic state is 67 kJ mol^{-1} higher than that of the end-on bonded complex. $[V(NN)_2]$ and a D_{2d}-symmetric $[V(NN)_4]$ complex have also been observed.

5.2.4. Group 6

$[CrN_2]^+$ undergoes photodissociation in the gas phase, and the onset of the diabatic dissociation energy threshold has been detected at 17100 cm^{-1}.[114] Dissociation leads to Cr^+ in the ^6D electronic state. By subtraction of the atomic promotion energy of Cr^+ from the observed dissociation limit, the binding energy in the $[CrN_2]^+$ ground state is found to be (58.9 ± 3.9) kJ mol^{-1}. IR and UV/Vis spectra that were measured for N_2 matrices containing thermally evaporated Cr atoms give evidence for $[Cr(N_2)_6]$[115] and bear comparison with the spectra of the formally valence-isoelectronic hexacarbonyl $[Cr(CO)_6]$. Moreover, $[Cr(N_2)_4]$ and $[Cr(N_2)_5]$ have been detected. In Ar matrices containing only small quantities of N_2, the species $[CrN_2]$, $[Cr(N_2)_2]$, and $[Cr(N_2)_3]$ are also formed. In matrix-isolation experiments in which laser-ablated Cr atoms are condensed in a solid N_2 matrix, complete cleavage of the N–N bond is realized in the detection of [NCrN]. The formation of this unusual species is, however, induced by the presence of the laser-ablated N atoms.[109] From the isotopic data the N-Cr-N angle in this

 © 2006 Wiley-VCH Verlag GmbH & Co. KGaA, Weinheim

species is estimated to be $(109 \pm 4)°$. DFT (BPL) calculations indicate a stable $^3B_2$ electronic state for this molecule.

IR spectra of laser-ablated Mo or W atoms isolated in solid N_2 matrices display bands attributable to $[W(NN)_6]$ and $[Mo(NN)_6]$.[116] The spectra are consistent with octahedral coordination of the N_2 ligands around the metal atom. The laser-ablation process gives rise to high-energy species which are presumably responsible for the formation of bent [NMoN]. From the Mo and N isotopic data, the N-Mo-N bond angle of this C_{2v}-symmetric molecule is estimated to be $(108 \pm 3)°$. In an N_2 matrix additional N_2 ligands are bound to the metal atom without changing the bond angle significantly. Activation of the metal atom through laser ablation is also necessary to generate [NWN]. The nitrogen isotopic splitting indicates an N-W-N bond angle of about 110°. The C_{2v}-symmetric side-on complex $[W(N_2)]$ is also formed. The isotopic shift upon $^{14}N/^{15}N$ substitution can be used to estimate an N-W-N bond angle of 105–110°. This finding argues for a $^1A_1$ state, although the $^3B_2$ state has a slightly lower energy according to DFT calculations. The bis(dinitrogen) complex $[Mo(NN)_2]$ has also been observed. Quantum chemical calculations show that the N_2 complexes of molybdenum and tungsten cannot be reliably described with single-reference methods.[117] According to CASPT2 calculations, end-on bonded, linear [MoNN] with a $^7\Sigma$ electronic ground state defines the energy-minimum form of all the possible $[MoN_2]$ geometries. Its energy is 21 kJ mol^{-1} below that of an isolated Mo atom and N_2. This is interesting as the coordination of dinitrogen to Mo complexes in homogeneous solution is much larger; in particular, coordination of dinitrogen to Schrock's trisamidoamine complex **1** amounts to -156.7 kJ mol^{-1} according to BP86 calculations.[20]

Next in increasing energy comes the side-on bonded [MoNN] complex with a $^5B_2$ electronic state having an energy of $+68$ kJ mol^{-1} relative to separated Mo and N_2. Two further electronic states, namely $^3B_2$ and $^1B_2$, have similar energies ($+84$ and $+95$ kJ mol^{-1}, respectively, relative to isolated Mo and N_2). At 96.7 and 96.6°, the N-Mo-N angles in the C_{2v}-symmetric species are quite large. As a consequence, the N···N separations are also very large (254.9 and 256.2 pm), and the Mo–N bond lengths short (170.1 and 171.7 pm). Finally, a $^1A_1$ state has an energy 222 kJ mol^{-1} above that of Mo and N_2. Hence only the weakly bound, end-on coordinated complex is stable with respect to Mo atoms and N_2 molecules.

Interestingly, the calculations indicate that the situation is different in the case of $[WN_2]$, for which the energies of the $^1B_2$ and $^3B_2$ states are below that of separated W and N_2 (relative energies -24 and -15 kJ mol^{-1}, respectively). This finding is astonishing because there is no direct N–N bond in these states (the N···N separations are 260.2 and 261.1 pm). The linear complex (the energetically lowest-lying state now being $^5\Sigma$) lies 42 kJ mol^{-1} above the energy of W and N_2.

5.2.5. Group 7

Bands in the IR spectrum of a solid N_2 matrix containing laser-ablated Mn atoms have been tentatively assigned to the mononuclear complex $[Mn(NN)_5]$ and the dinuclear complex $[Mn_2(NN)_{10}]$.[109] The conditions of the laser-ablation technique also lead to formation of the bent species [NMnN]. Isotopic data suggest an upper limit to the N-Mn-N bond angle of 127°. DFT (BPL) calculations predict this high-energy species to assume a $^4A_2$ electronic state. The energy of this species exceeds that of an end-on bonded, slightly bent [MnNN] complex by as much as 240 kJ mol^{-1}. In other calculations, the end-on bonded [MnNN] complex was reported to be linear ($^6\Pi$ electronic ground state).

5.2.6. Group 8

The N–N stretching mode of [FeNN] has been detected in matrix-isolation experiments.[118] According to DFT calculations, linear [FeNN] exhibits a triplet electronic ground state. Several electronic states of [FeNN] have been studied with CASSCF.[119] The $^3\Sigma^-$ state is found to have an energy 46 kJ mol^{-1} lower than that of Fe(^{3}F) and N_2. This value is not enough, however, to compensate for the energy needed to excite Fe from the ^{5}D into the ^{3}F electronic state (176 kJ mol^{-1}). In experiments with laser-ablated Fe atoms, the side-on coordinated complex $[Fe(N_2)]$ (also with a triplet electronic state) has been detected. It can be converted into the end-on bonded form by annealing of the matrix. In line with these findings, the side-on bonded complex is calculated to have an energy about 17 kJ mol^{-1} higher than that of the end-on bonded isomer. Furthermore, the experiments indicate that [FeNN] can take up another N_2 molecule in a slow reaction leading to linear [NNFeNN], again with a triplet electronic ground state. According to DFT calculations (which are not very reliable for this kind of molecule, as the authors admit[118]), this process is exothermic by as much as -151 kJ mol^{-1}. The conditions associated with laser-ablation of the metal also give rise to the high-energy species [NFeN]. On the basis of the collected isotopic data, it was possible to estimate an N-Fe-N angle in the range 110–121°. Calculations result in a triplet electronic state with an N-Fe-N angle of 114.4° and a Fe–N bond length of 158.0 pm. The calculated energy is 318 kJ mol^{-1} higher than that of the linear complex [FeNN]. This species is presumed to be formed by reaction of FeN with N atoms (both formed under the conditions of laser ablation).

5.2.7. Group 9

The $[CoN_2]$ complex has been studied by the matrix-isolation technique. The first experiments indicated a side-on bonded complex.[120] Later studies showed, however, that this assignment is incorrect, and that the complex is more likely to be linear (that is, with end-on coordination of the N_2 ligand).[121] DFT calculations indicate that the side-on bonded complex ($^2A'$ ground state) has an energy 38 kJ mol^{-1} higher than that of the end-on bonded complex ($^2\Delta$ ground state). Unfortunately, only one band of the complex in its $^2\Delta$ ground state (at 2109 cm^{-1} for a pure $^{14}N_2$ matrix) has been observed in the IR spectra. The cationic complex $[CoN_2]^+$ has been studied in the gas phase by ion cyclotron resonance mass spectrometry.[122] A ligand-substitution reaction (displacement of N_2 by CH_4) was used to

© 2006 Wiley-VCH Verlag GmbH & Co. KGaA, Weinheim

obtain information about the bond energies. From the rate constants of this substitution reaction a $\Delta G^{\neq}$ value of (4.2 ± 2.5) kJ mol^{-1} was estimated. With estimates of the thermal contributions to the reaction enthalpy and the change in free enthalpy, and by using the experimental value for the bond-dissociation energy D_0 of $[Co(CH_4)]^+$,[123] one then arrives at a D_0 value of (96.2 ± 7.1) kJ mol^{-1} for $[CoN_2]^+$. Coupled-cluster calculations indicate that a side-on bonded complex $[CoN_2]^+$ has an energy about 54 kJ mol^{-1} higher than that of the linear ground-state geometry.

Matrix-isolated dinitrogen complexes of the type $[Rh(N_2)_n]$ ($n = 1$–3) have been generated recently through reaction of laser-ablated Rh atoms with N_2 (in Ne, Ar, or N_2 matrices).[124] $[Rh(NN)_3]$ assumes a T-shaped geometry with a $^2A_1$ electronic ground state. $[Rh(NN)_2]$ ($^2\Sigma_g^+$ ground state) exhibits absorption bands at 2199.3 cm^{-1} in a Ne matrix and at 2185.9 cm^{-1} in an Ar matrix. According to B3LYP calculations, a nonlinear state ($^2B_2$)[125] is about 39 kJ mol^{-1} higher in energy. An IR band at 2162.0 cm^{-1} in Ne and 2153.5 cm^{-1} in Ar has been assigned to [RhNN], which has a $^2\Delta$ ground state. According to DFT (BPW91) calculations, the Rh–N bond length increases in the order [RhNN] (186.4 pm) < $[Rh(NN)_2]$ (193.9 pm) < $[Rh(NN)_3]$ (198.5/201.5 pm), whereas, as expected, the N–N bond lengths vary in the reverse order: $[Rh(NN)_3]$ (112.2/112.1 pm) < $[Rh(NN)_2]$ (112.5 pm) < [RhNN] (113.4 pm). Contrary to earlier reports,[126] the new experiments give no evidence of $[Rh(NN)_4]$. The magnitude of the energy change upon coordination of N_2 decreases in the series Rh > [RhNN] > $[Rh(NN)_2]$ > $[Rh(NN)_3]$, showing that the coordinated N_2 ligands make the binding of additional N_2 molecules less and less favorable.

Rhodium dinitrogen complexes can also be prepared in the cavities of zeolites.[127] Dealuminated Y zeolites have been impregnated with an ethanolic solution of $RhCl_3$. The solution was dried at 120 °C in air and subsequently treated in a flow of pure dioxygen at 400 °C. Dispersed Rh_2O_3 is formed in the pores of the zeolite and can be reduced at 150 °C by CO to give $[Rh(CO)_2]^+$ according to Equation (2), where O_z denotes oxygen in a structural acid site of the zeolite framework.

$$Rh_2O_3 + 6\,CO + 2\,O_zH \rightarrow 2\,[O_zRh^{I}(CO)_2] + 2\,CO_2 + H_2O \qquad (2)$$

This dicarbonyl complex is partly decarbonylated in an atmosphere of dilute hydrogen and finally transformed into dinitrogen complexes in a gas flow of dinitrogen; $[O_zRh(N_2)_2]^+$ and $[O_zRh(CO)N_2]$ have thus been characterized.

5.2.8. Group 10

For $C_{\infty v}$-symmetric $[NiN_2]$ ($^1\Sigma^+$ electronic ground state), formed by reaction between Ni and N_2 in an Ar matrix, IR measurements give evidence of all three vibrational fundamentals. The two σ^+ modes (which can be roughly described as the ν(N–N) and ν(Ni–N) fundamentals) occur at 2089.5 and 563.5 cm^{-1}, and the π mode (N-Ni-N bending) comes at 357.0 cm^{-1}.[128] The Ni–N stretching force constant at 360 N m^{-1}, as determined from these values, is only about 10% smaller than the corresponding Ni–C force constant of [NiCO] (407 N m^{-1}).[129] The dissociation energy D_e of $[NiN_2]$, estimated by coupled-cluster-related MCPF calculations, is 99 kJ mol^{-1}.[130] These results indicate that the bond strength in $[NiN_2]$ is comparable with that in [NiCO], a result which is at first glance surprising. Matrix experiments have shown that Ni atoms can take up four dinitrogen molecules.[131,132] The T_d-symmetric $[Ni(N_2)_4]$ complex, formally isoelectronic with the well-known benchmark system $[Ni(CO)_4]$, has been characterized by its vibrational (IR as well as Raman) and UV/Vis spectra. The new experiments[132] have succeeded in characterizing this interesting complex more completely. Comparison of the IR and Raman spectra (Figure 8a) confirms immediately its tetrahedral symmetry. In the low-frequency region, the totally symmetric Ni–N_2 stretching fundamental, which is Raman-active but IR-silent, and the triply degenerate Ni–N_2 stretching fundamental have both been located. Furthermore, the experiments give for the first time evidence of several overtones and combination modes (see Figure 8b). These data allow a first estimate of the Ni–N_2 bond strength. To retrieve information about the bonding, we again divide the dissociation into a fragmentation and a relaxation step (see Figure 9). The dominant part of the relaxation energy is now contained in the relaxation of the $[Ni(N_2)_3]$ fragment from its C_{3v}-symmetric to its lowest-energy D_{3h}-symmetric form. The measured data allow an estimation of the fragmentation energy on the basis of the local-mode model[133] to a value of about 120 kJ mol^{-1}. A corresponding analysis of $[Ni(CO)_4]$ yields a value of 148 kJ mol^{-1}, in good

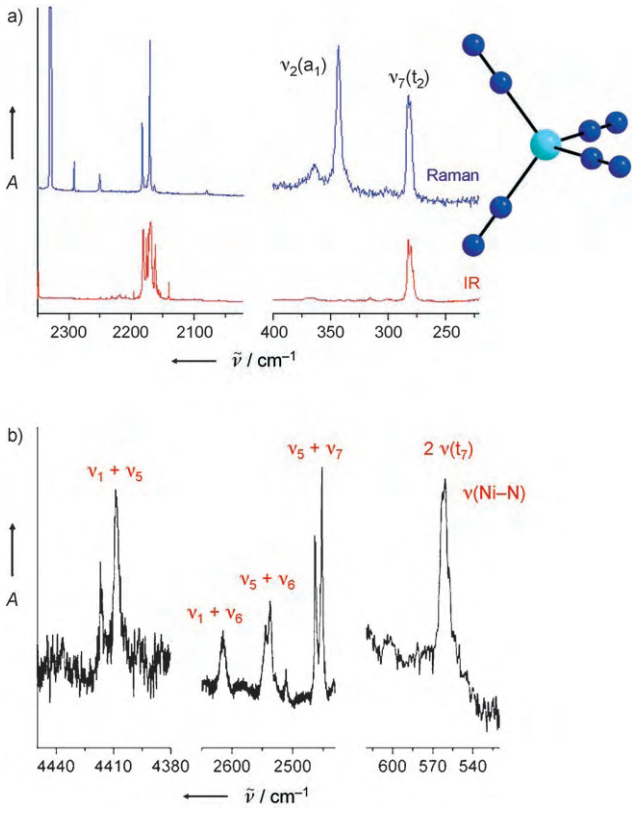

Figure 8. a) Comparison of the IR and Raman spectra of $[Ni(N_2)_4]$ in an N_2 matrix. b) A section of the IR spectrum of $[Ni(N_2)_4]$ in an Ar matrix shows combination bands and overtones.

 © 2006 Wiley-VCH Verlag GmbH & Co. KGaA, Weinheim

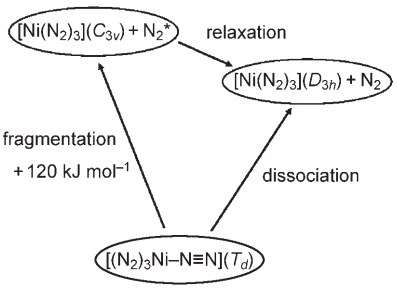

Figure 9. Illustration of the relationship between the dissociation energy and the fragmentation and relaxation energies in the case of $[Ni(N_2)_4]$.

agreement with that derived previously through a combination of experiment and calculation.[134] This means that the Ni–N_2 bond in $[Ni(N_2)_4]$ is much stronger (by a factor of about 10) than, for example, the Ga–N_2 bond in $[GaN_2]$. The stretching force constants f(N–N) and f(Ni–N) for $[Ni(N_2)_4]$, as determined by normal coordinate analysis of the experimentally observed wave numbers, are 2013 and 126 N m^{-1}, respectively. The massive increase of f(N–N) in $[Ni(N_2)_4]$ relative to $[NiN_2]$ (1800 N m^{-1}) might indicate that the degree of back-donation in $[Ni(N_2)_4]$ is significantly reduced. In the case of $[Ni(CO)_4]$ and [Ni(CO)], the increase is less dramatic (f(C–O) = 1540 N m^{-1} in [NiCO] vs. 1740 N m^{-1} in $[Ni(CO)_4]$).

It should be mentioned that another possible form of a molecule with the overall formula NiN_8 is $[Ni(N_4)_2]$, which features two N_4 rings coordinated to a Ni atom. This molecule can exhibit D_{4d} or D_{4h} symmetry, depending on the relative orientations of the two N_4 rings. Calculations indicate that the D_{4d}-symmetric form is slightly more stable than the D_{4h}-symmetric form.[135] However, although these forms are energy minima on the potential-energy hypersurface, they are about 300 kJ mol^{-1} higher in energy than that corresponding to the tetrakis(dinitrogen) complex $[Ni(N_2)_4]$.

Collision-induced dissociation (CID) experiments with $[Ni(N_2)_n]^+$ (n = 1–4) using Xe as the collision gas have been performed.[136] The cross sections at zero pressure (obtained by extrapolation of the cross sections measured for two different Xe pressures) were analyzed as a function of the kinetic and laboratory ion energies. The thresholds measured in the cross-section analysis indicate that the bond-dissociation energies are (111.0 ± 10.6), (111.0 ± 10.6), (56.0 ± 3.9), and (42.5 ± 9.6) kJ mol^{-1} for n = 1–4, respectively. In similar experiments, bond-dissociation energies of (174.6 ± 10.6), (167.9 ± 10.6), (91.7 ± 5.8), and (72.4 ± 2.9) kJ mol^{-1} were obtained for the series $[Ni(CO)_n]^+$ (n = 1–4). These trends show once again that the strength of the bonds depends critically on the number and nature of the other ligands in the complex.

Experiments indicate that Pd can take up only three N_2 molecules while Pt (in disagreement with earlier reports[131b]) appears to take up no more than two N_2 molecules.[137–138] $[Pt(N_2)_2]$ is a linear molecule ($D_{\infty h}$ symmetry and $^1\Sigma_g^+$ electronic ground state). $[PtN_2]$ is found to exhibit a $^1\Sigma^+$ electronic ground state ($C_{\infty v}$ symmetry). As anticipated, the Pt–N bonding appears to be stronger in the mono- than in the bis(dinitrogen) complex. DFT (BPW91) calculations suggest, in agreement with results of more recent experimental studies, that Pt atoms combine exothermally with two N_2 ligands but that attachment of a third ligand would be endothermic. Analysis of the metal–nitrogen stretching force constants of the mono(dinitrogen) complexes, derived from the experimentally observed vibrational wave numbers, shows a decrease in the order f(Ni–N) > f(Pt–N) > f(Pd–N). The relatively weak Pd–N_2 bond thus implied has been attributed to relativistic contraction effects and to differences in the electron affinity of Pd and Pt.

5.2.9. Group 11

Gas-phase experiments indicate a bond-dissociation energy of (88.7 ± 29.3) kJ mol^{-1} for the $[CuN_2]^+$ complex.[139] The bonding of Cu^+ and Cu^{2+} to N_2 has also been studied by quantum chemical calculations;[140] according to CCSD(T) calculations, the bond-dissociation energies are 93 kJ mol^{-1} in the case of $[CuN_2]^+$[140a] and 235 kJ mol^{-1} for $[CuN_2]^{2+}$.[140b] The linear complex $[ClCuN_2]$ has been generated in matrix-isolation experiments through the reaction of CuCl with N_2.[141] The experiments indicate end-on coordination of the N_2 ligand, leading to a linear complex with $C_{\infty v}$ symmetry. According to second-order Møller–Plesset (MP2) calculations, end-on coordination is exothermic by −121 kJ mol^{-1}, while side-on coordination is exothermic by only −54 kJ mol^{-1}. The value for end-on coordination is thus on the same order as that derived for $[CuN_2]^+$. In a normal coordinate analysis the force constants, f(Cu–N) and f(N–N) were determined to be 163 and 2173 N m^{-1}, respectively. Thus, f(N–N) for $[ClCuN_2]$ is slightly, but significantly, smaller than f(N–N) for free N_2 (2239 N m^{-1}). The neutral complex $[CuN_2]$ should exhibit a bent structure with a $^2A'$ electronic ground state.[142]

5.2.10. Group 12

The vibrational and rotational structures observed in the LIF spectra of $[HgN_2]$, formed in a supersonic free jet, have provided estimates of the dissociation energies and the distances between Hg and the center of mass of N_2 in two excited electronic states.[143] The absorption spectrum of Hg which is trapped in an N_2 matrix shows a band resulting from the 6^3P_1–6^1S_0 transition, which is strongly blue-shifted with respect to the corresponding transition of the Hg atom in the gas phase ($\Delta\tilde{\nu}$ = 800 cm^{-1}).[144] Excitation of the $^3P_1$ state with the aid of an excimer laser gives rise to a very strong broadband emission in the near-UV region which can be assigned to a $[HgN_2]$* exciplex.

6. General Discussion and Analysis

With the data accumulated for N_2 complexes at hand, an attempt can be made to understand the differences in the N_2 activation capacity of the various elements. Naturally, such a discussion can only be accomplished after the experimental and theoretical facts have been presented.

© 2006 Wiley-VCH Verlag GmbH & Co. KGaA, Weinheim

6.1. General Remarks

Understanding the binding and activation of dinitrogen to main-group and transition-metal atoms and complexes requires the adoption of a certain model, which serves the purpose of describing and eventually predicting the effect of a metal fragment on dinitrogen. In general, it is believed that we do already have these models at hand, and indeed we have already mentioned many references to a qualitative MO and atomic orbital picture. But these models are hampered by various drawbacks from the point of view of pure theory.

For the sake of simplicity, we may consider here only direct processes of dinitrogen activation. These are all chemical reactions which directly lead to an activated dinitrogen moiety. Thus, a substantially strong coordination without direct activation of dinitrogen by a metal fragment will be noted, but subsequent mechanisms for activation of such fixed dinitrogen units will not be considered here. The activation of inert dinitrogen may be best measured on the basis of well-defined observable properties like the N–N bond length or the N–N vibrational frequency. However, one may find additional measures like partial charges which may well serve as suitable descriptors but are not unambiguously defined. Finally, chemical reactivity should also be considered.

The next restriction which needs to be introduced in view of the scope of this review is the investigation of minimum and equilibrium structures only. The kinetic process of dinitrogen activation starting from the bare metal fragments is not considered with rigor. It should be emphasized that the discussion of equilibrium structures of coordinated dinitrogen complexes only allows us to understand the coordination and activation processes a posteriori.

We may divide the possible models to describe dinitrogen coordination and activation into four classes: a) largely phenomenological models based on comparatively crude approximations and chemical intuition (like discussions of charge transfer based on Pauling electronegativities), b) purely electrostatic interaction models from multipole analyses, c) MO-based interpretations, d) concepts based on the electronic charge density (like the concept of ligand-induced charge concentrations[145]). Here, we shall only consider models of classes (b) and (c) because class (a) may be useful only for first estimates and class (d) appears to be very promising but is not yet sufficiently well-developed.

Electrostatic models of type (b) are, of course, only of limited applicability as covalent effects are completely neglected. Also MO-type models of type (c) hardly provide quantitative understanding. This is because they are either based on semiempirical schemes, like extended Hückel theory (EHT), or on first-principles, single-determinant methods like Hartree–Fock or DFT. While semiempirical methods such as EHT may have nice features like occupation-number-independent MOs, these are necessarily accompanied with a loss of accuracy. Also the single-determinant methods possess drawbacks. As an independent particle model Hartree–Fock theory neglects electron-correlation effects, while Kohn–Sham DFT may be in principle exact, but suffers from approximations in present-day density functionals like BP86 or B3LYP. A further disadvantage of these canonical self-consistent field methods is that the sum of all orbital energies is not equal to the total energy. In other words, the resulting well-known MO diagrams are hardly predictive in a strict quantitative sense and have therefore been largely omitted in this review. Qualitative reasoning using MO terminology is, however, included but does not require MO diagrams for better comprehension.

It is noteworthy that multideterminantal approaches may be much more accurate but do not provide a single-particle picture as occupation numbers are no longer well-defined (or in other words, they are nonintegral), Koopmans' Theorem does not hold, and so on.

For the sake of brevity we use in the following presentation the well-known notation for atomic orbitals to describe those molecular orbitals which can by and large be represented by this atomic orbital. In fact, we have applied this terminology already in the previous sections.

6.2. Side-On versus End-On Bonding

There are two possible ideal binding modes for a [MNN] complex, namely the end-on bonded form **A** (with $C_{\infty v}$ or only C_s symmetry) and the side-on bonded form **B** (with C_{2v} or only C_s symmetry). Form **A** is clearly the preferred structure. However, under some circumstances **B** should be preferred. The most simple model to rationalize the bonding in the complex would be that of an ion pair $M^+(N_2^-)$. This model would favor form **B**. The distance between the two centers of charge is smaller in **B** than in **A**, thus implying stronger bonding. A complex which might fall into this category is [LiNN]. Matrix-isolation studies suggest ionic bonding and C_{2v} symmetry. Binding in this system can thus be understood solely on the grounds of electrostatic interactions according to model (b), whereby covalent contributions are negligible.

Electrostatic binding does not necessarily imply an interaction of monopoles as in the example above. If the system [MNN] cannot be decomposed into charged parts, multipole interactions may still play a role. An example is the HNN molecule, in which the dinitrogen fragment interacts through quadrupolar interactions with the hydrogen atom (in this case the interaction is important because of the absence of monopoles).

Of course, the electrostatic-bonding model works best if the ionization potential of the element is small, like in the case of Li, and if the energetic separation of the (fragment) orbitals on the M (or H) atom and the N_2 fragment is large enough to prevent strong covalent bonding, as covered in model (c).

However, the bonding in most other [MNN] complexes is certainly more complicated. An alternative explanation, following model (c) on the basis of qualitative MO theory, is given by the Dewar–Chatt–Duncanson model[10] and includes σ- and π-bond contributions. In analogy to the interpretation for CO complexes (Scheme 4), the σ bond should be formed from vacant s, p, $d_{x^2-y^2}$, or d_{z^2} orbitals on the metal and the σ_p orbital on N_2 in the case of **A** or one of the π orbitals on N_2 in the case of **B**. The π back-bond involves for both **A** and **B**

 © 2006 Wiley-VCH Verlag GmbH & Co. KGaA, Weinheim

an occupied d_{xz} or d_{yz} orbital on the metal and one of the π^* orbitals on N_2. The clear preference for **A** suggests that the σ orbital on N_2 is close in energy to a suitable vacant metal orbital, while the π orbital on N_2 is too low in energy to form a strong bonding combination with a vacant metal fragment orbital.[146]

To achieve a quantitative discussion we have carried out B3LYP/TZVPP calculations. Tables 4 and 5 summarize the essential results of our B3LYP/TZVPP calculations on first-row transition-metal dinitrogen complexes, which were conducted for all relevant spin states (however, only those spin states are listed which are sufficiently close in energy to that of the ground state). It can be seen that for both the end-on and the side-on bonded complexes generally high-spin states are preferred. In the case of the side-on bonded complexes, the low-spin states have a significantly larger N–N bond length and thus a higher degree of N_2 activation. For example, the N–N bond length changes by nearly 5 pm between the sextet and the doublet spin states of the side-on bonded $[VN_2]$ complex. For end-on bonded complexes, it seems to be generally

Table 4: N–N bond lengths [pm] and wave numbers of the ν(N–N) stretch [cm^{-1}] for end-on bonded N_2 complexes of transition-metal atoms, M–NN bond energies [$kJ\,mol^{-1}$], and the energy change [$kJ\,mol^{-1}$] for reactions with H^+.

M	$2S+1$ (ΔE)[a]	B3LYP d(N–N), ν(N–N)[b]	BP86 d(N–N), ν(N–N)	Literature values d(N–N), ν(N–N)	ΔE(M–NN)[c]	B3LYP $\Delta E(H^+)$
Sc	4	113.6, 1963	115.3, 1880	116.7, 1870[95]	−95 (−108)	−869
	2 (+6)	111.6, 2083				−914
Ti	5	112.5, 2053	114.5, 1941	115.8, 1941[98]	−86 (−94)	−824
	3 (+40)	112.1, 2008				−906
V	6	111.7, 2122	113.9, 1991	114.1, 1980[109]	−66 (−71)	−801
	4 (+40)	110.6, 2203				−873
Cr	5	110.0, 2300	112.9, –	116.2, –[109]	−24 (−25)	−870
	3 (+128)		113.9, 1952	115.1, 1923[109]		−865
Mn	6	112.5, –	113.6, 2056	115.6, 1933[109]	105 (97)[d]	−828
	4	112.4, 2080		115.4, 1869[109]		−852
	2					
Fe	3	111.5, 2146	113.5, 2071	115.2, 2023[118]	−40 (−44)	−847
	5 (+134)					−962
	1 (+138)					
Co	2	110.9, 2253	113.4, 2095	113.6, 2082[121]	−78 (−80)	−771
	4 (+11)	110.5, 2286				−776
Ni	1	111.3, 2248	113.4, 2127	115.0, 2105[128]	−185 (−189)	−736
	3 (+21)	109.7, 2355				−764
Cu	2[e]		112.2, 2128			−746
	4 (+142)		117.4, 1862			−917

[a] ΔE denotes the energy (in $kJ\,mol^{-1}$) relative to the electronic ground state. [b] For N_2, B3LYP calculations yield d(N–N) = 110.0 pm and $\tilde{\nu} = 2452\ cm^{-1}$ for ν(N–N). [c] Values with nonrelaxed N_2 in parenthesis (negative if complex formation exothermic). [d] The $[MnN_2]$ complex turned out to be difficult to optimize, shows spin contamination ($\langle S^*S\rangle = 9.1$), and tends to dissociate (endothermic). [e] Cu-N-N is nonlinear and not stable toward dissociation.

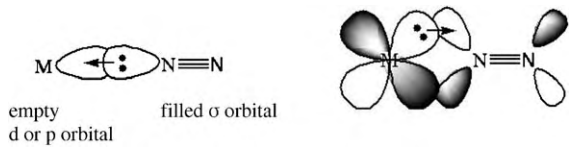

Scheme 4. σ Bond and π back-bond for a transition-metal dinitrogen complex.

the other way round: high-spin complexes exhibit the larger degree of N_2 activation according to the d(N–N) values; the changes are also smaller. Thus for end-on bonded [ScNN], the N–N bond length is elongated by 2 pm if the spin state changes from doublet to quartet. This elongation brings about a marked decrease in the wave number of the ν(N–N) mode (by more than $100\ cm^{-1}$). Thus, in general, we can conclude that changing the electronic state has a substantial effect on N_2 activation.

We also performed calculations with the BP86 functional on the most stable electronic states. The results are included in Table 4. It is apparent that the bond lengths as calculated with BP86 are larger than the ones calculated with B3LYP. Consequently, the wave number of the ν(N–N) stretch is smaller for BP86 than for B3LYP, owing to the different approximation of exchange and correlation effects in the two functionals. Nevertheless, since the trends are similar for both functionals, we decided to continue our discussion on the basis of the B3LYP data only as these will also correspond to more reliable relative energies of the various spin states.[155,156] Table 4 also includes comparison of our calculations with the

Table 5: Calculated B3LYP/TZVPP parameters of side-on bonded [MNN] complexes (d(N–N) [pm], $\tilde{\nu}$ of ν(N–N) [cm^{-1}]), energy change $\Delta E(H^+)$ [$kJ\,mol^{-1}$] as calculated for the reaction [MNN] + $H^+ \rightarrow [MNNH]^+$, and energy difference ΔE(side-on) [$kJ\,mol^{-1}$] between side-on and end-on bonded complexes with the same spin.[a]

M	$2S+1$ (ΔE)[b]	d(N–N)	ν(N–N)	$\Delta E(H^+)$	ΔE(side-end)[c]
Sc	4	116.0	1895.1		+6
	2 (+24)	116.2	1880.0	1004	+24
Ti	3	120.2	1674.0	943	−5
	5 (+3)	113.9	2012.5		+39
	1 (+103)			1011	
V	6	113.6	2022.3		+33
	4 (+30)	117.6	1808.7	922	+23
	2 (+65)	118.6	1730.3	913	
Cr	3	116.4	1858.9	824	+6
	1 (+143)	118.8	1733.7		
Mn	4	120.6	1601.1	912	+95
Fe	3	117.6	1788.0	886	+96
	1 (+174)	118.6	1711.7	908	+132
Co	2	112.5	2118.5	796	+56
Ni	1	114.9	1963.1	780	

[a] Spin states that are not quoted are either not stable (mostly by rearrangement to form the end-on bonded complex) or high in energy. [b]] ΔE denotes the energy (in $kJ\,mol^{-1}$) relative to the electronic ground state. [c] A positive energy means that the side-on bonded complex is less stable than the end-on bonded one.

results of previous calculations reported in the literature using pure density functionals. In Figure 10 the N–N bond lengths are plotted for end-on bonded complexes of first-row

© 2006 Wiley-VCH Verlag GmbH & Co. KGaA, Weinheim

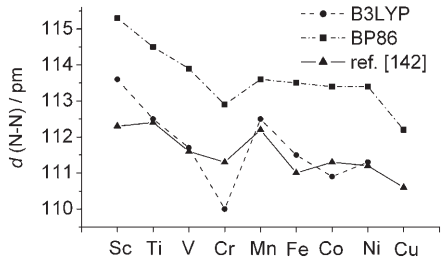

Figure 10. N–N bond lengths as calculated for end-on bonded [MNN] complexes.

transition metals. The values calculated using BP86 and those calculated in reference [142] using B3LYP are also included. Note that we cannot confirm the results in reference [142] for the end-on bonded N_2 complexes of Cr and Cu. In the case of Cu the N_2 complex dissociates in the doublet state while all states of higher spin are bound but much higher in energy compared with the dissociated doublet and can thus be neglected. For Cr, we found the quintet and not the septet spin state to be the more stable. The N–N bond length in this quintet state is very short (110.0 pm), but the Cr–N distance lies just above 200 pm.

As a general trend the N–N bond length decreases from left to right in the period. Two factors are responsible for this trend. The first is the decrease in energy of the d orbitals of the transition metal in the same sequence. This decrease reduces the chances for efficient overlap between the M and N_2 orbitals. The second effect, which is closely related to the first one, is the general decrease of the radii of the M atoms within the period. For efficient bonding the M and N_2 fragments generally have to come close together. However, there can be a repulsive interaction between the electrons in the valence s orbital at the metal atom and the electron in the σ orbital of N_2. The elements Cr and Mn, however, do not follow this general trend. In the case of the carbonyl complexes, it was shown that the charge transfer from the metal center to the CO group is smaller for Cr and Cu than for the other metals.[147] The same can be found for the N_2 complexes.[142] Thus Cr is not a good choice for the activation of N_2.

Generally, the N–N bond length in the side-on bonded version of $[MN_2]$ is larger than in the end-on bonded form. Most strikingly, for the triplet state of $[TiN_2]$, it is 112.1 pm for the end-on bonded form but 120.2 pm for the side-on bonded version. From Table 5 it can be seen that in general the energy difference between end-on and side-on bonded complexes, ΔE(side-end), is small for early transition metals, and larger for late transition metals of the same spin. Generally the end-on coordination mode is preferred, but the energy gap can be very small (for example, for Sc, Ti, V, and Cr).

6.3. Analysis of the Vibrational Frequencies

According to model (c), the MO view of the bonding situation, the bonding includes σ- and π-bond contributions. The σ bond should be formed by the σ_p bond of N_2 and a suitable vacant orbital on the metal. Thus electron density is transferred from the N_2 ligand to the metal center. To see the maximum effect this can have on the ν(N–N) stretching frequency, the frequency of the N_2^+ molecule is compared with that of neutral N_2 (see Table 1). For N_2^+ in its $^2\Sigma_g^+$ electronic ground state, a harmonic frequency of 2207.0 cm^{-1} was reported. This means that the σ bond alone could significantly lower the frequency. This situation is different from that in [MCO] complexes. CO^+ is found at a *higher* frequency than CO. Our B3LYP/TZVPP calculations yield wave numbers of 2452.3 cm^{-1} in the case of neutral N_2, and 2333.4 and 1892.2 cm^{-1} for N_2^+ and N_2^-, respectively.

In Table 6 experimentally observed ν(N–N) stretching frequencies are compared for some transition-metal [MNN] complexes. Some trends can be explained on the basis of model (c). For example, Pd has a closed and energetically low-lying d shell, and therefore the back-bonding can be expected to be relatively weak. Consequently, the ν(N–N) stretching frequency is higher for [PdNN] than for [NiNN]. The same trend can be seen for the CO complexes.

Table 6: Measured ν(N–N) stretching frequencies for some end-on bonded [MNN] complexes.

M	Configuration	I_1 [eV]	exp. ν(N-N) [cm^{-1}]	Environment	Ref.
Ga	$[Ar]3d^{10}4s^24p^1$	5.998	2324.2	N_2 matrix	[77]
C	$[He]2s^22p^2$	11.257	1235 (sym.) 1419 (asym.)	Ar matrix	[84]
Si	$[Ne]3s^23p^2$	8.151	1731.6 1754.7	Ar matrix N_2 matrix	[90]
Sc	$[Ar]3d^14s^2$	6.54	1902.0	Ar matrix	[95]
Fe	$[Ar]3d^64s^2$	7.869	2017.8 2017.8/2012.0	Ar matrix N_2 matrix	[118]
Co	$[Ar]3d^74s^2$	7.876	2100.9 2109	Ar matrix N_2 matrix	[121]
Ni	$[Ar]3d^84s^2$	7.635	2089.5	Ar matrix	[128]
Pd	$[Kr]4d^{10}$	8.34	2213	Ar matrix	[138]
Pt	$[Xe]4f^{14}5d^96s^1$	9.02	2168.5 2073.0	Ar matrix N_2 matrix	[138]

To analyze the trends, we have calculated the wave numbers of the ν(N–N) mode for several end-on bonded transition-metal dinitrogen complexes (Table 4). Naturally the absolute values of the experimentally measured anharmonic wave numbers differ from the calculated harmonic ones (apart from the fact that the potential-energy surface is modelled using a specific density functional and the harmonic frequencies were thus only approximated). Nevertheless, the trend is reproduced nicely in our calculations. Thus both calculations and experiment agree that the wave number increases in the order [ScNN] ≪ [FeNN] ≪ [NiNN] < [CoNN]. It can be seen that the wave numbers generally increase from left to right in the period. Again, [CrNN] stands out, having an unexpectedly high wave number, in line with the short N–N bond bond.

 © 2006 Wiley-VCH Verlag GmbH & Co. KGaA, Weinheim

6.4. Analysis of Differences in Chemical Reactivity

A chemical measure for the degree of dinitrogen activation is the energy change associated with the protonation reaction of N_2 that is bound to a complex relative to the protonation of free N_2. In Table 4 are summarized the energies calculated for the protonation reaction [MNN] + $H^+ \rightarrow [MNNH]^+$ for the isolated end-on bonded complexes. The reference system is $N_2 + H^+$. If the bond in N_2 is activated in a complex [MNN], a higher value is expected in the case of [MNN] + H^+. For the protonation of free N_2, our calculations yield an energy change of $-514\ kJ\,mol^{-1}$. This B3LYP estimate of the gas-phase proton affinity is close to the value calculated using MP3 ($-523\ kJ\,mol^{-1}$).[148] Generally, the protonation energy is higher for early transition metals than for late transition metals. This trend follows the trend of the N–N bond lengths, showing that large N–N bond lengths are associated with high protonation energy. However, there are some irregularities. For example, [CrNN] is predicted by the B3LYP calculations to have a surprisingly high protonation energy, which is difficult to explain.

Experiments with Lewis acids such as AlR_3 suggest that the terminal N basicity increases down a group in the periodic table (for example, [CrNN] vs. [MoNN]). Presumably the larger d orbitals permit delocalization of electrons to the periphery of the complex. This is in agreement with the finding that Mo (but not Cr) and Ru (but not Fe) complexes tend to be better systems for N_2 activation.

6.5. Differences between [MNN] and [L_nMNN] Complexes

Ligands L should have a large effect on the M–N_2 bond. The N–N bond lengths calculated for end-on bonded complexes [MNN], [HMNN], and [H_3PMNN] in their lowest-energy spin states are summarized in Table 7 and plotted in Figure 11. Values for the respective side-on bonded complexes are given in Table 8. Obviously, an electron-donating ligand such as a phosphine group should favor the π backbond. Phosphine ligands are most frequently used for the synthesis of new dinitrogen-binding transition-metal complexes. Of course phosphines such as PF_3 are π acceptors, but the donation should be larger in the case of PH_3. Indeed, in all cases the N–N bond length is larger in [H_3PMNN] complexes than in [HMNN] complexes. The influence of the H ligand (for the pair [HMNN]/[MNN]) is largest for early-transition-metal complexes. Qualitatively speaking, these elements do not have enough electron density to accommodate an electron-withdrawing ligand without becoming more inactive toward N_2 activation. The PH_3 ligand is most efficient in helping to activate N_2 for the elements V, Cr, Mn, and Fe (the elements in the middle of the period).

We also looked at differences in the LM–N_2 energies. Table 9 lists the differences in this energy between [HMN_2] and [H_3PMN_2]. To compare the different electronic situations the geometries of the HM and H_3PM fragments were not

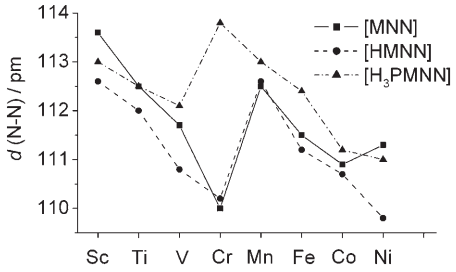

Figure 11. Comparison between the N–N bond lengths as calculated using B3LYP for end-on bonded [MNN], [HMNN], and [H_3PMNN] complexes.

Table 8: N–N bond lengths [pm] for side-on bonded [MNN], [HMNN], and [H_3PMNN] complexes in their electronic ground states (B3LYP/TZVPP calculations; the spin state is given in parentheses).

M	[MNN]	[HMNN]	[H_3PMNN]
Sc	116.0 (quartet)	116.6 (triplet)	115.7 (quartet)
Ti	120.2 (triplet)	114.1 (quartet)	114.4 (quintet)
V	113.6 (sextet)	112.7 (quintet)	–
Cr	116.4 (triplet)	116.6 (quartet)	117.1 (triplet)
Mn	120.6 (quartet)	114.8 (singlet)	116.0 (doublet)
Fe	117.6 (triplet)	–	113.8 (singlet)
Co	112.5 (doublet)	112.7 (triplet)	–
Ni	114.9 (singlet)	111.2 (doublet)	–
Cu	–	110.2 (singlet)	–

Table 7: N–N bond lengths [pm] for end-on bonded [MNN], [HMNN], and [H_3PMNN] complexes in their electronic ground states (B3LYP/TZVPP calculations; the spin state is given in parentheses).

M	[MNN]	[HMNN]	[H_3PMNN]
Sc	113.6 (quartet)	112.6 (triplet)	113.0 (quartet)
Ti	112.5 (quintet)	112.0 (quartet)	112.5 (quintet)
V	111.7 (sextet)	110.8 (quintet)	112.1 (sextet)
Cr	110.0 (quintet)	110.2 (sextet)	113.8 (quintet)
Mn	112.5 (sextet)	112.6 (quintet)	113.0 (quartet)
Fe	111.5 (triplet)	111.2 (quartet)	112.4 (triplet)
Co	110.9 (doublet)	110.7 (triplet)	111.2 (doublet)
Ni	111.3 (singlet)	109.8 (doublet)	111.0 (singlet)
Cu	–[a]	109.5 (singlet)	113.7 (doublet)

[a] Not stable toward dissociation.

Table 9: Differences between the changes in energy of the two reactions HM + $N_2 \rightarrow$[HMNN] (end-on) and H_3PM + $N_2 \rightarrow$[H_3PMNN] (end-on), $\Delta E(H,H_3P)$ [$kJ\,mol^{-1}$], as calculated with B3LYP/TZVPP. For HM and H_3PM the geometries are the same as after complex formation.

M	$2S+1$ [HMNN]	$2S+1$ [H_3PMNN]	$\Delta E(H,H_3P)$[a]
Sc	3	4	17 (20)
V	5	6	−26 (−22)
Cr	6	5	−15 (0)
Mn	5	4	59 (62)
Fe	4	3	−15 (−12)
Co	3	2	37 (39)
Ni	2	1	37 (39)
Cu	1	2	−74 (−59)

[a] A negative value of $\Delta E(H,H_3P)$ means that the bond energy is larger for [HMNN] than for [H_3PMNN]. Values for nonrelaxed N_2 are given in parentheses.

© 2006 Wiley-VCH Verlag GmbH & Co. KGaA, Weinheim

relaxed, and Table 9 contains the results both with and without relaxed N_2. Although the N_2 activation is larger in the [H_3PMNN] systems, the M–NN bond energy is in several cases larger for [HMNN]. In the case of Cr, the bond energy does not significantly change from L = H to L = PH_3, although the change in the N–N bond length is significant.

7. Conclusions and Future Perspectives

In this review article dinitrogen complexes of main-group and transition-element atoms and dimers have been discussed which resemble the generic systems for the study of intrinsic dinitrogen fixation and activation. These complexes are relatively simple systems and should thus be ideal for establishing and testing models of the bonding properties. However, because of the variety of different electronic states which are energetically close to the ground state, their interpretation is not simple and straightforward. Various electronic states produce differences in the degree of dinitrogen activation. Calculations allow the analysis of the influence of the spin state and ligand on dinitrogen activation.

As anticipated, neutral dinitrogen complexes of the atoms of main-group elements have generally only very weakly bound N_2. The dinitrogen ligand in cationic complexes such as $[KN_2]^+$ is significantly more strongly bound, owing to polarization of the electron density on the N_2 unit by the metal cation. For very weakly bound complexes (e.g. [GaN_2]), most of the intrinsic bond energy is consumed by the necessary slight elongation of the N–N bond. Accordingly, the magnitude of this relaxation energy is much greater than that of the dissociation energy. In the case of transition metals, low-spin side-on bonded complexes (which are however energy-rich species) activate the dinitrogen bond best. Both end-on and side-on complexes generally tend to occur as high-spin systems.

The analysis which is presented above highlights important similarities between the "worlds" of small dinitrogen complexes (those observed in the gas phase and through matrix isolation) and the synthetically obtained dinitrogen complexes. These similarities are maybe most pronounced in the case of ligand influence on N_2 activation. The experience-based rule that electron-donating groups which build up electron density on the metal increase N_2 activation is confirmed for the small systems. Consequently, end-on bonded [H_3PMNN] complexes feature a larger N–N bond length than [MNN] complexes. The influence of the electronic state of the metal atom on the N–N bond length was also analyzed. For complexes of later transition metals, for which the M–N bond lengths decrease and the σ repulsion increases, a destabilization of the complex is found. Finally, the change in energy that results from the protonation of a dinitrogen fragment was considered as a further gauge of N_2 activation.

New experiments show that the reactivity of metal dimers and clusters differs markedly from that of a single metal atom, thus providing an elementary link to heterogeneous dinitrogen activation at surfaces. Dimers and small clusters of certain elements are able to activate highly or even cleave the N_2 bond. Of the main-group-element dimers, Ge_2 was reported to react spontaneously with N_2 to give the dinuclear [GeNNGe] complex. In the case of the transition metals, it has been shown that a Ti atom in its electronic ground state does not react with N_2, while Ti_2 reacts spontaneously to give the cyclic compound [Ti(μ-N)$_2$Ti]. During this reaction the strong N–N triple bond is completely cleaved without any significant activation energy. The cyclic system resembles that formed in the reaction between synthetic dinuclear transition-metal complexes and N_2 (for example, the [Zr_2N_2] core described in reference [23]). Current work in our group is concerned with the stabilization of Ti_2 and small clusters in the cavities of zeolites in an effort to exploit the outstanding reactivity of these species in the development of new, ground-breaking synthetic options.[149] Ti clusters on the surface of carbon nanotubes or fullerences are also interesting in this context.[150]

Appendix: Quantum Chemical Methodology

To supplement the quantum chemical calculations from the literature, which are of varying quality (see also comments below) and often not available for the whole range of complexes, we carried out quantum chemical calculations for generic model complexes. For this purpose we chose a fast method for which a certain degree of experience with respect to its reliability has been gained, namely the "black-box" DFT method employing the B3LYP hybrid density functional[151] and a sufficiently large basis set (in order to reduce basis-set superposition effects to a large extent). All calculations were carried out with the Turbomole 5.71 package of DFT programs.[152] A TZVPP basis set as implemented in Turbomole was employed, which comprises the TZV core from Ahlrichs et al.[153] with polarization functions taken from the Dunning basis set.[154] For a comparison with reference data from the literature we carried out some BP86 calculations with the TZVPP basis set employing the resolution of the identity (RI) density-fitting technique for acceleration of the calculations.

Special care was taken with respect to the correct ground-state multiplicity of the complexes. As Harvey discusses in detail,[155] this is a notoriously complicated issue—especially in DFT calculations. We have noted in earlier work that these complications stem from systematic effects and that a reparameterized B3LYP functional (B3LYP*) is most appropriate in such cases.[156] However, the original B3LYP functional usually performs well (regardless of which version of the VWN functional it is combined with), and we employed this functional here because of the significant experience gained with B3LYP.

Vibrational analyses were performed within the harmonic approximation with the SNF package,[157] which uses numerical first derivatives of analytic gradients for the calculation of the Hessian matrix. Scaling of frequencies is not applied as the unscaled harmonic frequencies often agree very well with the experimental fundamentals.[158]

Finally, we add some general remarks on selected quantum chemical methods employed in the literature. These comments may be somewhat generalized, but should

 © 2006 Wiley-VCH Verlag GmbH & Co. KGaA, Weinheim

be understood as a caveat not to take the calculated properties as definitive since the complexes under study may feature electronic structures where a method may fail for some reason. By definition Hartree–Fock theory does not include electron correlation, although the treatment of correlation is essential for the description of chemical bonding and chemical reactivity. Post-Hartree–Fock methods such as configuration interaction (CI) or coupled cluster (CC), which do include electron-correlation effects, often suffer from restricted "excitations" in the ansatz for the wave function and from the lack of multideterminant character in the reference function. Such methods are moreover quite time-intensive, which often leads to limitations in precision (for example, through selection of a too small basis set).

For closed-shell references, that is, electronic structures which can be qualitatively well-described by Hartree–Fock theory, the CCSD(T) model, which is a coupled-cluster model that includes single- and double-excitation operators and treats the triple excitations perturbatively, is the currently accepted quantum chemical standard method to yield energetics, structures, and properties of unprecedented accuracy. However, the reliability of CCSD(T) results is significantly decreased if small, low-quality basis sets are used (a triple-zeta Dunning-type basis set is a recommended minimum choice[159]). Also, in cases of electronic structures with significant multireference character the standard coupled-cluster models cannot be expected to be reliable. We should emphasize that the CASSCF approach (often followed by a CASPT2 perturbation theory calculation) is currently the optimum choice for the treatment of near-degeneracies in open-shell transition-metal complexes. However, because of its very limited active space, also this approach can bear severe limitations. In such cases, DFT methods are usually the method of choice although their accuracy can neither be controlled nor systematically improved.

We thank the Deutsche Forschungsgemeinschaft (especially through the Schwerpunktprogramm "Experimentelle Ladungsdichte als Schlüssel zum Verständnis chemischer Wechselwirkung" and the collaborative research center SFB 436 "Metal-mediated Reactions modelled after Nature" at Jena) and the Fonds der Chemischen Industrie for their continuous support. M.R. thanks the Fonds der Chemischen Industrie for a generous Dozentenstipendium. H.-J.H. is grateful to Prof. Jon Dilworth and Tony Downs (both Oxford) and Hansgeorg Schnöckel (Karlsruhe) for useful discussions.

Received: August 15, 2005
Revised: January 25, 2006

[1] a) A. D. Allen, C. V. Senoff, *J. Chem. Soc. Chem. Commun.* **1965**, 621; b) A. D. Allen, F. Bottomley, R. O. Harris, V. P. Reinsalu, C. V. Senoff, *J. Am. Chem. Soc.* **1967**, *89*, 5595; c) see also: G. J. Leigh, *Can. J. Chem.* **2005**, *83*, 277.

[2] For some early reviews, see for example: a) J. Chatt, G. J. Leigh, *Chem. Soc. Rev.* **1972**, *1*, 121; b) D. Sellman, *Angew. Chem.* **1974**, *86*, 692; *Angew. Chem. Int. Ed. Engl.* **1974**, *13*, 639; c) J. Chatt, J. R. Dilworth, R. L. Richards, *Chem. Rev.* **1978**, *78*, 589.

[3] J. J. Turner, J. K. Burdett, *J. Chem. Soc Chem. Commun.* **1971**, *16*, 885.

[4] J. K. Burdett, M. A. Graham, J. J. Turner, *J. Chem. Soc. Dalton Trans.* **1972**, 1620.

[5] T. H. Rod, B. Hammer, J. K. Nørskov, *Phys. Rev. Lett.* **1999**, *82*, 4054.

[6] B. Hinnemann, J. K. Nørskov, *Phys. Chem. Chem. Phys.* **2004**, *6*, 843.

[7] M. Chen, G. Wang, M. Zhou, *Chem. Phys. Lett.* **2005**, *409*, 70.

[8] D. V. Fomitchev, K. A. Bagley, P. Coppens, *J. Am. Chem. Soc.* **2000**, *122*, 532.

[9] A. Cusanelli, D. Sutton, *J. Chem. Soc. Chem. Commun.* **1989**, 1719.

[10] a) J. S. Dewar, *Bull. Soc. Chim. Fr.* **1951**, *18*, C71; b) J. Chatt, L. A. Duncanson, *J. Chem. Soc.* **1953**, 2939.

[11] J. M. Manriquez, J. E. Bercaw, *J. Am. Chem. Soc.* **1974**, *96*, 6229.

[12] G. P. Pez, P. Apgar, R. K. Crissey, *J. Am. Chem. Soc.* **1982**, *104*, 482.

[13] H. Shan, Y. Yang, A. J. James, P. R. Sharp, *Science* **1997**, *275*, 1460.

[14] J. Kim, D. C. Rees, *Science* **2002**, *297*, 1696.

[15] a) H.-I. Lee, P. M. C. Benton, M. Laryukhin, R. Y. Igarashi, D. R. Dean, L. C. Seefeld, B. M. Hoffman, *J. Am. Chem. Soc.* **2003**, *125*, 5604; b) B. M. Barney, T.-C. Yang, R. Y. Igarashi, P. C. Dos Santos, M. Laryukhin, H.-I. Lee, B. M. Hoffman, D. R. Dean, L. C. Seefeldt, *J. Am. Chem. Soc.* **2005**, *127*, 14960.

[16] See, for example: a) B. Hinnemann, J. K. Nørskov, *J. Am. Chem. Soc.* **2003**, *125*, 1466; b) J. Schimpl, H. M. Petrilli, P. E. Blochl, *J. Am. Chem. Soc.* **2003**, *125*, 15772; c) T. Lovell, T. Liu, D. A. Case, L. Noodleman, *J. Am. Chem. Soc.* **2003**, *125*, 8377; d) I. Dance, *Chem. Commun.* **2003**, 324; e) V. Vrajmasu, E. Munch, E. L. Bominaar, *Inorg. Chem.* **2003**, *42*, 5974; f) B. Hinnemann, J. K. Nørskov, *J. Am. Chem. Soc.* **2004**, *126*, 3920; g) J. Kastner, P. E. Blochl, *Inorg. Chem.* **2005**, *44*, 4568; h) U. Huniar, R. Ahlrichs, D. Coucouvanis, *J. Am. Chem. Soc.* **2004**, *126*, 2588; i) L. C. Seefeldt, I. G. Dance, *Biochemistry* **2004**, *43*, 1401; j) F. Neese, *Angew. Chem.* **2006**, *118*, 202; *Angew. Chem. Int. Ed.* **2006**, *45*, 196.

[17] P. E. M. Siegbahn, J. Westerberg, M. Svensson, R. H. Crabtree, *J. Phys. Chem. B* **1998**, *102*, 1615.

[18] a) D. V. Yandulov, R. R. Schrock, *Science* **2003**, *301*, 76; b) D. V. Yandulov, R. R. Schrock, A. L. Rheingold, C. Ceccarelli, W. Davis, *Inorg. Chem.* **2003**, *42*, 796; c) V. Ritleng, D. V. Yandulov, W. W. Weare, R. R. Schrock, A. S. Hock, W. M. Davis, *J. Am. Chem. Soc.* **2004**, *126*, 6150; d) D. V. Yandulov, R. R. Schrock, *Inorg. Chem.* **2005**, *44*, 1103; e) R. R. Schrock, *Acc. Chem. Res.* **2005**, *38*, 955.

[19] a) Z. Cao, Z. Zhou, H. Wan, Q. Zhang, *Int. J. Quantum Chem.* **2005**, *103*, 344; b) F. Studt, F. Tuczek, *Angew. Chem.* **2005**, *117*, 5783; *Angew. Chem. Int. Ed.* **2005**, *44*, 5639.

[20] a) B. Le Guennic, B. Kirchner, M. Reiher, *Chem. Eur. J.* **2005**, *11*, 7448; b) M. Reiher, B. Le Guennic, B. Kirchner, *Inorg. Chem.* **2005**, *44*, 9640.

[21] Some recent review articles: a) M. Hidai, Y. Mizobe, *Chem. Rev.* **1995**, *95*, 1115; b) C. M. Kozak, P. Mountford, *Angew. Chem.* **2004**, *116*, 1206; *Angew. Chem. Int. Ed.* **2004**, *43*, 1186; c) M. D. Fryzuk, S. A. Johnson, *Coord. Chem. Rev.* **2000**, *200*, 379; d) S. Gambarotta, *J. Organomet. Chem.* **1995**, *500*, 117.

[22] F. Tuczek, N. Lehnert, *Angew. Chem.* **1998**, *110*, 2780; *Angew. Chem. Int. Ed.* **1998**, *37*, 2636.

[23] R. J. Deeth, *J. Organomet. Chem.* **2001**, *635*, 165.

[24] a) D. Rehder, C. Woitha, W. Priebsch, H. Gailus, *J. Chem. Soc. Chem. Commun.* **1992**, 364; b) H. Gailus, C. Woitha, D. Rehder, *J. Chem. Soc. Dalton Trans.* **1994**, 3471.

[25] See, for example: a) R. A. Henderson, G. J. Leigh, C. J. Pickett, *Adv. Inorg. Chem. Radiochem.* **1983**, *25*, 198; b) M. Hidai, Y. Mizobe, *Chem. Rev.* **1995**, *95*, 1115; c) R. R. Eady, *Chem. Rev.*

 © 2006 Wiley-VCH Verlag GmbH & Co. KGaA, Weinheim

1996, *96*, 3013; d) M. D. Fryzuk, S. A. Johnson, *Coord. Chem. Rev.* **2000**, *200–202*, 379; e) M. P. Shaver, M. D. Fryzuk, *Adv. Synth. Catal.* **2003**, *345*, 1061; f) D. C. Rees, J. B. Howard, *Science* **2003**, *300*, 929; g) M. Masanobu, Y. Mizobe, *Can. J. Chem.* **2005**, *83*, 358.

[26] P. Chen, Z. Xiong, J. Luo, J. Lin, K. L. Tan, *Nature* **2002**, *420*, 302.

[27] M. Mori, K. Hori, M. Akashi, M. Hori, Y. Sato, M. Nishida, *Angew. Chem.* **1998**, *110*, 659; *Angew. Chem. Int. Ed.* **1998**, *37*, 636.

[28] J. Ho, R. J. Drake, D. W. Stephan, *J. Am. Chem. Soc.* **1993**, *115*, 3792.

[29] a) T. E. Hanna, E. Lobkovsky, P. J. Chirik, *J. Am. Chem. Soc.* **2004**, *126*, 14688; b) T. E. Hanna, I. Keresztes, E. Lobkovsky, W. H. Bernskoetter, P. J. Chirik, *Organometallics* **2004**, *23*, 3448.

[30] S. M. Mullins, A. P. Duncan, R. G. Bergman, J. Arnold, *Inorg. Chem.* **2001**, *40*, 6952.

[31] R. Duchateau, S. Gambarotta, N. Beydoun, C. Bensimon, *J. Am. Chem. Soc.* **1991**, *113*, 8986.

[32] a) M. D. Fryzuk, J. B. Love, S. J. Rettig, V. G. Young, *Science* **1997**, *275*, 1445; b) H. Basch, D. G. Musaev, K. Morokuma, M. D. Fryzuk, J. B. Love, W. W. Seidel, A. Albinati, T. F. Koetzle, W. T. Klooster, S. A. Mason, J. Eckert, *J. Am. Chem. Soc.* **1999**, *121*, 523.

[33] F. Studt, L. Morello, N. Lehnert, M. D. Fryzuk, F. Tuczek, *Chem. Eur. J.* **2003**, *9*, 520.

[34] C. Janiak, U. Versteeg, K. C. H. Lange, R. Weiman, E. Hahn, *J. Organomet. Chem.* **1995**, *501*, 219.

[35] J. A. Pool, E. Lobkovsky, P. J. Chirik, *Nature* **2004**, *427*, 527.

[36] W. H. Bernskoetter, E. Lobkovsky, P. J. Chirik, *J. Am. Chem. Soc.* **2005**, *127*, 14051.

[37] a) N. Beydoun, R. Duchateau, S. Gambarotta, *J. Chem. Soc. Chem. Commun.* **1992**, 244; b) J.-K. F. Buijink, A. Meetsma, J. H. Teuben, *Organometallics* **1993**, *12*, 2004; c) R. Ferguson, E. Solari, C. Floriani, A. Chiesi-Villa, C. Rizzoli, *Angew. Chem.* **1993**, *105*, 453; *Angew. Chem. Int. Ed. Engl.* **1993**, *32*, 396.

[38] a) N. Re, M. Rosi, A. Sgamellotti, C. Floriani, E. Solari, *Inorg. Chem.* **1994**, *33*, 4390; b) N. Re, M. Rosi, A. Sgamellotti, C. Floriani, *Inorg. Chem.* **1995**, *34*, 3410.

[39] G. K. B. Clentsmith, V. M. E. Bates, P. B. Hitchcock, F. G. N. Cloke, *J. Am. Chem. Soc.* **1999**, *121*, 10444.

[40] a) M. D. Fryzuk, S. A. Johnson, O. B. Patrick, A. Albinati, S. A. Mason, T. F. Koetzle, *J. Am. Chem. Soc.* **2001**, *123*, 3960; b) F. Studt, B. A. MacKay, M. D. Fryzuk, F. Tuczek, *J. Am. Chem. Soc.* **2004**, *126*, 280; c) F. Studt, B. A. MacKay, M. D. Fryzuk, F. Tuczek, *Chem. Eur. J.* **2005**, *11*, 604.

[41] a) F. Tuczek, K. H. Horn, N. Lehnert, *Coord. Chem. Rev.* **2003**, *245*, 107; b) F. Tuczek, *Adv. Inorg. Chem.* **2004**, *56*, 27.

[42] M. Hidai, K. Tominari, Y. Uchida, A. Misono, *J. Chem. Soc. Chem. Commun.* **1969**, 1392.

[43] a) M. Hidai, K. Tominari, Y. Uchida, *J. Am. Chem. Soc.* **1972**, *94*, 110; b) T. A. George, R. C. Tisdale, *Inorg. Chem.* **1988**, *27*, 2909.

[44] Y. Nishibayashi, S. Iwai, M. Hidai, *Science* **1998**, *279*, 540.

[45] G. V. Leigh, *Science* **2003**, *301*, 55.

[46] B. E. Wiesler, N. Lehnert, J. Neuhausen, W. Tremel, F. Tuczek, *Angew. Chem.* **1998**, *110*, 856; *Angew. Chem. Int. Ed.* **1998**, *37*, 815.

[47] O. Franke, B. E. Wiesler, N. Lehnert, L. Näther, J. Neuhausen, V. Ksenofontov, F. Tuczek, *Inorg. Chem.* **2002**, *41*, 3491.

[48] O. Franke, B. E. Wiesler, N. Lehnert, F. Tuczek, *Z. Anorg. Allg. Chem.* **2002**, *628*, 2395.

[49] G. Moritz, M. Reiher, B. A. Hess, *Theor. Chem. Acc.* **2005**, *114*, 76.

[50] a) D. Sellmann, B. Hautsch, A. Rösler, F. W. Heinemann, *Angew. Chem.* **2001**, *113*, 1553; *Angew. Chem. Int. Ed.* **2001**, *40*, 1505; b) D. Sellmann, A. Hille, F. W. Heinemann, M. Moll, G. Brehm, M. Reiher, B. A. Hess, S. Schneider, *Inorg. Chim. Acta* **2003**, *348*, 194; c) D. Sellmann, A. Hille, A. Rösler, F. W. Heinemann, M. Moll, G. Brehm, S. Schneider, M. Reiher, B. A. Hess, W. Bauer, *Chem. Eur. J.* **2004**, *10*, 819; d) M. Reiher, B. A. Hess, *Adv. Inorg. Chem.* **2004**, *56*, 55; e) M. Reiher, B. Kirchner, J. Hutter, D. Sellmann, B. A. Hess, *Chem. Eur. J.* **2004**, *10*, 4443; f) B. Kirchner, M. Reiher, A. Hille, J. Hutter, B. A. Hess, *Chem. Eur. J.* **2005**, *11*, 574.

[51] B. K. Burgess, D. J. Low, *Chem. Rev.* **1996**, *96*, 2983.

[52] a) M. Grunze, M. Golze, W. Hirschwald, H.-J. Freund, H. Plum, U. Seip, M. C. Tsai, G. Ertl, J. Küppers, *Phys. Rev. Lett.* **1984**, *53*, 850; b) M. C. Tsai, U. Seip, I. C. Bassignana, J. Küppers, G. Ertl, *Surf. Sci.* **1985**, *155*, 387.

[53] C. W. Bauschlicher, Jr., L. G. M. Pettersson, P. E. M. Siegbahn, *J. Chem. Phys.* **1987**, *87*, 2129.

[54] R. C. Egeberg, S. Dahl, A. Logadottir, J. H. Larsen, J. K. Nørskov, I. Chorkendorff, *Surf. Sci.* **2001**, *491*, 183.

[55] I. Korobkov, S. Gambarotta, G. P. A. Yap, *Angew. Chem.* **2003**, *115*, 5108; *Angew. Chem. Int. Ed.* **2003**, *42*, 4958

[56] W. J. Evans, S. A. Kozimor, J. W. Ziller, *J. Am. Chem. Soc.* **2003**, *125*, 14264.

[57] S. P. Walch, *J. Chem. Phys.* **1991**, *95*, 4277, and references therein.

[58] S. F. Selgren, P. W. McLoughlin, G. I. Gellene, *J. Chem. Phys.* **1989**, *90*, 1624.

[59] S. P. Walch, R. J. Duchovic, C. M. Rohlfing, *J. Chem. Phys.* **1989**, *90*, 3230.

[60] a) B. E. Turner, *Astrophys. J.* **1974**, *193*, L83; b) S. Green, J. A. Montgomery, Jr., P. Thaddeus, *Astrophys. J.* **1974**, *193*, L89; c) P. Thaddeus, B. E. Turner, *Astrophys. J.* **1975**, *201*, L25.

[61] J. C. Owrutsky, C. S. Gudeman, C. C. Martner, L. M. Tack, N. H. Rosenbaum, R. J. Saykally, *J. Chem. Phys.* **1986**, *84*, 605.

[62] a) C. S. Gudeman, M. H. Begemann, J. Pfaff, R. J. Saykally, *J. Chem. Phys.* **1983**, *78*, 5837; b) S. C. Foster, A. R. W. McKellar, *J. Chem. Phys.* **1984**, *81*, 3424.

[63] R. C. Spiker, Jr., L. Andrews, C. Trindle, *J. Am. Chem. Soc.* **1972**, *94*, 2401.

[64] L. Manceron, M. Hawkins, L. Andrews, *J. Phys. Chem.* **1986**, *90*, 4987.

[65] M. F. Falcetta, P. E. Siska, *J. Chem. Phys.* **1998**, *109*, 6615.

[66] E. A. Gislason, P. Polak-Dingels, M. S. Rajan, *J. Chem. Phys.* **1990**, *93*, 2476.

[67] E. P. F. Lee, T. G. Wright, *Chem. Phys. Lett.* **2004**, *392*, 187.

[68] R. Goldstein, J. Grosser, O. Hoffmann, V. Schumann, D. Wößner, M. Jungen, M. Lehner, *J. Chem. Phys.* **2001**, *114*, 2144.

[69] See, for example: a) S. Kita, H. Tanuma, M. Izawa, *Chem. Phys.* **1988**, *125*, 415; b) A. W. Castleman, Jr., R. G. Keesee, *Chem. Rev.* **1986**, *86*, 589, zit. Lit.

[70] P. Soldán, V. Špirko, E. P. F. Lee, T. G. Wright, *J. Chem. Phys.* **1999**, *111*, 3420.

[71] A. W. Castleman, Jr., P. M. Holland, D. M. Lindsay, K. I. Peterson, *J. Am. Chem. Soc.* **1978**, *100*, 6039.

[72] E. P. F. Lee, Z. Almahdi, A. Musgrave, T. G. Wright, *Chem. Phys. Lett.* **2003**, *373*, 599.

[73] S. Ikuta, *Chem. Phys.* **1985**, *95*, 235.

[74] D. L. Robbins, L. R. Brock, J. S. Pilgrim, M. A. Duncan, *J. Chem. Phys.* **1995**, *102*, 1481.

[75] S. H. Pullins, J. E. Reddic, M. R. France, M. A. Duncan, *J. Chem. Phys.* **1998**, *108*, 2725.

[76] L. R. Brock, M. A. Duncan, *J. Phys. Chem.* **1995**, *99*, 16571.

[77] H.-J. Himmel, N. Hebben, *Chem. Eur. J.* **2005**, *11*, 4096.

[78] E. P. F. Lee, J. M. Dyke, *J. Phys. Chem. A* **2000**, *104*, 11810.

[79] G. M. Greetham, M. J. Hanton, A. M. Ellis, *Phys. Chem. Chem. Phys.* **1999**, *1*, 2709.

[80] H.-J. Himmel, A. J. Downs, T. M. Greene, *J. Am. Chem. Soc.* **2000**, *122*, 9793.

 © 2006 Wiley-VCH Verlag GmbH & Co. KGaA, Weinheim

[81] S. Li, G. K. Rothschopf, D. Pillai, B. R. Sohnlein, B. M. Wilson, D.-S. Yang, *J. Chem. Phys.* **2001**, *115*, 7968.
[82] L. R. Brock, M. A. Duncan, *J. Chem. Phys.* **1995**, *102*, 9498.
[83] E. Wasserman, L. Barash, W. A. Yager, *J. Am. Chem. Soc.* **1965**, *87*, 2075.
[84] B. E. Wurfel, A. Thoma, R. Schlachta, V. E. Bondybey, *Chem. Phys. Lett.* **1992**, *190*, 119, and references therein.
[85] D. E. Milligan, M. E. Jacox, *J. Chem. Phys.* **1966**, *44*, 2850.
[86] P. Rajendra, P. Chandra, *J. Chem. Phys.* **2001**, *114*, 1589.
[87] V. V. Melnikov, P. Jensen, *Chem. Phys. Lett.* **2004**, *394*, 171.
[88] E. P. Clifford, P. G. Wenthold, W. C. Lineberger, G. A. Petersson, K. M. Broadus, S. R. Kass, S. Kato, C. H. DePuy, V. M. Bierbaum, G. B. Ellison, *J. Phys. Chem. A* **1998**, *102*, 7100.
[89] R. R. Lemke, R. F. Ferrante, W. Weltner, Jr., *J. Am. Chem. Soc.* **1977**, *99*, 416.
[90] G. Maier, H. P. Reisenauer, J. Glatthaar, *Organometallics* **2000**, *19*, 4775.
[91] a) R. Janoschek, *Adv. Quantum Chem.* **1997**, *28*, 235; b) F. R. Ornellas, L. T. Ueno, S. Iwata, *J. Chem. Phys.* **1997**, *106*, 151.
[92] H.-J. Himmel, A. J. Downs, J. C. Green, T. M. Greene, *J. Phys. Chem. A* **2000**, *104*, 3642.
[93] A. J. Bridgeman, *J. Chem. Soc. Dalton Trans.* **1997**, 1323.
[94] M. Bahou, K. Sankaran, Y.-J. Wu, Y.-P. Lee, D. Rayner, B. Simard, *J. Chem. Phys.* **2003**, *118*, 9710.
[95] G. V. Chertihin, L. Andrews, C. W. Bauschlicher, Jr., *J. Am. Chem. Soc.* **1998**, *120*, 3205.
[96] M. Zhou, G. Wang, Y. Zhao, M. Chen, C. Ding, *J. Phys. Chem. A* **2005**, *109*, 5079.
[97] L. A. Barnes, C. W. Bauschlicher, Jr., *J. Chem. Phys.* **1989**, *91*, 314.
[98] G. P. Kushto, P. F. Souter, G. V. Chertihin, L. Andrews, *J. Chem. Phys.* **1999**, *110*, 9020.
[99] H.-J. Himmel, A. Bihlmeier, *Chem. Eur. J.* **2004**, *10*, 617.
[100] O. Hübner, H.-J. Himmel, L. Manceron, W. Klopper, *J. Chem. Phys.* **2004**, *121*, 7195.
[101] Some of these overtones were observed previously: C. Cossé, M. Fouassier, T. Mejean, M. Tranquille, D. P. DiLella, M. Moskovits, *J. Chem. Phys.* **1980**, *73*, 6076.
[102] B. H. Weiller, *J. Am. Chem. Soc.* **1996**, *118*, 4975.
[103] H.-J. Himmel, O. Hübner, W. Klopper, L. Manceron, *Angew. Chem.* **2006**, *118*, 2865; *Angew. Chem. Int. Ed.* **2006**, *45*, 2799.
[104] P. E. M. Siegbahn, *J. Chem. Phys.* **1991**, *95*, 364.
[105] Z. Y. Chen, A. W. Castleman, Jr., *J. Chem. Phys.* **1993**, *98*, 231.
[106] B. V. Reddy, S. N. Khanna, *Phys. Rev. B* **1996**, *54*, 2240.
[107] M. Chen, G. Wang, M. Zhou, *Chem. Phys. Lett.* **2005**, *409*, 70.
[108] H. Huber, T. A. Ford, W. Klotzbücher, G. A. Ozin, *J. Am. Chem. Soc.* **1976**, *98*, 3176.
[109] L. Andrews, N. D. Bare, G. V. Chertihin, *J. Phys. Chem. A* **1997**, *101*, 8417.
[110] S. H. Parrish, R. J. Van Zee, W. Weltner, Jr., *J. Phys. Chem. A* **1999**, *103*, 1025, and references therein.
[111] A. B. P. Lever, G. A. Ozin, *Inorg. Chem.* **1977**, *16*, 2012.
[112] S. W. Bratt, A. Kassik, R. N. Perutz, M. C. R. Symons, *J. Am. Chem. Soc.* **1982**, *104*, 490.
[113] E. Bernhardt, H. Willner, A. Kornath, J. Breidung, M. Buehl, V. Jonas, W. Thiel, *J. Phys. Chem. A* **2003**, *107*, 859.
[114] D. E. Lessen, R. L. Asher, P. J. Brucat, *Chem. Phys. Lett.* **1991**, *177*, 380.
[115] T. C. DeVore, *Inorg. Chem.* **1976**, *15*, 1315.
[116] L. Andrews, P. F. Souter, W. D. Bare, B. Liang, *J. Phys. Chem. A* **1999**, *103*, 4649.
[117] P. Pyykkö, T. Tamm, *J. Phys. Chem. A* **1997**, *101*, 8107.
[118] G. V. Chertihin, L. Andrews, M. Neurock, *J. Phys. Chem.* **1996**, *100*, 14609.
[119] P. E. M. Siegbahn, M. R. A. Blomberg, *Chem. Phys.* **1984**, *87*, 189.
[120] G. A. Ozin, A. Vander Voet, *Can. J. Chem.* **1973**, *51*, 637.
[121] L. Andrews, A. Citra, G. V. Chertihin, W. D. Bare, M. Neurock, *J. Phys. Chem. A* **1998**, *102*, 2561.
[122] C. Heinemann, J. Schwarz, H. Schwarz, *J. Phys. Chem.* **1996**, *100*, 6088.
[123] a) P. R. Kemper, J. Bushnell, P. A. M. van Koppen, M. T. Bowers, *J. Phys. Chem.* **1993**, *97*, 1810; b) C. L. Haynes, P. B. Armentrout, J. K. Perry, W. A. Goddard, *J. Phys. Chem.* **1995**, *99*, 6340.
[124] X. Wang, L. Andrews, *J. Phys. Chem. A* **2002**, *106*, 2457.
[125] M. L. McKee, S. D. Worley, *J. Phys. Chem. A* **1997**, *101*, 5600.
[126] G. A Ozin, A. Vander Voet, *Can. J. Chem.* **1973**, *51*, 3332.
[127] a) H. Miessner, *J. Am. Chem. Soc.* **1994**, *116*, 11522; b) E. A. Wovchko, J. T. Yates, Jr., *J. Am. Chem. Soc.* **1996**, *118*, 10250.
[128] L. Manceron, M. E. Alikhani, H. A. Joly, *Chem. Phys.* **1998**, *228*, 73.
[129] H. A. Joly, L. Manceron, *Chem. Phys.* **1998**, *236*, 61.
[130] C. W. Bauschlicher, Jr., S. R. Langhoff, L. A. Barnes, *Chem. Phys.* **1989**, *129*, 431.
[131] a) H. Huber, E. P. Kündig, M. Moskovits, G. A. Ozin, *J. Am. Chem. Soc.* **1973**, *95*, 332; b) W. Klotzbücher, G. A. Ozin, *J. Am. Chem. Soc.* **1975**, *97*, 2672.
[132] H.-J. Himmel, L. Manceron, *Dalton Trans.* **2005**, 2615.
[133] a) I. M. Mills, A. G. Robiette, *Mol. Phys.* **1985**, *56*, 743; b) I. M. Mills, *Mol. Phys.* **1987**, *61*, 711.
[134] R. J. McKinney, D. A. Peusak, *Inorg. Chem.* **1979**, *18*, 3413.
[135] Q. S. Li, J. Guan, *J. Phys. Chem. A* **2003**, *107*, 8584.
[136] F. A. Kahn, D. L. Steele, P. B. Armentrout, *J. Phys. Chem.* **1995**, *99*, 7819.
[137] D. W. Green, J. Thomas, D. M. Gruen, *J. Chem. Phys.* **1973**, *58*, 5453.
[138] A. Citra, X. Wang, W. D. Bare, L. Andrews, *J. Phys. Chem. A* **2001**, *105*, 7799.
[139] M. T. Rodgers, B. Walker, P. B. Armentrout, *Int. J. Mass Spectrom.* **1999**, *182/183*, 99.
[140] a) A. Delabie, K. Pierloot, *J. Phys. Chem. A* **2002**, *106*, 5679; b) J.-M. Ducéré, A. Goursot, D. Berthomieu, *J. Phys. Chem. A* **2005**, *109*, 400.
[141] H. S. Plitt, H. Schnöckel, M. Baer, R. Ahlrichs, *Z. Anorg. Allg. Chem.* **1992**, *607*, 45.
[142] J. Pilme, B. Silvi, M. E. Alikhani, *J. Phys. Chem. A* **2005**, *109*, 10028.
[143] K. Yamonouchi, S. Isogai, S. Tsuchiya, M.-C. Duval, C. Jouvet, O. Benoist d'Azy, B. Soep, *J. Chem. Phys.* **1988**, *89*, 2975.
[144] C. Crépin, F. Legay, N. Legay-Sommaire, A. Tramer, *Chem. Phys.* **1987**, *111*, 169.
[145] See, for example: W. Scherer, P. Sirsch, D. Shorokhov, M. Tafipolsky, G. S. McGrady, *Chem. Eur. J.* **2003**, *9*, 6057.
[146] See also the discussion in: K. I. Goldberg, D. M. Hoffman, R. Hoffmann, *Inorg. Chem.* **1982**, *21*, 3863.
[147] J. Pilmé, B. Silvi, M. Alikhani, *J. Phys. Chem. A* **2003**, *107*, 4506.
[148] S. Ikuta, *Chem. Phys.* **1985**, *95*, 235.
[149] See also the discussion in: H.-J. Himmel, *Z. Anorg. Allg. Chem.* **2005**, *631*, 1551.
[150] N. Kuganathan, J. C. Green, H.-J. Himmel, *New J. Chem.* **2006**, *30*, 1253.
[151] A. D. Becke, *J. Chem. Phys.* **1993**, *98*, 5648. P. J. Stephens, F. J. Devlin, C. F. Chabalowski, M. J. Frisch, *J. Phys. Chem.* **1994**, *98*, 11623.
[152] R. Ahlrichs et al., TURBOMOLE, http://www.cosmologic.de/turbomole.html.
[153] A. Schäfer, C. Huber, R. Ahlrichs, *J. Chem. Phys.* **1994**, *100*, 5829.
[154] T. H. Dunning, Jr., *J. Chem. Phys.* **1989**, *90*, 1007; D. E. Woon, T. H. Dunning, Jr., *J. Chem. Phys.* **1994**, *100*, 2975.
[155] J. N. Harvey, *Struct. Bonding (Berlin)* **2004**, *112*, 151.

 © 2006 Wiley-VCH Verlag GmbH & Co. KGaA, Weinheim

[156] M. Reiher, O. Salomon, B. A. Hess, *Theor. Chem. Acc.* **2001**, *107*, 48; M. Reiher, *Inorg. Chem.* **2002**, *41*, 6928; O. Salomon, M. Reiher, B. A. Hess, *J. Chem. Phys.* **2002**, *117*, 4729.
[157] J. Neugebauer, M. Reiher, C. Kind, B. A. Hess, *J. Comput. Chem.* **2002**, *23*, 895.
[158] a) M. Reiher, J. Neugebauer, B. A. Hess, *Z. Phys. Chem.* **2003**, *217*, 91; b) J. Neugebauer, B. A. Hess, *J. Chem. Phys.* **2003**, *118*, 7215; c) M. Reiher, G. Brehm, S. Schneider, *J. Phys. Chem. A* **2004**, *108*, 734.
[159] a) K. L. Bak, J. Gauss, P. Jørgensen, J. Olsen, T. Helgaker, J. F. Stanton, *J. Chem. Phys.* **2001**, *114*, 6548; b) F. Pawowski, A. Halkier, P. Jørgensen, K. L. Bak, T. Helgaker, W. Klopper, *J. Chem. Phys.* **2003**, *118*, 2539.

 © 2006 Wiley-VCH Verlag GmbH & Co. KGaA, Weinheim

Chemical Dynamics

DOI: 10.1002/anie.200601985

Intramolecular Orbital Alignment Observed in the Photodissociation of [D_1]Thiophenol**

Jeong Sik Lim, Ivan S. Lim, Kyoung-Seok Lee, Doo-Sik Ahn, Yoon Sup Lee, and Sang Kyu Kim**

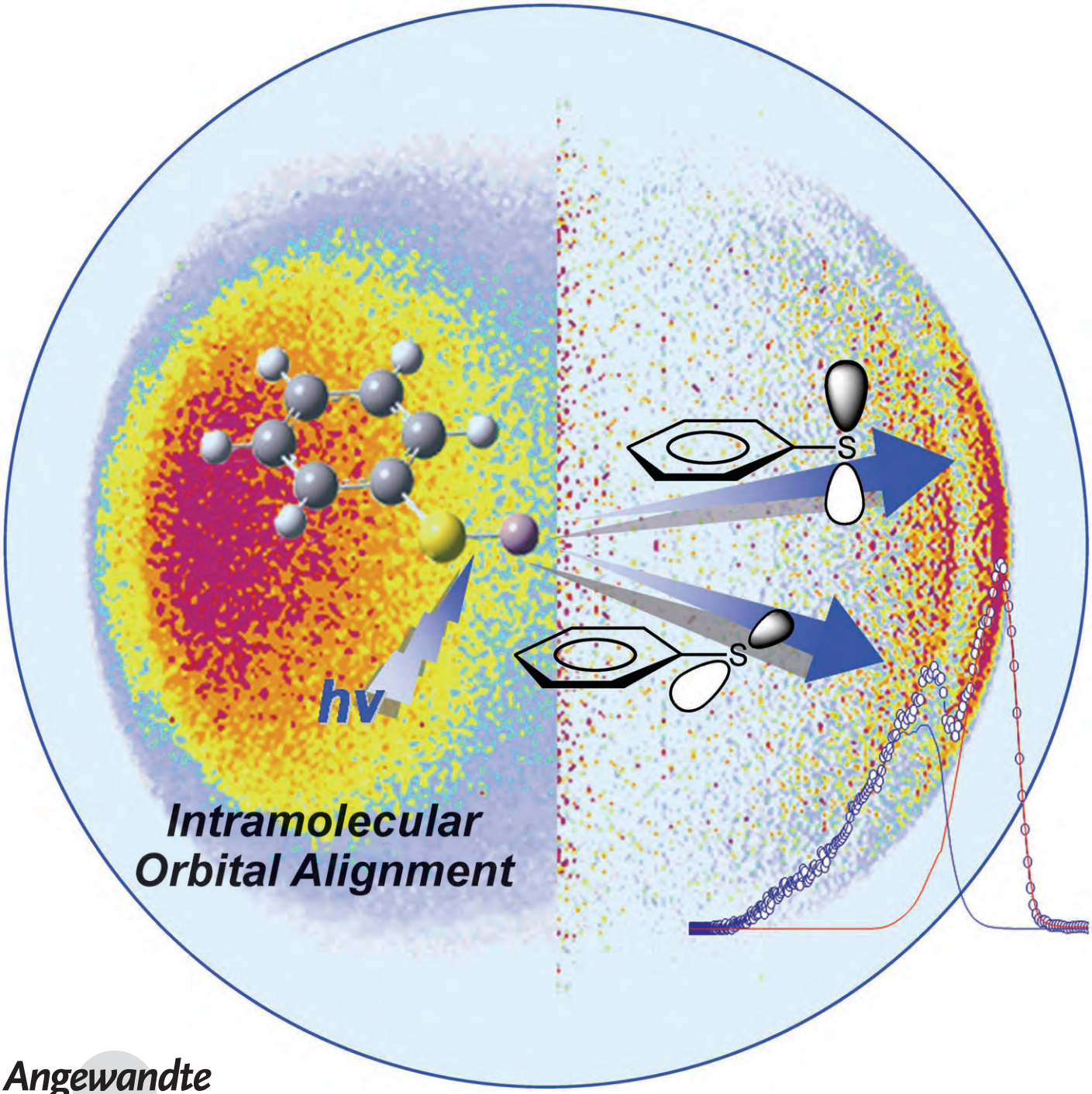

WILEY InterScience DISCOVER SOMETHING GREAT

© 2006 Wiley-VCH Verlag GmbH & Co. KGaA, Weinheim

One of the most active topics in stereodynamics is the orientation and alignment of molecules with respect to the laboratory or recoil frame. Steric effects have long been recognized as an important factor for the explanation of the experimentally measured rate constants with theoretical models based on the simple version of collision theory. The basic concept behind the steric factor is that the chemical reactivity in bimolecular reactions is significantly affected by the relative orientation of the reactants at the moment of collision.

Brilliant experiments have been carried out[1–11] to demonstrate the molecular alignment, and excellent review articles in the area of chemical dynamics have appeared.[12–20] In particular, a major effort has gone into the development of experimental and theoretical tools for the alignment of reactants in the laboratory frame. One of the most commonly utilized tools is based on the manipulation of the nuclear framework in the laboratory-fixed axes, which arise from the interaction of the molecular permanent (or transition) dipole moments with an external electric (or optical) field.[8] A typical example is the collision between a free metal atom and an oriented symmetric-top molecule, such as potassium or rubidium atoms and oriented methyl iodide.[9,14] In that case, one obtains a different yield according to the orientation of the symmetric-top molecule, which enables one to explore stereoselective chemistry in terms of the chemical shape.[17]

A conceptually different kind of alignment is known for open-shell systems.[10–13] In this case, the electronic orbital is aligned either in the laboratory or recoil frame subsequent to the reactive (or inelastic) collision, photodissociation, or gas–surface collision. Typically, diatomic molecules have been subjected to such experiments.[10,11] For example, the relative population in Λ-doublet states of diatomic fragments such as OH(…$\sigma^2\pi^3$;$X^2\Pi$), NO(…$\sigma^2\pi^1$;$X^2\Pi$), and NH*(…$\sigma^1\pi^3$;$c^1\Pi$) have been used as a clue for determining the planarity of the photodissociation process. This is attributed to the fact that the singly occupied molecular orbital (SOMO) in the classical limit is either parallel or perpendicular to the rotating plane.[11]

As an extension, one may consider a rather different case of orbital alignment. Here, one recognizes and maintains the essential ingredients of the recoil frame orbital alignment with the exception of the reference frame with respect to which the orbital alignment is achieved. In other words, one introduces a frame of reference within the molecule so that an intramolecular orbital alignment is achieved on the molecular frame defined by symmetry. As the orbital alignment is genuinely provided and maintained within the molecule, one eliminates the need to work with rotating planes. One of the easiest examples of such cases is hydrogen-abstracted planar aromatic radicals. These species have been known to exist in so-called π and σ structures,[21] which arise from the relative orientation of the SOMO with respect to the molecular plane defined by the benzene moiety. However, there is no report of experimental generation of such orbital-aligned species because an experimental observation of electronically forbidden transitions is difficult.[22]

Herein, we investigate the deuterium-detachment photodissociation of jet-cooled [D_1]thiophenol (C_6H_5SD) by the velocity map ion imaging technique using the (2+1) ionization of D at 243.0 nm. The speed and angular distribution of the nascent D fragment provide the first experimental observation for the photoinduced products of phenylthiyl radical (C_6H_5S) species. Through our theoretical work we show that these radical species are characterized by the relative orientation of the SOMO with respect to the molecular frame.

The raw and reconstructed images of the photodissociated deuterium ion are shown in Figure 1. A detailed description of the experimental setup and data analysis was reported earlier.[23] Both images consisting of two energy distributions give rise to two peaks in the total translational energy distribution which are located at 24.7 and 32.4 kcal mol^{-1}, respectively (Figure 2). The corresponding anisotropy parameters, β, are -1 and -0.76 for the respective large and small total translational energies.[24] It is inferred that the observed peaks arise from two different quantum states of phenylthiyl radical which may be reached by at least two distinct dissociation pathways. The observation of two different quantum states are clearly supported by the deconvoluted translational energy distribution plot shown in Figure 2, which was obtained using Equation (1), where $\beta(E)$ is the anisotropy parameter as a function of the translational energy E, $P_1(E)$ and $P_2(E)$ represent the population of the D fragment belonging to $\beta=-1$ and $\beta=-0.76$ channels, respectively, with $P_1(E) + P_2(E) = 1$.

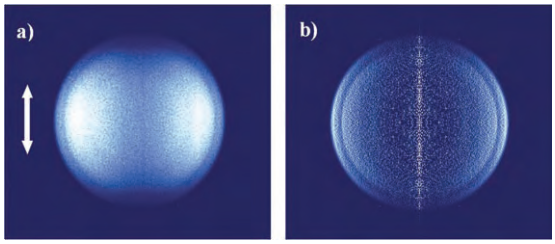

Figure 1. a) 2D projection of the raw 3D distribution and b) the central slice of the reconstructed 3D distribution of the deuterium ion from the photodissociation of C_6H_5SD at 243.0 nm. The vertical arrow indicates the polarization of the pump laser pulse.

[*] J. S. Lim, Dr. I. S. Lim, Dr. K.-S. Lee,[+] D.-S. Ahn, Prof. Y. S. Lee, Prof. S. K. Kim
Department of Chemistry and
School of Molecular Science (BK21)
Korea Advanced Institute of science and Technology (KAIST)
Daejoen 305-701 (Republic of Korea)
Fax: (+82) 42-869-2810
E-mail: yoonsuplee@kaist.ac.kr
sangkyukim@kaist.ac.kr

[+] Current address:
Korea Research Institute of Standards and Science

[**] This research was supported by the Pure Basic Science Research Groups of Korea Research Foundation (KRF-2005-070-C00063), CNMM of KIMM (M102KN010010-05K1401-01010), and the Supercomputing Center of KISTI.

 © 2006 Wiley-VCH Verlag GmbH & Co. KGaA, Weinheim

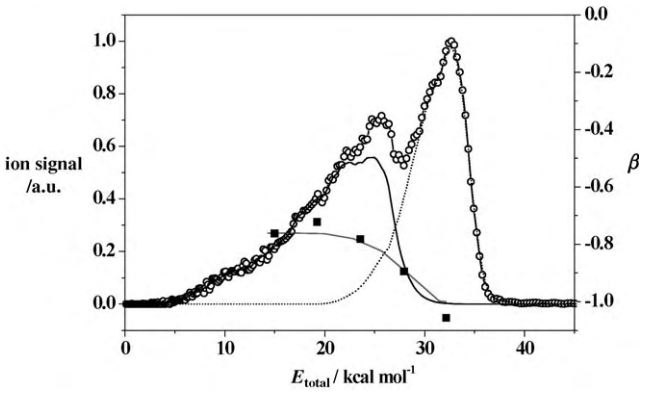

Figure 2. Plot of the total translational energy (E_{total}) distribution and the anisotropy parameter, β. The plot shows the overall distribution (○), deconvoluted $\tilde{X}(B_1)$ state (•••••), and $\tilde{A}(B_2)$ state (——) of the C_6H_5S radical. The averaged anisotropy parameter (β: ■) is plotted versus the transitional energy. The fit using Equation (1) is shown as a gray line.

$$\beta(E) = (-1.00)\,P_1(E) + (-0.76)\,P_2(E) \qquad (1)$$

Our multireference ab initio calculation revealed that there are indeed two close-lying electronic states of the phenylthiyl radical which correspond to the ground state, $\tilde{X}(B_1)$, and the first excited state, $\tilde{A}(B_2)$, separated by 2674 cm^{-1}, as determined at the CASPT2 (complete active space second-order perturbation theory) level in agreement with the experimental value of 2605 ± 84 cm^{-1}. As shown in Figure 3, the essential difference between the radical species arises from the relative orientation of the SOMO with respect to the benzene moiety that defines the molecular plane. The $\tilde{A}(B_2) \leftarrow \tilde{X}(B_1)$ transition is essentially a promotion of an electron from the nonbonding σ(HOMO−1) orbital to the nonbonding π(SOMO) orbital of the ground state. This transition results in an energetic promotion of the in-plane nonbonding orbital and a corresponding demotion of the out-of-plane orbital, which gives the in-plane SOMO for the excited state. During this process the partially bonding π(HOMO−2) orbital of the ground state participates and gives rise to the bonding π(HOMO−2) and antibonding π*(HOMO) orbitals of the excited states. In similar fashion to other hydrogen-detachment reactions of planar aromatic systems such as phenol,[26] there is a crossing of the potential energy curves (PECs) which leads to these two electronic states of the radical along the S–D dissociation coordinates owing to symmetry conservation. Although such an energetic ordering was predicted almost three decades ago,[25] the experimental observation in a photodissociation process is given here for the first time.

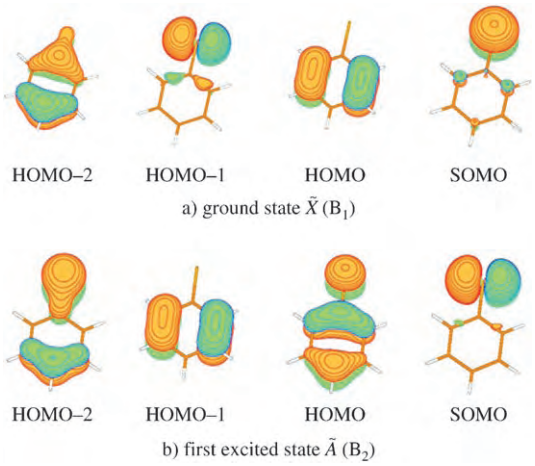

Figure 3. Natural orbitals obtained in a CASSCF(6,6) calculation for the singly occupied (SOMO) and highest doubly occupied molecular orbitals (HOMO), the second HOMO (HOMO−1), and the third HOMO (HOMO−2) of a) the ground state and b) the first electronically excited state of the phenylthiyl radical.

More striking, however, is the indication that the SOMOs of the phenylthiyl radical in both states are largely localized on the sulfur atom and show little π interaction with the adjacent benzene moiety, as depicted in Figure 3. These nonbonding SOMOs, therefore, maintain to a large degree the characteristics of the corresponding atomic p orbitals on sulfur whose relative orientation gives rise to either a perpendicular π(p_x) or a parallel σ(p_y) orbital alignment with respect to the molecular plane for the respective $\tilde{X}(B_1)$ and $\tilde{A}(B_2)$ state of the phenylthiyl radical. In contrast to the Λ-doublet species for which the orbital alignment is defined according to the virtual plane induced by a nuclei rotation, the present case reveals a situation where an orbital alignment occurs naturally as photodissociation products result from an electronic excitation (Figure 4). The chemical significance of this case lies in the expectation that the molecular-frame-aligned orbital may present a reactive center with atomic-orbital-like characteristics. This may lead to stereoselective chemical reactivity, thus introducing a new stereodynamic feature in chemical reactions. The orbital aligned with respect to the molecular frame can make experimental investigation of stereospecific dynamics quite simple because no laboratory-frame alignment or orientation is necessary.

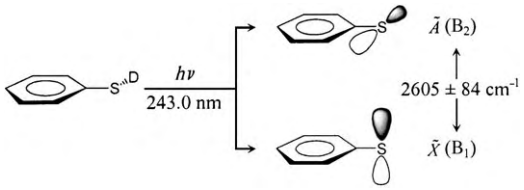

Figure 4. The two close-lying electronic states of the phenylthiyl radical corresponding to the ground and first excited states.

In conclusion, we have presented an example of a novel case of orbital alignment for the phenylthiyl radical generated by the photodissociation of thiophenol. Clear directionality with well-defined alignment of the orbital makes the present case stand out from the so-called π and σ structures of similar planar aromatic systems.[26] A small energy difference between the $\tilde{X}(B_1)$ and $\tilde{A}(B_2)$ states of the C_6H_5S radical suggests that the lifetime of the upper state should be long enough for further chemical reactions. Whether or not the intramolecular orbital alignment of the phenylthiyl radical will affect the chemical reactivity will be an important

 © 2006 Wiley-VCH Verlag GmbH & Co. KGaA, Weinheim

question, for instance, in bimolecular reactions. It will also be interesting to investigate the effect of orbital alignment in terms of the molecular structure and reactivity upon complexation of the phenylthiyl radical with a metal. A detailed theoretical investigation on the photodissociation dynamics of thiophenol is underway, and the results will be reported soon. This will serve as a guide in the controlled production of molecule-frame orbital-aligned radical species by, for example, tuning the excitation wavelength.

Experimental Section

[D_1]Thiophenol (>80%) was mixed with He to be expanded into vacuum through a nozzle orifice with a backing pressure of 3 atm. The wavelength of the pump/probe laser pulse ($\Delta t \approx 5$ ns) was continuously scanned over the entire Doppler width of the D fragment while the corresponding image was being taken. The image was averaged over 36000 laser shots. The three-dimensional image was reconstructed by using the BASEX algorithm.[27]

Received: May 18, 2006

Keywords: ab initio calculations · deuterium · molecular orbitals · photodissociation · radicals

[1] J. P. J. Driessen, S. R. Leone, *J. Phys. Chem.* **1992**, *96*, 6136 – 6146.
[2] H. Hou, S. J. Gulding, C. T. Rettner, A. M. Wodke, D. J. Auerbach, *Science* **1997**, *277*, 80 – 81.
[3] T. P. Rakitzis, A. J. van den Brom, M. H. M. Janssen, *Science* **2004**, *303*, 1852 – 1854.
[4] M. H. M. Janssen, J. W. G. Mastenbroek, S. Stolte, *J. Phys. Chem. A* **1997**, *101*, 7605 – 7613.
[5] A. G. Smolin, O. S. Vasyutinskii, E. R. Wouters, A. G. Suits, *J. Chem. Phys.* **2004**, *121*, 6759 – 6770.
[6] C. Murray, J. K. Pearce, S. Rudic, B. Retail, A. J. Orr-Ewing, *J. Phys. Chem. A* **2005**, *109*, 11093 – 11102.
[7] E. R. Wouters, M. Beckert, L. J. Russell, K. N. Rosser, A. J. Orr-Ewing, M. N. R. Ashfold, O. S. Vasyutinskii, *J. Chem. Phys.* **2002**, *117*, 2087 – 2096.
[8] a) K. H. Kramer, R. B. Bernstein, *J. Chem. Phys.* **1965**, *42*, 767 – 770; b) A. Lübbert, G. Rotzoll, F. Günther, *J. Chem. Phys.* **1978**, *69*, 5174 – 5179; c) U. Hefter, G. Ziegler, A. Mattheus, A. Fischer, K. Bergmann, *J. Chem. Phys.* **1986**, *85*, 286 – 302; d) M. J. J. Vrakking, S. Stolte, *Chem. Phys. Lett.* **1997**, *271*, 209 – 215; e) L. Cai, J. Marango, B. Friedrich, *Phys. Rev. Lett.* **2001**, *86*, 775 – 778; f) H. Stapelfeldt, T. Seideman, *Rev. Mod. Phys.* **2003**, *75*, 543 – 557.
[9] a) P. R. Brooks. , E. M. Jones, *J. Chem. Phys.* **1966**, *45*, 3449 – 3450; b) R. J. Beuhler, Jr., R. B. Bernstein, *J. Chem. Phys.* **1969**, *51*, 5303 – 5315; c) D. H. Parker, K. K. Chakravorty, R. B. Bernstein, *J. Phys. Chem.* **1981**, *85*, 466 – 468; d) H. J. Loesch, A. Remcheid, *J. Chem. Phys.* **1990**, *93*, 4779 – 4790; e) J. J. van Leuken, J. Bulthuis, S. Stoke, H. J. Loesch, *J. Phys. Chem.* **1995**, *99*, 13582 – 13590.
[10] a) J. Derouard, T. N. Nguyen, N. Sadeghi, *J. Chem. Phys.* **1980**, *72*, 6698 – 6705; b) R. P. Mariella, Jr., B. Lantzch, V. T. Maxson, A. C. Luntz, *J. Chem. Phys.* **1978**, *69*, 5411 – 5418; c) E. J. Murphy, J. H. Brophy, G. C. Arnold, W. F. Dimpfl, J. L. Kinsey, *J. Chem. Phys.* **1981**, *74*, 324 – 330.
[11] a) F. Alberti, A. E. Douglas, *Chem. Phys.* **1978**, *34*, 399 – 402; b) A. M. Quinton, J. P. Simons, *Chem. Phys. Lett.* **1981**, *81*, 214 – 217; c) P. Andersen, G. S. Ondrey, B. Titze, E. W. Rothe, *J. Chem. Phys.* **1984**, *80*, 2548 – 2569; d) R. Vasudev, R. N. Dixon, R. N. Zare, *J. Chem. Phys.* **1984**, *80*, 4863 – 4878; e) K.-H. Gericke, S. Klee, F. J. Comes, R. N. Dixon, *J. Chem. Phys.* **1986**, *85*, 4463 – 4479.
[12] R. B. Bernstein, D. R. Herschbach, R. D. Levine, *J. Phys. Chem.* **1987**, *91*, 5365 – 5377.
[13] J. P. Simons, *J. Phys. Chem.* **1987**, *91*, 5378 – 5387.
[14] D. H. Parker, H. Jalink, S. Stolte, *J. Phys. Chem.* **1987**, *91*, 5427 – 5437.
[15] R. D. Levine, *J. Phys. Chem.* **1990**, *94*, 8872 – 8880.
[16] A. J. Orr-Ewing, R. N. Zare, *Annu. Rev. Phys. Chem.* **1994**, *45*, 315 – 366.
[17] H. J. Loesch, *Annu. Rev. Phys. Chem.* **1995**, *46*, 555 – 594.
[18] A. J. Alexander, B. Mark, K. S. Kalogerakis, J. P. Simons, *Chem. Soc. Rev.* **1998**, *27*, 405 – 415.
[19] A. J. Orr-Ewing, *J. Chem. Soc. Faraday Trans.* **1996**, *92*, 881 – 900.
[20] V. Aquilanti, M. Bartolomei, F. Pirani, D. Cappelletti, F. Vecchiocattivi, Y. Shimizu, T, Kasai, *Phys. Chem. Chem. Phys.* **2005**, *7*, 291 – 300.
[21] E. M. Evleth, P. M. Horowitz, T. S. Lee, *J. Am. Chem. Soc.* **1973**, *95*, 7948 – 7955.
[22] a) K. Shibuya, M. Nemoto, A. Yanagibori, M. Fukushima, K. Obi, *Chem. Phys.* **1988**, *121*, 237 – 244; b) G. N. R. Tripathi, Q. Sun, D. A. Armstrong, D. M. Chipman, R. H. Schuler, *J. Phys. Chem.* **1992**, *96*, 5344 – 5350.
[23] K. S. Lee, J. S. Lim, D. S. Ahn, K. W. Choi, S. K. Kim, *J. Chem. Phys.* **2006**, *124*, 124307.
[24] An extreme β value for a fast channel means a direct dissociation on a repulsive PEC. On the other hand, slightly reduced β values may arise for a slow channel caused by a slightly longer lifetime owing to factors such as intersystem crossing to a lower triplet state, for example.
[25] E. M. Evleth, O. Chalvet, P. Balmiere, *J. Phys. Chem.* **1977**, *81*, 1913 – 1917.
[26] a) A. L. Sobolewski, W. Domcke, C. Dedonder-Lardeux, C. Jouvet, *Phys. Chem. Chem. Phys.* **2002**, *4*, 1093 – 1100; b) L. Zhenggang, W. Domcke, V. Vallet, A. L. Sobolewski, S. Mahapatra, *J. Chem. Phys.* **2005**, *122*, 224315.
[27] V. Dribinski, A. Ossadtchi, V. A. Mandelshtam, H. Reisler, *Rev. Sci. Instrum.* **2002**, *73*, 2634 – 2642.

 © 2006 Wiley-VCH Verlag GmbH & Co. KGaA, Weinheim

Polyaromatic Compounds

DOI: 10.1002/anie.200602428

Tandem Ring Expansion of Alkenyl Benzocyclobutenol Derivatives into Substituted Naphthols**

*Toshiyuki Hamura, Takeaki Suzuki, Takashi Matsumoto, and Keisuke Suzuki**

In our continuing studies on the synthesis of polyaromatic compounds,[1] we previously reported thermal conversion of alkenyl benzocyclobutene **A** into functionalized naphthol **C** by tandem electrocyclic reactions [Eq. (1)].[2] We report

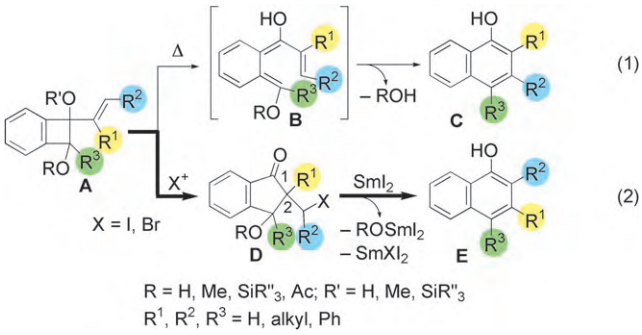

herein a process that is capable of converting the same starting material **A** into *isomeric* naphthol **E** [Eq. (2)]. The process involves two successive ring enlargements (**A**→**D**→**E**): the halonium ion (X^+) induces ring expansion of alkenyl benzocyclobutene **A** (four-membered ring) to indanone **D** (five-membered ring), and SmI_2 promotes expansion of **D** to naphthol **E** (six-membered ring) with concomitant elimination of $ROSmI_2$.

This tandem 4→5→6 ring-enlargement process starts with the 4→5 ring enlargement triggered by the halogenation of diol derivative **1** (Table 1).[3] When alcohol **1** was treated with ICl (1.5 equivalents) in THF (0°C→RT), the ring enlargement occurred smoothly to give iodomethyl indanone **2a** in 90% yield as a mixture of stereoisomers (Table 1, entry 1).[4] An NOE study showed that the major product of **2a** has the *cis* configuration with respect to the iodomethyl and the acetoxy groups. Similarly, bromination of **1** was also effective (1.5 equivalents NBS, CH_2Cl_2, −78→−10°C) and gave bromomethyl indanone **2b** in quantitative yield (Table 1, entry 2).

Table 1: 4→5 Ring enlargement triggered by the halogenation of diol derivative **1**.

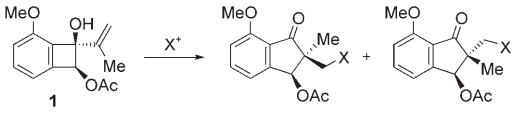

Entry	Conditions	Yield [%]	*cis*/*trans*
1	ICl, THF, 0°C→RT	90	1.6:1
2	NBS, CH_2Cl_2, −78→−10°C	quant.	3.2:1

Ac = acetyl, NBS = *N*-bromosuccinimide.

The second step, 5→6 ring enlargement, is the intramolecular Barbier-type reaction of halomethyl indanone and subsequent Grob fragmentation[5] of the resulting cyclopropanol intermediate (Table 2).[6]

Table 2: 5→6 Ring enlargement by an intramolecular Barbier-type reaction and subsequent Grob fragmentation of halomethyl indanone **2**.

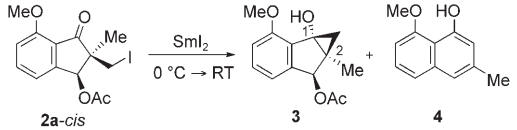

Entry	Conditions	*t* [h]	Yield of **3** [%]	Yield of **4** [%]
1	THF/HMPA[a]	8	15[d]	78
2	THF/HMPA,[a] $BF_3{\cdot}Et_2O$[b]	2.5	–	82
3	CH_3CN[c]	4	–	79

[a] 11–14% HMPA. [b] 2.0–2.5 equivalents. [c] SmI_2 in CH_3CN. [d] Cyclopropanol **3** has the *trans* configuration with respect to the hydroxy and acetoxy groups on the five-membered ring. HMPA = hexamethyl phosphoramide.

Indanone **2a**-*cis* was used for the initial model study, which revealed several sets of suitable conditions. Upon treatment of **2a**-*cis* with SmI_2 (0.1M in THF) in THF/HMPA, the starting material was quickly consumed, thereby giving naphthol **4** in 78% yield and a sizable amount of cyclopropanol **3** (Table 2, entry 1).[7] Monitoring of the reaction by TLC showed the initial formation of cyclopropanol **3**, which was gradually consumed to give naphthol **4**. The process is rationalized by selective cleavage of the C1−C2 bond and elimination of samarium acetate. Although prolonged reaction time and/or higher reaction temperature was incapable of driving the in situ conversion of cyclopropanol **3** to the final product **4**, we were pleased to find that the conversion was facilitated by the presence of $BF_3{\cdot}Et_2O$ (Table 2, entry 2) or by the use of CH_3CN *as the solvent* (Table 2, entry 3), thus giving naphthol **4** in high yield.[8,9]

With these results in hand, we attempted to carry out the two consecutive reactions *in one pot*, which proved to be successful. Thus, alcohol **1** was treated with ICl (1.4 equiv-

[*] Dr. T. Hamura, T. Suzuki, Dr. T. Matsumoto, Prof. Dr. K. Suzuki
Department of Chemistry
Tokyo Institute of Technology, and SORST
Japan Science and Technology Agency (JST)
2-12-1 O-okayama, Meguro-ku, Tokyo 152-8551 (Japan)
Fax: (+81) 3-5734-2788
E-mail: ksuzuki@chem.titech.ac.jp

[**] This research was partially supported by the 21st Century COE program and Grant-in-Aid for Young Scientists (B). T.S. is grateful to JSPS for a predoctoral fellowship.

Supporting information for this article is available on the WWW under http://www.angewandte.org or from the author.

InterScience
© 2006 Wiley-VCH Verlag GmbH & Co. KGaA, Weinheim

alents) in THF at 0 °C, and the reaction was stirred for 40 minutes at room temperature. The reaction mixture was again chilled to 0 °C, and 3.4 equivalents of SmI_2 (0.07 M in CH_3CN) was added. Subsequent stirring at room temperature for four hours cleanly gave naphthol **4** as the sole product in 97 % yield [Eq. (3)]. The almost quantitative yield in this

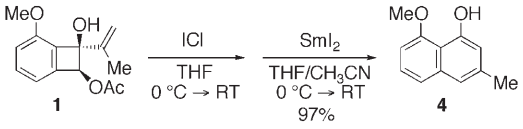

(3)

particular instance implies that both isomers of the initially formed indanones **2a**-*cis* and **2a**-*trans* took part in the second 5→6 ring enlargement. Importantly, this one-pot procedure gave a higher yield of **4** than the overall yield by the reactions that were performed separately.

Table 3 shows the application of this one-pot protocol to various substrates. Under the same conditions, the reaction of compound **5**, isomeric to **1**, also proceeded smoothly (Table 3,

Table 3: One-pot preparation of substituted naphthols.

Entry	Benzocyclobutene[a]	Product		Yield [%]
1	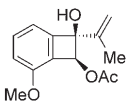	**5**	**10**	85
2	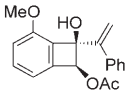	**6**	**11**	96
3	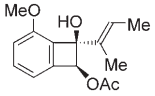	**7**	**12**	88
4	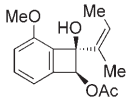	**8**	**12**	77
5	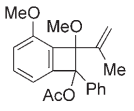	**9**	**13**	78

[a] Conditions: ICl, THF, 0 °C→RT (20–40 minutes), then SmI_2 in CH_3CN, 0 °C→RT (1.5–4 hours).

entry 1). Likewise, the reaction of α-styryl alcohol **6** gave naphthol **11** in 96 % yield (Table 3, entry 2). The reactions worked well with substrates **7** and **8**, which have one additional methyl group at the β position of the olefin with *E* or *Z* geometry, and afforded the tetrasubstituted naphthalene **12** in high yields (Table 3, entries 3 and 4).[10] Arylated substrate **9**[11] also underwent smooth ring expansion to give 78 % yield of aryl naphthalene **13** (entry 5).

Furthermore, the process of successive ring enlargement proved to be applicable to substrates with more highly substituted olefinic moieties [Eq. (4)]. Treatment of **14** with NBS in the presence of silica gel[12] gave the bromoisopropyl

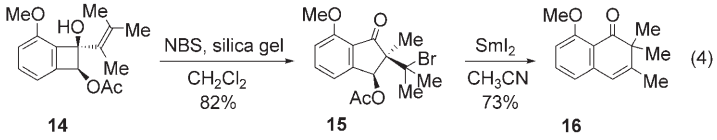

(4)

indanone **15**, which was smoothly converted into the corresponding ketone **16** by the Barbier reaction. ICl was ineffective in this case and gave only a complex mixture of products, presumably because of the instability of the intermediary tertiary alkyl iodide.

The process is applicable to the synthesis of natural-product-like structures, such as angucycline-type tetracycle **18** (Scheme 1).[13] After treatment of compound **17**,[11] which has

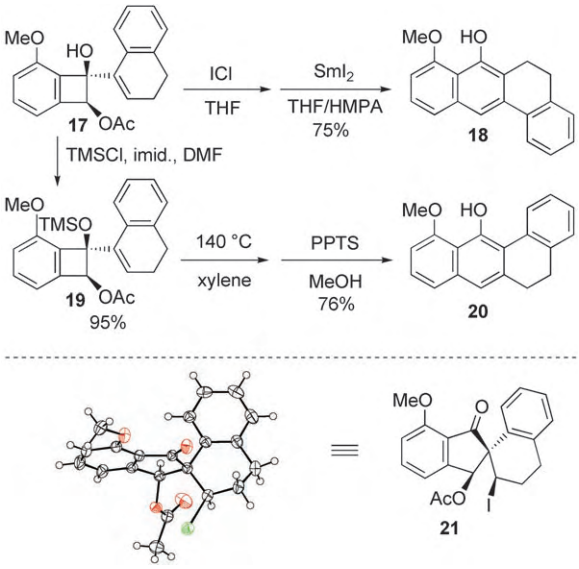

Scheme 1. Divergent sSynthesis of isomeric tetracyles **18** and **20**. Lower left: molecular structure of **21**; thermal ellipsoids set at 50 % probability (O red, I green). PPTS = pyridinium *p*-toluenesulfonate; imid. = imidazole.

a dihydronaphthalene substituent, with ICl (THF, 0 °C→RT, 0.5 hours), the reaction was warmed to 40 °C, and HMPA and subsequently SmI_2 (0.1 M in THF, 10 minutes) were added to afford the angular tetracycle **18**[11] in 75 % yield. It should be noted that this one-pot reaction proceeded smoothly even though the intermediates that are involved should have highly strained polycyclic structures.

It is thus interesting to note the X-ray structure of spiroketone **21**[14] (the major isomer), which was obtained by interception of the above process at the initial iodination stage (92 % yield, major/minor 2.4:1). The structure is intriguing in relation to the synthesis of polycyclic natural products containing a spiro center.[15] The stereoselectivity of the iodination was enhanced to 5.6:1 by employing $BnMe_3N^+ICl_2^-$ as the iodinating agent.

This process constitutes one of the two complementary processes that allow divergent syntheses of isomeric polyaromatic compounds from a single starting material. Indeed, the

 © 2006 Wiley-VCH Verlag GmbH & Co. KGaA, Weinheim

isomeric angular tetracycle **20**[11] was accessible from the same alcohol **17** in high yield by silylation, thermolysis, and desilylation of the initially formed ring-expanded product [see Eq. (1)].

In summary, we have described a facile synthesis of substituted polyaromatic compounds by successive ring expansion of alkenyl benzocyclobutenes. Further studies are currently in progress.

Experimental Section

General experimental procedures for the synthesis of naphthols (one-pot procedure): A solution of acetate **1** (121 mg, 0.489 mmol) in THF (2.0 mL) was added to a solution of ICl (114 mg, 0.702 mmol) in THF (1.5 mL) at 0 °C. The reaction was stirred for 40 min at room temperature. SmI_2 (0.07 M in CH_3CN, 24 mL, 1.7 mmol) was added to the reaction mixture at 0 °C, and the temperature raised to room temperature. After 4 h, the reaction was quenched with saturated aqueous NH_4Cl. The products were extracted with EtOAc (3 × 10 mL), and the combined organic extracts were washed with brine, dried over Na_2SO_4, and concentrated in vacuo. The residue was purified by silica gel flash column chromatography (hexane/EtOAc = 9:1) to give naphthol **4** (89.3 mg, 97.0 %).

Received: June 16, 2006
Published online: August 28, 2006

Keywords: halogenation · polyaromatic compounds · reductive coupling · ring expansion · strained molecules

[1] a) D. Astruc, *Modern Arene Chemistry*, Wiley-VCH, Weinheim, **2002**; b) C. B. de Koning, A. L. Rousseau, W. A. L. van Otterlo, *Tetrahedron* **2003**, *59*, 7 – 36.

[2] a) T. Matsumoto, T. Hamura, M. Miyamoto, K. Suzuki, *Tetrahedron Lett.* **1998**, *39*, 4853 – 4856; b) T. Hamura, M. Miyamoto, T. Matsumoto, K. Suzuki, *Org. Lett.* **2002**, *4*, 229 – 232; c) T. Hamura, M. Miyamoto, K. Imura, T. Matsumoto, K. Suzuki, *Org. Lett.* **2002**, *4*, 1675 – 1678; d) K. Ohmori, K. Mori, Y. Ishikawa, H. Tsuruta, S. Kuwahara, N. Harada, K. Suzuki, *Angew. Chem.* **2004**, *116*, 3229 – 3233; *Angew. Chem. Int. Ed.* **2004**, *43*, 3167 – 3171; e) A. K. Sadana, R. K. Saini, W. E. Billups, *Chem. Rev.* **2003**, *103*, 1539 – 1602, and references therein.

[3] Starting compounds were readily available from various benzocyclobutenones; see: a) T. Hosoya, T. Hasegawa, Y. Kuriyama, T. Matsumoto, K. Suzuki, *Synlett* **1995**, 177 – 179; b) T. Hamura, T. Hosoya, H. Yamaguchi, Y. Kuriyama, M. Tanabe, M. Miyamoto, Y. Yasui, T. Matsumoto, K. Suzuki, *Helv. Chim. Acta* **2002**, *85*, 3589 – 3604; see also references [2b], [2c].

[4] For a related iodonium-mediated ring expansion of alkenyl cyclobutanols, see: a) H. Nemoto, M. Shiraki, K. Fukumoto, *J. Org. Chem.* **1996**, *61*, 1347 – 1353; related acid-catalyzed ring expansions of alkenyl cyclobutenols and alkenyl benzocyclobutenols were also reported; see: b) G. B. Stone, L. S. Liebeskind, *J. Org. Chem.* **1990**, *55*, 4614 – 4622; c) H. Ziehe, R. Wartchow, H. Butenschön, *Eur. J. Org. Chem.* **1999**, 823 – 835.

[5] a) C. A. Grob, *Angew. Chem.* **1969**, *81*, 543 – 554; *Angew. Chem. Int. Ed. Engl.* **1969**, *8*, 535 – 622; b) C. A. Grob, W. Baumann, *Helv. Chim. Acta* **1955**, *38*, 594 – 603.

[6] For reviews of SmI_2-mediated Barbier reactions, see: a) G. A. Molander, C. R. Harris, *Chem. Rev.* **1996**, *96*, 307 – 338; b) A. Krief, A. M. Laval, *Chem. Rev.* **1999**, *99*, 745 – 777; related reductive cyclization of bromoalkyl ketones and subsequent ring opening of cycloalkanol derivatives were reported: c) E. Hasegawa, H. Tsuchida, M. Tamura, *Chem. Lett.* **2005**, 1688 – 1689; d) G. A. Molander, Y. L. Huérou, G. A. Brown, *J. Org. Chem.* **2001**, *66*, 4511 – 4516; e) P. Dowd, W. Zhang, *Chem. Rev.* **1993**, *93*, 2091 – 2115; related 5→6 ring enlargement of methanoindane to aryl naphthalene was also reported: f) K. Wakasugi, Y. Nishii, Y. Tanabe, *Tetrahedron Lett.* **2000**, *41*, 5937 – 5942; g) I. Takemura, T. Matsumoto, K. Suzuki, *Tetrahedron Lett.* **2006**, *47*, 6677 – 6679.

[7] When the reaction was performed without HMPA, the yield of **4** decreased to 46 % and was accompanied by cyclopropanol **3** (16 %).

[8] This 5→6 ring enlargement was applicable to the bromo substrate **2b** (SmI_2 in THF/HMPA, $BF_3{\cdot}Et_2O$), giving naphthalene **4** in 48 % yield.

[9] Concentration of SmI_2 in CH_3CN was 0.07 M (iodometric titration); recently, solvent effects of SmI_2-mediated reactions were reported: a) B. Hamann, J.-L. Namy, H. B. Kagan, *Tetrahedron* **1996**, *52*, 14225 – 14234; b) P. R. Chopade, T. A. Davis, E. Prasad, R. A. Flowers II, *Org. Lett.* **2004**, *6*, 2685 – 2688.

[10] Previously, we reported the thermolysis of alkenyl benzocyclobutenes that have alkyl groups at the β position of the olefin with *Z* geometry, whereby mainly a 1,7-hydrogen shift occurred to give the ring-opened 1,3-diene derivatives as the major products; see references [2c] and [2d].

[11] For details, see the Supporting Information.

[12] H. Konishi, K. Aritomi, T. Okano, J. Kiji, *Bull. Chem. Soc. Jpn.* **1989**, *62*, 591 – 593.

[13] a) J. Rohr, R. Thiericke, *Nat. Prod. Rep.* **1992**, *9*, 103 – 137; b) M. C. Carreño, A. Urbano, *Synlett*, **2005**, 1 – 25.

[14] CCDC-611287 (**21**) contains the supplementary crystallographic data for this paper. These data can be obtained free of charge from The Cambridge Crystallographic Data Centre via www.ccdc.cam.ac.uk/data_request/cif.

[15] M. Sannigrahi, *Tetrahedron* **1999**, *55*, 9007 – 9071.

 © 2006 Wiley-VCH Verlag GmbH & Co. KGaA, Weinheim

Conformational Switch

DOI: 10.1002/anie.200602084

A Photoswitchable Miniprotein Based on the Sequence of Avian Pancreatic Polypeptide**

Simon Jurt, Andreas Aemissegger, Peter Güntert, Oliver Zerbe, and Donald Hilvert**

Since the early work of Anfinsen, structural biology has been influenced by the dogma that proteins fold into unique structures dictated by their amino acid sequence.[1] However, the recent observation that prion proteins undergo spontaneous conversion from well-folded and soluble helical entities into insoluble β-sheet-containing aggregates suggests that this view is overly simplistic.[2] It also raises the intriguing possibility that conformational switches might be designed to transform proteins deliberately from one unique structure into another unique structure. Such switches could be quite valuable, for example, for studying folding in the absence of denaturants or for controlling receptor function or enzyme activity.

Photochromic compounds, which undergo large conformational changes when exposed to light of an appropriate wavelength, are interesting in this context as they might permit reversible conformational control. Of the many photochromic systems that have been described, azobenzenes are well suited for this type of application as they have been extensively characterized and are readily synthesized. Irradiation at the wavelength of the $\pi\rightarrow\pi^*$ transition converts the thermodynamically favored *trans* to the *cis* isomer, whereas the reverse process can be achieved either thermally or by irradiation at the wavelength of the $n\rightarrow\pi^*$ transition. Azobenzenes have been introduced into many peptides and proteins, both into side chains[3,4] and into the main chain.[5,6] For example, our research group[7] and Moroder and coworkers[8] have shown that the *meta*-substituted Fmoc-protected linker **1** (Scheme 1) can be inserted into a polypeptide backbone through solid-phase peptide synthesis and, in its *cis* configuration, serve as the β-turn-inducing segment in β-hairpin peptides. Thermally induced isomerization from *cis*-**1** to *trans*-**1** results in unfolding of the hairpin.

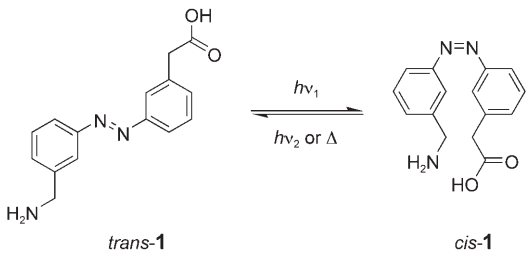

trans-**1** *cis*-**1**

Scheme 1. Interconversion of the *trans*- and *cis*-configured azobenzene derivative **1**. The amino acid sequence of the synthesized peptides is ^{1}GPSQPTYPG-**1**-^{13}PVEDLIRFYNDLQQYLNVVTRHRY-NH_2. For simplicity, the amino acids in the sequence are numbered as in wild-type aPP, with amino acid **1** replacing turn residues 10, 11, and 12.

In this study, we have extended our work to larger helical polypeptides. As a model system, we chose a derivative of avian pancreatic polypeptide (aPP). The 36 residue hormone was one of the first peptides for which a crystal structure was available.[9] It consists of a C-terminal α helix (residues 14–31) connected through a β turn (residues 9–13) to an N-terminal type-II polyproline helix, a structural motif known as the PP fold. In the solid state and in solution, two aPP polypeptides further associate to form a symmetric dimer.[10] Despite its small size, aPP thus displays the features of much larger proteins, that is, it a possesses secondary as well as tertiary and quaternary structure.

To allow switching of the aPP peptide from a back-folded (PP-folded) to an extended form, we replaced the β-turn segment between the helices, comprising residues Asp 10–Asp 11–Ala 12, with **1**. The resulting molecule, which exhibits similar helicity to natural aPP (as determined by circular dichroism spectroscopy), is readily interconverted between the *cis* and *trans* forms upon irradiation. At thermodynamic equilibrium, the *trans*/*cis* ratio is 90:10, but the fraction of *cis*-configured peptide can be increased up to about 85% in the photostationary state. Repeated interconversion between the two states ultimately results in peptide precipitation. However, thermal relaxation from the *cis* to the *trans* configuration is relatively slow in aqueous solution at room temperature (half-life > 2 weeks), enabling detailed biophysical characterization of the molecule. Sedimentation equilibrium analysis indicates that, in contrast to wild-type aPP, purified *cis*-**1**-PP is tetrameric in solution. A molecular weight of 16 kDa is determined assuming a single ideal species, which is in good agreement with the expected mass of 16.8 kDa for a tetramer. Detailed structural information on the effect of the linker on the PP fold was obtained by standard 2D NMR spectroscopic methods (Figure 1).[11]

As shown in Figure 1, *cis*-**1**-PP clearly adopts a back-folded PP structure. The C-terminal α helix, encompassing residues Val 14–Thr 32, exhibits a root-mean-square deviation (RMSD) of 0.67 ± 0.22 Å for all backbone atoms. However, introduction of the azobenzene shifts the position of the turn toward the C terminus, displacing the entire N-terminal

[*] S. Jurt, Priv.-Doz. Dr. O. Zerbe
Institute of Organic Chemistry
University of Zurich
8057 Zurich (Switzerland)
Fax: (+41) 44-635-6882
E-mail: oliver.zerbe@oci.unizh.ch
Dr. A. Aemissegger, Prof. Dr. D. Hilvert
Laboratory of Organic Chemistry
ETH Zurich
8093 Zurich (Switzerland)
Fax: (+41) 44-632-1486
E-mail: hilvert@org.chem.ethz.ch
Priv.-Doz. Dr. P. Güntert
RIKEN Genomic Sciences Center
1-7-22 Suehiro-cho, Tsurumi, Yokohama 230-0045 (Japan)

[**] We thank the ETH Zurich and the University of Zurich for financial support and Joris Beld for operating the analytical ultracentrifuge.

Supporting information for this article is available on the WWW under http://www.angewandte.org or from the author.

 © 2006 Wiley-VCH Verlag GmbH & Co. KGaA, Weinheim

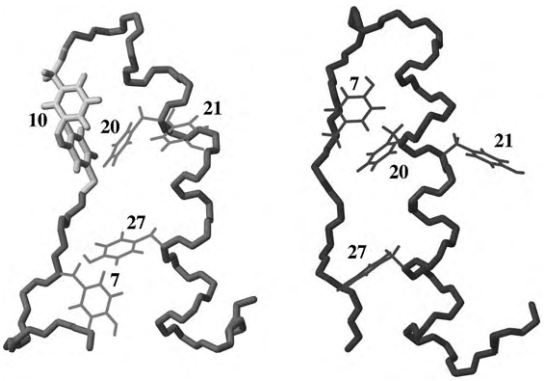

Figure 1. Backbone representation of the monomeric subunits of *cis*-**1**-PP (left) and aPP (right) including the side chains of aromatic residues. In *cis*-**1**-PP, the azobenzene moiety, residue 10, is depicted in pale gray.

segment along the axis of the α helix. The linker itself assumes a relatively extended conformation, despite its *cis* configuration, and forms an aromatic stacking interaction with Phe 20. As a consequence, Tyr 7, which normally contacts Phe 20 in aPP, is able to π stack with Tyr 27, reinforcing the back-fold (Figure 1). Furthermore, we observe a dense network of intermolecular NOEs that define a dimer interface similar to that seen in aPP (Figure 2). As is true for a number of other proteins,[12] aromatic ring-stacking interactions appear to be particularly important in stabilizing this interface. Although the experimental line widths for *cis*-**1**-PP are consistent with the presence of a tetrameric state in solution, we were unable to identify NOEs that allow unambiguous assignment of this higher-order structure. Nonetheless, formation of the tetramer is presumably mediated by the larger exposed hydrophobic surface generated upon replacement of the original Asp–Asp–Ala sequence (Figure 2 D) with the relatively hydrophobic azobenzene (Figure 2 B).

In contrast to *cis*-**1**-PP, *trans*-**1**-PP affords NMR spectra with extremely broad lines, indicating that it is highly aggregated in solution. As a consequence, complete sequential resonance assignment and full structure determination were not possible. Nevertheless, no NOEs were visible in the spectral region in which NOEs between resonances from N- and C-terminal residues were observed in *cis*-**1**-PP, suggesting that *trans*-**1**-PP is not back-folded. Consistent with this inference, other non-back-folded aPP homologues, such as neuropeptide Y,[13,14] are known to form higher-order aggregates at high concentrations.

Receptor binding by peptide hormones related to aPP has been proposed to occur through a mechanism involving initial association of the peptide with the membrane.[13,15] In this model, hydrophobic contacts between residues in the N- and C-terminal regions are replaced by hydrophobic contacts between the C-terminal helix and the membrane, leading to unfolding of the N terminus. As positioning of the N-terminal segment is likely to be the primary difference in the structure between *trans*-**1**-PP and *cis*-**1**-PP, binding of both species to a membrane model such as dodecylphosphocholine (DPC) micelles should result in very similar structures owing to removal of the back-fold in *cis*-**1**-PP. To test this hypothesis, we determined the structures of both *trans*-**1**-PP and *cis*-**1**-PP in the presence of DPC micelles. Strikingly, *trans*-**1**-PP displays line widths that are comparable to *cis*-**1**-PP under these conditions. A superposition of the ensemble of low-energy NMR conformers is depicted in Figure 3. The

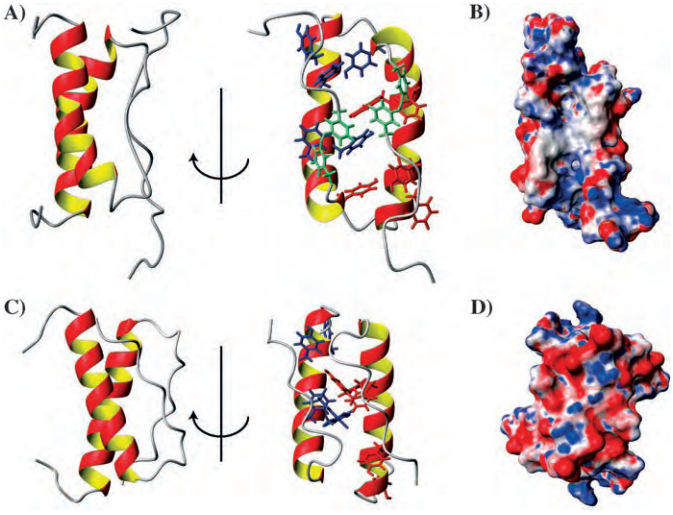

Figure 2. A) Structure of a low-energy NMR conformer of the *cis*-**1**-PP dimer in aqueous solution. The aromatic side chains contributing to the dimer interface are shown in the view at the right. B) Electrostatic surface of the *cis*-**1**-PP dimer with positively and negatively charged surface areas shown in red and blue, respectively. C) Crystal structure of the aPP dimer[9] with the corresponding electrostatic surface (D).

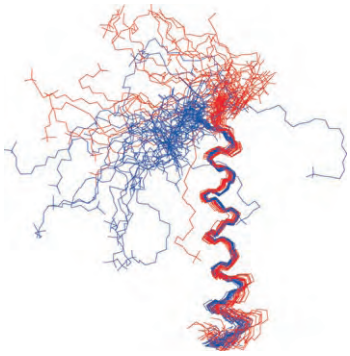

Figure 3. Superposition of the 20 lowest-energy conformers of *trans*-**1**-PP (red) and *cis*-**1**-PP (blue) determined in the presence of DPC micelles. Backbone atoms of residues 14–31 were superimposed in the fit.

structures are highly similar: the C-terminal helix extends over residues 15–28 in both peptides and hydrogen bonds typical for an α helix are populated to approximately the same extent. The N-terminal segment is flexible and no medium- or long-range NOEs were observed. In the absence of DPC micelles, such flexibility, together with exposure of hydrophobic helix residues to solvent, would be expected to promote the formation of aggregates, explaining the broad lines seen for *trans*-**1**-PP in solution.

 © 2006 Wiley-VCH Verlag GmbH & Co. KGaA, Weinheim

To conclude, we have demonstrated that a peptide capable of adopting different tertiary structures can be constructed by inserting an azobenzene linker into the polypeptide backbone, and that a simple transformation (irradiation or heating) can be used to switch from one form to the other. This approach thus complements related efforts to control helix conformation through azobenzene-based photo-cross-linkers between appropriately spaced cysteine side chains.[4] Extrapolating from this proof of principle, we envision that incorporation of amino acid **1** into larger polypeptides or proteins will provide a sensitive means of controlling both folding and function in more complex systems.

Experimental Section

Peptides were prepared by solid-phase peptide synthesis on a 0.1-mmol scale with double coupling of all amino acids except the azobenzene residue **1** by using standard 9-fluorenylmethoxycarbonyl (Fmoc) conditions (20% piperidine in *N*,*N*-dimethylformamide (DMF) for Fmoc deprotection, 1-hydroxy-benzotriazole (HOBt)/benzotriazol-1-yl-*N*-tetramethyluronium hexafluorophosphate (HBTU) for activation, *N*,*N*-diisopropylethylamine (DIPEA) as a base, and *N*-methylpyrrolidinone as solvent) and Ac_2O capping on a Rink amide resin. The peptides were cleaved from the resin with a solution of TFA:H_2O:TIPS (93:5:2; TFA = trifluoroacetic acid, TIPS = triisopropylsilane), purified by reverse-phase HPLC, and characterized by electrospray MS ($[M]^+$ *m*/*z* calcd 4187.7, found 4187.0). Although problems with silanes in the cleavage reaction for azobenzene-containing peptides have been reported,[6] good yields were obtained.

Analytical HPLC showed the presence of both the *trans* (90%) and *cis* (10%) isomers at thermodynamic equilibrium. After irradiation at 320 nm (Philips PL-S 9W/12 compact fluorescent tube), the *cis* content increased to 85%. Both isomers were obtained in greater than 99% purity by preparative HPLC (linear gradient of 5–60% MeCN in H_2O and 0.1% TFA, flow rate 10 mL min^{-1}, Macherey-Nagel Nucleosil 100–7 C18 21 × 250 mm^2 column). UV spectroscopy did not show significant isomerization under the conditions used for NMR measurements.

Sedimentation equilibrium experiments were performed with purified *cis*-**1**-PP on a Beckman Optima XL-A ultracentrifuge with an AnTi60 rotor and two channel Epon charcoal centerpieces at 4 °C and rotor speeds of 30, 35, 40, and 42 krpm in 20 mM acetate buffer solution (pH 4.1) with 80 mM NaCl. The partial specific volume was calculated from the amino acid composition, substituting the azobenzene linker by two phenylalanine residues. Runs were analyzed by using the Ultrascan II software package.[16]

Structure elucidation of the peptides in solution was performed on approximately 2 mM samples at 22 °C in 20 mM acetate buffer solution (pH 4.1) in $H_2O/^2H_2O$ (9:1) or at 37 °C in the presence of 300 mM dodecylphosphocholine micelles and 50 mM *N*-[2-morpholinoethane]sulfonic acid (MES) buffer solution (pH 6.0). Structural data were measured on Bruker DRX-600 and AV-700 instruments. Sequential resonance assignments were obtained by standard procedures by using clean-TOCSY spectra[17] with mixing times of 12 and 40 ms and a NOESY spectrum[18] recorded with 70 ms mixing time and a zero-quantum suppression filter.[19] Spectra were processed with the Bruker TOPSPIN software and transferred into the XEASY program[20] for data analysis. Structures were calculated by using a simulated-annealing protocol based on molecular dynamics in torsion-angle space as implemented in the program CYANA.[21] NOESY cross peaks for the homodimeric model of *cis*-**1**-PP were assigned by a combination of manual[20] and automated approaches[21] with a modified version of the program CYANA 2.1. The modified version takes the homodimer symmetry explicitly into account for the network anchoring of the NOE assignments and ensures an identical conformation of the two monomers by imposing dihedral-angle difference restraints for all corresponding torsion angles. This maintains a symmetric relative orientation of the two monomers by applying distance difference restraints between symmetry related intermolecular Cα–Cα distances.

The final input (including only meaningful restraints) for the structure calculations consisted of 940 upper distance limits in the case of *cis*-**1**-PP in the absence of DPC. Structure calculations were started from 100 starting conformers with random torsion-angle values and used 20000 torsion-angle dynamics steps per conformer. The 20 CYANA conformers with the lowest final target function values were subjected to restrained energy minimization in explicit water against the AMBER force field[22] by using the program OPALp.[23] The computed structures contained no consistent violation of experimental observables and displayed overall good geometric features as judged by the program PROCHECK.[24] Graphics were prepared with the program MOLMOL.[25] The coordinates of the structures have been deposited in the Protein Data Bank under access codes 2H4B (*cis*-**1**-PP), 2H3S (*cis*-**1**-PP bound to DPC micelles), and 2H3T (*trans*-**1**-PP bound to DPC micelles).

Received: May 24, 2006
Published online: August 25, 2006

Keywords: azobenzene · peptides · photochromic compounds · protein folding · tertiary structures

[1] C. B. Anfinsen, *Science* **1973**, *181*, 223.
[2] B. Caughey, *Trends Biochem. Sci.* **2001**, *26*, 235; S. B. Prusiner, M. R. Scott, S. J. DeArmond, F. E. Cohen, *Cell* **1998**, *93*, 337.
[3] O. Pieroni, J. L. Houben, A. Fissi, P. Costantino, F. Ciardelli, *J. Am. Chem. Soc.* **1980**, *102*, 5913; D. Liu, J. Karanicolas, C. Yu, Z. H. Zhang, G. A. Woolley, *Bioorg. Med. Chem. Lett.* **1997**, *7*, 2677; J. R. Kumita, O. S. Smart, G. A. Woolley, *Proc. Natl. Acad. Sci. USA* **2000**, *97*, 3803.
[4] G. A. Woolley, *Acc. Chem. Res.* **2005**, *38*, 486; L. Guerrero, O. S. Smart, C. J. Weston, D. C. Burns, G. A. Woolley, R. K. Allemann, *Angew. Chem.* **2005**, *117*, 7956; *Angew. Chem. Int. Ed.* **2005**, *44*, 7778; G. A. Woolley, A. S. I. Jaikaran, M. Berezovski, J. P. Calarco, S. N. Krylov, O. S. Smart, J. R. Kumita, *Biochemistry* **2006**, *45*, 6075.
[5] L. Ulysse, J. Cubillos, J. Chmielewski, *J. Am. Chem. Soc.* **1995**, *117*, 8466; C. Renner, R. Behrendt, S. Spörlein, J. Wachtveitl, L. Moroder, *Biopolymers* **2000**, *54*, 489; C. Renner, J. Cramer, R. Behrendt, L. Moroder, *Biopolymers* **2000**, *54*, 501.
[6] C. Renner, U. Kusebauch, M. Löweneck, A. G. Milbradt, L. Moroder, *J. Pept. Res.* **2005**, *65*, 4.
[7] A. Aemissegger, V. Kräutler, W. F. van Gunsteren, D. Hilvert, *J. Am. Chem. Soc.* **2005**, *127*, 2929; V. Kräutler, A. Aemissegger, P. H. Hünenberger, D. Hilvert, T. Hansson, W. F. van Gunsteren, *J. Am. Chem. Soc.* **2005**, *127*, 4935.
[8] S. L. Dong, M. Löweneck, T. E. Schrader, W. J. Schreier, W. Zinth, L. Moroder, C. Renner, *Chem. Eur. J.* **2006**, *12*, 1114.
[9] T. L. Blundell, J. E. Pitts, S. P. Tickle, C. W. Wu, *Proc. Natl. Acad. Sci. USA* **1981**, *78*, 4175.
[10] X. A. Li, M. J. Sutcliffe, T. W. Schwartz, C. M. Dobson, *Biochemistry* **1992**, *31*, 1245.
[11] K. Wüthrich, *NMR of Proteins and Nucleic Acids*, 1st ed., Wiley, New York, **1986**.
[12] S. K. Burley, G. A. Petsko, *Science* **1985**, *229*, 23; D. A. Dougherty, *Science* **1996**, *271*, 163; E. A. Meyer, R. K. Castellano, F. Diederich, *Angew. Chem.* **2003**, *115*, 1244; *Angew. Chem. Int. Ed.* **2003**, *42*, 1210.
[13] R. Bader, A. Bettio, A. G. Beck-Sickinger, O. Zerbe, *J. Mol. Biol.* **2001**, *305*, 307.

 © 2006 Wiley-VCH Verlag GmbH & Co. KGaA, Weinheim

[14] S. A. Monks, G. Karagianis, G. J. Howlett, R. S. Norton, *J. Biomol. NMR* **1996**, *8*, 379.
[15] R. Bader, O. Zerbe, *ChemBioChem* **2005**, *6*, 1520; M. Lerch, V. Gafner, R. Bader, B. Christen, G. Folkers, O. Zerbe, *J. Mol. Biol.* **2002**, *322*, 1117; M. Lerch, M. Mayrhofer, O. Zerbe, *J. Mol. Biol.* **2004**, *339*, 1153; M. Lerch, H. Kamimori, G. Folkers, M.-I. Aguilar, A. G. Beck-Sickinger, O. Zerbe, *Biochemistry* **2005**, *44*, 9255.
[16] B. Demeler, Ultrascan II 6.2, The University of Texas, San Antonio, http://www.ultrascan.uthscsa.edu/
[17] C. Griesinger, G. Otting, K. Wüthrich, R. R. Ernst, *J. Am. Chem. Soc.* **1988**, *110*, 7870.
[18] S. Macura, R. R. Ernst, *Mol. Phys.* **1980**, *41*, 95.
[19] G. Otting, *J. Magn. Reson.* **1990**, *86*, 496.
[20] C. Bartels, T.-h. Xia, M. Billeter, P. Güntert, K. Wüthrich, *J. Biomol. NMR* **1995**, *6*, 1.
[21] P. Güntert, *Methods Mol. Biol.* **2004**, *278*, 353.
[22] W. D. Cornell, P. Cieplak, C. I. Bayly, I. R. Gould, K. M. Merz, D. M. Ferguson, D. C. Spellmeyer, T. Fox, J. W. Caldwell, P. A. Kollman, *J. Am. Chem. Soc.* **1995**, *117*, 5179.
[23] R. Koradi, M. Billeter, P. Güntert, *Comput. Phys. Commun.* **2000**, *124*, 139.
[24] R. A. Laskowski, J. A. C. Rullmann, M. W. MacArthur, R. Kaptein, J. M. Thornton, *J. Biomol. NMR* **1996**, *8*, 477.
[25] R. Koradi, M. Billeter, K. Wüthrich, *J. Mol. Graphics* **1996**, *14*, 51.

 © 2006 Wiley-VCH Verlag GmbH & Co. KGaA, Weinheim

Clay Swelling

DOI: 10.1002/anie.200601740

A Thermodynamic Understanding of Clay-Swelling Inhibition by Potassium Ions**

*Xian-Dong Liu and Xian-Cai Lu**

Smectites are important in geological processes and have industrial and engineering applications.[1–3] They consist of negatively charged clay platelets and interlayer counterions. Water can enter the interlayer space and force the clay platelets apart, causing clay swelling.[2,4] Generally, this swelling behavior can be divided into two types: intracrystalline swelling, with a limited amount of adsorbed water, and osmotic swelling, which involves a much larger amount of water. This unique property has resulted in numerous studies because of its direct applicability in civil and petroleum engineering.[3,5] It has been found, for instance, that K-smectites do not expand to the osmotic regime and form crystalline hydrates even in aqueous suspension.[6,7] Thus, the K^+ ion can be used as a swelling inhibitor in drilling mud to prevent the well-bore collapse typically caused by the macroscopic swelling of Na-smectites.[7] However, the fundamental mechanisms of the inhibition of clay swelling by K^+ ions are not clear,[8–10] and the striking stability of the single-layer K-hydrate cannot yet be explained.[10,11]

Herein, we employ molecular simulations to study the thermodynamic constraints imposed by K^+ ions on clay-swelling inhibition, in comparison with the contrasting case of Na^+ ions. We find that the single-layer hydrate of K-smectites actually corresponds to the global minimum of the swelling energy curve and that expansion to the osmotic regime is, therefore, energetically unfavorable. In contrast, the double-layer state of Na-smectites corresponds to the global minimum of the energy curve, and osmotic swelling is easy to achieve. Furthermore, we examine the microstructure of the single-layer K-hydrate and find, for the first time, that the K^+ ions are all tightly confined in coordination cages above surface hexagons, which leads to this surprising stability.

We used Arizona montmorillonite as the smectite model.[12] Constant number pressure temperature (NPT) molecular dynamics simulations were performed using the LAMMPS code[13] to mimic the experimental environments (298 K, 1 atm). Clayff, which incorporates the simple point charge (SPC) water model, was used as the force field.[14] Details are given in the Supporting Information.

It has been shown that the energy contribution to free energy dominates clay swelling and that the entropy term plays only a secondary role.[15–17] The local minima of the swelling energy curve correspond to stable states, namely the single-, double-, or triple-layer hydrates. Hence, the relative stabilities of different states can be determined from Equation (1):[15,16]

$$Q = \langle U(N)\rangle - \langle U(N^0)\rangle - (N-N^0)U_{\mathrm{bulk}} \quad (1)$$

$\langle U(N)\rangle$ is the average potential energy of the hydrate with water content N, N^0 is the water content of the reference state, and U_{bulk} is the internal energy of bulk water. In this study, we selected the state with 425 milligrams of water per gram of clay as the reference. Q is often referred to as the "immersion energy", although it is difficult to compare the calculated results directly with experimentally measured data, owing to the formation of mixed-layer hydrates and external surface contributions.[15] The energy term can also be expressed as the "hydration energy" [Eq. (2)], where $\langle U(0)\rangle$ is the average potential energy of the dry clay.[15]

$$\Delta U = (\langle U(\mathrm{N})\rangle - \langle U(0)\rangle)/N \quad (2)$$

[*] X.-D. Liu, Prof. Dr. X.-C. Lu
Department of Earth Sciences
Nanjing University
and
State Key Laboratory of Mineral Deposit Research
Nanjing 210093 (China)
Fax: (+86) 25-8368-6016
E-mail: xcljun@nju.edu.cn

[**] The authors acknowledge financial support from the National Science Foundation of China (no. 40373024), and the kind help of Dr. T. J. Tambach from the Van't Hoff Institute for Molecular Sciences, Prof. H. Q. Zhou, Prof. J. Ma, Dr. X. Wang, and Dr. X. Zhang.

Supporting Information for this article is available on the WWW under http://www.angewandte.org or from the author.

WILEY InterScience DISCOVER SOMETHING GREAT
© 2006 Wiley-VCH Verlag GmbH & Co. KGaA, Weinheim

The hydration energy is an integral quantity and can be compared with the calorimetry data renormalized by adding the condensation heat of water.[9,18]

Table 1 shows an encouraging agreement between the simulated and experimental basal spacings. Figures 1 and 2 display the calculated hydration and immersion energies,

Table 1: A comparison of simulated basal spacings and measured ranges.

	Sim. [Å]	Exp. [Å]
Single-layer (K)	12.49	11.8–12.6[11,19,21,22]
Double-layer (K)	15.61	15.2–16.0[11,19,21]
Single-layer (Na)	12.19	12.2–12.6[19,21–24]
Double-layer (Na)	15.17	15.0–15.55[19,21–24]
Triple-layer (Na)	18.24	18.1–19.0[24]

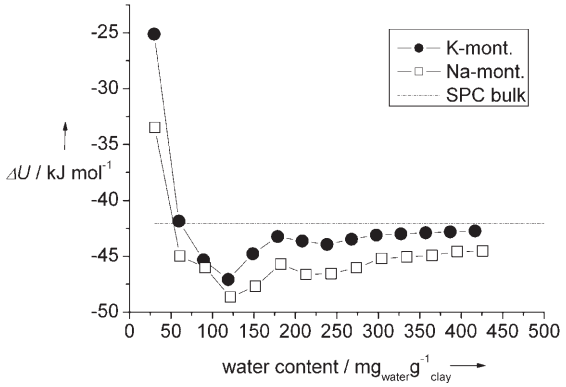

Figure 1. Hydration energy ΔU of K- and Na-montmorillonite.

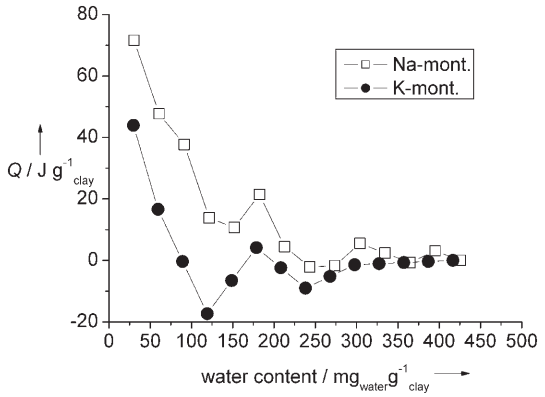

Figure 2. Swelling immersion energy Q of K- and Na-montmorillonite.

respectively. The simulated hydration energy of single-layer K-hydrate is $-47.0\ kJ\,mol^{-1}$ (approximately 120 milligrams of water per gram of clay), similar to the experimental value of $-45\ kJ\,mol^{-1}$ (approximately 100 milligrams of water per gram of clay).[9,19] The simulated value of single-layer Na-hydrate ($-48.6\ kJ\,mol^{-1}$) falls within the experimental range (-52 to $-48\ kJ\,mol^{-1}$).[4,20] These findings confirm that our simulations can reproduce both basal spacings and calorimetry data and thus suggest the reliability of our subsequent analyses.

Two local minima occur on the hydration energy curve for Na-montmorillonite, with the one with lower water content being the global minimum. Three local minima appear on the immersion energy curve, of which the double-layer state, which is similar to the triple-layer state in energy, is the global minimum. This result is exactly consistent with the experiments: Na-smectites prefer expanded states (double-layer, triple-layer, and fully expanded) to a single-layer hydrate.[6,7] The swelling energy can, therefore, reveal the relative stabilities of the different hydrate states. For K-montmorillonite, the swelling immersion energy curve presents two local minima, which correspond to single- and double-layer states, respectively. The single-layer state is the global minimum, with an energy much lower than that of the double-layer state. It is, therefore, more stable than the double-layer state. There is no local minimum at higher water contents; therefore, no triple-layer K-hydrate is formed even under aqueous conditions.[9]

The hydration energy approaches that of bulk water as the water content increases (Figure 1);[8,15] therefore, the hydration energy curve allows us to study the hydration potential at relatively high water contents. Thus, when the water content of Na-montmorillonite exceeds 370 milligrams of water per gram of clay (i.e. the triple-layer state), its hydration energy is still much lower than that of bulk water, which indicates that further swelling is still strongly preferred. For K-montmorillonite, however, when the water content is higher than the range of the double-layer hydrate, the hydration energy is very close to that of bulk water; therefore, its osmotic swelling is inhibited energetically. This means that K-hydrates never expand fully, even in aqueous suspension, whereas Na-hydrates do.

The interlayer structure and dynamic behavior of the single-layer K-hydrate were also investigated. The water molecules form a single layer and the K^+ ions bind to the clay surfaces (Figure 3a). A detailed analysis shows that all the K^+ ions are centered above the adjacent six-membered rings and present a cage-like coordination structure in which each K^+ ion is coordinated to six oxygen atoms of the hexagonal ring and five oxygen atoms from water (Figure 3b). Interestingly, two neighboring ions can share a water molecule. To study the mobility of the ions, a long simulation of 3500 ps was run. No macroscopic diffusion can be identified in the resulting mean square displacements (MSD; Figure 4).[25] The movement trajectories of the ions clearly show that every ion is restricted within a very limited space above the hexagon and that their actual motions are below the detectable limits of both length and time (Figure 5).[25] In other words, the K^+ ions are trapped and immobile within the coordination cages. We repeated the simulation with different initial states and always obtained the same coordination structure, which is similar to one of the patterns found on an open mica surface but without the reported mobility.[26] The fixed ions effectively screen the negative charges of the clay sheets so that further swelling is inhibited, just as neutral clay minerals (e.g. pyrophyllite) never swell. This microscopic mechanism verifies previous suggestions,[8,27] and clarifies the inherent "hydrophobicity" of K^+ ions.[28] The stable cage-like coordination structure indicates that K^+ ions strongly prefer binding to the clay

 © 2006 Wiley-VCH Verlag GmbH & Co. KGaA, Weinheim

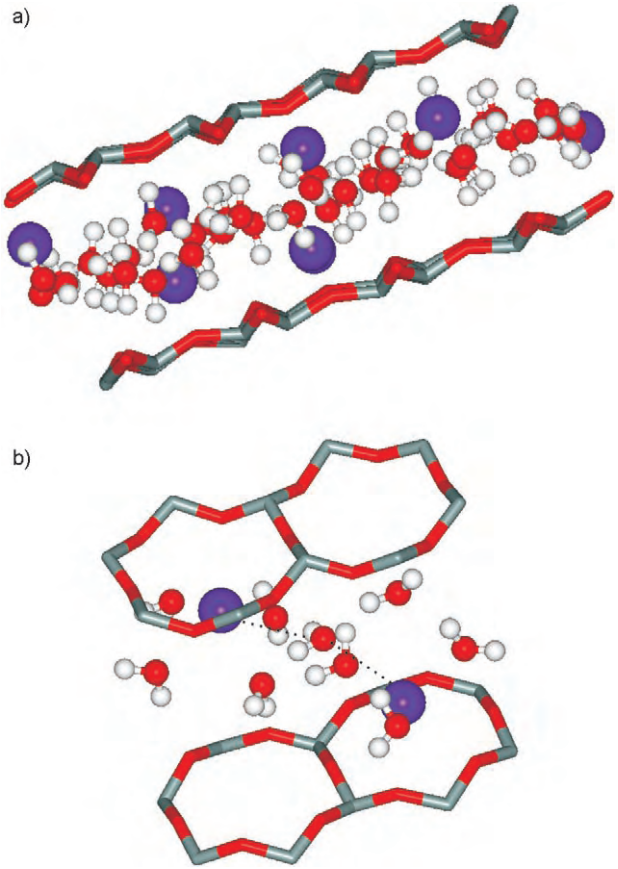

Figure 3. a) A snapshot of the equilibrated single-layer K-hydrate. b) An amplified snapshot of the cage-like coordination structures of two K^+ ions; dotted lines denote the shared water molecule. Sticks: clay framework, blue spheres: K, red spheres: water O, white spheres: water H.

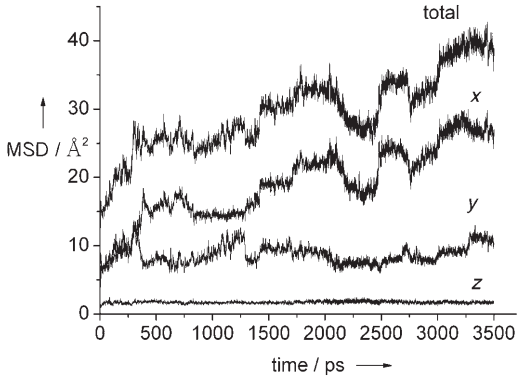

Figure 4. Mean square displacements (MSD) of K^+ ions during a simulation of 3500 ps in a single-layer K-hydrate. The *x*, *y*, and *z* components, and the total are plotted.

rather than being solvated, which results in the surprising stability of the single-layer hydrate.

In summary, we have presented a fundamental understanding of the inhibition of clay swelling by K^+ ions. The most stable single-layer state is found to correspond to the global minimum of the swelling energy curve, and the osmotic swelling is inhibited energetically. We have also found a novel microstructure of this single-layer K-hydrate that is responsible for the surprising stability: the K^+ ions are all fixed in coordination cages composed of surface oxygen atoms and water molecules.

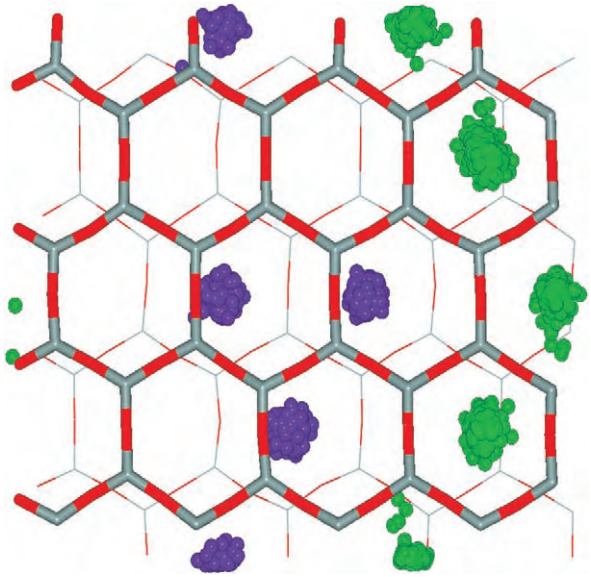

Figure 5. Trajectories of K^+ ions after 1000 ps in the simulation of a single-layer K-hydrate. The stick and line frameworks represent the upper and lower clay surfaces, respectively. The green and blue spheres represent K^+ ions close to the upper and lower surfaces, respectively. Each "cluster" represents the sampled trajectories of a single ion. The motions are so restricted that the ions can be viewed as being stationary.

Received: May 3, 2006
Published online: August 25, 2006

Keywords: clays · mobility · molecular dynamics · potassium · thermodynamics

[1] a) R. E. Grim, *Applied Clay Mineralogy*, McGraw-Hill, New York, **1962**; b) S. Karaborni, B. Smit, W. Heidug, J. Urai, E. Van Oort, *Science* **1995**, *271*, 1102–1104; c) M. M. Hanczyc, S. M. Fujikawa, J. W. Szostak, *Science* **2003**, *302*, 618–622.
[2] G. W. Brindley, G. Brown, *Crystal Structures of Clay Minerals and their X-ray Identification*, Mineralogical Society, London, **1980**.
[3] W. F. Bleam, *Rev. Geophys.* **1993**, *31*, 51–74.
[4] R. W. Mooney, A. G. Keenan, L. A. Wood, *J. Am. Chem. Soc.* **1952**, *74*, 1367–1371.
[5] a) N. T Skipper, *Min. Mag.* **1998**, *62*, 657–667; b) S.-H. Park, G. Sposito in *Handbook of Layered Materials Science & Technology* (Eds.: S. A. Auerbach, K. A. Carrado, P. K. Dutta), Marcel Dekker, New York, **2004**, Chapter 2.
[6] a) A. M. Posner, J. P. Quirk, *J. Colloid Sci.* **1964**, *19*, 798–812; b) D. J. Cebula, R. K. Thomas, J. W. White, *J. Chem. Soc., Faraday Trans. 1* **1980**, *76*, 314–321.
[7] J. H. Denis, M. J. Keall, P. L. Hall, G. H. Meeten, *Clay Miner.* **1991**, *26*, 255–268.
[8] E. S. Boek, P. V. Coveney, N. T. Skipper, *J. Am. Chem. Soc.* **1995**, *117*, 12608–12617.

 © 2006 Wiley-VCH Verlag GmbH & Co. KGaA, Weinheim

[9] F.-R. C. Chang, N. T. Skipper, G. Sposito, *Langmuir* **1998**, *14*, 1201 – 1207.
[10] G. Odriozola, J. F. Aguilar, *J. Theor. Comput. Chem.* **2005**, *1*, 1211 – 1220.
[11] R. Calvet, *Ann. Agron.* **1973**, *24*, 77 – 133.
[12] a) T. J. Tambach, P. G. Bolhuis, B. Smit, *Angew. Chem.* **2004**, *116*, 2704 – 2706; *Angew. Chem. Int. Ed.* **2004**, *43*, 2650 – 2652; b) T. J. Tambach, E. J. M. Hensen, B. Smit, *J. Phys. Chem. B* **2004**, *108*, 7586 – 7596.
[13] S. J. Plimpton, *J. Comput. Phys.* **1995**, *117*, 1 – 19; http://www.cs.sandia.gov/~sjplimp/lammps.html.
[14] R. T. Cygan, J.-J. Liang, A. G. Kalinichev, *J. Phys. Chem. B* **2004**, *108*, 1255 – 1266.
[15] D. E. Smith, *Langmuir* **1998**, *14*, 5959 – 5967.
[16] a) R. M. Shroll, D. E. Smith, *J. Chem. Phys.* **1999**, *111*, 9025 – 9033; b) D. A. Young, D. E. Smith, *J. Phys. Chem. B* **2000**, *104*, 9163 – 9170; c) H. D. Whitley, D. E. Smith, *J. Chem. Phys.* **2004**, *120*, 5387 – 5395.
[17] D. E. Smith, Y. Wang, H. D Whitley, *Fluid Phase Equilib.* **2004**, *222*, 189 – 194.
[18] a) N. T. Skipper, F.-R. C. Chang, G. Sposito, *Clays Clay Miner.* **1995**, *43*, 294 – 303; b) F.-R. C. Chang, N. T. Skipper, G. Sposito, *Langmuir* **1995**, *11*, 2734 – 2741.
[19] I. Bérend, J. M. Cases, M. François, J. P. Uriot, L. Michot, A. Masion, F. Thomas, *Clays Clay Miner.* **1995**, *43*, 324 – 336.
[20] W. H. Slabaugh, *J. Phys. Chem.* **1959**, *63*, 436 – 438.
[21] T. Sato, T. Watanabe, R. Otsuka, *Ann. Agron.* **1992**, *40*, 103 – 113.
[22] K. Tamura, H. Yamada, H. Nakazawa, *Clays Clay Miner.* **2000**, *48*, 400 – 404.
[23] M. H. Fu, Z. Z. Zhang, P. F. Low, *Clays Clay Miner.* **1990**, *38*, 485 – 492.
[24] K. Norrish, *Discuss. Faraday Soc.* **1954**, *18*, 120 – 133.
[25] N. T. Skipper, K. Refson, J. D. C. McConnell in *Geochemistry of Clay-Pore Fluid Interactions* (Eds.: D. C. Manning, P. L. Hall, C. R. Hughes), Chapman and Hall, London, **1993**, Chapter 3.
[26] S.-H. Park, G. Sposito, *Phys. Rev. Lett.* **2002**, *89*, 85501.
[27] T. J. Tambach, P. G. Bolhuis, E. J. M. Hensen, B. Smit, *Langmuir* **2006**, *22*, 1223 – 1234.
[28] a) G. Sposito, R. Prost, *Chem. Rev.* **1982**, *82*, 553 – 573; b) G. Sposito, N. T. Skipper, R. Sutton, S.-H. Peark, A. K. Soper, J. A. Greathouse, *Proc. Natl. Acad. Sci. USA* **1999**, *96*, 3358 – 3364.

 © 2006 Wiley-VCH Verlag GmbH & Co. KGaA, Weinheim

Layered Compounds

DOI: 10.1002/anie.200600321

Soft Synthesis of Single-Crystal Silicon Monolayer Sheets**

Hideyuki Nakano, Takuya Mitsuoka, Masashi Harada, Kayo Horibuchi, Hiroshi Nozaki, Naoko Takahashi, Takamasa Nonaka, Yoshiki Seno, and Hiroshi Nakamura*

Silicon-based nanoscale materials, such as nanotubes,[1] nanowires,[2] and nanoparticles,[3] have remarkable electronic and optical properties and are suitable for nanodevice applications owing to their extraordinary structures. While zero- or one-dimensional nanomaterials may be suitable for nanoscale fabrication, two-dimensional nanomaterials can bridge the gap between the quantum world and three-dimensional bulk because of their nanoscale thickness and microscale area. To synthesize two-dimensional nanomaterials, chemical exfoliation is performed artificially for several classes of layered materials by certain soft-chemistry procedures.[4] In a previous study,[5] we tried to prepare the two-dimensional silicon backbone of siloxene nanosheets (composition: $Si_6H_3(OH)_3$),[6] but the silicon skeleton was partially oxidized. Moreover, epitaxial films of siloxene are obtained on the silicon (111) surface by topochemical transformation of $CaSi_2$ (111) films.[7] Although many researchers have attempted to prepare two-dimensional silicon sheets, there have been no reports of a successful fabrication of silicon monolayer sheets.

We tried to prepare silicon sheets by chemical exfoliation of calcium disilicide, $CaSi_2$, which has a hexagonal layered structure consisting of alternating Ca layers and corrugated Si (111) planes in which the Si_6 rings are interconnected (Figure 1 a). One of the most important techniques to exfoliate precursor-layered crystals into their elementary layers is the adjustment of the charge on the silicon layer. Because $CaSi_2$ is ionic (i.e. $Ca^{2+}(Si^-)_2$) the electrostatic interaction between the Ca^{2+} and Si^- layers is strong and so it is very important to reduce the charge on the negatively charged silicon layers. Thus, we prepared Mg-doped $CaSi_2$ (mixture composition: $CaSi_{1.85}Mg_{0.15}$) in which Mg was doped successfully into the $CaSi_2$ (see Supporting Information). Then, we tried to prepare silicon monolayer sheets (Figure 1 b,c) through chemical exfoliation of $CaSi_{1.85}Mg_{0.15}$. When

[*] Dr. H. Nakano, T. Mitsuoka, Dr. M. Harada, Dr. K. Horibuchi, Dr. H. Nozaki, N. Takahashi, T. Nonaka, Dr. Y. Seno, H. Nakamura
Toyota Central R&D Labs., Inc.
Nagakute, Aichi, 480–1192 (Japan)
Fax: (+81) 561-63-6507
E-mail: hnakano@mosk.tytlabs.co.jp

[**] This work was supported by a Grant-in-Aid for Scientific Research from Ministry of Education, Science, Sports and Culture, Japan.

Supporting information for this article is available on the WWW under http://www.angewandte.org or from the author.

© 2006 Wiley-VCH Verlag GmbH & Co. KGaA, Weinheim

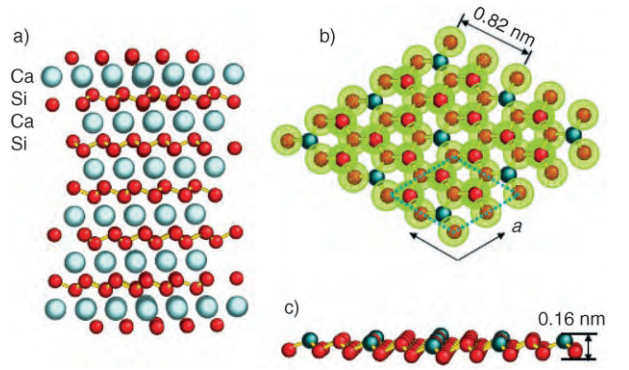

Figure 1. a) Structural model of $CaSi_2$. b) Top view of Mg-doped silicon sheet capped with oxygen; the axis notation follows that for the hexagonal crystal structure of the parent layered silicon. c) Side view of the core of the silicon sheet; the large yellow-green circles represent oxygen atoms, small red (Si) and green (Mg) circles represent the Si(111) plane in the layer below.

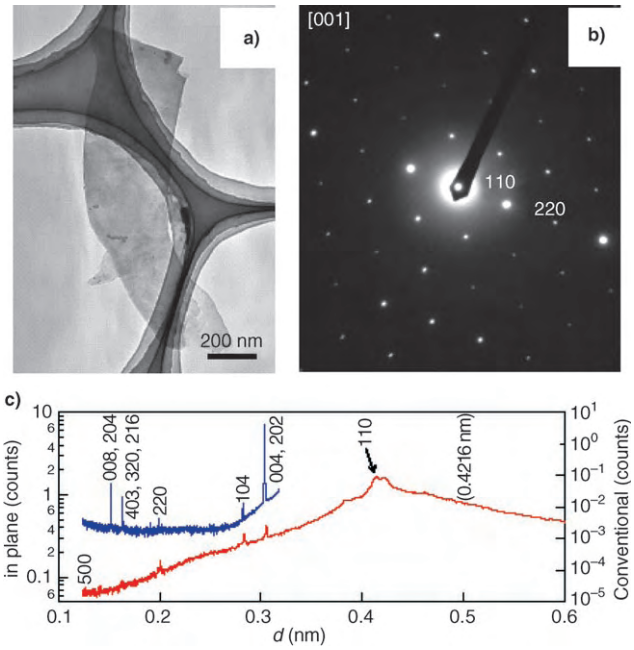

Figure 2. a) TEM image of the sheet. b) ED pattern recorded along the [001] zone axis perpendicular to the surface of the sheet. c) In-plane XRD scans with an incident angle of 0.2° (red line) and conventional θ-2θ scans (blue line) of the silicon sheets. The data was recorded at SPring-8 (BL16XU).

bulk $CaSi_{1.85}Mg_{0.15}$ is immersed in a solution of propylamine hydrochloride (PA·HCl), the calcium ions are deintercalated, which is accompanied by the evolution of hydrogen, and $CaSi_{1.85}Mg_{0.15}$ is converted into a mixture of silicon sheets and an insoluble black metallic solid. A light-brown suspension containing silicon sheets was obtained after the sediment was removed from the bottom of the flask.

To determine the binding energy and composition of silicon sheets, X-ray photoelectron spectroscopy (XPS) of the Si 2p orbitals on silicon sheets adsorbed on a positively charged graphite substrate was measured (see Supporting Information). The Si 2p peak has a binding energy of 102 eV. This energy is close to that of the Si^{II} oxidation state. From the XPS data, the molar ratio of Si:O is roughly 1:1, which is in good agreement with previous reports.[8] The composition of the adsorbed monolayer silicon sheets was determined to be Si:Mg:O = 7.0:1.3:7.5 by XPS measurement. The Si:Mg ratio is appreciably smaller in the starting material, $CaSi_{1.85}Mg_{0.15}$, which indicates that exfoliation into individual silicon sheets occurred preferentially in a section of the silicon layer where magnesium atoms were present. The bonding of oxygen onto the surface of the silicon sheets was confirmed by Fourier transform infrared spectroscopy (FTIR). The bands at 1050 cm^{-1} correspond to Si-O-Si stretching, which indicates that the sheets are capped with oxygen.[9] The overall exfoliation reaction comprises the following steps: 1) the oxidation of $CaSi_{1.85}Mg_{0.15}$ is initiated by the oxidation of the Ca atoms with PA·HCl, accompanied by the liberation of PA; 2) the resulting Mg-doped SiH is presumably very reactive and thus easily oxidized with water to form gaseous hydrogen; 3) Mg-doped layered silicon with capping oxygen atoms is exfoliated by the reaction with aqueous PA solution, which results in a stable colloidal suspension of silicon sheets.

The structure of the silicon sheets was confirmed by transmission electron microscopy (TEM). A TEM image of the silicon sheets, dropped on a carbon grid, which shows their general characteristics, reveals a two-dimensional structure with lateral dimensions in the range of 200 to 500 nm (Figure 2a). The sheet is almost transparent, thus indicating a high degree of exfoliation of the $CaSi_{1.85}Mg_{0.15}$ crystals, and it exhibits uniform and homogeneous contrast, which reflects its uniform thickness. A selected-area electron diffraction (ED) pattern of the *hk*0 layer is shown in Figure 2b. ED confirmed that the sheet is single-crystalline and gives a spot pattern. All the diffraction spots could be indexed as *hk* reflections of a hexagonal lattice with $a = 0.82$ nm, which corresponds to approximately twice that of the (111) plane structure of bulk silicon (0.38 nm). The arrangement is attributable to either a superlattice structure or a delamination effect. Figure 2c shows the in-plane X-ray diffraction (XRD) scan of the sheets with an incident angle of 0.2°. The sheets give rise to fundamental peaks at $d = 0.422$ nm that correspond to the (110) plane, which is also observed in the ED (Figure 2b). Moreover, although the in-plane diffraction pattern of the silicon sheet was compared with that of siloxene,[10] this diffraction pattern could not be assigned to any siloxene structures (see Supporting Information). Thus, these results can be explained by the silicon sheets having a superlattice structure with twice the period of the (111) plane structure of bulk silicon. Energy-dispersive X-ray spectroscopy (EDX) combined with TEM revealed the presence of Si and Mg atoms, which suggests successful Mg doping of the sheets. Taken together with the superlattice structure and the XPS data, the evidence shows the structure of the sheets to be that of the theoretical structure shown in Figure 1b, and the molar ratio of silicon sheet is consequently Si:Mg = 7:1. However, the position of the Mg site is questionable and will be investigated in more detail.

Atomic force microscopy (AFM) provided further evidence of monolayer sheets. Figure 3a shows a noncontact

 © 2006 Wiley-VCH Verlag GmbH & Co. KGaA, Weinheim

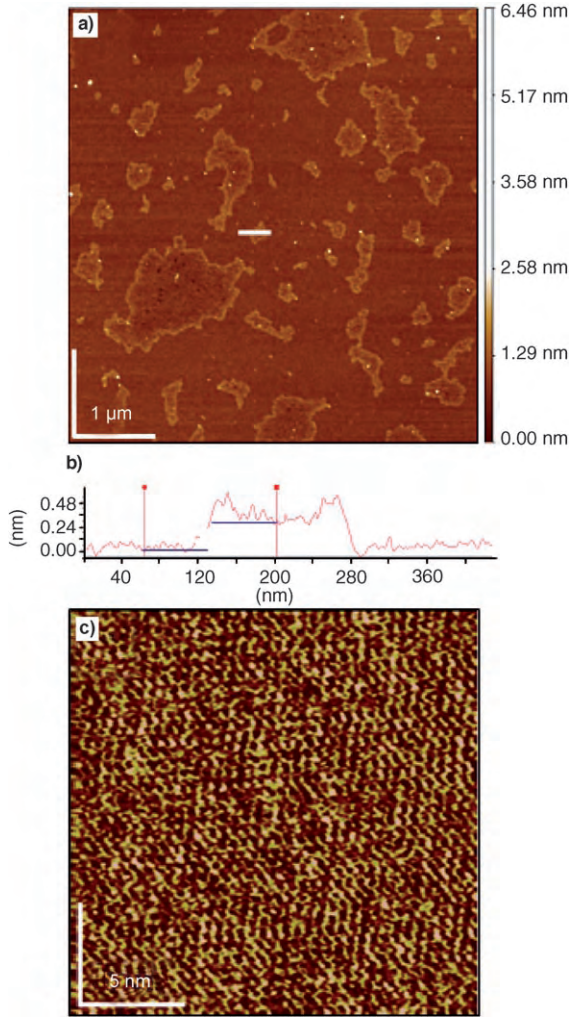

Figure 3. a) Noncontact mode AFM image of the silicon sheets, and b) its line profile taken along the white line in (a). c) Atomically resolved AFM image of silicon sheets.

mode AFM image of silicon sheets adsorbed electrostatically onto a positively charged mica substrate as the silicon sheets have a negative charge. The observation of breaks at the edges of the sheets suggests that they are ultrathin. The thickness of the sheets was measured at intervals between the sheets and the substrate surface and yielded an average value of 0.37 nm (Figure 3b). A thickness below 1 nm clearly demonstrates that the sample was composed of monolayer sheets. The crystallographic thickness of the silicon sheet was calculated to be 0.16 nm on the basis of its atomic architecture (Figure 1c). The difference between this value and that obtained by AFM indicates that the surface of the silicon sheet was stabilized by capping oxygen atoms, silicon nanowires,[2] and silicon nanoparticles.[3]

An atomically resolved AFM image of an individual sheet provided further insight into the structure (Figure 3c). The quality of the image was neither affected by the long duration of the experiment during which the sample was exposed to air nor by exposure of the sheet to air for several days before measurement. Thus, the oxygen-capped silicon sheets are resistant to air oxidation. A high-resolution AFM image reveals that the closest distance between the dotlike "atoms" is 0.41 ± 0.02 nm (Figure 3c). The lattice period of the sheet determined by this measurement is in agreement with that of the TEM observation. A structural model for the surface of the sheet is shown in Figure 1b. In this model, each silicon atom in the plane below is bonded to an oxygen atom, which may be accounted for by considering the resolution of AFM and the actual surface structure. Thus, the periodicity of the surface of the sheet is 0.41 nm, which is slightly larger than the distance between Si atoms in a Si (111) plane of bulk crystal, that is, 0.38 nm. On the basis of the high-resolution AFM image and the TEM observation, we conclude that the sheet cores consist of a single-crystalline silicon monolayer with the thickness of a slightly squashed Si (111) plane.

The absorption spectrum of the silicon sheets (Figure 4a) has a peak at 268 nm (4.8 eV) that corresponds to the L→L critical point in the silicon-band structure, which is strongly

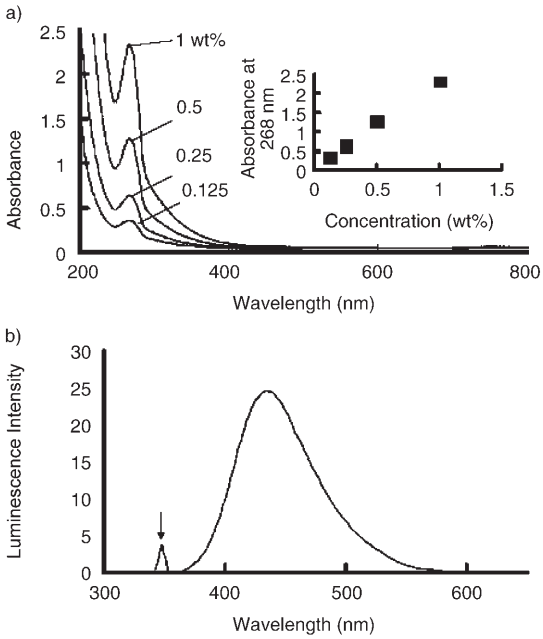

Figure 4. Room-temperature optical properties of the silicon sheets. a) UV/Vis spectra of suspensions of silicon sheets at various concentrations. Inset: the absorbance at 268 nm is plotted against the concentration of the sheets. b) PL spectra dispersed in water with an excitation wavelength of 350 nm (indicated by an arrow).

blue-shifted with respect to the bulk indirect band gap of 1.1 eV. The silicon sheets are thought to be predominantly ⟨110⟩ oriented. Normally, ⟨110⟩-oriented silicon nanowires exhibit a single sharp absorbance at 3.7 eV.[11] This difference in energy of about 1 ev maybe associated with the subnanometer thickness of the silicon sheets, which is about one order of magnitude smaller than the thickness of silicon nanowires (5 nm). The position of the absorbance was observed to be linearly dependent on the silicon content and excludes a possible association of nanosheets in this concentration range. The photoluminescence (PL) spectrum was obtained by using an excitation wavelength of 350 nm (Figure 4b). The emission has a peak at 434 nm (2.9 eV),

 © 2006 Wiley-VCH Verlag GmbH & Co. KGaA, Weinheim

which is direct evidence that the two-dimensional silicon backbone is maintained because the PL of the silicon quantum dots, with diameters smaller than 2 nm, has a peak at 3 eV and shifts to the red by as much as 1 eV after exposure to oxygen.[12] Moreover, the absence of PL from defect or trap-state recombination, which typically occurs near 600 nm, supports the notion that the observed PL is due to direct electron–hole recombination in the silicon sheets as occurs in silicon nanocrystals.[13]

In conclusion, we have obtained unique silicon sheets, whose thickness is an order of magnitude smaller than that previously reported for silicon nanomaterials. The ability to synthesize silicon sheets under the conditions presented will presumably broaden the applicability of these sheets in future optoelectronic devices.

Experimental Section

A stoichiometric mixture (Ca:Si:Mg = 1:1.85:0.15) of CaSi (99%), Si (99.99%), and Mg (99.9%) was melted by using a water-cooled copper crucible with radio-frequency (RF) heating under an Ar atmosphere and then slowly cooled to room temperature.

Preparation of silicon monolayer sheets through chemical exfoliation of $CaSi_{1.85}Mg_{0.15}$: PA·HCl (10 g) and water (50 mL) were added to platelike crystals of $CaSi_{1.85}Mg_{0.15}$ (0.1 g) several millimetres in width. The reaction mixture was stirred (100 rpm) at room temperature for ten days to yield a mixture of silicon sheets and an insoluble black metallic solid. A light-brown suspension containing silicon sheets was obtained after the sediment at the bottom of the flask was removed. The total yield of silicon sheets based on the starting materials ($CaSi_{1.85}Mg_{0.15}$) was less than 1%.

The monolayer sheets for the XPS and AFM measurements were prepared by a self-assembling layer-by-layer technique. The substrate was primed by treatment with a poly(diallyldimethylammonium chloride solution (PDADMAC, $M_w > 200000$; 1.0 g dm^{-3}) for 20 min to introduce a positive charge to the substrate surface. The substrate was deposited into a suspension of silicon sheets (0.5 g dm^{-3}) and after 20 min, the excess silicon sheets and other ions (e.g., PA and Ca^{2+} ions) were removed thoroughly by washing with water.

Received: January 25, 2006
Revised: July 6, 2006
Published online: August 30, 2006

Keywords: layered compounds · monolayers · scanning probe microscopy · semiconductors · silicon

[1] J. Sha, X. Niu, X. Ma, J. Xu, X. Zhang, Q. Yang, D. Yang, *Adv. Mater.* **2002**, *14*, 1219–1221.
[2] A. M. Morales, C. M. Lieber, *Science* **1998**, *279*, 208–211.
[3] R. D. Tilley, J. H. Warner, K. Yamamoto, I. Matsui, H. Fujimori, *Chem. Commun.* **2005**, 1833–1835.
[4] a) N. Miyamoto, H. Yamamoto, R. Kaito, K. Kuroda, *Chem. Commun.* **2002**, 2378–2379; b) T. Sasaki, M. Watanabe, H. Hashizume, H. Yamada, H. Nakazawa, *J. Am. Chem. Soc.* **1996**, *118*, 8329–8335; c) Y. Omomo, T. Sasaki, L. Wang, M. Watanabe, *J. Am. Chem. Soc.* **2003**, *125*, 3568–3575.
[5] H. Nakano, M. Ishii, H. Nakamura, *Chem. Commun.* **2005**, 2945–2947.
[6] A. Weiss, G. Beil, H. Meyer, *Z. Naturforsch. B* **1979**, *34*, 25–30.
[7] a) G. Vogg, M. S. Brandt, M. Stutxmann, M. Albrecht, *J. Cryst. Growth* **1999**, *203*, 570–581; b) G. Vogg, N. Zamanzadeh-Hanebuth, M. S. Brandt, M. Stutzmann, M. Albrecht, *Monatsh. Chem.* **1999**, *130*, 79–87.
[8] S. K. Tan, K. L. Yeo, T. S. Wee, *Surf. Interface Anal.* **2004**, *36*, 640–644.
[9] U. Dettlaff-Weglikowska, W. Honle, A. Molassioti-Dohms, S. Finkbeiner, J. Weber, *Phys. Rev. B* **1997**, *56*, 13132–13140.
[10] P. Deak, M. Posenbauer, M. Stutzmann, J. Weber, M. S. Brandt, *Phys. Rev. Lett.* **1992**, *69*, 2531–2534.
[11] J. D. Holmes, K. P. Johnston, R. C. Doty, B. A. Korgel, *Science* **2000**, *287*, 1471–1473.
[12] M. V. Wolkin, J. Jorne, P. M. Fauchet, *Phys. Rev. Lett.* **1999**, *82*, 197–200.
[13] J. P. Wilcoxon, G. A. Samara, P. N. Provencio, *Phys. Rev. B* **1999**, *60*, 2704–2714.

 © 2006 Wiley-VCH Verlag GmbH & Co. KGaA, Weinheim

Supramolecular Chemistry

DOI: 10.1002/anie.200600847

Molecular Self-Assembly of Macroporous Parallelogrammatic Pipes**

*Myungeun Seo, Gon Seo, and Sang Youl Kim**

Controlling the shape and symmetry of supramolecular materials is essential to express the desired functionalities of new materials. Most self-assembled materials have spherical or cylindrical morphologies, because soft amphiphilic molecules tend to aggregate to form spheres, which are the most thermodynamically stable shape.[1] Consequently, the generation of unique shapes with lower symmetries in self-assembled soft materials has been limited. We aimed to develop a strategy to control the shape and symmetry of the self-assembled materials by a taking two-step approach: First,

[*] M. Seo, Prof. S. Y. Kim
Department of Chemistry and School of Molecular Science (BK21)
Korea Advanced Institute of Science and Technology
373-1 Guseong-dong, Yuseong-gu, Daejeon, 305-701 (Korea)
Fax: (+82) 42-869-8177
E-mail: kimsy@kaist.ac.kr
Homepage: http://macro.kaist.ac.kr
Prof. G. Seo
School of Applied Chemical Engineering & The Research Institute for Catalysis
Chonnam National University
300 Yongbong-dong, Buk-gu, Gwangju, 500-757 (Korea)

[**] Financial support by the BK 21 program and by the Basic Research Program of the KOSEF (grant number R01-2006-000-11258-0) is acknowledged. The authors thank J. Lee for X-ray crystallography, Prof. C. Shin for CP-MAS ^{13}C NMR measurements and porosity evaluation, and Prof. T. Hayakawa and Photron Ltd. for the real-time imaging of the pipe growth.

Supporting information for this article is available on the WWW under http://www.angewandte.org or from the author.

 WILEY InterScience DISCOVER SOMETHING GREAT © 2006 Wiley-VCH Verlag GmbH & Co. KGaA, Weinheim

polymorphic molecular aggregates were constructed with highly directed noncovalent bonds and second, the evolution process was controlled by applying nonequilibrium conditions during the self-assembly.[2] As an example to show the potential of our strategy, we demonstrate the formation of hollow parallelogrammatic pipes through simple drying-mediated self-assembly of organic molecules.

We designed a molecular aggregate based on the hydrogen-bonded network of primary aromatic amides to achieve a parallelogrammatic shape. Primary aromatic amides are known to form 2-dimensional hydrogen-bonded networks through highly directional side-to-side and face-to-face hydrogen bonds involving anti (H_{anti}) and syn protons (H_{syn}), respectively.[3,4] In the present work, we synthesized 4-dodecyloxy-2-trifluoromethylbenzamide (**1**, Figure 1a),

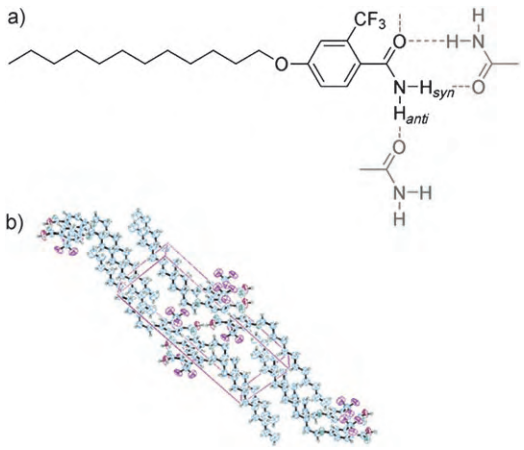

Figure 1. a) Molecular structure and hydrogen bonding pattern of **1**. b) ORTEP drawing of the crystal structure of **1L**.

which is highly crystalline as a result of the interaction between lipophilic alkyl chains and the strong hydrogen bonds. Compound **1** shows polymorphism: two different crystal structures were identified in the powder X-ray diffraction (XRD) patterns. The crystallization of **1** from *n*-hexane and solidification of the melt yielded a needlelike crystal with a small-angle peak at $d = 2.39$ nm (**1L** structure), whereas the crystallization in polar solvents such as ethanol, ethyl acetate, acetone, and diethyl ether produced rodlike crystals with a small-angle peak at $d = 1.48$ nm (**1S** structure).

The triclinic unit cell of the **1L** structure, obtained from the single crystal grown in *n*-hexane, is illustrated in Figure 1b.[5] The molecules form an intercalated head-to-head bilayer structure, and the primary amide groups form a hydrogen-bonded network that consists of side-to-side and face-to-face hydrogen bonds in the layer.

However, we were unable to grow a suitable single crystal of the **1S** structure. In ethanol, a powder precipitated at low concentration and the solution became a crystalline gel at concentrations greater than 15% w/v (see the Supporting Information). Thus we assumed that the **1S** structure is triclinic and assigned the three crystallographic axes as $a = 0.725$, $b = 1.13$, and $c = 1.48$ nm on the basis of the powder XRD pattern. Compared with the **1L** structure, the supposed unit cell has a considerably shorter c axis even though its volume is similar to that of the **1L** structure. This observation suggests that the alkyl chains in the **1S** structure are more disordered than those in the **1L** structure. ^{13}C cross-polarization magic-angle-spinning (CP-MAS) solid-state NMR spectra and FT-IR spectra reveal a large fraction of gauche conformations,[6,7] and a large red shift of the N–H symmetric stretching vibration to 3184 cm^{-1} (3196 cm^{-1} in the **1L** structure) indicates that the face-to-face hydrogen bond of the **1S** structure is much stronger than that of the **1L** structure (see the Supporting Information).[4a] These spectroscopic data suggest that the strong face-to-face hydrogen bond stabilizes the **1S** structure, whereas the rapid crystallization of the alkyl chains favors the **1L** structure. The fact that the **1S** structure grows only in polar solvents can be rationalized by the solvation of the H_{syn} atom by an O atom of the solvent molecule.

To utilize the difference between two polymorphs in the assembly, we irreversibly evaporated a solution of **1** in a polar solvent. Evaporation from a drop of solution on a substrate is a complex nonequilibrium process.[8,9b] The possibility of using evaporation to produce unique two-dimensional supramolecular patterns on a mesoscopic scale has been exploited recently.[8–12]

We found that evaporation resulted in unusual crystal growth when a hot solution of **1** in polar solvents was allowed to drop onto a substrate. In a typical experiment, a solution of **1** in ethanol at 96 °C was allowed to drop onto a silicon wafer at room temperature. The process of the structure evolution was imaged in real time by an optical microscope (a movie clip is available in the Supporting Information). Figure 2a

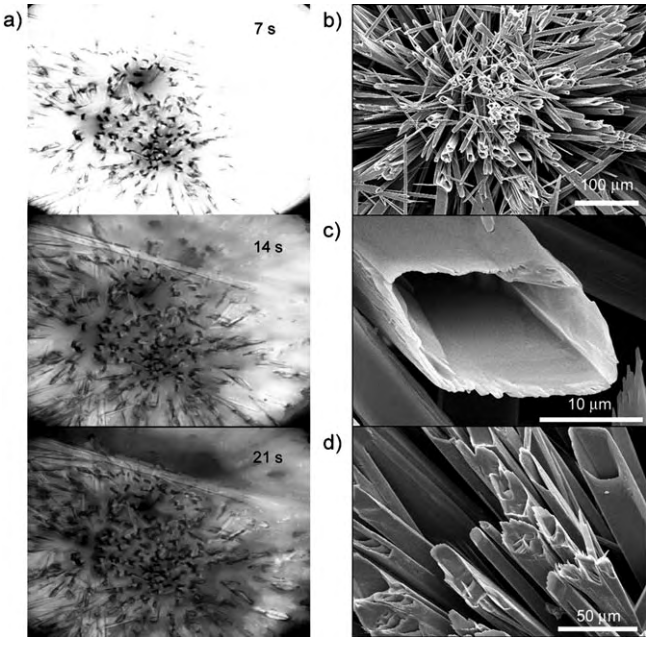

Figure 2. Drying-mediated assembly of **1** to generate a bundle of pipes: a) Snapshots of the pipe formation during the evaporation. The sample was prepared by allowing a hot solution of **1** (20% w/v) in ethanol to drop onto a silicon wafer at room temperature. The time lapse after the solution was dropped is given in the top left of each picture. b-d) SEM images of: b) a macroscopic view of the hemispherically formed pipes; c) an enlarged view of a typical pipe; d) some partitioned pipes.

 © 2006 Wiley-VCH Verlag GmbH & Co. KGaA, Weinheim

shows three snapshots taken during the process. As ethanol evaporated, rodlike crystals nucleated at the surface of the drop and grew inside to form three-dimensional hemispherical bundles. Field-emission scanning electron microscopy (FE-SEM) images show that bundles of micrometer-sized parallelogrammatic pipes were formed (Figure 2b–d). The pipes were about 1 mm high, and the cross section was about $20 \times 15\ \mu m^2$ with angles of 80 and 100°. The thickness of the wall was about 150 nm. Although most pipes were parallelogrammatic, some of the pipes consisted of more-complex shapes; platelike crystals were observed in regions around the bundle. The growth was completed within one minute.

Figure 3a depicts the powder XRD patterns of the solids that remained on the wafer. Series of peaks were assigned to the **1L** and **1S** structures. However, the pattern obtained from

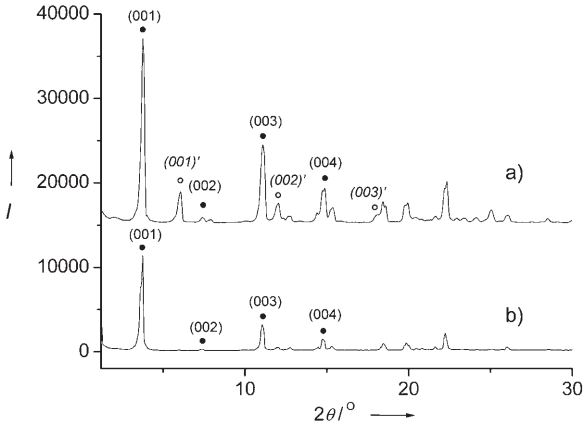

Figure 3. Powder XRD patterns of **1** formed on the silicon wafer: a) The whole solid after the complete evaporation. b) Carefully selected pipes. Filled circles: Bragg peaks with the spacing of 2.40 nm. Open circles: Bragg peaks with the spacing of 1.48 nm.

carefully selected pipes consisted almost solely of the **1L** structure (Figure 3b). Because the crystallization in ethanol yielded only the **1S** structure, the **1L** structure should be generated during the evaporation, when the alkyl chains crystallize rapidly. Indeed, dropping a hot solution of **1** in ethanol onto a silicon wafer at 96 °C yielded the **1L** structure.

We believe that the polymorphic transition of **1S** into **1L** during the evaporation is crucial in the formation of the unusual parallelogrammatic cross section of micrometer size. The formation of parallelogrammatic channels can not be explained by the bent backbone in the crystal structure because this backbone is restricted to within the nanometer scale.[13a] Some reports regard one-dimensional growth in the liquid crystalline (LC) medium and the filling of the cavity with LC fluid as a key mechanism in the formation of micrometer-sized tubes.[13b,c] However, the resulting tubes are highly symmetric (hexagonal), and the growth process is surprisingly slow relative to the present result. Thus, we suggest a different mechanism, which involves the transition between two polymorphs to give the self-templated hollow structure. Figure 4 summarizes the main features of this mechanism. A similar mechanism that involves organic crystals as templates in the formation of hollow fibers with parallelogrammatic cross section has been proposed.[14]

The whole drop is a dynamic system in which a Benárd convective flow occurs owing to the temperature difference between the surface and the bottom fo the drop.[8] This flow transports hot solution from the bottom toward the colder surface of the drop. The solution becomes saturated, and solvent-rich gel-like solid of **1S** structure forms. However, when the solid comes in contact with air during the evaporation, the rapid crystallization of alkyl chains induces the **1L** structure instantaneously and creates a wall around the gel-like solid. Then, solute flows toward the wall to compensate the solute consumed by crystallization of the **1L** structure. The concentration inside the wall decreases continuously as a result of consumption of the solute. Consequently, the solvent evaporates and leaves a parallelogrammatic channel resembling the shape of the **1S** crystal. The radial-bundle shape can be attributed to the radial convective flow. Platelike crystals of **1L** structure at the boundary of the droplet may appear because of the small temperature difference between the surface and the bottom of the drop. Residual **1S** structure may crystallize inside the drop near the bottom without the contact to air. To verify this hypothesis, we measured the powder XRD of a sample immediately quenched with liquid nitrogen after the dropping of the solution. The data show that the **1S** structure appears in high population at a very early stage of the growth process, which

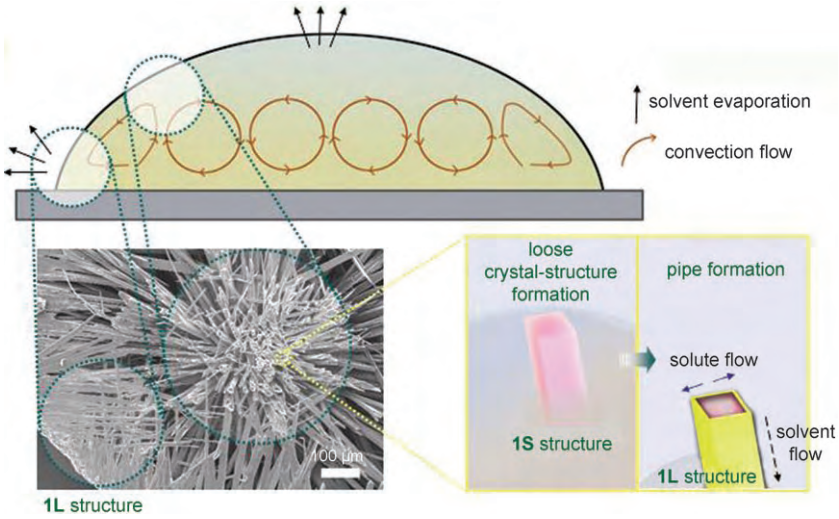

Figure 4. The proposed mechanism of pipe formation based on the polymorphic transition: The **1L** structure forms at the boundary of the droplet as a result of evaporation. Benárd convective flow around the center of the drop induces crystallization of the **1S** structure near the surface of the droplet. However, polymorphic transition from the **1S** to the **1L** structure yields a crystalline wall, the inside of which is hollow because of solute flow to the wall to compensate for the consumption of solute upon crystallization.

 © 2006 Wiley-VCH Verlag GmbH & Co. KGaA, Weinheim

supports the proposed mechanism (see the Supporting Information).

This organic supramolecular material can be regarded as a new type of macroporous material. We confirmed the existence of the macropores by using a mercury intrusion porosimeter (Figure 5a). The result shows the development

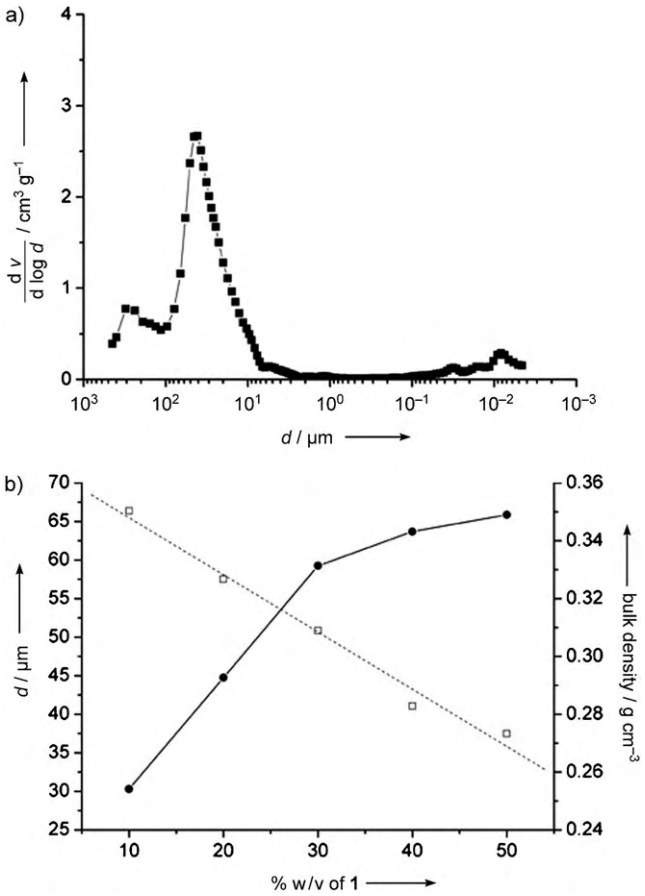

Figure 5. a) Typical pore-size distribution of the pipes. The sample was prepared from a 40% w/v solution in ethanol. Porosity: 73%. Maximum mean pore diameter: 41.1 µm. b) Plot of content (% w/v) of **1** in ethanol versus maximum mean pore diameter and bulk density of the pipes. Filled dots: bulk density. Empty squares: maximum pore diameter. Dashed line: least-squares fit of maximum pore diameter plot ($R = 99.2\%$).

of pipes with the average pore diameter of tens of micrometers, which corresponds to those observed by SEM. The average pore diameter of the pipes was gradually reduced with increases of the concentration of **1** (Figure 5b), which indicates that it is possible to tune the pore size.

In summary, we developed a novel self-templating technique between polymorphs and demonstrated the formation of organic macroporous parallelogrammatic pipes through drying-mediated assembly. We expect that this strategy to generate organic materials with lower symmetries in a macroscopic dimension will open a route to develop hollow macroscopic structures with unusual shapes.

Experimental Section

The detailed synthesis of **1** is provided in the Supporting Information. To generate parallelogrammatic pipes, 20% w/v solution of **1** in ethanol was prepared at 96°C and allowed to drop onto a silicon wafer that had been freshly washed with piranha solution. The drop was allowed to evaporate at RT. The process of the structure evolution was imaged by a Nikon ME600L microscope equipped with a Photron Focuscope all-in-focus system. FE-SEM studies were performed on Philips XL30S FE-SEM for Au-sputtered samples. Powder XRD patterns were obtained on Rigaku D/MAX Ultima diffractometer with scan speed of 2° min^{-1}, sampling width of 0.01°, and $Cu_{K\alpha}$ ($\lambda = 0.154$ nm) as a light source. Mercury porosimetry isotherms were obtained with an AutoPore III (Micromeritics). The samples were evacuated under vacuum (below 3×10^{-2} Torr) at room temperature prior to intrusion of mercury. The Kelvin equation was used to determine the pore-size distribution of the samples. The contact angle between sample and mercury was chosen as 140°.

Received: March 5, 2006
Revised: July 2, 2006
Published online: August 29, 2006

Keywords: crystal growth · polymorphism · self-assembly · X-ray diffraction

[1] T. Kunitake, Y. Okahata, M. Shimomura, S. Yasunami, K. Takarabe, *J. Am. Chem. Soc.* **1981**, *103*, 5401–5413; H.-A. Klok, S. Lecommandoux, *Adv. Mater.* **2001**, *13*, 1217–1229.

[2] G. M. Whitesides, B. Grzybowski, *Science* **2002**, *295*, 2418–2421; G. M. Whitesides, M. Boncheva, *Proc. Natl. Acad. Sci. USA* **2002**, *99*, 4769–4774.

[3] M. C. Etter, *Acc. Chem. Res.* **1990**, *23*, 120–126; M. C. Etter, *J. Phys. Chem.* **1991**, *95*, 4601–4610.

[4] a) L. S. Reddy, A. Nangia, V. M. Lynch, *Cryst. Growth Des.* **2004**, *4*, 89–94; b) C. M. Reddy, L. S. Reddy, S. Aitipamula, A. Nangia, C.-K. Lam, T. C. W. Mak, *CrystEngComm* **2005**, *7*, 44–52.

[5] Crystal data for **1L**: $C_{20}H_{30}F_3NO_2$, triclinic, space group $P\bar{1}$, scan range $3.4 < 2\theta < 56.3°$, $T = 293(2)$ K, $a = 4.9837(13)$, $b = 8.952(2)$, $c = 23.931(6)$ Å, $\alpha = 93.495(5)$, $\beta = 90.810(5)$, $\gamma = 93.460(5)°$, $V = 1063.5(5)$ Å^3, $Z = 2$, $\rho_{calcd} = 1.166$ g cm^{-3}, $\mu(Mo_{K\alpha}) = 0.092$ mm^{-1}, 12062 unique reflections, of which 4746 were taken as observed [$I > 2\sigma(I)$], $R\,|F^2| = 0.2093$, $wR = 0.1397$. CCDC-600374 contains the supplementary crystallographic data for this paper. These data can be obtained free of charge from The Cambridge Crystallographic Data Centre via www.ccdc.cam.ac.uk/data_request/cif.

[6] M. Pursch, R. Brindle, A. Ellwanger, L. C. Sander, C. M. Bell, H. Handel, K. Albert, *Solid State Nucl. Magn. Reson.* **1997**, *9*, 191–201.

[7] M. Matsuda, V. Volkmar, T. Shimizu, *J. Am. Chem. Soc.* **2000**, *122*, 12327–12333.

[8] M. Shimomura, T. Sawadaishi, *Curr. Opin. Colloid Interface Sci.* **2001**, *6*, 11–16.

[9] a) A. P. H. J. Schenning, F. B. G. Benneker, H. P. M. Geurts, X. Y. Liu, R. J. M. Nolte, *J. Am. Chem. Soc.* **1996**, *118*, 8549–8552; b) M. C. Lensen, K. Takazawa, J. A. A. W. Elemens, C. R. L. P. N. Jeukens, P. C. M. Christianen, J. C. Maan, A. E. Rowan, R. J. M. Nolte, *Chem. Eur. J.* **2004**, *10*, 831.

[10] a) J. Tang, G. Ge, L. E. Brus, *J. Phys. Chem. B* **2002**, *106*, 5653–5658; E. Rabani, D. R. Reichman, P. L. Geissler, L. E. Brus, *Nature* **2003**, *426*, 271; b) E. Lauga, M. P. Brenner, *Phys. Rev. Lett.* **2004**, *93*, 238301.

 © 2006 Wiley-VCH Verlag GmbH & Co. KGaA, Weinheim

[11] L. V. Govor, G. Reiter, J. Parisi, G. H. Bauer, *Phys. Rev. E* **2004**, *69*, 061 609; L. V. Gover, G. Reiter, G. H. Bauer, J. Parisi, *Appl. Phys. Lett.* **2004**, *84*, 4774 – 4776.
[12] a) A. P. Sommer, M. Ben-Moshe, S. Magdassi, *J. Phys. Chem. B* **2004**, *108*, 8 – 10; X. Chen. Z. Chen, B. Yang, G. Zhang, J. Shen, *J. Colloid Interface Sci.* **2004**, *269*, 79 – 83; K. Chen, A. Taflove, Y. L. Kim, V. Backman, *Appl. Phys. Lett.* **2005**, *86*, 033 101; b) H. Li, Q. Liu, L. Qin, M. Xu, X. Lin, S. Yin, L. Wu, Z. Su, J. Shen, *J. Colloid Interface Sci.* **2005**, *289*, 488 – 497.
[13] a) B. H. Hong, J. Y. Lee, C.-W. Lee, J. C. Kim, S. C. Bae, K. S. Kim, *J. Am. Chem. Soc.* **2001**, *123*, 10 748 – 10 749; b) S. Leclair, P. Baillargeon, R. Skouta, D. Gauthier, Y. Zhao, Y. L. Dory, *Angew. Chem.* **2004**, *116*, 353 – 357; *Angew. Chem. Int. Ed.* **2004**, *43*, 349 – 353; S. Leclair, P. Baillargeon, R. Skouta, D. Gauthier, Y. Zhao, Y. L. Dory, *Angew. Chem.* **2004**, *116*, 353 – 357; c) J.-S. Hu, Y.-G. Guo, H.-P. Liang, L.-J. Wan, L. Jiang, *J. Am. Chem. Soc.* **2005**, *127*, 17 090 – 17 095.
[14] a) H. Nakamura, Y. Matsui, *J. Am. Chem. Soc.* **1995**, *117*, 2651 – 2652; F. Miyaji, S. A. Davis, J. P. H. Charmant, S. Mann, *Chem. Mater.* **1999**, *11*, 3021 – 3024; b) F. Mallet, S. Petit, S. Lafont, P. Billot, D. Lemarchand, G. Coquerel, *Cryst. Growth Des.* **2004**, *4*, 965 – 969.

 © 2006 Wiley-VCH Verlag GmbH & Co. KGaA, Weinheim

Low-Dimensional Magnet

DOI: 10.1002/anie.200601349

Assembling Magnetic Nanowires into Networks: A Layered Co^{II} Carboxylate Coordination Polymer Exhibiting Single-Chain-Magnet Behavior**

*Yan-Zhen Zheng, Ming-Liang Tong, Wei-Xiong Zhang, and Xiao-Ming Chen**

Chemists and physicists have jointly pushed the rapid progress of molecule-based nanomagnets in recent years.[1] Since the first discovery of single-molecule magnets (SMMs) in the 1990s,[2] exciting discoveries in this area have included single-chain magnets (SCMs, or so-called magnetic nanowires)[3] and a hydrogen-bonded SMM dimer,[4] which can be regarded as expansions of SMMs by intermolecular magnetic interactions.[4,5] These observations have encouraged chemists to construct or tailor SMMs into an extended network with the hope that certain cooperative effects mediated by covalent linkers could improve the quantum properties of the original units.[5–7] This idea has led to a variety of interesting SMM networks exhibiting properties from classical to quantum magnetism[6,7] and provided useful subjects for studying the effects of intermolecular interactions on the behavior arising from the energy barrier to magnetization reversal.[4–7] In contrast to the rapid development of SMM networks, SCM networks are significantly restricted, which may be attributable to the difficulty in arranging these magnetic nanowires while maintaining a sufficiently large ratio of intra- to interchain magnetic interaction to "freeze in" one-dimensional (1D) magnetization and prevent 3D ordering.[3] Thus, it is important to use proper covalent linkers, which should have at least two features: 1) multitopic structure to covalently link the chains; 2) magnetically "inertness" to efficiently prevent magnetic interactions between the chains.

As σ-bonding linkers are significantly weaker mediators of the spin carriers,[8] crystal engineering with a judicious choice of σ-bonding ditopic linkers may allow us to covalently link 1D Ising ferro- or ferrimagnetic chains into 2D or 3D networks without significant deterioration of the one-dimensional magnetism of the SCMs in the 2D or 3D structures, although no genuine example has been reported so far. In this regard, *trans*-1,2-cyclohexanedicarboxylate (*trans*-1,2-chdc) is a good candidate, since it was demonstrated to be a very weak magnetic mediator[9] due to alternation effects.[8]

As part of our ongoing search for new magnetic coordination polymers,[10] we chose this ligand as a structural linker and magnetic separator to incorporate magnetic anisotropic chains into a higher dimensional network. We have used *trans*-1,2-chdc to prepare laminated coordination polymer $^{2}_{\infty}[Co^{II}_{3}(OH)_2(trans\text{-}1,2\text{-}chdc)_2]$ (**1**) exhibiting magnetism due to coexistent spin frustration and long-range magnetic ordering.[10a] Interestingly, at lower reaction pH value and temperature, we obtained the new laminated product $^{2}_{\infty}[Co^{II}(trans\text{-}1,2\text{-}chdc)]$ (**2**) as a pure phase, which consists of a parallel arrangement of carboxylate-bridged, paddle-wheel Co^{II} chains and shows interesting SCM behavior.

In the single-crystal structure of **2**, the Co^{II} atom (Figure 1 and Figure S1) adopts a slightly distorted square-pyramidal geometry with four basal oxygen atoms (Co–O 1.971(3)–2.210(3) Å) and one apical oxygen atom (Co–O 2.019(3) Å) giving a small τ value of 0.028 ($\tau = 0$ for an ideal square pyramid)[11] and slight displacement (0.34 Å) of the Co^{II} atom from the basal plane. A pair of inversely related Co^{II} ions are bridged by four μ-carboxylate groups into a paddle-wheel dimer with an intradimer $Co^{II}\cdots Co^{II}$ distance of 2.912(1) Å. Interestingly, a pair of such adjacent, inversely related Co^{II} dimers are bridged by a pair of μ-carboxylato-O bridges (Co-O-Co 101.1(1)°; interdimer $Co^{II}\cdots Co^{II}$ distance 3.269(1) Å) to form a chain that is structurally analogous to those observed previously for Cu^{II}, Rh^{II}, and Ni^{II}.[12] Adjacent chains are interlinked into layers by *trans*-1,2-chdc ligands with a shortest interchain $Co^{II}\cdots Co^{II}$ distance of about 5.5 Å. Such

[*] Y.-Z. Zheng, Prof. Dr. M.-L. Tong, W.-X. Zhang, Prof. Dr. X.-M. Chen
MOE Laboratory of Bioinorganic and Synthetic Chemistry
State Key Laboratory of Optoelectronic Materials and Technologies
School of Chemistry and Chemical Engineering
Sun Yat-Sen University
Guangzhou 510275 (China)
Fax: (+86) 20-8411-2245
E-mail: cxm@mail.sysu.edu.cn

[**] This work was supported by the NSFC (No. 20531070) and Science and Technology Department of Guangdong Province (No. 04205405). The authors are grateful to Prof. Song Gao and Dr. Wolfgang Wernsdorfer for fruitful discussions.

Supporting information for this article is available on the WWW under http://www.angewandte.org or from the author.

WILEY InterScience DISCOVER SOMETHING GREAT
© 2006 Wiley-VCH Verlag GmbH & Co. KGaA, Weinheim

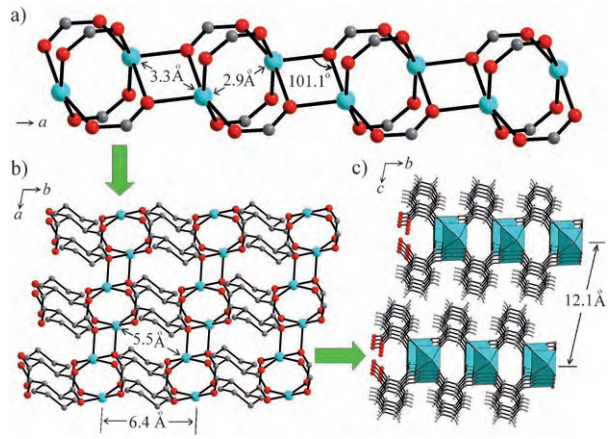

Figure 1. Perspective views of the a) paddle-wheel chain, b) layer, and c) crystal packing with the Co^{II} atoms highlighted as blue polyhedra in **2** (C gray, Co blue, O red).

layers are further stacked along the *c* axis solely by van der Waals interactions with a shortest interlayer $Co^{II}\cdots Co^{II}$ distance of about 12.1 Å.

The effect of this structural arrangement on the magnetism of **2** is evident. The dc susceptibility data (Figure 2) measured on a powder sample of **2** show that the χT value of **2**

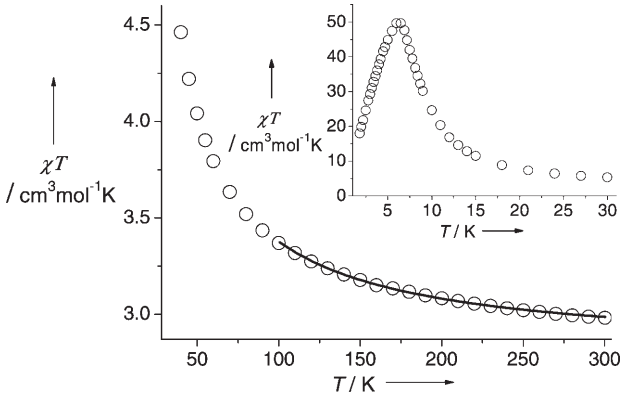

Figure 2. Plot of χT vs. *T* at an applied field of 500 Oe from 50 to 300 K; solid line: fitted by the modified Fisher model for 1D alternating chain ($S=^3/_2$). Inset: χT vs. *T* plot from 2 to 30 K.

at 300 K is 2.98 $cm^3 mol^{-1} K$ per Co^{II} ion, which is significantly larger than the spin-only value of 1.88 $cm^3 mol^{-1} K$ and hence indicates a large orbital contribution. On cooling, it gradually increases to about 30 K without the presence of a minimum, and the data in the range of 50–300 K obeys the Curie–Weiss law ($\chi_m = C/(T-\theta)$, with $C = 2.83\ cm^3 mol^{-1} K$ and $\theta = 15.87$ K). The set of data above 100 K were well fitted by the modified Fisher model for a 1D alternating chain ($S=^3/_2$), and the spin Hamiltonian[13] reads as Equation (1), where J_1 and J_2 are the intrachain alternating coupling constants, and the interchain interactions are described by the mean-field approximation: $\chi_M = \chi_{chain}/(1-zJ'\chi_{chain}/Ng^2\beta^2)$; for magneto-structural correlation, see Scheme S1. The best fit gave $J_1/k_B = 11.51$ K, $J_2/k_B = 3.95$ K, $g = 2.45$, $zJ'/k_B = -0.01$ K, and $R = 4.5\times10^{-5}$, where $R = S[(\chi_{mT})_{obs}-(\chi_{mT})_{calcd}]^2/[(\chi_{mT})_{obs}]^2$.[13]

$$H = -J_1 \sum S_{2i}\, S_{2i+1} - J_2 \sum S_{2i+1}\, S_{2i+2} \qquad (1)$$

The two positive values ($J_1 > J_2 > 0$) reveal that the intrachain interactions are ferromagnetic and inequivalent. Assuming the fitting results are correct, the ratio $|J'/J_{average}|$ (assuming $z=2$) of about 6.5×10^{-4} indicates that the magnetic interchain interactions are very weak compared with the intrachain interaction.[3a] The undoubtedly ferromagnetic coupling within the tetracarboxylate-bridged Co^{II} paddle wheels is unprecedented.[14] The data below 30 K (inset of Figure 2), however, show a not-so-round peak at 6.0 K (usually, a round peak correlates with 1D behavior, while a cusp suggests 3D ordering).[3j] Similar peaks were also observed in some previously reported SCMs[3b,f,k] and were explained as a short-range saturation effect[3f] or 1D Ising behavior.[3b] Since the magnetic field applied to **2** was only 500 Oe, this not-so-round peak is more likely to correlate with Ising-like ferromagnetic behavior rather than the saturation effect or a 3D ordered phase,[15] and this required further study.

Therefore, we performed magnetization measurements on an orientated single crystal of **2** in order to understand the low-temperature magnetism of **2** in more detail. As shown in Figure 3, the magnetization is significantly anisotropic below 50 K. Rotational measurements of magnetization on a single crystal of **2** (Figure S2) reveal an unambiguously uniaxial anisotropic magnetism.[16] The uniaxial anisotropic behavior is also reflected in the field dependence of magnetization along the easy-axis direction (inset of Figure 3), which quickly saturates at 4.10 μ_B per Co^{II} unit.

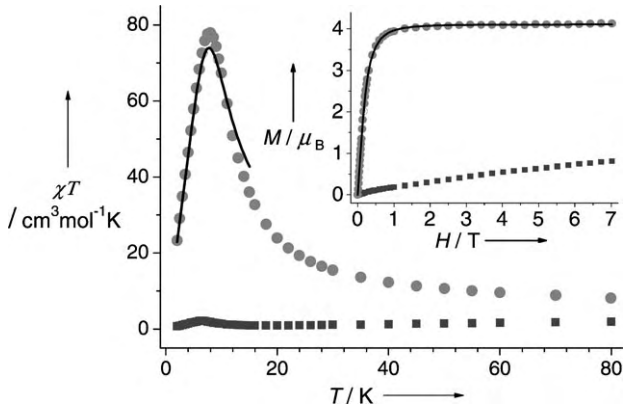

Figure 3. Field-cooled magnetization with an applied field of 2 KOe from 80 to 2 K of a single crystal of **2** along (●) and perpendicular to the easy-axis direction (■); solid line: best fit of the 1D Ising model. Inset: Field dependence of the magnetization at 10 K; solid line: best fit of the 1D Ising model.

To model these results, the simplest relevant approach is 1D Ising model with $S=^1/_2$ and anisotropic *g* value, since the Co^{II} ion is most frequently Ising-like with $S_{eff}=^1/_2$ at low temperatures (typically below 30 K),[16] the Hamiltonian

 © 2006 Wiley-VCH Verlag GmbH & Co. KGaA, Weinheim

can be written as Equation (2). To identify this expression with Glauber's notation,[17] one should introduce $\sigma_i = -2S_{Tz,i}$ ($=\pm 1$), and the Hamiltonian now is expressed by Equation (3).[3b,18]

$$H = -J_{\text{eff}} \sum S_{Tz,i} S_{Tz,i+1} + g_z \mu_B H_z \sum S_{Tz,i} \; ; J_{\text{eff}} = J_1 = J_2 \qquad (2)$$

$$H = -J'_{\text{eff}} \sum \sigma_i \sigma_{i,i+1} - \mu_{\text{eff}} H \sum \sigma_i \; ; J'_{\text{eff}} = {}^1\!/_4 J_{\text{eff}} \; , \mu_{\text{eff}} = {}^1\!/_2 g_z \mu_B \qquad (3)$$

This model gives the magnetization as the function of temperature and magnetic field [Equation (4)].[3b,18]

$$M = N \mu_{\text{eff}} \sin h(\mu_{\text{eff}} H/k_B T)/[\sin h^2(\mu_{\text{eff}} H/k_B T) + \exp(-4J'_{\text{eff}}/k_B T)]^{1/2} \qquad (4)$$

This expression was used to fit the data between 2 and 15 K (solid lines in Figure 3 and its inset), and this led to $g_z = 8.20$, $\mu_{\text{eff}}/\mu_B = {}^1\!/_2 g_z = 4.10$, $J'_{\text{eff}}/k_B = 8.89$ K, and $R = 8 \times 10^{-4}$. This satisfactory result confirms that the χT peak and the rapid saturation of the magnetization along the chain (inset of Figure 3) is compatible with 1D Ising behavior and does not imply long-range ordering.

Below 3.5 K, irreversibility effects are observed in static magnetic measurements as the discrepancy between zero-field-cooled (ZFC) and field-cooled (FC) magnetization in an applied external field (Figure S3). Furthermore, hysteresis loops clearly appear below 2.2 K with orientation- and temperature-dependent shape (Figure 4). Along the easy-axis direction, the coercive fields are 5, 31, and 165 Oe at 2.2, 2.0, and 1.8 K, respectively. Interestingly, the coercive field and the saturated magnetic moment along the easy-axis direction at 1.8 K are almost twice that of the powder sample (Figure S4). It is also noteworthy that the hysteresis loops along the easy-axis direction exhibit "steps" at the original region due to the effect of weak interchain interaction,[3j] which can be easily overcome by a small external field. The dM/dH curve at 1.8 K clearly shows that the critical field H_C is 45 Oe in this direction, which could be used to estimate the interchain interaction by the expression $g_z \mu_B H_C S_T = 2 |zJ'| S_T^2$,[19] giving $|zJ'| = 0.025$ K ($S_T = {}^1\!/_2$). This result is in agreement with the $|zJ'|$ value obtained from the alternating chain model with $S = {}^3\!/_2$ and provides further support for the weak interchain interaction. Even though such aforementioned behaviors are usually observed in ferro-/ferrimagnetically ordered magnetism, another possibility could be the presence of a frozen magnetized state caused by the strong anisotropy.[3b] To gain more insight into the magnetic properties of **2**, we performed detailed ac magnetic measurements.[20]

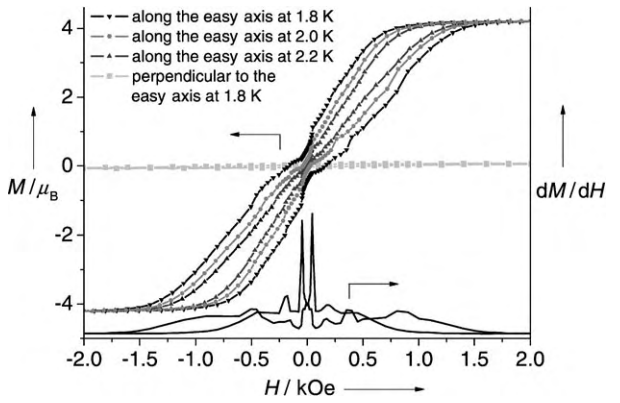

Figure 4. Top: hysteresis loops of a single crystal of **2**. Bottom: Plot of dM/dH vs. H at 1.8 K.

Below 6.5 K, the real (χ') and imaginary (χ'') components of the ac susceptibility are strongly frequency-dependent (Figure 5). This behavior precludes any significant 3D ordering, and confirms that the very "robust" Glauber dynamic region is unaffected by possible weak interchain interactions.[3j,21] The peak temperatures T_p of χ'' can be well fitted by the Arrhenius plot extracted from these data (inset of Figure 5, bottom), which shows the occurrence of a clear crossover between two different activated regions at $T^* = 4.4$ K ($1/T^* = 0.227$ K^{-1}), giving best-fit physical τ_0 values of 5.19×10^{-11} and 5.59×10^{-8} s for the high- and low-temperature regions, respectively, and two corresponding different barriers ($\Delta_{\tau 1}/k_B = 80.9$ and $\Delta_{\tau 2}/k_B = 50.2$ K). This result is in agreement with the observed finite-size effect (i.e., the presence of structural defects on the chain which limit the growth of the correlation)[22] halving the Glauber activation barrier for SCMs. This crossover behavior is also evident from the plot of ln(χT) versus 1/T. Figure S5 shows ln(χT) increas-

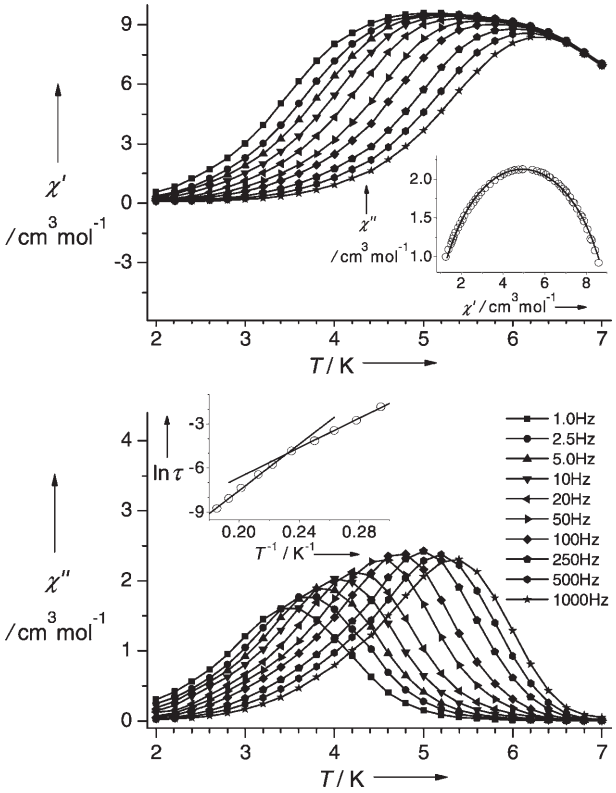

Figure 5. Top: Real part of ac susceptibility (inset: Cole–Cole diagram at 4.2 K). Bottom: Imaginary part of ac susceptibility (inset: peak temperatures of χ'' fitted by Arrhenius law for a powder sample of **2**).

 © 2006 Wiley-VCH Verlag GmbH & Co. KGaA, Weinheim

ing linearly between 40 and 10 K with an energy gap of $\Delta_\xi/k_B = 24.0$ K (the value obtained by fitting the expression $\chi T = C_{eff}\exp(\Delta_\xi/k_B T)$ between 10 to 40 K). In theory, the energy gap obtained by fitting the plot of $\ln(\chi T)$ versus $1/T$ should be equal to $\Delta_{\tau 1} - \Delta_{\tau 2}$.[22e] Some disagreement seems to exist compared to the previous perfect examples.[3b,h,22a] The obtained Δ_ξ values are probably indicative of a wide distribution of chain lengths or just within the reasonable scope of the experimental error, in accord with some previous reports.[3a,j] In addition, the peak temperatures T_p of χ' can be measured by the parameter $\phi = (\Delta T_p/T_p)/\Delta(\lg f) = 0.10$,[23] which is in the range of normal superparamagnets and precludes the possibility of a spin glass. Moreover, the shape of the Cole–Cole diagram (inset of Figure 5, top) obtained at 4.2 K, which can be fitted by a generalized Debye model with an α value of 0.10, indicates a narrow distribution of relaxation time,[24] in agreement with the observed crossover behavior.

In summary, the above evidence reveals an interesting SCM behavior for **2**. Such behavior is mainly caused by the strong anisotropic intrachain ferromagnetic interactions that significantly "freeze" the magnetization in one direction and prevent easy reversal of the spins or 3D ordering behavior induced by interchain interactions. More importantly, the covalent-linking strategy described here should be suitable for preparing other SCMs. Longer σ-bonding linkers should be better suited to obtaining ideal SCM behavior.

Experimental Section

2: In a typical hydrothermal reaction, a mixture of $CoCl_2{\cdot}6H_2O$ (0.237 g, 1 mmol), 1,2-chdcH_2 (0.172 g, 1 mmol), and triethylamine (0.200 g, 2.0 mmol) in deionized water (10 mL) was sealed in a 23-mL teflon-lined autoclave and heated at 160 °C for 5 d to give dark red platelike crystals of **2** (87% yield), which was verified by powder XRD to be a pure phase (Figure S6). IR data for **2**: $\tilde{\nu} = 2928$ (m), 2957(w), 1600 (vs), 1540 (s), 1448 (s), 1417 (s), 1336 (w), 1290 (w), 1238 (w), 1116 (w), 1039 (w), 932 (w), 860 (w), 773 (w), 707 (m), 615 (w), 529 (w), 447 cm^{-1} (w). Elemental analysis (%) calcd for **2**: C 41.94, H 4.40; found: C 41.88, H 4.38. A large single crystal of **2** (8.0 mg, $3.7 \times 2.1 \times 0.4$ mm, see Figure S7) used in anisotropic magnetic measurements was grown in one month.

Crystal data of **2**: triclinic, $P\bar{1}$ (no. 2); $a = 5.1528(4)$, $b = 6.5380(6)$, $c = 13.366(1)$ Å, $\alpha = 99.260(1)$, $\beta = 97.900(1)$, $\gamma = 102.229(1)°$, $V = 427.42(6)$ Å^3, $Z = 2$, $\rho = 1.78$ g cm^{-3}, $\mu = 1.98$ mm^{-1}, final $R_1 = 0.0473$ for $I \geq 2\sigma(I)$, $wR_2 = 0.1352$ for all data. The intensity data were recorded on a Bruker SMART Apex CCD system with $Mo_{K\alpha}$ radiation ($\lambda = 0.71073$ Å) at 293 K. The structure was solved by direct methods and refined by full-matrix least-squares techniques on F^2 using SHELXTL. CCDC-601744 contains the supplementary crystallographic data for this paper. These data can be obtained free of charge from The Cambridge Crystallographic Data Centre via www.ccdc.cam.ac.uk/data_request/cif.

Magnetic susceptibility measurements on **2** were performed with a Quantum Design MPMS-XL7 SQUID. Hysteresis loops were measured in the "hysteresis mode". Data were corrected for the diamagnetic contribution calculated from Pascal constants.

Received: April 5, 2006
Revised: May 26, 2006
Published online: August 25, 2006

Keywords: carboxylate ligands · cobalt · crystal engineering · hydrothermal synthesis · magnetic properties

[1] Review: a) D. Gatteschi, R. Sessoli, *Angew. Chem.* **2003**, *115*, 278; *Angew. Chem. Int. Ed.* **2003**, *42*, 268; and references therein.
[2] R. Sessoli, D. Gatteschi, A. Caneschi, M. A. Novak, *Nature* **1993**, *365*, 141.
[3] For examples, see a) A. Caneschi, D. Gatteschi, N. Lalioti, C. Sangregorio, R. Sessoli, G. Venturi, A. Vindigni, A. Rettori, M. G. Pini, M. A. Novak, *Angew. Chem.* **2001**, *113*, 1810; *Angew. Chem. Int. Ed.* **2001**, *40*, 1760; b) R. Clérac, H. Miyasaka, M. Yamashita, C. Coulon, *J. Am. Chem. Soc.* **2002**, *124*, 12837; c) R. Lescouëzec, J. Vaissermann, C. Ruiz-Pérez, F. Lloret, R. Carrasco, M. Julve, M. Verdaguer, Y. Dromzee, D. Gatteschi, W. Wernsdorfer, *Angew. Chem.* **2003**, *115*, 1521; *Angew. Chem. Int. Ed.* **2003**, *42*, 1483; d) T.-F. Liu, D. Fu, S. Gao, Y.-Z. Zhang, H.-L. Sun, G. Su, Y.-J. Liu, *J. Am. Chem. Soc.* **2003**, *125*, 13976; e) S. Wang, J.-L. Zuo, S. Gao, H.-C. Zhou, Y.-Z. Zhang, X.-Z. You, *J. Am. Chem. Soc.* **2004**, *126*, 8900; f) E. Pardo, R. Ruiz-Garća, F. Lloret, J. Faus, M. Julve, Y. Journaux, F. Delgado, C. Ruiz-Pérez, *Adv. Mater.* **2004**, *16*, 1597; g) N. E. Chakov, W. Wernsdorfer, K. A. Abboud, G. Christou, *Inorg. Chem.* **2004**, *43*, 5919; h) M. Ferbinteanu, H. Marilena, W. Wernsdorfer, K. Nakata, K.-i. Sugiura, M. Yamashita, C. Coulon, R. Clérac, *J. Am. Chem. Soc.* **2005**, *127*, 3090; i) T. Kajiwara, M. Nakano, Y. Kaneko, S. Takaishi, T. Ito, M. Yamashita, A. Igashira-Kamiyama, H. Nojiri, Y. Ono, N. Kojima, *J. Am. Chem. Soc.* **2005**, *127*, 10150; j) L. Bogani, C. Sangregorio, R. Sessoli, D. Gatteschi, *Angew. Chem.* **2005**, *117*, 5967; *Angew. Chem. Int. Ed.* **2005**, *44*, 5817; k) Z.-M. Sun, A. V. Prosvirin, H.-H. Zhao, J.-G. Mao, K. R. Dunbar, *J. Appl. Phys.* **2005**, *97*, 10B305; l) L. M. Toma, R. Lescouëzec, J. Pasán, C. Ruiz-Pérez, J. Vaissermann, J. Cano, R. Carrasco, W. Wernsdorfer, F. Lloret, M. Julve, *J. Am. Chem. Soc.* **2006**, *128*, 4842; m) X.-J. Li, X.-Y. Wang, S. Gao, R. Cao, *Inorg. Chem.* **2006**, *45*, 1508.
[4] a) W. Wernsdorfer, N. Aliaga-Alcalde, D. N. Hendrickson, G. Christou, *Nature* **2002**, *416*, 406; b) W. Wernsdorfer, S. Bhaduri, R. Tiron, D. N. Hendrickson, G. Christou, *Phys. Rev. Lett.* **2002**, *89*, 197201; c) S. Hill, R. S. Edwards, N. Aliaga-Alcade, G. Christou, *Science* **2003**, *302*, 1015.
[5] a) M. Murugesu, R. Clérac, W. Wernsdorfer, C. E. Anson, A. K. Powell, *Angew. Chem.* **2005**, *117*, 6836; *Angew. Chem. Int. Ed.* **2005**, *44*, 6678; b) R. Tiron, W. Wernsdorfer, N. Aliaga-Alcade, G. Christou, *Phys. Rev. B* **2003**, *68*, 140407; c) R. Tiron, W. Wernsdorfer, D. Foguet-Albiol, N. Aliaga-Alcade, G. Christou, *Phys. Rev. Lett.* **2003**, *91*, 227203; d) J. Larionova, M. Gross, M. Pilkington, H. Andres, H. Stoeckli-Evans, H. U. Güdel, S. Decurtins, *Angew. Chem.* **2000**, *112*, 1667; *Angew. Chem. Int. Ed.* **2000**, *39*, 1605; e) J. C. Goodwin, R. Sessoli, D. Gatteschi, W. Wernsdorfer, A. K. Powell, S. L. Heath, *J. Chem. Soc. Dalton Trans.* **2000**, 1835; f) M. Affronte, J. C. Lasjaunias, W. Wernsdorfer, R. Sessoli, D. Gatteschi, S. L. Heath, A. Fort, A. Rettori, *Phys. Rev. B* **2002**, *66*, 064408.
[6] a) H. Miyasaka, K. Nakata, L. Lollita, C. Coulon, Y. Nakazawa, T. Fujisaki, K.-i. Sugiura, M. Yamashita, R. Clérac, *J. Am. Chem. Soc.* **2006**, *128*, 3770; b) L. Lecren, O. Roubeau, C. Coulon, Y.-G. Li, X. F. L. Goff, W. Wernsdorfer, H. Miyasaka, R. Clérac, *J. Am. Chem. Soc.* **2005**, *127*, 17353; c) H. Miyasaka, K. Nakata, K.-i. Sugiura, M. Yamashita, R. Clérac, *Angew. Chem.* **2004**, *116*, 725; *Angew. Chem. Int. Ed.* **2004**, *43*, 707.
[7] C. Boskovic, R. Bircher, P. L. W. Tregenna-Piggott, H. U. Güdel, C. Paulsen, W. Wernsdorfer, A.-L. Barra, E. Khatsko, A. Neels, H. Stoeckli-Evans, *J. Am. Chem. Soc.* **2003**, *125*, 14046.
[8] P. Day, *J. Chem. Soc. Dalton Trans.* **1997**, 701.
[9] L. S. Kramer, A. W. Clauss, L. C. Francesconi, D. R. Corbin, D. N. Hendrickson, G. D. Stucky, *Inorg. Chem.* **1981**, *20*, 2070.

 © 2006 Wiley-VCH Verlag GmbH & Co. KGaA, Weinheim

[10] a) Y.-Z. Zheng, M.-L. Tong, W.-X. Zhang, X.-M. Chen, *Chem. Commun.* **2006**, 165; b) M.-H. Zeng, W.-X. Zhang, X.-Z. Sun, X.-M. Chen, *Angew. Chem.* **2005**, *117*, 3139; *Angew. Chem. Int. Ed.* **2005**, *44*, 3079.
[11] A. W. Addison, T. N. Rao, J. Reedijk, J. van Rijn, G. C. Verschoor, *J. Chem. Soc. Dalton Trans.* **1984**, 1349.
[12] a) B. Kozlevčar, I. Leban, M. Petrič, S. Petriček, O. Roubeau, J. Reedijk, P. Šegedin, *Inorg. Chim. Acta* **2004**, *357*, 4220; b) F. A. Cotton, E. V. Dikarev, S.-E. Stiriba, *Inorg. Chem.* **1999**, *38*, 4877; c) M. Dan, C. N. R. Rao, *Angew. Chem.* **2006**, *118*, 287; *Angew. Chem. Int. Ed.* **2006**, *45*, 281; d) E. V. Dikarev, A. S. Filatov, R. Clérac, M. A. Petrukhina, *Inorg. Chem.* **2006**, *45*, 744.
[13] Special care should be taken in using this fitting result because this Hamiltonian is based 1) on the classical spin operators (for details, see R. Cortés, M. Drillon, X. Solans, L. Lezama, T. Rojo, *Inorg. Chem.* **1997**, *36*, 677) and 2) also on the Heisenberg model, but single-crystal magnetic studies show that the system is highly anisotropic even up to 80 K.
[14] According to our search of the Cambridge Crystallographic Database: CSD version 5.27 updates (January 2006), 14 compounds with tetracarboxylate-bridged Co^{II} dimers were recorded, and only one of them was magnetically studied; it showed anitiferromagnetism: A. A. Pasynskii, T. C. Idrisov, V. M. Novotortsev, V. T. Kalinnikov, *Koord. Khim.* **1975**, *1*, 1059. The ferromagnetic coupling in this case probably arises from the orbital orthogonality of d_{xz} and d_{z^2} through the space of the dimer (see Scheme S2) However, the exact mechanism can not be concluded without theoretical calculations.
[15] a) O. Kahn, *Molecular Magnetism*, VCH, New York, **1993**; b) C. L. Carlin, *Magnetochemistry*, Springer, Berlin, **1986**.
[16] However, we are unable to directly correlate the easy axis with the crystallographic axes for such a triclinic crystal. The easy axis is probably along the direction of the most distorted Co–O bond (which is about 40° from the crystallographic *ab* plane, according to previous reports on SCMs with octahedrally coordinated Co^{II} atoms,[3a,c,d] in which the easy axes are usually referred to the most distorted bonds of the octahedra.
[17] R. J. Glauber, *J. Math. Phys.* **1963**, *4*, 294.
[18] C. J. Thompson, *Phase Transition and Critical Phenomena*, *Vol. 1* (Eds.: C. Domb, M. S. Green), Academic Press, London, **1972**, pp. 177–226.
[19] S. Chikazumi, *Physics of Ferromagnetism*, Clarendon Press, Oxford Science Publications, Oxford, **1997**, p. 521.
[20] Specific-heat variation is also a very sensitive method to determine the ordering state. Unfortunately, we cannot perform this measurement with our SQUID.
[21] S. Žumer, *Phys. Rev. B* **1980**, *21*, 1298.
[22] a) C. Coulon, R. Clérac, L. Lecren, W. Wernsdorfer, H. Miyasaka, *Phys. Rev. B* **2004**, *69*, 132408; b) H. Miyasaka, R. Clérac, K. Mizushima, K.-i. Sugiura, M. Yamashita, W. Wernsdorfer, C. Coulon, *Inorg. Chem.* **2003**, *42*, 8203; c) L. Bogani, A. Caneschi, M. Fedi, D. Gatteschi, M. Massi, M. A. Novak, M. G. Pini, A. Rettori, R. Sessoli, A. Vindigni, *Phys. Rev. Lett.* **2004**, *92*, 207204; d) L. Bogani, R. Sessoli, M. G. Pini, A. Rettori, M. A. Novak, P. Rosa, M. Massi, M. E. Fedi, L. Giuntini, A. Caneschi, D. Gatteschi, *Phys. Rev. B* **2005**, *72*, 064406; e) C. Coulon, H. Miyasaka, R. Clérac, *Struct. Bonding (Berlin)* **2006**, *122*, 163.
[23] $\phi = 0.01$ is a typical value for a spin glass. For details, see J. A. Mydosh, *Spin Glasses: An Experimental Introduction*, Taylor & Francis, London, **1993**.
[24] K. S. Cole, R. H. Cole, *J. Chem. Phys.* **1941**, *9*, 341.

 © 2006 Wiley-VCH Verlag GmbH & Co. KGaA, Weinheim

Conductive Polymers

DOI: 10.1002/anie.200601694

Processing of Polyacetylene from Aqueous Nanoparticle Dispersions**

*Johannes Huber and Stefan Mecking**

Conjugated, conductive polymers are the key component in the development of flexible displays, low-cost, large-scale displays, and thin-film transistors.[1] However, ever since the seminal discovery of the conductive nature of ("doped") polyacetylene by Heeger, McDiarmid, Shirakawa, and co-workers, the processing of conductive polymers into devices has been a critical issue.[2–7] The rigid conjugated polymer backbone results in very low solubilities in organic solvents and thermal properties that prohibit thermoplastic processing. These drawbacks can be overcome to some extent by introducing substituents as side chains, which, however, also alters the electronic properties and often requires additional synthetic effort.[1] Polyacetylene itself is still considered unprocessable.[4–8] Grafting to other polymers has been reported to result in processable materials.[9–11] We report a different approach, namely, the synthesis of aqueous dispersions of submicron polyacetylene particles by catalytic polymerization in emulsion. Such dispersions are suited for processing by printing techniques, as exemplified by the generation of a polyacetylene-based functioning electronic circuit by ink-jet printing as a straightforward and versatile technique.

The concept of processing polyacetylene from polymer particle dispersions was suggested early on, but hitherto has not been reported.[12,13,38] The few examples of polyacetylene particle dispersions reported to date are restricted to dispersions of polyacetylene in organic solvents.[12,14,15] The reported catalyst productivities are very low (35 mol acetylene per mol metal),[15] such that metal residues can be problematic for polymer stability and also for the electronic properties. It is well known that polymer particles can be stabilized in aqueous dispersions effectively by appropriate surfactants. Printing techniques are usually developed for aqueous systems. The insolubility of most polymers in water can be advantageous in the preparation of multilayer devices, in which the application of organic solvents often poses

[*] Dipl.-Chem. J. Huber, Prof. Dr. S. Mecking
Universität Konstanz
Lehrstuhl für Chemische Materialwissenschaft
Fachbereich Chemie
Universitätsstrasse 10, 78457 Konstanz (Germany)
Fax: (+49) 7531-88-5152
E-mail: stefan.mecking@uni-konstanz.de

[**] We thank Ralf Thomann (Freiburg) for TEM micrographs. S.M. is indebted to the Fonds der Chemischen Industrie for support.

Supporting information for this article (materials and methods; time course of acetylene polymerization; circuit diagram of the sound generator) is available on the WWW under http://www.angewandte.org or from the author.

InterScience
© 2006 Wiley-VCH Verlag GmbH & Co. KGaA, Weinheim

problems because of unwanted re-dissolution of already applied layers. For these reasons, we studied the approach of aqueous polyacetylene dispersions.

Aqueous polymer dispersions are traditionally prepared by free-radical routes.[16] However, the polymerization of acetylene is viable only catalytically. The sensitivity of catalysts towards water is a major issue for catalytic polymerizations in aqueous systems. The most common catalysts for insertion polymerization are based on early transition metals, most prominently complexes with d^0 metals such as titanium and zirconium. These complexes are highly oxophilic and very reactive towards water. By comparison, complexes of late transition metals, usually with d^8 metals, are softer Lewis acids and consequently less oxophilic.[9–11,17–20]

Cationic palladium diphosphine complexes are well known to copolymerize olefins with carbon monoxide by an insertion mechanism, and they have been noted to polymerize substituted acetylenes in non-aqueous systems.[21–24] However, in general, acetylene polymerization appears to be less viable than polymerization of substituted acetylenes in terms of catalysts suited and catalyst activity.[25–27] By studying different diphosphine-based catalysts, we found that a palladium(II) catalyst modified by 1,3-bis(di-*tert*-butyl)phosphinopropane (**1**)[28] is very active for the polymerization of acetylene in aqueous emulsion (Table 1).[29] To prepare a dispersion of small (submicron) particles, the initial reaction mixture including the hydrophobic catalyst must be highly disperse.[30–34] A mixture of **1** and $Pd(OAc)_2$ was dissolved in a small volume of hexane/ethanol, and mixed with an aqueous solution of sodium dodecylsulfate (SDS) surfactant and methane sulfonic acid.[35] Sonication of the mixture afforded a miniemulsion. Gentle stirring under an acetylene atmosphere at ambient pressure resulted in the formation of an intensely colored, black dispersion (Figure 1). TEM images (Figure 2) reveal unexpectedly small particle sizes of approximately 20 nm.

A possible mechanism for the particle formation involves polymerization starting in the hexane miniemulsion droplets. As polyacetylene is highly insoluble, it should precipitate rapidly during polymerization to form particles, which may exit the droplets and stabilize themselves by adsorption of surfactant. If the active sites remain within the hexane droplets, particles could form continuously. This assumption is supported by the observation that polymerization continues for hours, even though swelling of existing particles with monomer should be very low. Although speculative at this point, this mechanism would account for the unusually small particle sizes observed (much smaller than miniemulsion droplets).

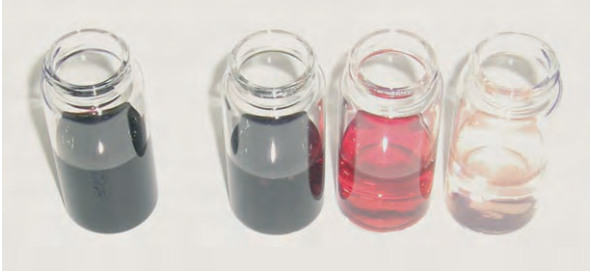

Figure 1. Appearance of a polyacetylene dispersion (polymer solids content 6.4%). Left to right: undiluted, 10^3-, 10^4-, and 10^5-fold dilution.

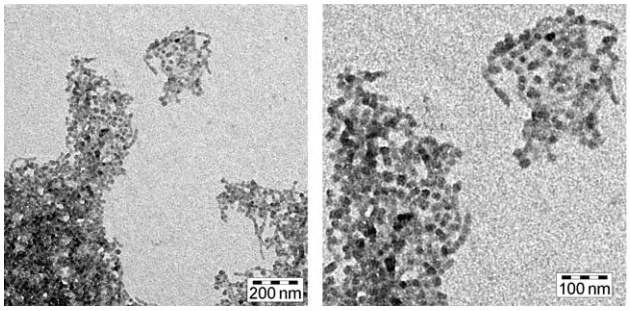

Figure 2. TEM images of polyacetylene particles (entry 3 in Table 1).

Table 1: Synthesis of polyacetylene dispersions.[a]

Entry	Pd [μmol]	Surfactant conc. [% w/w]	*T* [°C]	Reaction time [h]	Polymer solids content[b] [%]
1	78	1.0	25	1	0.7
2	90	2.5	25	3	4.2
3	90	2.5	25	6	6.5
4	90	4.0	25	6	6.9
5	90	2.0	50	2	2.2

[a] $Pd(OAc)_2/tBu_2P(CH_2)_3PtBu_2 = 1:3$; surfactant: SDS; total volume: 40 mL (entries 2, 4), 50 mL (entries 1, 3, 5). [b] Polymer solids content only, emulsifier excluded.

Optimization of the catalyst loading, surfactant concentration, and reaction time afforded dispersions with polyacetylene solids contents of 7% w/w (Table 1). Catalyst productivities correspond to 1.4×10^3 mol acetylene per mol Pd. Drawing samples from an ongoing reaction revealed the catalyst to be active for more than six hours in aqueous emulsion (see the Supporting Information).

No difference in polymer yield was observed when acetylene was polymerized as received (99%, delivered as a solution in acetone adsorbed in diatomaceous earth) or purified by various methods (passage through concentrated sulfuric acid and activated carbon), which reveals that the catalyst is rather insensitive to monomer purity.

IR spectroscopy on the isolated bulk polymer reveals the material to contain a mixture of *cis* and *trans* repeat units (60:40). Tempering at 120 °C results in complete conversion to the *trans* structure, as reported previously for polyacetylene prepared with Shirakawa-type catalysts.[36]

Continuous films with a metallic luster could be obtained on various substrates, such as glass and paper, by simple dip-coating or spreading of dispersions on the substrate and subsequent drying (Figure 3). The films on paper are flexible and stable against dynamic bending. An average thickness of 0.7 μm was determined from the weight of the dispersion applied for a film prepared by spreading of a dispersion on high-gloss ink-jet paper and drying in warm air. After doping the film with iodine, the conductivity was found to be approximately 50 $S\,cm^{-1}$. Reported conductivities of bulk

 © 2006 Wiley-VCH Verlag GmbH & Co. KGaA, Weinheim

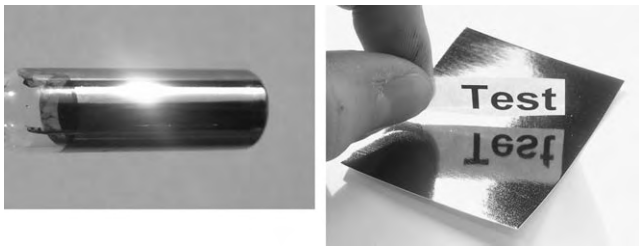

Figure 3. Polyacetylene film on glass formed by dip-coating into a dispersion (left), and film obtained by spreading on paper (right; smooth-surfaced paper for photo printing used).

polyacetylene vary considerably and are influenced by orientation induced by stretching and by the doping procedure. Values range from 10^2 to 10^5 $S\,cm^{-1}$.[3,6,37] In our films, the surfactant shell and possibly voids in the film may influence the conductivity. Polyacetylene is generally considered to be unstable in air.[4–6] Therefore, the conductivity of the films in air was measured over time. A decrease of conductivity to one fifth of the initial value was observed after 48 h. This result demonstrates a limited, but rather surprising, stability of the doped material in air, which is sufficient for the studies reported herein.

As a probe for facile processing into functional devices, the polyacetylene dispersions were printed by means of a commercial ink-jet printer. Dispersions were used as obtained with the addition of 5% v/v glycerol to adjust the drying rate. The printed films had an average thickness of around 10^2 nm. The circuit depicted in Figure 4 was printed on plain paper

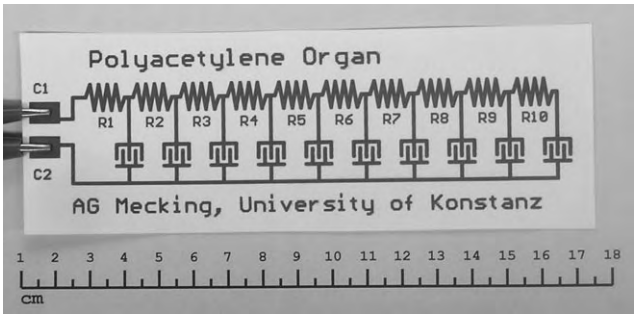

Figure 4. Ink-jet printed functional circuit board.

and subsequently doped. The polyacetylene circuit also fulfills the function of a resistor in this case. Upon contacting one of the comb-shaped "keypads" with a finger, the resistance between the two connectors of the board (C1, C2) drops to between 10^5 and 10^6 Ω, depending on the length of the circuit path (R1 to R10) of the individual key. The resistance can be translated into a tone by an appropriate circuit (see the Supporting Information), which allows simple tunes to be played.

In summary, we have demonstrated the facile processing of polyacetylene from aqueous dispersions of submicron particles. As an example, ink-jet printing provides functioning circuits composed of this conductive polymer, which is widely considered unprocessable. The key step that enables access to the required dispersions is catalytic polymerization in an aqueous emulsion, with a suitable late-transition-metal catalyst. This approach is also of interest for other conjugated hydrocarbon-backbone polymers, such as polyparaphenylenes or polyphenylenevinylidenes.

Experimental Section

Catalyst solution: Solutions of $Pd(OAc)_2$ (22.6 mg, 100 μmol) in acetonitrile (5 mL) and **1**[28] (99.7 mg, 300 μmol) in ethanol (5 mL) were mixed, and the solvent was evaporated in vacuo. The residue was dissolved in a mixture of ethanol (0.2 mL) and hexane (4.8 mL) to afford a catalyst solution with a concentration of 20 μmol Pd mL^{-1}. Solutions with up to 100 μmol Pd mL^{-1} were prepared in this fashion.

Polymerization procedure: A mixture of an aqueous solution (50 mL) of SDS (1.25 g), a drop of methane sulfonic acid, and catalyst solution (1.5 mL, 90 μmol Pd) was sonicated for 2 min in a 100-mL round-bottom Schlenk flask closed with a septum (Bandelin HD 2200 with a KE76 tip, operated at 120 W). The septum was replaced by a connector with a tube to a bubbler. Acetylene was gently streamed over the solution via the Schlenk stopcock under stirring for six hours.

Received: April 28, 2006
Revised: June 30, 2006
Published online: August 23, 2006

Keywords: conducting materials · conjugation · homogeneous catalysis · polyacetylenes · polymers

[1] *Handbook of Luminescence, Display Materials, and Devices* (Eds.: H. S. Nalwa, L. S. Rohwer), American Scientific Publishers, Stevenson Ranch, **2003**.
[2] H. Shirakawa, E. J. Louis, A. G. MacDiarmid, C. K. Chiang, A. J. Heeger, *J. Chem. Soc. Chem. Commun.* **1977**, 578–580.
[3] C. K. Chiang, M. A. Druy, S. C. Gau, A. J. Heeger, E. J. Louis, A. G. MacDiarmid, Y. W. Park, H. Shirakawa, *J. Am. Chem. Soc.* **1978**, *100*, 1013–1015.
[4] H. Shirakawa, *Angew. Chem.* **2001**, *113*, 2642–2648; *Angew. Chem. Int. Ed.* **2001**, *40*, 2574–2580.
[5] A. G. MacDiarmid, *Angew. Chem.* **2001**, *113*, 2649–2659; *Angew. Chem. Int. Ed.* **2001**, *40*, 2581–2590.
[6] A. J. Heeger, *Angew. Chem.* **2001**, *113*, 2660–2682; *Angew. Chem. Int. Ed.* **2001**, *40*, 2591–2611.
[7] L. M. Wilson in *Materials Science and Technology*, *Vol. 18* (Eds.: R. W. Cahn, P. Haasen, E. J. Kramer, E. H. Meijer), Wiley-VCH, Weinheim, **1997**, pp. 659–705.
[8] For example, to obtain a polyacetylene film, the polymer must be prepared directly in this shape by polymerization on a liquid surface[4] or a solid substrate: O. A. Sherman, R. H. Grubbs, *Synth. Met.* **2001**, *124*, 431–434.
[9] K. A. Ostoja-Starzewski in *Ziegler Catalysts* (Eds.: H.-H. Brintzinger, G. Fink, R. Mülhaupt), Springer, Berlin, **1995**, pp. 497–505.
[10] K. A. Ostoja Starzewski, G. M. Bayer, *Angew. Chem.* **1991**, *103*, 1012–1013; *Angew. Chem. Int. Ed. Engl.* **1991**, *30*, 961–962.
[11] K. A. Ostoja-Starzewski in *Late Transition Metal Polymerization Catalysis* (Eds.: B. Rieger, L. S. Baugh, S. Kacker, S. Striegler), Wiley-VCH, Weinheim, **2003**, pp. 1–26.
[12] J. Edwards, R. Fisher, B. Vincent, *Macromol. Rapid Commun.* **1983**, *4*, 393–397.
[13] B. Vincent, *Polym. Adv. Technol.* **1995**, *6*, 356–361.
[14] S. P. Armes, B. Vincent, *Synth. Met.* **1988**, *25*, 171–179.
[15] K. Müller, M. Klapper, K. Müllen, *Macromol. Rapid Commun.* **2006**, *27*, 586–593.

 © 2006 Wiley-VCH Verlag GmbH & Co. KGaA, Weinheim

[16] An alternative approach to polymer dispersions involves the dispersion of a pre-made polymer in water to so-called secondary dispersions. However, this approach again requires solubility of the polymer in an organic solvent or fusibility: see, for example, K. Landfester, R. Montenegro, U. Scherf, R. Güntner, U. Asawapirom, S. Patil, D. Neher, T. Kietzke, *Adv. Mater.* **2002**, *14*, 651 – 655.
[17] S. Mecking, *Angew. Chem.* **2001**, *113*, 550 – 557; *Angew. Chem. Int. Ed.* **2001**, *40*, 534 – 540.
[18] I. Amer, H. Schumann, V. Ravindar, W. Baidossi, N. Goren, J. Blum, *J. Mol. Catal.* **1993**, *85*, 163 – 171.
[19] E. Yashima, T. Matsushima, Y. Okamoto, *J. Am. Chem. Soc.* **1997**, *119*, 6345 – 6359.
[20] R. D'Amato, L. Medei, I. Venditti, M. V. Russo, M. Falconieri, *Mater. Sci. Eng. C* **2003**, *23*, 861 – 865.
[21] E. Drent, P. H. M. Budzelaar, *Chem. Rev.* **1996**, *96*, 663 – 681.
[22] E. Lindner, M. Schmid, J. Wald, J. A. Queisser, M. Geprägs, P. Wegner, C. Nachtigal, *J. Organomet. Chem.* **2000**, *602*, 173 – 187.
[23] E. Drent, D. H. L. Pello, Eur Pat. 576091 (Shell), **1993**.
[24] K. Li, G. Wei, J. Darkwa, S. K. Pollack, *Macromolecules* **2002**, *35*, 4573 – 4576.
[25] E. J. Ginsburg, C. B. Gorman, R. H. Grubbs in *Modern Acetylene Chemistry* (Ed.: P. J. Stang, F. Diederich), VCH, Weinheim, **1995**, pp. 353 – 383.
[26] N. Theophilou, R. Aznar, A. Munardi, J. Sledz, F. Schué, H. Naarmann, *J. Macromol. Sci. Part A* **1987**, *24*, 797 – 812.
[27] D. G. Belov, O. N. Efimov, G. P. Belov, *Plast. Eng.* **1998**, *45*, 297 – 330
[28] N. Carr, B. J. Dunne, L. Mole, A. G. Orpen, J. L. Spencer, *J. Chem. Soc. Dalton Trans.* **1991**, 863 – 868.
[29] The catalyst system also polymerizes phenylacetylene with very high activities in aqueous emulsion. Stable poly(phenylacetylene) dispersions with solids contents of up to 36% were obtained, with catalyst productivities of 2×10^5 mol phenylacetylene per mol Pd in a one-hour experiment.
[30] F. M. Bauers, S. Mecking, *Angew. Chem.* **2001**, *113*, 3112 – 3115; *Angew. Chem. Int. Ed.* **2001**, *40*, 3020 – 3022.
[31] R. Soula, C. Novat, A. Tomov, R. Spitz, J. Claverie, X. Drujon, J. Malinge, T. Saudemont, *Macromolecules* **2001**, *34*, 2022 – 2026.
[32] V. Monteil, P. Wehrmann, S. Mecking, *J. Am. Chem. Soc.* **2005**, *127*, 14568 – 14569.
[33] I. Göttker-Schnetmann, B. Korthals, S. Mecking, *J. Am. Chem. Soc.* **2006**, *128*, 7708 – 7709.
[34] S. Mecking, V. Monteil, J. Huber, L. Kolb, P. Wehrmann, *Macromol. Symp.* **2006**, *236*, 117 – 123.
[35] For a discussion of the function of acid in palladium(II)/phosphine catalysts, see reference [21].
[36] H. W. Gibson, S. Kaplan, R. A. Mosher, W. M. Prest, R. J. Weagley, *J. Am. Chem. Soc.* **1986**, *108*, 6843 – 6851.
[37] N. Basescu, Z.-X. Liu, D. Moses, A. J. Heeger, H. Naarmann, N. Theophilou, *Nature* **1987**, *327*, 403 – 405.
[38] Non-aqueous dispersions in mixtures of polar and nonpolar solvents reported very recently[15] can be processed by ink-jet printing: K. Müllen, personal communication.

 © 2006 Wiley-VCH Verlag GmbH & Co. KGaA, Weinheim

Photoisomerization

DOI: 10.1002/anie.200602088

Hierarchical Self-Assembly of Donor–Acceptor-Substituted Butadiene Amphiphiles into Photoresponsive Vesicles and Gels**

*N. S. Saleesh Kumar, Shinto Varghese, Gopinathan Narayan, and Suresh Das**

The construction of supramolecular architectures by the spontaneous self-assembly of molecules is currently a subject of great interest in areas that range from chemistry and biology to materials science.[1] Of particular interest is the design of externally addressable molecules that contain self-assembly elements, as these can give rise to so-called "smart materials".[2] Such addressable molecules could include among others, photochromics, which can be used to bring about light-induced changes in the self-assembly[3,4] or environment-sensitive luminophores, which can provide valuable insight into the nature of the molecular aggregation within such assemblies.[5] Herein, we present a novel class of donor–acceptor-substituted amphiphilic butadienes (Scheme 1) capable of undergoing spontaneous concentration-dependent hierarchical self-assembly from vesicles to gels. The self-assembly process was associated with unique changes in the fluorescence of the system. Moreover, the presence of a photoisomerizable chromophore makes these

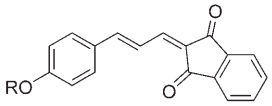

BINC8: R = C_8H_{17} BINC12: R = $C_{12}H_{25}$

BINC16: R = $C_{16}H_{33}$ BINC18: R = $C_{18}H_{37}$

Scheme 1. Structures of the molecules used in this study.

[*] N. S. S. Kumar, S. Varghese, G. Narayan, Dr. S. Das
Photosciences and Photonics Section
Chemical Sciences and Technology Division
Regional Research Laboratory, CSIR
Trivandrum, 695019 Kerala (India)
Fax: (+91) 471-249-1712
E-mail: sdaas@rediffmail.com

[**] This study was supported by the Department of Science and Technology (DST), Government of India (New Delhi), and Council of Scientific and Industrial Research (CSIR, Task Force Program, CMM 22). The authors thank Robert Philip for assistance with AFM studies, M. R. Chandran for SEM measurements, Dr. J. D. Sudha for the rheological studies, and Dr. M. R. Pillai (Director of the Rajiv Gandhi Centre for Biotechnology, Trivandrum) for TEM and confocal laser scanning microscopy experiments. N.S.S.K., S.V., and G.N. thank the CSIR (Government of India) for research fellowships (This is manuscript no. RRLT-PPS-218).

Supporting information for this article is available on the WWW under http://www.angewandte.org or from the author.

 © 2006 Wiley-VCH Verlag GmbH & Co. KGaA, Weinheim

materials photoresponsive. Such stimuli-responsive vesicles and gels are becoming increasingly important because of their obvious implications in controlled-release systems.[4d,6,7]

The butadiene derivatives were synthesized in a multistep process, and their structures were established by FTIR and ^{1}H and ^{13}C NMR spectroscopy, high-resolution mass spectrometry, and elemental analysis.[8] ^{1}H NMR spectroscopic analysis revealed that the compounds existed as their *E* isomers.[8] All the derivatives formed transparent gels in polar solvents, such as alcohols, acetonitrile, and dimethyl sulfoxide (DMSO).[8] As BINC18 gels were the most stable, detailed studies were carried out on this molecule. BINC18 was observed to be capable of gelating polar solvents at very low concentrations. Its critical gelator concentration (CGC), which ranged from 1.3 to 1.7×10^{-3} M,[8] was comparable to that of some of the best low-molecular-weight gelators.[5f,6i,9]

Microscopic investigations of solutions of BINC18 provided clear evidence for a hierarchical build-up of supramolecular assemblies, which started from small-sized vesicles at lower concentrations to larger vesicles at intermediate concentrations, until gel formation occurred in the millimolar concentration range. The formation of aggregates was spontaneous and did not require any special effects, such as ultrasonication or the use of mixed solvents. Atomic force microscopy (AFM) imaging of films deposited on mica sheets from freshly prepared 5×10^{-6} M solutions of BINC18 in methanol indicated the formation of small nanospheres of nearly uniform size, with an average diameter of 200 nm (Figure 1a). Films cast from the same solutions, but which were aged for about 24 hours, indicated the formation of much larger polydisperse spherical aggregates, with sizes that ranged from 1 to 2 μm, many of which were found to be adhered together (Figure 1b). Apart from aging, the size of the spherical aggregates was also observed to be dependent on the initial concentration of the solution. Thus AFM images of films deposited from a freshly prepared 1×10^{-4} M solution of BINC18 in methanol indicated the formation of polydisperse spherical structures, with an average diameter of about 500 nm.[8] Aging of these solutions also resulted in an increase in the size of the spherical aggregates from 1 to 2 μm.[8] In the millimolar concentration range, in which BINC18 formed transparent gels, AFM analysis indicated that the large spherical aggregates interconnected to form a continuous globular network (Figure 1c).

Scanning electron microscopy (SEM) and transmission electron microscopy (TEM) images indicated a vesicular structure for the spherical aggregates (Figure 1d,e). SEM analysis of samples prepared from 1×10^{-4} M aged solutions of BINC18 in methanol (Figure 1d) showed spheres with diameters that ranged from 1 to 2 μm, which was similar to that observed by AFM images under identical conditions.[8] In several cases, half-opened vesicular aggregates that resulted from wall collapse were observed, which can be attributed to the high vacuum applied during the preparation of the sample. In the millimolar concentration range, in which gelation occurred, the SEM images indicated a morphology that matched closely that of the AFM images.[8]

TEM images of samples prepared by drop-casting aged 1.2×10^{-4} M solutions onto a Formvar-coated copper grid also indicated circular structures with diameters in the range 1–1.5 μm (Figure 1e), similar to that observed by SEM and AFM. The hollow nature of the spherical aggregates was clearly indicated by the sharp contrast between the periphery and center.[6e,g] The images also revealed that the vesicles were sufficiently robust enough to retain their spherical shape under the conditions of the TEM experiments. Further support for the concentration-dependent hierarchical formation of vesicles, joined vesicles, and gels was obtained by confocal laser scanning microscopy (CLSM) (Figure 1f–h).

Self-assembly of BINC18 was also indicated by changes in the absorption and emission spectra as a function of temperature (Figure 2a). With decreasing temperature, a reduction in the intensity of the main peak at 432 nm and concomitant increase in absorption at 330 nm, with clear isosbestic points at 372 and 274 nm, were observed. The process was completely reversible on heating. The temperature-dependent changes in the absorption spectrum of BINC18 in methanol were also accompanied by changes in its fluorescence behavior. Whereas the solution of BINC18 (1.2×10^{-4} M) exhibited a weak fluorescence band centered at 540 nm at room temperature (quantum yield, $\Phi_f = 0.004$), a nearly 40-fold enhancement in fluorescence accompanied by a shift in the maximum to 602 nm was observed at 7 °C (Figure 2b). A significant enhancement in the fluorescence lifetimes was also observed with a decrease in temperature (Figure 2b, inset). Mainly a long-lived component with a lifetime of 1.0 ns was observed at 13 °C, whereas the lifetime of the species was within the time resolution of the instrument (< 100 ps) at 40 °C.[8] These effects can be attributed to the formation of H aggregates, which involves a parallel interaction mode of the chromophores.[10] Excitonic splitting in

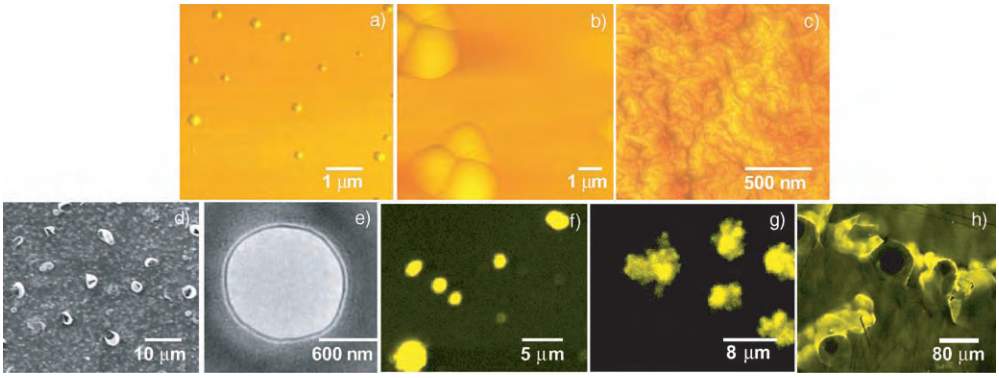

Figure 1. Microscopic images of aggregates of BINC18 deposited from methanolic solutions. The concentration of the solutions and conditions are indicated. (a–c) AFM height images on mica: a) 5×10^{-6} M; b) 5×10^{-6} M, aged 24 h; and c) 1.5×10^{-3} M. d) SEM image at 1×10^{-4} M, aged 24 h; e) TEM image at 1.2×10^{-4} M, aged 24 h. (f–h) CLSM images ($\lambda_{ex}=488$ nm; $\lambda_{em}=500$–800 nm): f) 1×10^{-4} M; g) 1×10^{-4} M, aged 24 h; and h) dried gel.

© 2006 Wiley-VCH Verlag GmbH & Co. KGaA, Weinheim

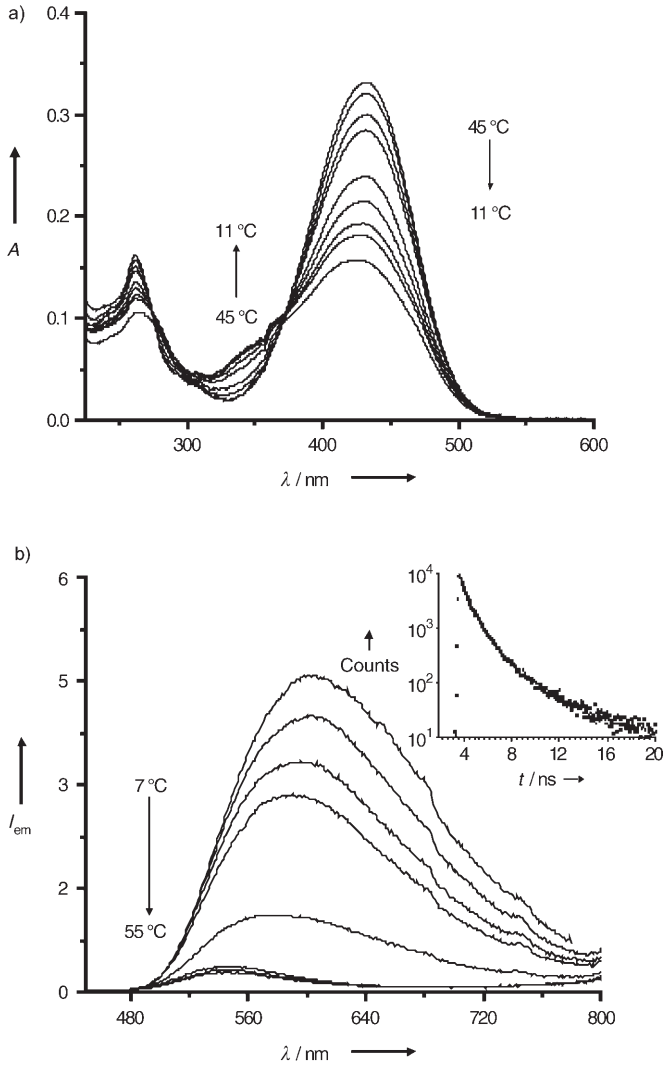

Figure 2. Temperature-dependent changes in a) absorption ($l = 1$ mm) and b) emission spectra ($\lambda_{ex} = 370$ nm; 1 cm × 1 cm) of a 1.2×10^{-4} M solution of BINC18 in methanol. The inset shows the fluorescence decay profile monitored at 13 °C ($\lambda_{ex} = 375$ nm; $\lambda_{em} = 600$ nm).

H aggregates is known to give rise to a high-energy allowed transition and a low-energy forbidden band. In such systems, absorption is dominated by the high-energy band, which results in a blue shift relative to the monomer absorption band, whereas long-lived and strongly red-shifted fluorescence occurs from the low-energy band.[5e,10]

The formation of H aggregates indicates a close π-stacked arrangement of the molecules. These results are also in support of the presence of an outer-membrane-like structure in the supramolecular aggregates.[11] The thickness of the wall of the vesicles (≈38 nm) measured from TEM images (Figure 1e) was almost ten times larger than the contour length of BINC18 (3.72 nm), thus suggesting a multilamellar structure for the walls of the vesicles. A model for the vesicle that is consistent with the spectroscopic studies and the TEM images would consist of about three to four closed bilayers, with the solvent layers existing in the center and between the bilayer membranes.[12] A schematic representation of the supramolecular assembly of BINC18 that leads to gel formation is provided in Figure 3.

Photoirradiation of a solution of BINC18 in methanol with 445-nm light resulted in a decrease in intensity of the main absorption band and was accompanied by a slight increase in absorption intensity at the lower wavelengths (Figure 4a). These changes can be attributed to a photoisomerization process (Figure 4b) similar to that reported earlier for donor–acceptor-substituted butadienes.[13] The rate of thermal reversal to the *E* isomer in such butadienes is known to depend on the electron-donating and -accepting strengths of the substituents.[13] For BINC18, a lifetime of 8.2×10^3 s was determined for the recovery of the *E* isomer by

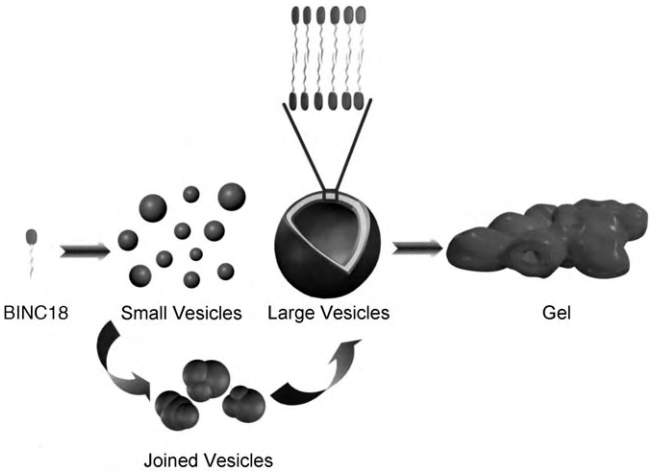

Figure 3. Schematic representation of the hierarchical organization from small to large vesicles and finally to gels. The molecular self-assembly of only one bilayer is indicated.

monitoring the growth of the 432-nm peak (Figure 4c). Photochemical isomerization and complete thermal reversal of BINC18 could be achieved over several cycles.

Photoirradiation of BINC18 also resulted in disruption of its supramolecular aggregates. Figure 5a,b depicts the effect of photoisomerization and thermal recovery of vesicles of BINC18. The AFM image of a film obtained from a non-irradiated aged 5×10^{-6} M solution of BINC18 showed the existence of large joined vesicular aggregates described earlier (Figure 1b). On irradiation, destruction of the larger vesicles and formation of small spherical aggregates was observed (Figure 5a), whereas AFM images obtained from the irradiated solutions kept in the dark for 24 hours clearly indicated recovery of the large vesicular aggregates (Figure 5b).

The effects of photoisomerization and thermal reversal on gel formation are shown in Figure 5c. Increased transparency and loss of fluorescence in a region of the gel photoirradiated at 445 nm through a mask (Figure 5c, film 2) suggested the destruction of the gel nature. Recovery of the fluorescence and scattering nature in the irradiated portion was observed on keeping the film in the dark for 24 hours, although persistence of a faint residual image indicated that the recovery was not complete under these conditions (Figure 5c, film 3).

 © 2006 Wiley-VCH Verlag GmbH & Co. KGaA, Weinheim

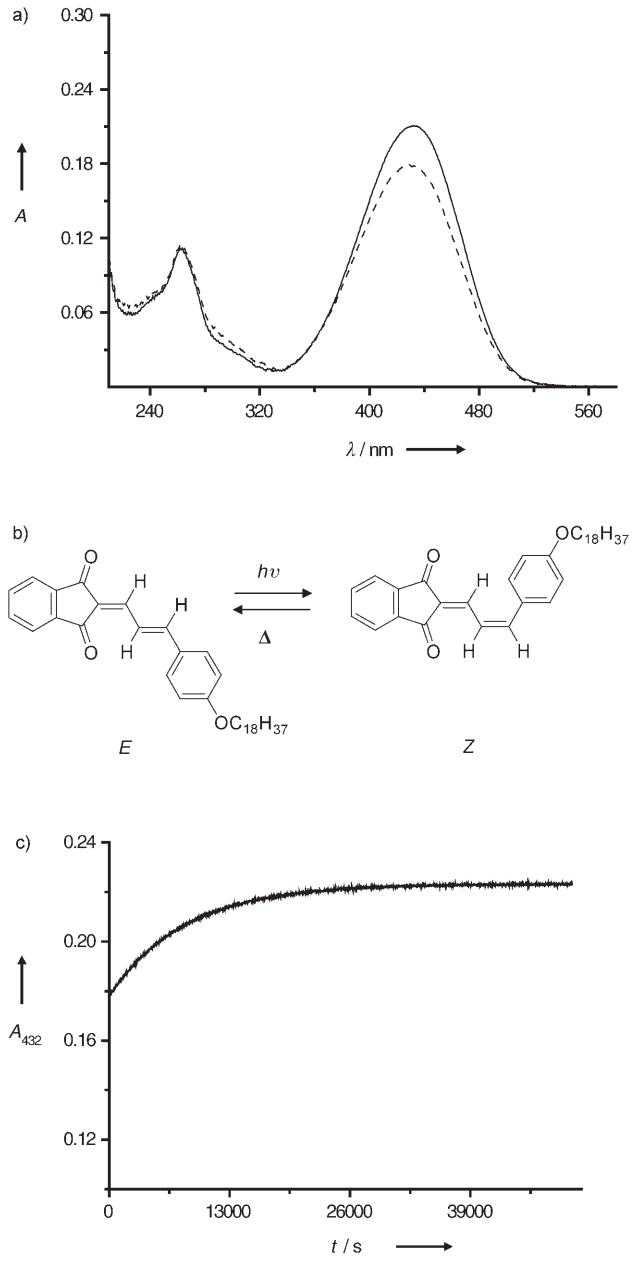

Figure 4. a) The effect of irradiation on the absorption spectrum of BINC18 in methanol (——) before and (-----) after irradiation with 445-nm light for 2 minutes ($c = 5 \times 10^{-6}$ M). b) Scheme depicting photo- and thermal isomerization of BINC18. c) Time-dependent recovery of the absorbance at 432 nm in the irradiated solution.

The reversible photoinduced destruction of the gel was also confirmed by viscosity measurements. Rheological studies on BINC18 (4×10^{-3} M) in *n*-butanol were indicative of the formation of fairly stable gels.[8] Frequency-sweep measurements showed that the elastic modulus (G′) and the loss modulus (G″) were almost independent of frequency over a wide range. The studies also indicated that these gels were not thixotropic, which is a common feature with most known low-molecular-weight gelators.[9a] Irradiation of BINC18 gels (3×10^{-3} M) in *n*-butanol at wavelengths greater than 385 nm from a 200-W mercury lamp for 3 hours resulted

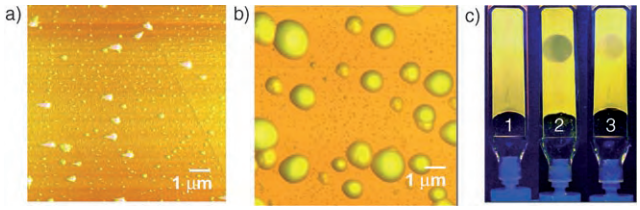

Figure 5. Effect of photoirradiation on vesicles and gels of BINC18. a) AFM tapping mode height image of film deposited from aged 5×10^{-6} M solution in methanol irradiated with 445-nm light for 2 minutes. b) AFM height image of film obtained from the same photoirradiated solution kept in the dark for 24 h. c) Photographic image of BINC18 gel in *n*-butanol kept under low-intensity 365-nm light which indicates yellow fluorescence of the gelated region ($l = 1$ mm, $c = 9.5 \times 10^{-3}$ M): 1) gel film before irradiation; 2) gel film irradiated with 445-nm light[8] for 30 minutes using a mask; and 3) irradiated gel film kept in the dark for 24 h.

in a gel-to-sol conversion, as observed by the free-flowing nature of the irradiated sample. The viscosity changes of the gel phase before and after irradiation were measured using a stress-controlled rheometer at low shear (0.02–1 s^{-1}) at 25 °C.[14] At a shear rate of 0.027 s^{-1}, the viscosity of the gel was 2.7×10^5 cP. Following irradiation, a considerable decrease in viscosity (5.1×10^4 cP) was observed at the same shear rate. Keeping the irradiated solution in the dark for 24 hours resulted in the reformation of the gel, as indicated by its nonflowing nature and increased viscosity (9.4×10^4 cP at a shear rate of 0.027 s^{-1}).

In conclusion, we have synthesized a novel class of amphiphilic donor–acceptor butadienes capable of spontaneous hierarchical self-assembly, which first involves the formation of smaller vesicles that merge to form larger ones until they finally link together to form gels that consist of globular aggregates with solvent entrapped within them. This type of gelation is rather uncommon, as with a very few recent exceptions[15] most reported gels are formed through self-aggregation of gelator molecules into long intertwined fibrous networks that hold the solvents in between predominantly by surface tension. The photoresponsive nature of these materials makes them potentially useful in controlled release systems, and we are currently exploring some of these possibilities.

Received: May 25, 2006
Published online: August 21, 2006

Keywords: gels · isomerization · photoresponsive materials · self-assembly · vesicles

[1] a) J.-M. Lehn, *Supramolecular Chemistry: Concepts and Perspectives*, VCH, Weinheim, **1995**.
[2] a) S. I. Stupp, V. Le Bonheur, K. Walker, L. S. Li, K. E. Huggins, M. Kesser, A. Amstutz, *Science* **1997**, *276*, 384–389; b) M. Muthukumar, C. K. Ober, E. L. Thomas, *Science* **1997**, *277*, 1225–1232; c) J. H. K. K. Hirschberg, L. Brunsveld, A. Ramzl, J. A. J. M. Vekemans, R. P. Sijbesma, E. W. Meijer, *Nature* **2000**, *407*, 167–170; d) T. Kato, *Science* **2002**, *295*, 2414–2418; e) G. M. Whitesides, B. Grzybowski, *Science* **2002**, *295*, 2418–

 © 2006 Wiley-VCH Verlag GmbH & Co. KGaA, Weinheim

2421; f) A. C. Grimsdale, K. Müllen, *Angew. Chem.* **2005**, *117*, 5732 – 5772; *Angew. Chem. Int. Ed.* **2005**, *44*, 5592 – 5629; g) T. Shimizu, M. Masuda, H. Minamikawa, *Chem. Rev.* **2005**, *105*, 1401 – 1443; h) J. M. J. Paulusse, R. P. Sijbesma, *Angew. Chem.* **2006**, *118*, 2392 – 2396; *Angew. Chem. Int. Ed.* **2006**, *45*, 2334 – 2337.

[3] a) K. Murata, M. Aoki, T. Suzuki, T. Harada, H. Kawabata, T. Komori, F. Ohseto, K. Ueda, S. Shinkai, *J. Am. Chem. Soc.* **1994**, *116*, 6664 – 6676; b) M. S. Vollmer, T. D. Clark, C. Steinem, M. R. Ghadiri, *Angew. Chem.* **1999**, *111*, 1703 – 1706; *Angew. Chem. Int. Ed.* **1999**, *38*, 1598 – 1601; c) S. A. Ahmed, X. Sallenave, F. Fages, G. Mieden-Gundert, W. M. Müller, U. Müller, F. Vögtle, J.-L. Pozzo, *Langmuir* **2002**, *18*, 7096 – 7101; d) L. Frkanec, M. Jokić, J. Makarević, K. Wolsperger, M. Žinić, *J. Am. Chem. Soc.* **2002**, *124*, 9716 – 9717; e) M. Moriyama, N. Mizoshita, T. Yokota, K. Kishimoto, T. Kato, *Adv. Mater.* **2003**, *15*, 1335 – 1338; f) F. Rakotondradany, M. A. Whitehead, A.-M. Lebuis, H. F. Sleiman, *Chem. Eur. J.* **2003**, *9*, 4771 – 4780.

[4] a) J. J. D. de Jong, L. N. Lucas, R. M. Kellogg, J. H. van Esch, B. L. Feringa, *Science* **2004**, *304*, 278 – 281; b) N. Koumura, M. Kudo, N. Tamaoki, *Langmuir* **2004**, *20*, 9897 – 9900; c) S. Yagai, T. Nakajima, K. Kishikawa, S. Kohmoto, T. Karatsu, A. Kitamura, *J. Am. Chem. Soc.* **2005**, *127*, 11134 – 11139; d) J. Eastoe, A. Vesperinas, *Soft Matter* **2005**, *1*, 338 – 347.

[5] a) C. Thalacker, F. Würthner, *Adv. Funct. Mater.* **2002**, *12*, 209 – 218; b) S.-J. Lim, B.-K. An, S. D. Jung, M.-A. Chung, S. Y. Park, *Angew. Chem.* **2004**, *116*, 6506 – 6510; *Angew. Chem. Int. Ed.* **2004**, *43*, 6346 – 6350; c) J. Wu, M. D. Watson, Li. Zhang, Z. Wang, K. Müllen, *J. Am. Chem. Soc.* **2004**, *126*, 177 – 186; d) T.-Q. Nguyen, R. Martel, P. Avouris, M. L. Bushey, L. Brus, C. Nuckolls, *J. Am. Chem. Soc.* **2004**, *126*, 5234 – 5242; e) B. W. Messmore, J. F. Hulvat, E. D. Sone, S. I. Stupp, *J. Am. Chem. Soc.* **2004**, *126*, 14452 – 14458; f) S. J. George, A. Ajayaghosh, *Chem. Eur. J.* **2005**, *11*, 3217 – 3227.

[6] a) K. Tsuda, G. C. Dol, J. Hofkens, L. Latterini, J. W. Weener, E. W. Meijer, F. C. De Schryver, *J. Am. Chem. Soc.* **2000**, *122*, 3445 – 3452; b) F. M. Menger, J. S. Keiper, *Angew. Chem.* **2000**, *112*, 1980 – 1996; *Angew. Chem. Int. Ed.* **2000**, *39*, 1906 – 1920; c) D. E. Discher, A. Eisenberg, *Science* **2002**, *297*, 967 – 973; d) Y. J. Jeon, P. K. Bharadwaj, S. W. Choi, J. W. Lee, K. Kim, *Angew. Chem.* **2002**, *114*, 4654 – 4656; *Angew. Chem. Int. Ed.* **2002**, *41*, 4474 – 4476; e) D. M. Vriezema, J. Hoogboom, K. Velonia, K. Takazawa, P. C. M. Christianen, J. C. Maan, A. E. Rowan, R. J. M. Nolte, *Angew. Chem.* **2003**, *115*, 796 – 800; *Angew. Chem. Int. Ed.* **2003**, *42*, 772 – 776; f) J.-H. Fuhrhop, T. Wang, *Chem. Rev.* **2004**, *104*, 2901 – 2937; g) M. Lee, S.-J. Lee, L.-H. Jiang, *J. Am. Chem. Soc.* **2004**, *126*, 12724 – 12725; h) R. Charvet, D.-L. Jiang, T. Aida, *Chem. Commun.* **2004**, 2664 – 2665; i) T. Ishi-i, S. Shinkai, *Top. Curr. Chem.* **2005**, *258*, 119 – 160.

[7] a) O. Uzun, A. Sanyal, H. Nakade, R. J. Thibault, V. M. Rotello, *J. Am. Chem. Soc.* **2004**, *126*, 14773 – 14777; b) Z. Hu, A. M. Jonas, S. K. Varshney, J.-F. Gohy, *J. Am. Chem. Soc.* **2005**, *127*, 6526 – 6527; c) T. Akutagawa, K. Kakiuchi, T. Hasegawa, S.-i. Noro, T. Nakamura, H. Hasegawa, S. Mashiko, J. Becher, *Angew. Chem.* **2005**, *117*, 7449 – 7453; *Angew. Chem. Int. Ed.* **2005**, *44*, 7283 – 7287; d) M. Yang, W. Wang, F. Yuan, X. Zhang, J. Li, F. Liang, B. He, B. Minch, G. Wegner, *J. Am. Chem. Soc.* **2005**, *127*, 15107 – 15111; e) B.-S. Kim, W.-Y. Yang, J.-H. Ryu, Y.-S. Yoo, M. Lee, *Chem. Commun.* **2005**, 2035 – 2037; f) F. J. M. Hoeben, I. O. Shklyarevskiy, M. J. Pouderoijen, H. Engelkamp, A. P. H. J. Schenning, P. C. M. Christianen, J. C. Maan, E. W. Meijer, *Angew. Chem.* **2006**, *118*, 1254 – 1258; *Angew. Chem. Int. Ed.* **2006**, *45*, 1232 – 1236; g) G. Ma, A. M. Müller, C. J. Bardeen, Q. Cheng, *Adv. Mater.* **2006**, *18*, 55 – 60; h) S. Wang, W. Shen, Y. Feng, H. Tian, *Chem. Commun.* **2006**, 1497 – 1499.

[8] See the Supporting Information.

[9] a) P. Terech, R. G. Weiss, *Chem. Rev.* **1997**, *97*, 3133 – 3159; b) J. H. van Esch, B. L. Feringa, *Angew. Chem.* **2000**, *112*, 2351 – 2354; *Angew. Chem. Int. Ed.* **2000**, *39*, 2263 – 2266; c) L. A. Estroff, A. D. Hamilton, *Chem. Rev.* **2004**, *104*, 1201 – 1217; d) N. M. Sangeetha, U. Maitra, *Chem. Soc. Rev.* **2005**, *34*, 821 – 836.

[10] a) M. Kasha, H. R. Rawls, M. A. El-Bayoumi, *Pure Appl. Chem.* **1965**, *11*, 371 – 392; b) D. G. Whitten, *Acc. Chem. Res.* **1993**, *26*, 502 – 509; c) K. C. Hannah, B. A. Armitage, *Acc. Chem. Res.* **2004**, *37*, 845 – 853; d) S. Y. Ryu, S. Kim, J. Seo, Y.-W. Kim, O.-H. Kwon, D.-J. Jang, S. Y. Park, *Chem. Commun.* **2004**, 70 – 71; e) H. Yao, K. Domoto, T. Isohashi, K. Kimura, *Langmuir* **2005**, *21*, 1067 – 1073.

[11] a) T. Kunitake, *Angew. Chem.* **1992**, *104*, 692 – 710; *Angew. Chem. Int. Ed. Engl.* **1992**, *31*, 709 – 726; b) D. G. Whitten, L. Chen, H. C. Geiger, J. Perlstein, X. Song, *J. Phys. Chem. B* **1998**, *102*, 10098 – 10111; c) J.-M. Pedrosa, M. T. M. Romero, L. Camacho, D. Möbius, *J. Phys. Chem. B* **2002**, *106*, 2583 – 2591.

[12] Y. Shang, Yi. Xu, H. Liu, Y. Hu, *J. Dispersion Sci. Technol.* **2006**, *27*, 105 – 108.

[13] a) H. Braatz, S. Hecht, H. Seifert, S. Helm, J. Bendig, W. Rettig, *J. Photochem. Photobiol. A* **1999**, *123*, 99 – 108; b) R. Davis, S. Das, M. George, S. Druzhinin, K. A. Zachariasse, *J. Phys. Chem. A* **2001**, *105*, 4790 – 4798; c) R. Davis, V. A. Mallia, S. Das, *Chem. Mater.* **2003**, *15*, 1057 – 1063.

[14] C. T. Lee, K. A. Smith, T. A. Hatton, *Macromolecules* **2004**, *37*, 5397 – 5405.

[15] a) J. H. Jung, Y. Ono, K. Sakurai, M. Sano, S. Shinkai, *J. Am. Chem. Soc.* **2000**, *122*, 8648 – 8653; b) F. M. Menger, A. V. Peresypkin, *J. Am. Chem. Soc.* **2003**, *125*, 5340 – 5345; c) G. Battaglia, A. J. Ryan, *Nat. Mater.* **2005**, *4*, 869 – 876; d) A. Ajayaghosh, R. Varghese, V. K. Praveen, S. Mahesh, *Angew. Chem.* **2006**, *118*, 3339 – 3342; *Angew. Chem. Int. Ed.* **2006**, *45*, 3261 – 3264.

 © 2006 Wiley-VCH Verlag GmbH & Co. KGaA, Weinheim

Biotechnology

DOI: 10.1002/anie.200602439

Control of the Yeast Cell Cycle with a Photocleavable α-Factor Analogue**

*Laurie L. Parker, Josh W. Kurutz, Stephen B. H. Kent, and Stephen J. Kron**

The budding yeast *Saccharomyces cerevisiae* is widely used as a model organism for studying many biological processes and systems, particularly for understanding the cell cycle. The yeast peptide pheromone α-factor (WHWLQLKPGQPMY) activates the mating pathway in MATa cells, arresting the cell cycle in the G1 phase. This arrest is used as a tool for synchronizing yeast cultures and for investigating signaling events involved in the pathway and other processes related to morphogenesis and transcription. Herein we report the synthesis and activity of an α-factor analogue designed to control the on/off state of the mating signal. Incorporating a photocleavable residue at a flexible site in the peptide allowed UV degradation in situ to mimic the natural protease degradation of this signaling peptide. The control over the α-factor signal achieved serves as proof of concept for use of this analogue as a tool. It also and allows access to previously impractical experiments that will yield highly time-resolved information about the yeast cell cycle and mating pathway.

The binding of the α-factor to its G-protein-coupled receptor Ste2p in haploid MATa yeast cells initiates a MAP kinase cascade that results in cell-cycle arrest, cell morphogenesis (to extend a cell-wall projection toward the source of the peptide), and mating-specific genes.[1,2] The peptide binds to the Ste2p receptor in a specific conformation, resulting in the termini being buried in the receptor with the central flexible region exposed.[1,3] Under normal circumstances, the Bar1 protease is excreted extracellularly to degrade excess peptide and to control the level of α-factor signaling.[4] Generally, α-factor-arrest experiments are performed in a liquid medium and require washing of cells in fresh buffer solution or medium to remove the α-factor peptide and allow release into the cell cycle.[5] However, precise temporal control of release is difficult to achieve in a multistep washing procedure and results in the loss of information about the initiation of the cell cycle. This also means that experiments involving arrest and release in formats other than liquid medium cannot be performed. An analogue of the α-factor, which could be degraded in a controlled manner in situ, would be useful for a better control of the release and more-rapid analysis of the physiological consequences of dropping below the pheromone-signaling threshold for the mating response. This will open the door to previously impractical experiments, such as microscopically studying the cytoskeletal changes that are the result of the change from pheromone-associated polarity to bud-site-selection polarity, or gene-expression analysis of the first few minutes after removal of the mating signal to obtain information about the switch that turns on cell-cycle-initiation factors such as cyclins and ultimately results in the decision to leave G1 arrest.

Although caging of bioactive molecules for subsequent activation by using UV light is a common strategy,[6–11] the use of photocleavable functionality for deactivation of peptides and proteins[12] is relatively unexplored. Backbone cleavage through 2-nitrophenyl amino acid derivatives provides an interesting way to specifically turn off a biological signal of interest. We show herein a successful proof of concept for applying this strategy to control the activity of a signaling peptide.

Substituting a position in the flexible region of the α-factor with an amino acid analogue that can be artificially cleaved should mimic Bar1 protease degradation at Lys-7 and results in "turning off" of the α-factor signal (Scheme 1 a). As the structure of this peptide is very important to its activity, selection of the mutation site was important. Extensive work by Naider and Becker has established the importance of particular residues to the activity, giving us a good basis on which to design the analogue.[1] For example, alanine scanning of this peptide with both L- and D-Ala showed that L-Ala at position 9 (Scheme 1 a) disrupted the binding of the peptide to the receptor and reduced the activity. Notably, however, at this position, D-Ala gave increased binding and a fivefold increase in activity. This suggested that, depending on the structural constraints imposed by the linkage, bulkier amino acids may be tolerated at position 9, for example, cleavable 2-nitrophenyl amino acid derivatives such as the commercially

[*] Dr. S. J. Kron
Department of Molecular Genetics and Cellular Biology
University of Chicago
924 East 57th Street, Knapp R322
Chicago, IL 60637 (USA)
Fax: (+1) 773-702-4394
E-mail: skron@uchicago.edu
Dr. L. L. Parker, Dr J. W. Kurutz, Prof. S. B. H. Kent
Department of Biochemistry and Molecular Biology
University of Chicago
929 E. 57th Street, CIS W201A, Chicago, IL 60637 (USA)

[**] L.P. gratefully acknowledges the NIH for a Ruth L. Kirschstein Individual Postdoctoral Fellowship (F32). S.J.K. is a Scholar of the Leukemia and Lymphoma Society.

Supporting information for this article is available on the WWW under http://www.angewandte.org or from the author.

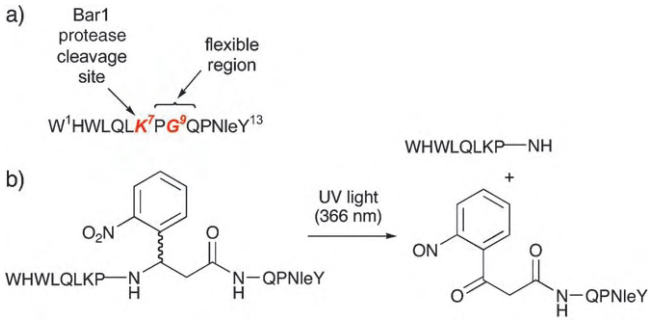

Scheme 1. a) Residues of interest in the α-factor sequence; b) UV cleavage of peptide **2**.

WILEY InterScience DISCOVER SOMETHING GREAT
© 2006 Wiley-VCH Verlag GmbH & Co. KGaA, Weinheim

available (2-nitro)-β-phenylalanine ([D/L]-(β)2-Npa; Scheme 1b).

With these design features in mind, we synthesized the photocleavable peptide **2** (see Table 1) and tested its activity to induce the mating response. In both **1** and **2**, the native

Table 1: Peptides synthesized in this study. (The bold text highlights the variation between the peptides.)

Peptide	Sequence
1	WHWLQLKPGQPNleY
2	WHWLQLKP-**[D/L-(β)2-Npa]**-QPNleY
2a	WHWLQLKP-**[D-(β)2-Npa]**-QPNleY
2b	WHWLQLKP-**[L-(β)2-Npa]**-QPNleY

Met12 was mutated to Norleucine (Nle), a common substitution that is reported to improve the stability of the peptide to oxidative damage.[1] Peptide **1** served as a "native" α-factor control. Peptide **2** was synthesized with racemic D/L-(2-nitro)-β-phenylalanine to provide a means for selective cleavage of the backbone, giving two diastereomeric products that were separated by reverse-phase HPLC into **2a** and **2b** (see the Supporting Information for characterization of all peptides). The rate of UV-induced cleavage for **2** (as shown in Scheme 1b) was determined at 366 nm, 5 mW cm^{-2} (5 μM, $t_{1/2} \approx 8$ min; see the Supporting Information). Although cleavage may be faster at shorter wavelengths (e.g. 237 nm), 366 nm is a safer wavelength for avoiding DNA damage in cells, so all characterization of UV treatment in biological assays was determined for 366-nm UV light.

Both diastereomers of **2** were tested for G1 arrest by using "shmoo" activity (to detect morphological changes resulting from activation of the mating pathway) and halo (disc diffusion, to determine the arrest-related growth inhibition) assays (see Figure 1 and the Supporting Information for images of arrest halos). Only one product was active, for which NOESY NMR spectroscopy supported the structural assignment as peptide **2a**, the diastereomer containing the D isomer of (2-nitro)-β-phenylalanine (see the Supporting Information and Table 1). Identifying compound **2a**, as the active diastereomer is consistent with previous data for bulky D- and L-amino acid substitutions at position 9 of this peptide, where L-amino acids tended to decrease activity, whereas D-amino acids improved activity.[1] The activity of **2a** in the halo assay was approximately 90% of the control peptide **1**, which is remarkably high activity for such a drastic change in backbone structure. As shown by Naider and Becker,[1] amino acid substitutions throughout this peptide affect the affinity for the receptor and show that it is normally necessary to increase the rigidity of the backbone in a favorable conformation for receptor binding to increase the activity. It is surprising that a β-amino acid with the backbone flexibility provided by the extra methylene group still results in a peptide with satisfactory activity.

The kinetics of release from G1 arrest for control α-factor **1** (after peptide washout by using standard conditions) and photocleavable peptide **2a** (after UV release) were characterized by using the α-factor/nocodozole trap assay (which discriminates with high resolution between cells that have and have not left G1 arrest) and analyzed by flow cytometry to determine the DNA content (fluorescence increases depending on the extent of DNA replication, indicating the progression of the cell cycle). Three hours of treatment at 25°C with 10 μM photocleavable analogue **2** was sufficient to obtain complete G1 arrest of a yeast culture (optical density at 600 nm $(OD)_{600} = 0.1$). After treating this culture for 5 min with UV light (20 mW cm^{-2}), the peptide was 75% degraded (as shown by the HPLC analysis of the supernatant medium, see the Supporting Information) and the synchronized cells were released into the cell cycle with kinetics comparable to those seen after washing out the control α-factor **1** (cells treated with 5 μM **1** to achieve G1 arrest; Figure 2).

This strategy for degradation in situ opens up exciting possibilities for G1 arrest and mating experiments in microscopy formats on solid media that were not possible before and

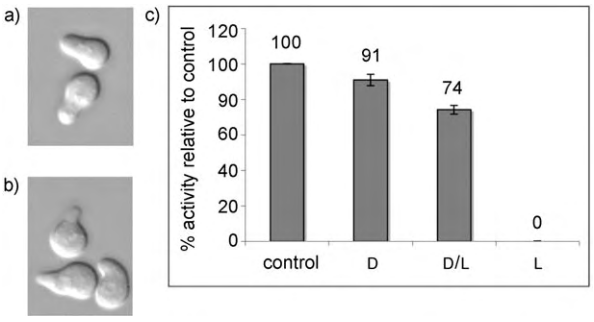

Figure 1. Shmooing of A cells induced by a) control peptide **1** (5 μM) compared with b) D-(β)2-Npa **2a** (10 μM); c) Halo assay for relative growth-arrest activity. All activity seen in the diastereomeric peptide mixture resulted from the D diastereomer.

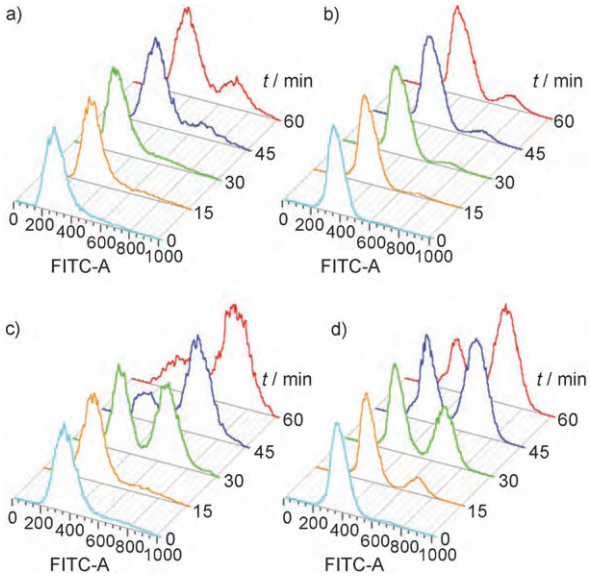

Figure 2. Flow cytometry analysis of the release from G1 arrest by a G1/G2 trap assay. The DNA content was determined as 1N (G1 trapped) or 2N (G2 trapped; SYTOX green staining). a) **1**, no release; b) **2a**, no release; c) **1**, washout; d) **2a**, UV (5 min, 366 nm, 20 mW cm^{-2}). FTIC-A = absorption of SYTOX green (fluorescein-based DNA stain).

 © 2006 Wiley-VCH Verlag GmbH & Co. KGaA, Weinheim

should lead to important, novel information about yeast mating and the cell cycle. For example, the rates of oscillations in expression of various genes between different phases of the cell cycle have been extensively characterized by using real-time PCR and microarray experiments.[13–16] However, the earliest times at which it has been possible to measure G1-arrest recovery-related gene induction have been after the first five to seven minutes—the typical time necessary for centrifugation and resuspension in pheromone-free medium. By this time, the cells have already made the decision to leave G1, and *CLN3/SWI4* expression levels are beginning to rise accordingly.[17] These genes are known to turn on the expression of *CLN1* and *CLN2*, cyclins that act with the cyclin-dependent kinase Cdc28p to drive the G1 to S transition. Owing to the practical constraints, it has not been possible to look for genes that change before that time frame, and questions remain about what defines the switch that is ultimately responsible for this process.[18,19]

Further to studying the normal cell-cycle recovery from G1 arrest, another intriguing possibility would be to cleave this peptide at 237-nm UV light to simultaneously induce damage and release cells from G1. This may provide new information about the G1 checkpoint mechanisms that delay entry into the cell cycle after DNA damage.[20] Another interesting application could involve the development of designer signaling mechanisms in mammalian cells by using chimeric receptors[21] that would respond to α-factors[22] (with photocleavable control of the signal) but stimulate pathways that are more relevant to other organisms.

In conclusion, we have shown that this peptide has sufficient activity to arrest cells in G1 at reasonable doses and that it can be specifically degraded by using relatively brief exposure to UV light at a wavelength that is "safe" for most cells. Its activity is related to the conformation of the peptide around its central loop region and agrees with literature data for other "constrained" versions of α-factors containing bulkier D-amino acids at position 9, even though this peptide contains a β-amino acid. We are currently investigating ways to use this cleavable α-factor to address the biological questions detailed above by using genome arrays and physiological and biochemical studies.

Experimental Section

Yeast strains and media: The strain used in this study was SKY809 (W303 background; MATa, ura3-1, can1-100, leu2-3,112 GAL+). Yeast cells were grown in standard rich YPD (1% yeast extract, 2% peptone, 2% dextrose) or a 2X synthetic media lacking tryptophan (2X-Trp) at 25 or 30°C. When necessary, cells were washed in standard rich YEP (1 % yeast extract, 2 % peptone).

Peptide synthesis and purification: Peptides were synthesized manually on a 0.1 mmol scale by using *tert*-butoxycarbonyl (Boc) solid-phase peptide synthesis, cleaved with anhydrous HF (*p*-cresol as scavenger), and purified by using reverse-phase HPLC (Grace Vydac C18 column, 10 mm ID × 250 mm L; solvent A: 0.1% aqueous TFA; solvent B: 0.1% TFA in acetonitrile). Peptides were analyzed by using an Agilent 1100 XCT ion trap LC/MS (C18 column, 2.1 mm ID × 50 mm L; gradient 5–65% B at 4% min^{-1}).

Halo disc diffusion assay[23]: Peptide dissolved in dimethylsulfoxide (DMSO; 15 μL total volume) was applied to sterile small paper discs (6.5 mm). wild-type (WT) W303 MATa yeast was grown overnight to saturation in YPD (10 μL), diluted into warm 0.5% agar in 2X-Trp medium (4 mL, dissolved by heating in the microwave and equilibrated in a water bath to 45°C), and poured onto the surface of YPD plates. After cooling briefly to set the agar, the peptide discs were laid on the surface and the plates incubated at 30°C overnight. Halos were visualized by digital photograph, the diameters measured and normalized to the paper disc diameters.

G1 arrest assay with an α-factor/nocodazole trap[20]: Yeast strain SKY809 was grown to saturation ($OD_{600} \approx 1.8$) overnight at room temperature in 2X-Trp medium. The culture was diluted in a 1:10 ratio and grown to the log phase at 30°C for 3 h (final $OD_{600} \approx 0.6$). This log phase culture was diluted to $OD_{600} = 0.1$ in 6-well plates (2.5 mL total volume) and treated with peptide **1** or **2** for 3 h at room temperature to arrest the cells in the G1 phase. Peptide **1** was removed by pelleting and washing the cells in YEP, then resuspending them in YPD. Peptide **2b** was degraded by treatment with a UVP Blak-Ray UV lamp (5 min, 20 mW cm^{-2}). Before and after UV treatment, 250 μl of the cell suspension was removed, pelleted, and the supernatant then removed and filtered for HPLC analysis (Waters 626 with Empower2 software system). After peptide removal, aliquots (250 μL) were quenched with trap medium (250 μL, 10 μM α-factor, 40 μg mL^{-1} nocodazole) after 0, 15, 30, 45 and 60 min and incubated for 1.5 h in a 24-well plate on a shaker at room temperature. Trapped cells were filtered in a 96-well filter bottom plate (MultiScreen, Millipore) and washed twice with 70% aqueous EtOH to fix them. After all time-point aliquots were finished being trapped, fixed cells were resuspended in 250 μL RNAse (0.25 μg $μL^{-1}$ in 50 mM tris(hydroxymethyl)aminomethane hydrochloride (Tris-Cl) buffer solution; pH 7.5) and incubated at 55°C for 2 h, followed by washing twice with Tris-Cl buffer solution (100 μL, 50 mM pH 7.5). Cells were then resuspended in 100 μL pepsin solution (5 μg $μL^{-1}$ in 4.5 mM HCl) and treated at 37°C for 1 h, washed twice with Tris-Cl buffer solution (as above), taken up in 100 μL Tris-Cl buffer solution (as in wash), and sonicated to deaggregate prior to analysis with flow cytometry. Cell suspensions were transferred to flow cytometry tubes containing 400 μL SYTOX green (Molecular Probes; final concentration 5 μM) and analyzed by using a BD FACSCanto flow cytometer.

Received: June 16, 2006
Published online: August 28, 2006

Keywords: biotechnology · peptides · peptidomimetics · pheromones · receptors

[1] F. Naider, J. M. Becker, *Peptides* **2004**, *25*, 1441.
[2] L. Bardwell, *Peptides* **2004**, *25*, 1465.
[3] B. K. Lee, S. Khare, F. Naider, J. M. Becker, *J. Biol. Chem.* **2001**, *276*, 37950.
[4] E. Ciejek, J. Thorner, *Cell* **1979**, *18*, 623.
[5] S. K. Raths, F. Naider, J. M. Becker, *J. Biol. Chem.* **1988**, *263*, 17333.
[6] Y. Shigeri, Y. Tatsu, N. Yumoto, *Pharmacol. Ther.* **2001**, *91*, 85.
[7] M. Matsumoto, J. Solzin, A. Helbig, V. Hagen, S. Ueno, O. Kawase, Y. Maruyama, M. Ogiso, M. Godde, H. Minakata, U. B. Kaupp, M. Hoshi, I. Weyand, *Dev. Biol.* **2003**, *260*, 314.
[8] G. Marriott, P. Roy, K. Jacobson, *Biophotonics Part A* **2003**, *360*, 274.
[9] D. M. Rothman, M. D. Shults, B. Imperiali, *Trends Cell Biol.* **2005**, *15*, 502.
[10] M. Toebes, M. Coccoris, A. Bins, B. Rodenko, R. Gomez, N. J. Nieuwkoop, W. van de Kasteele, G. F. Rimmelzwaan, J. Haanen, H. Ovaa, T. N. M. Schumacher, *Nat. Med.* **2006**, *12*, 246.
[11] A. Nguyen, D. M. Rothman, J. Stehn, B. Imperiali, M. B. Yaffe, *Nat. Biotechnol.* **2004**, *22*, 993.

 © 2006 Wiley-VCH Verlag GmbH & Co. KGaA, Weinheim

[12] P. M. England, H. A. Lester, N. Davidson, D. A. Dougherty, *Proc. Natl. Acad. Sci. USA* **1997**, *94*, 11025.
[13] J. Bahler, *Annu. Rev. Genet.* **2005**, *39*, 69.
[14] V. L. MacKay, X. H. Li, M. R. Flory, E. Turcott, G. L. Law, K. A. Serikawa, X. L. Xu, H. Lee, D. R. Goodlett, R. Aebersold, L. P. Zhao, D. R. Morris, *Mol. Cell. Proteomics* **2004**, *3*, 478.
[15] K. A. Serikawa, X. L. Xu, V. L. MacKay, G. L. Law, O. Zong, L. P. Zhao, R. Bumgarner, D. R. Morris, *Mol. Cell. Proteomics* **2003**, *2*, 191.
[16] P. T. Spellman, G. Sherlock, M. Q. Zhang, V. R. Iyer, K. Anders, M. B. Eisen, P. O. Brown, D. Botstein, B. Futcher, *Mol. Biol. Cell* **1998**, *9*, 3273.
[17] V. L. MacKay, B. Mai, L. Waters, L. L. Breeden, *Mol. Cell. Biol.* **2001**, *21*, 4140.
[18] S. B. Haase, S. I. Reed, *Nature* **1999**, *401*, 394.
[19] C. Wittenberg, S. I. Reed, *Oncogene* **2005**, *24*, 2746.
[20] R. Wysocki, A. Javaheri, S. Allard, F. Sha, J. Cote, S. J. Kron, *Mol. Cell. Biol.* **2005**, *25*, 8430.
[21] T. Jackson, *Pharmacol. Ther.* **1991**, *50*, 425.
[22] D. Z. Yin, S. Gavi, E. Shumay, K. Duell, J. B. Konopka, C. C. Malbon, H. Y. Wang, *Biochem. Biophys. Res. Commun.* **2005**, *329*, 281.
[23] G. A. Hoffman, T. R. Garrison, H. G. Dohlman, *G Protein Pathways Part B* **2002**, *344*, 617.

 © 2006 Wiley-VCH Verlag GmbH & Co. KGaA, Weinheim

Nanoelectronics

DOI: 10.1002/anie.200602215

Gold-Nanoparticle-Enhanced Current Transport through Nanometer-Scale Insulating Layers**

Yongdong Jin, David Cahen, Noga Friedman, and Mordechai Sheves*

We report herein how adding a monolayer of small ($\approx$2.5 nm diameter) Au nanoparticles (NPs) on top of an approximately 5-nm-thick insulating layer significantly enhances electronic current transport through the insulator. The insulating film is sandwiched between Au and Al or Si (degenerate) electrodes to give the following sandwich configuration: Au//Au NP monolayer/5-nm-thick insulating layer//Al or Si. Enhancement is found both with hard inorganic (SiO_2) and with soft organic insulators (lipid bilayers stabilized with bacteriorhodopsin (bR)).

Citrate-stabilized Au NPs ($\approx$2.5 nm diameter, unless stated otherwise) were synthesized as described elsewhere.[1] As a model insulating layer, we prepared SiO_2 layers on the surface of conducting, degenerate (100) *n*-Si substrates ($\approx 10^{-3}\,\Omega$ cm). The Si wafers with native oxide layer ($\approx$1.8 nm) were first cleaned with organic solvents, then an oxide layer of controlled thickness was grown on top of them by plasma-assisted oxidation. The oxide-layer thickness was determined by ellipsometry. Unless otherwise stated, we used oxide layers with a thickness of (5.4 $\pm$ 0.5) nm. These samples were then used in both test and control junctions. The oxide layer was modified with (3-aminopropyl)trimethoxysilane (APTMS)[1a] to assemble the Au NPs (from a suspension with pH 5) on the oxide by binding them to the exposed APTMS amino groups.[2] After formation of a saturated Au NP monolayer (incubation time $>$6 h), the NP-covered surface was treated with 20 mM aqueous cysteamine for 30 min to passivate the surface of the colloids. The junctions were prepared by depositing Au on top of the NP-covered surface. This deposition was done by floating preformed Au pads (60 nm thick, 0.5 mm diameter, 2×10^{-3} cm^2 area) onto the Au NP-covered surface in a nondestructive manner, using the "lift-off, float-on" technique (LOFO).[3] For control experiments we also evaporated Au onto the NP-covered surface. We constructed control junctions of the type Au pad// APTMS-SiO_2 ($\approx$5 nm)//Si in a similar manner.

Current–voltage (*I–V*) measurements were performed in a class 10000 clean room at 293 K and 40% relative humidity (RH). *I–V* characteristics were measured using a W needle connected to a micromanipulator to contact the Au pad—an InGa drop on the Au pad minimizes mechanical (pressure) damage to the film—and an HP 4155 semiconductor parameter analyzer. All *I–V* measurements were performed in the dark, unless noted otherwise. As shown in curve 1 of Figure 1, in the absence of the NP layer, the current that we measured through the approximately 5-nm-thick inorganic insulating layers is within the noise level ($\approx$100 pA). Adding the NP film changes this situation; typical currents through the Au pad//cysteamine/Au NP monolayer/APTMS-SiO_2 ($\approx$5 nm)// Si junctions were 0.3–2 nA at 1 V applied bias, as shown in curve 2 of Figure 1.

This result immediately suggested that the Au NPs are in direct contact with the Si substrate via pinholes or cracks in the oxide film. It therefore became important to investigate the topography of the oxide surface. Figure 2 (top) shows a typical tapping-mode AFM map of the Si/SiO_2 layer, which gives an average root-mean-square (rms) roughness of 0.10 nm, nearly identical to the roughness that we measured for the native oxide surface of Si. This result indicates that the as-grown SiO_2 layers form in a homogeneous fashion on the Si substrate. Figure 2 (middle) shows an AFM image of a densely packed monolayer of Au NPs on the APTMS-modified Si/SiO_2 surface. This AFM image is a tip–sample

[*] Dr. Y. Jin, Dr. N. Friedman, Prof. M. Sheves
Department of Organic Chemistry
Weizmann Institute of Science
Rehovot 76100 (Israel)
Fax: (+972) 8-934-4142
E-mail: yongdong.jin@weizmann.ac.il
Prof. D. Cahen
Department of Materials and Interfaces
Weizmann Institute of Science
Rehovot 76100 (Israel)

[**] We thank the Minerva Foundation (Munich), the Kimmel Center for Nanoscale Science, and the Grand Center for Sensors and Security for partial support, Harvey Scher for constructive criticism, and Oliver Seitz, Izhar Ron, and Hagay Shpaisman for their assistance and helpful discussions.

Supporting Information for this article is available on the WWW under http://www.angewandte.org or from the author.

 © 2006 Wiley-VCH Verlag GmbH & Co. KGaA, Weinheim

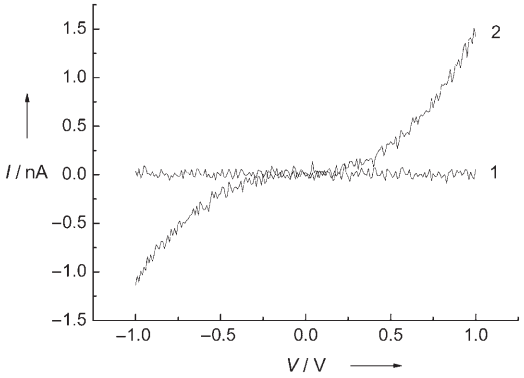

Figure 1. *I–V* curves of the Au pad (formed by LOFO or vacuum deposition)//APTMS-SiO_2 ($\approx$5 nm)//Si junctions (curve 1) and the Au pad (formed by LOFO)//cysteamine/Au NP monolayer/APTMS-SiO_2 ($\approx$5 nm)//Si junctions (curve 2), measured under ambient conditions and in the dark. The *I–V* curves of the Au pad (formed by vacuum deposition)//(nominal) Au NP monolayer/APTMS-SiO_2 ($\approx$5 nm)//Si junctions are similar to curve 1. Degenerate (100) *n*-Si was used ($\approx 10^{-3}\,\Omega$cm).

convolution. As a result of the tip size (>10 nm) and the dense packing of the NPs on the smooth substrate, the individual NPs cannot be resolved. However, section analysis of some defect sites in the NP layer shows that the average height of the features ($\approx$2.6 nm) is consistent with the known size of the Au NPs.

As a further check we prepared top contacts by electron-beam evaporation of Au onto both control samples and samples with NPs, and compared the properties of the samples with those prepared by LOFO. Firstly, evaporated Au is known to be able to penetrate through even small defects, therefore this technique will tell us to what depth the oxide layer is defect-free. Secondly, if the current enhancement is due to the Au NPs, then evaporating Au onto them will make them merge into an Au top contact film and should destroy any enhancement. Indeed, comparing samples with evaporated and LOFO-deposited Au reveals that both the control samples (without NPs) and the NP-containing samples with evaporated Au show only noise (similar to curve 1 in Figure 1), in contrast to the NP-containing sample with LOFO-deposited Au. The possibility that the changes in junction currents arise from the exposure of the insulating film to the solution used to prepare the Au NP monolayer was ruled out by comparing the *I–V* results of the NP-containing samples with LOFO-deposited and evaporated Au. Indeed, no significant change in insulator thickness was found by ellipsometry as a result of Au NP assembly or LOFO preparation using either an NP-free aqueous subphase with the same pH value or the LOFO aqueous subphase used for actual sample preparation.

At present we can only speculate on the underlying physical origins of the observed current enhancement, but it is tempting to invoke the strong, localized electromagnetic fields associated with Au NPs, that is, some form of electric-field-enhanced current. Possible reasons for such enhancement are field emission ("lightning-rod effect", Fowler–Nordheim tunneling), Poole–Frenkel hopping, or even the

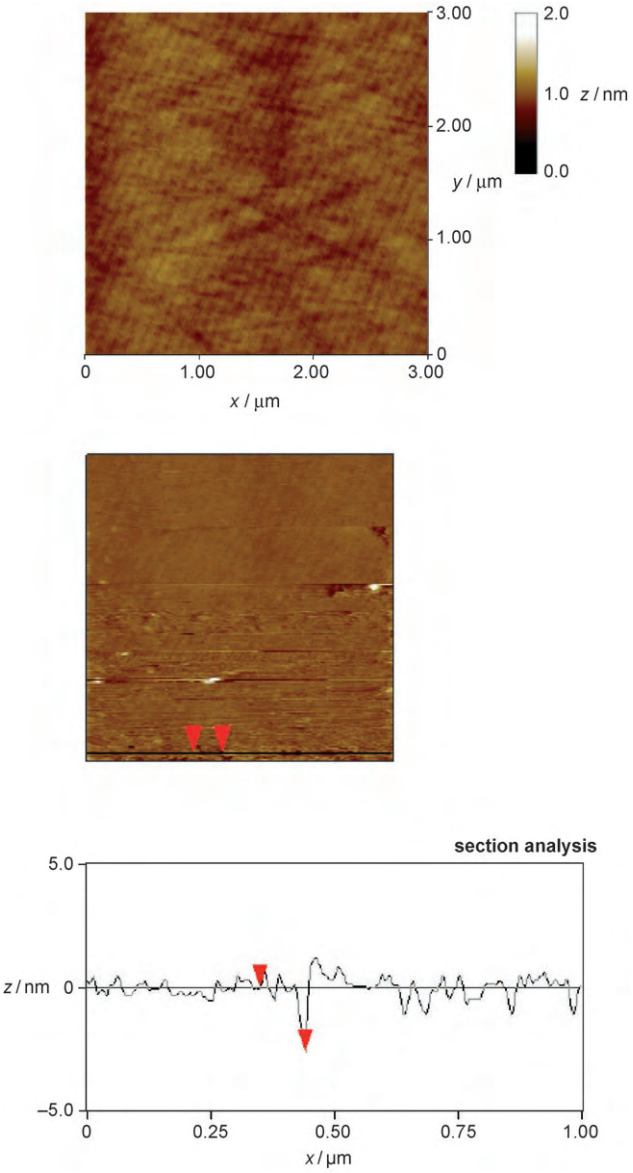

Figure 2. Representative AFM images of the oxide surface of the Si/SiO_2 ($\approx$5 nm) substrate (top; height scale given) and a saturated Au NP monolayer self-assembled on an APTMS-modified Si/SiO_2 ($\approx$5 nm) substrate (middle). A section analysis (bottom) shows that the average height of the Au NPs is approximately 2.6 nm (between the two red markers).

involvement of surface plasmon (SP) modes (see Supporting Information).

We note here that field enhancement increases with the inverse particle radius, so we can expect, up to a point, larger particles to show smaller effects. At the same time, in terms of optical efficiency, the propagation length of surface plasmon polaritons (SPPs) varies with the NP diameter and decays slowly (at least compared to tunneling) within the efficient propagation length (gap).[4,5]

As a preliminary check on the mechanism we used the same degenerate (100) *n*-Si as electrode ($\approx 10^{-3}\,\Omega$cm), but now with a native oxide layer of approximately 1.8 nm to construct Au pad//octadecanethiolate (C18SH)/Au NP mon-

 © 2006 Wiley-VCH Verlag GmbH & Co. KGaA, Weinheim

olayer//APTMS-SiO_x-Si junctions, with Au pad//cysteamine/Au NP monolayer//APTMS-SiO_x-Si junctions as control. The C18SH monolayers serve as spacer between the Au NPs and the Au pad (see Supporting Information for details on junction preparation and AFM images of the as-prepared monolayers). As seen from Figure 3a, microamp currents flow through this structure. These currents are only a few times smaller than those obtained for the control Au pad//cysteamine/Au NP monolayer//APTMS-SiO_x-Si junctions (Figure 3b). If the mechanism of current transport were normal tunneling through a rectangular barrier, the current should decay by some eight orders of magnitude because of the additional approximately 2-nm-thick C18SH layers.[6]

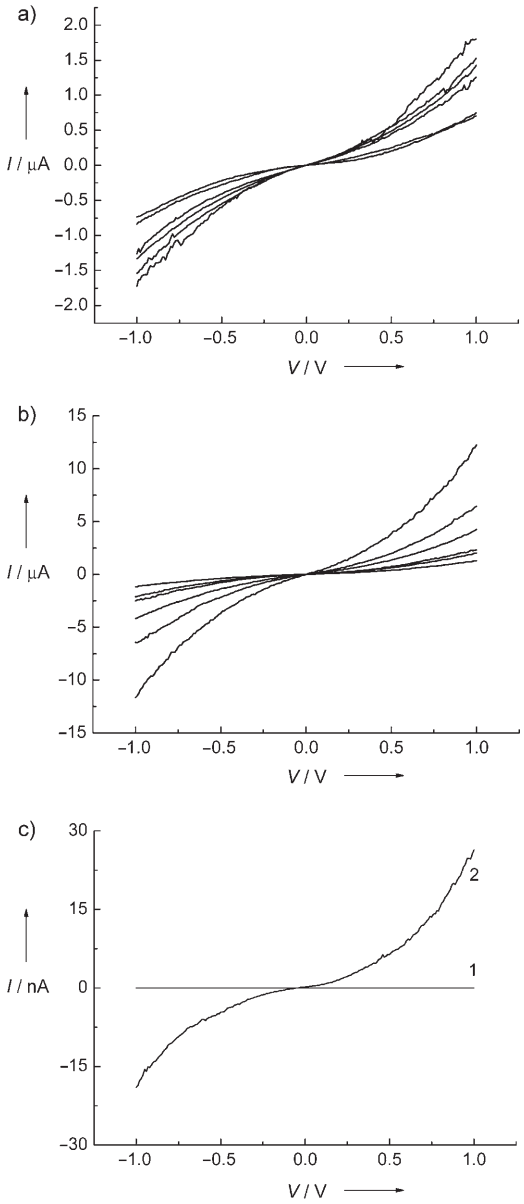

Figure 3. *I–V* curves of six independent junctions from three samples of a) Au pad//C18SH/Au NP monolayer//APTMS-SiO_x-Si junctions (currents: 0.73–1.7 μA) and b) Au pad//cysteamine/Au NP monolayer//APTMS-SiO_x-Si junctions (currents: 1.1–11.7 μA). All curves were measured under ambient conditions, and (100) *n*-Si ($\approx 10^{-3}$ Ω cm) was used. c) *I–V* curves of Au pad (formed by LOFO)//cysteamine/Au NP ($\approx$2.5 or 10 nm) monolayer/APTMS-SiO_2 (6.2 ± 0.2 nm)//Si junctions, measured under ambient conditions and in the dark. Curve 1: 2.5-nm Au NPs; curve 2: 10-nm Au NPs.

To see if the insulator thickness and NP size are independent parameters for the current enhancement, we varied both the SiO_2-layer thickness and the Au NP size. As shown in curve 1 of Figure 3c, if the SiO_2-layer thickness is increased to (6.2 ± 0.2) nm, the current flow drops to the picoamp range, even with an Au NP ($\approx$2.5 nm) monolayer. However, if we use larger Au NPs ($\approx$10 nm diameter, Sigma–Aldrich) a strong increase in current is seen, with typical currents through the (6.2 ± 0.2)-nm-thick oxide layers of 3–50 nA at 1 V applied bias, as shown in curve 2 of Figure 3c. These results can be construed as support for the involvement of SPs since the efficient propagation length of the SP field will depend on the NP size[4,5] and this length should limit the insulator thickness.

To what extent is current enhancement a general phenomenon? To explore this we looked for a soft material insulator. Because of the difficulty of preparing monolayers from pure lipid bilayers reproducibly,[7] we decided to use approximately 5-nm-thick bR-containing phospholipid bilayers as the insulator. We have previously reported the preparation of stable monolayers from these compounds, which we used to study their current transport behavior.[7] In this way we constructed Au pad//bR-lipid bilayer/Au NP ($\approx$2.5 nm) monolayer//APTMS-AlO_x-Al junctions, with Au pad//bR-lipid bilayer/APTMS-AlO_x-Al ones as control. The basic junction structure is shown in Figure 4. The description of the junction preparations and the AFM characterization of the as-prepared films can be found in the Supporting Information.

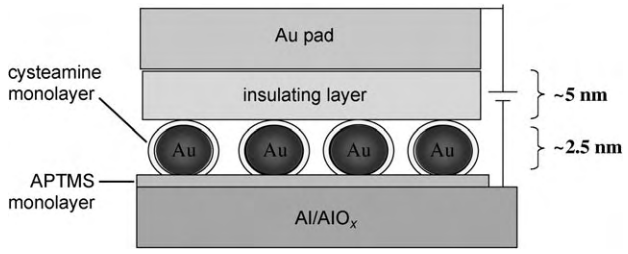

Figure 4. Schematic diagram of the Au pad//insulating layer/Au NP monolayer//APTMS-AlO_x-Al complex planar junction. An organic insulating layer is suspended over the surface of a colloidal Au monolayer by spreading negatively charged bR-containing proteoliposomes onto the positively charged colloidal Au monolayer.

The *I–V* characteristics of Au pad//bR-lipid bilayer/Au NP monolayer//APTMS-AlO_x-Al planar junctions are shown in curve 1 of Figure 5. The current is approximately (2 ± 1) μA at 1 V applied bias. For comparison, currents through control Au pad/bR-lipid bilayers/APTMS-AlO_x-Al junctions were typically (1 ± 0.5) nA at 1 V applied bias,[7] as shown in curve 2 and the inset of Figure 5. Although the currents vary slightly from junction to junction, owing to variation in effective contact area, the *I–V* measurements are reproducible with

 © 2006 Wiley-VCH Verlag GmbH & Co. KGaA, Weinheim

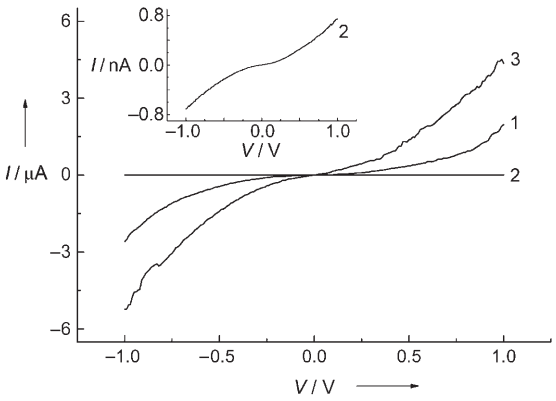

Figure 5. *I–V* curves of the Au pad//bR-lipid bilayer/Au NP monolayer//APTMS-AlO_x-Al complex planar junction (curve 1) and of the same junction without the NPs, that is, Au pad///bR-lipid bilayer/APTMS-AlO_x-Al (curve 2 and inset). Curve 3 shows a typical *I–V* curve of the control Au pad/Au NP monolayer/APTMS-AlO_x-Al junctions. All measurements were performed under ambient conditions and in the dark.

respect to the order of magnitude of the current. We can therefore state that current transport through the 5-nm-thick bR-lipid bilayers is also significantly enhanced by the introduction of an Au NP monolayer into the planar junction.

The current through control Au pad/Au NPs monolayer/APTMS-Alox-Al junctions is typically (4 ± 1) μA at 1 V applied bias,[8] as shown in curve 3 of Figure 5. Assuming that SPs on the Au NPs are involved, we note that plasmon-induced currents decay by a factor of approximately two over the 5-nm gap between the STM tip and the sample surface.[9] In such a scenario, the 4-μA current that flows through the control Au pad/Au NPs monolayer/APTMS-Alo_x-Al junction will decrease to 2 μA upon separating the Au NPs from the top electrode by a 5-nm-thick insulator, in close agreement with our experimental observations (curves 1 and 3 in Figure 5).

In view of the idea that SPs might be involved in the process, we checked the effect of illumination on current transport through the as-prepared junctions. We have previously found that the current of the Au pad/Au NP monolayer/APTMS-AlO_x-Al junctions can be significantly enhanced (the increment is approximately 3 μA at 1 V) by resonant excitation of the surface plasmon resonance (SPR) with green light ($\lambda > 550$ nm, which is close to the NP SPR wavelength).[8,10] While the current increment of the Au pad//bR-lipid bilayer/Au NP monolayer//APTMS-AlO_x-Al junctions upon irradiation with green light is typically 0.5 μA at 1 V applied bias (not shown), no pronounced light effect was observed for the Au//Au NP monolayer/$\approx$5 nm SiO_2 layer//Si junctions, and further experiments are underway to elucidate the mechanism that underlies the observed current enhancements.

In conclusion, we have found that even though adding Au NPs to a planar tunnel junction enlarges the distance between the two electrodes, it also enhances current transport significantly. Although the underlying physical origins of the observed current enhancement are not yet clear, our results suggest that strong, localized electromagnetic fields, associated with the Au NPs, play a role. If borne out by further experiments and by theory, such field effects on electronic current flow through ultra-thin insulators may also need to be considered when interpreting results for transport through insulating molecules in particular. They may well lead to interesting new avenues in nanoelectronics as, irrespective of the underlying physical picture, this enhancement may improve the sensitivity of devices like sensors.

Received: June 2, 2006
Revised: July 2, 2006
Published online: September 1, 2006

Keywords: current enhancement · current transport · electric-field effects · gold · nanostructures

[1] a) Y. D. Jin, X. F. Kang, Y. H. Song, B. L. Zhang, G. J. Cheng, S. J. Dong, *Anal. Chem.* **2001**, *73*, 2843–2849; b) Y. D. Jin, Y. Shen, S. J. Dong, *J. Phys. Chem. B* **2004**, *108*, 8142–8147.
[2] J. F. Geng, M. D. R. Thomas, D. S. Shephard, B. F. G. Johnson, *Chem. Commun.* **2005**, 1895–1897.
[3] A. Vilan, A. Shanzer, D. Cahen, *Nature* **2000**, *404*, 166–168.
[4] C. Sönnichsen, B. M. Reinhard, J. Liphardt, A. P. Alivisatos, *Nat. Biotechnol.* **2005**, *23*, 741–745.
[5] K. H. Su, Q. H. Wei, X. Zhang, J. J. Mock, D. R. Smith, S. Schultz, *Nano. Lett.* **2003**, *3*, 1087–1090.
[6] A. Salomon, D. Cahen, S. Lindsay, J. Tomfohr, V. B. Engelkes, C. D. Frisbie, *Adv. Mater.* **2003**, *15*, 1881–1890.
[7] Y. D. Jin, N. Friedmann, M. Sheves, T. He, D. Cahen, *Proc. Natl. Acad. Sci. USA* **2006**, *103*, 8601–8606.
[8] Y. D. Jin, N. Friedman, *J. Am. Chem. Soc.* **2005**, *127*, 11902–11903.
[9] R. Möller, U. Albrecht, J. Boneberg, B. Koslowski, P. Leiderer, K. Dransfeld, *J. Vac. Sci. Technol. B* **1991**, *9*, 506–509.
[10] The thin Au film top electrode is (semi)transparent to green light. For example, the transmittance of a 55-nm Au film is around 70% at a wavelength of about 550 nm (cf. M. F. Xiao, N. Rakov, *J. Phys. Condens. Matter* **2003**, *15*, L133–L137).

 © 2006 Wiley-VCH Verlag GmbH & Co. KGaA, Weinheim

Pure Silica Zeolites

DOI: 10.1002/anie.200602036

Mechanical and Dielectric Properties of Pure-Silica-Zeolite Low-*k* Materials**

*Zijian Li, Mark C. Johnson, Minwei Sun, E. Todd Ryan, David J. Earl, Wolfgang Maichen, Jeremy I. Martin, Shuang Li, Christopher M. Lew, Junlan Wang, Michael W. Deem, Mark E. Davis, and Yushan Yan**

The continuing evolution of microprocessors requires the timely development of low-dielectric-constant (low-*k*) materials to replace dense silica, which with a *k* value of about 4 has been the dielectric insulator of choice since the inception of the semiconductor industry.[1–4] One leading approach to lower the *k* value to the ultralow-*k* range (i.e. $k < 2.2$) is to introduce porosity into the silica by taking advantage of the low *k* value of air ($k \approx 1$).[3,4] Amorphous porous silicas such as sol–gel silica[5,6] and organic-templated mesoporous silica[7–10] have been suggested as possible low-*k* materials. High thermal and chemical stability of porous silicas and their similarity to dense silica in terms of chemical composition are some of their attractive features over polymeric low-*k* materials.[3,4] Porous silicas can also offer generational extendibility within the ultralow-*k* range.[2] However, the introduction of porosity into amorphous silicas thus far has been generally accompanied by a dramatic reduction in mechanical strength (commonly manifested in lower values of the elastic modulus, *E*),[3,4] which makes their survivability during chemical mechanical processing (CMP) and packaging questionable. Germane to ultralow-*k* applications, pure-silica-zeolites (PSZs) offer several potential advantages over amorphous silicas, including crystalline structure, intrinsically uniform and small pore size, and hydrophobicity. Here we hypothesize that PSZs exhibit a higher *E* value for any given *k* value than their amorphous counterparts because of their crystalline nature and provide support for this postulate below.

We have been investigating PSZs as possible low-*k* materials and have developed two film-deposition processes: in situ crystallization and spin-on of a zeolite nanoparticle suspension.[11–16] The in situ films are pure zeolitic silica films that are useful for revealing the intrinsic properties of zeolites. The spin-on films are composites of PSZs and amorphous silica, and, as such, their properties are not necessarily the intrinsic properties of the pure zeolites. However, the spin-on films have the advantage of providing a *k* value in the ultralow-*k* range. Moreover, the spin-on deposition process is more viable for the manufacturing of integrated circuits (ICs).

To provide evidence for the hypothesis that crystallinity is important to the mechanical strength of silicas, experimental data from in situ and spin-on PSZ films and amorphous silicas were compared in an *E* versus *k* plot, which is one of the most revealing engineering plots for the evaluation of low-*k* materials. The amorphous silica data were obtained from the literature (Figure 1, open circles and solid data fitted line).[17] Clearly, the *E* value of amorphous silicas drastically declines as the value of *k* is lowered. A similar and much larger data set was also reported recently.[18] The rapid deterioration of *E* as *k* is lowered raises significant concerns for integrating amorphous porous low-*k* materials with a *k* value of less than 2.5 into conventional IC fabrication

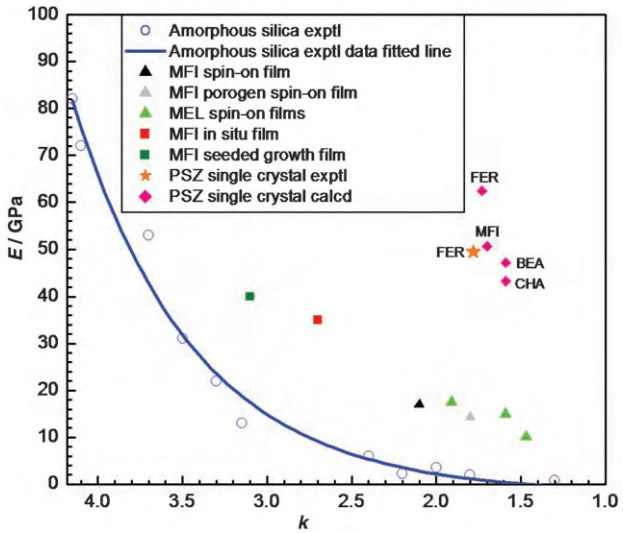

Figure 1. Elastic modulus (*E*) versus dielectric constant (*k*) for amorphous silicas and PSZs. The open circles and solid data fitted line correspond to experimental data taken from Xu et al.[17] Squares correspond to experimental data for polycrystalline PSZ MFI films; triangles correspond to experimental data for spin-on PSZ MFI and MEL films; diamonds correspond to calculations of PSZ single crystals; the star corresponds to experimental data for FER single crystals.

[*] Dr. Z. Li, M. Sun, Dr. S. Li, C. M. Lew, Prof. Y. S. Yan
Department of Chemical and Environmental Engineering
University of California, Riverside, CA 92521 (USA)
Fax: (+1) 951-827-5696
E-mail: yushan.yan@ucr.edu
M. C. Johnson, Prof. J. Wang
Department of Mechanical Engineering
University of California, Riverside, CA 92521 (USA)
Dr. E. T. Ryan, Dr. J. I. Martin
Advanced Micro Devices Inc.
Hopewell Junction, NY 12533 (USA)
Dr. D. J. Earl, Dr. M. W. Deem
Department of Bioengineering, Physics and Astronomy
Rice University, Houston, TX 77251 (USA)
Dr. W. Maichen
Teradyne Inc.
Agoura Hills, CA 91301 (USA)
Prof. M. E. Davis
Department of Chemical Engineering
California Institute of Technology
Pasadena, CA 91125 (USA)

[**] We acknowledge the NSF (CTS-0404376), Advanced Micro Devices Inc., Engelhard Corporation, and UC-Discovery Grant for their financial support. We thank Dr. S. I. Zones of ChevronTexaco for his help on B-CHA single-crystal synthesis. *k* = Dielectric constant.
Supporting information for this article is available on the WWW under http://www.angewandte.org or from the author.

© 2006 Wiley-VCH Verlag GmbH & Co. KGaA, Weinheim

processes because the E values fall in a range (e.g. $E < 6$ GPa) where CMP can be problematic and cracks can readily propagate during packaging.

The experimental data we have obtained thus far on PSZ films, in situ (Figure 1, red square) and spin-on (Figure 1, triangles), support the hypothesis that PSZ films have greater E values than amorphous silicas at comparable k values (Figure 1). However, several critical questions remain. First, the elastic modulus is measured by nanoindentation on thin films with a thickness of about or slightly less than 0.5 μm and could be influenced by the contributions from substrate effects. The substrate in these cases is a silicon wafer that has $E = 130$ GPa. Typically the indentation depth should be less than 10% of the film thickness to eliminate substrate effects. Depending on the modulus of the film and the geometry of the indenter tip, a thickness of greater than 1 μm is usually required. Second, these in situ and spin-on films are either polycrystalline or composites with amorphous silica, and thus it would be helpful to examine the intrinsic limiting values of k and E for PSZs from both experimental and theoretical perspectives to provide guidance for the development of spin-on films. To address these two questions, we initiated efforts on the preparation, characterization, and calculation of thick PSZ films and PSZ single crystals.

We synthesized polycrystalline PSZ MFI films with a thickness greater than 6 μm on silicon wafers by a seeded growth method.[19] Images corresponding to the top and cross-sectional views of a typical seeded growth film are shown in Figure 2 A and B. Unlike the polycrystalline *b*-oriented PSZ MFI films synthesized previously by in situ crystallization,[13] the seeded growth film has a majority of its crystals *c*-oriented.[19] After polishing, the film has a smooth surface free from cracks or delamination (Figure 2 A, inset), demonstrating the strong adhesion between the film and substrate. An image showing the cross-sectional view of the polished film (Figure 2 B) reveals that the film is dense without pinholes or microcracks between the individual crystals. The thickness is uniform over the entire substrate. The E value of the seeded growth PSZ MFI film is 41.8 GPa as measured by nanoindentation. Substrate effects can be neglected because the deepest indent is less than 200 nm, which is less than 3% of the film thickness. The k value of the film is 3.10. Note that the E value for the seeded growth film (Figure 1, green square) is well above the amorphous silica line, again supporting the hypothesis that PSZs are mechanically stronger than amorphous silicas.

We synthesized single crystals of PSZ FER with the largest dimension over 1 mm (Figure 2 C and E) following a published procedure.[20] These are the largest FER single crystals ever synthesized. The FER crystals have a thin-plate geometry, which is crucial for measurements of k values. The plates are not perfectly flat but have a flattened four-sided pyramidal shape on both sides of the thin plate (Figure 2 C). The orientations of three edges of the FER crystals are parallel to the respective directions of the crystallographic *a*, *b*, and *c* axes (Figure 2 E).[21] The crystals were indented along the *c* axis (i.e. [001] direction). The results obtained for the elastic modulus and the hardness of one typical FER crystal are shown in Figure 2 D. Many crystals were tested, each with

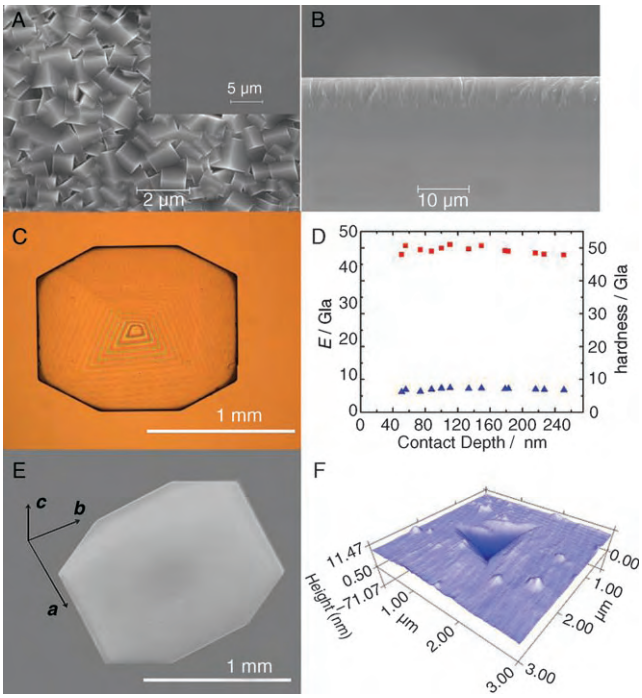

Figure 2. A) Top-view scanning electron microscopy (SEM) image of a seeded growth PSZ MFI film. The inset shows the surface of the film after polishing. B) Cross-sectional view of a polished film on a silicon substrate with a thickness of over 6 μm. C) Optical image of an FER single crystal. The rings seen in the image are light interference patterns showing the four-sided pyramidal shape on both sides of the thin-plate-shaped crystals. D) Nanoindentation results: red squares correspond to the elastic modulus (E), while blue triangles correspond to the hardness of PSZ FER crystals. E) SEM image of the FER crystal with the crystallographic orientation shown. F) Atomic force microscopy (AFM) 3D image of an indent scanned by the same Berkovich tip for indentation with a scan area of 3×3 μm^2.

numerous indents, and consistent results were obtained. The E value and the hardness of the FER single crystals are 49.4 and 7.2 GPa, respectively. A 3D image of an indent with an indentation depth of 250 nm is shown in Figure 2 F. Note that there are no cracks or pile-ups around the indents.

Measurements of k on zeolite single crystals are not currently available. Although 1-mm FER single crystals are sufficiently large for measurements of E values by nanoindentation, they are still too small for measurements of k values using routine impedance analyzers. The small electrode area (≈ 1 mm^2) and the large thickness (≈ 30 μm) of the crystal lead to a capacitance that is beyond the limit of most of the commonly used impedance analyzers. Thus a time domain reflectometry (TDR) technique[22] was chosen to measure the capacitance of the FER crystals and a k value of 2.18 was obtained at 1 MHz. Note that this k value for FER was obtained from noncalcined crystals. After over 100 attempts, it became clear that cracking is inevitable during the calcination process for crystals of this size and that the cracks can lead to unreliable k values. We have previously shown that removal of the organic structure-directing agent leads to a reduced k value (e.g. 3.4 to 2.7 for polycrystalline PSZ MFI films[13]), and we believe that the FER crystals, once

 © 2006 Wiley-VCH Verlag GmbH & Co. KGaA, Weinheim

the organic structure-directing agent is removed, will yield a k value of 1.78, assuming a dependence on porosity similar to MFI.

All of the k values for the PSZ films and amorphous silicas reported in Figure 1 were obtained under ambient conditions at 1 MHz, which is the most commonly used measurement frequency for low-k materials. The E value for single-crystal FER (Figure 1, orange star) is well above the amorphous silica line, once again supporting the hypothesis that PSZs are mechanically stronger than amorphous silicas at similar k values.

We examined computationally the limiting values of k and E for PSZ single crystals. The elastic constants for each of the zeolites were determined with the MPDyn simulation code[23] and the BKS force field.[24] The bulk modulus, shear modulus, elastic modulus, and Poisson's ratio were determined by the Voigt–Reuss–Hill method.[25] Dielectric constants were calculated from energy-minimized structures using the GULP simulation package.[26] An ion-pair shell-model force field by Jackson and Catlow[27] was used to represent the interactions between atoms. The calculated E and k (infinite frequency) values for MFI, FER, BEA, and CHA are presented in Table 1. The Poisson's ratio and E value for randomly oriented polycrystalline samples are also listed. The values of E and the high-frequency k are used in the E versus k plot shown in Figure 1 and in Figure 3. Note that the calculated data points for MFI, FER, BEA, and CHA once again are above amorphous silicas in the E versus k plot (Figure 1). For comparison, experimental data for single-crystal MFI (E), CHA (E), FER (E and k), polycrystalline MFI (E and k), and BEA (k) are included in Table 1 and Figures 1 and 3. Because of the geometries (non-thin-plate), it was not possible to measure the k values of single-crystal MFI, BEA, and CHA. The fact that the polycrystalline films have a much higher k value than calculated values for single crystals (2.70–3.10 versus 1.70 for MFI, and 2.30 versus 1.6 for BEA) suggests that grain boundaries and crystal defects play a major role in controlling the k value.

From the E versus k plot it is clear that zeolite materials significantly outperform amorphous porous silicas (Figure 1). Both E and k values depend on the porosity, and, it is fundamentally interesting and practically instructive to examine k versus porosity (Figure 3 A) and E versus porosity (Figure 3 B) for PSZs and amorphous silicas. For k versus porosity (Figure 3 A), most of the spin-on films (triangles) deviate little from amorphous silica (solid line), which is understandable because these films are a composite of zeolite and amorphous silica and contain a significant amount of amorphous silica. By contrast, when the spin-on films have higher crystallinity[12] (two gray triangles straying much below the solid line), the k value becomes significantly lower than that for amorphous silica. This result is consistent with the observations that polycrystalline in situ MFI (red square) and BEA (black square) films are below amorphous silicas, and FER single crystal is even lower (orange star). The polycrystalline seeded growth MFI film (green square) is above the

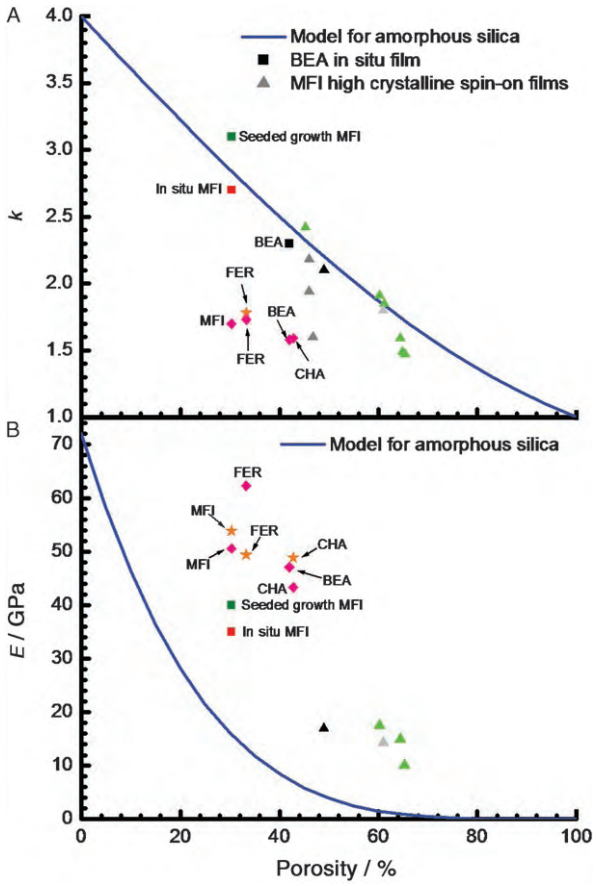

Figure 3. Dielectric constant (k) and elastic modulus (E) of PSZs versus porosity. A) k versus porosity; the solid line refers to a model for amorphous silica.[28] B) E versus porosity; the solid line corresponds to a model for amorphous silica.[29] Squares correspond to experimental data for polycrystalline PSZ MFI films; triangles correspond to experimental data for spin-on PSZ MFI and MEL films; diamonds correspond to calculations of PSZ single crystals; the stars correspond to experimental data for single crystals.

Table 1: Calculated and measured k and E values for different frameworks.

Framework code	MFI (monoclinic)			FER (orthorhombic)			CHA (monoclinic)			BEA (tetragonal)		
	x	y	z	x	y	z	x	y	z	x	y	z
k calcd (∞ MHz)	1.71	1.71	1.70	1.69	1.75	1.75	1.59	1.59	1.59	1.58	1.58	1.61
k exptl (1 MHz)	[a]	2.7[b]	3.1[c]	[a]	[a]	1.78	[a]	[a]	[a]	2.3[d]		
Poisson's ratio calcd	0.1666 ± 0.0080			0.1996 ± 0.0077			0.3845 ± 0.0012			0.3701 ± 0.0015		
E calcd [GPa]	50.6 ± 0.7			62.4 ± 0.7			43.3 ± 0.8			47.1 ± 0.6		
E exptl[e] [GPa]	53.9 ± 0.5			49.4 ± 1.1			48.9 ± 1.2[f]			[a]		

[a] Values not measurable due to experimental limitations. [b] Measured on in situ films. [c] Measured on seeded growth films. [d] Measured on randomly oriented films. [e] Measured on single crystals assuming a Poisson's ratio of 0.25. [f] Measured on boron chabazite single crystals.

© 2006 Wiley-VCH Verlag GmbH & Co. KGaA, Weinheim

amorphous silica line possibly because of its *c* orientation. For *E* versus porosity (Figure 3B), it is clear that that PSZ materials (spin-on, polycrystalline, and single crystals) are vastly superior to amorphous silicas. Overall, it is the higher *E* values of PSZs rather than their lower *k* values at a given porosity that positions the PSZs well above the amorphous silicas in the *E* versus *k* plot (Figure 1).

In summary, our experimental results provide definitive evidence for the hypothesis that PSZs offer a significantly superior elastic modulus to amorphous silicas at any given *k* value or porosity. The PSZ single crystals offer the exciting possibility to simultaneously achieve remarkably high *E* and low *k* values, as demonstrated by $E = 49.4$ GPa and $k = 1.78$ for PSZ FER. The results further suggest that improving crystallinity and decreasing crystal defects are critical for achieving a higher *E* value and lower *k* value for the spin-on film, a strategy that we have already started to explore.[12] Moreover, our theoretical calculations of PSZ single crystals validate our experimental results and further suggest that there is much room for improving both *k* and *E* values of PSZ low-*k* films.

Received: May 23, 2006
Published online: August 23, 2006

Keywords: mechanical properties · porous materials · silicates · thin films · zeolites

[1] *International Technology Roadmap for Semiconductors* **2005**.
[2] R. D. Miller, *Science* **1999**, *286*, 421.
[3] M. Morgen, E. T. Ryan, J. H. Zhao, C. Hu, T. H. Cho, P. S. Ho, *Annu. Rev. Mater. Sci.* **2000**, *30*, 645.
[4] K. Maex, M. R. Baklanov, D. Shamiryan, F. Iacopi, S. H. Brongersma, Z. S. Yanovitskaya, *J. Appl. Phys.* **2003**, *93*, 8793.
[5] L. W. Hrubesh, L. E. Keene, V. R. Latorre, *J. Mater. Res.* **1993**, *8*, 1736.
[6] S. Seraji, Y. Wu, M. Forbess, S. J. Limmer, T. Chou, G. Z. Cao, *Adv. Mater.* **2000**, *12*, 1695.
[7] D. Zhao, P. Yang, N. Melosh, J. Feng, B. F. Chmelka, G. D. Stucky, *Adv. Mater.* **1998**, *10*, 1380.
[8] D. A. Doshi, N. K. Huesing, M. C. Lu, H. Y. Fan, Y. F. Lu, K. Simmons-Potter, B. G. Potter, A. J. Hurd, C. J. Brinker, *Science* **2000**, *290*, 107.
[9] K. Landskron, B. D. Hatton, D. D. Perovic, G. A. Ozin, *Science* **2003**, *302*, 266.
[10] R. A. Pai, R. Humayun, M. T. Schulberg, A. Sengupta, J. N. Sun, J. J. Watkins, *Science* **2004**, *303*, 507.
[11] Z. J. Li, C. M. Lew, S. A. Li, D. I. Medina, Y. S. Yan, *J. Phys. Chem. B* **2005**, *109*, 8652.
[12] Z. J. Li, S. Li, Y. S. Yan, *Adv. Funct. Mater.* **2004**, *14*, 1019.
[13] Z. B. Wang, H. T. Wang, A. P. Mitra, L. M. Huang, Y. S. Yan, *Adv. Mater.* **2001**, *13*, 746.
[14] Z. B. Wang, A. P. Mitra, H. T. Wang, L. M. Huang, Y. H. Yan, *Adv. Mater.* **2001**, *13*, 1463.
[15] S. Li, Z. J. Li, Y. S. Yan, *Adv. Mater.* **2003**, *15*, 1528.
[16] S. Li, J. N. Sun, Z. J. Li, H. G. Peng, D. Gidley, E. T. Ryan, Y. S. Yan, *J. Phys. Chem. B* **2004**, *108*, 11689.
[17] G. Xu, J. He, E. Andideh, J. Bielefeld, T. Scherban, in *IEEE International Interconnect Technology Conference*, Piscataway, NJ, San Francisco, CA, **2002**, p. 57.
[18] E. T. Ryan, C. Labelle, S. Nitta, N. C. M. Fuller, G. Bonilla, K. McCullough, C. Taft, H. Lin, A. Simon, E. Simonyi, K. Malone, M. Sankarapandian, D. Dunn, M. A. Zaitz, S. Cohen, N. Klymko, B. K. Moon, Z. Li, S. L, Y. Yan, J. Liu, P. S. Ho, *Material Research Society Annual Conference, Vol. Materials, Technology and Reliability of Advanced Interconnects* (Eds.: P. R. Besser, A. J. McKerrow, F. Iacopi, C. P. Wong, J. Vlassak), San Francisco, CA, **2005**, p. B2.1.2.
[19] A. Gouzinis, M. Tsapatsis, *Chem. Mater.* **1998**, *10*, 2497.
[20] A. Kuperman, S. Nadimi, S. Oliver, G. A. Ozin, J. M. Garces, M. M. Olken, *Nature* **1993**, *365*, 239.
[21] J. E. Lewis, C. C. Freyhardt, M. E. Davis, *J. Phys. Chem.* **1996**, *100*, 5039.
[22] *TDR Impedance Measurements: A Foundation for Signal Integrity*, Application Note 55W-14601-0, **2001**.
[23] MPDyn is a freely available simulation package written by W. Shinoda and M. Shiga. See http://staff.aist.go.jp/w.shinoda/MPDyn.
[24] B. W. H. Van Beest, G. J. Kramer, R. A. Van Santen, *Phys. Rev. Lett.* **1990**, *64*, 1955.
[25] R. F. S. Hearmon, *Physics of the Solid State*, Academic, New York, **1969**.
[26] J. D. Gale, A. L. Rohl, *Mol. Simul.* **2003**, *29*, 291.
[27] R. A. Jackson, C. R. A. Catlow, *Mol. Simul.* **1988**, *1*, 207.
[28] D. Bruggeman, *Ann. Phys.* **1935**, *24*, 636.
[29] K. K. Phani, S. K. Niyogi, *J. Mater. Sci.* **1987**, *22*, 257.

 © 2006 Wiley-VCH Verlag GmbH & Co. KGaA, Weinheim

Acid–Base Catalysis

DOI: 10.1002/anie.200602243

Multifunctional Heterogeneous Catalysts: SBA-15-Containing Primary Amines and Sulfonic Acids**

*Ryan K. Zeidan, Son-Jong Hwang, and Mark E. Davis**

A current area of interest in the design and synthesis of solid catalysts is the creation of materials that contain multiple types of active centers. These functionalities may be used to perform several steps in a reaction sequence or work in a cooperative manner to alter the characteristics of a single reaction, for example, rates, selectivities, and so forth. Enzymes, such as aldolases, are interesting examples of multifunctional catalysts as they are capable of conducting multistep reactions. Enzymes immobilize mutually incompat-

[*] R. K. Zeidan, S.-J. Hwang, Prof. M. E. Davis
Division of Chemistry and Chemical Engineering
California Institute of Technology
Pasadena, CA 91125 (USA)
Fax: (+1) 626-568-8743
E-mail: mdavis@cheme.caltech.edu

[**] Technical assistance from Stacey Zones, Allen Barton, and Ken Ong of Chevron is gratefully acknowledged. This study was supported by a grant from the US Department of Energy. SBA-15 is a mesoporous silica (Santa Barbara Amorphous).

Supporting information for this article is available on the WWW under http://www.angewandte.org or from the author.

WILEY InterScience DISCOVER SOMETHING GREAT
© 2006 Wiley-VCH Verlag GmbH & Co. KGaA, Weinheim

ible functional groups in a manner that maintains their independent functionality, and as such, are able to carry out multistep reaction sequences with functionalities that would not be tolerated together in solution.

Previous work on bifunctional solid-catalyst synthesis largely involved the use of metal centers with acid sites. Recently, attention has been focused on combinations of organic functional groups. Immobilized organic amines (base) have been used with supported silanols (acid)[1] to perform bifunctional catalysis, and amine functional groups have been immobilized together with thiols.[2,3] Dufaud and Davis[4] reported on the positioning of adjacent sulfonic acid functional groups, and Zeidan et al.[5] have also incorporated sulfonic acids and thiols that exhibit a cooperative effect in a condensation reaction. Also, bifunctional catalysis with different active centers on separate supports[6–9] and hydrogen-bonding ureas with amine bases[10] have been investigated. However, no reports of a material containing an organic acid and organic base that are incorporated into the same material have appeared, presumably as a result of the incompatibility of these groups. Herein, we report a solid material that contains both organic acid and base groups that together exhibit a reactivity in the aldol condensation of acetone with 4-nitrobenzaldehyde that is not achievable with these same groups in solution.

A sulfonic acid and amine were incorporated into SBA-15 (Santa Barbara Amorphous) through a "one-pot" synthesis using poly(ethylene glycol)-*block*-poly(propylene glycol)-*block*-poly(ethylene glycol) (P123), HCl, H_2O, and tetraethoxysilane (TEOS; Scheme 1) to prepare the dual-functionalized mesoporous catalyst SBA-15-A/B.

Table 1: Acid–base aldol catalysis.

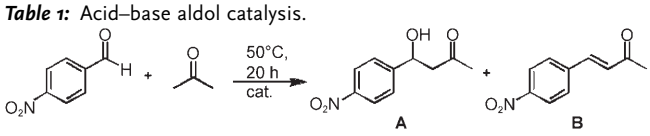

Entry	Catalyst (10 mol%)	**A** [%]	**B** [%]	Conv. [%][a]
1	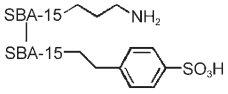	45	17	62
2	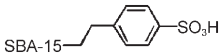	8	8	16
3		25	8	33
4	SBA-15-A/SBA-15-B[b]	30	14	44
5	SBA-15	0	0	0
6	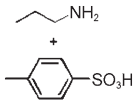	0	0	0
7		3	5	8
8	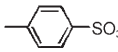	3	1	4

[a] Total conversion. Yields determined through ^{1}H NMR spectroscopic analysis with THF as the internal standard. [b] 1:1 mixture of sulfonic acid functionalized SBA-15 (SBA-15-A) and amine-functionalized SBA-15 (SBA-15-B).

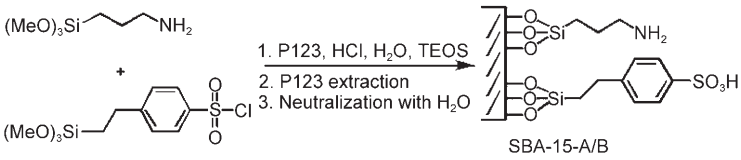

Scheme 1. Catalyst synthesis.

This material (as well as SBA-15 functionalized with sulfonic acid alone and propylamine alone) was analyzed by ^{13}C and ^{29}Si CP/MAS solid-state NMR spectroscopy, X-ray diffraction (XRD), N_2 adsorption, and thermogravimetric analysis (see Supporting Information).

The characterization data show that the functionalized materials have surface areas of between 600 and 800 $m^2 g^{-1}$ and pore sizes on the order of 40–60 Å, typical of SBA-15-type materials.[4,5] The ^{13}C NMR spectra indicate the presence of the intact organic functional groups, and the ^{29}Si NMR spectrum indicates the incorporation of organic functional groups.

The immobilized catalysts were tested for activity in the aldol condensation of 4-nitrobenzaldehyde with acetone to give the resulting aldol addition and dehydration products. SBA-15-A/B was used as a catalyst for this reaction (Table 1, entry 1), and in all experiments the total amount of amine and/or sulfonic acid functional groups was kept constant at 0.05 mmol. Significant production of both products occurred and gave a total conversion of 62%. Use of SBA-15 functionalized only with a sulfonic acid or amine functionality gave significantly lower levels of conversion (Table 1, entries 2 and 3). A physical mixture of acid-functionalized SBA-15 and amine-functionalized SBA-15 showed an intermediate level of conversion that was significantly lower than the dual-functionalized acid/base catalyst (Table 1, entry 4). The support alone caused no conversion (Table 1, entry 5). Interestingly, the homogeneous analogues of the sulfonic acid and amine showed no conversion of the starting materials into either product, as these functionalities apparently neutralize each other and salt out of the reaction mixture (Table 1, entry 6). Also, the individual acid and base homogeneous analogues gave rise to very low conversions (Table 1, entries 7 and 8), much less than the acid/base bifunctional catalyst. The observed cooperative effect indicates some level of acid/base pairing in this material. With the two functional groups being dispersed randomly in the synthesis, it was expected that there would be acid sites neighboring acid sites, base sites neighboring base sites, and some acid sites in proximity to base sites. If the catalytic activity is due to single acid or base sites, or neighboring acid/acid or base/base sites, the level of conversion in entries 2 and 3 (Table 1) would be the maximum

 © 2006 Wiley-VCH Verlag GmbH & Co. KGaA, Weinheim

achievable. The enhancement of reactivity beyond those cases is likely due to interactions between neighboring acid and base sites (see Supporting Information for the mechanism).

It is expected that the acid and base groups in SBA-15-A/B would be in equilibrium between the free acid and base and the ion pair that results from neutralization, and that the solvent would have a dramatic effect on this equilibrium, that is, protic solvents would confer different properties to aprotic solvents as a result of differing abilities to stabilize the neutralized ion pair. The equilibrium would lie towards the ion pair in polar, protic solvents, as proton exchange would be rapid and the protic solvent would stabilize the ion pair the most. Nonpolar, aprotic solvents would cause slower exchange of the protons and would stabilize an ion pair much less than a protic solvent, thus forcing the equilibrium in favor of the free acid and base. To investigate these possibilities, reactions were carried out in a variety of cosolvents to examine the effect of solvent polarity on conversion. The conversion into both products is nearly 30% in polar, protic solvents, such as water and methanol (Table 2, entries 1 and 2). The conversion more than doubles

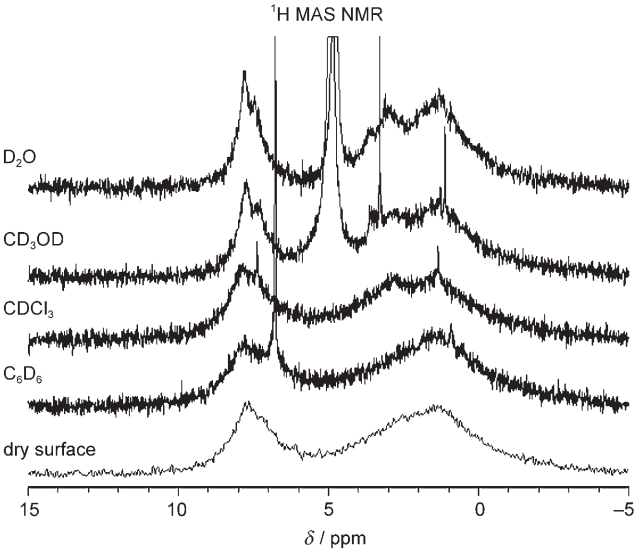

Figure 1. Solvent effect on the line shape of ^{1}H MAS NMR spectra. Sharp lines are due to incomplete deuteration of the solvents.

Table 2: Solvent effect on the catalysis.

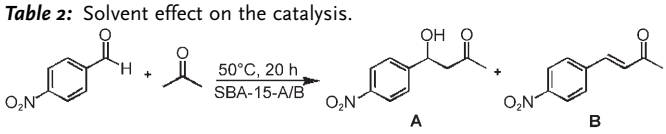

Entry	Cosolvent (1:1)[a]	**A** [%]	**B** [%]	Conv. [%][b]
1	H_2O	27	7	34
2	MeOH	14	9	23
3	Et_2O	52	13	65
4	$CHCl_3$	60	9	69
5	hexane	75	13	88
6	benzene	62	12	74

[a] 50:50 mixture of acetone/cosolvent. [b] Total conversion. Yields determined through ^{1}H NMR spectroscopic analysis with THF as the internal standard.

to about 70% upon moving to polar, aprotic solvents, such as diethyl ether and chloroform (Table 2, entries 3 and 4). Nonpolar, aprotic solvents, such as hexane and benzene (Table 2, entries 5 and 6), give further improvements in conversion, which approach 90% in the case of hexanes (Table 2, entry 5). Thus, there is a clear effect on conversion that is related to solvent polarity, thereby suggesting that the nature of the solvent does affect the equilibrium of proton exchange and hence the effective concentration of free acid and base.

Solid-state CP/MAS NMR spectroscopic analysis was used to probe the local motion of the bifunctional catalyst. SBA-15-A/B was fully deuterated and then slurried in different deuterated solvents to study the changes in motion of the functional groups in these different environments (Figure 1). The resolution of the ^{1}H NMR resonances in D_2O and CD_3OD (from non-exchanging protons in the organic functional groups) sharpened, thus indicating a more mobile structure. However, the resonances broadened in the nonpolar solvents CD_3Cl and C_6D_6, thus suggesting more restricted motion of the two groups as the acid and base functional groups associate to avoid unfavorable interactions with nonpolar solvents. The trend is in full agreement with the catalysis data as reactions in nonpolar solvents cause the polar acid and base groups to associate to a greater extent, thus allowing for an increased cooperative effect. The groups are more mobile in polar solvents as they favorably interact with the solvent and are less likely to interact with one another for cooperative catalysis to occur. Taken together, the catalytic and NMR spectroscopic data suggest that the catalytic behavior of SBA-15-A/B is clearly dictated by multiple factors, two of which seem to be the state of the equilibrium between the acid and base and the ion pair and the interactions between the two functional groups as caused by polar/nonpolar interactions with the solvent.

To probe the bifunctionality of the catalyst, SBA-15-A/B was treated with acid to neutralize the amine functional groups, thus leaving only the sulfonic acid sites. SBA-15-A/B was washed with 1M HCl or aqueous *para*-toluenesulfonic acid (*p*-TSA; Table 3, entries 1 and 2, respectively), and it is clear that the material behaves as the immobilized sulfonic acid alone (Table 1, entry 2). Likewise, SBA-15-A/B was treated with propylamine (Table 3, entry 3) and the resulting material, in which the sulfonic acid sites are neutralized, behaved the same as the amine-functionalized catalyst (Table 1, entry 3). These results illustrate the bifunctionality of SBA-15-A/B and the coexistent acidity and basicity. These experiments highlight the interesting properties achievable by immobilization of multiple functional group types. The amine and sulfonic acid salt out in solution and give rise to no conversion (Table 1, entry 6), and when the heterogeneous catalyst SBA-15-A/B is treated with homogeneous acids or bases the opposing functional group salts out and the respective behavior is lost. On the other hand, the two opposing functional groups do not lose catalytic activity when the amine and sulfonic acid are immobilized on SBA-15-A/B

 © 2006 Wiley-VCH Verlag GmbH & Co. KGaA, Weinheim

Table 3: Catalyst quenching experiments.

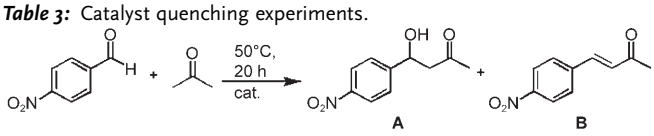

Entry	Catalyst	**A** [%]	**B** [%]	Conv. [%][a]
1	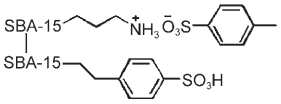	7	7	14
2	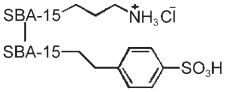	8	7	15
3	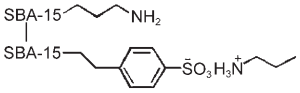	31	7	38

[a] Total conversion. Yields determined by ^{1}H NMR spectroscopic analysis with THF as the internal standard.

but rather function in a cooperative manner to give the most active catalyst used in this study.

In summary, a new approach to carrying out heterogeneous catalysis with functional groups that are incompatible and incapable of catalyzing reactions in solution has been reported. By immobilizing functional groups that can not coexist in solution as active catalytic sites, it has been demonstrated that reactivity can be restored and a cooperative, catalytic effect is observed between the functional groups. Advanced solid-state NMR experiments are in progress to study the proton motion and spacing of functional groups in these materials, and further catalytic applications are being investigated.

Experimental Section

"One-pot" synthesis of catalyst: HCl (120.0 mL, 240.0 mmol, 2.0 M) and H_2O (6.0 mL, 333.0 mmol) were added to triblock copolymer P123 (4.0 g, 0.688 mmol, $M_n = 5800$) and stirred at 40 °C until the P123 was fully dissolved. TEOS (8.2 mL, 37.8 mmol) was then added, and the reaction mixture was allowed to stir at 40 °C for 45 min. Then 2-(4-chlorosulfonylphenyl)ethyltrimethoxysilane (0.65 g) in dichloromethane (1.0 mmol, 50/50 (w/w)) was added followed by 3-aminopropyltrimethoxysilane (0.19 mL, 1.0 mmol). The reaction mixture was then stirred at 40 °C for 20 h, and then left at 100 °C for 24 h. The resulting solid was filtered and rinsed with excess H_2O (4 × 500 mL) until the slurry reached a neutral pH value. The solid was then allowed to dry overnight on a filter. The dried solid was then extracted with EtOH (400 mL per gram) by refluxing in EtOH for 24 h to remove the P123. The solid was filtered and rinsed repeatedly with EtOH (4 × 500 mL), washed with copious amounts of water until neutral, and dried overnight to obtain a dry white solid. The solid was then further dried at 80 °C under vacuum for 24 h.

Catalytic experiments (using the following general procedure for the aldol condensation):[10] Catalyst was added (0.05 mmol total amines and/or sulfonic acids) to a solution of 4-nitrobenzaldehyde (76 mg, 0.5 mmol) in acetone (10 mL), and the reaction flask was then sealed under Ar and heated at 50 °C for 20 h. Acetone was then removed in vacuo, and the product was analyzed by ^{1}H NMR spectroscopy in $CDCl_3$ with THF as an internal standard. In the case of the cosolvent studies, 10 mL of a 50:50 mixture of acetone and cosolvent was used.

Received: June 5, 2006
Revised: July 5, 2006
Published online: August 28, 2006

Keywords: aldol reaction · amines · heterogeneous catalysis · silica · sulfonic acids

[1] J. D. Bass, A. Solovyov, A. J. Pascall, A. Katz, *J. Am. Chem. Soc.* **2006**, *128*, 3737 – 3747.
[2] D. Coutinko, S. Madhugiri, K. J. Balkus, *J. Porous Mater.* **2004**, *11*, 239 – 254.
[3] J. D. Bass, A. Katz, *Chem. Mater.* **2006**, *18*, 1611 – 1620.
[4] V. Dufaud, M. E. Davis, *J. Am. Chem. Soc.* **2003**, *125*, 9403 – 9413.
[5] R. K. Zeidan, V. Dufaud, M. E. Davis, *J. Catal.* **2006**, *239*, 299 – 306.
[6] F. Gelman, J. Blum, D. Avnir, *Angew. Chem.* **2001**, *113*, 3759 – 3761; *Angew. Chem. Int. Ed.* **2001**, *40*, 3647 – 3649.
[7] B. Voit, *Angew. Chem.* **2006**, *118*, 4344 – 4346; *Angew. Chem. Int. Ed.* **2006**, *45*, 4238 – 4240.
[8] K. Motokura, N. Fujita, K. Mori, T. Mizugaki, K. Ebitani, K. Kaneda, *J. Am. Chem. Soc.* **2005**, *127*, 9674 – 9675.
[9] B. Helms, S. J. Guillaudeu, Y. Xie, M. McMurdo, C. J. Hawker, J. M. J. Frechet, *Angew. Chem.* **2005**, *117*, 6542 – 6545; *Angew. Chem. Int. Ed.* **2005**, *44*, 6384 – 6387.
[10] S. Huh, H. T. Chen, J. W. Wiench, M. Pruski, V. Lin, *Angew. Chem.* **2005**, *117*, 1860 – 1864; *Angew. Chem. Int. Ed.* **2005**, *44*, 1826 – 1830.

 © 2006 Wiley-VCH Verlag GmbH & Co. KGaA, Weinheim

Heterogenous Catalysis

DOI: 10.1002/anie.200602585

Intermolecular Rhodium-Catalyzed Carbometalation/Heck-Type Reaction in Water**

Takuya Kurahashi, Hiroshi Shinokubo, and Atsuhiro Osuka*

In recent years, organic reactions in aqueous media have received particular attention for environmental and safety reasons. Furthermore, water often exhibits profound effects on the rate and selectivity of organic reactions through enhanced hydrophobic interactions and the enrichment of organic substrates in the local environment as a result of its unique physical and chemical properties.[1,2] A recent report by Sharpless and co-workers clearly demonstrates that water can accelerate some types of intermolecular addition reactions, even under heterogeneous conditions with insoluble organic components.[3] Such an intriguing effect should also be valid for transition-metal-catalyzed reactions, thus leading to novel transformations that are difficult in conventional reaction media. Herein, we wish to describe a novel rhodium-catalyzed coupling reaction of aryl boronic acids with internal alkynes and acrylates in water to afford functionalized dienes through an aryl rhodation/Heck-type addition sequence. Although a number of rhodium-catalyzed domino processes with organoboron reagents and unsaturated functionalities have been reported,[4–6] a fully intermolecular version is quite rare.

α,β-Unsaturated carbonyl compounds are highly reactive substrates in the rhodium-catalyzed addition of boronic acid derivatives. Aryl rhodation also occurs to alkynes, but the reactivity is lower than that of conjugated enones and enoates. The rhodium-catalyzed addition of aryl boronic acids to α,β-unsaturated carbonyl compounds can proceed at room temperature, whereas the addition to alkynes often requires elevated temperatures.[7] Consequently, one can anticipate that an aryl rhodium intermediate predominantly adds to unsaturated carbonyl compounds, even in the presence of alkynes. Not surprisingly, the 1,4-addition product **4aa** was formed as the major product in 58% yield in organic solvents such as wet THF and dioxane. The reaction in a biphasic system (water/diisopropyl ether) yielded the Heck-type product **5aa** as the major product in 61% yield. Curiously, however, when the same reaction was conducted in aqueous media, a three-component assembly reaction took place to afford 1,3-diene **6aaa** in 81% yield along with the simple Heck-type product **5aa** (11%) and 1,4-addition product **4aa** (3%; Scheme 1): an emulsion of phenylboronic acid (**1a**), 5-decyne (**2a**), methyl acrylate (**3a**), and 4 mol% of $[\{Rh(OH)(cod)\}_2]$ (cod = 1,5-cyclooctadiene) in water was allowed to stand at ambient temperature for 12 h without stirring to provide 4-butyl-5-phenylnona-2,4-dienoic acid methyl ester (**6aaa**; see Supporting Information).[8] Note that arylation proceeds at ambient temperature with an unactivated alkyne. Importantly, the domino reaction takes place only in an emulsion of substrates with water, as far as we investigated. As Lautens et al. already reported, the use of surfactants (i.e., sodium decyl sulfate) to homogenize the reaction system resulted in the exclusive formation of the Heck product **5aa**.[9] Water-soluble phosphine ligands, such as trisodium triphenylphosphine-3,3′,3″-trisulfonate, disodium triphenylphosphine-4,4′-disulfonate, and cyclohexyl amphos chloride, were not effective. Thus, the course of the reaction was found to be quite sensitive to the conditions.

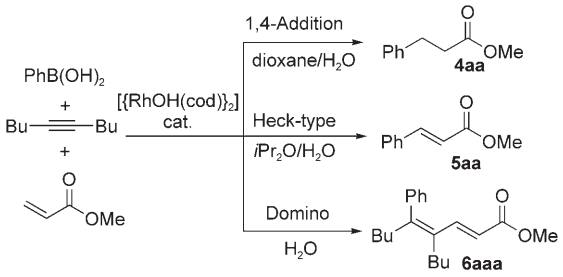

Scheme 1. Addition of phenylboronic acid to methyl acrylate and 5-decyne.

Boronic acids with electron-donating (**1b** and **1c**) or -withdrawing groups (**1d**) gave the corresponding product **6** as the predominant product in moderate yields (Table 1). 2-Naphthylboronic acid (**1e**) also reacted with **2a** and **3a** to furnish the corresponding diene **6eaa** in 45% yield. In this case, the emulsion of the substrates in water seemed not to be as stable as that obtained from **1a**. The reactions of **1a** and **3a** with various alkynes were also examined. Alkynes, such as 4-octyne, 6-dodecyne, and 7-tetradecyne, reacted to furnish the corresponding dienes **6**. The sparingly water-soluble tolane (**2e**) sluggishly reacted to give **6bea** in 31% yield. The miscibility of substrates seems to be critical for the successful reaction.[10] The configuration of diene **6bea** was unambiguously confirmed by an X-ray crystal structure analysis (see Supporting Information). Consequently, the arylation of alkynes in this reaction proceeds in a *syn* fashion.

We propose the following mechanism for this domino reaction (Scheme 2). Both the alkyne and acrylate coordinate to the aryl–rhodium species **B**, which is generated through the

[*] Dr. T. Kurahashi, Prof. Dr. H. Shinokubo, Prof. Dr. A. Osuka
Department of Chemistry
Graduate School of Science
Kyoto University, Sakyo-ku, Kyoto 606-8502 (Japan)
and
PRESTO
Japan Science and Technology Agency (JST)
Fax: (+81) 75-753-3970
E-mail: hshino@kuchem.kyoto-u.ac.jp

[**] We thank Yasuhide Inokuma for X-ray analysis and Katsuhiro Shimono for the mass spectrometric measurements. H.S. acknowledges the Takeda Science Foundation for Science and Technology and the Kurata Memorial Hitachi Science and Technology Foundation for financial support.

Supporting information for this article is available on the WWW under http://www.angewandte.org or from the author.

InterScience
© 2006 Wiley-VCH Verlag GmbH & Co. KGaA, Weinheim

Table 1: Rhodium-catalyzed domino carbometalation/Heck-type reaction of aryl boronic acids to alkynes and methyl acrylate in water.[a]

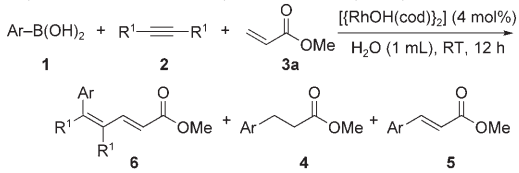

Ar	R^1	Yield [%]		
		6[b]	**4**[c]	**5**[c]
Ph (**1a**)	Bu (**2a**)	81 (**6aaa**)	3 (**4aa**)	11 (**5aa**)
4-Me-C_6H_4 (**1b**)	Bu (**2a**)	66 (**6baa**)	5 (**4ba**)	5 (**5ba**)
4-MeO-C_6H_4 (**1c**)	Bu (**2a**)	50 (**6caa**)	10 (**4ca**)	14 (**5ca**)
4-CF_3-C_6H_4 (**1d**)	Bu (**2a**)	72 (**6daa**)	12 (**4da**)	11 (**5da**)
2-Naphthyl (**1e**)	Bu (**2a**)	45 (**6eaa**)	3 (**4ea**)	44 (**5ea**)
Ph (**1a**)	Pr (**2b**)	61 (**6aba**)	3 (**4aa**)	7 (**5aa**)
Ph (**1a**)	C_5H_{11} (**2c**)	53 (**6aca**)	11 (**4aa**)	8 (**5aa**)
Ph (**1a**)	C_6H_{13} (**2d**)	57 (**6ada**)	6 (**4aa**)	5 (**5aa**)
4-Me-C_6H_4 (**1b**)	Ph (**2e**)	31 (**6bea**)	3 (**4ba**)	59 (**5ba**)

[a] The reaction was carried out with **1** (0.2 mmol), **2** (0.1 mmol), and **3** (0.2 mmol) in water (1 mL) in the presence of [{RhOH(cod)}$_2$] (0.004 mmol) at ambient temperature for 12 h. [b] Yield of the isolated products. [c] Yields were determined by the ^{1}H NMR signals of the crude products with dibromomethane as an internal standard.

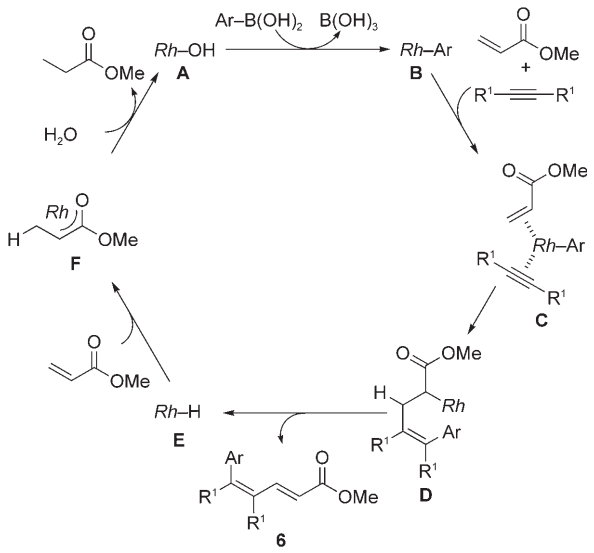

Scheme 2. A plausible mechanism for the rhodium-catalyzed domino reaction.

transmetalation of hydroxo–rhodium species **A** with aryl boronic acid **1**. The resulting complex **C** then undergoes an addition to the carbon–carbon triple bond of alkyne **2** and the double bond of acrylate **3** in either a concerted or stepwise manner to yield alkyl–rhodium species **D**.[11] We suppose that acrylate **3** acts not only as the third coupling component but also as a good π-acid ligand to promote the addition of aryl boronic acids to alkynes, as the reaction of **1a** and **2a** without **3** under the same conditions provided a trace of the phenylation product of **2a**. Compound **D** affords product **6** and hydrido–rhodium species **E** through β-hydride elimination. The hydrido–rhodium **E** reacts with **3** to form oxa-π-allyl–rhodium species **F**, which is hydrolyzed to complete the catalytic cycle. This mechanism is consistent with fact that quantitative formation of the 1,4-reduction product, methyl propanoate, was observed by ^{1}H NMR spectroscopic analysis in the reaction mixture.[12]

Although conclusive discussion of the role of water in this reaction is difficult at present, we performed several experiments to obtain some information. Whereas the reaction under solvent-free conditions provided the three-component coupling product **6aaa** in only 15% yield and Heck product **5aa** as the major product (31%), application of high pressure (140 atm) doubled the yield of **6aaa** under the same conditions but produced **5aa** (33%) in an unchanged yield (Scheme 3). The domino reaction is more pressure-dependent

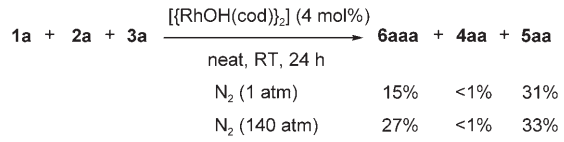

Scheme 3. Pressure dependence under neat conditions.

than the Heck-type reaction. This fact indicates that the rate-determining step of the domino reaction, which would be the C–C bond-forming step of the reaction of aryl rhodium with alkyne and acrylate species (**C**→**D**), has a negative activation volume ($\Delta V^{\neq}$). Importantly, water often enhances reaction rates for reactions, such as the Diels–Alder reaction and Claisen rearrangement, for which the activation volumes are negative.[13] This behavior implies that high internal pressure of water may be one of reasons for this phenomenon. However, the heterogeneous nature of the present reaction may call for other explanations, such as specific interactions between hydrophobic molecules at the microscopic water–oil phase boundary.

In summary, we have demonstrated that the reaction of aryl boronic acids with internal alkynes and acrylate units can be performed by rhodium catalysis in water to give the domino coupling products. Although the role of water is unclear at this stage, the present reaction demonstrates that water offers us not only the possibility to optimize known reactions but also to discover novel transformations. Investigations to expand the scope and limitations of this procedure along with the mechanistic elucidation are currently in progress.

Received: June 29, 2006
Published online: August 28, 2006

Keywords: alkynes · aqueous media · boron · domino reactions · rhodium

[1] a) R. Breslow, *Acc. Chem. Res.* **2004**, *37*, 471–478; b) U. M. Lindström, F. Andersson, *Angew. Chem.* **2006**, *118*, 562–565; *Angew. Chem. Int. Ed.* **2006**, *45*, 548–551.

[2] For transition-metal catalysis in an aqueous media, see: a) C.-J. Li, T. H. Chan, *Organic Reactions in Organic Media*, Wiley, New York, **1997**; b) B. Cornils, W. A. Herrmann, *Aqueous-Phase*

 © 2006 Wiley-VCH Verlag GmbH & Co. KGaA, Weinheim

Organometallic Chemistry: Concepts and Applications, Wiley-VCH, Weinheim, **1998**; c) *Organic Synthesis in Water* (Ed.: P. A. Grieco), Blacky Academic and Professional, London, **1998**; d) D. Sinou in *Modern Solvents in Organic Synthesis* (Ed.: P. Knochel), Springer, Berlin, **1999**, p. 41; e) C.-J. Li, *Chem. Rev.* **2005**, *105*, 3095 – 3165.

[3] S. Narayan, J. Muldoon, M. G. Finn, V. V. Fokin, H. C. Kolb, K. B. Sharpless, *Angew. Chem.* **2005**, *117*, 3339 – 3343; *Angew. Chem. Int. Ed.* **2005**, *44*, 3275 – 3279.

[4] For reviews on multicomponent reactions, see: a) P. A. Wender, *Chem. Rev.* **1996**, *96*, 1 – 2; b) M. Lautens, W. Klute, W. Tam, *Chem. Rev.* **1996**, *96*, 49 – 92; c) L. F. Tietze, *Chem. Rev.* **1996**, *96*, 115 – 136; d) A. Padwa, M. D. Weingarten, *Chem. Rev.* **1996**, *96*, 223 – 270; e) D. F. Harvey, D. M. Sigano, *Chem. Rev.* **1996**, *96*, 271 – 288; f) M. Malacria, *Chem. Rev.* **1996**, *96*, 289 – 306; g) E.-I. Negishi, C. Copéret, S. Ma, S.-Y. Liou, F. Liu, *Chem. Rev.* **1996**, *96*, 365 – 394; h) *Multicomponent Reactions* (Eds.: J. Zhu, H. Bienaymé), Wiley-VCH, Weinheim, **2005**.

[5] For reviews on Rh-catalyzed C–C bond formations, see: a) K. Fagnou, M. Lautens, *Chem. Rev.* **2003**, *103*, 169 – 196; b) T. Hayashi, K. Yamasaki, *Chem. Rev.* **2003**, *103*, 2829 – 2844; c) *Modern Rhodium-Catalyzed Organic Reactions* (Ed.: P. A. Evans), Wiley-VCH, Weinheim, **2005**.

[6] a) M. Lautens, J. Mancuso, *Org. Lett.* **2002**, *4*, 2105 – 2108; b) D. F. Cauble, J. D. Gipson, M. Kirsche, *J. Am. Chem. Soc.* **2003**, *125*, 1110 – 1111; c) M. Lautens, J. Mancuso, *J. Org. Chem.* **2004**, *69*, 3478 – 3487; d) M. Lautens, T. Marquardt, *J. Org. Chem.* **2004**, *69*, 4607 – 4614; e) R. Shintani, K. Okamoto, Y. Otamura, K. Ueyama, T. Hayashi, *J. Am. Chem. Soc.* **2005**, *127*, 54 – 55; f) T. Miura, M. Shimada, M. Murakami, *J. Am. Chem. Soc.* **2005**, *127*, 1094 – 1095; g) T. Miura, T. Sasaki, H. Nakazawa, M. Murakami, *J. Am. Chem. Soc.* **2005**, *127*, 1390 – 1391; h) T. Miura, H. Nakazawa, M. Murakami, *Chem. Commun.* **2005**, 2855 – 2856; i) T. Miura, M. Murakami, *Org. Lett.* **2005**, *7*, 3339 – 3341; j) T. Matsuda, M. Makino, M. Murakami, *Angew. Chem.* **2005**, *117*, 4684 – 4687; *Angew. Chem. Int. Ed.* **2005**, *44*, 4608 – 4611; k) T. Miura, M. Shimada, M. Murakami, *Angew. Chem.* **2005**, *117*, 7770 – 7772; *Angew. Chem. Int. Ed.* **2005**, *44*, 7598 – 7600; l) T. Matsuda, M. Makino, M. Murakami, *Chem. Lett.* **2005**, *34*, 1416 – 1417; m) T. Miura, T. Sasaki, T. Harumashi, M. Murakami, *J. Am. Chem. Soc.* **2006**, *128*, 2516 – 2517.

[7] For the Rh-catalyzed hydroarylation of alkynes, see: a) T. Hayashi, K. Inouen, N. Taniguchi, M. Ogasawara, *J. Am. Chem. Soc.* **2001**, *123*, 9918 – 9919; b) M. Lautens, M. Yoshida, *Org. Lett.* **2002**, *4*, 123 – 125; c) E. Genin, V. Michelet, J.-P. Genêt, *J. Organomet. Chem.* **2004**, *689*, 3820 – 3830; d) E. Genin, V. Michelet, J.-P. Genêt, *Tetrahedron Lett.* **2004**, *45*, 4157 – 4161.

[8] Initially, a mixture of **1a**, **2a**, **3a**, and the catalyst in water was sonicated for 1–2 minutes to form an emulsion; furthermore, vigorously stirring the emulsion resulted in decreased yield of **6**.

[9] a) M. Lautens, A. Roy, K. Fukuoka, K. Fagnou, B. Martín-Matute, *J. Am. Chem. Soc.* **2001**, *123*, 5358 – 5359; b) M. Lautens, J. Mancuso, H. Grover, *Synthesis* **2004**, 2006 – 2014; c) G. Zou, Z. Wang, J. Zhu, J. Tang, *Chem. Commun.* **2003**, 2438 – 2439; d) G. de la Herrán, C. Murcia, A. G. Csáky, *Org. Lett.* **2005**, *7*, 5629 – 5632.

[10] Triphenylboroxine and phenylboronate pinacol ester were inferior to phenylboronic acid and afforded **6aaa** in only moderate yields; in these cases, formation of a stable emulsion was not observed.

[11] Involvement of a rhodacyclopentene intermediate before the formation of **D** is also conceivable; however, the formation of such rhodacycles usually occurs in an intramolecular fashion.

[12] A. Mori, Y. Danda, T. Fujii, K. Hirabayashi, K. Osakada, *J. Am. Chem. Soc.* **2001**, *123*, 10774 – 10775.

[13] M. C. Pirrung, *Chem. Eur. J.* **2006**, *12*, 1312 – 1317.

 © 2006 Wiley-VCH Verlag GmbH & Co. KGaA, Weinheim

Silica Nanostructures

DOI: 10.1002/anie.200602274

Nanoscale Silica Capsules Ordered on a Substrate: Oxidation of Nanocellular Thin Films of Poly(styrene-*b*-dimethylsiloxane)**

*Lei Li and Hideaki Yokoyama**

The fabrication of nanoscale hollow particles has been receiving increasing attention in both academic and industrial fields. Various materials have been adopted to satisfy the growing needs for encapsulation,[1,2] and a variety of chemical and physicochemical methods have been developed in order to prepare hollow spheres with controlled size and shape, including colloid particle templating,[3] sol–gel synthesis,[4] layer-by-layer self-assembly,[5] and surface living polymerization.[6] Block copolymers are considered to be ideal candidates for the fabrication of nanoscale structures, owing to their predictable self-assembly in the size range 5–50 nm.[7,8] Our group recently reported a nondestructive CO_2 foaming method that introduces 15–30-nm voids into CO_2-philic fluorinated block copolymers.[9–12] Herein, we extend the same methodology to poly(styrene-*b*-dimethylsiloxane) (PS-PDMS), the PDMS domain of which is a CO_2-philic polymer,[13] to fabricate nanocells in thin films and to convert them into silica hollow particles (nanocapsules) ordered on substrates by oxidation.[14] Silica nanocapsules with a number density of $7.0 \times 10^{10}\,cm^{-2}$, a diameter of less than 40 nm, and a wall thickness of 2 nm were successfully synthesized.

We first made a PS-PDMS thin film with a thickness of 43 nm and a single layer of PDMS spherical domains on a silicon wafer. It is well known that PDMS can be easily converted into silica by exposure to UV light/ozone[15] and that PS is totally decomposed under these conditions. The PDMS nanodomains are therefore converted into silica particles, as shown schematically in Figure 1a,b. These particles were found to be spherical with a number density of $8.9 \times 10^{10}\,cm^{-2}$, as observed by atomic force microscopy (AFM; Figure 1c).

The oxidation process was monitored by X-ray photoelectron spectroscopy (XPS). The atomic fractions of C, Si, and O were determined from the intensities of the C1s, Si2p and O1s peaks, respectively, as a function of oxidation time. The Si2p peaks are shown in Figure 2a as an example. A single Si2p peak due to untreated PS-PDMS is found initially

[*] Dr. L. Li, Dr. H. Yokoyama
Nanotechnology Research Institute
National Institute of Advanced Industrial Science and Technology
1-1-1, Higashi, Tsukuba, Ibaraki 305-8565 (Japan)
Fax: (+81) 29-861-4432
E-mail: yokoyama@ni.aist.go.jp

[**] This research was partially funded by the Project on Nanostructured Polymeric Materials of New Energy and Industrial Technology Development Organization. L.L. thanks the Japan Society for the Promotion of Science for a fellowship.

WILEY InterScience DISCOVER SOMETHING GREAT
© 2006 Wiley-VCH Verlag GmbH & Co. KGaA, Weinheim

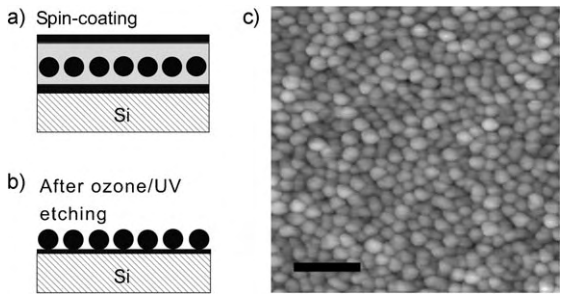

Figure 1. Formation of silica nanodots from a PS-PDMS thin film using UV light/ozone oxidation. a) Morphology of the as-cast PS-PDMS copolymer thin film. Spherical PDMS nanodomains are dispersed in a continuous PS matrix by micro-phase separation. The black and gray domains represent the PDMS and PS domains, respectively. b) The PS domains are decomposed, and the PDMS domains are converted into silica by UV light/ozone oxidation. c) Topographic AFM image of the silica nanodots after oxidation with UV light/ozone for 1 h (scale bar 200 nm).

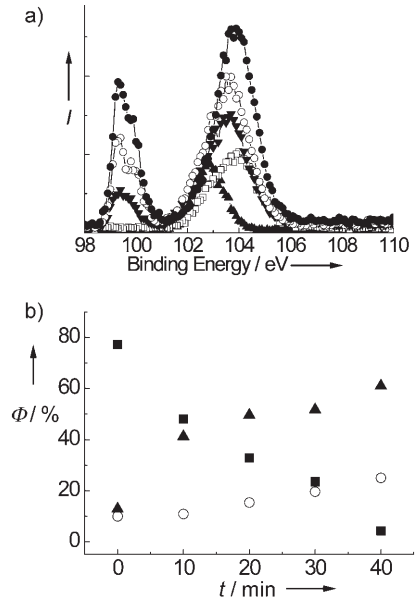

Figure 2. a) Photoelectron intensities, *I*, of the Si2p peaks from the PS-PDMS thin film, after oxidation with UV light/ozone for 0 (▲), 10 (□), 20 (▼), 30 (○), and 40 min (●). b) Atomic fractions, Φ, in the PS-PDMS thin film versus oxidation time, *t*, determined from the C1s (■), Si2p (○), and O1s (▲) XPS peaks. The atomic fraction of oxidized Si can be obtained from the Si2p binding-energy region 101–106 eV.

at 102.6 eV. This peak shifts to 104 eV after oxidation for 10 min with UV light/ozone, thereby indicating formation of silicon oxide.[16] After etching for 30 min, a peak at 99 eV due to elemental silicon from the silicon substrate appears; this is an indication of reduced film thickness.[16] The signal below 101 eV due to elemental silicon was therefore excluded from the analysis. The atomic fractions of Si, C, and O are plotted in Figure 2b. The atomic fraction of C decreases linearly with oxidation time and reaches 4.2% at 40 min, which indicates nearly perfect conversion. The O/Si ratio is 2.4:1, which approximates to that of silicon dioxide and indicates that the PDMS nanodomains have been successfully converted into silica particles that are ordered on the substrate.

We have previously reported a successful fabrication of nanocells in block-copolymer thin films by a process involving supercritical CO_2 ($scCO_2$).[9–12] A thin film of block copolymer with a CO_2-philic block was pressurized with CO_2 to localize it in the CO_2-philic nanodomains. Upon reducing the CO_2 pressure at reduced temperature, the volume of CO_2 in the CO_2-philic domains is converted into voids. In this study, we employ the same methodology with a PS-PDMS block copolymer instead of a fluorinated copolymer to fabricate nanocells in the CO_2-philic PDMS domains.[13]

A PS-PDMS thin film was placed in a high-pressure vessel at 20 MPa and 60 °C for 2 h; the temperature was then reduced isobarically to 0 °C. Subsequently, the pressure was released at a rate of 0.5 MPa min^{-1}. The whole process is the same as that used for the fluorinated block copolymers in our previous study.[9–12] Reducing the temperature to 0 °C freezes the surrounding PS matrix (T_g of PS in 20 MPa of CO_2 is approximately 30 °C)[17] and fixes the morphologies while a significant amount of CO_2 still remains in the PDMS domains. Analytical ellipsometry can be used to measure the thicknesses and refractive indices of the films before and after the CO_2 process, provided that the size of the nanocells is much smaller than the wavelength of light and the effective medium approximation is valid. The increment of thickness, Δd, after the $scCO_2$ process is 4.2 nm from the initial thickness of 43 nm. The porosity is 8.7%, assuming that the film size is fixed in the plane by the substrate and the mass is conserved. The refractive index decreases from 1.56 to 1.50, which corresponds to 9% porosity, according to the Lorentz–Lorenz equation [Eq. (1)].[18] Herein, n_f and n_s are the refractive

$$\frac{n_f^2-1}{n_f^2+2} = (1-V_c)\frac{n_s^2-1}{n_s^2+2} \quad (1)$$

indices of a nanocellular film and a solid skeleton, respectively, and V_c is the porosity. The good agreement between the porosities determined from the thickness and the refractive index indicates the successful introduction of nanocellular structures into the copolymer thin film using this CO_2 process.

This process forms a flat surface with no indication of cellular structures, as confirmed by both scanning electron microscopy (SEM) and AFM. To investigate the structures embedded in the film, reactive ion etching (RIE) with tetrafluoromethane (CF_4) gas was employed to etch the film at a controlled rate.[19,20] An AFM image of the nanocellular structure after 24-nm etching is shown in Figure 3a. The hole pattern in this figure is an evidence of nanocellular structures embedded in the film, as illustrated schematically in Figure 3b. The resulting nanocells have a number density of 7.0×10^{10} cm^{-2} and a spacing of 41.3 nm.

In the last step, nanocellular thin films were fully oxidized by exposure to UV light/ozone for 1 h. Spherical silica dots with an equivalent number density (7.2×10^{10} cm^{-2}) and spacing (40.0 nm) to those of the nanocells in Figure 3a were obtained. An AFM image of these dots, which have an average outer diameter of (29 ± 3) nm, is shown in Figure 3c. If the nanocells in the PDMS domains were still preserved after oxidation, the nanodots should have empty voids (capsules), as illustrated in Figure 3d. To probe the capsule

 © 2006 Wiley-VCH Verlag GmbH & Co. KGaA, Weinheim

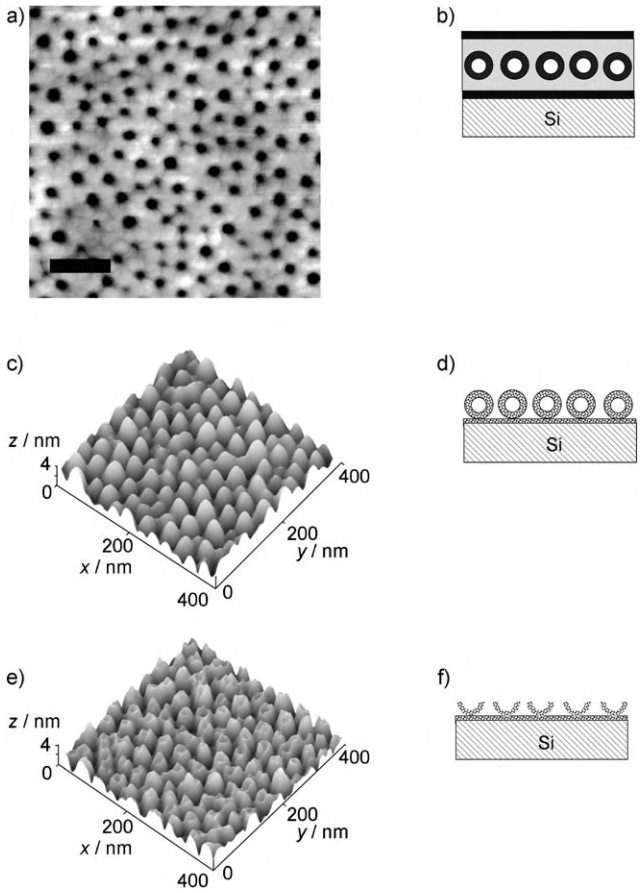

Figure 3. Topographic AFM images and schematic pictures of silica capsules on the substrate. a) Topographic image after RIE for 60 s (scale bar 100 nm), and b) schematic picture of the nanocellular structures on the block-copolymer film. The black and gray domains represent the PDMS and PS domains, respectively; the white part is air. c) Three-dimensional topographic image after oxidation by UV light/ozone, and d) schematic picture of the silica nanocapsules obtained. e) Three-dimensional topographic image after further RIE of 2-nm, and f) schematic picture showing the resulting caldera topography.

structure, the nanodots were etched for 2 min by RIE with a CF_4 rate of 1.5 mL min^{-1} and a powder density of 2 W cm^{-2}. Under these conditions, the etching rate for silica is 1 nm min^{-1}, which means that 2 nm of the silica layer was etched away from the surface. This etching removes the top skin of the capsules and converts them into calderas on the substrate, as shown in Figure 3e and illustrated in Figure 3f. This caldera morphology is clear evidence of a capsule structure before CF_4 etching. The top wall thickness of the silica nanocapsules is approximately 2 nm. The silica capsules were found to be tightly bound to the silicon substrate, even after a long ultrasonic rinse with organic solvents. This successful fabrication of silica nanocapsules provides strong evidence for the presence of CO_2-philic domains surrounding the voids.

In conclusion, we have synthesized silica nanocapsules that are ordered on a substrate by a nondestructive CO_2-foaming method that produces nanocells with the help of a block-copolymer template containing CO_2-philic PDMS domains. The nanocells are formed in the PDMS domains. The PDMS domains surrounding the empty cells are converted into hollow silica particles (nanocapsules) that are ordered on the substrate by oxidation with UV light/ozone. These nanocapsules with a number density of 7.0×10^{10} cm^{-2} have a diameter less than 40 nm and a wall thickness of 2 nm. An advantage of this method over others for the synthesis of nanocapsules is that the nanocapsules are two-dimensionally ordered and controlled using the domain structure of the block-copolymer template. The capsules are easily embedded by deposition after this process. The fabrication of more complex structures using the same method but with different block fractions is currently under investigation.

Experimental Section

A poly(styrene-*b*-dimethylsiloxane) block copolymer was purchased from Polymer Source Inc. The molecular weights of the PS and PDMS blocks are 57600 and 6500 g mol^{-1}, respectively. The silicon wafers were used as received. The PS-PDMS copolymer films were prepared by spin-casting a toluene solution onto silicon substrates. The film thickness was controlled by varying the concentration of the solutions and the rotation speed.

A high-pressure vessel for CO_2 processes was connected to a liquid chromatography pump (JASCO PU-2086 plus) fitted with a cooling head and to a back-pressure regulator (JASCO SCF-Bpg). The PS-PDMS films were placed in the high-pressure vessel at 60 °C for 2 h at a CO_2 pressure of 20 MPa. The vessel was then cooled to 0 °C in an ice bath whilst maintaining the pressure by means of the pump and regulator. The depressurization rate was controlled at 0.5 MPa min^{-1}.

Oxidation of the copolymer thin films by exposure to UV light/ozone was performed in a UVO cleaner 342-101 (Jelight, Inc.). The cleaner generates UV emissions at a wavelength of 254 nm (28 mW cm^{-2}). The distance between the UV source and the silicon wafers was 50 mm.

The film thickness and refractive index were measured with a JASCO M-220 ellipsometer with incident light in a wavelength range of 400–800 nm at an incident angle of 60° with respect to the surface normal. The etching process to expose the embedded cellular structures to the surface and open the hollow spherical structures was performed with a reactive ion etcher (FA-1, SAMCO) and tetrafluoromethane (CF_4) gas. Etching was performed with a CF_4 flow rate of 2 mL min^{-1}, a pressure of 10 Pa, and a power density of 10 W cm^{-2}. The etching rate for PS-PDMS copolymer thin films is approximately 0.4 nm s^{-1} under these conditions.

The surface topography due to the embedded cell structures revealed by RIE was characterized by AFM. AFM measurements were carried out in the tapping mode with an SII SPA300HV. We used a cantilever with a carbon nanotube tip (SII Co.) for the nanocellular PS-PDMS films. Silicon cantilevers (DF-20, SII Co.) were used for the observation of silica nanodots and nanocapsules.

XPS spectra were acquired with a PHI Quantum 2000 spectrometer using monochromated X-rays from an $Al_{K\alpha}$ source with a take-off angle of 45° from the surface plane. The X-ray beam was operating at 20 W and was focused to a diameter of about 100 μm rastered over a 500 μm × 500 μm area. The atomic fractions of carbon, oxygen, and silicon were computed using the attenuation factors provided by the supplier and the sum of these atomic fractions was normalized to unity.

Received: June 7, 2006
Published online: August 25, 2006

 © 2006 Wiley-VCH Verlag GmbH & Co. KGaA, Weinheim

Keywords: block copolymers · nanostructures · self-assembly · silica · template synthesis

[1] W. Schartl, *Adv. Mater.* **2000**, *12*, 1899 – 1908.
[2] F. Caruso, *Adv. Mater.* **2001**, *13*, 11 – 22.
[3] a) Z. Z. Yang, Z. W. Niu, Y. F. Lu, Z. B. Hu, C. C. Han, *Angew. Chem.* **2003**, *115*, 1987 – 1989; *Angew. Chem. Int. Ed.* **2003**, *42*, 1943 – 1945; b) E. Bourgeat-Lami, I. Tissot, F. Lefebvre, *Macromolecules* **2002**, *35*, 6185 – 6191; c) F. Caruso, R. A. Caruso, H. Möhwald, *Science* **1998**, *282*, 1111 – 1114.
[4] a) D. Y. Zhao, J. L. Feng, Q. S. Huo, N. Melosh, G. H. Fredrickson, B. F. Chmelka, G. D. Stucky, *Science* **1998**, *279*, 548 – 552; b) N. E. Botterhuis, Q. Y. Sun, P. C. M. M. Magusin, R. A. van Santen, N. A. J. M. Sommerdijk, *Chem. Eur. J.* **2006**, *12*, 1448 – 1456.
[5] M. Yang, J. Ma, C. L. Zhang, Z. Z. Yang, Y. F. Lu, *Angew. Chem.* **2005**, *117*, 6885 – 6888; *Angew. Chem. Int. Ed.* **2005**, *44*, 6727 – 6730.
[6] Y. W. Chen, E. T. Kang, K. G. Neoh, A. Greiner, *Adv. Funct. Mater.* **2005**, *15*, 113 – 117.
[7] M. Lazzari, M. A. Lopez-Quintela, *Adv. Mater.* **2003**, *15*, 1583 – 1594.
[8] C. Park, J. S. Yoon, E. L. Thomas, *Polymer* **2003**, *44*, 6725 – 6760.
[9] H. Yokoyama, L. Li, T. Nemoto, K. Sugiyama, *Adv. Mater.* **2004**, *16*, 1542 – 1546.
[10] L. Li, H. Yokoyama, T. Nemoto, K. Sugiyama, *Adv. Mater.* **2004**, *16*, 1226 – 1229.
[11] H. Yokoyama, K. Sugiyama, *Macromolecules* **2005**, *38*, 10516 – 10522.
[12] L. Li, H. Yokoyama, T. Nemoto, K. Sugiyama, *Macromolecules* **2006**, *39*, 4746 – 4755.
[13] Z. Bayraktar, E. Kiran, *J. Appl. Polym. Sci.* **2000**, *75*, 1397 – 1403.
[14] J. J. Robin, *Adv. Polym. Sci.* **2004**, *167*, 35 – 79.
[15] J. Morvan, M. Camelot, P. Zecchini, C. Roquescarmes, *J. Colloid Interface Sci.* **1984**, *97*, 149 – 156.
[16] J. F. Moulder, W. F. Stickle, P. E. Sobol, K. D. Bomben in *Handbook of X-ray Photoelectron Spectroscopy*, Physical Electronics Inc., Eden Prairie, MN, USA, **1995**, pp. 56 – 57.
[17] W. C. V. Wang, E. J. Kramer, W. H. Sachse, *J. Polym. Sci. Polym. Phys. Ed.* **1982**, *20*, 1371 – 1384.
[18] M. Born, E. Wolf in *Principles of Optics*, Cambridge University Press, Cambridge, UK, **1999**.
[19] H. Yokoyama, T. E. Mates, E. J. Kramer, *Macromolecules* **2000**, *33*, 1888 – 1898.
[20] R. Magerle, *Phys. Rev. Lett.* **2000**, *85*, 2749 – 2752.

 © 2006 Wiley-VCH Verlag GmbH & Co. KGaA, Weinheim

DOI: 10.1002/anie.200601988

N_2–Cu–F: A Complex of Dinitrogen and Cuprous Fluoride Characterized by Rotational Spectroscopy**

*Simon G. Francis, Steven L. Matthews, Oleg Kh. Poleshchuk, Nicholas R. Walker, and Anthony C. Legon**

From the viewpoint of the fixation of atmospheric nitrogen, there is a long-term general interest in the identification and characterization of compounds that result from the reaction of transition metals with dinitrogen. In addition, the investigation of the interaction of N_2 with transition-metal compounds has intrinsic significance because of the isoelectronic, isolobal nature of dinitrogen and carbon monoxide. There is a voluminous amount of literature[1] on transition-metal carbonyl compounds, from which it is concluded that the nature of the generally strong bonding interaction of CO with the transition-metal center in such compounds is well-understood.

Recently, a series of simple linear transition-metal carbonyl complexes of the type OC–M–X (M = Cu,[2] Ag,[3] or Au[4]; X = F, Cl, or Br) were thoroughly investigated in the gas phase by means of their rotational spectra to give details of their geometry and electronic structure. Information about the electric-charge redistribution at the metal center is contained in the nuclear quadrupole coupling constants for M = Cu or Au. The interaction between CO and M was also found to be strong in these transient species. On the other hand, the hydrogen-bonded species OC···H–X, which may be envisaged, formally at least, as generated from OC–M–X by replacement of M by H, have been investigated extensively by rotational spectroscopy.[5–7] Such complexes are weakly bound (here depicted with ···) with intermolecular binding energies of only a few kJ mol^{-1}. The dinitrogen complexes N_2···H–X have linear geometries similar to those of OC···H–X, but with slightly weaker hydrogen bonds.[8–10] The isostructural nature of OC···H–X and N_2···H–X can be understood by assuming that the electrophilic region of HX seeks the most nucleophilic region of CO or N_2 (namely, the axis of a nonbonding

[*] S. G. Francis, Dr. S. L. Matthews, Dr. N. R. Walker, Prof. A. C. Legon
School of Chemistry
University of Bristol
Bristol BS8 1TS (UK)
Fax: (+44) 117-925-0612
E-mail: a.c.legon@bristol.ac.uk
Prof. O. K. Poleshchuk
Tomsk State Pedagogical University
Komsomolskii 75, 634041 Tomsk (Russia)

[**] The authors thank the Engineering and Physical Sciences Research Council for supporting this work. N.R.W. thanks the Royal Society for the award of a Royal Society University Research Fellowship.

Supporting information for this article is available on the WWW under http://www.angewandte.org or from the author.

 © 2006 Wiley-VCH Verlag GmbH & Co. KGaA, Weinheim InterScience

electron pair).[11] A quantitative scale of nucleophilicities N(B) of Lewis bases B, developed from intermolecular stretching force constants, confirms the order $N(CO) > N(N_2)$.[12] The formal relationship between OC···H–X and OC–M–X and the similarity in the properties of OC···H–X and N_2···H–X raise interesting questions about N_2–M–X. Can these species be detected and identified? Are they isostructural with the corresponding carbonyl complexes? Are they less strongly bound than the carbonyl analogues? How does the electric-charge redistribution at the metal center upon formation of N_2–M–X compare with that when OC–M–X is formed? We report herein the experimental detection and characterization of an N_2–M–X analogue of OC–M–X, namely N_2–Cu–F, which has been observed in the gas phase through its rotational spectrum. The first report of an N_2–M–X species refers to N_2–Cu–Cl when isolated in a cryogenic matrix.[13]

The observed transitions of $^{15}N_2$–^{63}Cu–F and $^{15}N_2$–^{65}Cu–F exhibited a hyperfine structure that was attributed to coupling of the Cu nuclear spins (both the ^{63}Cu and ^{65}Cu nuclides have $I=\frac{3}{2}$) to the molecular rotation through the electric quadrupole and magnetic dipole (spin rotation) coupling mechanisms. A small additional splitting arising from the F ($I=\frac{1}{2}$) nuclear spin–rotation coupling and ^{n}Cu,^{19}F spin–spin coupling was also partially resolved. The magnetic moment of the ^{15}N nucleus ($I=\frac{3}{2}$) is too small to lead to additional hyperfine structure (see Figure 1). This fact was the reason for using $^{15}N_2$ in the initial search for the spectrum, for $^{14}N_2$ introduces two further quadrupole splittings from the ^{14}N nuclei ($I=1$) and consequently a spread of intensity over more hyperfine components.

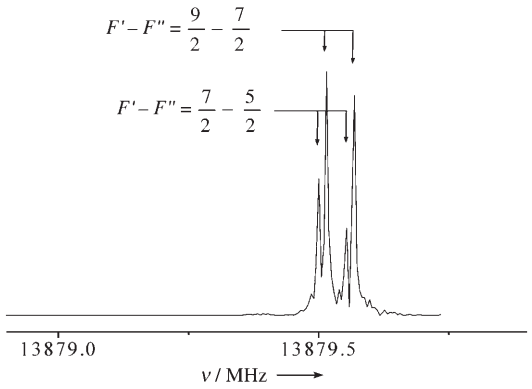

Figure 1. Two hyperfine components in the $J=3\leftarrow2$ transition of the isotopomer $^{15}N_2$–^{63}Cu–^{19}F (Note: Each component is a doublet as a result of a Doppler doubling effect. This is the larger of the two splittings shown.) The labels F' and F'' are those appropriate to the coupling of the ^{63}Cu nucleus only because the transitions shown are not split by the fluorine spin.

Observed frequencies of individual components (estimated accuracy 1 kHz) in the $J=2\leftarrow1$ and $J=3\leftarrow2$ transitions were fitted by using the program SPFIT[14] to give the rotational constant B_0, the centrifugal distortion constant D_J, the ^{n}Cu nuclear quadrupole $\chi_{aa}(^{n}Cu)$ and spin–rotation $M_{bb}(^{n}Cu)$ coupling constants, and the ^{19}F spin–rotation coupling constant $M_{bb}(^{19}F)$ for each of the isotopomers $^{15}N_2$–^{63}Cu–F and $^{15}N_2$–^{65}Cu–F. The ^{n}Cu,^{19}F spin–spin coupling constant $D_{aa}(^{n}Cu,^{19}F)$ was held fixed at its value for ^{n}Cu^{19}F[15] because this quantity depends only on the distance r(Cu–F), and we show below that this distance differs little from that in free CuF. The results are recorded in Table 1, which also

Table 1: Spectroscopic constants of three isotopomers of N_2–Cu–F.

Spectroscopic constant	$^{15}N_2$–^{63}Cu–^{19}F	$^{15}N_2$–^{65}Cu–^{19}F	$^{14}N_2$–^{63}Cu–^{19}F
B_0 [MHz]	2313.3839(2)	2311.0884(2)	2410.35(10)[a]
D_J [kHz]	0.351(8)	0.349(7)	–
χ_{aa}(Cu) [MHz]	61.8838(70)	57.2686(76)	–
M_{bb}(Cu) [kHz]	9.85(10)	10.51(10)	–
M_{bb}(F) [kHz]	−2.3(5)	−2.1(5)	–
D_{aa}(Cu,F) [kHz]	−10.3[b]	−10.3[b]	–
σ [kHz]	0.9	1.0	–
N	13	13	–

[a] Estimated by finding the center of the ^{14}N substructure in some of the ^{63}Cu hyperfine components of the $J=2\leftarrow1$ and $3\leftarrow2$ transitions and assuming χ_{aa}(Cu) and D_J to be unchanged from $^{15}N_2$–^{63}Cu–^{19}F. [b] This quantity was fixed at the value for free CuF from reference [15] (see text).

includes the standard deviation σ and the number of hyperfine components N included in each fit. We note that the ratios $\{\chi_{aa}(^{63}Cu)/\chi_{aa}(^{65}Cu)\} = 1.0806(3)$ and $\{M_{bb}(^{63}Cu)/M_{bb}(^{65}Cu)\} = 0.94(2)$ agree within experimental error with the ratios 1.08(2)and 0.935 of the electric quadrupole and magnetic dipole moments of the two Cu nuclides.[16] Moreover, the value of $M_{bb}(^{19}F)$ is identical within experimental error for the two isotopomers.

Rotational transitions of $^{14}N_2$–^{63}Cu–F were also observed but were weak. They carry a complex hyperfine structure arising from the presence of three quadrupolar nuclei (^{14}N, ^{14}N, and ^{63}Cu) and one $I=\frac{1}{2}$ nucleus, which is yet to be fully resolved and assigned. It is possible to estimate the unperturbed frequency of transitions with reasonable accuracy (as described in footnote [a] of Table 1), and this estimation leads to the approximate rotational constant for this species given in Table 1.

The observed spectra of N_2–Cu–F are consistent with a linear geometry (although a slightly bent arrangement with a low energy barrier to the linear conformation cannot be ruled out on the basis of ground-state spectroscopic constants alone). On the assumption of a linear geometry and an r_0(N–N) value (1.1000 Å) that is unchanged from free N_2,[17] the two bond lengths r(N–Cu) = 1.790(2) Å and r(Cu–F) = 1.739(3) Å were obtained by a least-squares fit to the rotational constants of the three isotopomers given in Table 1. We note that r(Cu–F) is close to the value r_0(Cu–F) = 1.74865 Å of free CuF. This agreement provides an a posteriori justification of the assumption that the r_0 bond length of N_2 is unchanged from the free N_2 molecule because the strong N–N triple bond is less likely to change than the CuF single bond when N_2–Cu–F is formed. We performed electronic-structure calculations at the QCISD/6-311G* level of theory with Gaussian 98,[18] with the results r_e(N–N) = 1.113 Å, r_e(N–Cu) = 1.761 Å, and r_e(Cu–F) = 1.743 Å, while

 © 2006 Wiley-VCH Verlag GmbH & Co. KGaA, Weinheim

for free N_2 and CuF calculations at the same level of theory gave 1.104 Å and 1.767 Å, respectively. This geometry leads to $B_e = 2434$ MHz, which is in good agreement with the observed quantity B_0 (Table 1).

The Cu nuclear quadrupole coupling constant $\chi_{aa}(^{63}Cu)$ carries information about the change in the electric-charge distribution near the Cu nucleus when N_2–Cu–F is formed from CuF. This quantity is proportional to the electric field gradient at the Cu nucleus along the internuclear axis *a*. The series Cu–F, Ar–Cu–F, N_2–Cu–F, and OC–Cu–F is of interest in this context. The values of $\chi_{aa}(^{63}Cu)$ are 21.9562(24),[15] 38.0556(15),[15] 61.8825(8), and 75.406(19) MHz,[2] respectively. These values show that the electric field gradient along the internuclear axis at the Cu nucleus increases smoothly along the series. The QCISD/6-311G* calculation predicts $\chi_{aa}(^{63}Cu) = 49.5$ and 21.3 MHz for N_2–Cu–F and Cu–F, respectively, thus indicating that this quantity is quite well accounted for at this level of theory. The calculation also indicates that the electric-charge redistribution on formation of N_2–Cu–F from the component molecules is small. Relative to the free molecules N_2 and Cu–F, the changes in the natural atomic charges on the atoms[19] N_{inner}, N_{outer}, Cu, and F are $\Delta q(N_i) = 0.142\,e$, $\Delta q(N_o) = -0.147\,e$, $\Delta q(Cu) = +0.014\,e$, and $\Delta q(F) = -0.009\,e$, respectively, which correspond to an intermolecular charge transfer $\Delta q(int)$ of only 0.005 e from N_2 to Cu–F. The binding energy relative to N_2 and Cu–F is 139 kJ mol^{-1} from these calculations. At the same level of theory, the corresponding results for OC–Cu–F are $\Delta q(Cu) = +0.023\,e$, $\Delta q(F) = -0.014\,e$, $\Delta q(int) = 0.009\,e$, and 203 kJ mol^{-1} for the binding energy. Evidently, there is a weaker interaction between N_2 and Cu–F than between CO and Cu–F. It is interesting to note that the ratio of the binding energies of N_2–Cu–F and OC–Cu–F is 0.68 while the ratio of the intermolecular stretching force constants for the corresponding hydrogen-bonded complexes N_2···HF and OC···HF is 0.65.[12] Given that the hydrogen-bonding interactions have a substantial electrostatic component and given the relatively small electric-charge redistribution that accompanies formation of the compounds of CO and N_2 with Cu–F, it is apparent that electrostatic interactions may also be significant in these metal complexes.

Experimental Section

$^{15}N_2$–Cu–F was synthesized by laser ablation of a copper rod over which a pulse of a gas mixture Ar/SF_6/$^{15}N_2$ (partial pressure ratio ≈ 100:0.5:2) was expanded into a vacuum. The pulse was formed with a solenoid valve from a stagnation pressure of 7 bar. A pulse of light (ca. 25 mJ) from a Nd–YAG laser operating at 532 nm was focused onto the rod to yield Cu vapor. The plume of ablated metal was immediately entrained by the supersonically expanded gas pulse, thereby producing CuF, which then combined with $^{15}N_2$ to form the desired product. The laser-ablation assembly has been described in detail elsewhere.[20] Its output feeds into a hole at the center of one of two mirrors that constitute the evacuated Fabry–Perot cavity of a Fourier-transform microwave spectrometer. Molecules of $^{15}N_2$–^{63}Cu–F and $^{15}N_2$–^{65}Cu–F were delivered thereby into the cavity, where they were polarized by pulses of microwave radiation and their $J = 2 \leftarrow 1$ and $J = 3 \leftarrow 2$ ground-state rotational transitions recorded in the usual way.[21]

Received: May 18, 2006
Published online: August 28, 2006

Keywords: copper · dinitrogen · electronic structure · fluorine · rotational spectroscopy

[1] F. A. Cotton, G. W. Wilkinson, *Advanced Inorganic Chemistry*, Wiley, London, **1988**.
[2] N. R. Walker, M. C. L. Gerry, *Inorg. Chem.* **2001**, *40*, 6158.
[3] N. R. Walker, M. C. L. Gerry, *Inorg. Chem.* **2002**, *41*, 1236.
[4] C. J. Evans, L. M. Reynard, M. C. L. Gerry, *Inorg. Chem.* **2001**, *40*, 6123.
[5] A. C. Legon, P. D. Soper, W. H. Flygare, *J. Chem. Phys.* **1981**, *74*, 4944.
[6] P. D. Soper, A. C. Legon, W. H. Flygare, *J. Chem. Phys.* **1981**, *74*, 2138.
[7] M. R. Keenan, T. K. Minton, A. C. Legon, T. J. Balle, W. H. Flygare, *Proc. Natl. Acad. Sci. USA* **1980**, *77*, 5583.
[8] P. D. Soper, A. C. Legon, W. G. Read, W. H. Flygare, *J. Chem. Phys.* **1982**, *76*, 292.
[9] R. S. Altmann, M. D. Marshall, W. Klemperer, *J. Chem. Phys.* **1983**, *79*, 57.
[10] N. W. Howard, A. C. Legon, *J. Chem. Phys.* **1989**, *90*, 672.
[11] A. C. Legon, D. J. Millen, *Faraday Discuss. Chem. Soc.* **1982**, *73*, 71.
[12] A. C. Legon, D. J. Millen, *J. Am. Chem. Soc.* **1987**, *109*, 356.
[13] H. S. Plitt, H. Schnöckel, M. Bärr, R. Ahlrichs, *Z. Anorg. Allg. Chem.* **1992**, *607*, 45.
[14] H. M. Pickett, *J. Mol. Spectrosc.* **1991**, *148*, 371.
[15] C. J. Evans, M. C. L. Gerry, *J. Chem. Phys.* **2000**, *112*, 9363.
[16] I. Mills, T. Civitas, K. Homann, N. Kallay, K. Kuchitsu, *IUPAC, Quantities, Units and Symbols in Physical Chemistry*, Blackwell Science, Oxford, **1993**.
[17] J. Bendtsen, *J. Raman Spectrosc.* **1974**, *2*, 133.
[18] Gaussian 98 (Revision A.6 and A.7), M. Frisch et al., Gaussian Inc., Pittsburgh PA, **1998**.
[19] E. D. Glendening, A. E. Reed, J. E. Carpenter, F. Weinhold, NBO Version 3.1.
[20] S. G. Batten, A. C. Legon, *Chem. Phys. Lett.* **2006**, *422*, 192.
[21] A. C. Legon in *Atomic and Molecular Beam Methods*, (Ed.: G. Scoles), Oxford University Press, New York, **1992**, chap. 9, p. 289.

 © 2006 Wiley-VCH Verlag GmbH & Co. KGaA, Weinheim

Template Synthesis

DOI: 10.1002/anie.200601845

Design and Implementation of a Highly Selective Minimal Self-Replicating System**

*Eleftherios Kassianidis and Douglas Philp**

The development and deployment of self-replicating[1] molecular architectures[2] can potentially revolutionize the fabrication of materials on the nanometer scale. The emergence of protocols based on molecular replication will deliver synthetic machinery[3] that is capable of directing its own synthesis and cooperating with other similar systems to create an organized hierarchy. Within this broad objective, the development of efficient protocols that allow self-replication, self-organization, and evolution[4] within synthetic supramolecular assemblies is essential. This approach to predetermined dynamic behavior has been termed "systems chemistry" by von Kiedrowski and co-workers.[5] Ultimately, we wish to exploit replicating systems in the construction, selection,[6] and amplification[7] of large molecular and supramolecular assemblies.

The minimal self-replicator model[8] (Figure 1) provides the framework for our studies. Paul and Joyce highlighted[9] three parameters within this model that must be optimized to ensure an efficient system: minimization of product inhibition arising from a stable **T**·**T** complex; the suppression of the reaction[10] through **A**·**B** to form $\mathbf{T}_{inactive}$, which is inert catalytically; and the catalytic efficiency within the key ternary complex **A**·**B**·**T**. Under ideal conditions, template **T** presents its recognition sites in the correct orientation, assembles **A** and **B**, and then connects these two molecules to form an exact copy of itself by transmitting structural information to the forming template. This process completes an autocatalytic cycle. It is useful to recognize that, unlike traditional catalysts, there is no requirement for **T** to achieve particularly high turnover numbers as the inherently nonlinear kinetics should achieve amplification of the template once autocatalysis has become established. Additionally, as long as the duplex **T**·**T** is not excessively stable, propagation of the template **T** is exponential. Despite concerted efforts, there are relatively few reports of synthetic self-replicating systems.[5,11]

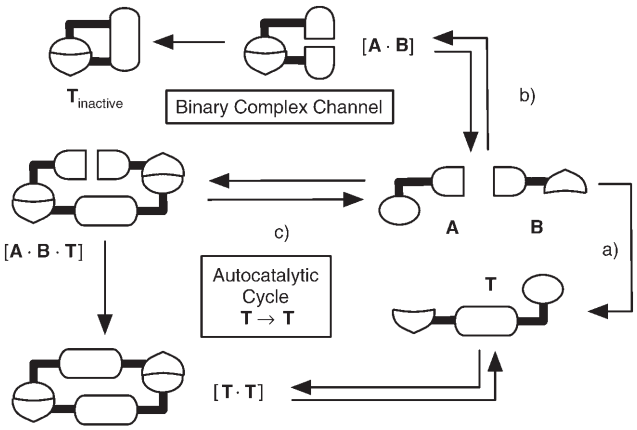

Figure 1. The minimal model of self-replication: Reagents **A** and **B** can react through three pathways: a) An uncatalyzed bimolecular reaction between **A** and **B** to give template **T**; b) a recognition-mediated reaction through the binary complex **A**·**B**; c) a recognition-mediated autocatalytic cycle through the ternary complex **A**·**B**·**T**.

In the context of our long-term goals, we must demonstrate that it is possible to exploit replication to amplify a single structure from a mixture based on its ability to guide its own formation through recognition processes, even when inherently unselective chemical reactions are used to covalently link the building blocks together. The reaction between an *N*-aryl nitrone and a maleimide is suitable for incorporation in a modular self-replicating system. The reaction proceeds readily at room temperature, and the rate and diastereoselectivity are almost immune to electronic substituent effects and adventitious catalysis by Brønsted acids. The two products (*endo* and *exo*) provide the means of exposing the efficiency of information transfer in any replicating system as the reaction is metronomic: the *endo*/*exo* ratio is always close to 3:1 in the absence of effects that arise from molecular recognition. Previous studies by us[12] demonstrated that this reaction can be incorporated into a replicating system, but that the levels of amplification achieved are poor.

We wished to develop a general protocol for optimizing the performance of replicating systems based on computational methods. Therefore, we identified **1** and **2** (Scheme 1) as suitable precursors for a successful replicating template by screening[13] a series of compounds computationally. We performed electronic structure calculations (see the Supporting Information for details) at the B3LYP/6-31G(d) level of theory on the two diastereoisomers *endo*-**3** and *exo*-**3** and the duplex *endo*-**3**·*endo*-**3**. These calculated structures reveal that *endo*-**3** has an open structure in which the two recognition sites are freely available to interact with other complementary species in solution (**T** in Figure 1). By contrast, the structure of *exo*-**3** is folded such that the recognition sites are placed in proximity to each other, thus rendering this product inert in a catalytic sense ($\mathbf{T}_{inactive}$ in Figure 1). Additionally, the calculated structure of the *endo*-**3**·*endo*-**3** duplex reveals a head-to-tail dimer whose assembly is driven by the self-complementarity of the template. We therefore expected that the *endo*-**3** template should accommodate the transition state that leads

[*] Dr. E. Kassianidis, Dr. D. Philp
EaStCHEM and Centre for Biomolecular Sciences
University of St Andrews
North Haugh, St Andrews, Fife KY16 9ST (UK)
Fax: (+44) 1334-463-808
E-mail: d.philp@st-andrews.ac.uk

[**] We thank the University of St Andrews and the EPSRC for financial support. We are grateful to Caroline Horsburgh (mass spectrometry) and Melanja Smith (NMR spectroscopy) for technical assistance. We thank Prof G. von Kiedrowski for providing us with a copy of his SimFit program.

Supporting information for this article is available on the WWW under http://www.angewandte.org or from the author.

InterScience
© 2006 Wiley-VCH Verlag GmbH & Co. KGaA, Weinheim

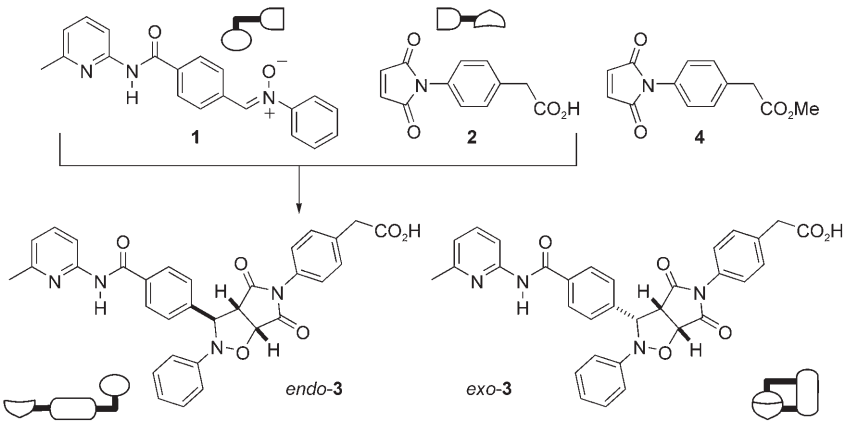

Scheme 1. Nitrone **1** and maleimide **2** can react to form two diastereoisomeric cycloadducts *exo*-**3** (an open template) and *endo*-**3** (a closed template). Schematic representations from Figure 1 are included to highlight the role of these components in the design of the replicating system.

to *endo*-**3** readily. This expectation proved correct: Calculations revealed the transition state **1**·**2**·*endo*-**3**‡ was readily accessible and similar in geometry to that calculated for the bimolecular reaction. In summary, our computational studies indicate that the formation of *endo*-**3** by reaction through a binary complex is impossible; however, *endo*-**3** should be capable of templating its own formation from nitrone **1** and maleimide **2** through the transition state **1**·**2**·*endo*-**3**‡. Our expectation was therefore that we had designed a synthetic system that should be capable of amplifying *endo*-**3** over *exo*-**3** through autocatalysis.

Template precursors **1** and **2**, together with the control compound **4**, in which the carboxylic acid recognition site is blocked, were synthesized by using standard methods. The kinetic behavior of the system was studied by measuring the kinetics of the reaction between **1** and **2** (or **4**) in a solution of $CDCl_3$ at various temperatures between −10 and 35 °C. The time course of the reactions was evaluated by ^{1}H NMR spectroscopic analysis (500 MHz), which monitored the disappearance of the resonance that arises from the maleimide protons present in **2** (or **4**) in the region $\delta = 6.70$–7.00 ppm and the simultaneous appearance of resonances that arise from the *endo* and *exo* cycloadducts in the region $\delta =$ 3.60–5.80 ppm. Profiles of concentration versus time for the formation of the two cycloadducts were constructed by deconvolution of these resonances. No decomposition or additional reaction products were detected in any of the experiments and the reaction was shown to be under kinetic control.[14] Experiments conducted at starting concentrations of **1** and **2** of 25 mM in $CDCl_3$ revealed that the recognition-mediated reactions were uniformly fast, reaching more than 85 % overall conversion ([*endo*] + [*exo*]) at all temperatures after 16 h, and, in all cases, the diastereoselectivity was greater than 33:1 in favor of *endo*-**3**. By contrast, in the control reaction between **1** and **4**, in which recognition cannot play a role, overall conversion after 16 h was around 30 % at 35 °C and only 9 % at −10 °C and, in all cases, the diastereoselectivity was only 3:1 in favor of *endo*-**3**. Clearly, the presence of recognition has a dramatic effect in this system.

Accordingly, we undertook a detailed kinetic analysis to demonstrate that the effects mediated by molecular recognition were indeed a result of the designed replication of *endo*-**3**. In the following discussion, we focus on the results obtained at −10 °C, as this temperature was the most convenient for measuring the reaction kinetics. The measured maximum rates[15] of reaction are summarized in Table 1. It is clear from these data that the bimolecular reaction between **1** and **4** (Table 1, entry 1) is slow and unselective. By contrast, the measured rates change significantly (Table 1, entry 2) when recognition is allowed to play a role in the reaction: the formation of *endo*-**3** is accelerated 13-fold. The small rate enhancement in the formation of *exo*-**3** is consistent with the computational results that indicate that reaction through a very weak binary complex may be possible. The rate enhancement in the formation of *endo*-**3** coupled with the observation of a sigmoidal rate profile (Figure 2), characteristic of autocatalysis, warranted further investigation. The role of hydrogen bonding in the formation of *endo*-**3** and *exo*-**3** could be demonstrated readily by the introduction of a competitive inhibitor. The association between **2** and any amidopyridine-bearing species present in the reaction mixture, including the template *endo*-**3**, can be disrupted through the addition of two equivalents of benzoic acid. Reaction between **1** and **2** in the presence of benzoic acid ([benzoic acid] = 50 mM) results in a significant decrease both in the rate of reaction and the diastereoselectivity (Table 1, entry 3). The final *endo*/*exo* ratio drops from 115:1 to only 17:1. These results demonstrate that the formation of *endo*-**3** is recognition-mediated.

Table 1: Maximum observed rates of reaction.[a]

Entry	Conditions	Maximum rate [nM s^{-1}]	
		endo-**3**	*exo*-**3**
1	[**1**] = [**4**] = 25 mM	39	13
2	[**1**] = [**2**] = 25 mM	528	21
3	[**1**] = [**2**] = 25 mM [benzoic acid] = 50 mM	105	17
4	[**1**] = [**2**] = 25 mM [*endo*-**3**] = 2.5 mM	561	< 1

[a] Maximum rates measured in $CDCl_3$ at −10 °C by ^{1}H NMR spectroscopic analysis.

A crucial experiment is the demonstration that *endo*-**3** is capable of accelerating its own formation. The injection of substoichiometric amounts of *endo*-**3** at the start of the reaction between **1** and **2** should result in an increase in the initial rate of formation of *endo*-**3**. Accordingly, we performed the reaction between **1** and **2** under identical conditions to those described previously, however, the reaction mixture

 © 2006 Wiley-VCH Verlag GmbH & Co. KGaA, Weinheim

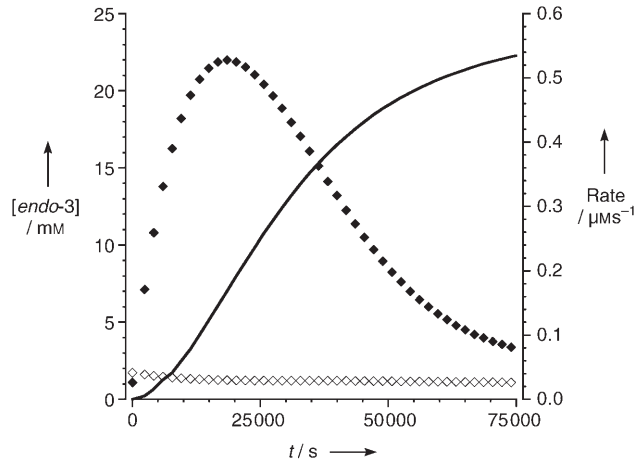

Figure 2. Variation of reaction rate for the formation of *endo*-**3** (◆, right axis) with time. The formation of the *endo* diastereoisomer in the control reaction between **1** and **4** is shown for comparison (◇, right axis). Experimental concentration–time data for *endo*-**3** (——, left axis) is also shown for comparison.

also contained 10 mol% of *endo*-**3**. The results of this experiment confirm the ability of *endo*-**3** to template its own formation (Table 1, entry 4). The maximum rate of formation of *endo*-**3** is now 14 times faster than the control and, pleasingly, almost exactly that observed for the reaction in the absence of the preformed template. This observation suggests that the maximum autocatalytic rate is reached immediately ($t=0$) on addition of this small amount of template. The *endo*/*exo* ratio is now at least 250:1,[16] compared with 115:1 in the absence of added *endo*-**3**. By contrast, the addition of 10 mol% of *exo*-**3** to the reaction mixture has no effect on the rate profile. From these observations, we conclude that the *exo*-**3** cycloadduct is completely incapable of competing with the efficient replication profile of *endo*-**3**. Therefore, it is this template that is amplified selectively through its monopolization of the precursors **1** and **2**.

The curve for the reaction rate versus time (Figure 2) confirms the autocatalytic behavior of *endo*-**3**, thus revealing that the reaction rate steadily increases, reaches a maximum, and then falls away. It is evident from Figure 2 that the maximal autocatalytic velocity is achieved at around five hours after the start of the reaction at a template concentration of around 7 mM. In fact, the maximum autocatalytic velocity is achieved in the time region in which $0.1<\rho<1.0$, where $\rho=$[template]/[precursors]. For our system, this region lies between 150 and 500 minutes, which corresponds to a concentration of *endo*-**3** between 2.5 and 12.5 mM. It is clear from this analysis of the kinetic data that autocatalyst saturation occurs at $t\approx10000$ s. The continuous increase of [*endo*-**3**] (and in turn the ρ value) during the course of the reaction does not increase reaction velocity further: within the concentration range 2.5–12.5 mM for *endo*-**3**, only a further 6% increase in reaction velocity is observed, whereas reaction velocity is considerably diminished at $\rho=1.0$ and beyond. These considerations explain the result of the template-injection experiment described above: employing an initial condition at which $\rho=0.1$ results in the system operating at the limit of its autocatalytic capacity from the start of the reaction. Indeed, exposure of reaction mixtures consisting of **1** and **2** to increasing initial concentrations of preformed *endo*-**3** (up to 7.5 mM or 30 mol%) results in rate profiles identical to those obtained when only 10 mol% of preformed *endo*-**3** is added, thus adding more template has no effect because the system is already operating at the limit of its autocatalytic capacity.

Ideally, to completely eradicate the formation of *exo*-**3** within this system, we must ensure that the contributions from the background bimolecular and binary complex modes of reactivity are removed. This objective cannot be achieved in this system by template injection. However, this goal can be accomplished by reducing the concentration of the reagents at the start of the reaction. Thus, employing initial concentrations of **1** and **2** of 15 mM results in an *endo*-**3**/*exo*-**3** ratio of 135:1, and employing initial concentrations of **1** and **2** of 5 mM results in an *endo*-**3**/*exo*-**3** ratio of more than 250:1; the concentration of *exo*-**3** is now below our limit of detection. On the basis of all of these observations, we believe that the formation of *endo*-**3** occurs principally through the iterative operation of an autocatalytic, self-replication cycle, which revolves around the assembly of the hydrogen-bonded ternary complex **1**·**2**·*endo*-**3**. In accordance with our electronic structure calculations, this assembly is capable of guiding the reaction of the nitrone and maleimide solely through the *endo* transition state, thereby allowing *endo*-**3** to create a new copy of itself.

We probed the stability of the *endo*-**3**·*endo*-**3** duplex to understand the apparent efficiency of autocatalysis in this system fully. The association constant (K_a) for the formation of the complex **1**·phenylacetic acid, a model for the binary associations in the system, was determined to be $1150\,M^{-1}$ at $-10\,^{\circ}C$ in $CDCl_3$ by using ^1H NMR titration methodology. Assuming simple additivity of interactions, we might therefore expect the *endo*-**3**·*endo*-**3** duplex to have an association constant in the region of $1.3\times10^6\,M^{-1}$.[17] We were unable, however, to directly measure the stability of the *endo*-**3**·*endo*-**3** duplex by ^1H NMR (500 MHz) dilution experiments as the ^1H NMR spectrum of *endo*-**3** showed no apparent dependence on concentration (100 μM < [*endo*-**3**] < 25 mM) at $-10\,^{\circ}C$ in $CDCl_3$). However, given the kinetic data, we reasoned that it should be possible to verify the relative stability of the *endo*-**3**·*endo*-**3** duplex through the simulation and fitting of the experimental datasets to an appropriate kinetic model (full details of this procedure are given in the Supporting Information). Our kinetic model requires that *exo*-**3** is formed exclusively through the bimolecular reaction channel and that *endo*-**3** is formed through the confluence of the bimolecular pathway and the autocatalytic self-replicating pathway. Estimates of the rate constant for the bimolecular reaction between **1** and **2** to form *exo*-**3** and *endo*-**3** were derived from experimental data for the reaction between **1** and methyl ester **4** and were used to describe all bimolecular processes that lead to the *exo* and *endo* cycloadducts, respectively. The association constant ($K_a=1150\,M^{-1}$) for the complex **1**·phenylacetic acid was used as a model for all binary complexes and the product complexes *exo*-**3**·*exo*-**3** and *exo*-

 © 2006 Wiley-VCH Verlag GmbH & Co. KGaA, Weinheim

3·*endo*-**3**. By using these fixed parameters and simplex optimization of the association constant for *endo*-**3**·*endo*-**3** and the rate constant for the reaction in the ternary complex **1**·**2**·*endo*-**3** to form *endo*-**3**·*endo*-**3**, excellent fits of the experimental data to this model were obtained ($R = 0.74\,\%$; see the Supporting Information for details). The optimized value of the association constant for [*endo*-**3**·*endo*-**3**] is $4.7 \times 10^6\,\text{M}^{-1}$, close to our original estimate. The optimized rate constant for the formation of *endo*-**3** within ternary complex [**1**·**2**·*endo*-**3**] is $1.22 \times 10^{-3}\,\text{s}^{-1}$, which corresponds to an effective molarity of just over 20 M.

It is clear from the results of the kinetic simulation and fitting of the experimental data that the major pathway for the formation of *exo*-**3** is simply the bimolecular reaction between **1** and **2**. The dominant pathway for the formation of *endo*-**3** is clearly a reaction through the ternary complex **1**·**2**·*endo*-**3**, which has a rather high effective molarity ($\approx$23 M) for such a simple system.[18] The **1**·**2**·*endo*-**3** complex drives the formation of *endo*-**3** almost exclusively, and the observed maximum rate at around 20000 s (Figure 2) corresponds to the maximum concentration of **1**·**2**·*endo*-**3** (420 μM). The interplay between this catalytic prowess and the high stability of the *endo*-**3**·*endo*-**3** duplex is intriguing. Despite the fact that the concentration of free *endo*-**3** never rises above 5 μM during the reaction, this structure is still capable of amplifying itself effectively to the exclusion of *exo*-**3**. The simulation and fitting of the data allows us to explore the effect of the stability of the *endo*-**3**·*endo*-**3** duplex on the rate profile of the system. The calculated reaction profile is altered dramatically by a modest reduction in the association constant for *endo*-**3**·*endo*-**3** from 10^6 to $10^5\,\text{M}^{-1}$. This change results in the curve of rate versus time becoming sharper and the maximum rate of formation of *endo*-**3** increasing. Although we cannot test this hypothesis directly at −10 °C, increasing the temperature[19] will lower the K_a value for *endo*-**3**·*endo*-**3**, and the expected effect on the curve of rate versus time is evident as we increase the reaction temperature from −10 to 10 °C (Figure 3).

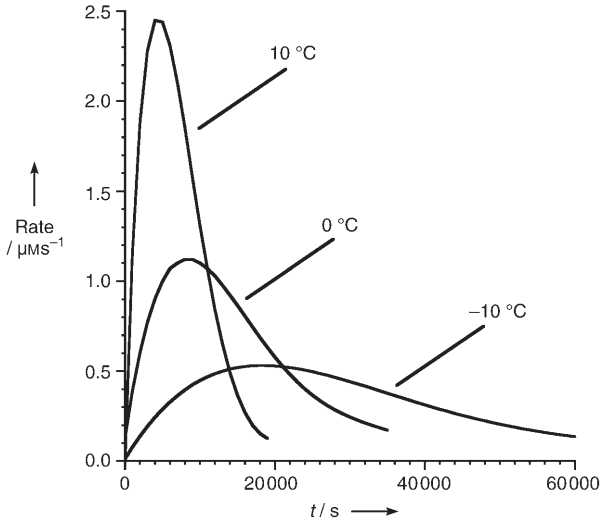

Figure 3. Observed rate versus time profiles for the reaction between **1** and **2** in $CDCl_3$ at −10, 0, and 10 °C.

Although conceptually simple, minimal self-replicating systems should require the optimization of the rate acceleration, or effective molarity, achieved by the ternary complex, the stability of the ternary complex, and the instability of the product duplex for efficient operation. We have demonstrated herein that it is possible to selectively amplify one of two possible products from a reaction mixture using a replication strategy in which only the first of these three parameters has been highly optimized through the logical application of computational methods. Therefore, although the stability of the catalytic ternary complex and product duplex are important, it is nevertheless possible to design and implement a synthetic system that is capable of highly selective amplification by focusing on templates that possess a high level of complementarity to transition states. We believe that the development of new replicating systems can be driven by aggressive optimization of the approach described herein.

Received: May 10, 2006
Revised: June 11, 2006
Published online: August 28, 2006

Keywords: kinetics · molecular modeling · self-replication · supramolecular chemistry · template synthesis

[1] For examples of complex replicable entities, see: a) L.-H. Eckardt, K. Naumann, W. M. Pankau, M. Rein, M. Schweitzer, N. Windhab, G. von Kiedrowski, *Nature* **2002**, *420*, 286; b) J. W. Szostak, D. P. Bartel, P. L. Luisi, *Nature* **2001**, *409*, 387–390; c) N. C. Seeman, P. S. Lukeman, *Rep. Prog. Phys.* **2005**, *68*, 237–270; d) R. Wick, P. Walde, P. L. Luisi, *J. Am. Chem. Soc.* **1995**, *117*, 1435–1436.

[2] a) A. Mulder, J. Huskens, D. N. Reinhoudt, *Org. Biomol. Chem.* **2004**, *2*, 3409–3424; b) G. M. Whitesides, M. Boncheva, *Proc. Natl. Acad. Sci. USA* **2002**, *99*, 4769–4774; c) G. M. Whitesides, B. Grzybowski, *Science* **2002**, *295*, 2418–2421; d) H. Cölfen, S. Mann, *Angew. Chem.* **2003**, *115*, 2452–2468; *Angew. Chem. Int. Ed.* **2003**, *42*, 2350–2365; e) I. W. Hamley, *Angew. Chem.* **2003**, *115*, 1730–1752; *Angew. Chem. Int. Ed.* **2003**, *42*, 1692–1712; f) G. W. Gokel, W. M. Leevy, M. E. Weber, *Chem. Rev.* **2004**, *104*, 2723–2750, and references therein; g) J. W. Lee, S. Samal, N. Selvapalam, H.-J. Kim, K. Kim, *Acc. Chem. Res.* **2003**, *36*, 621–630, and references therein; h) F. W. B. van Leeuwen, H. Beijleveld, H. Kooijman, A. L. Spek, W. Veboom, D. N. Reinhoudt, *J. Org. Chem.* **2004**, *69*, 3928–3936, and references therein; i) J. Rebek, Jr., *Angew. Chem.* **2005**, *117*, 2104–2115; *Angew. Chem. Int. Ed.* **2005**, *44*, 2068–2078; j) M. Ruben, J. Rojo, F. J. Romero-Salguero, L. H. Uppadine, J.-M. Lehn, *Angew. Chem.* **2004**, *116*, 3728–3747; *Angew. Chem. Int. Ed.* **2004**, *43*, 3644–3662; k) O. Lukin, F. Vögtle, *Angew. Chem.* **2005**, *117*, 1480–1501; *Angew. Chem. Int. Ed.* **2005**, *44*, 1456–1477; l) A. Carbone, N. C. Seeman, *Proc. Natl. Acad. Sci. USA* **2002**, *99*, 12577–12582; m) N. C. Seeman, A. M. Belcher, *Proc. Natl. Acad. Sci. USA* **2002**, *99*, 6451–6455; n) S. Liao, N. C. Seeman, *Science* **2004**, *306*, 2072–2074; o) H. Yan, *Science* **2004**, *306*, 2048–2049; p) B. Samori, G. Zuccheri, *Angew. Chem.* **2005**, *117*, 1190–1206; *Angew. Chem. Int. Ed.* **2005**, *44*, 1166–1181; q) K. V. Gothelf, R. S. Brown, *Chem. Eur. J.* **2005**, *11*, 1062–1069.

[3] a) G. Ashkenasy, R. Jegasia, M. Yadav, M. R. Ghadiri, *Proc. Natl. Acad. Sci. USA* **2004**, *101*, 10872–10877; b) G. Ashkenasy, M. R. Ghadiri, *J. Am. Chem. Soc.* **2004**, *126*, 11140–11141.

 © 2006 Wiley-VCH Verlag GmbH & Co. KGaA, Weinheim

[4] a) D. S. Watts, S. H. Strogatz, *Nature* **1998**, *393*, 440–442; b) S. H. Strogatz, *Nature* **2001**, *410*, 268–276; c) H. Jeong, B. Tombor, R. Albert, Z. N. Oltval, A. L. Barabasi, *Nature* **2000**, *407*, 651–654; d) E. Ravasz, A. L. Somera, D. A. Mongru, Z. N. Oltvai, A. L. Barabasi, *Science* **2002**, *297*, 1551–1555; e) M. Girvan, M. E. J. Newman, *Proc. Natl. Acad. Sci. USA* **2002**, *99*, 7821–7826; f) R. Guimerà, L. A. N. Amaral, *Nature* **2005**, *433*, 895–900; g) J. J. Perez, *Chem. Soc. Rev.* **2005**, *34*, 143–152; h) K. Ding, H. Du, Y. Yuan, J. Long, *Chem. Eur. J.* **2003**, *9*, 2872–2884; i) R. R. Breaker, *Nature* **2004**, *432*, 838–845; j) C. M. Dobson, *Nature* **2004**, *432*, 824–828; k) J. J. Lavigne, E. V. Anslyn, *Angew. Chem.* **2001**, *113*, 3212–3225; *Angew. Chem. Int. Ed.* **2001**, *40*, 3118–3130.

[5] M. Kindermann, I. Stahl, M. Reimold, W. M. Pankau, G. von Kiedrowski, *Angew. Chem.* **2005**, *117*, 6908–6913; *Angew. Chem. Int. Ed.* **2005**, *44*, 6750–6755.

[6] a) I. Saur, R. Scopelliti, K. Severin, *Chem. Eur. J.* **2006**, *12*, 1058–1066; b) A. Buryak, K. Severin, *Angew. Chem.* **2005**, *117*, 8149–8152; *Angew. Chem. Int. Ed.* **2005**, *44*, 7935–7938; c) L. Vial, J. K. M. Sanders, S. Otto, *New J. Chem.* **2005**, *29*, 1001–1003; d) P. T. Corbett, J. K. M. Sanders, S. Otto, *J. Am. Chem. Soc.* **2005**, *127*, 9390–9392; e) P. T. Corbett, L. H. Tong, J. K. M. Sanders, S. Otto, *J. Am. Chem. Soc.* **2005**, *127*, 8902–8903.

[7] a) J. D. Cheeseman, A. D. Corbett, J. L. Gleason, R. J. Kazlauskas, *Chem. Eur. J.* **2005**, *11*, 1708–1716; b) J. D. Cheeseman, A. D. Corbett, R. Shu, J. Croteau, J. L. Gleason, R. J. Kazlauskas, *J. Am. Chem. Soc.* **2002**, *124*, 5692–5701.

[8] a) G. von Kiedrowski, *Angew. Chem.* **1986**, *98*, 932–934; *Angew. Chem. Int. Ed. Engl.* **1986**, *25*, 932–935; b) G. von Kiedrowski, *Bioorg. Chem. Front.* **1993**, *3*, 113–146.

[9] N. Paul, G. F. Joyce, *Curr. Opin. Chem. Biol.* **2004**, *8*, 634–639.

[10] a) A. Robertson, D. Philp, N. Spencer, *Tetrahedron* **1999**, *55*, 11365–11384; b) R. M. Bennes, B. M. Kariuki, K. D. M. Harris, D. Philp, N. Spencer, *Org. Lett.* **1999**, *1*, 1087–1090; c) S. J. Howell, D. Philp, N. Spencer, *Tetrahedron* **2001**, *57*, 4945–4954; d) R. J. Pearson, E. Kassianidis, D. Philp, *Tetrahedron Lett.* **2004**, *45*, 4777–4780.

[11] Some recent examples include: a) E. Kassianidis; R. J. Pearson, D. Philp, *Chem. Eur. J.*, 10.1002/chem.200600460; b) R. J. Pearson, E. Kassianidis, A. M. Z. Slawin, D. Philp, *Chem. Eur. J.*, 10.1002/chem.200501189; c) E. Kassianidis, R. J. Pearson, D. Philp, *Org. Lett.* **2005**, *7*, 3833–3836; d) R. J. Pearson, E. Kassianidis, A. M. Z. Slawin, D. Philp, *Org. Biomol. Chem.* **2004**, *2*, 3434–3441; e) J. M. Quayle, A. M. Z. Slawin, D. Philp, *Tetrahedron Lett.* **2002**, *43*, 7229–7233; f) X. Li, J. Chmielewski, *J. Am. Chem. Soc.* **2003**, *125*, 11820–11821; g) S. Matsumura, T. Takahashi, A. Ueno, H. Mihara, *Chem. Eur. J.* **2003**, *9*, 4829–4837; h) R. Isaac, J. Chmielewski, *J. Am. Chem. Soc.* **2002**, *124*, 6808–6809; i) B. Wang, I. O. Sutherland, *Chem. Commun.* **1997**, 1495–1496.

[12] V. C. Allen, D. Philp, N. Spencer, *Org. Lett.* **2001**, *3*, 777–780.

[13] We screened a series of compounds in which *ortho*-, *meta*-, or *para*-disubstituted benzene rings connected the recognition sites to the reactive sites in both the nitrone and the maleimide building blocks of the prospective template. We calculated (AMBER* forcefield, GB/SA $CHCl_3$ solvation model, Macromodel, version 7.1, Schrodinger Inc., USA, 2000) the minimum energy conformations of the both the *endo* and *exo* cycloadducts from all of the possible combinations of these six building blocks. Of the possible cycloadducts, only one combination, *endo*-**3** from the reaction between **1** with **2**, had the desired open template structure required for replication and warranted further investigation.

[14] The ratio of *endo*-**3** and *exo*-**3** did not change upon heating the reaction mixtures to 60 °C; additionally, heating *endo*-**3** and *exo*-**3** with *N*-phenylmaleimide did not result in any crossover products being formed. These results suggest that no thermodynamic equilibration between *endo* and *exo* cycloadducts occurs within the temperature range and on the timescale of our investigations.

[15] Maximum rates (velocities) of reaction were calculated by determining the largest value of the first derivative of the function that describes the concentration–time profile for each reaction; for bimolecular reactions, this metric is equivalent to the initial rate; for autocatalytic reactions, this represents the point of inflection of the sigmoidal curve.

[16] On the basis of the observed signal-to-noise ratios in the ^{1}H NMR spectra (500 MHz) of the reaction mixtures, we estimate that our limit of detection for *exo*-**3** is 100 μM. This analysis places a lower limit of 250:1 on the *endo*/*exo* selectivity generated by the recognition-mediated reaction.

[17] The simple additivity calculation described herein will underestimate the stability of the duplex somewhat (C. A. Hunter, *Angew. Chem.* **2004**, *116*, 5424–5539; *Angew. Chem. Int. Ed.* **2004**, *43*, 5310–5324); however, it gives a reasonable first estimate for the K_a value of the duplex, which is then refined by iterative fitting.

[18] The value of 22.7 M is higher than many simple synthetic systems that exploit recognition processes to achieve rate accelerations in cycloaddition reactions; for some comparison data, see: R. Cacciapaglia, S. Di Stefano, L. Mandolini, *Acc. Chem. Res.* **2004**, *37*, 113–122. The effective molarity observed in the system reported herein is of the same order of magnitude as that observed (Ref. [5]) by von Kiedrowski and co-workers in an almost exponentially replicating system based on the Diels–Alder reaction.

[19] Raising the temperature will diminish the K_a value for the product duplex by increasing the magnitude of the $T\Delta S$ term in the free energy of binding. We recognize that the change in temperature will also affect the stability of other complexes in solution; however, as the behavior of the system is sensitive to the product duplex K_a value, we wished to use these means to explore this effect qualitatively. A detailed analysis of the effect of temperature on this system will be reported elsewhere. An alternative method of achieving the same effect is to change the solvent polarity; however, in practice, it is difficult to add a polar solvent without destroying recognition between the various components within the system completely.

 © 2006 Wiley-VCH Verlag GmbH & Co. KGaA, Weinheim

Supported Oligosaccharides

DOI: 10.1002/anie.200601128

Efficient Polymer-Assisted Strategy for the Deprotection of Protected Oligosaccharides**

*Hiroshi Tanaka, Tadasuke Ishida, Nobuatsu Matoba, Hirokazu Tsukamoto, Haruo Yamada, and Takashi Takahashi**

Oligosaccharides play important roles in cell-surface events through carbohydrate–protein and carbohydrate–carbohydrate interactions.[1] The chemical synthesis of structurally defined oligosaccharides would be highly desirable in structure–activity studies because oligosaccharides from natural sources can be produced in only limited qualities. Recent progress in oligosaccharide synthesis has resulted in a number of new and efficient glycosidation methodologies, which are amenable to the synthesis of protected oligosaccharides **1** by standardized and routine protocols.[2] However, deprotection of the protected oligosaccharides **1**→**2**, including the cleavage of various O-protecting groups and the replacement of N-protecting groups with *N*-acetyl groups is difficult to achieve by standardized protocols (Scheme 1). The complete deprotection of protected oligosaccharides frequently requires careful selection of the reaction solvents to prevent the partially deprotected intermediates from precipitating. Herein, we describe an efficient method for the deprotection of protected oligosaccharides based on a polymer-assisted strategy and its application to the synthesis of dimeric and trimeric Lewis X derivatives.

Our polymer-assisted strategy for the deprotection of protected oligosaccharides **1** is illustrated in Scheme 1. The solid-supported protected oligosaccharide **3** linked through a tetrahydropyranyl (THP) linker was designed as a key intermediate. The solid-supported complex oligosaccharides would smoothly undergo deprotection because they are aggregated to only a very limited extent. A Birch reduction was adapted for removing the solid-supported benzyl ethers and esters on **3**.[3] The THP linker would survive deprotection reactions and can be cleaved under mildly acidic conditions to release the fully deprotected oligosaccharide **2** without anomerization or cleavage of the glycosidic bonds.[4,5] The ease of handling of solid-supported compounds would be effective not only for the high-speed synthesis of a single target oligosaccharide but also for the deprotection of a protected oligosaccharide library.[6] The polymer-supported protected oligosaccharide **3** can be prepared using the following methodology: 1) acetal formation of the protected saccharides **1** with prelinker **4** containing a dihydropyranyl (DHP) moiety and an activated ester and 2) subsequent

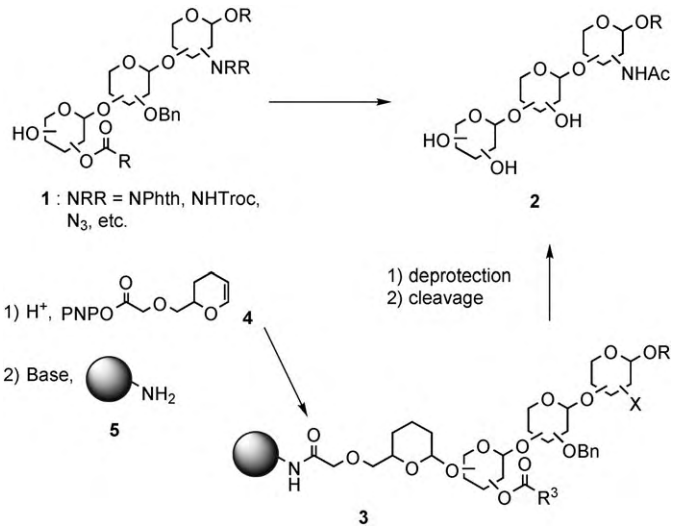

Scheme 1. Polymer-assisted strategy for deprotection of the protected oligosaccharides **1**. Bn = benzyl, PNP = *para*-nitrophenyl, Phth = phthalyl, Troc = 2,2,2-trichloroethoxycarbonyl.

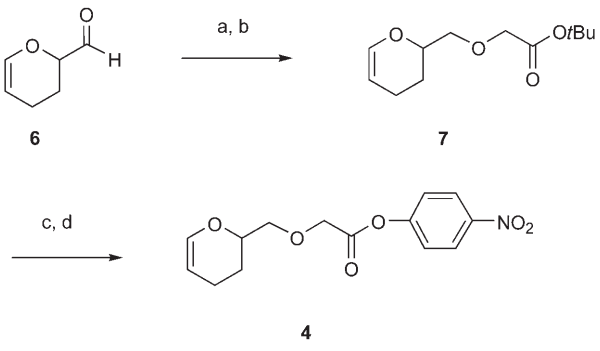

Scheme 2. Reagents and conditions: a) $LiAlH_4$, THF; b) *tert*-butyl bromoacetate, NaH, DMF; c) 1 N aq. NaOH, dioxane; d) 4-nitrophenol, EDCI, DIEA, CH_2Cl_2, 42% from **6**. DMF = *N*,*N*-dimethylformamide, EDCI = 1-ethyl-3-(3-dimethylaminopropyl)carbodiimide, DIEA = diisopropylethylamine.

[*] Dr. H. Tanaka, T. Ishida, Dr. N. Matoba, Dr. H. Tsukamoto,[+] Prof. Dr. H. Yamada,[#] Prof. Dr. T. Takahashi
Department of Applied Chemistry
Graduate School of Science and Engineering
Tokyo Institute of Technology
2-12-1 Ookayama, Meguro, Tokyo 152-8552 (Japan)
Fax: (+81) 3-5734-2884
E-mail: ttak@apc.titech.ac.jp
Homepage: www.apc.titech.ac.jp/≈ttakahas/index.html

[+] Current address:
Graduate School of Pharmaceutical Sciences, Tohoku University
Aobayama, Aoba-ku, Sendai 980-8578 (Japan)

[#] Current address:
Department of Chemistry, Faculty of Science
Okayama University of Science
Okayama, Ridai 1-1, Okayama 700-0005, Japan

[**] This work was supported by a Grant-in-Aid for Young Scientists (B) (grant-in-aid no. 16710155) from the Ministry of Education, Culture, Sports, Science, and Technology.

Supporting information for this article is available on the WWW under http://www.angewandte.org or from the author.

© 2006 Wiley-VCH Verlag GmbH & Co. KGaA, Weinheim

Table 1: Deprotection of the *O*-benzyl-protected glucose derivative **8** based on a polymer-assisted strategy.[a]

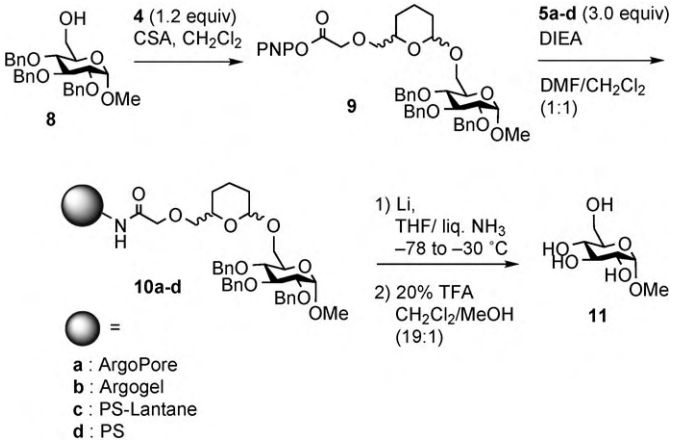

Entry	**10**	Loading yield (**8**→**10**) [%][b]	Conv. [%][c]	Purity of **11** [%][c]	Overall yield (**8**→**11**) [%]
1	**10a**	99	>99	>99	91
2	**10b**	97	59	58	–
3	**10c**	99	trace	trace	–
3	**10d**	93	3	3	–

[a] CSA = (+)-camphorsulfonic acid, PS = polystrene, TFA = trifluoroacetic acid. [b] The yield was estimated by the release of **8** from **10**. [c] The conversion and purity were estimated by HPLC analysis of the cleaved materials using ELSD.

amidation of the resulting activated ester with the solid-supported amines **5** to give **3**, irreversibly. The irreversible loading reaction would enable the complete immobilization of the protected oligosaccharides **1**.[7]

The preparation of prelinker **4** is outlined in Scheme 2. The reduction of aldehyde **6** followed by alkylation of the resulting alcohol with *tert*-butyl α-bromoacetate provided the *tert*-butyl ester **7**. Hydrolysis of the *tert*-butyl ester **7** under basic conditions followed by esterification with 4-nitrophenol afforded prelinker **4** in 42% overall yield from **6**.

We first examined the polymer-assisted deprotection of methyl 2,3,4-*O*-tribenzylglucoside (**8**) using the solid supports **5a–d** (Table 1). Treatment of **8** with 1.2 equiv of prelinker **4** under acidic conditions provided the protected glucoside **9**, which contains an activated ester, as a mixture of diastereomers. The subsequent amidation of **9** with 3.0 equiv of the solid-supported amines **5a–d** afforded the solid-supported protected glucoses **10a–d**. The yields of **10a–d** based on **8**, estimated by cleavage of **8** from **10**, were excellent. The removal of the benzyl ethers was achieved by treatment of the solid-supported protected glucose derivatives **10a–d** with lithium in liquid ammonia and tetrahydrofuran at −30 °C for 1 h.

Exposure of the solid-supported glucose derivatives to mildly acidic conditions permitted the products to be released. An HPLC analysis of the released products using an evaporative light-scattering detector (ELSD) revealed that only the benzyl ethers supported on the ArgoPore resin underwent complete reductive cleavage under the Birch reduction conditions (Table 1, entry 1). These results suggest that the substrates on the surface of the polymer might selectively undergo Birch reduction because the solution of liquid ammonia in THF did not cause the hydrophobic polymers to swell. Further purification of the product

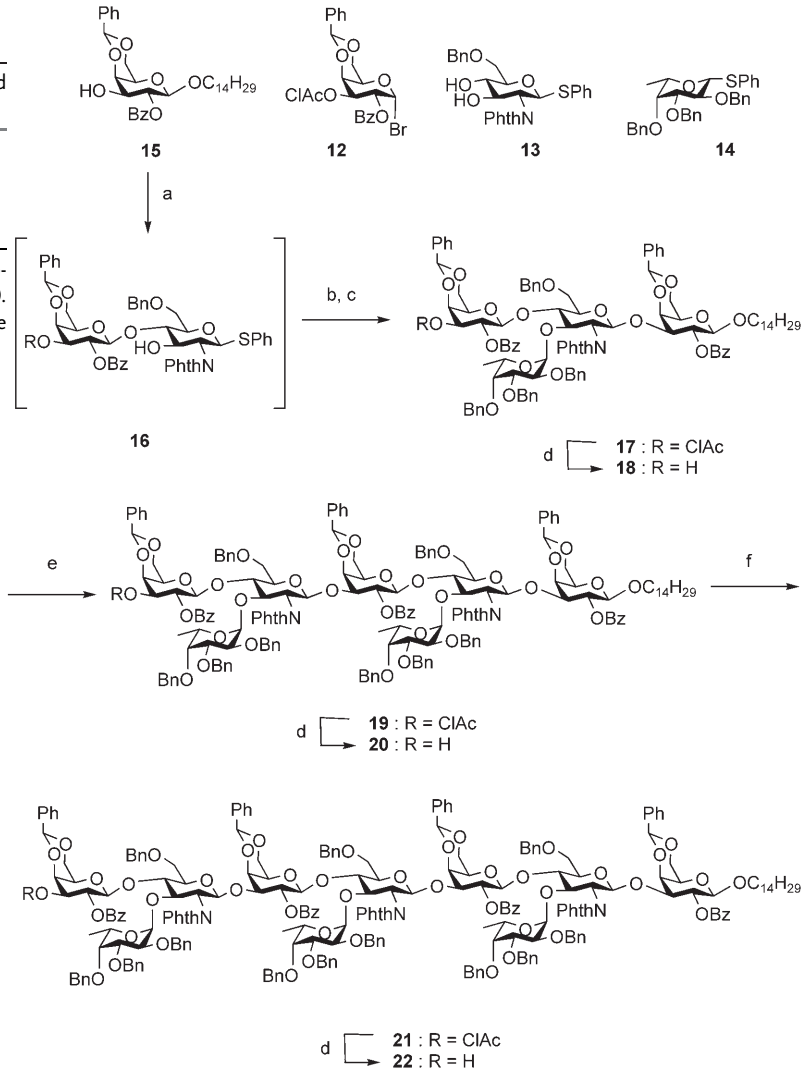

Scheme 3. Reagents and conditions: a) **12** (1.8 equiv), **13** (1.5 equiv), AgOTf (1.8 equiv), CH_2Cl_2, 4-Å M.S., −20 °C; b) **15** (1.0 equiv), NIS (1.5 equiv), −10 °C; c) **14** (5.0 equiv), NIS (5.5 equiv), 77% based on **15;** d) thiourea, 2,6-lutidine, DMF, 99% for **18**, 92% for **20**, 70% for **22**; e) **12** (1.8 equiv), **13** (1.5 equiv), AgOTf (1.5 equiv), CH_2Cl_2, 4-Å M.S., −20 °C, then **18** (1.0 equiv), NIS (1.5 equiv), −10 °C, then, **14** (5.0 equiv), NIS (5.5 equiv), 56% based on **18**; f) **12** (1.8 equiv), **13** (1.5 equiv), AgOTf (1.8 equiv), CH_2Cl_2, 4-Å M.S., −20 °C, then **20** (1.0 equiv), NIS (1.5 equiv), −10 °C, then, **14** (10 equiv), NIS (10.5 equiv), 44% based on **20**. Bz = benzoyl, M.S. = molecular sieves, NIS = *N*-iodosuccinimide, Tf = trifluoromethanesulfonyl.

 © 2006 Wiley-VCH Verlag GmbH & Co. KGaA, Weinheim

released from the ArgoPore resin provided α-methyl glucoside **11** in 91% yield based on **8** (Table 1, entry 1). These results indicate that the substrate on the ArgoPore resin was not released during the Birch reduction. To the best of our knowledge, this is the first report on an application of a Birch reduction to solid-phase synthesis.

We next synthesized the trimeric and dimeric Lewis X derivatives **29** and **30** by a one-pot glycosylation and the polymer-assisted deprotection procedure (Scheme 3). The hepta- and decasaccharides **29** and **30** are important tumor-associated antigens[8] and have served as effective synthetic targets for demonstrating the feasibility of new methodologies owing to the complexity of their branched structure, which contains both α- and β-glycosidic linkages.[9–11]

A one-pot glycosylation was used to prepare the protected hepta- and decasaccharides **20** and **22**, respectively (Scheme 3).[12] The chemo-, stereo-, and regioselective glycosylation of glucosamine **13** at the C4 hydroxy group with the galactosyl bromide **12** provided the glycosylated thioglycoside **16**. Subsequent activation of thioglycoside **16** to couple with alkyl galactoside **15** at the 3-position, followed by the α-selective glycosylation of the remaining hydroxy group at the C3 position with thiofucoside **14** provided tetrasaccharide **17** in 77% overall yield based on **15**. Removal of the chloroacetyl group at the C3 position on **17** provided alcohol **18** in 99% yield, which was used as an acceptor in the next one-pot glycosylation. A one-pot glycosylation using these three building blocks—**12**, **13**, and **14**—and acceptor **18** provided heptasaccharide **19** in 57% yield based on **18**. Subsequent deprotection of the C3 protecting group gave the heptasaccharide acceptor **20** in 92% yield. A one-pot glycosylation using the three building blocks **12**, **13**, and **14** and heptasaccharide **20** afforded the protected decasaccharide **21** in 44% yield based on **20**. Removal of the chloroacetyl protecting group gave the decasaccharide **22**, containing a hydroxy group, in 70% yield.

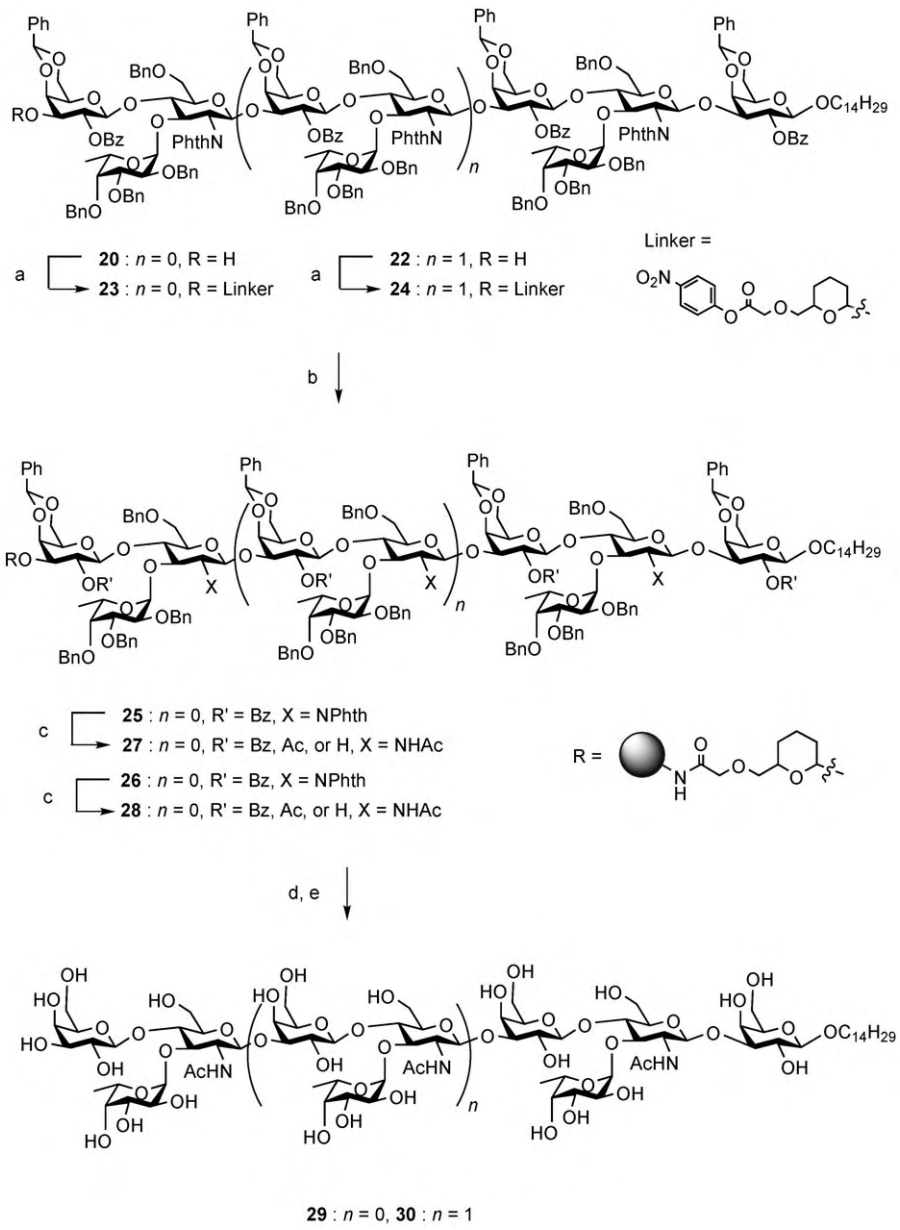

Scheme 4. Reagents and conditions: a) **4** (3 equiv), CSA, CH_2Cl_2, room temperature; b) aminomethyl ArgoPore **5a** (10 equiv), DIEA, DMF, room temperature, 12 h; c) $NH_2NH_2{\cdot}H_2O$/EtOH (1:5), reflux, 6 h, then AcOH, DIC, DIEA, room temperature, 6 h; d) lithium, THF, liq. NH_3, −78 °C, 1.5 h, reflux, 1 h, then MeOH, 12 h; (l); e) TFA, MeOH/CH_2Cl_2 (1:19), 58% yield for **20**→**29**, 58% yield for **22**→**30**. DIC = 1,3-diisopropylcarbodiimide.

Deprotection of the protected trimeric and dimeric Lewis X epitopes **20** and **22** based on the polymer-supported strategy was examined (Scheme 4). The treatment of **20** and **22** with 3 equiv of prelinker **4** in the presence of CSA at room temperature provided the protected oligosaccharides **23** and **24**, which contain an activated ester. After removal of the remaining prelinker **4** by flash column chromatography, the activated esters **23** and **24** were reacted with 10 equiv of the solid-supported amine **5a** in DMF under basic conditions for 12 h to give the solid-supported protected oligosaccharides **25** and **26**, respectively. The phthalyl groups of **25** and **26** were removed by treatment with $NH_2NH_2{\cdot}H_2O$/EtOH (1:5) at reflux for 6 h.[13] Acetylation of the resulting amines provided the solid-supported acetamides **27** and **28**, respectively. Oligosaccharides **27** and **28** were then subjected to Birch reduction conditions and then cleaved from the resin under mildly acidic conditions. ^{1}H NMR spectra of the released products revealed that most of the solid-supported benzyl esters on the complex oligosaccharides smoothly underwent cleavage in the Birch reduction. Purification of the released

 © 2006 Wiley-VCH Verlag GmbH & Co. KGaA, Weinheim

products afforded the fully deprotected trimeric and dimeric Lewis X epitopes **29** and **30**, each in 58% overall yield, based on **20** and **22**, respectively. Although the loading and release of these complex protected oligosaccharides would be difficult to achieve without loss of material, this method should be of practical use for the synthesis of oligosaccharide libraries.

In conclusion, an efficient polymer-assisted method for the deprotection of protected oligosaccharides has been demonstrated. The prelinker **4** composed of a DHP unit and an activated ester was effective not only for the loading of the protected oligosaccharides from the solution but also for the release of the fully deprotected oligosaccharide from the resin. ArgoPore was the best support for the cleavage of solid-supported benzyl ethers, which was achieved using Birch reduction conditions.

Received: March 22, 2006
Revised: May 30, 2006
Published online: August 17, 2006

Keywords: Birch reduction · glycoconjugates · glycosylation · oligosaccharides · solid-phase synthesis

[1] a) A. Varki, *Glycobiology* **1993**, *3*, 97–130; b) R. A. Dwek, *Chem. Rev.* **1996**, *96*, 683–720; c) S. Hakomori, *Arch. Biochem. Biophys.* **2004**, *426*, 173–181; d) I. Bucior, M. M. Burger, *Curr. Opin. Struct. Biol.* **2004**, *14*, 631–637.

[2] P. H. Seeberger, W.-C. Haase, *Chem. Rev.* **2000**, *100*, 4349–4393.

[3] The solid-supported benzyl ethers are known to be difficult to cleave. a) O. Kanie, G. Grotenbreg, C.-H. Wong, *Angew. Chem.* **2000**, *112*, 4719–4721; *Angew. Chem. Int. Ed.* **2000**, *39*, 4545–4547; b) M. Adinolfi, G. Barone, A. Iadonisi, M. Schiattarella, *Tetrahedron Lett.* **2001**, *42*, 5971–5972.

[4] L. A. Thompson, J. A. Ellman, *Tetrahedron Lett.* **1994**, *35*, 9333–9336.

[5] The THP linker is not amenable to the solid-phase synthesis of oligosaccharides because it is not stable under acidic glycosidation conditions.

[6] a) A. Matsuda, T. Doi, H. Tanaka, T. Takahashi, *Synlett* **2001**, 1101–1104; b) H. Tanaka, T. Zenkoh, H. Setoi, T. Takahashi, *Synlett* **2002**, 1427–1430.

[7] B. Meseguer, D. Alonso-Díaz, N. Griebenow, T. Herget, H. Waldmann, *Angew. Chem.* **1999**, *111*, 3083–3087; *Angew. Chem. Int. Ed.* **1999**, *38*, 2902–2906.

[8] S. Hakomori, Y. Zhang, *Chem. Biol.* **1997**, *4*, 97.

[9] For reports of the chemical synthesis of dimeric Lewis X, see a) S. Sato, Y. Ito, T. Ogawa, *Tetrahedron Lett.* **1988**, *29*, 5267–5270; b) A. Kameyama, T. Ehara, Y. Yamada, H. Ishida, M. Kiso, A. Hasegawa, *J. Carbohydr. Chem.* **1995**, *14*, 507.

[10] For reports of the chemical synthesis of trimeric Lewis X, see a) K. C. Nicolaou, T. J. Caulfield, H. Kataoka, N. A. Stylianides, *J. Am. Chem. Soc.* **1990**, *112*, 3693–3695; b) A. Toepfer, W. Kinzy, R. R. Schmidt, *Liebigs Ann. Chem.* **1994**, 449–464; c) W. Broder, H. Kunz, *Bioorg. Med. Chem.* **1997**, *5*, 1–19; d) K. M. Köeller, C.-H. Wong, *Chem. Eur. J.* **2000**, *6*, 1243–1251.

[11] a) T. Kanemitsu, O. Kanie, C.-H. Wong, *Angew. Chem.* **1998**, *110*, 3574–3577; *Angew. Chem. Int. Ed.* **1998**, *37*, 3415–3418; b) T. Zhu, G.-J. Boons, *J. Am. Chem. Soc.* **2000**, *122*, 10222–10223; c) K. R. Love, P. H. Seeberger, *Angew. Chem.* **2004**, *116*, 612–615; *Angew. Chem. Int. Ed.* **2004**, *43*, 602–605.

[12] H. Tanaka, N. Matoba, H. Tsukamoto, H. Takimoto, H. Yamada, T. Takahashi, *Synlett* **2005**, 824–828.

[13] Treatment of **10a** with $NH_2NH_2{\cdot}H_2O$/EtOH (1:5) at reflux for 12 h did not reduce the loading amount of the solid-supported **10a**. These results indicated that the THP linker could be stable during cleavage of the phthalyl groups.

 © 2006 Wiley-VCH Verlag GmbH & Co. KGaA, Weinheim

Selective Protein Recognition

DOI: 10.1002/anie.200601161

Tuning Linear Copolymers into Protein-Specific Hosts**

*Sebastian J. Koch, Christian Renner, Xiulan Xie, and Thomas Schrader**

The selective protein recognition by synthetic receptor molecules remains an important challenge for supramolecular and bioorganic chemistry. To distinguish between proteins of similar sizes and pI values (pI = isoelectric point), but of different biological function, an artificial host must be able to recognize the pattern of amino acid residues, that is, the topology, polarity, as well as the electrostatic potential of a protein surface. From protein–protein interactions, we can learn that nature prefers large contact areas (approximately 1500 $Å^2$) with an unusual amount of arginine and aromatic amino acid residues involved in polar interactions (Coulomb, π-cation). These interactions are complemented and enforced by hydrophobic attraction between approaching nonpolar domains or patches.[1] This combination is partly reflected in recent attempts to produce artificial protein binders that include secondary-structure mimetics,[2] multiplication of single specific[3] or unspecific binding sites,[4] evolutive optimization of biomacromolecular scaffolds,[5] and molecular

[*] S. J. Koch, C. Renner, X. Xie, Prof. T. Schrader
Philipps-Universität Marburg
Fachbereich Chemie
Hans-Meerwein-Strasse, 35032 Marburg (Germany)
Fax: (+49) 6421-28-25544
E-mail: schradet@staff.uni-marburg.de

[**] We thank Dr. J. Piehler (Biocenter Frankfurt University) for the opportunity to perform RIfS measurements in his group. C.R. is also indebted to the Deutsche Forschungsgemeinschaft for funding. We gratefully acknowledge generous support from Prof. Hynes (National University of Ireland, Galway) by providing his WinEQNMR program to evaluate 2:1 complexation events. The disclosure of preliminary results from a cell-wall degradation assay with lysozyme by Kirstin Wenck is also gratefully acknowledged.

Supporting information for this article is available on the WWW under http://www.angewandte.org or from the author.

WILEY InterScience DISCOVER SOMETHING GREAT
© 2006 Wiley-VCH Verlag GmbH & Co. KGaA, Weinheim

imprinting.[6] Herein, we introduce a new chemical concept that involves statistical copolymerization of simple binding monomers in defined stoichiometric ratios.[7]

The underlying idea is the following: for a given protein target, the chemist chooses from a preformed set of polymerizable binding sites those that match the majority of amino acid residues dominating the surface character of the protein. By statistical free-radical copolymerization, a flexible copolymer is produced that is capable of performing an extensive "induced-fit" procedure on top of the respective protein surface, and therefore reaching maximal attractive noncovalent interactions. No cross-linking is employed to guarantee perfect water solubility; no imprinting technique is used because the linear polymer is expected to adapt its shape to flat and rugged surface topologies. Thus, technical simplicity is maintained to accomplish a complex task. This modular approach deliberately avoids extensive design, requiring exact knowledge of protein-surface topology from crystal structures. Herein, we disclose preliminary, but highly promising, results.

According to the above-outlined concept, the whole procedure can be subdivided into three main steps: 1) A set of simple methacrylamide-based co-monomers is prepared; this ensemble is by itself capable of recognizing all proteinogenic basic, acidic, polar, aromatic, and nonpolar amino acid residues. 2) From this set, the co-monomers that are complementary to the most characteristic protein surface residues are copolymerized in an estimated appropriate stoichiometric ratio, with simultaneous incorporation of a small amount of polymerizable fluorophors (see Table 1). The new polymeric materials are conveniently characterized by ^{1}H and ^{31}P NMR spectroscopy, gel permeation chromatography, elemental analysis, as well as fluorescence properties. 3) In the last phase, affinities to very similar proteins are evaluated, at best in mixtures.

To demonstrate the feasibility of this concept, we faced the task of distinguishing between various basic proteins of similar size and pI value. To this end, we prepared four different binding monomers, tailored for basic, aliphatic, and aromatic residues; an amino sugar based component was added for increased water solubility. Further to the simple polymers **1** and **2**, four copolymers (**3**–**6**) were synthesized, each of which contained three different binding monomers in a 1:1:1 or 3:1:1 ratio and 10% of a dansyl fluorescence label. Free-radical copolymerization was conducted in *N*,*N*-dimethylformamide (DMF) and initiated by 0.5–0.7 mol% of azobisisobutyronitrile. Subsequent polymer-analogous reactions with LiBr led to mild dealkylation of the bisphosphonates and afforded the final receptor polymers. Their composition is depicted in Table 1. Molecular-weight determinations for **1** and **2** in DMF and water produced comparable results, excluding a potential ion-pair induced aggregation. For copolymer **5** with hydrophobic residues, very similar hydrodynamic radii were calculated from NMR spectroscopic diffusion experiments at varying concentrations (50 μM to 1.6 mM). These hydrodynamic radii also suggest monomeric species as do the symmetric M_w/M_n curves. Moreover, this copolymer displays a very compact nature—resembling a protein—most likely resulting from burial of dodecyl tails in its inner core while exposing the polar bisphosphonate head groups into the bulk solvent. Copolymerization parameters, determined for **2**, indicate a perfect statistical copolymerization, ruling out the formation of hydrophobic blocks or aggregated micelles.

Table 1: Modular set of methacrylamide-based co-monomers ($n = 1$ or 7) and polymers **1**–**6** derived thereof.[a]

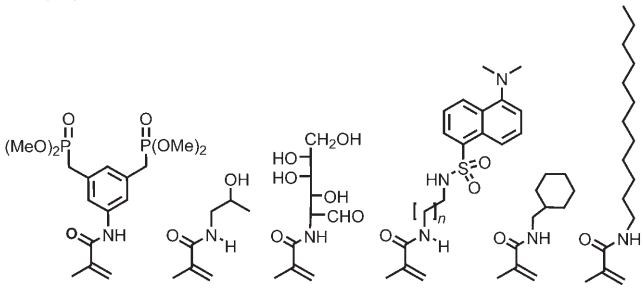

a **b** **c** **d** **e** **f**

Polymer	Bisphosphonate **a**	Alcohol **b**, **c**	Dansyl **d**	Cyclohexyl **e**	Dodecyl **f**
1	1	–	0.1	–	–
2	1	3[b]	0.4	–	–
3	1	1[c]	1	–	–
4	3	1[c]	0.5	1	–
5	1	1[c]	0.3	–	1
6	3	1[c]	0.5	–	1

[a] Each row indicates the relative ratio of co-monomers for a given copolymer. [b] Alcohol monomer from 2-hydroxypropylamine **b**. [c] Alcohol monomer from 2-glucosamine **c**.

In a systematic study, each fluorescent polymer was titrated with the same series of neutral and basic proteins.[8] In most cases, fluorescence emission intensities increased markedly on protein binding, presumably owing to reorientation of the polymer's binding sites towards the protein surface with concomitant deshielding of the fluorophor. Unfortunately, the most basic protein histone H1 formed insoluble complexes even at 10 nM concentrations, precluding the exact determination of its free binding energies. All of the other examined protein complexes, however, furnished binding isotherms with a perfect fit by nonlinear regression methods.[9] The respective association constants (K_a) are summarized in Table 2; they cover a relatively broad range from $10^4\,M^{-1}$ up to over $10^7\,M^{-1}$.

It is instructive to compare K_a values for a given protein among the various copolymers because they reveal the contribution of additional noncovalent interactions, especially in relation to pure polybisphosphonates. Thus, bovine serum albumin (BSA), a blood lipid carrier, is bound much more strongly if the polymer (**5**) also contains long aliphatic side chains for additional hydrophobic attraction (Figure 1). Most likely these imitate the natural binding mode inside the nonpolar cleft. Similarly, for all copolymers, the dansyl-containing **3** displays superior affinity towards trypsin with its unusually high content of aromatic residues (dissociation constant, $K_d = 170$ nM).[10] Clearly, additional π stacking renders complex formation even 100-times more efficient than the parent bisphosphonate copolymer **2**. Experimentally determined stoichiometries (Job plots) remain around 1:1

 © 2006 Wiley-VCH Verlag GmbH & Co. KGaA, Weinheim

Table 2: Protein affinities to hosts **1**–**6**, determined as $K_{1:1}$ values by fluorescence titrations in 30 mM phosphate buffer at pH 7.0.[a]

Polymer	Cytochrome c		Trypsin		Lysozyme		BSA	
	K_a [M^{-1}]	Ratio[b]	K_a [M^{-1}]	Ratio[b]	K_a [M^{-1}]	Ratio[b]	K_a [M^{-1}]	Ratio[b]
1	6×10^5	1:2.0	$>10^5$	–	$>10^5$	–	2×10^5	1:2.5
2	2×10^5	1:3.0	4×10^4	1:4.0	4×10^6	1:4.0	2×10^5	1:1.5
3	5×10^5	1.0:1	6×10^6	1.5:1	7×10^6	1:2.0	2×10^5	1:1.5
4	3×10^5	1.5:1	–	–	9×10^5	2.0:1	4×10^5	1.5:1
5	2×10^6	1.7:1	–	–	–	–	7×10^5	1.5:1
6	4×10^5	2.0:1	6×10^5	1.5:1	4×10^7	2.0:1	6×10^5	1.5:1

[a] Complex formation was assumed to occur without cooperativity and with uniform binding constants for each step. Standard deviations from the nonlinear regressions were calculated at 2–17%. [b] Polymer/protein stoichiometry.

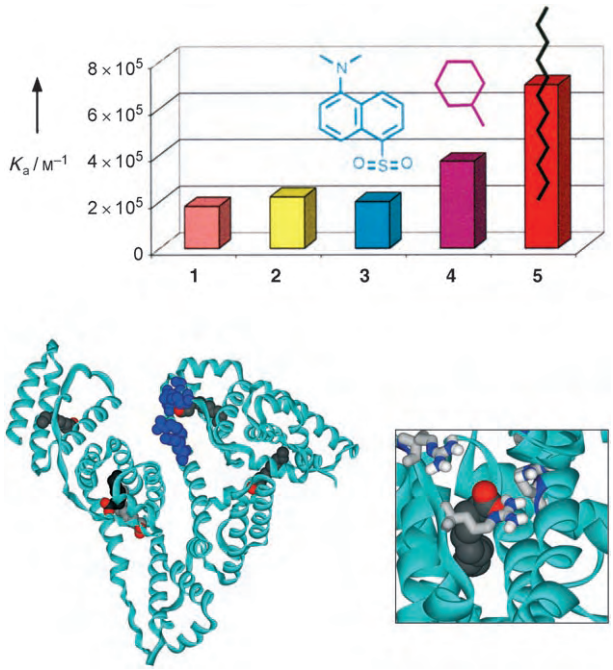

Figure 1. Top: Target optimization of homopolymer **1** into an efficient BSA binder **5** by incorporation of dodecyl co-monomers for additional hydrophobic interactions. Bottom: Crystal structure of human serum albumin with complexed lipids.[12] Note the basic residues (blue) at the entrance of the clefts, holding the myristic acid guest (black) in place (see zoom).

throughout the whole series, indicating optimal surface coverage of the protein.[11] To prove that cooperative effects are negligible, two more copolymers, **7** and **8**, were synthesized that were comprised of the same monomer composition but different molecular weights (see Supporting Information). Their bisphosphonate (BP) content (2:1:1 BP/dodecyl/sugar) lies between that of polymer **5** (1:1:1) and polymer **6** (3:1:1). This also implies that the amount of hydrophobic dodecylmethacrylamide co-monomers steadily increases from **6** over **7** and **8** to **5**. Intriguingly, the binding constants with cytochrome c follow the very same trend, indicating that, in this series, the number of hydrophobic interactions and not electrostatics determines the relative polymer affinities (**6**: 4×10^5; **8**: 6×10^5; **7**: 8×10^5; **5**: 2×10^6).

In our systematic binding study for representative basic proteins, we identified among polymers **1**–**6** a candidate with pronounced protein selectivity (Figure 2). Arginine-rich lysozyme is recognized by bisphosphonate-rich copolymer **6** with a remarkable K_d value of 25 nM, which is 100-times superior to cytochrome c (comparable in size and pI; Table 2). Close inspection of the electrostatic potential surface[13] reveals numerous hydrophobic patches between the Arg residues, ideal for van der Waals interactions with the copolymer's long aliphatic tails. Compared to protein complexes of **1** or **2**, the glucosamine content in **3**–**6** leads to markedly improved water solubilities.

Preliminary results from an enzyme assay measuring the kinetics of bacterial cell wall degradation by lysozyme (*Micrococcus lysodeicticus*) indicate a competitive inhibition of enzyme activity by bisphosphonate-containing copolymers. Intriguingly, the corresponding IC_{50} values follow the same order as their binding constants determined by fluorescence titration. Thus, polymers **4** ($K_a = 9\times10^5\,M^{-1}$), **3** ($K_a = 7\times10^6\,M^{-1}$), and **6** ($K_a = 4\times10^7\,M^{-1}$) produced IC_{50} values of roughly 20, 10, and 1 μM for enzymatic bacterial degradation, indicating, that 2 equivalents of polymer **6** suffice to completely shut down lysozyme activity, whereas polymer **4** needs about 50 equivalents for the same task (≈1 μM protein concentration).

Reflectometric interference spectroscopy (RIfS) measurements record the change of optical thickness for compound layers deposited successively on glass chips. A first layer of cationic polyethyleneimine (PEI) was coated with negatively charged copolymers **3** and **5**, followed by noncovalent immobilization of various proteins. The binding constants and dissociation rates derived thereof confirm the affinity and selectivity trends observed in solution (see Supporting Information for details).[14] More importantly, however, the amount of irreversible binding contributions compared to the parent polybisphosphonates **1** and **2** increased drastically (Figure 3). As the latter rely mostly on electrostatic interactions, this change strongly indicates

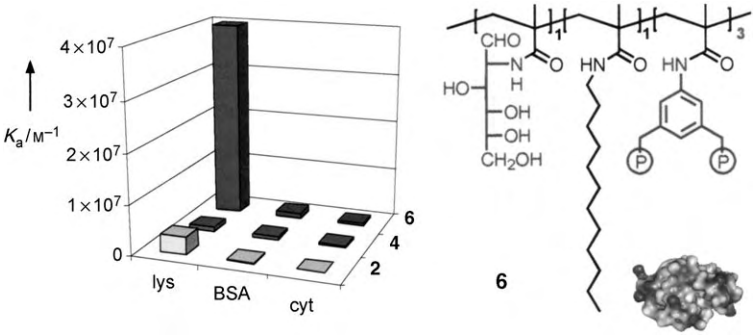

Figure 2. Drastic selectivity increase from copolymer **2** to lysozyme binder **6**. lys = lysozyme, cyt = cytochrome c, P = phosphonate.

 © 2006 Wiley-VCH Verlag GmbH & Co. KGaA, Weinheim

essential hydrophobic, van der Waals, or π-stacking interactions between the aliphatic and aromatic co-monomer residues and nonpolar protein surface areas. For a kinetically stable protein immobilization, low off-rates (dissociation rates) are mandatory; the new copolymers thus offer the

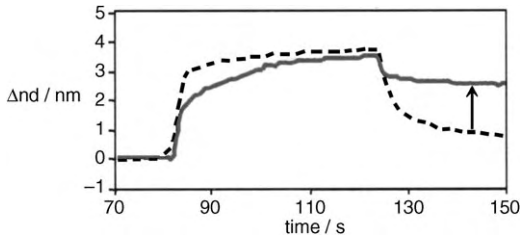

Figure 3. RIfS curves for lysozyme recognition on a polymer-coated PEI surface (solid line: homopolymer **1**; dashed line: dansyl copolymer **3**). Note the elevated level of irreversible binding with **3**. nd = optical thickness.

unique option of mild noncovalent protein attachment to the chip surface and its potential observation in a functional state (e.g., in new enzyme-sensor systems).

We are currently optimizing the above-introduced modular concept by creating diverse copolymer libraries with a representative pool of binding monomers for all important noncovalent interactions occurring in protein recognition events. A fast RIfS protocol will be useful for efficient screening. Optimized binding monomers for each class of amino acid residues may pave the way towards the ultimate goal—artificial antibodies.

Received: March 23, 2006
Revised: June 8, 2006
Published online: August 28, 2006

Keywords: copolymers · NMR spectroscopy · noncovalent interactions · protein recognition · reflectometric interference spectroscopy

[1] T. A. Larsen, A. J. Olsen, D. S. Goodsell, *Structure* **1998**, *6*, 421; J. Janin, S. Miller, C. Chothia, *J. Mol. Biol.* **1988**, *204*, 155; A. A. Bogan, K. S. Thorn, *J. Mol. Biol.* **1998**, *280*, 1; F. B. Sheinerman, R. Norel, B. Honig, *Curr. Opin. Struct. Biol.* **2000**, *10*, 153.

[2] α-helices: H. Yin, G. I. Lee, K. A. Sedey, J. M. Rodriguez, H. G. Wang, S. M. Sebti, A. D. Hamilton, *J. Am. Chem. Soc.* **2005**, *127*, 5463; β-turns: A. B. Smith, W. Y. Wang, P. A. Sprengeler, R. Hirschmann, *J. Am. Chem. Soc.* **2000**, *122*, 11037.

[3] L. Baldini, A. J. Wilson, J. Hong, A. D. Hamilton, *J. Am. Chem. Soc.* **2004**, *126*, 5656; E. A. Merritt, Z. Zhang, J. C. Pickens, M. Ahn, W. G. J. Hol, E. Fan, *J. Am. Chem. Soc.* **2002**, *124*, 8818; A. Ojida, Y. Miyahara, T. Kohira, I. Hamachi, *Biopolymers* **2004**, *76*, 177; Md. A. Fazal, B. C. Roy, S. Sun, S. Mallik, K. R. Rodgers, *J. Am. Chem. Soc.* **2001**, *123*, 6283.

[4] Gold clusters: N. O. Fischer, A. Verma, C. M. Goodman, J. M. Simard, V. M. Rotello, *J. Am. Chem. Soc.* **2003**, *125*, 13387; postsynthetically modified polymers: L. E. Strong, L. L. Kiessling, *J. Am. Chem. Soc.* **1999**, *121*, 6193.

[5] Protein grafting: S. E. Rutledge, H. M. Volkman, A. Schepartz, *J. Am. Chem. Soc.* **2003**, *125*, 14336; RNA aptamers: D. J. Schneider, J. Feigon, Z. Hostomsky, L. Gold, *Biochemistry* **1995**, *34*, 9599.

[6] Reconstructed liposomes: M. Santos, B. C. Roy, H. Goicoechea, A. D. Campiglia, S. J. Mallik, *J. Am. Chem. Soc.* **2004**, *126*, 10738; Cu^{II}-imprinted silica: S. Mallik, S. D. Plunkett, P. K. Dhal, R. D. Robinson, D. Pack, D. Shenk, F. H. Arnold, *New J. Chem.* **1994**, *18*, 299; saccharide/polymer coating: H. Q. Shi, W. B. Tsai, M. D. Garrison, S. Ferrari, B. D. Ratner, *Nature* **1999**, *398*, 593.

[7] It was reported that merely controlling the amount and nature of functional side chains yielded, in a combinatorial fashion, a polymer with remarkable phosphatase properties, although statistical distribution of catalytically active sites was allowed: F. M. Menger, A. V. Eliseev, V. A. Migulin, *J. Org. Chem.* **1995**, *60*, 6666.

[8] For an account on the parent bisphosphonate homopolymers as synthetic hosts for basic proteins, see: C. Renner, J. Piehler, T. Schrader, *J. Am. Chem. Soc.* **2006**, *128*, 620.

[9] K. A. Connors, *Binding Constants*, Wiley, New York, **1987**.

[10] Protein surface residue distributions were evaluated with the PROVE program (PROtein Volume Evaluation): J. Pontius, J. Richelle, S. J. Wodak, *J. Mol. Biol.* **1996**, *264*, 121.

[11] M. T. Blanda, J. H. Horner, M. Newcomb, *J. Org. Chem.* **1989**, *54*, 4626. Three independent titrations between polymer **1** and cytochrome c furnished identical stoichiometry factors and the following K_a values: a) $5.4\times10^5\,\text{M}^{-1}\pm3\,\%$ (1:2); b) $5.5\times10^5\,\text{M}^{-1}\pm2\,\%$ (1:2); $5.8\times10^5\,\text{M}^{-1}\pm9\,\%$ (1:1.9).

[12] S. Curry, H. Mandelkow, P. Brick, N. Franks, *Nat. Struct. Biol.* **1998**, *5*, 827.

[13] M. F. Sanner, J. C. Spehner, A. J. Olson, *Biopolymers* **1996**, *38*, 305.

[14] J. Piehler, A. Brecht, G. Gauglitz, M. Zerlin, C. Maul, R. Thiericke, S. Grabley, *Anal. Biochem.* **1997**, *249*, 94.

 © 2006 Wiley-VCH Verlag GmbH & Co. KGaA, Weinheim

Ligand Design

DOI: 10.1002/anie.200601229

A σ-Donor with a Planar Six-π-Electron $B_2N_2C_2$ Framework: Anionic N-Heterocyclic Carbene or Heterocyclic Terphenyl Anion? **

*Taryn D. Forster, Kelly E. Krahulic, Heikki M. Tuononen, Robert McDonald, Masood Parvez, and Roland Roesler**

Dedicated to Professor Tristram Chivers

The remarkable success of N-heterocyclic carbenes[1] (NHCs) as ligands in main-group and especially in transition-metal chemistry and catalysis[2] has prompted the synthesis and characterization of numerous representatives of this class of compounds. Derivatives with a five-membered framework (**A**) have been investigated most extensively. However, four-, six-, and seven-membered carbenes have also been reported. Emerging trends in carbene ligand design involve the replacement of one or both intraannular nitrogen atoms with elements such as carbon, phosphorus, and sulphur,[3] and the replacement of the carbon backbone with heteroelements (**B**–**D**).[4] In this way, the steric and electronic properties of the ligand can be effectively tuned. Although NHCs are traditionally neutral ligands, a few anionic derivatives have been prepared in which the charge is localized on an adjoining borate or cyclopentadienyl moiety.[5] Herein we report the synthesis of an anionic NHC (**3**) that has a six-π-electron system in which the charge is localized on the ring framework. This compound has the potential to coordinate in either σ (η^1) or π (η^6) fashion.

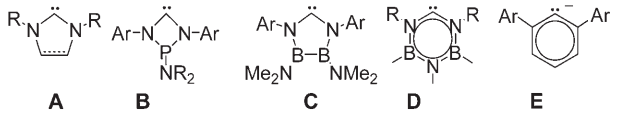

The reaction of the corresponding trimethylsilyl formamidinate[4c] with 1,1-bis(methylchloroboryl)ethane[6] in the presence of trimethylsilyl triflate (Scheme 1) yielded the zwitterionic ring compound **1**. Crystallographic analysis (Figure 1) revealed an iminium borate structure with the triflate group coordinated to one of the boron atoms.[7] The $B_2N_2C_2$ ring in **1** has a half-boat conformation with the sp^3-hybridized carbon C(2) situated outside the slightly twisted $B_2N_2C(1)$ plane. The B–C and B–N bonds to borate center B(1) are longer than the corresponding bonds to borane center B(2), and the two N–C(1) bonds within the ring are not equal. The ^{11}B NMR spectrum of **1** in benzene displayed only one signal at $\delta = 40.7$ ppm, which corresponds to a three-coordinated boron and indicates that the triflate dissociates in solution to form an ion pair. The ^1H and ^{13}C spectra are in agreement with C_s symmetry.

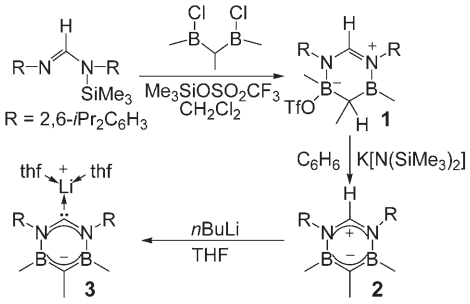

Scheme 1. Synthesis of derivatives **1**–**3**.

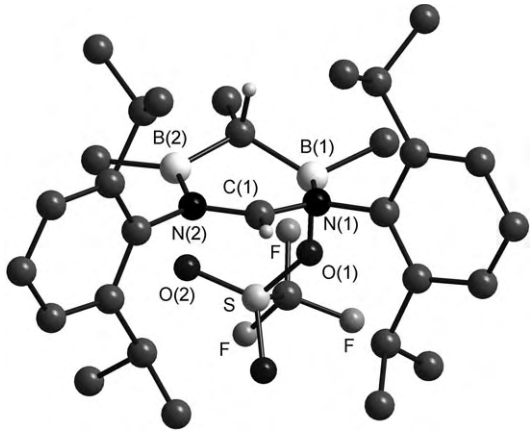

Figure 1. Molecular structure of **1**. Hydrogen atoms on the organic substituents have been omitted for clarity. Selected bond lengths [Å] and angles [°]: N(1)–C(1) 1.298(2), N(2)–C(1) 1.345(2), N(1)–B(1) 1.595(3), N(2)–B(2) 1.475(3), C(2)–B(1) 1.603(3), C(2)–B(2) 1.550(3), O(1)–B(1) 1.626(3); N(1)-C(1)-N(2) 125.74(17), C(1)-N(1)-B(1) 121.48(16), C(1)-N(2)-B(2) 122.23(16), B(1)-C(2)-B(2) 113.66(16).

[*] T. D. Forster, K. E. Krahulic, Dr. M. Parvez, Dr. R. Roesler
Department of Chemistry
University of Calgary
2500 University Dr. NW
Calgary, AB, T2N 1N4 (Canada)
Fax: (+1) 403-289-8141
E-mail: roesler@ucalgary.ca
Dr. H. M. Tuononen
Department of Chemistry
University of Jyväskylä
P.O. Box 35, 40014 Jyväskylä (Finland)
Dr. R. McDonald
Department of Chemistry
University of Alberta
11227 Saskatchewan Dr. NW
Edmonton, AB, T6G 2G2 (Canada)

[**] This work was supported by the Natural Sciences and Engineering Research Council of Canada, the Canada Foundation for Innovation, and the Alberta Science and Research Investments Program. K.E.K. thanks the NSERC and the Alberta Ingenuity Fund for doctoral scholarships.

Supporting information for this article is available on the WWW under http://www.angewandte.org or from the author.

InterScience
© 2006 Wiley-VCH Verlag GmbH & Co. KGaA, Weinheim

Deprotonation of **1** with an equimolar amount of K[N(SiMe$_3$)$_2$] cleanly yielded the 1,5-diaza-2,4-diborine **2**. Few carbaborazines have been described, and a derivative with this framework has not been reported; however, its stability and properties have been the object of theoretical calculations.[8] At −40 °C, the ^{13}C NMR spectrum features signals corresponding to the ring carbon atoms adjacent to nitrogen and boron at $\delta = 146.8$ and 119.2 ppm, respectively, in the typical range for benzene derivatives.

The X-ray structural determination of **2** (Figure 2) confirmed the proposed structure, which contains a planar $B_2N_2C_2$ ring with equivalent pairs of B–N, B–C, and N–C

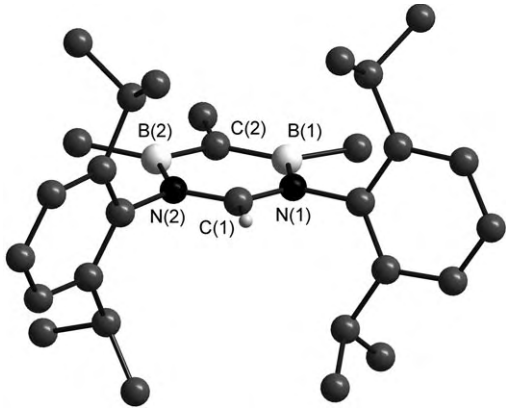

Figure 2. Molecular structure of **2**. Hydrogen atoms on the organic substituents have been omitted for clarity. Selected bond lengths [Å] and angles [°]: N(1)–C(1) 1.3264(17), N(2)–C(1) 1.3274(17), N(1)–B(1) 1.5027(19), N(2)–B(2) 1.4980(19), C(2)–B(1) 1.477(2), C(2)–B(2) 1.479(2); N(1)-C(1)-N(2) 122.83(12).

bond lengths.[7] The endocyclic N–C bond lengths (ca. 1.33 Å) are intermediate between the two values observed in **1** and practically identical to those observed in the cationic precursors to carbenes **B**–**D**.[4] The B–N bond lengths in **2** (1.50 Å) are similar to those observed in **C** and significantly longer than those in borazines (1.42–1.44 Å).[9] The intraannular B–C and N–C bonds (1.48 and 1.33 Å, respectively) are shorter than the corresponding bonds observed in the regioisomers 1,3-diaza-2,4-diborine and 1,4-diaza-2,3-diborine (ca. 1.53 and 1.38–1.40 Å, respectively).[10] The B–N bond lengths in the latter derivatives are equal with those in borazines. As proposed by Bertrand and co-workers for the cationic precursor to **D**,[4d] the six π electrons in **2** appear to be distributed over two allyl-like fragments (B_2C^- and N_2C^+) to form a zwitterionic structure, rather than delocalized over the entire ring framework.

Deprotonation of **2** with *n*BuLi produced the lithium salt **3**, which was stable in the solid state under an inert atmosphere but decomposed slowly in tetrahydrofuran (thf) through deprotonation of the solvent and reformation of the starting material. The crystallographic determination (Figure 3) revealed that **3** contains a planar $B_2N_2C_2$ ligand σ-coordinated to the lithium ion.[7] The distorted trigonal planar coordination environment of lithium center is completed by two thf molecules, and the ring carbon atoms and

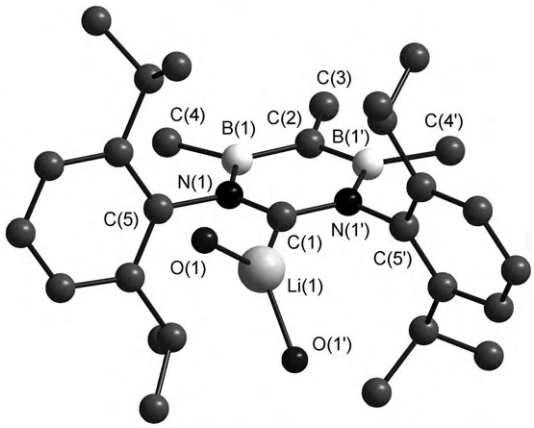

Figure 3. Molecular structure of **3**. Hydrogen atoms on the organic substituents and the carbon atoms in the thf molecules have been omitted for clarity. Selected bond lengths [Å] and angles [°]: C(1)–Li(1) 2.152(6), N(1)–C(1) 1.3627(19), N(1)–B(1) 1.495(3), C(2)–B(1) 1.475(3), N(1)–C(5) 1.450(2), C(4)–B(1) 1.599(3), C(2)–C(3) 1.518(4), O(1)–Li(1) 1.946(4); N(1)-C(1)-N(1′) 114.0(2), N(1)-C(1)-Li(1) 123.01(10), O(1)-Li(1)-C(1) 130.48(13), O(1)-Li(1)-O(1′) 99.0(3).

the lithium atom lie on a crystallographic C_2 axis. Consistent with other NHCs, deprotonation of **2** results in lengthening of the intraannular N–C bonds by approximately 0.03 Å to a value of 1.36 Å. The N(1)-C(1)-N(1′) angle in **3** (114.0°) is more acute than that in **2** (122.8°) and **1** (125.7°). This is a result of a lateral compression of the ring skeleton, which causes an increase of the C(1)···C(2) distance by 0.13 Å in **3** versus **2**. The overall geometry of **3** strongly resembles the structure of isoelectronic lithium terphenyl derivatives.[11] The planar six-π-electron σ-donating anion in **3** could therefore be seen as either an anionic NHC or a heterocyclic terphenyl anion (**E**).

The Li–C bond length and the chemical shift of the carbon atom connected to lithium center can be considered when comparing **3** to a lithium NHC complex and a lithium terphenyl. The Li(1)–C(1) bond measures 2.152(6) Å, which is typical for lithium NHC complexes. In representatives of this class, the substitution of the lithium center and the charge of the NHC ligand have little influence on the length of the Li–C bond (2.124(4)–2.197(4) Å).[12] Conversely, the length of the Li–C bond in trigonal-planar, three-coordinate terphenyl lithium derivatives falls within a narrow range (2.074(16)–2.128(4) Å).[13] The ^{13}C NMR signal corresponding to the carbene carbon atom could not be located in the spectrum of **3**. However, the potassium analogue, obtained by deprotonation of **2** with benzyl potassium, displayed a signal for the carbene carbon atom at 239.1 ppm, which is significantly downfield shifted relative to the ipso carbon atom in terphenyl lithium derivatives (175–201 ppm)[13] and the carbene carbon atom in NHC–Li (189–198 ppm)[12] and NHC–K complexes[14] (199–208 ppm). It is uncertain if this signal belongs to the free anionic carbene or the potassium-coordinated ligand. To our knowledge, potassium terphenyl derivatives have not been reported.

A density functional theory treatment of the simplified structures **I**–**III** showed an increase in the energy of both the

 © 2006 Wiley-VCH Verlag GmbH & Co. KGaA, Weinheim

highest occupied molecular orbitals (HOMOs; σ) and the lowest unoccupied molecular orbitals (LUMOs; π) in the order of **I** to **II** to **III**, which indicates that the σ-donating ability decreases in the order **III** > **II** ≫ **I** and the π-accepting ability decreases in the reverse order (Figure 4). NHCs are generally considered to be excellent σ donors and poor

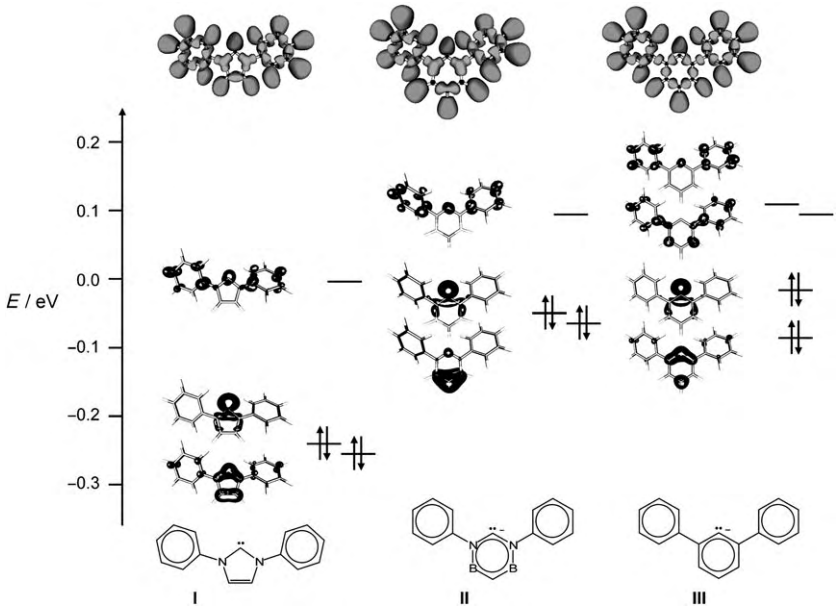

Figure 4. Frontier molecular orbitals and ELF diagrams for systems I–III.

π acceptors. Analysis of the electron localization function (ELF)[15] for the compounds in question gives occupancies of 2.28, 2.35, and 2.45 electrons for the carbon lone-pair basins in **III**, **II**, and **I**, respectively. Hence, the ELF analysis suggests that NHC **I** is a better σ donor than is predicted by the orbital energies alone. The same is implied by the trends in Mulliken atomic charges, which show that the carbene carbon atom in NHC **I** bears slightly more negative charge (−0.20) than that in **II** (−0.15) or **III** (−0.14). To fully resolve the issue of relative σ-donating ability of the studied systems, we performed charge decomposition analyses (CDA)[16] for complexes of **I**–**III** with Li^+ and CuCl. The results show that the σ-donating ability of ligands **I**–**III** follows the trend in orbital energies for the Li^+ complexes (total donation of σ electrons is 0.484, 0.566, and 0.622 for **I**, **II**, and **III**, respectively), but within the CuCl series ligand **II** has similar σ-donating ability to **I** (total donation of 0.236 and 0.233 electrons, respectively) and **III** has slightly less (0.206 electrons). Hence, the computational data indicate that the new anionic carbene **II** has similar or even greater σ-donating ability, depending on the metal fragment, than the traditional ligand **I**.

In summary, experimental and theoretical evidence indicates that the anionic carbene in **3** bridges the gap between two classical ligands that have quite different properties: NHCs and terphenyl anions. Its facile synthesis from the formally zwitterionic diazadiborine **2** renders the novel system a promising anionic ligand, with which both σ (η^1) and π (η^3 or η^6) coordination modes are possible. Its coordinating ability towards transition metals is currently being investigated.

Experimental Section

All operations were carried out with exclusion of air and moisture. The NMR spectra were measured on a Bruker Avance DRX-400 spectrometer. All chemicals were prepared according to reported procedures or purchased from commercial sources. Computational details are presented in the Supporting Information.

1: 1,1-Bis(chloromethylboryl)ethane (345 mg, 2.3 mmol) was added slowly to a solution of *N*,*N*′-bis(2,6-diisopropylphenyl)trimethylsilylformamidine (1.0 g, 2.3 mmol) in dichloromethane (20 mL) at room temperature. The solution was stirred for one hour, trimethylsilyltriflate (0.5 g, 2.2 mmol) was added, and the solution was stirred for an additional 30 minutes. Volatile substances were removed in vacuo and the oily residue was recrystallized from hexane to yield **1** as a colorless, crystalline solid (0.82 g, 1.14 mmol, 61 %). ^{1}H NMR (400 MHz, CD_2Cl_2, 25 °C): $\delta = 0.21$ (s, 6H, BCH_3), 0.87 (q, 1H, B_2CHCH_3, $^3J_{H,H} = 7.0$ Hz), 1.14, 1.15 (d, 6H, $CH(CH_3)_2$, $^3J_{H,H} = 6.9$ Hz), 1.24, 1.25 (d, 6H, $CH(CH_3)_2$, $^3J_{H,H} = 6.8$ Hz), 1.32 (d, 3H, B_2CHCH_3, $^3J_{H,H} = 7.0$ Hz), 2.94 (sept., 2H, $CH(CH_3)_2$, $^3J_{H,H} = 6.9$ Hz), 3.24 (sept., 2H, $CH(CH_3)_2$, $^3J_{H,H} = 6.8$ Hz), 7.23, 7.27 (dd, 2H, *m*-C_6H_3, $^3J_{H,H} = 7.8$ Hz, $^4J_{H,H} = 1.5$ Hz), 7.37 (t, 2H, *p*-C_6H_3, $^3J_{H,H} = 7.8$ Hz), 7.57 ppm (s, 1H, $N_2C(H)$); ^{13}C NMR (100 MHz, CD_2Cl_2, −50 °C): $\delta =$ 0.8 (B_2CHCH_3), 4.5 (BCH_3), 9.9 (B_2CHCH_3), 24.1, 24.2, 25.6, 25.8 ($CH(CH_3)_2$), 28.5, 29.4 ($CH(CH_3)_2$), 124.2, 124.6 (*m*-C_6H_3), 128.9 (*p*-C_6H_3), 136.6 (*i*-C_6H_3), 144.0, 144.8 (*o*-C_6H_3), 160.9 ppm (N_2CH); ^{11}B NMR (128 MHz, C_6D_6, 25 °C): $\delta = 40.7$ ppm; MS (EI, 70 eV): *m*/*z* 443(8) [$M^+ - O_3SCF_3$], 427(100) [$M^+ - O_3SCF_3 - CH_3$]; HRMS (EI, 70 eV): found *m*/*z* 443.3727 [$M^+ - O_3SCF_3$], calcd for $H_{45}C_{29}N_2{}^{11}B_2$ *m* = 443.3769.

2: A mixture of **1** (1.0 g, 1.69 mmol) and K[$N(SiMe_3)_2$] (0.36 g, 1.8 mmol) was stirred in toluene (30 mL) for 1 h at room temperature and then filtered. Volatile substances were removed in vacuo to leave behind **2** as a crystalline, colorless solid (0.64 g, 1.45 mmol, 86 %). ^{1}H NMR (400 MHz, CD_2Cl_2, 25 °C): $\delta = 0.26$ (s, 6H, BCH_3), 1.12, 1.18 (d, 12H, $CH(CH_3)_2$, $^3J_{H,H} = 6.8$ Hz), 2.06 (s, 3H, B_2CHCH_3), 2.75 (sept., 4H, $CH(CH_3)_2$, $^3J_{H,H} = 6.8$ Hz), 7.24 (d, 4H, *m*-C_6H_3, $^3J_{H,H} = 7.6$ Hz), 7.36 (t, 2H, *p*-C_6H_3, $^3J_{H,H} = 7.6$ Hz), 7.57 ppm (s, 1H, N_2CH); ^{13}C NMR (100 MHz, CD_2Cl_2, −40 °C): $\delta = 0.1$ (br, BCH_3), 16.9 (B_2CCH_3), 23.6, 24.8 ($CH(CH_3)_2$), 27.9 ($CH(CH_3)_2$), 119.2 (br, B_2CCH_3), 123.8 (*m*-C_6H_3), 128.2 (*p*-C_6H_3), 139.1 (*i*-C_6H_3), 144.1 (*o*-C_6H_3), 146.8 ppm (N_2CH); ^{11}B NMR (128 MHz, CD_2Cl_2, 25 °C): $\delta = 38.4$ ppm; MS (EI, 70 eV): *m*/*z* 442(24) [M^+], 427(80) [$M^+ - CH_3$]; HRMS (EI, 70 eV): found *m*/*z* 442.3656, calcd for $H_{44}C_{29}N_2{}^{11}B_2$ *m* = 442.3691.

3: Solid *n*BuLi (5 mg, 0.9 μmol) was added at room temperature to a solution of **2** (20 mg, 0.45 μmol) in THF (1 mL). The solvent was removed in vacuo, and the colorless product (19 mg, 0.32 μmol, 71 %) was recrystallized from toluene to yield colorless crystals. ^{1}H NMR (400 MHz, [D_8]THF, 25 °C): $\delta = 0.02$ (s, 6H, BCH_3), 1.09, 1.12 (d, 12H, $CH(CH_3)_2$, $^3J_{H,H} = 6.9$ Hz), 1.89 (s, 3H, B_2CHCH_3), 3.23 (sept., 4H, $CH(CH_3)_2$, $^3J_{H,H} = 6.9$ Hz), 7.15 ppm (s, 6H, C_6H_3); ^{13}C NMR (100 MHz, [D_8]THF, 25 °C): $\delta = 2.3$ (s, br, BCH_3), 17.8 (B_2CCH_3), 25.2, 25.4 ($CH(CH_3)_2$), 28.5 ($CH(CH_3)_2$), 124.1 (*m*-C_6H_3), 126.4 (*p*-C_6H_3), 146.2 (*o*-C_6H_3), 149.7 ppm (*i*-C_6H_3); ^{11}B NMR (128 MHz, [D_8]THF, 25 °C): $\delta = 36.3$ ppm; ^{7}Li NMR (155 MHz, [D_8]THF, 25 °C): $\delta = 0.15$ ppm.

Received: March 28, 2006
Revised: June 26, 2006
Published online: August 29, 2006

Keywords: aromaticity · boron · carbenes · heterocycles · lithium

 © 2006 Wiley-VCH Verlag GmbH & Co. KGaA, Weinheim

[1] a) D. Bourissou, O. Guerret, F. P. Gabbaï, G. Bertrand, *Chem. Rev.* **2000**, *100*, 39 – 91; b) *Carbene Chemistry* (Ed.: G. Bertrand), Marcel Dekker, New York, **2002**; c) R. W. Alder, M. E. Blake, L. Chaker, J. N. Harvey, F. Paolini, J. Schütz, *Angew. Chem.* **2004**, *116*, 6020 – 6036; *Angew. Chem. Int. Ed.* **2004**, *43*, 5896 – 5911; ; d) V. Nair, S. Bindu, V. Sreekumar, *Angew. Chem.* **2004**, *116*, 5240 – 5245; *Angew. Chem. Int. Ed.* **2004**, *43*, 5130 – 5135; ; e) D. Enders, T. Balensiefer, *Acc. Chem. Res.* **2004**, *37*, 534 – 541.

[2] a) L. Jafarpour, S. P. Nolan, *J. Organomet. Chem.* **2001**, *617–618*, 17 – 27; b) D. Enders, H. Gielen, *J. Organomet. Chem.* **2001**, *617–618*, 70 – 80; c) W. A. Herrmann, *Angew. Chem.* **2002**, *114*, 1342 – 1363; *Angew. Chem. Int. Ed.* **2002**, *41*, 1290 – 1309; ; d) A. C. Hillier, G. A. Grasa, M. S. Viciu, H. M. Lee, C. Yang, S. P. Nolan, *J. Organomet. Chem.* **2002**, *653*, 69 – 82; e) M. C. Perry, K. Burgess, *Tetrahedron: Asymmetry* **2003**, *14*, 951 – 961; f) E. Peris, R. H. Crabtree, *Coord. Chem. Rev.* **2004**, *248*, 2239 – 2246; g) C. M. Crudden, D. P. Allen, *Coord. Chem. Rev.* **2004**, *248*, 2247 – 2273; h) V. César, S. Bellemin-Laponnaz, L. H. Gade, *Chem. Soc. Rev.* **2004**, *33*, 619 – 636; i) N. M. Scott, S. P. Nolan, *Eur. J. Inorg. Chem.* **2005**, 1815 – 1828.

[3] a) F. E. Hahn, *Angew. Chem.* **2006**, *118*, 1374 – 1378; *Angew. Chem. Int. Ed.* **2006**, *45*, 1348 – 1352; ; b) H. Nikawa, T. Nakahodo, T. Tsuchiya, T. Wakahara, G. M. A. Rahman, T. Akasaka, Y. Maeda, M. T. H. Liu, A. Meguro, S. Kyushin, H. Matsumoto, N. Mizorogi, S. Nagase, *Angew. Chem.* **2005**, *117*, 7739 – 7742; *Angew. Chem. Int. Ed.* **2005**, *44*, 7567 – 7570; c) V. Lavallo, Y. Canac, C. Präsang, B. Donnadieu, G. Bertrand, *Angew. Chem.* **2005**, *117*, 5851 – 5855; *Angew. Chem. Int. Ed.* **2005**, *44*, 5705 – 5709; d) D. Martin, A. Baceiredo, H. Gornitzka, W. W. Schoeller, G. Bertrand, *Angew. Chem.* **2005**, *117*, 1728 – 1731; *Angew. Chem. Int. Ed.* **2005**, *44*, 1700 – 1703.

[4] a) E. Despagnet-Ayoub, R. H. Grubbs, *J. Am. Chem. Soc.* **2004**, *126*, 10198 – 10199; b) E. Despagnet-Ayoub, R. H. Grubbs, *Organometallics* **2005**, *24*, 338 – 340; c) K. E. Krahulic, G. D. Enright, M. Parvez, R. Roesler, *J. Am. Chem. Soc.* **2005**, *127*, 4142 – 4143; d) C. Präsang, B. Donnadieu, G. Bertrand, *J. Am. Chem. Soc.* **2005**, *127*, 10182 – 10183.

[5] a) R. Fränkel, C. Birg, U. Kernbach, T. Habereder, H. Nöth, W. P. Fehlhammer, *Angew. Chem.* **2001**, *113*, 1961 – 1964; *Angew. Chem. Int. Ed.* **2001**, *40*, 1907 – 1910; ; b) A. Wacker, C. G. Yan, G. Kaltenpoth, A. Ginsberg, A. M. Arif, R. D. Ernst, H. Pritzkow, W. Siebert, *J. Organomet. Chem.* **2002**, *641*, 195 – 202; c) A. Weiss, H. Pritzkow, W. Siebert, *Eur. J. Inorg. Chem.* **2002**, 1607 – 1614; d) A. Wacker, H. Pritzkow, W. Siebert, *Eur. J. Inorg. Chem.* **1998**, 843 – 849; e) U. Kernbach, M. Ramm, P. Luger, W. P. Fehlhammer, *Angew. Chem.* **1996**, *108*, 333 – 335; *Angew. Chem. Int. Ed. Engl.* **1996**, *35*, 310 – 312; f) A. J. Arduengo III, D. Tapu, W. J. Marshall, *Angew. Chem.* **2005**, *117*, 7406 – 7410; *Angew. Chem. Int. Ed.* **2005**, *44*, 7240 – 7244.

[6] a) T. Deforth, M. Kaschke, H. Stock, H. Pritzkow, W. Siebert, *Z. Naturforsch. B* **1997**, *52*, 823 – 830; b) M. Enders, B. Gangnus, R. Hettrich, Z. Magos-Martin, M. Stephan, H. Pritzkow, W. Siebert, U. Zenneck, *Chem. Ber.* **1993**, *126*, 2197 – 2203.

[7] Crystallographic data: **1**: $C_{30}H_{45}B_2F_3N_2O_3S$, 193 K, $0.31\times0.26\times0.21$ mm^3, monoclinic, space group $P2_1/c$, $a=19.2460(17)$, $b=10.6805(10)$, $c=15.7888(14)$ Å, $\alpha=\gamma=90°$, $\beta=90.9307(15)°$, $V=3245.01(5)$ Å^3, $Z=4$, $\rho_{calcd}=1.212$ g cm^{-3}, $2.30=\theta=25.86°$, $R_1=0.0507$ ($I>2\sigma(I)$), $wR_2=0.1330$ (all data); residual electron density: 0.280/−0.276 e Å^{-3}. **2**: $C_{29}H_{44}B_2N_2$, 193 K, $0.65\times0.57\times0.23$ mm^3, orthorhombic, space group $Pbca$, $a=15.6004(13)$, $b=21.0211(18)$, $c=17.1099(15)$ Å, $\alpha=\gamma=\beta=90°$, $V=5611.0(8)$ Å^3, $Z=8$, $\rho_{calcd}=1.047$ g cm^{-3}, $2.27=\theta=26.36°$, $R_1=0.0472$ ($I>2\sigma(I)$), $wR_2=0.1415$ (all data); residual electron density: 0.287/−0.224 e Å^{-3}. **3**: $C_{37}H_{59}B_2LiN_2O_2$, 173 K, $0.16\times0.12\times0.08$ mm^3, monoclinic, space group $C2/c$, $a=12.227(4)$, $b=18.309(6)$, $c=16.603(3)$ Å, $\alpha=\gamma=90°$, $\beta=97.74(2)°$, $V=3683.0(18)$ Å^3, $Z=4$, $\rho_{calcd}=1.068$ g cm^{-3}, $3.30=\theta=27.50°$, $R_1=0.070$ ($I>2\sigma(I)$), $wR_2=0.209$ (all data); residual electron density: 0.53/−0.37 e Å^{-3}. $Mo_{K\alpha}$ radiation ($\lambda=0.71073$ Å). Non-hydrogen atoms were refined anisotropically. Hydrogen atoms were included at geometrically calculated positions and refined by using the riding model. CCDC-602682–602684 (**1**–**3**) contain the supplementary crystallographic data for this paper. These data can be obtained free of charge from The Cambridge Crystallographic Data Centre via www.ccdc.cam.ac.uk/data_request/cif.

[8] a) I. V. Stankevich, E. G. Gal'pern, R. Seto, *Russ. J. Phys. Chem.* **2003**, *77*, 768 – 773; b) R. J. Doerksen, A. J. Thakkar, *J. Phys. Chem. A* **1998**, *102*, 4679 – 4686; c) T. Kar, D. E. Elmore, S. Scheiner, *J. Mol. Struct.* **1997**, *392*, 65 – 74; d) S. T. Massey, R. W. Zoellner, *Inorg. Chem.* **1991**, *30*, 1063 – 1066; e) R. Hoffmann, *J. Chem. Phys.* **1964**, *40*, 2474 – 2480.

[9] a) R. Boese, A. H. Maulitz, P. Stellberg, *Chem. Ber.* **1994**, *127*, 1887 – 1889; b) C. A. Jaska, K. Temple, A. J. Lough, I. Manners, *J. Am. Chem. Soc.* **2003**, *125*, 9424 – 9434; c) T. Jäschke, M. Jansen, *Z. Anorg. Allg. Chem.* **2004**, *630*, 239 – 243.

[10] P. Schreyer, P. Paetzold, R. Boese, *Chem. Ber.* **1988**, *121*, 195 – 205; C. J. Carmalt, W. Clegg, A. H. Cowley, F. J. Lawlor, T. B. Marder, N. C. Norman, C. R. Rice, O. J. Sandoval, A. J. Scott, *Polyhedron* **1997**, *16*, 2325 – 2328.

[11] a) P. P. Power, *Appl. Organomet. Chem.* **2005**, *19*, 488 – 493; b) P. P. Power, *Chem. Commun.* **2003**, 2091 – 2101; c) J. A. C. Clyburne, N. McMullen, *Coord. Chem. Rev.* **2000**, *210*, 73 – 99; d) B. Twamley, S. T. Haubrich, P. P. Power, *Adv. Organomet. Chem.* **1999**, *44*, 1 – 65.

[12] a) G. Boche, C. Hilf, K. Harms, M. Marsch, J. C. W. Lohrenz, *Angew. Chem.* **1995**, *107*, 509 – 511; *Angew. Chem. Int. Ed. Engl.* **1995**, *34*, 487 – 489; b) A. Wacker, H. Pritzkow, W. Siebert, *Eur. J. Inorg. Chem.* **1998**, 843 – 849; c) A. J. Arduengo III, M. Tamm, J. C. Calabrese, F. Davidson, W. J. Marshall, *Chem. Lett.* **1999**, 1021 – 1022; d) R. Fränkel, C. Birg, U. Kernbach, T. Habereder, H. Nöth, W. P. Fehlhammer, *Angew. Chem.* **2001**, *113*, 1961 – 1964; *Angew. Chem. Int. Ed.* **2001**, *40*, 1907 – 1910; e) P. L. Arnold, S. A. Mungur, A. J. Blake, C. Wilson, *Angew. Chem.* **2003**, *115*, 6163 – 6166; *Angew. Chem. Int. Ed.* **2003**, *42*, 5981 – 5984; f) S. A. Mungur, S. T. Liddle, C. Wilson, M. J. Sarsfield, P. L. Arnold, *Chem. Commun.* **2004**, 2738 – 2739; g) P. L. Arnold, M. Rodden, K. M. Davis, A. C. Scarisbrick, A. J. Blake, C. Wilson, *Chem. Commun.* **2004**, 1612 – 1613.

[13] a) T. Maetzke, D. Seebach, *Helv. Chim. Acta* **1989**, *72*, 624 – 631; b) G. W. Rabe, R. D. Sommer, A. L. Rheingold, *Organometallics* **2000**, *19*, 5537 – 5540; c) N. J. Hardman, B. Twamley, M. Stender, R. Baldwin, S. Hino, B. Schiemenz, S. M. Kauzlarich, P. P. Power, *J. Organomet. Chem.* **2002**, *643–644*, 461 – 467; d) G. E. Wegner, R. J. F. Berger, A. Schier, H. Schmidbaur, *Z. Naturforsch. B* **2000**, *55*, 995 – 999; e) R. C. Crittendon, B. C. Beck, J. Su, X.-W. Li, G. H. Robinson, *Organometallics* **1999**, *18*, 156 – 160; f) G. S. Girolami, M. E. Riehl, K. S. Suslick, S. R. Wilson, *Organometallics* **1992**, *11*, 3907 – 3910; g) M. M. Olmstead, P. P. Power, *J. Organomet. Chem.* **1991**, *408*, 1 – 6.

[14] a) P. L. Arnold, M. Rodden, C. Wilson, *Chem. Commun.* **2005**, 1743 – 1745; b) P. L. Arnold, S. T. Liddle, *Organometallics* **2006**, *25*, 1485 – 1491.

[15] For an account of ELF analysis in quantifying the σ-donating properties of NHCs, see: G. Frison, A. Sevin, *J. Phys. Chem. A* **1999**, *103*, 10998 – 11003.

[16] a) S. Dapprich, G. Frenking, *J. Phys. Chem.* **1995**, *99*, 9352 – 9362; b) C. Boehme, G. Frenking, *Organometallics* **1998**, *17*, 5801 – 5809; c) G. Frenking, M. Solà, S. F. Vyboishchikov, *J. Organomet. Chem.* **2005**, *690*, 6178 – 6204.

 © 2006 Wiley-VCH Verlag GmbH & Co. KGaA, Weinheim

Asymmetric Catalysis

DOI: 10.1002/anie.200601540

Rh-Catalyzed Asymmetric Hydrogenation of α-Aryl Imino Esters: An Efficient Enantioselective Synthesis of Aryl Glycine Derivatives**

*Gao Shang, Qin Yang, and Xumu Zhang**

Enantiomerically pure α-amino acids and their derivatives are of great importance in pharmaceutical, biological and synthetic chemistry. An interesting class of these compounds are the chiral aryl glycines, which are important building blocks for many bioactive molecules such as amoxicillins,[1] nocardicins,[2] cephalecins,[3] and glycopeptide antibiotics.[4] A number of methods have been applied to synthesize these intermediates,[5] such as the Sharpless asymmetric aminohydroxylation,[5b] the catalytic enantioselective amination of enolate intermediates,[5c] and the asymmetric Strecker reaction.[5d,e] However, achieving regioselectivity has been a challenge in the asymmetric aminohydroxylation reaction, and in the enantioselective amination of enolates, high catalyst loading has been used with only moderate success. These problems prompted us to seek for an alternative approach to synthesize chiral aryl glycines. Herein, we report a highly enantioselective synthesis of a series of chiral aryl glycine derivatives by using the asymmetric hydrogenation of α-aryl imino esters with a Rh–tangphos catalyst (tangphos = 1,1′-di-*tert*-butyl-(2,2′)-diphospholane, see Scheme 1).

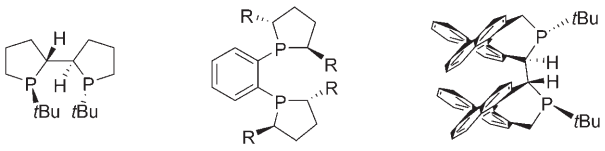

A: (*S,S,R,R*)-tangphos **B**: R = Et, (*R,R*)-Et-duphos **C**: R = Me, (*R,R*)-Me-duphos **D**: (*S*)-binapine

Scheme 1. Chiral ligands for asymmetric hydrogenation.

Asymmetric hydrogenation catalyzed by transition metals has been shown to be highly efficient in many syntheses.[6] A large number of α-alkyl amino acids and their derivatives have been prepared with high enantioselectivity from the asymmetric hydrogenation of α-dehydroamino acids or esters.[6] However, aryl glycines lacking the β-hydrogen atom cannot be synthesized in an analogous manner by hydrogenation of alkenes. Nevertheless, asymmetric hydrogenation of the C=N double bond in the corresponding α-imino acids or esters could be an alternative way to synthesize chiral aryl glycines. In fact, reduction of a C=N bond is the key step of transaminase in some biological transformations. Despite the great potential of this transformation, there have been very few reports of both good enantioselectivities and yields, because the imine substrates are difficult to prepare and also because the substrates show relatively poor reactivity toward hydrogenation.[7] Recently, Kadyrov et al. reported the synthesis of chiral α-*N*-benzylamino acids resulting from the reductive amination of keto acids, but the method proved less successful for aryl glycines.[7c] Amii and co-workers have also reported the asymmetric hydrogenation of α-fluorinated imino esters, but this method is successful for only a limited range of substrates.[7d]

We started our investigation using PMP-protected α-aryl imino esters **1** (Table 1) as the substrates, since they could be synthesized in one step and in high yield from the corresponding α-keto esters,[8] and the resulting products could be deprotected under mild conditions using cerium ammonium nitrate (CAN).[9] Moreover, the PMP-protected α-aryl imino esters are notably more stable than their corresponding imines. Key to achieving high enantioselectivity and turnover rates in the reduction of α-aryl imino esters is to find an effective catalyst. We initially examined the hydrogenation of **1a** using the Rh–tangphos catalyst, which was developed within our research group. Its electron-rich character and rigid, well-defined geometry offers both high activity and enantioselectivity in the asymmetric hydrogenation of a wide range of substrates.[6d,10]

Several commercially available chiral ligands were also screened for the hydrogenation of **1a** (Scheme 1). We achieved up to 93% *ee* with the Rh–tangphos catalyst,

Table 1: Asymmetric hydrogenation of α-imino ester **1a**.

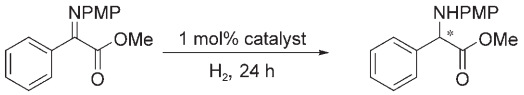

1a **2a**

Entry	Catalyst[a]	H_2 pressure [atm]	*T* [°C]	Solvent	Conv. [%][b]	*ee* [%][c]
1	**E**	30	25	CH_2Cl_2	>95	93
2	**F**	30	25	CH_2Cl_2	>95	83
3	**G**	30	25	CH_2Cl_2	29	75
4	**H**	30	25	CH_2Cl_2	70	85
5	**E**	50	25	CH_2Cl_2	>95	93
6	**E**	70	25	CH_2Cl_2	>95	93
7	**E**	50	50	CH_2Cl_2	>99	95
8	**E**	50	80	CH_2Cl_2	>99	91

[a] **E**: Rh[(*S,S,R,R*)-tangphos](cod)]BF_4; **F**: [Rh{(*S*)-binapine}(cod)]BF_4; **G**: [Rh{(*R,R*)-Me-duphos}(cod)]BF_4; **H**: [Rh{(*R,R*)-Et-duphos}(cod)]BF_4. [b] % Conversions were determined by ^1H NMR spectroscopy. [c] *ee* values were determined by chiral HPLC. PMP = *para*-methoxyphenyl, cod = cycloocta-1,5-diene.

[*] G. Shang, Q. Yang, Prof. X. Zhang
Department of Chemistry
The Pennsylvania State University
104 Chemistry Building, University Park, PA 16802 (USA)
Fax: (+1) 814-863-8403
E-mail: xumu@chem.psu.edu

[**] This work was supported by the National Institutes of Health (GM58832).

Supporting information for this article is available on the WWW under http://www.angewandte.org or from the author.

WILEY InterScience DISCOVER SOMETHING GREAT
© 2006 Wiley-VCH Verlag GmbH & Co. KGaA, Weinheim

(Table 1, entry 1), while 83% *ee* was obtained with the Rh–binapine catalyst (Table 1, entry 2). Hydrogenation with Me-duphos and Et-duphos offered moderate conversions and *ee* values (29% and 75% *ee* for **F**; 70% and 85% *ee* for **G**; Table 1, entries 3 and 4).

The effects of hydrogen pressure and reaction temperature on the hydrogenation were also studied. An increase in pressure from 30 to 70 atm had no apparent effect on the conversion or enantioselectivity of this transformation (Table 1, entries 1, 5, and 6). However, increasing the reaction temperature from 25 °C to 50 °C resulted in a slightly higher enantioselectivity (Table 1, entry 7), but the *ee* value dropped to 91% at 80 °C (Table 1, entry 8). An investigation into the effects of the solvent was also carried out. Common solvents such as THF, methanol, toluene, and acetone gave either poor conversion or low *ee* values. Only dichloromethane and trifluoroethanol resulted in both high conversion and enantioselectivity.

We examined the scope of the reaction using different α-imino esters under the optimized reaction conditions (Table 1, entry 7). Thus, we synthesized a number of α-imino esters **1a**–**1o** with various substituents on the aromatic ring or the ester group.[8] Asymmetric hydrogenation was performed using the [Rh{(*S*,*S*,*R*,*R*)-tangphos}(cod)]BF_4 complex as the catalyst precursor. Good conversions were observed for all substrates, with *ee* values ranging from 90% to 95%. Notably, 99% ee was achieved after one recrystallization when using **2a**. The electronic properties of the substituents had no apparent effect on the yields or the enantioselectivities. The presence of the sterically hindered naphthyl group resulted in slightly lower enantioselectivity (90% and 91% *ee*; Table 2, entries 11 and 12). A lower *ee* value was also observed with **1n** bearing an ethyl group at the R′ position (84% *ee*; Table 2, entry 14). To explore the efficiency of the catalyst for α-alkyl imino esters, **1o** was synthesized and hydrogenated under the optimized conditions. We were pleased to find that a high *ee* value was observed (94% *ee*; Table 2, entry 15).

To determine the potential of the asymmetric hydrogenation of α-aryl imino esters catalyzed by Rh–tangphos as a practical means to synthesize chiral α-aryl amino acid derivatives the hydrogenation of **1a** was carried out using a low catalyst loading (substrate/catalyst 1000:1) and a gram of the substrate (1.08 g, 4 mmol). Using catalyst made in situ and CH_2Cl_2 as the solvent, α-aryl amino ester **2a** was obtained in 82% yield (turnover number (TON) >820) and with 91% *ee*.[11] Moreover, the PMP group of **2a** could be easily removed by CAN in 86% yield, without affecting the *ee* value.[9]

In conclusion, a series of chiral aryl glycines were synthesized in high enantioselectivity in the first Rh-catalyzed asymmetric hydrogenation of the corresponding α-aryl imino esters using the tangphos ligand. This method is potentially useful for the preparation of a variety of chiral aryl glycines with high *ee* values and yields. However, the synthesis of the imine substrates and the relatively high catalytic loadings are limitations of this work. Further studies to improve the results and to expand the range of substrates that can be used will be reported in due course.

Table 2: Asymmetric hydrogenation of α-imino esters.

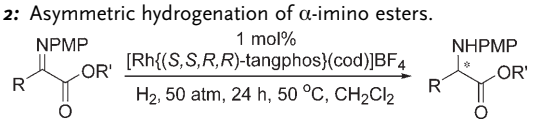

1a–o **2a–o**

Entry	R	R′	Product	Conv. [%][a]	*ee* [%][b]	Config.[c]
1	C_6H_5 (**1a**)	CH_3	**2a**	>99(99)	95(99)	*S*(−)
2	2-FC_6H_4 (**1b**)	CH_3	**2b**	>99	91	(−)
3	3-FC_6H_4 (**1c**)	CH_3	**2c**	>95	94	(−)
4	4-FC_6H_4 (**1d**)	CH_3	**2d**	>95	93	(−)
5	4-ClC_6H_5 (**1e**)	CH_3	**2e**	>99	92	(−)
6	4-BrC_6H_5 (**1f**)	CH_3	**2f**	>95	92	(−)
7	2-$CH_3OC_6H_4$ (**1g**)	CH_3	**2g**	>95	95	(−)
8	3-$CH_3OC_6H_4$ (**1h**)	CH_3	**2h**	>99	93	(−)
9	4-$CH_3OC_6H_5$ (**1i**)	CH_3	**2i**	>95	93	(−)
10	4-$CH_3C_6H_5$ (**1j**)	CH_3	**2j**	>99	93	(−)
11	*2*-naphthyl (**1k**)	CH_3	**2k**	>99	90	(−)
12	1-naphthyl (**1l**)	CH_3	**2l**	>95	91	(−)
13	3-nitro (**1m**)	CH_3	**2m**	>99	93	(−)
14	C_6H_5 (**1n**)	C_2H_5	**2n**	>95	84	(−)
15	cyclohexyl (**1o**)	CH_3	**2o**	84	94	(+)

[a] % Conversions were determined by ^{1}H NMR spectroscopy and the values in parentheses correspond to the yield of the isolated product. [b] *ee* values were determined by chiral HPLC and the value in parentheses corresponds to the *ee* value after one recrystallization. [c] Absolute configuration was determined by comparison of the sign of the optical rotation of the deprotected product (phenylglycine methyl ester) with (*S*)-phenylglycine methyl ester.

Experimental Section

General procedure for asymmetric hydrogenation of α-imino esters: $[Rh(cod)_2]BF_4$ (40.6 mg, 0.1 mmol) and (*S*,*S*,*R*,*R*)-tangphos (28.6 mg, 0.1 mmol) were dissolved in degassed dichloromethane (2 mL) in a Schlenk tube under N_2. After stirring the solution at room temperature for 1 h, degassed hexanes (10 mL) was added to precipitate the catalyst, which was filtered under nitrogen to give [Rh{(*S*,*S*,*R*,*R*)-tangphos}(cod)]BF_4 as an orange solid. The complex (52.0 mg, 88.9% yield) was stored in a nitrogen-filled glovebox until required. The complex (11.7 mg, 0.02 mmol) was dissolved in degassed dichloromethane (10 mL) in a glovebox and divided equally among 10 vials. To each of the vials was added **1** (0.2 mmol, substrate/catalyst 100:1) and the resulting mixture was transferred to an autoclave, which was then charged with H_2 (50 atm). The hydrogenation was performed at 50 °C for 24 h. After carefully releasing the hydrogen gas, the solvent was removed under reduced pressure. The crude product was purified through a plug of silica gel (eluting with a mixture of Hex/EtOAc, 10:1) to afford the aryl glycine **2**. The enantiomeric excess was determined by HPLC on a chiral stationary phase.

Received: April 19, 2006
Revised: July 11, 2006
Published online: August 28, 2006

Keywords: amino acids · asymmetric catalysis · enantioselectivity · hydrogenation · reduction

[1] E. M. Meyer, W. H. J. Boesten, H. E. Schoemaker, J. A. M. van Balken in *Biocatalysis in Organic Synthesis* (Eds.: J. Tramper,

 © 2006 Wiley-VCH Verlag GmbH & Co. KGaA, Weinheim

H. C. van der Plas, P. Linko), Elsevier, Amsterdam, **1985**, pp. 135 – 158.
[2] C. A. Townsend, A. M. Brown, *J. Am. Chem. Soc.* **1983**, *105*, 913 – 918.
[3] J. L. Spencer, E. H. Flynn, R. W. Roeske, F. Y. Siu, R. R. Chauvette, *J. Med. Chem.* **1966**, *9*, 746 – 750.
[4] A. V. Rama Rao, M. K. Gurjar, K. Laxma Reddy, A. S. Rao, *Chem. Rev.* **1995**, *95*, 2135 – 2167.
[5] a) R. M. Williams, J. A. Hendrix, *Chem. Rev.* **1992**, *92*, 889 – 917, and references therein; b) K. L. Reddy, K. B. Sharpless, *J. Am. Chem. Soc.* **1998**, *120*, 1207 – 1217; c) D. A. Evans, S. G. Nelson, *J. Am. Chem. Soc.* **1997**, *119*, 6452 – 6453, and references therein; d) M. S. Iyer, K. M. Gigstad, N. D. Namdev, M. Lipton, *J. Am. Chem. Soc.* **1996**, *118*, 4910 – 4911; e) C. A. Krueger, K. W. Kuntz, C. D. Dzierba, W. G. Wirschun, J. D. Gleason, M. L. Snapper, A. H. Hoveyda, *J. Am. Chem. Soc.* **1999**, *121*, 4284 – 4285; f) J. M. Vernier, L. S. Hegedus, D. B. Miller, *J. Org. Chem.* **1992**, *57*, 6914 – 6920; g) D. L. Boger, R. M. Borzilleri, S. Nukui, *J. Org. Chem.* **1996**, *61*, 3561 – 3565; h) H. Kunz, W. Sager, *Angew. Chem.* **1987**, *99*, 595 – 597; *Angew. Chem. Int. Ed. Engl.* **1987**, *26*, 557 – 559; i) M. J. O'Donnell, W. D. Bennett, *Tetrahedron* **1988**, *44*, 5389 – 5401; j) K. C. Nicolaou, H. J. Mitchell, N. F. Jain, N. Winssinger, R. Hughes, T. Bando, *Angew. Chem.* **1999**, *111*, 253 – 255; *Angew. Chem. Int. Ed.* **1999**, *38*, 240 – 244.
[6] a) P. A. Chaloner, M. A. Esteruelas, F. Joó, L. A. Oro, *Homogeneous Hydrogenation*, Kluwer, Dordrecht, **1994**; b) J. M. Brown, In *Comprehensive Asymmetric Catalysis*, *Vol. 1* (Eds.: E. N. Jacobsen, A. Pfaltz, H. Yamamoto), Springer, Berlin, **1999**, chap. 5.1; c) R. Noyori, *Asymmetric Catalysis in Organic Synthesis*, Wiley, New York, **1994**, chap. 2; d) W. Tang, X. Zhang, *Chem. Rev.* **2003**, *103*, 3029 – 3070.
[7] For reviews, see: a) F. Spindler, H.-U. Blaser in *Transition Metals for Organic Synthesis* (Eds.: M. Beller, C. Bolm), Wiley-VCH, Weinheim, **2004**, pp. 113 – 123; b) S. Kobayashi, H. Ishitani, *Chem. Rev.* **1999**, *99*, 1069 – 1094; c) R. Kadyrov, T. H. Riermeier, U. Dingerdissen, V. Tararov, A. Börner, *J. Org. Chem.* **2003**, *68*, 4067 – 4070; d) H. Abe, H. Amii, K. Uneyama, *Org. Lett.* **2001**, *3*, 313 – 315; e) M. J. Burk, J. E. Feaster, *J. Am. Chem. Soc.* **1992**, *114*, 6266 – 6267.
[8] Y. Niwa, M. Shimizu, *J. Am. Chem. Soc.* **2003**, *125*, 3720 – 3721.
[9] a) F. Palacios, D. Aparicio, J. García, E. Rodríguez, *Eur. J. Org. Chem.* **1998**, 1413 – 1423; b) D. Taniyama, M. Hasegawa, K. Tomioka, *Tetrahedron Lett.* **2000**, *41*, 5533 – 5536.
[10] a) W. Tang, X. Zhang, *Angew. Chem.* **2002**, *114*, 1682 – 1684; *Angew. Chem. Int. Ed.* **2002**, *41*, 1612 – 1614; b) Q. Dai, W. Yang, X. Zhang, *Org. Lett.* **2005**, *7*, 5343 – 5345; c) Q. Yang, W. Gao, J. Deng, X. Zhang, *Tetrahedron Lett.* **2006**, *47*, 821 – 823.
[11] See supporting information for more results and experimental details.

 © 2006 Wiley-VCH Verlag GmbH & Co. KGaA, Weinheim

Rearrangement

DOI: 10.1002/anie.200601959

Zirconocene-Catalyzed Reactions of Alkenyl-Substituted Enol Ethers**

José Barluenga, Lucía Álvarez-Rodrigo, Félix Rodríguez, and Francisco J. Fañanás*

Organozirconocene complexes[1] have become very useful tools in organic chemistry since the pioneering works of Schwartz[2] and Negishi.[3] Despite the extensive advances in this area that have been accomplished in recent years, very few catalytic processes involving the use of zirconocene complexes have been described.[4] Particularly noteworthy are those catalytic carbometalative processes developed mainly by Negishi[5] and Hoveyda.[6] Some years ago, we initiated a study of new cross-coupling reactions between organozirconocene complexes and heterosubstituted alkenes (principally enol ethers).[7] In this context, the extensive work by Marek and co-workers should also be remarked upon.[8] In an attempt to further develop this interesting chemistry, we decided to investigate intramolecular versions of the reaction of alkene–zirconocene complexes and enol ethers (Scheme 1).[9] Thus, we envisioned that alkenyl-substituted

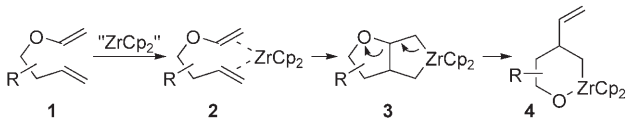

Scheme 1. Proposed intramolecular version of the reaction of alkene–zirconocene complexes and enol ethers. Cp = cyclopentadienyl.

enol ethers such as **1** could coordinate to a zirconocene complex generated in situ to give species **2**, which could react through a carbocyclization process to give **3**. These new complexes would evolve by a β-elimination of the alkoxy group to finally give **4,** which could be further functionalized by reaction with electrophiles. Thus, the general reaction from **1** to **4** would suppose an interesting isomerization–metalation

[*] Prof. Dr. J. Barluenga, L. Álvarez-Rodrigo, Dr. F. Rodríguez, Dr. F. J. Fañanás
Instituto Universitario de Química Organometálica "Enrique Moles", Unidad Asociada al C.S.I.C.
Universidad de Oviedo
Julián Clavería 8, 33006 Oviedo (Spain)
Fax: (+34) 98-510-3450
E-mail: barluenga@uniovi.es

[**] This research was supported by the DGICYT (BQU-2001-3853). The authors thank the MEC (FPU predoctoral grant for L.A.-R.) and the MEC and Fondo Social Europeo (contract under the "Ramón y Cajal" program for F.R.). Helpful comments from a referee are deeply acknowledged.

Supporting information for this article is available on the WWW under http://www.angewandte.org or from the author.

WILEY InterScience DISCOVER SOMETHING GREAT
© 2006 Wiley-VCH Verlag GmbH & Co. KGaA, Weinheim

process. The final goal of our investigation was the development of a catalytic method, and herein we describe a new zirconocene-catalyzed isomerization–magnesation reaction of alkene-substituted enol ethers.

At the outset of this study, the reaction was tested with stoichiometric amounts of zirconocene dichloride. Thus, the reactive low-valent zirconocene species were generated by the method developed by Negishi by mixing zirconocene dichloride [$ZrCl_2Cp_2$] with two equivalents of a Grignard or an organolithium reagent. This reaction gives the corresponding alkene–zirconocene complex, which after a ligand exchange reaction would generate the necessary complex **2**. Initially, the reaction was studied on the model alkenyl-substituted enol ether **1a** (Scheme 2 and Table 1). Thus, **1a** was treated with one equivalent of [$ZrCl_2Cp_2$] and two equivalents of different Grignard or organolithium reagents at −78 °C. The reaction was allowed to reach room temperature and after 1 h was quenched with silica gel. Thus, the expected alkenol **5a**, which is formed by simple hydrolysis of the corresponding zirconium complex **4** (see Scheme 1), was obtained together with different amounts of alcohol **6a**. Formation of **6a** could be explained by following the mechanism proposed by Marek and co-workers for the synthesis of alkenyl–zirconium complexes from acyclic enol ethers.[8c,i] Thus, we suppose the generation of vinyl–zirconium complex **7a**, as the by-product **6a** and a molecule of ethene are generated after hydrolysis.

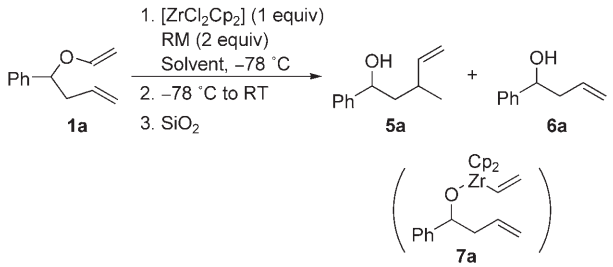

Scheme 2. Zirconocene-mediated reaction of enol ether **1a**.

Table 1: Products obtained from the zirconocene-mediated reaction of enol ether **1a** and different Grignard or organolithium reagents.

Entry	RM	Solvent	Product	Yield [%][a]	d.r. of **5a**[b]
1	EtMgBr	THF	**6a**	90	–
2	EtMgBr	Et_2O	**6a**	86	–
3	PrMgCl	THF	**5a/6a**	78/5	1:1
4	PrMgCl	Et_2O	**5a/6a**	66/5	1:1
5	BuLi	THF	**5a**	88	1:1
6	BuLi	Et_2O	**5a**	78	5:1[c]

[a] Yield based on starting material **1a**. [b] Determined by ^{1}H NMR spectroscopic analysis of the reaction crude product. [c] The major diastereoisomer was found to be the 1,3-*anti* isomer (see the Supporting Information).

As shown in Table 1, the formation of the desired compound **5a** or by-product **6a** was highly influenced by the structure of the Grignard or organolithium reagent used. Thus, we observed the exclusive formation of **6a** when ethylmagnesium bromide was used either in diethyl ether or THF (Table 1, entries 1 and 2). However, **5a** was obtained in 78% yield as a 1:1 mixture of diastereoisomers when propylmagnesium chloride was used in THF. A small amount of **6a** was also isolated (5% yield; Table 1, entry 3). Similar results, although with slightly lower yields, were obtained when this reaction was performed in diethyl ether (Table 1, entry 4). Finally, **5a** was obtained in 88% yield (1:1 mixture of diastereoisomers) by using butyllithium (Table 1, entry 5). However, the selectivity of the reaction improved and a 5:1 mixture of diastereoisomers was obtained when the reaction was carried out in diethyl ether (78% yield; Table 1, entry 6).[10] It is of note that formation of **6a** was completely suppressed by using butyllithium.

Once we had found the right conditions to direct the reaction to the isomerized compound **5a**, thus avoiding the formation of undesired **6a**, we decided to investigate the reaction under catalytic conditions with zirconium. We speculated that under catalytic conditions, the excess of organometallic reagents (Grignard or organolithium compounds) could react with intermediate **4** (see Scheme 1) through a double transmetalation reaction, thereby regenerating the catalytic zirconium species and forming a new organometallic reagent related to **4** (with magnesium or lithium instead of zirconium).

To find the optimum conditions, model compound **1a** was treated with an excess of the corresponding organometallic compound in the presence of catalytic amounts of commercially available zirconocene dichloride under various reaction conditions (Scheme 3 and Table 2). As the best results in the stoichiometric reactions were reached by using butyllithium, we started our catalytic studies with this organometallic ethylmagnesium bromide was used either in diethyl ether or THF (Table 2, entries 1 and 2). However, **5a** was obtained in 78% yield as a 1:1 mixture of diastereoisomers when propylmagnesium chloride was used in THF. A small amount of **6a** was also isolated (5% yield; Table 2, entry 3). Similar results, although with slightly lower yields, were obtained when this reaction was performed in diethyl ether (Table 2, entry 4). Finally, **5a** was obtained in 88% yield (1:1 mixture of diastereoisomers) by using butyllithium (Table 2, entry 5). However, the selectivity of the reaction improved and a 5:1 mixture of diastereoisomers was obtained when the reaction was carried out in diethyl ether (78% yield; Table 2, entry 6).[10] It is of note that formation of **6a** was completely suppressed by using butyllithium.

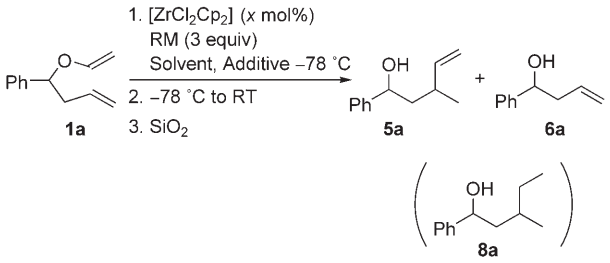

Scheme 3. Zirconocene-catalyzed reaction of enol ether **1a**.

Table 2: Zirconocene-catalyzed reaction of enol ether **1a** and different Grignard or organolithium reagents.

Entry	RM	[$ZrCl_2Cp_2$] [mol%]	Solvent	Additive	Products	Yield [%][a]	d.r. of **5a**
1	BuLi	5–25	THF[b]	–	polymer	–	–
2	EtMgBr	25	THF[b]	–	**6a/8a**	25/66	–
3	EtMgBr	5	THF[b]	–	**6a/8a**	5/85	–
4	PrMgCl	15	Et_2O	–	**5a/6a**	63/12	2:1
5	PrMgCl	15	THF	–	**5a/6a**	76/15	1:1
6	PrMgCl	5	Et_2O	PPh_3[c]	**5a**	62	2:1
7	PrMgCl	5	THF	PPh_3[c]	**5a**	82	1:1

[a] Yield of the isolated products based on starting material **1a**. [b] Similar results were found when Et_2O was used as the solvent. [c] 10 mol% of PPh_3 was used.

 © 2006 Wiley-VCH Verlag GmbH & Co. KGaA, Weinheim

reagent. However, we did not detect the formation of **5a** in any case attempted and mainly observed polymerization of the starting material (Table 2, entry 1). In consonance with the results of the stoichiometric reactions, by using ethylmagnesium bromide we observed the formation of **6a** along with different quantities of the new alcohol **8a**, depending on the amount of catalyst used (Table 2, entries 2 and 3). Formation of **8a** is easily explained by a simple zirconium-catalyzed carbomagnesiation of the double bond of **6a** and further hydrolysis. Fortunately, we observed the formation of the desired alkenol **5a** together with a small amount of **6a** (Table 2, entries 4 and 5) after only 1 h at room temperature when propylmagnesium chloride was employed in the presence of 20 mol% of $[ZrCl_2Cp_2]$. Both diethyl ether and THF were found to be appropriate solvents; however, a slightly higher diastereoselectivity was found in diethyl ether and higher yield in THF. The reaction times became longer when the amount of catalyst was lowered, and 24 h were required for complete conversion of the starting material when 5 mol% of $[ZrCl_2Cp_2]$ was used. We tried some reactions in the presence of an additive[11] in an attempt to totally avoid the formation of **6a** and to achieve complete conversions in shorter times. To our delight, under the optimal reaction conditions (5 mol% of $[ZrCl_2Cp_2]$, 10 mol% PPh_3), starting compound **1a** was completely transformed into isomerized alcohol **5a** after 8 h at room temperature in THF (82% yield of the isolated product, 1:1 mixture of diastereoisomers; Table 2, entry 7). The formation of **6a** was not observed under these conditions. Again, slightly higher selectivity, although lower yield, was found when diethyl ether was used as the solvent (Table 2, entry 6).

A proposed mechanism for the catalytic reaction is shown in Scheme 4. Initially, the zirconocene dichloride reacts with two equivalents of propylmagnesium chloride to form the corresponding dipropylzirconocene complex **9**, which further evolves, as described by Negishi, to give the propene–zirconocene complex **10** with the loss of a molecule of propane. This sixteen-electron complex reacts in the presence of the alkene-substituted enol ether **1a** through a ligand-exchange process, thus releasing a molecule of propene and forming the eighteen-electron zirconocene complex **2a**. A carbocyclization reaction furnishes the bicyclic complex **3a**. Subsequent elimination of zirconium alkoxide affords the intermediate **4a**.[12] Finally, a double magnesium–zirconium exchange gives the final organomagnesium compound **11** and regenerates the dipropylzirconocene complex **9**, which initiates a new catalytic cycle.[11]

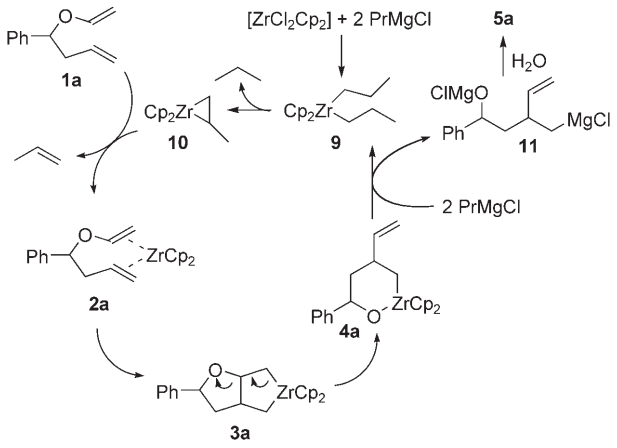

Scheme 4. Proposed mechanism for the zirconocene-catalyzed reaction of **1a**.

With an effective zirconocene-catalyzed reaction in hand, we investigated the scope of the process. Table 3 shows the results of the reactions performed under the optimized catalytic conditions previously found for **1a**. The reaction worked for a range of alkene-substituted enol ethers **1**, and the formed Grignard reagent could be trapped with different typical electrophiles for organomagnesium reagents. The final rearranged products **5** were isolated in high yield, but unfortunately the reaction gave mixtures of both possible diastereoisomers (d.r. ≈ 1:1, except for starting material **1e** d.r. = 14:1; however, the yield in this case was lower). Attempts to improve the selectivity by changing the reaction

Table 3: Zirconocene-catalyzed reaction of enol ethers **1** in the synthesis of functionalized alcohols **5**.

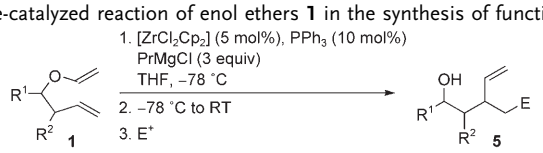

Entry	R^1	R^2	Starting diene	E^+(E)	Product	Yield [%][a]
1	Ph	H	**1a**	H_2O(H)	**5a**	82
2	Cy	H	**1b**	H_2O(H)	**5b**	93
3	Cy	H	**1b**	D_2O(D)	**5c**	85
4	Cy	H	**1b**	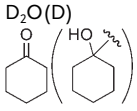	**5d**	56[b]
5	Cy	H	**1b**	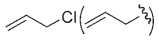	**5e**	67
5	heptyl	H	**1c**	H_2O(H)	**5f**	94
6	heptyl	H	**1c**	D_2O(D)	**5g**	84
7	heptyl	H	**1c**	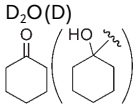	**5h**	64[b]
8	$Ph(CH_2)_2$	H	**1d**	H_2O(H)	**5i**	90
9	$Ph(CH_2)_2$	H	**1d**	D_2O(D)	**5j**	88
10	H	Ph	**1e**	H_2O(H)	**5k**	52[c]

[a] Yield of the isolated products based on starting material **1**; unless noted, an inseparable 1:1 mixture of the two possible diastereoisomers was obtained. [b] Both diastereoisomers from the 1:1 mixture were readily separated. [c] In this case, the formation of several other by-products was observed, and the major diastereoisomer was found to be (2*R**,3*R**)-3-methyl-2-phenyl-4-penten-1-ol (d.r. = 14:1; see the Supporting Information). E = electrophile.

 © 2006 Wiley-VCH Verlag GmbH & Co. KGaA, Weinheim

conditions were unsuccessful until now. For this reason, current efforts are being directed to find the appropriate catalyst or reaction conditions to achieve higher selectivities.

In summary, we have developed a new zirconocene-catalyzed isomerization–magnesation reaction of readily available alkene-substituted enol ethers.[13] The net process supposes the migration of the vinyl moiety of the enol ether to the internal position of the initial alkene and the magnesation of the terminal carbon atom of that initial alkene moiety (Scheme 5). The global reaction may also be considered as an

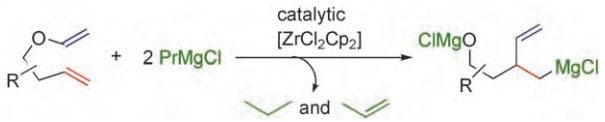

Scheme 5. General reaction of the zirconocene-catalyzed isomerization–magnesation process.

equivalent of the vinylmagnesation of terminal olefins, which is still a rather difficult challenge in the field of carbometallation of alkenes. This unprecedented process is one of the few examples of zirconocene-catalyzed reactions described in the literature. The reaction supposes a simple methodology to access to functionalized Grignard reagents which could find application in organic synthesis programs.

Received: May 17, 2006
Published online: August 23, 2006

Keywords: Grignard reagents · homogeneous catalysis · rearrangement · synthetic methods · zirconium

[1] a) *New Aspects of Zirconium-Containing Organic Compounds*, *Topics in Organomet. Chem.*, *Vol. 10* (Ed.: I. Marek), Springer, Berlin, **2005**; b) *Titanium and Zirconium in Organic Synthesis* (Ed.: I. Marek), Wiley-VCH, Weinheim, Germany, **2002**.

[2] For some representative examples, see: a) J. Schwartz, J. A. Labinger, *Angew. Chem.* **1976**, *88*, 402; *Angew. Chem. Int. Ed. Engl.* **1976**, *15*, 333; b) C. A. Bertelo, J. Schwartz, *J. Am. Chem. Soc.* **1976**, *98*, 262; c) D. W. Hart, T. F. Blackburn, J. Schwartz, *J. Am. Chem. Soc.* **1975**, *97*, 679; d) D. W. Hart, J. Schwartz, *J. Am. Chem. Soc.* **1974**, *96*, 8115.

[3] E. Negishi, T. Takahashi, *Acc. Chem. Res.* **1994**, *27*, 124, and references cited therein.

[4] Zirconocene complexes are known to catalyze polymerization reactions; for some other interesting zirconocene-catalyzed reactions, see: a) Y. Ikeuchi, T. Taguchi, Y. Hanzawa, *J. Org. Chem.* **2005**, *70*, 4354; b) J. Terao, S. A. Begum, A. Oda, N. Kambe, *Synlett* **2005**, 1783; c) V. Gandon, P. Bertus, J. Szymoniak, *Eur. J. Org. Chem.* **2001**, 3677; d) P. Wipf, S. Ribe, *Org. Lett.* **2001**, *3*, 1503; e) Y. Ura, R. Hara, T. Takahashi, *Chem. Commun.* **2000**, 875; f) F. Grepioni, S. Grilli, G. Martelli, D. Saoia, *J. Org. Chem.* **1999**, *64*, 3679; g) Y. Yamamura, M. Mori, *Tetrahedron Lett.* **1999**, *40*, 3221; h) K. Kasai, Y. Liu, R. Hara, T. Takahashi, *Chem. Commun.* **1998**, 1989; i) D. B. Millward, R. M. Waymouth, *Organometallics* **1997**, *16*, 1153; j) G. Dawson, C. A. Durrant, G. G. Kirk, R. J. Whitby, R. V. H. Jones, M. C. H. Standen, *Tetrahedron Lett.* **1997**, *38*, 2335; k) N. Uesaka, M. Mori, K. Okamura, T. Date, *J. Org. Chem.* **1994**, *59*, 4542; l) T. Takahashi, D. Y. Kondakov, N. Suzuki, *Organometallics* **1994**, *13*, 3411; m) D. P. Lewis, P. M. Muller, R. J. Whitby, R. V. H. Jones, *Tetrahedron Lett.* **1991**, *32*, 6797.

[5] For some recent papers, see: a) Z. Tan, E. Negishi, *Angew. Chem.* **2004**, *116*, 2971; *Angew. Chem. Int. Ed.* **2004**, *43*, 2911; b) E. Negishi, Z. Tan, B. Liang, T. Novak, *Proc. Natl. Acad. Sci. USA* **2004**, *101*, 5782; c) S. Huo, J. Shi, E. Negishi, *Angew. Chem.* **2002**, *114*, 2245; *Angew. Chem. Int. Ed.* **2002**, *41*, 2141.

[6] a) R. R. Cesati III, J. de Armas, A. H. Hoveyda, *Org. Lett.* **2002**, *4*, 395; b) J. de Armas, A. H. Hoveyda, *Org. Lett.* **2001**, *3*, 2097; c) J. de Armas, S. P. Kolis, A. H. Hoveyda, *J. Am. Chem. Soc.* **2000**, *122*, 5977; d) A. H. Hoveyda in *Titanium and Zirconium in Organic Synthesis* (Ed.: I. Marek), Wiley-VCH, Weinheim, Germany, **2002**, p. 180.

[7] a) J. Barluenga, F. Rodríguez, L. Álvarez-Rodrigo, F. J. Fañanás, *Chem. Soc. Rev.* **2005**, *34*, 762; b) J. Barluenga, A. Fernández, L. Álvarez-Rodrigo, F. Rodríguez, F. J. Fañanás, *Synlett* **2005**, 2513; c) J. Barluenga, L. Álvarez-Rodrigo, F. Rodríguez, F. J. Fañanás, *Angew. Chem.* **2004**, *116*, 4022; *Angew. Chem. Int. Ed.* **2004**, *43*, 3932; d) J. Barluenga, F. Rodríguez, L. Álvarez-Rodrigo, J. M. Zapico, F. J. Fañanás, *Chem. Eur. J.* **2004**, *10*, 109; e) J. Barluenga, F. Rodríguez, L. Álvarez-Rodrigo, F. J. Fañanás, *Chem. Eur. J.* **2004**, *10*, 101.

[8] a) N. Chinkov, A. Levin, I. Marek, *Angew. Chem.* **2006**, *118*, 479; *Angew. Chem. Int. Ed.* **2006**, *45*, 465; b) I. Marek, N. Chinkov, A. Levin, *Synlett* **2006**, 501; c) S. Farhat, I. Zouev, I. Marek, *Tetrahedron* **2004**, *60*, 1329; d) N. Chinkov, S. Majumdar, I. Marek, *J. Am. Chem. Soc.* **2003**, *125*, 13258; e) S. Farhat, I. Marek, *Angew. Chem.* **2002**, *114*, 1468; *Angew. Chem. Int. Ed.* **2002**, *41*, 1410; f) N. Chinkov, H. Chechik, S. Majumdar, A. Liard, I. Marek, *Synthesis* **2002**, 2473; g) N. Chinkov, S. Majumdar, I. Marek, *J. Am. Chem. Soc.* **2002**, *124*, 10282; h) A. Liard, J. Kaftanov, H. Chechik, S. Farhat, N. Morlender-Vais, C. Averbuj, I. Marek, *J. Organomet. Chem.* **2001**, *624*, 26; i) A. Liard, I. Marek, *J. Org. Chem.* **2000**, *65*, 7218.

[9] For interesting zirconocene-induced cocyclization–elimination reactions, see: a) D. R. Owen, R. J. Whitby, *Synthesis* **2005**, 2061; b) M. Kotora, G. Gao, Z. Li, T. Takahashi, *Tetrahedron Lett.* **2000**, *41*, 7905; c) D. B. Millward, R. M. Waymouth, *Organometallics* **1997**, *16*, 1153.

[10] The reaction led to a complex mixture of unidentified compounds when less polar solvents, such as toluene or hexane, were used. Similar variations on the diastereoselectivity by changing the solvent (from diethyl ether to THF) have been observed in related works; this solvent effect has been attributed to the chelation between the zirconium center and the solvent; for details, see: A. F. Houri, M. T. Didiuk, Z. Xu, N. R. Horan, A. H. Hoveyda, *J. Am. Chem. Soc.* **1993**, *115*, 6614.

[11] Addition of catalytic amounts of PPh_3 has led to important improvements in related processes; see for example ref. [4k]. The role played by the phosphine moiety in these processes is unclear; however, we hypothesize the possibility of a stabilization of sixteen-electron zirconocene complexes such as **9** and/or **10** (see Scheme 4). As these complexes are the real catalytic species of the reaction, their stabilization by coordination with the phosphine allows a longer half-life time of the catalyst and so, a lower zirconium loading is possible.

[12] Alternatively, a similar mechanism that involves the formation of a zirconate species by addition of PrMgCl to **3a** followed by Mg–Zr exchange, elimination of Mg alkoxide, further reaction with another molecule of PrMgCl, and a second transmetalation step to form **11** and **9** might also be suggested; see ref. [6].

[13] Starting enol ethers used in this work are very readily available on a large scale by Pd-catalyzed *O*-vinylation of the corresponding homoallyl alcohol; see: K. F. W. Hekking, F. L. van Delft, F. P. J. T. Rutjes, *Tetrahedron* **2003**, *59*, 6751.

 © 2006 Wiley-VCH Verlag GmbH & Co. KGaA, Weinheim

Organocatalysis

DOI: 10.1002/anie.200602221

A Chiral Primary Amine Thiourea Catalyst for the Highly Enantioselective Direct Conjugate Addition of α,α-Disubstituted Aldehydes to Nitroalkenes**

*Mathieu P. Lalonde, Yonggang Chen, and Eric N. Jacobsen**

The remarkable advances in the application of secondary amines as enantioselective catalysts are tied to the accessibility of divergent carbonyl activation pathways, either via nucleophilic enamines or electrophilic imminium ions, and to the highly effective stereoinduction that is achievable in reactions of such covalent intermediates.[1] By comparison, little progress has been made in the development of small-molecule chiral primary amine catalysts,[2] a fact that is attributable, at least in part, to unfavorable imine–secondary enamine equilibria.[3] Nevertheless, primary amine catalysis is effectively exploited by enzymes such as type I aldolases, decarboxylases, and dehydratases, each of which contain catalytically active lysine residues.[4] We became interested in the possible use of chiral primary amine thiourea derivatives in enamine catalysis motivated partly by their straightforward accessibility from chiral 1,2-diamines and partly by recent successes in the application of related tertiary amine thiourea frameworks as bifunctional catalysts in a wide variety of enantioselective catalytic reactions.[5–7] In this vein, Tsogoeva and Wei, as well as our own group, reported recently the successful application of primary amine thiourea catalysts to the addition of ketones to nitroalkenes.[8] The proven ability of secondary enamines to participate in conjugate addition reactions between sterically demanding partners[9] prompted us to examine the primary amine thiourea catalyzed addition of racemic α,α-disubstituted aldehydes to β-substituted Michael acceptors [Eq. (1); EWG = electron-withdrawing group] as a possible attractive solution to the challenging problem of generating chiral building blocks with contiguous quaternary and tertiary stereogenic centers.[10] We describe here the identification of primary amine thiourea derivatives as effective and general catalysts for the enantio- and diastereoselective conjugate addition of α,α-disubstituted aldehydes to nitroalkenes.

(1)

Despite extensive studies on secondary amine catalyzed conjugate additions of carbonyl compounds to nitroalkenes,[11,12] only two reports by Barbas and co-workers have addressed α,α-disubstituted aldehydes as potential nucleophilic partners.[13] We selected the challenging combination of 1-nitrohex-1-ene, a β-alkyl-substituted nitroalkene, and 2-phenylpropionaldehyde as model substrates for initial optimization studies,[14] with the hope that broad reaction scope would ensue. Among the primary amine thiourea catalysts examined, derivatives **1** and **3** were found to induce particularly high diastereo- and enantioselectivities (Table 1, entries 1 and 2). The best results were obtained using only a twofold excess of aldehyde relative to nitroalkene.[15,16] Diaminocyclohexane-derived catalyst **1** proved more broadly applicable and was selected for further optimization as catalyst **3**, derived from diphenylethylene diamine, was found subsequently to afford optimal results only in reactions involving 2-phenylpropionaldehyde.[17] Variation of standard reaction parameters (solvent, temperature, reagent ratios, concentration, catalyst loading) failed to improve the product yield, however, inclusion of controlled amounts of water led to significant improvements (Table 1, entry 1 vs 3–5, 2 vs 8).[18] Catalysts bearing a secondary amide (**1** and **3**) afforded higher levels of substrate conversion and product yields than their tertiary amide counterparts (e.g. **2**), while derivatives lacking an amide, as in **4**, were virtually inactive (Table 1, entry 7).

Table 1: Optimization studies.

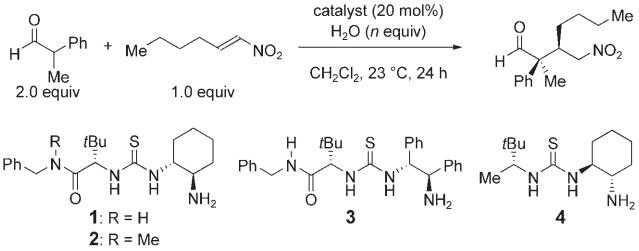

Entry	Catalyst	H_2O [equiv]	Yield [%][a]	d.r. (*syn*/*anti*)[a]	*ee* [%][b]
1	**1**	0	34	>10:1	96
2	**3**	0	93	>10:1	99
3	**1**	2.0	56	>10:1	96
4	**1**	5.0	64	>10:1	96
5	**1**	10	54	>10:1	96
6	**2**	5.0	31	>10:1	96
7	**4**	5.0	<5	–	–
8	**3**	5.0	100	>10:1	99

[a] Product yields determined by ^{1}H NMR spectroscopic analysis of the crude reaction mixture using trimethoxybenzene as an internal standard. [b] Determined by chiral HPLC analysis compared with authentic racemic material.

[*] M. P. Lalonde, Dr. Y. Chen, Prof. Dr. E. N. Jacobsen
Department of Chemistry and Chemical Biology
Harvard University
Cambridge, MA 02138 (USA)
Fax: (+1) 617-496-1880
E-mail: jacobsen@chemistry.harvard.edu

[**] This work was supported by the NIH (GM-43214 and P50 GM069721). M.P.L. gratefully acknowledges the NSERC and La Fondation Baxter et Alma Ricard for graduate scholarships. Dr. Richard Staples is acknowledged for the determination of the crystal structure of **22**.

Supporting information for this article is available on the WWW under http://www.angewandte.org or from the author.

InterScience
© 2006 Wiley-VCH Verlag GmbH & Co. KGaA, Weinheim

A wide range of α,α-disubstituted aldehyde/nitroalkene combinations were surveyed to determine the scope and limitations of the methodology. Excellent enantioselectivity and useful levels of diastereoselectivity were obtained with a variety of substrates by using catalyst **1** (Table 2). The highest levels of diastereoselectivity (>10:1 d.r.) were observed for aldehydes bearing phenyl or ethereal ($R^1 = OPh$ and *p*-$MeOC_6H_4CH_2O$) α-substituents. At the other extreme, only modest diastereoselectivities (2.1–4.7:1 d.r.) were obtained for adducts **9**, **10**, and **19–22**, results that were deemed

Table 2: Asymmetric addition of α,α-disubstituted aldehydes to nitroalkenes catalyzed by **1**.[26]

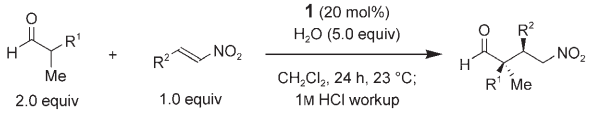

Product	Yield [%]	d.r. (*syn*/*anti*)	*ee* [%]	Product	Yield [%]	d.r. (*syn*/*anti*)	*ee* [%]
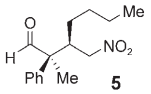 **5**	54	28:1	96 (*syn*)	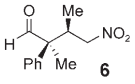 **6**	91	23:1	99 (*syn*)
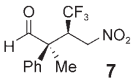 **7**	34	>50:1	97 (*syn*)	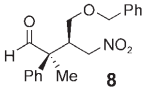 **8**	87	>50:1	99 (*syn*)
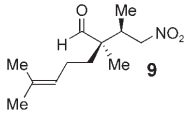 **9**	61	3.3:1	99 (*syn*) 99 (*anti*)	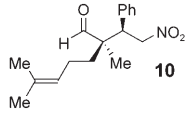 **10**	82	3.9:1	99 (*syn*) 99 (*anti*)
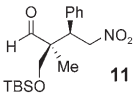 **11**	87	6.3:1	99 (*syn*) 98 (*anti*)	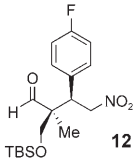 **12**	86	6.6:1	99 (*syn*) 94 (*anti*)
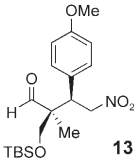 **13**	85	7.1:1	99 (*syn*) 95 (*anti*)	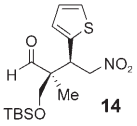 **14**	85	6.6:1	99 (*syn*) 97 (*anti*)
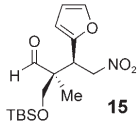 **15**	79	5.4:1	99 (*syn*) 95 (*anti*)	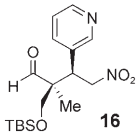 **16**	94	5.6:1	99 (*syn*) 96 (*anti*)
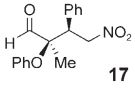 **17**	78	10.4:1	94 (*syn*) 92 (*anti*)	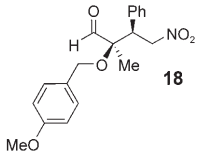 **18**	78	13:1	96 (*syn*)
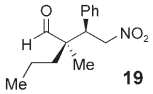 **19**	98	2.1:1	99 (*syn*) 97 (*anti*)	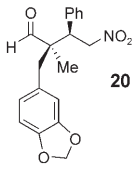 **20**	82	3.1:1	99 (*syn*) 99 (*anti*)
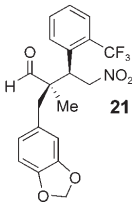 **21**	63	4.7:1	98 (*syn*) 92 (*anti*)	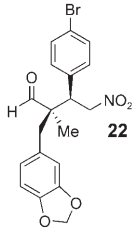 **22**	81	3.8:1	99 (*syn*) 99 (*anti*)

TBS = *tert*-butyldimethylsilyl.

© 2006 Wiley-VCH Verlag GmbH & Co. KGaA, Weinheim

satisfactory nonetheless given the minimal degree of steric differentiation between the aldehyde α-substituents. A variety of β-aryl-, β-heteroaryl-, and β-alkyl-substituted nitroalkenes underwent conjugate addition in good yields regardless of their electronic properties. The highly electrophilic 3,3,3-trifluoro-1-nitroprop-1-ene afforded adduct **7** in high *ee* and d.r. but only modest yield, a result ascribable to its susceptibility to effect alkylation of the primary amine group of **1**.[19,20]

As noted above, diphenylethylene diamine derivative **3** proved a more effective catalyst than **1** in conjugate additions involving 2-phenylpropionaldehyde as the nucleophilic partner. The effect was especially pronounced in additions to *trans*-β-nitrostyrene, which proceeded in substantially higher enantioselectivity and diastereoselectivity with catalyst **3** compared to **1** (Table 3, entries 1–2). Further modifications to the catalyst structure led to the observation that valine-derived catalyst **23** afforded almost identical results to *tert*-leucine-derived **3**, a significant outcome given the substantially lower cost of the precursor amino acid and also because this equivalence has not been observed in any other *tert*-leucine-derived thiourea-catalyzed reactions. The significantly diminished yield and *ee* values obtained with mismatched catalyst **24** point to the cooperative role of the stereochemistry of both the amino acid and the diamine in simultaneously defining conjugate addition selectivity and catalyst activity.

A catalytic cycle consistent with our experimental observations is depicted in Scheme 1. Tautomerization of imine **A**, resulting from the condensation of aldehyde and catalyst **1**, leads to the formation of an *E* or *Z* enamine. Preferred reaction via the thermodynamically favorable *E* enamine **B** is proposed to account for the observed diastereoselectivities.[21] Binding of the nitroalkene through only one oxygen atom allows the enamine to attain sufficiently close proximity for carbon–carbon bond formation to occur (intermediate **C**).[22] Proton transfer (**D** to **E**) followed by imine hydrolysis yields the product and regenerates the catalyst. Zwitterionic species analogous to **D** have been invoked in numerous studies concerning the mechanism of conjugate addition of enamines to nitroalkenes.[23] These intermediates may undergo hydrolysis to the nitroaldehyde product or collapse to 1,2-oxazine-*N*-oxide and cyclobutane intermediates **F** and **G**, respectively. Although 1,2-oxazine-*N*-oxides such as **F** undergo hydrolysis readily in the presence of atmospheric moisture,[23l] hydrolysis of cyclobutanes analogous to **G** requires strong aqueous acid.[23i,l] The beneficial role of water may lie in increasing turnover by eliminating a potential catalyst sink (formation of **F**) and accelerating imine (**E**) hydrolysis. However, cyclobutane **G** is unlikely to undergo hydrolysis under the catalytic conditions, and its irreversible formation may be responsible for catalyst deactivation.[24]

We have shown that chiral primary amine thiourea catalysts are highly effective in the addition of α,α-disubstituted aldehydes to nitroalkenes, generating synthetically versatile nitroaldehyde adducts. Simultaneous activation of both nucleophile and electrophile through a combination of effects typically associated with enzymes (approximation,

Table 3: Diphenylethylene diamine derived catalysts in the addition of 2-phenylpropionaldehyde to *trans*-β-nitrostyrene.

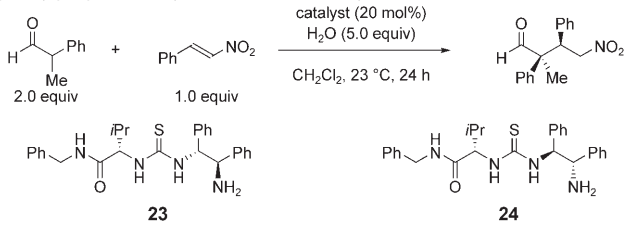

Entry	Catalyst	Yield [%][a]	d.r. (*syn*/*anti*)[a]	*ee* [%] (*syn*/*anti*)[b]
1	**1**	100	1.2:1	67:3
2	**3**	86	8.6:1	97:24
3	**23**	84	11.9:1	97:32
4	**24**	35	6.9:1	71:40[c]

[a] Product yields were determined by ^{1}H NMR spectroscopic analysis of the crude reaction mixture using trimethoxybenzene as an internal standard. [b] Determined by chiral HPLC analysis compared with authentic racemic material. [c] Products are of opposite absolute configuration to those in entries 1–3.

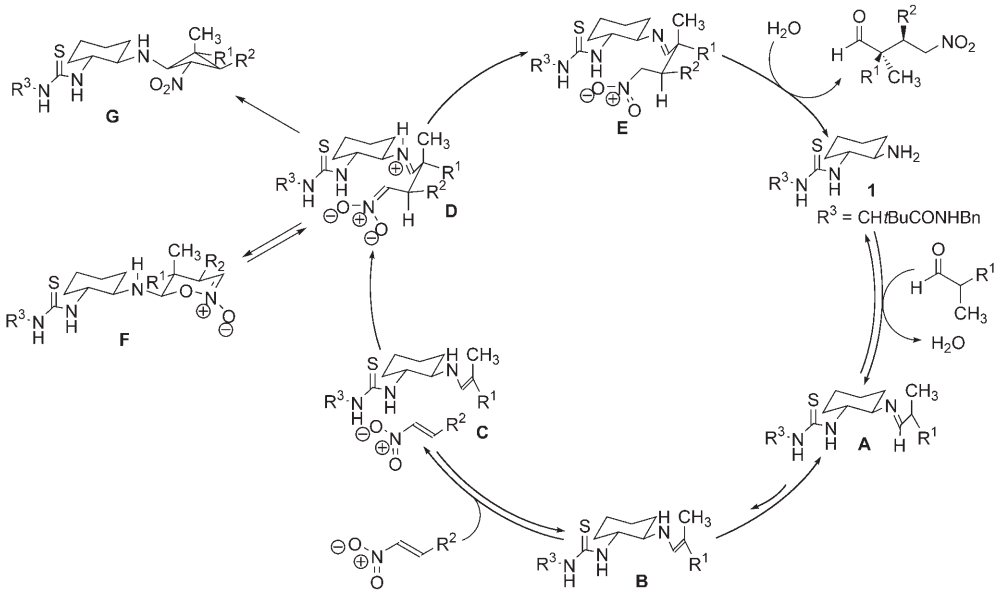

Scheme 1. Proposed mechanism for the asymmetric addition of α,α-disubstituted aldehydes to nitroalkenes catalyzed by **1**. Bn = benzyl.

© 2006 Wiley-VCH Verlag GmbH & Co. KGaA, Weinheim

hydrogen bonding, and covalent nucleophilic catalysis) allows this challenging transformation to take place under mild reaction conditions and with broad substrate scope. Interestingly, and in contrast to many enzymes, these bifunctional catalysts function by sequestering substrates from hydrophobic organic solvents into hydrophilic active sites. This study adds to a growing body of evidence suggesting that dual-activation catalysis with simple bifunctional organic frameworks holds substantial promise for asymmetric synthesis.[25] Our current efforts are focused on further development of conjugate addition reactions promoted by thiourea amine derivatives, as well as on the design of new bifunctional frameworks for use in asymmetric catalysis.

Experimental Section

(2*S*,3*R*)-2,3-Dimethyl-4-nitro-2-phenylbutanal (**6**): Under a positive pressure of nitrogen at room temperature, thiourea catalyst **1** (75.3 mg, 0.20 mmol, 20 mol%) was loaded into an oven-dried 25-mL round-bottomed flask equipped with a magnetic stir bar, rubber septum, and nitrogen inlet. The catalyst was dissolved in dichloromethane (6.7 mL). Water (90.1 μL, 5.0 mmol, 5.0 equiv) and 2-phenylpropionaldehyde (265.4 μL, 2.0 mmol, 2.0 equiv) were subsequently added by syringe. The resulting clear colorless solution was stirred for approximately 2 min. Addition of 1-nitropropene (87.1 mg, 1.0 mmol, 1.0 equiv) by syringe produced a light yellow solution. The rubber septum was quickly replaced with a yellow polyethylene stopper (to avoid absorption of dichloromethane by the septum), and the reaction mixture was stirred for 24 h at room temperature. Aqueous hydrochloric acid solution (1M, 7 mL) was added to the reaction flask, and the resulting biphasic mixture was stirred vigorously for 5 min at room temperature. The biphasic mixture was transferred to a separating funnel, and additional portions of dichloromethane (30 mL) and 1M HCl (30 mL) were added. The phases were separated, and the aqueous layer was washed with dichloromethane (30 mL). The organic layers were combined and washed with saturated aqueous sodium bicarbonate solution (30 mL), saturated aqueous sodium chloride solution (30 mL), dried over anhydrous sodium sulfate, filtered, and concentrated under reduced pressure. The resulting yellow residue was purified by chromatography on silica (8% diethyl ether/hexanes), providing the title compound as a colorless/light yellow liquid in 91% yield (201.1 mg) in 23:1 diastereomeric ratio and with 99% *ee* (major diastereomer) as determined by HPLC (Chiralpak AD-H, 2.0% propan-2-ol/hexanes, 1.0 mL min^{-1}, 230 nm; t_r(minor enantiomer, minor diastereomer) = 11.83 min, t_r(major enantiomer, minor diastereomer) = 12.87 min, t_r(minor enantiomer, major diastereomer) = 13.82 min, t_r(major enantiomer, major diastereomer) = 15.48 min). $[\alpha]_D^{25} = +88.6°$ (c = 0.0200 g/2.0 mL, chloroform); ^{1}H NMR (400 MHz, $CDCl_3$): $\delta = 9.47$ (1H, s), 7.42 (2H, t, $J = 7.3$ Hz), 7.34 (1H, t, $J = 7.3$ Hz), 7.24 (2H, d, $J = 7.3$ Hz), 4.57 (1H, dd, $J = 3.3$, 12.0 Hz), 4.19 (1H, dd, $J = 10.6$, 12.0 Hz), 3.17 (1H, m), 1.48 (3H, s), 0.81 ppm (3H, d, $J = 7.0$ Hz); ^{13}C NMR (100 MHz, $CDCl_3$): $\delta = 200.6$, 137.4, 129.4, 128.2, 127.4, 78.8, 55.9, 37.1, 14.6, 13.2 ppm; IR (neat): $\tilde{\nu} = 3060$ (w), 2981 (m), 2819 (w), 2719 (w), 1722 (s), 1533 (s), 1496 (m), 1446 (m), 1377 (s), 763 (m), 702 (m); HRMS (ESI): calcd for $[C_{12}H_{15}NO_3+NH_4]^+$: 239.1396; found: 239.1402.

Received: June 2, 2006
Published online: August 28, 2006

Keywords: amines · asymmetric catalysis · conjugate addition · organocatalysis

[1] For a timely review, see: B. List, *Chem. Commun.* **2006**, 819–824.

[2] a) S. Pizzarello, A. L. Weber, *Science* **2004**, *303*, 1151; b) F. Tanaka, R. Thayumanavan, N. Mase, C. F. Barbas III, *Tetrahedron Lett.* **2004**, *45*, 325–328; c) A. Córdova, I. Ibrahem, J. Casas, H. Sundén, M. Engqvist, E. Reyes, *Chem. Eur. J.* **2005**, *11*, 4772–4784; d) M. Amedjkouh, *Tetrahedron: Asymmetry* **2005**, *16*, 1411–1414; e) A. Córdova, W. Zou, I. Ibrahem, E. Reyes, M. Engqvist, W.-W. Liao, *Chem. Commun.* **2005**, 3586–3588; f) W. Zou, I. Ibrahem, P. Dziedzic, H. Sundén, A. Córdova, *Chem. Commun.* **2005**, 4946–4948; g) I. Ibrahem, W. Zou, M. Engqvist, Y. Xu, A. Córdova, *Chem. Eur. J.* **2005**, *11*, 7024–7029; h) A. Bassan, W. Zou, E. Reyes, F. Himo, A. Córdova, *Angew. Chem.* **2005**, *117*, 7190–7194; *Angew. Chem. Int. Ed.* **2005**, *44*, 7028–7032; i) Y. Xu, A. Córdova, *Chem. Commun.* **2006**, 460–462; j) Y. Xu, W. Zou, H. Sundén, I. Ibrahem, A. Córdova, *Adv. Synth. Catal.* **2006**, *348*, 418–424.

[3] a) E. D. Bergmann, E. Zimkin, S. Pinchas, *Rec. Trav. Chim.* **1952**, *71*, 168–191; b) E. D. Bergmann, Y. Hirshberg, E. Zimkin, S. Pinchas, *Rec. Trav. Chim.* **1952**, *71*, 192–199; c) E. D. Bergmann, E. Meeron, Y. Hirshberg, S. Pinchas, *Rec. Trav. Chim.* **1952**, *71*, 200–212; d) B. Witkop, *J. Am. Chem. Soc.* **1956**, *78*, 2873–2882; e) M. Pfau, C. Ribière, *J. Chem. Soc. D* **1970**, 66–67; f) R. A. Clark, D. C. Parker, *J. Am. Chem. Soc.* **1971**, *93*, 7257–7261; g) B. De Jeso, J.-C. Pommier, *J. Chem. Soc. Chem. Commun.* **1977**, 565–566; h) B. De Jeso, J.-C. Pommier, *J. Organomet. Chem.* **1977**, *137*, 23–29; i) R. Knorr, A. Weiss, P. Löw, E. Räpple, *Chem. Ber.* **1980**, *113*, 2462–2489; j) D. R. Boyd, W. B. Jennings, L. C. Waring, *J. Org. Chem.* **1986**, *51*, 992–995; k) B. Capon, Z.-P. Wu, *J. Org. Chem.* **1990**, *55*, 2317–2324.

[4] D. J. Hupe in *New Comprehensive Biochemistry, Vol. 6* (Ed.: M. I. Page), Elsevier, Amsterdam, **1984**, pp. 271–301.

[5] a) T. Okino, Y. Hoashi, Y. Takemoto, *J. Am. Chem. Soc.* **2003**, *125*, 12672–12673; b) T. Okino, S. Nakamura, T. Furukawa, Y. Takemoto, *Org. Lett.* **2004**, *6*, 625–627; c) Y. Hoashi, T. Yabuta, Y. Takemoto, *Tetrahedron Lett.* **2004**, *45*, 9185–9188; d) T. Okino, Y. Hoashi, T. Furukawa, X. Xu, Y. Takemoto, *J. Am. Chem. Soc.* **2005**, *127*, 119–125; e) A. Berkessel, F. Cleemann, S. Mukherjee, T. N. Müller, J. Lex, *Angew. Chem.* **2005**, *117*, 817–821; *Angew. Chem. Int. Ed.* **2005**, *44*, 807–811; f) Y. Hoashi, T. Okino, Y. Takemoto, *Angew. Chem.* **2005**, *117*, 4100–4103; *Angew. Chem. Int. Ed.* **2005**, *44*, 4032–4035; g) A. Berkessel, F. Cleemann, S. Mukherjee, *Angew. Chem.* **2005**, *117*, 7632–7635; *Angew. Chem. Int. Ed.* **2005**, *44*, 7466–7469; h) A. Berkessel, S. Mukherjee, F. Cleemann, T. N. Müller, J. Lex, *Chem. Commun.* **2005**, 1898–1900; i) A. P. Dove, R. C. Pratt, B. G. G. Lohmeijer, R. M. Waymouth, J. L. Hedrick, *J. Am. Chem. Soc.* **2005**, *127*, 13798–13799; j) B. Vakulya, S. Varga, A. Csámpal, T. Soós, *Org. Lett.* **2005**, *7*, 1967–1969; k) B.-J. Li, L. Jiang, M. Liu, Y.-C. Chen, L.-S. Ding, Y. Wu, *Synlett* **2005**, 603–606; l) S. H. McCooey, S. J. Connon, *Angew. Chem.* **2005**, *117*, 6525–6528; *Angew. Chem. Int. Ed.* **2005**, *44*, 6367–6370; m) J. Ye, D. J. Dixon, P. S. Hynes, *Chem. Commun.* **2005**, 4481–4483; n) D. E. Fuerst, E. N. Jacobsen, *J. Am. Chem. Soc.* **2005**, *127*, 8964–8965; o) J. Wang, H. Li, X. Yu, L. Zu, W. Wang, *Org. Lett.* **2005**, *7*, 4293–4296; p) J. Wang, H. Li, W. Duan, L. Zu, W. Wang, *Org. Lett.* **2005**, *7*, 4713–4716; q) X. Xu, T. Furukawa, T. Okino, H. Miyabe, Y. Takemoto, *Chem. Eur. J.* **2006**, *12*, 466–476.

[6] For reviews concerning asymmetric catalysis by chiral thioureas (including tertiary amine thiourea derivatives), see: a) S. J. Connon, *Chem. Eur. J.* **2006**, *12*, 5418–5427; b) M. S. Taylor, E. N. Jacobsen, *Angew. Chem.* **2006**, *118*, 1550–1573; *Angew. Chem. Int. Ed.* **2006**, *45*, 1520–1543; c) P. R. Schreiner, *Chem. Soc. Rev.* **2003**, *32*, 289–296; d) Y. Takemoto, *Org. Biomol. Chem.* **2005**, *3*, 4299–4306.

 © 2006 Wiley-VCH Verlag GmbH & Co. KGaA, Weinheim

[7] Although thorough mechanistic investigations have as yet not been reported, tertiary amine thiourea catalysts are generally proposed to function by cooperative general acid/general base mechanisms reminiscent of more complex enzymatic systems, wherein reactivity and selectivity are imparted through binding, activation, and proper positioning of distinct substrates. For a discussion of the aforementioned concepts in enzyme catalysis, see: a) T. C. Bruice in *Enzymes*, *Vol. 2*, 3rd ed. (Ed.: P. D. Boyer), Academic Press, New York, **1970**, pp. 217–279; b) R. A. Copeland, *Enzymes: A Practical Introduction to Structure, Mechanism, and Data Analysis*, 2nd ed., Wiley, New York, **2000**, pp. 146–187.

[8] a) S. B. Tsogoeva, S. Wei, *Chem. Commun.* **2006**, 1451–1453; b) H. Huang, E. N. Jacobsen, *J. Am. Chem. Soc.* **2006**, *128*, 7170–7171.

[9] J. d'Angelo, D. Desmaële, F. Dumas, A. Guingant, *Tetrahedron: Asymmetry* **1992**, *3*, 459–505, and references therein.

[10] For alternative asymmetric catalytic approaches to the preparation of compounds with contiguous quaternary and tertiary stereogenic centers, see: a) Y. Hamashima, D. Hota, M. Sodeoka, *J. Am. Chem. Soc.* **2002**, *124*, 11240–11241; b) M. S. Taylor, E. N. Jacobsen, *J. Am. Chem. Soc.* **2003**, *125*, 11204–11205; c) M. S. Taylor, D. N. Zalatan, A. M. Lerchner, E. N. Jacobsen, *J. Am. Chem. Soc.* **2005**, *127*, 1313–1317; d) H. Li, Y. Wang, L. Tang, F. Wu, X. Liu, C. Guo, B. M. Foxman, L. Deng, *Angew. Chem.* **2005**, *117*, 107–110; *Angew. Chem. Int. Ed.* **2005**, *44*, 105–108; e) F. Wu, H. Li, L. Deng, *Angew. Chem.* **2006**, *118*, 961–964; *Angew. Chem. Int. Ed.* **2006**, *45*, 947–950.

[11] For secondary amine catalyzed additions of unbranched aldehydes to nitroalkenes, see: a) J. M. Betancort, C. F. Barbas III, *Org. Lett.* **2001**, *3*, 3737–3740; b) A. Alexakis, O. Andrey, *Org. Lett.* **2002**, *4*, 3611–3614; c) O. Andrey, A. Alexakis, A. Tomassini, G. Bernardinelli, *Adv. Synth. Catal.* **2004**, *346*, 1147–1168; d) P. Kotrusz, S. Toma, H.-G. Schmalz, A. Adler, *Eur. J. Org. Chem.* **2004**, 1577–1583; e) W. Wang, J. Wang, H. Li, *Angew. Chem.* **2005**, *117*, 1393–1395; *Angew. Chem. Int. Ed.* **2005**, *44*, 1369–1371; f) Y. Hayashi, H. Gotoh, T. Hayashi, M. Shoji, *Angew. Chem.* **2005**, *117*, 4284–4287; *Angew. Chem. Int. Ed.* **2005**, *44*, 4212–4215.

[12] For a review of asymmetric conjugate additions to nitroalkenes, see: O. M. Berner, L. Tedeschi, D. Enders, *Eur. J. Org. Chem.* **2002**, 1877–1894.

[13] a) N. Mase, R. Thayumanavan, F. Tanaka, C. F. Barbas III, *Org. Lett.* **2004**, *6*, 2527–2530; b) N. Mase, K. Watanabe, H. Yoda, K. Tanabe, F. Tanaka, C. F. Barbas III, *J. Am. Chem. Soc.* **2006**, *128*, 4966–4967.

[14] Secondary enamines conjugated to aromatic systems are known to display low reactivity (see Ref. [9]). Relative to nitrostyrene derivatives, inferior product yields have been reported in additions of aldehydes to β-alkyl-substituted nitroalkenes (see Refs. [11a, c–e]).

[15] Direct Michael additions to nitroalkenes promoted by secondary amine catalysts typically require large (e.g. tenfold) excess of aldehyde due to competing aldol pathways (see Ref. [11]).

[16] 2-Phenylpropionaldehyde was recovered in 2.5% *ee*, thus indicating that a simple kinetic resolution mechanism is not operative.

[17] The addition of 2-methylvaleraldehyde to *trans*-β-nitrostyrene catalyzed by 20 mol% **3** proceeded with less than 10% conversion.

[18] The benefit of added water has been observed in other primary amine catalyzed transformations (see references [2c–j, 8a]).

[19] For the conjugate addition of α-amino acid esters to *trans*-3,3,3-trifluoro-1-nitropropene, see: M. Molteni, A. Volonterio, M. Zanda, *Org. Lett.* **2003**, *5*, 3887–3890.

[20] The addition of amines to nitroalkenes has been extensively studied with very few stable adducts isolated. Anilines and electron-deficient nitroalkenes lead to relatively stable adducts. For representative studies, see: a) D. E. Worrall, *J. Am. Chem. Soc.* **1927**, *49*, 1598–1605; b) R. L. Heath, J. D. Rose, *J. Chem. Soc.* **1947**, 1486–1489; c) F. Brower, H. Burkett, *J. Am. Chem. Soc.* **1953**, *75*, 1082–1084; d) J. C. Sowden, A. Kirkland, K. O. Lloyd, *J. Org. Chem.* **1963**, *28*, 3516–3518; e) É. S. Lipina, Z. F. Pavlova, T. Y. Paperno, V. V. Perekalin, L. V. Prikhod'ko, *Zh. Org. Khim.* **1970**, *6*, 1123–1129.

[21] Diastereomers are assumed to arise from competitive reaction of *E* and *Z* enamines rather than poor nitroalkene facial selectivity. Consistent with this notion, catalyst **1** promotes the reaction of nitrostyrene with isobutyraldehyde in 99% *ee* (see Supporting Information for details).

[22] For a relevant analysis, see: D. A. Yalalov, S. B. Tsogoeva, S. Schmatz, *Adv. Synth. Catal.* **2006**, *348*, 826–832.

[23] a) K. C. Brannock, A. Bell, R. D. Burpitt, C. A. Kelly, *J. Org. Chem.* **1964**, *29*, 801–812; b) M. E. Kuehne, L. Foley, *J. Org. Chem.* **1965**, *30*, 4280–4284; c) A. Risaliti, S. Fatutta, M. Forchiassin, E. Valentin, *Tetrahedron Lett.* **1966**, *7*, 1821–1825; d) A. Risaliti, M. Forchiassin, E. Valentin, *Tetrahedron Lett.* **1966**, *7*, 6331–6335; e) A. T. Nielsen, T. G. Archibald, *Tetrahedron* **1970**, *26*, 3475–3485; f) D. Seebach, J. Golinski, *Helv. Chim. Acta* **1981**, *64*, 1413–1423; g) S. J. Blarer, W. B. Schweizer, D. Seebach, *Helv. Chim. Acta* **1982**, *65*, 1637–1654; h) S. J. Blarer, D. Seebach, *Chem. Ber.* **1983**, *116*, 3086–3096; i) D. Seebach, A. K. Beck, J. Golinski, J. N. Hay, T. Laube, *Helv. Chim. Acta* **1985**, *68*, 162–172; j) F. Felluga, P. Nitti, G. Pitacco, E. Valentin, *Tetrahedron* **1989**, *45*, 2099–2108; k) F. Felluga, P. Nitti, G. Pitacco, E. Valentin, *Tetrahedron* **1989**, *45*, 5667–5678; l) F. Felluga, P. Nitti, G. Pitacco, E. Valentin, *J. Chem. Soc. Perkin Trans. 1* **1992**, 2331–2335.

[24] See Supporting Information for experimental evidence for the formation of **G**.

[25] For a discussion of dual activation within the context of asymmetric catalysis by chiral hydrogen-bond donors, see Ref. [6b].

[26] Yields are of isolated products after column chromatography. Diastereomeric ratios and enantiomeric excesses were determined by SFC or HPLC analysis compared with authentic racemic material. The absolute configuration of **22** was determined by X-ray crystallography, whereas those of **6–21** were inferred.

 © 2006 Wiley-VCH Verlag GmbH & Co. KGaA, Weinheim

Si–Si Multiple Bonds

DOI: 10.1002/anie.200602214

Fused Tricyclic Disilenes with Highly Strained Si–Si Double Bonds: Addition of a Si–Si Single Bond to a Si–Si Double Bond**

Ryoji Tanaka, Takeaki Iwamoto, and Mitsuo Kira**

Dimerization of a silylene (divalent silicon compound) to the corresponding disilene (silicon–silicon doubly bonded compound) and its reverse reaction constitute an important pair of chemical processes in organosilicon chemistry.[1] The first stable disilene, tetramesityldisilene, was synthesized by the dimerization of photochemically generated dimesitylsilylene by West et al. in 1981.[2] Okazaki, Tokitoh, et al. have reported that a stable tetraaryl disilene dissociates into the corresponding silylene in solution at higher temperatures.[3,4] We have found that isolable dialkyl silylene **1**,[5] which is protected kinetically by the bulky helmet substituent 1,1,4,4-tetrakis(trimethylsilyl)butane-1,4-diyl, does not dimerize to the corresponding disilene either in solution or in the solid state. During our efforts to obtain compounds tethering two dialkyl silylene moieties, we have achieved unexpectedly the synthesis of fused tricyclic disilenes with two dialkyl silylene units, *trans*- and *cis*-**2**. Neither *cis*-**2** nor *trans*-**2** dissociates into the corresponding silylene. Instead, upon heating, *trans*-**2** undergoes unprecedented intramolecular $[2_s+2_a]$ cycloaddition of the Si–Si single bond to the Si–Si double bond to give a tetracyclic compound.

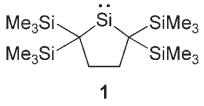

1

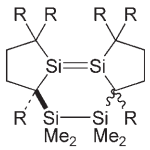

trans-**2**, *cis*-**2** (R = $SiMe_3$)

Fused tricyclic disilenes *trans*-**2** and *cis*-**2** were synthesized as red-purple crystals in 57% yield and yellow crystals in 44% yield, respectively, according to the reaction sequences shown in Scheme 1.[6] Disilenes *trans*-**2** and *cis*-**2** were identified by NMR spectroscopy and X-ray crystallographic analyses.

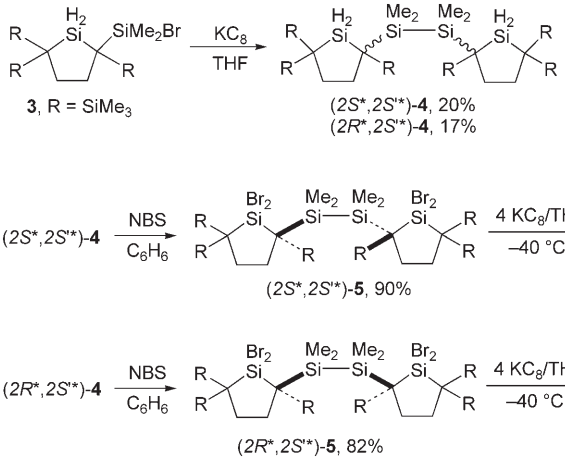

Scheme 1. Synthesis of tricyclic disilenes *trans*-**2** and *cis*-**2**. NBS = *N*-bromosuccinimide.

Figures 1 and 2 show ORTEP drawings of *trans*-**2** and *cis*-**2**, respectively.[7] The geometry around the Si=Si bond in *trans*-**2** is highly distorted. The Si=Si bond length of *trans*-**2** (2.2687(7) Å) is the second largest among all the reported disilenes; the largest was observed in (*Z*)-diaminodisilyl disilene **6** (2.2890(14) Å), reported by West and co-workers.[8]. The Si=Si bond in *trans*-**2** adopts a strongly *trans*-bent and twisted geometry with bent angles θ of 32.9 and 30.9° and a twist angle τ of 42.5°.[9,10] The central six-membered ring of *trans*-**2** adopts a twist-boat conformation. In contrast, the

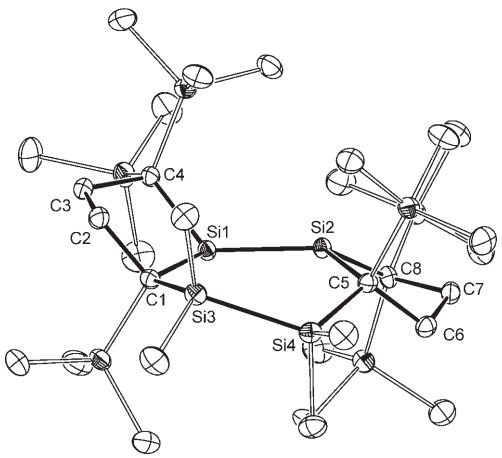

Figure 1. ORTEP drawing of *trans*-**2**. All hydrogen atoms are omitted for clarity. Thermal ellipsoids are shown at the 30% probability level. Selected bond lengths [Å] and angles [°]: Si1-Si2 2.2687(7), Si3-Si4 2.3745(8), Si1-C4 1.916(2), Si1-C1 1.937(2), Si2-C5 1.916(2), Si2-C8 1.936(2); Si1-Si2-C5 122.26(6), Si1-Si2-C8 126.31(6), Si2-Si1-C1 125.84(6), Si2-Si1-C4 120.62(6), C1-Si1-C4 98.58(9), C5-Si2-C8 97.93(9).

[*] Prof. Dr. T. Iwamoto, Prof. Dr. M. Kira
Department of Chemistry
Graduate School of Science
Tohoku University
Aoba-ku, Sendai 980-8578 (Japan)
Fax: (+81) 22-795-6589
E-mail: iwamoto@mail.tains.tohoku.ac.jp
mkira@mail.tains.tohoku.ac.jp
Dr. R. Tanaka, Prof. Dr. T. Iwamoto
PRESTO
Japan Science and Technology Agency
4-1-8 Honcho Kawaguchi, Saitama (Japan)

[**] This work was supported in part by the Ministry of Education, Culture, Sports, Science, and Technology of Japan (Specially Promoted Research, No. 17002005).

Supporting information for this article is available on the WWW under http://www.angewandte.org or from the author.

© 2006 Wiley-VCH Verlag GmbH & Co. KGaA, Weinheim

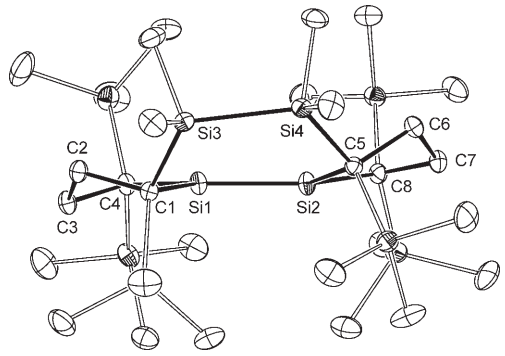

Figure 2. ORTEP drawing of *cis*-**2**. All hydrogen atoms are omitted for clarity. Thermal ellipsoids are shown at the 30% probability level. Selected bond lengths [Å] and angles [°]: Si1-Si2 2.1767(6), Si3-Si4 2.3752(7), Si1-C4 1.919(2), Si1-C1 1.920(2), Si2-C5 1.917(2), Si2-C8 1.924(2); Si1-Si2-C5 119.96(5), Si1-Si2-C8 137.21(6), Si2-Si1-C1 120.12(5), Si2-Si1-C4 139.38(5), C1-Si1-C4 100.26(7), C5-Si2-C8 100.57(7).

distortion around the Si=Si bond in *cis*-**2** is relatively small. In *cis*-**2**, the Si=Si bond length (2.1767(6) Å) is typical, and the θ and τ values are rather small ($\theta = 3.9°$ (Si1) and 12.4° (Si2); $\tau = 3.9°$). The central six-membered ring of *cis*-**2** exhibits a boat conformation.

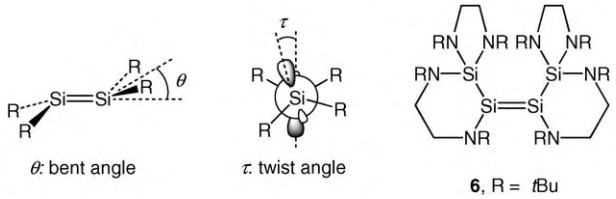

The longest-wavelength absorption band which was assignable to the $\pi \rightarrow \pi^*$ transition of *trans*-**2** ($\lambda_{max} = 517$ nm, $\varepsilon = 4800\ mol^{-1}\,L\,cm^{-1}$) is remarkably red-shifted from that of *cis*-**2** ($\lambda_{max} = 433$ nm, $\varepsilon = 8580\ mol^{-1}\,L\,cm^{-1}$) and that of structurally similar $\{(Me_3Si)_2CH\}_2Si{=}Si\{CH(SiMe_3)_2\}_2$ (**8**; $\lambda_{max} = 393$ nm, $\varepsilon = 12\,600\ mol^{-1}\,L\,cm^{-1}$).[11] The small $\pi \rightarrow \pi^*$ transition energy of *trans*-**2** can be explained by poor 3pπ–3pπ overlap as a result of the significant twist and elongation of the Si=Si bond. The distortion would be responsible for the smaller molar extinction coefficient of *trans*-**2** compared to that of *cis*-**2**. A similar tendency is observed between highly distorted $(tBu_2MeSi)_2Si{=}Si(SiMetBu_2)_2$ (**7**; $\tau = 54.5°$, $\lambda_{max} = 612$ nm, $\varepsilon = 1300\ mol^{-1}\,L\,cm^{-1}$)[10] and less distorted $(tBuMe_2Si)_2Si{=}Si(SiMe_2tBu)_2$ ($\tau = 8.9°$, $\lambda_{max} = 420$ nm, $\varepsilon = 2800\ mol^{-1}\,L\,cm^{-1}$).[12]

The NMR resonances for the unsaturated ^{29}Si nuclei, $\delta(Si_u)$, of these disilenes ($\delta = 135.9$ ppm (*trans*-**2**), 128.1 ppm (*cis*-**2**)) are considerably low-field-shifted compared with that for **8** ($\delta = 87.4$ ppm).[13] Because $\delta(Si_u)$ values in disilenes are known to be proportional to the reciprocal of the energy difference between the σ and π* orbitals of the Si=Si bond,[13] it is reasonable that the order of $\delta(Si_u)$, *trans*-**2** > *cis*-**2** > **8**, is the same as that of λ_{max} of the π–π* transition bands among these disilenes.

Although both *trans*-**2** and *cis*-**2** are intramolecular dimers of two apparently isolable dialkyl silylene units, they do not dissociate into the corresponding tethered bis(dialkyl silylene) compounds upon heating at 100 °C or upon irradiation with a monochromated Xe lamp. The results indicate that the dissociation of the Si=Si bond in *trans*- and *cis*-**2** to give the bis(dialkyl silylene) compounds is energetically unfavorable though the disilenes have twisted Si=Si bonds and strained rings. In comparison with the steric repulsion between the trimethylsilyl groups for the hypothetical dimer of **1**, this repulsion for *trans*- and *cis*-**2** would be significantly reduced by tethering. However, upon heating at 110 °C in $[D_{10}]p$-xylene or in the solid state, *trans*-**2** isomerized stereospecifically into tetracyclic compound **9** in quantitative yield [Eq. (1)]. The structure of product **9** was determined by NMR spectroscopy and X-ray analysis (Figure 3). To the best of our knowledge, compound **9** is the first tetracyclo[7.3.0.0^{3,6}.0^{3,9}]dodecane derivative.

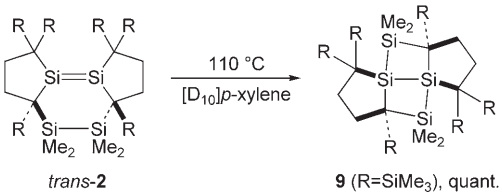

(1)

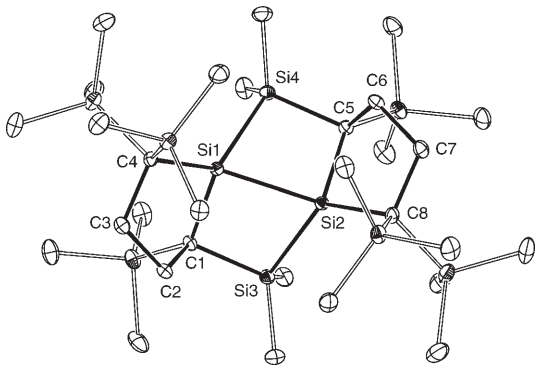

Figure 3. ORTEP drawing of **9**. All hydrogen atoms are omitted for clarity. Thermal ellipsoids are shown at the 30% probability level. Selected bond lengths [Å] and angles [°]: Si1-Si2 2.4536(9), Si2-Si3 2.3601(8), Si1-Si4 2.3677(8); Si1-Si2-C8 141.65(3), Si2-Si1-C4 142.05(7), Si4-Si1-Si2-Si3 −115.20(3).

The X-ray analysis of **9** shows that two terminal five-membered rings in **9** are fused to the central bicyclo-[2.2.0]hexane skeleton in an *anti* fashion, thus indicating that the isomerization is the *antarafacial* [2+2] addition of the Si–Si bond to the Si=Si bond. The central Si1–Si2 bond is considerably elongated (2.4536(9) Å) compared with the peripheral Si–Si bonds (2.3601(8) and 2.3677(8) Å). The Si1-Si2-C8 (141.65(3)) and Si2-Si1-C4 (142.05(7)°) bond angles are unusually large. These structural distortions could be caused by the steric repulsion between the trimethylsilyl groups on the C4 and C8 atoms. The tetrasilane unit in **9** adopts an almost eclipsed conformation with an Si4-Si1-Si2-Si3 dihedral angle of 115.20(3)°.

 © 2006 Wiley-VCH Verlag GmbH & Co. KGaA, Weinheim

The first-order rate constants and the activation parameters for the isomerization of *trans*-**2** to **9** were determined by monitoring the decrease of the UV/Vis absorbance at 517 nm of *trans*-**2** at various temperatures: $k = 2.68 \pm 0.02\ s^{-1}$ at 351 K, $\Delta H^{\neq} = 19.0 \pm 1.2$ kcal mol^{-1}, $\Delta S^{\neq} = -21 \pm 3$ cal mol^{-1} K^{-1}. The $\Delta H^{\neq}$ value is slightly smaller than that for the bond dissociation of the Si=Si bond in Tbt(Mes)Si=Si(Mes)Tbt (Tbt = 2,4,6-{$(Me_3Si)_2$-CH}$_3C_6H_2$; Mes = 2,4,6-$Me_3C_6H_2$) reported by Suzuki, Tokitoh, and Okazaki (ca. 26 kcal mol^{-1})[4] and much smaller than that of the Si–Si bond in hexamethyldisilane (79 kcal mol^{-1}).[14] The large negative $\Delta S^{\neq}$ value suggests that the transition-state structure of the thermal isomerization is considerably restricted, and therefore, multistep mechanisms involving dissociation into the corresponding silylenes or the Si–Si bond cleavage may be ruled out. Stereospecific formation of **9** and the activation parameters indicate that the thermal isomerization is regarded as the first symmetry-allowed thermal $[2_s+2_a]$ intramolecular cycloaddition between Si–Si double and single bonds as proposed for the thermal isomerization of cyclobutene to bicyclo-[1.1.0]butane.[15]

Further work on the reactivity of *cis*- and *trans*-**2** are currently in progress.

Experimental Section

trans-**2**: A mixture of (2*S**,2′*S**)-**5** (273 mg, 0.264 mmol) and KC_8 (157 mg, 1.16 mmol) in dry THF (25 mL) was stirred at −40 °C for 48 h, and a brown solution was obtained. The solvent was removed in vacuo, and dry hexane was added to the resulting residue. Filtration of the resulting mixture and concentration of the filtrate under −20 °C gave pure *trans*-**2** as red-purple crystals (107 mg, 57% yield). M.p. 182 °C (decomp); ^{1}H NMR (400 MHz, [D$_6$]benzene): $\delta = 0.306$ (s, overlap, 24H, 2 $SiMe_3$ + $SiMe_2$), 0.357 (s, overlap, 36H, 4 $SiMe_3$), 0.396 (s, 6H, $SiMe_2$), 1.80–1.97 (m, 4H), 2.13–2.20 ppm (m, 4H); ^{13}C NMR (100 MHz, [D$_6$]benzene): $\delta = 2.75$, 3.47 ($SiMe_2$), 4.37, 4.88, 5.07 ($SiMe_3$), 17.62, 22.34 (C), 34.89, 35.43 ppm (CH_2); ^{29}Si NMR (79 MHz, [D$_6$]benzene): $\delta = -19.51$ ($SiMe_2$), 2.44, 3.48, 3.61 ($SiMe_3$), 135.90 ppm (Si=Si); MS (30 eV): *m*/*z* (%): 714 (100) [M^+]; UV/Vis (hexane) λ_{max} (ε in mol^{-1} L cm^{-1}): 517 (4800), 334 nm (6830). Elemental analysis (%) calcd for $C_{30}H_{74}Si_{10}$: C 50.34, H 10.42; found: C 50.36, H 10.18.

cis-**2**: Similarly to the synthesis of *trans*-**2**, reaction of (2*R**,2′*S**)-**5** (94 mg, 91 mmol) and KC_8 (54 mg, 400 mmol) in dry THF (10 mL) gave pure *cis*-**2** as yellow crystals (29 mg, 44% yield). M.p. 208 °C (decomp); ^{1}H NMR (400 MHz, [D$_6$]benzene): $\delta = 0.281$ (s, 18H, $SiMe_3$), 0.323 (s, 6H, $SiMe_2$), 0.351 (s, 18H, $SiMe_3$), 0.375 (s, 6H, $SiMe_2$), 0.398 (s, 18H, $SiMe_3$), 1.75–2.20 ppm (m, 8H); ^{13}C NMR (100 MHz, [D$_6$]benzene): $\delta = 1.73$, 3.30 ($SiMe_2$), 4.40, 5.03, 5.08 ($SiMe_3$), 15.64, 19.05, 35.38, 36.56 ppm (CH_2); ^{29}Si NMR (79 MHz, [D$_6$]benzene): $\delta = -11.78$ ($SiMe_2$), 2.98, 3.10, 3.84 ($SiMe_3$), 128.07 ppm (Si=Si); MS (30 eV) *m*/*z* (%): 714 (93) [M^+], 357 (70), 73 (100); UV/Vis (hexane) λ_{max} (ε in mol^{-1} L cm^{-1}): 433 (8580), 353 nm (12800). Elemental analysis (%) calcd for $C_{30}H_{74}Si_{10}$: C 50.34, H 10.42; found: C 50.35, H 10.39.

9: A solution of *trans*-**2** (1.9 mg) in [D$_{10}$]*p*-xylene (0.4 mL) was sealed in an NMR tube and was heated at 110 °C for 3 h. Removal of the solvent from the resulting solution gave **9** as colorless crystals (1.9 mg, 100% yield). M.p. 243–245 °C; ^{1}H NMR (400 MHz, [D$_6$]benzene): $\delta = 0.221$ (s, 18H, $SiMe_3$), 0.282 (s, 36H, $SiMe_3$), 0.401 (s, 6H, $SiMe_2$), 0.854 (s, 16, $SiMe_2$), 1.80–2.25 ppm (m, 8H, CH_2); ^{13}C NMR (100 MHz, [D$_6$]benzene): $\delta = 0.95$, 2.96, 3.85, 4.16, 5.33, 13.55, 17.63, 34.65, 36.36 ppm; ^{29}Si NMR (79 MHz, [D$_6$]benzene): $\delta = 0.72$, 2.23, 2.35, 2.64, 37.99 ppm; UV/Vis (hexane) λ_{max} (ε in mol^{-1} L cm^{-1}): 301 (8310), 242 (16500), 234 nm (16600). Elemental analysis (%) calcd for $C_{30}H_{74}Si_{10}$: C 50.34, H 10.42; found: C 50.12, H 10.12.

Received: June 2, 2006
Published online: August 21, 2006

Keywords: cycloaddition · disilene · silicon · silylene · structure elucidation

[1] R. Okazaki, R. West, *Adv. Organomet. Chem.* **1996**, *39*, 231; M. Weidenbruch in *The Chemistry of Organic Silicon Compounds*, *Vol. 3* (Eds.: Z. Rappoport, Y. Apeloig), Wiley, Chichester, **2001**, p. 391; R. West, *Polyhedron* **2002**, *21*, 467; M. Kira, T. Iwamoto, *Adv. Organomet. Chem.* **2006**, *54*, 73.
[2] R. West, M. J. Fink, J. Michl, *Science* **1981**, *214*, 1343.
[3] N. Tokitoh, H. Suzuki, R. Okazaki, K. Ogawa, *J. Am. Chem. Soc.* **1993**, *115*, 10428.
[4] H. Suzuki, N. Tokitoh, R. Okazaki, *Bull. Chem. Soc. Jpn.* **1996**, *68*, 2471.
[5] M. Kira, S. Ishida, T. Iwamoto, C. Kabuto, *J. Am. Chem. Soc.* **1999**, *121*, 9722.
[6] See the Supporting Information for the details of the preparations of **4** and **5**.
[7] CCDC-609692, 609693, and 609694 (*trans*-**2**, *cis*-**2**, and **9**) contain the supplementary crystallographic data for this paper. These data can be obtained free of charge from The Cambridge Crystallographic Data Centre via www.ccdc.cam.ac.uk/data_request/cif.
[8] T. A. Schmedake, M. Haaf, Y. Apeloig, T. Müller, S. Bukalov, R. West, *J. Am. Chem. Soc.* **1999**, *121*, 9479.
[9] Bent angle θ is defined as the angle between the axis through the Si=Si bond and R-Si(sp^2)-R plane, and twist angle τ is defined as the angle between the two axes that bisect the R-Si(sp^2)-R angles as viewed along the Si=Si axis. Bent angles θ of *trans*-**2** are comparable to those of **6** ($\theta = 32.3$ and 33.8°) and the twist angle τ of *trans*-**2** is the next largest to that in (tBu$_2$MeSi)$_2$Si=Si(SiMetBu$_2$)$_2$ (**7**; $\tau = 54.5$°). For compound **7**, see reference [10].
[10] A. Sekiguchi, S. Inoue, M. Ichinohe, *J. Am. Chem. Soc.* **2004**, *126*, 9626.
[11] S. Masamune, Y. Eriyama, T. Kawase, *Angew. Chem.* **1987**, *99*, 601; *Angew. Chem. Int. Ed. Engl.* **1987**, *26*, 584.
[12] M. Kira, T. Maruyama, C. Kabuto, K. Ebata, H. Sakurai, *Angew. Chem.* **1994**, *106*, 1575; *Angew. Chem. Int. Ed. Engl.* **1994**, *33*, 1489.
[13] R. West, J. D. Cavalieri, J. J. Buffy, C. Fly, K. W. Kurt, J. C. Duchamp, M. Kira, T. Iwamoto, T. Müller, Y. Apeloig, *J. Am. Chem. Soc.* **1997**, *119*, 4972.
[14] W. J. Bullock, R. Walsh, K. D. King, *J. Phys. Chem.* **1994**, *98*, 2595.
[15] R. B. Woodward, R. Hoffmann, *Angew. Chem.* **1969**, *81*, 797; *Angew. Chem. Int. Ed. Engl.* **1969**, *8*, 781; R. B. Woodward, R. Hoffmann, *The Conservation of Orbital Symmetry*, Verlag Chemie, Weinheim, **1970**.

 © 2006 Wiley-VCH Verlag GmbH & Co. KGaA, Weinheim

Protein Binding

DOI: 10.1002/anie.200602227

Contribution of Ligand Desolvation to Binding Thermodynamics in a Ligand–Protein Interaction**

*Natalia Shimokhina, Agnieszka Bronowska, and Steve W. Homans**

Despite enormous advances in the structure determination of protein complexes, our ability to predict binding affinity from structure remains severely limited. Affinities are governed by both structure and dynamics, including solvent rearrangement. Although a number of studies have examined the contribution of water molecules in the protein binding pocket,[1–11] ligand solvation has received little attention. Herein, we examine the latter contribution in the major urinary protein (MUP), an abundant pheromone-binding protein for which the subtle recognition of a series of related compounds is essential to its biological function.[12–14] Our approach involves the experimental determination of solvation thermodynamics of relevant ligands by measuring air/water partition coefficients. These measurements are interpreted in the context of thermodynamic binding data[15] and allow the interaction thermodynamics to be resolved to a level of detail unreported for any system.

We determined experimental standard free energies of solvation for a pyrazine-derived ligand of MUP, namely 2-methoxy-3-isopropylpyrazine (IPMP). We also determined solvation thermodynamics for methylpyrazine (MP), for which data have been reported previously, to assess the validity of our approach (see the Experimental Section). In each case we found that the temperature dependence of the standard free energy of solvation is approximately linear and the value for MP at 25 °C (-24.4 ± 0.1 kJ mol^{-1}, Table 1) is very close to that obtained previously by Buttery et al. (-23.1 kJ mol^{-1}).[16] Standard enthalpy and entropy values derived from the temperature dependence of the standard free energy are given in Table 1.

Table 1: Solvation thermodynamic parameters (in kJ mol^{-1}) of pyrazine derivatives at 298 K.

Ligand	ΔG^0_{solv} [a]	ΔH^0_{solv}	$T\Delta S^0_{solv}$
MP	-24.4 ± 0.1	-50.5 ± 0.96	-26.1 ± 0.99
IPMP	-17.0 ± 0.04	-43.8 ± 8.2	-26.7 ± 8.4

[a] Errors are reported for duplicate experiments.

[*] N. Shimokhina, Dr. A. Bronowska, Prof. S. W. Homans
Institute of Molecular and Cellular Biology
University of Leeds
Mount Preston Street, Leeds LS2 9JT (UK)
Fax: (+44) 113-343-3167
E-mail: S.W.Homans@leeds.ac.uk

[**] This work was supported by the BBSRC (grant numbers 24/B19388 and BB/C500679/1) and by The Wellcome Trust (grant numbers 062164 and 072568).

It is convenient to represent the binding process in terms of a conventional Born–Haber cycle (Scheme 1).[17] Since G is a state function, the observed standard free energy of binding

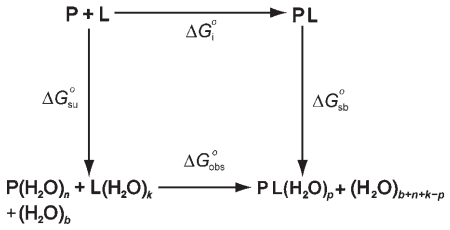

Scheme 1. Born–Haber cycle for ligand L binding to protein P, showing the relationship between the observed free energy of binding ΔG^0_{obs}, the "intrinsic" (solute–solute) term ΔG^0_i, and the solvation free energies of unbound (ΔG^0_{su}) and bound (ΔG^0_{sb}) species.

is given by Equation (1), in which ΔG^0_i represents the "intrinsic" solute–solute contribution, and the quantity in braces contains solvation processes, that is, the standard free energies of solvation of the ligand (ΔG^0_{solL}) and the protein (ΔG^0_{solP}), which together comprise ΔG^0_{su}, and the standard free energy of solvation of the complex ΔG^0_{solPL}, which is equivalent to ΔG^0_{sb}.

$$\Delta G^0_{obs} = \Delta G^0_i + \{\Delta G^0_{sb} - \Delta G^0_{su}\} \quad (1)$$

Thus Equation (1) can be rewritten as Equation (2). A similar equation can be written for the standard enthalpy and entropy of binding.

$$\Delta G^0_{obs} = \Delta G^0_i + \{\Delta G^0_{solPL} - (\Delta G^0_{solP} + \Delta G^0_{solL})\} \quad (2)$$

We consider first ΔS^0_i. This term comprises changes in the dynamics of the protein and the ligand following association. The entropic contribution from protein degrees of freedom to the binding of IPMP to MUP determined from NMR relaxation measurements is zero within experimental error.[15] Furthermore, we have estimated the entropic contribution from the loss of translational and rotational degrees of freedom of a ligand in earlier work on the binding of an oligosaccharide to cholera toxin B-subunit.[18] Since this entropic component depends on the logarithm of the molecular mass, this loss of degrees of freedom represents an unfavorable contribution of approximately -25 kJ mol^{-1}. If the internal degrees of freedom of the ligand are assumed to be essentially "frozen" on binding, the corresponding unfavorable contribution from the two internal degrees of freedom of IPMP amount to approximately -12 kJ mol^{-1}.[19] Herein, we ignore degrees of freedom about the symmetry axis of methyl groups since rotation about the latter will not be frozen on binding. The crystallographic B factors for the ligand, which are lower than those for the protein backbone, show that the ligand degrees of freedom are indeed frozen on binding.[15] From these data together with the standard entropy of solvation of IPMP determined in the present

 InterScience © 2006 Wiley-VCH Verlag GmbH & Co. KGaA, Weinheim

study, the breakdown of the standard entropy of binding is shown in Table 2.

The term $T\Delta S^0_{solvPL} - T\Delta S^0_{solvP}$ is inaccessible experimentally, but can be inferred by comparison of the sum of the above contributions with $T\Delta S^0_{obs}$. Remarkably, these data suggest that the entropic contribution from desolvation of the protein is small or zero. It has been surmised that the release of ordered water molecules from the binding pocket of a protein following ligand binding gives rise to a substantial favorable entropic contribution to binding. However, the binding pocket of MUP is suboptimally hydrated, which results in a dearth of well-ordered water molecules.[11,20] Thus, the characteristic entropy-driven thermodynamic signature of "hydrophobic binding" is not realized, since the favorable entropic contribution arising from ligand desolvation is insufficient to overcome the unfavorable contribution from "freezing" the protein and ligand degrees of freedom on binding.

Table 2: Breakdown of the thermodynamics of binding of IPMP to MUP at 298 K.

Description	Value [kJ mol^{-1}]	Description	Value [kJ mol^{-1}]
$T\Delta S^0_i$		ΔH^0_i	
protein degrees of freedom	-0.8 ± 3.8[a]	new solute–solute interactions	ca. -76
ligand degrees of freedom $-T\Delta S^0_{solvL}$	ca. -37	changes in ligand/protein structure $-\Delta H^0_{solvL}$	ca. 0
ligand desolvation $T\Delta S^0_{solvPL} - T\Delta S^0_{solvP}$	$+26.7 \pm 8.4$	ligand desolvation $\Delta H^0_{solvPL} - \Delta H^0_{solvP}$	$+43.8 \pm 8.2$
desolvation of protein/complex $T\Delta S^0_{obs}$	$+0.4 \pm 9.2$	desolvation of protein/complex ΔH^0_{obs}	-12.3 ± 8.4
observed entropy	-10.7 ± 0.5[a]	observed enthalpy	-44.5 ± 0.4[a]

[a] From reference [15].

The term ΔH^0_i comprises changes in the structure of the protein and the ligand, together with the formation of new solute–solute nonbonded interactions following association. There are no significant changes in the structure of MUP on binding either pyrazine-derived or alternative surrogate ligands.[11,20] Moreover, quantum chemical calculations at the 6-31G* level indicate that IPMP is bound in a low-energy conformation that is energetically indistinguishable from the global minimum-energy conformation. Thus ΔH^0_i can be equated with the formation of new solute–solute interactions. In a recent study on the binding of aliphatic primary alcohols to MUP, we concluded that binding was driven by favorable solute–solute interactions.[20] The linear relationship between ΔH^0_i and the length of the carbon chain enabled an estimate of the contribution from a methylene group (-8.4 ± 0.2 kJ mol^{-1}). Assuming this contribution is proportional to the van der Waals surface area of the ligand, we estimate $\Delta H^0_i \approx -76$ kJ mol^{-1} for the association of IPMP with MUP. Given a desolvation enthalpy $-\Delta H^0_{solvL} = +43.8 \pm 8.2$ kJ mol^{-1} for IPMP as above together with $\Delta H^0_{obs} = -44.5 \pm 0.4$ kJ mol^{-1},[15] the contribution from desolvation of the protein on formation of the complex $\Delta H^0_{solvPL} - \Delta H^0_{solvP}$ can be estimated as approximately -12.3 ± 8.4 kJ mol^{-1} (Table 2).

In summary, the favorable entropic contribution arising from desolvation of IPMP on binding to MUP is insufficient to overcome the strongly unfavorable component arising from "freezing" of ligand degrees of freedom. These data thus explain the unfavorable global entropy of binding $T\Delta S^0_{obs}$, which is paradoxical in view of the hydrophobic nature of the interaction. The enthalpic contribution to binding is more difficult to deconvolute with accuracy, but the data above indicate that the unfavorable enthalpic contribution arising from desolvation of the ligand is offset both by favorable solute–solute dispersive interactions,[20] with a contribution from desolvation of the protein binding pocket.[11]

Experimental Section

A microfuge tube containing ligand solution (1.5 mL) of known concentration (0.4–4 mM) in water was placed in a closed glass bottle (25 L) at a constant temperature (6, 13, and 20 °C for IPMP and 13, 20, and 27 °C for MP). Trial experiments were used to find the appropriate equilibration period, which ranged from 7 to 14 days. The pressure was kept constant by means of a conventional 50-mL glass gas syringe connected through the screw-top lid. Initial and equilibrated ligand concentrations were determined from optical-density measurements at 220 nm ($\varepsilon_{220} = 144\,\text{M}^{-1}\text{cm}^{-1}$ for MP and $4590\,\text{M}^{-1}\text{cm}^{-1}$ for IPMP). The mass of each microfuge tube was recorded before and after the equilibration period to account for evaporation. The equilibrium constant K for $L_{air} \rightleftharpoons L_{sol}$ (L = ligand) in this experiment is given by Equation (3).

$$K = \frac{[L]_{sol}}{[L]_{gas}} = \frac{[L]_{sol}}{[L]_0\, m_0 - [L]_{sol}\, m_{sol}} V_{bottle}\, \rho_{water} \quad (3)$$

In Equation (3), $[L]_{sol}$ and $[L]_{gas}$ are the ligand concentrations in solution and gas phase, respectively, after equilibration, $[L]_0$ is the initial ligand concentration, m_0 and m_{sol} are the masses of the initial and equilibrated solutions, V_{bottle} is the volume of the bottle with syringe attachment, and ρ_{water} is the density of water at the relevant temperature.

Standard free energies of solvation of each ligand were calculated according to Equation (4).

$$\Delta G^0_{solv} = -R\,T \ln K \quad (4)$$

Standard enthalpies and entropies of solvation were determined from plots of the standard free energy versus temperature in a conventional van't Hoff analysis.

Global binding thermodynamics data were obtained from a previous report.[15]

Received: June 3, 2006
Published online: August 14, 2006

Keywords: noncovalent interactions · solvation · thermodynamics

[1] M. A. Williams, J. M. Goodfellow, J. M. Thornton, *Protein Sci.* **1994**, *3*, 1224.
[2] L. Zhang, J. Hermans, *Proteins* **1996**, *24*, 433.
[3] K. Venu, V. P. Denisov, B. Halle, *J. Am. Chem. Soc.* **1997**, *119*, 3122.

 © 2006 Wiley-VCH Verlag GmbH & Co. KGaA, Weinheim

[4] V. P. Denisov, K. Venu, J. Peters, H. D. Horlein, B. Halle, *J. Phys. Chem. B* **1997**, *101*, 9380.
[5] G. A. Holdgate, A. Tunnicliffe, W. H. J. Ward, S. A. Weston, G. Rosenbrock, P. T. Barth, I. W. F. Taylor, R. A. Pauptit, D. Timms, *Biochemistry* **1997**, *36*, 9663.
[6] C. Clarke, R. J. Woods, J. Gluska, A. Cooper, M. A. Nutley, G.-J. Boons, *J. Am. Chem. Soc.* **2001**, *123*, 12238.
[7] Z. Li, T. Lazaridis, *J. Am. Chem. Soc.* **2003**, *125*, 6636.
[8] R. M. Levy, L. Y. Zhang, E. Gallicchio, A. K. Felts, *J. Am. Chem. Soc.* **2003**, *125*, 9523.
[9] S. D. Sharrow, K. A. Edmonds, M. A. Goodman, M. V. Novotny, M. J. Stone, *Protein Sci.* **2005**, *14*, 249.
[10] P. Connelly, R. A. Aldape, F. J. Bruzzese, S. P. Chambers, M. J. Fitzgibbon, M. A. Fleming, S. Itoh, D. J. Livingston, M. A. Navia, J. A. Thomson, K. P. Wilson, *Proc. Natl. Acad. Sci. USA* **1994**, *91*, 1964.
[11] E. Barratt, R. Bingham, D. J. Warner, C. A. Laughton, S. E. V. Phillips, S. W. Homans, *J. Am. Chem. Soc.* **2005**, *127*, 11827.
[12] Z. Bocskei, C. R. Groom, D. R. Flower, C. E. Wright, S. E. V. Phillips, A. Cavaggioni, J. B. C. Findlay, A. C. T. North, *Nature* **1992**, *360*, 186.
[13] L. Zídek, M. V. Novotny, M. J. Stone, *Nat. Struct. Biol.* **1999**, *6*, 1118.
[14] L. Zídek, M. J. Stone, S. M. Lato, M. D. Pagel, Z. S. Miao, A. D. Ellington, M. V. Novotny, *Biochemistry* **1999**, *38*, 9850.
[15] R. Bingham, G. Bodenhausen, J. H. B. C. Findlay, S.-Y. Hsieh, A. P. Kalverda, A. Kjellberg, C. Perazzolo, S. E. V. Phillips, K. Seshadri, W. B. Turnbull, S. W. Homans, *J. Am. Chem. Soc.* **2004**, *126*, 1675.
[16] R. G. Buttery, J. L. Bomben, D. G. Guadagni, L. C. Ling, *J. Agric. Food Chem.* **1971**, *19*, 1045.
[17] M. C. Chervenak, E. J. Toone, *J. Am. Chem. Soc.* **1994**, *116*, 10533.
[18] W. B. Turnbull, B. L. Precious, S. W. Homans, *J. Am. Chem. Soc.* **2004**, *126*, 1047.
[19] J. J. Lundquist, S. D. Debenham, E. J. Toone, *J. Org. Chem.* **2000**, *65*, 8245.
[20] R. Malham, S. Johnstone, R. J. Bingham, E. Barratt, S. E. V. Phillips, C. A. Laughton, S. W. Homans, *J. Am. Chem. Soc.* **2005**, *127*, 17061.

 © 2006 Wiley-VCH Verlag GmbH & Co. KGaA, Weinheim

Natural Product Synthesis

DOI: 10.1002/anie.200602507

Formal Total Synthesis of (+)-Zaragozic Acid C through an Ireland–Claisen Rearrangement**

*Jens O. Bunte, Anthony N. Cuzzupe, Alica M. Daly, and Mark A. Rizzacasa**

The zaragozic acids[1] and squalestatins[2] are structurally related fungal metabolites isolated independently by several industrial research groups in the early 1990s.[3] These compounds were identified as potent inhibitors[4] of squalene synthase and showed promise as cholesterol-lowering compounds.[5] In addition, some zaragozic acids inhibit farnesyl protein transferase and thus show potential as antitumor agents.[6] The engrossing, highly oxygenated 2,8-dioxabicyclo-[3.2.1]octane core present in these compounds coupled with their biological activity sparked great interest within the synthetic community which, to date, has culminated in five total syntheses[7] of zaragozic acid C (**1**),[8] three syntheses of its congener zaragozic acid A,[9] and one synthesis of the related 6,7-dideoxysqualestatin H5.[10] Herein, we report a synthesis of an advanced intermediate which has been converted into **1**.

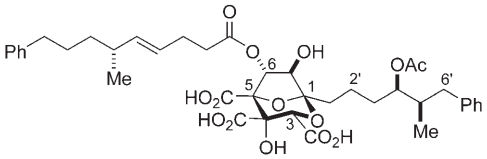

1: Zaragozic acid C

Our retrosynthetic analysis of **1** is shown in Scheme 1. The primary target was known intermediate **2**, which was converted into zaragozic acid C (**1**) in four steps.[8a] It was envisaged that triacetate **2** could be formed by methanolysis[10] of the spirolactone acetal **3** and subsequent acid-mediated cyclization to secure the 2,8-dioxabicyclo-[3.2.1]octane core. Functional-group manipulations would

[*] Dr. J. O. Bunte, Dr. A. N. Cuzzupe, A. M. Daly, Prof. Dr. M. A. Rizzacasa
School of Chemistry
The University of Melbourne
Bio21 Institute, 30 Flemmington Road
Melbourne, Victoria 3010 (Australia)
Fax: (+61) 3-9347-8396
E-mail: masr@unimelb.edu.au
Homepage: http://www.chemistry.unimelb.edu.au/staff/masr/research/MARHomepage.html

[**] Financial support for this study was provided by the Australian Research Council: Discovery-Grants Program and the Deutsche Forschungsgemeinschaft (DFG postdoctoral fellowship to J.O.B.).

Supporting information for this article is available on the WWW under http://www.angewandte.org or from the author.

© 2006 Wiley-VCH Verlag GmbH & Co. KGaA, Weinheim

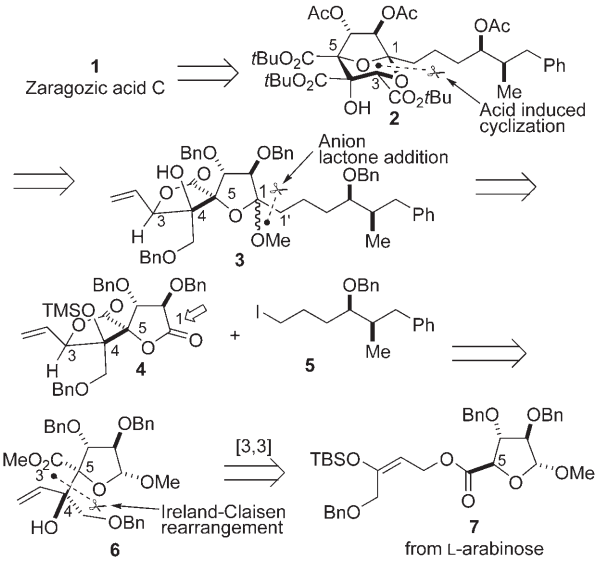

Scheme 1. Retrosynthetic analysis of zaragozic acid C (**1**). Bn = benzyl, TBS = *tert*-butyldimethylsilyl, TMS = trimethylsilyl.

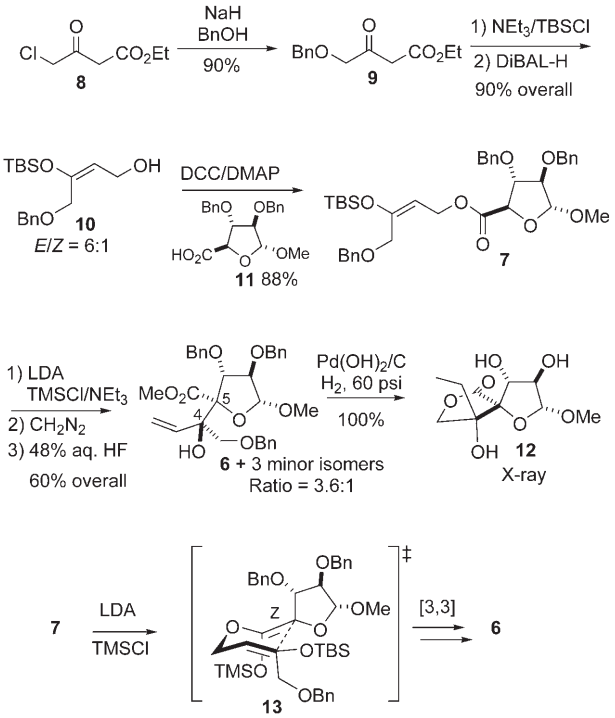

Scheme 2. Synthesis of ester **6**. DCC = dicyclohexylcarbodiimide, DiBAL-H = diisobutylaluminum hydride, DMAP = 4-dimethylaminopyridine, LDA = lithium diisopropylamide.

then give the triacetate **2**. The acetal **3** could be formed by regioselective addition[11] of the lithium anion derived from the side-chain iodide **5** to the less-hindered C1 carbonyl group[12] of the spirobislactone **4**. Compound **4** could be obtained from tertiary alcohol **6**, which in turn would be formed by an Ireland–Claisen rearrangement in the presence of a β leaving group[13] of the sensitive allylic ester **7** derived from L-arabinose. This key transformation would form the C4–C5 bond and the two quaternary asymmetric centers simultaneously.[14] Furthermore, intermediate **6** contains all the asymmetric centers required for the core system apart from that at C3. We have previously utilized the Ireland–Claisen rearrangement of allyl furanosiduronates in the presence of a β leaving group for the synthesis of related 2-alkylcitrate natural products, such as cinatrins B,[15] C_1, and C_3,[16] as well as trachyspic acid[17] and a model zaragozic acid A system devoid of substituents at C4.[18]

The synthesis of the key intermediate **6** is outlined in Scheme 2. Treatment of ethyl 4-chloroacetoacetate (**8**) with the anion derived from benzyl alcohol afforded ether **9**.[19] Exposure of **9** to TBSCl and NEt_3[20] in THF at 50 °C followed by reduction with DiBAl-H gave the alcohol **10** as a 6:1 mixture of geometric isomers. DCC-mediated coupling of this alcohol with the L-arabinose derived acid **11**[21] afforded the Ireland–Claisen precursor **7**, which could be purified by rapid chromatography on silica gel. Treatment of a solution of the ester **7** in THF/hexamethylphosphoramide (HMPA) and the centrifugate from a 1:1 (v/v) mixture of TMSCl and NEt_3 with LDA at −100 °C[13b,c] gave the silyl ketene acetal, which underwent stereoselective [3,3] rearrangement upon warming to room temperature. Hydrolysis of the crude TMS ester followed by methylation and removal of the TBS group provided ester **6** as the major product along with three other minor diastereoisomers in 60% yield for the three steps and a ratio of 3.6:1, respectively. The desired ester **6** was readily separated from the other minor isomers by flash chromatography. One minor isomer (stereochemistry undetermined) was obtained pure, whereas the other two were isolated as a 63:37 mixture. The stereochemistry of **6** was determined by its conversion into the crystalline spirolactone **12** (Scheme 2). A single-crystal X-ray structure[22] was obtained for **12**, which confirmed the stereochemistry of the major product **6** of the Ireland–Claisen rearrangement. Interestingly, attempted rearrangement of the ester synthesized from the *para*-methoxybenzyl (PMB)-protected analogue of allyl alcohol **10** and acid **11** failed completely.

The outcome of the [3,3] rearrangement can be explained by considering the chairlike transition state **13** in which it is assumed that the geometry of the major ketene acetal formed is *Z*[23] (Scheme 2). The C5 stereochemistry results from rearrangement from the face opposite the β-benzyloxy group, whereas the C4 stereochemistry arises from the chairlike transition state as shown.

The conversion of the Claisen product **6** into the spirobislactone core precursor **4** is outlined in Scheme 3. We initially investigated the dihydroxylation of the alkene functionality in **6** as a means of introducing the C3 stereochemistry. Unfortunately, both simple catalytic[24] or asymmetric[25] dihydroxylation of **6** resulted in preferential formation of the isomer with undesired stereochemistry at C3. This result led to an alternative method for the introduction of the C3 stereochemistry. Ozonolysis of the alkene **6** provided an aldehyde and chelation-controlled addition[9e] of vinylmagnesium bromide and gave the desired lactone **14** in a stereoselective manner (90% d.r.) after acid treatment to complete lactonization. The stereochemistry for spirolactone

 © 2006 Wiley-VCH Verlag GmbH & Co. KGaA, Weinheim

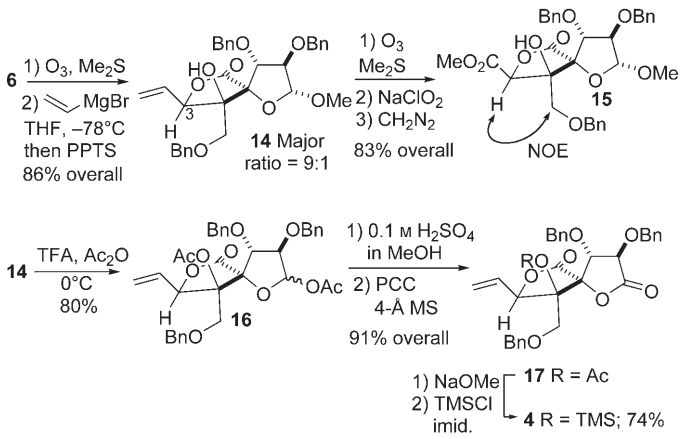

Scheme 3. Synthesis of spirobislactone **4**. imid. = imidazole, MS = molecular sieves, PCC = pyridinium chlorochromate, PPTS = pyridinium *p*-toluenesulfonate, TFA = trifluoroacetic acid.

14 was assigned based on NOE interactions observed between H3 and the C4 methylene group in the derived C3 methyl ester **15**.

The hydrolysis of the methyl ketal in **14** proved troublesome as most acidic methods caused extensive decomposition of the substrate. Eventually, we found that acetolysis (Ac_2O, TFA, 0 °C)[26] cleanly gave the diacetate **16** as a 2:1 mixture of anomers. Higher temperatures also resulted in acetolysis of the benzyl groups. The anomeric acetate could now be readily cleaved with dilute acid and oxidation gave the lactone **17**. Selective acetate methanolysis followed by TMS protection provided the spirobislactone core precursor **4** in good yield.

With the required spirobislactone **4** in hand, we then synthesized the iodide **5** required for the C1 side chain as outlined in Scheme 4. Thus, an Evans aldol reaction[27] between the boron enolate derived from oxazolidinone **18** and aldehyde **19**[28] proceeded in excellent yield and stereoselectivity (> 95 % *de*) to afford adduct **20**. Reductive

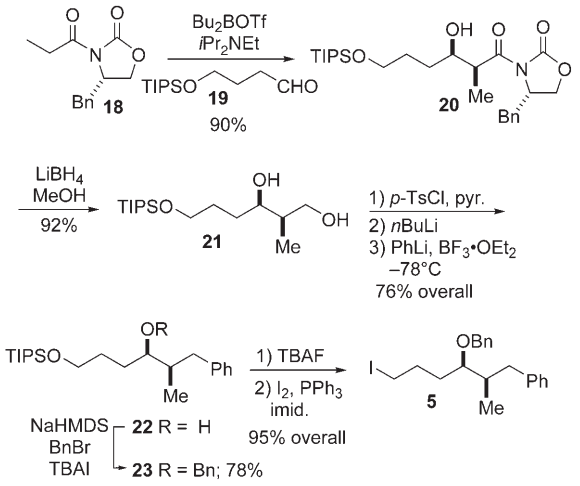

Scheme 4. Synthesis of the side-chain iodide **5**. OTf = triflate, pyr. = pyridine, NaHMDS = sodium hexamethyldisilazane, TBAI = tetrabutylammonium iodide, TBAF = tetrabutylammonium fluoride, TIPS = triisopropylsilyl, *p*-TsCl = *p*-toluenesulfonyl chloride.

removal of the chiral auxiliary provided diol **21**, which was converted into the primary monotosylate and treatment of this with *n*BuLi resulted in oxetane formation.[8a] Ring opening of the oxetane with PhLi in the presence of a Lewis acid gave alcohol **22** in good overall yield. We found that the synthesis and isolation of the oxetane gave better yields than the one-pot process reported by Carreira and Du Bois.[8a] Benzyl group protection proceeded best with NaHMDS as the base to afford ether **23**, and fluoride-induced desilylation followed by conversion of the primary alcohol into the iodide[29] gave the side-chain fragment **5** in excellent yield.

The final steps to the zaragozic acid C intermediate **2** are outlined in Schemes 5 and 6. Treatment of **5** with *t*BuLi[30] in a Et_2O/hexane solvent mixture at −78 °C generated the lithium

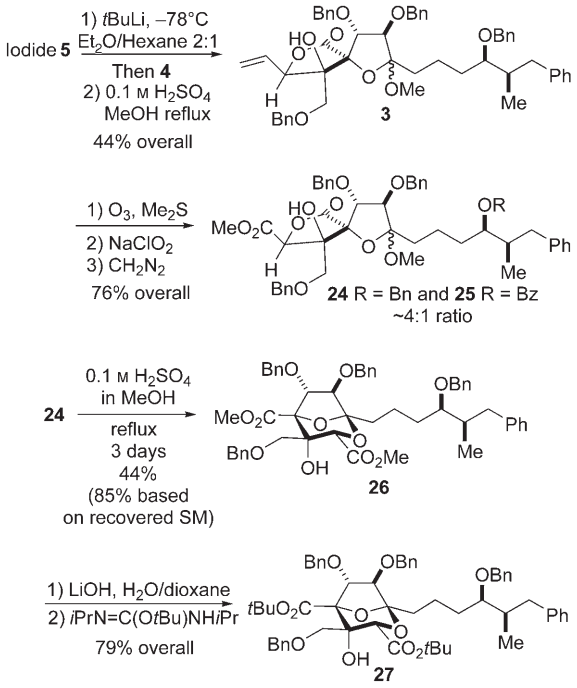

Scheme 5. Synthesis of the 2,8-dioxabicyclo[3.2.1]octane **27**. SM = starting material, Bz = benzoyl.

anion, which selectively added to spirolactone **4** at the C1 carbonyl group (2.2:1 ratio of addition products; 72 % yield). Treatment of the C1 addition product with acidic methanol, however, gave the methyl ketals **3** as a separable mixture and only a trace (2 % yield) of the desired 2,8-dioxa-[3.2.1]bicyclooctane. We surmised that the slow step in the acid-catalyzed process may be opening of the lactone ring and therefore decided that a decrease in electron density would assist the methanolysis. Therefore, alkene **3** was oxidatively cleaved and oxidation[31] followed by methylation afforded methyl ester **24** along with a by-product **25**, as a result of oxidation of the side-chain O4′ benzyl protecting group.[32] To our delight, treatment of a mixture of ketals **24** with 0.1 M sulfuric acid in boiling methanol resulted in the formation of the desired zaragozic acid core system **26** in 44 % yield along with recovered methyl ketals **24** (85 % based on recovered

 © 2006 Wiley-VCH Verlag GmbH & Co. KGaA, Weinheim

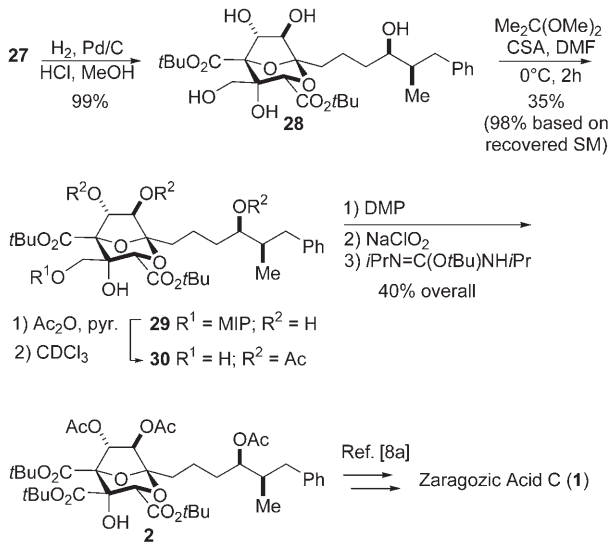

Scheme 6. Completion of the formal total synthesis of zaragozic acid C (**1**). CSA = 10-camphorsulfonic acid, DMP = Dess–Martin periodinane, DMF = *N*,*N*-dimethylformamide, MIP = methoxyisopropyl.

24). Hydrolysis of the methyl esters and formation[33] of the di-*tert*-butyl ester gave bicycle **27**.

The final major synthetic challenge was the selective functionalization of the C4 primary alcohol. This quest began with global debenzylation through hydrogenolysis to give pentol **28** in high yield.[34] Numerous experiments to selectively protect the C4 primary alcohol failed. In one case, to form the dimethylacetonide of the 1,2-diol at C4, pentol **28** was exposed to 2,2-dimethoxypropane in DMF in the presence of catalytic CSA, which resulted in the formation of an undesired acetonide between the primary alcohol and the C7 hydroxy group. However, during the course of monitoring this reaction by TLC, we initially noticed the selective formation of a spot at a higher R_f value which slowly disappeared and a spot at a lower R_f value, which corresponds to the undesired acetonide, was formed. Treatment of **28** with the same reagents as above, but at 0 °C for a shorter time, selectively afforded the compound with a higher R_f value, which was identified as methoxyisopropyl (MIP) ether **29**, along with recovered starting material **28**, which could readily be recycled. This serendipitous discovery led to the monoprotection of pentol **28** with a highly acid-labile protecting group. Acetylation of **29** and treatment with mild acid[35] gave alcohol **30**, which upon two-stage oxidation and ester formation yielded the target compound **2**, the physical data for which were identical to those reported.[8a,c]

In conclusion, we have completed a synthesis the precursor of zaragozic acid C (**1**), in which the C4–C5 bond was formed in a stereoselective manner with concomitant formation of the quaternary asymmetric centers by an Ireland–Claisen rearrangement of the sensitive allylic ester **7**. Other highlights of this route include a novel acetolysis of the methyl ketal **15**, selective carbanion addition to the spirobislactone **4**, methanolysis of lactone **24**, subsequent formation of the zaragozic acid bicycle **26**, and a selective MIP group protection of pentol **28**. Studies towards the synthesis of other members of the zarazozic acid/squalestatin family are underway.

Received: June 22, 2006
Published online: August 30, 2006

Keywords: Ireland–Claisen rearrangement · lactones · natural products · total synthesis · zaragozic acid

[1] a) K. E. Wilson, R. M. Burk, T. Biftu, R. G. Ball, K. Hoogsteen, *J. Org. Chem.* **1992**, *57*, 7151–7158; b) J. D. Bergstrom, M. M. Kurtz, D. J. Rew, A. M. Amend, J. D. Karkas, R. G. Bosterdor, V. S. Dansal, C. Dufresne, F. L. V. Middlesworth, O. D. Hensens, J. M. Liesch, D. L. Zink, K. E. Wilson, J. Onishi, J. A. Millifan, G. Bills, L. Kaplan, M. Nallin-Omstead, R. G. Jenkins, L. Huang, M. S. Meinz, L. Quinn, R. W. Burg, Y. L. Kong, S. Mochales, M. Mojena, I. Martin, F. Pelaez, M. T. Diez, A. W. Alberts, *Proc. Natl. Acad. Sci. USA* **1993**, *90*, 80–84.

[2] M. J. Dawson, J. E. Farthing, P. S. Marshall, R. F. Middleton, M. J. O'Neill, A. Shuttleworth, C. Stylli, R. M. Tait, P. M. Taylor, H. G. Wildman, A. D. Buss, D. Langley, M. V. Hayes, *J. Antibiot.* **1992**, *45*, 639–647.

[3] Reviews: U. Koert, *Angew. Chem.* **1995**, *107*, 849–855; *Angew. Chem. Int. Ed. Engl.* **1995**, *34*, 773–778; A. Nadin, K. C. Nicolaou, *Angew. Chem.* **1996**, *108*, 1372–1766; *Angew. Chem. Int. Ed. Engl.* **1996**, *35*, 1622–1656; N. Jotterand, P. Vogel, *Curr. Org. Chem.* **2001**, *5*, 637–661; A. Armstrong, T. J. Blench, *Tetrahedron* **2002**, *58*, 9321–9349.

[4] A. Baxter, B. J. Fitzgerald, J. L. Hutson, A. D. McCarthy, J. M. Motteram, B. C. Ross, M. Sapra, M. A. Snowden, N. S. Watson, R. J. Williams, C. Wright, *J. Biol. Chem.* **1992**, *267*, 11705–11708.

[5] Review: N. S. Watson, P. A. Procopiou, *Prog. Med. Chem.* **1996**, *33*, 331–378.

[6] J. B. Gibbs, D. L. Pompliano, S. D. Mosser, E. Rands, R. B. Lingham, S. B. Singh, E. M. Scolnick, N. E. Kohl, A. Oliff, *J. Biol. Chem.* **1993**, *268*, 7617–7620.

[7] Review: S. Nakamura, *Chem. Pharm. Bull.* **2005**, *53*, 1–10.

[8] a) E. M. Carreira, J. Du Bois, *J. Am. Chem. Soc.* **1994**, *116*, 10825–10826; E. M. Carreira, J. Du Bois, *J. Am. Chem. Soc.* **1995**, *117*, 8106–8125; b) D. A. Evans, J. C. Barrow, J. L. Leighton, A. J. Robichaud, M. Sefkow, *J. Am. Chem. Soc.* **1994**, *116*, 12111–12112; c) H. Sato, S. Nakamura, N. Watanabe, S. Hashimoto, *Synlett* **1997**, 451–454; S. Nakamura, H. Sato, Y. Hirata, N. Watanabe, S. Hashimoto, *Tetrahedron* **2005**, *61*, 11078–11106; d) A. Armstrong, L. H. Jones, P. A. Barsanti, *Tetrahedron Lett.* **1998**, *39*, 3337–3340; A. Armstrong, P. A. Barsanti, L. H. Jones, G. Ahmed, *J. Org. Chem.* **2000**, *65*, 7020–7032; e) S. Nakamura, Y. Hirata, T. Kurosaki, M. Anada, O. Kataoka, S. Kitagaki, S. Hashimoto, *Angew. Chem.* **2003**, *115*, 5509–5513; *Angew. Chem. Int. Ed.* **2003**, *42*, 5351–5355.

[9] a) K. C. Nicolaou, A. Nadin, J. E. Leresche, E. W. Yue, S. La Greca, *Angew. Chem.* **1994**, *106*, 2312–2313; *Angew. Chem. Int. Ed. Engl.* **1994**, *33*, 2190–2191; K. C. Nicolaou, E. W. Yue, S. La Greca, A. Nadin, Z. Yang, J. E. Lereshe, T. Tsuri, Y. Naniwa, F. De Riccardis, *Chem. Eur. J.* **1995**, *1*, 467–494; b) D. Stoermer, S. Caron, C. H. Heathcock, *J. Org. Chem.* **1996**, *61*, 9115–9125; S. Caron, D. Stoermer, A. K. Mapp, C. H. Heathcock, *J. Org. Chem.* **1996**, *61*, 9126–9134; c) K. Tomooka, M. Kikuchi, K. Igawa, M. Suzuki, P.-H. Keong, T. Nakai, *Angew. Chem.* **2000**, *112*, 4676–4679; *Angew. Chem. Int. Ed.* **2000**, *39*, 4502–4505.

[10] S. F. Martin, S. Naito, *J. Org. Chem.* **1998**, *63*, 7592–7593; S. Naito, M. Escobar, P. R. Kym, S. Liras, S. F. Martin, *J. Org. Chem.* **2002**, *67*, 4200–4208.

 © 2006 Wiley-VCH Verlag GmbH & Co. KGaA, Weinheim

[11] For the selective addition of sulfone carbanions to a spirobislactone, see Ref. [10]; for the addition of carbanions to a lactone in the presence of *tert*-butyl esters, see Refs. [8b] and [9c].
[12] Numbering based on zaragozic acid C is used throughout.
[13] a) R. E. Ireland, D. W. Norbeck, *J. Am. Chem. Soc.* **1985**, *107*, 3279 – 3285; b) L. M. McVinish, M. A. Rizzacasa, *Tetrahedron Lett.* **1994**, *35*, 923 – 926; R. W. Gable, L. M. McVinish, M. A. Rizzacasa, *Aust. J. Chem.* **1994**, *47*, 1537 – 1544; c) R. Di Florio, M. A. Rizzacasa, *J. Org. Chem.* **1998**, *63*, 8595 – 8598; d) B. Werschkun, J. Thiem, *Synthesis* **1999**, 121 – 137.
[14] Other approaches that formed the C4–C5 bond and two quaternary asymmetric centers simultaneously: a) aldol reaction: Ref. [8c]; b) acetal [1,2] Wittig rearrangement: Ref. [9c].
[15] A. N. Cuzzupe, R. Di Florio, M. A. Rizzacasa, *J. Org. Chem.* **2002**, *67*, 4392 – 4398.
[16] A. N. Cuzzupe, R. Di Florio, J. M. White, M. A. Rizzacasa, *Org. Biomol. Chem.* **2003**, *1*, 3572 – 3577.
[17] S. C. Zammit, M. A. Rizzacasa, J. M. White, *Org. Biomol. Chem.* **2005**, *3*, 2073 – 2074.
[18] R. K. Mann, J. G. Parsons, M. A. Rizzacasa, *J. Chem. Soc. Perkin Trans. 1* **1998**, 1283 – 1293.
[19] T. Meul, R. Miller, L. Tenud, *Chimia* **1987**, *41*, 73 – 76.
[20] J.-M. Poirier, L. Hennequin, *Tetrahedron* **1989**, *45*, 4191 – 4202.
[21] Synthesized in six steps from L-arabinose in an identical manner to that reported for the enantiomer: see Ref. [15].
[22] CCDC-234390 contains the supplementary crystallographic data for this paper. These data can be obtained free of charge from The Cambridge Crystallographic Data Centre via www.ccdc.cam.ac.uk/data_request/cif.
[23] R. E. Ireland, P. Wipf, J. D. Armstrong III, *J. Org. Chem.* **1991**, *56*, 650 – 657.
[24] V. VanRheenen, R. C. Kelly, D. Y. Cha, *Tetrahedron Lett.* **1976**, *17*, 1973 – 1976.
[25] K. B. Sharpless, W. Amber, Y. L. Bennani, G. A. Crispino, J. Hartung, K. Jeong, H. Kwong, K. Morikawa, Z. Wang, D. Xu, X. Zhang, *J. Org. Chem.* **1992**, *57*, 2768 – 2771.
[26] F. Nicotra, L. Panza, G. Russo, L. Zucchelli, *J. Org. Chem.* **1992**, *57*, 2154 – 2158.
[27] D. A. Evans, J. Bartroli, T. L. Shih, *J. Am. Chem. Soc.* **1981**, *103*, 2127 – 2129.
[28] S. Venel, P. Knochel, *Tetrahedron Lett.* **1994**, *35*, 5849 – 5892; M. Delgado, J. D. Martin, *J. Org. Chem.* **1999**, *64*, 4798 – 4816.
[29] P. J. Garegg, B. Samuelsson, *J. Chem. Soc. Perkin Trans. 1* **1980**, 2866 – 2869.
[30] W. F. Bailey, E. R. Punzalan, *J. Org. Chem.* **1990**, *55*, 5404 – 5406.
[31] B. O. Lindgren, T. Nilsson, *Acta Chem. Scand.* **1973**, *27*, 888 – 890.
[32] This selective benzylic oxidation appears to occur during ozonolysis; we could neither suppress this reaction or increase the conversion.
[33] L. J. Mathias, *Synthesis* **1979**, 561 – 576.
[34] The use of acidic methanol was essential for effective global debenzylation; in the absence of acid, only the O4′ benzyl group was removed at an acceptable rate.
[35] $CDCl_3$ untreated with base was used for this transformation; for an example see Ref. [1a].

 © 2006 Wiley-VCH Verlag GmbH & Co. KGaA, Weinheim

Drug Polymorphism

DOI: 10.1002/anie.200601468

New News about an Old Drug: Investigations on the Polymorphism of Triamcinolone Acetonide**

Christian Näther and Inke Jeß*

Polymorphism, defined as the ability of a compound to exist in more than one crystalline modification, is a widespread phenomenon and of extreme importance in a number of areas like material science and pharmaceutical development.[1,2] For polymorphic drugs several aspects are of importance:[2] Before a new drug is approved by the authorities for sale, it is subjected to a battery of tests, also including investigations of its polymorphism. In addition, information on the influence of a particular corresponding phase on the chemical, biological, and physical properties of a drug are needed, and under certain circumstances different modifications can be patented separately.

The glucocorticoid triamcinolone acetonide (**1**) is an extremely versatile and effective drug and has been used, for example, for treating autoimmune diseases for several years.[3]

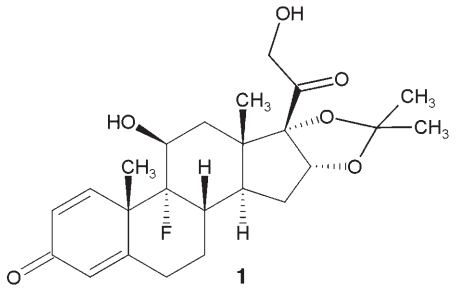

1

In most cases it is administered as a suspension of a crystalline form and hence marketed in glass ampules. In the preparation of its dosage form the drug must be sterilized, and different methods exist. Sterile filtration is a very interesting method in which the compound is dissolved in a given solvent, filtered off, recrystallized, and dried. After the drug has been ground into a fine powder it must be guaranteed that the phase formed is exactly that used in therapy or preferred by the producer. Surprisingly there are very few investigations on the polymorphism of this drug, and the only crystal structure available in the CSD is that of the methanol solvate.[4,5]

We started our research by recording powder diffraction data for several batches of commercially available triamcinolone acetonide prepared by sterile filtration.[6,7] While most batches were found to contain the form used in therapy (modification **I**), one batch exhibited an additional reflection indicating the presence of a second form. To determine the thermodynamically most stable modification at room temperature, we stirred suspensions of the crystalline form of the drug in several solvents, and the products were examined by powder diffraction. In most solvents, for example, acetone, modification **I** was obtained, whereas in ethanol a new and hitherto unknown modification was discovered (form **II**). Interestingly, this form corresponds to that observed as a contamination in one of the batches investigated. Modification **I** crystallizes in different morphologies, whereas form **II** crystallizes mostly as plates (Figure 1).

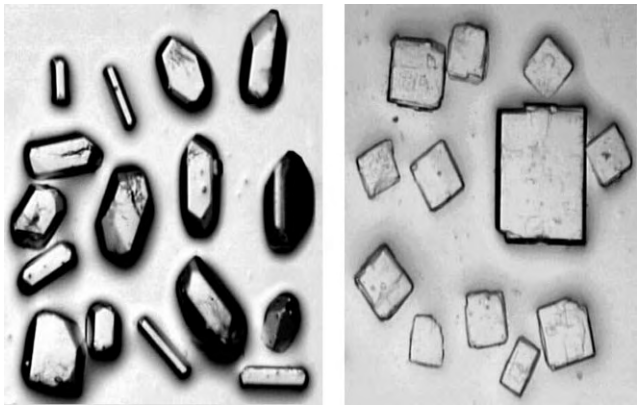

Figure 1. Microscopic images of crystals of modifications **I** (left) and **II** (right).

Differential scanning calorimetry (DSC) shows that form **II** melts at about 288 °C without any further transformation, while the DSC curve of form **I** exhibits a very broad signal only in a few cases before its melting point at 288 °C (Figure 2).[7] The powder pattern of the residue of modification **I** obtained at 220 °C unambiguously shows the formation of form **II**. Thermogravimetric (TG) measure-

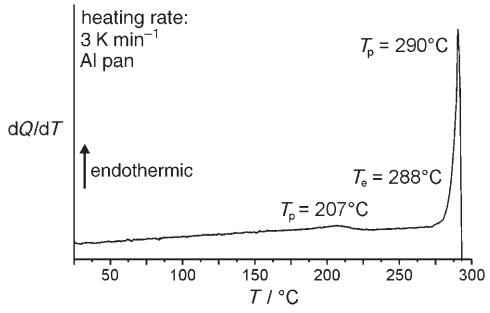

Figure 2. DSC curve of modification **I** (T_p = peak temperature, T_e = onset temperature).

[*] Dr. C. Näther, I. Jeß
Institut für Anorganische Chemie
Christian-Albrechts-Universität zu Kiel
Olshausenstrasse 40, 24098 Kiel (Germany)
Fax: (+49) 431-880-1520
E-mail: cnaether@ac.uni-kiel.de

[**] This work was supported by the State of Schleswig-Holstein. We thank Prof. Dr. Wolfgang Bensch for allowing us to use his equipment and Dr. Michael Bolte, Institute of Inorganic Chemistry Frankfurt, for collecting the data of modification **II**.

Supporting information for this article is available on the WWW under http://www.angewandte.org or from the author.

© 2006 Wiley-VCH Verlag GmbH & Co. KGaA, Weinheim

ments of form **I** using small sample weights did not show appreciable weight loss.

Crystal structure analysis of **I** shows that it crystallizes in space group $R3$.[8] In the structure the molecules are connected by O–H···O hydrogen bonds into layers, which are parallel to (001). This arrangement leads to the formation of trigonal channels in the direction of [001], within which two small residual electron density peaks were found after refinement which were assigned to water (Figure 3). Form **II** crystallizes in space group $P4_12_12$ with the molecules connected by O–H···O hydrogen bonds into layers parallel to (001) (Figure 3).[8] In contrast to form **I** a dense structure is observed.

As the structural results indicated that form **I** is a hydrate, transformation of **I** into **II** in ethanol can be explained if one assumes that the dry solvent dehydrates form **I**. To prove this, a suspension of crystalline **I** was stirred in ethanol until form **II** formed. Afterwards a few drops of water were added, and the suspension was stirred for a few hours. As expected, the powder diffraction pattern of the product thus obtained corresponds to that of form **I**. In addition, **I** can also be transformed to **II** by evacuation at room temperature or by storage at about 100 °C. TG measurements of form **I** in combination with mass spectrometry using large sample weights show clearly that this form contains 1.7 % water (Figure 4).[7] Further investigations using microgravimetry under controlled humidity add credence to our findings.

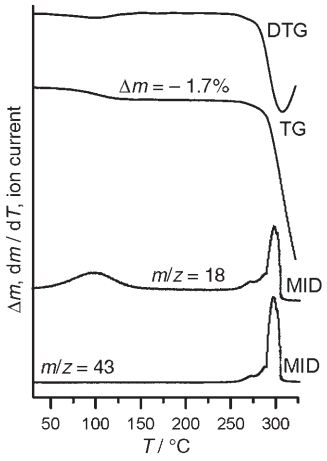

Figure 4. DTG, TG and MS trend-scan curves of **I** (m/z 18 (water and triamcinolone acetonide); m/z 43 (triamcinolone acetonide). MID: multiple-ion detection.

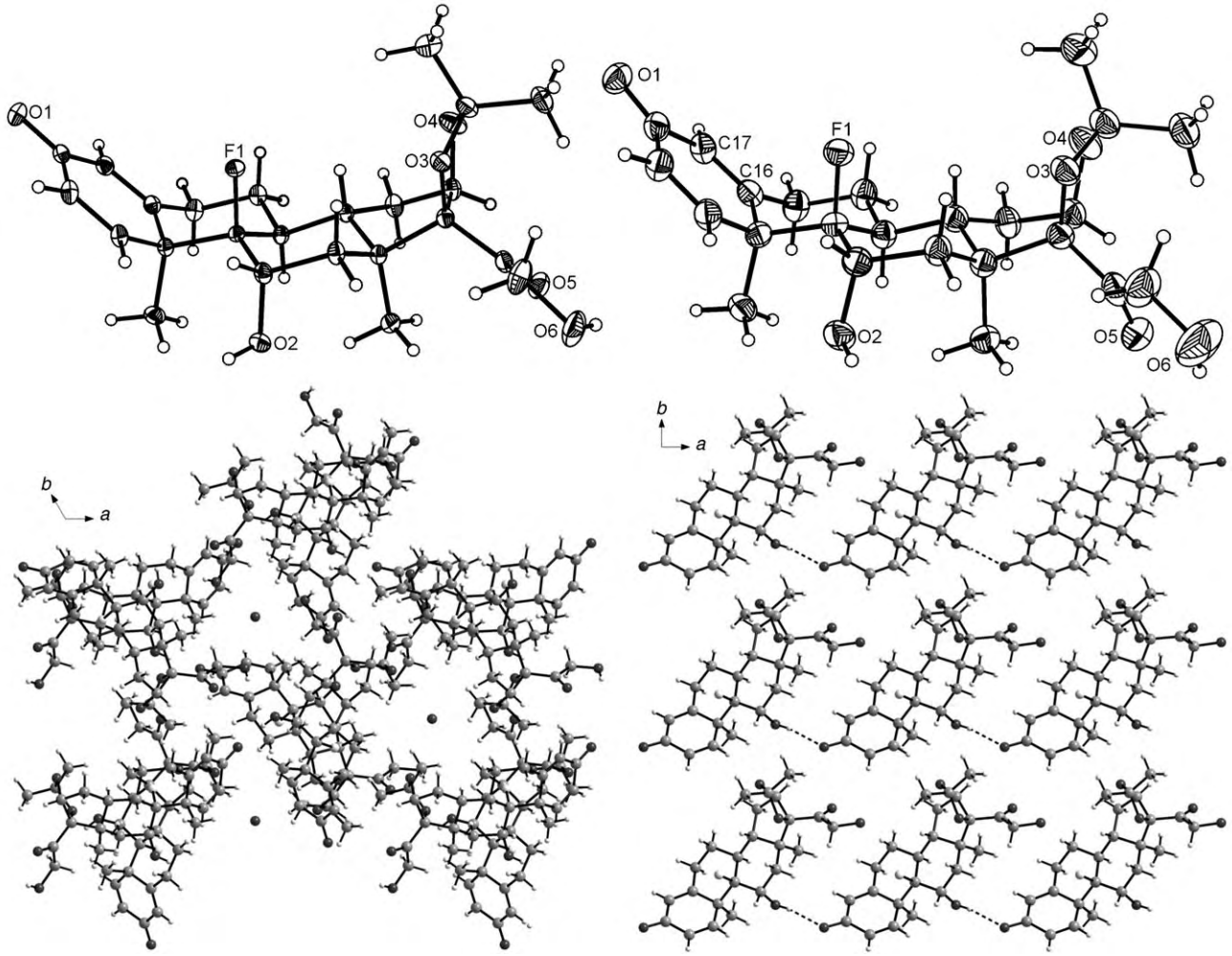

Figure 3. Crystal structures of modifications **I** (left) and **II** (right) (ellipsoids at 50 % probability).

 © 2006 Wiley-VCH Verlag GmbH & Co. KGaA, Weinheim

In summary, our investigations clearly show that the modification of triamcinolone acetonide used in therapy is a hydrate and contains a small amount of water, which is responsible for the stability of this form. When the water is removed, a transformation into the new and hitherto unkown form **II** was observed. It is to be noted that the melting point given in the patent of this drug does not correspond to that of **I**; it actually corresponds to that of **II**. Based on our results the entire process of sterile filtration was improved so as to yield form **I** as a pure phase. Since this drug is mainly used as a suspension of the crystalline form in water, our results indicate that **II** can also be used as it will transform in water into modification **I**. We note, however, that the stability of the suspension depends, for example, on the particle size, which is difficult to control if the hydrate is formed in situ by transformation of modification **II**.

Received: April 13, 2006
Published online: August 29, 2006

Keywords: drugs · hydrates · polymorphism · structure elucidation · transition behavior

[1] a) "Crystal Engineering": in *Mater. Sci. Monogr.* (Ed.: G. R. Desiraju), Elsevier, Amsterdam, **198**; b) J. Bernstein in *Organic Solid State Chemistry: Conformational Polymorphism* (Ed.: G. R. Desiraju), Elsevier, Amsterdam, **1987**, p. 471; c) J. Bernstein, R. Davey, O. Henck, *Angew. Chem.* **1999**, *111*, 3646 – 3669; *Angew. Chem. Int. Ed.* **1999**, *38*, 3440 – 3461; d) J. Bernstein in *X-Ray Crystallography and Drug Action* (Eds.: A. S. Horn, C. J. De Ranter), Clarendon, Oxford, **1984**, p. 23; e) J. D. Dunitz, *Acta Crystallogr. Sect. B* **1995**, *51*, 619 – 631; f) J. D. Dunitz, J. Bernstein, *Acc. Chem. Res.* **1995**, *28*, 193 – 200; g) C. Näther, I. Jeß, Z. Havlas, N. Nagel, M. Bolte, S. Nick, *Solid State Sci.* **2002**, *4*, 859 – 871.

[2] a) *Polymorphism in Pharmaceutical Solids* (Ed.: H. G. Brittain), Marcel Dekker, New York, **1999**; b) S. R. Vippagunta, H. G. Brittain, D. J. W. Grant, *Adv. Drug Delivery Rev.* **2001**, *48*, 3 – 26; c) H. G. Brittain, *Am. Pharm. Rev.* **2000**, *3*, 67 – 68; d) K. R. Morris, U. J. Griesser, C. J. Eckhardt, J. G. Stowell, *Adv. Drug Delivery Rev.* **2001**, *48*, 91 – 114; e) B. Bechtlov, S. Nordhoff, J. Ulrich, *Cryst. Res. Technol.* **2001**, *36*, 1315 – 1328.

[3] a) H. J. Hatz, *Glucocorticoide*, Wissenschaftliche Verlagsgesellschaft, Stuttgart, **2005**; b) P. J. Barnes, *Clin. Sci.* **1998**, *94*, 557 – 572; c) F. Buttgereit, *Z. Rheumatol.* **2000**, *59*, 119 – 123; d) E. Falkenstein, H. C. Tilmann, M. Christ, M. Feuring, M. Wehling, *Pharmacol. Rev.* **2000**, *52*, 513 – 556.

[4] a) *Analytical Profiles of Drug Substances*, *Vol. 11* (Ed.: K. Florey), Academic Press, New York, **1982**; b) J. Fried, A. Borman, W. B. Kessler, P. Grabowich, E. F. Sabo, *J. Am. Chem. Soc.* **1958**, *80*, 2338 – 2339; c) S. Bernstein, R. H. Lenhard, W. S. Allen, M. Heller, R. Littel, S. M. Stolar, L. Feldman, R. H. Blank, *J. Am. Chem. Soc.* **1959**, *81*, 1689 – 1696; d) M. Heller, S. Stolar, S. Bernstein, *J. Org. Chem.* **1961**, *26*, 5044 – 5046.

[5] a) E. Surcouf, *Acta Crystallogr. Sect. B* **1979**, *35*, 2638 – 2642; b) C. Näther, I. Jeß, *Acta Crystallogr. Sect. E* **2005**, *62*, 0960 – 0962.

[6] The sterilzed material was obtained from HPP Pharmaceutical Products (Magdeburg, Germany).

[7] X-Ray powder diffraction experiments were performed using a STOE STADI P transmission powder diffractometer ($Mo_{K\alpha}$ radiation) equipped with a position-sensitive detector (scan range: 5–45°) from STOE & CIE. DSC experiments were performed on a DSC 204/1/F instrument from Netzsch. DTA-TG-MS measurements were performed using the STA-409CD with Skimmer coupling from Netzsch, which is equipped with a quadrupole mass spectrometer from Balzers. The MS measurements were performed in analog and trend-scan mode (Al_2O_3 crucibles, dynamic helium atmosphere, heating rate: 4 K min^{-1}).

[8] **I**: $C_{24}H_{31.82}FO_{6.41}$ ($M_w = 441.89$), $a = b = 17.684(1)$, $c = 18.143(1)$ Å, $V = 4913.6(4)$ Å^3 (170 K), $\rho_{calcd} = 1.344$ g cm^{-3}, trigonal, $R3$, $Z = 9$, STOE IPDS-1, $Mo_{K\alpha}$ radiation, $\mu = 0.102$ mm^{-1}, 9159 measured ($5° \le 2\theta \ge 56°$) and 2628 independent reflections ($R_{int} = 0.0299$ %), structure solution: SHELXS-97, structure refinement: SHELXL-97, 295 parameters, $R1$ for 2491 reflections with $I > 2\sigma(I) = 0.0298$, $wR2$ for all data = 0.0778, GOF = 1.055, residual electron density: 0.22/−0.20 e Å^{-3}. **II**: $C_{24}H_{31}FO_6$ ($M_w = 434.49$), $a = b = 9.1692(4)$ Å, $c = 49.946(4)$ Å, $V = 4199.1(4)$ Å^3 (170 K), $\rho_{calcd} = 1.375$ g cm^{-3}, tetragonal, $P4_12_12$, $Z = 8$, STOE IPDS-2, $Mo_{K\alpha}$ radiation, $\mu = 0.103$ mm^{-1}, 24250 measured ($5° \le 2\theta \ge 51°$) and 2418 independent reflections ($R_{int} = 0.1099$ %), structure solution: SHELXS-97, structure refinement: SHELXL-97), 287 parameters, $R1$ for 1601 reflections with $I > 2\sigma(I) = 0.0352$, $wR2$ for all data = 0.0698, GOF = 0.834, residual electron density: 0.15/−0.15 e Å^{-3}. Non-hydrogen atoms were refined anisotropic. C–H and O–H hydrogen atoms were positioned with idealized geometry (the position was optimized for OH) and refined using a riding model. The hydrogen atoms of water in form **I** were not located. Friedel opposites were merged in the refinement. CCDC 604474 (**I**) and CCDC 604475 (**II**) contain the supplementary crystallographic data for this paper. These data can be obtained free of charge from The Cambridge Crystallographic Data Centre via www.ccdc.cam.ac.uk/data_request/cif.

 © 2006 Wiley-VCH Verlag GmbH & Co. KGaA, Weinheim

Carboxyborates

DOI: 10.1002/anie.200601870

$[B(CO_2H)_4]^-$ and $[B(CNCH_3)_4]^{3+}$: Homoleptic Boron Complexes Containing Carboxy and Methylisocyanide Ligands**

Eduard Bernhardt, David J. Brauer, Maik Finze, and Helge Willner**

Since the synthesis of the first carboxyborane $Me_3NBH_2CO_2H$[1] the interest in boron compounds containing one or more carboxy ligands has increased because of

[*] Dr. E. Bernhardt, Prof. Dr. D. J. Brauer, Prof. Dr. H. Willner
Fachbereich C—Anorganische Chemie
Bergische Universität Wuppertal
Gaussstrasse 20, 42097 Wuppertal (Germany)
Fax: (+49) 202-439-3052
E-mail: edbern@uni-wuppertal.de
willner@uni-wuppertal.de

Dr. M. Finze
Institut für Anorganische Chemie und Strukturchemie II
Heinrich-Heine-Universität Düsseldorf
Universitätsstrasse 1, 40225 Düsseldorf (Germany)

[**] Financial support by the Deutsche Forschungsgemeinschaft (DFG) and Merck KGaA, Darmstadt, is gratefully acknowledged.

© 2006 Wiley-VCH Verlag GmbH & Co. KGaA, Weinheim

their potential medical applications.[2–4] Cyanoborates are used as starting materials for the synthesis of the corresponding carboxyborates by ethylation and subsequent hydrolysis.[1,4–10] A further synthetic route to carboxyboron complexes such as $[(CF_3)_3BCO_2H]^-$[11,12] and $[1,12\text{-}(HO_2C)_2\text{-}B_{12}H_{10}]^{2-}$[13,14] is by the addition of water to boron carbonyls. So far, the simplest carboxyborate anion $[H_3BCO_2H]^-$ is unknown, whereas the dianion $[H_3BCO_2]^{2-}$ forms stable salts.[15] To the best of our knowledge, boron complexes containing three or even more carboxy ligands have not been described.

In recent years we have been interested in the chemistry of borates with four boron–carbon bonds and have succeeded in the first syntheses of tetracyanoborates.[16–18] In comparison to organic nitriles[19–21] and to cyano complexes of transition metals,[22,23] cyanoboranes and -borates are unexpectedly chemically inert; for example, in basic media organic nitriles are hydrolyzed by H_2O_2, whereas the $[B(CN)_4]^-$ ion is stable under comparable conditions.[18] The reason for this stability is the lower positive charge of the carbon atoms of the cyano groups in contrast to organic nitriles, such that a nucleophilic attack at the carbon atoms is prevented. The synthesis of the tetrakis(trifluoromethyl)borate anion [Eq. (1)] in anhydrous HF was the first example of a ligand transformation of the $[B(CN)_4]^-$ anion.[24]

$$[B(CN)_4]^- + 4\,ClF_3 \xrightarrow[-40\,^\circ C \rightarrow RT]{HF} [B(CF_3)_4]^- + 2\,Cl_2 + 2\,N_2 \qquad (1)$$

In the series of the homoleptic borate anions $[B(CN)_4]^-$, $[B(CO_2H)_4]^-$, and $[B(CF_3)_4]^-$, with electron-poor ligands coordinated to the boron atom, the tetrakis(carboxy)borate anion is the only missing member. Herein we report on the preparation of salts of the $[B(CO_2H)_4]^-$ ion in a three-step procedure. In the first step the four cyano ligands of the $[B(CN)_4]^-$ anion are activated by alkylation. From the reaction mixture of $[n\mathrm{Bu}_4\mathrm{N}][B(CN)_4]$ and $[Et_3O][BF_4]$ in dichloromethane $[B(CN)(CNEt)_3][BF_4]_2$ precipitates at 40 °C, and no further ethylation takes place. In contrast, using CF_3SO_3Me gives the triflate salt of the homoleptic $[B(CNMe)_4]^{3+}$ ion in good yields (70–90 %) [Eq. (2)].

$$[n\mathrm{Bu}_4\mathrm{N}][B(CN)_4] + 4\,CF_3SO_3Me \xrightarrow[60\,^\circ C,\ 4\ days]{CF_3SO_3Me} [B(CNMe)_4][CF_3SO_3]_3 + [n\mathrm{Bu}_4\mathrm{N}][CF_3SO_3] \qquad (2)$$

The isolation of $[B(CNMe)_4][CF_3SO_3]_3$ is accomplished by filtration and subsequent washing with CH_2Cl_2. $[B(CNMe)_4][CF_3SO_3]_3$ is soluble in CH_3CN (≈ 10 g/100 mL) without decomposition, but is insoluble in CH_2Cl_2, diethyl ether, monoglyme, and pentane. In the absence of moisture $[B(CNMe)_4][CF_3SO_3]_3$ can be stored at room temperature without decomposition. The $[B(CNMe)_4]^{3+}$ ion is hydrolyzed under acidic conditions to $[B\{C(O)NHMe\}_n\{C(OH)NHMe\}_{4-n}]^{3-n}$ ($n = 0$–4) [Eq. (3)].

$$[B(CNMe)_4]^{3+} + 4\,H_2O \xrightarrow{H_2O} [B\{C(O)NHMe\}_n\{C(OH)NHMe\}_{4-n}]^{3-n} + n\,H^+ \qquad (3)$$

When the aqueous solution is placed in an NO/NO_2 atmosphere, the $[B(CO_2H)_4]^-$ ion is formed [Eq. (4)]. Also addition of $NaNO_2$ leads to transformation of -C(O)NHMe or -C(OH)NHMe ligands to $-CO_2H$. The reaction proposed in Equation (4), with HNO_2 in equilibrium, remains tentative.

$$[B\{C(O)NHMe\}_n\{C(OH)NHMe\}_{4-n}]^{3-n} + 4\,HNO_2 \xrightarrow{H_2O} [B(CO_2H)_4]^- + 4\,[MeHN_2O]^+ + (3-n)\,H^+ \qquad (4)$$

After the reaction is complete, the mixture is neutralized with Na_2CO_3. Addition of ethanol precipitates $Na_3[B(CO_2)_2(CO_2H)_2]\cdot 2\,H_2O$, which is thermally stable up to 100 °C. In a metathesis reaction $[Co(NH_3)_6][B(CO_2)_2(CO_2H)_2]\cdot 2\,H_2O$ is obtained from an aqueous solution of the sodium borate.

Single crystals of $[Co(NH_3)_6][B(CO_2)_2(CO_2H)_2]\cdot 2\,H_2O$ were obtained from an aqueous solution that was acidified with acetic acid. The salt crystallizes in the triclinic space group $P\bar{1}$ with two formula units in the unit cell.[25] The two crystallographically independent $[Co(NH_3)_6]^{3+}$ ions possess crystallographic C_i symmetry with small deviations from D_{3d} symmetry in the solid state. While the borate anion has crystallographic C_1 symmetry, its deviation from C_2 symmetry is not large (Figure 1). The two hydrogen atoms of the anion

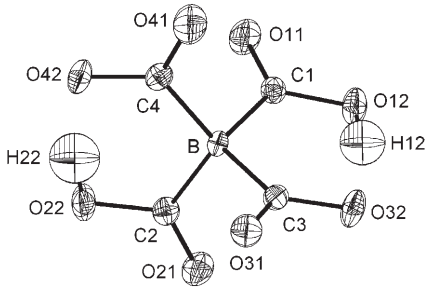

Figure 1. Structure of the $[B(CO_2)_2(CO_2H)_2]^{3-}$ ion in $[Co(NH_3)_6][B(CO_2)_2(CO_2H)_2]\cdot 2\,H_2O$ (thermal ellipsoids set at 50 % probability). Bond lengths [Å]: B-C1 1.635(3), B-C2 1.630(3), B-C3 1.631(3), B-C4 1.631(3), C1-O11 1.227(2), C1-O12 1.332(2), C2-O21 1.231(3), C2-O22 1.332(3), C3-O31 1.262(2), C3-O32 1.290(2), C4-O41 1.251(3), C4-O42 1.296(2), O12-H12 0.86(4),; O22-H22 0.91(4); H12···O32 1.63(4), H22···O42 1.60(4), O12···O32 2.470(2), O22···O42 2.497(2).

were located empirically and refined isotropically without constraints. The protons in the anion link pairs of carboxy groups by strong asymmetric hydrogen bonds. The carboxy groups also participate in weaker hydrogen bonding by accepting protons from the cations and the water molecules. No direct interactions are observed between the anions. Crystal structures of $Na_3[B(CO_2)_2(CO_2H)_2]\cdot 2\,H_2O$ and $[Co(NH_3)_6][B(CO_2)(CO_2H)_3][B(CO_2H)_4]$, the latter of which was obtained as a side product in the synthesis of single crystals of $[Co(NH_3)_6][B(CO_2)_2(CO_2H)_2]\cdot 2\,H_2O$, will be presented elsewhere.

The titration curve of aqueous solutions of $[B(CO_2)_2(CO_2H)_2]^{3-}$ salts with acids and bases exhibits three equivalence points [Eq. (5)]:

The pK_{S2} and pK_{S3} values were obtained from the titration curve. The protonation of $[B(CO_2H)_4]^-$ to $B(CO_2H)_3\{C(OH)_2\}$ and the deprotonation of the trianion $[B(CO_2)_2$-

 © 2006 Wiley-VCH Verlag GmbH & Co. KGaA, Weinheim

$$B(CO_2H)_3\{C(OH)_2\} \underset{+H^+}{\overset{-H^+}{\rightleftharpoons}} [B(CO_2H)_4]^- \underset{+H^+}{\overset{-H^+}{\rightleftharpoons}} [B(CO_2)(CO_2H)_3]^{2-}$$
$$pK_{S1} < 1.5 \qquad pK_{S2} = 4.2 \qquad (5)$$
$$\underset{+H^+}{\overset{-H^+}{\rightleftharpoons}} [B(CO_2)_2(CO_2H)_2]^{3-} \underset{+H^+}{\overset{-H^+}{\rightleftharpoons}} [B(CO_2)_3(CO_2H)]^{4-}$$
$$pK_{S3} = 6.6 \qquad pK_{S4} > 12.5$$

$(CO_2H)_2]^{3-}$ were not observed, and the pK_S values were estimated to be $pK_S < 1.5$ and $pK_S > 12.5$, respectively. The significantly smaller difference between pK_{S2} and pK_{S3} (2.4) than between pK_{S3} and pK_{S4} (> 5.9) is probably a result of the stabilization of $[B(CO_2)_2(CO_2H)_2]^{3-}$ by the intramolecular hydrogen bonds (Figure 1). The $[B(CO_2H)_4]^-$ ion represents the strongest carboxyborate acid known so far ($pK_{S2} = 4.2$).[26] Its acidity is higher than that of the neutral carboxyboranes that have been described so far, and it is similar in acidity to the $[(CH_2NMe_2)_2BrB(CO_2H)]^+$ ion ($pK_s = 4.17$), the strongest carboxyborane acid known.[26] The pK_{S3} value for the deprotonation of $[B(CO_2)(CO_2H)_3]^{2-}$ is comparable to the value of the $[(CF_3)_3BCO_2H]^-$ anion ($pK_S = 7.0$).[12]

In Table 1 the NMR data of $[B(CNCH_3)_4]^{3+}$, the intermediate $[B(CN)(CNCH_3)_3]^{2+}$, and $[B(CN)_4]^-$[16,17] are shown. A higher degree of methylation results in an increase in the resonance frequency of the ^{11}B nuclei while $\delta(^{13}C)$ decreases. The very small line width of the ^{11}B NMR signal of the $[B(CN)_4]^-$ ion (0.2 Hz) shows that quadrupole broadening is unimportant because of the small electric field gradient at the ^{11}B nucleus.[27–29] A similarly sharp signal is observed for the ^{11}B NMR resonance of the $[B(CNCH_3)_4]^{3+}$ ion, whereas for $[B(CN)(CNCH_3)_3]^{2+}$ a broader signal is found.

Table 1: NMR data[a,b] of $[B(CNCH_3)_4]^{3+}$, $[B(CN)(CNCH_3)_3]^{2+}$, and $[B(CN)_4]^-$.[16,17]

Parameter[b]	$[B(CNCH_3)_4]^{3+}$	$[B(CN)(CNCH_3)_3]^{2+}$	$[B(CN)_4]^-$
$\delta(^{11}B)$	−30.6	−32.9	−38.5
$\sigma(^{11}B)$	1.5	33	0.2
$\delta(^{1}H)$	3.88	3.83	
$^{1}J(^{11}B,^{13}C)$	94.6	n.o.[c]	70.9
$^{1}J(^{1}H,^{13}C)$	152.0	151.9	
$^{4}J(^{11}B,^{1}H)$	1.2	n.o.	
$\delta(^{13}C, CN)$	104.5	n.o.	122.3
$\delta(^{13}C, CH_3)$	32.8	n.o.	
$^{1}\Delta^{11}B(^{12/13}C)$	3.9	n.o.	4.9
$^{1}\Delta^{1}H(^{12/13}C)$	2.6	2.7	

[a] Measured in CD_3CN at room temperature. [b] δ in ppm, σ and J in Hz, Δ in ppb. [c] n.o. = not observed.

The ^{11}B and ^{13}C NMR spectra of the $[B(CO_2H)_4]^-$ ion were analyzed at different pH values in D_2O (Table 2). Both $\delta(^{11}B)$ and $\delta(^{13}C)$ are strongly dependent on the pH value owing to varying degrees of protonation. The chemical shift of the ^{11}B nucleus increases with increasing basicity of the solution, from −20.2 ppm in strongly acidic media and up to −14.0 ppm in very basic solution. A reverse trend was observed for $\delta(^{13}C)$. The ^{13}C chemical shifts are comparable to values reported for carboxylic acids.[30] A strong dependency on the pH value is also found for the line widths of the ^{11}B and ^{13}C NMR signals.

Table 2: NMR data[a] of $[B(CO_2H)_4]^-$ in D_2O at different pH values.

Parameter[a]	pH < 0	0 < pH < 3	pH ≈ 10[b]	pH > 14
$\delta(^{11}B)$	−20.2	−19.3	−19.1	−14.0
$\sigma(^{11}B)$	2	0.5	5	8
$^{1}J(^{11}B,^{13}C)$	63.4	63.5	60.7	60.7
$^{1}\Delta^{11}B(^{12/13}C)$	5.2	5.4	5.2	5
$\delta(^{13}C)$	193.7	n.o.[c]	201.4	208.1
$\sigma(^{13}C)$	2.4	n.o.	2.8	6
$^{1}\Delta^{13}C(^{10/11}B)$	n.o.	n.o.	3.7	n.o.

[a] δ in ppm, σ and J in Hz, Δ in ppb. [b] $Na_3[B(CO_2)_2(CO_2H)_2]\cdot 2H_2O$ (0.1 M). [c] n.o. = not observed.

The synthesis of tetrakis(carboxy)borates, $M[B(CO_2H)_4]$, and a tetrakis(methylisocyanide) complex of boron, $[B(CNCH_3)_4][CF_3SO_3]_3$, by employing $[nBu_4N][B(CN)_4]$ as a starting material demonstrates once again the synthetic potential of the tetracyanoborate anion. Furthermore, the series $[B(CN)_4]^-$, $[B(CO_2H)_4]^-$, and $[B(CF_3)_4]^-$ has been completed with the synthesis of salts of the $[B(CO_2H)_4]^-$ ion. Such compounds are promising starting materials for the preparation of further homoleptic boron complexes with four ligands bound to boron through carbon.

Experimental Section

$[B(CNCH_3)_4][CF_3SO_3]_3$: $Bu_4N[B(CN)_4]$ (12.3 g, 34.4 mmol) and $CF_3SO_3CH_3$ (106.6 g, 650 mmol) were placed into a round-bottom flask (250 mL) equipped with a PTFE valve and warmed to 60 °C for 4 days. After 2 and 3 days the reaction mixture was treated in an ultrasonic bath for 5 hours and 1 hour, respectively. The precipitate was separated by filtration, washed with anhydrous CH_2Cl_2 (200 mL), and dried in vacuum. Yield: 19.8 g (31.8 mmol, 92 %). The excess $CF_3SO_3CH_3$ (64.0 g, 390 mmol) was recovered.

$Na_3[B(CO_2)_2(CO_2H)_2]\cdot 2H_2O$: $[B(CNCH_3)_4][CF_3SO_3]_3$ (0.52 g, 0.84 mmol) was dissolved in water (20 mL), and the solution was cooled to 0 °C. A mixture of NO and NO_2, prepared from $NaNO_2$ (30 g, 435 mmol), H_2SO_4 (60 mL, 1.1 mol), and water (80 mL, 4.4 mol), was added over a span of 4 h to the reaction mixture. At room temperature the reaction mixture was further stirred for 16 h. Upon addition of Na_2CO_3 (3.2 g, 30 mmol) and ethanol (300 mL) the crude product precipitated and was separated by filtration. The precipitate was dissolved in water (15 mL), the solution was saturated with CO_2, and ethanol (200 mL) was added. After filtration the product was washed with ethanol (20 mL) and diethyl ether (20 mL). Yield: 0.25 g (0.84 mmol, 100 %).

$[Co(NH_3)_6][B(CO_2)_2(CO_2H)_2]\cdot 2H_2O$: $Na_3[B(CO_2)_2(CO_2H)_2]\cdot 2H_2O$ (0.15 g, 0.5 mmol) was dissolved in water (25 mL) and treated with a solution of $[Co(NH_3)_6]Cl_3$ (0.25 g, 1 mmol) in water (25 mL). Immediately, an orange solid was formed which recrystallized after 2–3 h to yield orange needles of $[Co(NH_3)_6][B(CO_2)_2(CO_2H)_2]\cdot 2H_2O$. The crystals were isolated by filtration, washed with water (10 mL), ethanol (10 mL), and diethyl ether (10 mL), and dried in air. Yield: 0.18 g (0.45 mmol, 90 %).

Received: May 11, 2006
Published online: August 29, 2006

Keywords: boron · isocyanide · ligand transformations · NMR spectroscopy · structure elucidation

 © 2006 Wiley-VCH Verlag GmbH & Co. KGaA, Weinheim

[1] B. F. Spielvogel, L. Wojnowich, M. K. Das, A. T. McPhail, K. D. Hargrave, *J. Am. Chem. Soc.* **1976**, *98*, 5702.
[2] B. F. Spielvogel, A. Sood, I. H. Hall, WO 9309,123, **1993**.
[3] I. H. Hall, E. S. Hall, M. C. I. Miller, A. Sood, B. F. Spielvogel, *Amino Acids* **1993**, *4*, 287.
[4] B. Györi, Z. Berente, *Inorg. Chem.* **2001**, *40*, 1770.
[5] J. H. Hall, C. O. Starnes, B. F. Spielvogel, P. Wisian-Neilson, M. K. Das, L. Wojnowich, *J. Pharm. Sci.* **1979**, *68*, 685.
[6] B. F. Spielvogel, F. U. Ahmed, A. T. McPhail, *Inorg. Synth.* **1989**, *25*, 79.
[7] M. Mittakanti, K. W. Morse, *Inorg. Chem.* **1990**, *29*, 554.
[8] A. Sood, B. F. Spielvogel, *Inorg. Chem.* **1992**, *31*, 2654.
[9] C. H. Sutton, M. W. Baize, L. J. Todd, *Inorg. Chem.* **1994**, *33*, 4221.
[10] Z. Berente, B. Györi, *Chem. Commun.* **1997**, 1799.
[11] A. Terheiden, E. Bernhardt, H. Willner, F. Aubke, *Angew. Chem.* **2002**, *114*, 823; *Angew. Chem. Int. Ed.* **2002**, *41*, 799.
[12] M. Finze, E. Bernhardt, A. Terheiden, M. Berkei, H. Willner, D. Christen, H. Oberhammer, F. Aubke, *J. Am. Chem. Soc.* **2002**, *124*, 15385.
[13] W. H. Knoth, J. C. Sauer, J. H. Balthis, H. C. Miller, E. L. Muetterties, *J. Am. Chem. Soc.* **1967**, *89*, 4842.
[14] M. A. Fox, J. A. K. Howard, J. M. Moloney, K. Wade, *Chem. Commun.* **1998**, 2487.
[15] L. J. Malone, R. W. Parry, *Inorg. Chem.* **1967**, *6*, 817.
[16] E. Bernhardt, G. Henkel, H. Willner, *Z. Anorg. Allg. Chem.* **2000**, *626*, 560.
[17] E. Bernhardt, M. Berkei, H. Willner, M. Schürmann, *Z. Anorg. Allg. Chem.* **2003**, *629*, 677.
[18] E. Bernhardt, M. Finze, H. Willner, *Z. Anorg. Allg. Chem.* **2003**, *629*, 1229.
[19] E. Müller, *Sauerstoff-Verbindungen III*, *Methoden der organischen Chemie (Houben-Weil)*, *Vol. 8*, Georg Thieme, Stuttgart, **1952**.
[20] J. Falbe, *Carbonsäuren und Carbonsäure-Derivate*, *Methoden der organischen Chemie (Houben-Weil)*, *Vol. E5*, Georg Thieme, Stuttgart, **1985**.
[21] U. Bergsträßer, S. J. Collier, Y. Ito, S. Kanemasa, P. Langer, S.-I. Murahashi, M. North, J. Podlech, A. Schmidt, L. R. Subramanian, M. Suginome, *Science of Synthesis*, *Three Carbon–Heteroatom Bonds: Nitriles, Isocyanides, and Derivatives*, *Vol. 19*, Georg Thieme, Stuttgart, **2004**.
[22] *Topics in Inorganic and General Chemistry*, *Chemistry of Pseudohalides*, *Vol. 21* (Eds.: A. M. Holub, H. Köhler, V. V. Skopenko), Elsevier, Amsterdam, **1986**, p. 77.
[23] Y. N. Kukushkin, *Reactivity of Coordination Compounds. (Reaktsionnaya Sposobnost' Koordinatsionnykh Soedinenii)*, Khimiya, Leningrad. Otd., Leningrad, **1987**.
[24] E. Bernhardt, G. Henkel, H. Willner, G. Pawelke, H. Bürger, *Chem. Eur. J.* **2001**, *7*, 4696.
[25] Crystal structure analysis of $[Co(NH_3)_6][B(CO_2)_2(CO_2H)_2]\cdot 2H_2O$: $C_4H_{24}BCoN_6O_{10}$, Bruker AXS P4-Smart 1 K; $Mo_{K\alpha}$ radiation ($\lambda = 0.71073$ Å), graphite monochromator; measurement temperature 20 °C. Orange crystals ($0.4 \times 0.1 \times 0.1$ mm^3) obtained from water, triclinic, space group $P\bar{1}$ (No. 2), $a = 7.0039(4)$, $b = 7.2994(4)$, $c = 15.1293(9)$ Å, $\alpha = 77.359(1)$, $\beta = 79.466(1)$, $\gamma = 77.000(1)$°, $V = 728.09(13)$ Å^3, $Z = 2$, $\rho_{calcd} = 1.761$ Mg m^{-3}, $\mu(Mo_{K\alpha}) = 1.24$ mm^{-1}, $F(000) = 404$, 5332 measured reflections ($2.2 < \theta < 28.28$°), integration with SAINT (V6.45A, 1997–9 Bruker Analytical X-ray Systems), structure solution by direct methods and refinement against F^2 with 3362 independent reflections (3147 independent reflections with $I > 2\sigma(I)$), 298 variables and 0 restraints (SHELXS-97).[31] All atoms (except for hydrogen) were refined anisotropically. $R_1 = 0.0340$ ($I > 2\sigma(I)$).[32] CCDC-600354 contains the supplementary crystallographic data for this paper. These data can be obtained free of charge from The Cambridge Crystallographic Data Centre via www.ccdc.cam.ac.uk/data_request/cif.
[26] B. Györi, Z. Berente, Z. Kovacs, *Inorg. Chem.* **1998**, *37*, 5131.
[27] P. S. Hubbard, *J. Chem. Phys.* **1970**, *53*, 985.
[28] T. K. Halstead, P. A. Osment, B. C. Sanctuary, J. Tagenfeldt, I. J. Lowe, *J. Magn. Reson.* **1986**, *67*, 267.
[29] B. Wrackmeyer, *Nuclear Magnetic Resonance Spectroscopy of Boron Compounds Containing Two-, Three- and Four-Coordinate Boron*, *Annual Reports on NMR Spectroscopy*, *Vol. 20* (Ed.: G. A. Webb), Academic Press, London, UK, **1988**, p. 61.
[30] H.-O. Kalinowski, S. Berger, S. Braun, *^{13}C-NMR-Spektroskopie*, Georg Thieme, Stuttgart, **1984**.
[31] G. M. Sheldrick, SHELXS-97, Programm for Crystal Structure Solution, Universität Göttingen, **1997**.
[32] G. M. Sheldrick, SHELXL-97, Programm for Crystal Structure Refinement, Universität Göttingen, **1997**.

 © 2006 Wiley-VCH Verlag GmbH & Co. KGaA, Weinheim

Allylations

DOI: 10.1002/anie.200600447

High-Yield Ruthenium-Catalyzed Friedel–Crafts-Type Allylation Reactions Using Dicationic Ru^{IV} Catalysts**

Ignacio Fernández, René Hermatschweiler, Frank Breher, Paul S. Pregosin, Luis F. Veiros, and Maria José Calhorda*

The organometallic catalytic chemistry of ruthenium continues to expand with applications in organic synthesis involving

[*] Dr. I. Fernández, R. Hermatschweiler, Prof. Dr. P. S. Pregosin
Laboratory of Inorganic Chemistry
ETHZ
Hönggerberg, 8093 Zürich (Switzerland)
Fax: (+41) 446-331-071
E-mail: pregosin@inorg.chem.ethz.ch
Prof. Dr. F. Breher
Institut für Anorganische Chemie
Universität Karlsruhe
Engesserstrasse 15, 76131 Karlsruhe (Germany)
Prof. Dr. L. F. Veiros
Centro de Química Estrutural
Complexo I
Instituto Superior Técnico
Av. Rovisco Pais 1, 1049-001 Lisbon (Portugal)
Prof. Dr. M. J. Calhorda
Departamento de Química e Bioquímica
Faculdade de Ciências
Universidade de Lisboa, 1749-016 Lisbon (Portugal)

[**] P.S.P. thanks the Swiss National Science Foundation, the Bundesamt für Bildung und Wissenschaft, and the ETHZ for financial support. I.F. thanks the Junta de Andalucía for a research contract. We also thank Johnson Matthey for the loan of precious metals.

Supporting information for this article is available on the WWW under http://www.angewandte.org or from the author.

WILEY InterScience DISCOVER SOMETHING GREAT
© 2006 Wiley-VCH Verlag GmbH & Co. KGaA, Weinheim

hydroamination,[1] isomerization,[2–4] kinetic resolution,[5] hydrogenation,[6] metathesis,[7] a variety of multiple C–C bond-formation reactions,[8] and allylic alkylation.[9,10]

With respect to allylation chemistry, several Cp*Ru precursors (Cp* = C_5Me_5) have been suggested as catalysts. These include the tris(acetonitrile) complex [Ru(Cp*)-$(CH_3CN)_3$]PF_6 (**1**) from Trost et al.,[9] complexes containing bidentate nitrogen ligands,[10] and the Ru^{IV} carbonate complex **2** reported by us.[11] The latter complex[11b] was shown to be an interesting alternative to **1** in the allylic alkylation of

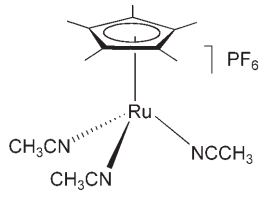

1

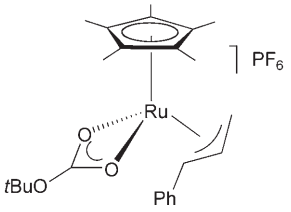

2

phenylallyl-*tert*-butyl carbonate with sodium dimethyl malonate. Complex **2** can also be used successfully in allylic amination[12a] and phenolation[12b] reactions.

If **2** were to decompose to afford CO_2 and *t*-butoxide, the Ru^{IV} solvate complexes, for example **3** and **4**, would be

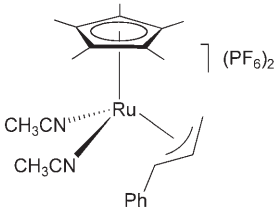

3

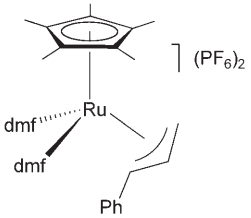

4

formed. Consequently, we prepared these dicationic complexes and show herein that **3**, in contrast to **2**, represents a novel catalyst for Friedel–Crafts-type allylation and catalyzes unexpected C–C couplings. Specifically, different arene compounds can be selectively allylated under relatively mild conditions in very good yield without the use of Lewis acidic main-group compounds or other additives.

Complexes **3** and **4** were prepared from our previously reported Ru^{IV} chlorido complex [Ru(Cp*)Cl$(CH_3CN)(\eta^3$-$PhCHCHCH_2)$]PF_6 [**5**, see Eq. (1)][11a] by treatment with $AgPF_6$ in the appropriate solvent.[13a] Table 1 shows the

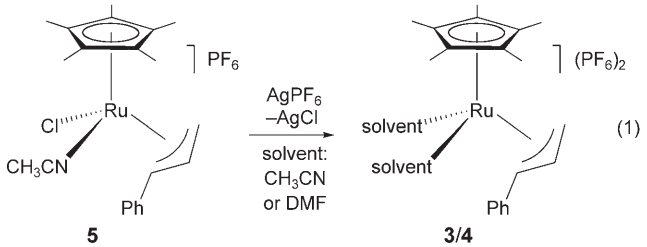

5 **3/4**

Table 1: Selected ruthenium-catalyzed carbon–carbon bond formations in acetonitrile at 353 K using the catalyst precursor **4** with the branched allyl carbonate substrate **6**.[a]

Entry	Arene	*t* [min]	Product	% C–C (*o*/*m*/*p*)[b]
1	phenol	72	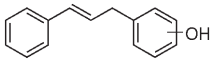	100 (10:6:84)
2	2,6-Me_2-phenol	58	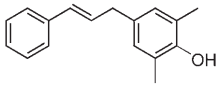	100 (0:0:100)
3	4-Me-phenol	1	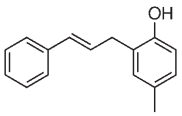	100 (82:18:0)
4	2-naphthol	4	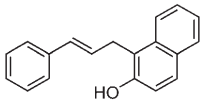	94
5	6-Br-2-naphthol (5 equiv)	4	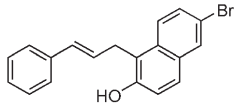	100
6	6-Br-2-naph-thoxysilane	5	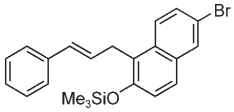	100
7	anisole	205	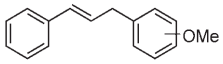	100 (5:2:93)
8	thioanisol	425	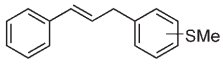	74 (16:0:84)
9	*p*-xylole[c]	16 h	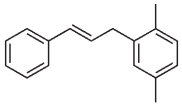	73
10	*o*-xylole[c]	92	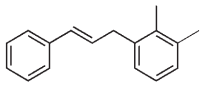	81 (20:80)

[a] Conditions: 0.07 mmol of allyl substrate **6**, 0.21 mmol of the corresponding arene derivative, 0.002 mmol of catalyst (3 mol%), in 0.5 mL of acetonitrile. [b] The *o*/*m*/*p* ratios were determined by ^{1}H NMR spectroscopy. [c] 30 equivalents.

Friedel–Crafts-type products from the reaction of the branched phenylallyl carbonate $PhCH(OCO_2tBu)CHCH_2$ (**6**) with a variety of electron-rich aromatic substrates at 353 K with **4** as the catalyst (which in acetonitrile solution reverts to **3**).

In all the examples shown, the conversion to product is high, and ^{1}H NMR spectroscopic data show only linear and no branched isomer. For a few of the arene compounds *only one isomer* is observed in very high yield (Table 1, entries 2, 5, and 6); however, for several of the arene compounds, one does find a mixture of *ortho*, *meta*, and *para* isomers. For the phenol compounds,[13b] the reaction is quite rapid, and in some cases complete conversion is observed in less than 10 minutes.

 © 2006 Wiley-VCH Verlag GmbH & Co. KGaA, Weinheim

With chlorobenzene, however, there is no allylation after about 24 hours. We were also able to show that the solvent can have a significant influence on the reaction. With dimethylformamide (DMF) as the solvent and precursor **4**, the reaction of a naphthol substrate affords both C–C (36%) and C–O (64%) coupling products.

To further test the generality of the catalyst precursors for Friedel–Crafts reactions, we used **3** to catalyze the reaction of 6-bromo-2-naphthol with several differently substituted carbonates [Eq. (2)]. For all of the reactions leading to **7**, the

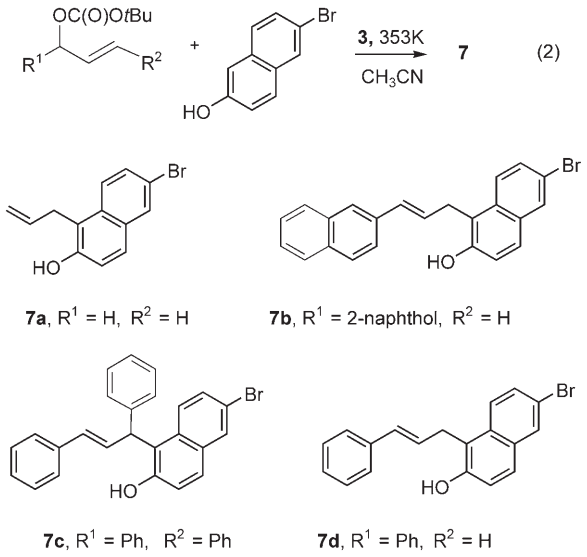

conversion is 100%, and the yield of product is greater than 80%. The reactions leading to **7b–7d** were complete within less than 10 minutes, whereas 100% conversion to **7a** required about two hours.

The Friedel–Crafts reaction has a long history.[14] Recently, it has been shown that a number of late-transition-metal complexes[15,16] are capable of condensing arene compounds with a suitable electrophile (for example, hexanoic acid anhydride[15]), and this area has recently been reviewed.[17] We are aware of several reports in which Ru compounds have been employed.[15,18] Two of these studies[18] use a dinuclear Ru^{III} species at about 413 K (fairly harsh conditions), and the yields are often only moderate. Fürstner and co-workers have employed $RuCl_3$ in the acylation of hexanoic acid anhydride with anisole; however, this catalyst seems to be relatively slow. Our catalyst represents a significant improvement relative to these Ru sources in that we use less catalyst and have faster reactions under milder conditions.

It is important to note that the related catalyst **2**[11b,12b] forms only C–O and no C–C bonds with phenol and the same branched allyl substrate [Eq. (3)], so that by a slight modification of the catalyst, one can completely redirect the nature of the organic product formed. Given this useful flexibility, we considered it appropriate to study aspects of these ruthenium catalysts.

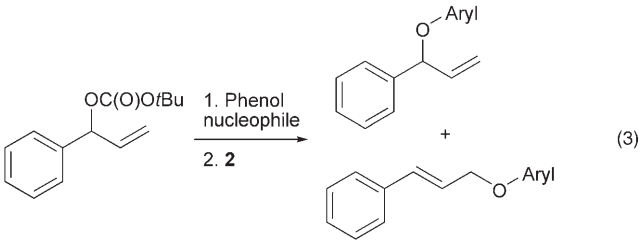

The molecular structures of the two dications of **3** and **4**[13] are shown in Figures 1 and 2. A selection of bond angles and bond lengths are given in the captions of the figures. Both

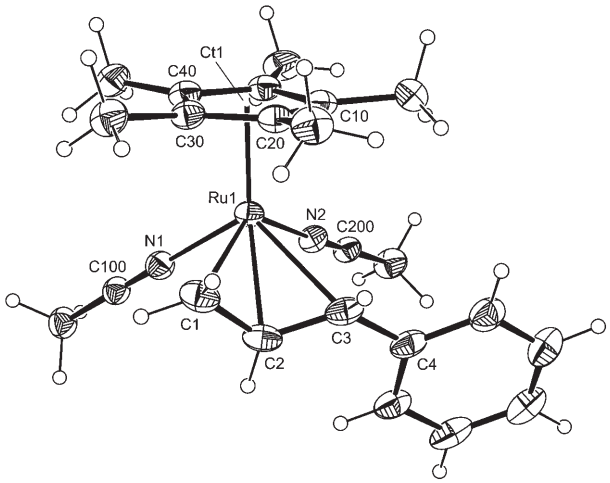

Figure 1. Structure of the dication $[Ru(Cp^*)(\eta^3\text{-}CH_2CHCHPh)(MeCN)_2]^{2+}$ in **3**. Thermal ellipsoids are drawn at 30% probability; PF_6 anions are omitted for clarity. Bond lengths [pm] and angles [°]: Ru1-N1 207.8(3), Ru1-N2 208.1(3), Ru1-C1 218.0(3), Ru1-C2 218.9(3), Ru1-C3 238.2(3), Ru1-Ct1 185.9(3), Ru1-C10 219.1(3), Ru1-C20 220.6(3), Ru-C30 221.4(3), Ru1-C40 225.7(3), Ru1-C50 223.9(3), N1-C100 112.3(4), N2-C200 112.4(4); C1-C2-C3 119.4(3), N1-Ru1-N2 82.6(1); $\phi = 70.3°$; Ct1 = centroid of the Cp* ligand; ϕ is the intersection of the planes described by C1, C2, C3 and the five atoms of the Cp* ring.

complexes show the Ru atom complexed by the Cp* ligand, the phenylallyl ligand, and two solvent molecules. As expected, the dmf ligands are complexed through the amide oxygen atoms. The most interesting features in these dications involve the various Ru–C(allyl) bond lengths. Specifically, the Ru–C3 bonds (238.2(3) (**3**) and 232.3(4) pm (**4**)) are relatively long with the former separation exceptionally large. We have observed this type of long Ru–C(allyl) bond in both the Ru^{IV} chlorido complex **5** (Ru–C3 235.1(2) pm)[11a] and Ru^{IV} carbonate complex **2** (Ru–C3 230.3(5) pm).[11b] However, for the acetonitrile complex **3**, this bond is the longest of the set.

We have previously suggested that this long bond arises from relatively weak π back-bonding.[11a] The observed ^{13}C NMR chemical shift of C3 in **3** ($\delta = 103.3$ ppm) appears at higher frequency than that in the monocation **5** ($\delta =$ 91.0 ppm) and is thus consistent with this suggestion.

 © 2006 Wiley-VCH Verlag GmbH & Co. KGaA, Weinheim

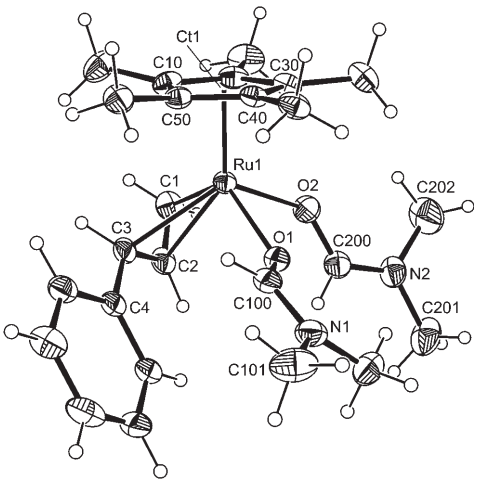

Figure 2. Structure of the dication $[Ru(Cp^*)(\eta^3\text{-}CH_2CHCHPh)(dmf)_2]^{2+}$ in **4**. Thermal ellipsoids are drawn at 30% probability; PF_6 anions are omitted for clarity. Bond lengths [pm] and angles [°]: Ru1-O1 211.0(3), Ru1-O2 212.6(3), Ru1-C1 218.4(4), Ru1-C2 215.5(4), Ru1-C3 232.3(4), Ru1-Ct1 186.0(4), Ru1-C10 220.1(4), Ru1-C20 216.3(4), Ru-C30 222.9(4), Ru1-C40 228.1(4), Ru1-C50 223.6(4), O1-C100 123.7(5), O2-C200 125.8(5), N1-C100 133.2(6), N2-C200 129.6(6); C1-C2-C3 117.0(4), O1-Ru1-O2 79.7(1); $\phi = 68.2°$; Ct1 = centroid of the Cp* ligand; ϕ is the intersection of the planes described by C1, C2, C3 and the five atoms of the Cp* ring.

To understand the chemistry of these salts a bit further, we performed DFT calculations[19] for the three model cations $[Ru(Cp)(CH_3CN)_2(\eta^3\text{-}PhCHCHCH_2)]^{2+}$, $[Ru(Cp)(dmf)_2(\eta^3\text{-}PhCHCHCH_2)]^{2+}$, and $[Ru(Cp)(CH_3OCO_2)(\eta^3\text{-}PhCHCHCH_2)]^{+}$ ($Cp = C_5H_5$). The results reveal that the Ru–C bond lengths for the substituted, terminal allyl carbon atom decrease as follows: 264 pm for the acetonitrile complex, 252 pm for the dmf complex, and 233 pm for the carbonate species. The remaining Ru–C(allyl) bond lengths are all in the range 210–222 pm. Although the separations of 264 pm and 252 pm are longer than the X-ray values, they are qualitatively consistent with the solid-state structures. Furthermore, natural population analysis (NPA) reveals the negative charges on the three terminal phenylallyl carbon atoms to be −0.05, −0.08, and −0.15, respectively, that is, the acetonitrile dication has the least amount of negative charge on this carbon atom. A possible reason can be deduced from the three molecular orbitals in Figure 3a, which represent the bonding metal–allyl π interactions. While the dmf and carbonate donors contribute to the orbital of the π interaction, this is not the case for the acetonitrile donors. This observation suggests an electron flow from the oxygen donors to the allyl ligand in the carbonate and dmf complexes, thus rationalizing the charges on the allyl carbon atoms.

The LUMO of the acetonitrile complex shows a greater participation of the substituted carbon atom (Figure 3b). If our reaction were orbital-controlled, one would expect attack at the *substituted*, terminal carbon and not, as found, at the allylic CH_2 carbon atom. Interestingly, there is less positive charge on the Ru atom in the acetonitrile complex (+0.34) than for the dmf (+0.49) and carbonate complexes (+0.51). This difference is consistent with the better donor ability of

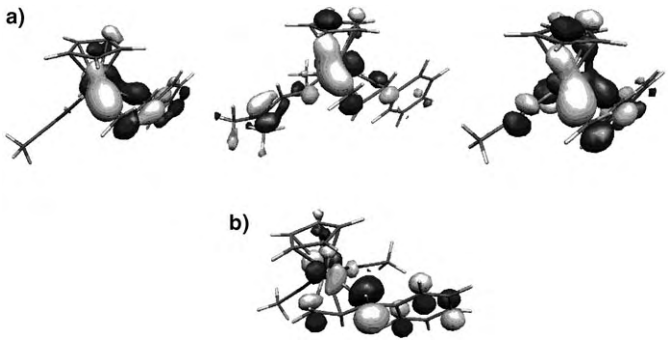

Figure 3. a) Bonding Ru allyl π orbitals. Left: HOMO−4 of $[Ru(Cp)(CH_3CN)_2(\eta^3\text{-}PhCHCHCH_2)]^{2+}$, with no contribution from the acetonitrile orbitals; middle: HOMO−5 of $[Ru(Cp)(dmf)_2(\eta^3\text{-}PhCHCHCH_2)]^{2+}$; right: HOMO−4 of $[Ru(Cp)(CH_3OCO_2)(\eta^3\text{-}PhCHCHCH_2)]^{+}$. b) LUMO of $[Ru(Cp)(CH_3CN)_2(\eta^3\text{-}PhCHCHCH_2)]^{2+}$, with a large contribution from the Ph–C allyl carbon atom.

the acetonitrile ligand than either of the oxygen ligands. Although the dicationic acetonitrile complex is substantially different from the other two cations, it is not clear from the X-ray and DFT data why the *linear* allyl product (namely, Ph-CH=CH-CH_2-Ar) is formed preferentially. Indeed, relative to palladium, ruthenium catalysts in allylation chemistry are interesting because they can favor the formation of the branched products.[9,10]

A partial answer to this question is given by diffusion data from pulsed-gradient spin echo (PGSE) NMR measurements for complexes **3** and **5** (Table 2). This diffusion methodology[20] allows one to estimate molecular volumes and ion pairing in solution. From the measured diffusion coefficient values D for the cation of **5**, we estimate the hydrodynamic radius r_H (using the Stokes–Einstein equation) to be about 4.7 Å, in good agreement with estimates of the size of this cation (4.5 Å) from our crystallographic data.[21] For the

Table 2: D and r_H values for the ruthenium complexes in acetonitrile at 299 K.[a]

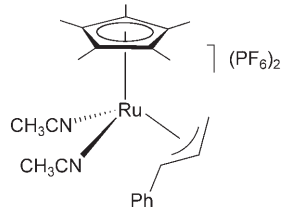

3

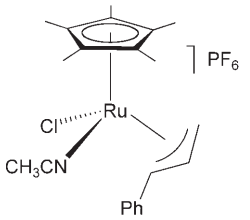

5

	Nucleus	D[b]	r_H[c] [Å]
3	^1H (cation)	12.07	5.4
	^{19}F (anion)	23.50	2.8
	^1H (free CH_3CN)	40.35	1.6
5	^1H (cation)	13.72	4.7
	^{19}F (anion)	24.76	2.6
	^1H (free CH_3CN)	40.34	1.6

[a] All at 2 mM. [b] ±2%, $\times 10^{10}\ m^2\,s^{-1}$. [c] $\eta(CH_3CN, 299\ K) = 0.3377 \times 10^{-3}\ kg\,s^{-1}\,m^{-1}$.

 © 2006 Wiley-VCH Verlag GmbH & Co. KGaA, Weinheim

cation of **3**, we obtain a much larger r_H value of about 5.4 Å, which can be the result of ion pairing.[20] However, the diffusion data from the PF_6 anions of **3** suggest that this is not the case. The r_H values for the PF_6 anions of both **3** and **5** (2.6–2.8 Å) are typical of what one finds in a polar solvent such as methanol. We suggest that the larger r_H value of 5.4 Å for the cation of **3** arises as a result of some charge-induced aggregation.[20d,e] The presence of an aggregate may make it more difficult to attack the substituted allylic carbon, so that we tentatively attribute the observed regioselectivity to steric effects as a result of aggregation.[22]

Perhaps there is a transition state in which the O (or S) donor approaches the Ph–C(allyl) position, but is hindered so that the C–C coupling is favored. To test this aggregation assumption we have carried out a catalytic reaction at tenfold dilution using 6-bromo-2-naphthol as the substrate. Indeed, whereas we had previously found no C–O product, we found 13% C–O bond formation in the diluted reaction mixture.

In conclusion, we have found that a new dicationic Ru^{IV} salt is a very efficient and mild catalyst for the Friedel–Crafts-type allylation of various electron-rich arene substrates. This C–C coupling reaction is in contrast to the selective C–O bond-forming reactions observed with related catalysts.

Received: February 2, 2006
Revised: May 22, 2006
Published online: August 23, 2006

Keywords: allylations · density functional calculations · NMR spectroscopy · ruthenium · structure elucidation

[1] J. Takaya, J. F. Hartwig, *J. Am. Chem. Soc.* **2005**, *127*, 5756.
[2] B. M. Trost, M. T. Rudd, *J. Am. Chem. Soc.* **2005**, *127*, 4763; B. M. Trost, M. U. Frederiksen, M. T. Rudd, *Angew. Chem.* **2005**, *117*, 6788; *Angew. Chem. Int. Ed.* **2005**, *44*, 6630.
[3] M. Ito, S. Itahara, T. Ikariya, *J. Am. Chem. Soc.* **2005**, *127*, 6172.
[4] R. C. van der Drift, M. Gagliardo, H. Kooijman, A. L. Spek, E. Bouwman, E. Drent, *J. Organomet. Chem.* **2005**, *690*, 1044.
[5] S. Hashiguchi, A. Fujii, K. J. Haack, K. Matsumura, T. Ikariya, R. Noyori, *Angew. Chem.* **1997**, *109*, 300; *Angew. Chem. Int. Ed. Engl.* **1997**, *36*, 288.
[6] a) T. Ohkuma, H. Ooka, T. Ikariya, R. Noyori, *J. Am. Chem. Soc.* **1995**, *117*, 10417; b) T. Ohkuma, H. Ooka, M. Yamakawa, T. Ikariya, R. Noyori, *J. Org. Chem.* **1996**, *61*, 4872; c) K. J. Haack, S. Hashiguchi, A. Fujii, T. Ikariya, R. Noyori, *Angew. Chem.* **1997**, *109*, 297; *Angew. Chem. Int. Ed. Engl.* **1997**, *36*, 285.
[7] R. H. Grubbs, *Tetrahedron* **2004**, *60*, 7117; A. Hejl, O. A. Scherman, R. H. Grubbs, *Macromolecules* **2005**, *38*, 7214.
[8] a) P. H. Dixneuf, C. Bruneau in *Organic Synthesis via Organometallics OSM 5* (Eds.: D. Helmchen, J. Dibo, J. Flubacher, B. Wiese), Friedr. Vieweg, Braunschwewig, **1997**, p. 1; b) S. Derien, P. H. Dixneuf, *J. Organomet. Chem.* **2004**, *689*, 1382; c) E. Bustelo, P. H. Dixneuf, *Adv. Synth. Catal.* **2005**, *347*, 393; T. Murahashi, *Ruthenium in Organic Synthesis*, Wiley-VCH, Weinheim, **2004**.
[9] a) B. M. Trost, P. L. Fraisse, Z. T. Ball, *Angew. Chem.* **2002**, *114*, 1101; *Angew. Chem. Int. Ed.* **2002**, *41*, 1059; b) B. M. Trost, M. L. Crawley, *Chem. Rev.* **2003**, *103*, 2921.
[10] a) M. D. Mbaye, B. Demerseman, J. L. Renaud, L. Toupet, C. Bruneau, *Angew. Chem.* **2003**, *115*, 5220; *Angew. Chem. Int. Ed.* **2003**, *42*, 5066; b) J. L. Renaud, C. Bruneau, B. Demerseman, *Synlett* **2003**, 408; c) M. D. Mbaye, J. L. Renaud, B. Demerseman, C. Bruneau, *Chem. Commun.* **2004**, 1870; d) M. D. Mbaye, B. Demerseman, J. L. Renaud, L. Toupet, C. Bruneau, *Adv. Synth. Catal.* **2004**, *346*, 835; e) N. Gurbuz, I. Ozdemir, B. Cetinkaya, J. L. Renaud, B. Demerseman, C. Bruneau, *Tetrahedron Lett.* **2006**, *47*, 535.
[11] a) R. Hermatschweiler, I. Fernandez, P. S. Pregosin, E. J. Watson, A. Albinati, S. Rizzato, L. F. Veiros, M. J. Calhorda, *Organometallics* **2005**, *24*, 1809; b) R. Hermatschweiler, I. Fernandez, F. Breher, P. S. Pregosin, L. F. Veiros, M. J. Calhorda, *Angew. Chem.* **2005**, *117*, 4471; *Angew. Chem. Int. Ed.* **2005**, *44*, 4397.
[12] a) I. Fernandez, R. Hermatschweiler, P. S. Pregosin, A. Albinati, S. Rizzato, *Organometallics* **2006**, *25*, 323; b) R. Hermatschweiler, I. Fernandez, P. S. Pregosin, F. Breher, *Organometallics* **2006**, *25*, 1440.
[13] a) Synthesis of **3**: $AgPF_6$ (48 mg, 0.174 mmol) was added to a solution of $[Ru(Cp^*)Cl(CH_3CN)(\eta^3\text{-}PhCHCHCH_2)]PF_6$ (100 mg, 0.174 mmol) in a mixture of toluene and acetonitrile (2 mL:2 mL). The reaction mixture was stirred for 16 h after which time the solution was filtered and then slowly concentrated under vacuum. The resulting crude solid was washed with diethyl ether to afford an oil, which was dissolved in dichloromethane, filtered, and dried under vacuum to afford a brown-yellow solid. This solid was dissolved in dichloromethane, filtered, and dried under vacuum. This sequence was repeated one more time. Yield: 78% (98 mg). An acetone solution of this solid was layered with *n*-pentane and stored at 5°C to afford air-sensitive crystals of **3**, which were suitable for X-ray diffraction. ^{1}H NMR ([D$_6$]acetone, 298 K, 400.13 MHz): $\delta = 1.96$ (s, 15H), 2.37 (s, 3H), 2.68 (s, 3H), 3.41 (d, 1H, $J = 10.4$ Hz), 4.87 (d, 1H, $J = 6.4$ Hz), 5.31 (d, 1H, $J = 12.0$ Hz), 6.59 (ddd, 1H, $J = 12.0$, 10.4, 6.4 Hz), 7.58 (m, 2H, $J = 7.6$, 7.2 Hz), 7.74 (m, 2H, $J = 7.6$, 1.4 Hz), 7.90 ppm (m, 2H, $J = 7.2$ Hz); ^{13}C NMR: $\delta = 3.7$ (CH_3), 4.0 (CH_3), 9.2 (CH_3), 66.3 (H_2C_{allyl}), 108.8 (C), 94.1 (HC_{allyl}), 103.3 (HC_{allyl}), 129.1 ($C_{nitrile}$), 129.2 ($C_{nitrile}$), 129.9 (HCAr), 131.1 (HCAr), 132.6 (HCAr), 133.6 ppm (C_{ipso}). Elemental analysis (%) calcd for $C_{23}H_{30}F_{12}N_2P_2Ru$: C 38.08, H 4.17, N 3.86; found: C 38.46, H 4.38, N 3.20; ESI-MS: *m/z*: 436.1 [M^+], 354.1 [$M^+ - 2CH_3CN$], 237.0 [$M^+ - 2CH_3CN - PhCHCHCH_2$]. Synthesis of **4**: $AgPF_6$ (48 mg, 0.174 mmol) was added to a solution of $[Ru(Cp^*)Cl(CH_3CN)(\eta^3\text{-}PhCHCHCH_2)]PF_6$ (100 mg, 0.174 mmol) in DMF (2 mL). The reaction mixture was stirred for 16 h after which time the solution was filtered and then slowly concentrated under vacuum. The resulting crude mixture was washed with diethyl ether. The resulting red oil was dissolved in dichloromethane, filtered, and dried under vacuum to afford a red-purple solid. This solid was dissolved in dichloromethane, filtered, and dried under vacuum. This sequence was repeated one more time. Yield: 84% (115 mg). A dichloromethane solution of this solid was then layered with *n*-pentane and stored at −30°C to afford red air-sensitive crystals of **4**, which were suitable for X-ray diffraction. ^{1}H NMR ([D$_6$]acetone, 298 K, 400.13 MHz): $\delta = 1.76$ (s, 15H), 2.60 (d, 3H, $J = 1.0$ Hz), 3.05 (s, 3H), 3.13 (d, 3H, $J = 1.0$ Hz), 3.28 (s, 3H), 3.64 (dd, 1H, $J = 10.0$, 0.9 Hz), 4.70 (dd, 1H, $J = 6.5$, 0.9 Hz), 5.49 (d, 1H, $J = 11.0$ Hz), 6.48 (ddd, 1H, $J = 11.0$, 10.0, 6.5 Hz), 7.12 (s, 1H), 7.50 (m, 2H, $J = 7.8$, 7.5 Hz), 7.72 (m, 1H, $J = 7.8$, 1.5 Hz), 7.75 (m, 2H, $J = 7.5$ Hz), 7.95 ppm (s, 1H); ^{13}C NMR: $\delta = 8.9$ (CH_3), 33.2 (CH_3), 33.8 (CH_3), 39.2 (CH_3), 39.4 (CH_3), 66.0 (H_2C_{allyl}), 107.9 (C), 96.9 (HC_{allyl}), 98.4 (HC_{allyl}), 129.9 (HCAr), 131.5 (HCAr), 131.6 (HCAr), 134.0 (C_{ipso}), 166.5 (C_{dmf}), 167.8 ppm (C_{dmf}); ESI-MS: *m/z*: 459.1 [$M^+ - Me_2NCHO + MeOH$), 427.1 [$M^+ - Me_2NCHO$], 354.1 [$M^+ - 2Me_2NCHO$]. Catalysis: In a typical experiment, the Ru catalyst precursor **3** or **4** (0.002 mmol, 3 mol%) was added to a mixture consisting of acetonitrile (0.5 mL) and the allylic

 © 2006 Wiley-VCH Verlag GmbH & Co. KGaA, Weinheim

carbonate substrate (0.07 mmol) in an oven-dried 5-mm NMR tube. The arene derivative (0.21 mmol) was added, and the mixture was monitored by ^{1}H NMR spectroscopy at 353 K. Crystal structure of **3**: Yellow crystals of [Ru(Cp*)(η^3-$CH_2CHCHPh$)$(MeCN)_2$]$(PF_6)_2$·acetone were obtained from an acetone solution of **3** which was layered with *n*-hexane; $C_{26}H_{36}F_{12}N_2OP_2Ru$, triclinic, space group $P\bar{1}$; $a = 9.535(1)$, $b = 11.750(1)$, $c = 15.879(1)$ Å, $\alpha = 109.395(1)$, $\beta = 96.719(1)$, $\gamma = 100.965(1)°$, $V = 1615.8(2)$ Å^3, $Z = 2$, $\rho_{calcd} = 1.611$ Mg m^{-3}, crystal dimensions $0.48 \times 0.27 \times 0.23$ mm, Bruker SMART Apex diffractometer with CCD detector, $Mo_{K\alpha}$ radiation (0.71073 Å), 200 K, $2\Theta_{max} = 56.68°$, 16798 reflections, 7984 independent ($R_{int} = 0.0217$), empirical absorption correction SADABS (ver. 2.03), direct methods, refinement against full matrix (versus F^2) with SHELXTL (ver. 6.12) and SHELXL-97, 406 parameters, $R1 = 0.0504$ and w$R2$ (all data) $= 0.1363$, max./min. residual electron density 1.106/−0.464 e Å^{-3}. All non-hydrogen atoms were refined anisotropically; the contribution of the hydrogen atoms, in their calculated positions, was included in the refinement using a riding model. Crystal structure of **4**: Red crystals of [Ru(Cp*)(η^3-$CH_2CHCHPh$)$(dmf)_2$]-$(PF_6)_2$·CH_2Cl_2·alkane were obtained from a methylene chloride solution, which was layered with *n*-hexane; $C_{28}H_{40}Cl_2F_{12}N_2O_2P_2Ru$, orthorhombic, space group *Pccn*; $a = 21.369(1)$, $b = 22.712(1)$, $c = 15.580(1)$ Å, $V = 7561.4(6)$ Å^3, $Z = 8$, $\rho_{calcd} = 1.579$ Mg m^{-3}, crystal dimensions $0.44 \times 0.42 \times 0.32$ mm, Bruker CCD1k diffractometer, $Mo_{K\alpha}$ radiation (0.71073 Å), 200 K, $2\theta_{max} = 52.74°$, 58019 reflections, 7735 independent ($R_{int} = 0.0272$), empirical absorption correction SADABS (ver. 2.03), direct methods, refinement against full matrix (versus F^2) with SHELXTL (ver. 6.12) and SHELXL-97, 515 parameters, $R1 = 0.0457$ and w$R2$ (all data) $= 0.1558$, max./min. residual electron density 1.193/−0.568 e Å^{-3}. All non-hydrogen atoms were refined anisotropically; the contribution of the hydrogen atoms, in their calculated positions, was included in the refinement using a riding model. One CH_2Cl_2 molecule could be refined. Presumably owing to solvent loss or incomplete incorporation, additional crystal solvent molecule(s) could only be refined by positioning two carbon atoms ($\times 0.5\,C_4$), one of which had to be split over two positions and refined using the ISOR restraint. One of the PF_6^- anions was disordered. Each of the fluorine atoms was split over two positions, which were refined against each other (FVAR = 0.53). CCDC- 295048 and 295049 contain the supplementary crystallographic data for this paper. These data can be obtained free of charge from The Cambridge Crystallographic Data Centre via www.ccdc.cam.ac.uk/data_request/cif. b) A reviewer has correctly suggested that the Friedel–Crafts chemistry might arise from a rearrangement of the branched organic product PhCH(OPh)$CHCH_2$ formed from the nucleophilic attack of phenol on the Ru^{IV} allyl complex. To test this we allowed this product, PhCH-(OPh)$CHCH_2$, to react with catalyst **3** under our standard conditions (CH_3CN at 353 K). After 12 h, that is, more than one order of magnitude longer than necessary for 100% conversion, we did find about 60% of the Friedel–Crafts product. However, this reaction is much too slow to be relevant.

[14] G. Olah, *J. Org. Chem.* **2001**, *66*, 5943.

[15] A. Fürstner, D. Voigtlander, W. Schrader, D. Giebel, M. T. Reetz, *Org. Lett.* **2001**, *3*, 417.

[16] a) I. Shimizu, T. Sakamoto, S. Kawaragi, Y. Maruyama, A. Yamamoto, *Chem. Lett.* **1997**, 137; b) A. V. Malkov, S. L. Davis, I. R. Baxendale, W. L. Mitchell, P. Kocovsky, *J. Org. Chem.* **1999**, *64*, 2751, and references therein; c) J. Choudhury, S. Podder, S. Roy, *J. Am. Chem. Soc.* **2005**, *127*, 6162.

[17] M. Bandini, A. Melloni, A. Umani-Ronchi, *Angew. Chem.* **2004**, *116*, 560; *Angew. Chem. Int. Ed.* **2004**, *43*, 550.

[18] a) Y. Nishibayashi, M. Yamanashi, Y. Takagi, M. Hidai, *Chem. Commun.* **1997**, 859; b) G. Onodera, H. Imajima, M. Yamanashi, Y. Nishibayashi, M. Hidai, S. Uemura, *Organometallics* **2004**, *23*, 5841, and references therein.

[19] DFT calculations were performed with the Gaussian 98 software package using the mPW1PW91 hybrid functional. The basis set that was used included a standard SDD which was augmented with an *f*-polarization function for Ru and 4-31G(d) for the other atoms. The atomic charges resulted from a natural population analysis (NPA). Computational details and the corresponding list of references are given as Supporting Information.

[20] a) M. Valentini, H. Rüegger, P. S. Pregosin, *Helv. Chim. Acta* **2001**, *84*, 2833; b) P. S. Pregosin, E. Martinez-Viviente, P. G. A. Kumar, *Dalton Trans.* **2003**, 4007; c) P. S. Pregosin, P. G. A. Kumar, I. Fernandez, *Chem. Rev.* **2005**, *105*, 2977; d) F. Q. Song, S. J. Lancaster, R. D. Cannon, M. Schormann, S. M. Humphrey, C. Zuccaccia, A. Macchioni, M. Bochmann, *Organometallics* **2005**, *24*, 1315; e) D. Zuccaccia, E. Clot, A. Macchioni, *New J. Chem.* **2005**, *29*, 430.

[21] The radii from the X-ray data for the cations in **3**, **4**, and **5** are 4.6, 4.8, and 4.5 Å, respectively.

[22] In a typical catalytic experiment the concentration of the catalyst precursor is 4.2 mM. The PGSE diffusion studies were performed at 2 mM, so that, in the catalytic solution, even more aggregation is expected.

 © 2006 Wiley-VCH Verlag GmbH & Co. KGaA, Weinheim

Copper Catalysts

DOI: 10.1002/anie.200601880

Structure Identification of Precatalytic Copper Phosphoramidite Complexes in Solution**

*Hongxia Zhang and Ruth M. Gschwind**

Copper salts and organocopper(I) compounds are widely used for stoichiometric and catalytic additions and substitutions.[1–3] The high synthetic potential of copper(I) complexes or metal organocuprate clusters and the difficulty in designing new active copper systems are both based on the ability of these complexes to form supramolecular clusters, which represent an intricate example of molecular recognition.[1,4] The complexity in determining the structures of these supramolecular species in solution,[4] the existence of dynamic

[*] MSc H. Zhang, Prof. Dr. R. M. Gschwind
Institut für Organische Chemie
Universität Regensburg
Universitätsstrasse 31, 93053 Regensburg (Germany)
Fax: (+49) 941-943-4617
E-mail: ruth.gschwind@chemie.uni-regensburg.de

[**] This work has been supported by the Fonds der Chemischen Industrie.

Supporting information (including experimental details) for this article are available on the WWW under http://www.angewandte.org or from the author.

© 2006 Wiley-VCH Verlag GmbH & Co. KGaA, Weinheim
InterScience

equilibria between several species,[5] and the resulting sensitivity of the reaction to solvent and salt effects[1,2] have so far been a hindrance to a rational design capable of tapping the full potential of copper reagents.

In the case of stoichiometric, diastereoselective lithium diorganocuprate reagents, we were able to shed some light on their supramolecular structures in solution as well as the resulting structure–reactivity correlations.[6] However, in the vast field of catalytic, asymmetric conjugate addition reactions that use copper salts and chiral ligands, very little is known about the structures of the precatalytic copper complexes or the active catalytic species.[1] For example, for the ground-breaking system for enantioselective additions to enones (by use of phosphoramidite ligands for copper-catalyzed additions of dialkylzinc),[2,7] only two crystal structures of copper complexes with less selective phosphoramidite ligands are known (Figure 1).[8,9]

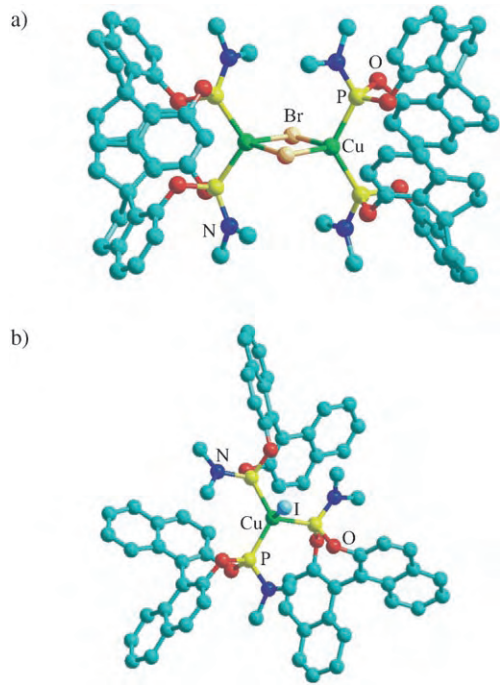

Figure 1. Known crystal structures of copper phosphoramidite complexes. a) [{CuBr(*O*,*O*′-(*R*)-(1,1′-spirobiindane-7,7′-diyl)-*N*,*N*′-dimethylphosphoramidite)$_2$}$_2$],[9] b) [CuI(*O*,*O*′-(*S*)-(1,1′-dinaphthyl-2,2′-diyl)-*N*,*N*′-dimethylphosphoramidite)$_3$].[8] For schematic drawings, see **8** and **7** in Scheme 2.

Herein, we present the first structural information about a precatalytic copper complex with phosphoramidite ligands in solution under standard conditions as used in synthetic protocols. The proposed structure is derived from a combination of ^{31}P NMR spectra, NMR spectroscopic diffusion experiments, elemental analyses, mass-spectrometric investigations, and crystal structures of related compounds. The presented binuclear copper complex with a mixed trigonal/tetrahedral coordination environment represents a new structural type of precatalytic copper complexes. This finding explains for the first time the observations of synthetic optimization procedures and supports a rational design for further catalytically active ligands.

To investigate the structures of copper phosphoramidite complexes in solution, two phosphoramidite ligands that are highly efficient in 1,4-additions to enones were selected

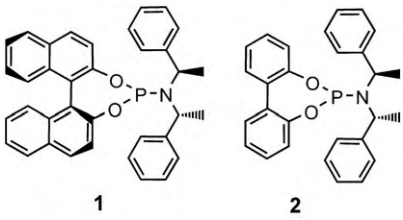

Scheme 1. Selected phosphoramidite ligands as representatives for the binaphthol- and biphenol-based ligands developed in the groups of Feringa[3] and Alexakis.[10]

(Scheme 1): the binaphthol-based ligand **1** developed by Feringa and co-workers[3,8] and the biphenol-based ligand **2** developed by Alexakis et al.[10,11] Cu^{I}Cl was chosen as the copper salt since it gives complete conversion and high *ee* values in several solvents[10] and produces very stable and diamagnetic NMR samples.

The ^{31}P NMR spectra of **2** and CuCl in different solvents are presented in Figure 2a. A 2:1 ratio between ligand and CuCl was selected, which was found to be the optimal ratio in synthetic procedures.[3,8,10] Under standard conditions, only one complex species (C2) and free ligand are observed in CD_2Cl_2 and $CDCl_3$, thus indicating C2 to be the active precatalytic complex. In [D$_8$]THF and [D$_8$]toluene, the ^{31}P NMR spectra show broad signals that correspond to

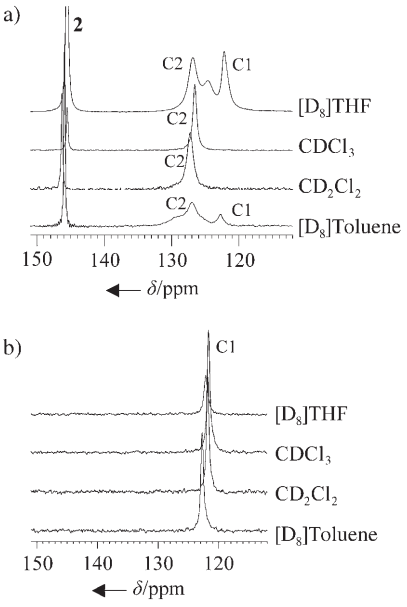

Figure 2. ^{31}P NMR spectra of the complexes built by **2** and CuCl (0.02 M) at a ratio of 2:1 (a) and 1:1 (b) in different solvents at 220 K (the two predominant complex species are labelled as C1 and C2).

 © 2006 Wiley-VCH Verlag GmbH & Co. KGaA, Weinheim

several complex species. Nevertheless, two key complexes can be identified, which are labeled as C1 and C2. Upon reducing the ligand/CuCl ratio to 1:1 or lower, only C1 is observed in all solvents (Figure 2b), independent of temperature and concentration (for details see the Supporting Information). Thus, in chloroform and dichloromethane, the two key complexes C1 and C2 can be investigated separately.

Figure 3 summarizes the appearance of complexes C1 and C2 as a function of the ligand/CuCl ratio.[12] For an excess of

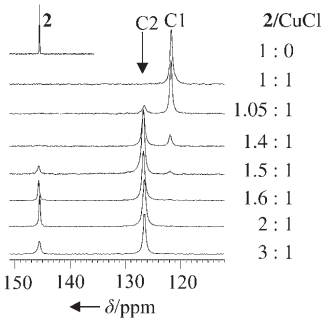

Figure 3. ^{31}P NMR spectra of **2** and mixtures of **2** and CuCl at varying ratios in $CDCl_3$ at 220 K.

CuCl and up to a ratio of 1:1, only C1 ($\delta = 121.7$ ppm) is observed. Starting from 1.05 equivalents of **2**, the signal for C2 emerges at $\delta = 126.6$ ppm. Between 1.05 and 1.5 equivalents of **2**, the ^{31}P NMR signal of C2 increases continuously, and the signal of C1 decreases. At ratios higher than 1.5 equivalents of **2**, C2 and increasing amounts of free ligand are observed. Identical measurements using the ligand **1** instead of **2** led to very similar ^{31}P NMR spectra in $CDCl_3$, thus indicating that similar complexes are formed (spectra not shown).

Because of the highly efficient quadrupole relaxation of copper and dynamic processes within the complexes, very broad ^{31}P NMR signals ($\nu_{1/2} \approx 120$ Hz) without $^{1}J_{Cu,P}$ or $^{2}J_{P,P}$ coupling patterns were observed, and diffusion measurements on ^{31}P NMR resonances were thus not applicable. Therefore, ^{1}H diffusion experiments were performed to obtain information about the hydrodynamic radius of C1 and C2. The viscosity-corrected diffusion coefficients of **1**, **2**, and their complexes C1 and C2 are listed in Table 1. The ligand **1** and the complexes containing **1** show lower diffusion coefficients compared to the compounds with **2**, which is consistent with the larger molecular size of **1** and its complexes. Surprisingly, the *D* values of C1 and C2 with the same ligand do not differ significantly.

The information about the molecular size and the composition of the complexes can be combined to elucidate the complex species C2 and C1. The first step is to examine whether the number of ligands and the amount of CuCl in the complexes can be determined from the diffusion coefficients. For this purpose, four model complexes were selected which represent all possible $L_m(CuCl)_n$ stoichiometries with two or three ligands as well as ligand/CuCl ratios between 1:1 and 2:1. Schematic drawings of model complexes **3**–**6** with typical configurations of Cu^I complexes[13] are shown in Scheme 2. Furthermore, the two known crystal structures are included as model complexes **7** and **8**. The volumes of C1, C2, and the model complexes **3**–**8** are given in

Table 1: Diffusion coefficients D[a] (10^{-10} m^2 s^{-1}) of the free ligands and complexes C1 and C2 (CuCl and **1** or **2**).

	Free ligand	C1	C2
1	2.30	1.60	1.62
2	2.68	1.81	1.83

[a] Experimental error ±2%, 0.02 M in $CDCl_3$ at 220 K.

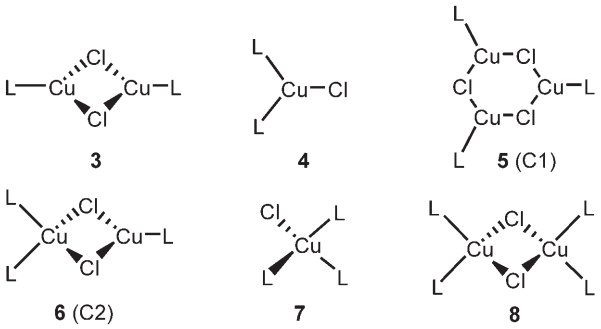

Scheme 2. Mono-, bi-, and trinuclear model complexes including the proposed structures of C1 and C2.

Table 2 (for experimental details, see the Supporting Information). A comparison of the volumes of **3**–**8** shows significant differences for complexes with 2, 3, or 4 ligands; however, varying the number of CuCl units induces only marginal changes. Thus, a comparison of the volumes of **3**–**8** with those of C1 and C2 reveals that: a) both complexes C1 and C2 are composed of three ligands, independent of the kind of ligand; b) diffusion-ordered NMR spectroscopy (DOSY) does not allow for determining the absolute number of CuCl units attached; and c) slightly lower volumes of C2 compared to C1 hint at a lower amount of CuCl in C2.

The missing information about the ratio between ligand and CuCl in the complexes C1 and C2 is found in Figure 3. Since we found that the solubility of pure CuCl in $CHCl_3$ or CH_2Cl_2 is very low (about 1 mM at room temperature), the given ligand/CuCl ratio represents the composition of the copper complex. [12] Thus, C1 has a ligand/CuCl ratio of 1:1 and the formula $[(LCuCl)_3]$, and C2 has a ratio of 1.5:1 and the formula $[L_3Cu_2Cl_2]$. The crystal structures of similar complexes with the identical stoichiometry, $[(PPh_3)_2Cu_2X_2$-

Table 2: Experimental (C1, C2)[a] and calculated (**3**–**8**) volumes [Å^3] of complexes composed of CuCl and ligands **1** or **2**.[b]

Ligand	C1	C2	**3** (1:1) $[L_2Cu_2Cl_2]$	**4** (2:1) $[L_2CuCl]$	**5** (1:1) $[L_3Cu_3Cl_3]$	**6** (1.5:1) $[L_3Cu_2Cl_2]$	**7** (3:1) $[L_3CuCl]$	**8** (2:1) $[L_4Cu_2Cl_2]$
1	2305[c]	2228[d]	1595	1565	2393	2363	2333	3131
2	1588[e]	1525[f]	1018	989	1528	1498	1468	1977

[a] Calculated from the experimental diffusion coefficients in Table 1. [b] For each model complex the ligand/CuCl ratio is given in brackets. [c] +383, −314. [d] +371, −303. [e] +264, −216. [f] +254, −207. Calculated from ±5% error in the diffusion coefficient (±2% experimental error plus ±3% possible systematic error).

© 2006 Wiley-VCH Verlag GmbH & Co. KGaA, Weinheim

(PPh_3)] (X = Cl, Br, I)[14] and a $[L_3Cu_2Br_2]$ complex with a cyclic phosphorous ligand,[15] both exhibit the typical configuration of binuclear complexes with three- and four-coordinate copper centers. Therefore, a binuclear complex with a mixed trigonal/tetrahedral copper geometry is proposed for the precatalyst C2 (see **6** in Scheme 2).

Trinuclear copper complexes like C1 are much less common than binuclear and tetranuclear complexes of Cu^I, and there is a lack of X-ray structures of trinuclear copper complexes with monodentate, nonchelating phosphorous ligands. Thus, it is only possible to suppose for C1 a planar hexagonal ring structure (see **5** in Scheme 2) or a triangular structure from related copper complexes.[13] In agreement with these proposed structures, the electrospray mass spectra of a 1:1 mixture of **2** and CuCl in CH_2Cl_2 show a dominant fragment-ion peak at *m*/*z* 605 ($[\mathbf{2}\cdot Cu_2Cl]^+$) as the base peak, whereas a 2:1 mixture produces the fragment-ion peak at *m*/*z* 941 ($[\mathbf{2}_2\cdot Cu]^+$) as the base peak and the molecular-ion peak of free ligand **2** at *m*/*z* 438 (see the Supporting Information).

With the identification of C1 and C2, it is now possible to understand some observations of synthetic optimization procedures, to propose a refinement of the catalytic cycle, and thus to support a rational design of further catalytically active ligands. 1) In conjugate additions to enones, ratios of ligand to copper salt of less than 1.5:1 were found to be detrimental,[2] thus suggesting that C2 rather than C1 is the precursor for the actual enantioselective catalyst (see Figure 3). 2) The substitution pattern of the amine moiety of the ligands was found to be decisive for the *ee* values; substituents that are too small (for example, methyl groups) and groups that are too large (for example, 1-naphthyl instead of the phenyl groups in **1**) both lead to reduced *ee* values.[3] A comparison of C2 with the crystal structures in Figure 1 shows that amine moieties that are too small may lead to tetrahedral coordination of both copper atoms, whereas substituents that are too large may hinder the formation of a binuclear structure. 3) In the catalytic cycle for copper-catalyzed 1,4-additions of R_2Zn reagents, as based on the mononuclear crystal structure (Figure 1b), an initial alkyl transfer from zinc to copper is proposed to be followed by a substitution of one of the ligands by the π-coordinated enone.[16] Alternatively, based on the 2:1 ratio of ligand to copper salt that was used in the synthesis and the observed negative nonlinear effects, dimeric $[L_2CuX]_2$ or mononuclear $[L_2CuX]$ precatalysts were proposed,[1,3,7] the latter of which has a coordination number of three, which is quite uncommon for mononuclear Cu^I complexes.[13]

The mixed trigonal/tetrahedral configuration of C2 seems to answer several advantages of the catalysts studied. The open coordination site on one of the copper centers may explain the strongly ligand-accelerated catalysis. The three ligands may account for the observed negative nonlinear effect,[3] the bridging anions may explain the strong sensitivity to the copper salt used,[2] and the aggregation level may illustrate the influence of the solvent.[2] Furthermore, π–π stacking within the $\{L_2Cu\}$ moiety together with nitrogen–zinc interactions may orient the amine moieties towards the free coordination site, thus explaining the decisive role of its configuration and the steric demand of the amine fragment.

By combining information from NMR spectroscopy, mass spectrometry, and elemental analysis, we were able to propose for the first time the structure of a precatalytic copper complex with phosphoramidite ligands in solution, which represents a new structural motif for catalytically active copper complexes. The identification of a mixed trigonal/tetrahedral precatalyst not only provides an explanation for the known synthetic optimization procedures and the reduction of the ligand/copper ratio from 2:1 to 1.6:1, but also offers the basis for designing new improved catalysts.

Received: May 12, 2006
Published online: August 23, 2006

Keywords: asymmetric catalysis · copper · NMR spectroscopy · phosphorous · structure elucidation

[1] N. Krause, *Modern Organocopper Chemistry*, Wiley-VCH, Weinheim, **2002**.
[2] A. Alexakis, C. Benhaim, *Eur. J. Org. Chem.* **2002**, 3221.
[3] L. A. Arnold, R. Imbos, A. Mandoli, A. H. M. de Vries, R. Naasz, B. L. Feringa, *Tetrahedron* **2000**, *56*, 2865.
[4] E. Nakamura, S. Mori, *Angew. Chem.* **2000**, *112*, 3902; *Angew. Chem. Int. Ed.* **2000**, *39*, 3750.
[5] N. Krause, A. Gerold, *Angew. Chem.* **1997**, *109*, 194; *Angew. Chem. Int. Ed. Engl.* **1997**, *36*, 186.
[6] a) M. John, C. Auel, C. Behrens, M. Marsch, K. Harms, F. Bosold, R. M. Gschwind, P. R. Rajamohanan, G. Boche, *Chem. Eur. J.* **2000**, *6*, 3060; b) R. M. Gschwind, X. Xie, P. R. Rajamohanan, C. Auel, G. Boche, *J. Am. Chem. Soc.* **2001**, *123*, 7299; c) X. Xie, C. Auel, W. Henze, R. M. Gschwind, *J. Am. Chem. Soc.* **2003**, *125*, 1595; d) W. Henze, A. Vyater, N. Krause, R. M. Gschwind, *J. Am. Chem. Soc.* **2005**, *127*, 17335.
[7] B. L. Feringa, *Acc. Chem. Res.* **2000**, *33*, 346.
[8] A. H. M. de Vries, A. Meetsma, B. L. Feringa, *Angew. Chem.* **1996**, *108*, 2526; *Angew. Chem. Int. Ed. Engl.* **1996**, *35*, 2374.
[9] W. Shi, L. Wang, Y. Fu, S. Zhu, Q. Zhou, *Tetrahedron: Asymmetry* **2003**, *14*, 3867.
[10] A. Alexakis, C. Benhaim, S. Rosset, M. Humam, *J. Am. Chem. Soc.* **2002**, *124*, 5262.
[11] A. Alexakis, S. Rosset, J. Allamand, S. March, F. Guillen, C. Benhaim, *Synlett* **2001**, 1375.
[12] The ratio stated in Figure 2 is identical with the actual ratio in solution. This was verified on selected samples by elemental analyses of the filtered solutions.
[13] G. Wilkinson, R. Gillard, J. McCleverty, *Comprehensive Coordination Chemistry*, *Vol. 5*, Pergamon, New York, **1987**.
[14] a) J. T. Gill, J. J. Mayerle, P. S. Welcker, D. F. Lewis, D. A. Ucko, D. J. Barton, D. Stowens, S. J. Lippard, *Inorg. Chem.* **1976**, *15*, 1155; b) J. C. Dyason, L. M. Engelhardt, C. Pakawatchai, P. C. Healy, A. H. White, *Aust. J. Chem.* **1985**, *38*, 1243.
[15] Juan Frutos, Ph.D. thesis, Université Pierre et Marie Curie, Paris, **1995**.
[16] B. L. Feringa, R. Naasz, R. Imbos, L. A. Arnold in *Modern Organocopper Chemistry* (Ed.: N. Krause), Wiley-VCH, Weinheim, **2002**, p. 234.

 © 2006 Wiley-VCH Verlag GmbH & Co. KGaA, Weinheim

Cover Picture

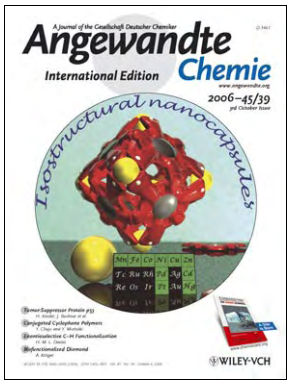

Shuichi Hiraoka, Koji Harano, Motoo Shiro, Yoshiki Ozawa, Nobuhiro Yasuda, Koshiro Toriumi, and Mitsuhiko Shionoya*

An isolated space for size- or shape-selective dynamic molecular recognition and metal-triggered chemical reactions is offered by the cavity within nanocapsules. In their Communication on page 6488 ff., M. Shionoya and co-workers describe a series of isostructural octahedral capsules prepared from a common tridentate ligand and ten different transition-metal ions, as highlighted in green in the cover picture, and demonstrate site-specific exchange of the anions coordinated within the cavity to the metal centers.

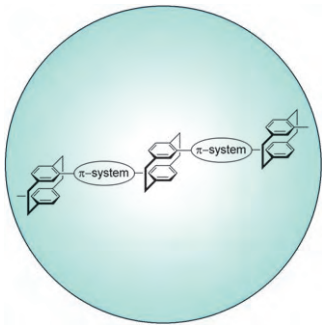

Cyclophane Polymers
Conjugated polymers that contain cyclophane units in the main chain are promising materials as molecular wires. In their Minireview on page 6430 ff., Y. Morisaki and Y. Chujo give an overview of recent developments in this class of polymer.

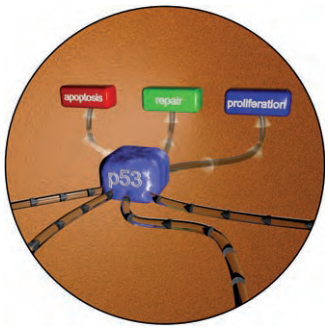

A Natural Cancer Suppressor
Many cells have a control system based on the tumor-suppressor protein p53 to prevent cancer development. In their Review on page 6440 ff., H. Kessler, J. Buchner, et al. describe the structure and regulation of p53 as well as new therapy possibilities.

Nanostructures
In their Communication on page 6462 ff., M. Y. Gao and H. Niu report the synthesis of cadmium thiolate nanowires, whose diameters can be tuned by using poly(acrylic acid), and their use as sacrificial templates for the preparation of long CdTe nanotubes.

Contents

VIP *The following Communications have been judged by at least two referees to be "very important papers" and will be published online at www.angewandte.org soon:*

*C. M. Erben, R. P. Goodman, A. J Turberfield**
Single-Molecule Protein Encapsulation in a Rigid DNA Cage

F. D. Lewis, H. Zhu, P. Daublain, B. Cohen, M. R. Wasielewski**
Hole Mobility in DNA A-Tracts

*S. Sekharan, M. Sugihara, V. Buss**
Origin of Spectral Tuning in Rhodopsin: It is Not the Binding Pocket

*H. Ma, T. P. Spaniol, J. Okuda**
Highly Heteroselective Ring-Opening Polymerization of *rac*-Lactide Initiated by Bis(phenolato) Scandium Complexes

H. Braunschweig, T. Kupfer, M. Lutz, K. Radacki, F. Seeler, R. Sigritz*
Metal-Mediated Diboration of Alkynes with [2]Borametalloarenophanes under Stoichiometric, Homogeneous, and Heterogenous Conditions

*M. E. Chiu, D. J. Watson, G. Kyriakou, M. S. Tikhov, R. M. Lambert**
Tilt the Molecule and Change the Chemistry: Mechanism of S-Promoted Chemoselective Catalytic Hydrogenation of Crotonaldehyde on Cu(111)

Meeting Reviews

Crosslinking in Molecular Main Group Element Chemistry — *R. Streubel* — **6418**

Books

Isotope Effects in Chemistry and Biology — Amnon Kohen, Hans-Heinrich Limbach — *reviewed by T. Strassner* — **6420**

Reagents for Glycoside, Nucleotide, and Peptide Synthesis — David Crich — *reviewed by C. Vogel* — **6421**

Highlights

Synthetic Methods

H. M. L. Davies* — **6422 – 6425**

Recent Advances in Catalytic Enantioselective Intermolecular C–H Functionalization

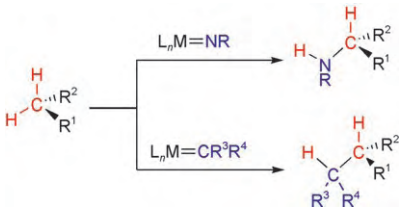

Bonds activated: In recent years, C–H insertion by metal-bound carbenes or nitrenes has come to the forefront as the most promising approach for the development of practical intermolecular methods for selective C–H functionalization. Recent examples demonstrate the spectacular regio-, diastereo-, and enantioselectivity that is possible in this methodology.

Functionalization of Diamond

A. Krüger* — **6426 – 6427**

Hard and Soft: Biofunctionalized Diamond

Exploring orientation: With the help of atomic force microscopy, the linkage and orientation of covalently bound surface molecules can be investigated (see picture). Nebel and co-workers applied this technique to the characterization of DNA films covalently bound to a diamond surface for the first time.

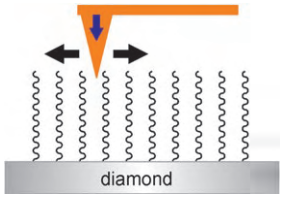

InterScience
© 2006 Wiley-VCH Verlag GmbH & Co. KGaA, Weinheim

Minireviews

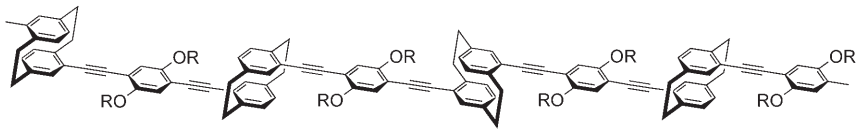

Down to the wire: Despite the recent remarkable progress in the chemistry of conjugated polymers, the synthesis of conjugated polymers that contain cyclophane units in the main chain (see picture) is limited. The Minireview discusses the synthesis and properties of through-space conjugated polymers based on cyclophanes and gives insight into their potential applications, for example, as molecular wires.

Cyclophane Polymers

Y. Morisaki, Y. Chujo* ____ **6430 – 6437**

Through-Space Conjugated Polymers Based on Cyclophanes

Reviews

Front and center: The tumor-suppressor protein p53 is the central element of the control system that many cells use to prevent the development of cancer. An intact p53 network ensures that DNA damage is detected early on. In-depth concepts and the newest advancements in the understanding of the structure and regulation of p53 are discussed. The picture shows the binding of the DNA binding domain of p53 (blue) to the DNA consensus sequence (orange).

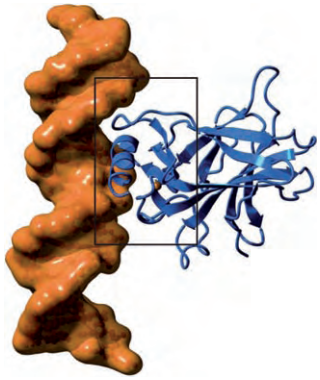

Tumor-Suppressor Protein

L. Römer, C. Klein, A. Dehner, H. Kessler,* J. Buchner* ____ **6440 – 6460**

p53—A Natural Cancer Killer: Structural Insights and Therapeutic Concepts

Communications

Self-sacrifice: Poly(acrylic acid) was used to tune the diameter of 1D nanowires prepared from linear Cd^{2+}/thioglycolic acid coordination polymer chains. The nanowires were then employed as sacrificial templates for preparing long CdTe nanotubes of different diameters (see the TEM images).

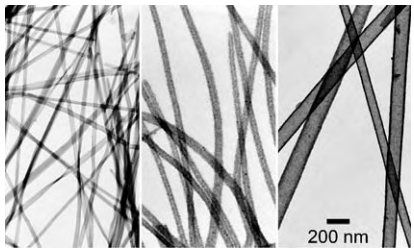

Nanostructures VIP

H. Niu, M. Y. Gao* ____ **6462 – 6466**

Diameter-Tunable CdTe Nanotubes Templated by 1D Nanowires of Cadmium Thiolate Polymer

For the USA and Canada:
ANGEWANDTE CHEMIE International Edition (ISSN 1433-7851) is published weekly by Wiley-VCH PO Box 191161, D 69451 Weinheim, Germany. Air freight and mailing in the USA by Publications Expediting Inc. 200 Meacham Ave., Elmont, NY 11003. Periodicals postage paid at Jamaica NY 11431. US POSTMASTER: send address changes to *Angewandte Chemie*, Wiley-VCH, 111 River Street, Hoboken, NJ 07030. Annual subscription price for institutions: US$ 5685/5168 (valid for print and electronic / print or electronic delivery); for individuals who are personal members of a national chemical society prices are available on request. Postage and handling charges included. All prices are subject to local VAT/sales tax.

© 2006 Wiley-VCH Verlag GmbH & Co. KGaA, Weinheim

The best in chemistry –

for more than a hundred years

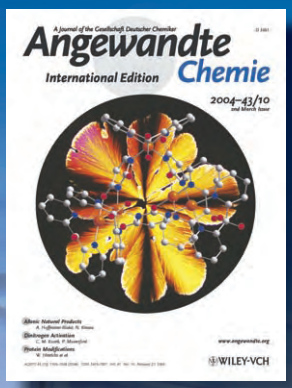

A Journal of the Gesellschaft Deutscher Chemiker

Angewandte
International Edition **Chemie**

www.angewandte.org

1888: ***The beginning of a success story***

Constant Innovations

1962: *First issue of the International Edition*
1976: *Graphical abstracts*
1979: *Cover pictures*
1988: *Centenary of Angewandte*
1989: *Routine use of color*
1991: *New section: Highlights*
1992: *Computerized editorial tracking system*
1995: *Internet service for readers*
1998: *Regular press service; full-text online*
2000: *New section: Essays; EarlyView: Communications available online ahead of the printed version*
2001: *New section: Minireviews*
2002: *Online submission of manuscripts*
2003: *Weekly publication; new section: News; new layout*
2004: *Backfiles (1962-1997); ManuscriptXpress: Online system for authors and referees*

Angewandte's advisors...

Rolf Thauer
MPI für terrestrische Mikrobiologie, Marburg

» *In 1970 Karl Decker, Kurt Jungermann, and I published a review on "Energy Production in Anaerobic Organisms" in* ***Angewandte Chemie****. We were soon surprised how many scientists from all over the world had read the article. Ever since then I have admired the broad scope, the high impact, and internationality of this Journal and I am therefore very proud, as a "chemical microbiologist", to be a member of its Editorial Board.* «

Angewandte Chemie International Edition *is a journal of the German Chemical Society (GDCh)*

GDCh

WILEY InterScience® DISCOVER SOMETHING GREAT

WILEY-VCH

1199404_gu

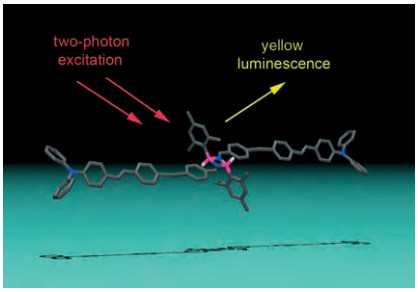

Through-bond coupling across a cyclodiborazane core results in large absorption cross sections in a new type of boron-containing two-photon-absorbing chromophore (see picture; B pink, N blue, C gray, H other than BH (white) omitted). This is a first step in the design of new dual-property chromophores for applications in biological science or medicine (e.g., two-photon imaging and boron neutron capture therapy).

Two-Photon Absorption

A. Hayek, J.-F. Nicoud,* F. Bolze, C. Bourgogne, P. L. Baldeck **6466 – 6469**

Boron-Containing Two-Photon-Absorbing Chromophores: Electronic Interaction through the Cyclodiborazane Core

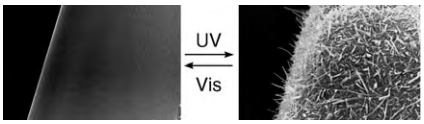

In a different light: A photoinduced change in surface morphology provides reversible changes in the superhydrophobic properties of a photochromic diarylethene film. The effect is achieved by the reversible formation of fine fibril structures on the coated microcrystalline surface upon irradiation by UV or visible light (see picture).

Superhydrophobic Effect

K. Uchida,* N. Izumi, S. Sukata, Y. Kojima, S. Nakamura,* M. Irie **6470 – 6473**

Photoinduced Reversible Formation of Microfibrils on a Photochromic Diarylethene Microcrystalline Surface

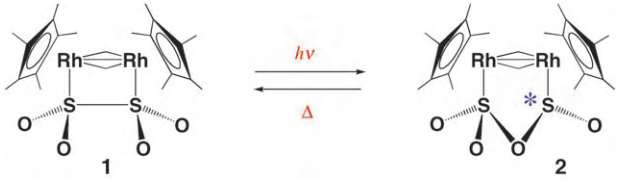

Fully reversible crystal photochromism between the μ-O_2SSO_2 (**1**) and μ-O_2SOSO (**2**) forms of a dinuclear rhodium complex has been observed. The photochromic reaction, including stereoselective oxygen-atom transfer and stereospecific transformation of photochemically generated μ-O_2SOSO isomers into the most stable isomer, was directly followed by conventional single-crystal X-ray diffraction.

Photochromic Crystals

H. Nakai, M. Mizuno,* T. Nishioka,* N. Koga, K. Shiomi, Y. Miyano, M. Irie, B. K. Breedlove, I. Kinoshita, Y. Hayashi, Y. Ozawa,* T. Yonezawa, K. Toriumi, K. Isobe* **6473 – 6476**

Direct Observation of Photochromic Dynamics in the Crystalline State of an Organorhodium Dithionite Complex

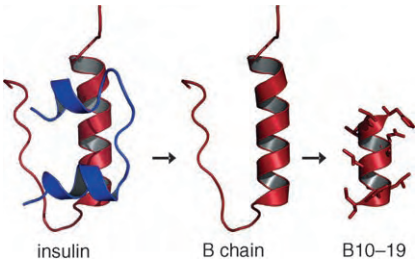

Nature's route for amyloid prevention: Insulin is a natural inhibitor of amyloid formation by the islet amyloid polypeptide (IAPP). The interacting domains of both proteins were identified by using a reductionist approach (see scheme). An understanding of the molecular mechanism of this physiological interaction may lead to the design of peptidomimetic drugs for type II diabetes.

Molecular Recognition

S. Gilead, H. Wolfenson, E. Gazit* **6476 – 6480**

Molecular Mapping of the Recognition Interface between the Islet Amyloid Polypeptide and Insulin

© 2006 Wiley-VCH Verlag GmbH & Co. KGaA, Weinheim

Contents

Helical Structures

J. Xu, K. N. Raymond* ——— **6480 – 6485**

Structurally Characterized Quadruple-Stranded Bisbidentate Helicates

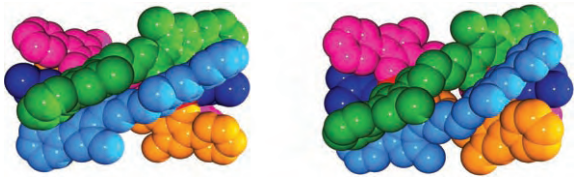

Let's twist again: Actinide quadruple-stranded helical supramolecular architectures were synthesized in which two capped square-antiprismatic Th^{IV} centers are coordinated by four bis(bidentate) 4-acylpyrazolone chelating strands. This example shows a cluster formation caused by incommensurate coordination numbers.

Carbohydrate Sensors

J. W. Lee, J.-S. Lee, Y.-T. Chang* ——— **6485 – 6487**

Colorimetric Identification of Carbohydrates by a pH Indicator/pH Change Inducer Ensemble

The sweet-test thing! Carbohydrate discrimination is highly challenging as a result of the similarity in their functional groups. A series of pH sensor/pH change inducer ensembles has been developed as an artificial "tongue" for the identification of carbohydrates. The optimized sensor array with six probe pairs demonstrated full discrimination of 23 carbohydrates.

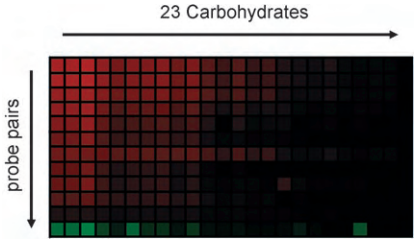

Molecular Capsules

S. Hiraoka, K. Harano, M. Shiro, Y. Ozawa, N. Yasuda, K. Toriumi, M. Shionoya* ——— **6488 – 6491**

Isostructural Coordination Capsules for a Series of 10 Different d^5–d^{10} Transition-Metal Ions

Ten of a kind: A series of $\{M_6L_8\}$ octahedral metallocapsules that are structurally identical except for the metal at the apexes was quantitatively prepared from tris-monodentate ligands L and ten divalent d^5–d^{10} transition-metal ions (see picture). Six $CF_3SO_3^-$ anions coordinated inside the capsules can be site-selectively replaced with other anionic ligands to functionalize the cavity.

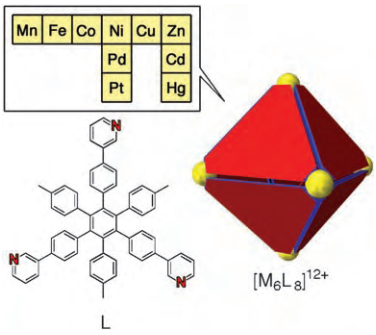

Composites

M. Ikeda, Y. Furusho,* K. Okoshi, S. Tanahara, K. Maeda, S. Nishino, T. Mori, E. Yashima* ——— **6491 – 6495**

A Luminescent Poly(phenylenevinylene)–Amylose Composite with Supramolecular Liquid Crystallinity

Going straight: A luminescent composite of poly(*p*-phenylenevinylene) (PPV) and amylose was synthesized by direct polymerization of the precursor monomer in aqueous media in the presence of amylose. The PPV–amylose composite consists of a rigid-rod PPV segment threaded into a flexible amylose tube and self-assembles into liquid-crystalline phases.

© 2006 Wiley-VCH Verlag GmbH & Co. KGaA, Weinheim

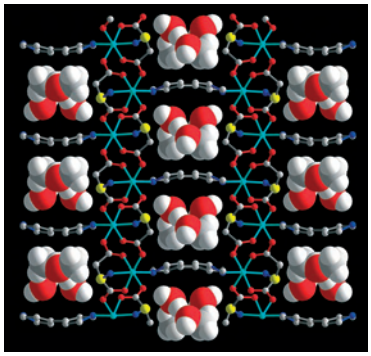

In the pocket: A nanoporous framework with internal surfaces lined with amino acid residues (see structure; Ni cyan, C gray (chiral centers yellow), H white, N blue, O red) is produced by the pillaring of nickel–aspartate layers by 4,4′-bipyridine. The presence of pockets capable of multiple interactions with guest species permits the enantioselective sorption of short-chain diols.

Metal–Organic Frameworks

R. Vaidhyanathan, D. Bradshaw, J.-N. Rebilly, J. P. Barrio, J. A. Gould, N. G. Berry, M. J. Rosseinsky* _____ **6495 – 6499**

A Family of Nanoporous Materials Based on an Amino Acid Backbone

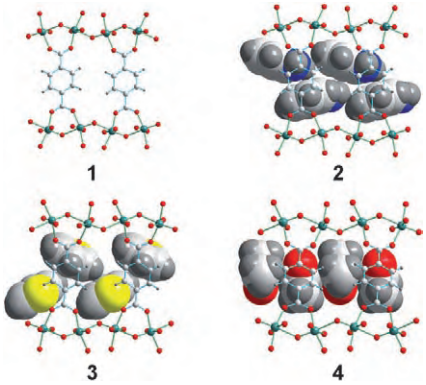

A very good host: The guest acid molecules of hydrothermally synthesized $[V(O)(bdc)](H_2bdc)_{0.71}$ (bdc = benzenedicarboxylate) are removed to give high-quality single crystals of $[V(O)(bdc)]$ (**1**). On absorption of guest molecules from the liquid phase, **1** undergoes crystal-to-crystal transformations (aniline: **2**; thiophene: **3**; acetone: **4**). Furthermore, complex **1** also selectively absorbs thiophene and dimethyl sulfide from methane.

Host–Guest Systems

X. Wang, L. Liu, A. J. Jacobson* _____ **6499 – 6503**

Intercalation of Organic Molecules into Vanadium(IV) Benzenedicarboxylate: Adsorbate Structure and Selective Absorption of Organosulfur Compounds

Going bananas: In a twisted geometry, an extrinsically chiral supermolecular structure was obtained in the calamitic phase. Upon cooling down to form the B_x phase, imbalanced growth of an intrinsic preferential chiral structure was attained. The preferential chiral handedness of the banana mesophase can be also controlled by the handedness of the twisted configuration.

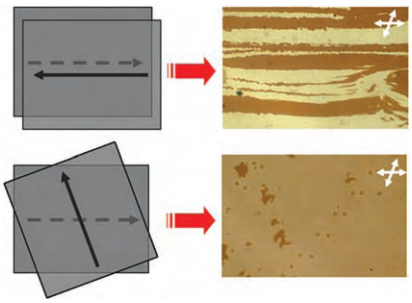

Liquid Crystals

S.-W. Choi, S. Kang, Y. Takanishi, K. Ishikawa, J. Watanabe, H. Takezoe* _____ **6503 – 6506**

Intrinsic Chirality in a Bent-Core Mesogen Induced by Extrinsic Chiral Structures

Unusual storage: An organic nonporous material, *p-tert*-butylcalix[4]arene, sorbs acetylene with high storage density under ambient conditions. It is presumed that gas molecules diffuse through the seemingly nonporous lattice without disrupting the arrangement of the host molecules (see picture; red O, blue C, gray H, yellow void space).

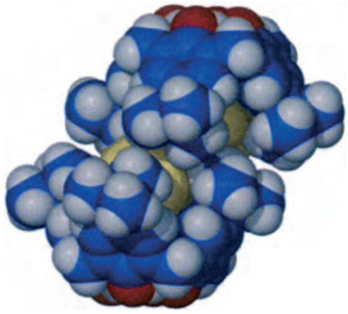

Gas Storage

P. K. Thallapally, L. Dobrzańska, T. R. Gingrich, T. B. Wirsig, L. J. Barbour,* J. L. Atwood* _____ **6506 – 6509**

Acetylene Absorption and Binding in a Nonporous Crystal Lattice

© 2006 Wiley-VCH Verlag GmbH & Co. KGaA, Weinheim

Contents

Chiral Grignard Reagents

J. Beckmann, D. Dakternieks, M. Dräger, A. Duthie* ——— **6509 – 6512**

New Insights into the Classic Chiral Grignard Reagent (1*R*,2*S*,5*R*)-Menthylmagnesium Chloride

Two in one: An equimolar mixture of the diastereomers (1*R*,2*S*,5*R*)-MenMgCl and (1*S*,2*S*,5*R*)-NeomMgCl is formed from reaction of Mg with either menthyl (Men) or neomenthyl (Neom) chloride. Once formed, each component of the Grignard reagent is configurationally stable. Reaction with electrophiles generally yields products from attack by the more nucleophilic menthyl portion of the Grignard reagent.

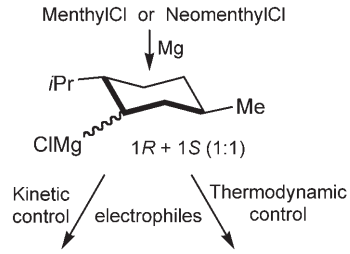

Methanol-to-Olefin Process

Z.-M. Cui, Q. Liu, W.-G. Song,* L.-J. Wan* ——— **6512 – 6515**

Insights into the Mechanism of Methanol-to-Olefin Conversion at Zeolites with Systematically Selected Framework Structures

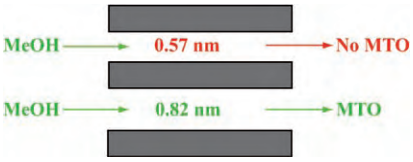

Com-paring mechanisms: The so-called hydrocarbon pool mechanism does not operate with zeolite ZSM-22 in the methanol-to-olefin (MTO) conversion process as a result of the narrow channels (0.57 nm) in its framework structure. However, this provided a condition free of secondary reactions for detailed mechanistic studies, with H/D exchange patterns of toluene suggesting a paring mechanism.

Mesoporous Crystals

K. Miyasaka, L. Han, S. Che, O. Terasaki* ——— **6516 – 6519**

A Lesson from the Unusual Morphology of Silica Mesoporous Crystals: Growth and Close Packing of Spherical Micelles with Multiple Twinning

Putting two and two together: An ordered mesoporous silica crystal of the cage type with cubic $Fm\bar{3}m$ symmetry was prepared by using a gemini surfactant as template. Icosahedral, decahedral, and plate morphologies are discussed (see SEM image). The structure is explained by the occurrence of multiple twinning during the formation of mesostructures.

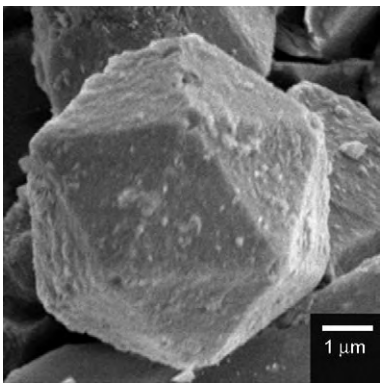

Radical Reactions

N. Charrier, D. Gravestock, S. Z. Zard* ——— **6520 – 6523**

Radical Additions of Xanthates to Vinyl Epoxides and Related Derivatives: A Powerful Tool for the Modular Creation of Quaternary Centers

An open relationship: The triethylborane/O_2-mediated addition of xanthates to vinyl epoxides and derivatives represents an efficient process to form carbon–carbon bonds. Complex structures can be rapidly assembled in a modular, convergent manner, under mild conditions, using readily available reagents (see scheme, Bn = benzyl). The formation of quaternary centers proved especially facile.

© 2006 Wiley-VCH Verlag GmbH & Co. KGaA, Weinheim

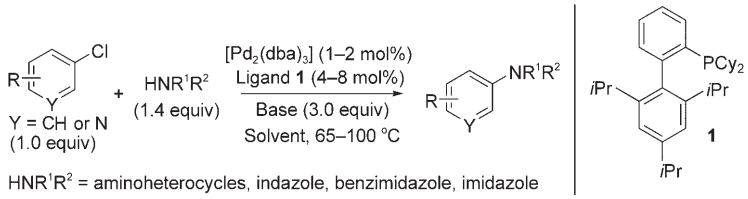

A good alternative: Highly reactive catalysts based on palladium and dialkylbiarylphosphino ligands provide unprecedented reactivity and selectivity in C–N bond-forming processes. The bulky monophosphine catalyst system Pd/**1** was effective for the reaction of aryl/heteroaryl halides bearing primary amides and 2-aminoheterocycles (see scheme; dba = dibenzylideneacetone, R = $CONH_2$, NH_2), thus showing that monodentate phosphines are viable alternatives to, and sometimes superior to, chelating ligands.

Amination

K. W. Anderson, R. E. Tundel, T. Ikawa, R. A. Altman, S. L. Buchwald* _____ **6523 – 6527**

Monodentate Phosphines Provide Highly Active Catalysts for Pd-Catalyzed C–N Bond-Forming Reactions of Heteroaromatic Halides/Amines and (H)N-Heterocycles

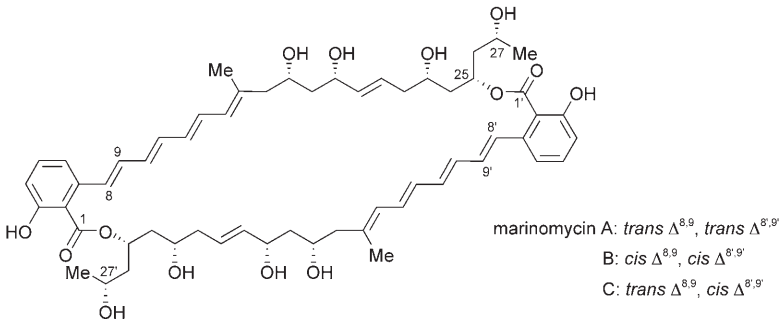

Ocean's three: Unearthed from the bottom of the ocean off the coast of La Jolla (California, USA), marinomycins A–C, which differ in geometry about the C8–C9 and C8′–C9′ double bonds, have been prepared by total synthesis through a strategy that features a Suzuki coupling reaction to forge their remarkable polyunsaturated 44-membered-ring systems (see picture).

Natural Product Synthesis

K. C. Nicolaou,* A. L. Nold, R. R. Milburn, C. S. Schindler _____ **6527 – 6532**

Total Synthesis of Marinomycins A–C

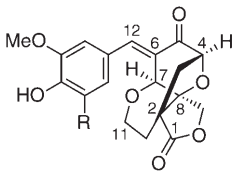

Carbonyl ylides to the fore: the first total synthesis of polygalolides A (**1**) and B (**2**) has been achieved by exploiting a tandem carbonyl ylide formation/1,3-dipolar cycloaddition to construct the unprecedented 5,10-dioxatricyclo-[6.2.1.0]undecane core structure of these molecules in a single step.

Total Synthesis

S. Nakamura, Y. Sugano, F. Kikuchi, S. Hashimoto* _____ **6532 – 6535**

Total Synthesis and Absolute Stereochemistry of Polygalolides A and B

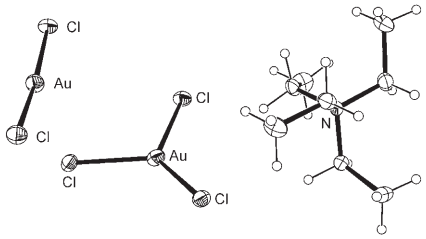

Caught between two geometries: The solid-state structure of $[NEt_4][AuCl_2]$-$[AuCl_3]$ (see picture) shows a geometry in $AuCl_3$ that is representative of a Y-shaped transition state as a result of Jahn–Teller distortion. Calculations by others indicate that the observed orientation is an intermediate geometry between two T-shaped structures with C_{2v} symmetry.

Jahn–Teller Distortion in Gold

K. R. Flower,* R. G. Pritchard, A. T. McGown _____ **6535 – 6537**

$[NEt_4][AuCl_2][AuCl_3]$: Solid-State Evidence of Essentially Y-Shaped Jahn–Teller-Distorted $AuCl_3$

© 2006 Wiley-VCH Verlag GmbH & Co. KGaA, Weinheim

Contents

Surface Chemistry

D. Loffreda* ——— **6537 – 6540**

Structural Identification of Conjugated Molecules on Metal Surfaces by Means of Soft Vibrations

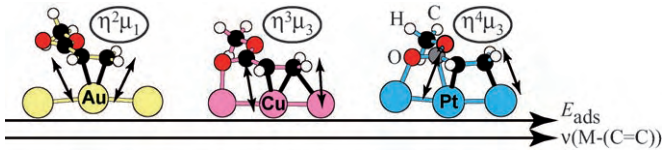

Adsorption structures of multifunctional molecules: A DFT study of four conjugated molecules on six metals showed that molecule–metal vibrations correlate with adsorption structure and strength (see picture). The $\eta^2\mu_1$ structure on Ag and Au is weakly adsorbed and has softer vibrations, but the $\eta^4\mu_3$ structure on Ni, Pd, and Pt is strongly stabilized and these modes are strengthened. An intermediate $\eta^3\mu_3$ structure occurs on Cu.

Heterogeneous Catalysis

F. Li, G. Yuan* ——— **6541 – 6544**

Hydrated Dibromodioxomolybdenum(VI) Supported on Zn-MCM-48 for Facile Oxidation of Methane

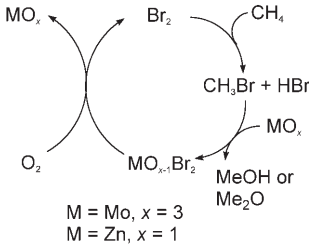

Three in one: The oxidation of methane to methyl derivatives, conversion of the methyl derivatives into oxygenated compounds, and regeneration of the oxidation media are the three steps involved in the catalytic partial oxidation of methane by MoO_2Br_2 supported on Zn-MCM-48 (see scheme). Reversible bromine metathesis between MoO_2Br_2 and MoO_3 is key to the efficient catalytic process.

Corroles

A. Mahammed, Z. Gross* ——— **6544 – 6547**

Iron and Manganese Corroles Are Potent Catalysts for the Decomposition of Peroxynitrite

Ring cycle: Iron and manganese corroles are among the most efficient decomposition catalysts of peroxynitrite reported to date. The catalytic rate of the iron complex is higher than that of analogous porphyrins, and the manganese complex operates through the catalytic disproportionation cycle shown in the picture.

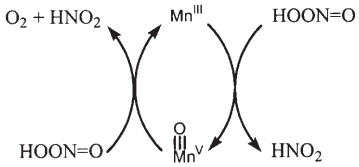

Metalation

W. Clegg, S. H. Dale, E. Hevia, L. M. Hogg, G. W. Honeyman, R. E. Mulvey,* C. T. O'Hara ——— **6548 – 6550**

Alkali-Metal-Mediated Zincation of Polycyclic Aromatic Hydrocarbons: Synthesis and Structures of Mono- and Dizincated Naphthalenes

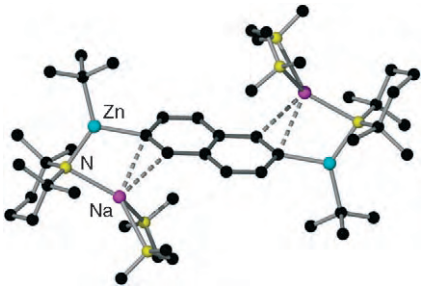

Zinc twice: Naphthalene is attacked and doubly deprotonated at the 2,6-position by a synergic sodium zincate base to generate a centrosymmetric dizincated molecule. The approach of alkali-metal-mediated zincation can effect dimetalation as well as monometalation of polycyclic aromatic hydrocarbons, thus providing access to new zincated naphthalenes that are inaccessible directly through mainstream organozinc reagents.

© 2006 Wiley-VCH Verlag GmbH & Co. KGaA, Weinheim

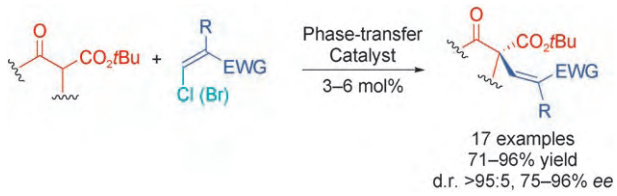

The clash of hybridizations: A tailored phase-transfer organocatalyst merges sp^3- and sp^2-hybridized carbon atoms by catalyzing the first enantioselective vinylic substitution (see scheme; EWG = electron-withdrawing group). The method provides access to optically active compounds possessing vinyl-substituted quaternary stereocenters with control of the alkene configuration.

Organocatalysis

T. B. Poulsen, L. Bernardi, M. Bell, K. A. Jørgensen* ——— **6551 – 6554**

Organocatalytic Enantioselective Nucleophilic Vinylic Substitution

---

Belt holes: By heating chromium under an ethanol atmosphere, nanobelts and nanorods of oxygen-deficient chromia (Cr_2O_{3-x}) are prepared for the first time (see image). The nanobelts exhibit two types of superlattice structures that arise from different orderings of the oxygen defects. Folding observed in some of the nanobelts is a result of twinning.

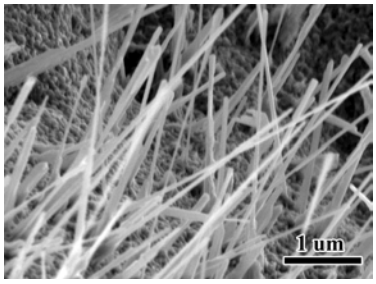

Nanostructures

W.-Q. Han,* L. J. Wu, A. Stein, Y. M. Zhu, J. Misewich, J. Warren ——— **6554 – 6558**

Oxygen-Deficiency-Induced Superlattice Structures of Chromia Nanobelts

---

Rings from light: Irradiation of acetonitrile solutions containing 1-cyano-2-(4-pentenyl)naphthalene derivatives afforded benzotetra- and benzopentacyclic compounds with tri- and tetraquinane skeletons in high yields, through intramolecular [2+3] photocycloaddition of the alkene at the 2,4-positions of the cyanonaphthalene (see scheme; $n = 1, 2$). The structures of these adducts were confirmed by their spectral properties and by X-ray crystallographic analyses.

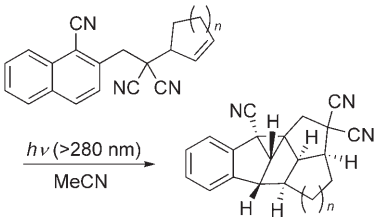

Polyquinane Synthesis

H. Mukae, H. Maeda, K. Mizuno* ——— **6558 – 6560**

One-Step Synthesis of Benzotetra- and Benzopentacyclic Compounds through Intramolecular [2+3] Photocycloaddition of Alkenes to Naphthalene

---

Three into one will go! A three-component coupling of a hydroxylamine, an aldehyde, and a cyclopropane diester provides the tetrahydro-1,2-oxazine scaffold necessary for completion of the first total synthesis of the natural product phyllantidine.

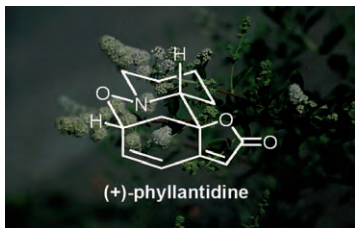

Total Synthesis

C. A. Carson, M. A. Kerr* ——— **6560 – 6563**

Total Synthesis of (+)-Phyllantidine

© 2006 Wiley-VCH Verlag GmbH & Co. KGaA, Weinheim

Contents

Perovskite Nanoparticles

R. L. Brutchey, D. E. Morse* **6564 – 6566**

Template-Free, Low-Temperature Synthesis of Crystalline Barium Titanate Nanoparticles under Bio-Inspired Conditions

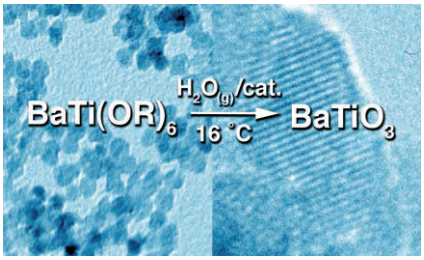

Mimicking sponges: Well-defined crystalline nanoparticles of cubic $BaTiO_3$ are prepared at a very low temperature by using a bio-inspired methodology. A bimetallic alkoxide is used as a single-source precursor in a vapor-diffusion sol–gel synthesis. Water and catalyst (HCl) are delivered in a spatial and temporal gradient to promote the slow growth of nanoparticles.

Asymmetric Catalysis

A. Berkessel,* M. L. Sebastian-Ibarz, T. N. Müller **6567 – 6570**

Lipase/Aluminum-Catalyzed Dynamic Kinetic Resolution of Secondary Alcohols

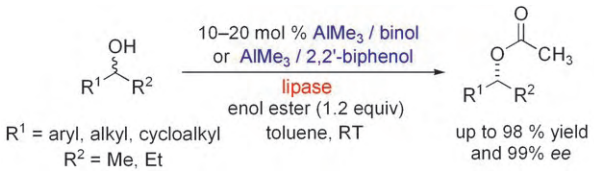

Racemization wanted: The dynamic kinetic resolution of secondary alcohols can be achieved by a simple and readily available catalyst system. Substrate racemization is effected at room temperature by a combination of (racemic) 1,1′-bi-2-naphthol (binol) or 2,2′-biphenol with $AlMe_3$, and a lipase performs enantiospecific acylation (see scheme).

Tumor Therapeutics

L. F. Tietze,* B. Krewer, H. Frauendorf, F. Major, I. Schuberth **6570 – 6574**

Investigation of Reactivity and Selectivity of DNA-Alkylating Duocarmycin Analogues by High-Resolution Mass Spectrometry

DNA alkylation: The reactivity and selectivity of DNA-alkylating duocarmycin analogues were determined by direct ESI-FTICRMS (negative-ion mode) measurements. The high efficiency of a new seco drug for the alkylation of duplex DNA has been determined in this way for the first time (picture: drug bound covalently to an oligodeoxynucleotide). The corresponding, less toxic prodrug and the enantiomer of the seco drug show, in contrast, only a very low alkylation tendency.

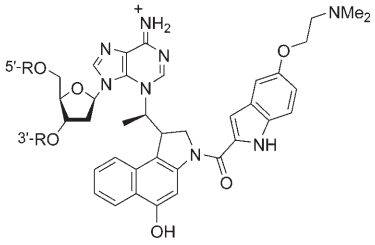

Prodrugs

L. F. Tietze,* F. Major, I. Schuberth **6574 – 6577**

Antitumor Agents: Development of Highly Potent Glycosidic Duocarmycin Analogues for Selective Cancer Therapy

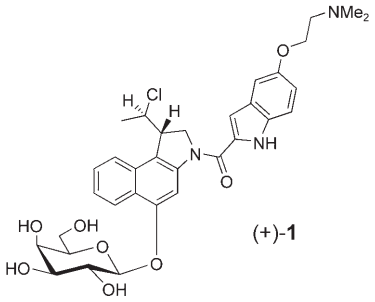

(+)-**1**

Better and better: The glycosidic prodrug (+)-**1**, which is based on duocarmycin antibiotics, was synthesized for selective cancer therapy. The drug was developed within the context of "antibody-directed enzyme prodrug therapy" (ADEPT). As a result of its outstanding QIC_{50} values, its excellent solubility, and easy synthesis it exceeds all other prodrugs produced to date. QIC_{50} = comparative toxicity value between the prodrug and the drug.

© 2006 Wiley-VCH Verlag GmbH & Co. KGaA, Weinheim

Designer jackets: Polydentate amino-functionalized poly(ethylene oxide)s with various block lengths are synthesized and used for ligand exchange and phase transfer of quantum dots and magnetic nanoparticles (see scheme; TEM images of the particles before and after the exchange are also shown). The ligands enable the transfer of the previously water-insoluble particles into aqueous media.

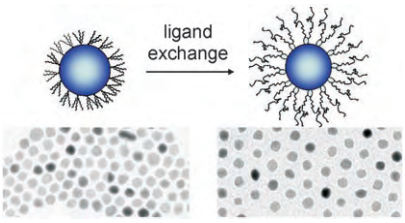

Nanomaterials

M. S. Nikolic, M. Krack, V. Aleksandrovic, A. Kornowski, S. Förster, H. Weller* ——— **6577 – 6580**

Tailor-Made Ligands for Biocompatible Nanoparticles

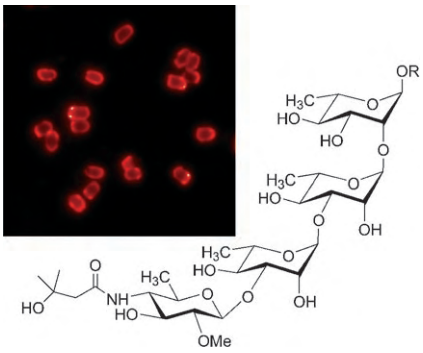

Sweet traitor: Monoclonal antibodies against a tetrasaccharide that contains the unique monosaccharide anthrose, which is found on the surface of *B. anthracis* spores, are used to selectively detect this biowarfare threat.

Pathogen Detection

M. Tamborrini, D. B. Werz, J. Frey, G. Pluschke, P. H. Seeberger* ——— **6581 – 6582**

Anti-Carbohydrate Antibodies for the Detection of Anthrax Spores

Alternative mimetics: Short cyclic hexapeptides (see picture; blue N, red O, white H, gray C) can be effective for oligosaccharide mimicry. The individual contributions of cyclization, amino acid stereochemistry, turn position, and side-chain functionality to the glycomimetic properties of the peptides were identified. Two peptides proved to be high-affinity ligands for the 412 antibody and also showed enhanced functional activity as HNK-1 mimetics.

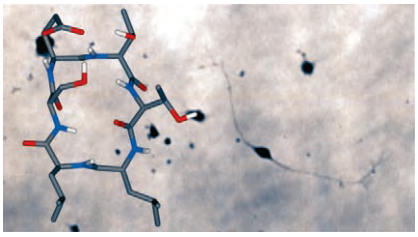

Neurochemistry

D. Bächle, G. Loers, E. W. Guthöhrlein, M. Schachner, N. Sewald* ——— **6582 – 6585**

Glycomimetic Cyclic Peptides Stimulate Neurite Outgrowth

Looking for outstanding employees?

Do you need another expert for your excellent team?
... Chemists, PhD Students, Managers, Professors, Sales Representatives...

Place an advert in the printed version and have it made available online for 1 month, free of charge!

Angewandte Chemie International Edition
Advertising Sales Department: Marion Schulz
Phone: 0 62 01 - 60 65 65
Fax: 0 62 01 - 60 65 50
E-Mail: MSchulz@wiley-vch.de

Service

Keywords ——— ***6588***

Authors ——— ***6589***

Angewandte's Sister Journals ——— ***6586 – 6587***

Preview ——— ***6591***

© 2006 Wiley-VCH Verlag GmbH & Co. KGaA, Weinheim

Crosslinking in Molecular Main Group Element Chemistry**

Rainer Streubel

Over the last forty to fifty years, important research areas of molecular main-group-element chemistry have been driven apart by focusing (too much) on themselves and have thereby missed benefiting interactions. These areas involve the study of neutral and ionic species such as compounds with high- and/or low-coordinated centers, reactive intermediates, transition-metal-stabilized unusual molecules, novel heterocycles, and last, but not least, applications in various fields of homogeneous catalysis, hybrid and/or inorganic polymers, functional molecules (sensors, molecular magnets, OLEDs, ionic liquids, etc.), and single-source precursors for new materials. This fact, together with the advance of more elaborate computational methods and programs that are able to tackle ever more complicated problems and real-size large molecules, has increased attention and created the wish to merge these fields of molecular main-group-element chemistry.

An initiative entitled *"Innovative Synthesis of Novel Main-Group Compounds and Its Application"*, proposed by a group of internationally renowned scientists headed by Yohsuke Yamamato (University of Hiroshima, Japan) who recognized this challenge in the field, was approved by the Japan Society for the Promotion of Science (JSPS) within the Core-to-Core Program—this initiative represents the only proposal on fundamental research in chemistry. The center of this network is in Japan, and it has two other main contributing countries: United States and Germany. Each has a national coordinator (Y. Yamamoto/Japan, A. J. Arduengo/USA, K. Seppelt/Germany) and additional cooperative members in these countries as well as others such as Canada, France, Switzerland, the Netherlands, New Zealand, UK, and Finland, thus altogether connecting 26 research teams outside Japan.

According to this background and the principal ideas outlined above, the Second Core-to-Core Symposium comprised single sessions each day with a total of 24 plenary lectures, nine short lectures, and a poster session (49 contributions). The opening lecture entitled *"The Strongest (yet Gentlest) Acid"* was given by C. A. Reed (Riverside, USA), who demonstrated the versatile applicability of $H(CHB_{11}Cl_{11})$, for example, for the protonation of C_{60}, C_6H_6, or R_3Si^+ ions, by virtue of the inertness of the corresponding anion. J. G. Verkade (Iowa, USA) presented long-awaited applications, following many years of fundamental research, of azaphosphatranes in various fields of organocatalysis, such as C–C and C–N coupling reactions.

K. Lammertsma (Amsterdam, The Netherlands) reported on novel functionality in organophosphorus chemistry and showed the importance of nucleophilic and electrophilic terminal phosphinidene complexes, the latter of which are especially useful in P,C-heterocyclic chemistry. D. A. Dixon (Tuscaloosa, USA) explained and illustrated new advances in computational main-group chemistry by predicting, for example, $(CF_3SO_2)_3CH$ as a promising new superacid. H.-J. Grützmacher (Zürich, Switzerland) showed how to make the true (monocoordinated and anionic) "CP" (cyaphide) ligand by using C–Si bond cleavage of a Ru-coordinated silyl-substituted phosphaalkyne, thus opening a new avenue in coordination chemistry.

Three short lectures gave insights into recent advances in experimental and theoretical areas: M. Yoshifuji (Tuscaloosa, USA) showed that the chemistry of 1,3-diphosphacyclobutane-2,4-diyls, which are fascinating heterocyclic singlet diradicaloids (first reported by E. Niecke in 1995), gives access to new heterocyclic radical cations. M. Ochiai (Tokushima, Japan) discussed hypervalent alkynyl- and alkenyl(aryl)-λ^3-bromanes and their broad applications in organic synthesis. S. Nagase (Okazaki, Japan) reported on the effects of bulky groups on the triple bonding in REER (R = alkyl; E = Si, Ge, Sn) compounds and the short distance in Na_2[RGaGaR]", thus convincingly demonstrating current computing abilities and their utility in the understanding of structure and bonding. The last lecture of the first day was given by F. Mathey (Riverside, USA), who described the way from 2*H*-phospholes to phosphaporphyrins, which illustrated again how long it can take to make use of once curious findings, such as the 1*H*-/2*H*-phosphole rearrangement.

The second day started with a lecture by D. Lentz (Berlin, Germany) on the synthesis and structure determination of tellurium(IV) compounds, in which he described cyanide and mixed fluoride/cyanide species of tellurium and showed the structural influence of solvates. J. Escudie (Toulouse, France) illustrated the synthetic pathways necessary to access heteroallenes containing low-coordinated heavy elements of Groups 14 and 15 and their use in heterocyclic chemistry. R. Réau (Rennes, France) demonstrated how new OLED materials can be designed based on fundamental knowledge of organophosphorus π-conjugated systems that comprise phospholes as a central building block. R. Streubel (Bonn, Germany) described new syntheses and bond-selective ring-expansions of oxaphosphirane complexes, thus

[*] Prof. Dr. R. Streubel
Institut für Anorganische Chemie
Rheinische Friedrich-Wilhelms-Universität Bonn
Gerhard-Domagk-Strasse 1
53121 Bonn (Germany)
E-mail: r.streubel@uni-bonn.de

[**] Second Core-to-Core Symposium on Main Group Element Chemistry, August 26–28, 2006, University of Tokyo.

InterScience
© 2006 Wiley-VCH Verlag GmbH & Co. KGaA, Weinheim

Dateiname: T603708E
Pfad: L:/daten/verlage/vch/ach/Hefte/0639/
Status Neusatz
Datum: 40 KW., 28. September 2006 (Donnerstag)
Pagina: 6418
Seite: 1 te von 2
Umfang (Seiten): 2
Zeit: 6:38:47 Uhr

presenting therein the first reactions of these epoxide analogues in phosphorus heterocyclic chemistry. F. P. Gabbai (College Station, USA) discussed polyfunctional and cationic boranes, focusing on their reduction chemistry and anion complexation, and also described novel boron-containing radicals.

A special minisymposium comprising eight lectures was integrated to celebrate the 70th birthday of Kin-ya Akiba. The opening short lecture of this minisymposium was given by the chairman Y. Yamamoto with a short report entitled *"Hypervalent Chemistry: From Bond Switching to Penta- and Hexacoordinate Carbon Compounds"* that discussed the most recent results from a collaboration with C. A. Reed on the use of weakly coordinating anions. K. Seppelt (Berlin, Germany) described reactions of the organoselenonium (telluronium) cation in his plenary lecture, which also discussed the first synthesis of tellurirenium ions. A stimulating short talk was given by K. Tamao (Saitama, Japan), who showed how organoelemental chemistry can be directed towards material science as exemplified by the chemistry of siloles. The lecture by M. Mikolajczyk (Łódź, Poland) was more devoted to "pure" organic synthesis, with a demonstration of how α-phosphorylvinyl sulfoxides can be successfully employed in asymmetric synthesis. The topic of the lecture by N. Tokitoh (Kyoto, Japan) was how to obtain various forms of kinetically stabilized tin–carbon double-bond systems. A highlight of this short talk was discussion of a 2-stanna-naphthalene derivative. "Going supramolecular" was the motto of W.-W. du Mont (Braunschweig, Germany), who used unusual soft–soft interactions to build up extended networks based on triisopropylphosphane selenide and telluride ligands. How to gain access to photocontrollable properties and reactivities of Si and P compounds was discussed by T. Kawashima (Tokyo, Japan). The final contribution in this session was a plenary lecture that could have been entitled *"The Music Plays in the Ligand"* delivered by A. J. Arduengo (Tuscaloosa, USA), who explained how N-heterocyclic carbenes can be tuned and used to realize unusual valence states of carbon and other main-group elements.

The final day of this marathon of excellence was opened by L. J. Wright (Auckland, New Zealand), who presented results in the area of metallabenzenoids that (again) probed the understanding of aromaticity. I. Manners (Bristol, UK) gave insights into catalytic routes to rings, chains, and macromolecules based on inorganic elements, thus illustrating the progress in this field towards applications. More fundamentally oriented was the plenary lecture by R. Laitinen (Oulu, Finland), who focused on recent progress in imidoselenium and –tellurium chemistry as the "partly forgotten relatives" of sulfurimides.

The subsequent three lectures built bridges between common and highly unusual main-group ligand chemistry and showed their impact in transition-metal chemistry. P. W. Roesky (Berlin, Germany) started with bis(diphosphanylamides) and moved on to discuss [η^5-C_5Me_5Al] as a ligand system. F. E. Hahn (Münster, Germany) continued by describing a tetracarbene ligand with crown ether topology. M. Kira (Sendai, Japan) focused on transition-metal complexes of disilenes and digermenes and their reactions, such as ligand exchange and cycloaddition with phenylacetylene.

A. Sekiguchi (Tsukuba, Japan) described the reactivity of stable disilyene compounds towards organic nucleophiles and various π systems. The bonding in heavier Group 14 element alkynes was impressively explained by P. P. Power (Davies, USA), who revealed how tiny changes in the ligands of REER (R = alkyl; E = Si, Ge, Sn, Pb) might result in surprising structural changes and bring some unexpected chemistry to the fore, such as spontaneous reaction of a Ge^{II} species with elemental hydrogen at ambient temperature! M. Driess (Berlin, Germany) focused the attention on heterofulvene-like silylenes and germylenes with ambivalent reactivity, thus also leading to the first intramolecular donor-stabilized silaformamide. The final speaker of the session and symposium was D. Tilley (Berkeley, USA), who reported on bond activations and catalytic transformations involving transition-metal–silicon systems in his plenary lecture, which demonstrated that substrate activation is not necessarily and intimately intertwined with metals (or metal centers).

In summary, this scientific meeting was truly at the frontiers of research in molecular main-group chemistry (centered around Group 14 and 15 elements) and very inspiring in fields such as unusual open-shell systems, novel low-valent compounds, and organoelemental catalysis including hydrogen activation (and maybe storage in the future). The meeting was perfectly suited to create and/or strengthen research networks internationally. There was also something special in the air besides chemistry, including enjoyable cultural efforts such as the exchange of scientific *Haikus* (a Japanese lyric verse form with three unrhymed lines of five, seven, and five syllables that traditionally invokes an aspect of nature or the seasons).

Tell your dream to flasks,
pour your love to reagents,
and I believe individual persons are most important.
(Kin-ya Akiba, 1980;
translated by Y. Yamamoto, 2006)

Bonds break, atoms fly,
elemental arrays inspire.
Glimpses of the future.
(Don Tilley, 2006)

DOI: 10.1002/anie.200603708

 © 2006 Wiley-VCH Verlag GmbH & Co. KGaA, Weinheim

Dateiname: T603708E
Pfad: L:/daten/verlage/vch/ach/Hefte/0639/
Status Neusatz
Datum: 40 KW., 28. September 2006 (Donnerstag)
Pagina: 6419
Seite: 2 te von 2
Umfang (Seiten): 2
Zeit: 6:38:48 Uhr

Synthetic Methods

DOI: 10.1002/anie.200601814

Recent Advances in Catalytic Enantioselective Intermolecular C–H Functionalization**

*Huw M. L. Davies**

Keywords:
amination · C–H activation · enantioselectivity · insertion · rhodium

The selective functionalization of C–H bonds is an area of intense current interest because such reactions offer new strategies for the synthesis of complex organic targets.[1] One of the major challenges in this field is the development of broadly applicable enantioselective intermolecular C–H functionalization methods. This would require the design of reagents that are reactive enough to cleave relatively strong C–H bonds but still sufficiently selective to distinguish between the variety of different C–H bonds seen in typical organic substrates.

In recent years, two types of transition-metal-mediated transformations have come to the forefront as the most promising approaches for the development of practical methods for selective C–H functionalization in complex organic substrates. The first method, typically described as C–H activation, involves insertion of a metal into a C–H bond, which then activates the substrate for further functionalization (Scheme 1 a).[2] The second method is the C–H insertion of metal-bound carbenes[3] or nitrenes,[4] which leads directly to the functionalized products (Scheme 1 b).

Excellent progress has been made in developing enantioselective variants of both types of transformations over the last few years. Murai and Kakiuchi pioneered a strategy of using coordinating groups to direct the site of C–H activation,[5] and this approach has been beautifully extended to steadily more elaborate systems by several groups.[6] Once the C–H activation has been achieved with the aid of the directing group, further transformations can be readily accomplished. Enantioselective variants of this process are now appearing, as seen in the recent example from Bergman, Ellman, and co-workers (Scheme 2).[7]

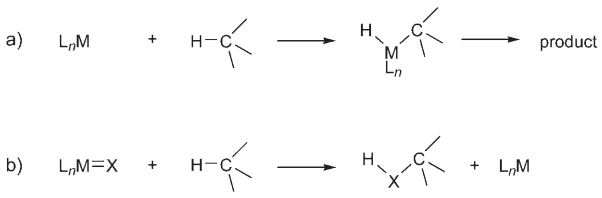

Scheme 1. C–H functionalization strategies (L = ligand; M = metal; X = NR or CR^1R^2): a) C–H activation; b) C–H insertion.

C–H functionalization by means of insertion of metal-bound carbenes and nitrenes into C–H bonds has been extensively applied to natural product synthesis.[3,4] As a result of the challenges of controlling the regioselectivity of the C–H functionalization, most of the applications have been directed towards intramolecular processes and a variety of efficient chiral catalysts have been developed for these systems.[3] A much more challenging scenario has been the development of practical intermolecular reactions, but several breakthroughs in this area have been made recently.[3,4] To achieve this, the reactivity of the metal-bound carbene or nitrene needs to be tuned carefully (Figure 1). Modulation of reactivity is possible by altering the structure of the metal and the carbene. Dirhodium complexes have been established as the most generally useful in this chemistry, and some of the most significant catalysts are shown in Figure 2. An electron-withdrawing substituent is required on the carbene or nitrene to have a sufficiently reactive electrophilic species for the C–H functionalization. The second substituent on the carbene gives a further control element, but this additional flexibility is not available with the nitrenes.

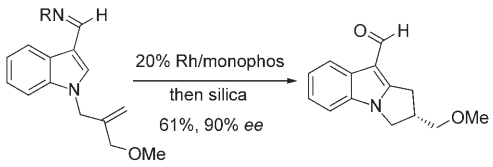

Scheme 2. Enantioselective C–H activation (monophos = (*R*)-(−)-(3,5-dioxa-4-phosphacyclohepta[2,1-*a*;3,4-*a*′]dinaphthalen-4-yl)dimethylamine).

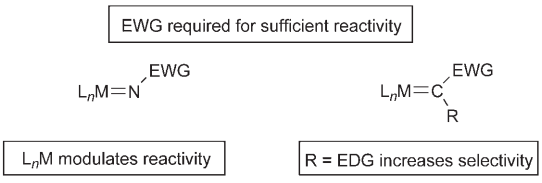

Figure 1. Controlling influences in metal-bound carbenes and nitrenes (EWG = electron-withdrawing group; EDG = electron-donating group).

[*] Prof. H. M. L. Davies
Department of Chemistry
University at Buffalo
The State University of New York
Buffalo, NY 14260-3000 (USA)
Fax: (+1) 716-645-6547
E-mail: hdavies@buffalo.edu

[**] This work was supported by the National Science Foundation (CHE-0350536).

InterScience
© 2006 Wiley-VCH Verlag GmbH & Co. KGaA, Weinheim

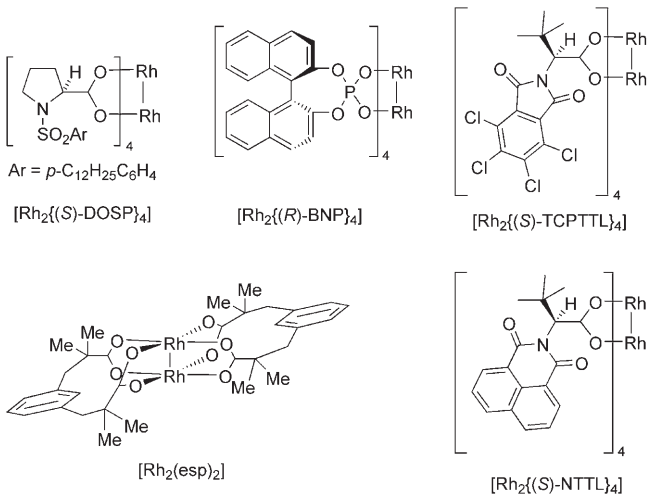

Figure 2. Dirhodium catalysts.

Intermolecular C–H insertions by rhodium-stabilized carbenoids were first reported nearly thirty years ago with ethyl diazoacetate used as the carbene source.[8] Owing to the limited selectivity of this carbenoid, this early version of the chemistry was not applied to any complex target synthesis. Altering the catalyst to bulky copper and silver complexes has improved the chemistry,[9] but the major breakthrough in this field was the discovery that a donor substituent such as an aryl or vinyl group on the carbene generates stabilized intermediates capable of highly regioselective transformations.[3] When these reactions are conducted in the presence of the dirhodium tetraprolinate catalyst, $[Rh_2\{(S)\text{-DOSP}\}_4]$, high asymmetric induction is possible as illustrated in the reaction with cyclohexane (Scheme 3).[10]

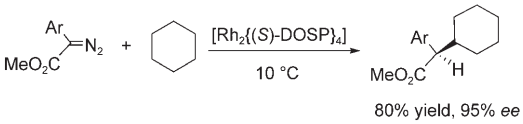

Scheme 3. Enantioselective carbenoid C–H insertion of cyclohexane.

The intermolecular C–H insertion by these donor/acceptor carbenoids has been shown to be a powerful strategic reaction applicable to a variety of substrates.[3] Excellent control of regioselectivity is possible through a delicate balance between steric and electronic effects. Complementary reactions can be achieved to some of the classic transformations of organic synthesis such as the Mannich reaction, aldol reaction, Michael addition, and the Claisen rearrangement.[3] An example of a Mannich reaction equivalent is shown in Scheme 4a.[11] In this case, not only is there excellent regiocontrol but also high kinetic resolution is possible, and the C–H insertion product **2** is produced with 98% *ee* even though the starting material **1** is racemic. Another example of the potential of this chemistry as a strategic reaction is the combined C–H activation/Cope rearrangement of the dihydronaphthalene **3** to form **4**,[12] a key step in the synthesis of colombiasin A (Scheme 4b). In this case, an enantiomer differentiation occurs whereby (*S*)-**3** undergoes C–H functionalization to form **4**, while (*R*)-**3** is cyclopropanated.

The enantioselective C–H functionalization by metal nitrenes has been a more intractable problem than the parallel reaction with metal carbenes because less options are available for modulating the reactivity of the metal nitrenes. The first example of an enantioselective reaction used the dirhodium catalyst $[Rh_2\{(R)\text{-BNP}\}_4]$,[13] and this was followed by a study using Hashimoto's catalyst $[Rh_2\{(S)\text{-TCPTTL}\}_4]$ (Scheme 5).[14] The nitrene source was

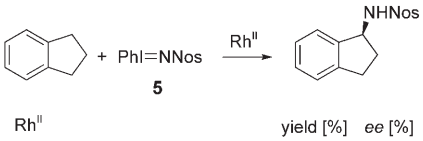

Rh^{II}	yield [%]	*ee* [%]
$[Rh_2\{(R)\text{-BNP}\}_4]$	71	33
$[Rh_2\{(S)\text{-TCPTTL}\}_4]$	51	73

Scheme 5. Enantioselective C–H amination of indane (Nos = *p*-nitrobenzenesulfonyl).

the arylsulfonyliminoiodinanes, and the *p*-nitro derivative **5** gave the highest-yielding reactions, but even so, the use of at least five equivalents of trapping agent was required. Similarly large excesses of trapping agents were required in enantioselective reactions catalyzed by chiral manganese and ruthenium complexes.[15] Thus, in this early devel-

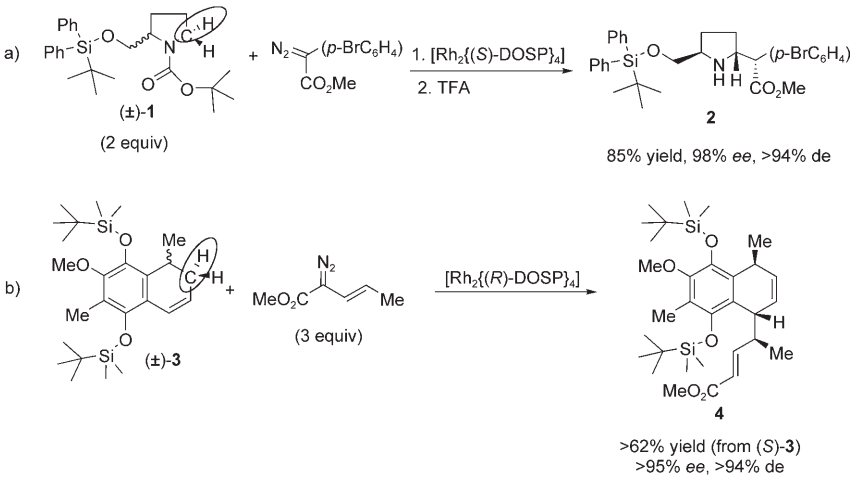

Scheme 4. Examples of highly regioselective and enantioselective intermolecular carbenoid C–H insertions.

© 2006 Wiley-VCH Verlag GmbH & Co. KGaA, Weinheim

opment stage it was demonstrated that reasonable levels of enantioselectivity could be achieved in this chemistry but still the practicality of the reaction required improvement.[3c]

For the C–H amination chemistry to develop further, a more selective nitrene system would need to be developed. Du Bois and co-workers demonstrated that the trichloroethylsulfamate **7** in the presence of phenyliodinane diacetate could be used as an effective nitrene source (Scheme 6).[16] Furthermore, when $[Rh_2(esp)_2]$ was used as catalyst, effective amination of ethylanisole (**6**) was achieved without resorting to an excess of the trapping agent. The application of this nitrene source to enantioselective C–H functionalization has not been reported.

The recent report by Müller, Dodd, Dauban and co-workers that the tosylsulfonylimidamide (*S*)-**8** is an effective

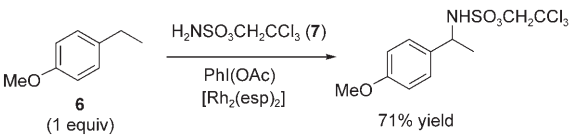

Scheme 6. C–H amination using a stoichiometric amount of trapping agent.

C–H aminating agent[17] is a major advance because it demonstrates a new approach for controlling the reactivity of the metal nitrene such that highly efficient reactions can be achieved without resorting to excess of trapping agent. High asymmetric induction was achieved in $[Rh_2\{(S)\text{-NTTL}\}_4]$-catalyzed reactions with a range of benzylic substrates, as illustrated by the representative examples shown in Scheme 7. These are the first examples of C–H aminations occurring in high yield and with high asymmetric induction in which the trapping agent is used as the limiting agent. The matching of the chiral aminating agents with the chiral catalyst is very pronounced because the high asymmetric induction is only obtained when the reactions of (*S*)-**8** is catalyzed by $[Rh_2\{(S)\text{-NTTL}\}_4]$. Very poor yields and asymmetric induction are obtained when the reaction is catalyzed by either $[Rh_2\{(R)\text{-NTTL}\}_4]$ or $Rh_2(OAc)_4$. The most impressive results were obtained at benzylic sites, while the asymmetric induction was considerably lower at allylic sites.

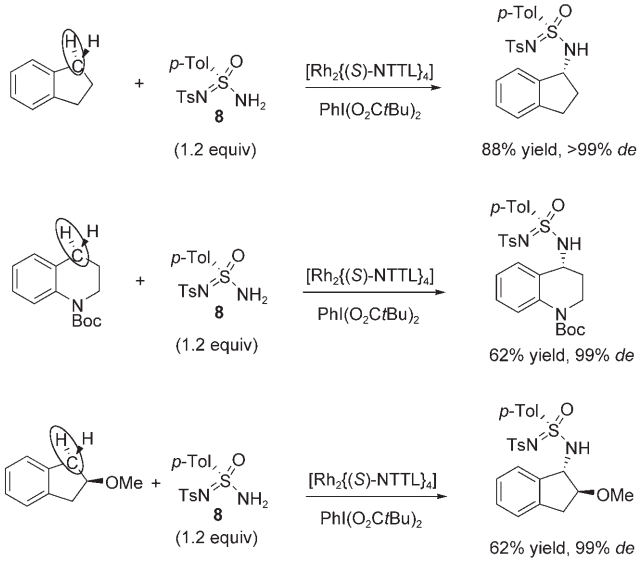

Scheme 7. Highly regioselective and enantioselective intermolecular C–H aminations (Tol = tolyl; Ts = *p*-toluenesulfonyl; Boc = *tert*-butyloxycarbonyl).

In conclusion, the stage is set for the rapid development of enantioselective intermolecular C–H functionalizations as powerful strategic reactions for organic synthesis. Impressive results have already been obtained in ligand-directed C–H activation and rhodium-carbenoid-induced C–H functionalizations. The identification of a nitrene source capable of intermolecular C–H amination with high asymmetric induction offers exciting opportunities for its application towards the synthesis of natural products and pharmaceutical targets.

Published online: September 13, 2006

[1] K. Godula, D. Sames, *Science* **2006**, *312*, 67.

[2] B. A. Arndtsen, R. G. Bergman, T. A. Mobley, T. H. Peterson, *Acc. Chem. Res.* **1995**, *28*, 154.

[3] H. M. L. Davies, R. E. J. Beckwith, *Chem. Rev.* **2003**, *103*, 2861.

[4] a) C. G. Espino, J. Du Bois in *Modern Rhodium-Catalyzed Organic Reactions* (Ed.: P. A. Evans), Wiley-VCH, Weinheim, **2005**, pp. 379–416; b) H. M. L. Davies, M. S. Long, *Angew. Chem.* **2005**, *117*, 3584; *Angew. Chem. Int. Ed.* **2005**, *44*, 3518; c) P. Müller, C. Fruit, *Chem. Rev.* **2003**, *103*, 2905.

[5] F. Kakiuchi, S. Murai, *Acc. Chem. Res.* **2002**, *35*, 826.

[6] a) B. D. Dangel, J. A. Johnson, D. Sames, *J. Am. Chem. Soc.* **2001**, *123*, 8149; b) D. Kalyani, N. R. Deprez, L. V. Desai, M. S. Sanford, *J. Am. Chem. Soc.* **2005**, *127*, 7330; c) K. M. Waltz, J. F. Hartwig, *J. Am. Chem. Soc.* **2000**, *122*, 11358.

[7] R. M. Wilson, R. K. Thalji, R. G. Bergman, J. A. Ellman, *Org. Lett.* **2006**, *8*, 1745.

[8] R. Paulissen, E. Hayez, A. J. Hubert, P. Teyssié, *Tetrahedron Lett.* **1974**, *43*, 607.

[9] a) H. V. R. Dias, H.-L. Lu, H.-J. Kim, S. A. Polach, T. K. H. H. Goh, R. G. Browning, C. J. Lovely, *Organometallics* **2002**, *21*, 1466; b) M. M. Diaz-Requejo, T. R. Belderrain, M. C. Nicasio, S. Trofimenko, P. J. Perez, *J. Am. Chem. Soc.* **2002**, *124*, 896.

[10] H. M. L. Davies, T. Hansen, M. R. Churchill, *J. Am. Chem. Soc.* **2000**, *122*, 3063.

[11] H. M. L. Davies, C. Venkataramani, T. Hansen, D. W. Hopper, *J. Am. Chem. Soc.* **2003**, *125*, 6462.

[12] H. M. L. Davies, X. Dai, M. S. Long, *J. Am. Chem. Soc.* **2006**, *128*, 2485.

[13] I. Nägeli, C. Baud, G. Bernardinelli, Y. Jacquier, M. Moraon, P. Müller, *Helv. Chim. Acta* **1997**, *80*, 1087.

[14] M. Yamawaki, H. Tsutsui, S. Kitagaki, M. Anada, S. Hashimoto, *Tetrahedron Lett.* **2002**, *43*, 9561.

[15] a) J.-L. Liang, S.-X. Yuan, J.-S. Huang, W.-Y. Yu, C.-M. Che, *Angew. Chem.* **2002**, *114*, 3615; *Angew. Chem. Int. Ed.*

 © 2006 Wiley-VCH Verlag GmbH & Co. KGaA, Weinheim

2002, *41*, 3465; b) Y. Kohmura, T. Katsuki, *Tetrahedron Lett.* **2001**, *42*, 3339.

[16] C. G. Espino, K. W. Fiori, M. Kim, J. Du Bois, *J. Am. Chem. Soc.* **2004**, *126*, 15378.

[17] C. Liang, F. Robert-Peillard, C. Fruit, P. Müller, R. H. Dodd, P. Dauban, *Angew. Chem.* **2006**, *118*, 4757; *Angew. Chem. Int. Ed.* **2006**, *45*, 4641.

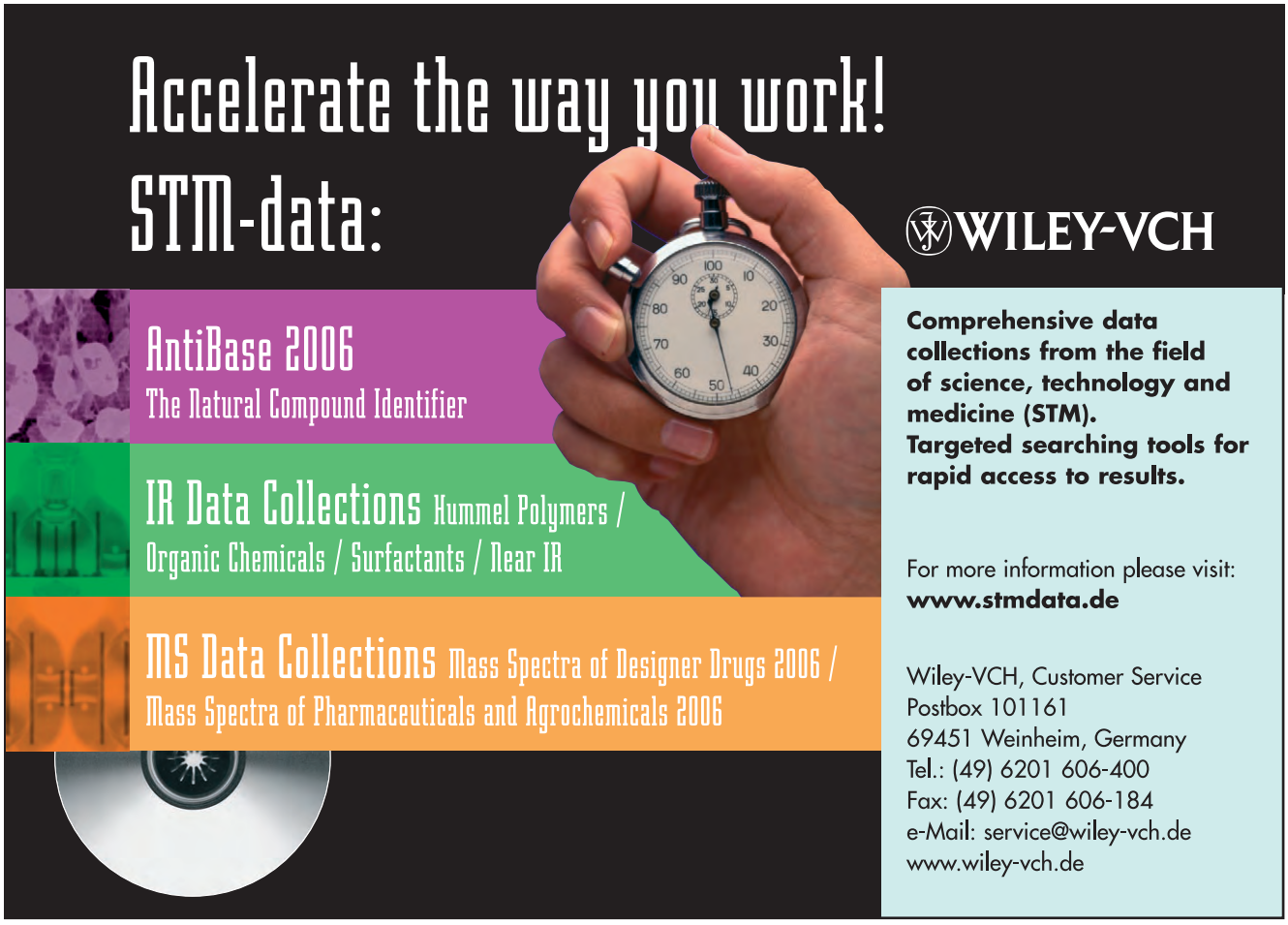

 © 2006 Wiley-VCH Verlag GmbH & Co. KGaA, Weinheim

Functionalization of Diamond

DOI: 10.1002/anie.200602509

Hard and Soft: Biofunctionalized Diamond**

*Anke Krüger**

Keywords:
diamond · DNA · nanostructures · surface chemistry · thin films

Dedicated to Professor Henning Hopf on the occasion of his 65th birthday

In recent years, the functionalization of semiconductor and carbon materials has developed into an active field of research at the border between organic chemistry and materials science. Thus, numerous studies on the surface modification of diamond have been published. Diamond, owing to its dopability, biocompatibility, and mechanical and chemical stability, is a versatile material for many applications.

Diamond materials can be produced by various established techniques.[1] Methods exist for the synthesis of single-crystalline and polycrystalline diamond films, as well as the production of nano- to microscopic diamond particles. Depending on the chosen synthetic method, diamond materials exhibit significantly different surface properties. For example, hydrogenated diamond films have a highly hydrophobic character, which hinders the nonspecific adsorption of polar biomolecules.[2] In contrast, poly-L-lysine, enzymes, or antibodies can be adsorbed on polar diamond surfaces coated with oxygen-containing groups. These noncovalently modified diamond materials are being investigated for sensors and other biomedical applications.[3] The presence of functional groups on the diamond surface also enables the covalent bonding of various moieties. Depending on the original surface coverage, different functionalization strategies, such as silanization, esterification, amidation, and direct C–C coupling have been applied. These techniques have been used for the modification of hydrogenated, halogenated, carboxylated, and hydroxylated diamond surfaces.[4]

The aim of many of these investigations is the grafting of biologically active moieties, such as DNA oligonucleotides, peptides, enzymes, or antibodies.[5] The application of biofunctionalized diamond in, for example, bioassays or "lab on the chip" devices has been considered.[6] Recently, the inherent fluorescence of defective diamond has been used for the fluorescence marking of drugs. The N-V centers (isolated nitrogen defects with adjacent vacancies) of diamond emit a characteristic red fluorescence,[7] which is suitable for fluorescence microscopy, including the examination of living cells.[8] The advantages of such a diamond marker, in addition to its favorable emission wavelength, are the high stability of the emission and the biocompatibility of the material.

The covalent attachment of DNA molecules to modified diamond surfaces has been described by several groups. Takahashi and co-workers used terminal carboxyl groups to connect the DNA molecules through the formation of amide linkages.[9] Ando and co-workers described the grafting of DNA molecules through thymidines immobilized by ester bridges.[10] A much more stable coupling can be achieved by the formation of direct C–C bonds. Hamers and co-workers introduced a very flexible technique that uses hydrogenated diamond films as the starting material.[11] In a photochemical reaction, the terminal vinyl group of a bifunctional organic moiety is connected to the diamond surface. After the deprotection of a terminal amino group, a subsequent reaction with sulfosuccinimidyl-4-(*N*-maleimidomethyl)cyclohexane-1-carboxylate (SSMCC) yields a modified diamond surface that is ready to be grafted with DNA. The grafting is then carried out using thiol-modified DNA (Scheme 1).

Recently, Nebel and co-workers reported the microscopic characterization of DNA-modified diamond surfaces.[12] Using the technique described above, the authors produced a continuous, covalently bound DNA film on a structured, partly hydrogenated (100) diamond surface. Subsequent reaction with fluorescence-labeled complementary oligonucleotides yielded functionalized diamond films, which were characterized by fluorescence microscopy. In this study, only the areas that were initially hydrogenated exhibited a strong fluorescence, whereas oxidized areas exhibited only weak fluorescence, owing to nonspecific adsorption of the marker.

The morphology of the DNA-modified diamond surface was studied using atomic force microscopy (AFM). By performing the measurements in a buffered solution, the natural conformation of the DNA molecules was conserved. Binding-force measurements demonstrated the covalent bonding of the DNA strands (Figure 1). Information on the thickness and orientation of the DNA layer was also obtained: the molecules form a pinhole-free film with a thickness of 76 Å and are arranged at an angle of approximately 36° relative to the diamond surface. The authors have, thus, performed the first microscopic characterization of a biofunctionalized diamond film. This characterization method is of crucial significance for the development of diamond-based sensors, as only a reliable and established ana-

[*] Dr. A. Krüger
Otto-Diels-Institut für Organische Chemie
Christian-Albrechts-Universität zu Kiel
Otto-Hahn-Platz 3, 24098 Kiel (Germany)
Fax: (+49) 431-880-1558
E-mail: akrueger@oc.uni-kiel.de

[**] A.K. gratefully acknowledges the Fonds der Chemischen Industrie for a Liebig habilitation scholarship.

InterScience
© 2006 Wiley-VCH Verlag GmbH & Co. KGaA, Weinheim

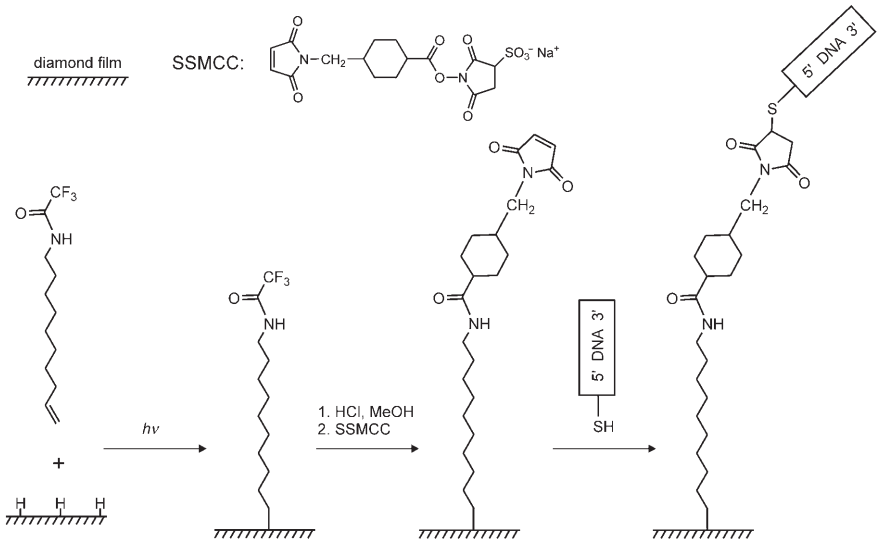

Scheme 1. Functionalization of a diamond surface with DNA oligonucleotides. See text for details.

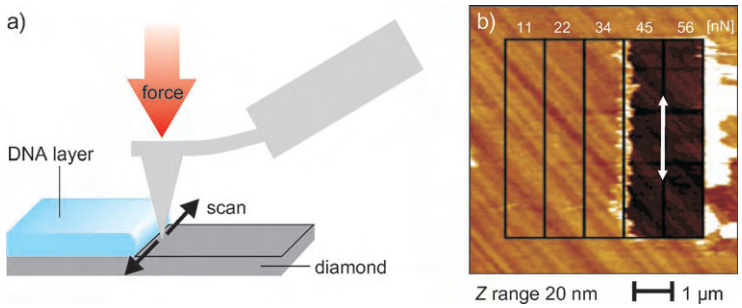

Figure 1. a) Schematic representation of binding-force measurements on a DNA-functionalized diamond surface using an AFM tip. b) In these measurements, the DNA layer is removed by scratching with the tip at increasing applied force (11–56 nN). (Adapted, with kind permission, from reference [12].)

lytical technique can ensure that surface coverage is complete and that the orientation of grafted molecules is correct.

In addition to the sensor arrays mentioned above, functionalized diamond materials are promising candidates for applications in targeted drug delivery and fluorescence diagnostics. Whether functionalized diamond will replace other materials, such as gold, silica, and quantum dots, in this field remains to be seen, but without question, diamond represents an attractive and complementary alternative.

Published online: September 4, 2006

[1] M. N. R. Ashfold, P. W. May, C. A. Rego, N. M. Everitt, *Chem. Soc. Rev.* **1994**, *23*, 21–30; T. R. Anthony, *Vacuum* **1990**, *41*, 1356–1359; O. A. Shenderova, V. V. Zhirnov, D. W. Brenner, *Crit. Rev. Solid State Mater. Sci.* **2002**, *27*, 227–356; J. B. Donnet, C. Lemoigne, T. K. Wang, C.-M. Peng, M. Samirant, A. Eckhardt, *Bull. Soc. Chim. Fr.* **1997**, *134*, 875–890.

[2] D. Delabouglise, B. Marcus, M. Mermoux, P. Bouvier, J. Chane-Tune, J.-P. Petit, P. Mailley, T. Livache, *Chem. Commun.* **2003**, 2698–2699; T. L. Clare, B. H. Clare, B. M. Nichols, N. L. Abbott, R. J. Hamers, *Langmuir* **2005**, *21*, 6344–6355.

[3] T. S. Huang, Y. Tzeng, Y. K. Liu, Y. C. Chen, K. R. Walker, R. Guntupalli, C. Liu, *Diamond Relat. Mater.* **2004**, *13*, 1098–1102; L.-C. L. Huang, H.-C. Chang, *Langmuir* **2004**, *20*, 5879–5884; X. Kong, L.-C. L. Huang, S.-C. V. Liau, C.-C. Han, H.-C. Chang, *Anal. Chem.* **2005**, *77*, 4273–4277.

[4] V. F. Loktev, V. I. Makal'ski, I. V. Stoyanova, A. V. Kalinkin, V. A. Likholobov, *Carbon* **1990**, *28*, 817–819; Y. Liu, Z. Gu, J. L. Margrave, V. N. Khabashesku, *Chem. Mater.* **2004**, *16*, 3924–3930; T. Nakamura, M. Ishihara, T. Ohana, Y. Koga, *Chem. Commun.* **2003**, 900–901; T. Tsubota, O. Hirabayashi, S. Ida, S. Nagaoka, M. Nagata, Y. Matsumoto, *Phys. Chem. Chem. Phys.* **2002**, *4*, 806–811.

[5] A. Härtl, E. Schmich, J. A. Garrido, J. Hernando, S. C. R. Catharino, S. Walter, P. Feulner, A. Kromka, D. Steinmüller, A. Stutzmann, *Nat. Mater.* **2004**, *3*, 736–742; A. Krüger, Y. Liang, G. Jarre, J. Stegk, *J. Mater. Chem.* **2006**, *16*, 2322–2328; G.-J. Zhang, K.-S. Song, Y. Nakamura, T. Ueno, T. Funatsu, I. Ohdomari, H. Kawarada, *Langmuir* **2006**, *22*, 3728–3734.

[6] K.-S. Song, H. Kawarada, *New Diamond Front. Carbon Technol.* **2005**, 5, 325–335; G. M. Swain, *Semicond. Semimetals* **2004**, *77*, 121–148.

[7] A. Gruber, A. Dräbenstedt, C. Tietz, L. Fleury, J. Wrachtrup, C. von Borczyskowski, *Science* **1997**, *276*, 2012–2014.

[8] S.-J. Yu, M.-W. Kang, H.-C. Chang, K.-M. Chen, Y.-C. Yu, *J. Am. Chem. Soc.* **2005**, *127*, 17604–17605.

[9] K. Takahashi, M. Tanga, O. Takai, H. Okamura, *Diamond Relat. Mater.* **2003**, *12*, 572–576.

[10] K. Ushizawa, Y. Sato, T. Mitsumori, T. Machinami, T. Ueda, T. Ando, *Chem. Phys. Lett.* **2002**, *351*, 105–108.

[11] W. Yang, O. Auciello, J. E. Butler, W. Cai, J. A. Carlisle, J. E. Gerbi, D. M. Gruen, T. Knickerbocker, T. L. Lasseter, J. N. Russel, Jr., L. M. Smith, R. J. Hamers, *Nat. Mater.* **2002**, *1*, 253–257.

[12] B. Rezek, D.-C. Shin, T. Nakamura, C. E. Nebel, *J. Am. Chem. Soc.* **2006**, *128*, 3884–3885.

© 2006 Wiley-VCH Verlag GmbH & Co. KGaA, Weinheim

Cyclophane Polymers

DOI: 10.1002/anie.200600752

Through-Space Conjugated Polymers Based on Cyclophanes

*Yasuhiro Morisaki and Yoshiki Chujo**

Keywords:
conjugated polymers · cyclophanes · fluorescence · through-space interactions

Conjugated polymers display unique electronic and optical properties, which favor their use in applications as optoelectronic materials and molecular devices. Despite the recent remarkable progress in the chemistry of conjugated polymers, the synthesis of conjugated polymers containing cyclophane units in the main chain is limited to only a few examples. This Minireview presents recent developments in the synthesis, properties, and applications of through-space conjugated polymers based on cyclophanes.

1. Introduction

Over the past three decades, a considerable amount of interest has emerged in the construction of novel conjugated polymers[1] as a result of their fascinating properties such as electrical conductivity,[1,2] electroluminescence,[3] liquid-crystallinity,[4] third-order nonlinear optical properties,[5] and chemical sensing properties.[6] The most prominent example is poly(arylenevinylene)s (PAVs), which, after the first report on poly(*p*-phenylenevinylene)s (PPVs) in 1990, have been used in polymer-based light-emitting diodes (LEDs) for displays and other applications.[7] Additionally, poly(aryleneethynylene)s (PAEs)[8] are promising candidates for molecular wires and as active components in polymer-based electronic and photonic devices. Current research on conjugated polymers including PAVs and PAEs is focused on the tuning of their spectral and electrical properties. To this end, aromatic compounds are incorporated into the backbone of conjugated polymers and the physical properties of these derivatives are investigated.

In the field of organic chemistry, cyclophane derivatives, particularly those that comprise intramolecular face-to-face π-conjugated systems, have been widely acknowledged.[9] Central to the study of cyclophane chemistry are the [*n.n*]cyclophanes ($n = 2$ or 3), which have overlapping π-electron clouds. A variety of [*n.n*]cyclophane derivatives have been prepared. Their unique structural and electronic properties result from the characteristic interactions between the two cofacial π-electron systems.[9,10] However, considerably less attention has been paid to the synthesis of conjugated polymers that contain cyclophane units in the main chain.

In this Minireview, we focus on the synthesis, properties, and applications of linear conjugated polymers with a cyclophane skeleton in their main chain. Polymers containing cyclophane units in the side chain are not discussed here.

[*] Dr. Y. Morisaki, Prof. Dr. Y. Chujo
Department of Polymer Chemistry
Graduate School of Engineering
Kyoto University
Katsura, Nishikyo-ku
Kyoto 615-8510 (Japan)
Fax: (+81) 75-383-2605
E-mail: chujo@chujo.synchem.kyoto-u.ac.jp

2. [2.2]Metacyclophane-Containing Polymers

The earliest examples of cyclophane-containing conjugated polymers were reported by Mizogami and Yoshimura in 1985.[11] It was demonstrated that the oxidative coupling reaction of 8,16-dihydroxy[2.2]metacyclophane **1** gave polymer **2**, which contained repeating diphenoquinone units (Scheme 1).[11a] In another reaction, the oxidative dimer **3** of **1** underwent polycondensation to give poly-[2.2]metacyclophane **4**.[11b] Both the polymers **2** and **4** were characterized by IR spectroscopy and elemental analysis. Doping poly[2.2]metacyclophane **4** with H_2SO_4 vapor led to an increase in its electrical conductivity from 10^{-9} to 10^{-1} S cm^{-1}.[11b]

3. [2.2]Paracyclophane-Containing Polymers

The incorporation of [2.2]paracyclophane into the conjugated polymer backbone was successfully achieved by the following three synthetic approaches.

InterScience DISCOVER SOMETHING GREAT

© 2006 Wiley-VCH Verlag GmbH & Co. KGaA, Weinheim

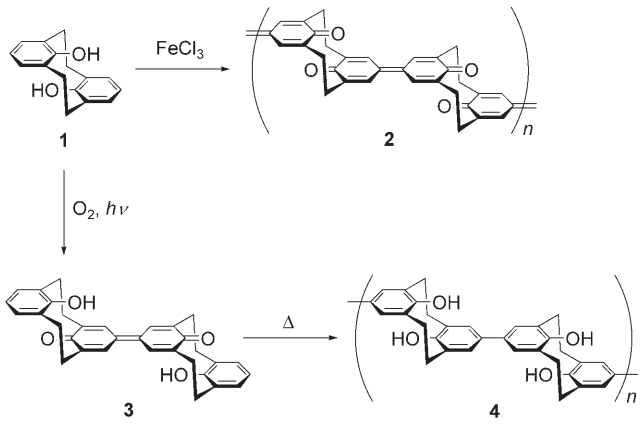

Scheme 1.

3.1. Electrochemical Polymerization

The electrochemical polymerization of oligothienyl-substituted [2.2]paracyclophanes was described by two research groups (Table 1).[12,13] Substituted thiophene rings were oxidized electrochemically, and the corresponding conjugated polymers were deposited on the electrode surface. The cyclic voltammogram (CV) of the polymers exhibited a broad reversible redox wave with $E_{1/2}$ at approximately 1.0 V. The absorption maximum of a thin film of polymer **12** was red-shifted by 44 nm in comparison to that of polymer **14**.[13b] This shift is due to the twisted form of the thiophene units, which results from the head-to-head linkage of octylthiophenes. Polymer **14** was also obtained by chemical oxidation polymerization using $FeCl_3$ in $CHCl_3$.[13b] This polymer was soluble in organic solvents such as hexane and $CHCl_3$, and the weight-average molecular weight (M_w) of the $CHCl_3$-soluble part of **14** was determined by gel permeation chromatography (GPC) to be 50000 g mol^{-1}.

3.2. Transition-Metal-Catalyzed Polymerization

Palladium-catalyzed coupling is a powerful method for preparing conjugated polymers such as PAEs, PAVs, and polyarylenes (PAs). Table 2 shows the successful synthetic results of the first well-defined [2.2]paracyclophane-containing conjugated polymers prepared by us.[14,15] The synthesis of PAE-type copolymer **17** was carried out through the Sonogashira coupling reaction[16] of pseudo-*p*-dibromo-[2.2]paracyclophane **15** with 2,5-didodecyloxy-1,4-diethynylbenzene (**16**; Table 2, entry 1).[14a] As another synthetic route to **17**, the reaction of pseudo-*p*-diethynyl[2.2]paracyclophane **18**[14g,15,17] with 2,5-didodecyloxy-1,4-diiodobenzene (**19**) proceeded more smoothly and yielded a polymer with a number-average molecular weight (M_n) of 14000 g mol^{-1} (Table 2,

Table 1: Electrochemical polymerization of oligothiophene-functionalized [2.2]paracyclophanes.

Monomer	Polymer	$E_{1/2}$ [V]	λ_{max} [nm]	Ref.
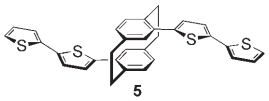 5	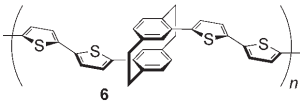 6	1.0[a]	398[b]	[12a]
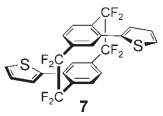 7	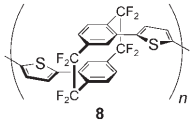 8	2.0[c]	–	[12b]
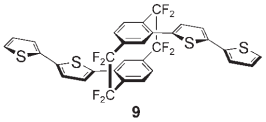 9	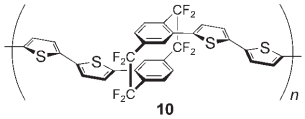 10	1.0[d]	–	[12b]
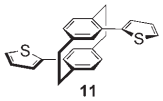 11	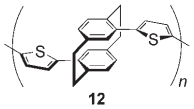 12	1.0[e]	380[b]	[13a,b]
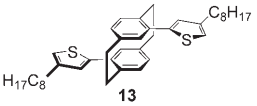 13	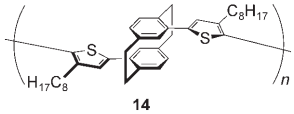 14	1.0[e]	336[b]	[13b]

[a] 1 V s^{-1} in CH_3CN (0.1 mol L^{-1} Bu_4NPF_6) versus Ag/Ag$^+$. [b] Deposited on an ITO electrode. [c] Peaks are ill-defined, which impedes the determination of $E_{1/2}$. [d] 2 V s^{-1} in CH_3CN (Et_4NClO_4) versus SCE. [e] 0.1 V s^{-1} in CH_2Cl_2 (0.1 mol L^{-1} Bu_4NPF_6) versus SCE.

Yoshiki Chujo completed his PhD at Kyoto University in 1980 and then joined Nagoya University as an assistant professor in 1981. In 1983, he joined J. McGrath at Virginia Polytechnic Institute as a postdoctoral research fellow. He returned to Kyoto University as a lecturer in 1986 and has been Professor of Polymer Chemistry there since 1994. His research interests focus on polymer synthesis, inorganic polymers, and polymeric hybrid materials.

Yasuhiro Morisaki was born in Osaka, Japan. He received his PhD from Kyoto University in 2000 under the direction of T.-a. Mitsudo. After a six-month postdoctoral stay with Y. Souma at Osaka National Research Institute, he joined the group of Yoshiki Chujo as an Assistant Professor at Kyoto University in 2000. He recently carried out postdoctoral work with R. R. Tykwinski at the University of Alberta (2004–5). His research interests focus on polymer synthesis and organic chemistry.

© 2006 Wiley-VCH Verlag GmbH & Co. KGaA, Weinheim

Table 2: Transition-metal-catalyzed polymerization and optical properties of [2.2]paracyclophane-containing conjugated polymers.

Entry	Monomers		Catalyst[a]	Polymer	Yield [%]	M_n[b]	M_w/M_n[b]	A λ_{max} [nm][c]	PL λ_{max} [nm][c] (Φ)[d]	Ref.
1	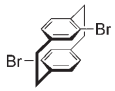 **15**	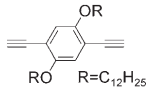 **16** $R=C_{12}H_{25}$	A	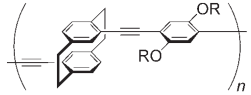 **17**	98	8000	1.8	384	460 (0.30)	[14a]
2	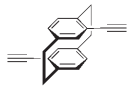 **18**	**19a** $R=C_{12}H_{25}$	B	**17**	95	14500	2.4	387	–	[14b]
3	**18**	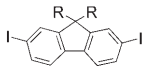 **20a** $R=C_{12}H_{25}$	B	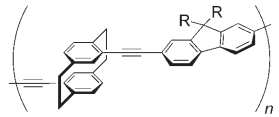 **21**	76	26400	2.5	370	415 (0.58) 418 (film)	[14c]
4	**18**	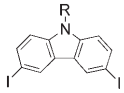 **22** $R=C_8H_{17}$	B	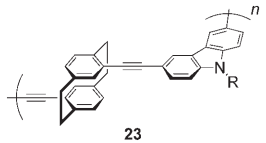 **23**	54	4400	1.9	353	413 (0.64) 450 (film)	[14d]
5	**18**	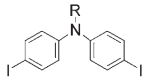 **24** $R=C_8H_{17}$	B	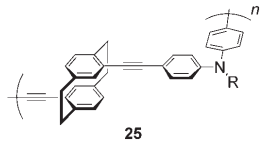 **25**	94	4300	3.1	373	410 (0.65)	[14e]
6	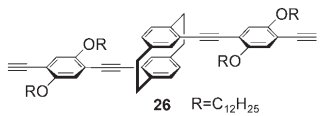 **26** $R=C_{12}H_{25}$	**27**	B	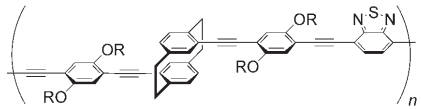 **28**	96	29700	2.6	470	565 (0.13) 565 (film)	[14f]
7	**26**	**29**	B	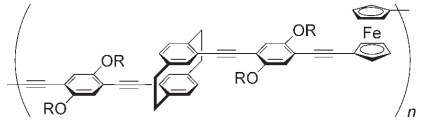 **30**	93	24500	2.7	384	475 (0.04)	[14g]
8	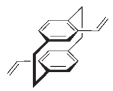 **31**	**19b** $R=C_6H_{13}$	C	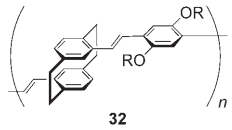 **32**	69	4200	2.0	398	462 (0.92) 507 (film)	[14h]

© 2006 Wiley-VCH Verlag GmbH & Co. KGaA, Weinheim

Table 2: (Continued)

Entry		Monomers	Catalyst[a]	Polymer	Yield [%]	M_n[b]	M_w/M_n[b]	A λ_{max} [nm][c]	PL λ_{max} [nm][c] (Φ)[d]	Ref.
9	**31**	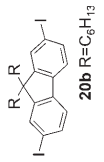 **20b** R=C_6H_{13}	D	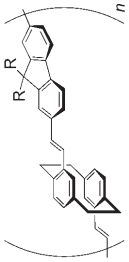 **33**	96	5200	1.9	372	426 (0.70) 484 (film)	[14i]
10	**15**	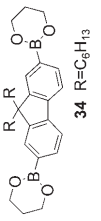 **34** R=C_6H_{13}	E	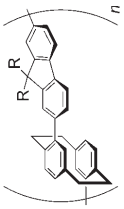 **35**	89	2600	2.5	340	392 (0.81) 415 (film)	[14j]
11	**26**	–	F	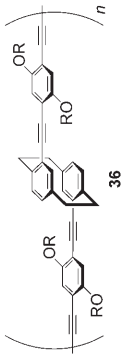 **36**	50	63000	1.6	406	442 (0.45) 497 (film)	[15]

[a] System A: $[PdCl_2(PPh_3)_2]/PPh_3/CuI$ in $THF/HNiPr_2$; system B: $[PdCl_2(PPh_3)_2]/PPh_3/CuI$ in THF/NEt_3; system C: $[PdCl_2(PPh_3)_2]/Bu_4NI/K_2CO_3$ in DMF; system D: $[PdCl_2(PPh_3)_2]/P(o\text{-Tol})_3/Bu_3N$ in DMF; system E: $[Pd(PPh_3)_4]/Na_2CO_3$ (aq) in toluene; system F: CuCl/TMEDA/O_2 in PhCl. [b] GPC ($CHCl_3$ or THF, polystyrene standards). [c] Dilute solution in $CHCl_3$ (ca. 10^{-5} M). [d] Fluorescence quantum yield in solution.

entry 2)[14b] It appears that dibromo[2.2]paracyclophane **15** is relatively inert for the oxidative addition to palladium, as a result of the steric hindrance and the electron-rich properties of the paracyclophane moiety. Fluorene,[14c] carbazole,[14d] phenylamine,[14e] benzothiadiazole,[14f] and ferrocene (Table 2, entries 3–7)[14g] can be incorporated alternately into the PAE-conjugated backbone with [2.2]paracyclophane by the Sonogashira coupling reaction to obtain the corresponding polymers.

Pseudo-*p*-divinyl[2.2]paracyclophane **31** was also polymerized with diiodobenzene **19b** and diiodofluorene **20b** through the Heck coupling reaction[18] to produce corresponding PAV-type conjugated polymers **32**[14h] and **33**,[14i] respectively (Table 2, entries 8, 9). Also, the palladium-catalyzed Suzuki–Miyaura coupling reaction[19] of **15** with **34** gave the corresponding PA-type conjugated polymer, which contains [2.2]paracyclophane and fluorene units in the main chain (Table 2, entry 10).[14j] [2.2]Paracyclophane-containing conjugated polymer **36**, which has a butadiyne unit, was prepared by the copper-catalyzed oxidative polycondensation of monomer **26** (Table 2, entry 11).[15]

The presence of long alkyl chains on the benzene ring makes it possible to confirm the structure of the obtained polymer and also results in good solubility of the polymer in common organic solvents which helps in the evaluation of their properties. All the polymers listed in Table 2 were characterized by ^1H and ^{13}C NMR spectroscopy, FTIR spectroscopy, and GPC analysis. [2.2]Paracyclophane-containing conjugated polymers could be processed into a thin film by casting or spin-coating from toluene solution and were found to be stable against air, moisture, and heat. For example, polymer **33** displayed good thermal stability, with thermogravimetric analysis (TGA) in air revealing a 10% weight loss at 433 °C.[14i]

The face-to-face arrangement of the benzene rings of [2.2]paracyclophane leads to through-space interaction and thus to an extension of the π-conjugation length of the polymer. The absorption spectrum of polymer **35**, as a representative polymer, is shown in Figure 1.[14j] At room temperature in $CHCl_3$, polymer **35** showed a strong absorp-

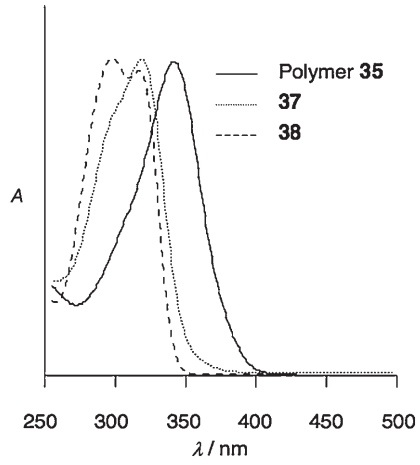

Figure 1. UV/Vis spectra of polymer **35** and the two model compounds **37** and **38** in $CHCl_3$ solution measured at room temperature.

© 2006 Wiley-VCH Verlag GmbH & Co. KGaA, Weinheim

tion peak at $\lambda_{max} = 340$ nm, which was red-shifted relative to those values for two model compounds, **37** ($\lambda_{max} = 315$ nm)

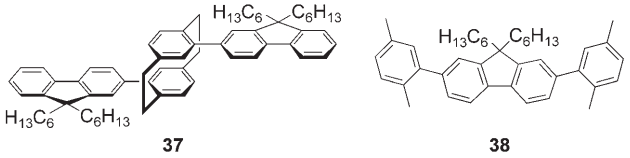

37 **38**

and **38** ($\lambda_{max} = 314$ nm; Figure 1). The fluorescence emission peak of polymer **35** in $CHCl_3$ was observed at approximately 390 nm in the visible purple-blue region with a high quantum efficiency of 0.81 (Table 2, entry 10). On the other hand, the emission of model compound **38** was slightly blue-shifted as compared to that of **35**, while the absorption maximum of **38** exhibited a stronger blue shift of approximately 25 nm. These results imply that the emission of polymer **35** occurs from the monomer (chromophore) state rather than the cyclophane state (Scheme 2).[9c,10a–c,20]

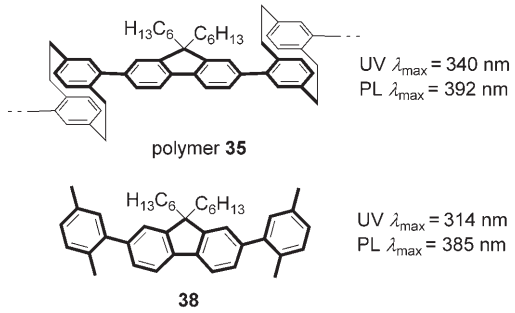

Scheme 2.

The through-space conjugation is not as effective as the through-bond conjugation for π-electron delocalization. For example, polymer **17** exhibits an absorption maximum at $\lambda_{max} \approx 385$ nm, whereas in general the absorption maxima of PPEs appear at over 400 nm.[8a]

The electroluminescent (EL) properties of a multilayered device of polymer **33** were also examined.[14i] The EL spectrum showed a maximum peak at 490 nm and a shoulder peak at approximately 510 nm, values which are very similar to the photoluminescence spectrum of the corresponding polymer film. The device emitted blue-green light with a turn-on voltage of 13 V when the thickness of the emissive polymer layer was approximately 110 nm. The luminescence brightness reached 150 cd m^{-2} at a drive voltage of 19 V and a current density of 546 A m^{-2}. The external quantum efficiency of the device of polymer **33** was found to be 0.88% at 38 cd m^{-2} with a bias of 14 V. The onset potential, brightness, and quantum efficiency are expected to be enhanced by optimizing parameters such as the thickness of the emissive layer, the combination of each charge-transporting layer, and the alkyl substituent at the C9 position of the fluorene unit in the polymer backbone.

3.3. Polycondensation Using Butyllithium

The σ–π-conjugated polymer **39**, which has organosilicon and [2.2]paracyclophane repeating units in the polymer backbone, was synthesized by the polycondensation of dichlorodisilanes with difunctional lithium acetylide derived from pseudo-*p*-diethynyl[2.2]paracyclophane **15** and butyllithium (Scheme 3) and their optical and thermal properties

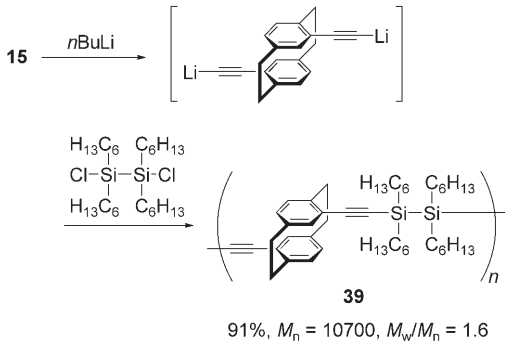

39

91%, M_n = 10700, M_w/M_n = 1.6

Scheme 3.

were investigated.[21] This polymer exhibited delocalization of π electrons through the Si–Si bonds and the through-space interaction of the [2.2]paracyclophane moiety. However, the σ–π-conjugation between the disilanylene unit and the π-electron system with a paracyclophane core was not particularly effective.

4. Linear Conjugated Polymers Containing Pendant Aromatic Rings

Lai and co-workers designed and synthesized a new type of linear conjugated polymer, which has other benzene rings appended to its main chain (type B in Scheme 4).[22] Examples of this type of polymer are fluorenedithia[3.3]paracyclophane polymers **40a–c**, which were prepared by the Suzuki–Miyaura coupling reaction.[22a] The electronic and optical properties of the polymer backbone can be altered through transannular π–π interactions from the external benzene group. In dilute THF solution, polymer **40a** emitted blue light with a fluorescence

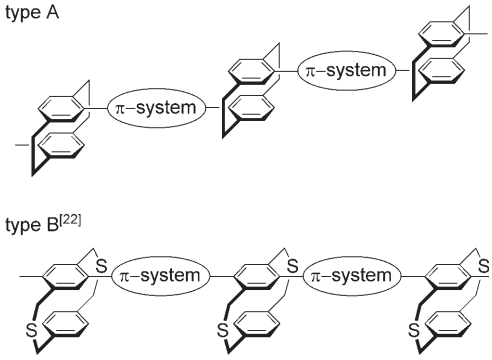

Scheme 4.

© 2006 Wiley-VCH Verlag GmbH & Co. KGaA, Weinheim

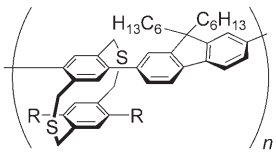

40a R = H, M_n = 2320, M_w/M_n = 1.39, PL efficiency = 75%*
40b R =OMe, M_n = 1700, M_w/M_n = 1.35, PL efficiency = 36%*
40c R = CN, M_n = 2780, M_w/M_n = 1.22, PL efficiency = 0%* * in THF

quantum yield of 75%, while the photoluminescence of polymer **40c** was completely quenched. Intramolecular electron transfer from the polymer main chain to the dicyanobenzene units occurred by through-space interactions.

The application of PAEs to chemo- and biosensors was pioneered by Swager and co-workers.[6,23] In their studies, cyclophane macrocycles were incorporated into the conjugated polymer backbone as a receptor for the methyl viologen salt **41** (MV^{2+}; Scheme 5). For example, the photoluminescence of polymer **42a** was highly quenched by the addition of MV^{2+}. The formation of a pseudopolyrotaxane from **42a** and MV^{2+} caused a 67-fold increase in the quenching efficiency owing to excellent signal amplification.[23a,c] Bis(thiophene)-cyclophane receptors of **42c** were also able to form pseudorotaxane complexes with MV^{2+}, and a resulting decrease in the carrier mobility and conductivity was observed.[23b,c] Other important studies on chemo- and biosensing, including signal amplification based on PAEs, have been recently reviewed by Swager and co-workers.[6b,c]

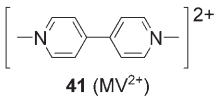

41 (MV^{2+})

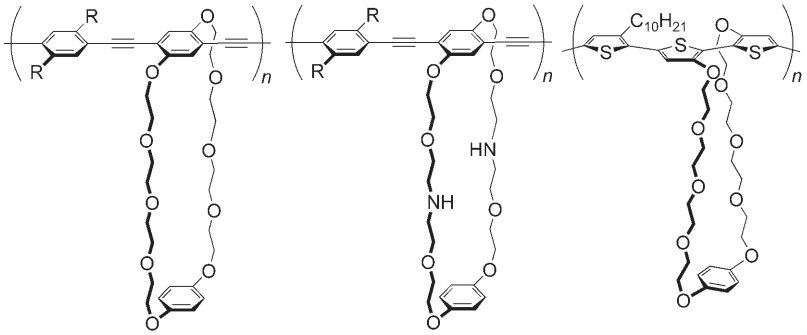

42a[23a,c], R = $CON(C_8H_{17})_2$ **42b**[23d], R = $C_{16}H_{33}$ **42c**[23b,c]

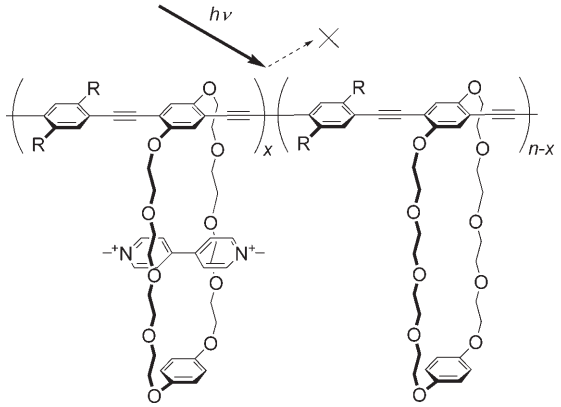

Scheme 5.

5. [3.3]Metaphane-Containing Polymers

[3.3]Metacyclophane and its derivatives contain two aromatic groups bridged by three atoms at each *meta*-position. They are of considerable interest not only as a result of the interesting transannular π–π interaction between the two aromatic rings but also because of their conformational flexibility.[9,24] The structure of [3.3]metacyclophanes in solution reveals that two aromatic rings are flipped by *syn*–[*anti*]–*syn* isomerization and bridged methylenes are wobbled by chair–boat isomerization;[24,25] their general crystal structure in the solid state shows a *syn* conformation.

This section presents the synthesis and characterization of dithia[3.3]metacyclophane-[26a] and dithia[3.3]metapyridinophane-containing zigzag polymers.[26b]

5.1. Dithia[3.3]metacyclophane-Containing Zigzag Polymers

As part of our studies on cyclophane chemistry, PAE-type polymer **43** consisting of dithia[3.3]metacyclophane in a conjugated polymer main chain was synthesized (Scheme 6).[26a] This polymer **43** also revealed an extension of π conjugation as a result of through-space interactions, and it gave a fluorescence emission at 439 nm ($\Phi = 0.51$ in $CHCl_3$ solution) in the visible blue region. Although dithia[3.3]metacyclophane moieties are incorporated in the conjugated polymer main chain, rapid *syn*–[*anti*]–*syn* conformational changes in solution were observed even at −80 °C (Scheme 6).

5.2. Dithia[3.3](2,6)pyridinophane-Containing Polymers

Recently, we developed dithia[3.3]-(2,6)pyridinophane-containing polymer **44** (Scheme 7), by replacing the benzene rings in [3.3]metacyclophane units in polymer **43** with pyridine rings.[26b] It was found that polymer **44** ($M_n = 4200$) also flipped rapidly in the same manner as polymer **43** as a result of *syn*–[*anti*]–*syn* isomerization.

It is established that dithia[3.3]-(2,6)pyridinophane acts as a bidentate nitrogen ligand with the palladium complex $[PdCl_2(PhCN)_2]$ to give [$PdCl_2$(dithia[3.3]-(2,6)pyridinophane)].[27] Polymer **44** was

 © 2006 Wiley-VCH Verlag GmbH & Co. KGaA, Weinheim

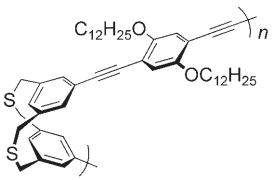

43 M_n = 7500, M_w/M_n = 1.8

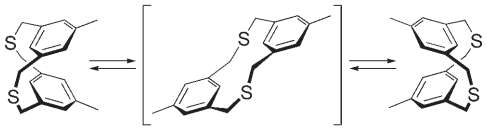

syn *[anti]* *syn*

Scheme 6.

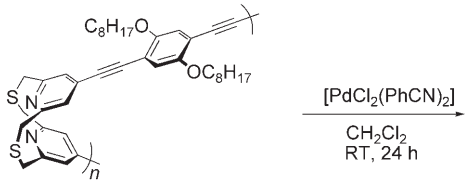

44 M_n = 4200, M_w/M_n = 2.7

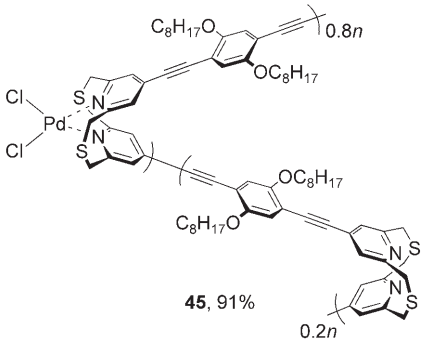

Scheme 7.

treated with an equimolar amount of $[PdCl_2(PhCN)_2]$ in CH_2Cl_2 to give the polymer complex $[PdCl_2(\mathbf{44})]$ (**45**) in 91% yield (Scheme 7).[26b] The ^{1}H NMR spectrum of **45** revealed that 80% of the dithia[3.3](2,6)pyridinophane units had a fixed *syn* geometry as a result of complexation. Polymer complex **45** was found to be a highly efficient catalyst for the Heck coupling reaction carried out in air (Scheme 8)[26b] and could be easily retrieved by a simple reprecipitation method and reused repeatedly without a significant loss in the catalytic activity.

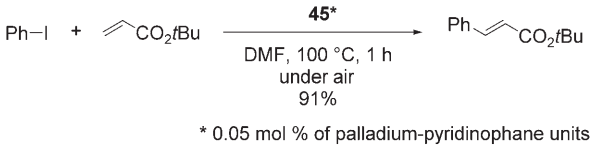

Scheme 8.

6. Conclusions and Outlook

In this Minireview, we have disclosed the synthesis, properties, and applications of a new class of through-space conjugated polymers, which comprise cyclophane derivatives as key components in their main chain. Despite the recent remarkable progress in the chemistry of conjugated polymers as mentioned above, only a few studies on cyclophane-containing conjugated polymers have been reported to date. Charge transfer and energy transfer are achieved effectively in such polymers by means of the through-space interaction in these π-conjugated systems. The incorporation of compounds with π-stacked benzene rings, that is, cyclophane skeletons, into the conjugated polymer backbone is expected to result in highly efficient charge-hopping as well as energy transfer. Recently, there has been considerable interest in the synthesis of molecular wires using rigid-rod π-conjugated oligomers. Therefore, through-space conjugation—besides through-bond conjugation—is a promising property for the construction of molecular wires. Further investigations into the design and construction of cyclophane-containing polymers will undoubtedly lead to their application in optoelectronic materials and molecular devices.

Received: February 27, 2006
Published online: August 14, 2006

[1] *Handbook of Conducting Polymers* (Eds.: T. A. Skothim, R. L. Elsenbaumer, J. R. Reynolds), 2nd ed., Marcel Dekker, New York, **1998**.

[2] a) H. Shirakawa, *Angew. Chem.* **2001**, *113*, 2642; *Angew. Chem. Int. Ed.* **2001**, *40*, 2574; b) A. G. MacDiarmid, *Angew. Chem.* **2001**, *113*, 2649; *Angew. Chem. Int. Ed.* **2001**, *40*, 2581; c) A. J. Heeger, *Angew. Chem.* **2001**, *113*, 2660; *Angew. Chem. Int. Ed.* **2001**, *40*, 2591.

[3] a) A. Kraft, A. C. Grimsdale, A. B. Holmes, *Angew. Chem.* **1998**, *110*, 416; *Angew. Chem. Int. Ed.* **1998**, *37*, 402; b) R. H. Friend, R. W. Gymer, A. B. Holmes, J. H. Burroughes, R. N. Marks, C. Taliani, D. D. C. Bradley, D. A. Dos Santos, J. L. Bredas, M. Lögdlund, W. R. Salaneck, *Nature* **1999**, *397*, 121; c) U. Mitschke, P. Bäuerle, *J. Mater. Chem.* **2000**, *10*, 1471; d) M. T. Bernius, M. Inbasekaran, J. O'Brien, W. Wu, *Adv. Mater.* **2000**, *12*, 1737; e) L. Akcelrud, *Prog. Polym. Sci.* **2003**, *28*, 875.

[4] a) J. Nehring, H. Amstutz, P. A. Holmes, A. Nevin, *Appl. Phys. Lett.* **1987**, *51*, 1283; b) A. Moll, N. Siegfried, W. Heitz, *Makromol. Chem. Rapid Commun.* **1990**, *11*, 485; c) H. Witteler, G. Lieser, G. Wegner, M. Schulze, *Makromol. Chem. Rapid Commun.* **1993**, *14*, 471.

[5] a) *Nonlinear Optical Effects in Organic Polymers* (Eds.: J. Messier, F. Kajzar, P. N. Prasad, D. R. Ulrich), Kluwer, Dordrecht, **1989** (*NATO ASI Ser., Ser. E: Appl. Sci., Vol. 162*); b) P. N. Prasad, D. J. Williams, *Introduction to Nonlinear Optical Effects in Molecules and Polymers*, Wiley-Interscience, New York, **1991**; c) J. L. Bredas, C. Adant, P. Tackx, A. Persoons, *Chem. Rev.* **1994**, *94*, 243.

[6] a) D. T. McQuade, A. E. Pullen, T. M. Swager, *Chem. Rev.* **2000**, *100*, 2537; b) Z. Juan, T. M. Swager, *Adv. Polym. Sci.* **2005**, *177*, 151; c) T. M. Swager in *Acetylene Chemistry* (Eds.: F. Diederich, P. J. Stang, R. R. Tykwinski), Wiley-VCH, Weinheim, **2005**, pp. 233–258.

[7] J. H. Burroughes, D. D. C. Bradley, A. R. Brown, R. N. Marks, K. Mackay, R. H. Friend, P. L. Burns, A. B. Holmes, *Nature* **1990**, *347*, 539.

 © 2006 Wiley-VCH Verlag GmbH & Co. KGaA, Weinheim

[8] a) U. H. F. Bunz, *Chem. Rev.* **2000**, *100*, 1605; b) *Poly(arylene ethynylene)s* (Ed.: C. Weder), Springer, Heidelberg, **2005** (*Adv. Polym. Sci., Vol 177*).

[9] a) F. Vögtle, *Cyclophane Chemistry*, Wiley, New York, **1993**; b) J. Shultz, F. Vögtle, *Top. Curr. Chem.* **1994**, *172*, 42; c) *Modern Cyclophane Chemistry* (Eds.: R. Gleiter, H. Hopf), Wiley-VCH, Weinheim, **2004**.

[10] For example, see: a) W. J. Oldham, Y. J. Miao, R. J. Laghicotte, G. C. Bazan, *J. Am. Chem. Soc.* **1998**, *120*, 419; b) G. C. Bazan, W. J. Oldham Jr., R. J. Lachicotte, S. Tretiak, V. Chernyak, S. Mukamel, *J. Am. Chem. Soc.* **1998**, *120*, 9188; c) S. Wang, G. C. Bazan, S. Tretiak, S. Mukamel, *J. Am. Chem. Soc.* **2000**, *122*, 1289; d) J. Zyss, I. Ledoux, S. Volkov, V. Chernyak, S. Mukamel, G. P. Bartholomew, G. C. Bazan, *J. Am. Chem. Soc.* **2000**, *122*, 11956; e) G. P. Bartholomew, G. C. Bazan, *Acc. Chem. Res.* **2001**, *34*, 30; f) G. P. Bartholomew, G. C. Bazan, *Synthesis* **2002**, 1245; g) G. P. Bartholomew, G. C. Bazan, *J. Am. Chem. Soc.* **2002**, *124*, 5183; h) G. P. Bartholomew, M. Rumi, S. J. K. Pond, J. W. Perry, S. Tretiak, G. C. Bazan, *J. Am. Chem. Soc.* **2004**, *126*, 11529; i) H. Y. Woo, J. W. Hong, B. Liu, A. Mikhailovsky, D. Korystov, G. C. Bazan, *J. Am. Chem. Soc.* **2005**, *127*, 820.

[11] a) S. Mizogami, S, Yoshimura, *J. Chem. Soc. Chem. Commun.* **1985**, 427; b) S. Mizogami, S, Yoshimura, *J. Chem. Soc. Chem. Commun.* **1985**, 1736.

[12] a) L. Guyard, P. Audebert, *Electrochem. Commun.* **2001**, *3*, 164; b) L. Guyard, P. Audebert, W. R. Dolbier, Jr., J.-X. Duan, *J. Electroanal. Chem.* **2002**, *537*, 189.

[13] a) F. Salhi, B. Lee, C. Metz, L. A. Bottomley, D. M. Collard, *Org. Lett.* **2002**, *4*, 3195; b) F. Salhi, D. M. Collard, *Adv. Mater.* **2003**, *15*, 81.

[14] Poly(aryleneethylene)s: a) Y. Morisaki, Y. Chujo, *Macromolecules* **2002**, *35*, 587; b) Y. Morisaki, Y. Chujo, unpublished results; c) Y. Morisaki, Y. Chujo, *Chem. Lett.* **2002**, 194; d) Y. Morisaki, N. Wada, Y. Chujo, *Polym. Bull.* **2005**, *53*, 73; e) Y. Morisaki, N. Wada, Y. Chujo, *Polymer* **2005**, *46*, 5884; f) Y. Morisaki, T. Ishida, H. Tanaka, Y. Chujo, *J. Polym. Sci. Part A* **2004**, *42*, 5891; g) Y. Morisaki, Y. Chujo, *Macromolecules* **2003**, *36*, 9319; poly(arylenevinylene)s: h) Y. Morisaki, T. Ishida, Y. Chujo, *Macromolecules* **2002**, *35*, 7872; i) Y. Morisaki, Y. Chujo, *Macromolecules* **2004**, *37*, 4099; polyarylenes: j) Y. Morisaki, Y. Chujo, *Bull. Chem. Soc. Jpn.* **2005**, *78*, 288.

[15] Y. Morisaki, Y. Chujo, *Polym. Bull.* **2002**, *49*, 209.

[16] a) Y. Tohda, K. Sonogashira, N. Hagihara, *Synthesis* **1977**, 777; b) K. Sonogashira in *Handbook of Organopalladium Chemistry for Organic Synthesis* (Ed.: E. Negishi), Wiley-VCH, New York, **2002**, pp. 493–529.

[17] Several ethynyl[2.2]paracyclophanes were prepared as building blocks for carbon-rich systems: L. Bondarenko, I. Dix, H. Hinrichs, H. Hopf, *Synthesis* **2004**, *16*, 2751.

[18] a) R. F. Heck, *J. Am. Chem. Soc.* **1968**, *90*, 5518; b) S. Bräse, A. de Meijere in *Metal-Catalyzed Cross-coupling Reactions* (Eds.: F. Diederich, P. J. Stang), Wiley-VCH, New York, **1998**, pp. 99–166.

[19] a) N. Miyaura, A. Suzuki, *J. Chem. Soc. Chem. Commun.* **1979**, 866; b) N. Miyaura, A. Suzuki, *Chem. Rev.* **1995**, *95*, 2457.

[20] M. Leung, M. B. Viswanath, P.-T. Chou, S.-C. Pu, H.-C. Lin, B.-Y. Jin, *J. Org. Chem.* **2005**, *70*, 3560.

[21] Y. Morisaki, F. Fujimura, Y. Chujo, *Organometallics* **2003**, *22*, 3553.

[22] a) W. Wang, J. Xu, Y.-H. Lai, *Org. Lett.* **2003**, *5*, 2765; b) W. Wang, J. Xu, Y.-H. Lai, F. Wang, *Macromolecules* **2004**, *37*, 3546.

[23] a) Q. Zhou, T. M. Swager, *J. Am. Chem. Soc.* **1995**, *117*, 7017; b) M. J. Marsella, P. J. Carroll, T. M. Swager, *J. Am. Chem. Soc.* **1995**, *117*, 9832; c) Q. Zhou, T. M. Swager, *J. Am. Chem. Soc.* **1995**, *117*, 12593; d) R. Deans, J. Kim, M. R. Machacek, T. M. Swager, *J. Am. Chem. Soc.* **2000**, *122*, 8565; e) A. Rose, C. G. Lugmair, T. M. Swager, *J. Am. Chem. Soc.* **2001**, *123*, 11298.

[24] a) R. H. Mitchell, *J. Am. Chem. Soc.* **2002**, *124*, 2352; b) M. F. Semmelhack, J. J. Harrison, D. C. Young, A. Gutiérrez, S. Raffi, J. Clardy, *J. Am. Chem. Soc.* **1985**, *107*, 7508.

[25] Ring-flipping and bridge-wobbling systems of [3.3]phanes have been studied in detail; for 2,11-dithia[3.3]metacyclophane, see Ref. [24a]; for dithia[3.3]metacyclophane derivatives, see: a) K. K. Laali, T. Okazaki, R. H. Mitchell, *J. Chem. Soc. Perkin Trans. 2* **2001**, 745; for 2,11-diaza[3.3](3,5)pyridinophane, see: b) T. Satou, T. Shinmyouzu, *J. Chem. Soc. Perkin Trans. 2* **2002**, 393; for 9-nitro- and 9-amino-2,11-dithia[3.3]metacyclophane, see: c) T. Moriguchi, K. Sakata, A. Tsuge, *Chem. Lett.* **1999**, 167; d) T. Moriguchi, K. Sakata, A. Tsuge, *J. Chem. Soc. Perkin Trans. 2* **2001**, 934; for [3.3]metacyclophane-2,11-dione derivatives, see: e) T. Yamato, K. Tsuchihashi, N. Nakamura, M. Hirahara, K. Tanaka, *Can. J. Chem.* **2002**, *80*, 510; f) H. Isaji, M. Yasutake, H. Takemura, K. Sako, H. Tatemitsu, T. Inazu, T. Shinmyozu, *Eur. J. Org. Chem.* **2001**, 2487; for 2,11-dithia[3.3](2,6)pyridinophane and 1,3,10,12-tetrathia[3.3](2,6)pyridinophane, see: g) G. R. Newkome, S. Pappalardo, F. R. Fronczek, *J. Am. Chem. Soc.* **1983**, *105*, 5152.

[26] a) Y. Morisaki, T. Ishida, Y. Chujo, *Polym. J.* **2003**, *35*, 501; b) Y. Morisaki, T. Ishida, Y. Chujo, *Org. Lett.* **2006**, *8*, 1029.

[27] T. Moriguchi, S. Kitamura, K. Sakata, A. Tsuge, *Polyhedron* **2001**, *20*, 2315.

© 2006 Wiley-VCH Verlag GmbH & Co. KGaA, Weinheim

DOI: 10.1002/anie.200600611

Tumor-Suppressor Protein

p53—A Natural Cancer Killer: Structural Insights and Therapeutic Concepts

Lin Römer, Christian Klein, Alexander Dehner, Horst Kessler, and Johannes Buchner**

Keywords:
apoptosis · molecular chaperones · protein folding · protein stability · tumor therapy

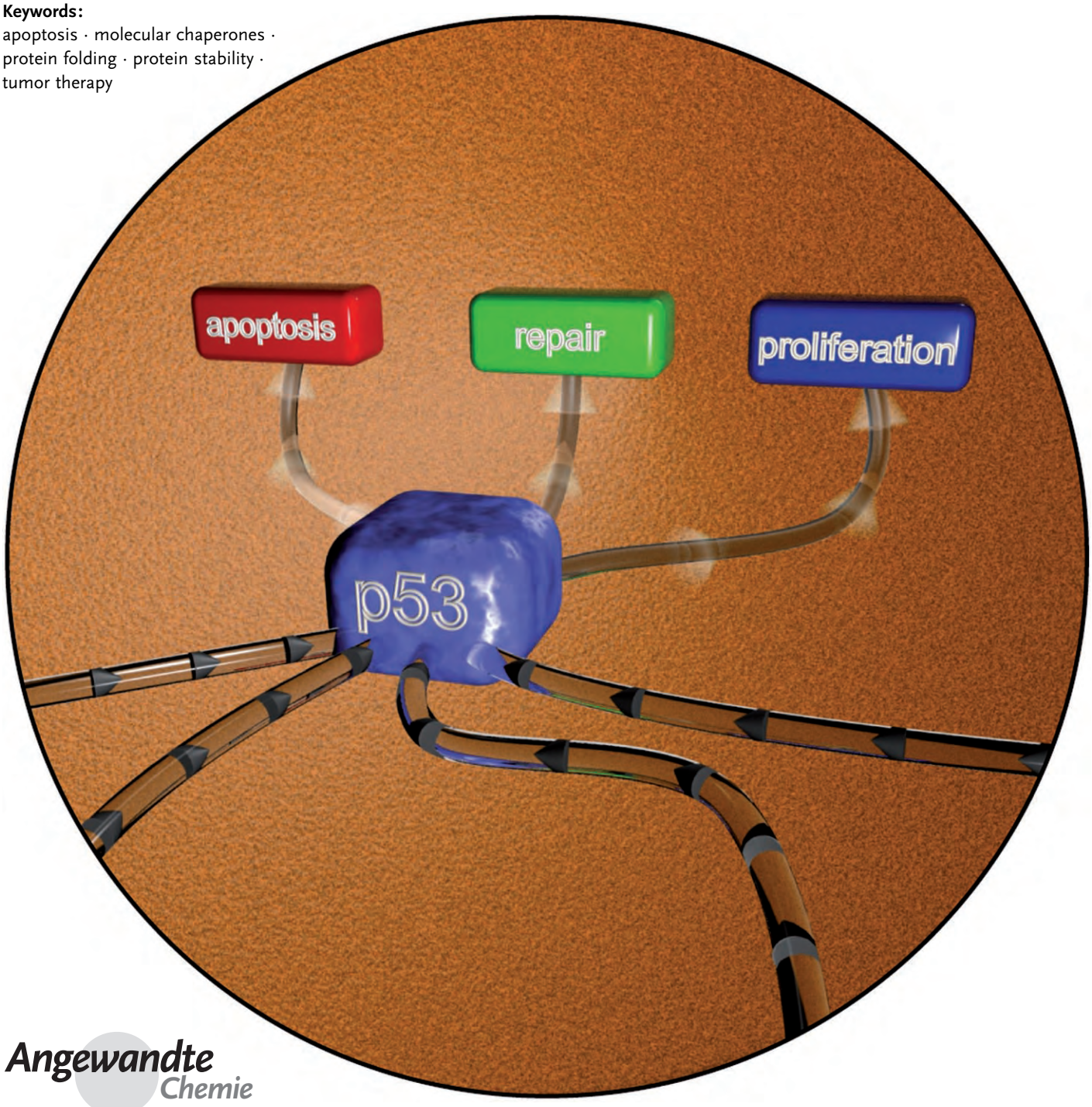

© 2006 Wiley-VCH Verlag GmbH & Co. KGaA, Weinheim

Every single day, the DNA of each cell in the human body is mutated thousands of times, even in absence of oncogenes or extreme radiation. Many of these mutations could lead to cancer and, finally, death. To fight this, multicellular organisms have evolved an efficient control system with the tumor-suppressor protein p53 as the central element. An intact p53 network ensures that DNA damage is detected early on. The importance of p53 for preventing cancer is highlighted by the fact that p53 is inactivated in more than 50% of all human tumors. Thus, for good reason, p53 is one of the most intensively studied proteins. Despite the great effort that has been made to characterize this protein, the complex function and the structural properties of p53 are still only partially known. This review highlights basic concepts and recent progress in understanding the structure and regulation of p53, focusing on emerging new mechanistic and therapeutic concepts.

From the Contents

1. The Tumor-Suppressor Protein p53	6441
2. Structure and Stability of p53	6441
3. DNA Binding of p53	6444
4. Regulation of p53	6446
5. Interaction with Chaperones	6448
6. Functions of p53	6450
7. p53 and Cancer Therapy	6451
8. Outlook	6455

1. The Tumor-Suppressor Protein p53

p53 is the major tumor-suppressor protein of the body. It was initially discovered as an oncogene that was responsible for various kinds of cancer.[1–3] During the following years it became evident that wild-type p53 acts as a tumor suppressor and that inactive p53 is responsible for the damaging effects.[4,5] Since then, its crucial role in the prevention of cancer and the underlying functional principles have been further investigated. However, despite an enormous number of publications, the complex functionality and the structural properties of p53 as the "guardian of the genome" are just beginning to be understood.[6,7]

p53 is a transcription factor involved in cell-cycle regulation, the initiation of apoptotic cell death, and of DNA repair. Inactivation of p53 is mainly due to mutations that interfere with the DNA-binding ability of the protein.[8,9] Mutated or otherwise deactivated p53 is observed in the majority of human cancers.[4,5] p53 is in the center of a huge network of proteins that allow integration of a variety of signals.[10,11] Cellular stress, such as DNA damage or the presence of oncogenes, results in the activation of this network. After activation, p53 binds to specific DNA consensus sequences of promoter regions to stimulate transcription of the corresponding target genes. The products of these genes are responsible for the induction of DNA repair mechanisms—or, if repair is not successful, for the induction of programmed cell death (Figure 1). p53 is not just responsible for the interactions with DNA, it is also involved in the initiation of apoptosis in the cytosol (see Section 6.3).

p53 is the central signaling system in which dozens (or maybe hundreds) of proteins are interconnected. A signal is often delivered to p53 through a cascade of three or more proteins. The direct analysis in vitro of p53 and (activating) partner proteins is therefore often hard to perform. Additionally, the connections between the nodes of this network shift as a result of several forms of cellular damage. Therefore, a direct connection between p53 and a particular signal is not easy to elucidate.

2. Structure and Stability of p53

As expected for a key regulatory protein, the normal concentration of p53 is kept very low and is regulated by several independent mechanisms (see Section 4).[12] Further to the regulation by other proteins, the structural stability and integrity of the protein itself is of major importance for its functionality. Interestingly, p53 turned out to be a very labile protein with a high turnover rate.

2.1. The Domain Structure of p53

The human p53 gene[13–15] codes for a protein of 393 amino acids that are organized in a modular structure consisting of four functional domains (Figure 2A). The amino-terminal transactivation domain (NTD) comprises the transcriptional

[*] Dr. L. Römer, Prof. Dr. H. Kessler, Prof. Dr. J. Buchner
Department Chemie
Technische Universität München
Lichtenbergstr. 4, 85747 Garching (Germany)
Fax: (+49) 89-289-13345 (Buchner)
Fax: (+49) 89-289-13210 (Kessler)
E-mail: kessler@ch.tum.de
johannes.buchner@ch.tum.de
Dr. C. Klein
Roche Diagnostics GmbH
Pharma Research
Molecular Biology
Nonnenwald 2, 82372 Penzberg (Germany)
Dr. A. Dehner
Tripos GmbH
Martin-Kollar-Straße 17, 81829 München (Germany)

 © 2006 Wiley-VCH Verlag GmbH & Co. KGaA, Weinheim

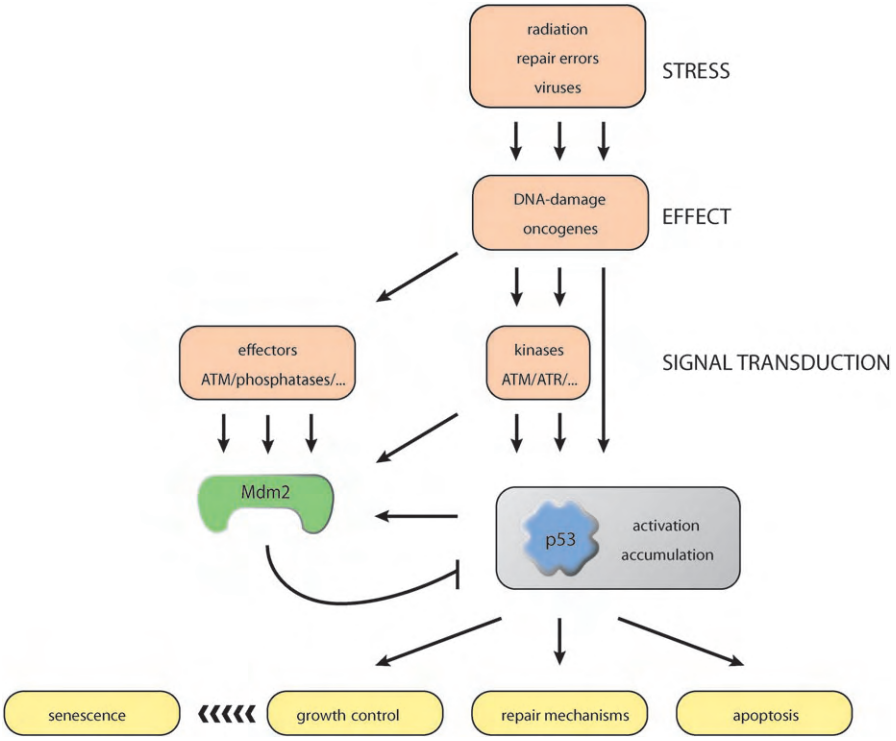

Figure 1. Simplified schematic view of the p53 pathway. p53 integrates a number of signals that report the status of the cell, most notably DNA damage. If activated, p53 induces different sets of genes depending on the input signal. Mdm2 is the negative regulator of p53 (see Section 4.3.1).

function of p53 (amino acids 1–42) and a proline-rich SH3 target-region (amino acids 60–97). The major part of the protein is the DNA binding domain of p53 (DBD; amino acids 102–292), also known as the "core" domain. This domain is responsible for the specific DNA-binding ability of p53. The vast majority of p53 mutations are located in this domain (see box 2). Adjacent to the core domain is the tetramerization domain (TD; amino acids 323–356), which is followed by a carboxy-terminal regulatory domain (RD; amino acids 360–393). Five regions of p53 are highly conserved throughout all multicellular organisms. These patches (13–26, 117–142, 171–181, 234–250, 270–286) do not correspond to stable folded regions (Figure 2 A).[16,17]

2.1.1. *The Amino-Terminal Domain of p53 (NTD)*

The NTD of p53 consists of two parts, the transcriptional activation region and the so-called SH3-target sequence. This proline-rich region is recognized by proteins containing SH3 domains (Src homology 3 domain). SH3 domains are about 60 amino acid residues long and were first identified as a conserved sequence in the noncatalytic part of several cytoplasmic tyrosine kinases such as Abl and Src. They are found in proteins that bind to proline-rich peptides in their respective binding partners, thereby increasing the substrate specificity of tyrosine kinases.[18] The SH3-target subdomain of p53 contains five copies of the amino acid sequence PXXP, which is thought to play an important role in the apoptotic functions of p53 (see Section 6.1).[19–21]

Several proteins of the transcription machinery bind to the transcription activation domain of p53 and activate the expression of various target genes.[22–24] Negative regulators of p53, such as Mdm2 (see Section 4.3), the hepatitis B virus X protein Hbx,[25] or the adenovirus E1B protein, bind to the same site in the NTD.[26–29] The interaction with proteins regulating the transcriptional activity and the turnover rate of p53 seems to be modified by posttranslational modifications like phosphorylation of the NTD (see Section 4.1).[30,31]

The NTD of p53 is unstructured.[32–34] At the level of the primary structure, the NTD shows the typical amino acid composition of "natively unfolded proteins" or "intrinsically unstructured proteins" (IUP).[33] In IUPs, the formation of secondary-structure elements and hydrophobic cores is disfavored by the amino acid composition.[35,36] Unstructured regions are a common motif of transcription factors.[37] It was shown that the interaction between transcription factors and target proteins induces conformational changes in a small amino acid patch in the unstructured region and leads to increased binding and a broad specificity for target mole-

Johannes Buchner holds the chair of Biotechnology at the Technische Universität of München (Germany). He studied biology and biochemistry at the University of Regensburg. In his PhD studies under the supervision of R. Rudolph and R. Jaenicke, he examined the mechanisms of molecular chaperones. After a postdoctoral stay in the group of I. Pastan at the National Cancer Institute in Bethesda (USA), he was an independent group leader at Regensburg before becoming full professor in Munich in 1998. He is a member of the Akademie Leopoldina. Professor Buchner's research is focused on molecular chaperones and on basic and applied aspects of protein folding.

Horst Kessler was born in 1940 in Suhl, Thuringia (Germany). He studied chemistry in Leipzig and Tübingen, where he received his PhD degree for work with E. Müller in 1966 and was promoted to professor in 1969. He was appointed as full professor for organic chemistry at the J. W. Goethe Universität in Frankfurt in 1971 and moved to the Technische Universität München in 1989. He is a member of the Bavarian Academy of Science and the Leopoldina, and was head of the editorial board of Angewandte Chemie from 2001–2005. His research activities are in the development and application of NMR spectroscopic methods for the investigation of biomolecules, as well as drug design and the application of integrin ligands.

 © 2006 Wiley-VCH Verlag GmbH & Co. KGaA, Weinheim

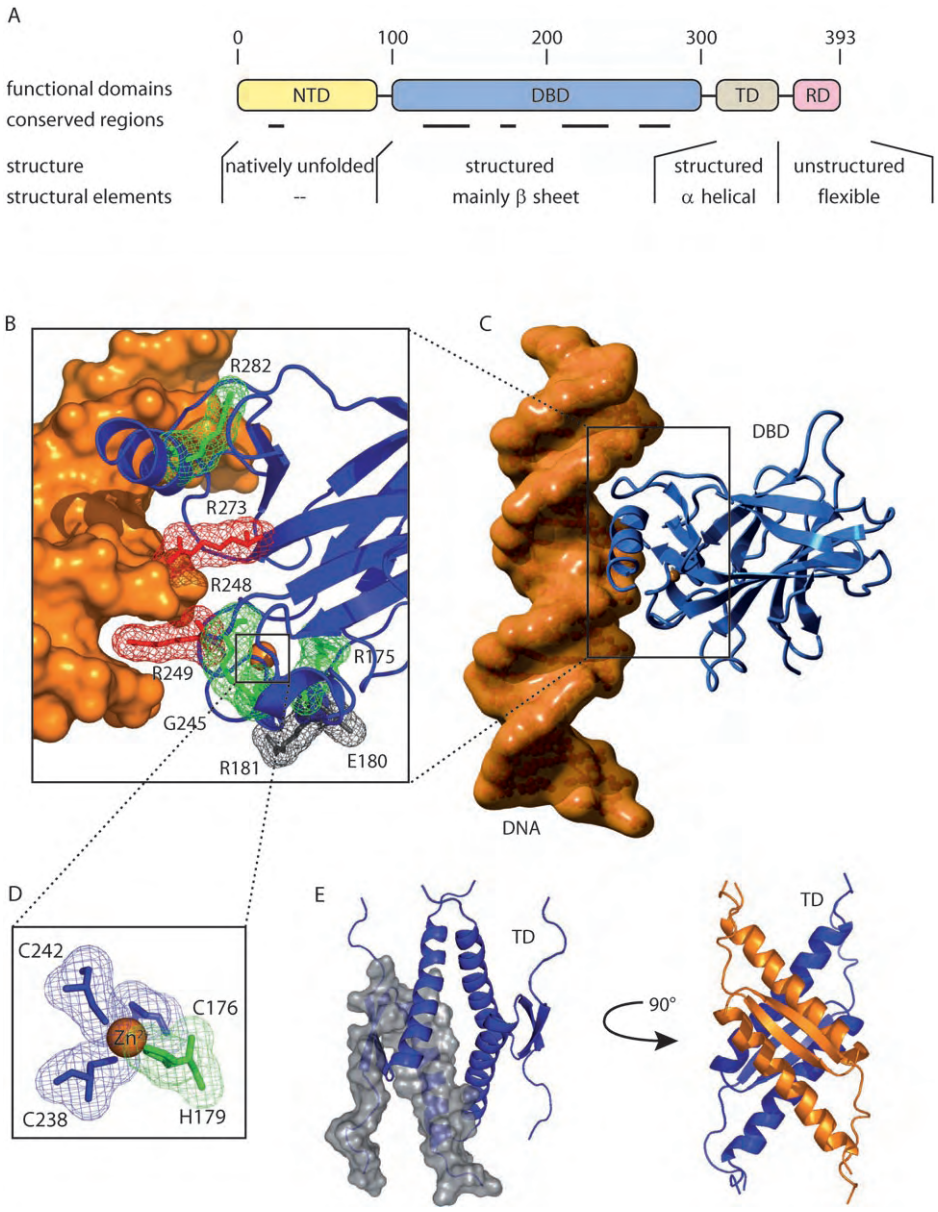

Figure 2. A) Domain organization of p53: The amino-terminal transactivation domain (NTD) is natively unfolded and interacts with components of the transcriptional machinery and includes the Mdm2 binding site. The central DNA binding "core" domain (DBD) holds 95.1% of the oncogenetic mutations. The carboxy-terminal region of p53 consists of a tetramerization domain (TD) and a regulatory domain (RD). B) Hot-spot mutations in the DBD. DNA-contact mutants are depicted in red and structural mutants in green. The amino acids responsible for cooperative DNA binding are depicted in gray. The molecular surface of the amino acids are drawn as meshes to enhance clarity. PDB code: 1TSR. C) Crystal structure of the DBD. The DNA binding domain of p53 (blue) bound to its consensus DNA sequence (orange). PDB: 1TSR. D) Coordination of the zinc ion. The essential Zn^{2+} ion (orange) is coordinated between a histidine (green) and three cysteine (blue) residues. E) The tetramerization domain of p53. Structure of four TDs that form a dimer of dimers (orange/blue). PDB: 1OLG.

cules.[38] This concept also seems to be true for the built-in transcription-factor domain of p53, and it was concluded that, in p53, unstructured and structured parts function synergistically.[33] It was also assumed that, depending on the partner proteins, several different short amino acid patches are able to form local substructures when interacting with partner proteins, thus creating a vast diversity of binding motifs. Recently, the natively unstructured part of p53 was used for novel biosensors. Insertion of random peptides generated variants that were specifically activated up to 100-fold more by novel effectors, suggesting that the molecular recognition pattern of IUPs is relatively easy to engineer and to use as a molecular sensor.[39]

2.1.2. *The DNA-Binding Domain (DBD)*

The central "core" region of p53, the sequence-specific DBD (amino acids 102–292), is of crucial importance for DNA-binding activity of the full-length protein. Over 90% of all known tumorigenic mutations are located in this part of the protein (see box 2). The DBD is highly resistant to proteolytic digestion and is one of the most-stable regions in the protein.[40,41] A more-detailed consideration of the structural and functional properties of this domain is given in Section 3.

2.1.3. *The Tetramerization Domain (TD)*

The quaternary structure of p53 is mediated by a defined TD.[42,43] The tetrameric state is important for functional DNA binding and for the affinity of p53 for specific consensus DNA.[44] The isolated TD is remarkably stable compared to the remainder of the protein (see Section 2.2).[45–47]

Analysis of the NMR spectroscopic and X-ray crystal structures of the isolated TD (Figure 2E) showed that the tetramer is composed of a dimer of dimers.[48–50] The isolated TD of p53 dimerizes through a native-like transition state with the primary dimers fully folded but the interdimer interactions only partially formed.[47]

There seems to be an equilibrium between dimers and tetramers of full-length p53 in solution, but the presence of a specific p53 DNA-binding sequence dramatically increases the tetramerization of p53.[51] On the other hand, the ability of the DBD to form dimers upon DNA binding is important for the function of p53 (see Section 3). An artificial variant of p53 with point mutations in the TD no longer forms a tetramer.

 © 2006 Wiley-VCH Verlag GmbH & Co. KGaA, Weinheim

Instead, this mutant forms dimers that retain half of the DNA-binding activity of the wild-type protein.[52] Hence, cooperativity in the DNA binding of the DBD (see Section 3) is followed by a second cooperativity in the TD forming tetrameric complexes.

2.1.4. The Regulatory Domain (RD)

The carboxy-terminal RD is connected to the tetramerization domain through a basic linker region. This linker hosts the nuclear localization sequence of p53.[53] The RD is, as the name implies, of major importance for the regulation of the protein.[54] This short domain seems to have a negative effect on specific DNA-binding of the full-length protein, and direct binding between the carboxy-terminal region and the DBD was not detectable by NMR spectroscopic titration experiments.[55] Thus, the effect of the RD on the sequence-specific DNA-binding ability of p53 is still enigmatic.

Furthermore, the carboxy-terminal RD itself is also able to bind to DNA nonspecifically. Posttranslational modifications such as phosphorylation and acetylation in this domain stabilize and activate p53.[56,57] Similar effects are achieved by binding of other proteins, such as specific antibodies, or by binding of nonspecific complementary DNA (cDNA) to the RD.[58,59] These interactions or modifications are thought to result in conformational changes that affect the sequence-specific binding to consensus DNA.[60,61] This aspect is discussed in more detail in Section 4.2.

2.2. Stability of p53

p53 has a very high turnover rate (half-life < 20 min) and therefore only small amounts of active protein reside in the cell (compare Section 4.3.1).[62] Several mechanisms control and maintain the level of p53. The interaction with kinases (see Section 4.1), molecular chaperones (see Section 5), and the functional antagonist Mdm2 (see Section 4.3) are of major importance. Apart from the interaction with regulating proteins, the intrinsic structural properties of p53 are decisive for the stability and activity of the protein.[32,33] Isolated, tetrameric p53 is a fragile protein that is very sensitive towards thermal denaturation. In vitro, the protein spontaneously unfolds at physiological temperatures[63,64] and aggregates rapidly at temperatures above 40 °C.[65]

The loss of tertiary and secondary structure is accompanied by the loss of its DNA-binding ability.[63,65,66] Surprisingly, the stability of the individual domains is strikingly different from that of the full-length protein. Both the isolated DBD and TD domains are more stable than the full-length protein.[32] Recently, it was shown that the NTD of p53 could be classified as an intrinsically unstructured protein.[33] Therefore, this domain only has a minor influence on the stability of the full-length protein.[32] To date, there is very little information available about the structural properties of the RD (see Section 2.1.4). This domain seems to be largely unstructured in the absence of modifications. However, phosphorylation and/or mutations in this area enhance the stability of the full-length protein.[67–69] In response to DNA damage, for example, phosphorylation of serine 392 increases the stability of the protein and activates p53 (see Section 4.1).

Taken together, it is obvious that in p53, unstructured and structured parts function synergistically, influencing the activity of the whole protein. As the isolated, unmodified protein is not able to maintain structural integrity at physiological temperatures,[32,65] the question of how p53 can be active in vivo is raised. It is likely that interactions with other proteins are essential for the survival of p53. In this context, it was shown recently that the molecular chaperone Hsp90 (see Section 5.3) is of crucial importance for the stability and integrity of p53 in vitro[65,66,70] and in vivo.[66,71,72] The emerging view is that p53 has evolved as an extremely labile protein to allow tight regulation of its activity and its levels in the cell.

Box 1: p53 Family Members: p63, p73

Twenty years after the discovery of the p53 tumor suppressor gene, Kaghad et al. reported the existence of a new p53 family member in humans, called p73.[73] A year later, another homologue, p63, was identified.[74] All members of the p53 family possess the same modular architecture with an amino-terminal transactivation domain, a DNA binding domain followed by a tetramerization domain, and a regulatory carboxy-terminal domain.[75,76]

Although p53 has only a single promoter, p63 and p73 each have two promotors, resulting in different isoforms and splice variants.[77,78] Several isoforms of p63 and p73 contain a conserved carboxy-terminal extension of about 100 residues that is not present in p53. Some of the isoforms contain so-called sterile-alpha-motif (SAM) domains are known to associate with other SAM domains, forming oligomers. Thus, SAM domains may provide the scaffold for the construction of large protein complexes in the cell. In addition, the p73 SAM domain is able to bind to lipid membranes.[82]

Another remarkable difference between p53 and its homologues concerns their degradation induced by Mdm2 (see Section 4.3). In contrast to the short-lived p53 protein, which is regulated by Mdm2-mediated ubiquitinylation and degradation by the proteasome, the interaction of p73 with Mdm2 leads to the inactivation of transcription and apoptosis but does not result in p73 degradation by the proteasome.[83,84] Surprisingly, Mdm2 does not bind to p63 at all.[85]

In activating transcription, p63 and p73 function similarly to p53. NMR spectroscopic investigations of the p63 DBD have shown a fold similar to that found in this region of p53.[86] On the basis of structural similarity, it was expected that their function, regarding tumor suppression, induction of apoptosis, and cell-cycle control, would also be similar to that of p53.[87,88] In contrast to p53 knockout mice, p63 and p73 knockout mice do not develop spontaneous tumors.[89] However, in response to various stresses (drugs, γ-irradiation), p53 requires p73, as well as p63, to initiate apoptosis.[90] Homologues of p53 were found in all multicellular organisms studied so far, including *C. elegans* and *D. melanogaster*.[91–95] This finally proved that efficient tumor suppression is important in all multicellular organisms.

3. DNA Binding of p53

A basic understanding of the DNA-binding ability of p53 is provided by the crystal structure of the DNA-bound DBD and NMR spectroscopic studies of the DNA interactions (Figure 2C). However, in the crystal, only one of three DBDs in the asymmetric unit binds to DNA,[96] whereas dimeriza-

 © 2006 Wiley-VCH Verlag GmbH & Co. KGaA, Weinheim

tion and tetramerization are needed for the functionality of p53. The DBD consists of a four- and five-stranded antiparallel β sheet and a loop–sheet–helix motif, which comprises a loop (residues 113–123), a three-stranded β sheet, and an α helix (residues 278–286). A second loop (residues 164–194), which is interrupted by the short helix, and the third loop (residues 237–250) are stabilized by a zinc ion.[96,97] This ion is coordinated between three cysteine residues and one histidine residue (Figure 2D).

More than 500 DNA-binding loci of p53 have been identified with high level of accuracy.[98] p53 binds specifically to a palindromic double-stranded DNA-promotor consensus site, which may be separated by up to 13 bp from a second copy (Figure 3). A stable p53–DNA complex contains a tetramer of p53, which binds to one full-length recognition element. Binding of p53 causes bending and twisting of the bound DNA.[99,100] It was shown, that the C_2 symmetry of the specific dimeric DNA binding and the D_2 symmetry of the TD can only be explained by binding of the tetramer between two strands that run in opposite directions.[55] As the recognition element in the DNA is palindromic, it suggests that the proposed binding is not consecutive along the sequence (as it was thought to be), but rather on two opposite strands of a single DNA molecule that has changed its direction. Interestingly, it was reported that p53 binds with higher affinity to the recognition elements of genes involved in cell-cycle control than to genes involved in apoptosis—suggesting regulation of transcriptional activity based on the recognition elements of p53 target genes.[101] A recent NMR spectroscopic and mutational study of full-length p53 protein implies the existence of a previously uncharacterized core–core interaction within the tetrameric complex.[102] A model was proposed in which the ligand-free tetramer has a DNA binding site that is more open than the DNA-bound tetrameric complex. This is required as the binding of DNA requires a rotation of 70° to form the known protein–protein interface. At present, however, no crystal structure is available for tetrameric full-length p53 bound to DNA, possibly owing to the high flexibility of the protein.

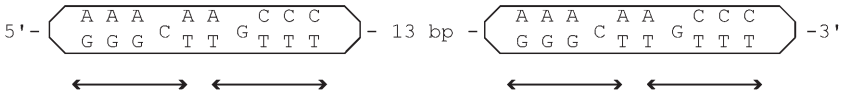

Figure 3. The DNA consensus sequence of p53. p53 binds specifically to two copies of a double-stranded DNA-promotor consensus site. The motifs may be separated by up to 13 bp.

In solution, DNA binding of the DBD is highly cooperative,[55,99,103–105] even when excess DNA is present.[106] Several reports discuss interdomain contacts in p53.[96,107–112] Interactions observed in the crystal structures of the p53 DBD are, however, most likely packing artifacts that are not compatible with cooperative DNA binding as it occurs in the native p53–DNA complex.[112] NMR and X-ray experiments identified a dimerization site in the DBD in the presence of DNA.[55,106] It has been shown earlier that the DBD of the homologue p63 (see box 1) fails to bind consensus DNA cooperatively[105] even though p53 and p63 contain a similar TD (see Section 2.1.3),[48–50] form homotetramers, and bind specifically to DNA.[11]

Interestingly, a stabilizing dimerization interface (double salt bridge, Figure 4)[108] within the p53 DBD, which is not present in the p63 DBD, seems to be responsible for the observed cooperativity in DNA binding. This dimerization is independent of the tetramerization of full-length p53.[103] Mutational analysis of the dimerization interface localized the salt bridge to residues E180 and R181 of p53.[108] In the homologue p63, the highly conserved amino acid R181 is replaced by a leucine residue. Thus, it is likely to be the reason for the observed lack in selective and cooperative DNA binding of the isolated p63 DBD.[55] These results support the idea that the additional dimerization interface of the DBD consists mainly of two intermolecular E180–R181 salt bridges between monomers (Figure 4). This is in agreement with a C_2 symmetric model complex as shown by Lebrun et al.[111] and Klein et al.[55,108]

Recently, the crystal structure of the DBD dimer bound to DNA was presented.[114] The potential role of the identified dimerization interface for p53 function is underlined by the naturally occurring E180K[115,116] and R181X[117] mutations, which are associated with the Li-Fraumeni syndrome, a rare autosomal-dominant hereditary disorder that is associated with early development of cancer.[116,118] This kind of oncogenic mutation cannot be assigned to any of the major p53 mutation classes (see Section 3).[97] This represents a new class of p53 mutations that lack p53 activity owing to a reduced cooperativity of DNA binding.[108] It is interesting to note that the same binding site of the DBD is used for binding to DNA as well as for the binding to Bcl2 (see Section 6.3) in the mitochondrial apoptotic pathway.[119]

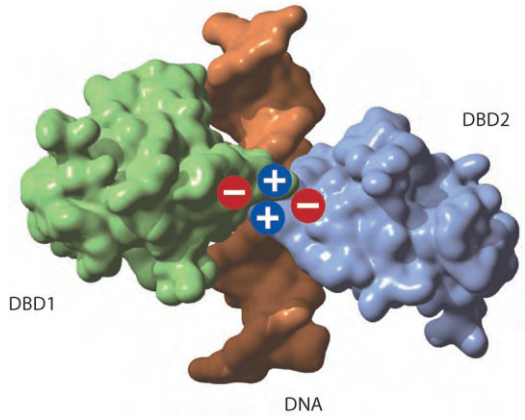

Figure 4. The dimerization interface between two DBDs. Model complex for the dimerization interface of the p53 DBD upon cooperative DNA binding. The dimerization interface is stabilized by a double intermolecular salt bridge between the E180 (−) and R181 (+) residues. The model is based on the structure with the PDB code 1TSR (adapted from Klein et al.[55]).

© 2006 Wiley-VCH Verlag GmbH & Co. KGaA, Weinheim

Most of the mutations of p53 involved in cancer and virtually all hot-spot mutations (see box 2) are located within the DBD.[120–122] This illustrates the importance of correct DNA recognition and binding for the transcriptional activation of target genes.[7,123] The hot-spot amino acids R273 and R248 directly contact the major and minor groove of bound DNA (Figure 2B). The four remaining hot-spot mutations are involved in stabilizing the surrounding structure through a hydrogen-bond network. Thus, there are three major classes of mutations that prevent DNA binding: 1) Mutations involved in direct DNA contact, 2) mutations that destabilize the structural integrity of the DNA binding region and/or cause a global unfolding of the DBD—both result in a loss of DNA binding affinity,[97] and 3) mutations in the helix region that prevent cooperative binding.[108]

In 2000, it was proposed that some mutants of p53, for example, R175H, not only loose their original sequence-specific DNA-binding ability, but also become able to induce or repress genes that are different from that of the wild-type protein.[124] The molecular basis for transcriptional modulation by mutant p53 is not fully understood, but increasing evidence in vivo[125] and in vitro[126]suggests that specific interactions of mutant p53 with DNA play an important role. Additionally, it was shown that mutant p53 binds non-B-DNA in a structure-selective way. This binding seems to be the basis for the selective transcriptional activity.[126]

Box 2: Mutations in p53

Intact p53 is of central importance for initiating responses to cellular stress in multicellular organisms. In consequence, mutations in p53 are often deleterious for the cell. If a certain mutation in p53 shifts the activity of p53 out of balance, the cell is then not able to react to cellular stress and tumorigenesis is favored. Today, more than 20000 different mutations of p53 are known[116] and most of these mutations (>95%) are located in the DBD of p53. Of special interest are the most frequently occurring hot-spot mutations R175, G245, R248, R249, R273, and R282 (see Section 3), which make up about a quarter of all analyzed p53 mutations. The data set[116] contains somatic mutations that have been identified by sequencing. This includes mutations reported in human tumor samples as well as in human cell lines. Further to somatic mutations, germline mutations are found in Li-Fraumeni syndrome, a rare disease in which half of the afflicted patients will get cancer before they reach the age of 30.[116,118]

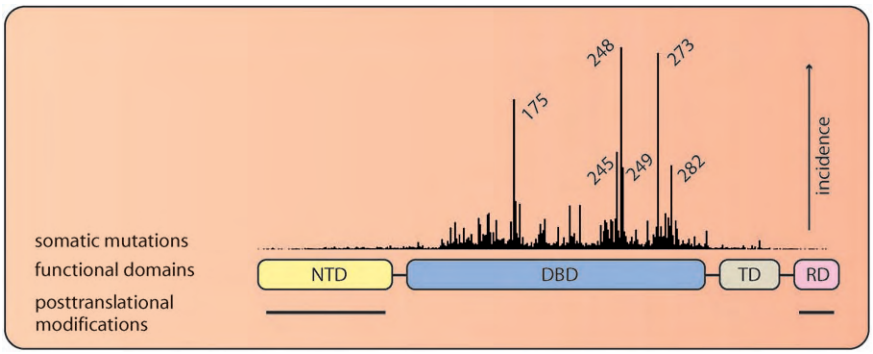

Box 3: "Mutant p53"

The term "mutant p53" often refers to the functional conformation of the protein. Mutant p53 is not able to bind to its consensus DNA efficiently and is therefore inactive. Initially, the term was coined because antibodies were found that were able to distinguish between the active and the mutant form regardless of the primary structure of p53.[129] Later on, it became evident that most point mutations destabilize the DBD of p53 thermodynamically. Apart from the DNA-contact mutants, which directly interfere with DNA binding, most other mutations change the overall conformational state of the DBD[130] thereby rendering the whole protein inactive. However, several of these inactive p53 mutants are thought to recover at least some level of activity under certain conditions, thus adopting a nativelike, active conformation.[131] The shift between an active "wild-type" conformation and an inactive "mutant" conformation can be regulated by certain drugs (see Section 7.1), temperature, and molecular chaperones (see Section 5).

Although the DBD displays sequence specificity for promotors of p53 target genes, the RD binds with high affinity to a large variety of DNA structures, including short single strands and irradiated DNA.[127,128] This feature of the RD is discussed in Section 4.2 in more detail.

4. Regulation of p53

4.1. Posttranslational Modifications

Owing to its potential toxicity for nontumorigenic cells, the activity of p53 is tightly controlled under physiological conditions. Cellular stress signals are required for p53 to activate and accumulate in its active form. Regulation and activation of p53 occurs through interaction with various partner proteins and several posttranslational mechanisms.[132–134]

4.1.1. Phosphorylation

The p53 protein contains 17 serine and threonine residues as possible phosphorylation sites. These sites include serines and threonines in the NTD, the carboxy-terminal domain, and the DBD. None of the tyrosine residues seem to be phosphorylated.[133,135] The most-prominent signal-transduction pathways are mediated by the ataxia-telangiectasia mutated gene product (ATM) and ATR (ATM- and Rad3-related protein kinase) kinases. The ATM kinase, which becomes activated by DNA damage and ionizing radiation, activates the downstream kinase Chk2.[135] ATM itself targets p53 at residue serine 15, whereas Chk2 phosphorylates residue serine 20. Both modifications are required not only to decrease p53 turnover but also to increase its affinity for specific promoter sequences.[136] ATR, together with the downstream kinase Chk1, phosphorylates p53 at various sites in response to UV-induced damage.[137]

 © 2006 Wiley-VCH Verlag GmbH & Co. KGaA, Weinheim

In general, phosphorylation of p53 in the amino- and carboxy-terminal domains (NTD and RD, respectively) is induced as a result of cellular stress, for example, DNA damage or activation of oncogenes. It often results in the stabilization (thermodynamic stabilization and decreased turnover rate) and activation of p53.[133,138] There are, however, also reports that phosphorylation may not be required for activation of p53.[139,140]

4.1.2. Acetylation

This modification is another important mechanism for the regulation and activation of p53 and affects different lysine residues in the carboxy-terminal domain.[133,141–143] DNA damage and phosphorylation can induce a cascade of acetylation events during which histone acetyltransferases are recruited to regulate the transcriptional function of p53.[144,145] The deacetylation of p53 is mediated by histone deacetylases.[146–148]

4.1.3. Ubiquitinylation

The half-life of p53 is regulated by ubiquitin modification of p53 on lysine residues in the carboxy-terminal region and subsequent degradation through the proteasome pathway.[149] The key component for the ubiquitinylation of p53 is its natural antagonist, the E3 ligase and oncoprotein Mdm2.[150] This interaction results in a negative feedback loop between p53 and Mdm2 (see Section 4.3).[151–153] It was suggested that low levels of Mdm2 induce monoubiquitinylation, nuclear export, and trafficking of p53, whereas high levels of Mdm2 promote polyubiquitinylation of p53 and nuclear degradation (see Section 4.3).[154] Ubiquitinylated p53 can be directly deubiquitinylated through the herpes-virus-associated ubiquitin-specific protease.[155,156] Recently, additional p53-specific ubiquitin ligases, were identified,[157–160] making the regulation of p53 degradation even more complex than previously thought.

4.1.4. Sumoylation

Further to ubiquitinylation, p53 is also regulated by modification of lysine residues in the carboxy-terminal domain by the SUMO1 (**s**mall **u**biqutin-related **mo**difier **1**)[161–163] and the ubiquitin-like protein NEDD8.[164,165]

The modifications discussed so far do not seem to be the end of the story. Several novel modifications of the p53 protein have been reported including glycosylation[166] and ADP ribosylation.[167] Their relative importance for regulating p53, however, requires further analysis to be fully explained.

4.2. Functions of the RD

Initial observations showed that the basic 30 amino acid region localized at the carboxy-terminal end of p53 has a strong regulatory effect on the ability of the DBD to bind specifically to its consensus DNA.[42] There are several possibilities to abolish the negative effect of the RD on DNA binding: Binding of a monoclonal antibody (PAb421) to these carboxy-terminal residues, phosphorylation of a serine residue (S392), or the deletion of the whole region. These possibilities result in stimulation of the DNA-binding activity of the DBD.[42,56] Acetylation of various residues in the carboxy-terminal region leads to a strong increase in specific DNA binding of the DBD in vitro[68,145] and in vivo.[168,169] Additionally, it was recently shown that acetylation of specific residues in the carboxy-terminal domain weakens nonspecific DNA binding by two- to threefold, whereas phosphorylation of serine 392 did not alter the nonspecific DNA binding of p53 at all.[61]

The specific mechanism involved in the activation of latent p53 through posttranslational modifications is still controversial. According to the allosteric model by Hupp and Lane, the carboxy-terminal region influences the conformation towards an active tetrameric p53.[56] In terms of negative regulation, it was suggested that the RD locks the DBD into an inactive/latent conformation until activating modifications, such as phosphorylation, acetylation, binding of a monoclonal antibody, or the complete removal of the carboxy-terminal domain, results in disruption of the interaction between these two domains, allowing the DBD to adopt an active conformation. A reinterpretation of the experimental data has now established a second model, in which nonspecific DNA binding competes with the specific DNA binding of the core domain.[58,60]

4.3. The Antagonist Mdm2

The cellular oncoprotein Mdm2 (**m**ouse **d**ouble **m**inute **2**, also termed HDM2 in humans)[*] acts as the major cellular regulator of the p53 tumor-suppressor protein.[5,7,170] Mdm2 is upregulated in human tumors and tumor cell lines.[171] It was originally identified as an oncoprotein that binds to p53 and inhibits p53-mediated transactivation.[172] The multidomain structure of Mdm2 (Figure 5 A) allows further regulation by a number of effector proteins that bind to different parts of Mdm2.

4.3.1. Mdm2 and the p53–Mdm2 Feedback Loop

Mdm2 blocks activation of p53 on the one hand by direct physical interaction and, on the other hand, by targeting p53 for degradation by ubiquitinylation through its E3 ligase activity. As a consequence, p53 exhibits a short half-life and the concentration of active p53 is kept at low levels (Figure 6). Moreover, as the Mdm2 gene itself contains two p53-responsive elements in its promoter region, Mdm2 transcription is induced after p53 activation. This coupling is the basis of a negative regulatory feedback loop that tightly controls the concentration of p53 and Mdm2 in cells.[173,174] In tumors that overexpress Mdm2, this feedback loop is deregulated so that even upon p53 activation, levels of p53 are no longer sufficient to exert the tumor-suppressive

[*] Mdm2 is used throughout the text regardless of the organism that this protein came from.

© 2006 Wiley-VCH Verlag GmbH & Co. KGaA, Weinheim

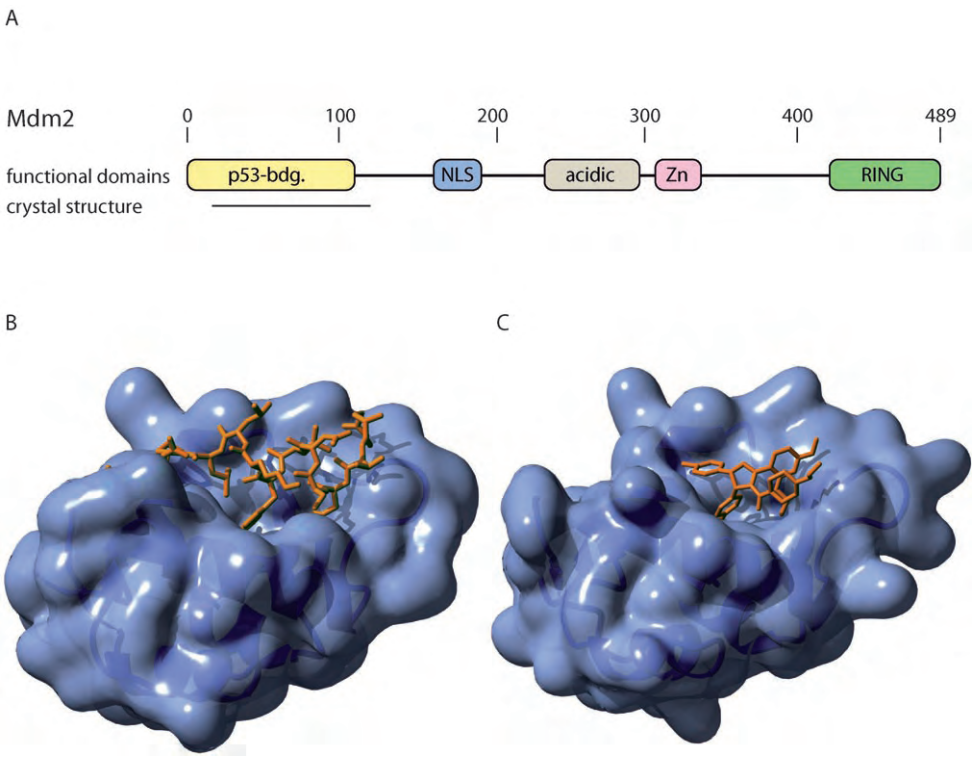

Figure 5. A) Domain structure of Mdm2. p53 bdg = p53 binding region; NLS = nuclear localization signal; Zn = zinc-finger domain; RING = ring-finger domain (zinc binding motif). B) Crystal structure of Mdm2 in complex with a p53 peptide. PDB code: 1YCR. C) Crystal structure of Mdm2 in complex with the inhibitor Nutlin. The structure of Mdm2 is slightly changed in comparison with the apo form. PDB code: 1RV1.

function. Antagonists of the p53–Mdm2 interaction are expected to overcome the oncogenic consequences of Mdm2 overexpression and to stabilize p53 (see Section 7.3).

4.3.2. The p53–Mdm2 Interaction

Genetic and biochemical studies mapped the p53–Mdm2 interaction site to the amino terminal domain of Mdm2 and the amino-terminal part of the transactivation domain of p53 (residues 15–29).[167–169,174–176] The crystal structure of the amino terminal domain of Mdm2 in complex with short peptides derived from the NTD of p53 (Figure 5B) revealed the structural basis of the interaction between p53 and Mdm2:[26] Upon binding to Mdm2, a segment of eight amino acids within the unstructured NTD of p53[33,34] forms an amphiphilic α helix that projects its hydrophobic residues into a deep hydrophobic binding pocket of Mdm2.[26] Mdm2 binding inhibits the transcriptional activity of p53 as the Mdm2 binding site on p53 is also responsible for interaction with factors of the transcriptional machinery.[177]

Upon binding with a ligand, the p53 binding domain of Mdm2 exhibits significant changes in its dynamics.[178,179] NMR spectroscopic studies of the p53-binding domain of human Mdm2 (apo-Mdm2) showed that residues 16–24 in Mdm2 form a lid that closes over the p53 binding pocket and might help to stabilize apo-Mdm2.[180] Posttranslational modification, for example, phosphorylation of the Mdm2 lid, may disrupt the p53–Mdm2 interaction and result in p53 stabilization.[180] In addition, the Mdm2 lid might help to explain how Mdm2 can be differentiated from its close homologue Mdm4 (MdmX). Mdm4 binds and inhibits p53 transcriptional activity and acts as a critical regulator of p53 in vivo.[180] Unlike Mdm2, however, Mdm4 does not cause nuclear export or ubiquitinylation and degradation of p53.[181–184] Mdm2 and Mdm4 show their highest level of sequence similarity in the p53 binding site;[27] however, the Mdm2 lid is not conserved, suggesting that lid modifications may be responsible for differences in the binding of Mdm2 and Mdm4 to p53.[180]

Recently, the structure of human apo-Mdm2 was solved by NMR spectroscopy.[185] Comparison of the apo-Mdm2 structure with that of Mdm2 in complex with a p53 peptide confirmed that binding of the peptide is accompanied by the displacement of the flexible lid and adjustment in the secondary structure. Furthermore, human Mdm2 becomes more rigid and stable upon binding to p53.

Surprisingly, the results indicate that the binding pocket of human apo-Mdm2 itself is shallow and thus not likely to provide much opportunity for ligand design, whereas Mdm2, both in complex with peptides[26] or with small-molecule antagonists,[186,187] exhibits a binding pocket with conformational plasticity.[185] As a consequence, the structure of ligand-complexed Mdm2, but not apo-Mdm2 could serve as a template for rational drug design.

5. Interaction with Chaperones

5.1. Overview

In the past years, a distinct interaction between p53 and the molecular chaperones Hsp70 and Hsp90 has been reported. The findings that p53 is a remarkably unstable and conformationally flexible protein (see Section 2.2) suggests that chaperones (see box 4) are an important element for the regulation and maintenance of the pool of active p53.

5.2. Hsp40/Hsp70

The Hsp70 heat-shock proteins are a family of ubiquitously expressed proteins and are an important part of the cell's machinery for protein folding.[191] They consist of a protein-binding and an ATPase domain that influence each other.[192] It has been shown that Hsp70 binds promiscuously to a wide variety of newly synthesized or unfolded pro-

 © 2006 Wiley-VCH Verlag GmbH & Co. KGaA, Weinheim

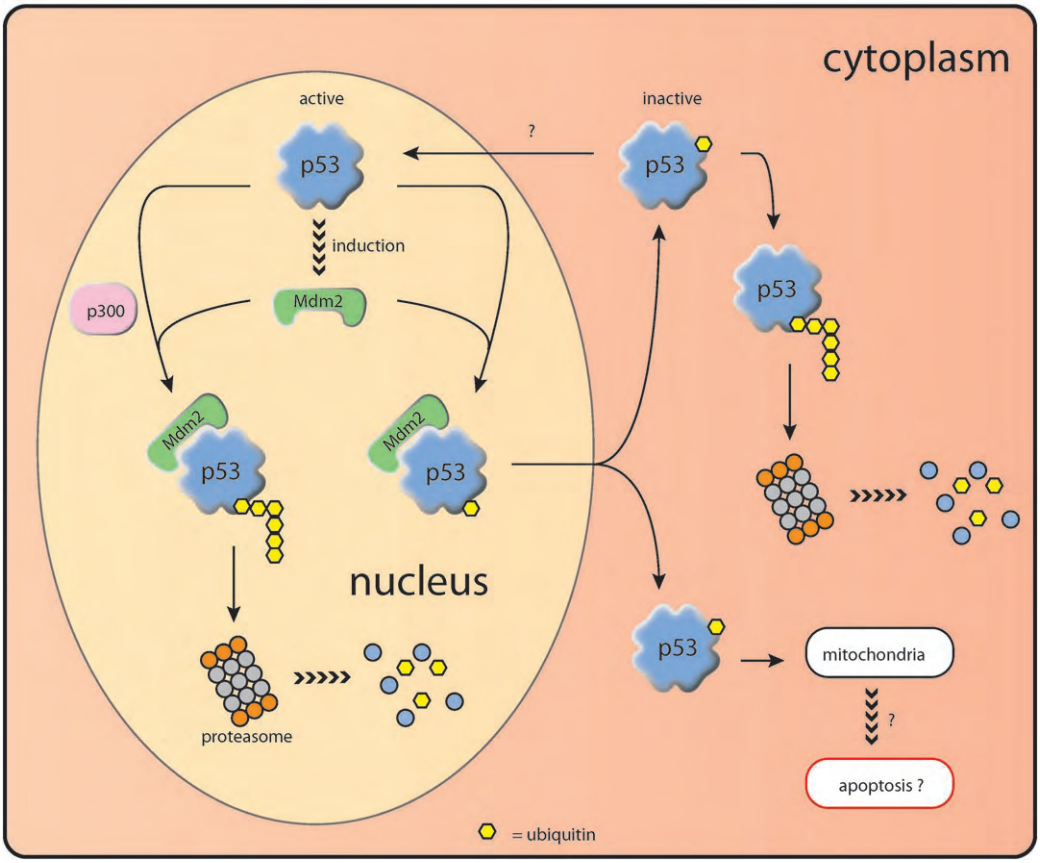

Figure 6. Schematic view of the interplay between Mdm2 and p53. Active p53 induces the regulator protein Mdm2. Single ubiquitinylation results in an export of p53 into the cytoplasm, whereas multiple ubiquitinylation steps (the E4-like histone acetyltransferase p300 can extend single p53-conjugated ubiquitin moieties into a polyubiquitin tree)[324] direct p53 to the proteasome in the nucleus.[325] Cytoplasmic, single-ubiquitinylated p53 may be able to re-enter the nucleus, but the major part of the protein will be degraded in the proteasome. Recent studies propose that p53 interacts with anti-apoptotic BclX and Bcl2 and thus induces the release of cytochrome *c* from mitochondria, which ultimatively leads to apoptosis.

teins.[193–196] Binding occurs, regardless of the secondary and tertiary structure, by recognition of hydrophobic sequences.[197] ATP binding and hydrolysis by Hsp70 are important for regulating the affinity for substrate proteins.

The molecular chaperone Hsp70 was identified in complex with mutated, but not wild-type p53.[198] Further components of this complex are the chaperone Hsp90 (see Section 5.3) and the Hsp70 cochaperone, Hsp40.[199,200] The major task of Hsp70 in this context seems to be the regulation of the translocation of p53 into and out of the nucleus.[201] Hsp70 masks the nuclear localization sequence of the tumor-suppressor protein and therefore inhibits its importation into the nucleus only when it is complexed with mutated p53.[202] The unmasked wild-type p53, however, is still able to enter the nucleus and to induce or downregulate its target genes. Furthermore, Hsp70 was reported to enhance the accumulation of cytosolic p53 in specific tumor cells.[203] As a result, cytosolic p53 is no longer degraded or marked for proteolysis by Mdm2 and therefore aggregates.[204] This consequently negatively influences the cellular control of DNA damage in these tumor cells.[205]

Although Hsp70 seems to be important for translocation and accumulation of p53, the stabilization and activation of p53 has to be performed by another chaperone (see Section 5.3).

5.3. Hsp90

The molecular chaperone Hsp90 is responsible for the late-state folding of fragile substrate proteins such as protein kinases and transcription factors.[197] Hsp90 is one of the most-abundant proteins in eukaryotes (1–2% of the total cellular proteins).[206,207] It has a low ATPase activity[208] and consists of three functional domains.[197] Several small-molecule drugs that target Hsp90 have been identified as potential anticancer agents. These drugs indirectly alter the activity of numerous kinases and transcription factors that are known to be involved in oncogenesis.[209]

Some years ago, Hsp90 was identified in complex with mutated p53 in tumor cells.[210–213] Hsp90 seems to bind to mutated or otherwise deactivated p53 irreversibly. This was monitored by translation experiments in vitro and by immunoprecipitation from human tumor cell lines.[71] It could also be shown that treatment of these cells with the Hsp90 inhibitor geldanamycin leads to the degradation of p53.[71]

 © 2006 Wiley-VCH Verlag GmbH & Co. KGaA, Weinheim

Box 4: Chaperones

Molecular chaperones assist other proteins to reach and maintain their native and active conformation.[188,189] Partially unfolded or misfolded proteins are often prone to nonspecific aggregation. The interaction of these proteins with molecular chaperones leads to suppression of aggregation, and the proteins are guided to their native/active state. A conserved feature of this class of proteins is a shift between high-affinity and low-affinity states for binding proteins. In many cases, this shift is initiated by ATP binding and hydrolysis. Almost all chaperones show enhanced expression rates under nonphysiological conditions, such as high temperatures or cellular stress. Therefore, most chaperones belong to the group of heat-shock proteins (Hsps).[190] There are several universal classes of molecular chaperones, they are functionally related but show little homology in sequence and structure. Chaperones recognize a large variety of proteins in non-native states. This promiscuous behavior together with the cooperation of different chaperones ensures protein homeostasis under conditions of stress. Besides the general house-keeping functions, chaperones seem to be utilized for adding an additional layer of regulation for a number of signaling proteins.

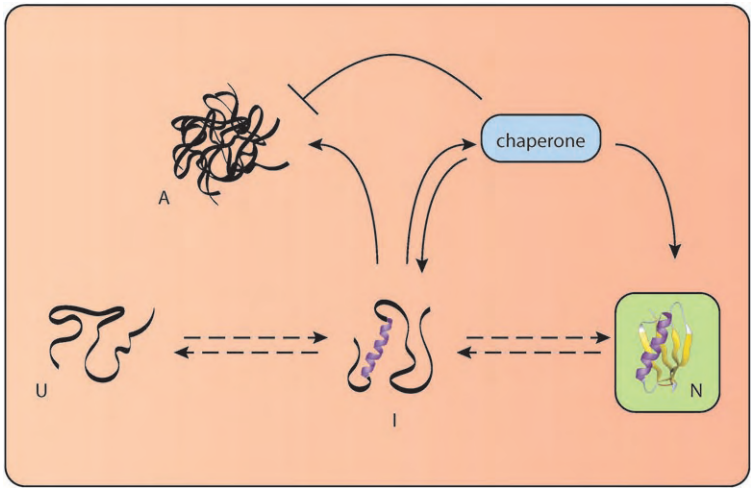

Functions of molecular chaperones. Newly synthesized or unfolded proteins (U) have to follow a certain pathway to achieve their native state (N), often through specific folding intermediates (I). Without the help of molecular chaperones, partially folded proteins would ultimately lead to aggregation (A). The main task of molecular chaperones is to support proteins on their way to the native folded active state—by preventing side reactions such as aggregation.

Geldanamycin releases Hsp90 from the Mdm2–p53 complex and p53 is then ubiquitinylated and dismantled from the proteosome. Hsp90 therefore indirectly stabilizes p53. Recently, there has also been evidence that Hsp90 directly stabilizes wild-type p53 in vivo and in vitro.[65,66] The binding to the wild-type protein seems to be weaker than that to the mutant protein. Hsp90 binds in vitro to the native form of p53 with micromolar affinity.[65] The interaction between the two proteins involves the DBD of p53 and the middle domain of Hsp90.[65,70] This interaction preserves the DNA-binding activity of p53 efficiently and prevents aggregation of p53 (Figure 7).[65,66] Similar results could be obtained in vivo.[66,72] Taken together, Hsp90 is required to ensure the functionality of wild-type p53 at physiological and heat-shock temperatures. These results are in agreement with a model in which Hsp90 helps to maintain the folded, active state of p53 by a reversible interaction, thus introducing an additional level of regulation.[65,66]

6. Functions of p53

Since the early 1990s, it has been known that target genes of p53 facilitate cell-cycle arrest and DNA repair mechanisms.[214–216] In a simplified view, the activation of p53-regulated genes by DNA damage results either in cell-cycle arrest allowing DNA repair mechanisms to occur or in apoptotic cell death (if DNA damage was too severe to be repaired).[170,217] A relatively new aspect is the involvement of p53 in replicative senescence (in somatic cells only a limited amount of cell division can occur) and aging.[218] There is also evidence that p53 is capable of performing transcription-independent reactions, such as the direct induction of apoptosis (Figure 8).[219] In spite of its central function during tumor suppression, p53 is not essential and p53-deficient mice show normal embryonic development, although they develop multiple tumors early on.[220,221] Transgenic mice with increased p53 activity exhibit resistance to spontaneous tumors but also display an early onset of phenotypes associated with senescence (see Section 6.2).[222,223]

6.1. Apoptosis

One of the most prominent functions of p53 is its ability to initiate apoptosis directly (through interaction of the DBD with BclX)[224] or indirectly (through transcription of genes involved in apoptosis). Although the second way has been known for a long time (for a review, see Vousden et al. 2002),[170] the direct interference with the BclX/Bax system was discovered only recently (see Section 6.3). Apoptosis is activated as soon as the cell and/or DNA are severely damaged and the repair mechanisms of the cell are unable to counteract efficiently. Programmed cell death is a complex mechanism and a large number of proteins are involved in the process.[225] If the apoptotic functions of cells are inhibited, they may proliferate indefinitely and give rise to a tumor, or will reside in a senescent state, if the cell cycle is also blocked (see Section 6.2).

6.2. p53-Related Senescence and Aging

Some years ago, several independent studies described that overexpression or hyperactivity of p53 in mice lead to an increased resistance against tumor growth.[222,226] This is consistent with the role of p53 as the tumor-suppressor protein of multicellular organisms. Surprisingly, the overall lifespan of these modified mice was significantly shorter when

 © 2006 Wiley-VCH Verlag GmbH & Co. KGaA, Weinheim

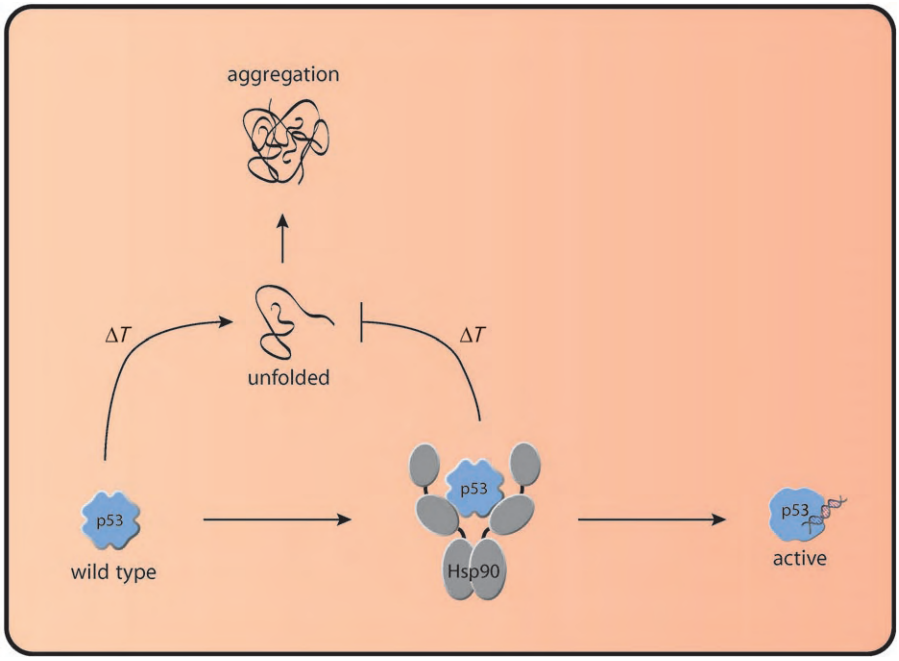

Figure 7. Simplified view of the influence of Hsp90 on the stability and activity of p53. Wild-type p53 interacts with Hsp90 reversibly. At higher temperatures, isolated p53 would denature and, as a consequence, aggregate irreversibly. Hsp90, however, is able to protect the protein from thermal unfolding and therefore prevent aggregation and inactivation. After posttranslational modifications, such as phosphorylation, p53 becomes activated and starts its transcriptional activity.

compared with the normal, more-cancer-prone animals. Moreover, mice with elevated p53 levels showed several signs of premature aging.[227]

It has been known for many years that p53 is able to induce transient cell-cycle arrest.[228] Since then, a lot of evidence has been accumulated that p53 is also responsible for an irreversible cell-cycle arrest, which is characteristic for senescent cell phenotypes.[229,230] Thus, p53 seems to be responsible for the decision to undergo apoptosis or cellular senescence.[227]

Cellular senescence may suppress the onset of cancer during the reproductive years of human life, and, as a pay-off, cancer and aging is promoted as the organism reaches the end of its life.[218,231]

6.3. Transcription-Independent Function of p53

As one of the key functions of p53 is the regulation of transcription, its localization in the nucleus plays an important role. Active transport of p53 towards the nucleus by dynein and the microtubule network has been described.[232–235] Contrary to this, the p53 protein contains two nuclear export sequences, one in the TD[236] and the other in the amino-terminal, Mdm2-binding region.[237] The ability of p53 to be exported is greatly enhanced by the action of Mdm2,[238] although export is not absolutely dependent on the presence of Mdm2. Nuclear export is not only required for p53 degradation, but also for transcription-independent aspects of the apoptotic response.[219] Mutations that abolish the transactivating function of p53 or prevent its nuclear localization do not suppress its apoptogenic potential. In addition, p53 can promote cell death even in the presence of transcriptional or translational inhibitors. Mitochondria also play a central role in apoptotic events through the release of pro-apoptotic factors such as cytochrome *c* and others. It has been shown recently that p53 can localize in mitochondria and directly interact with antiapoptotic BclX and Bcl2 proteins, finally leading to the release of cytochrome *c*.[239] Recent NMR chemical-shift-perturbation experiments with the DBD and BclX protein provided additional evidence for interaction of these antiapoptotic Bcl2 family members with the DBD of p53.[240] Interestingly, Bcl2 directly binds to the DNA binding site of p53.[119]

7. p53 and Cancer Therapy

For decades, scientists have been trying to cure or avoid cancer by altering the activity of p53. As a result, different approaches have been established. One important aspect is to reactivate mutant or inactive p53. This can be done by small molecules, enzymes, or gene therapy (see Section 7.1). In some cases, it is even necessary to inhibit the functionality of p53 (see Section 7.2). A very promising approach is to focus on the interaction between p53 and partner proteins. Only recently, small-molecule inhibitors were identified that block the interaction between Mdm2 and p53 (see Section 7.3.1). As a result, the level of active p53 inside the nucleus rises—leading to an increased protection against cancer. However, only the small number of patients with imbalanced p53–Mdm2 equilibrium will benefit from this progress.

7.1. Reactivation of Mutant p53 in Tumors

Obviously, one of the most-attractive approaches in cancer therapy is the restoration of wild-type-p53 function in tumors that have lost p53 activity by mutation. One strategy to achieve this is the introduction of wild-type p53 in tumors with mutated p53 by gene therapy. In 2003, p53 gene therapy for the treatment of certain carcinomas was approved in China. Thus, the first gene therapy ever approved for use in humans is based on p53, and further p53-based gene therapies are currently in clinical phase II and III trials.[240,242] The future will show whether p53-based gene therapies can succeed in a clinical setting.

A more conventional approach is the identification of small-molecule drugs that can activate p53 in human tumors. Based on a detailed thermodynamic and biophysical analysis

 © 2006 Wiley-VCH Verlag GmbH & Co. KGaA, Weinheim

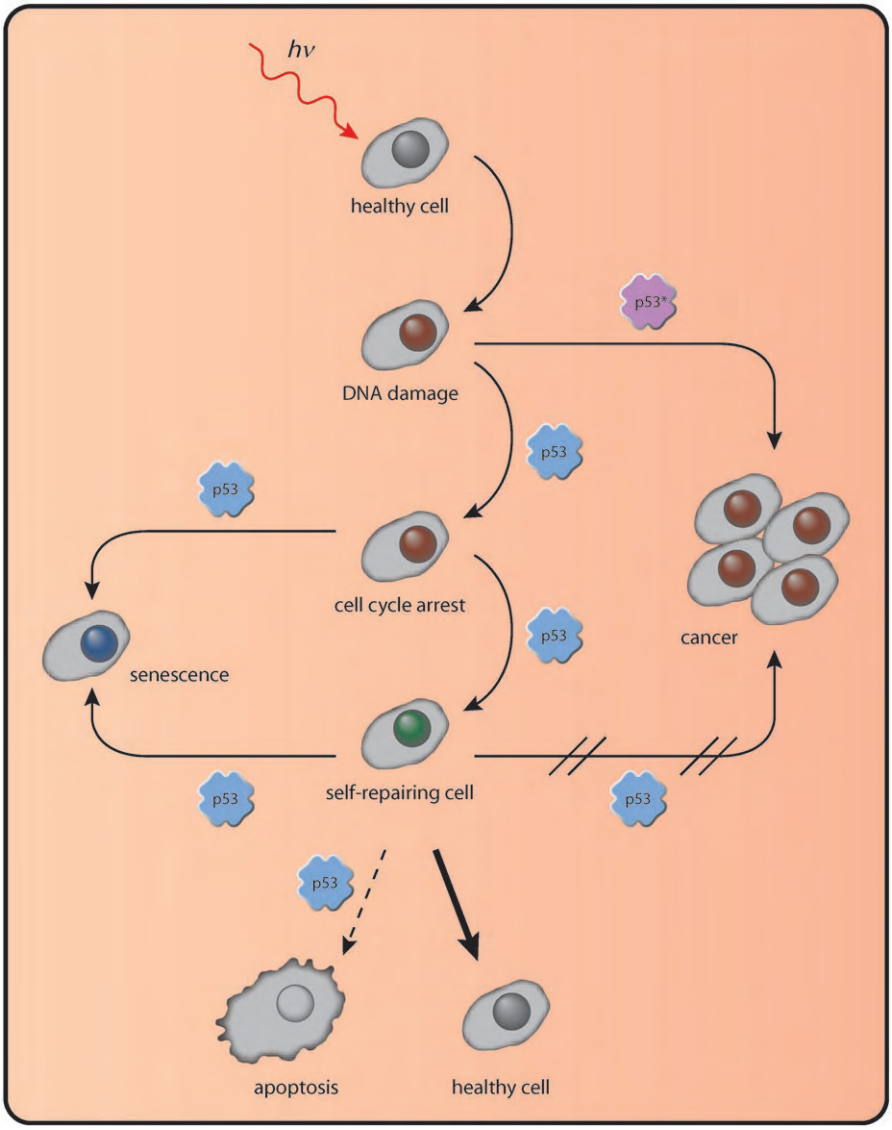

Figure 8. p53 and its role in repair, apoptosis, and senescence. Influence of active, wild-type p53 (blue) and mutant p53 (pink) on damaged eukaryotic cells.

of p53 mutants, three phenotypes were distinguished: 1) DNA-contact mutations that have little or no effect on folding; 2) mutations that disrupt the local structure, and 3) mutations that prevent cooperative binding to DNA (see Section 3). The division of these phenotypes into states where DNA binding is possible and not possible defines the distinct classes of p53 mutations.[97,108,130,243] There are two principle mechanisms to achieve activation of mutant p53 by small molecules: The largest proportion of p53 structural mutants can adopt both mutant and wild-type conformations (see box 3). The mutant conformation is characterized by a decreased or completely lost DNA-binding ability. Whenever mutant p53 is capable of adopting a wild-type conformation, it would be possible, in principle, to rescue its functionality by small molecules that bind to and stabilize the wild type and thus shift the conformational equilibrium in favor of this conformation. For a small proportion of DNA-contact mutants or more-heavily destabilized p53 variants, however, small molecules might be required that recognize a specific mutant conformation and induce a wild-type-like conformation, for example, by forming additional stabilizing interactions.[97]

Restoration of the wild-type conformation and function of mutant p53 by small molecules is demanding from a technical point of view. Nevertheless, early proof-of-concept studies showed that the wild-type p53 conformation can be restored by several means. Basic residues were introduced into the DBD, based on structural information, to establish novel contacts between p53 and the DNA phosphate backbone. In three of the seven most common p53 mutants, replacement of Thr284 with Arg significantly enhanced the DNA-binding affinity and rescued their transactivation and tumor-suppressor functions.[244] Second-site suppressor mutants that were able to overcome the deleterious effects of common p53 cancer mutations in human cells were identified[8] and their mechanisms analyzed. Specific second-site mutants for selected p53 mutants were identified and the authors came to the conclusion that the function of p53 mutants analogues could be restored by small molecules that bind to and hence stabilize the native structure.[245] Finally, a superstable quadruple mutant of the p53 DBD was designed.[246] This mutant contains the second-site suppressor mutations N239Y and N268D, which specifically restore activity and stability in several oncogenic mutants. The crystal structure of this mutant illustrated how an increase in rigidity results in increased thermostability.[247] It was also shown that the addition of consensus DNA and heparin resulted in a thermodynamic stabilization of the p53 DBD.[246,248] Further to the intrinsic stabilization by mutation, solvent additives, such as glycerol, trimethylamine *N*-oxide (TMAO), and the aminothiol WR1065, can stabilize the active wild-type conformation of temperature-sensitive p53 mutants in vivo.[249–254] Specific stabilization by peptides and small molecules should thus be possible.[255]

Screening of a large compound library of small molecules that could stabilize wild-type p53 against thermal denaturation identified several ligands of which CP-31398 (Figure 9) was the most potent representative.[256] It was pharmacologically active in cellular assays and showed antitumor activity in xenograft models. In addition, CP-31398 induced a specific

 © 2006 Wiley-VCH Verlag GmbH & Co. KGaA, Weinheim

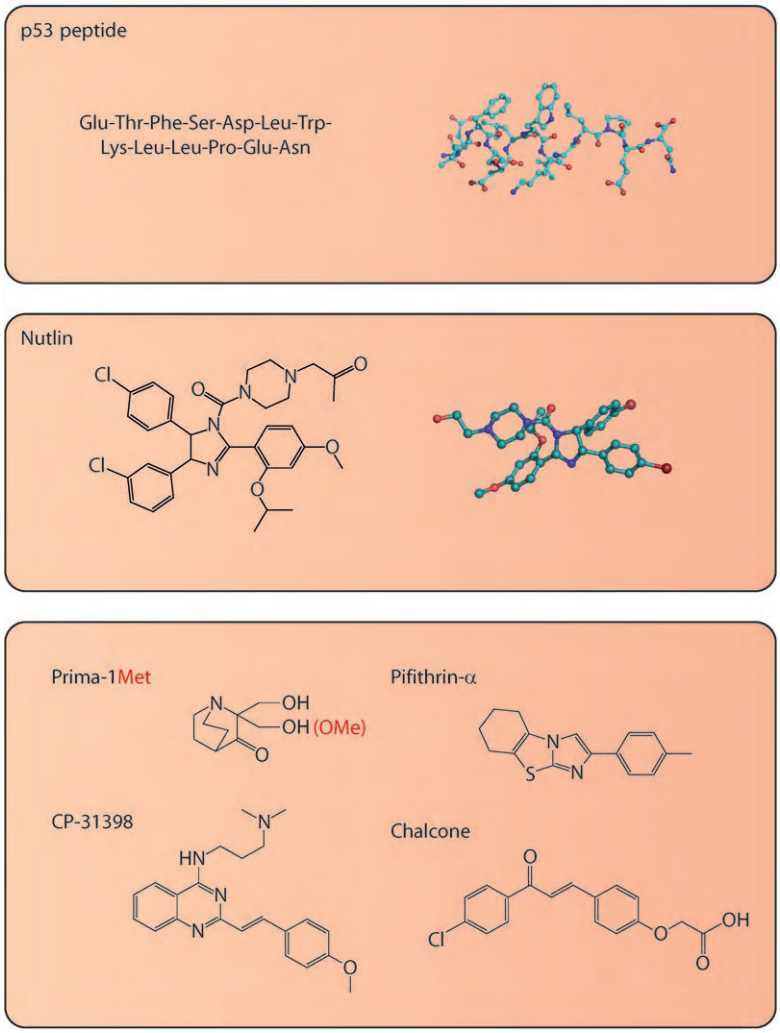

Figure 9. Mdm2 and p53 inhibitors. The conformations of the p53 peptide and of Nutlin were taken from their crystal structures with Mdm2: 1YCR and 1RV1, respectively. O = red, N = blue, C = green, Cl = dark red.

p53 response and apoptosis in tumor cells.[257–262] However, since its discovery, no data on the direct interaction with p53 have been reported.[263] In contrast, it was found that CP-31398 did not stabilize p53 thermodynamically, but intercalated with DNA. It was also unable to reactivate the mutant p53 protein.[264] It did, however, induce native p53 in cells that also express mutant p53. Thus, CP-31398 might exclusively act on newly synthesized p53, which would also explain why no direct interaction can be detected with purified p53 domains. Taken together, the mode of action of CP-31398 remains controversial and requires further studies.

Another promising compound is called Prima-1 (for **p**53 **r**eactivation and **i**nduction of **m**assive **a**poptosis; Figure 9). It was found to inhibit several tumor cell lines with different p53 statuses by restoring p53-dependent apoptosis[265] and DNA-binding activity and to exhibit antitumor activity in xenograft models.[266] In contrast to CP-31398, it was also reported to restore wild-type p53 conformation of both DNA contact and structural mutants in vitro and in vivo. It was shown that Prima-1 selectively eliminated mutant p53 cells. The methylated form, Prima-1MET, is more active than Prima-1 and synergizes with chemotherapeutic agents such as cisplatin.[267] Recently, a family of p53 reactivators derived from the backbone of Prima-1 was described.[268]

A maleimide analogue with similar activity, which originated from the same screening campaign, called MIRA-1 (**m**utant p53-dependent **i**nduction of **r**apid **a**poptosis) was shown to reactivate DNA binding and preserve the active conformation and transcriptional function of mutant p53 in vitro and in living cells.[269] However, restoration of wild-type conformation in vitro could not be detected. As for CP-31398, the mode of action of Prima-1 and derivatives has yet to be clarified.

The first biochemical and biophysical proof-of-principle experiments for the direct rescue of mutant p53 mutation came from studies with the nine-residue peptide CDB3 (REDED-EIEW).[270] The CDB3 peptide binds specifically to the DBD and stabilizes it against thermal unfolding.[271] NMR spectroscopy proved that CDB3 reverts the chemical shifts of the hot-spot mutant R249S back towards the wild-type conformation.[272] Finally, it was shown that the CDB3 peptide also induced the active wild-type conformation of the p53 hot-spot mutants His175 and His273 in vivo. This resulted in the expression of p53 target genes accompanied by p53-dependent partial restoration of apoptosis.[273] Based on their experiments, the authors concluded that potential drugs with a mode of action comparable to that of CDB3 have to act during or immediately after biosynthesis to rescue the conformation of unstable p53 mutants.[274]

In summary, the studies described above show that the restoration of wild-type p53 function in tumors with mutant p53 is, in principle, feasible. Nevertheless, all molecules described so far exhibit low-to-moderate potency and inappropriate physicochemical properties and will therefore probably not qualify as therapeutics. One focus in the future search for p53 reactivators has to be the elucidation of this mode of action and the structural mechanisms resulting in the rescue of p53 mutants.

7.2. Inhibition of p53 Activity in Nontumor Tissue After Genotoxic Stress

It might be surprising to hear that inhibition of p53 represents another therapeutic strategy that seems to be useful under conditions in which p53 accumulates and becomes activated in non-tumor tissue, such as hypoxia as a consequence of stroke,[275] conventional chemotherapeutic agents (e.g. DNA-damaging agents, antimetabolites, proteasome inhibitors), or radiotherapy. Induction of apoptosis

 © 2006 Wiley-VCH Verlag GmbH & Co. KGaA, Weinheim

following activation of p53 in normal tissue is one of the reasons for neurodegeneration or the severe side effects observed with conventional broad-spectrum tumor therapy.[276] Thus, inhibition of p53 activity by cytoprotective agents might be an interesting option to protect normal tissue from the harmful consequences of stroke or cancer treatment.[277]

Screening for compounds that inhibit the transcriptional activity of p53 identified Pifithrin-α (**p-fi**fty **thr**ee **in**hibitor).[278] Pifithrin-α is able to reduce the side effects of chemo- and radiotherapy in vivo without lowering the efficacy of therapy for p53-mutant tumors and without promoting the formation of tumors in the short term.[278–281] It must be noted, however, that inhibition of p53 activity in normal tissue following treatment with Pifithrin-α might increase the incidence of tumors in the long term.[282] Interestingly, the p53 protein itself does not appear to be the target of Pifithrin and the mode of action remains unknown.[283] Further to its application for the treatment of tumors with mutant p53, inhibition of p53 activity might also be of use for several other pathological states such as stroke, severe burns, heart infarct, or wound healing.[283,284]

7.3. Mdm2 and Cancer Therapy

Because of the significance of Mdm2 as a negative regulator of p53 and the existence of a defined hydrophobic p53-binding pocket on Mdm2, there was a major interest to employ this interaction for therapeutic intervention.[38,97,285–292,326,327] In recent years, a variety of approaches proved that Mdm2 represents a valuable target.[285–291] The deletion of the Mdm2 gene in mice results in embryonic lethality, which can be overcome by simultaneous loss of p53, substantiating the importance of the negative regulation of p53 by Mdm2.[293,294] Even the partial inhibition of Mdm2 is sufficient to activate the p53 pathway in vivo.[295]

An alternative route to Mdm2 inhibition might be the E3 ubiquitin ligase activity of Mdm2.[296,297] Its inhibition should result in diminished degradation of p53 and increased p53 levels (see Section 7.3.2). Just recently, the first selective antagonists of Mdm2 with potency in vitro and in vivo were described.[186]

7.3.1. Targeting the p53–Mdm2 Interaction with Peptides and Small-Molecule Antagonists

The affinity of the native p53 peptide for Mdm2 could be enhanced by introduction of hydrophobic residues.[298] The alignment of optimized peptide sequences allowed identification of PxFxDYWxxL (x = any amino acid) as the consensus motif for binding to Mdm2.[298,299] Semirational design in combination with NMR spectroscopy generated very potent derivatives of this motif.[300] Artificial amino acids were introduced that entropically stabilize the helical conformation of the peptide and form additional polar and hydrophobic van der Waals interactions with Mdm2. This optimization enhanced the affinity of the peptide almost 2000-fold when compared with the native p53 peptide.[300]

Potential low-molecular-weight antagonists of the p53–Mdm2 interaction were identified from different compound classes.[301–304] The first small-molecule Mdm2 antagonists were identified as derivatives of phenoxy acetic acid and phenoxymethyl tetrazole as well as chalcones (Figure 9).[305] However, they exhibit only moderate potency and also inhibit glutathione-S-transferase activity.[305] Recently, novel boronic chalcone derivatives were described as potential Mdm2 antagonists with fewer significant side reactivities.[306] Other approaches to target the Mdm2–p53 interaction are still in their infancy: By using computer-aided design, nonpeptidic polycyclic Mdm2 antagonists were synthesized. These inhibitors seem to have moderate affinity for Mdm2 and can induce the p53 pathway in tumor cell lines.[307] By using protein grafting (a strategy that involves dissecting a functional recognition epitope from its native helical or polyproline type II (PPII) helical context and presenting it on a small but structured protein scaffold), Mdm2 ligands were described that have high affinities and are thought to exhibit inhibitory potencies.[308] These ligands can be readily synthesized and are easy to modify. Another promising compound is the fungal cyclic chlorofusin. It was selected as an inhibitor of the p53–Mdm2 interaction by screening of a library of microbial extracts.[309]

Recently, *cis*-imidazolines, also called Nutlins, were identified as potent and selective small-molecule antagonists of Mdm2.[186] The lead compounds were improved by multidimensional optimization of different parameters, such as binding affinity, solubility, reactivity, and pharmacokinetics, and rational structure-based design. Interaction studies and the first crystal structure of Mdm2 in complex with a small-molecule antagonist confirmed that these compounds bind Mdm2 in the p53-binding pocket with submicromolar affinities (Figure 5C). The cellular analysis confirmed that Nutlins activate the p53 pathway and induce apoptosis in wild-type p53 cancer cells but not in mutant p53 cancer cells—indicating that especially cancer that is caused by Mdm2 overreactivity can be treated with this drug. Furthermore, these compounds exhibit antitumor acivity in xenograft models without major signs of toxicity.[186]

Together, these studies have provided proof of principle that the p53–Mdm2 interaction can in fact be inhibited by small molecules, and that disruption of the p53–Mdm2 interaction induces the phenotype expected for the action of Mdm2 antagonists.[310] Following the paper by Vassilev et al.,[186] several reports have been published that describe novel peptide-based and small-molecule antagonists of Mdm2 with in vitro and partly also cellular activity.[311] The structure-based optimization of a novel series of benzodiazepinedione antagonists of the Mdm2–p53 interaction was described. These 1,4-benzodiazepin-2,5-diones induce stabilization of p53 in cells, subsequent transcription of p53 target genes, and inhibit the proliferation of tumor cells.[312–314] In addition, there are is a growing number of potent and promising peptidic and nonpeptidic inhibitors of the p53–Mdm2 interaction. However, there is so far primarily biochemical and a limited set of cellular data reported for them, for example, spiro(oxindole-3,3'-pyrrolidine) derivatives,[315] isoindolinone derivatives,[316] terphenyl-based α-helical mimetics,[157,317] β-

 © 2006 Wiley-VCH Verlag GmbH & Co. KGaA, Weinheim

hairpin peptidomimetics,[318–320] and retroinverso p53 peptides.[321] There was also a 2,5-bis(5-hydroxymethyl-2-thienyl)furan derivative (called RITA) reported that was found to block the p53–MDM2 interaction by binding to p53.[273] However, actual NMR spectroscopic data indicate that RITA works through a different mechanism.[322]

Given the high amount of data supporting the therapeutic concept of p53 activation by Mdm2 antagonists, there is a realistic chance that Mdm2 antagonists will be experimentally validated in a clinical setting in the near future.

7.3.2. Inhibition of p53 Ubiquitinylation by Mdm2

An alternative route for activation of p53 by inhibition of Mdm2 is to block the E3 ubiquitin ligase activity of Mdm2.[296,323] Inhibition of the E3 ligase activity results in diminished degradation of p53 by the ubiquitin-proteasome pathway and thus should lead to p53 activation in tumor cells. It has yet to be shown whether inhibitors of the Mdm2 E3 ligase can exhibit efficacy that is comparable to direct inhibitors of the p53–Mdm2 interaction. In addition, as ubiquitin ligases target a plethora of cellular proteins, it might be more difficult to find selective enzymatic inhibitors of the Mdm2 E3 ligase function than it is to target the unique p53-binding pocket on Mdm2. On the other hand, one can argue that there is a proven track record for the clinical development of enzymatic inhibitors, whereas the development of inhibitors of protein–protein interactions is a new concept. The biochemical feasibility to block Mdm2-mediated ubiquitinylation of p53 with small-molecule inhibitors was already established, however, no data on the cellular or pharmacological potency of these compounds were reported.[296]

8. Outlook

More than 25 years after the discovery of p53 and despite remarkable progress, our knowledge of its structure, dynamics, and its interaction with DNA or cellular interaction partners is still very limited. In this context, it only recently became evident that a large part of the protein is natively unfolded. This region seems to adopt a structure first when bound to partner proteins. So far, the influence of only a few interactors on the structure of this region has been analyzed.

Surprisingly, even the details of how p53 takes part in recognizing DNA damage are not yet fully understood, and a comprehensive analysis of the genes regulated by p53 is still missing. Similarly, the regulation of p53 by nonspecific DNA binding, as well as by modifications such as phosphorylation and acetylation, remains to be elucidated in more detail. Finally, the complex network of interactions of p53 in the nucleus as well as in the cytosol, together with the regulation of transport between the compartments, adds another dimension of complexity that needs to be addressed. Understanding the function of p53, among other things, requires further detailed structural information; the crystal structure of the tetrameric p53 in complex with DNA would be highly desirable.

This short enumeration exemplifies clearly that central aspects of the p53 machinery are still uncharted territory. The more we learn about the basic aspects of p53 function by a combination of techniques in vivo and in vitro, the easier it will be to tailor novel therapeutics. Clearly, exciting times lie ahead in this field.

Abbreviations

DBD	central DNA binding "core" domain of p53
Hsp	heat-shock protein
IUP	intrinsic unstructured protein
Mdm2	Mouse double minute 2; in the text, Mdm2 is used independent of the originating organism of the protein, this also applies for the human version Hdm2
NTD	amino-terminal transactivation domain of p53
RD	carboxy-terminal regulatory domain of p53
TD	tetramerization domain of p53

Financial support by the DFG and the Fonds der chemischen Industrie to J.B. and H.K. is gratefully acknowledged. We thank Marco Retzlaff for comments on the manuscript and Titus Franzmann for comments on artwork. The authors apologize to all authors whose work could not be cited due to space limitations.

Received: February 15, 2006
Published online: September 19, 2006

[1] C. Chang, D. T. Simmons, M. A. Martin, P. T. Mora, *J. Virol.* **1979**, *31*, 463–471.
[2] D. P. Lane, L. V. Crawford, *Nature* **1979**, *278*, 261–263.
[3] D. I. Linzer, A. J. Levine, *Cell* **1979**, *17*, 43–52.
[4] T. Soussi, Y. Legros, R. Lubin, K. Ory, B. Schlichtholz, *Int. J. Cancer* **1994**, *57*, 1–9.
[5] B. Vogelstein, D. Lane, A. J. Levine, *Nature* **2000**, *408*, 307–310.
[6] D. P. Lane, *Nature* **1992**, *358*, 15–16.
[7] A. J. Levine, *Cell* **1997**, *88*, 323–331.
[8] R. K. Brachmann, K. Yu, Y. Eby, N. P. Pavletich, J. D. Boeke, *EMBO J.* **1998**, *17*, 1847–1859.
[9] T. Hernandez-Boussard, P. Rodriguez-Tome, R. Montesano, P. Hainaut, *Hum. Mutat.* **1999**, *14*, 1–8.
[10] S. Jin, A. J. Levine, *J. Cell Sci.* **2001**, *114*, 4139–4140.
[11] G. I. Evan, K. H. Vousden, *Nature* **2001**, *411*, 342–348.
[12] W. Maltzman, L. Czyzyk, *Mol. Cell. Biol.* **1984**, *4*, 1689–1694.
[13] S. Benchimol, P. Lamb, L. V. Crawford, D. Sheer, T. B. Shows, G. A. Bruns, J. Peacock, *Somatic Cell Mol. Genet.* **1985**, *11*, 505–510.
[14] C. Miller, T. Mohandas, D. Wolf, M. Prokocimer, V. Rotter, H. P. Koeffler, *Nature* **1986**, *319*, 783–784.
[15] D. Reisman, M. Greenberg, V. Rotter, *Proc. Natl. Acad. Sci. USA* **1988**, *85*, 5146–5150.
[16] T. Soussi, C. Caron de Fromentel, P. May, *Oncogene* **1990**, *5*, 945–952.
[17] T. Soussi, P. May, *J. Mol. Biol.* **1996**, *260*, 623–637.
[18] B. J. Mayer, R. Gupta, *Curr. Top. Microbiol. Immunol.* **1998**, *228*, 1–22.
[19] D. Sakamuro, P. Sabbatini, E. White, G. C. Prendergast, *Oncogene* **1997**, *15*, 887–898.

 © 2006 Wiley-VCH Verlag GmbH & Co. KGaA, Weinheim

[20] K. K. Walker, A. J. Levine, *Proc. Natl. Acad. Sci. USA* **1996**, *93*, 15335 – 15340.
[21] C. Venot, M. Maratrat, C. Dureuil, E. Conseiller, L. Bracco, L. Debussche, *EMBO J.* **1998**, *17*, 4668 – 4679.
[22] S. Fields, S. K. Jang, *Science* **1990**, *249*, 1046 – 1049.
[23] H. Lu, A. J. Levine, *Proc. Natl. Acad. Sci. USA* **1995**, *92*, 5154 – 5158.
[24] C. J. Thut, J. L. Chen, R. Klemm, R. Tjian, *Science* **1995**, *267*, 100 – 104.
[25] S. G. Lee, H. M. Rho, *Oncogene* **2000**, *19*, 468 – 471.
[26] P. H. Kussie, S. Gorina, V. Marechal, B. Elenbaas, J. Moreau, A. J. Levine, N. P. Pavletich, *Science* **1996**, *274*, 948 – 953.
[27] V. Bottger, A. Bottger, C. Garcia-Echeverria, Y. F. Ramos, A. J. van der Eb, A. G. Jochemsen, D. P. Lane, *Oncogene* **1999**, *18*, 189 – 199.
[28] M. Uesugi, G. L. Verdine, *Proc. Natl. Acad. Sci. USA* **1999**, *96*, 14801 – 14806.
[29] R. Truant, J. Antunovic, J. Greenblatt, C. Prives, J. A. Cromlish, *J. Virol.* **1995**, *69*, 1851 – 1859.
[30] S. Banin, L. Moyal, S. Shieh, Y. Taya, C. W. Anderson, L. Chessa, N. I. Smorodinsky, C. Prives, Y. Reiss, Y. Shiloh, Y. Ziv, *Science* **1998**, *281*, 1674 – 1677.
[31] W. L. Liu, C. Midgley, C. Stephen, M. Saville, D. P. Lane, *J. Mol. Biol.* **2001**, *313*, 711 – 731.
[32] S. Bell, C. Klein, L. Muller, S. Hansen, J. Buchner, *J. Mol. Biol.* **2002**, *322*, 917 – 927.
[33] R. Dawson, L. Muller, A. Dehner, C. Klein, H. Kessler, J. Buchner, *J. Mol. Biol.* **2003**, *332*, 1131 – 1141.
[34] H. Lee, K. H. Mok, R. Muhandiram, K. H. Park, J. E. Suk, D. H. Kim, J. Chang, Y. C. Sung, K. Y. Choi, K. H. Han, *J. Biol. Chem.* **2000**, *275*, 29426 – 29432.
[35] A. K. Dunker, J. D. Lawson, C. J. Brown, R. M. Williams, P. Romero, J. S. Oh, C. J. Oldfield, A. M. Campen, C. M. Ratliff, K. W. Hipps, J. Ausio, M. S. Nissen, R. Reeves, C. Kang, C. R. Kissinger, R. W. Bailey, M. D. Griswold, W. Chiu, E. C. Garner, Z. Obradovic, *J. Mol. Graphics Modell.* **2001**, *19*, 26 – 59.
[36] V. N. Uversky, J. R. Gillespie, A. L. Fink, *Proteins* **2000**, *41*, 415 – 427.
[37] H. J. Dyson, P. E. Wright, *Curr. Opin. Struct. Biol.* **2002**, *12*, 54 – 60.
[38] P. Chene, *Nat. Rev. Cancer* **2003**, *3*, 102 – 109.
[39] M. L. Geddie, T. L. O'Loughlin, K. K. Woods, I. Matsumura, *J. Biol. Chem.* **2005**, *280*, 35641 – 35646.
[40] J. Bargonetti, J. J. Manfredi, X. Chen, D. R. Marshak, C. Prives, *Genes Dev.* **1993**, *7*, 2565 – 2574.
[41] N. P. Pavletich, K. A. Chambers, C. O. Pabo, *Genes Dev.* **1993**, *7*, 2556 – 2564.
[42] T. R. Hupp, D. W. Meek, C. A. Midgley, D. P. Lane, *Cell* **1992**, *71*, 875 – 886.
[43] P. Wang, M. Reed, Y. Wang, G. Mayr, J. E. Stenger, M. E. Anderson, J. F. Schwedes, P. Tegtmeyer, *Mol. Cell. Biol.* **1994**, *14*, 5182 – 5191.
[44] P. Hainaut, A. Hall, J. Milner, *Oncogene* **1994**, *9*, 299 – 303.
[45] C. R. Johnson, P. E. Morin, C. H. Arrowsmith, E. Freire, *Biochemistry* **1995**, *34*, 5309 – 5316.
[46] M. G. Mateu, A. R. Fersht, *EMBO J.* **1998**, *17*, 2748 – 2758.
[47] M. G. Mateu, M. M. Sanchez Del Pino, A. R. Fersht, *Nat. Struct. Biol.* **1999**, *6*, 191 – 198.
[48] G. M. Clore, J. Ernst, R. Clubb, J. G. Omichinski, W. M. Kennedy, K. Sakaguchi, E. Appella, A. M. Gronenborn, *Nat. Struct. Biol.* **1995**, *2*, 321 – 333.
[49] W. Lee, T. S. Harvey, Y. Yin, P. Yau, D. Litchfield, C. H. Arrowsmith, *Nat. Struct. Biol.* **1994**, *1*, 877 – 890.
[50] P. D. Jeffrey, S. Gorina, N. P. Pavletich, *Science* **1995**, *267*, 1498 – 1502.
[51] R. L. Weinberg, D. B. Veprintsev, A. R. Fersht, *J. Mol. Biol.* **2004**, *341*, 1145 – 1159.
[52] T. S. Davison, X. Nie, W. Ma, Y. Lin, C. Kay, S. Benchimol, C. H. Arrowsmith, *J. Mol. Biol.* **2001**, *307*, 605 – 617.
[53] G. Shaulsky, N. Goldfinger, A. Ben Ze'ev, V. Rotter, *Mol. Cell. Biol.* **1990**, *10*, 6565 – 6577.
[54] J. Ahn, C. Prives, *Nat. Struct. Biol.* **2001**, *8*, 730 – 732.
[55] C. Klein, E. Planker, T. Diercks, H. Kessler, K. P. Kunkele, K. Lang, S. Hansen, M. Schwaiger, *J. Biol. Chem.* **2001**, *276*, 49020 – 49027.
[56] T. R. Hupp, D. P. Lane, *Cold Spring Harbor Symp. Quant. Biol.* **1994**, *59*, 195 – 206.
[57] T. R. Hupp, A. Sparks, D. P. Lane, *Cell* **1995**, *83*, 237 – 245.
[58] M. E. Anderson, B. Woelker, M. Reed, P. Wang, P. Tegtmeyer, *Mol. Cell. Biol.* **1997**, *17*, 6255 – 6264.
[59] R. L. Weinberg, S. M. Freund, D. B. Veprintsev, M. Bycroft, A. R. Fersht, *J. Mol. Biol.* **2004**, *342*, 801 – 811.
[60] P. May, E. May, *Oncogene* **1999**, *18*, 7621 – 7636.
[61] A. Friedler, D. B. Veprintsev, S. M. Freund, K. I. von Glos, A. R. Fersht, *Structure* **2005**, *13*, 629 – 636.
[62] W. Maltzman, L. Czyzyk, *Mol. Cell. Biol.* **1984**, *4*, 1689 – 1694.
[63] S. Hansen, T. R. Hupp, D. P. Lane, *J. Biol. Chem.* **1996**, *271*, 3917 – 3924.
[64] S. Hansen, D. P. Lane, C. A. Midgley, *J. Mol. Biol.* **1998**, *275*, 575 – 588.
[65] L. Muller, A. Schaupp, D. Walerych, H. Wegele, J. Buchner, *J. Biol. Chem.* **2004**, *279*, 48846 – 48854.
[66] D. Walerych, G. Kudla, M. Gutkowska, B. Wawrzynow, L. Muller, F. W. King, A. Helwak, J. Boros, A. Zylicz, M. Zylicz, *J. Biol. Chem.* **2004**, *279*, 48836 – 48845.
[67] N. M. Nichols, K. S. Matthews, *Biochemistry* **2002**, *41*, 170 – 178.
[68] K. Sakaguchi, H. Sakamoto, M. S. Lewis, C. W. Anderson, J. W. Erickson, E. Appella, D. Xie, *Biochemistry* **1997**, *36*, 10117 – 10124.
[69] Y. Y. Kim, B. J. Park, D. J. Kim, W. H. Kim, S. Kim, K. S. Oh, J. Y. Lim, J. Kim, C. Park, S. I. Park, *FEBS Lett.* **2004**, *572*, 92 – 98.
[70] S. Rudiger, S. M. Freund, D. B. Veprintsev, A. R. Fersht, *Proc. Natl. Acad. Sci. USA* **2002**, *99*, 11085 – 11090.
[71] Y. Peng, L. Chen, C. Li, W. Lu, J. Chen, *J. Biol. Chem.* **2001**, *276*, 40583 – 40590.
[72] C. Wang, J. Chen, *J. Biol. Chem.* **2003**, *278*, 2066 – 2071.
[73] M. Kaghad, H. Bonnet, A. Yang, L. Creancier, J. C. Biscan, A. Valent, A. Minty, P. Chalon, J. M. Lelias, X. Dumont, P. Ferrara, F. McKeon, D. Caput, *Cell* **1997**, *90*, 809 – 819.
[74] A. Yang, M. Kaghad, Y. Wang, E. Gillett, M. D. Fleming, V. Dotsch, N. C. Andrews, D. Caput, F. McKeon, *Mol. Cell* **1998**, *2*, 305 – 316.
[75] U. M. Moll, N. Slade, *Mol. Cancer Res.* **2004**, *2*, 371 – 386.
[76] G. Melino, X. Lu, M. Gasco, T. Crook, R. A. Knight, *Trends Biochem. Sci.* **2003**, *28*, 663 – 670.
[77] B. Trink, K. Okami, L. Wu, V. Sriuranpong, J. Jen, D. Sidransky, *Nat. Med.* **1998**, *4*, 747 – 748.
[78] A. Yang, M. Kaghad, D. Caput, F. McKeon, *Trends Genet.* **2002**, *18*, 90 – 95.
[79] S. W. Chi, A. Ayed, C. H. Arrowsmith, *EMBO J.* **1999**, *18*, 4438 – 4445.
[80] W. K. Wang, M. Bycroft, N. W. Foster, A. M. Buckle, A. R. Fersht, Y. W. Chen, *Acta Crystallogr. Sect. D* **2001**, *57*, 545 – 551.
[81] J. Schultz, C. P. Ponting, K. Hofmann, P. Bork, *Protein Sci.* **1997**, *6*, 249 – 253.
[82] F. N. Barrera, J. A. Poveda, J. M. Gonzalez-Ros, J. L. Neira, *J. Biol. Chem.* **2003**, *278*, 46878 – 46885.
[83] E. Balint, S. Bates, K. H. Vousden, *Oncogene* **1999**, *18*, 3923 – 3929.
[84] H. Lu, X. Zeng, L. Chen, C. A. Jost, R. Maya, D. Keller, X. Wang, W. G. Kaelin, M. Oren, J. Chen, *FASEB J.* **1999**, *13*, A1538.

 © 2006 Wiley-VCH Verlag GmbH & Co. KGaA, Weinheim

[85] M. Dohn, S. Z. Zhang, X. B. Chen, *Oncogene* **2001**, *20*, 3193 – 3205.
[86] J. Furrer, A. Enthart, A. Kühlewein, A. Dehner, C. Klein, S. Hansen, M. Schwaiger, H. Kessler, G. Gemmecker, *J. Biomol. NMR* **2003**, *26*, 377 – 378.
[87] C. Maisse, P. Guerrieri, G. Melino, *Biochem. Pharmacol.* **2003**, *66*, 1555 – 1561.
[88] N. Mondal, J. D. Parvin, *Cancer Biol. Ther.* **2005**, *4*, 414 – 418.
[89] E. R. Flores, S. Sengupta, J. B. Miller, J. J. Newman, R. Bronson, D. Crowley, A. Yang, F. McKeon, T. Jacks, *Cancer Cell* **2005**, *7*, 363 – 373.
[90] E. R. Flores, K. Y. Tsai, D. Crowley, S. Sengupta, A. Yang, F. McKeon, T. Jacks, *Nature* **2002**, *416*, 560 – 564.
[91] M. H. Brodsky, W. Nordstrom, G. Tsang, E. Kwan, G. M. Rubin, J. M. Abrams, *Cell* **2000**, *101*, 103 – 113.
[92] W. B. Derry, A. P. Putzke, J. H. Rothman, *Science* **2001**, *294*, 591 – 595.
[93] S. Jin, S. Martinek, W. S. Joo, J. R. Wortman, N. Mirkovic, A. Sali, M. D. Yandell, N. P. Pavletich, M. W. Young, A. J. Levine, *Proc. Natl. Acad. Sci. USA* **2000**, *97*, 7301 – 7306.
[94] M. Ollmann, L. M. Young, C. J. Di Como, F. Karim, M. Belvin, S. Robertson, K. Whittaker, M. Demsky, W. W. Fisher, A. Buchman, G. Duyk, L. Friedman, C. Prives, C. Kopczynski, *Cell* **2000**, *101*, 91 – 101.
[95] B. Schumacher, K. Hofmann, S. Boulton, A. Gartner, *Curr. Biol.* **2001**, *11*, 1722 – 1727.
[96] Y. Cho, S. Gorina, P. D. Jeffrey, N. P. Pavletich, *Science* **1994**, *265*, 346 – 355.
[97] A. Bullock, A. Fersht, *Nat. Rev. Cancer* **2001**, *1*, 68 – 76.
[98] C. L. Wei, Q. Wu, V. B. Vega, K. P. Chiu, P. Ng, T. Zhang, A. Shahab, H. C. Yong, Y. Fu, Z. Weng, J. Liu, X. D. Zhao, J. L. Chew, Y. L. Lee, V. A. Kuznetsov, W. K. Sung, L. D. Miller, B. Lim, E. T. Liu, Q. Yu, H. H. Ng, Y. Ruan, *Cell* **2006**, *124*, 207 – 219.
[99] A. K. Nagaich, V. B. Zhurkin, S. R. Durell, R. L. Jernigan, E. Appella, R. E. Harrington, *Proc. Natl. Acad. Sci. USA* **1999**, *96*, 1875 – 1880.
[100] P. Balagurumoorthy, H. Sakamoto, M. S. Lewis, N. Zambrano, G. M. Clore, A. M. Gronenborn, E. Appella, R. E. Harrington, *Proc. Natl. Acad. Sci. USA* **1995**, *92*, 8591 – 8595.
[101] R. L. Weinberg, D. B. Veprintsev, M. Bycroft, A. R. Fersht, *J. Mol. Biol.* **2005**, *348*, 589 – 596.
[102] D. B. Veprintsev, S. M. Freund, A. Andreeva, S. E. Rutledge, H. Tidow, J. M. Canadillas, C. M. Blair, A. R. Fersht, *Proc. Natl. Acad. Sci. USA* **2006**, *103*, 2115 – 2119.
[103] K. G. McLure, P. W. K. Lee, *EMBO J.* **1998**, *17*, 3342 – 3350.
[104] K. G. McLure, P. W. K. Lee, *EMBO J.* **1999**, *18*, 763 – 770.
[105] C. Klein, G. Georges, A. P. Künkele, R. Huber, R. A. Engh, S. Hansen, *J. Biol. Chem.* **2001**, *276*, 37390 – 37401.
[106] T. M. Rippin, S. M. V. Freund, D. B. Veprintsev, A. R. Fersht, *J. Mol. Biol.* **2002**, *319*, 351 – 358.
[107] K. Zhao, X. Chai, K. Johnston, A. Clements, R. Marmorstein, *J. Biol. Chem.* **2001**, *276*, 12120 – 12127.
[108] A. Dehner, C. Klein, S. Hansen, L. Muller, J. Buchner, M. Schwaiger, H. Kessler, *Angew. Chem.* **2005**, *117*, 5381 – 5386; *Angew. Chem. Int. Ed.* **2005**, *44*, 5247 – 5251.
[109] C. Prives, J. Bargonetti, G. Farmer, E. Ferrari, P. Friedlander, Y. Wang, L. Jayaraman, N. Pavletich, U. Hubscher, *Cold Spring Harbor Symp. Quant. Biol.* **1994**, *59*, 207 – 213.
[110] C. H. Arrowsmith, P. Morin, *Oncogene* **1996**, *12*, 1379.
[111] A. Lebrun, R. Lavery, H. Weinstein, *Protein Eng.* **2001**, *14*, 233 – 243.
[112] B. Ma, Y. Pan, K. Gunasekaran, R. B. Venkataraghavan, A. J. Levine, R. Nussinov, *Proc. Natl. Acad. Sci. USA* **2005**, *102*, 3988 – 3993.
[113] P. N. Friedman, X. Chen, J. Bargonetti, C. Prives, *Proc. Natl. Acad. Sci. USA* **1993**, *90*, 3319 – 3323.
[114] W. C. Ho, M. X. Fitzgerald, R. Marmorstein, *J. Biol. Chem.* **2006**, *281*, 20494 – 20502.
[115] X. Wang, D. C. Christiani, J. K. Wiencke, M. Fischbein, X. Xu, T. J. Cheng, E. Mark, J. C. Wain, K. T. Kelsey, *Cancer Epidemiol. Biomarkers Prev.* **1995**, *4*, 543 – 548.
[116] M. Olivier, R. Eeles, M. Hollstein, M. A. Khan, C. C. Harris, P. Hainaut, *Hum. Mutat.* **2002**, *19*, 607 – 614.
[117] J. M. Varley, *Hum. Mutat.* **2003**, *21*, 313 – 320.
[118] P. Campomenosi, P. Monti, A. Aprile, A. Abbondandolo, T. Frebourg, B. Gold, T. Crook, A. Inga, M. A. Resnick, R. Iggo, G. Fronza, *Oncogene* **2001**, *20*, 3573 – 3579.
[119] Y. Tomita, N. Marchenko, S. Erster, A. Nemajerova, A. Dehner, C. Klein, H. Pan, H. Kessler, P. Pancoska, U. M. Moll, *J. Biol. Chem.* **2006**, *281*, 8600 – 8606.
[120] M. Hollstein, D. Sidransky, B. Vogelstein, C. C. Harris, *Science* **1991**, *253*, 49 – 53.
[121] M. Hollstein, K. Rice, M. S. Greenblatt, T. Soussi, R. Fuchs, T. Sorlie, E. Hovig, B. Smith-Sorensen, R. Montesano, C. C. Harris, *Nucleic Acids Res.* **1994**, *22*, 3551 – 3555.
[122] P. Hainaut, T. Soussi, B. Shomer, M. Hollstein, M. Greenblatt, E. Hovig, C. C. Harris, R. Montesano, *Nucleic Acids Res.* **1997**, *25*, 151 – 157.
[123] W. D. Funk, D. T. Pak, R. H. Karas, W. E. Wright, *Mol. Cell. Biol.* **1992**, *12*, 2866 – 2871.
[124] A. Sigal, V. Rotter, *Cancer Res.* **2000**, *60*, 6788 – 6793.
[125] G. A. Lang, T. Iwakuma, Y. A. Suh, G. Liu, V. A. Rao, J. M. Parant, Y. A. Valentin-Vega, T. Terzian, L. C. Caldwell, L. C. Strong, A. K. El Naggar, G. Lozano, *Cell* **2004**, *119*, 861 – 872.
[126] T. Gohler, S. Jager, G. Warnecke, H. Yasuda, E. Kim, W. Deppert, *Nucleic Acids Res.* **2005**, *33*, 1087 – 1100.
[127] L. Jayaraman, C. Prives, *Cell. Mol. Life Sci.* **1999**, *55*, 76 – 87.
[128] J. H. Bayle, B. Elenbaas, A. J. Levine, *Proc. Natl. Acad. Sci. USA* **1995**, *92*, 5729 – 5733.
[129] J. Milner, *Trends Biochem. Sci.* **1995**, *20*, 49.
[130] A. N. Bullock, J. Henckel, A. R. Fersht, *Oncogene* **2000**, *19*, 1245 – 1256.
[131] C. J. Di Como, C. Prives, *Oncogene* **1998**, *16*, 2527 – 2539.
[132] C. L. Brooks, W. Gu, *Curr. Opin. Cell Biol.* **2003**, *15*, 164 – 171.
[133] A. M. Bode, Z. Dong, *Nat. Rev. Cancer* **2004**, *4*, 793 – 805.
[134] E. Appella, C. W. Anderson, *Eur. J. Biochem.* **2001**, *268*, 2764 – 2772.
[135] W. T. Steegenga, A. J. van der Eb, A. G. Jochemsen, *J. Mol. Biol.* **1996**, *263*, 103 – 113.
[136] C. E. Helt, W. Wang, P. C. Keng, R. A. Bambara, *Cell Cycle* **2005**, *4*, 529 – 532.
[137] T. Caspari, *Curr. Biol.* **2000**, *10*, R315-R317.
[138] S. Y. Shieh, M. Ikeda, Y. Taya, C. Prives, *Cell* **1997**, *91*, 325 – 334.
[139] C. Blattner, E. Tobiasch, M. Litfen, H. J. Rahmsdorf, P. Herrlich, *Oncogene* **1999**, *18*, 1723 – 1732.
[140] T. Thompson, C. Tovar, H. Yang, D. Carvajal, B. T. Vu, Q. Xu, G. M. Wahl, D. C. Heimbrook, L. T. Vassilev, *J. Biol. Chem.* **2004**, *279*, 53015 – 53022.
[141] W. Gu, X. L. Shi, R. G. Roeder, *Nature* **1997**, *387*, 819 – 823.
[142] W. Gu, R. G. Roeder, *Cell* **1997**, *90*, 595 – 606.
[143] S. R. Grossman, *Eur. J. Biochem.* **2001**, *268*, 2773 – 2778.
[144] N. A. Barlev, L. Liu, N. H. Chehab, K. Mansfield, K. G. Harris, T. D. Halazonetis, S. L. Berger, *Mol. Cell* **2001**, *8*, 1243 – 1254.
[145] C. Prives, J. L. Manley, *Cell* **2001**, *107*, 815 – 818.
[146] J. Luo, A. Y. Nikolaev, S. Imai, D. Chen, F. Su, A. Shiloh, L. Guarente, W. Gu, *Cell* **2001**, *107*, 137 – 148.
[147] H. Vaziri, S. K. Dessain, E. E. Ng, S. I. Imai, R. A. Frye, T. K. Pandita, L. Guarente, R. A. Weinberg, *Cell* **2001**, *107*, 149 – 159.
[148] W. Gu, J. Luo, C. L. Brooks, A. Y. Nikolaev, M. Li, *Novartis Found. Symp.* **2004**, *259*, 197 – 205.
[149] V. Jesenberger, S. Jentsch, *Nat. Rev. Mol. Cell Biol.* **2002**, *3*, 112 – 121.

© 2006 Wiley-VCH Verlag GmbH & Co. KGaA, Weinheim

[150] S. Fang, J. P. Jensen, R. L. Ludwig, K. H. Vousden, A. M. Weissman, *J. Biol. Chem.* **2000**, *275*, 8945 – 8951.
[151] C. J. Sherr, *Nat. Rev. Mol. Cell Biol.* **2001**, *2*, 731 – 737.
[152] M. H. Kubbutat, K. H. Vousden, *Mol. Med. Today* **1998**, *4*, 250 – 256.
[153] S. L. Harris, A. J. Levine, *Oncogene* **2005**, *24*, 2899 – 2908.
[154] M. Li, C. L. Brooks, F. Wu-Baer, D. Chen, R. Baer, W. Gu, *Science* **2003**, *302*, 1972 – 1975.
[155] M. Li, D. Chen, A. Shiloh, J. Luo, A. Y. Nikolaev, J. Qin, W. Gu, *Nature* **2002**, *416*, 648 – 653.
[156] M. Li, C. L. Brooks, N. Kon, W. Gu, *Mol. Cell* **2004**, *13*, 879 – 886.
[157] D. Chen, N. Kon, M. Li, W. Zhang, J. Qin, W. Gu, *Cell* **2005**, *121*, 1071 – 1083.
[158] D. Dornan, I. Wertz, H. Shimizu, D. Arnott, G. D. Frantz, P. Dowd, O. R. K, H. Koeppen, V. M. Dixit, *Nature* **2004**, *429*, 86 – 92.
[159] R. P. Leng, Y. Lin, W. Ma, H. Wu, B. Lemmers, S. Chung, J. M. Parant, G. Lozano, R. Hakem, S. Benchimol, *Cell* **2003**, *112*, 779 – 791.
[160] A. Shmueli, M. Oren, *Cell* **2005**, *121*, 963 – 965.
[161] M. S. Rodriguez, J. M. Desterro, S. Lain, C. A. Midgley, D. P. Lane, R. T. Hay, *EMBO J.* **1999**, *18*, 6455 – 6461.
[162] M. Gostissa, A. Hengstermann, V. Fogal, P. Sandy, S. E. Schwarz, M. Scheffner, G. Del Sal, *EMBO J.* **1999**, *18*, 6462 – 6471.
[163] F. Melchior, L. Hengst, *Cell Cycle* **2002**, *1*, 245 – 249.
[164] J. W. Harper, *Cell* **2004**, *118*, 2 – 4.
[165] D. P. Xirodimas, M. K. Saville, J. C. Bourdon, R. T. Hay, D. P. Lane, *Cell* **2004**, *118*, 83 – 97.
[166] P. Shaw, J. Freeman, R. Bovey, R. Iggo, *Oncogene* **1996**, *12*, 921 – 930.
[167] J. Wesierska-Gadek, A. Bugajska-Schretter, C. Cerni, *J. Cell. Biochem.* **1996**, *62*, 90 – 101.
[168] K. Sakaguchi, J. E. Herrera, S. Saito, T. Miki, M. Bustin, A. Vassilev, C. W. Andersen, E. Appella, *Genes Dev.* **1998**, *12*, 2831 – 2841.
[169] J. Luo, M. Li, Y. Tang, M. Laszkowska, R. G. Roeder, W. Gu, *Proc. Natl. Acad. Sci. USA* **2004**, *101*, 2259 – 2264.
[170] K. H. Vousden, X. Lu, *Nat. Rev. Cancer* **2002**, *2*, 594 – 604.
[171] J. Momand, D. Jung, S. Wilczynski, J. Niland, *Nucleic Acids Res.* **1998**, *26*, 3453 – 3459.
[172] J. Momand, H. H. Wu, G. Dasgupta, *Gene* **2000**, *242*, 15 – 29.
[173] T. Juven-Gershon, M. Oren, *Mol. Med.* **1999**, *5*, 71 – 83.
[174] D. A. Freedman, C. B. Epstein, J. C. Roth, A. J. Levine, *Mol. Med.* **1997**, *3*, 248 – 259.
[175] S. M. Picksley, B. Vojtesek, A. Sparks, D. P. Lane, *Oncogene* **1994**, *9*, 2523 – 2529.
[176] J. Chen, V. Marechal, A. J. Levine, *Mol. Cell. Biol.* **1993**, *13*, 4107 – 4114.
[177] M. Uesugi, G. L. Verdine, *Proc. Natl. Acad. Sci. USA* **1999**, *96*, 14801 – 14806.
[178] O. Schon, A. Friedler, M. Bycroft, S. M. Freund, A. R. Fersht, *J. Mol. Biol.* **2002**, *323*, 491 – 501.
[179] O. Schon, A. Friedler, S. Freund, A. R. Fersht, *J. Mol. Biol.* **2004**, *336*, 197 – 202.
[180] M. A. McCoy, J. J. Gesell, M. M. Senior, D. F. Wyss, *Proc. Natl. Acad. Sci. USA* **2003**, *100*, 1645 – 1648.
[181] M. W. Jackson, S. J. Berberich, *Mol. Cell. Biol.* **2000**, *20*, 1001 – 1007.
[182] R. Stad, N. A. Little, D. P. Xirodimas, R. Frenk, A. J. van der Eb, D. P. Lane, M. K. Saville, A. G. Jochemsen, *EMBO Rep.* **2001**, *2*, 1029 – 1034.
[183] J. Parant, A. Chavez-Reyes, N. A. Little, W. Yan, V. Reinke, A. G. Jochemsen, G. Lozano, *Nat. Genet.* **2001**, *29*, 92 – 95.
[184] J. C. Marine, A. G. Jochemsen, *Biochem. Biophys. Res. Commun.* **2005**, *331*, 750 – 760.
[185] S. Uhrinova, D. Uhrin, H. Powers, K. Watt, D. Zheleva, P. Fischer, C. McInnes, P. N. Barlow, *J. Mol. Biol.* **2005**, *350*, 587 – 598.
[186] L. T. Vassilev, B. T. Vu, B. Graves, D. Carvajal, F. Podlaski, Z. Filipovic, N. Kong, U. Kammlott, C. Lukacs, C. Klein, N. Fotouhi, E. A. Liu, *Science* **2004**, *303*, 844 – 848.
[187] D. C. Fry, S. D. Emerson, S. Palme, B. T. Vu, C. M. Liu, F. Podlaski, *J. Biomol. NMR* **2004**, *30*, 163 – 173.
[188] J. Buchner, *Cell. Mol. Life Sci.* **2002**, *59*, 1587 – 1588.
[189] S. Walter, J. Buchner, *Angew. Chem.* **2002**, *114*, 1142 – 1158; *Angew. Chem. Int. Ed.* **2002**, *41*, 1098 – 1113.
[190] C. Georgopoulos, W. J. Welch, *Annu. Rev. Cell Biol.* **1993**, *9*, 601 – 634.
[191] B. Bukau, A. L. Horwich, *Cell* **1998**, *92*, 351 – 366.
[192] J. Jiang, K. Prasad, E. M. Lafer, R. Sousa, *Mol. Cell* **2005**, *20*, 513 – 524.
[193] R. P. Beckmann, L. E. Mizzen, W. J. Welch, *Science* **1990**, *248*, 850 – 854.
[194] J. Frydman, E. Nimmesgern, K. Ohtsuka, F. U. Hartl, *Nature* **1994**, *370*, 111 – 117.
[195] J. P. Hendrick, F. U. Hartl, *Annu. Rev. Biochem.* **1993**, *62*, 349 – 384.
[196] A. Mogk, T. Tomoyasu, P. Goloubinoff, S. Rudiger, D. Roder, H. Langen, B. Bukau, *EMBO J.* **1999**, *18*, 6934 – 6949.
[197] H. Wegele, L. Muller, J. Buchner, *Rev. Physiol. Biochem. Pharmacol.* **2004**, *151*, 1 – 44.
[198] T. R. Hupp, D. P. Lane, K. L. Ball, *Biochem. J.* **2000**, *352 Pt 1*, 1 – 17.
[199] F. W. King, A. Wawrzynow, J. Hohfeld, M. Zylicz, *EMBO J.* **2001**, *20*, 6297 – 6305.
[200] K. Sugito, M. Yamane, H. Hattori, Y. Hayashi, I. Tohnai, M. Ueda, N. Tsuchida, K. Ohtsuka, *FEBS Lett.* **1995**, *358*, 161 – 164.
[201] M. Zylicz, F. W. King, A. Wawrzynow, *EMBO J.* **2001**, *20*, 4634 – 4638.
[202] S. Akakura, M. Yoshida, Y. Yoneda, S. Horinouchi, *J. Biol. Chem.* **2001**, *276*, 14649 – 14657.
[203] K. Helmbrecht, E. Zeise, L. Rensing, *Cell Proliferation* **2000**, *33*, 341 – 365.
[204] A. Zaika, N. Marchenko, U. M. Moll, *J. Biol. Chem.* **1999**, *274*, 27474 – 27480.
[205] U. M. Moll, A. G. Ostermeyer, R. Haladay, B. Winkfield, M. Frazier, G. Zambetti, *Mol. Cell. Biol.* **1996**, *16*, 1126 – 1137.
[206] B. T. Lai, N. W. Chin, A. E. Stanek, W. Keh, K. W. Lanks, *Mol. Cell. Biol.* **1984**, *4*, 2802 – 2810.
[207] W. J. Welch, J. R. Feramisco, *J. Biol. Chem.* **1982**, *257*, 14949 – 14959.
[208] T. Scheibel, S. Neuhofen, T. Weikl, C. Mayr, J. Reinstein, P. D. Vogel, J. Buchner, *J. Biol. Chem.* **1997**, *272*, 18608 – 18613.
[209] L. Whitesell, S. L. Lindquist, *Nat. Rev. Cancer* **2005**, *5*, 761 – 772.
[210] M. V. Blagosklonny, J. Toretsky, S. Bohen, L. Neckers, *Proc. Natl. Acad. Sci. USA* **1996**, *93*, 8379 – 8383.
[211] B. Sepehrnia, I. B. Paz, G. Dasgupta, J. Momand, *J. Biol. Chem.* **1996**, *271*, 15084 – 15090.
[212] L. Whitesell, P. D. Sutphin, E. J. Pulcini, J. D. Martinez, P. H. Cook, *Mol. Cell. Biol.* **1998**, *18*, 1517 – 1524.
[213] Y. Nagata, T. Anan, T. Yoshida, T. Mizukami, Y. Taya, T. Fujiwara, H. Kato, H. Saya, M. Nakao, *Oncogene* **1999**, *18*, 6037 – 6049.
[214] S. Adimoolam, J. M. Ford, *DNA Repair* **2003**, *2*, 947 – 954.
[215] H. Offer, R. Wolkowicz, D. Matas, S. Blumenstein, Z. Livneh, V. Rotter, *FEBS Lett.* **1999**, *450*, 197 – 204.
[216] J. Zhou, J. Ahn, S. H. Wilson, C. Prives, *EMBO J.* **2001**, *20*, 914 – 923.
[217] S. A. Amundson, T. G. Myers, A. J. Fornace, Jr., *Oncogene* **1998**, *17*, 3287 – 3299.

 © 2006 Wiley-VCH Verlag GmbH & Co. KGaA, Weinheim

[218] L. A. Donehower, *J. Cell. Physiol.* **2002**, *192*, 23 – 33.
[219] N. D. Marchenko, A. Zaika, U. M. Moll, *J. Biol. Chem.* **2000**, *275*, 16202 – 16212.
[220] G. Lozano, G. P. Zambetti, *J. Pathol.* **2005**, *205*, 206 – 220.
[221] L. D. Attardi, L. A. Donehower, *Mutat. Res.* **2005**, *576*, 4 – 21.
[222] S. D. Tyner, S. Venkatachalam, J. Choi, S. Jones, N. Ghebranious, H. Igelmann, X. Lu, G. Soron, B. Cooper, C. Brayton, P. S. Hee, T. Thompson, G. Karsenty, A. Bradley, L. A. Donehower, *Nature* **2002**, *415*, 45 – 53.
[223] I. Varela, J. Cadinanos, A. M. Pendas, A. Gutierrez-Fernandez, A. R. Folgueras, L. M. Sanchez, Z. Zhou, F. J. Rodriguez, C. L. Stewart, J. A. Vega, K. Tryggvason, J. M. Freije, C. Lopez-Otin, *Nature* **2005**, *437*, 564 – 568.
[224] U. M. Moll, S. Wolff, D. Speidel, W. Deppert, *Curr. Opin. Cell Biol.* **2005**, *17*, 631 – 636.
[225] L. J. Hofseth, A. I. Robles, Q. Yang, X. W. Wang, S. P. Hussain, C. Harris, *Chest* **2004**, *125*, 83S-85S.
[226] I. Garcia-Cao, M. Garcia-Cao, J. Martin-Caballero, L. M. Criado, P. Klatt, J. M. Flores, J. C. Weill, M. A. Blasco, M. Serrano, *EMBO J.* **2002**, *21*, 6225 – 6235.
[227] J. Campisi, *Nat. Rev. Cancer* **2003**, *3*, 339 – 349.
[228] M. B. Kastan, O. Onyekwere, D. Sidransky, B. Vogelstein, R. W. Craig, *Cancer Res.* **1991**, *51*, 6304 – 6311.
[229] A. Di Leonardo, S. P. Linke, K. Clarkin, G. M. Wahl, *Genes Dev.* **1994**, *8*, 2540 – 2551.
[230] S. P. Linke, K. C. Clarkin, G. M. Wahl, *Cancer Res.* **1997**, *57*, 1171 – 1179.
[231] N. F. Mathon, A. C. Lloyd, *Nat. Rev. Cancer* **2001**, *1*, 203 – 213.
[232] P. Giannakakou, D. L. Sackett, Y. Ward, K. R. Webster, M. V. Blagosklonny, T. Fojo, *Nat. Cell Biol.* **2000**, *2*, 709 – 717.
[233] R. M. Buey, J. F. Diaz, J. M. Andreu, A. O'Brate, P. Giannakakou, K. C. Nicolaou, P. K. Sasmal, A. Ritzen, K. Namoto, *Chem. Biol.* **2004**, *11*, 225 – 236.
[234] P. Giannakakou, M. Nakano, K. C. Nicolaou, A. O'Brate, I. Yu, M. V. Blagosklonny, U. F. Greber, T. Fojo, *Proc. Natl. Acad. Sci. USA* **2002**, *99*, 10855.
[235] A. O'Brate, P. Giannakakou, *Drug Resist. Updates* **2003**, *6*, 313 – 322.
[236] J. M. Stommel, N. D. Marchenko, G. S. Jimenez, U. M. Moll, T. J. Hope, G. M. Wahl, *EMBO J.* **1999**, *18*, 1660 – 1672.
[237] Y. P. Zhang, Y. Xiong, *Science* **2001**, *292*, 1910 – 1915.
[238] D. A. Freedman, A. J. Levine, *Cancer Res.* **1999**, *59*, 1 – 7.
[239] M. Mihara, U. M. Moll, *Methods Mol. Biol.* **2003**, *234*, 203 – 209.
[240] A. M. Petros, A. Gunasekera, N. Xu, E. T. Olejniczak, S. W. Fesik, *FEBS Lett.* **2004**, *559*, 171 – 174.
[241] J. Edelman, J. Nemunaitis, *Curr. Opin. Mol. Ther.* **2003**, *5*, 611 – 617.
[242] A. G. Zeimet, K. Riha, J. Berger, M. Widschwendter, M. Hermann, G. Daxenbichler, C. Marth, *Biochem. Pharmacol.* **2000**, *60*, 1153 – 1163.
[243] A. C. Joerger, H. C. Ang, D. B. Veprintsev, C. M. Blair, A. R. Fersht, *J. Biol. Chem.* **2005**, *280*, 16030 – 16037.
[244] A. M. Wieczorek, J. L. Waterman, M. J. Waterman, T. D. Halazonetis, *Nat. Med.* **1996**, *2*, 1143 – 1146.
[245] P. V. Nikolova, K. B. Wong, B. DeDecker, J. Henckel, A. R. Fersht, *EMBO J.* **2000**, *19*, 370 – 378.
[246] P. V. Nikolova, J. Henckel, D. P. Lane, A. R. Fersht, *Proc. Natl. Acad. Sci. USA* **1998**, *95*, 14675 – 14680.
[247] A. C. Joerger, M. D. Allen, A. R. Fersht, *J. Biol. Chem.* **2004**, *279*, 1291 – 1296.
[248] A. N. Bullock, J. Henckel, B. S. DeDecker, C. M. Johnson, P. V. Nikolova, M. R. Proctor, D. P. Lane, A. R. Fersht, *Proc. Natl. Acad. Sci. USA* **1997**, *94*, 14338 – 14342.
[249] C. R. Brown, L. Q. Hong-Brown, W. J. Welch, *J. Clin. Invest.* **1997**, *99*, 1432 – 1444.
[250] D. Maurici, P. Monti, P. Campomenosi, S. North, T. Frebourg, G. Fronza, P. Hainaut, *Oncogene* **2001**, *20*, 3533 – 3540.
[251] S. North, O. Pluquet, D. Maurici, F. El Ghissassi, P. Hainaut, *Mol. Carcinog.* **2002**, *33*, 181 – 188.
[252] K. Ohnishi, I. Ota, A. Takahashi, T. Ohnishi, *Br. J. Cancer* **2000**, *83*, 1735 – 1739.
[253] T. Ohnishi, K. Ohnishi, X. Wang, A. Takahashi, K. Okaichi, *Radiat. Res.* **1999**, *151*, 498 – 500.
[254] T. Ohnishi, H. Matsumoto, X. Wang, A. Takahashi, T. Tamamoto, K. Ohnishi, *Int. J. Radiat. Biol.* **1999**, *75*, 1095 – 1098.
[255] V. J. Bykov, G. Selivanova, K. G. Wiman, *Eur. J. Cancer* **2003**, *39*, 1828 – 1834.
[256] B. A. Foster, H. A. Coffey, M. J. Morin, F. Rastinejad, *Science* **1999**, *286*, 2507 – 2510.
[257] M. L. Smith, A. J. Fornace, *Cancer Biol. Ther.* **2002**, 47 – 55.
[258] Y. Luu, G. Li, *J. Invest. Dermatol.* **2002**, *119*, 1207 – 1209.
[259] Y. Luu, J. Bush, K. J. Cheung, Jr., G. Li, *Exp. Cell Res.* **2002**, *276*, 214 – 222.
[260] R. Takimoto, W. Wang, D. T. Dicker, F. Rastinejad, J. Lyssikatos, W. S. El-Deiry, *Cancer Biol. Ther.* **2002**, 47 – 55.
[261] M. J. Demma, S. Wong, E. Maxwell, B. Dasmahapatra, *J. Biol. Chem.* **2004**, *279*, 45887 – 45896.
[262] J. Wischhusen, U. Naumann, H. Ohgaki, F. Rastinejad, M. Weller, *Oncogene* **2003**, *22*, 8233 – 8245.
[263] T. M. Rippin, V. J. Bykov, S. M. Freund, G. Selivanova, K. G. Wiman, A. R. Fersht, *Oncogene* **2002**, *21*, 2119 – 2129.
[264] S. Tanner, A. Barberis, *J. Negat. Results Biomed.* **2004**, *3*, 5.
[265] Y. Li, Y. Mao, P. W. Brandt-Rauf, A. C. Williams, R. L. Fine, *Mol. Cancer Ther.* **2005**, *4*, 901 – 909.
[266] V. J. Bykov, N. Issaeva, G. Selivanova, K. G. Wiman, *Carcinogenesis* **2002**, *23*, 2011 – 2018.
[267] V. J. Bykov, N. Zache, H. Stridh, J. Westman, J. Bergman, G. Selivanova, K. G. Wiman, *Oncogene* **2005**, *24*, 3484 – 3491.
[268] M. C. Myers, J. Wang, J. A. Iera, J. K. Bang, T. Hara, S. Saito, G. P. Zambetti, D. H. Appella, *J. Am. Chem. Soc.* **2005**, *127*, 6152 – 6153.
[269] V. J. Bykov, N. Issaeva, N. Zache, A. Shilov, M. Hultcrantz, J. Bergman, G. Selivanova, K. G. Wiman, *J. Biol. Chem.* **2005**, *280*, 30384 – 30391.
[270] S. Gorina, N. P. Pavletich, *Science* **1996**, *274*, 1001 – 1005.
[271] A. Friedler, L. O. Hansson, D. B. Veprintsev, S. M. Freund, T. M. Rippin, P. V. Nikolova, M. R. Proctor, S. Rudiger, A. R. Fersht, *Proc. Natl. Acad. Sci. USA* **2002**, *99*, 937 – 942.
[272] A. Friedler, B. S. DeDecker, S. M. Freund, C. Blair, S. Rudiger, A. R. Fersht, *J. Mol. Biol.* **2004**, *336*, 187 – 196.
[273] N. Issaeva, A. Friedler, P. Bozko, K. G. Wiman, A. R. Fersht, G. Selivanova, *Proc. Natl. Acad. Sci. USA* **2003**, *100*, 13303 – 13307.
[274] A. Friedler, D. B. Veprintsev, L. O. Hansson, A. R. Fersht, *J. Biol. Chem.* **2003**, *278*, 24108 – 24112.
[275] A. Lakkaraju, J. M. Dubinsky, W. C. Low, Y. E. Rahman, *J. Biol. Chem.* **2001**, *276*, 32000 – 32007.
[276] M. V. Blagosklonny, *Int. J. Cancer* **2002**, *98*, 161 – 166.
[277] E. A. Komarova, A. V. Gudkov, *Semin. Cancer Biol.* **1998**, *8*, 389 – 400.
[278] P. G. Komarov, E. A. Komarova, R. V. Kondratov, K. Christov-Tselkov, J. S. Coon, M. V. Chernov, A. V. Gudkov, *Science* **1999**, *285*, 1733 – 1737.
[279] E. A. Komarova, A. V. Gudkov, *Biochemistry* **2000**, *65*, 41 – 48.
[280] C. Culmsee, X. Zhu, Q. S. Yu, S. L. Chan, S. Camandola, Z. Guo, N. H. Greig, M. P. Mattson, *J. Neurochem.* **2001**, *77*, 220 – 228.
[281] A. Gudkov, P. Komarov, E. Komarova, *Patentschrift* **2000**, 00-02104.
[282] L. Bassi, M. Carloni, E. Fonti, N. Palma de la Pena, R. Meschini, F. Palitti, *Mutat. Res.* **2002**, *499*, 163 – 176.
[283] A. V. Gudkov, E. A. Komarova, *Biochem. Biophys. Res. Commun.* **2005**, *331*, 726 – 736.

© 2006 Wiley-VCH Verlag GmbH & Co. KGaA, Weinheim

[284] E. A. Komarova, A. V. Gudkov, *Biochem. Pharmacol.* **2001**, *62*, 657 – 667.
[285] J. P. Blaydes, V. Gire, J. M. Rowson, D. Wynford-Thomas, *Oncogene* **1997**, *14*, 1859 – 1868.
[286] A. Bottger, V. Bottger, A. Sparks, W. L. Liu, S. F. Howard, D. P. Lane, *Curr Biol* **1997**, *7*, 860 – 869.
[287] L. Chen, W. Lu, S. Agrawal, W. Zhou, R. Zhang, J. Chen, *Mol. Med.* **1999**, *5*, 21 – 34.
[288] T. Geiger, D. Husken, J. Weiler, F. Natt, K. A. Woods-Cook, J. Hall, D. Fabbro, *Anti-Cancer Drug Des.* **2000**, *15*, 423 – 430.
[289] H. Wang, X. Zeng, P. Oliver, L. P. Le, J. Chen, L. Chen, W. Zhou, S. Agrawal, R. Zhang, *Int. J. Oncol.* **1999**, *15*, 653 – 660.
[290] H. Wang, L. Nan, D. Yu, S. Agrawal, R. Zhang, *Clin. Cancer Res.* **2001**, *7*, 3613 – 3624.
[291] Z. Zhang, M. Li, H. Wang, S. Agrawal, R. Zhang, *Proc. Natl. Acad. Sci. USA* **2003**, *100*, 11636 – 11641.
[292] U. M. Moll, O. Petrenko, *Mol. Cancer Res.* **2003**, *1*, 1001 – 1008.
[293] R. Montes de Oca Luna, D. S. Wagner, G. Lozano, *Nature* **1995**, *378*, 203 – 206.
[294] S. N. Jones, A. E. Roe, L. A. Donehower, A. Bradley, *Nature* **1995**, *378*, 206 – 208.
[295] S. M. Mendrysa, M. K. McElwee, J. Michalowski, K. A. O'Leary, K. M. Young, M. E. Perry, *Mol. Cell. Biol.* **2003**, *23*, 462 – 472.
[296] Z. Lai, K. V. Ferry, M. A. Diamond, K. E. Wee, Y. B. Kim, J. Ma, T. Yang, P. A. Benfield, R. A. Copeland, K. R. Auger, *J. Biol. Chem.* **2001**, *276*, 31357 – 31367.
[297] I. V. Davydov, D. Woods, Y. J. Safiran, P. Oberoi, H. O. Fearnhead, S. Fang, J. P. Jensen, A. M. Weissman, J. H. Kenten, K. H. Vousden, *J. Biomol. Screening* **2004**, *9*, 695 – 703.
[298] V. Bottger, A. Bottger, S. F. Howard, S. M. Picksley, P. Chene, C. Garcia-Echeverria, H. K. Hochkeppel, D. P. Lane, *Oncogene* **1996**, *13*, 2141 – 2147.
[299] A. Bottger, V. Bottger, C. Garcia-Echeverria, P. Chene, H. K. Hochkeppel, W. Sampson, K. Ang, S. F. Howard, S. M. Picksley, D. P. Lane, *J. Mol. Biol.* **1997**, *269*, 744 – 756.
[300] C. Garcia-Echeverria, P. Chene, M. J. Blommers, P. Furet, *J. Med. Chem.* **2000**, *43*, 3205 – 3208.
[301] M. R. Arkin, J. A. Wells, *Nat. Rev. Drug Discovery* **2004**, *3*, 301 – 317.
[302] P. L. Toogood, *J. Med. Chem.* **2002**, *45*, 1543 – 1558.
[303] A. G. Cochran, *Chem. Biol.* **2000**, *7*, 85 – 94.
[304] H. Yin, A. D. Hamilton, *Angew. Chem.* **2005**, *117*, 4200 – 4235; *Angew. Chem. Int. Ed.* **2005**, *44*, 4130 – 4163.
[305] R. Stoll, C. Renner, S. Hansen, S. Palme, C. Klein, A. Belling, W. Zeslawski, M. Kamionka, T. Rehm, P. Muhlhahn, R. Schumacher, F. Hesse, B. Kaluza, W. Voelter, R. A. Engh, T. A. Holak, *Biochemistry* **2001**, *40*, 336 – 344.
[306] S. K. Kumar, E. Hager, C. Pettit, H. Gurulingappa, N. E. Davidson, S. R. Khan, *J. Med. Chem.* **2003**, *46*, 2813 – 2815.
[307] J. Zhao, M. Wang, J. Chen, A. Luo, X. Wang, M. Wu, D. Yin, Z. Liu, *Cancer Lett.* **2002**, *183*, 69 – 77.
[308] J. A. Kritzer, R. Zutshi, M. Cheah, F. A. Ran, R. Webman, T. M. Wongjirad, A. Schepartz, *ChemBioChem* **2006**, *7*, 29 – 31.
[309] S. J. Duncan, M. A. Cooper, D. H. Williams, *Chem. Commun.* **2003**, 316 – 317.
[310] D. P. Lane, P. M. Fischer, *Nature* **2004**, *427*, 789 – 790.
[311] N. Fotouhi, B. Graves, *Curr. Top. Med. Chem.* **2005**, *5*, 159 – 165.
[312] P. Raboisson, J. J. Marugan, C. Schubert, H. K. Koblish, T. Lu, S. Zhao, M. R. Player, A. C. Maroney, R. L. Reed, N. D. Huebert, J. Lattanze, D. J. Parks, M. D. Cummings, *Bioorg. Med. Chem. Lett.* **2005**, *15*, 1857 – 1861.
[313] B. L. Grasberger, T. Lu, C. Schubert, D. J. Parks, T. E. Carver, H. K. Koblish, M. D. Cummings, L. V. LaFrance, K. L. Milkiewicz, R. R. Calvo, D. Maguire, J. Lattanze, C. F. Franks, S. Zhao, K. Ramachandren, G. R. Bylebyl, M. Zhang, C. L. Manthey, E. C. Petrella, M. W. Pantoliano, I. C. Deckman, J. C. Spurlino, A. C. Maroney, B. E. Tomczuk, C. J. Molloy, R. F. Bone, *J. Med. Chem.* **2005**, *48*, 909 – 912.
[314] D. J. Parks, L. V. LaFrance, R. R. Calvo, K. L. Milkiewicz, V. Gupta, J. Lattanze, K. Ramachandren, T. E. Carver, E. C. Petrella, M. D. Cummings, D. Maguire, B. L. Grasberger, T. Lu, *Bioorg. Med. Chem. Lett.* **2005**, *15*, 765 – 770.
[315] K. Ding, Y. Lu, Z. Nikolovska-Coleska, S. Qiu, Y. Ding, W. Gao, J. Stuckey, K. Krajewski, P. P. Roller, Y. Tomita, D. A. Parrish, J. R. Deschamps, S. Wang, *J. Am. Chem. Soc.* **2005**, *127*, 10130 – 10131.
[316] I. R. Hardcastle, S. U. Ahmed, H. Atkins, A. H. Calvert, N. J. Curtin, G. Farnie, B. T. Golding, R. J. Griffin, S. Guyenne, C. Hutton, P. Kallblad, S. J. Kemp, M. S. Kitching, D. R. Newell, S. Norbedo, J. S. Northen, R. J. Reid, K. Saravanan, H. M. Willems, J. Lunec, *Bioorg. Med. Chem. Lett.* **2005**, *15*, 1515 – 1520.
[317] H. Yin, A. D. Hamilton, *Angew. Chem.* **2005**, *117*, 4200 – 4235; *Angew. Chem. Int. Ed.* **2005**, *44*, 4130 – 4163.
[318] R. Fasan, R. L. Dias, K. Moehle, O. Zerbe, J. W. Vrijbloed, D. Obrecht, J. A. Robinson, *Angew. Chem.* **2004**, *116*, 2161 – 2164; *Angew. Chem. Int. Ed.* **2004**, *43*, 2109 – 2112.
[319] J. A. Kritzer, J. D. Lear, M. E. Hodsdon, A. Schepartz, *J. Am. Chem. Soc.* **2004**, *126*, 9468 – 9469.
[320] J. A. Kritzer, M. E. Hodsdon, A. Schepartz, *J. Am. Chem. Soc.* **2005**, *127*, 4118 – 4119.
[321] K. Sakurai, H. S. Chung, D. Kahne, *J. Am. Chem. Soc.* **2004**, *126*, 16288 – 16289.
[322] M. Krajewski, P. Ozdowy, L. D'Silva, U. Rothweiler, T. A. Holak, *Nat. Med.* **2005**, *11*, 1135 – 1136.
[323] Y. Yang, R. L. Ludwig, J. P. Jensen, S. A. Pierre, M. V. Medaglia, I. V. Davydov, Y. J. Safiran, P. Oberoi, J. H. Kenten, A. C. Phillips, A. M. Weissman, K. H. Vousden, *Cancer Cell* **2005**, *7*, 547 – 559.
[324] S. R. Grossman, M. E. Deato, C. Brignone, H. M. Chan, A. L. Kung, H. Tagami, Y. Nakatani, D. M. Livingston, *Science* **2003**, *300*, 342 – 344.
[325] A. Shmueli, M. Oren, *Mol. Cell* **2004**, *13*, 4 – 5.
[326] D. P. Lane, T. R. Hupp, *Drug Discov. Today* **2003**, *8*, 347 – 55.
[327] D. Lane, *Carcinogenesis* **2004**, *25*, 1077 – 1081.

 © 2006 Wiley-VCH Verlag GmbH & Co. KGaA, Weinheim

VIP Nanostructures

DOI: 10.1002/anie.200601779

Diameter-Tunable CdTe Nanotubes Templated by 1D Nanowires of Cadmium Thiolate Polymer**

*Haijun Niu and Mingyuan Gao**

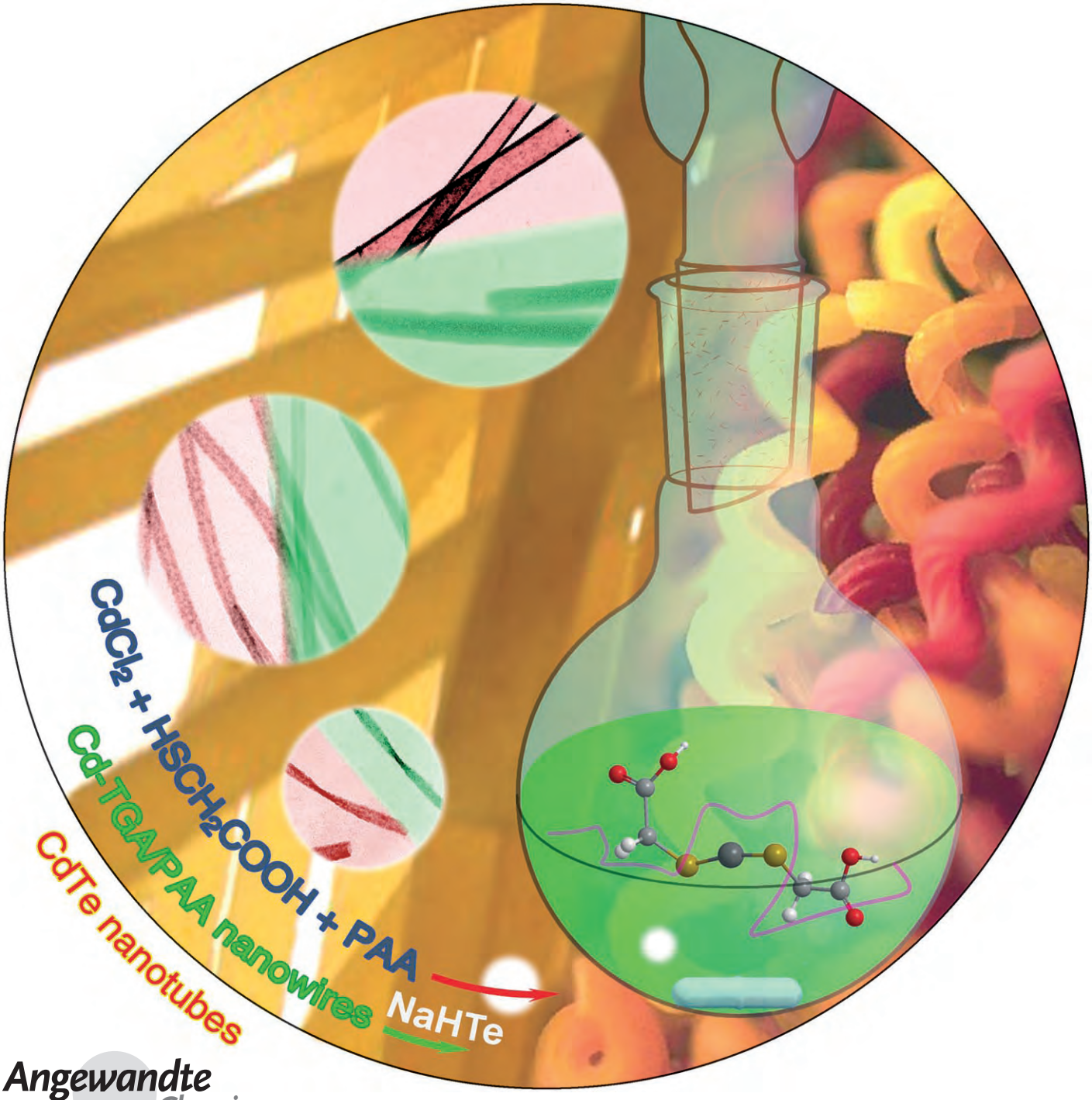

WILEY InterScience DISCOVER SOMETHING GREAT

© 2006 Wiley-VCH Verlag GmbH & Co. KGaA, Weinheim

Nanotubes are intensively investigated owing to their potential applications in electronics, optoelectronics, energy storage, sensing, and nanodevices.[1] Different types of inorganic nanotubes have so far been prepared by various approaches including vapor–liquid–solid,[2] hydrothermal,[3] and high-temperature methods,[4] as well as template methods based on hard mesoporous materials,[5] soft self-organized nanostructures,[6] or low-dimensional sacrificial precursors.[7] Among them, the sacrificial template approach offers such advantages as 1) by consuming the template upon replacement reactions, hollow products with the original shape of the templates can be prepared; 2) many reactions taking place under mild conditions in solution can be adopted; 3) the approach is typically characterized by a one-step process, which can lead to relatively pure products in comparison with the hard-template route that requires additional post-processing procedures to remove the templates; and 4) massive products can principally be produced, which is important with respect to technical applications. However, only very few 1D nanomaterials have so far been found to be suitable as sacrificial templates for nanotubes in comparison with their spherical counterparts.[7]

The design and synthesis of metal-driven 1D supramolecular structures has been of increasing interest owing to their potential applications.[8] Though 1D coordination chains are commonly seen as the structural motifs of bulk crystals, some isolated single coordinate chains with distinct 1D structures and even bundles of them can be formed in solution by interchain interactions.[9] Therefore, isolated 1D coordination polymer chains or chain bundles could reasonably be expected to act as a new type of sacrificial templates for 1D inorganic nanostructures upon further chemical reactions using the metal ions in the 1D chains as precursors.

Since the first report on the use of thioglycolic acid as the stabilizing agents for highly fluorescent water-soluble CdTe nanocrystals,[10] different types of mercaptocarboxylic acids have widely been adopted in the syntheses of CdTe quantum dots[11] and CdTe nanowires.[12] Previous studies have demonstrated that some mercaptocarboxylic acids can form complicated complexes with cadmium ions, with primary coordination of cadmium ions to the thiol groups and a secondary coordination to the carboxylic groups.[13] This dual coordination not only plays an important role in enhancing the fluorescence efficiency of the CdTe nanocrystals but also has an impact on the formation of 1D CdTe nanowires.[11,12b]

Following on from these investigations, we report herein the preparation of isolated 1D nanostructures with controllable diameters and morphologies formed by Cd^{2+} ions and thioglycolic acid (TGA) complexes and demonstrate that the resultant 1D Cd–TGA nanowires are suitable sacrificial templates for synthesizing long CdTe nanotubes.

In a typical synthesis, equimolar quantities of $CdCl_2$ and thioglycolic acid were mixed in water at a concentration of 6.5×10^{-3} M. The resultant turbid solution was heated at reflux after its pH value was adjusted to 11 using 1M NaOH. Nanowires were gradually formed in the solution at reflux (see Supporting Information for more details). Transmission electron microscopy (TEM) investigations demonstrated that the sample obtained after 3 hours of heating at reflux (sample 1) appeared as nanobelts, with a relatively uniform thickness of about 8 nm (Figure 1a). The typical width of the belts was in the range of 19–40 nm. Additionally, a high percentage of the nanobelts exhibited a helical structure.

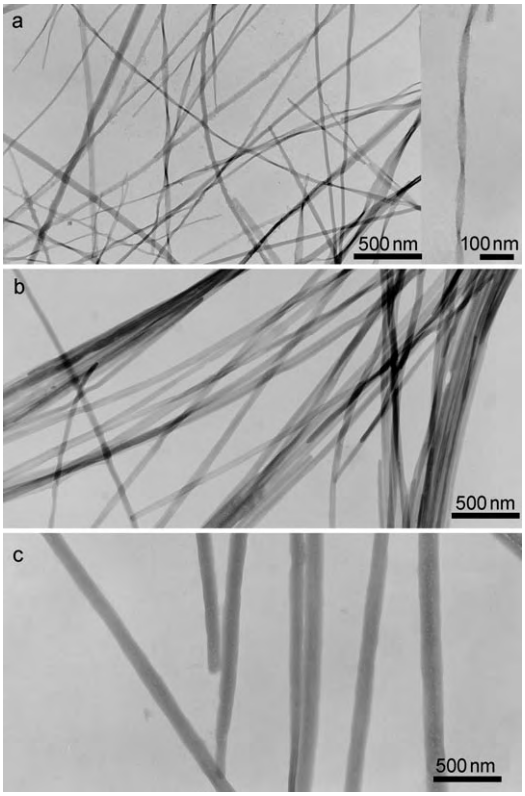

Figure 1. TEM images of 1D Cd–TGA nanowires prepared a) in the absence of PAA (sample 1) and b,c) in the presence of PAA using Cd/TGA/AA molar ratios of 1:1:0.1 (b; sample 2) and 1:1:0.3 (c; sample 3). The inset in part (a) shows a typical helical Cd–TGA nanobelt obtained in sample 1.

To further tune the diameter of the 1D Cd–TGA structures, poly(acrylic acid) sodium salt (PAA, $M_w = 5100$) was introduced into the reaction system. Figure 1b and c show the TEM images of two additional samples prepared in the presence of PAA by using molar ratios of Cd/TGA/AA (AA is the repeat unit of PAA) of 1:1:0.1 (sample 2) and 1:1:0.3 (sample 3). As expected, the average diameter of the nanowires could substantially be increased as a function of the amount of PAA. The average diameters of the nanowires in

[*] H. Niu, Prof. M. Y. Gao
Institute of Chemistry, CAS
Zhong Guan Cun, Bei Yi Jie 2
Beijing 100080 (P.R. China)
Fax: (+86) 108-261-3214
E-mail: gaomy@iccas.ac.cn

[**] The current investigations were financially supported by NSFC projects (20225313, 90206024).

Supporting information for this article is available on the WWW under http://www.angewandte.org or from the author.

 © 2006 Wiley-VCH Verlag GmbH & Co. KGaA, Weinheim

samples 2 and 3 were 55 ± 12 nm and 132 ± 25 nm, respectively. Moreover, these nanowires did not show helical structures such as those in sample 1.

Upon introduction of NaHTe, the aqueous dispersion of the aforementioned Cd–TGA nanobelts became dark brown, indicating the formation of nanometer-sized CdTe. TEM results demonstrated that the nanobelts were completely converted into tubular structures after reacting with NaHTe, as can be seen from the broken end of the 1D structures shown in the insets of Figure 2a. In general, the nanotubes

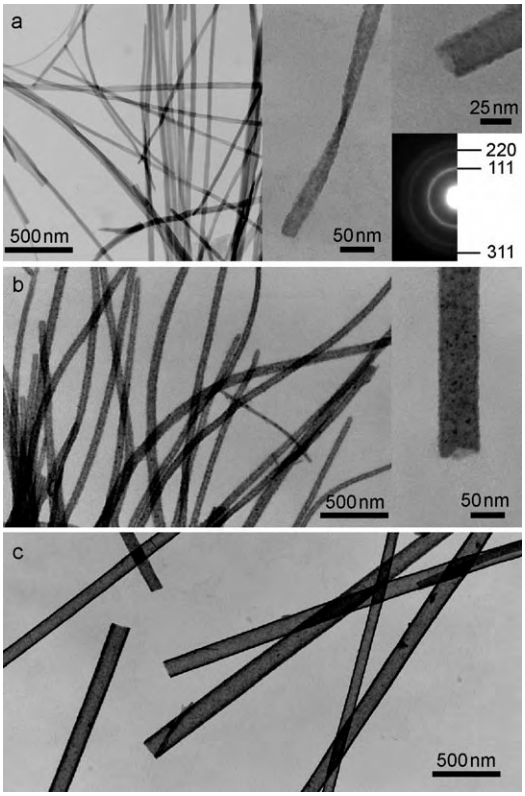

Figure 2. TEM images of CdTe nanotubes obtained by introducing NaHTe into the aqueous dispersions of samples a) 1, b) 2, and c) 3. The insets show TEM images taken under higher magnifications as well as an electron diffraction pattern of the nanotubes presented in part (a).

preserved the initial sizes and morphologies of their precursors. In some cases, the helical feature of the precursors was also retained. Statistical results indicated that the inner and outer diameters of the nanotubes were in the ranges of 12–20 nm and 30–50 nm, respectively. The electron diffraction patterns of these nanotubes suggest that the CdTe adopts a cubic structure. The atomic ratio of Cd to Te in these nanotubes was determined to be roughly 1:1.1 by energy dispersive X-ray spectroscopy. Note that the preparative procedures for CdTe nanotubes described here are significantly different from those reported by Wang and co-workers for CdTe nanowires,[12b] even though similar reaction conditions were used. In that case, however, NaHTe was introduced prior to the formation of the Cd–TGA nanowires.

Further experimental results also demonstrated that the 1D Cd–TGA precursors obtained in the presence of PAA (samples 2 and 3) could also be converted into CdTe nanotubes (Figure 2b and c), independent of the initial diameter. The length of these tubes was typically hundreds of micrometers, quite similar to the initial length of the precursors. It is reasonable to suggest that the formation of CdTe nanotubes generally follows the mechanism for the sacrificial template approach, as the Cd–TGA complex is a common precursor for CdTe nanocrystals.[10–12] During the formation of CdTe, 1D Cd–TGA precursors were gradually consumed, which finally led to the hollow structures shown in Figure 2, while the original shape of the 1D templates was preserved.

In fact, cadmium thiolates have been intensively investigated. 1D chainlike structures formed by cadmium ions and various types of thiol ligands have been found in the macrocrystals of cadmium coordination polymers.[13–14] Typically, the molar ratio of cadmium to thiol ligand in such 1D chainlike coordination polymers is universally 1:2; that is, cadmium atoms are linked by pairs of doubly bridging thiolate ligands. However, additional coordination may also exist. For example, Dance et al. demonstrated that in the linear chain structures formed by $[Cd^{II}(\mu\text{-}SCH_2COOCH_2CH_3)_2]_\infty$, the primary coordination of each cadmium atom is $Cd(\mu\text{-}SR)_4$.[13] In addition, four carboxylic oxygen atoms coordinate with cadmium forming dodecahedrons alternated by tetrahedrons of $Cd(\mu\text{-}SR)_4$.[13] According to their calculations, the two CdS_2 primary coordination planes in the dodecahedron are almost orthogonal (87.1°). As TGA is structurally very similar to $HSCH_2COOCH_2CH_3$, it is reasonable to believe that the Cd–TGA complexes here adopt a similar coordination structure in which the carboxylic groups will be concentrated along the *a* axis as shown in Figure 3. Therefore,

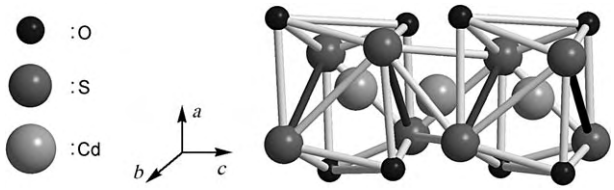

Figure 3. Illustration of the possible coordination structures in 1D Cd–TGA complexes, according to the crystalline structure of $[Cd(\mu\text{-}SCH_2COOCH_2CH_3)_2]_\infty$.[13]

the single Cd–TGA polymeric chains quite possibly present anisotropic aggregation behaviors along the *a* and *b* axes, which leads to the formation of the belt structure (Figure 1a). On the other hand, the helix in the nanobelts is introduced by the non-perpendicular intersection between the two adjacent CdS_2 primary coordination planes along each single Cd–TGA polymer chain.

Although the crystalline structure of the $[Cd(\mu\text{-}SCH_2COOCH_2CH_3)_2]_\infty$ coordination polymer can explain the formation of one-dimensional and helical belt structures in Cd–TGA, such 1D coordination polymer chains were previously observed only in bulk crystals with a Cd/S ratio of 1:2. However, our experimental studies revealed that the

 © 2006 Wiley-VCH Verlag GmbH & Co. KGaA, Weinheim

isolated 1D Cd–TGA nanowires were better formed under a Cd/S feed ratio of 1:1, independent of the presence of PAA. Therefore, it is important to know the Cd/S ratio in the different types of nanowires shown in Figure 1. X-ray photoelectron spectroscopy (XPS) was employed initially to determine the compositional evolution in the helical nanowires during their formation. The results shown in Table 1

Table 1: Variation of the Cd/S atomic ratio in Cd–TGA complexes with the duration of heating at reflux.

t [h]	Cd/S ratio (XPS)
0.0	1:1.0
0.5	1:1.2
1.0	1:1.4
2.0	1:1.7
3.0	1:2.1

reveal that the Cd/S ratio decreases with the reflux time and approaches 1:2.1 for those nanowires shown in Figure 1a. It can thus be concluded that Cd^{2+} and TGA tend to form 1:2 linear coordination structures, similar to $[Cd(\mu\text{-}SCH_2COOCH_2CH_3)_2]_\infty$, and that the non-stoichiometric addition of Cd^{2+} and TGA leads to isolated 1D nanowires rather than bulk crystals. Such non-stoichiometric addition of cationic and anionic ions is commonly adopted for synthesizing inorganic nanoparticles.

In principle, PAA can not only form hydrogen bonds with Cd–TGA chains but also coordinate with cadmium ions on the polymer backbone by replacing the carboxylic groups from TGA. Such a process enabled the diameter of the 1D Cd–TGA chain bundles to be tunable in the presence of PAA. Because PAA is a multichelating agent and as cadmium ions were present in excess in the reaction mixture, additional cadmium ions were brought into the gaps between Cd–TGA chains. As a result, the ordering level in pure Cd–TGA chain bundles decreased as demonstrated by powder X-ray diffraction studies (see Supporting Information). In the meantime, the Cd/S ratio in the resultant nanowires increased against the feeding amount of PAA (see Table 2). All these experimental

Table 2: Variation of Cd/S atomic ratio in 1D Cd–TGA nanowires shown in Figure 1 with the amount of PAA.

Sample	Cd/TGA/AA (feed molar ratio)	Cd/S ratio (XPS)
1	1:1:0.0	1:2.1
2	1:1:0.1	1:1.3
3	1:1:0.3	1:1.2

results suggest that PAA cross-links the 1D Cd–TGA chains in perpendicular directions by introducing additional Cd^{2+} ions into the gaps of Cd–TGA chains. Consequently, the helical structure formed by pure Cd–TGA complexes is lost.

To further demonstrate the potential of the diameter-tunable 1D Cd–TGA nanowires, they were also employed as sacrificial templates in preparing CdS and HgS nanotubes. With respect to the preparations of CdS nanotubes, Na_2S was introduced instead of NaHTe into an aqueous dispersion of sample 2. TEM measurements demonstrated that hollow nanotubes formed by cubic CdS were successfully obtained. By introducing $HgCl_2$ into the aqueous dispersion of CdS nanotubes under stirring, HgS nanotubes were formed through cation exchange (solubility product constants: $K_{sp}(HgS) = 1.6 \times 10^{-52}$; $K_{sp}(CdS) = 8 \times 10^{-27}$). The resultant HgS nanotubes were also of cubic structure (see Supporting Information for more details).

In summary, we have synthesized diameter-tunable 1D nanowires formed from Cd–TGA coordination polymer and PAA, and further demonstrated that these 1D nanowires can be used as sacrificial templates for synthesizing long CdTe nanotubes of different diameters. The key point for synthesizing the isolated 1D metal-driven nanowires is the non-stoichiometric addition of metal ions and thiolic ligands. The diameter tunability by PAA mainly relies on the weak intermolecular interactions between PAA and Cd–TGA polymer chains. To put the present results into greater perspective, many types of supramolecular structures formed by metal-coordination compounds could be tailored in a similar way to form low-dimensional sacrificial precursors for hollow inorganic nanostructures.

Received: May 6, 2006
Revised: June 27, 2006
Published online: August 9, 2006

Keywords: cadmium · coordination polymers · nanostructures · nanotubes · template synthesis

[1] a) T. W. Ebbesen, H. J. Lezec, H. Hiura, J. W. Bennett, H. F. Ghaemi, T. Thio, *Nature* **1996**, *382*, 54; b) P. M. Ajayan, *Chem. Rev.* **1999**, *99*, 1787; c) J. Kong, N. R. Franklin, C. Zhou, M. G. Chapline, S. Peng, K. Cho, H. Dai, *Science* **2000**, *287*, 622; d) J. Chen, S. L. Li, Z. L. Tao, Y. T. Shen, C. X. Cui, *J. Am. Chem. Soc.* **2003**, *125*, 5284.
[2] E. P. A. M. Bakkers, M. A. Verheijen, *J. Am. Chem. Soc.* **2003**, *125*, 3440.
[3] a) X. Wang, J. Zhuang, J. Chen, K. Zhou, Y. D. Li, *Angew. Chem.* **2004**, *116*, 2051; *Angew. Chem. Int. Ed.* **2004**, *43*, 2017; b) A. W. Xu, Y. P. Fang, L. P. You, H. Q. Liu, *J. Am. Chem. Soc.* **2003**, *125*, 1494.
[4] M. Nath, C. N. R. Rao, *J. Am. Chem. Soc.* **2001**, *123*, 4841.
[5] G. Wu, L. Zhang, B. Cheng, T. Xie, X. Yuan, *J. Am. Chem. Soc.* **2004**, *126*, 5976.
[6] M. Harada, M. Adachi, *Adv. Mater.* **2000**, *12*, 839.
[7] a) J. J. Miao, T. Ren, L. Dong, J. J. Zhu, H. Y. Chen, *Small* **2005**, *1*, 802; b) X. Li, H. Chu, Y. Li, *J. Solid State Chem.* **2006**, *179*, 96; c) Y. Sun, B. Mayers, Y. Xia, *Adv. Mater.* **2003**, *15*, 641; d) Y. Yin, R. M. Rious, C. K. Erdonmez, S. Hughes, G. A. Somorjai, A. P. Alivisatos, *Science* **2004**, *304*, 711.
[8] a) O. Kahn, C. J. Martinez, *Science* **1998**, *279*, 44; b) K. T. Wong, J. M. Lehn, S. M. Peng, G. H. Lee, *Chem. Commun.* **2000**, 2259; c) K. Kuroiwa, T. Shibata, A. Takada, N. Nemoto, N. Kimizuka, *J. Am. Chem. Soc.* **2004**, *126*, 2016.
[9] a) D. Olea, S. S. Alexandre, P. Ano-Ochoa, A. Guijarro, F. Jesús, J. M. Soler, P. J. Pablo, F. Zamora, J. Gómez-Herrero, *Adv. Mater.* **2000**, *12*, 1761; b) X. Zhang, Y. Xie, Q. Zhao, Y. Tian, *New J. Chem.* **2003**, *27*, 827; c) N. Kimizuka, N. Oda, T. Kunitake, *Inorg. Chem.* **2000**, *39*, 2684.

 © 2006 Wiley-VCH Verlag GmbH & Co. KGaA, Weinheim

[10] M. Y. Gao, S. Kirstein, H. Möhwald, *J. Phys. Chem. B* **1998**, *102*, 8360.
[11] a) H. Zhang, Z. Zhou, B. Yang, M. Y. Gao, *J. Phys. Chem. B* **2003**, *107*, 8; b) N. Gaponik, D. V. Talapin, A. L. Rogach, K. Hoppe, E. V. Shevchenko, A. Kornowski, A. Eychmüller, H. Weller, *J. Phys. Chem. B* **2002**, *106*, 7177.
[12] a) Z. Tang, N. A. Kotov, M. Giersig, *Science* **2002**, *297*, 237; b) H. Zhang, D. Wang, H. Möhwald, *Angew. Chem.* **2006**, *118*, 762; *Angew. Chem. Int. Ed.* **2006**, *45*, 748.
[13] I. G. Dance, M. L. Scudder, R. Secomb, *Inorg. Chem.* **1983**, *22*, 1794.
[14] a) O. F. Z. Khan, P. O'Brien, *Polyhedron* **1991**, *10*, 325; b) J. C. Bayón, M. C. Briansó, J. L. Briansó, P. González Duarte, *Inorg. Chem.* **1979**, *18*, 3478.

 © 2006 Wiley-VCH Verlag GmbH & Co. KGaA, Weinheim

Two-Photon Absorption

DOI: 10.1002/anie.200602266

Boron-Containing Two-Photon-Absorbing Chromophores: Electronic Interaction through the Cyclodiborazane Core**

Ali Hayek, Jean-François Nicoud, Frédéric Bolze, Cyril Bourgogne, and Patrice L. Baldeck*

Conception of novel chromophores exhibiting two-photon absorption (TPA) is of growing importance nowadays due to the great variety of applications of this nonlinear optical (NLO) property,[1] which include two-photon excited fluorescence (TPEF) microscopy of biological systems,[2] three-dimensional microfabrication,[3] optical limiting,[4] data storage, and photodynamic therapy.[5] Since the prediction of this phenomenon by Göppert-Mayer in 1931,[6] many theoretical studies have been made on mono- and multidimensional chromophores.[7] Experimentally, symmetrical one-dimensional chromophores typically consist of two donor or acceptor groups that interact through a conjugated system. For example, the donor–acceptor–donor and acceptor–donor–acceptor chromophores described by Marder et al. can be regarded as π-conjugated molecules that undergo large changes in quadrupole moment on excitation.[8] Another approach was proposed by Andraud, Baldeck et al., who pointed out that TPA cross sections of oligomers are enhanced by biexcitonic coupling between two weakly conjugated monomers.[9] This theoretical approach led to the molecular engineering of several new efficient TPA chromophores and, in our hands, to water-soluble TPEF chromophores for bioimaging.[10]

In most cases the electronic interaction proceeds via conjugated systems. Recently, some computational studies have shown that the traditional π-conjugated transmitter in hyperpolarizable donor–acceptor systems could be replaced by a system of σ bonds to give π–σ–π through-bond coupling.[11] Furthermore, experimental data on 1,3-bis(diphenylmethylene)cyclobutane (Scheme 1a) have shown that

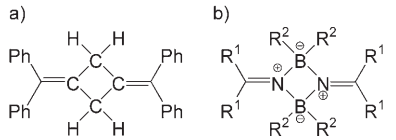

Scheme 1. 1,3-Bis(diphenylmethylene)cyclobutane (a) and cyclodiborazanes (b).

in such a structure the two π systems interact electronically through the 1,3-dimethylenecyclobutane core.[12] Cyclodiborazanes (Scheme 1b), widely studied by Chujo et al., mainly for the preparation of conjugated polymers, are heteroatomic analogues of 1,3-dimethylenecyclobutane derivatives.[13] Many of the cyclodiborazane-based polymers are fluorescent and electroluminescent. They were also expected to show interesting third-order NLO properties.[13b] These experimental results suggested that the cyclodiborazane core maintains some kind of conjugation (1,3-π-type interaction) between the π systems across its square structure.

We report here the synthesis and characterization of a new TPA chromophore containing a cyclodiborazane central core. Our aim was to check the influence of this unusual structure on the efficiency of TPA properties due to electronic coupling through such a pseudoconjugated system. Our target chromophore **1** is shown in Figure 1.

Bis(4-iodophenyl)cyclodiborazane core **4** was obtained in 60% yield by classical hydroboration dimerization of 4-iodobenzonitrile (**2**) with mesitylborane (**3**; Scheme 2).[13a] Product **4** was obtained as a mixture of two stereoisomers in a 1:1 ratio (^{1}H NMR spectrum in the Supporting Information). Considering the different substituents in the cyclodiborazane structure, **4** can exist as four stereoisomers (Scheme 3).[14] The mesityl groups can be *cis* or *trans* with respect to each other, and the Ar groups can be in *syn* or *anti* configurations. Thus, *cis-syn* (**A**), *cis-anti* (**B**), *trans-syn* (**C**),

[*] A. Hayek, Prof. Dr. J.-F. Nicoud, Dr. F. Bolze, Dr. C. Bourgogne
Institut de Physique et Chimie des Matériaux de Strasbourg
Groupe des Matériaux Organiques (UMR 7504)
23 rue du Loess, BP 43, 67034 Strasbourg cedex 2 (France)
Fax: (+33) 388-107-246
E-mail: nicoud@ipcms.u-strasbg.fr
Dr. P. L. Baldeck
Laboratoire de Spectrométrie Physique
Université Joseph Fourier, CNRS (UMR 5588)
BP 87, 38402 Saint Martin d'Hères (France)
Fax: (+33) 476-635-495
E-mail: baldeck@ujf-grenoble.fr

[**] Boron-Containing Two-Photon-Absorbing Chromophores, Part 1. This work was supported by the CNRS and University Louis Pasteur of Strasbourg. A.H. is grateful to the French ministry of research for a fellowship. We thank Prof. Dr. R. Welter and Dr. A. De Cian for the solution of the X-ray crystal structure.

Supporting information for this article is available on the WWW under http://www.angewandte.org or from the author.

InterScience
© 2006 Wiley-VCH Verlag GmbH & Co. KGaA, Weinheim

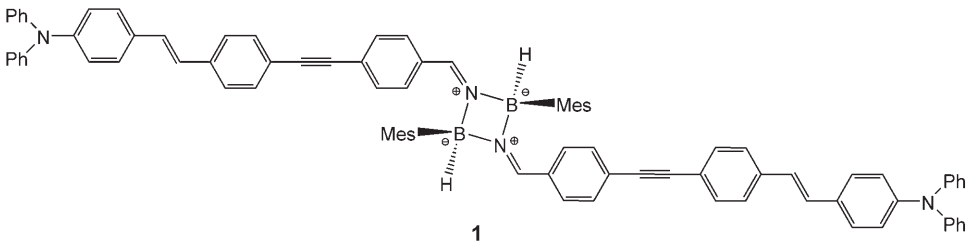

Figure 1. Structure of chromophore **1**.

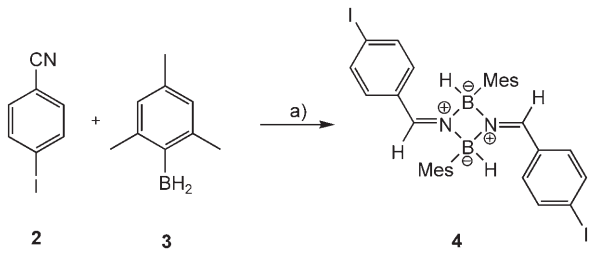

Scheme 2. Synthesis of bis(4-iodophenyl)cyclodiborazane core **4**. a) THF, 0 °C, 15 min; 25 °C, 12 h; 60%.

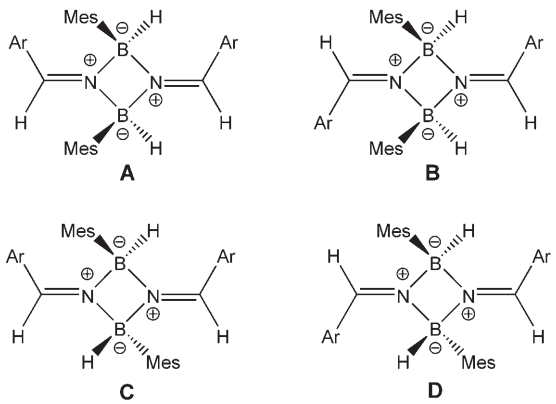

Scheme 3. Possible stereoisomers of tetrasubstituted cyclodiborazanes.

and *trans-anti* (**D**) stereoisomers are possible. The *trans-syn* and *trans-anti* isomers (**C** and **D**) have been proposed as the most stable, but with no experimental evidence. We calculated the heats of formation for each stereoisomer by the AM1 method and found 269.0, 247.5, 238.7, and 232.0 kJ mol^{-1} for **A**, **B**, **C**, and **D** respectively.[15] These computational results clearly show that the *cis* arrangement of the mesityl groups in **A** and **B** is disfavored. Since we obtained only two stereoisomers for **4**, we can deduce that it consists of a mixture of **C** and **D**.

The synthesis of chromophore **1** is shown in Scheme 4. (*E*)-4-Iodo-4′-diphenylaminostilbene (**7**) was prepared by Wadsworth–Emmons condensation between commercially available 4-(diphenylamino)benzaldehyde (**5**) and diethyl 4-iodobenzylphosphonate (**6**) in the presence of sodium hydride. Trimethylsilylacetylene was subjected to Sonogashira coupling with **7** to give **8** in 85% yield. The trimethylsilyl (TMS) group was removed by tetrabutylammonium fluoride (TBAF) in THF to yield ethynyl derivative **9**. Sonogashira coupling of **4** with 4-diphenylamino-4′-ethynylstilbene (**9**) led to a mixture of two stereoisomers, from which stereopure chromophore **1** was isolated in 55% yield after

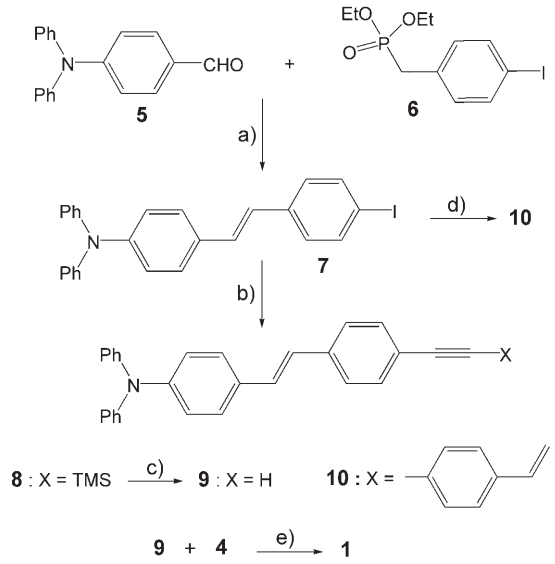

Scheme 4. Synthesis of chromophore **1** and model compound **10**. a) NaH, THF, 3 h, 55→66 °C, 85%; b) $Me_3SiC{\equiv}CH$, $[PdCl_2(PPh_3)_2]$ 6 mol%, CuI 10 mol%, THF/iPr_2NH, RT, 48 h, 90%; c) TBAF, THF, 15 min, RT, 80%; d) 4-ethynylstyrene, $[PdCl_2(PPh_3)_2]$ 6 mol%, CuI 10 mol%, NEt_3, RT, 70%; e) $PdCl_2$ 10 mol%, $Cu(OAc)_2{\cdot}H_2O$ 1.5 mol%, PPh_3 40 mol%, THF, Et_3N, 80 °C, 12 h, 70%.

column chromatography. It was fully characterized by ^{1}H, ^{11}B, and ^{13}C NMR and IR spectroscopy and HRMS. In the ^{1}H NMR spectrum, the imino resonance is located at $\delta =$ 8.1 ppm, as already reported for other cyclodiborazane structures.[16] The protons linked to boron give a very broad signal around 5.3 ppm. The ^{11}B NMR signal appears at $\delta =$ 5.6 ppm. Complete NMR characteristics are given in the Supporting Information. In the IR spectrum, the C=N band at 1641 cm^{-1} and B–H band at 2390 cm^{-1} are in agreement with previous reports.[14a] The stereochemistry of **1** was definitively proved by X-ray crystallography. X-ray-quality crystals were grown by slow diffusion of pentane into a concentrated chloroform solution. It was identified as the *trans-anti* **D**-type isomer. This confirms the stereochemistry of the most stable isomer predicted by our computational studies and the earlier predictions by Hawthorne.[14a] An ORTEP plot of **1** is presented in Figure 2. Color figures are available in the Supporting Information.[17]

This is, to our knowledge, the first structure showing the actual stereochemistry of a tetrasubstituted cyclodiborazane. The central square ring is totally planar (torsion angle B1-N1-

 © 2006 Wiley-VCH Verlag GmbH & Co. KGaA, Weinheim

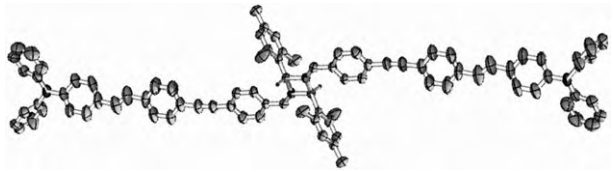

Figure 2. ORTEP plot of chromophore **1** showing the **D**-type stereochemistry.

B2-N2 0.0°). The phenyl rings attached to the cyclodiborazane moiety slightly deviate from planarity (torsion angle B1-N1-C1-C2 7.2°). The N–N distance of 2.17 Å is short enough to permit electronic coupling between the two conjugated systems. This N–N distance is similar to those reported for symmetric cyclodiborazanes and is close to the C_{sp^2}–C_{sp^2} distance of 2.12 Å reported for 1,3-dialkylidene cyclobutanes.[18]

Given that the starting diiodo compound **4** is most probably a mixture of **C** and **D** structures, we can assume that the other stereoisomer of **1** has **C** stereochemistry. It has been isolated and its study is in progress.

The optical properties of **1** were investigated in CH_2Cl_2 by UV/Vis absorption and fluorescence emission spectroscopy (all spectra in the Supporting Information). For comparison we also prepared the styrene "monomer" **10**, that is, a conjugated system linked to the nitrogen atoms of the cyclodiborazane core by a double bond. Compound **10** was obtained from **7** by Sonogashira coupling with 4-ethynylstyrene (Scheme 4). The absorption maxima are located at 403 nm ($\varepsilon = 1.0\times10^5\,M^{-1}cm^{-1}$) and 392 nm ($\varepsilon = 4.3\times10^4\,M^{-1}cm^{-1}$) for **1** and **10**, respectively. Thus, chromophore **1** exhibits a slight bathochromic shift of 11 nm in comparison with the model "monomer" **10**. Both chromophores are luminescent: $\lambda_{max} = 557$ nm for **1** and $\lambda_{max} = 491$ nm for **10**. A marked bathochromic shift of the emission band is observed for **1** in comparison with **10**. These results show a large difference ($\Delta = 1718\ cm^{-1}$) in the Stokes shifts of **1** and **10**. This indicates that the two conjugated systems linked to the cyclodiborazane core are strongly coupled in the excited state, but weakly coupled in the ground state. Such behavior has already been reported for the coupling of phenylacetylene chromophores in *meta* conjugation around a phenyl ring.[19] This led us to consider the photophysical properties of chromophore **1** in the light of the exciton model. The use of the exciton model to understand the photophysics of covalently bonded conjugated molecules is not new.[20]

According to the theory, purely excitonic coupling should lead to large shifts in both absorption and emission spectra. Since we observed a large shift only for the emission, it appears that a through-bond electronic interaction likely occurs essentially in the excited state.[19] This interaction was evidenced by molecular modeling. Selected AM1 calculated molecular orbitals of **1** are depicted in Figure 3. The HOMO−1 and HOMO are quasidegenerate in energy, and this is also the case for the LUMO and LUMO + 1. These two pairs of orbitals differ essentially in symmetry properties. We can observe from the HOMOs that in the fundamental state the electronic density is located around the terminal diphenylamino moieties, while the LUMOs show clearly that an electronic delocalization actually occurs along the whole conjugation pathway of the molecule. In the LUMO + 1 (Figure 3 a) orbital overlap is present across the cyclodiborazane ring and thus allows conjugation between the two donor groups in the excited state.

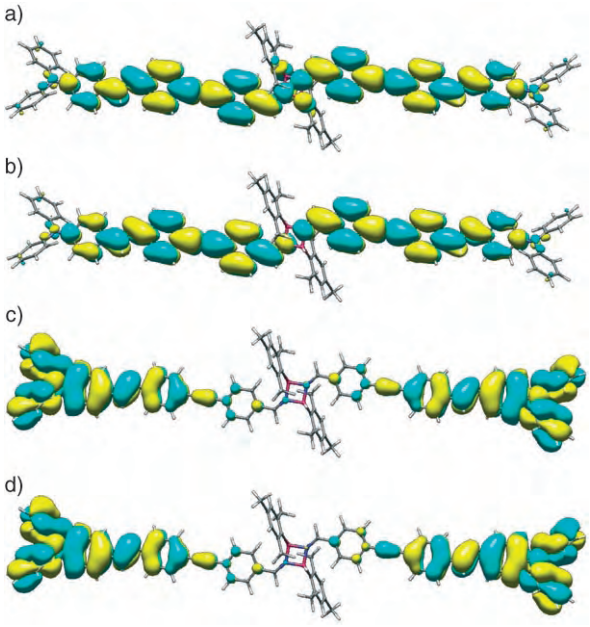

Figure 3. AM1 calculated molecular orbitals of chromophore **1**: a) LUMO + 1 ($E = -0.9984$ eV); b) LUMO ($E = -1.0054$ eV); c) HOMO ($E = -7.8874$ eV); d) HOMO−1 ($E = -7.8885$ eV).

Two-photon absorption properties are directly related to the third-order nonlinearity γ. Thus, we calculated the hyperpolarizability γ of chromophore **1** using the finite-field method, which has been already used to calculate the hyperpolarizabilities of boron-containing NLO chromophores.[21] We found $\gamma_0 \approx 1730\times10^{-36}$ esu. This high γ value is in agreement with the TPA cross section σ_2 of **1** that was experimentally determined in dichloromethane by the way of its two-photon induced fluorescence emission.[22] Indeed, **1** exhibits a strong two-photon absorption band in the near-IR region, centered at 830 nm with $\sigma_2 = 1350$ GM (1 GM = $10^{-50}\ cm^4\,s\,photon^{-1}$). The TPA spectrum is shown in Figure 4.

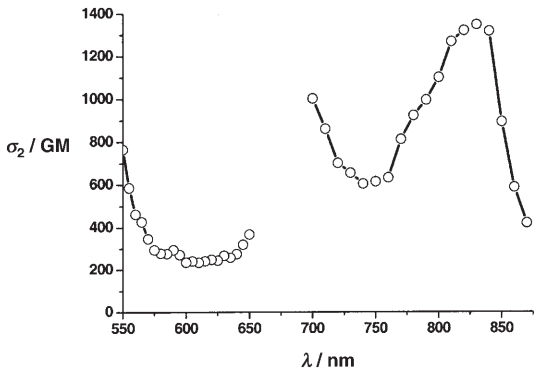

Figure 4. Two-photon absorption cross section of **1** in CH_2Cl_2.

 © 2006 Wiley-VCH Verlag GmbH & Co. KGaA, Weinheim

A TPA chromophore having the same carbon skeleton as **1**, but without the cyclodiborazane central core and with $NOct_2$ donor groups in place of NPh_2, has $\sigma_2 = 950$ GM at 800 nm.[23] Given that NR_2 instead of NAr_2 does not affect significantly the TPA cross section,[8b] we conclude that the electronic effect induced by the cyclodiborazane core significantly increases the TPA cross section in comparison with two conjugated systems linked only by a σ bond.

In conclusion, we have prepared a new type of efficient centrosymmetric one-dimensional TPA chromophore based on the interaction between two donor groups through the incompletely conjugated cyclodiborazane core (π–σ–π through-bond coupling). This strategy afforded a fluorophore with a TPA maximum in the range of laser wavelengths used in two-photon microscopy. This opens the way to the use of new boron-containing TPA chromophores in biological sciences. The *trans-anti* stereochemistry around the central core was proved by X-ray crystallography. The study of the other stereoisomer of chromophore **1** that is in progress will provide information on geometrical effects on the electronic coupling and its influence on the TPA properties.

Experimental Section

Syntheses: Full synthetic experimental details and analytical data can be found in the Supporting Information.

X-ray crystal structure of chromophore **1**: Details on data collection, structure solution, and additional ORTEP plots are given in the Supporting Information.

Computational studies: Geometry optimization of the chromophore was performed with the MOPAC program within the InsightII and Cerius^2 interfaces from Accelrys (http://www.accelrys.com) with the AM1 Hamiltonian. Static hyperpolarizabilities were calculated by the finite-field method incorporated in the MOPAC program.

The TPA cross-section spectra were obtained by up-conversion fluorescence measurements (details in the Supporting Information).[22]

Received: June 6, 2006
Published online: September 4, 2006

Keywords: boron · donor–acceptor systems · heterocycles · luminescence · nonlinear optics

[1] S. R. Marder, *Chem. Commun.* **2006**, 131 – 134.
[2] a) W. Denk, J. H. Strickler, W. W. Webb, *Science* **1990**, *248*, 73 – 76; b) J. D. Bhawalkar, A. Shih, S. J. Pan, W. S. Liou, J. Swiatkiewicz, B. A. Reinhardt, P. N. Prasad, P. C. Cheng, *Bioimaging* **1996**, *4*, 168 – 178; c) W. R. Zipfel, R. M. Williams, W. W. Webb, *Nat. Biotechnol.* **2003**, *21*, 1368 – 1376.
[3] a) S. Kawata, H. B. Sun, T. Tanaka, K. Takada, *Nature* **2001**, *412*, 697 – 698; b) S. M. Kuebler, M. Rumi, T. Watanabe, K. Braune, B. H. Cumpston, A. A. Heikal, L. L. Erskine, S. Thayumanadan, S. Barlow, S. R. Marder, J. W. Perry, *J. Photopolym. Sci. Technol.* **2001**, *14*, 657 – 668; c) I. Wang, M. Bouriau, P. L. Baldeck, C. Martineau, C. Andraud, *Opt. Lett.* **2002**, *27*, 1348 – 1350.
[4] a) J. E. Ehrlich, X. L. Wu, I. Y. S. Lee, Z. Y. Hu, H. Rockel, S. R. Marder, J. W. Perry, *Opt. Lett.* **1997**, *22*, 1843 – 1845; b) P. L. Baldeck, Y. Morel, C. Andraud, J.-F. Nicoud, A. Ibanez, *Photonics Sci. News* **1999**, *4*, 5 – 8.
[5] J. Liu, Y. W. Zhao, J. Q. Zhao, A. D. Xia, L. J. Jiang, S. Wu, L. Ma, Y. Q. Dong, Y. H. Gu, *J. Photochem. Photobiol. B* **2002**, *68*, 156 – 164.
[6] M. Göppert-Mayer, *Ann. Phys.* **1931**, *9*, 273 – 294.
[7] a) M. Barzoukas, M. Blanchard-Desce, *J. Chem. Phys.* **2000**, *104*, 2396 – 2401; b) S. K. Pati, T. J. Marks, M. A. Ratner, *J. Am. Chem. Soc.* **2001**, *123*, 7287 – 7291.
[8] a) M. Albota, D. Beljonne, J.-L. Brédas, J. E. Ehrlich, J.-Y. Fu, A. A. Heikal, S. E. Hess, T. Kogej, M. D. Levin, S. R. Marder, D. McCord-Maughon, J. W. Perry, H. Röckel, M. Rumi, G. Subramaniam, W. W. Webb, X.-L. Wu, C. Xu, *Science* **1998**, *281*, 1653 – 1656; b) M. Rumi, J. E. Ehrlich, A. A. Heikal, J. W. Perry, S. Barlow, Z.-Y. Hu, D. McCord-Maughon, T. C. Parker, H. Röckel, S. Thayumanavan, S. R. Marder, D. Beljonne, J.-L. Brédas, *J. Am. Chem. Soc.* **2000**, *122*, 9500 – 9510.
[9] a) R. Anémian, J.-C. Mulatier, C. Andraud, O. Stéphan, J.-C. Vial, *Chem. Commun.* **2002**, 1608 – 1609; b) Y. Morel, A. Irimia, P. Najechalski, Y. Kervella, O. Stephan, P. L. Baldeck, C. Andraud, *J. Chem. Phys.* **2001**, *114*, 5391 – 5396; c) C. Martineau, G. Lemercier, C. Andraud, *Opt. Mater.* **2002**, *21*, 555 – 557.
[10] a) R. Anémian, Y. Morel, P. L. Baldeck, B. Paci, K. Kretsch, J.-M. Nunzi, C. Andraud, *J. Mater. Chem.* **2003**, *13*, 2157 – 2163; b) A. Hayek, F. Bolze, J.-F. Nicoud, P. L. Baldeck, Y. Mély, *Photochem. Photobiol. Sci.* **2006**, *5*, 102 – 106.
[11] S. Sitha, J. L. Rao, K. Bhanuprakash, B. M. Choudary, *J. Phys. Chem. A* **2001**, *105*, 8727 – 8733.
[12] a) G. W. Griffin, A. F. Vellturo, *J. Org. Chem.* **1961**, *26*, 5183 – 5185; b) M. Simonetta, S. Carra, *Tetrahedron Lett.* **1965**, 913 – 919.
[13] a) N. Matsumi, T. Umeyama, Y. Chujo, *Macromolecules* **2000**, *33*, 3956 – 3957; b) F. Matsumoto, Y. Chujo, *J. Organomet. Chem.* **2003**, *680*, 27 – 30.
[14] a) M. F. Hawthorne, *Tetrahedron* **1962**, *17*, 117 – 122; b) Y. Chujo, I. Tomita, N. Murata, H. Mauermann, T. Saegusa, *Macromolecules* **1992**, *25*, 27 – 32.
[15] M. J. S. Dewar, E. G. Zoebisch, E. F. Healy, J. J. P. Stewart, *J. Am. Chem. Soc.* **1985**, *107*, 3902 – 3919.
[16] N. Matsumi, T. Umeyama, Y. Chujo, *Macromolecules* **2001**, *34*, 3510 – 3511.
[17] CCDC-609596 (**1**) contains the supplementary crystallographic data for this paper. These data can be obtained free of charge from The Cambridge Crystallographic Data Centre via www.ccdc.cam.ac.uk/data_request/cif.
[18] a) J. R. Jennings, R. Snaith, M. M. Mahmoud, S. C. Wallwork, S. J. Brian, J. Halfpenney, E. A. Petch, K. Wad, *J. Organomet. Chem.* **1983**, *249*, C1 – C5; b) E. Bustelo, C. Guérot, A. Hercouet, B. Carboni, L. Toupet, P. H. Dixneuf, *J. Am. Chem. Soc.* **2005**, *127*, 11582 – 11583.
[19] a) K. M. Gaab, A. L. Thompson, J. Xu, T. J. Martinez, C. J. Barbeen, *J. Am. Chem. Soc.* **2003**, *125*, 9288 – 9289; b) A. L. Thompson, K. M. Gaab, J. Xu, T. J. Martinez, C. J. Barbeen, *J. Phys. Chem. A* **2004**, *108*, 671 – 682.
[20] M. Kasha, H. R. Rawls, M. A. El-Bayoumi, *Pure Appl. Chem.* **1965**, *11*, 371 – 392.
[21] a) Z. Yuan, N. J. Taylor, R. Ramachandran, T. B. Marder, *Appl. Organomet. Chem.* **1996**, *10*, 305 – 316; b) Z. Yuan, J. C. Collings, N. J. Taylor, T. B. Marder, C. Jardin, J.-F. Halet, *J. Solid State Chem.* **2000**, *154*, 5 – 12.
[22] C. Xu, W. W. Webb, *J. Opt. Soc. Am. B* **1996**, *13*, 481 – 491.
[23] O. Mongin, L. Porrès, L. Moreaux, J. Mertz, M. Blanchard-Desce, *Org. Lett.* **2002**, *4*, 719 – 722.

 © 2006 Wiley-VCH Verlag GmbH & Co. KGaA, Weinheim

Superhydrophobic Effect

DOI: 10.1002/anie.200602126

Photoinduced Reversible Formation of Microfibrils on a Photochromic Diarylethene Microcrystalline Surface**

Kingo Uchida, Norikazu Izumi, Shinichiro Sukata, Yuko Kojima, Shinichiro Nakamura,* and Masahiro Irie*

Lotus and taro leaves have hydrophobic surfaces, which in nature consist of micrometer-scale rods or projections that exhibit a super water-repellent property called the lotus effect. The contact angle of a water droplet on such surfaces is $161.0 \pm 2.7°$. Recently, many reports concerning changes in water droplet contact angle as a result of changes in surface morphology and surface polarity have been published.[1] Additionally, changes in photoresponsive wettability have also been reported.[2]

Herein, we report a new photoinduced change in surface morphology that provides superhydrophobic properties, obtained by the photoinduced reversible formation of fine fibril structures on coated microcrystalline surfaces. The origin of the reversible formation of fibrils is the photoisomerization of a photochromic diarylethene molecule **1** (see Scheme 1) of a thin film. The reversible changes in surface morphology of a thin film made from photochromic diarylethene **1** were followed by scanning electron microscopy (SEM), optical microscopy, and contact angle measurements of a water droplet. The film was prepared by coating a solution of **1** in chloroform onto a substrate, which gave a contact angle of the water droplet of around 120°. Upon irradiation with UV light, the film surface became superhydrophobic (contact angle 163°). SEM images showed that the surface was covered with microfibrils of diameter around 1 μm. Upon irradiation with visible light, the surface again became flat and recovered the initial contact angle of 120°.

Diarylethene derivatives are promising artificial photoresponsive molecules that show reversible transformation between open- and closed-ring isomers with different absorption spectra.[3] As they also show thermally irreversible and fatigue-resistant photochromic performance,[4] intensive studies have aimed at applications such as molecular memories and switches.[5–13] Herein, we report a new function for the cast film of a derivative.

There are two approaches to controlling surface wettability. One is to change the surface morphology, because it is known that increasing surface roughness results in a superhydrophobic surface, an effect that is widely observed on lotus leaves.[14,15] Such micrometer-scale rugged or fractal structures were also artificially prepared to make superhydrophobic surfaces.[1b,16,17] The other approach is a change of polarity.[18–22] Several reports have attempted to control surface wettability by using photochromic compounds that change the surface polarity.[21] We report changes in photoinduced wettability based on the changes in morphology of a photochromic diarylethene crystal and thin film.

The photochromism of a diarylethene, 1,2-bis(2-methoxy-5-trimethylsilylthien-3-yl)perfluorocyclopentene (**1o**; Scheme 1), in a hexane solution is shown in the Supporting Information. The open-ring isomer is colorless, and absorption maxima of the spectrum were observed at $\lambda = 255$ ($\varepsilon = 2.8 \times 10^4\,\mathrm{M^{-1}cm^{-1}}$) and 325 nm ($\varepsilon = 7.7 \times 10^3\,\mathrm{M^{-1}cm^{-1}}$). Upon UV irradiation (254 nm), the solution turned blue and a new band was observed at 599 nm ($\varepsilon = 5.2 \times 10^3\,\mathrm{M^{-1}cm^{-1}}$). Upon irradiation with visible light, the color disappeared and the bands of the open-ring isomer were regenerated (see Scheme 1). The coloration and discoloration quantum yields were 0.37 and 0.0015, respectively. The reversible formation of the two isomers was not only observed in solution but also in the crystalline phase.

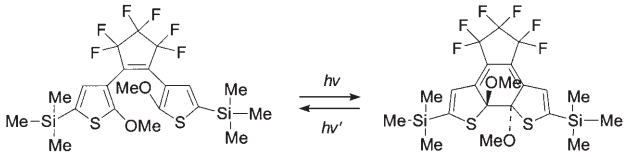

Open-ring isomer **1o** Closed-ring isomer **1c**

Scheme 1. Reversible formation of open-ring isomer **1o** and closed-ring isomer **1c**.

An SEM image of the crystalline surface is shown in Figure 1a. Upon UV irradiation (254 nm), the color became deep blue within 5 min, yet no change in surface morphology was observed at this moment at room temperature. After irradiation for 10 min the crystal was stored in the dark, but 5 min later small microfibrils had already started to grow (see

[*] Prof. K. Uchida, N. Izumi, S. Sukata
Department of Materials Chemistry
Faculty of Science and Technology, Ryukoku University and
CREST, Japan Science and Technology Corporation
Seta, Otsu 520-2194 (Japan)
Fax: (+81) 77-543-7483
E-mail: uchida@chem.ryukoku.ac.jp
Homepage: http://www.chem.ryukoku.ac.jp/~uchida/UchidaLab5a.htm

Dr. Y. Kojima, Dr. S. Nakamura
Mitsubishi Chemical Group
Science and Technology Research Center, Inc. and
CREST, Japan Science and Technology Corporation
1000 Kamoshida, Yokohama 227–8502 (Japan)
E-mail: shin@cc.m-kagaku.co.jp

Prof. M. Irie
Department of Chemistry and Biochemistry
Graduate School of Engineering, Kyushu University
6-10-1 Hakozaki, Fukuoka 812-8581 (Japan)

[**] This work was partly supported by Grants-in-Aid for Scientific Research (B) (18350101) from the Ministry of Education, Culture, Sports, Science, and Technology (MEXT) of the Japanese Government. We thank Prof. Takahiro Seki and Mitsuo Hara for the powder X-ray analysis. We also express thanks to Prof. Hiroshi Komatsu, Prof. Tsuyoshi Tsujioka, Dr. Takao Matsuzaki, Prof. Nobuo Niimura, Dr. Seiya Kobatake, and S. Matsumoto for their helpful discussions.

Supporting information for this article is available on the WWW under http://www.angewandte.org or from the author.

 InterScience © 2006 Wiley-VCH Verlag GmbH & Co. KGaA, Weinheim

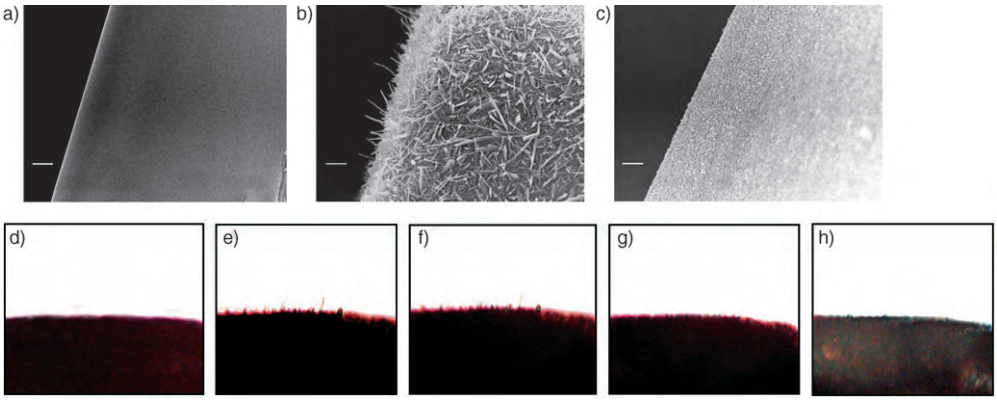

Figure 1. Reversible changes in surface morphology of a single crystal of **1** (scale bar: 10 μm). a) SEM image of the crystal surface of **1o** from a side view (×1000) before UV irradiation (254 nm). b) SEM image from a side view (×1000) of the surface after UV irradiation (254 nm, 12 W, 10 min) and storage in the dark for 24 h. c) SEM image from a side view (×1000) of the surface after irradiation with visible light ($\lambda > 500$ nm, 500 W, 20 min) and storage in the dark for 24 h. d–h) Optical microscopic images (×500) of the appearance and disappearance of fibrils upon irradiation with UV and visible light (500-W Xe lamp, $\lambda > 500$ nm). d) Before irradiation with UV light, the surface was flat. e) After UV irradiation (254 nm, 10 min) and storage in the dark for 5 h at room temperature, microfibrils were generated. Irradiation with visible light for f) 5, g) 10, and h) 60 min.

Supporting Information). After storage for 24 h, the surface was covered with many microfibrils, as shown in Figure 1b. Upon irradiation of the surface with visible light ($\lambda > 500$ nm), the blue color and the microfibrils disappeared (see Figure 1c). The surface changes at the same point were also monitored from a side view by using an optical microscope (see Figure 1d–h). The disappearance process (Figure 1e–h) of the fibrils was well monitored.

Measurement of the contact angle of a water droplet is a simple and direct method for evaluating wettability. The contact angle of the film surface before UV irradiation was 120° (Figure 2a). Upon irradiation of the surface with UV light (254 nm), the color became blue and the angle was reduced to around 90° (Figure 2b) after a short irradiation time (1–2 min). After 24 h the angle had gradually increased to 163° (Figure 2c and d).

The colored surface was irradiated with visible light to regenerate the open-ring isomer. After 20 min the blue color disappeared. The contact angle was also monitored during the fibril disappearing process. It gradually decreased and finally recovered to the initial 120° (Figure 2e).

Powder X-ray diffraction measurements were carried out to elucidate the composition of the microfibrils. Figure 3 shows a comparison of the measured powder diffraction patterns and estimated patterns from single-crystal structure analysis of the open- (**1o**) and closed-ring (**1c**) isomers. The fibril pattern was in good agreement with that of the closed-ring isomer. Diffraction peaks at 5.1, 7.7, and 15.0° are appropriate for the (001), (010), and ($1\bar{1}\bar{1}$) lattice planes of the closed-ring isomer crystal, respectively. Ordinarily, closed-ring isomers formed in the crystal of open-ring isomers are strained by the lattice and have different structures from closed-ring isomer crystals obtained by recrystallization in solution.[23,24] The above results indicate that the fibril crystal formed on the film grew freely from the crystal lattice of the open-ring isomer.

The phase diagram of photoirradiated crystals was measured to investigate why microfibrils grew after UV irradiation (Figure 4). The melting points of the open- and closed-ring isomers are 99.8–100.3 and 143.2–144.1 °C, respectively, whereas the melting point of the mixture of open- and closed-ring isomers decreased to around 30 °C at a certain ratio (24:76 open-ring/closed-ring isomers). The result suggests that a homocrystal of the closed-ring isomer is formed from the melting of the crystal at this ratio.

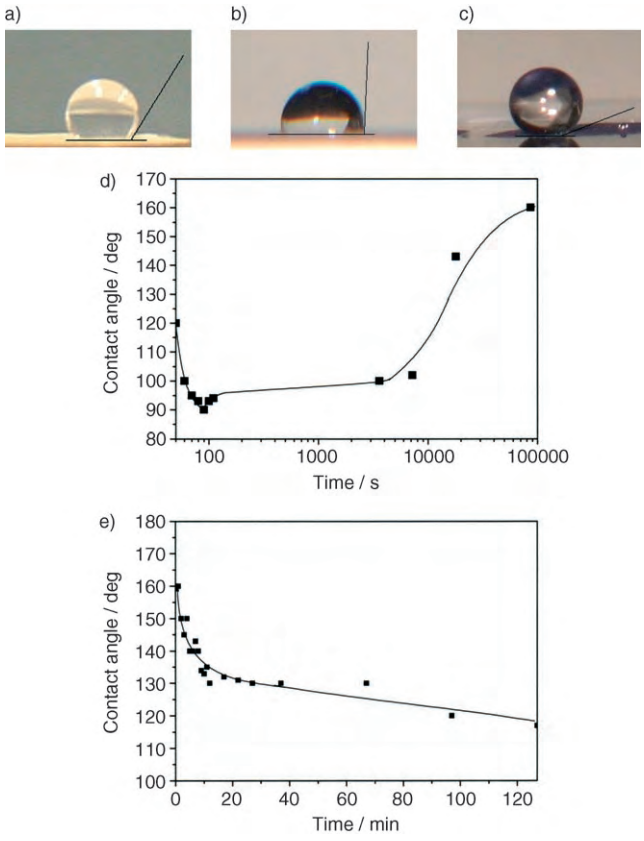

Figure 2. Contact angles of a water droplet on a microcrystalline film of diarylethene **1**. a) Water droplet (1.2 mm ∅) on the microcrystalline surface before irradiation with UV light (254 nm, 12 W). The contact angle was 120 ± 2°. b) Water droplet after UV irradiation for a short time (1–2 min). The contact angle changed to 92 ± 2°. c) Water droplet after irradiation (10 min) with light and storage in the dark at room temperature for 24 h. The contact angle increased to 163 ± 2°. d) Time profile of the contact angle during the fibril generation process after UV irradiation. e) Profile during fibril disappearance upon irradiation of the colored fibril structured surface with visible light.

 © 2006 Wiley-VCH Verlag GmbH & Co. KGaA, Weinheim

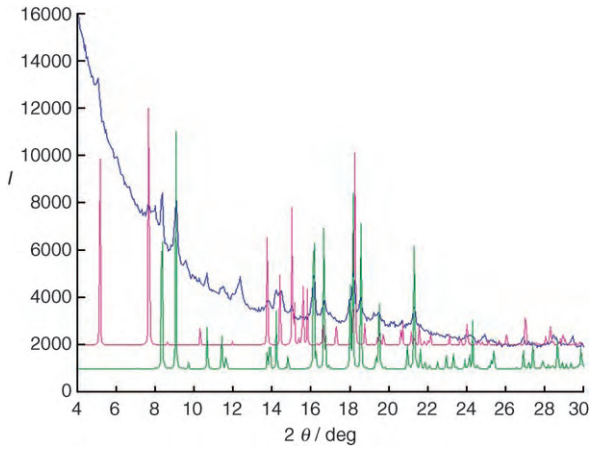

Figure 3. X-ray diffraction patterns of needles obtained from the surface by scratching (blue line), and of **1o** (green line) and **1c** (pink line) derived from single-crystal analysis.

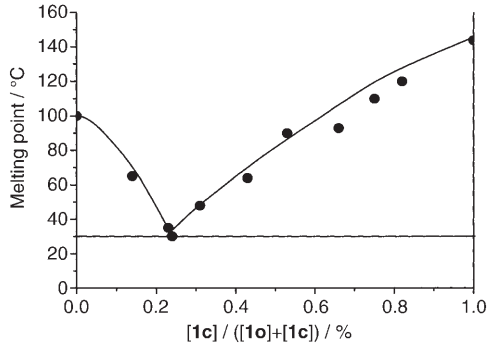

Figure 4. Phase diagram of mixtures of open- (**1o**) and closed-ring isomers (**1c**) formed by irradiation of diarylethene crystals with UV light (313 nm).

The shape of the crystals of the closed-ring isomer was a needle or fibril when obtained by recrystallization from a solution containing this isomer. The crystal shape tends to grow in one direction along the *a* axis. Upon UV irradiation, the open-ring isomer is converted to the closed-ring isomer. When conversion exceeds 24%, crystal growth of the closed-ring isomer starts to form fibril structures on the film surface. To confirm this mechanism, the sample was kept in air and water at different temperatures. Below around 0°C the fibril did not grow, but we found fibril formation in water and in air around 30°C. The results also support the melt mechanism as depicted in the phase diagram. Fibril growth was not only observed on glass and metal substrates but also on plastics and paper. The film will be applicable to materials with photoinduced reversible surface water repellency.

Experimental Section

The preparation of **1o** and **1c** is described in detail in the Supporting Information. Single crystals of **1o** and **1c** were obtained by recrystallization from ethanol. A solution of **1o** in chloroform (100 mg mL^{-1}) was coated on the substrate (glass, resin, or metal), and the solvent was evaporated. The film thickness was approximately 20–30 μm and was measured by observing the scratched surface by SEM.

A scanning electron microscope (JEOL JSM-5200) and an optical microscope (Leica DMLP) were used to study the surface microstructure. Photoirradiation (visible light: $\lambda > 500$ nm) was carried out using a Ushio 500-W xenon lamp with a cutoff filter (Toshiba color filter Y-50), and UV irradiation was carried out by using a Topcon UV lamp PU-2 (12 W). X-ray crystallographic analysis was performed using a Bruker SMART CCD X-ray diffractometer. Suitable colorless prism-shaped (**1o**) and dark blue needle crystals (**1c**) were obtained by recrystallization from ethanol. Crystals with dimensions of $0.5 \times 0.4 \times 0.15$ mm^3 (**1o**) and $0.5 \times 0.1 \times 0.05$ mm^3 (**1c**) were mounted on a glass fiber and aligned on a Bruker SMART 1000 CCD diffractometer (platform with full three-circle goniometer) at room temperature. The diffractometer was equipped with a 1K CCD detector set 50.0 mm from each crystal. Intensity measurements were performed using graphite-monochromated $Mo_{K\alpha}$ radiation from a sealed ceramic diffraction tube (Siemens). Generator settings were 50 kV/40 mA. SMART was used for preliminary determination of the unit cell constants and data collection control. The intensities of the reflections of the hemisphere were collected by a combination of three sets of exposures (frames). Each set had a different angle ϕ for the crystal and each exposure covered a range of 0.3° in ω; 1800 frames were collected for each crystal with an exposure time of 5.0 s per frame for **1o** and 10.0 s per frame for **1c**. Data integration and global cell refinement was performed with SAINT. The final unit cells were obtained after integration from the *xyz* centroids of 2912 reflections for **1o** and 1352 reflections for **1c**. Intensity data were corrected for Lorentz and polarization effects, scale variation, and decay and absorption; based on the intensities of symmetry-related reflections measured at different angular settings (SADABS), multiscan absorption correction was applied and reduced to F_o^2.

Crystal data and structural refinement parameters for **1o**: $C_{21}H_{26}F_6O_2S_2Si_2$, $M_r = 544.72$, triclinic, space group $P\bar{1}$, $a = 10.122(6)$, $b = 11.268(6)$, $c = 12.814(7)$ Å, $\alpha = 103.355(11)$, $\beta = 94.298(13)$, $\gamma = 74.981(12)°$, $V = 1373.3(13)$ Å^3, $Z = 2$, $\rho_{calcd} = 1.317$ g cm^{-3}, $\mu(Mo_{K\alpha}) = 0.337$ mm^{-1}, $T = 298(2)$ K, $F(000) = 564$, $R1 = 0.0685$ ($wR2 = 0.2056$) for 5717 unique reflections ($R_{int} = 0.0172$) with a GOF of 0.927. Crystal data and structural refinement parameters for **1c**: $C_{21}H_{26}F_6O_2S_2Si_2$, $M_r = 544.72$, triclinic, space group $P\bar{1}$, $a = 6.697(2)$, $b = 11.777(4)$, $c = 17.470(6)$ Å, $\alpha = 96.899(6)$, $\beta = 96.993(6)$, $\gamma = 98.472(6)°$, $V = 1339.2(8)$ Å^3, $Z = 2$, $\rho_{calcd} = 1.351$ g cm^{-3}, $\mu(Mo_{K\alpha}) = 0.346$ mm^{-1}, $T = 298(2)$ K, $F(000) = 564$, $R1 = 0.0791$, ($wR2 = 0.1898$) for 4496 unique reflections ($R_{int} = 0.0359$) with a GOF of 0.883. Data were collected on a Bruker SMART 1000 CCD diffractometer with graphite-monochromated $Mo_{K\alpha}$ radiation ($\lambda = 0.71073$ Å). The structure was solved by direct methods using SHELXS97 and refined by full-matrix least-squares against F^2 with SHELXL97.[25] CCDC 293161 (**1o**) and 293162 (**1c**) contain the supplementary crystallographic data for this paper. These data can be obtained free of charge from the Cambridge Crystallographic Data Centre via www.ccdc.cam.ac.uk/data_request/cif.

Received: May 28, 2006
Published online: August 22, 2006

Keywords: crystal growth · hydrophobic effect · photochromism · thin films

[1] a) H. Y. Erbil, A. L. Demirel, Y. Avci, O. Mert, *Science* **2003**, *299*, 1377–1380; b) T. Onda, S. Shibuichi, N. Satoh, K. Tsujii, *Langmuir* **1996**, *12*, 2125–2127.

[2] a) S. Wang, X. Feng, J. Yao, L. Jiang, *Angew. Chem.* **2006**, *118*, 1286–1289; *Angew. Chem. Int. Ed.* **2006**, *45*, 1264–1267; b) H. Liu, L. Feng, J. Zhai, L. Jiang, D. Zhu, *Langmuir* **2004**, *20*, 5659–5661.

 © 2006 Wiley-VCH Verlag GmbH & Co. KGaA, Weinheim

[3] a) G. H. Brown, *Photochromism*, Wiley-Interscience, New York, **1971**; b) H. Duerr, H. Bouas-Laurent, *Photochromism: Molecules and Systems*, Elsevier, Amsterdam, **1990**.
[4] a) M. Irie, *Chem. Rev.* **2000**, *100*, 1685 – 1716; b) M. Irie, K. Uchida, *Bull. Chem. Soc. Jpn.* **1998**, *71*, 985 – 996.
[5] M. Irie, K. Uchida, T. Eriguchi, H. Tsuzuki, *Chem. Lett.* **1995**, 899 – 900.
[6] S. Kobatake, T. Yamada, K. Uchida, N. Kato, M. Irie, *J. Am. Chem. Soc.* **1999**, *121*, 2380 – 2386.
[7] S. Kobatake, M. Yamada, T. Yamada, M. Irie, *J. Am. Chem. Soc.* **1999**, *121*, 8450 – 8456.
[8] T. Yamada, S. Kobatake, K. Muto, M. Irie, *J. Am. Chem. Soc.* **2000**, *122*, 1589 – 1592.
[9] M. Irie, T. Lifka, S. Kobatake, N. Kato, *J. Am. Chem. Soc.* **2000**, *122*, 4871 – 4876.
[10] S. Kobatake, K. Shibata, K. Uchida, M. Irie, *J. Am. Chem. Soc.* **2000**, *122*, 12135 – 12141.
[11] S. Kobatake, K. Uchida, E. Tsuchida, M. Irie, *Chem. Commun.* **2002**, 2804 – 2805.
[12] M. Morimoto, S. Kobatake, M. Irie, *Chem. Rec.* **2004**, *4*, 23 – 38.
[13] M. Irie, S. Kobatake, M. Horichi, *Science* **2001**, *291*, 1769 – 1772.
[14] W. Barthlott, C. Neinhuis, *Planta* **1997**, 202, 1 – 8.
[15] C. Neinhuis, W. Barthlott, *New Phytol.* **1998**, *138*, 91 – 98.
[16] H. Y. Erbil, A. L. Demirel, Y. Avci, O. Mert, *Science* **2003**, *299*, 1377 – 1380.
[17] S. Shibuichi, T. Onda, N. Satoh, K. Tsujii, *J. Phys. Chem.* **1996**, *100*, 19512 – 19517.
[18] X. Feng, J. Zhai, L. Jiang, *Angew. Chem.* **2005**, *117*, 5245 – 5248; *Angew. Chem. Int. Ed.* **2005**, *44*, 5115 – 5118.
[19] S. Abbott, J. Ralston, G. Reynolds, R. Hayes, *Langmuir* **1999**, *15*, 8923 – 8928.
[20] J. Lahann, S. Mitragotri , T.-N. Tran, H. Kaido, J. Sundaram, I. S. Choi, S. Hoffer, G. A. Somorjai, R. Langer, *Science* **2003**, *299*, 371 – 374.
[21] K. Ichimura, S.-K. Oh, M. Nakagawa, *Science* **2000**, *288*, 1624 – 1626.
[22] B. S. Gallardo, V. K. Gupta, F. D. Eagerton, L. I. Jong, V. S. Craig, R. R. Shah, N. L. Abbott, *Science* **1999**, *283*, 57 – 60.
[23] T. Yamada, S. Kobatake, M. Irie, *Bull. Chem. Soc. Jpn.* **2000**, *73*, 2179 – 2184.
[24] S. Kobatake, M. Morimoto, Y. Asano, A. Murakami, S. Nakamura, M. Irie, *Chem. Lett.* **2002**, *31*, 1224 – 1225.
[25] SHELXS97 and SHELXL97, G. M. Sheldrick, Programs for Crystal Structure Analysis, University of Göttingen, Germany, **1997**.

 © 2006 Wiley-VCH Verlag GmbH & Co. KGaA, Weinheim

Photochromic Crystals

DOI: 10.1002/anie.200601702

Direct Observation of Photochromic Dynamics in the Crystalline State of an Organorhodium Dithionite Complex**

Hidetaka Nakai, Motohiro Mizuno, Takanori Nishioka,* Nobuaki Koga, Kimie Shiomi, Yousuke Miyano, Masahiro Irie, Brian K. Breedlove, Isamu Kinoshita, Yoshihito Hayashi, Yoshiki Ozawa,* Takae Yonezawa, Koshiro Toriumi, and Kiyoshi Isobe**

One of the essential approaches to developing molecular memory devices and switching materials is to synthesize molecules with highly efficient switching functions based on reversible isomerization reactions that respond to external stimuli.[1–3] Among these, photoinduced crystalline-state reac-

[*] Dr. H. Nakai, Prof. M. Mizuno, Y. Miyano, Prof. Y. Hayashi, Prof. K. Isobe
Department of Chemistry
Graduate School of Natural Science & Technology
Kanazawa University
Kakuma-machi, Kanazawa 920-1192 (Japan)
Fax: (+81) 76-264-5742
E-mail: mizuno@wriron1s.kanazawa-u.ac.jp
isobe@cacheibm.s.kanazawa-u.ac.jp

Prof. T. Nishioka, K. Shiomi, Dr. B. K. Breedlove, Prof. I. Kinoshita
Department of Material Science
Graduate School of Science
Osaka City University
Sumiyoshi-ku, Osaka 558-8585 (Japan)
Fax: (+81) 6-6605-2569
E-mail: nishioka@sci.osaka-cu.ac.jp

Prof. Y. Ozawa, T. Yonezawa, Prof. K. Toriumi
Department of Material Science
Graduate School of Material Science
University of Hyogo
3-2-1 Kouto, Kamigori-cho, Ako-gun, Hyogo 678-1297 (Japan)
Fax: (+81)-791-58-0154
E-mail: ozawa@sci.u-hyogo.ac.jp

Prof. N. Koga
Graduate School of Information Science
Nagoya University
Chikusa-ku, Nagoya 464-8601 (Japan)

Prof. M. Irie
Department of Chemistry and Biochemistry
Graduate School of Engineering
Kyushu University
Hakozaki 6-10-1, Higashi-ku, Fukuoka 812-8581 (Japan)

[**] This work was financially supported by the Grant-in-Aids for Scientific Research (KAKENHI) in Priority Area "Molecular Nano Dynamics", "Dynamic Complex", and "Chemistry of Coordination Space" and by the Grant-in-Aids "15350036" and "Nanotechnology Support Project" from Ministry of Education, Culture, Sports, Science and Technology (MEXT), Japan, and "Tokuyama Science Foundation". We thank Professor P. Coppens (State University of New York) for valuable discussions.

Supporting information for this article is available on the WWW under http://www.angewandte.org or from the author.

© 2006 Wiley-VCH Verlag GmbH & Co. KGaA, Weinheim

tions proceeding with regio-, stereo-, and even enantiospecificity are the most promising tools for constructing high-density recording media and smart switching materials.[4,5] To date, only a limited number of synthetic methodologies and crystalline-state photochromic compounds have been reported, and their photochromic reaction mechanisms and dynamics are not well analyzed as a result of the low degree of isomerization and instability of the photochromic compounds in the solid phase.[6–10] Our coordination-chemistry approach towards the synthesis of new switching-functional molecular crystals using the $(RhCp^*)_2(\mu\text{-}CH_2)_2$ fragment ($Cp^* = \eta^5\text{-}C_5Me_5$), which can accept two sulfur atoms coordinated parallel to the Rh–Rh bond,[11] and the external-stimulus-responsive $S_2O_4^{2-}$ ion as ligand[12] led successfully to the formation of uniquely photoresponsive and first side-on dithionite complex $[(RhCp^*)_2(\mu\text{-}CH_2)_2(\mu\text{-}O_2SSO_2)]$ (**1**). Herein we disclose the following two processes in single crystals of **1** (Figure 1): 1) fully reversible crystalline-state

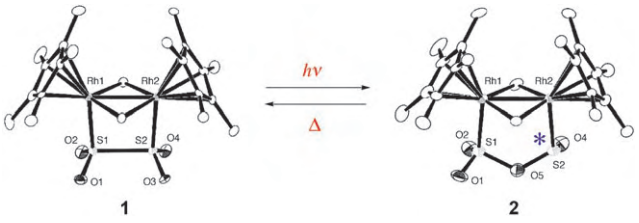

Figure 1. Two processes in a crystal: 1) fully reversible crystalline-state photochromism between $\mu\text{-}O_2SSO_2$ and $\mu\text{-}O_2SOSO$ complexes (red), and 2) stereoselective oxygen-atom transfer and stereospecific transformation of the photochemically generated $\mu\text{-}O_2SOSO$ isomers into the most stable isomer (blue). ORTEP plots of **1** and **2** with 50% probability ellipsoids. Hydrogen atoms are omitted for clarity.

photochromism between $\mu\text{-}O_2SSO_2$ and $\mu\text{-}O_2SOSO$ complexes (red), and 2) stereoselective oxygen-atom transfer and stereospecific transformation of the photochemically generated $\mu\text{-}O_2SOSO$ isomers into the most stable one (blue).

Crystals of **1** suitable for X-ray diffraction analysis were grown from a solution in ethyl acetate/dichloromethane at room temperature. Figure 1 (left) shows the ORTEP plot of **1**. The $\mu\text{-}O_2SSO_2$ ligand in **1** has a weak S–S bond of 2.330(2) Å. On irradiation with the light from two halogen lamps (12 V, 75 W) for 140 h, the red-orange crystals ($\lambda_{max} = 510$ nm, crystal size: $0.08 \times 0.06 \times 0.02$ mm) of **1** change to yellow-orange crystals ($\lambda_{max} = 475$ nm) of a new isomer, $[(RhCp^*)_2(\mu\text{-}CH_2)_2(\mu\text{-}O_2SOSO)]$ (**2**), with almost 100% interconversion ratio (to our knowledge, crystalline-state photochromism usually proceeds with considerably lower interconversion ratios of less than 15%[7–9]) and with about 1% expansion in unit-cell volume from 2319.2(10) to 2334(1) Å^3. Complex **2** contains new oxysulfide species O_2SOSO with an oxo bridge between the two S atoms: S1 has two terminal O atoms, while S2 has only one terminal O atom and is asymmetric (Figure 1, right). The O_2SOSO type of oxysulfur and oxysulfide compounds is unknown to date but has been theoretically calculated[13]. The bridging S1–O5 and S2–O5 bonds in **2** differ significantly in length (S1–O5 1.709(5), S2–O5 1.636(6) Å), and the latter has double-bond character. Although **2** has an asymmetric sulfur atom S2, the reaction gives pairs of enantiomers in crystals because of the centrosymmetric space group $P2_1/n$. On leaving crystals of **2** in the dark for three weeks at room temperature, the back reaction takes place and leads to complete regeneration of crystals of **1** (exothermic reaction with liberation of about 4.5 kcal mol^{-1} of heat according to differential scanning calorimetry). The bonding character in **2** indicates that selective cleavage of the weak S1–O5 bond is the lowest-energy path for returning to complex **1**; this may be the only path for isomerization to **1**.

Thus, unusual unimolecular type T inverse photochromism [i.e., the back reaction occurs thermally, $\lambda_{max}(\mathbf{1}) > \lambda_{max}(\mathbf{2})$][14] in the crystal has been observed for an organorhodium compound. The photochromic system is stable and repeatable in the crystalline state. In contrast, in solution the photoreaction gives a mixture of **2** and further oxidation products such as $[(RhCp^*)_2(\mu\text{-}CH_2)_2(\mu\text{-}SO_3)]$.[15] It is noteworthy that the absorption coefficient of λ_{max} in **2** is smaller than that in **1** by about one-third (see the Supporting Information): as the photoreaction proceeds, light is able to pass more easily through the crystal.[16] These physical properties result in the unique full reversibility, which is advantageous for clarifying the reaction dynamics by spectroscopic methods (see the Supporting Information) and other techniques.

The crystalline-state photochromic process can be directly followed by conventional single-crystal X-ray diffraction. During the photoreaction positional disorder of the oxygen atoms (see the Supporting Information) and occupancy changes with irradiation time are observed in X-ray diffraction analyses. In contrast, the thermal back reaction does not show any disorder phenomena except for that due to the formation of **1**. This observation is consistent with the bonding character in **2**. A careful analysis of time dependence of the positional disorder[17–19] and the S···S distance during photoreaction at 20 °C indicates that at the initial stage of the reaction (unconverted starting complex exists to 72%) four species **2a–d** that cause the positional disorder of the oxygen atoms are generated in respective yields of 10, 8, 5, and 5% (Figure 2 and Table 1). In the present treatment only one asymmetric unit in the crystal was considered.

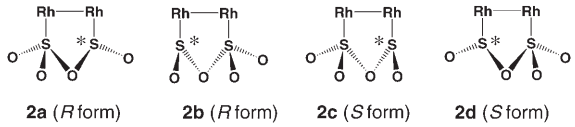

Figure 2. Stereoisomers of **2**. The Cp* and $\mu\text{-}CH_2$ ligands are omitted for clarity.

Isomers **2a** and **2c** are a pair of enantiomers, **2a** and **2b** are identical species but differ orientationally in the cavity, and **2c** and **2d** are also identical but differ in orientation. Isomers of **2a–d** exist in the *trans* form. We found no evidence for the existence of the *cis* isomer in the disorder analysis, and DFT calculations also suggest that the *cis* isomer is energetically less stable than the *trans* isomer by 2.0 kcal mol^{-1} (see the Supporting Information). The population of **2a** increases

 © 2006 Wiley-VCH Verlag GmbH & Co. KGaA, Weinheim

Table 1: Percentage population of photochemically generated isomers[a] in one asymmetric unit in the crystal.

Entry[b]	t [h][c]	T [°C][c]	**1**	**2a**	**2b**	**2c**	**2d**
1	0	20	100	0	0	0	0
2	2	20	72	10	8	5	5
3	6	20	32	35	23	4	6
4	18	20	7	62	25	2	4
5	40	20	2	77	15	3	3
6	98	20	1	86	7	4	2
7	140	20	0	100	0	0	0
8	12	−158	72	5	12	8	3
9	149	−158	6	43	25	20	6

[a] All the parameters, except for entries 1 and 7, have errors of ±1% according to the estimated standard deviations of the occupancy parameters of the oxygen atoms. [b] X-ray crystallographic data were recorded at −173 °C. Crystal sizes: 0.08×0.06×0.02 mm^3 (entries 1 and 7), 0.10×0.08×0.06 mm^3 (entries 2, 3, 4, 5, and 6), and 0.08×0.06×0.02 mm^3 (entries 8 and 9). [c] Irradiation conditions.

with increasing irradiation time, and in the final stage of the reaction only **2a** is formed and the positional disorder disappears. This disappearance means that the thermodynamically unstable μ-O_2SOSO isomers generated in the crystal are converted under irradiation to the most stable species **2a**. In contrast, the photoreaction at −158 °C clearly shows a different reaction rate and population from those at 20 °C (Table 1, entries 8 and 9). The dependence of the population of the photochemically generated isomers at −158 °C on irradiation time shows that the most stable product **2a** is not necessarily generated in the highest population in the initial stage of the reaction (Table 1 and Figure 3). In the dark, the temperature dependence of the

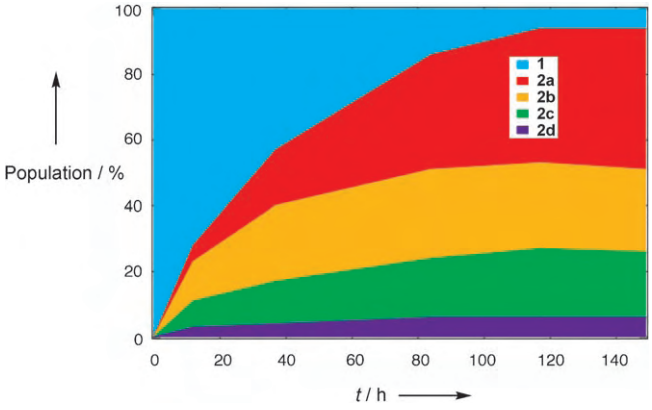

Figure 3. Change in population of the photochemically generated isomers with irradiation time at −158 °C.

population of the isomers generated at −158 °C after 149 h of irradiation shows that isomer **2c** is directly transformed into **2a** without irradiation (see the Supporting Information). These results strongly indicate that at −158 °C mainly the kinetically controlled reaction takes place. What is responsible for the selectivity of the photoreaction at the initial stage at −158 °C and the specific formation of only **2a** in the final stage at 20 °C?

We investigated possible causes for this. Since the crystals of **1** and **2** have the same space group and molecular arrangement, by comparison of a certain molecule in the unit cell of **1** with that in **2**, it can be readily seen which terminal oxygen atom in the μ-O_2SSO_2 ligand of **1** is transformed into the bridging oxygen atom in **2** (see the Supporting Information). It is the O3 atom (Figure 1). In the μ-O_2SSO_2 ligand, the four oxygen atoms are stereochemically nonequivalent in the cavity formed by six Cp* ligands: they do not have an equal chance to undergo transfer. The O3 atom is the most congested by methyl groups of the Cp* ligands (see the Supporting Information). Thus, migration of the O3 atom is more difficult compared with the other O atoms. This is the origin of the kinetically controlled reaction at −158 °C (Figure 3): the population reflects the selectivity based on the shape of the cavity in the crystal, that is, **2a** is the kinetically unfavorable product. Since **2a** accumulates through the repetitive photochromic process (**2b** (or **2d**)→**1**→**2a**, Table 1) and direct thermal conversion from **2c** to **2a** (see the Supporting Information), specificity of oxygen transfer is observed at 20 °C: **2a** is the thermodynamically favorable product. Further low-temperature X-ray analysis is in progress to elucidate whether direct thermal conversion process of **2b** (or **2d**) to **2a** is present or not.

In conclusion, we have demonstrated that a new class of photochromic compounds, a rhodium dinuclear complex **1** with the photoreactive dithionite ligand, undergoes a fully reversible crystalline-state photochromic reaction with stereoselective oxygen-atom transfer and thermodynamically controlled isomerization. This photochromic process is a repetitive crystalline-state reaction accompanied by, in addition to the color change, 1) alternating expansion–shrinkage of the crystal lattice with about 1% change in volume, 2) alternating gain–loss of the asymmetric center but with retention of the space group $P2_1/n$. Our findings offer attractive new prospects for the construction of functional molecular crystals.

Experimental Section

Detailed synthetic procedures for **1** and **2** are described in the Supporting Information.

X-ray crystallographic analysis was carried out on a Rigaku RAXIS-RAPID Imaging Plate diffractometer with $Mo_{K\alpha}$ radiation ($\lambda = 0.71073$ Å). Crystal data for **1**: $C_{22}H_{34}O_4Rh_2S_2$, $M = 632.44$, monoclinic, space group $P2_1/n$, $Z = 4$, $T = 100$ K, $a = 8.394(2)$, $b = 36.532(8)$, $c = 8.430(2)$ Å, $\beta = 116.213(10)°$, $V = 2319.2(10)$ Å^3, GOF = 1.024, $R1 = 0.0567$ ($I > 2\sigma(I)$), $wR2 = 0.1039$ (all data). Crystal data for **2**: $C_{22}H_{34}O_4Rh_2S_2$, $M = 632.44$, monoclinic, space group $P2_1/n$, $Z = 4$, $T = 100$ K, $a = 8.339(2)$, $b = 36.750(9)$, $c = 8.447(2)$ Å, $\beta = 115.594(10)°$, $V = 2334(1)$ Å^3, GOF = 1.039, $R1 = 0.0650$ ($I > 2\sigma(I)$), $wR2 = 0.1365$ (all data). CCDC-603301 (**1**), -603302 (**2**), -612865 (entry 3 in Table 1), and -612866 (entry 9 in Table 1) contain the supplementary crystallographic data for this paper. These data can be obtained free of charge from The Cambridge Crystallographic Data Centre via www.ccdc.cam.ac.uk/data_request/cif.

Received: April 29, 2006
Revised: July 1, 2006
Published online: September 4, 2006

 © 2006 Wiley-VCH Verlag GmbH & Co. KGaA, Weinheim

Keywords: photochemistry · photochromism · rhodium · S ligands · solid-state reactions

[1] Special edition: *Photochromism: Memories and Switches* (Ed.: M. Irie), *Chem. Rev.* **2000**, *100*.
[2] *Molecular Switches* (Ed.: B. L. Feringa), Wiley-VCH, Weinheim, **2001**.
[3] J. J. D. de Jong, L. N. Lucas, R. M. Kellogg, J. H. van Esch, B. L. Feringa, *Science* **2004**, *304*, 278.
[4] M. Irie, S. Kobatake, M. Horichi, *Science* **2001**, *291*, 1769.
[5] S. Yamamoto, K. Matsuda, M. Irie, *Angew. Chem.* **2003**, *115*, 1589; *Angew. Chem. Int. Ed.* **2003**, *42*, 1636.
[6] E. V. Boldyreva, *Mol. Cryst. Liq. Cryst.* **1994**, *242*, 17.
[7] J. Harada, H. Uekusa, Y. Ohashi, *J. Am. Chem. Soc.* **1999**, *121*, 5809.
[8] T. Yamada, S. Kobatake, K. Muto, M. Irie, *J. Am. Chem. Soc.* **2000**, *122*, 1589.
[9] T. Yamada, S. Kobatake, M. Irie, *Bull. Chem. Soc. Jpn.* **2000**, *73*, 2179.
[10] M. Morimoto, M. Irie, *Chem. Commun.* **2005**, 3895.
[11] T. Nishioka, H. Kitayama, B. K. Breedlove, K. Shiomi, I. Kinoshita, K. Isobe, *Inorg. Chem.* **2004**, *43*, 5688.
[12] F. A. Cotton, G. Wilkinson, *Advanced Inorganic Chemistry*, 5th ed., Wiley-Interscience, New York, **1988**, p. 522.
[13] S. Lacombe, M. Loudet, A. Dargelos, E. Robert-Banchereau, *J. Org. Chem.* **1998**, *63*, 2281.
[14] H. Dürr, H. Bouas-Laurent, *Photochromism: Molecules and Systems*, Elsevier, Amsterdam, **2003**, p. 1032.
[15] Results on the photoreactivity of **1** in solution will be published elsewhere.
[16] The absorption spectra in Figure S1 in the Supporting Information were measured on the same sample before and after irradiation.
[17] Y. Ohashi, *Acta Crystallogr. Sect. A* **1998**, *54*, 842.
[18] P. Coppens, I. Novozhilova, A. Kovalevsky, *Chem. Rev.* **2002**, *102*, 861.
[19] A. Y. Kovalevsky, K. A. Bagley, J. M. Cole, P. Coppens, *Inorg. Chem.* **2003**, *42*, 140.

 © 2006 Wiley-VCH Verlag GmbH & Co. KGaA, Weinheim

Molecular Recognition

DOI: 10.1002/anie.200602034

Molecular Mapping of the Recognition Interface between the Islet Amyloid Polypeptide and Insulin**

*Sharon Gilead, Haguy Wolfenson, and Ehud Gazit**

The self-assembly of endogenous proteins into amyloid fibrils is the hallmark of a group of diverse human disorders including Alzheimer's disease, Parkinson's disease, and type II diabetes.[1] Many inhibition strategies have been developed in attempts to prevent this key process.[2] A leading approach is the search for natural agents that inhibit amyloid formation. Although most of the studied amyloidogenic proteins can readily form amyloid fibrils in vitro, they are normally stable and physiologically functional, even though there is no sequence diversity between healthy individuals and most of the affected patients. This raises the question as to what prevents these proteins from forming amyloid fibrils in normal situations. A possible explanation is the presence of natural stabilizing agents that prevent these aggregation-prone proteins from adopting the pathological amyloidal conformation. For example, the islet amyloid polypeptide (IAPP) hormone can rapidly form amyloid fibrils in vitro at concentrations that are 100-fold lower than those inside the secretory granules where it is stored. IAPP accumulates into amyloid deposits in the pancreas of type II diabetes patients, whereas in healthy individuals it is functional and soluble.[3] It has previously been shown that insulin is a highly efficient inhibitor of IAPP amyloid formation.[4] Insulin is colocalized and cosecreted with IAPP and it is suggested to stabilize IAPP inside the pancreatic cell. The physical interaction between IAPP and insulin has previously been characterized.[4] However, the molecular elements that mediate this highly important interaction remain to be identified.

In this study we used the natural inhibition mechanism that was selected by an elaborate evolutionary process as a basis to identify a novel and very effective inhibitory module. We performed a systematic reductionist analysis and used peptide-array methodology to identify the molecular determinants within insulin that facilitate the interaction with IAPP and vice versa.

[*] S. Gilead, H. Wolfenson, Prof. E. Gazit
Department of Molecular Microbiology and Biotechnology
Tel Aviv University
Tel Aviv 69978 (Israel)
Fax: (+972) 3-6409407
E-mail: ehudg@post.tau.ac.il

[**] We thank Steve Manch for editing the manuscript, Michal Sadovnic for graphical artwork, and members of the Gazit laboratory for helpful discussions. Support from the BIO-DISC Research and Development program is gratefully acknowledged.

Supporting information for this article is available on the WWW under http://www.angewandte.org or from the author.

WILEY InterScience DISCOVER SOMETHING GREAT
© 2006 Wiley-VCH Verlag GmbH & Co. KGaA, Weinheim

Insulin is composed of two chains, A and B, crosslinked by two disulfide bridges. As a first step, we evaluated the effect of each of the separated chains on IAPP amyloid formation. IAPP was allowed to form amyloid fibrils alone or in the presence of insulin chains. The fibrilization process was monitored by using the thioflavin T (ThT) fluorescence assay (see the Supporting Information). The inhibition abilities of human and bovine insulin were monitored as controls. Both bovine and human insulin exhibited a strong inhibitory effect on the aggregation of the highly amyloidogneic IAPP (Figure 1). The reductionist analysis allowed us to specifically

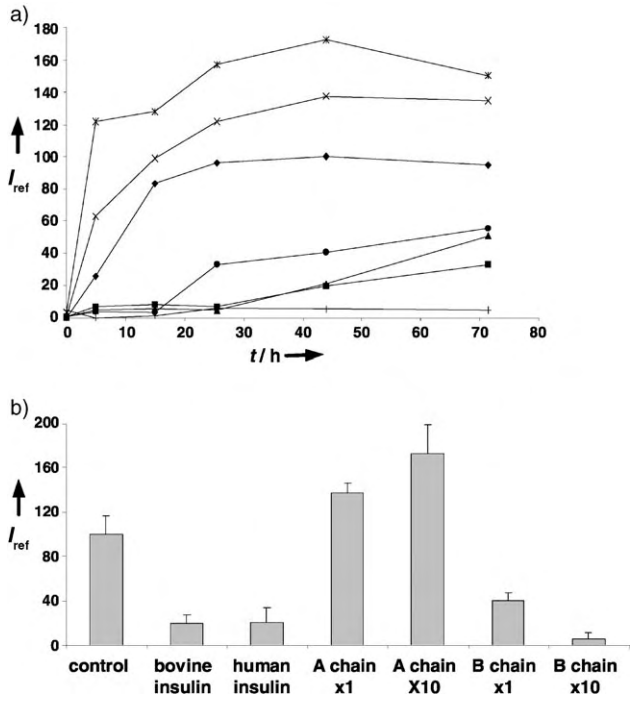

Figure 1. Influence of insulin chains on IAPP amyloid formation as assessed by a ThT-binding fluorescence assay. a) Kinetics of amyloid fibril formation by IAPP (◆) and by IAPP in the presence of bovine insulin (■), human insulin (▲), the insulin A chain at a onefold ratio (×) and at a tenfold ratio (*), and the insulin B chain at a onefold ratio (●) and at a tenfold ratio (+). Human and bovine insulin were added for comparison at a onefold ratio. Each graph represents the average of four independent repeats. b) Presentation of the relative fluorescence values I_{ref} of the samples after 44 h, when IAPP alone reached maximal ThT binding. Each column represents the average of four independent repeats; error bars represent the standard deviation.

pinpoint the B chain as a potent inhibitor which works in a dose-dependent manner. Its inhibition appears to be similar to that of the intact insulin molecule. At a 10-fold ratio, B-chain inhibition seems to be absolute throughout the course of the experiment. Conversely, no inhibition was observed in the presence of the A chain, but the aggregation was instead accelerated. Hence, we propose that the inhibition of IAPP by insulin is predominantly mediated by the B chain.

In order to confirm our assumption, we assessed the ability of the insulin chains to inhibit the IAPP structural transition from random coils into β sheets, a transition that is characteristic of amyloid formation, by using far-UV circular dichroism (CD) analysis (see the Supporting Information). IAPP was incubated alone or in the presence of the A chain, the B chain, or insulin at a 1:1 ratio. CD spectra were recorded after 0, 24, and 48 h (Figure 2).

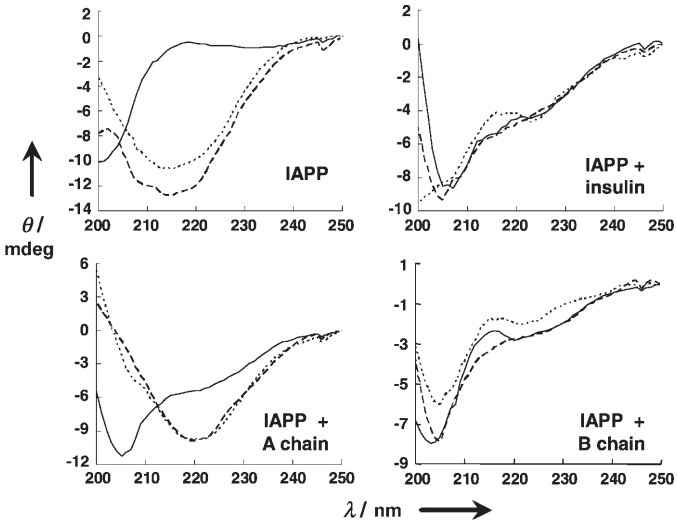

Figure 2. Influence of insulin chains on the IAPP structural transition. CD spectra (200–250 nm) of IAPP alone and in the presence of bovine insulin, the A chain, and the B chain. Changes in the IAPP secondary structure, as a result of amyloid formation, were tracked by measuring samples immediately after preparation (——), after 24 h (-----), and after 48 h (•••••).

The spectra of IAPP alone showed a clear transition from a random-coil conformation at zero time (minimum in the vicinity of 200 nm) to a β-sheet conformation (minimum in the vicinity of 217 nm) after 24 h. However, when the IAPP was incubated with insulin, this transition was not observed. This confirms the efficient insulin inhibition at a very early stage of the structural transition. The CD analyses of IAPP incubated with the B chain indicated a random-coil conformation without a transition over time, as observed in the presence of insulin. By contrast, when IAPP was incubated with the A chain, a structural transition was observed after 24 h, as in the case of IAPP alone. Accordingly, as observed for the formation of ThT-positive fibrils, only the B chain (and not the A chain) inhibits the process of structural transition by IAPP.

We further continued our reductionist analysis by mapping the recognition site within the B chain. To this end, we used an overlapping peptide array for a fine molecular mapping.[5] Briefly, 21 decamer peptides corresponding to consecutive overlapping fragments of the B chain were synthesized on a cellulose membrane. The membrane was incubated with biotinyl-IAPP, and IAPP-binding peptides were detected by dye precipitation with alkaline phosphatase conjugated avidin (see the Supporting Information). A large binding region was observed between residues 8 and 25 (Figure 3a). A second strong binding site was observed at the C-terminus spanning residues 20–30.

Next, we determined whether the peptide fragments of the B chain that bind IAPP are also capable of inhibiting

 © 2006 Wiley-VCH Verlag GmbH & Co. KGaA, Weinheim

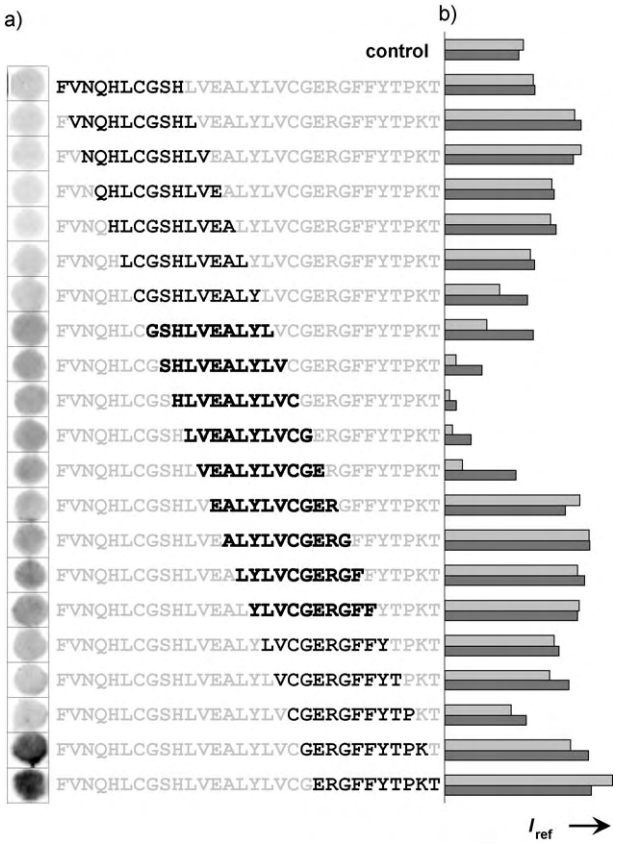

Figure 3. Screen for IAPP-binding and -inhibiting sequences within the insulin B chain. a) Decamer peptides corresponding to consecutive overlapping sequences of the B chain were synthesized on a cellulose membrane and incubated with biotinyl-IAPP. The sequence (black) of each spot and the position of each within the complete B chain sequence (gray) are presented. The sequences corresponding to the spots that exhibited binding are denoted in bold. b) The same peptides were cleaved from the membrane and then transferred onto a microtiter plate. Amyloid fibril formation by IAPP in the presence of the B chain peptides was assessed by the ThT-binding assay. Peptides were added at a 10-fold excess and ThT fluorescence was measured after 48 h (light gray) and 70 h (dark gray).

amyloid formation. We used ThT fluorescence as a complementary assay and searched for the inhibiting region within the B chain. IAPP fibrilization was performed in the presence of the same consecutive overlapping peptides, free in solution. Inhibition was observed with a set of peptides corresponding to residues 9–20 (Figure 3b). This region is included within the large region observed to bind IAPP. On the other hand, the peptides corresponding to the C-terminus sequence did not exhibit any inhibition effect. In addition, it was previously reported that insulin with a truncated B chain (lacking residues 23–30) also binds IAPP.[4e] Thus, the combination of the two assays points toward one central domain within the B chain that is responsible for binding to IAPP and preventing its aggregation.

To further pinpoint the region within IAPP to which insulin binds, we performed a reciprocal peptide-array analysis. 28 decamer peptides corresponding to consecutive overlapping fragments of IAPP were synthesized on a cellulose membrane and incubated with insulin (see the Supporting Information). A single binding domain spanning residues 7–19 was detected (Figure 4). Intriguingly, we previously identified this same region as the major recognition domain of IAPP fibrilization by using the same peptide-array method.[5] In addition, short peptide fragments derived from this region were found to associate into amyloid-like fibrils. Thus, insulin appears to interact with IAPP at the same region as that where IAPP self-interacts to form ordered amyloid assemblies.

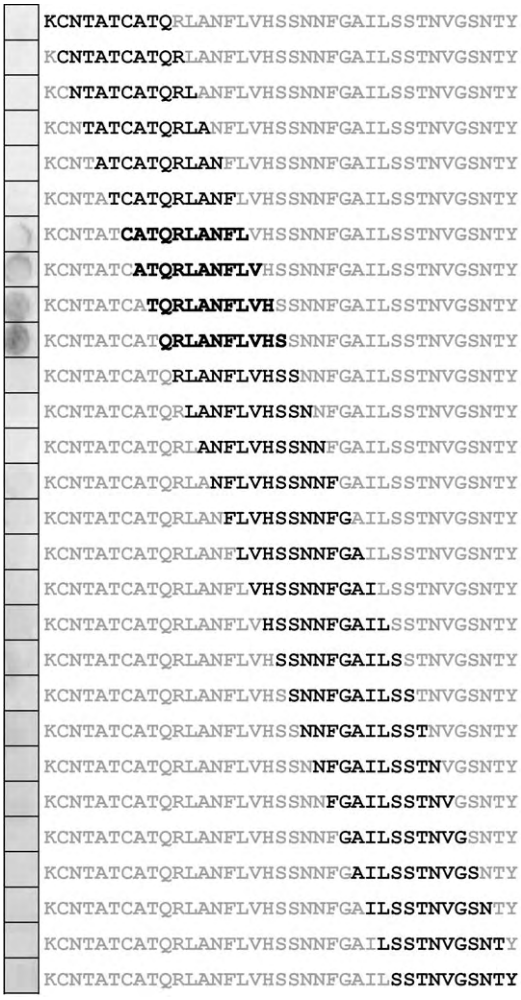

Figure 4. Screen for insulin-binding sequences within IAPP. Decamer peptides corresponding to consecutive overlapping sequences of IAPP were synthesized on a cellulose membrane and incubated with insulin. The sequence (black) of each spot and the position of each within the IAPP sequence (gray) are presented. Sequences corresponding to the spots that exhibited binding are denoted in bold.

To conclude, by a systematic biochemical reductionist approach we have identified a single domain within insulin that binds to IAPP and also inhibits IAPP amyloid formation. This domain is located at the center of the insulin B chain and spans residues 9–20. Moreover, we have identified a single domain within IAPP that binds insulin in the vicinity of residues 7–19. We propose that these two domains compose

 © 2006 Wiley-VCH Verlag GmbH & Co. KGaA, Weinheim

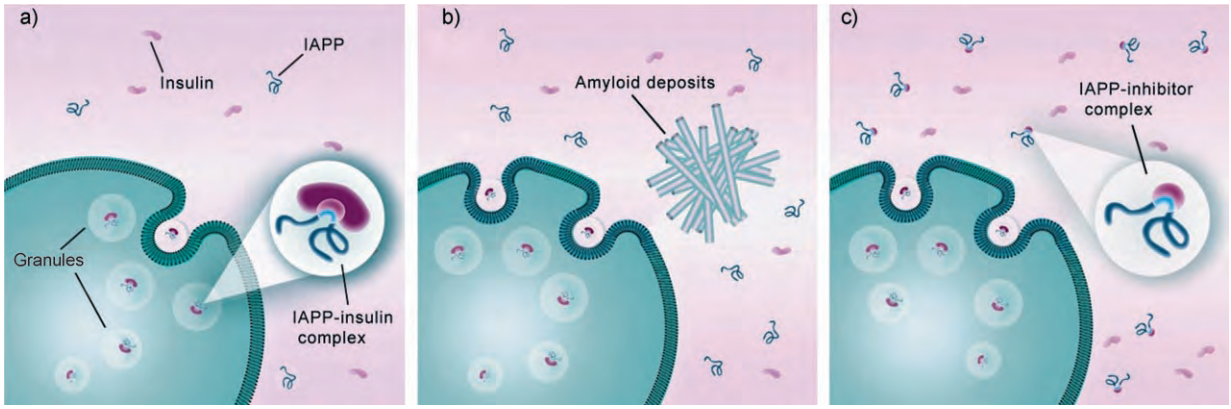

Figure 5. A possible model for IAPP and insulin behavior under different physiological conditions. a) In a healthy individual, IAPP and insulin form a complex within the secretory granules. When secreted, they disassociate and circulate in the blood. Random-coiled IAPP is shown in blue, globular insulin is shown in magenta. The magnification of the IAPP–insulin complex is depicted in the light circle with the recognition sites highlighted. b) In type II diabetes, secretion of IAPP and insulin is accelerated and the IAPP local concentration is increased. As a result, amyloid fibrils are deposited. c) Hypothetical strategy for treating type II diabetes: A short peptide, corresponding to the insulin recognition site, binds to secreted IAPP and prevents it from adopting the β-sheet conformation and accumulating into amyloid fibrils. The magnification of the IAPP–peptide inhibitor complex is depicted in the light circle.

the recognition interface that mediates the IAPP–insulin interaction.

Interestingly, the results are in good agreement with previous data and theories regarding amyloid formation and inhibition. First, as mentioned above, the identified domain within IAPP is the recognition site that is responsible for amyloid formation. It is very plausible that this domain will also be the target of insulin. Second, the two regions share sequence homology, as previously reported.[4e] The results directly support one of the proposals that was raised on the basis of sequence alignment. The two sequences are ANFLV, at positions 13–17 of IAPP, and ALYLV, at positions 14–18 of the insulin B chain. This homology probably allows the specific recognition between the domains. Third, according to the three-dimensional structure of insulin, the recognition region is organized in an α-helix conformation. It is possible that, in the context of the entire insulin molecule, this domain mediates inhibition by structure restriction, that is, by disabling the conversion into a β-sheet conformation. The β-breaking methodology is a central strategy of amyloid inhibition.[2b,c,f] We have previously exemplified this mechanism, when IAPP fibrilization was strongly inhibited by using α-aminoisobutyric acid (Aib) modified peptides, which also display a helical conformation.[6] Possibly, a similar mechanism underlies insulin inhibition. However, this suggestion should be further studied. Fourth, the identified region of the B chain contains an aromatic amino acid, tyrosine (at position 16), which is located opposite the phenylalanine residue of IAPP in the sequence alignment. We speculate that the tyrosine mediates IAPP–insulin recognition through π stacking with the phenylalanine. This assumption is based on our hypothesis regarding the key role of aromatic interactions in the process of amyloid formation[7] by providing directionality and stability to the assembled ultrastructural fibril.[8] Here, the tyrosine residue might play a similar role in the IAPP–insulin interaction.

Taken together, the results and characteristics discussed above clearly describe a putative molecular mechanism underlying insulin inhibition of IAPP fibrilization. Insulin binds to the amyloid-formation recognition site of IAPP through a specific recognition mechanism that is based on sequence homology and is possibly mediated by aromatic interactions. In this way, insulin blocks the ability of IAPP to assemble into amyloid fibrils through structure constraints.

Based on our conclusions, we suggest a hypothetical physiological mechanism for the IAPP–insulin interaction and a therapeutic approach of using insulin-derived peptides as amyloid inhibitors for type II diabetes (Figure 5). Within the secretory granule, insulin is found in 10–50-fold molar excess over IAPP. At this concentration ratio, kinetic inhibition is calculated to be maintained for several months, whereas the lifetime of a granule is several hours.[4d] This provides a reasonable explanation for the lack of amyloid fibrils inside the cell. When secreted, the IAPP–insulin complex dissociates, probably as a result of dilution beyond the association-constant concentration (Figure 5a). In the case of type II diabetes, the insulin and IAPP secretion is greatly accelerated due to insulin resistance. The amount of unbound IAPP outside the cell is augmented, which induces transient local high concentrations. As a result, IAPP associates into amyloid deposits (Figure 5b).

Due to the global prevalence of type II diabetes, there is a growing need to develop effective therapeutic agents to treat it. Since insulin is an excellent natural inhibitor, it may be very worthwhile to imitate its mechanism. We hypothesize that a properly designed peptide inhibitor, based on the insulin recognition module, might be an attractive drug lead for treating type II diabetes. Such a peptide inhibitor would bind to secreted IAPP in the same manner that insulin does and prevent its accumulation into amyloid fibrils (Figure 5c).

Received: May 22, 2006
Revised: July 2, 2006
Published online: September 8, 2006

 © 2006 Wiley-VCH Verlag GmbH & Co. KGaA, Weinheim

Keywords: amyloids · insulin · molecular recognition · peptides · protein–protein interactions

[1] a) J. C. Rochet, P. T. Lansbury, Jr., *Curr. Opin. Struct. Biol.* **2000**, *10*, 60–68; b) C. Soto, *Nat. Rev. Neurosci.* **2003**, *4*, 49–60; c) C. M. Dobson, *Nature* **2003**, *426*, 884–890.

[2] a) L. O. Tjernberg, J. Näslund, F. Lindqvist, J. Johansson, A. R. Karlström, J. Thyberg, L. Terenius, C. Nordstedt, *J. Biol. Chem.* **1996**, *271*, 8545–8548; b) C. Soto, E. M. Sigurdsson, L. Morelli, R. A. Kumar, E. M. Castano, B. Frangione, *Nat. Med.* **1998**, *4*, 822–826; c) T. L. Lowe, A. Strzelec, L. L. Kiessling, R. M. Murphy, *Biochemistry* **2001**, *40*, 7882–7889; d) L. A. Scrocchi, Y. Chen, S. Waschuk, F. Wang, S. Cheung, A. A. Darabie, J. McLaurin, P. E. Fraser, *J. Mol. Biol.* **2002**, *310*, 697–706; e) H. M. Petrassi, S. M. Johnson, H. E. Purkey, K. P. Chiang, T. Walkup, X. Jiang, E. T. Powers, J. W. Kelly, *J. Am. Chem. Soc.* **2005**, *127*, 6662–6671; f) L. M. Yan, M. Tatarek-Nossol, A. Velkova, A. Kazantzis, A. Kapurniotu, *Proc. Natl. Acad. Sci. USA* **2006**, *103*, 2046–2051.

[3] a) P. Westermark, C. Wernstedt, E. Wilander, K. Sletten, *Biochem. Biophys. Res. Commun.* **1986**, *140*, 827–831; b) A. Kapurniotu, *Biopolymers* **2001**, *60*, 438–459; c) E. T. Jaikaran, A. Clark, *Biochim. Biophys. Acta* **2001**, *1537*, 179–203; d) A. E. Butler, J. Jang, T. Gurlo, M. D. Carty, W. C. Soeller, P. C. Butler, *Diabetes* **2004**, *53*, 1509–1516.

[4] a) P. Westermark, Z. C. Li, G. T. Westermark, A. Leckstrom, D. F. Steiner, *FEBS Lett.* **1996**, *379*, 203–206; b) S. Janciauskiene, S. Eriksson, E. Carlemalm, B. Ahren, *Biochem. Biophys. Res. Commun.* **1997**, *236*, 580–585; c) Y. C. Kudva, C. Mueske, P. C. Butler, N. L. Eberhardt, *Biochem. J.* **1998**, *331*, 809–813; d) J. L. Larson, A. D. Miranker, *J. Mol. Biol.* **2004**, *335*, 221–231; e) E. T. Jaikaran, M. R. Nilsson, A. Clark, *Biochem. J.* **2004**, *377*, 709–716.

[5] Y. Mazor, S. Gilead, I. Benhar, E. Gazit, *J. Mol. Biol.* **2002**, *322*, 1013–1024.

[6] S. Gilead, E. Gazit, *Angew. Chem.* **2004**, *116*, 4133–4136; *Angew. Chem. Int. Ed.* **2004**, *43*, 4041–4044.

[7] E. Gazit, *FASEB J.* **2002**, *16*, 77–83.

[8] a) R. Azriel, E. Gazit, *J. Biol. Chem.* **2001**, *276*, 34156–34161; b) S. Jones, J. Manning, N. M. Kad, S. E. Radford, *J. Mol. Biol.* **2003**, *325*, 249–257; c) G. G. Tartaglia, A. Cavalli, R. Pellarin, A. Caflisch, *Protein Sci.* **2004**, *13*, 1939–1941; d) O. S. Makin, E. Atkins, P. Sikorski, J. Johansson, L. C. Serpell, *Proc. Natl. Acad. Sci. USA* **2005**, *102*, 315–320; e) A. P. Pawar, K. F. Dubay, J. Zurdo, F. Chiti, M. Vendruscolo, C. M. Dobson, *J. Mol. Biol.* **2005**, *350*, 379–392; f) C. Wu, H. Lei, Y. Duan, *Biophys. J.* **2005**, *88*, 2897–2906; g) H. Inouye, D. Sharma, W. J. Goux, D. A. Kirschner, *Biophys. J.* **2006**, *90*, 1774–1789; h) F. G. De Felice, M. N. Vieira, L. M. Saraiva, J. D. Figueroa-Villar, J. Garcia-Abreu, R. Liu, L. Chang, W. L. Klein, S. T. Ferreira, *FASEB J.* **2004**, *18*, 1366–1372; i) Y. Porat, Y. Mazor, S. Efrat, E. Gazit, *Biochemistry* **2004**, *43*, 14454–14462.

 © 2006 Wiley-VCH Verlag GmbH & Co. KGaA, Weinheim

Helical Structures

DOI: 10.1002/anie.200602060

Structurally Characterized Quadruple-Stranded Bisbidentate Helicates**

*Jide Xu and Kenneth N. Raymond**

Although examples preceded the definition, the term "helicate" was introduced by Lehn et al. in 1987 for metal complexes that contain two or more metal centers bridged by one or more ligand strands.[1] Helicates are the simplest and most fundamental supramolecular architectures.[2–3] The formation of different types of helicates is a consequence of the combination of the information intrinsic to the helicate components. Since this self-assembly process is also the basis for the formation of other supramolecular architectures and devices, helicates in particular have received much attention.[2–3] For example, early work in this laboratory on M^{III} triple-stranded helicates[4] elucidated structural principles that have allowed the development of a versatile class of inorganic supramolecular structures.[5] While numerous single-, double-, and triple-stranded helicates have been well documented,[2–4,6] there are only a few examples of quadruple-stranded helicates,[7–9] as a result of the increased complexity of this architecture in relation to other helicates.

As predicted,[2] most reported saturated quadruple-stranded helicates have been achieved by employing a combination of square-planar metal centers with oligomonodentate bridging ligands.[8] Recently, the formulation of the first quadruple-stranded bisbidentate helicate was confirmed[9] by electrospray mass spectrometry as a double-charged anion, which was composed of two Eu^{III} ions and four bis(β-diketone) ligands. However, there have been no reports of fully characterized fourfold-symmetric oligobidentate quadruple-stranded helicates, nor reports of quadruple-stranded actinide helicates. The design and synthesis of oligobidentate quadruple-stranded helicates has remained a challenge.

A continuing goal in our group has been the development of chelating agents for lanthanide and actinide ions.[10] The lanthanide and actinide ions generally display high, variable (8, 9, or higher) coordination numbers which makes them excellent candidates for matching the coordination require-

[*] Dr. J. Xu, Prof. K. N. Raymond
Department of Chemistry
University of California
Berkeley, CA 94720-1460 (USA)
Fax: (+1) 510-486-5283
E-mail: raymond@socrates.berkeley.edu

[**] Coordination Number Incommensurate Cluster Formation part 33. This research was supported by the Director, Office of Science, Office of Advanced Scientific Computing Research, Office of Basic Energy Sciences (U.S. Department of Energy) under contract DE-AC02-05CH11231. The authors would like to thank Modi Wetzler, Matt Stavis, Geza Szigethy, Dr. Christoph Jocher, and Dr. Michael Seitz for helpful discussions and suggestions.

 WILEY InterScience DISCOVER SOMETHING GREAT

© 2006 Wiley-VCH Verlag GmbH & Co. KGaA, Weinheim

ment (8 or higher) of oligobidentate quadruple-stranded helicates. Indeed, the high coordination number of lanthanide and actinide ions potentially permits greater versatility in the design and construction of supramolecular edifices, of which quadruple-stranded helicates represent the important first step. However, the high and variable coordination number also presents a challenge along with complicated coordination geometries.

It has been suggested[2] that the synthesis of a quadruple-stranded helicate might be achieved by employing a combination of square-antiprismatic metal centers with oligobidentate bridging ligands. A metal ion with fourfold coordination geometry, such as square antiprism or monocapped square antiprism, would be a good candidate for a saturated quadruple-stranded helicate. However, quadruple-stranded helicates based on eight-coordinate square-antiprism metal ions may leave relatively large openings at both ends of the helicate, thus causing undesirable high repulsion energy between the donor atoms (Figure 1 a). As a result, we

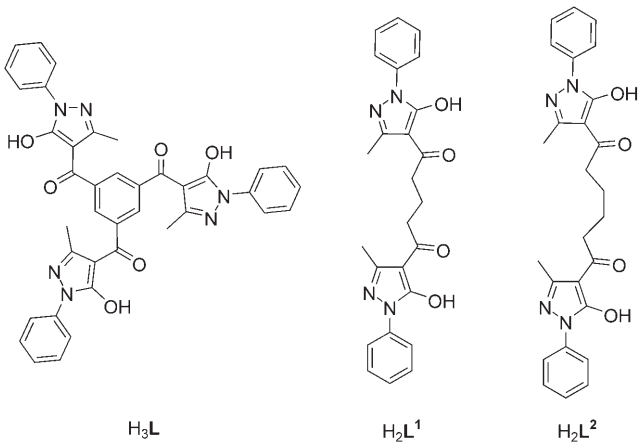

$H_3\mathbf{L}$ $H_2\mathbf{L}^1$ $H_2\mathbf{L}^2$

Scheme 1. Tris-β-diketonate $H_3\mathbf{L}$ and bis-diketonate 4-acyl-2-pyrazolin-5-one ligands $H_2\mathbf{L}^1$ and $H_2\mathbf{L}^2$ with three and four methylene linear scaffolds, respectively.

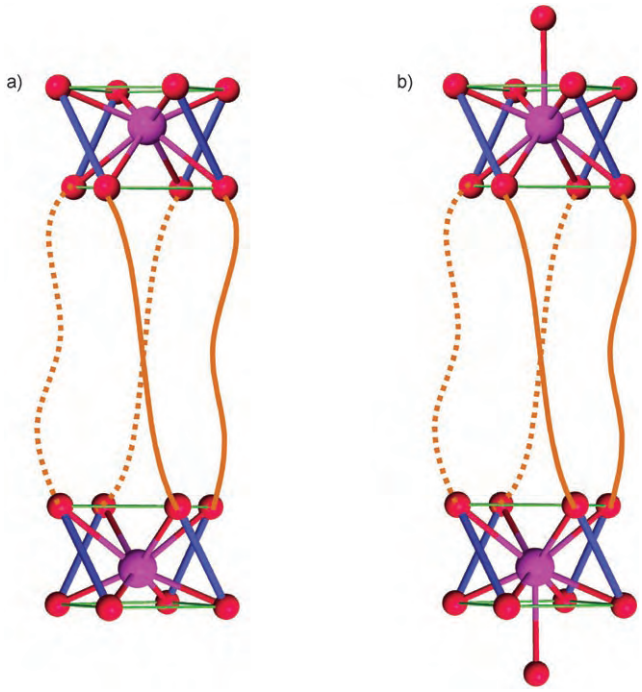

Figure 1. Schematic view of quadruple-stranded helicates based on a) square-antiprism (C.N.: 8) and b) monocapped square-antiprism (C.N.: 9) metal centers (purple, donor atoms red) and bisbidentate ligand strands (orange). C.N. = coordination number.

concluded that nine-coordinate metal ions, with monocapped square-antiprism geometry, in which the donors are distributed more evenly around the central metal ion, would be the better choice for designing a quadruple-stranded helicate (Figure 1 b).

We previously reported that the tris-β-diketonate type hexadentate 4-acyl-2-pyrazolin-5-one ligand, $H_3\mathbf{L}$ (Scheme 1), forms a supramolecular lanthanide complex $[La_8\mathbf{L}_8]$.[11] The bisbidentate 4-acyl-2-pyrazolin-5-one ligands were first synthesized about two decades ago.[12] The avidity of 4-acyl-2-pyrazolin-5-one ligands towards lanthanide and actinide ions has long been recognized.[13] One such bisbidentate ligand $H_2\mathbf{L}^1$ (Scheme 1), for example, forms triple-stranded dinuclear lanthanide complexes $[Ln_2(\mathbf{L}^1)_3(dmf)_4]$ (dmf = *N*,*N*,-dimethylformamide), in which each lanthanide ion is eight-coordinate with three bidentate ligand moieties and two solvent DMF molecules.[13] It was therefore reasoned that these bisbidentate pyrazolonate ligands, in combination with eight- or nine-coordinate tetravalent ions, such as Th^{IV}, would lead to quadruple-stranded helicates, because the high charge (4+) would encourage four monoanionic bidentate pyrazolone ligand moieties to bind at each central metal ion. In addition, repulsion energy calculations predicted that the capped square antiprism isomer with a C_4 symmetry axis is the discrete potential energy minimum for $[M^{IV}(bidentate)_4(monodentate)]$ complexes.[14,15] In such a geometry, the monodentate ligand occupies the cap position and the four equivalent bidentate ligands are wrapped around the nine-coordinate M^{IV} atoms, thus forming capped square antiprisms with the bidentate ligands spanning the edges linking the two square faces of the square antiprism (Figure 1 b).

A series of bisbidentate pyrazolone ligands with systematically varied lengths of the linear ligand scaffold was prepared according to reported procedures.[12,13] Scheme 1 shows two examples, $H_2\mathbf{L}^1$ and $H_2\mathbf{L}^2$, with a linear scaffold of three and four methylene groups, respectively.

The Th^{IV} quadruple-stranded helicate complexes were prepared by treatment of Th^{IV} tetrakisacetylacetonate with two equivalents of bisbidentate pyrazolone ligands $H_2\mathbf{L}^1$ or $H_2\mathbf{L}^2$ in a solution of MeOH/$CHCl_3$ (1:1). FAB(+) mass spectrometric analysis indicated that both Th^{IV} complexes have the expected $M_2\mathbf{L}_4$ stoichiometry. The ^{1}H NMR spectra of these complexes in [D_6]DMSO are consistent with the formation of highly symmetrical quadruple-stranded helicates with average D_4 symmetry on the NMR timescale. For example, the ^{1}H NMR spectrum of $[Th_2(\mathbf{L}^1)_4]$ shows only one multiplet for the protons of the central methylene units of the ligand (Figure 2, upper panel). After crystallization from

 © 2006 Wiley-VCH Verlag GmbH & Co. KGaA, Weinheim

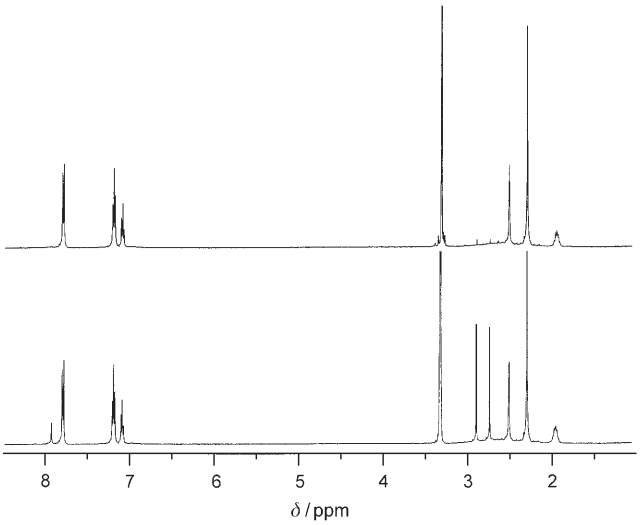

Figure 2. Proton NMR spectra of a[$Th_2(\mathbf{L}^1)_4$] (upper panel) and [$Th_2(\mathbf{L}^1)_4(dmf)_2$] (lower panel) in [$D_6$]DMSO.

DMF, the NMR spectra of the complex indicated the presence of two DMF molecules associated with the complex, and only one set of the DMF peaks is apparent (Figure 2, lower panel). The high symmetry of the original molecule is retained, which implies that the two DMF molecules are located on the C_4 axis, at the termini of the helicate, as it seems unlikely that full scrambling at the position of the bisbidentate ligand occurs on the NMR timescale.

As a result of the high nuclear quadrupole moment of thorium (Q(mbarn) = 4300),[16] the NMR signals of the ligand spacer methylene groups adjacent to the thorium coordination centers are broadened and can be detected only at elevated temperatures (Figure 3).

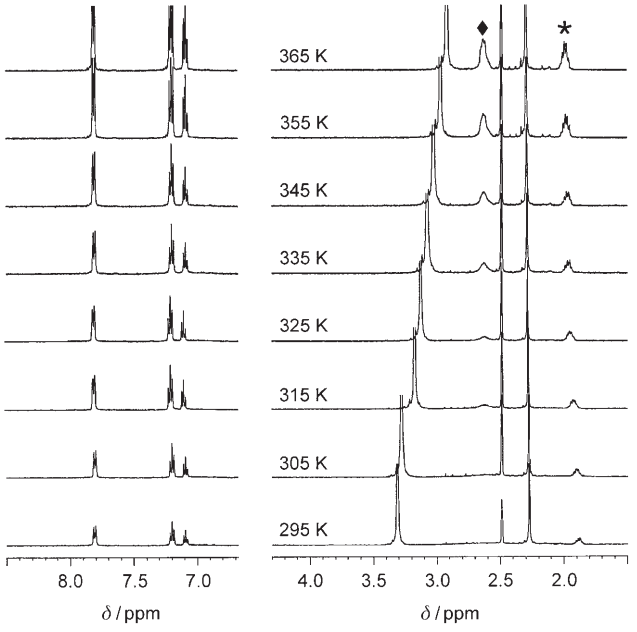

Figure 3. Variable-temperature NMR spectra of [$Th_2(\mathbf{L}^1)_4$] in [D_6]DMSO. The signal labeled with the diamond represents the central methylene, and the star represents the methylene groups of the scaffold adjacent to the coordination centers.

Single-crystal X-ray structure analyses were carried out to determine the solid-state structures of [$Th_2(\mathbf{L}^1)_4$] and [$Th_2(\mathbf{L}^2)_4$].[17] X-ray quality crystals of [$Th_2(\mathbf{L}^1)_4(dmf)_2$] were grown by slow evaporation of its wet DMF solution (1% H_2O in DMF), while those of [$Th_2(\mathbf{L}^2)_4(dmf)_2$] were grown from wet DMF solution by diffusion of diethyl ether. The crystal structures of both helical complexes are shown in Figures 4 and 5. These structures indicate that both of the quadruple helicates are homochiral, which implies that there might be

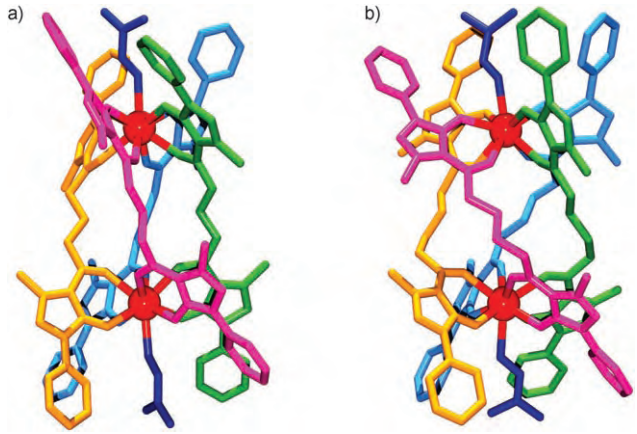

Figure 4. Frame-and-sphere representations of the crystal structure of a) [$Th_2(\mathbf{L}^1)_4(dmf)_2$] and b) [$Th_2(\mathbf{L}^2)_4(dmf)_2$] as viewed perpendicular to the twofold axis of the quadruple-stranded helicate. For clarity, each ligand is represented in a different color, with thorium ions represented by dark red spheres, coordinated dmf dark blue.

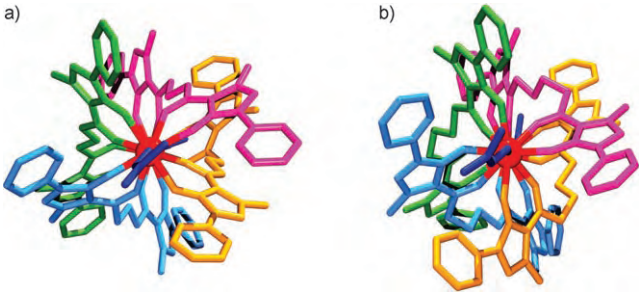

Figure 5. Frame-and-sphere representations of the crystal structure of a) [$Th_2(\mathbf{L}^1)_4(dmf)_2$] and b) [$Th_2(\mathbf{L}^2)_4(dmf)_2$] as viewed down the fourfold axis of the quadruple-stranded helicate. For clarity, each ligand is represented in a different color, with thorium ions represented by dark red spheres, coordinated dmf dark blue.

mechanical coupling between the two centers of each helicate such that the chirality at one can be transmitted to the second.[2]

In both helicates, [$Th_2(\mathbf{L}^1)_4(dmf)_2$] and [$Th_2(\mathbf{L}^2)_4(dmf)_2$], the Th^{IV} ions are nine-coordinate. This coordination number has several idealized coordination geometries. The tricapped trigonal prism (D_{3h}) and capped square antiprism (C_{4v}) are the most stable geometries, and the energy difference between the two is very small as predicted by repulsion energy calculations.[14,15] We thus employed the shape measure S to assess this subtle difference[18] and found that in both helicates

 © 2006 Wiley-VCH Verlag GmbH & Co. KGaA, Weinheim

the nine-coordinate geometries can be assigned as being closest to the monocapped square antiprism (C_{4v}) based on the shape measure calculation.

As expected from repulsion energy calculations and previous observations,[14,15] the bidentate units are symmetrically bonded in a capped square-antiprism geometry (Figure 1b), with the donor atoms that form the capped face (O_{cf}) experiencing considerably less repulsion than those that form the uncapped face (O_{uf}), in agreement with the observed average Th–O lengths in the quadruple helicates. The Th^{IV}–O_{cf} bond lengths are 2.41(1) and 2.40(1) Å and the Th^{IV}–O_{uf} bond lengths are 2.47(3) and 2.48(3) Å in $[Th_2(\mathbf{L}^1)_4(dmf)_2]$; the Th–$O_{cf}$ bond lengths are 2.38(3) and 2.41(2) Å and the Th–O_{uf} bond lengths are 2.49(6) and 2.47(2) Å in $[Th_2(\mathbf{L}^2)_4(dmf)_2]$. Note that in the 10-coordinate Th^{IV} complex of bis(4-benzoyl-2,4-dihydro-5-methyl-2-phenyl-3-*H*-pyrazolonato-*O*,*O*′)-bis(nitrato-*O*,*O*′)-bis(triphenylphosphine oxide-*O*) complex,[19] the bond lengths between the Th^{IV} ion and the two oxygen donors of a bidentate 4-acyl-pyrazolonate ligand are quite similar at 2.435 and 2.447 Å, respectively.

The pitch L of a helicate is defined by Equation 1,[2] where d is the distance (Å) between the upper and bottom surfaces

$$L = d/(\omega_1/360) \quad (1)$$

of the helicate cylinder and ω_1 is the twist angle (in degrees) of the upper and bottom surfaces. An ideal helicate should be palindromic (constant pitch), which is not the case with $[Th_2(\mathbf{L}^1)_4(dmf)_2]$ and $[Th_2(\mathbf{L}^2)_4(dmf)_2]$, and three subpitches L_1, L_2, and L_3 compose the total pitch L_T (Figure 6). The two subpitches (L_1 and L_3) of both capped square antiprisms of the helicate are different from that of the bridging part (L_2; see Table 1).

Previous studies have found that the stereoselective formation of triple-stranded helicate complexes from linear alkyl-bridged ligands depends, to a large extent, on the preferred conformation of the spacers. An odd number of methylene units yields a molecule with an internal mirror plane, thus producing an achiral *meso* helicate. In the case of an even number of methylene units, the favored conformation imposes a C_2 axis upon complex formation and will lead to a chiral helicate.[3] In the case of bisbidentate quadruple-stranded helicate complexes formed from linear alkyl-bridged ligands, the preferred conformation of the spacer does not significantly affect the stereochemistry of the complexes. With both three and four (odd or even) methylene spacers, the complexes are all homochiral helicates. However, the alkyl-bridge pitch (L_2) in $[Th_2(\mathbf{L}^1)_4(dmf)_2]$ ($n=3$, odd) is much longer than that in $[Th_2(\mathbf{L}^2)_4(dmf)_2]$ ($n=4$, even), which suggests a trend similar to that observed in the triple-stranded helicates. Given the important role of chirality in the application of supramolecular compounds in catalysis, the difference between the observed behavior of the triple- and quadruple-helicate complexes is significant.

In summary, new actinide quadruple-stranded helical supramolecular architectures have been synthesized in which two capped square-antiprismatic Th^{IV} centers are coordinated by four bisbidentate 4-acylpyrazolone chelating strands. These complexes are the first two structurally characterized examples of bisbidentate quadruple-stranded helical complexes and are another remarkable example of cluster formation by incommensurate coordination number. These helicates and the previous $[La_8\mathbf{L}_8]$ complex ("The Lord of Rings")[11] highlight the versatility of 4-acylpyrazolone ligands in lanthanide and actinide coordination chemistry, with implications ranging beyond the field of supramolecular chemistry.

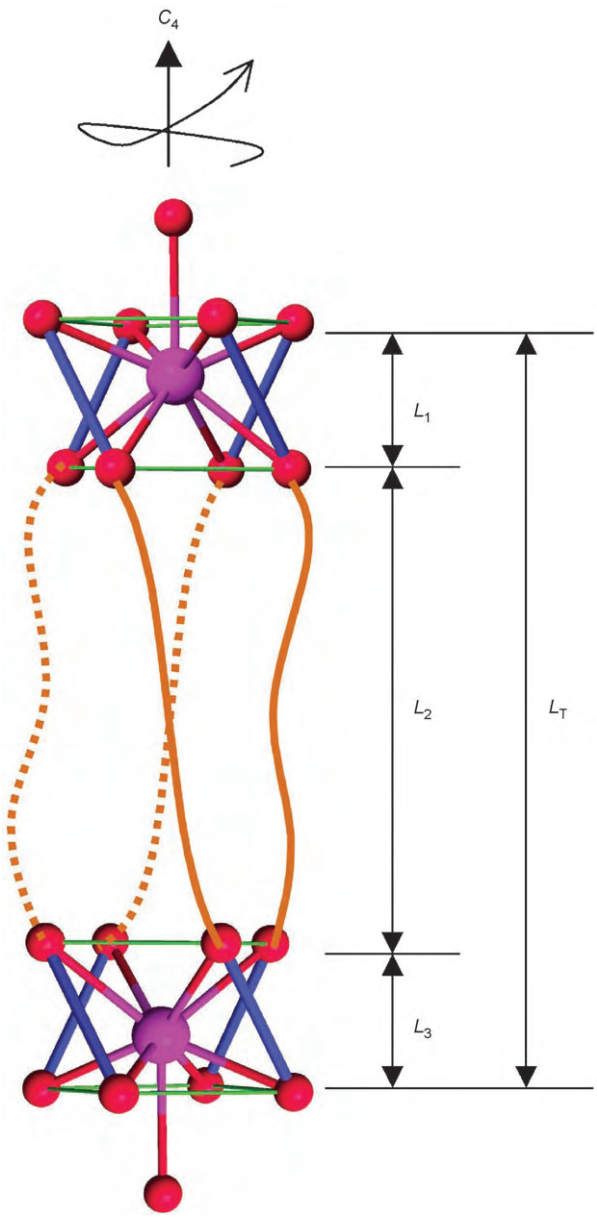

Figure 6. Different subpitches (L_1–L_3) in a quadruple-stranded helicate, in which the height of the helicate (L_T) is defined as the distance between the centroids of the outer square faces. Colors as in Figure 1. The thick edges of the polyhedra represent the bidentate spanning edges.

Experimental Section

$[Th_2(\mathbf{L}^1)_4]$: A solution of $[Th(acac)_4]$ (acac = acetylacetone; 0.05 mmol) in absolute methanol (10 mL) was added to a solution of $H_2\mathbf{L}^1$ (0.11 mmol) in $CHCl_3$ (10 mL). The reaction mixture was

 © 2006 Wiley-VCH Verlag GmbH & Co. KGaA, Weinheim

Table 1: Twist angles and helical pitches in $[Th_2(L^1)_4(dmf)_2]$ and $[Th_2(L^2)_4(dmf)_2]$.

Complex	$[Th_2(L^1)_4(dmf)_2]$	$[Th_2(L^2)_4(dmf)_2]$
Th(1)–Th(2) distance (Å)	8.304	8.151
Height of the upper square antiprism (Å)	2.367	2.328
Average twist angle of the upper square antiprism (°)	40.5	43.8
Pitch of the upper square antiprism L_1 (Å)	21.04	19.13
Height of the alkyl bridge (Å)	5.282	5.206
Average twist angle of the alkyl bridge (°)	4.3	37.5
Pitch of the alkyl bridge part L_2 (Å)	442.21	49.98
Height of the bottom square antiprism (Å)	2.367	2.376
Average twist angle of the lower square antiprism (°)	40.5	39.5
Pitch of the bottom square antiprism L_3 (Å)	21.04	21.65
Average total twist angle (°)	85.2	120.6
Distance between the outer faces of upper and lower square antiprisms (Å)	10.01	9.86
Total pitch L_T (Å)	42.3	29.6

heated at reflux under N_2 with stirring for 16 h, during which time a beige precipitate formed. The solid was collected by filtration, washed with methanol, and dried under vacuum to yield 88 mg (0.039 mmol, 78%) of $[Th_2(\mathbf{L}^1)_4]$ based on $[Th(acac)_4]$. Elemental analysis (%) calcd for $C_{100}H_{88}N_{16}O_{16}Th_2$ (2233.99 g mol^{-1}): C 53.76, H 3.97, N 10.03; found: C 53.47, H 4.11, N 10.22; ^{1}H NMR (500 MHz, [D$_6$]DMSO, 25 °C): $\delta = 1.93$ (qt, 8H, $J = 7.0$ Hz; CH_2), 2.27 (s, 24H; CH_3), 7.09 (t, $J =$ 7.5 Hz, 8H; ArH), 7.20 (t, $J = 7.7$ Hz, 16H; ArH), 7.80 ppm (d, $J =$ 8.0 Hz, 16H; ArH); (+)FAB-MS [MH$^+$] m/z 2193.7. This compound was recrystallized from wet DMF (containing 1% H_2O) to provide X-ray-quality colorless crystals of $[Th_2(\mathbf{L}^1)_4(dmf)_2]\cdot 6\,DMF\cdot 0.5\,H_2O$.

$[Th_2(\mathbf{L}^2)_4]$: This compound was prepared by a similar procedure as above, except $H_2\mathbf{L}^2$ was used instead of $H_2\mathbf{L}^1$, and yielded 84 mg (0.037 mmol, 74%) based on $[Th(acac)_4]$. Elemental analysis (%) calcd for $C_{104}H_{96}N_{16}O_{16}Th_2$ (2290.05 g mol^{-1}): C 54.55, H 4.23, N 9.79; found: C 54.22, H 4.33, N 9.82; ^{1}H NMR(500 MHz, [D$_7$]DMF, 25 °C): $\delta = 1.20$ (s, br, 8H, CH_2), 1.92 (s, br, 8H, CH_2), 2.41 (s, 24H, CH_3), 7.09 (t, $J = 7.5$ Hz, 8H, ArH), 7.22 (t, $J = 7.7$ Hz, 16H, ArH), 7.94 ppm (d, $J = 8.0$ Hz, 16H, Ar H); (+)FAB-MS [MH$^+$] m/z 2289.6. Colorless X-ray-quality crystals $[Th_2(\mathbf{L}^2)_4(dmf)_2]\cdot 0.5\,DMF\cdot 1.5\,C_4H_{10}O$ were obtained form diffusion of its DMF solution into diethyl ether.

Received: May 23, 2006
Published online: September 4, 2006

Keywords: actinides · helical structures · self-assembly · shape analysis · supramolecular chemistry

[1] J.-M. Lehn, A. Rigault, J. Siegel, J. Harrowfield, B. Chevrier, D. Moras, *Proc. Natl. Acad. Sci. USA* **1987**, *84*, 2565 – 2569.
[2] C. Piguet, G. Bernardinelli, G. Hopfgartner, *Chem. Rev.* **1997**, *97*, 2005 – 2062; J.-C. G. Bünzli, C. Piguet, *Chem. Rev.* **2002**, *102*, 1897 – 1928, and references therein.
[3] a) M. Albrecht, *Chem. Rev.* **2001**, *101*, 3457 – 3497; b) M. Albrecht, *Chem. Soc. Rev.* **1998**, *27*, 281 – 288, and references therein.
[4] R. C. Scarrow, D. L. White, K. N. Raymond, *J. Am. Chem. Soc.* **1985**, *107*, 6540 – 6546.
[5] a) A. V. Davis, K. N. Raymond, *J. Am. Chem. Soc.* **2005**, *127*, 7912 – 7919; b) D. Fiedler, R. G. Bergman, K. N. Raymond, *Angew. Chem.* **2006**, *118*, 759 – 762; *Angew. Chem. Int. Ed.* **2006**, *45*, 745 – 748; c) D. H. Leung, D. Fiedler, R. G. Bergman, K. N. Raymond, *Angew. Chem.* **2004**, *116*, 981 – 984; *Angew. Chem. Int. Ed.* **2004**, *43*, 963 – 966; d) D. L. Caulder, K. N. Raymond, *J. Chem. Soc. Dalton Trans.* **1999**, 1185 – 1200; e) T. Beissel, R. E. Powers, K. N. Raymond, *Angew. Chem.* **1996**, *108*, 1166 – 1170; *Angew. Chem. Int. Ed. Engl.* **1996**, *35*, 1084 – 1086.
[6] a) E. C. Constable in *Comprehensive Supramolecular Chemistry*, *Vol. 9* (Eds.: J.-M. Lehn, J.-P. Sauvage, M. W. Hosseini), Pergamon, Oxford, **1996**, p. 213; b) A. Williams, *Chem. Eur. J.* **1997**, *3*, 15 – 19; c) A. E. Rowan, R. J. M. Nolte, *Angew. Chem.* **1998**, *110*, 65 – 71; *Angew. Chem. Int. Ed.* **1998**, *37*, 63 – 68, and references therein.
[7] a) S. J. Shieh, C. C. Chou, G. H. Lee, C. C. Wang, S. M. Peng, *Angew. Chem.* **1997**, *109*, 57 – 59; *Angew. Chem. Int. Ed. Engl.* **1997**, *36*, 56 – 59; b) A. F. Cotton, L. M. Daniels, G. T. Jordan, C. A. Murillo, *J. Am. Chem. Soc.* **1997**, *119*, 10377 – 10381; c) Y.-H. Chen, C.-C. Lee, C.-C. Wang, G.-H. Lee, S.-Y. Lai, F.-Y. Li, C.-Y. Mou, S.-M. Peng, *Chem. Commun.* **1999**, 1667 – 1668; d) H. A. Burkill, R. Vilar, A. J. P. White, D. J. Williams, *J. Chem. Soc. Dalton Trans.* **2002**, 837 – 839.
[8] a) L. J. Barbour, G. W. Orr, J. L. Atwood, *Nature* **1998**, *393*, 671 – 673; b) D. A. McMorran, P. J. Steel, *Angew. Chem.* **1998**, *110*, 3495 – 3497; *Angew. Chem. Int. Ed.* **1998**, *37*, 3295 – 3297; c) P. N. W. Baxter, J.-M. Lehn, G. Baum, D. Fenske, *Chem. Eur. J.* **2000**, *6*, 4510 – 4517; d) C.-Y. Su, Y.-P. Cai, C.-L. Chen, H.-X. Zhang, B.-S. Kang, *J. Chem. Soc. Dalton Trans.* **2001**, 359 – 361; e) T. D. Owens, F. J. Hollander, A. G. Oliver, J. A. Ellman, *J. Am. Chem. Soc.* **2001**, *123*, 1539 – 1540; S. L. Castro, O. Just, W. S. Rees, Jr., *Angew. Chem.* **2000**, *112*, 963 – 965; *Angew. Chem. Int. Ed.* **2000**, *39*, 933 – 935.
[9] A. P. Basset, S. W. Megennis, P. B. Glover, D. J. Lewis, N. Spencer, S. Parsons, R. M. Williams, L. De Cola, Z. Pikramenou, *J. Am. Chem. Soc.* **2004**, *126*, 9413 – 9424.
[10] a) A. E. V. Gorden, D. K. Shuh, B. E. F. Tiedemann, R. E. Wilson, J. Xu, K. N. Raymond, *Chem. Eur. J.* **2005**, *11*, 2842 – 2848; b) S. Petoud, S. M. Cohen, J.-C. G. Bünzli, K. N. Raymond, *J. Am. Chem. Soc.* **2003**, *125*, 13324 – 13325; c) J. Xu, D. W. Whisenhunt, Jr., A. C. Veeck, C. U. Linda, K. N. Raymond, *Inorg. Chem.* **2003**, *42*, 2665 – 2674.
[11] J. Xu, K. N. Raymond, *Angew. Chem.* **2000**, *112*, 2857 – 2859; *Angew. Chem. Int. Ed.* **2000**, *39*, 2745 – 2747.
[12] X. C. Dong, F. C. Liu, Y. L. Zhao, *Acta Chim. Sin.* **1983**, *41*, 848 – 850.
[13] L. Yang, R. Yang, *Polyhedron* **1995**, *14*, 507 – 510; Y. Xing, X. Li, L. Yan, R. Yang, *Chem. J. Chin. Univ.* **1992**, *13*, 14 – 18; D. Zhou, Q. Li, C. Huang, G. Yao, S. Umetani, M. Matsui, L. Ying, A. Yu, X. Zhao, *Polyhedron* **1997**, *16*, 1381 – 1389.

 © 2006 Wiley-VCH Verlag GmbH & Co. KGaA, Weinheim

[14] a) D. L. Kepert, *Prog. Inorg. Chem.* **1977**, *23*, 1–65; b) T. W. Hambley, D. L. Kepert, C. L. Raston, A. H. White, *Aust. J. Chem.* **1978**, *31*, 2635–2640.
[15] J. Xu, D. W. Whisenhunt, Jr., A. C. Veeck, L. C. Uhlir, K. N. Raymond. *Inorg. Chem.* **2003**, *42*, 2665–2674.
[16] P. Pyykkö, *Mol. Phys.* **2001**, *99*, 1617–1629.
[17] Crystallographic data: The X-ray diffraction data for $[Th_2(\mathbf{L}^1)_4(dmf)_2]$ and $[Th_2(\mathbf{L}^2)_4(dmf)_2]$ were collected on a Bruker SMART diffractometer by using graphite-monochromated $Mo_{K\alpha}$ radiation. The structures were solved by using direct methods, expanded by Fourier techniques, and refined with the SHELX software package (G. M. Sheldrick, SHELX-97 Universität Göttingen, **1997**). All non-hydrogen atoms were refined anisotropically. Hydrogen atoms were placed in idealized positions and induced in the structure factor calculations. CCDC-200541 and -200542 contain the supplementary crystallographic data for this paper. These data can be obtained free of charge from The Cambridge Crystallographic Data Centre via www.ccdc.cam.ac.uk/data_request/cif. Crystal data for $[Th_2(\mathbf{L}^1)_4(dmf)_2]\cdot 6\,DMF\cdot 0.5\,H_2O$: $Th_2C_{106}H_{102}N_{18}O_{18}\cdot 6\,C_3H_7NO\cdot 0.5\,H_2O$, $M_r = 2827.70$, colorless crystal, crystal dimension $0.32\times 0.27\times 0.20\,mm^3$, monoclinic, space group $P2(1)/c$ (#14), $a = 24.7142(3)$, $b = 14.9788(3)$, $c = 37.4021(8)$ Å, $\beta = 105.447(1)°$, $V = 13\,345.7(4)$ Å^3, $Z = 4$, $F(000) = 5724$, $\rho_{calcd} = 1.406\,g\,cm^{-3}$, $\mu Mo_{K\alpha} = 2.301\,mm^{-1}$, radiation λ ($Mo_{K\alpha}$) = 0.71073 Å, $T = 181(2)$ K, 58 075 reflections collected ($2\theta_{max} = 51.26°$), of which 22 237 unique ($R_{int} = 0.0545$). Data/restrains/parameters of 22 237/0/1481, $R_1 = 0.0487$ ($wR_2 = 0.1218$, $I > 2\sigma(I)$), $R_1 = 0.0698$ ($wR_2 = 0.1293$, all data), GOF = 1.005. Crystal data for $[Th_2(\mathbf{L}^2)_4(dmf)_2]\cdot 0.5\,DMF\cdot 1.5\,C_4H_{10}O$: $Th_2C_{110}H_{110}N_{18}O_{18}\cdot 0.5\,C_3H_7NO\cdot 1.5\,C_4H_{10}O$, $M_r = 2583.97$, colorless crystal, crystal dimension $0.12\times 0.05\times 0.04$, triclinic, space group $P\bar{1}$ (#2), $a = 18.0226(19)$, $b = 19.107(2)$, $c = 20.390(8)$ Å, $\alpha = 110.845(2)$, $\beta = 114.358(2)$, $\gamma = 90.431(2)°$, $V = 5879.0(11)$ Å^3, $Z = 2$, $F(000) = 2606$, $\rho_{calcd} = 1.460\,g\,cm^{-3}$, $\mu Mo_{K\alpha} = 2.301\,mm^{-1}$, radiation λ ($Mo_{K\alpha}$) = 0.71073 Å, $Mo_{K\alpha}$, $T = 179(2)$ K, 18 500 reflections collected ($2\theta_{max} = 49.46°$), of which 12 701 unique ($R = 0.0504$), data/restrains/parameters of 12 701/0/1392. $R_1 = 0.0528$ ($I > 2\sigma(I)$), $wR_2 = 0.1195$, $R_1 = 0.0920$ ($wR_2 = 0.11368$, all data), GOF = 0.968.
[18] J. Xu, E. Radkov, M. Ziegler, K. N. Raymond, *Inorg. Chem.* **2000**, *39*, 4156–4164.
[19] G. D. Jarvinen, A. J. Zozulin, E. M. Larson, R. R. Ryan, *Acta Crystallogr. Sect. C* **1991**, *47*, 262–263.

 © 2006 Wiley-VCH Verlag GmbH & Co. KGaA, Weinheim

DOI: 10.1002/anie.200602055

Colorimetric Identification of Carbohydrates by a pH Indicator/pH Change Inducer Ensemble**

*Jae Wook Lee, Jun-Seok Lee, and Young-Tae Chang**

Carbohydrates are one of the primary biological materials, along with proteins and nucleic acids. Although automatic analyses have been fully developed and routinely used for proteins and nucleic acids, carbohydrate analysis remains a highly challenging process.[1] Unlike other biomolecules, most carbohydrates have only one kind of functional group (hydroxy) with different stereochemistry, making the recognition of different carbohydrates extremely difficult. While biosensors[2] and chemical receptors[3] for carbohydrate recognition have been extensively studied, most research has been focused on a target-oriented approach to discover a selective sensor/probe for a given carbohydrate target. As a result of the similarity of the chemical nature between different carbohydrates, many of these selective sensor molecules suffer from cross-reactivity. With such technical difficulties, a systematic study to distinguish a broad range of carbohydrates is even more challenging.

The human tongue uses an array of receptors combined with a pattern analysis to distinguish, in principle, unlimited numbers of different tastes.[4] Inspired by nature's combinatorial sensing approach, many chemosensor arrays have been developed as artificial sensory systems.[5,6] Recently, an indicator displacement assay (IDA) based on organometallic receptors was reported for amino sugar discrimination,[7] but no practical sensing method for the discrimination of large numbers of conventional carbohydrates (with only hydroxy groups) is available yet. Herein, we report the successful recognition of 23 different carbohydrates by using a new strategy based on a pH indicator/pH change-inducer ensemble.

We recently developed an off-the-shelf dye array (NYT-1 with 47 dyes) for the discrimination of 44 metal ions both in identity and quantity.[8] Although NYT-1 can discriminate many different analytes, when we tried carbohydrates in this

[*] J. W. Lee, J.-S. Lee, Prof. Dr. Y.-T. Chang
Department of Chemistry
New York University
New York, NY 10003 (USA)
Fax: (+1) 212-995-4203
E-mail: yt.chang@nyu.edu

[**] This work was supported by the National Science Foundation (CHE-0449139). Components of this work were conducted in a Shared Instrumentation Facility constructed with support from Research Facilities Improvement Grant C06 RR-16572 from the NCRR/NIH. J.-S.L. was supported by the Korea Research Foundation Grant funded by the Korean Government (MOEHRD, Basic Research Promotion Fund: KRF-2005-C00088).

Supporting information for this article is available on the WWW under http://www.angewandte.org or from the author.

 © 2006 Wiley-VCH Verlag GmbH & Co. KGaA, Weinheim

system, the discriminating power was not satisfactory, reflecting the challenging nature of this work.

Among the known chemical recognition motifs for carbohydrates, boronic acids have been the most popular and successful since they were first reported by Lorand and Edwards in 1959.[9a] Most of these types of carbohydrate sensors are dye-conjugated boronic acid molecules. Upon carbohydrate binding, the dye generates readouts as changes in absorbance or fluorescence. Alternatively, diol-containing dyes have been used as carbohydrate competitors against boronic acid receptors to measure glucose concentrations[10] or to study carbohydrate–boronic acid binding.[11] Boronic acid forms reversible cyclic ester complexes with diols, which are abundant in carbohydrates, and undergoes an acid–base reaction with water as a conjugate acid (Scheme 1). Typically, boronic ester is more acidic than boronic acid ($pK_{a1}-pK_{a2} \approx 3$),[12] and ester formation is preferred at higher pH values by an equilibrium shift to the conjugate base releasing a proton.[13]

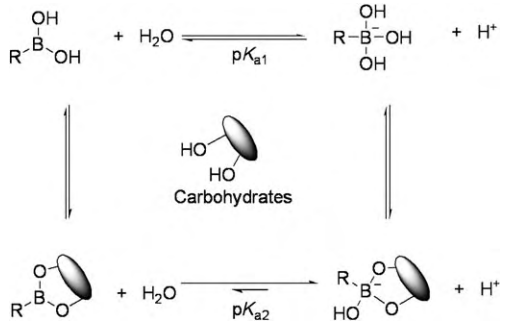

Scheme 1. Boric/boronic acid equilibria in water in both the absence and presence of carbohydrate.

Utilizing the well-known fact that different carbohydrates exhibit different binding constants to boronic acid, thus generating diverse changes in pH, two key components were devised to maximize the sensitivity and the discrimination power. To enhance the resolution of the pH change readout, we used an array of pH indicators instead of a pH meter. Another key component is the diversity of the boronic acid partner. Although the general binding constant of carbohydrates and boronic acid mainly depends on the pK_a value of boronic acid and the pH value of the solution, it is also affected by other unknown factors.[13] Thus, diverse boronic acids would further discriminate the carbohydrates by generating more unique response patterns per carbohydrate.

We tested more than 100 organic indicator dyes and over 10 boronic acids at various pH values with various buffers using conventional carbohydrates, and narrowed the choice down to 12 dyes and phenylboronic acid/boric acid as the best probe set. The optimized buffer was a sodium phosphate buffer (10 mM) with boric acid ($pK_a = 9.2$)[14] or phenylboronic acid ($pK_a = 8.8$).[13] In the absence of carbohydrate (water control), the final pH values were 8.0 and 7.9, respectively.

We tested 23 different carbohydrates, including 14 mono-, seven di-, and two trisaccharides, at a concentration of 100 mM. The absorbance spectra were collected using a 384-well microtiter plate reader, and the change in absorbance was calculated for further analysis following the previously reported procedure.[8] Ten independent measurements were performed for the statistical data process.

First, we visualized the probe responses by using a heat map plot (Figure 1). In general, a greater fold change of absorbance is correlated to a larger change in pH induced by

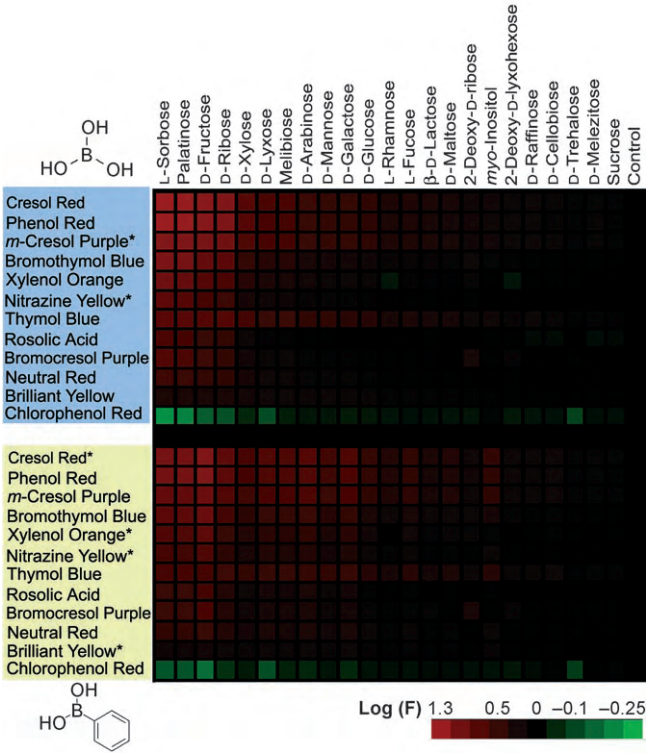

Figure 1. Heat map plot of the 23 carbohydrates (red: increase; green: decrease). F = fold change of absorbance (see the Supporting Information for the full definition). The dyes highlighted on a blue background were tested with boric acid, while those highlighted on a yellow background were tested with phenylboronic acid. Asterisks (*) indicate the six probes selected for minimally requested probe sets.

easier formation of the ester.[13] It seems that unrestrained vicinal diols that contain anomeric hydroxy groups (e.g. in L-sorbose, palatinose, and D-fructose) form the strongest esters, followed by the vicinal diol of furanose (D-ribose). While full analysis of the molecular recognition between each sugar and boric/boronic acids is complicated, several case studies have cast molecular bases for the structural discrimination.[15]

For pattern analysis and predictive ability determination, we used linear discriminant analysis (LDA) combined with a "jackknifed" classification matrix.[16] Surprisingly, 100% accurate discrimination was achieved for all 23 carbohydrates from this cross-validation routine, which we had expected to be highly challenging to achieve.

Encouraged by this result, we next examined how many probes are minimally required for full discrimination out of a total of 24 probe pairs (12 pH indicators and two pH-change inducers). Selection was performed by a variable selection

 © 2006 Wiley-VCH Verlag GmbH & Co. KGaA, Weinheim

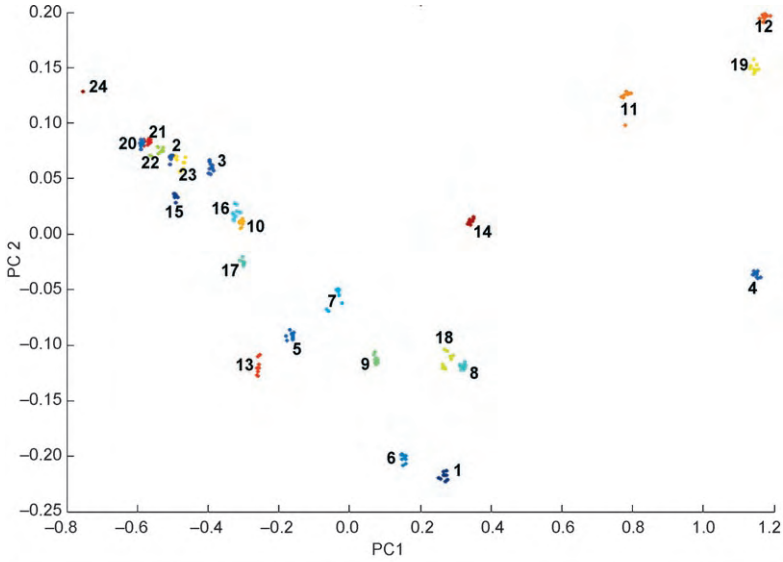

1: D-Arabinose	7: D-Glucose	13: *myo*-Inositol	19: Palatinose
2: 2-Deoxy-D-lyxohexose	8: D-Lyxose	14: D-Xylose	20: Sucrose
3: 2-Deoxy-D-ribose	9: D-Mannose	15: D-Cellobiose	21: D-Trehalose
4: D-Fructose	10: L-Rhamnose	16: β-D-Lactose	22: D-Melezitose
5: L-Fucose	11: D-Ribose	17: D-Maltose	23: D-Raffinose
6: D-Galactose	12: L-Sorbose	18: Melibiose	24: Control

Figure 2. Principal component analysis (PCA) plot for the identification of the 23 carbohydrates using six probe pairs. PC1 variance = 95.4%; PC2 variance = 3.4%.

algorithm using SYSTAT (version 11.0). Six probe pairs (marked with asterisks in Figure 1) were selected as a minimum probe set for full discrimination of the 23 carbohydrates by using stepwise forward algorithms with restricted iteration number. Note that probe sets using only boric acid or only phenylboronic acid could not distinguish all 23 carbohydrates at any combination, which clearly demonstrated the critical synergy effect of the boric/phenylboronic acid combination. The discrimination of 23 carbohydrates using the six probe pair minimum set were visualized by a principal component analysis (PCA; Figure 2). Within the two principal components, over 98% of all discriminatory information is contained and most of the carbohydrates are visually distinguishable in this two-dimensional plot.

In conclusion, a colorimetric discrimination of 23 carbohydrates was successfully demonstrated by using a pH indicator/pH change inducer array. The practical application of this new approach in to real samples is under study.

Received: May 24, 2006
Revised: July 10, 2006
Published online: September 15, 2006

Keywords: boronic acids · carbohydrates
pH indicators · sensors · UV/Vis spectroscopy

[1] J. F. Kennedy, M. F. Chaplin, *Carbohydrate Analysis: A Practical Approach*, IRL, Oxford, **1986**.
[2] R. Jelinek, S. Kolusheva, *Chem. Rev.* **2004**, *104*, 5987.
[3] S. Shinkai, M. Takeuchi, *Biosens. Bioelectron.* **2004**, *20*, 1250.
[4] D. Drayna, *Annu. Rev. Genomics Hum. Genet.* **2005**, *6*, 217.
[5] K. J. Albert, N. S. Lewis, C. L. Schauer, G. A. Sotzing, S. E. Stitzel, T. P. Vaid, D. R. Walt, *Chem. Rev.* **2000**, *100*, 2595.
[6] J. J. Lavigne, E. V. Anslyn, *Angew. Chem.* **2001**, *113*, 3212; *Angew. Chem. Int. Ed.* **2001**, *40*, 3119.
[7] F. Zaubitzer, A. Buryak, K. Severin, *Chem. Eur. J.* **2006**, *12*, 3928.
[8] J. W. Lee, J. S. Lee, M. Kang, A. I. Su, Y. T. Chang, *Chem. Eur. J.* **2006**, *12*, 5691.
[9] a) J. P. Lorand, J. O. Edwards, *J. Org. Chem.* **1959**, *24*, 769; b) T. D. James, K. R. A. S. Sandanayake, S. Shinkai, *Angew. Chem.* **1996**, *108*, 2038; *Angew. Chem. Int. Ed. Engl.* **1996**, *35*, 1911; c) T. D. James, S. Shinkai, *Top. Curr. Chem.* **2002**, *218*, 159; d) *Boronic acids: Preparation and Applications in Organic Synthesis and Medicine* (Ed.: D. G. Hall), Wiley-VCH, Weinheim, **2005**, pp. 441 – 480.
[10] S. Boduroglu, J. M. El Khoury, D. Venkat Reddy, P. L. Rinaldi, J. Hu, *Bioorg. Med. Chem. Lett.* **2005**, *15*, 3974.
[11] G. Springsteen, B. H. Wang, *Chem. Commun.* **2001**, 1608.
[12] R. Badugu, J. R. Lakowicz, C. D. Geddes, *Anal. Chem.* **2004**, *76*, 610.
[13] a) G. Springsteen, B. H. Wang, *Tetrahedron* **2002**, *58*, 5291; b) J. Yan, G. Springsteen, S. Deeter, B. H. Wang, *Tetrahedron* **2004**, *60*, 11205; c) L. I. Bosch, T. M. Fyles, T. D. James, *Tetrahedron* **2004**, *60*, 11175.
[14] W. T. Wofford, E. F. Gloyna, K. P. Johnston, *Ind. Eng. Chem. Res.* **1998**, *37*, 2045.
[15] a) M. Dowlut, D. G. Hall, *J. Am. Chem. Soc.* **2006**, *128*, 4226; b) J. C. Norrild, H. Eggert, *J. Am. Chem. Soc.* **1995**, *117*, 1479; c) M. Bielecki, H. Eggert, J. C. Norrild, *J. Chem. Soc. Perkin Trans. 2* **1999**, 449; d) J. C. Norrild, H. Eggert, *J. Chem. Soc. Perkin Trans. 2* **1996**, 2583.
[16] a) P. C. Jurs, G. A. Bakken, H. E. McClelland, *Chem. Rev.* **2000**, *100*, 2649; b) D. R. Burgard, J. T. Kuznicki, *Chemometrics: Chemical and Sensory Data*, CRC, Boca Raton, **1990**; c) B. K. Lavine, *Chemometrics and Chemoinformatics*, American Chemical Society, Washington DC, **2005**; d) B. Efron, *Ann. Stat.* **1979**, *7*, 1.

 © 2006 Wiley-VCH Verlag GmbH & Co. KGaA, Weinheim

Molecular Capsules

DOI: 10.1002/anie.200601431

Isostructural Coordination Capsules for a Series of 10 Different d^5–d^{10} Transition-Metal Ions**

*Shuichi Hiraoka, Koji Harano, Motoo Shiro, Yoshiki Ozawa, Nobuhiro Yasuda, Koshiro Toriumi, and Mitsuhiko Shionoya**

Supramolecular assembly of predesigned organic and inorganic building blocks has been recognized as an excellent tool in constructing well-defined nanosized molecules for potential application in molecular devices.[1] In particular, discrete hollow structures such as capsules[2] formed by metal-mediated assembly of organic ligands are of great interest because of the chemical phenomena that may occur in their inner space.[3] However, the number of metals used to maintain the shapes of metal-assembled architectures is still limited. Metal-exchangeable coordination architectures with a series of transition-metal ions would give rise to a large number of metal-dependent functions. Here we present a novel disk-shaped tris-monodentate ligand **1** that forms 10 structurally equivalent coordination capsules, $[M_6(\mathbf{1})_8]^{12+}$, with a series of divalent d^5–d^{10} transition-metal ions, M^{2+} (M = Mn, Fe, Co, Ni, Pd, Pt, Cu, Zn, Cd, and Hg) through self-assembly protocols. The resulting complexes have an octahedron-shaped structure in which the six metal ions lie on the apexes and the eight sides are occupied with eight ligands **1**. X-ray structural analysis of a single crystal of $[Hg_6(\mathbf{1})_8(CF_3SO_3)_{12}]$ revealed a 3-nm-sized octahedron-shaped capsule structure, with sides of 1.8 nm in length. Some of these complexes have two axial ligands at each hexacoordinate metal center, one each from inside and outside the cavity. Note that the inner space of the capsule was successfully decorated with other anionic ligands as a result of the site-selective replacement of the six $CF_3SO_3^-$ ligands coordinated from inside the capsule.

The disk-shaped C_3-symmetric tris-monodentate ligand **1** comprises a central hexaphenylbenzene core whose six peripheral rings are alternately 4-substituted with 3-pyridyl and methyl groups (Figure 1). The distance between the two neighboring pyridyl nitrogen atoms is approximately 1.8 nm.

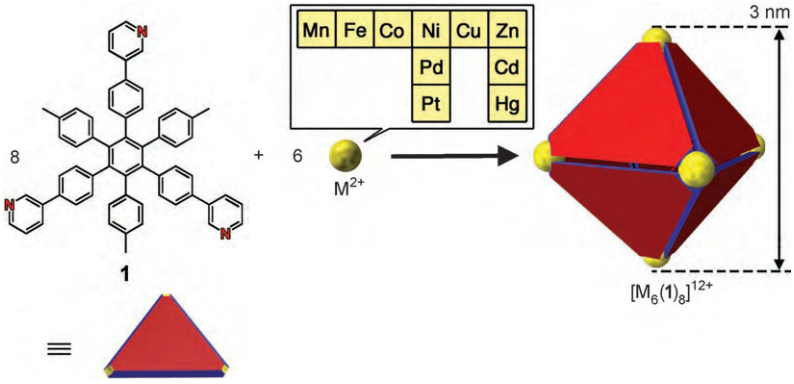

Figure 1. Schematic representation of the formation of $[M_6(\mathbf{1})_8]^{12+}$ coordination capsules formed from eight disk-shaped tris-monodentate ligands **1** and six divalent d^5–d^{10} transition-metal ions, M^{2+}.

Titrimetric complexation studies with a series of transition-metal ions revealed that 10 different $[M_6(\mathbf{1})_8]^{12+}$ complexes are formed from **1** and 10 divalent d^5–d^{10} transition-metal ions which prefer a square-planar or an octahedral coordination geometry (M = Mn, Fe, Co, Ni, Pd, Pt, Cu, Zn, Cd, and Hg).

The most studied example was that with M = Hg. The ^{1}H NMR spectrum of the $[Hg_6(\mathbf{1})_8]^{12+}$ complex is given in Figure 2b. A ^{1}H NMR titration study of ligand **1** with $Hg(CF_3SO_3)_2$ in CD_3CN at 293 K revealed that a highly symmetrical complex is quantitatively constructed when **1** and Hg^{2+} are mixed in a ratio of 4:3. All the proton signals for phenylene and *p*-tolyl groups (H_e–H_h) were divided into two sets (H_{e1}, H_{e2}, H_{f1}, H_{f2}, H_{g1}, H_{g2}, H_{h1}, and H_{h2}) at the same integral ratio, indicating that all the pyridyl nitrogen atoms are directed towards Hg^{2+}. Note that the signals for the methyl protons (H_i) were shifted upfield as a result of shielding effects from the neighboring ligands assembled by Hg^{2+}. The ESI-TOF mass spectrum of this solution showed five signals at *m*/*z* 1202.1, 1426.9, 1742.3, 2215.1, and 3003.2. These signals are all assignable to positively charged $\{Hg_6(\mathbf{1})_8\}$ complexes with the loss of $CF_3SO_3^-$ anions (Figure 3), and this result is in good agreement with the convergence ratio 4:3 for **1**/Hg^{2+} observed in the ^{1}H NMR titration study. Thus, a discrete, highly symmetrical $[Hg_6(\mathbf{1})_8]^{12+}$ complex was quanti-

[*] Dr. S. Hiraoka, K. Harano, Prof. Dr. M. Shionoya
Department of Chemistry, Graduate School of Science
The University of Tokyo
Hongo, Bunkyo-ku, Tokyo 113-0033 (Japan)
Fax: (+81) 3-5841-8061
E-mail: shionoya@chem.s.u-tokyo.ac.jp
Dr. M. Shiro
Rigaku Corporation
3-9-12 Matsubaracho, Akishima, Tokyo 196-8666 (Japan)
Dr. Y. Ozawa, Prof. Dr. K. Toriumi
Graduate School of Material Science, University of Hyogo
Harima Science Garden City, Kamigori, Hyogo 678-1297 (Japan)
Dr. N. Yasuda
Japan Synchrotron Radiation Research Institute
Spring-8 1-1-1 Kouto, Mikazuki, Sayo, Hyogo 679-5198 (Japan)

[**] We thank Dr. Misako Imachi (Bruker BioSpin K.K.) for useful discussions and technical support for DOSY measurements. This work was supported by a Grant-in-Aid for The 21st Century COE Program for Frontiers in Fundamental Chemistry; a Grant-in-Aid for Scientific Research (S) to M.S. (no. 16105001); a Grant-in-Aid for Young Scientists (A) to S.H. (no. 17685005) from the Ministry of Education, Culture, Sports, Science, and Technology of Japan; a PRESTO (Precursory Research for Embryonic Science and Technology) project from the Japan Science and Technology Agency; and the Kurata Foundation.

Supporting information for this article is available on the WWW under http://www.angewandte.org or from the author.

InterScience
© 2006 Wiley-VCH Verlag GmbH & Co. KGaA, Weinheim

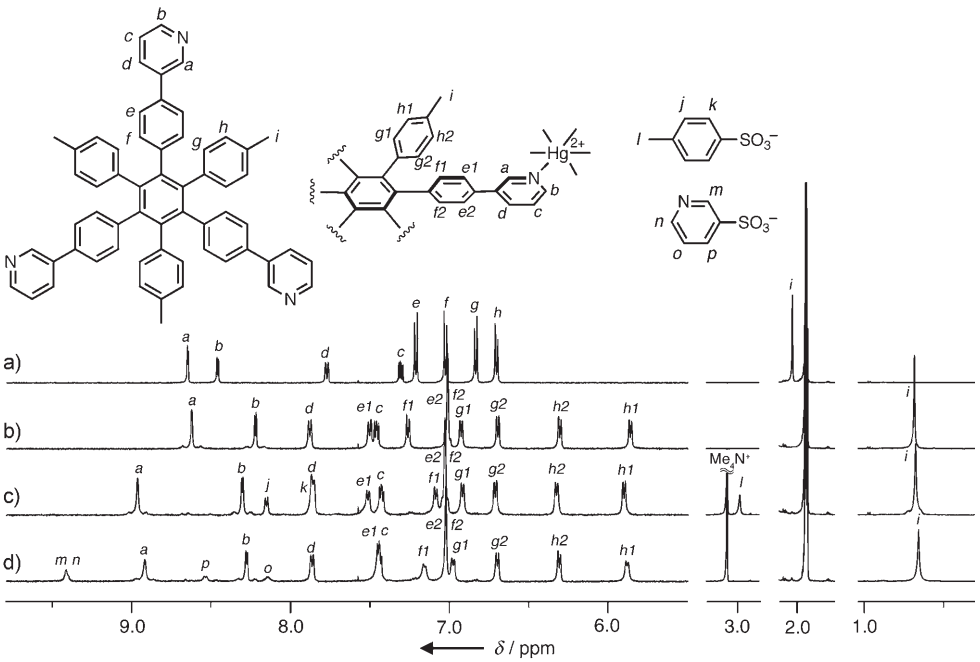

Figure 2. ^{1}H NMR spectra for complexation of Hg^{2+} with **1** in CD_3CN at 293 K ([**1**] = 3.0 mM). a) Metal-free ligand **1**; b) Hg^{2+} complex (**1**/$Hg(CF_3SO_3)_2$ = 4:3); c) Hg^{2+} complex with added *p*-$MeC_6H_4SO_3NMe_4$ (**1**/$Hg(CF_3SO_3)_2$/*p*-$MeC_6H_4SO_3NMe_4$ = 4:3:3); and d) Hg^{2+} complex with added tetramethylammonium 3-pyridinesulfonate (**1**/$Hg(CF_3SO_3)_2$/tetramethylammonium 3-pyridinesulfonate = 4:3:3).

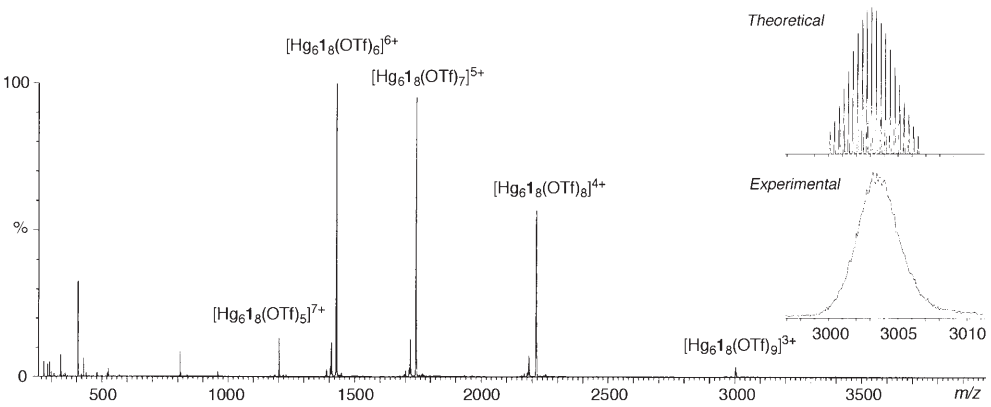

Figure 3. ESI-TOF mass spectrum of the Hg^{2+} complex in CD_3CN ([**1**] = 3.0 mM, [Hg^{2+}] = 2.3 mM). Inset: expansion and simulation of the signal at *m*/*z* 3003.2. OTf = $CF_3SO_3^-$.

tatively formed in solution. The formation of the $[M_6(\mathbf{1})_8]^{12+}$ complexes with other diamagnetic divalent transition-metal ions (Pd^{2+}, Pt^{2+}, Zn^{2+}, and Cd^{2+}) in solution was demonstrated in the same way.

Single-crystal X-ray structural analysis demonstrated an octahedron-shaped capsule structure of the $[Hg_6(\mathbf{1})_8(CF_3SO_3)_{12}]$ complex (Figure 4). The complex cocrystallized with a non-metallated ligand cluster (see Supporting Information), and a crystal cell contains four such units. As for the $[Hg_6(\mathbf{1})_8]^{12+}$ part, eight ligands are arranged into an octahedron-shaped framework in which six Hg^{2+} ions occupy the six apexes. Each Hg^{2+} is hexacoordinate and bound by four pyridyl nitrogen atoms of four separate ligands and two oxygen atoms of the axial $CF_3SO_3^-$ ligands, one each from inside and outside the capsule (Figure 4b). The distances between two neighboring Hg^{2+} ions and two diagonal Hg^{2+} ions are on average 17.9 Å and 25.4 Å, respectively. The eight tris-monodentate ligands **1** in $[Hg_6(\mathbf{1})_8]^{12+}$ are densely arranged through π–π stacking of the *p*-tolyl rings and a close contact between the methyl groups of the *p*-tolyl and the phenylene rings. As a result, the inner space of the capsule is almost completely isolated from outside. The inner volume was estimated to be approximately 2700 Å^3.

As for paramagnetic $[M_6(\mathbf{1})_8]^{12+}$ complexes (M = Mn, Fe, Co, Ni, and Cu), the signals in the ^{1}H NMR spectra for metal-free ligand **1** completely disappeared when 0.75 equiv of metal ions (**1**/M^{2+} = 4:3) were added to the solutions and broadened signals for metal complexes appeared with a significant shift to lower magnetic field. Their complexation in solution was then examined by UV titration experiments and ESI-TOF mass measurements.[4] ^{1}H DOSY measurement is a powerful tool to estimate the size of macromolecules in solution and can be utilized even for paramagnetic metal species. The diffusion coefficients (D) of $[M_6(\mathbf{1})_8]^{12+}$ complexes in solutions were estimated as $D = 3.8 \pm 0.4 \times 10^{-10}$ m^2 s^{-1} (except for M = Mn^{2+}),[5] which corresponds to a 3-nm-sized spherical structure, as confirmed by the X-ray crystal structure analysis of the $[Hg_6(\mathbf{1})_8(CF_3SO_3)_{12}]$ capsule.

The metals used in this study can be divided according to their coordination geometries, namely octahedral and square-planar. The coordination exchange of two axial ligands at each octahedral metal center is of great interest because these two ligands are more labile than equatorial ligands and hence are placed in inequivalent circumstances. For example, as seen in the X-ray crystal structure analysis, two inequivalent $CF_3SO_3^-$ ions coordinate to each Hg^{2+} ion of the $[Hg_6(\mathbf{1})_8(CF_3SO_3)_{12}]$ capsule complex, that is, one from inside and the other from outside. To investigate the dynamic behaviors of these axial ligands in solution, we measured the ^{19}F NMR

 © 2006 Wiley-VCH Verlag GmbH & Co. KGaA, Weinheim

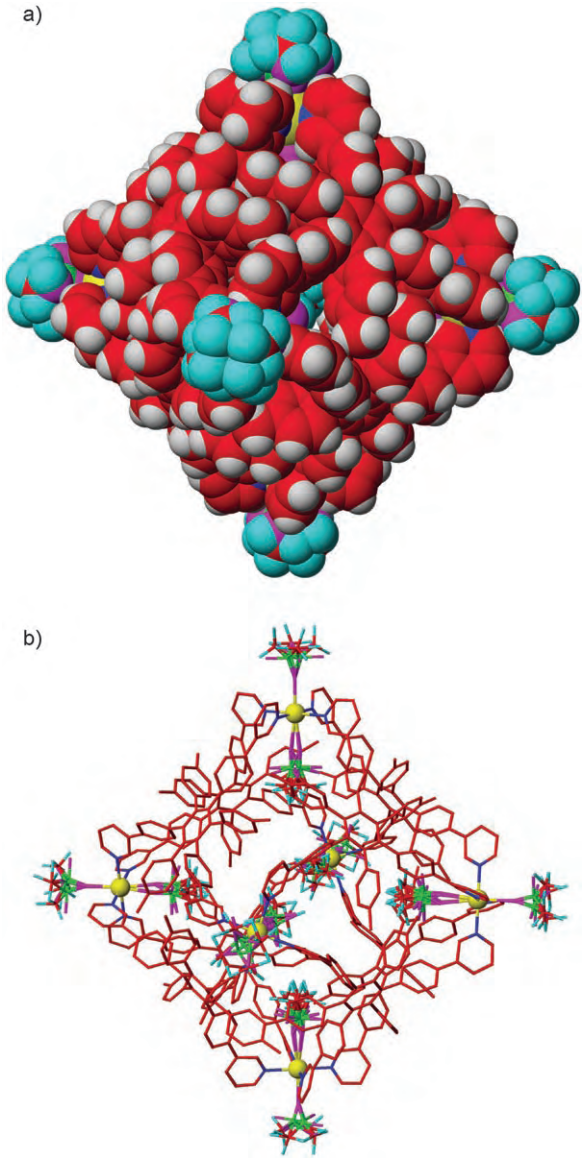

Figure 4. Crystal structure of $[Hg_6(\mathbf{1})_8(CF_3SO_3)_{12}]$. Axially coordinated $CF_3SO_3^-$ ions are disordered. a) Space-filling model; b) cylinder model (hydrogen atoms are omitted for clarity). C red, Hg yellow, N blue, O purple, S green, F cyan, H white.

spectrum of the $[Hg_6(\mathbf{1})_8(CF_3SO_3)_{12}]$ complex. Two broadened signals were observed at 293 K in a 1:1 integral ratio at $\delta =$ 85.2 and 86.1 ppm, which are assignable to the outer and the inner $CF_3SO_3^-$ ligands, respectively.[6] The axial ligand exchange between both sides was slightly slower than the NMR timescale. This result clearly indicates that each Hg^{2+} center of the complex is in an octahedral coordination geometry with two axial $CF_3SO_3^-$ ligands in solution.[7] Furthermore, all six $CF_3SO_3^-$ axial ligands coordinating from inside the capsule were site-selectively replaced by six *p*-$MeC_6H_4SO_3^-$ ligands upon addition of 6 equiv of *p*-$MeC_6H_4SO_3NMe_4$ to a solution of the $[Hg_6(\mathbf{1})_8(CF_3SO_3)_{12}]$ complex. Aromatic ^{1}H NMR signals for the $[Hg_6(\mathbf{1})_8]^{12+}$ capsule (H_a, H_b, and H_f) as well as both aromatic and methyl signals for *p*-$MeC_6H_4SO_3^-$ were shifted to lower magnetic field as compared to the original signals (Figure 2c) upon addition of 6 equiv of *p*-$MeC_6H_4SO_3NMe_4$. The ^{19}F NMR spectrum showed only one sharp signal at $\delta =$ 85.1 ppm, which coincides with the chemical shift of $Hg(CF_3SO_3)_2$ at $\delta = 85.1$ ppm, indicating that all the $CF_3SO_3^-$ ligands exist outside the capsule. ESI-TOF mass measurement of the mixed solution showed distinct signals which are assignable to $[Hg_6(\mathbf{1})_8(p\text{-}MeC_6H_4SO_3)_6(CF_3SO_3)_n]^{6-n}$ ($n = 0$–2). This finding would allow us to utilize the six metal centers at the apexes of the capsule for chemical modification of the inner space with functional anionic molecules or for the hub of signal transfer between the inner and outer spaces. For example, the inner space of the $[Hg_6(\mathbf{1})_8]^{12+}$ capsule was decorated with six 3-pyridinesulfonate groups coordinated to the Hg^{2+} centers (Figure 2d).

In summary, we have demonstrated that a series of 10 isostructural octahedron-shaped coordination nanocapsules $[M_6(\mathbf{1})_8]^{12+}$ can be constructed from disk-shaped tris-monodentate ligands **1** and 10 divalent d^5–d^{10} transition-metal ions. One can anticipate their ability to fine-tune metal-dependent functions such as magnetic, redox, optical, and dynamic properties because the metal ions at the six apexes can be exchanged with preservation of the structure. Moreover, site-specific replacement of the internal axial ligands of the six metal centers would allow functionalization of the interior of the coordination capsule. Such metal-exchangeable capsules that have a large hollow structure surrounded by organic and inorganic components would, therefore, be endowed with an isolated space for size- or shape-selective dynamic molecular recognition and metal-triggered chemical reactions.

Experimental Section

A single crystal of $[Hg_6(\mathbf{1})_8(CF_3SO_3)_{12}]$ suitable for X-ray crystal structure analysis was obtained by slow diffusion of diethyl ether into a solution of **1** (5.7 mg, 7.1 μmol) and $Hg(CF_3SO_3)_2$ (2.6 mg, 5.4 μmol) in CH_3CN. After 2 days, colorless cubic crystals appeared. The crystals were collected and then dried in vacuo to obtain $[Hg_6(\mathbf{1})_8(CF_3SO_3)_{12}]\cdot 8(\mathbf{1})$ (5.7 mg, 0.36 μmol, 81%). Crystallographic data: $C_{972}H_{744}F_{36}Hg_6N_{48}O_{48}S_{12}$ ($[Hg_6(\mathbf{1})_8(CF_3SO_3)_{12}]\cdot 8C_{60}H_{45}N_3\cdot 12H_2O$), $M_r = 16137.06$, colorless block ($0.25\times0.20\times0.10$ mm^3), density 0.964, cubic, space group $F432$, $a = b = c = 48.0818(13)$ Å, $V =$ 111158(5) Å^3, $Z = 4$, $R_1(I>2\sigma(I)) = 0.0901$, $wR(F_o^2) = 0.2868$, GOF = 0.968. As the reflections in the range of high 2θ angle are very weak, the positional and thermal parameters are not accurate. Large R and wR values might be due to a poor quality of the crystal used and the disordered structure. CCDC-295986 contains the supplementary crystallographic data for this paper. These data can be obtained free of charge from The Cambridge Crystallographic Data Centre via www.ccdc.cam.ac.uk/data_request/cif.

Received: April 11, 2006
Revised: June 13, 2006
Published online: August 14, 2006

Keywords: molecular capsules · NMR spectroscopy · self-assembly · supramolecular chemistry · transition metals

[1] a) J.-M. Lehn, *Science* **2002**, *295*, 2400–2403; b) J.-M. Lehn, *Supramolecular Chemistry: Concepts and Perspectives*, Wiley-VCH, Weinheim, **1995**.

 © 2006 Wiley-VCH Verlag GmbH & Co. KGaA, Weinheim

[2] a) N. Takeda, K. Umemoto, K. Yamaguchi, M. Fujita, *Nature* **1999**, *398*, 794 – 796; b) D. Chand, K. Biradha, M. Fujita, S. Sakamoto, K. Yamaguchi, *Chem. Commun.* **2002**, 2486 – 2487; c) M. Tominaga, K. Suzuki, M. Kawano, T. Kusukawa, T. Ozeki, S. Sakamoto, K. Yamaguchi, M. Fujita, *Angew. Chem.* **2004**, *116*, 5739 – 5743; *Angew. Chem. Int. Ed.* **2004**, *43*, 5621 – 5625; d) L. R. MacGillivray, J. L. Atwood, *Angew. Chem.* **1999**, *111*, 1018 – 1033; *Angew. Chem. Int. Ed.* **1999**, *38*, 1018 – 1033; e) R. M. McKinlay, G. W. V. Cave, J. L. Atwood, *Proc. Natl. Acad. Sci. USA* **2005**, *102*, 5944 – 5948; f) B. Olenyuk, J. A. Whiteford, A. Fechtenkotter, P. J. Stang, *Nature* **1999**, *398*, 796 – 799; g) A. Müller, S. Roy, *Coord. Chem. Rev.* **2003**, *245*, 153 – 166; h) A. Müller, L. Toma, H. Bögge, C. Schäffer, A. Stammler, *Angew. Chem.* **2005**, *117*, 7935 – 7939; *Angew. Chem. Int. Ed.* **2005**, *44*, 7757 – 7761; i) R. W. Saalfrank, H. Glaser, B. Demleitner, F. Hampel, M. M. Chowdhry, V. Schünemann, A. X. Trautwein, G. M. Vaughan, R. Yeh, A. V. Davis, K. N. Raymond, *Chem. Eur. J.* **2002**, *8*, 493 – 497; j) M. Albrecht, I. Janser, S. Meyer, P. Weis, R. Fröhlich, *Chem. Commun.* **2003**, 2854 – 2855; k) M. Albrecht, I. Janser, S. Kamptmann, P. Weis, B. Wibbeling, R. Fröhlich, *Dalton Trans.* **2004**, 37 – 43; l) D. Moon, S. Kang, J. Park, K. Lee, R. P. John, H. Won, G. H. Seong, Y. S. Kim, G. H. Kim, H. Rhee, M. S. Lah, *J. Am. Chem. Soc.* **2006**, *128*, 3530 – 3531; m) S. Aoki, M. Zulkefeli, M. Shiro, E. Kimura, *Proc. Natl. Acad. Sci. USA* **2002**, *99*, 4894 – 4899; n) A. Ikeda, H. Udzu, Z. Zhong, S. Shinkai, S. Sakamoto, K. Yamaguchi, *J. Am. Chem. Soc.* **2001**, *123*, 3872 – 3877; o) T. Haino, M. Kobayashi, M. Chikaraishi, Y. Fukazawa, *Chem. Commun.* **2005**, *18*, 2321 – 2323; p) T. Haino, M. Kobayashi, Y. Fukazawa, *Chem. Eur. J.* **2006**, *12*, 3310 – 3319; q) M. Yamanaka, Y. Yamada, Y. Sei, K. Yamaguchi, K. Kobayashi, *J. Am. Chem. Soc.* **2006**, *128*, 1531 – 1539; r) S. J. Park, D. M. Shin, S. Sakamoto, K. Yamaguchi, Y. K. Chung, M. S. Lah, J.-I. Hong, *Chem. Eur. J.* **2005**, *11*, 235 – 241; s) S. P. Argent, H. Adams, T. Riis-Johannessen, J. C. Jeffery, L. P. Harding, M. D. Ward, *J. Am. Chem. Soc.* **2006**, *128*, 72 – 73.

[3] a) M. Yoshizawa, T. Kusukawa, M. Fujita, *J. Am. Chem. Soc.* **2000**, *122*, 6311 – 6312; b) D. Fiedler, R. G. Bergman, K. N. Raymond, *Angew. Chem.* **2004**, *116*, 6916 – 6919; *Angew. Chem. Int. Ed.* **2004**, *43*, 6748 – 6751.

[4] ^{1}H NMR spectra, ESI-TOF mass spectra, and changes in UV absorption for the complexation of **1** with metal ions (Mn^{2+}, Fe^{2+}, Co^{2+}, Ni^{2+}, Cu^{2+}) are summarized in the Supporting Information.

[5] DOSY spectra of the complexes are shown in the Supporting Information. For the Mn^{2+} complex, no cross peaks were observed at the signals for **1** because of the significantly broadened ^{1}H NMR signals.

[6] The assignment of the two ^{19}F NMR signals was conducted by ^{19}F DOSY measurement. ^{19}F DOSY measurement of $[Zn_6(\mathbf{1})_8(CF_3SO_3)_{12}]$ was used to determine the diffusion coefficient from the signal at the lower field as $D = 2.8 \times 10^{-10}\,m^2 s^{-1}$, which is comparable to that of the $\{Zn_6(\mathbf{1})_8\}$ capsule determined by ^{1}H DOSY measurement ($D = 4.2 \times 10^{-10}\,m^2 s^{-1}$) and significantly smaller than that determined from the signal at higher field ($D = 1.2 \times 10^{-9}\,m^2 s^{-1}$). The ^{19}F DOSY spectrum is shown in the Supporting Information.

[7] The ^{19}F NMR spectrum of the $[Zn_6(\mathbf{1})_8(CF_3SO_3)_{12}]$ complex showed two relatively sharp signals at $\delta = 85.9$ and 85.1 ppm, indicating its much slower coordination exchange at the axial ligands of each metal center as compared with the $[Hg_6(\mathbf{1})_8(CF_3SO_3)_{12}]$ complex. The ^{19}F NMR spectrum of $[Cu_6(\mathbf{1})_8(CF_3SO_3)_{12}]$ showed two signals in a 1:1 integral ratio, indicating an octahedral coordination geometry of Cu^{2+} centers in the complex.

 © 2006 Wiley-VCH Verlag GmbH & Co. KGaA, Weinheim

Composites

DOI: 10.1002/anie.200602134

A Luminescent Poly(phenylenevinylene)–Amylose Composite with Supramolecular Liquid Crystallinity

Masato Ikeda, Yoshio Furusho, Kento Okoshi, Sayaka Tanahara, Katsuhiro Maeda, Shunsuke Nishino, Tatsuo Mori, and Eiji Yashima**

Poly(*p*-phenylenevinylene) (PPV) is the first π-conjugated polymer used as the emissive layer in light-emitting diodes (LEDs).[1] However, PPV is insoluble in solvents, and therefore a two-step synthesis is required for the fabrication of the PPV thin films for LEDs; the synthesis of a solution-processable precursor polymer **2** by polymerization of the disulfonium salts of α,α′-dichloro-*p*-xylene (**1**), followed by thermal conversion of the precursor to the PPV film at high temperature (Figure 1 a).[1,2] To improve its processability, numerous soluble PPV derivatives have been synthesized by a side-chain functionalization.[3] Another attractive alternative is "encapsulation or wrapping" of conjugated polymers by organic hosts through noncovalent bonding interactions, thus leading to soluble and processable insulated molecular wires.[4] Cyclodextrins[5] and polysaccharides, such as amylose[6] and schizophyllan,[4c,6c,d,7] have been extensively used for these purposes. They possess a chiral hydrophobic cavity that forms inclusion complexes or polyrotaxanes with soluble conjugated polymers[4,6c,d,7] and carbon nanotubes[6a,b] that fit the cavity size in solution.[4b,8] However, the wrapping approach cannot be applicable to PPV because it is totally insoluble and intractable. Herein, we demonstrate that PPV can be encapsulated in amylose during the polymerization of monomer **1** in aqueous media at ambient temperature (ca. 20–25 °C), thus resulting in a soluble, PPV-based lumi-

[*] Dr. M. Ikeda, Dr. Y. Furusho, Dr. K. Okoshi, Prof. E. Yashima
Yashima Super-structured Helix Project
Exploratory Research for Advanced Technology (ERATO)
Japan Science and Technology Agency (JST)
101 Creation Core Nagoya, Shimoshidami
Moriyama-ku, Nagoya 463-0003 (Japan)
Fax: (+81) 52-739-2081
E-mail: furusho@yp-jst.jp
yashima@apchem.nagoya-u.ac.jp
Homepage: http://helix.mol.nagoya-u.ac.jp/
http://helix.mol.nagoya-u.ac.jp/

S. Tanahara, Dr. K. Maeda, Prof. E. Yashima
Department of Molecular Design and Engineering
Graduate School of Engineering, Nagoya University
Chikusa-ku, Nagoya 464-8603 (Japan)
Fax: (+81) 52-789-3185

S. Nishino, Prof. T. Mori
Department of Electrical Engineering and Computer Science
Graduate School of Engineering, Nagoya University
Chikusa-ku, Nagoya 464-8603 (Japan)

Supporting information for this article is available on the WWW under http://www.angewandte.org or from the author.

 © 2006 Wiley-VCH Verlag GmbH & Co. KGaA, Weinheim

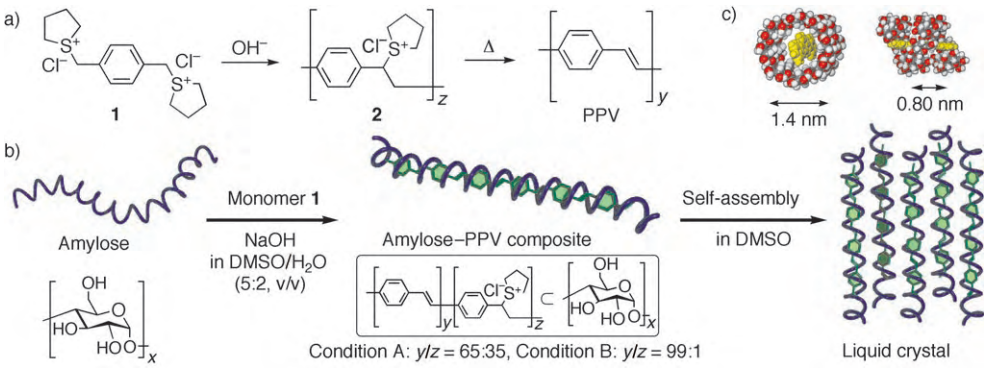

Figure 1. a) Scheme showing the synthesis of PPV. b) Schematic illustration of the synthesis of a green-luminescent amylose–PPV composite, which further self-assembles into a molecular ordering in LC phases. Condition A: NaOH (1 M), DMSO/H_2O (5:2 v/v; [NaOH]/[amylose] = 4:1) at room temperature for 30 min; Condition B: NaOH (1 M), DMSO/H_2O (5:2 v/v; [NaOH]/[amylose] = 10:1) at 0 °C for 0.5 h and then at 20 °C for 48 h. c) Calculated structure of amylose (15 glucose units)–PPV (3 mer) shown using a space-filling model in the top (left) and side (right) views; PPV yellow, amylose red, white, and gray.

nescent polymer composite (Figure 1 b). Moreover, amylose, which is too flexible to form a liquid crystal (LC),[9] exhibits an liquid crystallinity when the PPV is threaded into the amylose tube, thereby resulting in a rigid-rod supramolecular assembly.

The amylose–PPV composites were synthesized by polymerization of monomer **1** (5 mM) in a mixture of dimethyl sulfoxide (DMSO) and alkaline water (5:2 v/v; [NaOH]/[**1**] = 4:1) in the presence of amyloses (45 mM based on the glucose units; molecular weight (M_W) = 15000, 24000, and 50000 with a polydispersity index (PDI) of 1.05).[10] The polymerization proceeded homogeneously at 25 °C and quantitatively produced the luminescent composites (92–95 % yield) within 30 minutes without heat treatment after quenching the reaction with aqueous HCl followed by precipitation into acetone (condition A).[11] The resulting composites are soluble in water and organic solvents and show typical absorption and photoluminescence (PL) spectra in water (3 % DMSO) as a result of the conjugated phenylenevinylene (PV) units (see Supporting Information), but the solution ^1H and solid-state ^{13}C NMR spectra of the composites (see Figure 2 and Supporting Information)[11] suggest that the core polymer contains approximately 35 mol % of the precursor units.[12] Further heat treatment of the amylose–PPV composites in DMSO/water (5:2 v/v) at 100 °C for 4 hours did not improve the PV content because of the intermolecular cross-linking between the remaining reactive precursor units and the OH groups of amylose inside the cavity (see Supporting Information).

The amylose–PPV composites are quite stable as evidenced by the size-exclusion chromatography (SEC) analyses (see Supporting Information). Three amyloses with different molecular weights showed unimodal SEC curves detected only by a refractive index (RI), whereas the amylose–PPV composites exhibited similar SEC curves detected by both the RI and visible light (400 nm); the molecular-weight distribution remained unimodal, thus indicating that the PPV cores hardly unthread from the tube, even in the absence of stoppers at the ends.[5a–e] These SEC results also support the proposed structure (Figure 1 b), in which the PV segments are encapsulated in the amylose cavity.

To decrease the defect (precursor units), we investigated the effects of the polymerization temperature (0–30 °C), time (0.5–48 h) and the concentrations of amylose (45–90 mM), **1** (5–10 mM), and NaOH ([NaOH]/[**1**] = 4:1–20:1 (molar ratio)) on the content of PV units in the resulting polymer composites, from which we determined the optimized conditions. We found that the polymerization of **1** (5 mM) in DMSO/alkaline water (5:2 v/v; [NaOH]/[**1**] = 10:1) in the

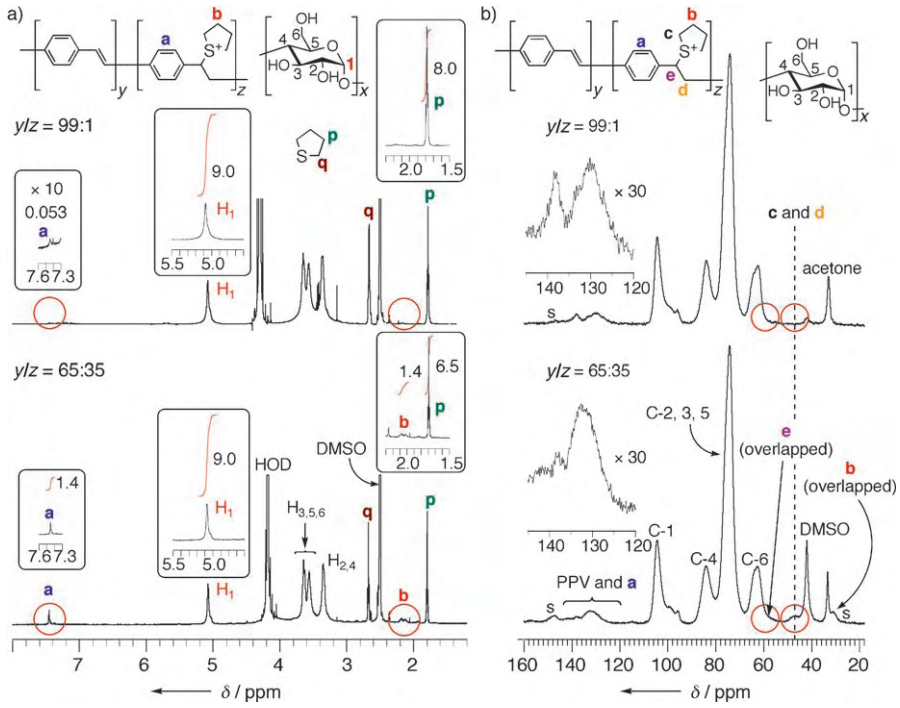

Figure 2. a) ^1H NMR spectra ([D_6]DMSO/D_2O (5:2 v/v), 25 °C) of the polymerization mixtures under condition A (bottom) and B (top) after addition of 1 M DCl. b) ^{13}C CP–MAS NMR spectra of the amylose (15000)–PPV composites prepared under condition A (bottom) and B (top) measured at 5.5 kHz at 25 °C. s = spinning side bands.

© 2006 Wiley-VCH Verlag GmbH & Co. KGaA, Weinheim

presence of amylose (45 mM) at 0 °C for 30 min and then at 20 °C for 48 h quantitatively gave an almost defect-free amylose–PPV composite (99 % PV units and [glucose units of amylose]/[PV] = 9:1) based on its solution ^{1}H and solid-state ^{13}C NMR spectra and elemental analysis (see Figure 2 and Supporting Information).[12,14] The solid-state ^{13}C NMR resonance peak pattern that arose from the PV part at around $\delta = 120$–140 ppm (see Figure 2b and Supporting Information) and the absorption spectral pattern and the maximum wavelengths in the PL spectra (509 and 544 nm; Figure 3) for the

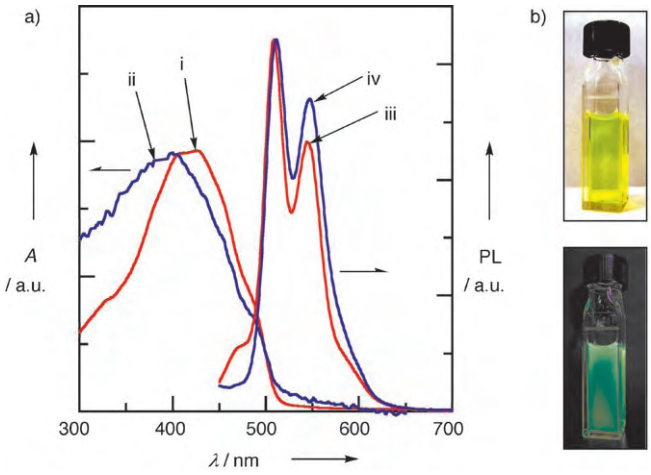

Figure 3. a) Absorption (i, ii), photoluminescence (excitation wavelength = 425 (iii) and 400-nm (iv)) spectra of the amylose (24 000)–PPV composite prepared under condition B in DMSO (1.0 (i) and 0.1 mg mL^{-1} (iii) red trace) and in the film state (ii, iv) blue trace. b) Photographs of the amylose (24 000)–PPV composite under white (top) and UV light at 365 nm (bottom).

amylose–PPV composite obtained under the optimized condition (condition B) are similar to those of a typical PPV reported previously.[15] The Raman spectrum of the composite film also supports the structure of PPV (see Supporting Information); the composite exhibited characteristic Raman bands that result from the stretching vibration of the vinyl groups (1328 and 1626 cm^{-1}) and phenyl rings (1173, 1548, and 1585 cm^{-1}) of the PV units. The intensity ratio of the C=C stretching vibration of the phenyl ring (1585 cm^{-1}) and vinyl group (1626 cm^{-1}; I_{1548}/I_{1626}) is higher than one with excitation at 785 nm, thus suggesting that the conjugation segment of the PPV in the amylose–PPV composite appears to be long for a typical PPV.[16]

The mechanism of the in situ encapsulation of PPV in the amylose tube during the polymerization of **1** in DMSO/alkaline water and the structure of the composites have not been clearly elucidated so far, but a possible mechanism can be proposed as follows: First, monomer **1** generates, through base catalysis, an intermediate quinodimethane species, which then polymerizes to produce the water-soluble sulfonium precursor oligomer or polymer **2**.[17] These species are too hydrophilic to be included in the hydrophobic amylose interior.[8,18] We, therefore, consider that once the precursor polymer or oligomer is generated in DMSO/alkaline water, part of the precursor units may be converted into the luminescent PV segments, which are highly hydrophobic and immediately entrapped in the hydrophobic amylose tube. These conversion and encapsulation processes may be accelerated in the presence of amylose and/or DMSO with excess NaOH, as any soluble PPVs could not be detected by photoluminescence in the absence of amylose or in the presence of maltohexaose and β-cyclodextrin under the identical polymerization conditions. According to this mechanism, the amylose–PPV composite containing 35 mol % of the precursor units prepared under condition A may have a random distribution of the two segments, which may further slowly convert into the PPV segments in the presence of excess NaOH.

Amylose is known to adopt a left-handed helix with a 0.8-nm pitch of six glucose units per turn in aqueous solution (see Figure 1c and Supporting Information).[8,18] Combined with computer modeling, a sixfold amylose of $M_w = 15\,000$ (93 glucose units) can be calculated to accommodate approximately 18 PV units. The obtained amylose (15 000)–PPV composite ([glucose]/[PV] = 9:1) may be able to accommodate approximately 11 PV units, but when the feed molar ratio increased during the polymerization, the amylose–PPV composite precipitated and became insoluble. The matrix-assisted laser desorption/ionization time-of-flight (MALDI-TOF) mass spectra of PPVs obtained by acid hydrolysis of the amylose (15 000)–PPV composites (conditions A and B) showed a molecular-mass distribution that ranged from approximately 500 to 1600 Da, which corresponds to a 5 mer to 14 mer of PV units (see Supporting Information).

Biological[19] and synthetic[20] rigid-rod helical polymers often form lyotropic LCs, but helical amylose shows no LC phases as a result of an overall flexible-chain characteristic in solution and films.[9] However, we anticipated that when a stiff, rodlike polymer is threaded into the flexible amylose tube, the resulting complex might become a rigid-rod, thus showing LCs in concentrated solutions. Figure 4a shows a polarizing optical micrograph of the amylose (24 000)–PPV composite prepared under the optimized conditions in a concentrated solution of DMSO (ca. 60 wt %). The observed Schlieren-like texture suggests a typical LC of nematic order. The reason why the optically active amylose-based complexes did not show a chiral LC such as a cholesteric LC is not clear at present.[21] An analogous nematic order occurs in colloidal solutions of the biological tobacco mosaic virus.[22] The solution of higher-molecular-weight amylose (50 000)–PPVs in DMSO (ca. 50 wt %; conditions A and B) also showed a similar nematic LC (see Supporting Information). Films prepared by solvent evaporation of the solutions of the amylose–PPVs in DMSO on a Teflon sheet and fibers that showed a green luminescence (Figure 4b and c) retained their molecular ordering, as evidenced by the polarizing optical microscopy (Figure 4d).

In summary, we have synthesized the first water-soluble, luminescent PPV-based polymer composite by polymerization of the precursor monomer in aqueous media in the presence of amylose. PPV encapsulated in an amylose tube can be further processed into luminescent films and fibers. Moreover, amylose, which is too flexible to form an LC,

 © 2006 Wiley-VCH Verlag GmbH & Co. KGaA, Weinheim

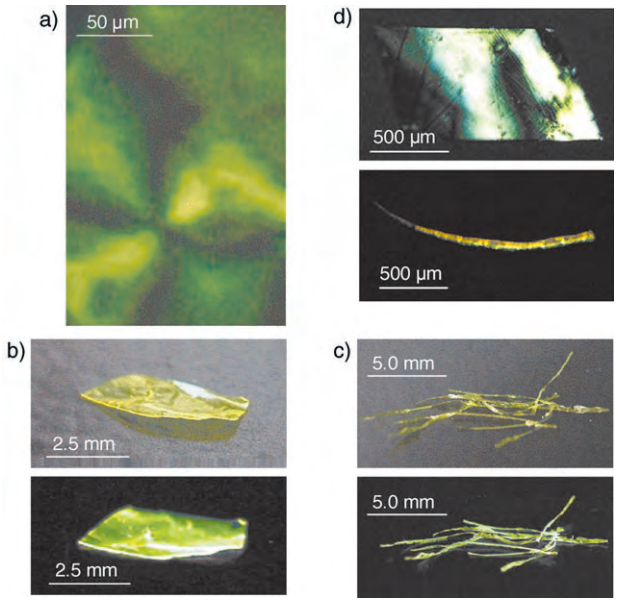

Figure 4. a) Polarizing optical micrograph of approximately 60 wt% solution of the amylose (24000)–PPV in DMSO. Photographs of an amylose–PPV b) film and c) fiber under white (top) and UV light at 365 nm (bottom). d) Polarizing optical micrographs of the amylose–PPV film (top) and fiber (bottom) are also shown.

exhibits an LC when the PPV is threaded into the amylose tube, thus resulting in a rigid-rod assembly. This supramolecular liquid-crystal formation is conceptually new and the polymer lengths of the amylose can be controlled by using the enzymatic polymerization technique.[10] Therefore, this approach will provide luminescent PPV-based amyloses with controlled molecular lengths and aspect ratios and will promise access to potentially valuable optoelectronic, chiral, and biocompatible materials with a controlled molecular order.

Received: May 29, 2006
Published online: September 8, 2006

Keywords: amylose · helical structures · liquid crystals · poly(phenylenevinylene) · supramolecular chemistry

[1] J. H. Burroughes, D. D. C. Bradley, A. R. Brown, R. N. Marks, K. Mackay, R. H. Friend, P. L. Burns, A. B. Holmes, *Nature* **1990**, *347*, 539–541.
[2] R. A. Wessling, *J. Polym. Sci. Polym. Symp.* **1985**, *72*, 55–66.
[3] a) C. L. Gettinger, A. J. Heeger, J. M. Drake, D. J. Pine, *J. Chem. Phys.* **1994**, *101*, 1673–1678; b) F. Hide, M. A. D. García, B. J. Schwartz, A. J. Heeger, *Acc. Chem. Res.* **1997**, *30*, 430–436; c) A. Kraft, A. C. Grimsdale, A. B. Holmes, *Angew. Chem.* **1998**, *110*, 416–443; *Angew. Chem. Int. Ed.* **1998**, *37*, 402–428; for recent examples of oligo-PPVs, see: d) S. J. George, A. Ajayaghosh, P. Jonkheijm, P. H. J. Schenning, E. W. Meijer, *Angew. Chem.* **2004**, *116*, 3504–3507; *Angew. Chem. Int. Ed.* **2004**, *43*, 3422–3425; e) J. F. Hulvat, M. Sofos, K. Tajima, S. I. Stupp, *J. Am. Chem. Soc.* **2005**, *127*, 366–372, and references therein.
[4] For reviews, see: a) K. Tajima, T. Aida, *Chem. Commun.* **2000**, 2399–2412; b) D. J. Cardin, *Adv. Mater.* **2002**, *14*, 553–563; c) K. Sakurai, K. Uezu, M. Numata, T. Hasegawa, C. Li, K. Kaneko, S. Shinkai, *Chem. Commun.* **2005**, 4383–4398.
[5] a) P. N. Taylor, M. J. O'Connell, L. A. McNeill, M. J. Hall, R. Aplin, H. L. Anderson, *Angew. Chem.* **2000**, *112*, 3598–3602; *Angew. Chem. Int. Ed.* **2000**, *39*, 3456–3460; b) K. Yoshida, T. Shimomura, K. Ito, R. Hayakawa, *Langmuir* **1999**, *15*, 910–913; c) F. Cacialli, J. S. Wilson, J. J. Michels, C. Daniel, C. Silva, R. H. Friend, N. Severin, P. Samori, J. P. Rabe, M. J. O'connell, P. N. Taylor, H. L. Anderson, *Nat. Mater.* **2002**, *1*, 160–164; d) I. Yamaguchi, K. Kashiwagi, T. Yamamoto, *Macromol. Rapid Commun.* **2004**, *25*, 1163–1166; e) J. S. Wilson, M. J. Frampton, J. J. Michels, L. Sardone, G. Mealetta, R. H. Friend, P. Samori, H. L. Anderson, F. Cacialli, *Adv. Mater.* **2005**, *17*, 2659–2663; for encapsulation of PPV in nanoporous materials, see: f) R. C. Smith, W. M. Fischer, D. L. Gin, *J. Am. Chem. Soc.* **1997**, *119*, 4092–4093; g) M. Álvaro, A. Corma, B. Ferrer, M. S. Galletero, H. García, E. Peris, *Chem. Mater.* **2004**, *16*, 2142–2147.
[6] a) A. Star, D. W. Steuerman, J. R. Heath, J. F. Stoddart, *Angew. Chem.* **2002**, *114*, 2618–2622; *Angew. Chem. Int. Ed.* **2002**, *41*, 2508–2512; b) O.-K. Kim, J. Je, J. W. Baldwin, S. Kooi, P. E. Pehrsson, L. J. Buckley, *J. Am. Chem. Soc.* **2003**, *125*, 4426–4427; c) T. Sanji, N. Kato, M. Kato, M. Tanaka, *Angew. Chem.* **2005**, *117*, 7467–7470; *Angew. Chem. Int. Ed.* **2005**, *44*, 7301–7304; d) T. Sanji, N. Kato, M. Tanaka, *Org. Lett.* **2006**, *8*, 235–238.
[7] a) M. Numata, T. Hasegawa, T. Fujisawa, K. Sakurai, S. Shinkai, *Org. Lett.* **2004**, *6*, 4447–4450; b) C. Li, M. Numata, A.-H. Bae, K. Sakurai, S. Shinkai, *J. Am. Chem. Soc.* **2005**, *127*, 4548–4549; c) S. Haraguchi, T. Hasegawa, M. Numata, M. Fujiki, K. Uezu, K. Sakurai, S. Shinkai, *Org. Lett.* **2005**, *7*, 5605–5608.
[8] Y. Hui, W. Zou in *Frontiers in Supramolecular Organic Chemistry and Photochemistry* (Eds.: H.-J. Schneider, H. Dürr), VCH, Weinheim, **1991**, pp. 203–221.
[9] a) Y. Nakanishi, T. Norisuye, A. Teramoto, S. Kitamura, *Macromolecules* **1993**, *26*, 4220–4225; b) P. Roger, M. A. V. Axelos, P. Colonna, *Macromolecules* **2000**, *33*, 2446–2455.
[10] a) S. Kitamura, H. Yunokawa, S. Mitsuie, T. Kuge, *Polym. J.* **1982**, *14*, 93–99; b) N. Enomoto, S. Furukawa, Y. Ogasawara, H. Akano, Y. Kawamura, E. Yashima, Y. Okamoto, *Anal. Chem.* **1996**, *68*, 2798–2804.
[11] See Supporting Information for details of the synthesis, structures, and characterization of the amylose–PPV composites.
[12] The molar proportion of amylose (x), the PV part (y), and the precursor part (z) was estimated from the ^{1}H NMR spectra during the in situ polymerization of **1** in the presence of amylose in [D$_6$]DMSO/D$_2$O (5:2 v/v; Figure 2a). The proportion was estimated based on the relative peak integrals of the signal H$_l$ of amylose, the phenyl signal H$_a$ of the precursor part, and the released tetrahydrothiophene signal H$_p$ after the polymerization, as the signals that arose from the PV part were greatly broadened, presumably as a result of its restricted motion on encapsulation in the amylose tube; hence, the signals of the PV part could not be used for the estimation. The molar proportions of the PV part relative to the precursor part were calculated to be 65:35 and 99:1 for the composites prepared under conditions A and B, respectively.[11] In the ^{13}C CP–MAS NMR spectra (B), the absence of the precursor part in the amylose (15000)–PPV composite obtained under condition B (top) was confirmed from the disappearance of a broad signal at around $\delta = 40$–50 ppm as a result of the precursor part (c and d; bottom).[13] We note that the peak pattern from the PV part at around $\delta = 120$–140 ppm for the amylose (15000)–PPV composite obtained under condition B (top) is similar to that of a typical PPV previously reported.[13]
[13] E. R. de Azevedo, R. W. A. Franco, A. Marletta, R. M. Faria, T. J. Bonagamba, *J. Chem. Phys.* **2003**, *119*, 2923–2934.

 © 2006 Wiley-VCH Verlag GmbH & Co. KGaA, Weinheim

[14] The solution finally became slightly turbid under these optimized conditions. After centrifugation, soluble components (ca. 60–70%) were obtained. The same elemental analyses were obtained for the soluble and insoluble fractions, thus showing the molar composition of glucose units of amylose to PV units to be 9:1, which is identical to the feed molar ratio.[11] We then attempted to estimate the molecular weights of the composites by SEC with the same aqueous eluent system for those prepared under condition A. However, it was difficult to conduct SEC analysis because of strong adsorption on an SEC column or aggregation of the polymers.
[15] A. B. Holmes, D. D. C. Bradley, A. R. Brown, P. L. Burn, J. H. Burroughes, R. H. Friend, N. C. Greenham, R. W. Gymer, D. A. Halliday, R. W. Jackson, A. Kraft, J. H. F. Martens, K. Pichler, I. D. W. Samuel, *Synth. Met.* **1993**, *55–57*, 4031 – 4040.
[16] E. Mulazzi, A. Ripamonti, J. Wery, B. Dulieu, S. Lefrant, *Phys. Rev. B* **1999**, *60*, 16519 – 16525.
[17] A. C. Grimsdale in *Organic Light-Emitting Devices* (Eds.: K. Müllen, U. Scherf), Wiley-VCH, Weinheim, **2006**, pp. 215 – 243.
[18] a) R. Bishop, I. G. Dance, *Top. Curr. Chem.* **1988**, *149*, 137 – 188; b) S. Kubik, O. Höller, A. Steinert, M. Tolksdorf, G. Wulff, *Macromol. Symp.* **1995**, *99*, 93 – 102; c) O.-K. Kim, L.-S. Choi, H.-Y. Zhang, X.-H. He, Y.-H. Shin, *J. Am. Chem. Soc.* **1996**, *118*, 12220 – 12221.
[19] a) C. Robinson, J. C. Ward, *Nature* **1957**, *180*, 1183 – 1184; b) Y. Tsujita, I. Yamanaka, A. Takizawa, *Polym. J.* **1979**, *11*, 749 – 754; c) F. Livolant, Y. Bouligand, *J. Phys.* **1986**, *47*, 1813 – 1827; d) T. E. Strzelecka, M. W. Davidson, R. L. Rill, *Nature* **1988**, *331*, 457 – 460; e) F. Livolant, A. M. Levelut, J. Doucet, J. P. Benoit, *Nature* **1989**, *339*, 724 – 726; f) S. Fortin, G. Charlet, *Macromolecules* **1989**, *22*, 2286 – 2292; g) S. Inatomi, Y. Jinbo, T. Sato, A. Teramoto, *Macromolecules* **1992**, *25*, 5013 – 5019; h) S. M. Yu, V. P. Conticello, G. Zhang, C. Kayser, M. J. Fournier, T. L. Mason, D. A. Tirrell, *Nature* **1997**, *389*, 167 – 170.
[20] a) T. Sato, Y. Sato, Y. Umemura, A. Teramoto, Y. Nagamura, J. Wagner, D. Weng, Y. Okamoto, K. Hatada, M. M. Green, *Macromolecules* **1993**, *26*, 4551 – 4559; b) M. M. Green, N. C. Peterson, T. Sato, A. Teramoto, R. Cook, S. Lifson, *Science* **1995**, *268*, 1860 – 1866; c) J. Watanabe, H. Kamee, M. Fujiki, *Polym. J.* **2001**, *33*, 495 – 497; d) J. J. L. M. Cornelissen, J. J. J. M. Donners, R. de Gelder, W. S. Graswinckel, G. A. Metselaar, A. E. Rowan, N. A. J. M. Sommerdijk, R. J. M. Nolte, *Science* **2001**, *293*, 676 – 680; e) J. Kim, B. M. Novak, A. J. Waddon, *Macromolecules* **2004**, *37*, 1660 – 1662; f) K. Maeda, Y. Takeyama, K. Sakajiri, E. Yashima, *J. Am. Chem. Soc.* **2004**, *126*, 16284 – 16285.
[21] X-ray diffraction studies of the LC films showed diffuse reflections.
[22] R. Oldenbourg, X. Wen, R. B. Meyer, D. L. D. Casper, *Phys. Rev. Lett.* **1988**, *61*, 1851 – 1854.

 © 2006 Wiley-VCH Verlag GmbH & Co. KGaA, Weinheim

Metal–Organic Frameworks

DOI: 10.1002/anie.200602242

A Family of Nanoporous Materials Based on an Amino Acid Backbone**

*Ramanathan Vaidhyanathan, Darren Bradshaw, Jean-Noel Rebilly, Jorge P. Barrio, Jamie A. Gould, Neil G. Berry, and Matthew J. Rosseinsky**

Biological molecules interact with substrates with exquisite precision and (stereo)chemical selectivity, because of their ability to generate suitable receptor sites for substrate molecules. These sites have sufficient diversity in their bonding capabilities to allow subtle differentiation between molecular geometries. There is, thus, considerable interest in the preparation of synthetic materials with aspects of this function.[1] One approach is to use biologically derived components in the assembly of such materials. Amino acid residues are the origin for the functional properties and highly selective substrate-binding ability of many extended biological structures, and so are an attractive option as chiral building blocks for the preparation of bio-analogous materials. Herein, we report a family of synthetic crystalline nanoporous materials in which the internal surface is provided by the amino acid aspartic acid. These materials display enantioselective sorption that is strongly dependent on the spatial distribution of functional groups within the guest molecule.

Aspartic acid ($NH_2CH(COOH)CH_2COOH$, $aspH_2$) is an acidic amino acid with one amine and two carboxylic acid groups. As each of these functional groups is capable of binding to metal centers, the aspartate anion has a variety of coordination modes.[2] This polyfunctionality makes it a suitable organic node for the construction of porous metal–organic open-framework materials.[3–6] Extended frameworks based on metal aspartates have recently been reported;[2] however, the structural motifs in these frameworks are too dense to generate guest-accessible volume. The lactate[7] and tartrate[8] anions have also been used in the construction of metal–organic frameworks.

We have sought to generate porosity by connecting metal-aspartate units with suitable bidentate linker molecules. This objective requires a synthetic route that avoids the presence

[*] Dr. R. Vaidhyanathan, Dr. D. Bradshaw, Dr. J.-N. Rebilly, J. P. Barrio, J. A. Gould, Dr. N. G. Berry, Prof. M. J. Rosseinsky
Department of Chemistry
University of Liverpool
Liverpool, L69 7ZD (UK)
Fax: (+44) 151-794-3587
E-mail: m.j.rosseinsky@liv.ac.uk
Homepage: http://www.liv.ac.uk/Chemistry/Postgraduate/portfolio.html

[**] We thank the EPSRC for funding under EPSRC/C511794 and for access to the SRS, and the Leverhulme Trust for support of J.N.R.

Supporting information for this article is available on the WWW under http://www.angewandte.org or from the author.

© 2006 Wiley-VCH Verlag GmbH & Co. KGaA, Weinheim

of competing anions in the framework-forming step. This precaution is necessary to prevent structures that do not contain the amino acid from being templated by the counterion of the nickel source, and to prevent channel blockage by charge-balancing anions. The use of the preformed Ni(asp)·3 H_2O salt as a source of both cation and anion avoids this type of complication. Solvothermal reaction of Ni(L-asp)·3 H_2O with the bidentate aromatic nitrogen donor 4,4′-bipyridine (bipy) as the framework-forming linker in a water/methanol mixture at 150 °C affords the open-framework material [Ni_2(L-asp)$_2$(bipy)]·guests (**1**). Chiral gas chromatography (GC) confirms that the enantiopurity of the starting amino acid is delivered to the product by this route when either D- or L-aspartate is used as the starting material. Containing only one enantiomer of the amino acid, **1** adopts the chiral $P2_12_12$ space group, as indicated by the systematic absences in diffraction patterns produced by single crystals selected from the homochiral product.[18]

In **1**, neutral chiral Ni(L-asp) layers are connected by 4,4′-bipyridine linkers to afford a pillared structure with one-dimensional channels defined by the length of the 4,4′-bipyridine ligand and the separation between the nickel centers in the Ni(L-asp) layer (Figure 1 a). The chiral Ni(L-asp) layers are formed by octahedrally coordinated nickel centers linked by aspartate molecules, which each bind to one nickel center in a tridentate fac mode (by the amine and the α- and β-carboxylate groups) and to two other nickel centers in a monodentate mode (by the α- and β-carboxylate groups). The geometries of the resulting five- and six-membered chelate rings are comparable with those found in other materials featuring tridentate aspartate ligands.[9] The carboxylate groups each bridge two nickel centers in the syn–anti mode.

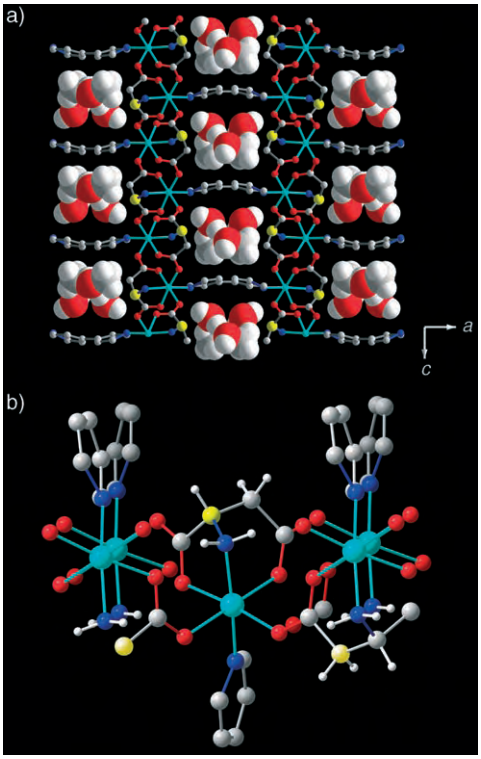

Figure 1. a) The connection of chiral Ni(L-asp) layers by 4,4′-bipyridine ligands produces framework **1**, which contains channels lined with amino acid residues. The disordered methanol and water guests that occupy the channels are represented with space-filling spheres. Hydrogen atoms and the minor disorder component of the 4,4′-bipyridine ligands are omitted for clarity. b) Part of the Ni(L-asp) layer of **1**, showing the coordination environments of the nickel centers. Ni cyan, C gray (chiral centers yellow), H white, N blue, O red.

In the octahedral coordination environment of the nickel cations, one triangular face comprises the amine nitrogen atom and oxygen atoms from both carboxylate functions of one aspartate molecule (Figure 1 b). The position trans to the amine group is occupied by a nitrogen atom from a 4,4′-bipyridine ligand. The two remaining coordination sites are occupied by oxygen atoms from carboxylate groups of two other aspartate molecules within the layer. Each nickel cation, thus, binds to three aspartate anions. The aspartate anions, in turn, link the metal center to four other nickel cations, which are coplanar and at a different height (along the *a* direction) to the central nickel cation, thus, imparting a corrugated nature to the layers. The tridentate aspartate anion links the nickel cation to two others by its two bridging carboxylate groups, while the two monodentate aspartate anions link the nickel cation to two further metal centers.

This corrugation requires that the 4,4′-bipyridine ligand bound to the central nickel cation and those bound to its four neighboring cations project outwards on opposite sides of the Ni(L-asp) layer. The distance (along the *c* direction) between the 4,4′-bipyridine pillars connecting two Ni(L-asp) layers is 7.73 Å, and the interlayer distance (along the *a* direction) between the nickel cations linked by the 4,4′-bipyridine molecules is 9.5 Å. The resulting channels (see Supporting Information), which run along the *b* direction, have a narrowest cross section of 3.8 × 4.7 Å (including van der Waals radii) and account for a solvent-accessible volume of 23.1 % of the total volume of **1**. The projection of the chiral carbon atoms of the aspartate units into the channels imparts chiral functionality to the internal surface of the material (Figure 1 b). In the as-prepared material, the channels are occupied by disordered water and methanol guest molecules (Figure 1 a). The composition of **1** refined from single-crystal X-ray diffraction data is [Ni_2(L-asp)$_2$(bipy)]·1.28 CH_3OH·0.72 H_2O.

Careful control over the water to methanol ratio is needed to achieve a homochiral material, as a competing achiral structure, [Ni_2(L,D-asp)$_2$(bipy)]·2 H_2O (**2**), forms by the racemization of the starting amino acid at higher water concentrations. Scanning electron microscope (SEM) images reveal considerable differences between the orthorhombic morphology of the chiral phase and the truncated polyhedral morphology of the racemic phase (see Supporting Information). The crystal structure of the racemic form **2** (space group $P2_1/n$) features similar Ni(asp) layers linked by 4,4′-bipyridine pillars, but successive layers are related by inversion symmetry.

The solvothermal synthesis based on Ni(L-asp)·3 H_2O is a generic route to a family of pillared open-framework materials with biologically derived internal surfaces. The replacement of 4,4′-bipyridine with related, but longer,

 © 2006 Wiley-VCH Verlag GmbH & Co. KGaA, Weinheim

bridging nitrogen-donor ligands generates analogous materials with larger channels (see Supporting Information).

The phase purity of bulk **1** obtained from the solvothermal reaction between Ni(L-asp)·3 H_2O and 4,4′-bipyridine was established by powder X-ray diffraction (see Supporting Information). The phase purity is consistent with the homogeneous appearance of the material under SEM examination. Elemental analysis provided the composition $[Ni_2(L\text{-asp})_2(bipy)]\cdot CH_3OH\cdot H_2O$ (elemental analysis (%) calcd: C 38.96, H 4.13, N 9.56; found: C 38.94, H 4.11, N 9.64; inductively coupled plasma (ICP) analysis (%) calcd: Ni 20.04; found: Ni 20.12), which is in good agreement with the crystallographically derived formula.

The extended array of Ni–N and Ni–O bonds within the material confers thermal stability and robustness, such that **1** retains its open-framework structure upon loss of the methanol and water guest molecules from the channels. Thermogravimetric analysis of **1** under a nitrogen flow reveals a weight loss of 8.48% between room temperature and 200 °C (see Supporting Information), which is attributed to the removal of methanol and water molecules (calcd weight loss 8.55% from the analyzed composition). The similarity of the powder X-ray diffraction patterns of the as-prepared and the desolvated material demonstrates that the framework of **1** is stable to guest loss (see Supporting Information). The permanent porosity of **1** is demonstrated by the CO_2 sorption isotherm (see Supporting Information), from which a BET surface area of 247(3) $m^2 g^{-1}$ is obtained.

The detailed structural consequences of desolvation can be followed by single-crystal X-ray diffraction at 100 °C under a nitrogen flow (crystals of **1** remain stable and diffracting up to 200 °C). The desolvated crystal retains the framework structure of **1** (space group $P2_12_12$), but with no significant electron density in the channels.[18] Elemental analysis of the desolvated material corresponds to the composition $[Ni_2(L\text{-asp})_2(bipy)]$. The geometry of the Ni(L-asp) layers does not change markedly upon loss of the guests: the bond lengths and angles involving the nickel centers and the carbon, nitrogen, and oxygen atoms of the aspartate ligands are almost unchanged, within error, and the N-C-C-O torsion angle within the five-membered chelate ring remains 18.0(4)°.

Vapor sorption isotherms demonstrate that cyclohexane is not sorbed by **1**, placing an upper limit of 4.982 × 6.580 Å[10] on guest dimensions. Given the homochiral nature of the biologically derived internal surface of **1**, the extent of enantioselectivity possible in guest sorption is clearly of interest. We probed enantioselective sorption by using a library of small chiral molecules with closely related functionalities and found that there is a geometry-dependent interaction between the nanoporous material and the small-molecule guests. Table 1 lists the enantiomeric excess (*ee*) values found for the sorption of small chiral diols by **1** at 278 K, compared to those of the racemic standards. In all cases, the opposite enantiomer was enhanced by sorption when a host derived from D-aspartate, rather than L-aspartate, was used. The host samples were verified to be greater than 95% enantiopure before use in the tests; the use of host samples of lower enantiopurity reduced the observed *ee* value, in all cases.

Table 1: Sorption of chiral diols by **1** at 278 K.[a]

Diol	Extracted *ee* value[b]	Standard *ee* value[c]
1,2-propanediol	5.35	0.16
1,3-butanediol	17.93	0.62
1,2-butanediol	5.07	0.88
2,3-butanediol	1.5[d]	0.5
1,2-pentanediol	13.9[e]	0.34
2,4-pentanediol	24.5	0.00
2-methyl-2,4-pentanediol	53.77	0.46
2,5-hexanediol	3.4[f]	0.0
1,2-hexanediol	5	0.09

[a] The enantiomeric excess $ee = (R-S)/(R+S)*100$ was determined for the trifluoroacetic anhydride derivatives of the diols on a Lipodex-E capillary GC column (Machery Nagel). See Supporting Information for details. [b] For the guest diols recovered by distillation from **1**, after exposure of **1** to the liquid diol for 16 h. [c] For the racemic diol standard. [d] Extracted 71.4% meso; standard 65.7% meso. [e] Extracted 45.1% meso; standard 50.7% meso. [f] Extracted 58.5% meso; standard 53.6% meso.

The levels of enantioselection for the sorption of these small molecules are significant, but it is the differentiation between diols with similar chain lengths but differing separations between the hydroxyl groups which is particularly striking. Considering a fixed chain length of four carbon atoms, 1,2-butanediol and 2,3-butanediol display considerably reduced enantioselection relative to 1,3-butanediol. The favorable nature of the 1,3-disposition of the diol units is further demonstrated by the high *ee* value of 2,4-pentanediol, in comparison with those of 1,2-pentanediol and 2,5-hexanediol. The highest sorption *ee* value observed within the library of diol guests studied was 53.7% for 2-methyl-2,4-pentanediol, a monosubstituted derivative of 2,4-pentanediol with only one chiral center.

The characteristics of the interactions between a diol guest and the internal surface of a porous material composed of Ni(asp) layers and 4,4′-bipyridine pillars are revealed by the crystal structure of $[Ni_2(L,D\text{-asp})_2(bipy)]\cdot CH_2(OH)CH(OH)CH_3$ (**3**),[18] which was prepared solvothermally in 1,2-propanediol. The framework of **3** adopts the racemic structure of **2**, as the conditions required to grow crystals of suitable size and quality from the diol solvent result in the racemization of the aspartate anion. However, given the similarity in structure between **1** and **2**, the structure of **3** can serve as a model for the guest binding motifs in the chiral host **1** as well. In the refined structure of **3**, the guest is located in a pocket defined by two neighboring 4,4′-bipyridine molecules and adopts an extended conformation, with the diol groups hydrogen bonded to the oxygen atoms of β-carboxylate groups in two Ni(asp) layers (Figure 2).

It was not possible to grow analogues of **1** with chiral guests; therefore, we used computational approaches to identify different modes of interaction between the guests and **1** that might explain the pronounced differences in enantioseparation. The efficient center-of-mass and conformational searching of a docking routine based on molecular mechanics was combined with higher-level quantum-mechanical calculations (see Supporting Information). Such docking

 © 2006 Wiley-VCH Verlag GmbH & Co. KGaA, Weinheim

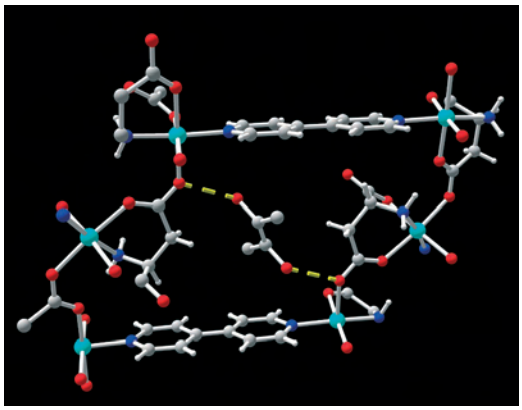

Figure 2. Location of 1,2-propanediol within the channels of **3**. As the 1,2-propanediol molecule is disordered over a crystallographic inversion center, each of the methyl groups shown has an occupancy of 50%; further disorder involving the methyl groups is omitted for clarity. Hydrogen bonds are represented by dashed yellow lines. Ni cyan, C gray, H white, N blue, O red.

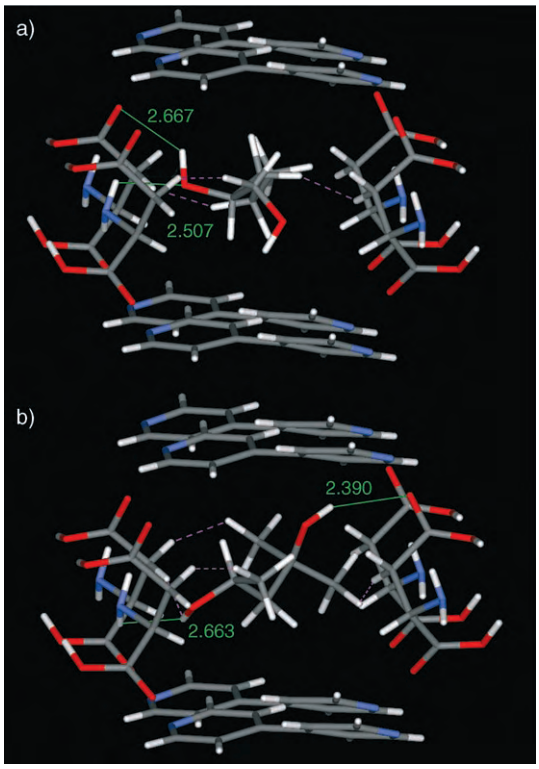

Figure 3. Location of a) (*S*)-1,2-pentanediol and b) (*S*)-2-methyl-2,4-pentanediol within the channels of **1**, as determined by the combination of molecular-mechanics docking and semi-empirical quantum-mechanical optimization. Hydrogen bonds are represented by solid green lines; potentially unfavorable contacts (with distances of less than 84% of the sums of the van der Waals radii) are represented by dashed pink lines. C gray, H white, N blue, O red; Ni atoms are omitted.

approaches have been extensively validated in the study of drug–receptor interactions in proteins and other biomolecules[11,12] and involve genetic-algorithm-driven searches of the conformational and positional space of guest species. These methods were tested by successfully reproducing the location of the 1,2-propanediol guest in **3**. The docking procedure was then applied to the interaction of **1** with the two guest molecules 1,2-pentanediol (13.9% *ee*, Table 1) and 2-methyl-2,4-pentanediol (53.77% *ee*, Table 1). These guests were chosen to investigate the factors responsible for enantioselection, as they have alkyl backbones of the same length. However, the *ee* values observed indicate that the differential free energy of sorption of enantiomers of the two guests differ by a factor of four. The molecular-mechanics docking procedures indicated differing modes of interaction for the 2-methyl-2,4-pentanediol and 1,2-pentanediol guests with the framework. The most popular docked pose of each enantiomer of the guests was then optimized within the framework using semi-empirical quantum-mechanical calculations at the PM3 level; this quantum mechanical optimization did not greatly change the geometry or location of the guest (the largest root-mean-square deviation between the docked and PM3-optimized structures was 0.68 Å).

As expected, given their equal alkyl-chain lengths, both 2-methyl-2,4-pentanediol and 1,2-pentanediol sit in essentially identical sorption sites within the framework of **1** (Figure 3). The guest pocket is defined by two aspartate residues on opposite sides of the channel and by two 4,4′-bipyridine molecules on opposite sides of the channel. However, within this pocket, the two guests interact in different ways with the framework. The approach geometries are similar for both enantiomers in each case (for example, the difference between the sorption energies of the enantiomers of 2-methyl-2,4-pentanediol is 2.8 kJ mol^{-1}). As the small differences between the interactions of the enantiomers of each guest cannot be reliably addressed by the present calculations, we instead use the calculations to identify the different modes of interaction of the two guests (*S* enantiomers) with the framework. The secondary alcohol group of (*S*)-1,2-pentanediol interacts with the framework of **1** by hydrogen bonding with the β-carboxylate group of an aspartate residue (OH···O 2.667 Å) and the amine group of another aspartate residue (O···HN 2.507 Å). The primary alcohol group is located at the center of the channel and does not hydrogen bond to the framework (Figure 3a). In contrast, both alcohol groups of (*S*)-2-methyl-2,4-pentanediol (which is sorbed by **1** with a higher *ee* value) participate in hydrogen bonds with the framework (Figure 3b). The tertiary alcohol group forms hydrogen bonds with the β-carboxylate group of an aspartate residue (OH···O 2.390 Å), and the secondary alcohol group forms a hydrogen bond with the amine group of another aspartate residue (O···HN 2.663 Å). The very different modes of interaction of the two guest molecules may produce the observed differences in enantioselection. The differentiation of substrates on the basis of multiple interactions within a compositionally complex pocket is reminiscent of the selective function of enzymes.

The dimensions of the channels in this amino acid derived open-framework material are on the order of those found in zeolites, but are smaller than the largest found in metal–organic frameworks (of nm-scale diameter).[13,14] For molecular recognition applications, such as chiral sorption, a good match of size and shape between the desired guest and the

 © 2006 Wiley-VCH Verlag GmbH & Co. KGaA, Weinheim

host is important; large-pore homochiral frameworks cannot separate small-molecule guests in this way.[15] This observation demonstrates that not only channel size, but also channel surface chemistry is important for functional behavior in metal–organic frameworks. The preparation of frameworks with internal surfaces derived from amino acids opens up the possibility of new classes of nanoporous materials for chiral catalysis and sorption,[16,17] and will enhance efforts to establish and understand solid-state geometries for bio-analogous recognition behavior.

Experimental Section

Experimental details are given in the Supporting Information.

Received: June 5, 2006
Published online: September 7, 2006

Keywords: amino acids · chirality · metal–organic frameworks · nanoporous materials · sorption

[1] M. Yoshizawa, M. Tamura, M. Fujita, *Science* **2006**, *312*, 251.
[2] E. V. Anokhina, A. J. Jacobson, *J. Am. Chem. Soc.* **2004**, *126*, 3044.
[3] B. F. Abrahams, B. F. Hoskins, D. M. Michail, R. Robson, *Nature* **1994**, *369*, 727.
[4] O. M. Yaghi, M. O'Keeffe, N. W. Ockwig, H. K. Chae, M. Eddaoudi, J. Kim, *Nature* **2003**, *423*, 705.
[5] N. Guillou, C. Livage, M. Drillon, G. Férey, *Angew. Chem.* **2003**, *115*, 5472; *Angew. Chem. Int. Ed.* **2003**, *42*, 5314.
[6] R. Matsuda. R. Kitaura, S. Kitagawa, Y. Kubota, R. V. Belosludov, T. C. Kobayashi, H. Sakamoto, T. Chiba, M. Takata, Y. Kawazoe, Y. Mita, *Nature* **2005**, *436*, 238.
[7] D. N. Dybtsev, A. L. Nuzhdin, H. Chun, K. P. Bryliakov, E. P. Talsi, V. P. Fedin, K. Kim, *Angew. Chem.* **2006**, *118*, 930; *Angew. Chem. Int. Ed.* **2006**, *45*, 916.
[8] S. Thushari, J. A. K. Cha, H. H.-Y. Sung, S. S.-Y. Chui, A. L.-F. Leung, Y.-F. Yen, I. D. Williams, *Chem. Commun.* **2005**, 5515.
[9] L. P. Battaglia, A. Bonamartini Corradi, L. Antolini, G. Marcotrigiano, L. Menabue, G. C. Pellacani, *J. Am. Chem. Soc.* **1982**, *104*, 2407.
[10] C. E. Webster, R. S. Drago, M. C. Zerner, *J. Am. Chem. Soc.* **1998**, *120*, 5509.
[11] C. Hetényi, D. V. D. Spoel, *Protein Sci.* **2002**, *11*, 1729.
[12] G. M. Morris, D. S. Goodsell, R. S. Halliday, R. Huey, W. E. Hart, R. K. Belew, A. J. Olson, *J. Comput. Chem.* **1998**, *19*, 1639.
[13] G. Férey, C. Mellot-Draznieks, C. Serre, F. Millange, J. Dutour, S. Surblé, I. Margiolaki, *Science* **2005**, *309*, 2040.
[14] H. K. Chae, D. Y. Siberio-Pérez, J. Kim, Y.-B. Go, M. Eddaoudi, A. J. Matzger, M. O'Keeffe, O. M. Yaghi, *Nature* **2004**, *427*, 523.
[15] D. Bradshaw, T. J. Prior, E. J. Cussen, J. B. Claridge, M. J. Rosseinsky, *J. Am. Chem. Soc.* **2004**, *126*, 6106.
[16] C.-D. Wu, A. Hu, L. Zhang, W. Lin, *J. Am. Chem. Soc.* **2005**, *127*, 8940.
[17] J. S. Seo, D. Whang, H. Lee, S. I. Jun, J. Oh, Y. J. Jeon, K. Kim, *Nature* **2000**, *404*, 982.
[18] Crystallographic data for solvated **1** ($[Ni_2(L\text{-asp})_2(bipy)]\cdot 1.28\,CH_3OH\cdot 0.72\,H_2O$): $C_{19.28}H_{24.56}N_4Ni_2O_{10}$, $M_r = 589.84$, orthorhombic, space group $P2_12_12$, $a = 22.2721(13)$, $b = 6.8371(4)$, $c = 7.7308(5)$ Å, $V = 1177.22(12)$ Å^3, $Z = 2$, $\lambda = 0.84600$ Å, $T = 150(2)$ K, $R_1 = 0.0432$, $R_w = 0.1128$. For desolvated **1** ($[Ni_2(L\text{-asp})_2(bipy)]$): $C_{18}H_{18}N_4Ni_2O_8$, $M_r = 535.78$, orthorhombic, space group $P2_12_12$, $a = 22.245(2)$, $b = 6.7907(7)$, $c = 7.7387(8)$ Å, $V = 1169.0(2)$ Å^3, $Z = 2$, $\lambda = 0.84600$ Å, $T = 373(2)$ K, $R_1 = 0.0350$, $R_w = 0.0809$. For **3** ($[Ni_2(L,D\text{-asp})_2(bipy)]\cdot CH_2(OH)CH(OH)CH_3$): $C_{21}H_{26}N_4Ni_2O_{10}$, $M_r = 611.87$, monoclinic, space group $P2_1/n$, $a = 6.5697(4)$, $b = 22.6167(13)$, $c = 7.8511(5)$ Å, $\beta = 90.1540(10)°$, $V = 1166.55(12)$ Å^3, $Z = 2$, $\lambda = 0.67270$ Å, $T = 100(2)$ K, $R_1 = 0.0390$, $R_w = 0.0950$. CCDC-607296 (solvated **1**, 150 K), CCDC-607297 (desolvated **1**, 373 K), and CCDC-607295 (**3**) contain the supplementary crystallographic data for this paper. These data can be obtained free of charge from The Cambridge Crystallographic Data Centre via www.ccdc.cam.ac.uk/data_request/cif.

 © 2006 Wiley-VCH Verlag GmbH & Co. KGaA, Weinheim

Host–Guest Systems

DOI: 10.1002/anie.200602556

Intercalation of Organic Molecules into Vanadium(IV) Benzenedicarboxylate: Adsorbate Structure and Selective Absorption of Organosulfur Compounds**

*Xiqu Wang, Lumei Liu, and Allan J. Jacobson**

The capacity and selectivity of nanoporous materials in the absorption and separation of molecular mixtures depend on specific interactions between the host frameworks and removable guest species, and in some cases the degree to which the structure of the host lattice can relax as the molecular species are intercalated. The classical zeolite frameworks are relatively rigid and exhibit little deformation upon loading and unloading of various guest species.[1] On the other hand, intercalation into layered structures leads to expansion of the interlayer separation because of the very weak interlayer bonding and can lead to complete exfoliation of the layers.[2]

Flexibility without loss of crystallinity is expected for structures containing rigid building blocks linked by relatively deformable hingelike units. Examples of framework flexibility have been found in a number of metal–organic frameworks (MOFs).[3] Among them, a group of compounds first reported by Férey and co-workers,[4] based on chains of *trans* corner-sharing octahedra $\{MO_6\}$ (M = V,[4] Cr,[5] Al,[6] Fe,[7] and In[8]) cross-linked by 1,4-benzenedicarboxylate (bdc) upon removal or absorption of guest species, show remarkable framework flexibility. The first member of the group $[\{V(OH)(bdc)\}(H_2bdc)_x]$[4] loses the guest acid on heating in

[*] Dr. X. Wang, Dr. L. Liu, Prof. A. J. Jacobson
Department of Chemistry
University of Houston
Houston, TX 77204-5003 (USA)
Fax: (+1) 713-743-2787
E-mail: ajjacob@uh.edu

[**] The Robert A. Welch Foundation is acknowledged for support of this work.

© 2006 Wiley-VCH Verlag GmbH & Co. KGaA, Weinheim

air, and at the same time the framework V^{3+} ions are oxidized to V^{4+} without changing the topology of the framework.

Sorption studies of these MOFs have focused on H_2 adsorption,[9] but some studies of the absorption of CO_2[10] and CH_4[11] have been reported. Of particular relevance to this study is the report by Férey and co-workers on the adsorption of CH_4 and CO_2 by [M(OH)(bdc)] (M = Cr, Al) and [V(O)(bdc)].[11a] The V^{IV} phase [V(O)(bdc)] shows some differences in the absorption isotherms relative to the trivalent compounds, but the amounts of CO_2 adsorbed above 10 bar are comparable. The relatively weak enthalpy of adsorption suggested that [V(O)(bdc)] has no specific adsorption sites for CO_2.[11a]

Herein, we report the synthesis of single crystals of $[V(O)(bdc)](H_2bdc)_{0.71}$ (**1**) directly. After removal of the guest acid molecules by heating **1** in air, we show that the [V(O)(bdc)] structure is sufficiently flexible to undergo single-crystal-to-single-crystal transformations upon absorption of aniline, thiophene, and acetone from the liquid phase, thus enabling the details of the guest structure, framework–guest interactions, and framework deformations to be determined from single-crystal X-ray diffraction data. Furthermore, we have observed rapid and highly selective gas-phase absorption of thiophene from methane by [V(O)(bdc)], a process relevant to natural-gas clean-up. This application and others of MOFs have been described in a recent review.[12]

The octahedral chain in the structure of $[V(O)(bdc)](H_2bdc)_{0.71}$ (**1**) contains a -V=O–V=O- backbone with alternating short and long V–O apical bonds of the $\{VO_6\}$ octahedra. The equatorial corners of the $\{VO_6\}$ octahedra are shared with the bdc ligands that cross-link the octahedral chains to form 1D rhombshaped tunnels, which are each filled by two columns of guest H_2bdc. Assuming that the H_2bdc molecules in each column are linked by hydrogen bonds similar to those in $[In(OH)(bdc)]\cdot(H_2bdc)_{0.75}$[8] and that a H_2bdc molecule has a length of 9.6 Å, a theoretical number of 0.71 guest H_2bdc molecules per vanadium atom can be derived from the lattice constants. This guest-acid content is confirmed by chemical analysis and structure refinements.[13] The columns of the guest H_2bdc molecules in different tunnels are found randomly disordered over positions shifted relative to each other along the tunnel axis in steps of approximately 1.4 Å. Thermal removal of the guest H_2bdc led to crystals of [V(O)(bdc)] (**2**) suitable for single-crystal X-ray measurement.[14] Our determination of the structure of **2** is in agreement with that reported earlier by Férey and co-workers.[4]

Although the structures of **2** and [M(OH)(bdc)] (M = Al^{3+}, Cr^{3+}, and V^{3+}) have the same topology and belong to the same space group, *Pnma*, they show important differences in local symmetry. In the latter structure, the metal atom is located at an inversion center, whereas the symmetry mirror planes are perpendicular to the octahedral chain and pass through the centers of the bdc ligands. The inversion symmetry center in **2** is shifted to the center of the bdc ligand because the V^{4+} ion is displaced from the center of a $\{VO_6\}$ octahedron to form a V–O double bond. The mirror plane is parallel to the octahedral chain and runs through the -V=O–V=O- backbone. This symmetry difference between the frameworks naturally leads to different space-group symmetries of the corresponding compounds intercalated by the guest H_2bdc molecules.

The $[M(OH)(bdc)](H_2bdc)_x$ phases have the same space-group symmetry as [M(OH)(bdc)], with the guest H_2bdc molecules in neighboring tunnels oriented perpendicular to each other. The same arrangement of the guest molecules is found in **1**, probably because this pattern allows all columns of guest H_2bdc molecules to have favorable π–π interactions with the framework bdc molecules. This arrangement of the guest H_2bdc molecules is not compatible, however, with the symmetry of **2**. The space-group symmetry of **1** is lowered to the non-centrosymmetric $P2_12_12_1$, which was confirmed by structure refinements and by second harmonic generation (SHG) measurements. The SHG efficiency measured on a powder sample of **1** is comparable to that of quartz.

Upon immersion in liquid aniline, thiophene, and acetone, the crystals of **2** transformed into the intercalation compounds [V(O)(bdc)](aniline) (**3**), $[V(O)(bdc)](thiophene)_{0.91}$ (**4**), and [V(O)(bdc)](acetone) (**5**), respectively, without losing their single-crystallinity. Part of each structure, drawn to emphasize the guest-molecule orientations, is shown in Figure 1. The aniline molecule (ca. 7.5 Å long) is much shorter than H_2bdc but still longer than the period (6.8 Å) of the [V(O)(bdc)] framework along the tunnel axis. The

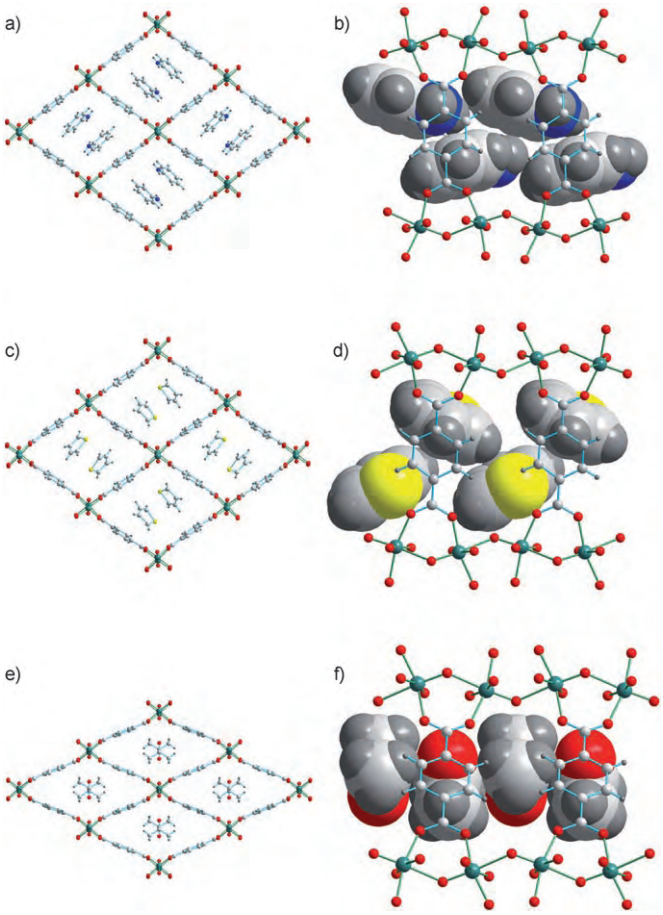

Figure 1. The structures of a, b) [V(O)(bdc)](aniline) (**3**); c, d) [V(O)(bdc)](thiophene)$_{0.91}$ (**4**); and e, f) [V(O)(bdc)](acetone) (**5**). b), d), f) Guest molecules in space-filling representation.

© 2006 Wiley-VCH Verlag GmbH & Co. KGaA, Weinheim

intercalated aniline molecules in **3** form angles of ±17° to the tunnel axis, which can be considered as a compromise between adapting to the framework period, maximizing packing efficiency, and facilitating π–π interactions with the framework bdc ligands. The shortest distance between the benzene-ring center of aniline and the carbon atoms of the bdc benzene ring is 3.507(1) Å, and the distance between their benzene-ring centers is 4.43(1) Å, which indicates a π–π interaction with substantial ring–ring offset.[15] The π–π interactions are complemented by weak C–H···π and N–H···π interactions between the aniline molecules and the bdc ligands. The packing of thiophene molecules in **4** is similar to aniline in **3**, but the angles between the thiophene molecules and the tunnel axis are changed to ±26°, probably as a result of the smaller molecular size. A clear C–H···π interaction between the thiophene molecules and the framework bdc molecule seems to play a major rule in dictating the thiophene orientation.[16] The occupancy of the thiophene position was refined to 0.91(1) in agreement with the absorption measurements (see below). Similar to **1**, the guest-molecule packing in **3** and **4**, which results from the weak interactions between the guest molecules and the host framework, is not compatible with the space-group symmetry of [V(O)(bdc)]. The centrosymmetric space group *Pnma* of [V(O)(bdc)] changes to the chiral space group $P2_12_12_1$ upon loading of the guest aniline or thiophene molecules.

Unlike the aniline and thiophene molecules that form two columns in each tunnel, the acetone molecules in **5** are stacked into one column along the tunnel axis with an antiparallel packing pattern. The intermolecular C=O···C=O distances 3.506(1)–3.510(1) Å within the column indicate weak dipolar carbonyl–carbonyl interactions between the acetone molecules, which probably dictate the packing pattern.[17] The [V(O)(bdc)] tunnel is too small to host two columns of the antiparallel-packed acetone molecules. With only one column of acetone molecules in each tunnel, the framework deforms so that the rhombshaped tunnel section flattens substantially. The flattening not only improves packing efficiency of the whole structure but also facilitates dipolar interactions between the carbonyl group of acetone and the carboxylate groups of the framework bdc ligands (C=O···CO_2: 3.267(1) Å). The packing of the acetone molecules is compatible with the symmetry of the [V(O)(bdc)] framework; therefore, **5** has the same space-group symmetry as **2**.

Upon intercalation of the guest molecules, the tunnel openings in [V(O)(bdc)] systematically shrink because of the interactions between the guest molecules and the host framework. This behavior is illustrated by the ratio of the two diagonals of the tunnel section, which changes from 13.99:16.06 (0.87) in **2** to 13.03:16.85 (0.77) in **3**, 12.62:17.09 (0.74) in **4**, 12.42:17.17 (0.72) in **1**, and 10.21:18.41 (0.55) in **5**. For comparison, the shrinkage on going from [Al(OH)(bdc)]·H_2bdc to [Al(OH)(bdc)]·H_2O is even larger 7.61:19.51 (0.39). The deformations are realized mainly through changes of the torsion angle V–O=C–C, which is the most flexible component of the framework. The packing density calculated for the guest-molecule column of **5** is 122.2 $Å^3$ per acetone molecule, which is almost identical to that of liquid acetone. In contrast, the guest-packing densities calculated for **3** and **4** are both approximately 21% lower than the corresponding liquid densities of the guest molecules, assuming a full occupancy, probably because the oriented interactions between the guest molecules and the framework bdc ligands also dictate the stoichiometry of the intercalated compounds.

Thiophene is also absorbed by [V(O)(bdc)] directly from the gas phase (Figure 2). Single crystals of [V(O)(bdc)]-$(H_2bdc)_{0.71}$ were heated on a thermobalance in flowing air to 350 °C to remove the H_2bdc guest molecules. After cooling to room temperature, the gas stream was switched to a 5% CH_4/He stream. The data in Figure 2 show that methane is not absorbed under these conditions. The gas stream was switched to a 5% CH_4/He stream saturated with thiophene at ambient temperature and 1 atm (10 kPa at 20 °C). Rapid absorption occurs on exposure to methane/thiophene/He corresponding to the uptake of 0.88 molecules of thiophene per [V(O)(bdc)], in agreement with the liquid-phase uptake. The inset in Figure 2 shows that the uptake kinetics are fast. Similar results were obtained for the uptake of dimethyl sulfide and thiophene at 1 kPa (see Table 1).

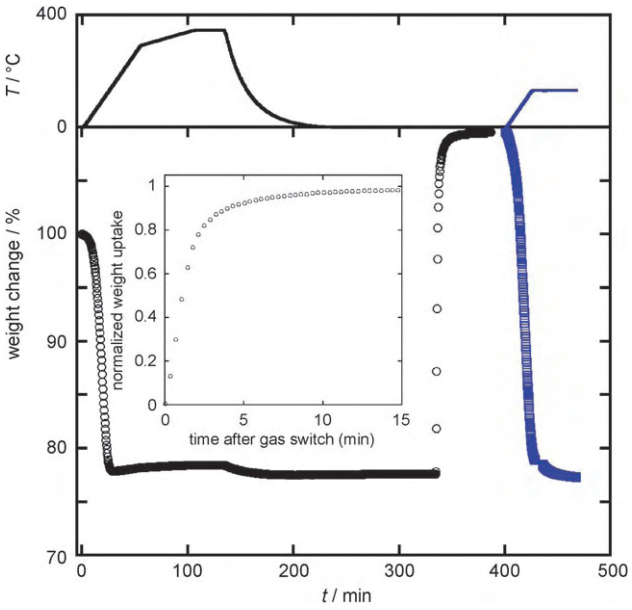

Figure 2. Thiophene uptake by [V(O)(bdc)] from methane saturated with thiophene at ambient temperature. The temperature profile is shown in the top panel and the corresponding weight change in the bottom panel. The inset shows an expanded view of the thiophene uptake kinetics. The data in blue show a second experiment in which a sample saturated with thiophene at ambient temperature is heated to 150 °C.

Table 1: Gas-phase adsorption by [V(O)(bdc)].

Formula	Δwt%	Molecules [f.u.][a]	*P* [kPa][b]
$(CH_3)_2S$	+34.0	1.12	66.9
C_4H_4S	+31.9	0.88	10.0
C_4H_4S	+23.4	0.65	1.0

[a] Formula unit. [b] Partial pressure.

 © 2006 Wiley-VCH Verlag GmbH & Co. KGaA, Weinheim

The reversibility of thiophene uptake was investigated thermogravimetrically and by X-ray diffraction studies. A sample was saturated with thiophene on a thermobalance following the procedure described above. When the sample reached constant weight at ambient temperature, the temperature was raised to 150 °C. Thiophene desorbed and the sample weight returned to its initial value (blue data points in Figure 2). An X-ray powder pattern of the final sample indicated complete retention of crystallinity. A single crystal of [V(O)(bdc)](thiophene) was heated to 200 °C for 30 min to remove the thiophene. The results show that the structure reverts to space group *Pnma*, and the complete absence of any electron density in the channels indicates complete desorption of thiophene. The lattice parameters are $a = 6.813(2)$, $b = 16.248(4)$, and $c = 13.749(3)$ Å, which indicate a 1% smaller cell volume than **2** and suggest that annealing at over 200 °C is necessary to allow the framework to completely relax.

The structural details of the four intercalated compounds presented herein, and the selective and reversible removal of sulfur-containing molecules from methane, show the importance of noncovalent oriented weak interactions in the packing of organic molecules within channels of a specific metal–organic framework. Such interactions, although relatively weak, can readily cause remarkable deformation and symmetry changes in the framework, thus pointing to effective ways of manipulating known materials or designing new materials with targeted properties through intercalation chemistry.

Experimental Section

$[V(O)(bdc)](H_2bdc)_{0.71}$ (**1**) was synthesized by hydrothermal reaction from a mixture of VO_2, HCl, H_2bdc, and H_2O (molar ratio = 1:2:0.5:77). The mixture was heated at 220 °C in a sealed teflon vessel for 3 days. By using vacuum filtration and drying in air, red-brown prisms of **1** were recovered as a major phase together with dark-green impurities, which were readily removed by washing with methanol. For the absorption measurements, red prism crystals of **1** were heated in air to 350 °C at a rate of 3 °C min^{-1} to form [V(O)(bdc)] (**2**). Intercalation experiments were carried out by immersing crystals of **2** in liquid aniline, thiophene, and acetone. For gas-phase absorption, crystals of **1** were heated on a thermobalance to 350 °C in air to remove H_2bdc. The sample was maintained at constant temperature for 30 min and then cooled to 28 °C. When the weight was constant at 28 °C, the air flow was switched to 5% CH_4/He. After the weight became constant, the flow of 5% CH_4/He was passed through a bubbler containing liquid $(CH_3)_2S$. After a short time, the weight of [V(O)(bdc)] increased dramatically.

Received: June 26, 2006
Published online: September 13, 2006

Keywords: host–guest systems · intercalation · metal–organic frameworks · selective absorption · vanadium

[1] a) D. W. Breck, *Zeolite Molecular Sieves*, Wiley, New York, **1974**; b) M. E. Davis, *Nature* **2002**, *417*, 813; c) H. van Koningsveld, F. Tuinstra, H. van Bekkum, J. C. Jansen, *Acta Crystallogr. Sect. B* **1989**, *45*, 423; d) G. Binder, L. Scandella, J. Kritzenberger, J. Gobrecht, J. H. Koegler, R. J. Prins, *J. Phys. Chem. B* **1997**, *101*, 483; e) E. Y. Choi, Y. Kim, K. J. Seff, *J. Phys. Chem. B* **2002**, *106*, 5827; f) C. A. Fyfe, A. C. Diaz, H. Grondey, A. R. Lewis, H. J. Forster, *J. Am. Chem. Soc.* **2005**, *127*, 7543.

[2] M. S. Whittingham, A. J. Jacobson, *Intercalation Chemistry*, Academic Press, New York, **1982**.

[3] a) C. J. Kepert, M. J. Rosseinsky, *Chem. Commun.* **1999**, 375; b) H. Li, M. Eddaoudi, M. O'Keeffe, O. M. Yaghi, *Nature* **1999**, *402*, 276; c) K. Biradha, M. Fujita, *Angew. Chem.* **2002**, *114*, 3542; *Angew. Chem. Int. Ed.* **2002**, *41*, 3392; d) M. P. Suh, J. W. Ko, H. J. Choi, *J. Am. Chem. Soc.* **2002**, *124*, 10976; e) S. Takamizawa, E. Nakata, H. Yokoyama, K. Mochizuki, W. Mori, *Angew. Chem.* **2003**, *115*, 4467; *Angew. Chem. Int. Ed.* **2003**, *42*, 4331; f) B. F. Abrahams, M. Moylan, S. D. Orchard, R. Robson, *Angew. Chem.* **2003**, *115*, 1892; *Angew. Chem. Int. Ed.* **2003**, *42*, 1848; g) B. Rather, M. J. Zaworotko, *Chem. Commun.* **2003**, 830; h) S. Takamizawa, E. Nakata, T. Saito, *Angew. Chem.* **2004**, *116*, 1392; *Angew. Chem. Int. Ed.* **2004**, *43*, 1368; i) S. Kitagawa, R. Kitaura, S. Noro, *Angew. Chem.* **2004**, *116*, 2388; *Angew. Chem. Int. Ed.* **2004**, *43*, 2234; j) S. Kitagawa, K. Uemura, *Chem. Soc. Rev.* **2005**, *34*, 109; k) A. J. Fletcher, E. J. Cussen, D. Bradshaw, M. J. Rosseinsky, K. M. Thomas, *J. Am. Chem. Soc.* **2004**, *126*, 9750.

[4] K. Barthelet, J. Marrot, D. Riou, G. Férey, *Angew. Chem.* **2002**, *114*, 291; *Angew. Chem. Int. Ed.* **2002**, *41*, 281.

[5] a) F. Millange, C. Serre, G. Férey, *Chem. Commun.* **2002**, 822; b) C. Serre, F. Millange, C. Thouvenot, M. Nogues, G. Marsolier, D. Louër, G. Férey, *J. Am. Chem. Soc.* **2002**, *124*, 13519.

[6] T. Loiseau, C. Serre, C. Huguenard, G. Fink, F. Taulelle, M. Henry, T. Bataille, G. Férey, *Chem. Eur. J.* **2004**, *10*, 1373.

[7] a) T. R. Whitfield, X. Wang, L. Liu, A. J. Jacobson, *Solid State Sci.* **2004**, *7*, 1096; b) T. R. Whitfield, X. Wang, A. J. Jacobson, *Mater. Res. Soc. Symp. Proc.* **2003**, *755*, 191.

[8] E. V. Anokhina, M. Vougo-Zanda, X. Wang, A. J. Jacobson, *J. Am. Chem. Soc.* **2005**, *127*, 15001.

[9] a) G. Férey, M. Latroche, C. Serre, F. Millange, T. Loiseau, A. Percheron-Guégan, *Chem. Commun.* **2003**, 2976; b) N. L. Rosi, J. Eckert, M. Eddaoudi, D. T. Vodak, J. Kim, M. O'Keeffe, O. M. Yaghi, *Science* **2003**, *300*, 1127.

[10] a) D. N. Dybtsev, H. Chun, S. H. Yoon, D. Kim, K. Kim, *J. Am. Chem. Soc.* **2004**, *126*, 32; b) A. C. Sudik, A. R. Millward, N. W. Ockwig, A. P. Cöte, J. Kim, O. M. Yaghi, *J. Am. Chem. Soc.* **2005**, *127*, 7110; c) L. Pan, K. M. Adams, H. X. Wang, C. Zheng, Y. Hattori, K. Kaneko, *J. Am. Chem. Soc.* **2003**, *125*, 3062.

[11] a) S. Bourrelly, P. L. Llewellyn, C. Serre, F. Millange, T. Loiseau, G. Férey, *J. Am. Chem. Soc.* **2005**, *127*, 13519; b) K. Seki, *Phys. Chem. Chem. Phys.* **2002**, *4*, 1968; c) T. Düren, L. Sarkisov, O. M. Yaghi, R. Q. Snurr, *Langmuir* **2004**, *20*, 2683.

[12] U. Mueller, M. Schubert, F. Teich, H. Puetter, K. Schierle-Arndt, J. Pastre, *J. Mater. Chem.* **2006**, *16*, 626.

[13] **1**: Elemental analysis (%) calcd for $[V(O)(bdc)](H_2bdc)_{0.71}$: V 14.6, C 47.08, H 2.37; found: 14.8; C 47.10, H 2.68; crystal data: space group $P2_12_12_1$, $a = 6.8094(3)$, $b = 12.4220(6)$, $c = 17.1733(8)$ Å, $V = 1452.6(1)$ Å^3, $Z = 4$, $T = 223$ K, $d_{calcd} = 1.593$ g cm^{-3}; single-crystal data were collected on a Siemens SMART/CCD diffractometer (14526 reflections total, 3498 unique, $R_{int} = 0.0478$); the structure was solved and refined with the SHELXTL software package; final refinements converged at $R1 = 0.0394$ for all 3498 reflections and 188 parameters.

[14] Thermogravimetric analyses of **1** carried out in air at 3 °C min^{-1} showed two weight-loss events. The first between 320 and 400 °C corresponds to the loss of the guest H_2bdc. The second between 440 and 480 °C corresponds to the loss of framework bdc. A sample heated at 390 °C for 10 h was confirmed to be identical to MIL-47 by IR spectroscopy (disappearance of the band at ca. 1700 cm^{-1} characteristic of free −C=O species) and single-crystal X-ray diffraction ([V(O)(bdc)] (**2**): space group *Pnma*, $a = 6.8249(8)$, $b = 16.073(2)$, $c = 13.995(2)$, $T = 293$ K, $d_{calcd} =$

 © 2006 Wiley-VCH Verlag GmbH & Co. KGaA, Weinheim

1.000 g cm^{-3}, $R1 = 0.0443$ for all 1904 unique reflections and 67 parameters). After immersing the [V(O)(bdc)] crystals in the corresponding guest liquid in air at room temperature for approximately 1 h, a suitable crystal for each intercalation phase was selected and sealed in a capillary together with the guest liquid in air and mounted on a Siemens SMART/CCD diffractometer for X-ray data collection. **3**: space group $P2_12_12_1$, $a = 6.785(1)$, $b = 13.031(2)$, $c = 16.851(2)$ Å, $V = 1489.8(4)$ Å^3, $Z = 4$, $T = 223$ K, $d_{calcd} = 1.445$ g cm^{-3}. 12940 reflections total, 3511 unique, $R_{int} = 0.0698$; $R1 = 0.0394$ for all 3511 unique reflections and 180 parameters. **4**: space group $P2_12_12_1$, $a = 6.786(1)$, $b = 12.618(2)$, $c = 17.086(3)$ Å, $V = 1463.0(4)$ Å^3, $Z = 4$, $T = 223$ K, $d_{calcd} = 1.503$ g cm^{-3}; 8691 reflections total, 3368 unique, $R_{int} = 0.0641$; $R1 = 0.0695$ for all 3368 unique reflections and 174 parameters. **5**: space group *Pnma*, $a = 6.796(3)$, $b = 18.410(8)$, $c = 10.214(4)$ Å, $V = 1278.0(9)$ Å^3, $Z = 4$, $T = 223$ K, $d_{calc} = 1.431$ g cm^{-3}; 7544 reflections total, 1006 unique, $R_{int} = 0.2022$; $R1 = 0.134$ for all 1006 unique reflections and 43 parameters. The crystal quality of **5** is comparatively poor probably because of the large unit-cell changes during intercalation. CCDC 619387–619391 (**1**–**5**, respectively) contain the supplementary crystallographic data for this paper. These data can be obtained free of charge from the Cambridge Crystallographic Data Centre via www.ccdc.cam.ac.uk/data_request/cif.

[15] C. Janiak, *J. Chem. Soc. Dalton Trans.* **2000**, 3885.

[16] H. Suezawa, T. Yoshida, Y. Umezawa, S. Tsuboyama, M. Nishio, *Eur. J. Inorg. Chem.* **2002**, 3148.

[17] a) D. R. Allan, S. J. Clark, R. M. Ibberson, S. Parsons, C. R. Pulham, L. Sawyer, *Chem. Commun.* **1999**, 751; b) F. H. Allan, C. A. Baalham, J. P. M. Lommerse, P. R. Raithby, *Acta Crystallogr. Sect. B* **1998**, *54*, 320.

 © 2006 Wiley-VCH Verlag GmbH & Co. KGaA, Weinheim

Liquid Crystals

DOI: 10.1002/anie.200601129

Intrinsic Chirality in a Bent-Core Mesogen Induced by Extrinsic Chiral Structures**

*Suk-Won Choi, Sungmin Kang, Yoichi Takanishi, Ken Ishikawa, Junji Watanabe, and Hideo Takezoe**

Chirality has been one of the most attractive subjects in chemistry since Pasteur's famous experiment showing the chirality of tartaric acid.[1] It is particularly interesting that some mesogenic phases of achiral, banana-shaped molecules[2] were found to be spontaneously segregated into two chiral domains.[3,4] Herein we report a simple but efficient method of obtaining a high excess of one handedness of chiral domains in a novel, substituted oxadiazole achiral banana-shaped molecule (Figure 1 a), which exhibits liquid-crystal (LC) polymorphism including both the calamitic (nematic) and undesignated banana smectic phase (B_x phase).[5] From an extrinsically chiral supermolecular structure in the nematic phase,[6] an intrinsically chiral conglomerate with one handedness of the B_x phase could be obtained. Moreover, the preferential chiral handedness can be controlled by the handedness of the twisted configuration.

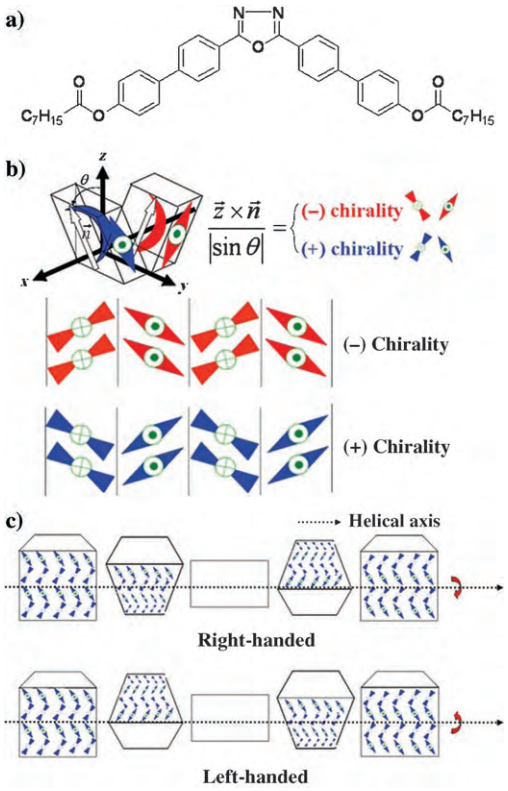

Figure 1. a) The achiral, banana-shaped substituted oxadiazole molecule used. b) Illustration of layer chirality induced by molecular tilting, and layer degeneracy in the B_2 phase of banana-shaped molecules; two layer structures may be observed which correspond to the two possible supermolecular-layer-stacking structures with opposite chirality (in the case of SmC_AP_A structure). c) Two possible TGB structures with opposite helix handedness in the B_4 phase. The tilted version of the TGB structure is drawn, as the present B_x phase is a tilted smectic phase.

Inherent chirality in achiral banana-shaped molecular systems has generated much attention because of a variety of unusual chirality-related phenomena, namely, large optical rotation (OR)[7,8] and chiral nonlinear optical (NLO) effects,[9,10] enhanced twisting power,[11–13] and induced blue phase[14] by doping conventional chiral systems with achiral banana-shaped molecules. Typical phases that exhibit macroscopic chiral separation are the B_2 phase,[7,8,15,16] and the complicated glasslike B_4 phase, as well as analogous uniden-

[*] S.-W. Choi, S. Kang, Dr. Y. Takanishi, Prof. Dr. K. Ishikawa, Prof. Dr. J. Watanabe, Prof. Dr. H. Takezoe
Department of Organic and Polymeric Materials
Tokyo Institute of Technology
O-okayama, Meguro-ku, Tokyo 152-8552 (Japan)
Fax: (+81) 3-5734-2876
E-mail: htakezoe@o.cc.titech.ac.jp

[**] This work was supported in part by Grants-in-Aid for Scientific Research (16105003) by the Ministry of Education, Culture, Sports, Science and Technology, Japan. We acknowledge Dr. Y. Saitoh and Dr. H. Satoh for kindly supplying glass substrates with DLC films.

© 2006 Wiley-VCH Verlag GmbH & Co. KGaA, Weinheim

tified phases.[3,4,16–18] The spontaneous chirality in the B_2 phase originates from breaking of the symmetry by the tilt of banana-shaped molecule with respect to the layer normal (Figure 1b). In contrast, conformational molecular chirality in the B_4 phase is believed to be nucleated, which results in some helical superstructures such as a twist-grain-boundary (TGB) structure with the helix parallel to the layer (Figure 1c).[17] As the system is achiral, it behaves like a racemic mixture when spontaneous symmetry breaking occurs; spontaneous degeneracy is inevitably formed (Figure 1b,c).[19] So far, the degeneracy has been successfully lifted by at least four methods, namely, by using: 1) chiral molecules;[19] 2) a template for macroscopically chiral structure;[20] 3) chiral surfaces;[21] and 4) circularly polarized light.[22] Herein, we demonstrate a fifth method for breaking this inevitable degeneracy. This method is based on the LC alignment technique twisted configuration field and is simple and efficient.

Recently, it was found that oxadiazole-based molecules[23] show an interesting polymorphism in which the banana mesophase is formed in a lower temperature region than well-known calamitic phases (i.e., nematic, SmA, and SmC phases).[5] Such a polymorphism including both banana and calamitic mesophases is attributed to a bend angle of oxadiazole cores (135°) which is a little larger than that of the classic banana-shaped molecules based on a resorcinol core (120°).[24]

We prepared the banana-shaped compound 2,5-bis(*p*-nonaloyloxybiphenyl)-1,3,4-oxadiazole (Figure 1a). The detailed syntheses and properties of homologous molecules are described elsewhere.[5] Polymorphism is clearly observed for this compound, with the calamitic phase (conventional nematic phase) in a higher temperature region and the undesignated banana smectic phase (B_x phase) in a lower temperature region (phase transition: isotropic-(266 °C)-nematic-(252 °C)-B_x-(193 °C)-cryst.). The B_x phase has a layered structure in which the molecules are packed in a liquidlike manner and are tilted with respect to the layer by 28°. It is thus similar to the well-known banana smectic B_2 phase in classic banana-shaped molecules, but is completely different from the typical B_2 phase. The most striking feature of this phase is a spontaneous chiral segregation that exhibits a transparent texture exactly like that of the typical B_4 phase. Thus, the B_x phase has the characteristics of not only the B_2 but also B_4 phases.

First, we confirmed good alignment in the nematic phase by alignment techniques such as homogeneous and twisted nematic (TN) treatment. Next, the clockwise- or counter-clockwise-TN cells were cooled down to form the B_x phase at a rate of $-1\,°C\,min^{-1}$. Figure 2a–d shows the textures observed with slightly (=10°) decrossed polarizers at twist angles of $\alpha = 0°$, $\alpha = -60°$, $-80°$ (corresponding to a counter-clockwise, right-handed twist), and $\alpha = 80°$ (corresponding to a clockwise, left-handed twist), respectively. The two chiral domains become apparent as bright and dark regions, and the brightness of the two domains interchanges when the polarizer is decrossed in the opposite direction. For $\alpha = 0°$, a large-scale heterogeneity caused by the degeneracy of the chiral structure was seen clearly (Figure 2a). Heterogeneity was

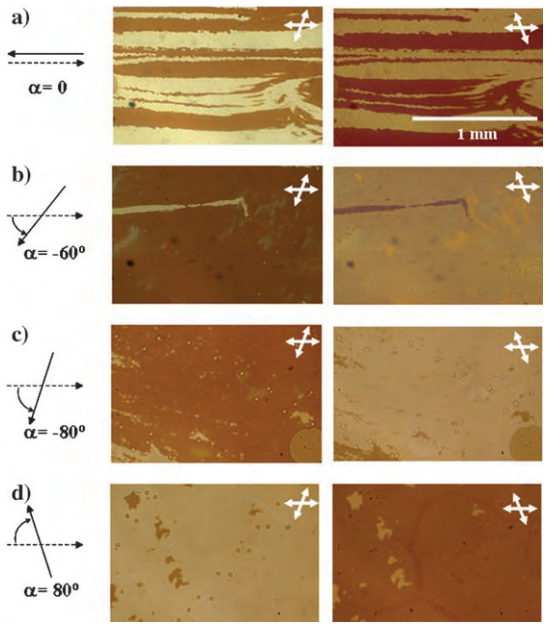

Figure 2. Polarizing optical microphotographs of the banana B_x phases in cells with several twisted configuration treatments. Twist angles were chosen to be a) $\alpha = 0°$, b) $\alpha = -60°$, c) $\alpha = -80°$, and d) $\alpha = 80°$.

also observed in cells with $\alpha < |40°|$. In contrast, the degeneracy is lifted by means of the twisted configuration with $\alpha > |50°|$ and almost complete symmetry breaking is observed in cells with $\alpha = -60°$ and $-80°$, if appropriate chiral domains are chosen (Figure 2b,c). In a cell with $\alpha = 80°$, the predominant domain was reversed with respect to that of the cell with $\alpha = -80°$ (Figure 2d). This indicates that a preferentially chiral conglomerate with one handedness can be regulated selectively by the twisted handedness (right-handed or left-handed twist) of the fabricated cell.

Circular dichroism (CD) measurements were carried out to confirm the occurrence of intrinsic chirality in the B_x phase. Figure 3 shows typical CD spectra observed in the B_x phase of cells with several twist angles. The CD measurements were repeated after several cycles of heating the cell to form the nematic phase and then cooling to form the B_x phase. In the B_x phase with $\alpha < |40°|$, a CD spectrum with negligible positive or negative signals was observed and the CD intensity was almost zero as a result of two chiral domains with

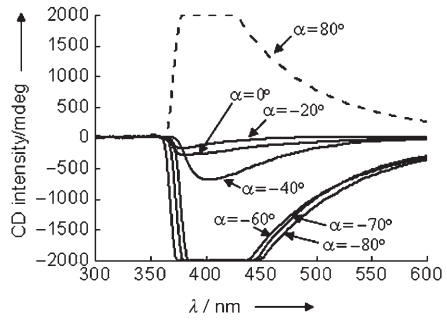

Figure 3. Typical CD spectra of the B_x phase in cells with several twist angles ($\alpha = 0°$, $-60°$, $-80°$, and 80°).

 © 2006 Wiley-VCH Verlag GmbH & Co. KGaA, Weinheim

opposite chiral structures coexisting with equal probability. In contrast, an enormous CD signal was observed around 400 nm in the twisted cells with $\alpha > |60°|$. The CD intensity of nearly perfect degeneracy-breaking domains exceeded the range of our CD instrument (i.e., > 2000 mdeg). To evaluate the CD intensity per unit μm, we assembled thinner cells (2 μm and 4 μm) with $\alpha = -80°$, which gave CD intensities of about 1000 mdeg and 2000 mdeg, respectively, at about 400 nm. The CD intensity is proportional to the cell thickness in the range 2–6 μm, (500 mdeg μm^{-1}) owing to the intrinsically chiral conglomerate, and a CD intensity of about 3000 mdeg is expected in a 6-μm-thick cell. However, the critical twist angle (between 50° and 60° in our case for 6-μm-thick cells) becomes larger for thicker cells.

These CD signals result from an induced circular dichroism (ICD) in the wavelength region in which the compound exhibits an absorption band, which indicates that a macroscopic chiral structure exists. The observed CD signals from oppositely twisted geometries are perfect mirror images (Figure 3), which indicates that mirror-image chiral structures were produced by twisted cell configurations of opposite handedness. The CD signal intensity obtained is comparable to that obtained from theoretical predictions,[7,8] which indicates the existence of an intrinsically chiral conglomerate with one handedness.

The fundamental difference between the nematic phase and the B_x phase of a compound is that, in the nematic phase, if the molecules are in a geometrically chiral configuration (i.e., TN structure), the structure is regarded as extrinsically chiral,[6] as it results from only the influences of surface treatment. In this case, a CD signal due to birefringence is observed. In contrast, the B_x phase is known to exhibit spontaneous symmetry breaking, and a huge CD signal due to intrinsic chirality is observed. The origin for this intrinsic chirality could be: 1) the tilt of the bent molecules within the layers,[15] 2) twist conformation of molecules[11,19] and so on, thus leading to the TGB-like model structure; the blocks of B_2 layers are twisted about the axis parallel to the layer plane.[3–4,25] In any event, such intrinsically chiral conglomerates originate from molecular axial chirality or chiral assemblies of such molecules.

Why can twisting give rise to degeneracy breaking in the B_x phase of the achiral banana-shaped compound? We can draw equal-energy minima for generating two possible chiral conglomerates in the B_x phase.[19] The clockwise (left-handed) or counterclockwise (right-handed) twisted field is considered to be the origin of the symmetry breaking. Moreover, this degeneracy-breaking is observed only in systems exhibiting polymorphism between the calamitic and banana phases, thus a well-developed TN configuration plays a key role in this phenomenon. If the banana-shaped molecules are incorporated into a well-developed TN configuration, that is, under a degeneracy-breaking field, then upon cooling down to form the B_x phase, chiral interactions are formed between the extrinsically chiral configuration and intrinsically chiral segregation of banana-shaped molecules. Thus, this preference triggers and accelerates a preferential formation of one of the two possible chiral conglomerates and is fixed when the system is brought into the B_x phase. Although, this phenomenon is the first example of a macroscopic geometric chiral perturbation biasing the formation of one handedness of an LC conglomerate, several similar phenomena[26–28] have been reported in the solid or solution state. Particularly, Ribo et al.[26] reported that achiral diprotonated porphyrins, which self-associate in aqueous solution, lead to spontaneous chiral symmetry breaking by vortex motion during the aggregation process. This chiral vortex is analogous to the twisted nematic geometry of the LC cell in our case.

In conclusion, under the degeneracy-breaking field, we demonstrated a preferential formation of LC conglomerate with one handedness in the B_x phase of an oxadiazole-based banana-shaped molecule, which exhibits liquid-crystal polymorphism involving both the calamitic and banana phases. The collective net chirality and orientation of the molecules into a single-handed domain of the B_x phase is the origin of the optical activity and CD behavior observed. The homochiral films obtained by achiral molecules open up the possibility for a wide range of practical applications, such as chiral separation and enzyme adsorption through chiral molecular recognition.

Experimental Section

We fabricated well-aligned cells by using inorganic (diamond-like carbon (DLC)) films with low-energy ion beams impinging at a glancing angle.[29] The DLC films were used for TN cells, as the used compound showed a high transition temperature from the nematic phase to the B_x phase (> 250 °C) and rubbed-organic polyimide films show poorer thermal stability than the DLC film. The nominal cell thickness was maintained by columnar spacers (5–6 μm in height) made by photolithography.

Degeneracy breaking was evaluated by means of direct texture observation under a polarizing microscope (Nikon, OPTIPHOT-POL) with uncrossed polarizer combinations and circular dichroism (CD) spectroscopic analysis (JASCO J-720WI).

Received: March 22, 2006
Revised: July 22, 2006
Published online: September 5, 2006

Keywords: chirality · circular dichroism · liquid crystals · mesophases

[1] L. Pasteur, *Ann. Chim. Phys.* **1848**, *24*, 442 – 459.
[2] T. Niori, T. Sekine, J. Watanabe, T. Furukawa, H. Takezoe, *J. Mater. Chem.* **1996**, *6*, 1231 – 1233.
[3] R. A. Reddy, C. Tschierske, *J. Mater. Chem.* **2006**, *16*, 907 – 961.
[4] H. Takezoe, Y. Takanishi, *Jpn. J. Appl. Phys.* **2006**, *45*, 597 – 625.
[5] S. Kang, Y. Saito, N. Watanabe, M. Tokita, Y. Takanishi, H. Takezoe, J. Watanabe, *J. Phys. Chem. B* **2006**, *110*, 5205 – 5214.
[6] F. D. Saeva, G. R. Olin, *J. Am. Chem. Soc.* **1976**, *98*, 2709 – 2711.
[7] J. Ortega, C. L. Folcia, J. Etxebarria, N. Gimeno, M. B. Ros, *Phys. Rev. E* **2003**, *68*, 011707 – 1–4.
[8] L. E. Hough, N. A. Clark, *Phys. Rev. Lett.* **2005**, *95*, 107802 – 1–4.
[9] F. Araoka, Y. Takanishi, H. Takezoe, A. Kim, B. Park, J. W. Wu, *J. Opt. Soc. Am. B* **2003**, *20*, 314 – 320.
[10] F. Araoka, N. Y. Ha, Y. Kinoshita, B. Park, J. W. Wu, H. Takezoe, *Phys. Rev. Lett.* **2005**, *94*, 137801 – 1–4.
[11] J. Thisayukta, H. Niwano, H. Takezoe, J. Watanabe, *J. Am. Chem. Soc.* **2002**, *124*, 3354 – 3358.

 © 2006 Wiley-VCH Verlag GmbH & Co. KGaA, Weinheim

[12] E. Gorecka, M. Cepic, J. Mieczkowski, M. Nakata, H. Takezoe, B. Zeks, *Phys. Rev. E* **2003**, *67*, 061794 – 1–5.
[13] D. J. Earl, M. A. Osipov, H. Takezoe, Y. Takanishi, M. R. Wilson, *Phys. Rev. E* **2005**, *71*, 021706 – 1–11.
[14] M. Nakata, Y. Takanishi, J. Watanabe, H. Takezoe, *Phys. Rev. E* **2003**, *68*, 041710 – 1–6.
[15] D. R. Link, G. Natale, R. Shao, J. E. Maclennan, N. A. Clark, E. Korblova, D. M. Walba, *Science* **1997**, *278*, 1924 – 1927.
[16] H. Niwano, M. Nakata, J. Thisayukta, D. R. Link, H. Takezoe, J. Watanabe, *J. Phys. Chem. B* **2004**, *108*, 14889 – 14896.
[17] J. Thisayukta, H. Takezoe, J. Watanabe, *Jpn. J. Appl. Phys.* **2001**, *40*, 3277 – 3287.
[18] D. M. Walba, L. Eshdat, E. Korblova, R. K. Shoemaker, *Cryst. Growth Des.* **2005**, *5*, 2091 – 2099.
[19] J. Thisayukata, H. Niwano, H. Takezoe, J. Watanabe, *J. Mater. Chem.* **2001**, *11*, 2717 – 2721.
[20] A. Jakli, G. G. Nair, C. K. Lee, R. Su, L. C. Chien, *Phys. Rev. E* **2001**, *63*, 061710 – 1–4.
[21] K. Shiromo, D. A. Sahade, T. Oda, T. Nihira, Y. Takanishi, K. Ishikawa, H. Takezoe, *Angew. Chem.* **2005**, *117*, 1984 – 1987; *Angew. Chem. Int. Ed.* **2005**, *44*, 1948 – 1951.
[22] S.-W. Choi, T. Izumi, Y. Hoshino, Y. Takanishi, K. Ishikawa, J. Watanabe, H. Takezoe, *Angew. Chem.* **2006**, *118*, 1410 – 1413; *Angew. Chem. Int. Ed.* **2006**, *45*, 1382 – 1385.
[23] a) B. R. Acharya, A. Primak, S. Kumar, *Phys. Rev. Lett.* **2004**, *92*, 145506-1-4; b) L. A. Madsen, T. J. Dingemans, M. Nakata, E. T. Samulski, *Phys. Rev. Lett.* **2004**, *92*, 145505-1-4.
[24] T. J. Dingemans, N. S. Murthy, E. T. Samulski, *J. Phys. Chem. B* **2001**, *105*, 8845 – 8860.
[25] W. Weissflog, S. Sokolowski, H. Dehne, B. Das, S. Grande, M. W. Schroder, A. Eremin, S. Diele, G. Pelzl, H. Kresse, *Liq. Cryst.* **2004**, *31*, 923 – 933.
[26] J. M. Ribo, J. Crusats, F. Sagues, J. Claret, R. Rubires, *Science* **2001**, *292*, 2063 – 2066.
[27] D. K. Kondepudi, R. J. Kaufman, N. Singh, *Science* **1990**, *250*, 975 – 976.
[28] J. M. McBride, R. L. Carter, *Angew. Chem.* **1991**, *103*, 298 – 300; *Angew. Chem. Int. Ed. Engl.* **1991**, *30*, 293 – 295.
[29] P. Chaudhari, J. Lacey, J. Doyle, E. Galligan, S. C. A. Lien, A. Callegari, G. Hougham, N. D. Lang, P. S. Andry, R. John, K. H. Yang, M. H. Lu, C. Cai, J. Speidell, S. Purushothaman, J. Ritsko, M. Samant, J. Stohr, Y. Nakagawa, Y. Katoh, Y. Saitoh, K. Sakai, H. Satoh, S. Odahara, H. Nakano, J. Nakagaki, Y. Shioda, *Nature* **2001**, *411*, 56 – 59.

 © 2006 Wiley-VCH Verlag GmbH & Co. KGaA, Weinheim

Gas Storage

DOI: 10.1002/anie.200601391

Acetylene Absorption and Binding in a Nonporous Crystal Lattice**

Praveen K. Thallapally, Liliana Dobrzańska, Todd R. Gingrich, Trevor B. Wirsig, Leonard J. Barbour, and Jerry L. Atwood**

Finding an economical and technologically viable way to capture highly flammable gases such as acetylene, hydrogen, and methane is very important for their production, transportation, and delivery.[1] Several methods have been proposed based on physical adsorption by activated carbon,[2] zeolites,[3] carbon nanotubes,[4] metal–organic frameworks,[5] and other porous and nonporous materials.[6] However, each method has its technical challenges and no ideal method has emerged thus far. Although storage in compressed cylinders provides an alternate technology,[7] acetylene gas, a key component for the synthesis of diverse organic compounds, petrochemicals, electric and electronic materials, cannot be compressed above 30 psia or 15 psig at room temperature or it explodes, even in the absence of oxygen.[8] Acetylene dissolves readily in acetone and is delivered in a steel cylinder containing acetone along with other porous materials to prevent polymerization when the gas is stored under pressure (solubility of acetylene in acetone at 1 atm and 15 °C equals 20 liters per liter of acetone). Therefore the search has begun to find a method of storing acetylene gas at room temperature while compressed well above its critical limits.[9]

In this context, metal–organic frameworks are well-investigated for storage and separation of gases[10] whereas organic crystals assembled by means of noncovalent forces and van der Waals interactions have largely been neglected as gas sorption substrates owing to close packing phenomena which generally do not lead to conventionally porous structures. Many inclusion compounds often possess zero-,

[*] Dr. P. K. Thallapally,[+] T. R. Gingrich, T. B. Wirsig, Prof. J. L. Atwood
Department of Chemistry
University of Missouri-Columbia
Columbia, MO 65211 (USA)
Fax: (+1) 573-882-2754
E-mail: atwoodj@missouri.edu

Dr. L. Dobrzańska, Prof. L. J. Barbour
Department of Chemistry
University of Stellenbosch
Matieland, 7602 (South Africa)
Fax: (+27) 21-808-3849
E-mail: ljb@sun.ac.za

[+] Current address:
Pacific Northwest National Laboratory
Richland, WA 99254 (USA)

[**] We acknowledge the Department of Energy (USA) and the National Research Foundation (South Africa) for support of this work.

Supporting information for this article is available on the WWW under http://www.angewandte.org or from the author.

 WILEY InterScience DISCOVER SOMETHING GREAT

© 2006 Wiley-VCH Verlag GmbH & Co. KGaA, Weinheim

one-, two-, or three-dimensional solvent-accessible space with guest molecules located in cavities or channels. It is therefore attractive to envision facile removal of the solvent molecules from these materials to yield highly porous host lattices analogous to those of zeolites. In reality, the process of desolvation is almost always accompanied by reassembly of the host molecules in the solid state to form one or more so-called apohost phases, where the pure compound is once again efficiently packed. However, a few organic compounds are exceptions to this phenomenon[6,11] (e.g. tris-*o*-phenylenedioxycyclotriphosphazine, which forms a porous hexagonal host framework stabilized by weak intermolecular interactions with a minimum pore diameter of 4.6 Å). These nanoporous crystals show high sorption capacity values for methane and carbon dioxide at 195 K.[11b] Calix[4]arene has the ability to entrap highly volatile guests such as CF_3Br, CF_4, and CH_4 well beyond their normal boiling points such that the host lattice must disassemble itself to release the guest molecules.[12] In a continuation of this work, we have extended our sorption studies on the low-density polymorph of *p-tert*-butylcalix[4]arene (**1**) to entrap the highly flammable gas acetylene, and to compare these results to those for carbon dioxide.

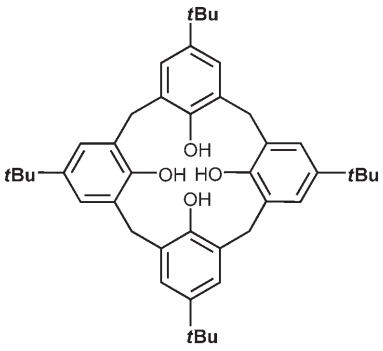

1

Acetylene and carbon dioxide sorption experiments were conducted volumetrically using a specially constructed device.[13] A sample of 1.5 g of **1** was placed in the sample chamber ($V_s = 10.93$ cm^3) and evacuated for several hours to remove any trace amount of gas. In separate experiments, acetylene and CO_2 were introduced at an initial pressure of 800 torr. Gas was absorbed over 3 h until equilibrium was reached (Figure 1). An occupancy study (Figure 2, that is, percentage occupancy versus equilibrium pressure) shows that the uptake of acetylene at standard temperature and pressure (STP) is approximately 2% by weight. This value corresponds to 39 cm^3 g^{-1} and is comparable to, or exceeds the values obtained for carbon nanotubes and inorganic zeolites such as Zeolite 4 A.[14] The seemingly nonporous crystals absorb 0.515 mol of acetylene per mol of host at 298 K and 1 atm pressure indicating complete filling of the available volume in the crystal structure (i.e. because two calixarenes are required to form one lattice void). The absorption and desorption isotherms for acetylene and CO_2 indicate a type I relationship between the equilibrium pressure and percentage

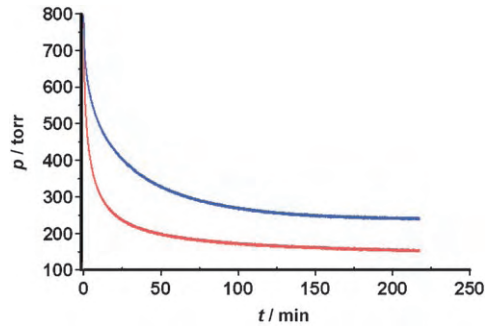

Figure 1. Sorption of acetylene (blue) and carbon dioxide (red) at room temperature and approximately 1 atm initial pressure.

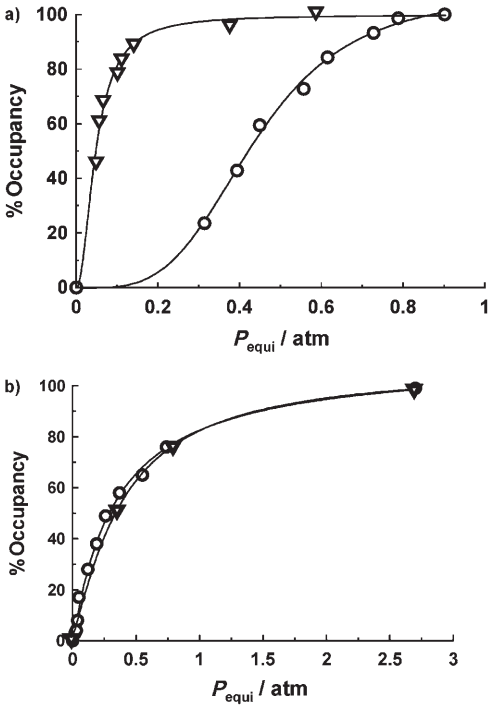

Figure 2. Absorption and desorption isotherms of acetylene and carbon dioxide at room temperature. a) Absorption values for acetylene are shown as circles while triangles represent desorption. Hysteresis in the sorption–desorption curves implies strong affinity towards acetylene. b) Sorption (circles) and desorption (triangles) isotherms for CO_2. Full occupancy of CO_2 was obtained at 3 atm pressure and no hysteresis is observed.

of calixarene lattice voids occupied by the two gases. It appears that the occupancy of acetylene is 100% (Figure 2a) at 1 atm pressure whereas 80% of the cavities are filled by CO_2 at this pressure (3 atm of CO_2 pressure is required to fill the cavities completely, see Figure 2b). Interestingly, the absorption–desorption process for CO_2 is fast and no hysteresis was observed. However, acetylene shows a significant hysteresis effect (acetylene desorption is slower than absorption), implying considerable stabilization of the gas in the nonporous material.

The calculated density of the absorbed acetylene at STP (using a void volume of 235 Å^3) is estimated to be 0.18 g cm^{-3}, which is equivalent to acetylene at 18 MPa and 90 times the

 © 2006 Wiley-VCH Verlag GmbH & Co. KGaA, Weinheim

compression limit for the safe storage of acetylene (0.2 MPa = 0.0021 g cm^{-3}; the density of the absorbed acetylene in the bulk material is 0.02 g cm^{-3} and is equivalent to 2 MPa at room temperature). To our knowledge this is the first report of an organic material which absorbs acetylene at room temperature and 1 atm pressure.

Although several attempts to collect single-crystal X-ray diffraction data for **1** with included acetylene failed, the remarkable stability of the acetylene in the host lattice facilitated identification of the gas in the crystal using solid-state NMR spectroscopy at ambient conditions (Supporting Information).[15] The resonance of the stored acetylene in the ^{13}C magic-angle spinning (MAS) NMR spectrum appears as a sharp signal at $\delta = 66.2$ ppm compared to free acetylene at $\delta = 71.8$ ppm. The exceptional upfield shift of -5.6 ppm is consistent with stronger binding of the acetylene in the host lattice and is shifted further upfield than any reported resonance of acetylene (Figure 3a and b). Similarly, the ^{13}C

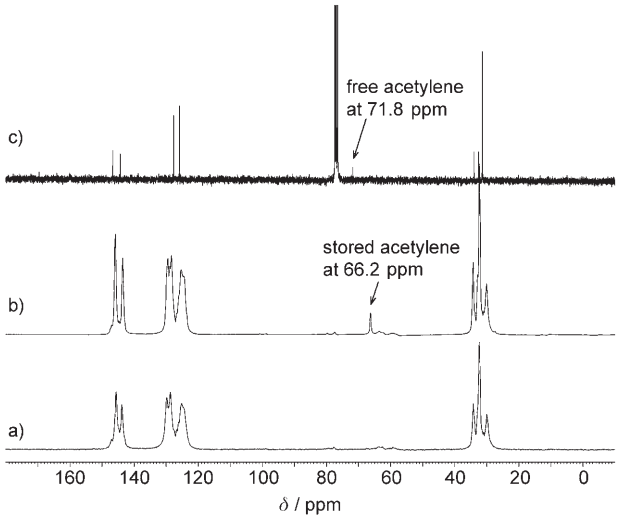

Figure 3. a) ^{13}C MAS NMR spectrum of sample **1**. b) Sharp signal at $\delta = 66.2$ ppm indicates the stored acetylene in **1**. c) ^{13}C NMR spectrum in chloroform, free acetylene at $\delta = 71.8$ ppm.

MAS NMR spectrum of the sample containing CO_2 shows a signal for stored CO_2 at $\delta = 121.9$ ppm. An upfield shift of -3.5 ppm occurs for the stored gas compared to the gas phase CO_2, which appears at $\delta = 125.4$ ppm. However, the signal is close to that for one of the carbon atoms of the host molecule and this problem was overcome by performing a non-quaternary suppression (NQS) experiment in which suitable conditions were found to suppress the protonated carbon atoms of the host. A neat signal at $\delta = 121.9$ ppm was assigned to the non-protonated carbon of CO_2 stored in the crystal (Figure 4b and c).

The solid-state structure of **1** features the calixarene molecules arranged in an up–down bilayer packing motif. The dimeric capsules are slightly offset relative to one another, and each dimeric capsule has an estimated free volume of approximately 235 Å^3 (Supporting Information). Our previous studies on a low-density polymorph of **1** and related

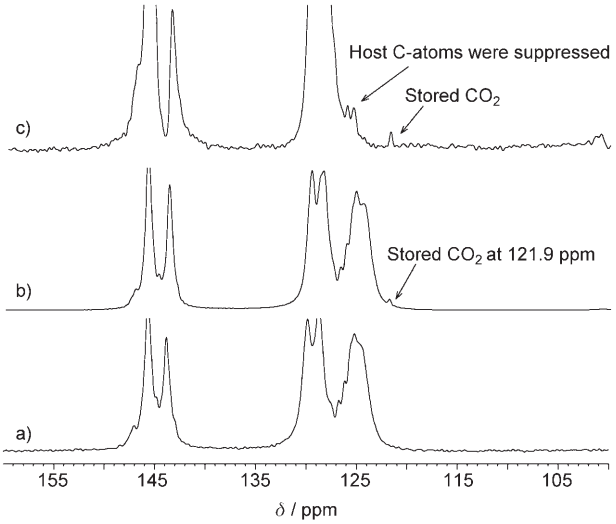

Figure 4. a) Solid-state NMR spectrum of sample **1**. For clarity, only part of the spectrum is shown. b) With stored CO_2 which give rise to the signal at $\delta = 121.9$ ppm. c) After host carbon atoms are suppressed using non-quaternary suppression.

calix[4]arene derivatives, obtained by vacuum sublimation at 280 °C, show absorption of various gases under ambient temperature and sub-ambient pressure.[6a,b,12] We also showed that immersion of this polymorph in liquid vinyl bromide for 15 minutes results in a single-crystal to single-crystal phase transition in which vinyl bromide diffuses through the crystal. The phase transition is characterized by an approximately 6 Å lateral shift of the bilayers relative to one another to allow guest diffusion and to achieve the thermodynamically most stable form.[6a] Unlike conventional porous materials that take up and release guest molecules, no channels are found in **1**. However, gas molecules diffuse through the seemingly nonporous lattice without disrupting the arrangement of the host molecules. To rationalize the occurrence of gas sorption, it is presumed that the upper-rim *tert*-butyl groups of the calixarenes play a critical role in gas uptake. In the solid state, the hydroxy groups at the lower rim of the calixarene have well-defined thermal ellipsoids and appear to be rigid, while the *tert*-butyl groups of the upper rim may rotate about the C(ar)–C(sp^3) bond, as evidenced by crystallographic disorder. The cooperative rotation of the *tert*-butyl groups would allow the gas molecules to diffuse through the crystals.[13,16]

In conclusion, although metal–organic frameworks have been shown to facilitate the concentration of acetylene well beyond its normal safe limit, we have now shown that low-density organic materials can also be exploited as promising substrates for acetylene storage.

Received: April 7, 2006
Revised: June 9, 2006
Published online: September 5, 2006

Keywords: acetylene · calixarenes · nonporous materials · sorption · supramolecular chemistry

 © 2006 Wiley-VCH Verlag GmbH & Co. KGaA, Weinheim

[1] Special issue on Hydrogen Economy: *Science* **2004**, *305*, 957, and other articles in this issue.

[2] V. C. Menon, S. Komarneni, *J. Porous Mater.* **1998**, *5*, 43.

[3] a) D. W. Breck, *Zeolite Molecular Sieves: Structure, Chemistry, and Use*, Wiley, New York, **1974**; b) A. Corma, *Chem. Rev.* **1997**, *97*, 2373.

[4] A. C. Dillon, K. M. Jones, T. A. Bekkedahl, C. H. Kiang, D. S. Bethune, M. J. Heben, *Nature* **1997**, *386*, 377.

[5] a) O. M. Yaghi, M. O'Keeffe, N. W. Ockwig, H. K. Chae, M. Eddaoudi, J. Kim, *Nature* **2003**, *423*, 705; b) S. Kitagawa, R. Kitaura, S.-I. Noro, *Angew. Chem.* **2004**, *116*, 2388; *Angew. Chem. Int. Ed.* **2004**, *43*, 2334.

[6] a) J. L. Atwood, L. J. Barbour, A. Jerga, B. L. Schottel, *Science* **2002**, *298*, 1000; b) J. L. Atwood, L. J. Barbour, A. Jerga, *Angew. Chem.* **2004**, *116*, 3008; *Angew. Chem. Int. Ed.* **2004**, *43*, 2948; c) P. K. Thallapally, G. O. Lloyd, J. L. Atwood, L. J. Barbour, *Angew. Chem.* **2005**, *117*, 3916; *Angew. Chem. Int. Ed.* **2005**, *44*, 3848; d) P. K. Thallapally, G. O. Lloyd, T. B. Wirsig, M. W. Bredenkamp, J. L. Atwood, L. J. Barbour, *Chem. Commun.* **2005**, 5272; e) J. A. Riddle, J. C. Bollinger, D. Lee, *Angew. Chem.* **2005**, *117*, 6847; *Angew. Chem. Int. Ed.* **2005**, *44*, 6689; f) L. Dobrzańska, G. O. Lloyd, H. G. Raubenheimer, L. J. Barbour, *J. Am. Chem. Soc.* **2006**, *128*, 698.

[7] "National Hydrogen Energy Roadmap", United States Department of Energy, results from the National Hydrogen Energy Roadmap Workshop, Washington DC, April 2–3, **2003**.

[8] a) P. J. Stang, F. Diederich, *Modern Acetylene Chemistry*, VCH, New York, **1995**; b) J. C. W. Chien, *Polyacetylene: Chemistry, Physics, and Material Science*, Academic Press, New York, **1984**.

[9] We note that the current method of storing acetylene involves dissolution of the gas in acetone.

[10] R. Matsuda, R. Kitaura, S. Kitagawa, Y. Kubota, R. V. Belosludov, T. C. Kobayashi, H. Sakamoto, T. Chiba, M. Takata, Y. Kawazoe, Y. Mita, *Nature* **2005**, *436*, 238.

[11] a) J. L. Atwood, L. J. Barbour, A. Jerga, *Chem. Commun.* **2002**, 2952; b) P. Sozzani, S. Bracco, A. Comotti, L. Ferretti, R. Simonutti, *Angew. Chem.* **2005**, *117*, 1850; *Angew. Chem. Int. Ed.* **2005**, *44*, 1816; c) C. Tedesco, I. Immediata, L. Gregoli, L. Viragilano, A. Immizi, P. Neri, *CrystEngComm* **2005**, *35*, 449; d) L. J. Barbour, *Chem. Commun.* **2006**, 1163.

[12] J. L. Atwood, L. J. Barbour, A. Jerga, *Science* **2002**, *296*, 2367.

[13] J. L. Atwood, L. J. Barbour, P. K. Thallapally, T. B. Wirsig, *Chem. Commun.* **2005**, 51.

[14] N. D. Lazo, J. L. White, E. J. Munson, M. Lambregts, J. F. Haw, *J. Am. Chem. Soc.* **1990**, *112*, 1990.

[15] ^{13}C MAS NMR spectra were recorded at 7.04 T static magnetic field on a Bruker Avance 300 spectrometer at 75.5 MHz at a spinning speed of 15 kHz obtained with 7 mm zirconia rotors (see Supporting Information).

[16] J. L. Atwood, L. J. Barbour, G. O. Lloyd, P. K. Thallapally, *Chem. Commun.* **2004**, 922.

 © 2006 Wiley-VCH Verlag GmbH & Co. KGaA, Weinheim

Chiral Grignard Reagents

DOI: 10.1002/anie.200602091

New Insights into the Classic Chiral Grignard Reagent (1*R*,2*S*,5*R*)-Menthylmagnesium Chloride**

*Jens Beckmann, Dainis Dakternieks, Martin Dräger, and Andrew Duthie**

A broad range of phosphines with chiral substituents have been used in asymmetric synthesis for many years. Some of these chiral substituents are derived from menthol, for example, the diastereomeric phosphines $MenPh_2P$ and $NeomPh_2P$ (Men = menthyl, Neom = neomenthyl).[1] Organotin hydrides that contain menthyl groups (for example, $MenPh_2SnH$ and Men_2PhSnH) are also known, and have shown promise as chirality-transfer reagents in enantioselective reductions involving free radicals.[2] The reaction of MenCl with Mg to form the menthyl Grignard reagent directly appeared to be atypical for this type of reaction, because subsequent reactions with Ph_2PCl and Me_3SnCl resulted in exclusive formation of the products $MenPh_2P$[3] and $MenMe_3Sn$,[4] respectively, with complete retention of all stereogenic centers within the menthyl substituents.[5] Although (1*R*,2*S*,5*R*)-menthylmagnesium chloride (**1**) is listed in the CAS structure database, there is no mention of (1*S*,2*S*,5*R*)-neomenthylmagnesium chloride (**2**). $NeomPh_2P$ has been synthesized, but from reaction of Ph_2PNa with MenCl.[8]

Our attempts to prepare menthyltriphenyltin, $MenPh_3Sn$, from the reaction between the menthyl Grignard reagent and Ph_3SnCl led to the formation of mixtures of $MenPh_3Sn$ and $NeomPh_3Sn$, the latter apparently resulting from epimerization at the C1 position in the original menthyl moiety.[9] At that time, we believed that the menthyl Grignard reagent was

[*] Prof. Dr. D. Dakternieks, A. Duthie
School of Life and Environmental Sciences
Deakin University
Geelong 3217 (Australia)
Fax: (+61) 352-271-040
E-mail: aduthie@deakin.edu.au
Prof. Dr. J. Beckmann
Institut für Chemie und Biochemie
Freie Universität Berlin
14195 Berlin (Germany)
Prof. Dr. M. Dräger
Institut für Anorganische Chemie und Analytische Chemie
Johannes Gutenberg Universität
55099 Mainz (Germany)

[**] The Centre for Chiral and Molecular Technologies, Deakin University and Chirogen Pty. Ltd. are acknowledged for financial support. We thank Dr. I. Barta of Ubichem for useful discussions regarding the attempted synthesis of Men_2Ph_2Sn (**1**) on larger scales. We are grateful to the Alexander von Humboldt Foundation for providing a Feodor Lynen Scholarship (to J.B.).

Supporting information for this article is available on the WWW under http://www.angewandte.org or from the author.

 © 2006 Wiley-VCH Verlag GmbH & Co. KGaA, Weinheim

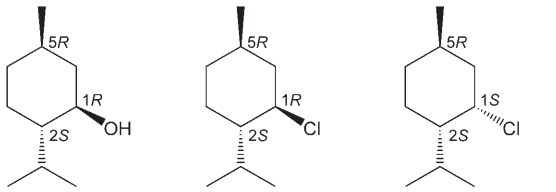

formed with complete retention of configuration, and that epimerization occurred during subsequent reaction of the Grignard reagent with some electrophiles.[9] Recently, Hoffmann proposed a single-electron-transfer (SET) mechanism for this type of reaction, in which triphenyltin and menthyl radicals would be formed and subsequently would recombine with little or no diastereoselectivity.[7] This mechanism appeared to provide a rational explanation for our observation of the formation of both $MenPh_3Sn$ and $NeomPh_3Sn$.

However, during studies to optimize the yield of Men_2Ph_2Sn (**3**) formed from the reaction between Ph_2SnCl_2 and the Grignard reagent derived from MenCl, we observed the formation of $NeomMenPh_2Sn$ (**4**), a product in which one of the menthyl groups had undergone epimerization at the C1 carbon atom. Interestingly, the reaction between menthyl Grignard reagent and Ph_2SnCl_2 has been previously reported to yield Men_2Ph_2Sn,[10] although the physical properties reported for the product, including the optical rotation (an oil, $[\alpha]_D^{20} = -30.5°$), differ significantly from those we found for **3**. A crystal structure of **3** was obtained and has confirmed the stereogenic centers in the menthyl groups to indeed be those of Men_2Ph_2Sn.[11]

These observations provoked a more detailed investigation of the stereochemical integrity in the reactions of Grignard reagents derived from MenCl (1*R*) and its epimerization partner, NeomCl (1*S*).[12] The two major conformations[14] are shown in Scheme 1.

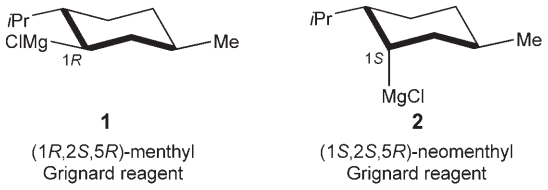

Scheme 1. The two major conformations of the Grignard reagent: equatorial (left) and axial (right).

In an attempt to obtain $Neom_2Ph_2Sn$, we reacted the Grignard reagent prepared from NeomCl with Ph_2SnCl_2. Surprisingly, this reaction gave products **3** and **4** in similar yields to those obtained from reaction of the Grignard reagent prepared from MenCl. We found no evidence for the formation of the anticipated product, $Neom_2Ph_2Sn$. These observations suggest that magnesium reacts with either MenCl or NeomCl to give an identical mixture of Grignard reagents. The results of quenching the reactions with D_2O were particularly informative. Quenching each of the Grignard reagents formed from MenCl and NeomCl with D_2O gave identical results, in each case a 1:1 ratio of [D]menthane and [D]neomenthane.

On reexamination of the reaction between the Grignard reagent mixture and Ph_2PCl, we gained additional information. The reaction between an approximately equimolar ratio of the Grignard reagent and Ph_2PCl had been reported to give $MenPh_2P$ in 51% yield.[3] We repeated this reaction and after quenching with D_2O, investigated the product array by NMR spectroscopy. We found that half of the Grignard reagent was consumed to form $MenPh_2P$ and the remaining half reacted with D_2O to form NeomD. Apparently only MenMgCl (**1**) is a sufficiently strong Lewis acid to lower the relatively high-energy LUMO of Ph_2PCl, which is attacked along the axial plane (opposite chloride) by the strongly nucleophilic menthyl group. NeomMgCl (**2**) appears to be more involved in the Schlenk equilibrium because of its axial magnesium chloride group, with a concomitant decrease in its Lewis acidity and shielding of its carbocation. Hence, in addition reactions, MenMgCl (**1**) acts simultaneously as a strong Lewis catalyst and as a strong nucleophile towards substrates.[15] As a result, we found no evidence for $NeomPh_2P$, which is consistent with **2** being much less nucleophilic than **1**.

Closer inspection of experimental details in the original report for the synthesis of $MenMe_3Sn$[4] revealed that reaction between the Grignard reagent and Me_3SnCl in a 2:1 stoichiometric ratio produced $MenMe_3Sn$ in 94% yield (based on Me_3SnCl). This observation is consistent with preferential reaction of the menthyl component **1** of the Grignard reagent (that is, half of the total Grignard reagent originally formed). The fate or nature of the unreacted Grignard reagent, presumably the neomenthyl component **2**, remained unaccounted for, and **2** was most likely hydrolyzed during the workup. Additional experiments involving the reaction of Me_3SnCl with a limited amount of Grignard reagent revealed that $NeomMe_3Sn$ was not formed at all, an observation similar to those made from the reaction of the Grignard reagent with Ph_2PCl.

The strong Lewis acidity of Ph_2SnCl_2, combined with the preferential attack by the more reactive MenMgCl, means that it is not possible to selectively form $NeomPh_2SnCl$ from a Grignard reaction. However, the weaker acidity of the triorganotin species results in lower rate discrimination between the menthyl and neomenthyl components of the Grignard reagent. Consequently, increasing the ratio of the Grignard reagent to Ph_3SnCl from 1:1 to 4:1 resulted in an increase in the product ratio of $MenPh_3Sn$ to $NeomPh_3Sn$ from 65:35 to 99:1.

When the Grignard reagent and Ph_2SnCl_2 are reacted together, depending on the reaction conditions, two different products can be obtained, namely Men_2Ph_2Sn (**3**) and $NeomMenPh_2Sn$ (**4**); these products were crystallized and isolated in yields of 32% (m.p. 75–76 °C, $[\alpha]_D^{25} = -50.2°$) and 21% (m.p. 58–59 °C, $[\alpha]_D^{25} = -13.9°$), respectively from separate reactions.[16] The identity of the novel compound $NeomMenPh_2Sn$ (**4**) was unambiguously confirmed by ^1H and ^{13}C NMR spectroscopy as well as by X-ray crystallography. The molecular structure of one of the two crystallographically independent conformers of **4** is shown in Figure 1.

 © 2006 Wiley-VCH Verlag GmbH & Co. KGaA, Weinheim

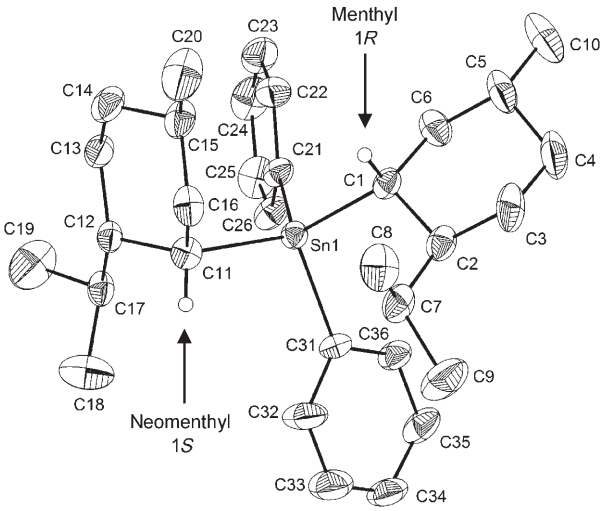

Figure 1. Molecular structures of one of the two crystallographically independent conformers of **4**, showing 30% probability displacement ellipsoids and the crystallographic numbering scheme. For clarity, only the hydrogen atoms connected to the C1 and C11 atoms are shown.

The ratio of products **3** and **4** could be significantly altered by changing the temperature, solvent, and the amount of Grignard reagent. Hence, when a hot solution of Ph_2SnCl_2 in toluene was added to a hot THF solution of Grignard reagent prepared from five equivalents of MenCl, and the reaction was stirred at reflux for two hours, Men_2Ph_2Sn (**3**) formed as the major product;[17] ^{119}Sn NMR spectroscopy showed the ratio of **3** and **4** to be 93:7 [Eq. (1)]. When a cold solution

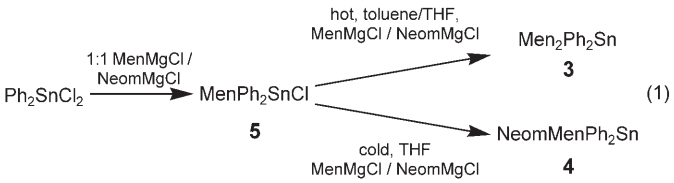

(1)

(0 °C) of Ph_2SnCl_2 in THF was added to a cold THF solution (0 °C) of Grignard reagent prepared from 2.5 equivalents of MenCl, and the reaction mixture was stirred for two days at room temperature, $NeomMenPh_2Sn$ (**4**) formed predominately [Eq. (1)]; ^{119}Sn NMR spectroscopy showed the ratio of **3** and **4** to be 28:72.[18] Significantly, there was no evidence for formation of either $Neom_2Ph_2Sn$ or $(NeomPh_2Sn)_2$, which suggests that under both hot and cold reaction conditions, the first substitution reaction affords exclusively the intermediate $MenPh_2SnCl$ (**5**).[19] These observations are consistent with a mechanism in which the first step is nucleophilic attack by the more reactive menthyl component of the Grignard reagent on the Lewis acidic tin species to give **5**. The second substitution is slower because of the decreased Lewis acidity and increased steric bulk of **5**, and thus, depending on the reaction conditions, either **3** or **4** is obtained. It may therefore be possible to prepare $Neom_2Ph_2Sn$ by first removing the more reactive MenMgCl (**1**) by reaction with Ph_2PCl.

In conclusion, direct synthesis of Grignard reagents from enantiomerically pure alkyl halides will always result in a 1:1 ratio of the two possible epimers. Once formed, the two components of the reagent are configurationally stable—there is no equilibrium between them. If the reactivity of the two epimers differs significantly, as in the case of MenMgCl (**1**) and NeomMgCl (**2**), it is possible to selectively use each component in reactions with electrophiles. This can be achieved by using thermodynamic/kinetic control of the reaction, altering temperature, solvent polarity, and stoichiometry. These findings reveal possible uses of Grignard reagents in asymmetric synthesis. Full consumption of the more reactive epimer (for example, **1**) by reaction with an appropriate electrophile (for example, Ph_2PCl) results in a reaction mixture that contains a pure chiral Grignard reagent (for example, **2**). Subsequent reaction with carbonyl groups opens the pathway to chiral alcohols. Fine-tuning of the reaction conditions will no doubt permit the application of pairs of Grignard epimers in which the difference in the reactivity is not as pronounced as in the case of **1** and **2**.

Received: May 25, 2006
Published online: September 5, 2006

Keywords: asymmetric synthesis · chiral Grignard reagents · Grignard reaction · kinetics

[1] The substituent names menthyl (Men) and neomenthyl (Neom) stand for the (1*R*,2*S*,5*R*)- and the (1*S*,2*S*,5*R*)-2-isopropyl-5-methylcyclohexyl group, respectively.
[2] "Asymmetric Free-Radical Reductions Mediated by Chiral Stannanes, Germanes and Silanes": J. Beckmann, D. Dakternieks, C. H. Schiesser in *Handbook of Chiral Chemicals* (Ed.: D. Ager), Marcel Dekker, New York, **2005**, chap. 27, pp. 531–538.
[3] M. Tanaka, I. Ogata, *Bull. Chem. Soc. Jpn.* **1975**, *48*, 1094.
[4] a) H. Schumann, B. C. Wassermann, *J. Organomet. Chem.* **1989**, *365*, C1; b) H. Schumann, B. C. Wassermann, F. E. Hahn, *Organometallics* **1992**, *11*, 2803.
[5] The formation of Grignard reagents by direct synthesis at a magnesium surface proceeds via alkyl radicals and furnishes racemic Grignard reagents, even when the precursor (in this case MenCl) is enantiomerically pure.[6] The preparation of true chiral Grignard reagents would require a route that avoids any intermediates radicals.[7]
[6] H. M. Walborsky, A. E. Young, *J. Am. Chem. Soc.* **1964**, *86*, 3288.
[7] R. W. Hoffmann, *Chem. Soc. Rev.* **2003**, *32*, 225, and references therein.
[8] J. D. Morrison, W. F. Masler, *J. Org. Chem.* **1974**, *39*, 270.
[9] D. Dakternieks, K. Dunn, D. J. Henry, C. H. Schiesser, E. R. T. Tiekink, *Organometallics* **1999**, *18*, 3342.
[10] C. Lucas, C. C. Santini, M. Prinz, M.-A. Cordonnier, J.-M. Basset, M.-F. Connil, B. Jousseaume, *J. Organomet. Chem.* **1996**, *520*, 101.
[11] D. Dakternieks, K. Dunn, B. R. Vincent, E. R. T. Tiekink, *Main Group Met. Chem.* **2000**, *23*, 329.
[12] The Grignard reagent was freshly prepared from the reaction of enantiomerically pure MenCl or NeomCl with Mg in THF; the reaction temperature was allowed to rise to the boiling point of THF and then kept there for 2 h. The Grignard reagent was typically found by titration to be formed in greater than 85% yield.[13]

 © 2006 Wiley-VCH Verlag GmbH & Co. KGaA, Weinheim

[13] "Wet Analysis of Grignard Reagents": G. S. Silverman in *Handbook of Grignard Reagents* (Eds.: G. S. Silverman, P. E. Rakita), Marcel Dekker, New York, **1996**, chap. 6, 89 – 92.
[14] D. H. R. Barton, *Experientia* **1950**, *6*, 316.
[15] P. Sykes, *A Guidebook to Mechanism in Organic Chemistry*, 6th ed., Longman Scientific & Technical, **1986**, chap. 8, pp. 221 – 223. The reaction involves a concerted polar mechanism via a six-membered cyclic transition state in which two molecules of RMgX are implicated. The second molecule of RMgX acts as a Lewis catalyst.
[16] The optical rotations of isolated **1** and **2** suggest that the material described in Ref. [6] was actually a mixture of **1** and **2**, with a ratio of approximately 54:46.
[17] There is an additional minor signal in the ^{119}Sn NMR spectrum (ca. 18%), which is attributed to the ditin species $MenPh_2SnSnPh_2Men$. This species was formed from an alternative six-membered transition state containing two molecules of $MenPh_2SnCl$ and one molecule of RMgCl.[15] RMgCl acts as a simultaneous acidic catalyst towards one moiety of $MenPh_2SnCl$ (**5**) (ClRMg→Cl-Sn) and as a basic catalyst towards the other moiety of **5** (RMgCl→Sn). The resulting stannyl anion carried out a nucleophilic attack at the axial site of the activated **5** (formally reductive elimination). This competitive reaction was favored by the reduced polarity of the solvent, which had been chosen to slow down the attack of the unwanted Neom carbanion.
[18] Under both hot and cold reactions conditions, a few additional minor ^{119}Sn NMR signals (total integral value of approximately 6%) were observed and remain unassigned.
[19] To support this theory, two equivalents of the Grignard reagent prepared from MenCl were added to a cold solution of Ph_2SnCl_2 in THF, and the mixture was immediately quenched with water. After workup, the ^{119}Sn NMR spectrum of the crude reaction mixture showed four signals at $\delta = -0.5$ (integral 27%), −54.6 (integral 62%), −89.3 (integral 4%), and −50.8 (integral 7%), corresponding to $MenPh_2SnCl$ (**5**), $(MenPh_2Sn)_2O$ (**6**), Men_2Ph_2Sn (**3**), and an unidentified component, respectively (Figure 2). Clearly most of **5** had been converted into **6** on workup. We converted (−)-$MenPh_2SnI$[9] into **5** by halogen exchange[20] and then into **6** by base hydrolysis to confirm the assignment of these signals from the NMR spectrum.
[20] B. Zobel, A. E. K. Lim, K. Dunn, D. Dakternieks, *Organometallics* **1999**, *18*, 4889.

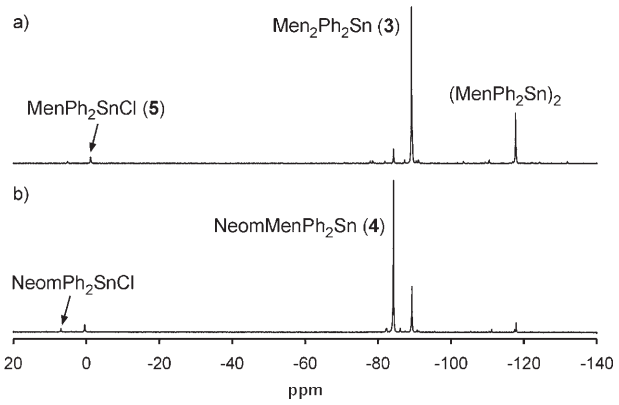

Figure 2. ^{119}Sn NMR spectrum of the crude reaction mixture prepared from the reaction of Grignard reagent with Ph_2SnCl_2 under a) hot (reflux) and b) cold (ice bath) conditions.

 © 2006 Wiley-VCH Verlag GmbH & Co. KGaA, Weinheim

Methanol-to-Olefin Process

DOI: 10.1002/anie.200602488

Insights into the Mechanism of Methanol-to-Olefin Conversion at Zeolites with Systematically Selected Framework Structures**

Zhi-Min Cui, Qiang Liu, Wei-Guo Song, and Li-Jun Wan**

Methanol-to-olefin (MTO) conversion[1,2] is essentially about how an initial ethylene C–C bond is formed from a C_1 species. In recent years, a hydrocarbon pool mechanism proposed by Dahl and Kolboe[3] has gained wide supports for post-induction-time MTO chemistry.[4–13] The organic intermediates, which are referred to as the hydrocarbon pool, serve as platforms to which C_1 species can bind and from which primary olefin products can dissociate. Polymethyl benzenes are the most active hydrocarbon pool species on HSAPO-34.[8,11,13,14] On ZSM-5, cyclopentenyl cations play an important role.[4] Though there is little doubt that ethylene is dissociated from some much larger organic species when the reaction proceeds beyond induction time, with possible routes include paring and side-chain-growth mechanisms,[6,10,15,16] the exact mechanism of how ethylene is formed is still not clear largely as a result of complications from secondary reactions, which make it hard to differentiate primary products from secondary products.

There is an ongoing debate about what happens during the induction time.[13,17–21] Besides the hydrocarbon pool mechanism, several direct mechanisms have been proposed to explain at least the initial olefin formation during the induction time.[2] A direct mechanism involves only C_1 species to form the C–C bond. Haw and co-workers argued that organic impurities in the methanol feed were responsible for forming the initial small amount of hydrocarbon pool species.[19] The contribution from certain direct mechanisms was questioned by H/D exchange studies on dimethyl ether.[21] A recent theoretical study by Waroquier and co-workers found a prohibitively high energy barrier for direct C–C bond formation from various C_1 species.[20] In contrast,

[*] Z.-M. Cui, Q. Liu, Prof. W.-G. Song, Prof. L.-J. Wan
Beijing National Laboratory for Molecular Sciences (BNLMS)
Institute of Chemistry
The Chinese Academy of Sciences
Beijing, 100080 (P.R. China)
Fax: (+86) 10-6255-7908
E-mail: wsong@iccas.ac.cn
wanlijun@iccas.ac.cn

[**] The authors thank the Natural Science Foundation of China (20121301), the Ministry of Science and Technology of China (2006CB806101), and the Chinese Academy of Sciences for financial support. Z.-M.C. and Q.L. thank Professor Chun-Li Bai for valuable advice.

Supporting information for this article is available on the WWW under http://www.angewandte.org or from the author.

InterScience
© 2006 Wiley-VCH Verlag GmbH & Co. KGaA, Weinheim

Hunger and co-workers contended that C–C bonds could be formed directly from surface methoxy groups.[17,18]

Herein, we approach these issues from a new angle by using zeolites with systematically selected framework structures. We report that the MTO reaction takes place only on zeolites that allow the hydrocarbon pool mechanism to work. In the absence of complications from secondary reactions, H/D exchange was observed on toluene even when no olefins were produced, thus implying a paring-type mechanism for the MTO process.

The zeolites used in this study included ZSM-11 (MEL), ZSM-22 (TON), SAPO-34 (CHA), and SAPO-5 (AFI). The pore structures of these zeolites are schematically illustrated to highlight the essence of each framework in Figure 1. These

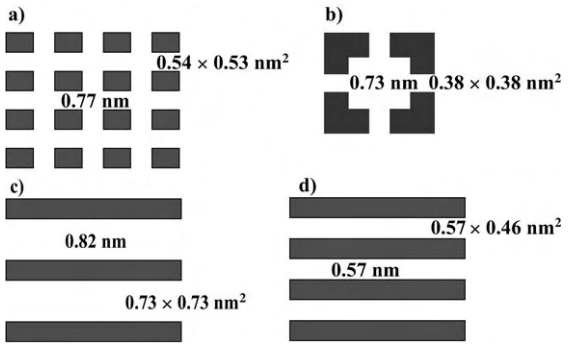

Figure 1. Illustration of zeolite pore structures: a) MEL structure of ZSM-11; b) CHA structure of SAPO-34; c) AFI structure of SAPO-5; and d) TON structure of ZSM-22. The values inside the pores indicate the maximum diameter of a sphere that can be included in the framework, and those outside the pores indicate the size of the pore openings.[22]

zeolites were selected on the basis of the maximum diameter of a sphere that could be included in the framework.[22] ZSM-11 and ZSM-22 have similar pore openings; however, the channel intersections in ZSM-11 enable it to accommodate a sphere with a diameter of 0.77 nm, as compared to 0.57 nm for ZSM-22, which has parallel channels. SAPO-5 also has parallel channels, but a sphere as big as 0.82 nm can be fitted into the framework. SAPO-34 has small pore openings of 0.38 nm, yet its cagelike framework allows a sphere with a diameter of 0.73 nm to be encapsulated.

Gas chromatography (GC) profiles following the 20th pulse of methanol on zeolites at 400 °C are depicted in Figure 2. Prior to that, the catalysts were pretreated with 19 identical pulses of methanol to ensure that the catalysts were in stable working conditions. ZSM-11, SAPO-34, and SAPO-5 showed various MTO activities. Methanol conversion on SAPO-34, ZSM-11, and SAPO-5 was about 80 %, 90 %, and 70 %, respectively (Figure 2 a–c). Meanwhile, methanol conversion on the TON framework (ZSM-22) was dramatically different from the other three catalysts. ZSM-22 showed a low but appreciable production of olefins during the first few pulses of methanol, probably as a result of an impurity ZSM-11 phase and/or external acid sites. However, the amount of olefins quickly decreased to essentially zero when most of

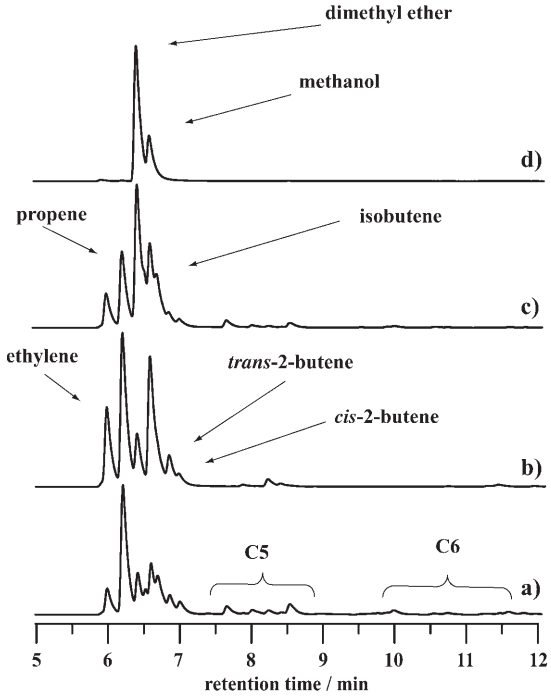

Figure 2. GC profiles of methanol pulsed onto various zeolites at 400 °C. a) ZSM-11; b) SAPO-34; c) SAPO-5; and d) ZSM-22. Samples were taken 8 seconds after methanol pulses. All signals are from a FID detector.

those active sites were deactivated after a few pulses (Figure 2 d).

A mixture of methanol and toluene (10:1 v/v) was pulsed onto SAPO-5, ZSM-11, and ZSM-22 at different temperatures (SAPO-34 was excluded from these experiments because its channel opening of 0.38 nm did not allow toluene to enter its cage). At 250 °C, essentially no olefin was produced using any of the catalysts, although various aromatics were detected from the gas stream or from acid-digested catalysts. At 350 °C and 400 °C, methanol conversion was about 90 % on SAPO-5 and ZSM-11. However, no olefins were detected from ZSM-22; only a small amount of xylene was detected.

The failure of ZSM-22 to convert methanol into olefins even with toluene present is mechanistically significant. Parker and Bibby reported that KZ-2 (a zeolite that also has a TON framework) did not show appreciable MTO activity,[23] but at the time of that study the authors could not relate its inactivity to its implication in the MTO mechanism. Mole et al. proposed that toluene takes on a role as co-catalyst in the MTO process,[24] which may explain the high conversions on SAPO-5 and ZSM-11 (90 %) at 350 °C. The major difference between a very active MTO catalyst, ZSM-11, and a non-active MTO catalyst, ZSM-22, is the absence of channel intersections on the latter, which limits the size of the intermediates that can be formed inside the pores to 0.57 nm or less. The hydrocarbon pool mechanism is a space-demanding process, which involves cyclic organic intermediates that require a space larger than that which ZSM-22 can

 © 2006 Wiley-VCH Verlag GmbH & Co. KGaA, Weinheim

offer (0.57 nm). Thus, ZSM-22 cannot accommodate a complete hydrocarbon pool mechanism cycle and consequently is not an active MTO catalyst. Meanwhile, SAPO-5 has the same type of 1D channel as ZSM-22 but with much larger pore sizes (0.82 nm), thus it is a very active MTO catalyst.

Zeolites are known for their shape selectivity, and the present results are an elegant example of transition-state shape selectivity. ZSM-22 failed as an MTO catalyst because the hydrocarbon pool mechanism did not work on this catalyst. These findings further support the arguments that the hydrocarbon pool mechanism might be the only working mechanism for methanol conversion under these reaction conditions.[19–21] Thus, ZSM-22 provides a pore system to study MTO mechanisms in detail without complications from secondary reactions.

CD_3OH was used to study H/D exchange in methanol and toluene co-injection experiments. A very informative H/D exchange pattern was observed on toluene in the volatile products. At 250 °C, when no olefin was produced from any of the catalysts, no H/D exchange of toluene was observed on SAPO-5, but substantial H/D exchange was observed with ZSM-11 and ZSM-22. The ion-mass distribution of toluene at 250 °C is shown in Figure 3. At higher temperatures, toluene showed more extensive H/D exchange; for example, on ZSM-22 more than half of the toluene molecules present contained one or more deuterium atoms at 350 °C. Table 1 reveals the temperature dependence of H/D exchange of toluene on ZSM-22, ZSM-11, and SAPO-5.

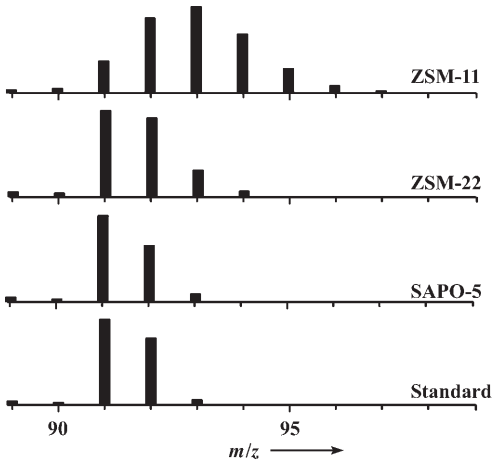

Figure 3. Mass distributions of toluene ions obtained from co-injection of CD_3OH and toluene at 250 °C onto various zeolites.

These findings, especially from the toluene H/D exchange study on ZSM-22 at all temperatures at which no olefin was produced, might provide clues to the detailed mechanism of MTO conversion. 1) As surface methoxy groups or the methyl group on methanol cannot directly undergo H/D exchange with acid-site protons,[25] toluene H/D exchange did not result from direct H/D exchange between protons on the benzene ring and deuterated acid sites. 2) As no olefin was produced on ZSM-22, partially deuterated toluene could not be derived from other highly methylated benzenes that have undergone H/D exchange.[11] 3) The deuterium atoms were incorporated into toluene one by one and not as CD_3 (Figure 3 shows that the $[M+3]$ peak did not dominate). This means that, aided by toluene, the C–D bond on CD_3OH was activated for H/D exchange, but the process did not produce any olefin.

Table 1: Isotopic distribution of deuterium on toluene from H/D scrambling at different temperatures.

Zeolite	T [°C]	Distribution of $[D_n]$toluene [%]					
		$[D_0]$	$[D_1]$	$[D_2]$	$[D_3]$	$[D_4]$	$[D_5]$
ZSM-22	250	75.4	20.5	3.5	0.3	0	0.3
	350	41.8	39.3	14.7	3.7	0.5	0
	400	25.8	40.6	23.0	4.6	6.0	0
ZSM-11	250	17.7	34.2	30.1	14.3	3.7	0
	350	10.4	23.4	32.6	23.4	0.6	1.3
	400	0.8	19.5	32.2	25.9	11.1	2.5
SAPO-5	250	100	0	0	0	0	0
	350	59.6	16.9	17.2	3.0	3.3	0
	400	28.0	24.3	24.4	16.3	5.5	1.5

Here we propose an indirect mechanism for toluene H/D exchange on ZSM-22. The simplified mechanism is illustrated in Scheme 1. CD_3OH readily forms surface methoxy groups on ZSM-22 acid sites.[13] When toluene is adsorbed inside the pore, because of the confinement effect due to the well-matched sizes of the toluene molecule and the ZSM-22 pore,[26] some of the toluene undergoes methyl exchange with surface methoxy groups to produce $[D_3]$toluene ($C_6H_5CD_3$). This then undergoes a partial paring mechanism, that is, ring contraction and expansion (steps 2 and 3 in Scheme 1), but stops short of producing any olefin. Steps 2 and 3 involve multiple proton- and hydride-transfer steps, and D^+ and D^- in step 3 could also undergo H/D exchange with toluene. Indeed, deuterium atoms were thus incorporated into toluene as observed in the H/D exchange study. The extent of H/D scrambling increased significantly from 250 °C to 400 °C, as expected from the process shown in Scheme 1. The choice of CD_3OH as donor of deuterium atoms was crucial in

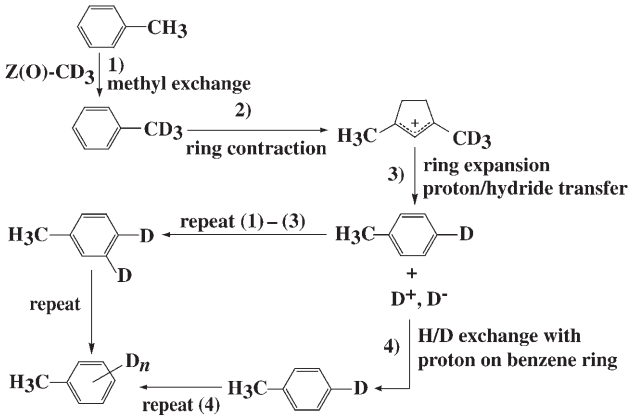

Scheme 1. Mechanism for toluene H/D exchange. Z = zeolite.

 © 2006 Wiley-VCH Verlag GmbH & Co. KGaA, Weinheim

experimental design; facile exchange between acid-site protons, benzene protons, and methanol hydroxy protons was not observed as it involved the same isotope.

The same mechanism could be applied to ZSM-11 at 250 °C. No H/D exchange on toluene was observed on SAPO-5 at 250 °C, probably because the pore size of SAPO-5 was too large and the benefit of the confinement effect was minimal. Weaker acid sites on SAPO-5 might also lead to no H/D exchange. At higher temperatures, owing to complications from secondary reactions, results from ZSM-11 and SAPO-5 were difficult to interpret.

Scheme 1 suggests that C–H bonds on methanol groups were activated—which is an essential step in the MTO process—in the presence of toluene through a paring mechanism. The paring mechanism is thus supported as a possible mechanism for MTO conversions. Kolboe and Haw have speculated on the role of the paring mechanism for the MTO process.[6,10,16] In the present study, parts of the paring mechanism were observed in the MTO process for the first time in the absence of complications from secondary reactions.

More detailed studies are underway for a better understanding of MTO mechanisms. It seems that on ZSM-22 and similar zeolites, as a result of their pore structures, the hydrocarbon pool mechanism could proceed to a certain extent depending on the reaction conditions, but stops prior to the olefin formation step. It might be possible to find more detectable intermediates that are involved in hydrocarbon pool mechanisms without complications from secondary reactions, so as to develop a more detailed MTO reaction sequence. This invites joint efforts from both theoretical and experimental studies.

Experimental Section

All zeolite samples were synthesized according to reported methods.[8,27,28] See Supporting Information for details.

The MTO reaction was conducted on a home-built pulse quench reactor. In a typical pulse experiment, 30-mg samples of catalyst were loaded into a 6-mm (OD) stainless-steel tube, which was then heated to reaction temperature and maintained at that temperature for 1 hour under 100 SCCM nitrogen flow prior to the reaction. In pulse experiments, methanol (2 equiv) was pulsed onto the catalyst and GC samples were taken 8 seconds after the injections. The volatile compounds were analyzed with an Agilent 6890 GC equipped with a 50-m capillary column and a FID detector using published response factors.

In H/D scrambling studies, samples were analyzed offline. Volatile products were collected by bubbling exhaust gas into a liquid chloroform trap, while five identical pulses were injected into the reactor. Samples were analyzed with a Shimazu QP2010 GC-MS system equipped with a DB-5 30-m capillary column.

Received: June 21, 2006
Revised: July 21, 2006
Published online: September 13, 2006

[1] C. D. Chang, A. J. Silvestri, *J. Catal.* **1977**, *47*, 249.
[2] M. Stocker, *Microporous Mesoporous Mater.* **1999**, *29*, 3.
[3] I. M. Dahl, S. Kolboe, *Catal. Lett.* **1993**, *20*, 329.
[4] J. F. Haw, J. B. Nicholas, W. Song, F. Deng, Z. Wang, T. Xu, C. S. Heneghan, *J. Am. Chem. Soc.* **2000**, *122*, 4763.
[5] M. Hunger, *Catal. Today* **2004**, *97*, 3.
[6] J. F. Haw, D. M. Marcus, *Top. Catal.* **2005**, *34*, 41.
[7] J. F. Haw, W. Song, D. M. Marcus, J. B. Nicholas, *Acc. Chem. Res.* **2003**, *36*, 317.
[8] W. Song, J. F. Haw, J. B. Nicholas, C. S. Heneghan, *J. Am. Chem. Soc.* **2000**, *122*, 10726.
[9] W. Song, H. Fu, J. F. Haw, *J. Phys. Chem. B* **2001**, *105*, 12839.
[10] U. Olsbye, M. Bjorgen, S. Svelle, K. P. Lillerud, S. Kolboe, *Catal. Today* **2005**, *106*, 108.
[11] B. Arstad, S. Kolboe, *J. Am. Chem. Soc.* **2001**, *123*, 8137.
[12] M. Bjorgen, U. Olsbye, S. Svelle, S. Kolboe, *Catal. Lett.* **2004**, *93*, 37.
[13] W. Wang, Y. J. Jiang, M. Hunger, *Catal. Today* **2006**, *113*, 102.
[14] M. Hunger, *Microporous Mesoporous Mater.* **2005**, *82*, 241.
[15] B. Arstad, S. Kolboe, O. Swang, *J. Phys. Chem. A* **2005**, *109*, 8914.
[16] J. F. Haw, W. G. Song, D. M. Marcus, J. B. Nicholas, *Acc. Chem. Res.* **2003**, *36*, 317.
[17] Y. J. Jiang, W. Wang, V. R. R. Marthala, J. Huang, B. Sulikowski, M. Hunger, *J. Catal.* **2006**, *238*, 21.
[18] W. Wang, A. Buchholz, M. Seiler, M. Hunger, *J. Am. Chem. Soc.* **2003**, *125*, 15260.
[19] W. Song, D. M. Marcus, H. Fu, J. O. Ehresmann, J. F. Haw, *J. Am. Chem. Soc.* **2002**, *124*, 3844.
[20] D. Lesthaeghe, V. Van Speybroeck, G. B. Marin, M. Waroquier, *Angew. Chem.* **2006**, 118, 1746; *Angew. Chem. Int. Ed.* **2006**, *45*, 1714.
[21] D. M. Marcus, K. A. McLachlan, M. A. Wildman, J. O. Ehresmann, P. W. Kletnieks, J. F. Haw, *Angew. Chem.* **2006**, *118*, 3205; *Angew. Chem. Int. Ed.* **2006**, *45*, 3133.
[22] http://www.iza-online.org.
[23] L. M. Parker, D. M. Bibby, *Zeolites* **1983**, *3*, 8.
[24] T. Mole, G. Bett, D. Seddon, *J. Catal.* **1983**, *84*, 435.
[25] D. M. Marcus, M. J. Hayman, Y. M. Blau, D. R. Guenther, J. O. Ehresmann, P. W. Kletnieks, J. F. Haw, *Angew. Chem.* **2006**, *118*, 1967; *Angew. Chem. Int. Ed.* **2006**, *45*, 1933.
[26] E. G. Derouane, C. D. Chang, *Microporous Mesoporous Mater.* **2000**, *35–36*, 425.
[27] E. W. Valyocsik, US 4,902,406, **1990**.
[28] D. M. Marcus, W. G. Song, S. M. Abubakar, E. Jani, A. Sassi, J. F. Haw, *Langmuir* **2004**, *20*, 5946.

Keywords: heterogeneous catalysis · isotopic labeling · methanol-to-olefin process · reaction mechanisms · zeolites

 © 2006 Wiley-VCH Verlag GmbH & Co. KGaA, Weinheim

Mesoporous Crystals

DOI: 10.1002/anie.200601451

A Lesson from the Unusual Morphology of Silica Mesoporous Crystals: Growth and Close Packing of Spherical Micelles with Multiple Twinning**

*Keiichi Miyasaka, Lu Han, Shunai Che, and Osamu Terasaki**

Ordered mesoporous silicas synthesized through the self-assembly of amphiphilic surfactants are of great interest because of their potential for new applications, for which the control of particle shape and size are vital. Some mesoporous crystals show characteristic morphology, such as MCM-48 crystals ($Ia\bar{3}d$) with truncated rhombic dodecahedra;[1] HMM-3/SBA-1 ($Pm\bar{3}n$) with well-defined decaoctahedra[2,3] and 74 faces as well as 54 faces with crystal-like shape;[4] SBA-7 ($P6_3/mmc$) with 20 distinct crystal faces with one sixfold axis;[5] and FDU-1 ($Im\bar{3}m$) with rhombododecahedra.[6] Furthermore, morphological evolution of SBA-1 was investigated with respect to various synthetic parameters such as temperature, acidity, time, concentration, and so on.[7] All morphologies reported in the above references were commensurate with crystallographic point-group symmetries, and were observed from the crystals synthesized under well-controlled conditions for crystal growth processes.

Recently, we have synthesized a crystal that shows a well-resolved powder X-ray diffraction (XRD) profile, but its morphology does not fit any crystallographic point-group symmetry. Herein, we present a structural solution for a well-ordered mesoporous silica crystal of the cage type with cubic $Fm\bar{3}m$ symmetry, and its structural description for the morphologies involved. The study was performed by powder XRD, scanning electron microscopy (SEM), and high-resolution transmission electron microscopy (HRTEM). Morphologies such as an icosahedron or a decahedron of cubic $Fm\bar{3}m$ structure seem to be inconsistent with the corresponding point-group symmetry, $m\bar{3}m$. However, the structure is explained in terms of the occurrence of multiple twinning during the formation of mesostructures. This behavior has been observed for face-centered cubic (FCC) metals.

Highly ordered mesoporous silica was prepared using the gemini cationic surfactant, $C_{16\text{-}3\text{-}1}$ (see Experimental Section), as template with a very low surfactant concentration of 0.36 wt %. The surfactant $C_{16\text{-}3\text{-}1}$ has two head groups and one tail, which makes the effective area of the critical packing parameter larger than that of normal surfactants used for conventional mesoporous silicas. Therefore, micelles form a lyotropic, liquid-crystal mesophase with high curvatures. Figure 1 shows the XRD pattern of the calcined sample,

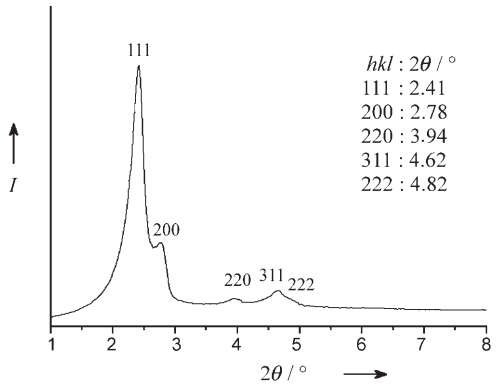

Figure 1. Powder XRD pattern of the calcined silica mesoporous crystal recorded in the region of $2\theta = 1.0$–$8.0°$. The pattern was indexed assuming a cubic lattice.

which is indexable with the cubic lattice, as supported by the TEM observations discussed below. The pattern shows two well-resolved sharp peaks indexed as 111 and 200 reflections in the region of $2\theta = 1.5$–$3.0°$, and three additional weak peaks indexed as 220, 311, and 222 reflections in the range of $2\theta = 3.5$–$6.0°$. The unit cell parameter a is 63 Å. The nitrogen adsorption–desorption isotherm of this sample is provided in the Supporting Information, together with the pore-size distribution analysis using nonlocal density functional theory. The Brunauer–Emmett–Teller (BET) surface area and the total pore volume are 778 $m^2 g^{-1}$ and 0.345 $cm^3 g^{-1}$, respectively. In the isotherm, the capillary condensation step observed at lower relative pressure ($P/P_0 < 0.2$) is analogous to that of high-quality MCM-41 with small pores templated by short-chain surfactants.

SEM images showed unusual morphologies from the point-group symmetry $m\bar{3}m$ expected from the space-group symmetry $Fm\bar{3}m$. Such morphologies can be categorized into two types: "plate" and "polyhedron" (see Figure 2a,b). The plate category normally showed a threefold triangular shape truncated at its vertices. For the polyhedron category, an icosahedral shape was typically observed. For the observed shapes of relevance, decahedral, Wulff, and D-Wulff polyhedrons can be categorized (see Figure 2c–e), although these were observed less often. The particle size of the icosahedron tended to be relatively smaller ($< 10\ \mu m$) than that of the other shapes, where plate-type particles show a variety of

[*] K. Miyasaka, Prof. O. Terasaki
Structural Chemistry, Arrhenius Laboratory
Stockholm University
10691 Stockholm (Sweden)
Fax: (+46) 816-3118
E-mail: terasaki@struc.su.se
L. Han, Prof. S. Che
School of Chemistry and Chemical Technology
State Key Laboratory of Composite Materials
Shanghai Jiao Tong University
800 Dongchuan Road, Shanghai, 200240 (P.R. China)

[**] O.T. thanks the Swedish Science Research Council (VR) and the Japan Science and Technology Agency (JST) for financial support. This work was also supported by the National Natural Science Foundation of China (Grant Nos. 20425102 and 20521140450), the China Ministry of Education, and the Shanghai Science Foundation (0452nm061 and 05XD14010).

Supporting information for this article is available on the WWW under http://www.angewandte.org or from the author.

WILEY InterScience DISCOVER SOMETHING GREAT
© 2006 Wiley-VCH Verlag GmbH & Co. KGaA, Weinheim

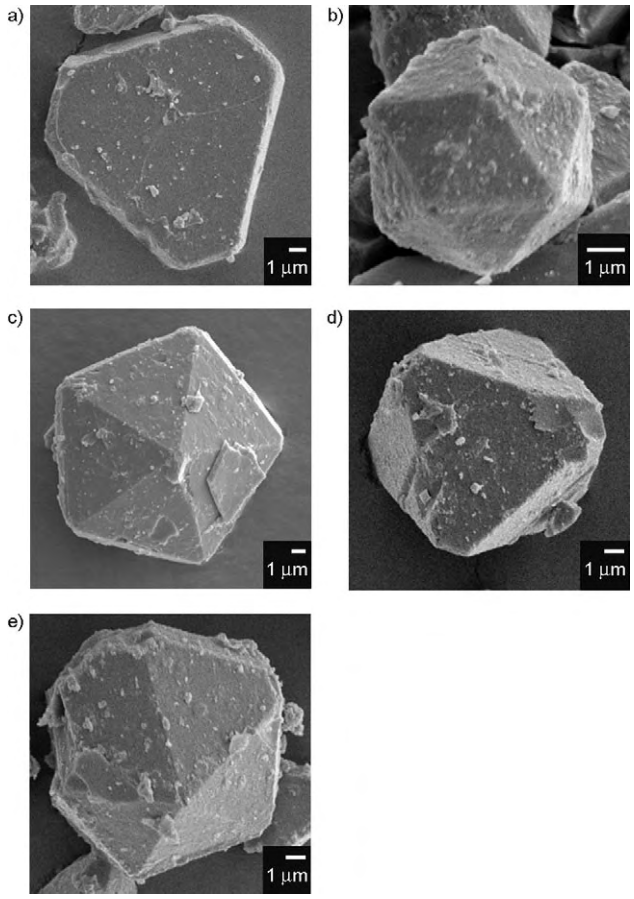

Figure 2. Typical SEM images of calcined silica mesoporous crystals coated by gold. a) Particle of plate type; its vertices are often truncated. b) Icosahedral shape. c) Decahedral shape. d) Particle showing the Wulff polyhedron. e) Particle showing the D-Wulff polyhedron.

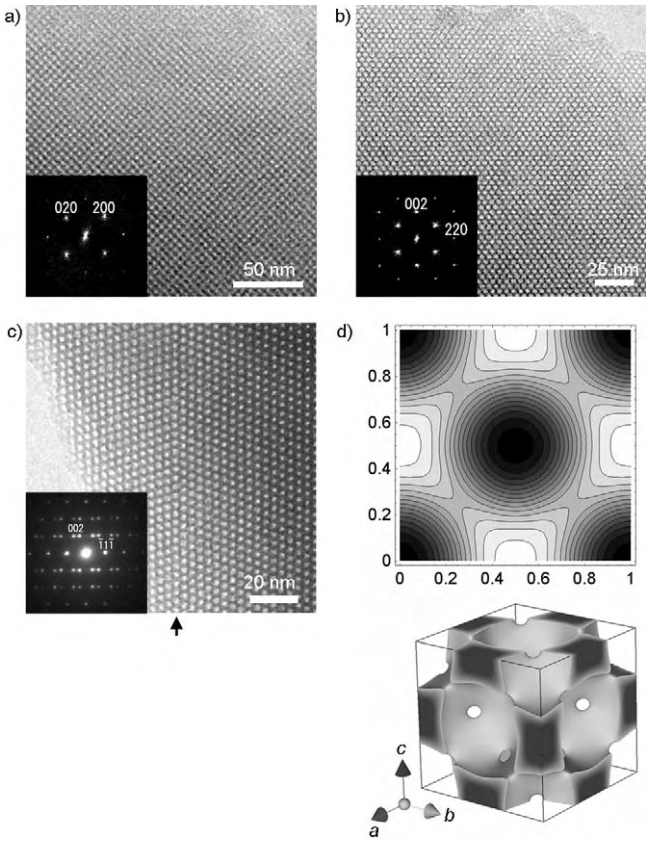

Figure 3. HRTEM images with the corresponding Fourier diffractograms inset, taken from a) [001] and b) [110] incidence. c) HRTEM image showing an occasional single twin boundary (indicated by an arrow) observed along [110]. The corresponding ED pattern (inset) is indexed based on the rightward region. d) The resultant structure of the calcined silica mesoporous crystal through the electron crystallographic process. Top: contour plot sliced perpendicular to [001] at $z=0$, where white and black correspond to the silica wall and the pore, respectively. Bottom: 3D representation of one unit cell of the crystal with $Fm\bar{3}m$ symmetry.

sizes up to 20 μm and decahedral particles sit around 10 μm. These morphological features will be discussed later in combination with the TEM results.

HRTEM images of the crystal demonstrate the pore arrangement covering a large area with beautiful crystallinity (see Figure 3a,b). We observed the sequential presence of four-, two-, and sixfold rotational symmetries in the projected images taken with [100], [110], and [111] incidences by tilting the specimen. The reflection conditions derived from the Fourier diffractograms of the HRTEM images are summarized as $\{hkl: h+k, k+l, l+h=2n; 0kl: k, l=2n; hhl: h+l=2n; 00l: l=2n\}$, which provide the possible space groups $F432$ (No. 209), $F\bar{4}3m$ (No. 216), and $Fm\bar{3}m$ (No. 225). However, the first option is excluded when taking into account the Wulff polyhedral single crystal observed (Figure 2d), because the symmetry group of a regular octahedron is $S_4 \times C_2$ which the first option does not possess. We conclusively chose $Fm\bar{3}m$ rather than $F\bar{4}3m$ because of its higher symmetry. Twinnings are occasionally observed in the image. A typical image is shown in Figure 3c, with the inset showing the electron diffraction (ED) pattern taken from the corresponding selected area. In this image, it is clear that there is merely a single twin boundary halving the field (indicated by an arrow).

Fourier analysis of HRTEM images based on electron crystallography was performed to elucidate the structural details, such as the pore shape and the possible pore connectivity. The details of the process can be found elsewhere.[3,8] The resultant Fourier coefficients (FCs) are tabulated in the Supporting Information. The electrostatic potential distribution, $\rho(x,y,z)$, is three-dimensionally built by Fourier synthesis from a set of FCs by taking into account $Fm\bar{3}m$ symmetry [Eq. (1)].

$$\rho(x,y,z) = \sum_{hkl} F_{hkl} \cos(2\pi h x) \cos(2\pi k y) \cos(2\pi l z) \quad (1)$$

The contour plot for the plane of $\rho(x,y,z)$ sliced at $z=0$, perpendicular to [001], is shown in Figure 3d together with a three-dimensional (3D) structural representation. We took the crystallographic origin at the center of the cage. One cage has 12 nearest neighbors. Mesocaged porous silicas comprising a cubic close-packed (CCP) arrangement have been reported previously, for example, as SBA-2[9] and SBA-12.[10]

 © 2006 Wiley-VCH Verlag GmbH & Co. KGaA, Weinheim

It is known that CCP stacking of spherical micelles stays next to hexagonal close-packed (HCP) stacking, and the HCP domain is often found in HRTEM images in the literature as random mixtures of both stacking (SBA-2) and segregated domains (SBA-12). In comparison with these, our sample showed overwhelming CCP over HCP stacking, and HCP stacking was observed only at the twin boundaries. The effect of HCP stacking on the XRD pattern as a result of twinning will be discussed below in terms of the formation of the particles and their size.

Nowadays the morphologies included herein are known as a remarkable feature of FCC crystals. A plate can be explained by the presence of single twinning in a tetrahedral/octahedral single FCC crystal (see Figure 4a), whilst particular polyhedrons can be multiply twinned particles (MTPs). The MTP model was first introduced by Ino[11] in the 1960s. It was applied to the epitaxial growth of metal particles and successfully explained the presence of the icosahedral or decahedral shape of those particles possessing a FCC structure. Based on the geometrical consideration, Ino discussed the stability of MTPs comprising icosahedrons and decahedrons in terms of the specific surface energy, the twin boundary energy, the elastic strain energy, and the adhesive energy to the substrate. The occurrence of MTPs is now a common phenomenon in nanoparticles with FCC structure. Correspondingly, the MTP model gives us an account of the existing behavior in morphologies of mesoporous materials. Namely, icosahedral and decahedral shapes are expected to consist of twin-related tetrahedrons packed along (111) faces. In the case of an icosahedron, for instance, the whole structure contains one primary, three secondary, six tertiary, six quartic, three quintic, and one sextic tetrahedral units (see Figure 4b). Representations of the other shapes are shown in Figure 4c–e.

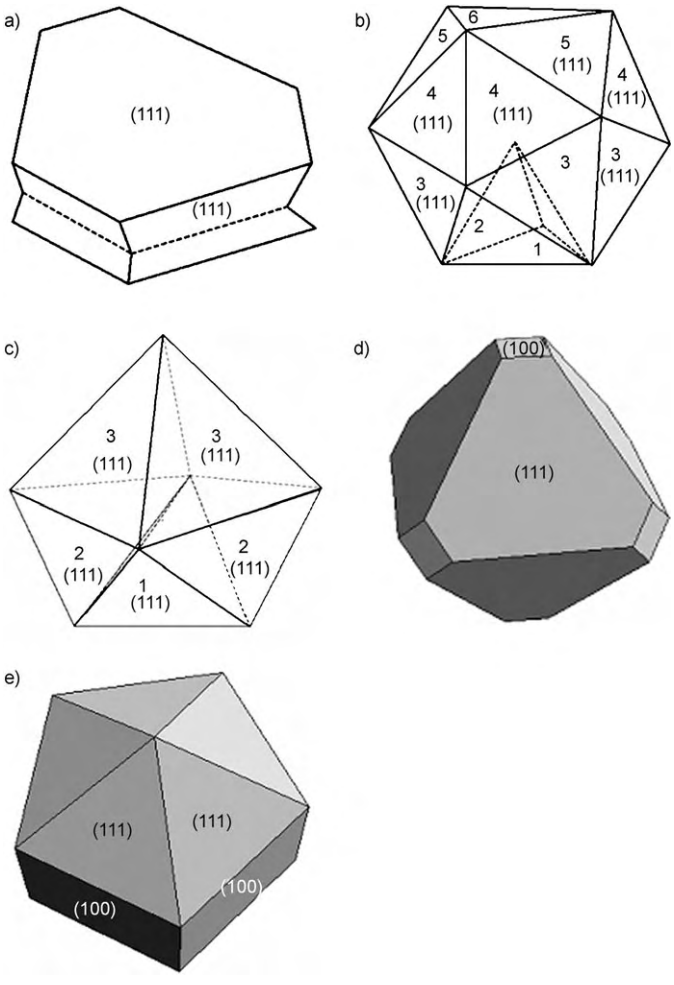

Figure 4. Schematic representations with Miller indices for the morphologies discussed. a) Triangular plate type; the dotted line represents a twin boundary. b) MTPs forming an icosahedron composed of 20 tetrahedrons, where the numbers specify the multiplicity of the twinning starting with the tetrahedron at the bottom. c) MTPs forming a decahedron composed of 5 five tetrahedrons. The multiplicity is indicated likewise. d) Wulff polyhedral single crystal. e) D-Wulff polyhedron.

Since the discovery of MTPs, various theoretical and experimental investigations have been reported[12] and different types of mechanisms have been proposed. As an example, Marks commented that the nucleation and growth of the particle are dominated by the probability of morphologies at a given condition, and are thus history-dependent.[13] In general, MTPs are not capable of growth to a large size because of the internal elastic strain arising from angular misfits of tetrahedral single crystals. According to the original evaluation by Ino,[14] it was suggested that the icosahedral MTP is the most stable in the region where the length of one edge r is short enough, while the energy rapidly increases with increasing r because of the internal elastic strain from misfits between tetrahedral building units. Thus, the particle size of icosahedrons should be smaller than that of decahedrons. Our SEM observations agree with this evaluation, as we observed that icosahedrons tended to be smaller compared to decahedrons. Meanwhile, the plate-type particle grows two dimensionally parallel to the twin boundary, and ends up with a variation of particle sizes.

The effect of the number of constituents (N) on the stability of MTPs should be discussed. The MTPs of the silica mesoporous crystal show a remarkably large N in comparison with those of FCC metals. Simple geometrical consideration gives the estimated value of N for both icosahedrons and decahedrons, since the relation between the edge length (r) of a tetrahedron built with a single FCC structure and a unit cell parameter (a) of the FCC lattice can be expressed by $N = \sqrt{2}r^3/3a^3$. In our case of an icosahedron composed of 20 tetrahedrons and a decahedron composed of 5 tetrahedrons, N is expected to be approximately 10^9, while $N < 10^5$ for Au MTPs as an example. This finding suggests that surfactant micelles are more flexible constituents compared with metal atoms, which can compensate the internal strain energy during the formation of MTPs. In this respect, the effect of HCP stacking arising from twinnings on measured XRD patterns is suppressed, because the number of FCC constituents exceeds hexagonal close packing by $r^{3/2}$ as r increases.

The use of gemini surfactant generally affords the SBA-2 type of structure as a mixture of 3D hexagonal and $Fm\bar{3}m$ symmetry.[15] However, the pure $Fm\bar{3}m$ mesostructure was

 © 2006 Wiley-VCH Verlag GmbH & Co. KGaA, Weinheim

achieved under extremely low reactant concentrations starting with a clear solution (see Experimental Section). Synthesis under low-concentration conditions would make micelles in the solution more diffuse, and crystallization more kinetically controlled. As suggested from the reconstructed 3D structure, the shape of the micelles is highly spherical. By analogy with metal nanoparticles, we speculate that such a spherical shape of the surfactant aggregates should be a key to open the door to a pure FCC phase and the occurrence of multiple twinning during self-assembly with silica precursors. Although the formation energy of CCP stacking would be expected to be close to that of HCP stacking, our results suggested that micellar constituents should prefer to stack not by hexagonal close packing but by cubic close packing. This evokes the notion that the particle morphologies result in an icosahedral or decahedral shape with multiple twinning, and a triangular plate with single twinning.

Finally, MTPs can give 10-fold symmetry in their diffraction patterns as well as quasi-crystals, and thus the structural determination of quasi-crystals would be difficult using only diffraction techniques. As the existence of quasi-crystals in the liquid-crystalline phase (liquid quasi-crystals) has been revealed recently for 12-fold symmetry,[16] further discussions are required to clarify liquid quasi-crystals on the mesoscopic scale.[17]

Experimental Section

Mesoporous silica was synthesized by using gemini surfactant $[C_{16}H_{33}N(CH_3)_2(CH_2)_3(CH_3)_3N]Br_2$ (termed $C_{16\text{-}3\text{-}1}$) and tetraethyl orthosilicate (TEOS; from China Chemical Reagent Corporation) as a silica source in the presence of sulfuric acid.

Synthesis of mesoporous silica: The surfactant $C_{16\text{-}3\text{-}1}$, distilled water, and sulfuric acid were mixed to obtain a homogeneous solution, which was allowed to react at 0 °C prior to the addition of the silica source TEOS. After the addition of TEOS, the mixture was stirred for 3 min and then the reaction was continued at 0 °C under static conditions for 3 days. The resultant white precipitate was isolated by filtration (without washing) and dried at 100 °C overnight. The as-synthesized sample was calcined in air under static conditions at 630 °C for 4 h. The molar composition of the $C_{16\text{-}3\text{-}1}$/TEOS/H_2SO_4/H_2O reaction mixture was 1:10:160:8000.

Characterization: The powder XRD pattern of the mesoporous silica was recorded on a STOE STADI powder diffractometer with $Cu_{K\alpha 1}$ (wavelength 1.5406 Å) radiation in the step-scan mode with tension = 40 kV and current = 50 mA. The rate of the measuring step was 0.02° min^{-1}. The scan range was $2\theta = 1.0$–8.0°.

Nitrogen adsorption–desorption measurements were conducted at −196 °C on an ASAP2020 Micromeritics instrument. The sample was outgassed for 6 h at 200 °C. The BET surface area was calculated from the relative pressure range of 0.05–0.20 on the adsorption branch. The total pore volume was estimated from the amount adsorbed at a relative pressure of 0.96. The pore-size distribution was analyzed using nonlocal density functional theory assuming the Tarazona model.

A JEOL JEM-2000FX microscope was used to obtain both HRTEM images and ED patterns at an accelerating voltage of 200 kV. The spherical aberration, convergence of angle, and spread of defocus were 1.00 mm, 0.50 mrad, and 80.00 Å, respectively. Images were recorded with a CCD camera (model Keen View, SIS analysis) with an image size of 1376 × 1032 pixels (pixel size = 23.5 × 23.5 μm^2). The observation was carried out at × 40000–120000 magnification under low-dose conditions of beam intensity.

After spattering gold particles on the specimen, SEM images were recorded by a JEOL 820 instrument operating at an accelerating voltage of 5 kV.

A 3D reconstruction technique using the HRTEM images obtained was carried out on the basis of the Fourier analysis, which enabled us to look into the features of the structure involved. CRISP (Calidris, version 2.1a) and Mathematica (Wolfram Research, version 5.0) software were used to extract FCs from the HRTEM images and for Fourier synthesis of FCs, respectively.

Received: April 12, 2006
Revised: July 7, 2006
Published online: September 5, 2006

Keywords: crystal growth · electron microscopy · mesoporous materials · silica · surfactants

[1] J. M. Kim, S. K. Kim, R. Ryoo, *Chem. Commun.* **1998**, 259.
[2] S. Guan, S. Inagaki, T. Ohsuna, O. Terasaki, *J. Am. Chem. Soc.* **2000**, *122*, 5660.
[3] O. Terasaki, T. Ohsuna; Z. Liu, Y. Sakamoto, A. E. Garcia-Bennett, *Stud. Surf. Sci. Catal.* **2004**, *148*, 261.
[4] a) S. Che, S. Kamiya, O. Terasaki, T. Tatsumi, *J. Am. Chem. Soc.* **2001**, *123*, 12089; b) S. Kamiya, H. Tanaka, S. Che, T. Tatsumi, O. Terasaki, *Solid State Sci.* **2003**, *5*, 197; c) S. Che, H. Li, S. Lim, Y. Sakamoto, O. Terasaki, T. Tatsumi, *Chem. Mater.* **2005**, *17*, 4103.
[5] S. Che, S. H. Lim, M. Kaneda, H. Yoshitake, O. Terasaki, T. Tatsumi, *J. Am. Chem. Soc.* **2002**, *124*, 13962.
[6] C. Yu, B. Tian, J. Fan, G. D. Stucky, D. Zhao, *J. Am. Chem. Soc.* **2002**, *124*, 4556.
[7] S. Che, Y. Sakamoto, O. Terasaki, T. Tatsumi, *Microporous Mesoporous Mater.* **2005**, *85*, 207.
[8] a) A. Carlsson, M. Kaneda, Y. Sakamoto, O. Terasaki, R. Ryoo, S. H. Joo, *J. Electron Microsc.* **1999**, *48*, 795; b) Y. Sakamoto, M. Kaneda, O. Terasaki, D. Zhao, J.-M. Kim, G. D. Stucky, H. J. Shin, R. Ryoo, *Nature* **2000**, *408*, 449.
[9] Q. Huo, R. Leon, P. M. Petroff, G. D. Stucky, *Science* **1995**, *268*, 1324.
[10] Y. Sakamoto, I. Diaz, O. Terasaki, D. Y. Zhao, J. Perez-Pariente, J. M. Kim, G. D. Stucky, *J. Phys. Chem. B* **2002**, *106*, 3118.
[11] S. Ino, *J. Phys. Soc. Jpn.* **1966**, *21*, 346.
[12] N. Doraiswamy, L. D. Marks, *Philos. Mag. B* **1995**, *71*, 291.
[13] L. D. Marks, *Rep. Prog. Phys.* **1994**, *57*, 603.
[14] S. Ino, *J. Phys. Soc. Jpn.* **1969**, *27*, 941.
[15] W. Zhou, H. M. A. Hunter, P. A. Wright, Q. Ge, J. M. Thomas, *J. Phys. Chem. B* **1998**, *102*, 6933.
[16] X. B. Zeng, G. Ungar, Y. S. Liu, V. Percec, A. E. Dulcey, J. K. Hobbs, *Nature* **2004**, *428*, 157.
[17] A. E. Garcia-Bennett, N. Kupferschmidt, Y. Sakamoto, S. Che, O. Terasaki, *Angew. Chem.* **2005**, *117*, 5451; *Angew. Chem. Int. Ed.* **2005**, *44*, 5317.

 © 2006 Wiley-VCH Verlag GmbH & Co. KGaA, Weinheim

Radical Reactions

DOI: 10.1002/anie.200601567

Radical Additions of Xanthates to Vinyl Epoxides and Related Derivatives: A Powerful Tool for the Modular Creation of Quaternary Centers**

*Nicolas Charrier, David Gravestock, and Samir Z. Zard**

Over the past ten years, we have developed a new radical chain process based on the degenerative exchange of a thiocarbonyl thio group (Z-C(=S)S-), and especially of xanthates (or dithiocarbonates, **1**).[1] This chemistry has provided a simple, efficient, and reasonably general solution to a longstanding problem in organic synthesis, namely the intermolecular creation of carbon–carbon bonds on non-activated alkenes. This degenerative exchange also constitutes the basis of the extremely powerful reversible addition fragmentation chain transfer/macromolecular design through interchange of xanthates (RAFT/MADIX) technology for the synthesis of block polymers.[2]

We have mainly used peroxides to initiate the radical addition, although irradiation with a tungsten halogen lamp was used when lower reaction temperatures were desired. The autooxidation of boranes, first reported by Brown and Midland,[3] and ingeniously exploited as a reaction initiating system by Oshima and co-workers,[4a,b] also proved to be quite efficient with xanthates, thereby allowing reactions to be performed at room temperature or below.[5,6] We have now found that the application of organoboranes to mediate the xanthate transfer is in fact far more powerful than initially anticipated. In particular, additions to vinyl epoxides and related derivatives have proved especially useful.

As outlined in Scheme 1, the addition of a radical R· derived from the xanthate **1** to the vinyl epoxide leads to opening of the epoxide ring and the formation of an alkoxy radical. The latter is rapidly intercepted by triethylborane to give a borinate and an ethyl radical, which propagates the chain reaction by reacting with the starting xanthate. Xanthates are highly radicophilic and a chain process can be readily sustained. As for the borinate intermediate, it is hydrolyzed on aqueous workup to afford the allylic alcohol **2**. Overall, combining the efficacious xanthate-transfer process with the use of triethylborane as both an initiator and controlling agent for quenching the highly reactive alkoxy radical results in a powerful C–C bond-forming process that is especially effective for the creation of quaternary centers.

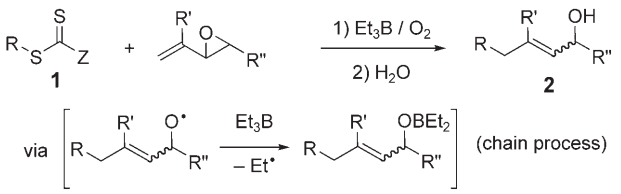

Scheme 1. Triethylborane-mediated radical addition of a xanthate to a vinyl epoxide.

Preliminary examples of this approach are shown in Scheme 2. Thus, exposure of the commercially available butadiene monoepoxide (**3**) and xanthate **4** to triethylborane and air gave rise to the corresponding allylic alcohol **5** in 60% yield (Scheme 2). This transformation parallels the ones reported by Brown and co-workers,[7] and later by the research groups of Oshima,[8] Roberts,[9a] and Kim.[9b] However, these pioneering studies were of rather limited synthetic scope because of severe constraints in the choice of substrates. Xanthates, in contrast, do not suffer from such limitations, as demonstrated by the other examples shown in Scheme 2. For example, reaction of xanthate **6** directly furnished the Weinreb amide **7** (in similar yield to that of the reaction that gave **5**), whereas the formation of allylic alcohols **9** and **11**, both containing a newly created quaternary center, proved to be even more efficient.

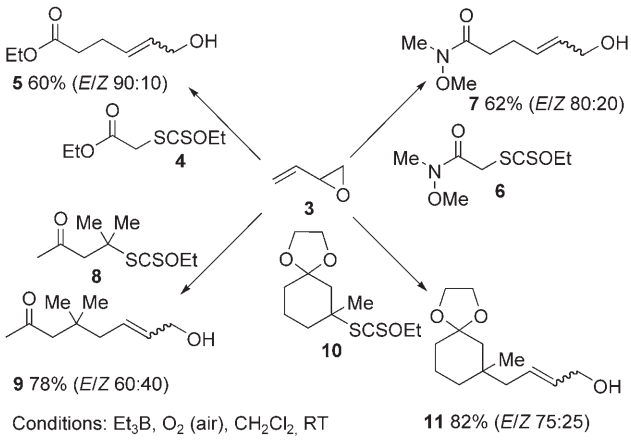

Scheme 2. Addition of various xanthates to butadiene monoepoxide.

The vinyl epoxide can be varied substantially, thus allowing the synthesis of more complex structures. Three such examples are shown in Scheme 3, in which xanthate **13**, a compound readily available by Michael addition of potassium *O*-ethyl xanthate to the cyclobutenone **12**[10] under acidic conditions, is used as the starting material.[11] The radical addition to epoxides **3**, **14**, and **15** provided the corresponding functionalized cyclobutanones **16**, **17**, and **18** in good yield, each containing a new quaternary center.

[*] N. Charrier, Dr. D. Gravestock, Prof. S. Z. Zard
Laboratoire de Synthèse Organique associé au CNRS (UMR 7652)
Département de Chimie
Ecole Polytechnique
91128 Palaiseau Cedex (France)
Fax: (+33) 1-6933-3851
E-mail: zard@poly.polytechnique.fr

[**] N.C. thanks the Ministère de l'Education Nationale, de la Recherche et de la Technologie (France) for a fellowship.

Supporting information for this article is available on the WWW under http://www.angewandte.org or from the author.

© 2006 Wiley-VCH Verlag GmbH & Co. KGaA, Weinheim

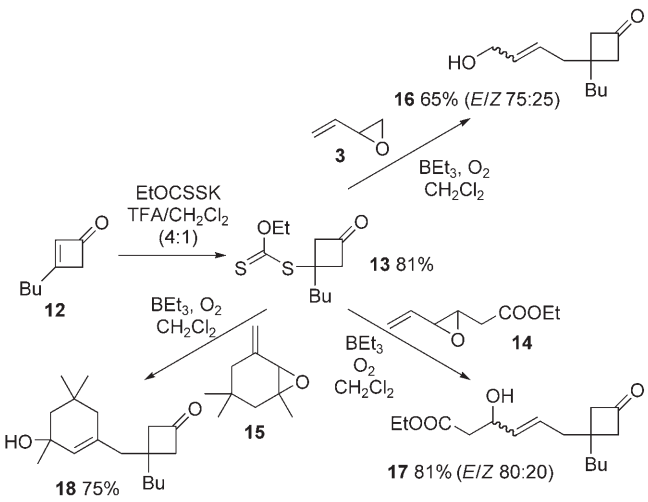

Scheme 3. Addition of a cyclobutanone xanthate to vinyl epoxides. TFA = trifluoroacetic acid.

The rapid assembly of intricate architectures can also be made by using a modular approach that depends on the unique ability of xanthates to add across non-activated olefins. This strategy is illustrated by the two sequences in Scheme 4. Thus, addition of xanthate **19** derived from

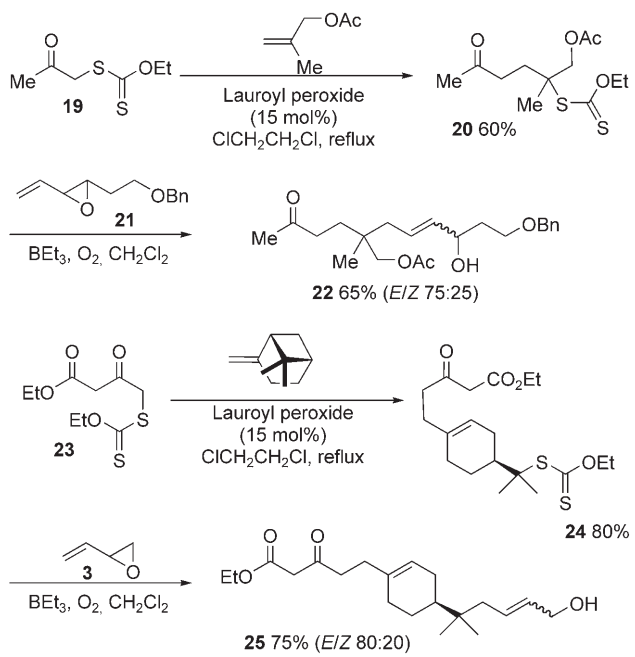

Scheme 4. Creation of quaternary centers by a modular approach. Bn = benzyl.

chloroacetone to methallyl acetate gave adduct **20** in 60% yield. Triethylborane-mediated addition to the functionalized vinyl epoxide **21** gave triol **22**, in which two of the alcohol groups are differentially protected. The xanthate entity has thus served to create two carbon–carbon bonds and at the same time to generate a quaternary center. Overall, the synthesis of triol **22** required just two steps from simple substrates. The second transformation leading to optically pure **25** incorporates a fragmentation of the cyclobutane ring of (−)-β-pinene. It was notable that the first addition of the ketoester xanthate **23** leading to the cyclohexene **24** occurs smoothly at the carbon atom bearing the least acidic hydrogen atoms. The ketoester motif in the final product **25** can be used for further manipulation.

This modular approach is not limited to the formation of quaternary centers; for example, it could be applied to alkenes bearing an ester or a carbonate as shown by the two transformations in Scheme 5. Radical addition of phenacyl

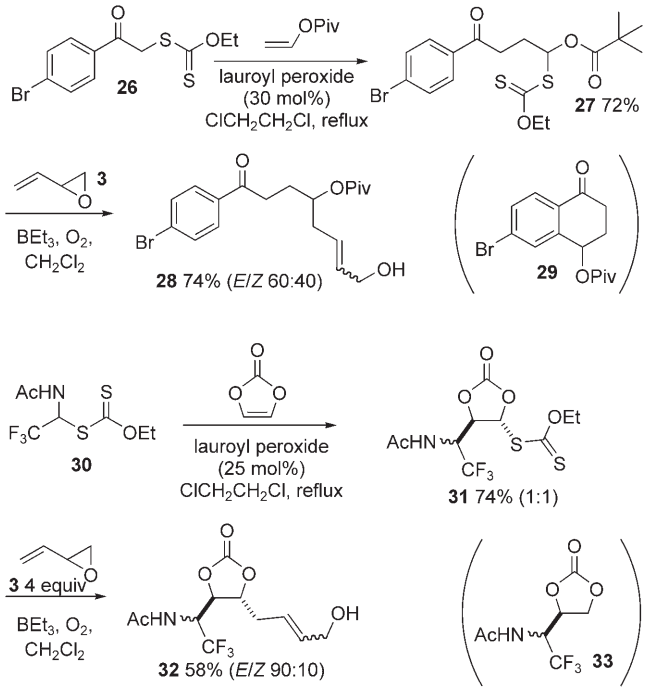

Scheme 5. Further modular assembly of complex structures. Piv = pivaloyl.

xanthate **26** to vinyl pivalate furnished adduct **27** in high yield, and exposure of the latter to vinyl epoxide **3** in the presence of triethylborane and air resulted in the clean formation of allylic alcohol **28**. Interestingly, no tetralone **29** was observed, indicating that the intermolecular addition of the intermediate radical to the vinyl epoxide **3** is faster than the intramolecular ring closure onto the aromatic nucleus, despite the modest radicophilicity of the non-activated vinyl group. We had previously reported that tetralones can be readily obtained by treatment of xanthates such as **27** with peroxide.[12] There is thus a considerable degree of flexibility in the way xanthates may be employed.

A more significant competition between the intermolecular addition process and intramolecular ring closure was observed with adduct **31**, derived from the addition of xanthate **30** to vinylidene carbonate.[13] The mixture of the two diastereoisomers of adduct **31** could be separated, but the subsequent triethylborane-mediated allylation of one of the two epimers to afford **32** occurred in only moderate yield

 © 2006 Wiley-VCH Verlag GmbH & Co. KGaA, Weinheim

(40%; *E*/*Z* 80:20), because of a competing hydrogen abstraction from the solvent to give **33** as the main side product. The reaction was repeated on the other epimer, but with the amount of vinyl epoxide increased to four equivalents and with the solvent 1,2-dichloroethane replaced by chloroform. The yield of **32** could thereby be improved to 58%. Interestingly, there was also a slight change in the ratio of the geometrical isomers (*E*/*Z* 90:10, Scheme 5).

By analogy with earlier studies by Brown and co-workers in which the addition of ethyl and cyclopentyl radicals (generated from the corresponding boranes) to alkynes was described,[14] we attempted a similar transformation involving the highly functionalized xanthate **34** derived from levulinic acid (Scheme 6).[15] The reaction with alkyne epoxide **35** was

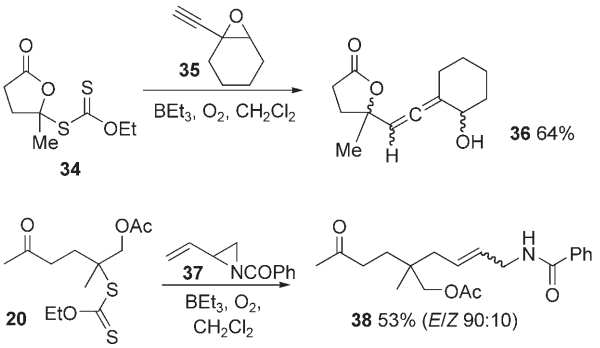

Scheme 6. Additions to an alkyne epoxide and to a vinyl aziridine.

somewhat sluggish, although clean and gave rise to the unusual allene **36**, which was isolated as a mixture of diastereoisomers. We also found it was possible to replace the epoxide by an aziridine ring (Scheme 6). The reaction of adduct **20** with aziridine **37** was also slow, but furnished **38** in useful yield (53%). As far as we are aware, vinylic aziridines have not hitherto been used in this manner.

It is clear from this preliminary study that the triethylborane-mediated radical reaction of xanthates with vinyl epoxides and vinyl aziridines represents a very powerful tool for the formation of carbon–carbon bonds under mild conditions. The approach is flexible, convergent, very easy to implement experimentally, and involves readily available starting materials and reagents. It is also worth noting that nonracemic products could be prepared by starting with optically pure vinyl epoxides, obtained for example by the kinetic resolution procedure developed by Jacobsen and co-workers.[16]

Experimental Section

Typical procedure for the radical addition on vinyl epoxides and aziridine: Triethylborane (1.0 M solution in hexane, 2 equiv) was added every 30 minutes over two hours to a stirred solution of the xanthate (1 equiv) and vinyl epoxide (2 equiv) in CH_2Cl_2 (1 mL mmol^{-1}) under nitrogen at room temperature. During the addition, the syringe needle was lowered into the solution. Furthermore, a small volume of air (about a quarter of the volume of the borane solution) was introduced by syringe following each addition of triethylborane. After stirring the reaction mixture overnight, the mixture was diluted with CH_2Cl_2 and then washed once with water and once with brine. The organic phase was dried over anhydrous $MgSO_4$, filtered, and concentrated. The residue was purified by chromatography on silica gel to give the desired products.

Received: April 20, 2006
Revised: August 5, 2006
Published online: September 14, 2006

Keywords: allylation · allylic alcohols · radical reactions · vinyl epoxides · xanthates

[1] a) B. Quiclet-Sire, S. Z. Zard, *Top. Curr. Chem.* **2006**, *264*, 201–236; b) S. Z. Zard in *Radicals in Organic Synthesis, Vol. 1* (Eds: P. Renaud, M. P. Sibi), Wiley-VCH, Weinheim, **2001**, pp. 90–108; c) B. Quiclet-Sire, S. Z. Zard, *Phosphorus Sulfur Silicon Relat. Elem.* **1999**, *153–154*, 137–154; d) B. Quiclet-Sire, S. Z. Zard, *J. Chin. Chem. Soc.* **1999**, *46*, 139–145; e) S. Z. Zard, *Angew. Chem.* **1997**, *109*, 724–737; *Angew. Chem. Int. Ed. Engl.* **1997**, *36*, 672–685.

[2] a) For recent reviews on RAFT/MADIX polymerization, see: G. Moad, E. Rizzardo, S. H. Thang, *Aust. J. Chem.* **2005**, *58*, 379–410; S. Perrier, P. Takolpuckdee, *J. Polym. Sci. Part A* **2005**, *43*, 5347–5393; b) for the original patents, see: P. Corpart, D. Charmot, T. Biadatti, S. Z. Zard, D. Michelet, Int. Pat. 9858974 [*Chem. Abstr.* **1999**, *130*, 82018]; T. P. Le, G. Moad, E. Rizzardo, S. H. Thang, Int. Pat. 9801478 [*Chem. Abstr.* **1998**, *128*, 115390].

[3] a) H. C. Brown, M. M. Midland, *Angew. Chem.* **1972**, *84*, 702–710; *Angew. Chem. Int. Ed. Engl.* **1972**, *11*, 692–700; b) M. M. Midland, H. C. Brown, *J. Am. Chem. Soc.* **1973**, *95*, 4069–4070.

[4] a) K. Nozaki, K. Oshima, K. Utimoto, *J. Am. Chem. Soc.* **1987**, *109*, 2547–2550; b) K. Nozaki, K. Oshima, K. Utimoto, *Bull. Chem. Soc. Jpn.* **1987**, *60*, 3465–3467; for recent and comprehensive reviews on organoboranes as a source of radicals, see: c) C. Ollivier, P. Renaud, *Chem. Rev.* **2001**, *101*, 3415–3434; d) V. Darmency, P. Renaud, *Top. Curr. Chem.* **2006**, *263*, 71–106.

[5] a) N. Legrand, PhD Thesis, Ecole Polytechnique (France), **2001**; b) M. E. Briggs, S. Z. Zard, *Synlett* **2005**, 334–337; c) L. Jean-Baptiste, S. Yemets, R. Legay, T. Lequeux, *J. Org. Chem.* **2006**, *71*, 2352–2359.

[6] The use of triethylborane/O_2 worked efficiently for most xanthates, except α-xanthyl ketones, which proved to be capricious. The problem was traced to an unexpected reduction which gave the parent ketone. It appears that the spin density on the oxygen atom in the intermediate α-ketoradical is sufficient to induce attack on triethylborane before the addition to the olefin actually occurs. Hydrolysis upon workup of the enol boronate gave the ketone. Analogous reduction of iodides were previously observed by Oshima and co-workers and very recently exploited by Lambert and Danishefsky in the total synthesis of UCS1025A: a) K. Nozaki, K. Oshima, K. Utimoto, *Bull. Chem. Soc. Jpn.* **1991**, *64*, 403–409; b) T. H. Lambert, S. J. Danishefsky, *J. Am. Chem. Soc.* **2006**, *128*, 426–427.

[7] A. Suzuki, N. Miyaura, M. Itoh, H. C. Brown, G. W. Holland, E.-I. Negishi, *J. Am. Chem. Soc.* **1971**, *93*, 2792–2793.

[8] a) Y. Ichinose, K. Oshima, K. Utimoto, *Chem. Lett.* **1988**, 1437–1440; b) S. Tanaka, T. Nakamura, H. Yorimitsu, K. Oshima, *Synlett* **2002**, 569–572.

[9] a) H.-S. Dang, B. P. Roberts, *Tetrahedron Lett.* **1992**, *33*, 6169–6172; b) S. Kim, S.-Y. Jon, *Bull. Korean Chem. Soc.* **1995**, *16*, 472–474.

[10] For the preparation of cyclobutenone **12**, see: A. A. Frimer, H. Pizem, *Tetrahedron* **1999**, *55*, 12175–12186.

[11] G. Binot, B. Quiclet-Sire, T. Saleh, S. Z. Zard, *Synlett*, **2003**, 382–387.

 © 2006 Wiley-VCH Verlag GmbH & Co. KGaA, Weinheim

[12] a) A. Cordero Vargas, B. Quiclet-Sire, S. Z. Zard, *Org. Lett.* **2003**, *5*, 3717 – 3719; b) N. Legrand, B. Quiclet-Sire, S. Z. Zard, *Tetrahedron Lett.* **2000**, *41*, 9815 – 9818; c) A. Liard, B. Quiclet-Sire, R. N. Saicic, S. Z. Zard, *Tetrahedron Lett.* **1997**, *38*, 1759 – 1762.
[13] F. Gagosz, S. Z. Zard, *Org. Lett.* **2003**, *5*, 2655 – 2657.
[14] A. Suzuki, N. Miyaura, M. Itoh, H. C. Brown, *Synthesis* **1973**, 305 – 306.
[15] S. K. Bagal, L. Tournier, S. Z. Zard, *Synlett* **2006**, 1485 – 1490.
[16] M. Tokunaga, J. F. Larrow, F. Kakiuchi, E. N. Jacobsen, *Science* **1997**, *277*, 936 – 938.

 © 2006 Wiley-VCH Verlag GmbH & Co. KGaA, Weinheim

Amination

DOI: 10.1002/anie.200601612

Monodentate Phosphines Provide Highly Active Catalysts for Pd-Catalyzed C–N Bond-Forming Reactions of Heteroaromatic Halides/Amines and (H)N-Heterocycles**

*Kevin W. Anderson, Rachel E. Tundel, Takashi Ikawa, Ryan A. Altman, and Stephen L. Buchwald**

Despite advances in the scope of palladium-catalyzed C–N bond-forming reactions through the development of more active catalysts,[1,2] limitations to the method still remain: 1) In many cases the coupling of substituted heteroaryl halides with amines is still problematic; 2) the N-arylation reactions of nitrogen heterocycles is limited in scope with respect to both coupling partners; 3) chemoselectivity in C–N bond-forming processes has not been explored in great detail.

Palladium catalysts based on dialkylphosphinobiaryl ligands[1b,3] have not only been shown to display high stability, but also have manifested increased reactivity in palladium-catalyzed carbon–carbon,[4] carbon–nitrogen,[1b,3] and carbon–oxygen[1b,5] bond-forming reactions. Our previous studies indicated that a catalyst system based on Pd/2-dicyclohexylphosphino-2′,4′,6′-triisopropylbiphenyl (XPhos; **1**; Cy = cyclohexyl) demonstrated both a greater degree of activity and stability than those derived from our previous generations of ligands.[6] The substitution of the 2′,2′-positions on the lower aromatic ring prevents palladacycle formation,[7] and the added bulk causes the equilibrium to shift from that favoring [L_2Pd^0] to one in which [L_1Pd^0] predominates, thus facilitating all steps in the catalytic cycle.[7–10]

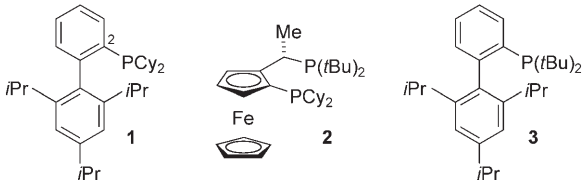

Recently, a long-lived catalyst based on the combination of a Pd precatalyst and bidentate Josiphos-type ligand **2** was shown to provide good results for the coupling of highly functionalized aryl/heteroaryl chlorides and primary amines.[11] It was postulated that the high reactivity of the system was, to a significant extent, as a result of the tight chelation of **2** to the Pd center, thus decreasing the chance for the binding of a heterocycle or basic amine, which may facilitate the loss of the ligand or otherwise deactivate the catalyst. Although this is an extremely reasonable supposition, we wondered whether, in fact, the use of chelating ligands was necessary for successful reactions with substrates of this type. Herein, we report our results which indicate that monodentate phosphines are viable alternatives to and are sometimes superior to chelating ligands in Pd-catalyzed C–N bond-forming processes.

We first explored the coupling of 4-chlorophenol and *n*-hexylamine (Table 1). Ligand **1** proved to be ineffective for this reaction, with its use resulting in incomplete conversion and lower yields as a result of diarylation (Table 1, entries 1 and 2). Interestingly, we found that the combination of **3** as the ligand and lithium hexamethyldisilazide (LiHMDS)[12] as the base was the most effective for this transformation at 50 °C, thus providing the product in 94 % yield in 2 h (Table 1, entry 6). This system is also proficient at room temperature, as the aryl amine is provided in 94 % yield, although the reaction required 46 h to go to completion (Table 1, entry 4). While Josiphos-type ligand **2** was reported to perform well at 100 °C for a similar transformation, its efficiency was far less than **3** at 40 °C (Table 1, compare entry 3 vs entry 5).

We previously disclosed that a catalyst system comprised of a Pd precatalyst and **1** displayed excellent chemoselectivity for reaction at an aniline NH_2 group over that of a primary amide.[6a] We have found that use of [$Pd_2(dba)_3$]/**1** (dba = dibenzylideneacetone) and LiHMDS allows the reaction of aliphatic primary and cyclic secondary amines with a substrate containing a primary amide (3-chlorobenzamide), which has been problematic with previous catalyst systems

[*] K. W. Anderson, R. E. Tundel, T. Ikawa, R. A. Altman, Prof. Dr. S. L. Buchwald
Department of Chemistry, Room 18–490
Massachusetts Institute of Technology
Cambridge, MA 02139 (USA)
Fax: (+1) 617-253-3297
E-mail: sbuchwal@mit.edu

[**] We thank the National Institutes of Health (GM 58160) and the National Cancer Institute (Cancer Training Grant GM 5-T32-CAO9112-30) for support of this work. R.E.T. would like to thank Pfizer for a SURF fellowship and MIT (UROP) for financial support. T.I. thanks the Uehara Memorial Foundation for a fellowship. We are grateful to Merck, Amgen, and Engelhard ($Pd(OAc)_2$) for additional support. The Bruker Advance 400 MHz instrument used in this study was purchased with funding from the National Institutes of Health (GM 1S10RR13886-01), and the Varian 300 and 500 MHz instruments were purchased with funding from the National Science Foundation (CHE 9808061 and DBI 9729592).

Supporting information for this article is available on the WWW under http://www.angewandte.org or from the author.

 © 2006 Wiley-VCH Verlag GmbH & Co. KGaA, Weinheim

Table 1: Ligands used for the coupling of 4-chlorophenol and *n*-hexylamine.

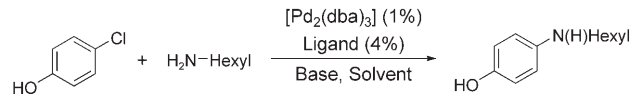

Entry	Ligand	Base	Solvent	*T* [°C]	*t* [h]	Conv. [%]	Yield [%][a]
1	**1**	$LiN(TMS)_2$	THF	40	24	84	31[b]
2	**1**	NaO*t*Bu	toluene	100	24	44	15[b]
3[c]	**2**	$LiN(TMS)_2$	THF	40	24	17	2[b]
4	**3**	$LiN(TMS)_2$	THF	RT	46	>99	94
5	**3**	$LiN(TMS)_2$	THF	40	24	>99	94
6	**3**	$LiN(TMS)_2$	toluene	50	2	>99	94
7	**3**	NaO*t*Bu	toluene	100	24	>99	89

[a] Yield of the isolated product. [b] Yield determined by GC analysis. [c] Reagents and condition: ligand **2**, octylamine, $LiN(TMS)_2$, 1,4-dioxane, 100 °C; yield = 72 %.[11] TMS = trimethylsilyl.

(Table 2).[12] 2-Aminohaloheterocycles have previously been inefficient electrophilic components for C–N bond-forming processes with monophosphine ligands. Thus, we examined the coupling of 2-amino-5-chloropyridine with aniline and morpholine (with **1**) and benzylamine (with **3**) and were pleased to find that these reactions proceeded in good yield.

The use of 2-aminoheterocycles as a nucleophilic component had only successfully been accomplished with aryl bromides utilizing a Pd/XantPhos[13] or binaphthol (BINAP)[14] catalyst system. A common belief is that using a bidentate ligand would prevent any coordination to a Pd^{II} species of the "guanidine-like" moiety of these substrates. Thus, the discovery that a catalyst comprised of $[Pd_2(dba)_3]$ and **3** was effective in the N-arylation of 2-aminopyridine was somewhat surprising. We explored the use of Pd/**3** for a diverse array of reaction combinations.[15] Substrates bearing a free hydroxy and indole –NH group react well with 2-aminopyridine and 2-aminopyrimidine, respectively, providing 92 and 57 % of the resultant diaryl amines (Table 3). In accord with the previous results, reaction at the heteroaromatic $-NH_2$ group prevails over that at a primary amide and provides 94 % yield in the coupling of 5-bromonicotinamide and 2-aminopyridine.[15]

Table 2: Chemoselectivity in Pd-catalyzed amination.

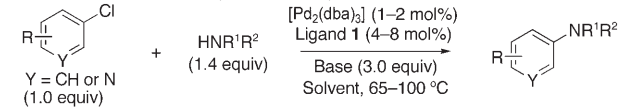

Product	Yield [%]
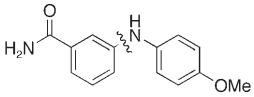	79[a,b] 82[a,c]
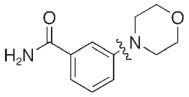	81[d]
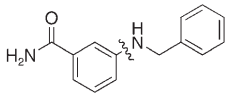	83[d]
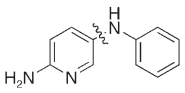	89[d]
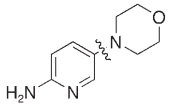	79[d]
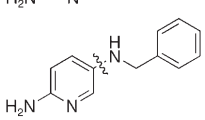	77[d,e]

[a] Previously reported, see Ref. [6a]. [b] K_2CO_3 in *t*BuOH, 100 °C, 20 h. [c] NaO*t*Bu in toluene, 100 °C, 18 h. [d] $LiN(TMS)_2$ in THF, 65 °C, 16–24 h. [e] Ligand **3** was used.

Table 3: Palladium-catalyzed N-arylation of aminoheterocycles.

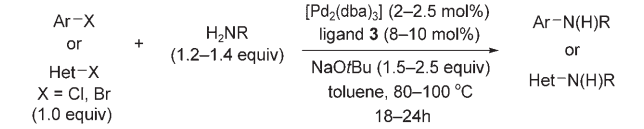

Product	X	Yield [%]
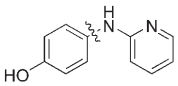	Cl	92
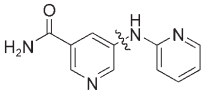	Br	94
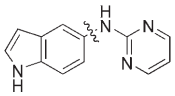	Br	57[a]
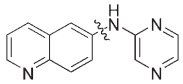	Cl	60[a]
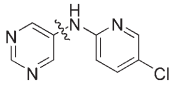	Br	75
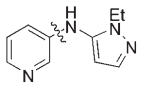	Cl	74[b]

[a] Cs_2CO_3 and *N*,*N*-dimethylformamide used as base and solvent, respectively. [b] 1,4-Dioxane used as solvent.

Prior work on the N-arylation of indoles and pyrroles revealed that catalytic systems based on monophosphinobiaryl ligands were somewhat effective.[16] In contrast, more acidic heterocycles, such as indazole or pyrazole, have not been reported to be coupling partners in palladium-based methods. Given our success with the Pd/**3** combination for the coupling of less basic 2-aminoheterocycles (Table 3), we felt that it might also be quite effective for the coupling of these nitrogen heterocycles. Indazole/pyrazole are expected to be less basic than their indole/pyrrole counterparts,[17] thus a more bulky phosphine moiety might speed up reductive elimination from a Pd aryl/amido intermediate.[18]

We first explored the N-arylation of indazole with 3-bromoanisole using Pd/**3** with K_3PO_4 in 1,4-dioxane at 100 °C. This system provided 52 % conversion and 48 % yield (GC) of the N1-arylated product exclusively; a result which is also

 © 2006 Wiley-VCH Verlag GmbH & Co. KGaA, Weinheim

observed for the coupling of aryl iodides using Cu-catalysis methodology.[19] Optimization of the reaction conditions revealed that use of the bases NaO*t*Bu (toluene, 80 °C) and Cs_2CO_3 (1,4-dioxane, 105 °C) provided the N1-arylated indazole in excellent yields using $[Pd_2(dba)_3]$/**3**. Interestingly, when NaO*t*Bu is used as the base at 100 °C, mixtures of the N1- and N2-arylated products were observed. One explanation for this result is that **I** (Scheme 1) is the kinetically

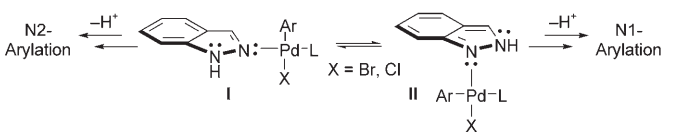

Scheme 1. Hypothesis for chemoselectivity in the N-arylation of indazole.

formed species (binding at the lone pair of electrons on N1 would disrupt the aromaticity, **I'**). At 80 °C (with NaO*t*Bu) or 105 °C with Cs_2CO_3, conversion into **II** occurs faster than deprotonation. As is seen in Table 4, indazole is arylated with

Table 4: Palladium-catalyzed N-arylation of indazole and pyrazole.

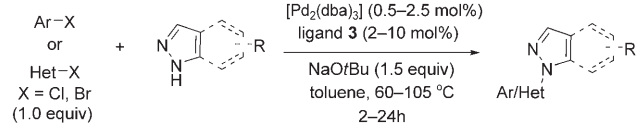

Product	R	X	*T* [°C]	Yield [%]
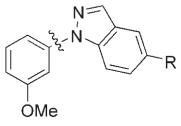	H	Cl	80	97
	NO_2	Br	80	91
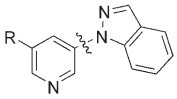	H	Cl	80	97
	CN	Br	60	62
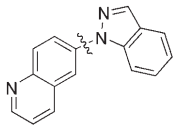	–	Cl	80	99
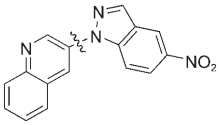	–	Br	90	92
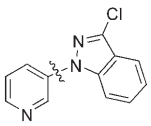	–	Br	60	79
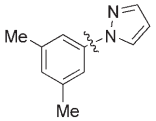	–	Br	80	88
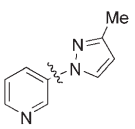	–	Cl	105	76

3-chloroanisole, 3-chloropyridine, 5-bromonicotinonitrile, and 6-chloroquinoline in respectable yields. Also, 5-nitroindazole is effectively treated with 3-bromoanisole and 3-bromoquinoline, thus providing the N-arylated heterocycles in 93 and 89% yields, respectively. Further, for the first time, pyrazole is efficiently combined with an aryl bromide and aryl chloride using a palladium catalyst.

To our knowledge, palladium-catalyzed amination reactions of benzimidazole and/or imidazole with unactivated aryl halides have not been accomplished.[20] As is seen in Table 5, the use of the especially hindered ligand **4** facilitates C–N bond-formation of these weakly basic nitrogen nucleophiles. Benzimidazole is coupled with 3-bromoquinoline and 4-chlorotoluene and provides the

Table 5: Palladium-catalyzed *N*-arylation of imidazole and benzimidazole.

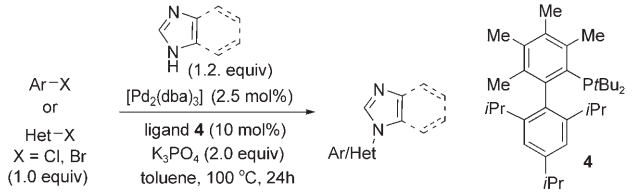

Product	X	Yield [%]
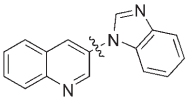	Br	94
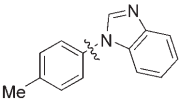	Cl	97
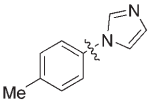	Br	70[a]

[a] With *N*,*N*-dimethylaniline used as solvent.

N-arylated products in 94 and 97% yields, respectively (Table 5). Imidazole is combined with 4-bromotoluene in a 70% yield, thus representing the first known palladium-catalyzed example of this coupling with an unactivated aryl bromide. Here the use of **4** may be necessary to facilitate the rate of reductive elimination from a $[L_1Pd(Ar)(N\text{-}Het)]$ intermediate.[21]

We have also explored the coupling of some amino-heterocycles and/or pyrazole substrates (Table 6). The results that we have obtained, in some cases, complement those previously seen with Cu-catalyzed protocols. The chemoselectivity of the aniline NH_2 group causes it to react in preference to the indazole –NH group, thus providing a 67% yield in the reaction of 5-aminoindazole with 5-bromo-*m*-xylene. We were particularly surprised to find that 5-amino-3-phenylpyrazole could be selectively arylated at the primary amino group, which is the first time, to our knowledge, that an unprotected aminopyrazole has ever reacted with this mode

 © 2006 Wiley-VCH Verlag GmbH & Co. KGaA, Weinheim

Table 6: Interesting chemoselectivity in palladium-catalyzed C–N bond formation.

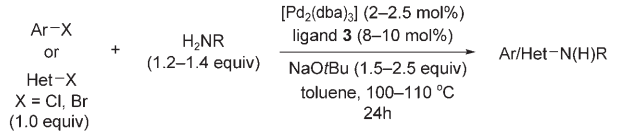

Product	Yield [%]	Product	Yield [%]
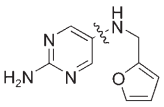	72	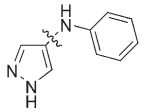	94
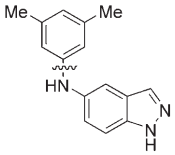	67	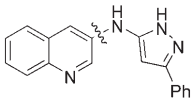	88

of chemoselectivity in a metal-catalyzed C–N bond-forming process. For example, we have previously shown with Cu catalysts that aminopyrazoles react preferentially at the pyrazole –NH group, thus representing complementarity between the Pd- and Cu-based methods.[19] Finally, for the first time a free (H)N-bromopyrazole can be successfully aminated, in this case with aniline as shown.

In conclusion, we have developed highly reactive catalysts based on palladium and dialkylbiarylphosphino ligands, particularly **1**, **3**, or **4**. These provide unprecedented reactivity and selectivity in C–N bond-forming processes. The bulky monophosphine catalyst system Pd/**1** was effective for the reaction of aryl/heteroaryl halides bearing primary amides and 2-aminoheterocycles. Also, the more sterically encumbered catalyst systems based on Pd and ligands **3** or **4** were found to be more proficient for the arylation of 2-aminoheterocycles and weakly basic HN heterocycles: pyrazoles, indazole, benzimidazole, and imidazole. The chemoselectivity of these catalysts was explored and the rough order of reactivity for amines follows the general trend: aryl amines $\gg$ primary and secondary aliphatic amines $>$ 2-aminoheteroaromatics $>$ primary amides $\approx$ HN heterocycles. We hypothesize that the efficacy of palladium catalysts based on ligands **1**, **3**, or **4** is attributed to a combination of factors: 1) A maximization of the amount of L_1Pd intermediates, thus speeding the desired catalytic process relative to different modes of catalyst decomposition; 2) providing quasi-stable [L_1Pd], [$L_1Pd(Ar)X$], and [$L_1Pd(Ar)$amido] intermediates because the size of these complexes slows bimolecular decomposition processes and because of stabilizing Pd/arene interactions; 3) providing [$L_1Pd(Ar)$amido] intermediates with especially sterically demanding ligand L_1 facilitates the rate of reductive elimination in forming the product. Further, this study demonstrates that monodentate ligands are viable alternatives to and sometimes superior to chelating ligands in Pd-catalyzed C–N bond-forming processes.

Received: April 24, 2006
Published online: September 6, 2006

Keywords: amination · chemoselectivity · palladium · phosphines

[1] a) J. F. Hartwig in *Handbook on Organopalladium Chemistry for Organic Synthesis* (Ed.: E. Negishi), Wiley-Interscience, New York, **2002**, p. 1051; b) L. Jiang, S. L. Buchwald in *Metal-Catalyzed Cross-Coupling Reactions* (Eds.: A. de Meijere, F. Diederich), 2nd ed., Wiley-VCH, Weinheim, **2004**, p. 699.
[2] a) D.-Y. Lee, J. F. Hartwig, *Org. Lett.* **2005**, 7, 1169; b) M. W. Hooper, M. Utsunomiya, J. F. Hartwig, *J. Org. Chem.* **2003**, *68*, 3861; c) S. Harkal, F. Rataboul, A. Zapf, C. Fuhrmann, T. Riermeier, A. Monsees, M. Beller, *Adv. Synth. Catal.* **2004**, *346*, 1742; d) M. V. Nandakumar, J. G. Verkade, *Angew. Chem.* **2005**, *117*, 5040; *Angew. Chem. Int. Ed.* **2005**, *44*, 3115; e) M. S. Viciu, R. M. Kissling, E. D. Stevens, S. P. Nolan, *Org. Lett.* **2002**, *4*, 2229.
[3] J. P. Wolfe, H. Tomori, J. Yin, J. Sadighi, S. L. Buchwald, *J. Org. Chem.* **2000**, *65*, 1158.
[4] S. D. Walker, T. E. Barder, J. R. Martinelli, S. L. Buchwald, *Angew. Chem.* **2004**, *116*, 1907; *Angew. Chem. Int. Ed.* **2004**, *43*, 1871.
[5] A. V. Vorogushin, X. Huang, S. L. Buchwald, *J. Am. Chem. Soc.* **2005**, *127*, 8146.
[6] a) X. Huang, K. W. Anderson, D. Zim, L. Jiang, A. Klapars, S. L. Buchwald, *J. Am. Chem. Soc.* **2003**, *125*, 6653; b) E. R. Strieter, D. G. Blackmond, S. L. Buchwald, *J. Am. Chem. Soc.* **2003**, *125*, 13978.
[7] E. R. Strieter, S. L. Buchwald, *Angew. Chem.* **2006**, *118*, 939; *Angew. Chem. Int. Ed.* **2006**, *45*, 925.
[8] a) F. Paul, J. Patt, J. F. Hartwig, *J. Am. Chem. Soc.* **1994**, *116*, 5969; b) J. F. Hartwig, F. Paul, *J. Am. Chem. Soc.* **1995**, *117*, 5373.
[9] For other studies with aryl chlorides, see: a) M. Portnoy, D. Milstein, *Organometallics* **1993**, *12*, 1665; b) A. F. Littke, G. C. Fu, *Angew. Chem.* **2002**, *114*, 4350; *Angew. Chem. Int. Ed.* **2002**, *41*, 4176.
[10] E. Galardon, S. Ramdeehul, J. M. Brown, A. Cowley, K. K. Hii, A. Jutand, *Angew. Chem.* **2002**, *114*, 1838; *Angew. Chem. Int. Ed.* **2002**, *41*, 1760.
[11] Q. Shen, S. Shekhar, J. P. Stambuli, J. F. Hartwig, *Angew. Chem.* **2005**, *117*, 1395; *Angew. Chem. Int. Ed.* **2005**, *44*, 1371.
[12] For the use of $LiN(TMS)_2$ to enhance the substrate scope, see: M. C. Harris, X. Huang, S. L. Buchwald, *Org. Lett.* **2002**, *4*, 2885.
[13] J. Yin, M. M. Zhao, M. A. Huffman, J. M. McNamara, *Org. Lett.* **2002**, *4*, 3481.
[14] T. H. M. Jonckers, B. U. W. Maes, G. L. F. Lemiere, R. Dommisse, *Tetrahedron* **2001**, *57*, 7027.
[15] To date, 2-aminobenzothiazole and 2-aminothiazole could not be N-arylated by using Pd/**3** or other monophosphine catalyst systems; these amino heterocycles inhibit the normally successful coupling of simple aryl halides and aniline, thus indicating their roles as catalyst poisons.
[16] a) G. Mann, J. F. Hartwig, M. S. Driver, C. Fernandez-Rivas, *J. Am. Chem. Soc.* **1998**, *120*, 827; b) J. F. Hartwig, M. Kawatsura, S. I. Hauck, K. H. Shaughness, L. M. Alcazar-Roman, *J. Org. Chem.* **1999**, *64*, 5575; c) D. W. Old, M. C. Harris, S. L. Buchwald, *Org. Lett.* **2000**, *2*, 1403.
[17] Pyrrole: $K_a = 23.0$ (DMSO); indole: $K_a = 20.95$ (DMSO); pyrazole: $K_a = 19.8$ (DMSO); see: F. G. Bordwell, *Acc. Chem. Res.* **1988**, *21*, 456.
[18] a) J. F. Hartwig, S. Richards, D. Baranano, F. Paul, *J. Am. Chem. Soc.* **1996**, *118*, 3626; b) M. S. Driver, J. F. Hartwig, *J. Am. Chem. Soc.* **1997**, *119*, 8232; c) A. H. Roy, J. F. Hartwig, *J. Am. Chem. Soc.* **2001**, *123*, 1232.
[19] J. C. Antilla, J. M. Baskin, T. E. Barder, S. L. Buchwald, *J. Org. Chem.* **2004**, *69*, 5578.

 © 2006 Wiley-VCH Verlag GmbH & Co. KGaA, Weinheim

[20] For two examples of N-arylation of imidazole using palladium catalysts of an activated aryl/heteroaryl halide, see: a) Y. Wan, M. Alterman, A. Hallberg, *Synthesis* **2002**, 1597; b) M. B. Andrus, S. N. Mettath, C. Song, *J. Org. Chem.* **2002**, *67*, 8284.
[21] a) C. H. Burgos, T. E. Barder, H. Huang, S. L. Buchwald, *Angew. Chem.* **2006**, *118*, 4427; *Angew. Chem. Int. Ed.* **2006**, *45*, 4321; b) M. C. Willis, G. N. Brace, I. P. Holmes, *Synthesis* **2005**, 3229.

 © 2006 Wiley-VCH Verlag GmbH & Co. KGaA, Weinheim

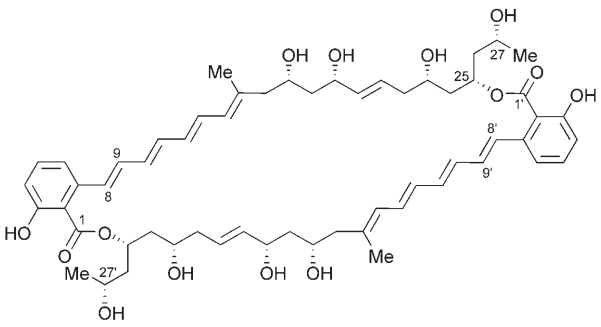

1: marinomycin A (*trans* $\Delta^{8,9}$, *trans* $\Delta^{8',9'}$)
2: marinomycin B (*cis* $\Delta^{8,9}$, *cis* $\Delta^{8',9'}$)
3: marinomycin C (*trans* $\Delta^{8,9}$, *cis* $\Delta^{8',9'}$)

Scheme 1. Structures of marinomycins A–C (**1**–**3**).

Natural Product Synthesis

DOI: 10.1002/anie.200601867

Total Synthesis of Marinomycins A–C**

K. C. Nicolaou, Andrea L. Nold, Robert R. Milburn, and Corinna S. Schindler*

Marinomycins A–C (**1**–**3**, Scheme 1) are recently discovered natural products with imposing molecular architectures and impressive biological properties.[1] Isolated from actinomycete *Marinispora* strain CNQ-140 cultured from a sediment collected from the bottom of the ocean offshore of La Jolla, California (USA), by Fenical and co-workers,[1] these novel compounds exhibit significant antibiotic activities (minimum inhibitory concentration, MIC = 0.1–0.6 μM) against methicillin-resistant *Staphylococcus aureus* (MRSA) and vancomycin-resistant *Enterococcus faecium* (VREF), and inhibit cancer cell proliferation against the National Cancer Institute's 60 cancer cell line panel (LC_{50} = 0.2–2.7 μM). In particular, these marinomycins **1**–**3** showed potent and selective cytotoxicities against six of the eight melanoma cell lines of that panel.[1] Their novel and sensitive polyunsaturated structures coupled with their potentially useful biological activities prompted our interest in these molecules. Herein, we report the total synthesis of marinomycins A–C (**1**–**3**) and of two of their hitherto unknown monomeric homologues, mono-marinomycin A (**m-1**) and *iso*-mono-marinomycin A (**m-2**, Scheme 7).

Given that **1**, the most abundant of the marinomycins, is photolytically convertible to a mixture of all three (i.e. **1**, **2**, and **3**),[1] a total synthesis of marinomycin A (**1**) would constitute syntheses of **2** and **3** as well. Scheme 2 depicts our

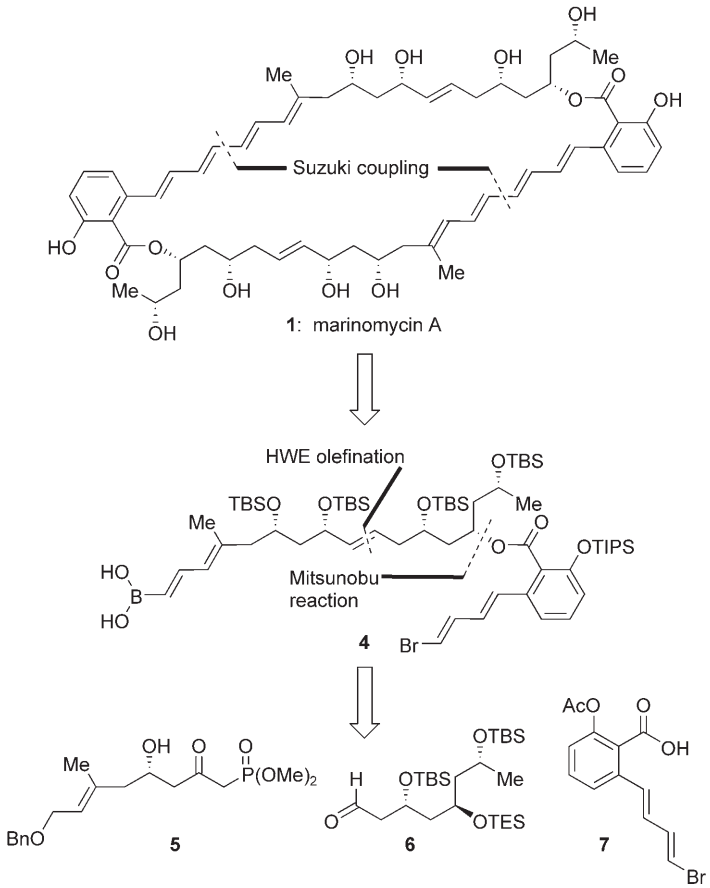

Scheme 2. Retrosynthetic analysis of marinomycin A (**1**). HWE = Horner–Wadsworth–Emmons, TBS = *tert*-butyldimethylsilyl, TES = triethylsilyl.

[*] Prof. Dr. K. C. Nicolaou, A. L. Nold, Dr. R. R. Milburn, C. S. Schindler
Department of Chemistry and
The Skaggs Institute for Chemical Biology
The Scripps Research Institute
10550 North Torrey Pines Road, La Jolla, CA 92037 (USA)
Fax: (+1) 858-784-2469
E-mail: kcn@scripps.edu
and
Department of Chemistry and Biochemistry
University of California, San Diego
9500 Gilman Drive, La Jolla, CA 92093 (USA)

[**] We thank Professor William Fenical for helpful discussions and Dr. Hak Cheol Kwon for assistance in the HPLC purification of synthetic marinomycins A–C. The assistance of Dr. D. H. Huang and Dr. R. Chadha with spectroscopic and X-ray crystallographic analyses, respectively, is also acknowledged. Financial support for this work was provided by a grant from the National Institutes of Health (USA) and the Skaggs Institute of Chemical Biology, the Pfeiffer Foundation (predoctoral fellowship to A.L.N.), and the Kurt Fordan Foundation (Germany) (fellowship to C.S.S.).

Supporting information for this article is available on the WWW under http://www.angewandte.org or from the author.

© 2006 Wiley-VCH Verlag GmbH & Co. KGaA, Weinheim

original retrosynthetic analysis of marinomycin A (**1**). The symmetrical structure of the molecule renders it suitable for several retrosynthetic disconnections; the one shown in Scheme 2 was chosen to highlight and test the Suzuki reaction as a means to construct large and complex macrocycles.[2] The appropriately functionalized vinyl boronic acid vinyl bromide **4** needed for the originally intended dimerization was traced to the three key building blocks ketophosphonate **5**, aldehyde **6**, and carboxylic acid **7**, through the indicated Horner–Wadworth–Emmons (HWE) olefination and Mitsunobu reactions. It was expected that dimer versus monomer formation in the cyclization process would be subject to concentration conditions.

The required building blocks **5**–**7** were synthesized in their enantiomerically pure forms as summarized in Schemes 3–5. Starting with the construction of ketophosphonate **5** (Scheme 3), the enantiomerically pure epoxide **8**[3] was regioselectively opened in the presence of $BF_3{\cdot}OEt_2$ with the lithium reagent derived from propargylic ether **9**[4] and *n*BuLi at −78 °C, leading to the corresponding secondary alcohol (89 % yield), whose silylation (TBSCl, 96 % yield) and de-*p*-methoxybenzylation (DDQ, 79 % yield) afforded the chain-extended propargylic alcohol **10**. Exposure of the latter compound to Red-Al, followed by addition of NIS, furnished the corresponding hydroxy vinyl iodide (66 % yield), whose temporary silylation (TMSCl) and subsequent coupling with $ZnMe_2$ in the presence of $[Pd(dppf)Cl_2]$ (cat.) gave, upon basic (K_2CO_3, MeOH) workup, the corresponding primary allylic alcohol (81 % yield). Benzylation of the latter compound (88 % yield) followed by desilylation (HF·py, 77 % yield) and oxidation with PCC afforded aldehyde **13** (73 % yield). Reaction of aldehyde **13** with the lithium species derived from dimethyl methyl phosphonate and *n*BuLi followed by oxidation (PDC) of the resulting epimeric mixture of alcohols led to ketophosphonate **14** in 64 % overall yield (two steps). Finally, fluoride-induced (aq HF/MeCN) desilylation of **14** gave the desired hydroxy ketophosphonate **5** in 92 % yield.

The synthesis of fragment **6** began with the readily available aldehyde **15**[5] and involved two iterations of Brown allylation[6] [(+)-$(ipc)_2$B-allyl]/ozonolysis (PPh_3) sequences with appropriate protections of the resulting secondary alcohols (Scheme 4). Proceeding through intermediates **16**–**18**, this sequence afforded the desired compound **6** in good overall yield (47 % from **15**, six steps) and with high diastereoselectivity (>40:1 d.r.).

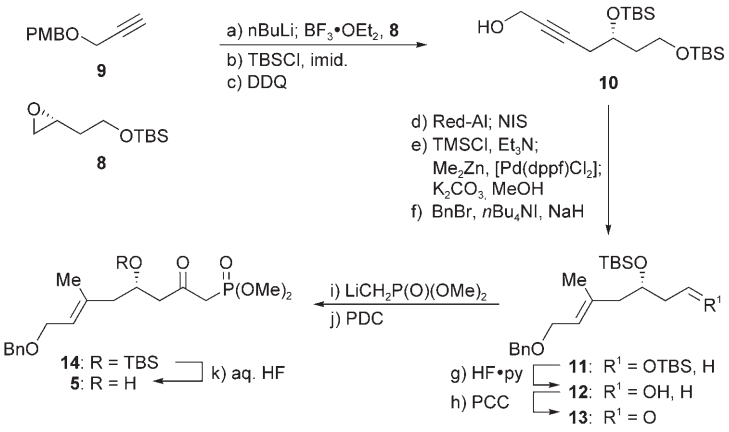

Scheme 3. Preparation of ketophosphonate **5**. Reagents and conditions: a) **9** (2.0 equiv), *n*BuLi (2.5 M in hexanes, 2.0 equiv), THF, −78 °C, 45 min; then $BF_3{\cdot}OEt_2$ (1.2 equiv), **8** in THF, −78 °C, 4 h, 89 %; b) TBSCl (1.2 equiv), imid. (3.0 equiv), DMF, 25 °C, 6 h, 96 %; c) DDQ (1.5 equiv), CH_2Cl_2, pH 7 phosphate buffer, 25 °C, 3 h, 79 %; d) Red-Al (3.33 M in toluene, 1.7 equiv), THF, 25 °C, 45 min; then NIS (1.8 equiv), THF, −78 °C, 30 min, 66 %; e) TMSCl (2.0 equiv), Et_3N (5.0 equiv), 25 °C, 2 h; then $[Pd(dppf)Cl_2]$ (0.05 equiv), Me_2Zn (2.0 equiv), THF, 65 °C, 12 h; then K_2CO_3 (0.1 equiv), MeOH, 25 °C, 4 h, 81 %; f) NaH (1.6 equiv), BnBr (1.7 equiv), nBu_4NI (0.1 equiv), THF, 25 °C, 6 h, 88 %; g) HF·py, THF, 0 °C, 3 h, 77 %; h) PCC (2.0 equiv), $NaHCO_3$ (0.5 equiv), 25 °C, 3 h, 73 %; i) $CH_3P(O)(OMe)_2$ (4.0 equiv), *n*BuLi (2.5 M in hexanes, 4.0 equiv), THF, −78 °C, 2 h; then **13** in THF, −78 °C, 2 h; j) PDC (2.1 equiv), 4-Å M.S., DMF, 25 °C, 12 h, 64 % over two steps; k) HF (48 % aq), MeCN, 25 °C, 3 h, 92 %. Bn = benzyl, DDQ = 2,3-dichloro-5,6-dicyano-1,4-benzoquinone, dppf = bis(diphenylphosphino)ferrocene, DMF = *N*,*N*-dimethylformamide, imid. = imidazole, PMB = *p*-methoxybenzyl, M.S. = molecular sieves, NIS = *N*-iodosuccinimide, PCC = pyridinium chlorochromate, PDC = pyridinium dichromate, py = pyridine, THF = tetrahydrofuran, TMS = trimethylsilyl.

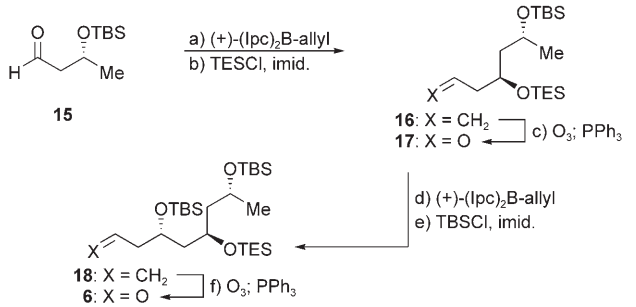

Scheme 4. Preparation of aldehyde **6**. Reagents and conditions: a) (−)-B(Ipc)$_2$OMe (1.7 equiv), allylMgBr (1.0 M in Et_2O, 1.7 equiv), Et_2O, −78→25 °C, 2 h; then **15** in Et_2O, −78 °C, 4 h, −78→25 °C, 1 h, 95 % (>40:1 d.r.); b) TESCl (1.8 equiv), imid. (4.0 equiv), DMF, 25 °C, 4 h; c) O_3, CH_2Cl_2, −78 °C, 4 h; then PPh_3 (1.3 equiv), −78 °C, 2 h, −78→25 °C, 1 h, 64 % over two steps; d) (−)-B(Ipc)$_2$OMe (1.7 equiv), allylMgBr (1.0 M in Et_2O, 1.7 equiv), Et_2O, −78→25 °C, 2 h; then **17** in Et_2O, −78 °C, 4 h, −78→25 °C, 1 h, 85 % (>40:1 d.r.); e) TBSCl (2.0 equiv), imid. (5.0 equiv), DMF, 25 °C, 4 h; f) O_3, CH_2Cl_2, −78 °C, 4 h; then PPh_3 (1.3 equiv), −78 °C, 2 h, −78→25 °C, 1 h, 91 % over two steps. Ipc = isopinocampheyl.

The dienyl bromide carboxylic acid **7** was synthesized from known acetonide acetylene **19**[7] (Scheme 5). Thus, **19** was reacted with the adduct of $BH_3{\cdot}THF$ with 2,5-dimethylhexa-2,4-diene,[8] and the resulting borane (87 % yield) was coupled with commercially available TMS vinyl bromide **20** in the presence of $[Pd(PPh_3)_4]$ (cat.) and Cs_2CO_3 to afford TMS diene **21** (89 % yield). Exposure of the latter compound, **21**, to NBS gave bromide **22** (88 % yield), which was converted into acetoxy carboxylic acid **7** through saponification (KOH, 87 % yield) and acetylation (Ac_2O, $Mg(ClO_4)_2$;[9] 96 % yield).

The assembly of fragments **5**–**7** and elaboration of the growing molecule to the targeted enyne bromide **28** is shown in Scheme 6. Thus, coupling of ketophosphonate **5** and aldehyde **6** proceeded smoothly under the influence of $Ba(OH)_2$ to afford the enone in 95 % yield. Hydroxy-directed reduction of this enone with Et_2BOMe and $NaBH_4$[10] at

 © 2006 Wiley-VCH Verlag GmbH & Co. KGaA, Weinheim

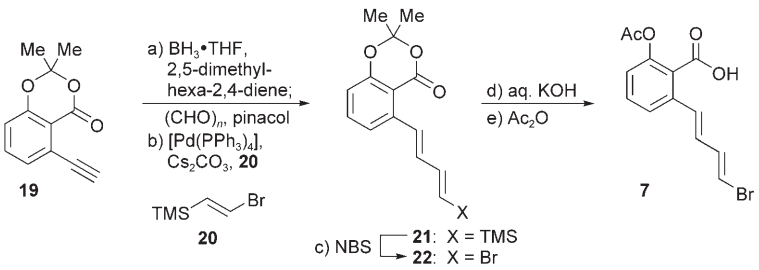

Scheme 5. Preparation of aryl diene fragment **7**. Reagents and conditions: a) 2,5-dimethylhexa-2,4-diene (5.5 equiv), BH_3·THF (2.5 equiv), THF, 0 °C, 3 h; then **19**, 0 °C, 1.5 h; then H_2O, 0→25 °C, 1 h; then $(CH_2O)_n$, 25 °C, 1 h; then pinacol (2.0 equiv), 25 °C, 24 h, 87%; b) $[Pd(PPh_3)_4]$ (0.1 equiv), Cs_2CO_3 (10 equiv), **20** (1.3 equiv), THF/H_2O (2:1), 55 °C, 1 h, 89%; c) NBS (1.2 equiv), MeCN, 25 °C, 15 min, 88%; d) KOH (5.0 equiv), THF/H_2O (1:1), 55 °C, 18 h, 87%; e) $Mg(ClO_4)_2$ (0.03 equiv), Ac_2O (1.1 equiv), 25 °C, 48 h, 96%. NBS = *N*-bromosuccinimide.

ized in pure form by preparative plate chromatography (silica, CH_2Cl_2/MeOH 93:7, two elutions) in the dark, followed by HPLC (C18-Dynamax column, 60 Å, 10 mm × 250 mm, 45% MeCN in H_2O). *iso*-Mono-marinomycin A (**m-2**) yielded crystals (mp: 213 °C (dec.), $CDCl_3$-D_3COD) that were suitable for X-ray crystallographic analysis (see ORTEP representation, Figure 1),[13] which confirmed its assigned structure as well as that of its sibling, mono-marinomycin A (**m-1**) and their precursors. The NOESY, ROESY, and COSY NMR data were also consistent with the assigned structures of **m-1** (Table 1) and **m-2**.

Having realized the propensity of dienyl bromide boronic acid **4** to cyclize before dimerization, −78 °C resulted in the exclusive formation of the corresponding allylic alcohol (89% yield), whose silylation (TBSCl) led to the fully protected hexaol **23** (89% yield). The benzyl group was then cleaved from the terminal oxygen atom of this compound, **23**, with Ca in liquid NH_3 (75% yield), and the resulting primary alcohol was oxidized with DMP to furnish aldehyde **25** (87% yield). Enyne **26** was then generated from aldehyde **25** upon acetylene installment ($TMSCHN_2$-LDA;[11] 85% yield) and selective desilylation (TES) with PPTS in ethanol (77% yield). Accompanied by inversion of configuration at C25 (marinomycin numbering scheme), the Mitsunobu reaction between hydroxy compound **26** and carboxylic acid **7** (DEAD, PPh_3) proceeded in 93% yield to afford ester **27**. Exchanging the Ac groups for a TIPS group (K_2CO_3, MeOH; TIPSOTf, 2,6-lut.) then furnished the targeted bromo enyne **28** in excellent yield (92% overall). This latter switch of protecting groups was necessary because of difficulties encountered in the subsequent hydroboration and Suzuki coupling steps using the Ac-protected and free phenol carboxylic acid variants of **28**.

The stage was now set for the anticipated Suzuki dimerization/cyclization in the hope of reaching marinomycins A–C (see Scheme 7). Thus, the required boronic acid **4** was generated from enyne **28** by reaction with catecholborane and catalytic amounts of dicyclohexylborane (THF, 25 °C; then H_2O) and exposed to the action of TlOEt (4.0 equiv) and $[Pd(PPh_3)_4]$ (cat.) in THF/H_2O (4:1) at ambient temperature[12] and 0.01 M concentration, to afford, much to our surprise, only the monomeric product **29** (72% yield over the two steps). Increasing the concentration (up to 1.0 M) did not have much effect on the outcome of this reaction, suggesting that the precursor had a well-preorganized disposition towards cyclization once the palladium species was inserted. However, the use of 300 equivalents of TlOEt produced, in addition to **29**, the dimeric product **1** in approximately 2% yield (see Scheme 6), after global desilylation. Fluoride-induced global desilylation (TBAF) of **29** (see Scheme 7) gave the all-*trans* 22-membered ring **m-1** (mono-marinomycin A) and the all-*trans* 24-membered ring **m-2** (*iso*-mono-marinomycin A), where the lactone had shifted during desilylation, in 85% yield as a separable 1:1 mixture. The mono-marinomycins A (**m-1** and **m-2**) were isolated and character-

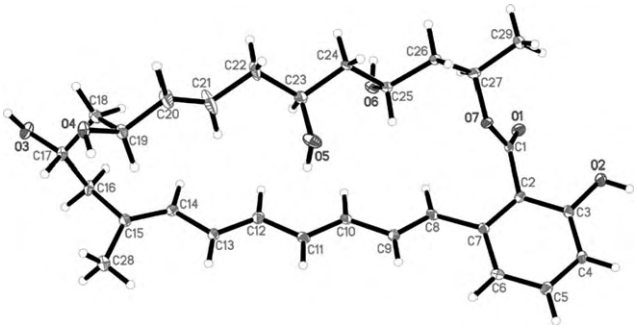

Figure 1. ORTEP representation of *iso*-mono-marinomycin A (**m-2**) with thermal ellipsoids shown at the 30% probability level. Hydrogen atoms are shown as white spheres.

we resorted to a stepwise approach to marinomycins A–C. The same key building blocks, **7** (Scheme 5), **26** (Scheme 6), and **28** (Scheme 6) were required, and the revised strategy is continued in Scheme 6. Thus, regioselective hydroboration of hydroxy enyne **26** with catecholborane catalyzed by dicyclohexylborane gave the corresponding boronic acid, whose Suzuki coupling (KOH (10 equiv), $[Pd(PPh_3)_4]$ (cat.), THF/H_2O (4:1)) with dienyl bromide **28** (0.67 equiv) led to hydroxy polyene **30** (63% yield based on **28**). Mitsunobu reaction of the latter compound, **30**, with carboxylic acid **7** proceeded with inversion of configuration at C25′ to afford, after exchange of the Ac group for a TIPS group, enyne ester **31** (78% overall yield for the three steps; Table 1).

Reaction of enyne **31** with catecholborane under the catalytic influence of dicyclohexylborane (THF, 25 °C) furnished, after H_2O quench, the corresponding boronic acid, which was, without isolation, treated with $[Pd(PPh_3)_4]$ (stoichiometric) and TlOEt (300 equiv) at ambient temperature to afford the fully protected macrocycle **32**. The product was used without purification in the next step, which involved global deprotection of **32** to give marinomycin A (**1**) in 23% overall yield for the three steps from **31**. Synthetic marinomycin A (**1**) was purified by HPLC (C8-Luna 5μ column, 100 Å, 250 mm × 10 mm, 60% MeCN in H_2O) and exhibited identical physical properties (R_f, R_t, UV spectral, α_D^{25}, mass

 © 2006 Wiley-VCH Verlag GmbH & Co. KGaA, Weinheim

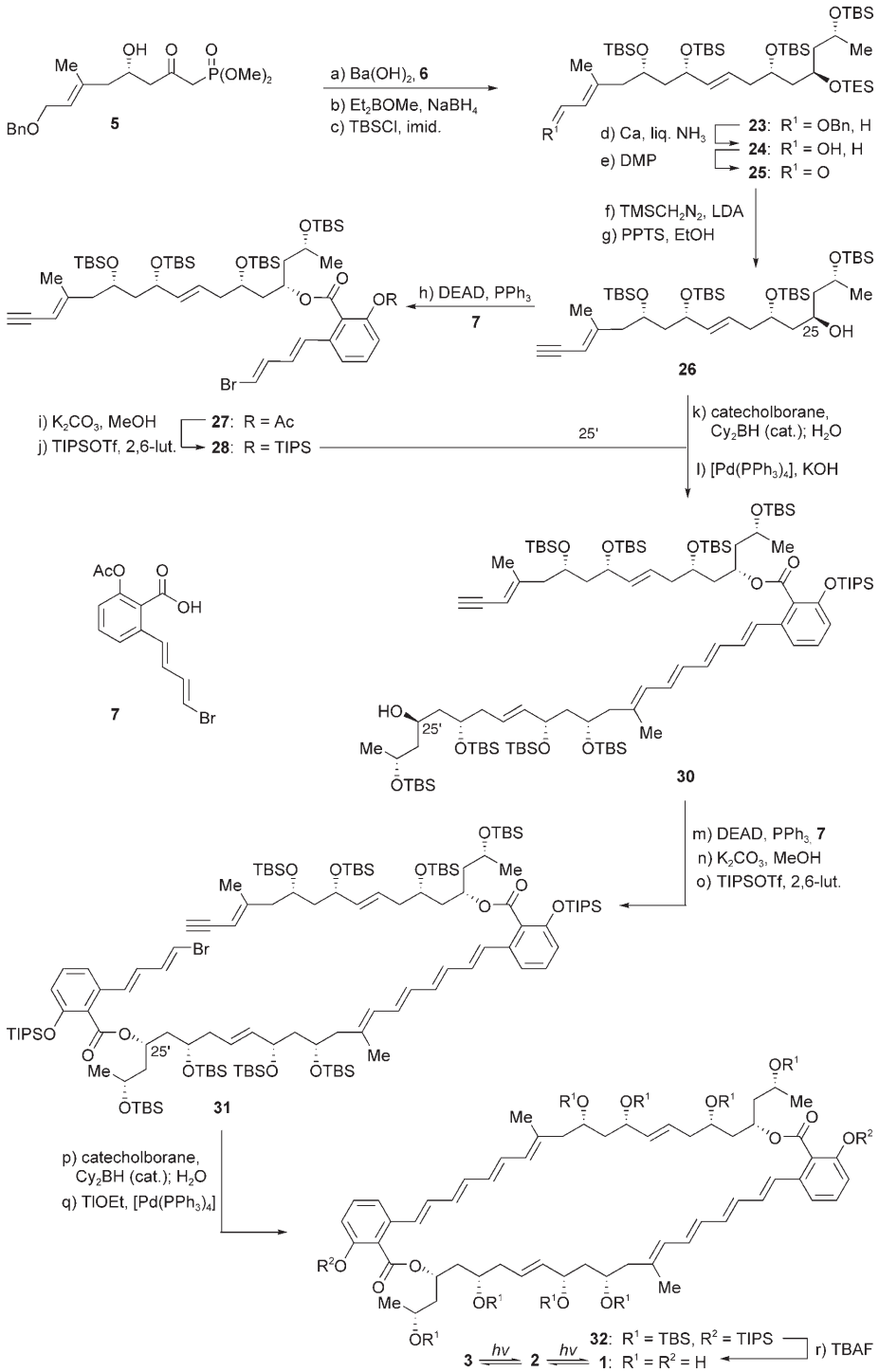

Scheme 6. Preparation of Suzuki coupling precursor **28** and completion of the total synthesis of marinomycins A–C (**1**–**3**). Reagents and conditions: a) **5** (1.0 equiv), **6** (1.1 equiv), $Ba(OH)_2{\cdot}H_2O$ (0.75 equiv), THF/H_2O (20:1), 25 °C, 1 h, 95%; b) Et_2BOMe (1.0 M in THF, 1.1 equiv), $NaBH_4$ (1.1 equiv), THF/MeOH (4:1), −78 °C, 3 h, 89%; c) TBSCl (4.0 equiv), imid. (8.0 equiv), DMF, 25 °C, 8 h, 89%; d) **23** in THF/*i*PrOH (3:1); then liq. NH_3; then Ca (30 equiv), −78 °C, 1 h, 75%; e) DMP (1.6 equiv), $NaHCO_3$ (10 equiv), CH_2Cl_2, 25 °C, 30 min, 87%; f) iPr_2NH (1.8 equiv), *n*BuLi (2.5 M in hexanes, 1.5 equiv), THF, −78→0 °C, 30 min, $TMSCH_2N_2$ (1.5 equiv), THF, −78 °C, 30 min; then **25**, −78 °C , 1 h, −78→25 °C, 2 h, 85%; g) PPTS (0.1 equiv), EtOH, 25 °C, 3 h, 77%; h) DEAD (6.0 equiv), PPh_3 (6.0 equiv), **7** (6.0 equiv), THF, 25 °C , 1 h, 93%; i) K_2CO_3 (0.05 equiv), THF/MeOH (1:1), 25 °C, 15 min; j) TIPSOTf (30 equiv), 2,6-lut. (60 equiv), CH_2Cl_2, 25 °C, 18 h, 92% over two steps; k) catecholborane (3.0 equiv), Cy_2BH (0.1 M in THF, 0.2 equiv), THF, 25 °C, 1 h; then H_2O (5.0 equiv); l) KOH (10 equiv), $[Pd(PPh_3)_4]$ (0.1 equiv), THF/H_2O (4:1), 25 °C, 1 h, 63% based on **28**; m) DEAD (6.0 equiv), PPh_3 (6.0 equiv), **7** (6.0 equiv), THF, 25 °C, 1 h; n) K_2CO_3 (0.05 equiv), THF/MeOH (1:1), 25 °C, 15 min; o) TIPSOTf (30 equiv), 2,6-lut. (60 equiv), CH_2Cl_2, 25 °C, 18 h, 78% over three steps; p) catecholborane (3.0 equiv), Cy_2BH (0.1 M in THF, 0.2 equiv), THF, 25 °C, 1 h; then H_2O (5.0 equiv); q) TlOEt (300 equiv), $[Pd(PPh_3)_4]$ (1.0 equiv), THF/H_2O (10:1), 25 °C, 4 h; r) TBAF (50 equiv), THF, 25 °C, 18 h, 23% over three steps. Cy = cyclohexyl, DMP = Dess–Martin periodinane, DEAD = diethyl azodicarboxylate, LDA = lithium diisopropylamide, lut. = lutidine, PPTS = pyridinium *p*-toluenesulfonate, TBAF = tetra-*n*-butylammonium fluoride, Tf = trifluoromethanesulfonyl, TIPS = triisopropylsilyl.

 © 2006 Wiley-VCH Verlag GmbH & Co. KGaA, Weinheim

Table 1: Selected physical properties for compounds **m-1** and **31**.

m-1: $R_f = 0.54$ (silica gel, $CHCl_3$/MeOH/H_2O 40:9:1); $[\alpha]_D^{37} = -276.6$ ($c = 0.06$, $CDCl_3$); IR (film): $\tilde{\nu}_{max} = 3352, 2926, 2851, 1709, 1656, 1595, 1449, 1376, 1259, 1218, 1118, 1065, 999\ cm^{-1}$; ^1H NMR (600 MHz, $CDCl_3$): $\delta = 7.35$ (t, $J = 7.8$ Hz, 1H), 7.13 (d, $J = 14.4$ Hz, 1H), 6.92 (d, $J = 8.4$ Hz, 1H), 6.77 (d, $J = 7.2$ Hz, 1H), 6.47 (dd, $J = 14.4$, 11.4 Hz, 1H), 6.34 (t, $J = 11.4$ Hz, 1H), 6.16–6.03 (m, 3H), 5.91 (d, $J = 10.8$ Hz, 1H), 5.38–5.20 (m, 3H); 4.16 (br, 1H, OH), 4.06 (m, 1H), 3.95 (m, 1H), 3.71 (t, $J = 9.0$ Hz, 1H), 3.65 (m, 1H), 3.58 (br, 1H, OH), 3.29 (br, 1H, OH), 2.56 (d, $J = 10.8$ Hz, 1H), 2.19 (d, $J = 13.8$ Hz, 1H), 2.14 (t, $J = 10.8$ Hz, 1H), 1.97–1.85 (m, 4H), 1.88 (s, 3H), 1.79–1.75 (m, 2H), 1.70–1.62 (m, 3H), 1.20 ppm (d, $J = 6.0$ Hz, 3H); ^{13}C NMR (150 MHz, $CDCl_3$): $\delta = 171.9, 162.4, 141.7, 135.8, 135.3, 134.6, 134.5, 133.3, 132.8, 131.9, 131.1, 130.3, 129.7, 128.2, 120.1, 117.0, 73.1, 72.5, 66.4, 65.8, 65.6, 50.4, 48.3, 45.5, 43.8, 42.5, 23.4, 17.8, 14.2$ ppm; HRMS (ESI-TOF) calcd for $C_{29}H_{38}O_7Na$ [M+Na^+]: 521.2510; found: 521.2530.

31: $R_f = 0.57$ (silica gel, hexanes/EtOAc, 8:1); $[\alpha]_D^{37} = -98.8$ ($c = 0.09$, CH_2Cl_2); IR (film): $\tilde{\nu}_{max} = 2952, 2828, 2856, 1729, 1570, 1465, 1255, 835, 775\ cm^{-1}$; ^1H NMR (600 MHz, C_6D_6, mixture of two rotamers around the aryl–carbonyl bond, ca. 1:1 ratio): $\delta = 7.15$ ($J = 8.4$ Hz, 1H), 7.11 (d, $J = 8.4$ Hz, 1H), 7.03–6.96 (m, 2H), 6.94–6.89 (m, 3H), 6.85 (dd, $J = 15.6$, 10.8 Hz, 1H), 6.75 (d, $J = 7.8$ Hz, 1H), 6.72 (d, $J = 7.8$ Hz, 1H), 6.61 (dd, $J = 13.2$, 13.2 Hz, 1H), 6.55 (dd, $J = 13.8$, 11.4 Hz, 1H), 6.49–6.37 (m, 2H), 6.31 (dd, $J = 15.6$, 10.8 Hz, 1H), 6.16 (d, $J = 11.4$ Hz, 1H), 6.03 (d, $J = 13.8$ Hz, 1H), 5.85 (dt, $J = 15.0$, 7.2 Hz, 1H), 5.83 (dt, $J = 15.0$, 7.2 Hz, 1H), 5.66 (dd, $J = 15.6$, 7.2 Hz, 1H), 5.59 (dd, $J = 15.6$, 7.2 Hz, 1H), 5.51–5.45 (m, 2H), 5.46 (s, 1H), 4.38 (q, $J = 7.2$ Hz, 1H), 4.28 (q, $J = 7.2$ Hz, 1H), 4.16–4.05 (m, 6H), 2.83 (d, $J = 2.4$ Hz, 1H), 2.49–2.40 (m, 4H), 2.33–2.25 (m, 2H), 2.23–2.10 (m, 6H), 2.05–1.92 (m, 5H), 2.04 (s, 3H), 1.86 (s, 3H), 1.85–1.79 (m, 2H), 1.70 (ddd, $J = 13.2$, 7.2, 4.8 Hz, 1H), 1.35–1.28 (m, 12H), 1.19–1.16 (m, 36H), 1.07 (s, 9H), 1.06 (s, 9H), 1.06 (s, 27H), 1.05 (s, 9H), 1.02 (s, 9H), 1.01 (s, 9H), 0.28 (s, 3H), 0.26 (s, 6H), 0.23 (s, 3H), 0.21 (s, 3H), 0.20 (s, 3H), 0.19 (s, 3H), 0.19 (s, 3H), 0.19 (s, 3H), 0.16 (s, 6H), 0.15 (s, 3H), 0.15 (s, 3H), 0.14 (s, 3H), 0.14 (s, 3H), 0.12 ppm (s, 3H); ^{13}C NMR (150 MHz, C_6D_6, mixture of rotamers around the aryl–carbonyl bond, ca. 1:1 ratio): $\delta = 167.4$ (0.5 C), 167.4 (0.5 C) 167.1, 153.9, 153.8 (0.5 C), 153.8 (0.5 C), 150.8, 137.8 (3 C), 137.7, 137.2, 137.1, 136.4, 136.2 (0.5 C), 136.2 (0.5 C), 135.7, 132.4 (0.5 C), 132.3 (0.5 C), 131.5 (0.5 C), 130.9 (0.5 C), 130.9, 130.1, 130.1 (0.5 C), 130.0, 129.9 (0.5 C), 129.1, 129.0, 126.5 (0.5 C), 126.4 (0.5 C), 126.3 (0.5 C), 126.2 (0.5 C), 118.1, 117.9, 117.9, 117.4, 110.6, 110.4 (0.5 C), 110.3 (0.5 C), 107.8, 81.9, 80.7, 72.0, 71.9 (0.5 C), 71.8 (0.5 C), 71.5, 71.4, 69.8 (0.5 C), 69.7 (0.5 C), 68.7, 68.2, 66.5, 66.4 (2 C), 51.7, 48.6, 47.4, 47.2, 46.7, 45.6, 45.5, 42.6, 42.5, 41.0, 30.2, 26.3 (9 C), 26.2 (9 C), 26.2 (3 C), 26.2 (3 C), 24.5, 24.4, 20.3, 18.3 (8 C), 17.9 (12 C), 12.7 (6 C), −3.4, −3.4, −3.8 (2 C), −3.9 (3 C), −3.9, −4.0, −4.1 (4 C), −4.2, −4.3, −4.4 ppm; HRMS (ESI-TOF) calcd for $C_{124}H_{226}BrO_{14}Si_{10}$ [$M-H^-$]: 2298.3853; found: 2298.3852.

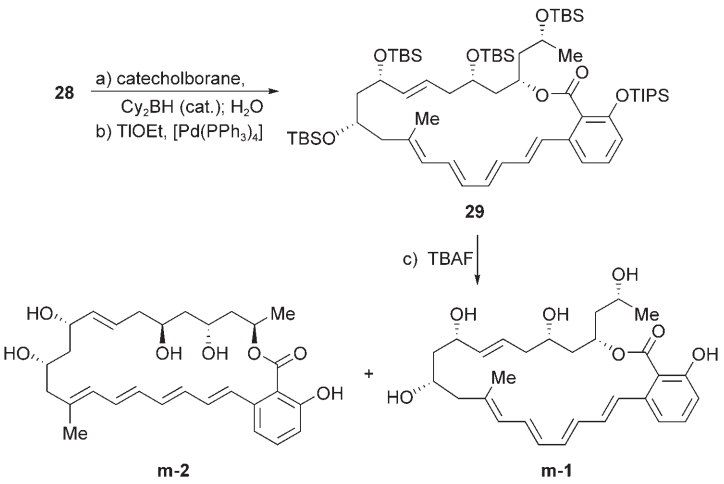

Scheme 7. Formation of mono-marinomycins **m-1** and **m-2**. Reagents and conditions: a) catecholborane (3.0 equiv), Cy_2BH (0.1 M in THF, 0.2 equiv), THF, 25 °C, 1 h; then H_2O (5.0 equiv); b) TlOEt (4.0 equiv), [$Pd(PPh_3)_4$] (0.1 equiv), THF/H_2O (4:1), 25 °C, 30 min, 72% over two steps; c) TBAF (30 equiv), THF, 18 h, 85% yield.

spectrometric, and ^1H and ^{13}C NMR spectral data) to those recorded for the naturally occurring substance.[1,14] When allowed to isomerize in ambient light, marinomycin A (**1**) formed mixtures with marinomycins B (**2**) and C (**3**) as previously reported (**1**/**2**/**3** ≈ 16:2:9 after 30 min; ca. 1:1:1 after 2 h by HPLC).[1,15]

The success of the Suzuki reaction in these syntheses underscores its usefulness in the construction of complex molecules. Besides rendering the naturally occurring marinomycins A–C (**1**–**3**) readily available, the described synthetic technology also provides access to their monomeric derivatives, mono-marinomycin A (**m-1**) and its isomer *iso*-mono-marinomycin A (**m-2**), and opens the way to the construction of other members of the class of natural or designed origins.

Received: May 11, 2006
Revised: June 28, 2006
Published online: September 15, 2006

Keywords: antibiotics · antitumor agents · natural products · Suzuki coupling · total synthesis

[1] H. C. Kwon, C. A. Kauffman, P. R. Jensen, W. Fenical, *J. Am. Chem. Soc.* **2006**, *128*, 1622. We thank Professor William Fenical for a preprint of this article.
[2] For selected examples of Suzuki macrocyclizations, see: a) J. D. White, R. Hanselmann, R. W. Jackson, W. J. Porter, Y. Ohba, T. Tiller, S. Wang, *J. Org. Chem.* **2001**, *66*, 5217; b) J. T. Njardarson, K. Biswas, S. Danishefsky, *Chem. Commun.* **2002**, *23*, 2759; c) G. A. Molander, F. Dehmel, *J. Am. Chem. Soc.* **2004**, *126*, 10313; d) B. Wu, Q. Liu, G. A. Sulikowski, *Angew. Chem.* **2004**, *116*, 6841; *Angew. Chem. Int. Ed.* **2004**, *43*, 6673.
[3] D. R. Williams, S. V. Plummer, S. Patnaik, *Angew. Chem.* **2003**, *115*, 4064; *Angew. Chem. Int. Ed.* **2003**, *42*, 3934.
[4] J. A. Marshall, E. A. Van Devender, *J. Org. Chem.* **2001**, *66*, 8037.
[5] Prepared from commerically available ethyl-(*R*)-(−)-3-hydroxybutyrate (Aldrich, 99% *ee*) according to a published method: K. Ohta, O. Miyagawa, H. Tsutsui, O. Mitsunobu, *Bull. Chem. Soc. Jpn.* **1993**, *66*, 523.
[6] U. S. Racherla, H. C. Brown, *J. Org. Chem.* **1991**, *56*, 401.
[7] G. A. Molander, F. Dehmel, *J. Am. Chem. Soc.* **2004**, *126*, 10313.
[8] A. V. Kalinin, S. Scherer, V. Snieckus, *Angew. Chem.* **2003**, *115*, 3521; *Angew. Chem. Int. Ed.* **2003**, *42*, 3399.
[9] A. K. Chakraborti, L. Sharma, R. Gulhane, Shivani, *Tetrahedron* **2003**, *59*, 7661.
[10] K.-M. Chen, G. E. Hardtmann, K. Prasad, O. Repič, M. J. Shapiro, *Tetrahedron Lett.* **1987**, *28*, 155; see also: K. Narasaka, F.-C. Pai, *Tetrahedron* **1984**, *40*, 2233.

 © 2006 Wiley-VCH Verlag GmbH & Co. KGaA, Weinheim

[11] S. Ohira, K. Okai, T. Moritani, *J. Chem. Soc. Chem. Commun.* **1992**, 721; for a review of trimethylsilyldiazomethane, see: T. Shiori, T. Aoyama, *J. Synth. Org. Chem. Jpn.* **1986**, *44*, 149.
[12] S. A. Frank, H. Chen, R. K. Kunz, M. J. Schnaderbeck, W. R. Roush, *Org. Lett.* **2000**, *2*, 2691; see also: J.-i. Uenishi, J.-M. Beau, R. W. Armstrong, Y. Kishi, *J. Am. Chem. Soc.* **1987**, *109*, 4756.
[13] CCDC-607141 (**m-2**) contains the supplementary crystallographic data for this paper. These data can be obtained free of charge from The Cambridge Crystallographic Data Centre via www.ccdc.cam.ac.uk/data_request/cif.
[14] We thank Professor William Fenical and Dr. Hak Cheol Kwon for an authentic sample and spectra of marinomycins A–C (**1**–**3**).
[15] Exact ratios of marinomycins A–C (**1**–**3**) varied from one experiment to another.

 © 2006 Wiley-VCH Verlag GmbH & Co. KGaA, Weinheim

Total Synthesis

DOI: 10.1002/anie.200602030

Total Synthesis and Absolute Stereochemistry of Polygalolides A and B**

*Seiichi Nakamura, Yukihito Sugano, Fumiaki Kikuchi, and Shunichi Hashimoto**

In 2003, Wei and co-workers reported the isolation and structural elucidation of the polygalolides A (**1**) and B (**2**) obtained from *Polygala fallax* Hemsl., a medicinal plant from which extracts are used as tonics and antihepatitis drugs in China.[1] The structure and relative configuration of the polygalolides were determined on the basis of NMR spectroscopic data. However, the issue of the absolute stereochemistry of the molecules has not been resolved. The structural complexity of these molecules, which include an unprecedented trioxatetracyclic ring system and contiguous quaternary stereogenic centers at C2 and C8, poses a considerable synthetic challenge. Herein, we describe the first total synthesis of (−)-polygalolides A (**1**) and B (**2**). The synthesis takes advantage of a transformation consisting of a tandem carbonyl ylide formation/1,3-dipolar cycloaddition, which has been extensively studied, especially in the research group of Padwa.[2–5]

Our retrosynthetic analysis of the polygalolides is illustrated in Scheme 1. We elected to introduce the arylmethylidene moiety at a late stage in the synthesis, and the

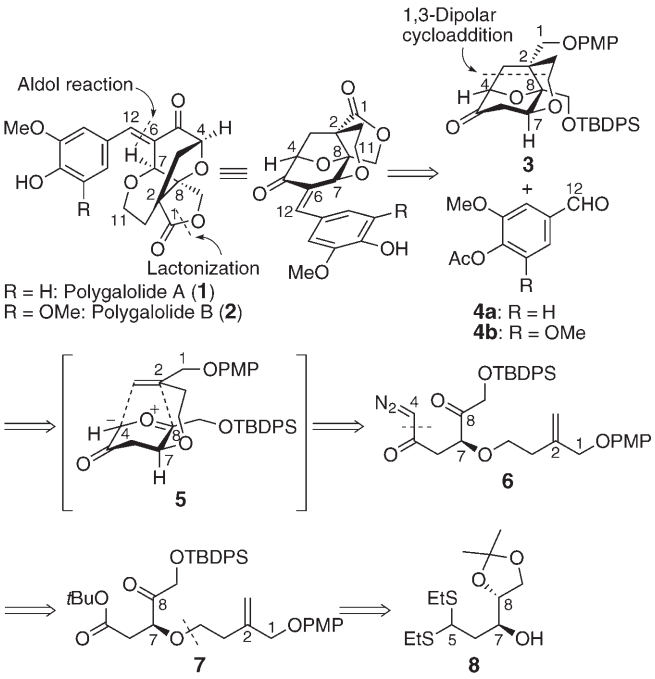

Scheme 1. Retrosynthetic analysis of polygalolides A and B. PMP = *p*-methoxyphenyl, TBDPS = *tert*-butyldiphenylsilyl.

scission of the lactone ring provided **3** as a common intermediate. The tricyclic compound **3** was assumed to arise from an intramolecular 1,3-dipolar cycloaddition of carbonyl ylide **5**, generated from α-diazoketone **6** in the presence of a Rh^{II} catalyst. Compound **6** arises from homologation of the *tert*-butyl ester **7**, which would be elaborated from the known alcohol **8**,[6] which in turn can readily be obtained from D-arabinose.

We initiated the synthesis by alkylating alcohol **8** with (*Z*)-1-bromo-4-(*tert*-butyldiphenylsilyl)oxy-2-butene[7] to provide the allyl ether **9** in 98% yield (Scheme 2). The oxidative hydrolysis of the dithioacetal with iodine was followed by oxidation with $NaClO_2$ and esterification with $(Boc)_2O$[8] to give *tert*-butyl ester **10** in 70% yield over three steps. Catalytic hydrogenation of alkene **10** provided the TBDPS ether **11** in 95% yield, and **11** was then treated with Bu_4NF in the presence of AcOH to give alcohol **12** in 96% yield. Installation of the C2=C3 bond was accomplished by employing a modification of the procedure reported by Ogasawara and co-workers,[9] and subsequent reduction with $NaBH_4$ gave alcohol **13** in 81% yield over both steps. A two-step sequence involving mesylation and nucleophilic substitution with *p*-methoxyphenol was used to convert the allyl alcohol **13** into the PMP ether **14** in 78% overall yield. The acetonide was

[*] Dr. S. Nakamura, Y. Sugano, F. Kikuchi, Prof. Dr. S. Hashimoto
Faculty of Pharmaceutical Sciences
Hokkaido University
Sapporo 060-0812 (Japan)
Fax: (+81) 11-706-3236
E-mail: hsmt@pharm.hokudai.ac.jp

[**] This research was in part supported by a Grant-in-Aid for Scientific Research on Priority Areas 17035002 from the Ministry of Education, Culture, Sports, Science and Technology (MEXT). We are grateful to Dr. X. Wei for providing spectra of the natural products. We thank H. Matsumoto, A. Maeda, S. Oka, M. Kiuchi, and T. Hirose of the Center for Instrumental Analysis, Hokkaido University, for technical assistance in obtaining MS and elemental analyses.

Supporting information for this article is available on the WWW under http://www.angewandte.org or from the author.

InterScience
© 2006 Wiley-VCH Verlag GmbH & Co. KGaA, Weinheim

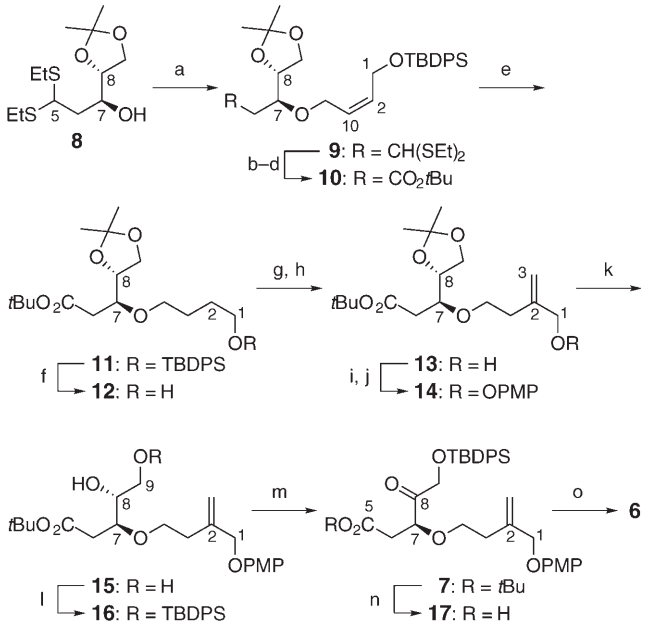

Scheme 2. Synthesis of cyclization precursor **6**. a) (*Z*)-1-bromo-4-(*tert*-butyldiphenylsilyl)oxy-2-butene, NaH, THF/DMF (10:1), 1.5 h, 98%; b) I_2, $NaHCO_3$, aq acetone, −25 °C, 5 min, 88%; c) $NaClO_2$, NaH_2PO_4, 2-methyl-2-butene, aq *t*BuOH, 6 h; d) $(Boc)_2O$, DMAP, *t*BuOH, 1 h, 80% (2 steps); e) H_2, 10% Pd/C, EtOAc, 13 h, 95%; f) Bu_4NF, AcOH, THF, 15 h, 96%; g) $(COCl)_2$, DMSO, Et_3N, CH_2Cl_2, −78→0 °C, then $Me_2N{=}CH_2I$, DBU, 20 h, 85%; h) $NaBH_4$, EtOH, 0 °C, 30 min, 95%; i) MsCl, Et_3N, CH_2Cl_2, 0 °C, 10 min; j) 4-$MeOC_6H_4OH$, K_2CO_3, MeCN, reflux, 6 h, 78% (2 steps); k) AcOH/THF/H_2O (3:1:1), 40 °C, 4 h, 95%; l) TBDPSCl, imidazole, CH_2Cl_2, 1 h, 92%; m) Dess–Martin periodinane, CH_2Cl_2, 1 h, 93%; n) TFA/CH_2Cl_2 (1:10), 0 °C, 1 h; o) $ClCO_2iBu$, Et_3N, Et_2O, 0 °C, 10 min, then CH_2N_2, 90 min, 55% (2 steps). Boc = *tert*-butoxycarbonyl, DMAP = 4-dimethylaminopyridine, DBU = 1,8-diazabicyclo[5.4.0]undec-7-ene, Ms = methanesulfonyl, TFA = trifluoroacetic acid.

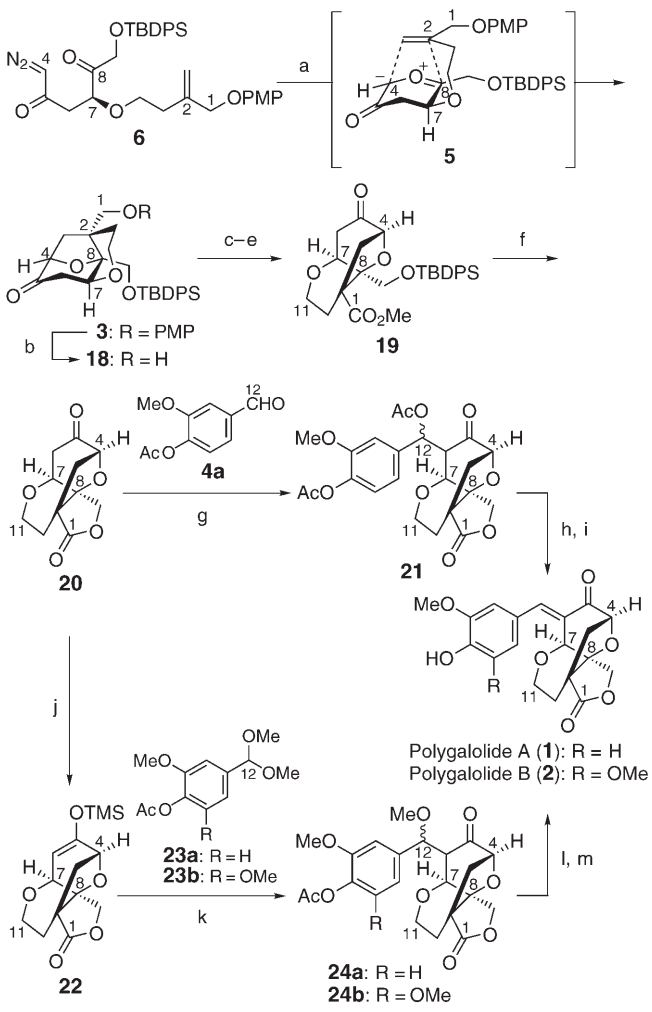

Scheme 3. Total synthesis of polygalolides A (**1**) and B (**2**). a) $Rh_2(OAc)_4$ (5 mol%), $PhCF_3$, 100 °C, 5 min, 73%; b) $(NH_4)_2Ce(NO_3)_6$, pyridine, aq MeCN, 0 °C, 2 h, 91%; c) Dess–Martin periodinane, CH_2Cl_2, 2 h, 92%; d) $NaClO_2$, NaH_2PO_4, 2-methyl-2-butene, aq *t*BuOH, 6 h; e) CH_2N_2, Et_2O, 0 °C, 30 min, 85% (2 steps); f) Bu_4NF, AcOH, THF, 20 h, 93%; g) LDA, $ZnCl_2$, THF, −78 °C, 1 h, aldehyde **4a**, −78 °C, 30 min, then Ac_2O, 0 °C, 1 h; h) SiO_2, CH_2Cl_2, 24 h; i) $NaHCO_3$, aq MeOH, 18% (3 steps); j) TMSOTf, Et_3N, CH_2Cl_2, 0 °C, 5 h, 90%; k) **23a** or **23b** (5 equiv), TMSOTf, molecular sieves (3 Å), CH_2Cl_2, −78 °C, 30 min, 58% (for **24a**) or 57% (for **24b**); l) DBU, CH_2Cl_2, 10 min; m) $NaHCO_3$, aq MeOH, 85% (for **1**) or 72% (for **2**). LDA = lithium diisopropylamide; TMS = trimethylsilyl; Tf = trifluoromethanesulfonyl.

removed using AcOH in aqueous THF at 40 °C to afford the diol **15** in 95% yield. Selective silylation of the C9 hydroxy group in **15** furnished the TBDPS ether **16** in 92% yield, and **16** was oxidized with Dess–Martin periodinane to give ketone **7**[10] in 93% yield. A carboxylic acid function at C5, available for a one-carbon homologation, was liberated upon exposure of the *tert*-butyl ester **7** to TFA. Although the carboxyl group in **17** could not be converted into the acid chloride because of the inevitable formation of the corresponding pseudochloride,[11] activation of the acid through the intermediacy of its mixed anhydride and subsequent treatment with CH_2N_2 afforded α-diazoketone **6** in 55% yield over the two steps.

With the cyclization precursor **6** in hand, we set out to investigate the critical carbonyl ylide formation/intramolecular 1,3-dipolar cycloaddition reaction sequence (Scheme 3). The reaction involved the addition of α-diazoketone **6** (ca. 30 mg) over five minutes to a solution of a Rh^{II} catalyst. Although **6** was completely consumed even at room temperature in the presence of $Rh_2(OAc)_4$, the reaction gave a complex mixture of products.[12] After some experimentation, we found that cycloadduct **3**[10] was produced as a single isomer in 36% yield at 60 °C in toluene; the product yield was improved to 68% by an increase in reaction temperature to 110 °C. We screened the solvents and Rh^{II} catalysts[13] and found $Rh_2(OAc)_4$ in benzotrifluoride[14] to be optimal, affording cycloadduct **3** in 73% yield.[15] After oxidative removal of the PMP group at C1 with $(NH_4)_2Ce(NO_3)_6$,[16] two successive oxidations and an esterification with CH_2N_2 gave the methyl ester **19** in 78% yield over three steps. Desilylation and concomitant lactone formation was effected with Bu_4NF in the presence of AcOH to provide the tetracyclic lactone **20**.

With the construction of the common tetracyclic core accomplished, we addressed the late-stage installation of the arylmethylidene moiety. Our initial attempts focused on the aldol reaction of ketone **20** with aldehyde **4a** under basic

 © 2006 Wiley-VCH Verlag GmbH & Co. KGaA, Weinheim

conditions. The formation of the aldol adduct was detected by ^{1}H NMR spectroscopy of the crude mixture when the zinc enolate derived from **20** was reacted with **4a**, but the desired product readily underwent retroaldol reaction upon exposure to silica gel. The coupling product **21** could be obtained along with considerable amounts of starting material **20** when the reaction mixture was treated with Ac_2O. Although the total synthesis of polygalolide A (**1**) could be completed through exposure of the mixture to silica gel followed by deacetylation, the low efficiency of this sequence (18% yield over three steps without intervening purification) left room for improvement. Accordingly, the decision was made to employ the Mukaiyama aldol-type reaction using dimethyl acetal **23a**.[17] Ketone **20** was easily converted into the silyl enol ether **22**. Gratifyingly, the TMSOTf-promoted coupling of **22** with **23a** in CH_2Cl_2 in the presence of molecular sieves (3 Å) at −78 °C proceeded to provide coupling product **24a** in 58% yield. The β-methoxyketone **24a** was smoothly converted into polygalolide A (**1**) by treatment with DBU, followed by deacetylation. Polygalolide B (**2**) was also synthesized in 41% yield from intermediate **22** following an identical reaction sequence. The spectroscopic data (^{1}H and ^{13}C NMR, IR, UV, and HRMS) of the products resulting from these syntheses correspond to those reported for the natural products, except for their specific rotations, which were equal in sign, but with magnitudes inconsistent with those previously reported: $[\alpha]_D = -499.9$ ($c = 0.022$ in MeOH) and −505.2 ($c = 0.018$ in MeOH) compared with $[\alpha]_D = -14.4$ ($c = 0.018$ in MeOH) and −21.3 ($c = 0.015$ in MeOH).[1] This difference suggests that polygalolides might be biosynthesized in near-racemic form. In this context, it is interesting that Snider and Grabowski recently proposed in their total syntheses of (±)-cartorimine and (±)-descurainin that the 8-oxabicyclo[3.2.1]octenone skeleton of these molecules would be biosynthesized by a [5+2] cycloaddition between a oxypyrylium zwitterion and an alkene.[5e,f] They speculated that [5+2] cycloadditions in a chiral environment could lead to optically enriched products as the very small $[\alpha]_D$ values of these natural products indicate that they are not completely racemic. We surmise that polygalolides would also be synthesized in the medicinal plant through [5+2] cycloaddition of the fructose-derived oxypyrylium zwitterion **25** with an isoprene derivative, followed by an intramolecular hetero-Michael addition, a lactone formation, and an aldol reaction with vanillin derivatives.[18] Our result would provide an experimental proof for the intriguing speculation by the Snider group.

In conclusion, we have accomplished the first total synthesis of polygalolides A (**1**) and B (**2**) from alcohol **8**, with a longest linear sequence of 25 steps and with overall yields of 3.8% and 3.2%, respectively. This total synthesis serves to confirm the absolute stereochemistry of these natural products. The synthesis illustrates the power of the carbonyl ylide cycloaddition methodology for the rapid assembly of the unusual dioxatricyclic ring system, which is difficult to construct by other means.

Received: May 22, 2006
Published online: September 5, 2006

Keywords: aldol reaction · carbonyl ylides · cycloaddition · diazo compounds · total synthesis

[1] W. Ma, X. Wei, T. Ling, H. Xie, W. Zhou, *J. Nat. Prod.* **2003**, *66*, 441 – 443.
[2] A. Padwa, G. E. Fryxell, L. Zhi, *J. Am. Chem. Soc.* **1990**, *112*, 3100 – 3109.
[3] For recent reviews, see: a) M. C. McMills, D. Wright in *Synthetic Applications of 1,3-Dipolar Cycloaddition Chemistry toward Heterocycles and Natural Products* (Eds.: A. Padwa, W. H. Pearson), Wiley, New York, **2002**, pp. 253 – 314; b) G. Mehta, S. Muthusamy, *Tetrahedron* **2002**, *58*, 9477 – 9504; c) A. Padwa, *Helv. Chim. Acta* **2005**, *88*, 1357 – 1374.
[4] For recent studies on the synthesis of bioactive molecules using a carbonyl ylide cycloaddition strategy, see: a) H. Koyama, R. G. Ball, G. D. Berger, *Tetrahedron Lett.* **1994**, *35*, 9185 – 9188; b) A. Padwa, M. A. Brodney, J. P. Marino, Jr., S. M. Sheehan, *J. Org. Chem.* **1997**, *62*, 78 – 87; c) C. S. Straub, A. Padwa, *Org. Lett.* **1999**, *1*, 83 – 85; d) D. M. Hodgson, C. Villalonga-Barber, *Tetrahedron Lett.* **2000**, *41*, 5597 – 5600; e) J. L. Wood, B. D. Thompson, N. Yusuff, D. A. Pflum, M. S. P. Matthäus, *J. Am. Chem. Soc.* **2001**, *123*, 2097 – 2098; f) F. Liu, D. J. Austin, *Org. Lett.* **2001**, *3*, 2273 – 2276; g) D. M. Hodgson, T. D. Avery, A. C. Donohue, *Org. Lett.* **2002**, *4*, 1809 – 1811; h) B. Chen, R. Y. Y. Ko, M. S. M. Yuen, K.-F. Cheng, P. Chiu, *J. Org. Chem.* **2003**, *68*, 4195 – 4205; i) S. Nakamura, Y. Hirata, T. Kurosaki, M. Anada, O. Kataoka, S. Kitagaki, S. Hashimoto, *Angew. Chem.* **2003**, *115*, 5509 – 5513; *Angew. Chem. Int. Ed.* **2003**, *42*, 5351 – 5355; j) T. Graening, V. Bette, J. Neudörfl, J. Lex, H.-G. Schmalz, *Org. Lett.* **2005**, *7*, 4317 – 4320; k) H. Oguri, S. L. Schreiber, *Org. Lett.* **2005**, *7*, 47 – 50.
[5] For representative works on the related [5+2] cycloadditions between oxypyrylium ylides and alkenes, see: a) P. A. Wender, H. Y. Lee, R. S. Wilhelm, P. D. Williams, *J. Am. Chem. Soc.* **1989**, *111*, 8954 – 8957; b) D. R. Williams, J. W. Benbow, E. E. Allen, *Tetrahedron Lett.* **1990**, *31*, 6769 – 6772; c) W. E. Bauta et al., see Supporting Information; d) P. Magnus, L. Shen, *Tetrahedron* **1999**, *55*, 3553 – 3560; e) B. B. Snider, J. F. Grabowski, *Tetrahedron Lett.* **2005**, *46*, 823 – 825; f) B. B. Snider, J. F. Grabowski, *Tetrahedron* **2006**, *62*, 5171 – 5177.
[6] M. Y. H. Wong, G. R. Gray, *J. Am. Chem. Soc.* **1978**, *100*, 3548 – 3553.
[7] R. M. Lemieux, P. N. Devine, M. F. Mechelke, A. I. Meyers, *J. Org. Chem.* **1999**, *64*, 3585 – 3591.
[8] K. Takeda, A. Akiyama, H. Nakamura, S. Takizawa, Y. Mizuno, H. Takayanagi, Y. Harigaya, *Synthesis* **1994**, 1063 – 1066.
[9] S. Takano, K. Inomata, K. Samizu, S. Tomita, M. Yanase, M. Suzuki, Y. Iwabuchi, T. Sugihara, K. Ogasawara, *Chem. Lett.* **1989**, 1283 – 1284.
[10] The homochirality of ketone **7** and cycloadduct **3** was confirmed by HPLC on a chiral stationary phase.
[11] W. J. Elliott, J. Fried, *J. Org. Chem.* **1978**, *43*, 2708 – 2710. We thank a referee for bringing the reference to our attention.
[12] The intermolecular reaction of diazoketone **6** with dimethyl acetylenedicarboxylate occurred in the presence of $Rh_2(OAc)_4$ at room temperature to provide a 1:1 mixture of diastereomeric cycloadducts in 35% yield, indicating that carbonyl ylide **5** was formed under these conditions. Heating is required to promote the intramolecular cycloaddition with a nonactivated alkene.
[13] Product yields obtained with $Rh_2(OAc)_4$ in other solvents: benzene (57%), $(CH_2Cl)_2$ (31%). Other Rh^{II} catalysts afforded lower product yields: $Rh_2(OCOC_7H_{15})_4$ (trace), $Rh_2(OCOC_3F_7)_4$ (complex mixture), $Rh_2(OCOCPh_3)_4$ (24%), $Rh_2(NHAc)_4$ (41%).
[14] For the use of benzotrifluoride as an effective solvent in Rh^{II}-catalyzed carbonyl ylide formation/1,3-dipolar cycloaddition

 © 2006 Wiley-VCH Verlag GmbH & Co. KGaA, Weinheim

reactions, see: S. Kitagaki, M. Anada, O. Kataoka, K. Matsuno, C. Umeda, N. Watanabe, S. Hashimoto, *J. Am. Chem. Soc.* **1999**, *121*, 1417 – 1418.

[15] The cycloaddition is not scale dependent and the cycloadduct **3** was obtained in 70 % yield when the reaction was performed on a 500-mg scale.

[16] T. Fukuyama, A. A. Laird, L. M. Hotchkiss, *Tetrahedron Lett.* **1985**, *26*, 6291 – 6292.

[17] a) T. Mukaiyama, M. Hayashi, *Chem. Lett.* **1974**, 15 – 16; b) S. Murata, M. Suzuki, R. Noyori, *J. Am. Chem. Soc.* **1980**, *102*, 3248 – 3249; for a review, see: T. Mukaiyama, M. Murakami, *Synthesis* **1987**, 1043 – 1054.

[18] A plausible biogenesis of polygalolides is illustrated schematically below.

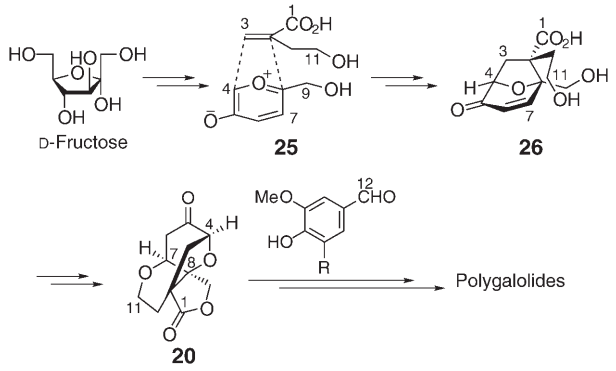

 © 2006 Wiley-VCH Verlag GmbH & Co. KGaA, Weinheim

Retraction

Since publication of this Communication, it has come to the authors' attention that the crystallographically determined structure of $[NEt_4][HgCl_2][HgCl_3]$ has been described previously (*Acta Cryst. E* **2002**, *58*, m534). The cell parameters and structural data are consistent with those of the compound that the authors reported as being $[NEt_4][AuCl_2][AuCl_3]$. Clearly the structure of the mercury compound as an impurity in the reaction product has been determined. Thus, all the conclusions drawn from this data are invalid, although several gold-containing products were derived from the reaction in high overall yields. Accordingly, the authors withdraw this Communication, apologize for these mistakes and that the readership of *Angewandte Chemie* has been mislead by the publication of this Communication. They would like to thank Prof. H. Schmidbaur for initially drawing their attention to this matter.

October 31, 2006

Jahn–Teller Distortion in Gold

DOI: 10.1002/anie.200602092

$[NEt_4][AuCl_2][AuCl_3]$: Solid-State Evidence of Essentially Y-Shaped Jahn–Teller-Distorted $AuCl_3$**

Kevin R. Flower, Robin G. Pritchard, and Alan T. McGown*

Gold halides are of considerable interest to computational and synthetic chemists alike owing to their interesting structural and bonding characteristics.[1–4] Of particular interest is the first-order Jahn–Teller distortion of the AuX_3 molecules (X = F, Cl, Br, I). Calculations have shown that the D_{3h} trigonal-planar structure is not the lowest-energy structure for AuL_3. Rather it distorts to T-, Y-, or even L-shaped geometries.[1,5] Looking at the frontier orbitals for the AuL_3 d^8 system with $D_{3h}(^1E')$ symmetry, there are two electrons in a doubly degenerate e′ orbital. Bending of the AuL_3 system breaks the degeneracy, thereby causing the formation of a doubly occupied b_2 (HOMO) and an empty a_1 (LUMO) orbital for a distorted $C_{2v}(^1A_1)$ symmetry: a first-order Jahn–Teller effect.[5]

This T-shaped geometry has been found to be the minimum for the Jahn–Teller surface of AuF_3, $AuCl_3$, and $AuBr_3$, with a Y-shaped geometry as the high-lying transition state between two T-shaped geometries such that the D_{3h} geometry is a second-order saddle point (Mexican hat with three bumps). Calculations have also been carried out on AuH_3[5] and $Au(CH_3)_3$,[6] and they also predict T-shaped ground-state geometries. Experimental data is available[3] for AuF_3 (electron diffraction) and shows clearly that it has T-shaped geometry in the gas phase. In a recent study combining matrix-isolation electronic absorption, IR, and AuL_3-edge EXAFS, it was shown that $AuCl_3$ also has a T-shaped geometry as a result of Jahn–Teller distortion.[7] This observation is consistent with the suggestion of Schultz and Hargittai that AuF_3 and $AuCl_3$ are static Jahn–Teller systems.[1] The related[1,4] molecules AuX_3 (X = Br and I) were found to have relatively flat potential-energy surfaces, and the energetic gain from Jahn–Teller distortion is small for these dynamic systems.

The solid-state structures of $[Au_2X_6]$ (X = F, Cl, Br) have also been described.[5,8–10] In all cases the gold center is found in the expected square-planar arrangement for a late-transition-metal d^8 cation.[11] For $[Au_2F_6]$, however, the square-planar $\{AuF_4\}$ units are linked by μ-F bridges in *cis* positions, thus affording an extended helical structure.[8] These solid-state intermolecular interactions are 0.7 Å longer than those observed in the $[Au_2F_6]$ moiety. The crystal and molecular structure of the mixed Au^I/Au^{III} compound $Cs_2[AuCl_2][AuCl_4]$ has also been described, and it contains a square-planar Au^{III} center with a linear Au^I center as expected.[12] Herein, we report the solid-state structure of $[NEt_4][AuCl_2][AuCl_3]$, which contains essentially Y-shaped $AuCl_3$, thus affording the first solid-state evidence for first-order Jahn–Teller distortion in $AuCl_3$.

Treatment of $[NEt_4][AuCl_4]$ with $Hg(C_6H_4\text{-}4\text{-}OMe)_2$ in acetonitrile afforded, after recrystallization, $[NEt_4][AuCl_2][AuCl_3]$ (**1**) and 4,4′-$(MeO)_2$-$C_{12}H_8$. Recrystallization of **1** from $NCMe/CH_2Cl_2$ at 277 K afforded crystals of **1** suitable for an X-ray diffraction study (Figure 1). Of particular note are the non-square-planar Au^{III} chloride fragment and the shorter Au^I–Cl bonds (av 2.322 Å) versus the Au^{III}–Cl bonds (av 2.441 Å). The latter is a direct result of relativistic effects, which dominate the chemistry of gold.[13] This property mirrors the shorter Au^I–Cl bond length observed in the crystallographically determined structure of $Cs_2[AuCl_2][AuCl_4]$.[9] The structure of the $AuCl_3$ fragment in **1** has a geometry intermediate (**B**) between the trigonal planar (D_{3h}, **A**) and T-shaped (C_{2v}, **C**) geometries (Figure 2).

[*] Dr. K. R. Flower, Dr. R. G. Pritchard
School of Chemistry
University of Manchester
Sackville Street, Manchester (UK)
Fax: (+44) 161-306-4459
E-mail: k.r.flower@manchester.ac.uk
Prof. A. T. McGown
Drug Discovery Unit
University of Salford
Frederick Street Campus, Salford (UK)

[**] The financial support of UMIP is acknowledged.

 © 2006 Wiley-VCH Verlag GmbH & Co. KGaA, Weinheim

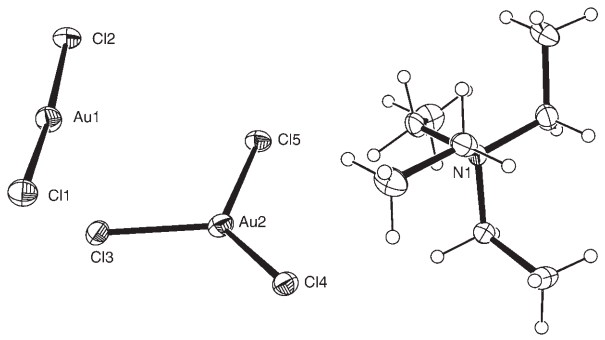

Figure 1. ORTEP representation of the molecular structure of **1**. Thermal ellipsoids are set at 30% probability. Selected bond lengths [Å] and angles [°]: Au1-Cl1 2.311(4), Au1-Cl2 2.334(4), Au2-Cl3 2.452(4), Au2-Cl4 2.454(4), Au2-Cl5 2.417(4); Cl1-Au1-Cl2 170.53(11), Cl3-Au2-Cl4 118.21(13), Cl3-Au2-Cl5 111.42(13), Cl4-Au2-Cl5 127.89(13).

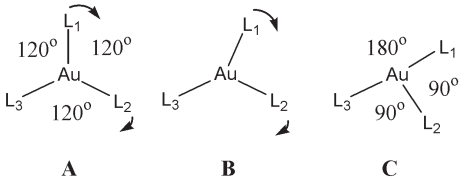

Figure 2. Pictorial representation of the bending in the AuL_3 fragments: **A** trigonal-planar; **B** Y-shaped; **C** T-shaped.

The structural features of the $[NEt_4][AuCl_2]$ portion of the structure are comparable to those that have been previously crystallographically determined for $[NEt_4][AuCl_2]$.[14]

By increasing the acceptable bonding radius of Cl to 1.20 Å from 0.99 Å, it becomes evident that Cl4 asymmetrically bridges two gold centers (Au2–Cl4 2.454(3) Å, Au2–Cl4_2 2.822(3) Å). This bridging affords an $\{Au_2Cl_6\}$ unit (Figure 3), which clearly differs from the previously reported structure of $[Au_2Cl_6]$ in which the Au^{III} atoms display the expected square-planar geometry with symmetric Au-Cl-Au bridges (Au–Cl 2.334(10) Å). The closest nonbonding approach in the square-planar structure is 3.487(10) Å. Schwerdtfeger et al. suggested[5] that the dimerization of the $AuCl_3$ fragments to give $[Au_2Cl_6]$ could easily be visualized as the bridging of equatorial ligands in the C_{2v}-symmetric T-shaped Jahn–Teller-distorted $AuCl_3$ fragments. The dimer

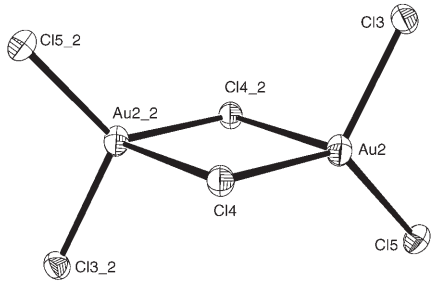

Figure 3. ORTEP representation of the $\{Au_2Cl_6\}$ fragment in **1**. Selected bond lengths [Å] and angles [°]: Au2-Cl4 2.454(4), Au2-Cl4_2 2.822(3); Cl4-Au2-Cl4_2 85.53(10), Au2-Cl4-Au2_2 94.47(10).

reported here can be visualized in a similar fashion in that two essentially Y-shaped fragments sit tail-to-tail, one on top of the other. The overall geometry is now closer to that observed for other $[M_2X_6]$ systems, which are described as two tetrahedra sharing one edge.[15]

Upon increasing further the acceptable covalent radius of Cl to 1.30 Å, an additional weak interaction between Cl3 and Au1 is observable (2.907(4) Å, Figure 4). A similar bridging

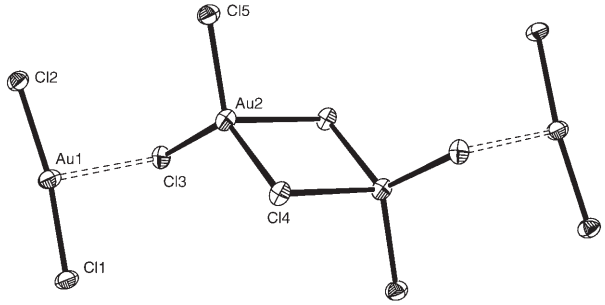

Figure 4. ORTEP representation of the $[AuCl_2][Au_2Cl_6][AuCl_2]$ chain in **1**. Selected bond lengths [Å] and angle [°]: Au1-Cl3 2.907(4), Au2-Cl3 2.452(4); Au2-Cl3-Au1 103.17(13).

interaction (Cl5–Au1 3.208(5) Å, Au2-Cl5-Au1 95.81(13)°) is also evident and is within the sum of the accepted van der Waals radii.[16] Finally, the extended structure is shown in Figure 5 and is best considered as a chain of repeating {-Cl-

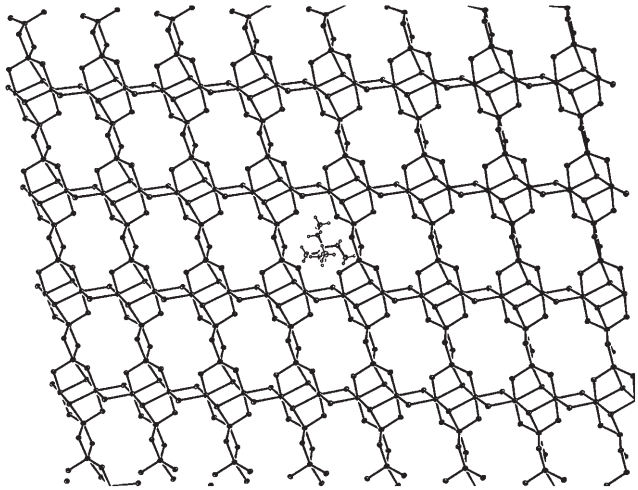

Figure 5. ORTEP representation of the extended structure of **1**.

Au^{III}-Cl-Au^{III}-Cl-Au^{I}-} units running from top to bottom of the diagram and a chain of alternating {-Cl-Au^{I}-Cl-} units running from right to left that creates channels in the structure that are occupied by the $[NEt_4]^+$ countercations. In the {-Cl-Au^{I}-Cl-} chain there are two possible $Au^{I}\cdots Au^{I}$ interactions. They are found to have separations of 4.104(12) and 4.210(14) Å and are longer than the Au2···Au2_2 separation of 3.881(16) Å. This finding means that there are no aurophilic interactions in this structure,[17] the most likely

 © 2006 Wiley-VCH Verlag GmbH & Co. KGaA, Weinheim

reason being the octahedral coordination geometry at the Au^I atom in the extended structure.

In conclusion, the solid-state structure of **1** gives the first solid-state evidence for Jahn–Teller distortion in a structure containing $AuCl_3$. The distortion observed is more representative of the Y-shaped transition state, in which two Au–X bonds are 120° or greater (127°, 118°, 111° for **1**), that is predicted by theoretical calculations than the expected T-shaped geometry with idealized angles of 180°, 90°, and 90°. In the extended structure there is clear evidence for asymmetric bridging of two $AuCl_3$ units to give an $\{Au_2Cl_6\}$ unit that does not show the expected square-planar geometry at the d^8 gold(III) center, but is more representative of other $[M_2X_6]$ systems.

Experimental Section

1 (Caution! Use of an organomercurial compound): $Hg(C_6H_4$-4-$OMe)_2$ (89 mg, 0.213 mmol) was added to a solution of $[NEt_4][AuCl_4]$ (100 mg, 0.213 mmol) in NCMe (25 mL) with continuous stirring at 273 K. After 3 h the solution was filtered through celite, and the solvent was removed in vacuo. Extraction of the crude product with hexane afforded 4,4′-$(MeO)_2$-$C_{12}H_{10}$ (42 mg, 92 %). Recrystallization of the remaining material from $NCMe/CH_2Cl_2$ (1:3) afforded **1** (48 mg, 75 %).

Crystallography: A suitable crystal of **1** was grown from $NCMe/CH_2Cl_2$ (1:3) at 277 K. The X-ray diffraction data were collected at 200 K with a Nonius Kappa CCD 4-circle diffractometer using graphite-monochromated $Mo_{K\alpha}$ radiation ($\lambda = 0.71073$ Å); CCD rotation images, thick slices, scans performed to $2\theta_{max} = 52°$.

Crystal data for $[C_8H_{20}N]^+[Au_2Cl_5]^-$, $C_8H_{20}Au_2Cl_5N$, $M_r = 701.43$, crystal dimensions $0.1 \times 0.1 \times 0.05$ mm^3, triclinic, space group $P\bar{1}$ (No. 2), $a = 8.2871(1)$, $b = 10.4086(2)$, $c = 10.9548(2)$ Å, $\alpha = 105.697(1)$, $\beta = 96.636(1)$, $\gamma = 108.756(1)°$, $V = 839.85(2)$ Å^3, $Z = 2$, $\rho_{calcd} = 2.774$ Mg m^{-3}, $\mu = 18.221$ mm^{-1}, $F(000) = 636$, 13366 reflections collected, 3262 unique [$R_{int} = 0.082$], 2569 [$I > 2\sigma(I)$], Lp and absorption corrections (semiempirical from equivalents, max/min transmission 0.463, 0.263). The structure was solved by direct methods using SHELXS-97[18] and refined against F^2 using SHELXL-97 (142 parameters). $wR_2 = 0.1654$ (all data), $R_1 = 0.0589$ [$I > 2\sigma(I)$]. Difference map max/min 3.36, −2.78 e Å^{-3}. CCDC-608090 contains the supplementary crystallographic data for this paper. These data can be obtained free of charge from The Cambridge Crystallographic Data Centre via www.ccdc.cam.ac.uk/data_request/cif.

Received: May 25, 2006
Revised: July 7, 2006
Published online: August 17, 2006

Keywords: crystal engineering · gold · halogens · Jahn–Teller distortion · structure elucidation

[1] A. Schulz, M. Hargittai, *Chem. Eur. J.* **2001**, *7*, 3657 – 3670.
[2] M. Hargittai, A. Schultz, B. Réffey, M. Kolonits, *J. Am. Chem. Soc.* **2001**, *123*, 1449 – 1450.
[3] B. Réffey, M. Kolonits, A. Schultz, T. M. Klapötke, M. Hargittai, *J. Am. Chem. Soc.* **2000**, *122*, 3127 – 3134.
[4] T. Söhnel, R. Brown, L. Kloo, P. Schwerdtfeger, *Chem. Eur. J.* **2001**, *7*, 3167 – 3173.
[5] P. Schwerdtfeger, P. D. W. Boyd, S. Brienne, A. K. Burrell, *Inorg. Chem.* **1992**, *31*, 3411 – 3422.
[6] S. Komiya, T. A. Albright, R. Hoffmann, J, Kochi, *J. Am. Chem. Soc.* **1976**, *98*, 7255 – 7265; S. Komiya, T. A. Albright, R. Hoffmann, J, Kochi, *J. Am. Chem. Soc.* **1977**, *99*, 8440 – 8447; K. Tatsumi, R. Hoffmann, A. Yamamoto, J. K. Stille, *Bull. Chem. Soc. Jpn.* **1981**, *54*, 1857 – 1867.
[7] I. J. Blackmore, A. J. Bridgeman, N. Harris, M. A. Holdaway, J. F. Rooms, E. L. Thompson, N. A. Young, *Angew. Chem.* **2005**, *117*, 6904 – 6908; *Angew. Chem.* **2005**, *117*, 6746 – 6750.
[8] F. W. B. Einstein, P. R. Rao, J. Trotter, N. Bartlett, *J. Chem. Soc. A* **1967**, 478 – 482; B. Zemva, K. Lutar, A. Jeshi, W. J. Casteel, A. P. Wilkinson, D. E. Cox, R. B. von Dreele, H. Bormann, N. Bartlett, *J. Am. Chem. Soc.* **1991**, *113*, 4192 – 4198.
[9] E. S. Clark, D. H. Templeton, C. H. MacGillavry, *Acta Crystallogr.* **1958**, *11*, 284 – 288.
[10] K. P. Lörcher, J. Strähle, *Z. Naturforsch. B* **1975**, *30*, 662 – 664.
[11] C. J. Jones, *d- and f- Block Chemistry*, Royal Society of Chemistry, Cambridge, UK, **2001**.
[12] J. C. M. Tindemans, V. Eijndhoven, G. C. Verschoor, *Mater. Res. Bull.* **1974**, *9*, 1667 – 1670.
[13] P. Schwerdtfeger, *Heteroat. Chem.* **2002**, *13*, 578 – 584.
[14] G. Helgesson, S. Jagner, *Acta Chem. Scand. Ser. A* **1987**, *41*, 556 – 561.
[15] M. Hargittai, *Chem. Rev.* **2000**, *100*, 2233 – 2301.
[16] A. Bondi, *J. Phys. Chem.* **1964**, *68*, 441 – 451.
[17] P. Pyykkö, *Angew. Chem.* **2004**, *116*, 4512 – 4557; *Angew. Chem. Int. Ed.* **2004**, *43*, 4412 – 4456.
[18] G. M. Scheldrick, SHELXL97, University of Göttingen, Germany, **1997**.

 © 2006 Wiley-VCH Verlag GmbH & Co. KGaA, Weinheim

Surface Chemistry

DOI: 10.1002/anie.200602105

Structural Identification of Conjugated Molecules on Metal Surfaces by Means of Soft Vibrations**

*David Loffreda**

Identification of molecular structures in nature remains a tremendous challenge. In heterogeneous catalysis, single-molecule vibrational spectroscopy and microscopy have progressively led to a better understanding of surface chemistry at the atomic level.[1] Inelastic electron tunneling spectroscopy and scanned energy photoelectron diffraction have exhibited great capabilities to characterize NO and CO

[*] Dr. D. Loffreda
Laboratoire de Chimie
UMR CNRS 5182
Ecole Normale Supérieure de Lyon
46 Allée d'Italie, 69364 Lyon, Cedex 07 (France)
Fax: (+33) 472-728-860
E-mail: David.Loffreda@ens-lyon.fr

[**] Dr. M.-L. Bocquet and Dr. F. Delbecq are acknowledged for helpful discussions, and Dr. J. Pilmé for valuable discussions about ELF interpretation. I thank IDRIS and PSMN for CPU time and assistance.

Supporting information for this article is available on the WWW under http://www.angewandte.org or from the author.

© 2006 Wiley-VCH Verlag GmbH & Co. KGaA, Weinheim

adsorption and dehydrogenation products of alkenes and aromatic molecules.[2–4] However, for these latter compounds, the analysis of the spectra is rendered difficult by the large number of possibilities. In this case, theoretical simulations have recently opened exciting perspectives.[5]

Powerful techniques such as high-resolution electron energy loss spectroscopy (HREELS) and synchrotron far-infrared reflection absorption spectroscopy (IRAS) have provided complementary measurements of CO and NO vibrations on various metal surfaces.[6,7] The adsorption modes were essentially elucidated on the basis of the analogy of the high frequency modes with those of organometallic compounds. Although the analysis of low-frequency molecule–metal bands has also been achieved and recently corroborated by theory,[8,9] the assignment is rarely simple, and the customary analogy with organometallic compounds has been questioned several times.[10,11] Moreover, interpretation of the spectra becomes particularly tough for multifunctional molecules.

The identification of the adsorption structures of conjugated molecules on metal surfaces is a probative example for which IRAS investigations have provided limited conclusions.[12–14] Competitive flat adsorption forms were suggested from a similar analogy without clearly answering the question of molecular coordination to the surface with typical π or di-σ structures.[12,13] A recently proposed promising route compared experimental and theoretical HREELS results for acrolein on Pt(111).[15] However, additional references for the low-frequency modes are missing so far for identifying unambiguously the adsorption structures of such complex multifunctional molecules.

In this work soft molecule–metal vibrations were unveiled by a systematic density functional theory (DFT) study. To investigate a significant number of adsorption structures, four conjugated molecules and six metal surfaces were selected (see Figure 1). The relationships between adsorption structure and strength, molecular conjugation, and soft molecule–metal vibrations are examined hereinafter.

The edges of supported metallic particles, which are relevant to catalysis, were modeled by Au, Ag, Cu, Pt, Pd, and Ni(110)-(1 × 2) missing-row surfaces with slabs of six metal layers in thickness. All the calculations are performed with VASP under accurate conditions (see Supporting Information for details). The four unsaturated molecules are defined in Figure 2a: a carboxylic acid (carboxy), an ester (acetoxy), an

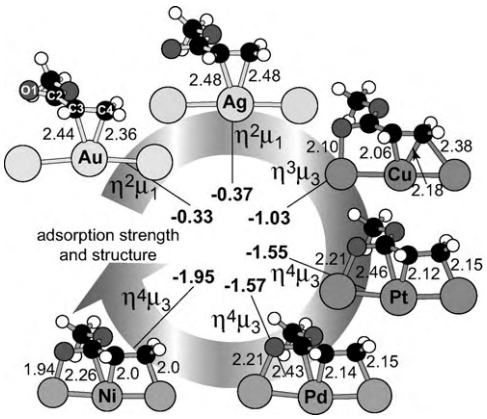

Figure 1. Mean adsorption strength [eV] and stable adsorption structures (distances in Å) of the multifunctional molecules on the ridge of the (110)-(1 × 2) metal surfaces. The *s-trans* ester (acetoxy) compound is chosen here for illustration.

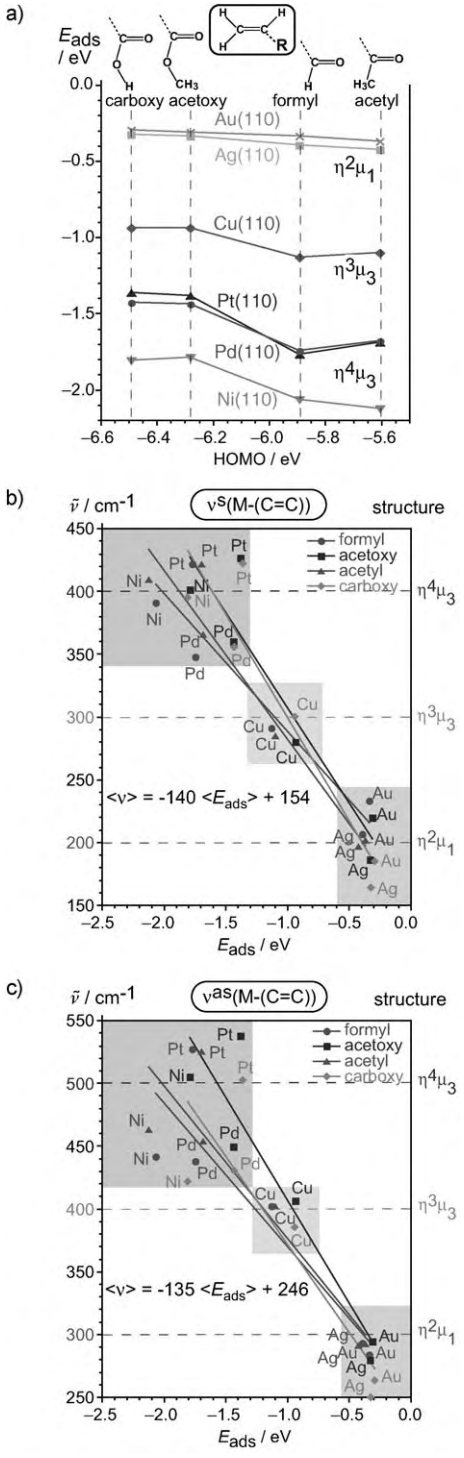

Figure 2. a) Adsorption energy E_{ads} [eV] of the *trans* conjugated molecules on six metal surfaces as a function of gas-phase HOMO energy [eV]. b) Symmetric ν^s(M–(C=C)) and c) antisymmetric ν^{as}(M–(C=C)) stretching frequency [cm^{-1}] as a function of E_{ads} [eV] and structure $\eta^i\mu_j$.

 © 2006 Wiley-VCH Verlag GmbH & Co. KGaA, Weinheim

aldehyde (formyl), and a ketone (acetyl). These flat compounds, which have conjugated C=C and C=O bonds, exhibit *s-cis* and *s-trans* conformations. After adsorption, both conformations may compete, as shown previously for π(C=C) and di-σ(C=C) structures on Au(110) and Pt(110) surfaces respectively.[16] To simplify the analysis, only the results of the *s-trans* adsorbates are discussed here.

Adsorption strength and molecular structure are intimately correlated, and the evolution from sp noble metal (Au, Ag, Cu) to d transition metal (Pt, Pd, Ni) surfaces is revealed in Figure 1. For all the considered adsorbates, DFT shows that the most stable adsorption geometries are $\eta^2\mu_1$ [π(C=C)] on Au(110) and Ag(110), $\eta^3\mu_3$ on Cu(110), and $\eta^4\mu_3$ [η^4(C=C,C=O)] on Pt(110),[17] Pd(110), and Ni(110). Figure 2a shows the adsorption energy of these stable structures for the six metals. The mean adsorption strength increases from Au (−0.33 eV) to Ni surfaces (−1.95 eV). The $\eta^3\mu_3$ structure on Cu(110) is atypical, since the C4 carbon atom shares formally five bonds with the Cu surface, the H atoms, and C3. This peculiar structure is discussed below on the basis of an electronic analysis.

The loss of conjugation, which is characterized by breaking of the molecular plane and progressive opening of the CH_2 moiety, is linked to the adsorption strength (see Figure 1). As shown in Figure 2a, the DFT adsorption energy E_{ads} decreases on the six metal surfaces with increasing depth of the HOMO in the gas phase. Hence, the greater the donor ability of the substituent (acetyl), the higher the HOMO, and the more stable the adsorbate. This effect, which is rather moderate on sp metals (60–190 meV), becomes stronger on d metal surfaces (330–410 meV).

Having determined the stable structures, molecular recognition based on vibrational characterization appeared to be a natural further step. Assignment of the low-frequency vibrations requires preliminary analysis of the normal modes (see Figure 3). Beside the external vibrations (frustrated translations and rotations of the adsorbate not reported here), several metal–molecule stretching modes appear in an intermediate frequency range (170–630 cm^{-1} for all the adsorption states) between the surface metal phonons (0–250 cm^{-1}) and the high molecular frequencies. To illustrate this result, the calculated EELS spectra of one molecule (acetoxy) on the six metal surfaces are presented in Figure 4 (see Supporting Information for all the other spectra). The

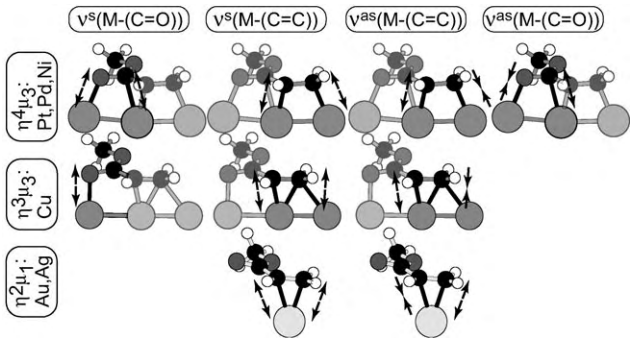

Figure 3. Molecule–metal stretching vibrations: symmetric ν^s(M−(C=O)), ν^s(M-(C=C)) and antisymmetric ν^{as}(M−(C=C)), ν^{as}(M−(C=O)).

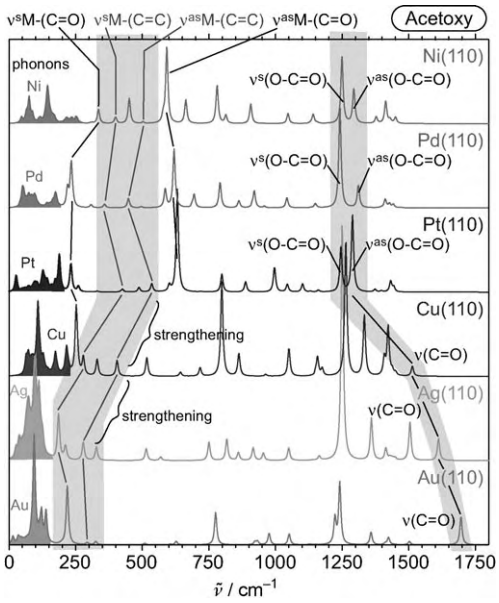

Figure 4. DFT EELS spectra of the most stable adsorption structures of the *trans* ester (acetoxy) compound on all the (110)-(1×2) surfaces.

number of normal modes intrinsically depends on the adsorption structure. Since the C=C bond systematically interacts with the metal, the symmetric ν^s(M−(C=C)) and antisymmetric ν^{as}(M−(C=C)) stretching modes are common characteristic vibrations for all surfaces (see Figure 3). On Cu(110), the additional Cu−O bond appearing in the $\eta^3\mu_3$ form provides a third ν(Cu−O) stretching mode. Moreover, the additional M−(C=O) bonds of the $\eta^4\mu_3$ structures on Pt, Pd, and Ni(110) give two supplementary vibrations: the symmetric ν^s(M−(C=O)) and antisymmetric ν^{as}(M−(C=O)) modes.

First, the type of adsorption structure determines the range of molecule–substrate frequencies. This result is demonstrated in Figure 2b and c by focusing the analysis on the symmetric and antisymmetric M−(C=C) vibrations. On Au and Ag, the weakly coordinated adsorbates ($\eta^2\mu_1$) are associated with softer mean ν^s(M−(C=C)) vibrations (210 and 189 cm^{-1}, respectively). In contrast, on Pt, Pd, and Ni, the multicoordinated molecules ($\eta^4\mu_3$) are associated with stronger mean stretching frequencies of 423, 357, and 399 cm^{-1} respectively. The intermediate $\eta^3\mu_3$ structure on Cu(110) has a medium averaged frequency of 289 cm^{-1}.

Hence, this clear-cut separation allows the definition of specific frequency ranges for each structure: 165–234 cm^{-1} for π, 280–300 cm^{-1} for $\eta^3\mu_3$, and 348–427 cm^{-1} for η^4 (see the shaded areas in Figure 2b). This analysis is supported by the results for the ν^{as}(M−(C=C)) vibrations with a systematic mean frequency shift of + 100 cm^{-1} (Figure 2c).

Second, the low molecule–metal frequencies are correlated with the adsorption strength, as shown in Figure 2b and c. A crude model averaged over the four molecules shows that the soft ν^s(M−(C=C)) and ν^{as}(M−(C=C)) vibrations are strengthened when the adsorption energy increases from noble metals (Au, Ag, Cu) to transition metals (Pd, Ni, Pt). This vibrational strengthening is indicated in the DFT EELS

 © 2006 Wiley-VCH Verlag GmbH & Co. KGaA, Weinheim

spectra of Figure 4. The mean slopes γ of the correlations are similar ($-140 \le \gamma \le -135\ cm^{-1}\ eV^{-1}$) for both M–(C=C) vibrations, which are separated by a mean vertical frequency shift of $+92\ cm^{-1}$. Beyond these correlations, the soft M–(C=C) vibrations are easily identifiable in the EELS spectra, since they are active and dominate the frequency range of 200–$600\ cm^{-1}$ with the M–(C=O) modes (left gray area in Figure 4). On sp metals ($\eta^2\mu_1$ and $\eta^3\mu_3$ structures), the M–(C=C) vibrations are intense at low frequencies, whereas they appear at higher frequencies for the $\eta^4\mu_3$ structures on d metals. In contrast, the C=O stretching mode can be recognized in the high-frequency region *only* if the C=O bond does not interact strongly with the metal surface (see the bands in the right gray area of Figure 4 at 1702, 1618, and $1519\ cm^{-1}$ for Au, Ag, and Cu respectively). In fact for strong adsorption on Pt, Pd, and Ni, the ν(C=O) vibration is coupled with ν(C–O) and appears at lower frequencies (1200–$1300\ cm^{-1}$). Such a frequency shift results in decreased coupling with the δ(CH) bending modes at 1300–$1450\ cm^{-1}$ and consequent attenuation of these latter vibrations.

The peculiar structure on Cu(110) is qualitatively explained by an electronic analysis based on the electron localization function (ELF). After adsorption on Au (see Figure 5a), the C=O and C=C bonds preserve a dominant

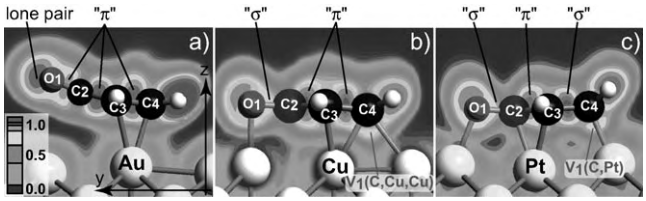

Figure 5. Two-dimensional sections in the *yz* plane of the isosurfaces of the ELF for adsorption of the *trans* aldehyde (formyl) on a) Au, b) Cu, and c) Pt.

π character, as shown by the presence of two disjointed disynaptic basins along the z axis (see the Supporting Information for more details). Conversely, the strong adsorption on Pt completely changes the picture in favor of a dominant σ character, as shown by the unique disynaptic basins around the bonds (Figure 5c). The pairing region with the metal is clearly revealed below the terminal C4 atom by the presence of a single disynaptic basin V_1(C,Pt). The intermediate structure on Cu is undeniably peculiar. The anomaly at C4 is explained as follows: Lateral shift of the C=C moiety results in loss of its π character. This favors the formation of an atypical pseudometallic three-centered bond between C4 and two Cu atoms characterized by one trisynaptic basin V_1(C,Cu,Cu) just below C4 (Figure 5b).

In summary, I have reported on a systematic theoretical investigation of the EELS spectra of multifunctional molecules on metal surfaces. Density functional theory calculations demonstrate that the low-frequency molecule–metal vibrations are strongly correlated with adsorption strength and structure, in agreement with previous results for CO and NO.[8,9] Weak adsorption on noble metals (Au, Ag) is associated with weakly coordinated π structures and provides softer molecule–metal stretching modes. Conversely, strong adsorption on transition metals (Pt, Pd, Ni) is stabilized by highly coordinated η^4 forms and results in harder M–(C=C) vibrations. The structure on Cu is an intermediate case in which the C=C bond forms an atypical multicentered bond with the surface. The calculated EELS spectra support the argument for possible recognition of the molecular structure on the basis of the frequency ranges of the soft vibrations. Future comparisons between new highly resolved spectroscopic investigations extended to low frequencies and the present theoretical results open exciting and promising perspectives for the structural identification of reactants in heterogeneous catalysis.

Received: May 26, 2006
Revised: July 10, 2006
Published online: September 6, 2006

Keywords: adsorption · density functional calculations · surface chemistry · transition metals · vibrational spectroscopy

[1] B. C. Stipe, M. A. Rezaei, W. Ho, *Science* **1998**, *280*, 1732.
[2] M. C. Asensio, D. P. Woodruff, A. W. Robinson, K.-M. Schindler, P. Gardner, D. Ricken, A. M. Bradshaw, J. C. Conesa, A. R. Gonzalez-Elipe, *Chem. Phys. Lett.* **1992**, *192*, 259.
[3] K.-M. Schindler, P. Hofmann, V. Fritzsche, S. Bao, S. Kulkarni, A. M. Bradshaw, D. P. Woodruff, *Phys. Rev. Lett.* **1993**, *71*, 2054.
[4] L. J. Lauhon, W. Ho, *J. Phys. Chem. A* **2000**, *104*, 2463.
[5] M.-L. Bocquet, H. Lesnard, N. Lorente, *Phys. Rev. Lett.* **2006**, *96*, 096101.
[6] W. A. Brown, D. A. King, *J. Phys. Chem. B* **2000** *104*, 2578.
[7] G. P. Williams, *J. Phys. Condens. Matter* **2001**, *13*, 11367.
[8] M. Gajdos, A. Eichler, J. Hafner, *J. Phys. Condens. Matter* **2004**, *16*, 1141.
[9] M. Gajdos, J. Hafner, A. Eichler, *J. Phys. Condens. Matter* **2006**, *18*, 13.
[10] K.-M. Schindler, P. Hofmann, K.-U. Weiss, R. Dippel, P. Gardner, V. Fritzsche, A. M. Bradshaw, D. P. Woodruff, M. E. Davila, M. C. Asensio, J. C. Conesa, A. R. Gonzalez-Elipe, *J. Electron Spectrosc. Relat. Phenom.* **1993**, *64*/65, 75.
[11] D. Loffreda, D. Simon, P. Sautet, *Chem. Phys. Lett.* **1998**, *291*, 15.
[12] F. Bournel, C. Laffon, P. Parent, G. Tourillon, *Surf. Sci.* **1996**, *350*, 60.
[13] F. Bournel, C. Laffon, P. Parent, G. Tourillon, *Surf. Sci.* **1996**, *359*, 10.
[14] J. C. de Jesus, F. Zaera, *Surf. Sci.* **1999**, *430*, 99.
[15] D. Loffreda, Y. Jugnet, F. Delbecq, J.-C. Bertolini, P. Sautet, *J. Phys. Chem. B* **2004**, *108*, 9085.
[16] D. Loffreda, *Surf. Sci.* **2006**, *600*, 2103.
[17] The η^2 structure reported previously[16] is metastable on Pt(110), Au(110), and Ag(110) and does not exist on Cu(110), Pd(110), and Ni(110).

 © 2006 Wiley-VCH Verlag GmbH & Co. KGaA, Weinheim

Heterogeneous Catalysis

DOI: 10.1002/anie.200600830

Hydrated Dibromodioxomolybdenum(VI) Supported on Zn-MCM-48 for Facile Oxidation of Methane**

*Fengbo Li and Guoqing Yuan**

Methane is the most abundant and low cost C_1 feedstock and is considered to be a clean substitute for dwindling petroleum resources. However, its efficient transformation to more valuable liquid products remains a great challenge.[1] The current route is a multistep and energy-intensive conversion that involves the incipient generation of syngas from methane.[2] With potentially many benefits, much effort has been directed towards the exploration of direct methods to partially oxidize and selectively functionalize one of the C–H bonds of methane, to convert it into valuable oxygenated and unsaturated compounds more efficiently, economically, and cleanly. As methane is an unreactive molecule, it reacts only under extreme conditions. Some methyl derivatives such as methanol,[3] methane sulfonic acid,[4] methane sulfonyl chlorides,[5] methyl bisulfate,[6] and acetic acid,[7] can be synthesized through the activation of methane in strong acid solvents with oxidants and radicals. Methane can also be activated over some solid catalysts with oxygen at high temperature, but selectivity towards valuable oxygenated products is poor. Catalytic methane-activation systems under mild conditions are all based on intricate metal complexes[8] and enzymes,[9] and their applications are limited to very small-scale syntheses.

Methane can be converted into oxygenates under mild conditions through a three-step catalytic recycling of the oxidation mediator by using oxygen as the ultimate oxidant: 1) oxidizing methane to methyl derivatives by an oxidation mediator; 2) converting the methyl derivatives into oxygenated compounds; 3) regenerating the oxidation mediator. We have reported a series of catalysts for the low-temperature vapor-phase conversion of methane to methanol via methyl bisulfate with supported concentrated sulfuric acid as the oxidation mediator.[10] Others have considered halogens as the oxidation mediator. Olah et al. described selective monohalogenation of methane over supported acid and platinum-metal catalysts followed by hydrolysis of methyl halides over γ-alumina-supported metal-oxide/hydroxide catalysts to convert methane into methanol and dimethyl ether.[11] Lorkovic and co-workers proposed a process for the functionalization of methane and ethane by using bromine as the mediator.[12] The process was carried out in a sequential zone-flow reactor (SZFR) that consisted of two serial reactors. In this process, the three-step conversions are actually carried out separately, and it is difficult to recycle the halogens.

Herein, we report the design and preparation of a novel multifunction methane-activation catalyst, hydrated dibromodioxomolybdenum(VI) supported on Zn-MCM-48 (a zinc-modified mesoporous silica), which integrates the three catalytic steps to transform methane into oxygenated products at a relatively low temperature ($<250\,^{\circ}C$). Bromine is derived from dibromodioxomolybdenum and can be recycled in the catalyst bed through bromine metathesis of metal bromide/metal oxide pairs. Bromine acts as the oxidation mediator and has advantages over other halogens; methane bromination is less exothermic than chlorination and proceeds spontaneously to completion. Bromine metathesis of metal bromide/metal oxide pairs can be accomplished under relatively mild conditions through the deoxidization of metal bromide with oxygen (the reduction potential of Br_2 (to Br^-) is 1.07 V versus a normal hydrogen electrode (NHE), and that of O_2 is 1.23 V).

MoO_2Br_2 is a useful precursor for the preparation of many excellent oxotransfer catalysts for chemical and biochemical processes.[13] Molybdenum in the MoO_2Br_2 core is on the borderline of stability between the V and VI oxidation states of the metal, which makes these compounds useful models for redox studies.[14] $MoO_2Br_2(H_2O)_2$ occurs in solutions of alkali molybdates, in concentrated hydrobromic acid, and it can be extracted with diethyl ether. Yellow crystals of $MoO_2Br_2(H_2O)_2{\cdot}2\,(Et)_2O$, which is the precursor for the preparation of $MoO_2Br_2(H_2O)_2$ supported on Zn-MCM-48, are obtained by cooling a solution of $MoO_2Br_2(H_2O)_2$ in diethyl ether to $-5\,^{\circ}C$.[15]

The catalytic cycles for the partial oxidation of methane are initiated by the decomposition of $MoO_2Br_2(H_2O)_2$. MoO_2Br_2 reacts readily with O_2 to release Br_2, which oxidizes C–H bonds to form HBr and a C–Br bond with higher selectivity than O_2. MoO_3 then scavenges the bromine atoms from HBr and the C–Br functionality to yield the oxidized products and regenerate MoO_2Br_2. The ultimate oxidant is oxygen, and bromine acts as the oxidation mediator. Figure 1 shows the test results for the partial oxidation of methane with $MoO_2Br_2(H_2O)_2$ supported on Zn-MCM-48-*N* (where *N* is the molar ratio of Si/Zn). The time-on-stream data (Figure 1a) show that zinc content has a great influence on the stability of the catalyst. Moreover, the zinc content provides control over the product distribution (Figure 1b). The presence of ZnO in the support induces the formation of dimethyl ether, which indicates that the product of the catalytic cycle involving $ZnBr_2$/ZnO pairs is different from that of MoO_2Br_2/MoO_3 pairs. The former affords predominantly dimethyl ether and the latter proceeds to yield methanol. With increasing zinc content the propensity towards deactivation is reduced gradually and the selectivity

[*] F. Li, Prof. G. Yuan
Beijing National Laboratory for Molecular Sciences
Laboratory of New Materials
Institute of Chemistry
Chinese Academy of Sciences
Beijing, 100080 (China)
Fax: (+88) 10-6255-9373
E-mail: yuangq@iccas.ac.cn

[**] This work supported by Sopu Chemical Co. China.

Supporting information for this article is available on the WWW under http://www.angewandte.org or from the author.

 © 2006 Wiley-VCH Verlag GmbH & Co. KGaA, Weinheim

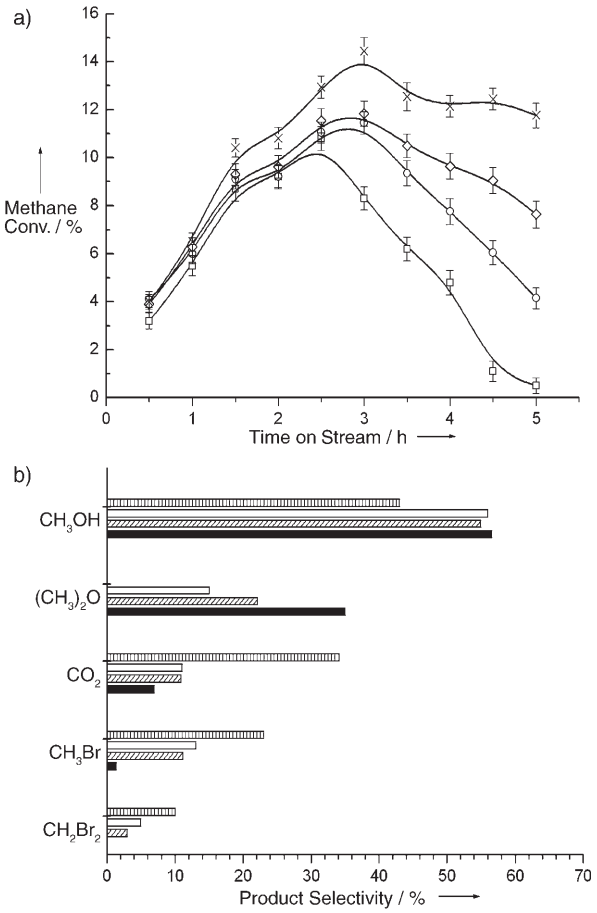

Figure 1. a) Time-on-stream data from catalytic-activity tests on $MoO_2Br_2(H_2O)_2$/MCM-48 (□), $MoO_2Br_2(H_2O)_2$/Zn-MCM-48-60 (○), $MoO_2Br_2(H_2O)_2$/Zn-MCM-48-40 (◇), and $MoO_2Br_2(H_2O)_2$/Zn-MCM-48-20 (×). The data are one-pass methane conversions, with error bars indicated. b) Product distribution after 2.5 h on the reaction stream for $MoO_2Br_2(H_2O)_2$/Zn-MCM-48-20 (black), $MoO_2Br_2(H_2O)_2$/Zn-MCM-48-40 (diagonal stripes), $MoO_2Br_2(H_2O)_2$/Zn-MCM-48-60 (white), and $MoO_2Br_2(H_2O)_2$/MCM-48 (vertical stripes).

towards the halocarbon species (CH_3Br and CH_2Br_2) dwindles. Bromine may leach from the catalyst column in the form of unconverted halocarbon species and bromine fumes, and this leaching is the main reason for the reduction in activity. Facile bromine metathesis of MoO_2Br_2/MoO_3 pairs increases the possibility of bromine leaching. The involvement of ZnO in the bromine metathesis of metal-bromide/metal-oxide pairs (Scheme 1) increases the chances of bromine being scavenged from HBr and the C–Br bond to yield the oxidized products. The moderate rate of bromine metathesis of the $ZnBr_2$/ZnO pair is an important factor for holding bromine in the catalyst column, and the promoting effects of $ZnBr_2$ on C–H bond bromination may also reduce the leaching of unconverted bromine.[16]

$$CH_4 + Br_2 \xrightarrow{ZnBr_2} CH_3Br + HBr \quad (1)$$
$$CH_3Br + HBr + ZnO \longrightarrow ZnBr_2 + CH_3OH \quad (2)$$
$$2\,CH_3Br + 2\,HBr + 2\,ZnO \longrightarrow 2\,ZnBr_2 + CH_3OCH_3 + H_2O \quad (3)$$
$$ZnBr_2 + 1/2\,O_2 \longrightarrow Br_2 + ZnO \quad (4)$$

$$CH_4 + 1/2\,O_2 \longrightarrow CH_3OH$$
or
$$2\,CH_4 + O_2 \longrightarrow CH_3OCH_3 + H_2O$$

Scheme 1. Proposed mechanism for the role of the zinc species in the catalytic cycle.

To obtain direct information about the role of bromine as mediator in the catalytic cycle, we have compared the catalytic conversion of methane by MoO_3 supported on Zn-MCM-48-20 and by MCM-48 before and after the introduction of bromine to the catalytic systems. Figure 2a shows that the catalytic systems have negligible methane conversion with the feed gas comprising methane, oxygen, and argon (Stage 1). After 2 h on the reaction stream, bromine is injected into the feed gas, which results in a sharp increase in methane conversion (Stage 2). This rise in activity clearly demonstrates the mediator role of bromine in the catalytic

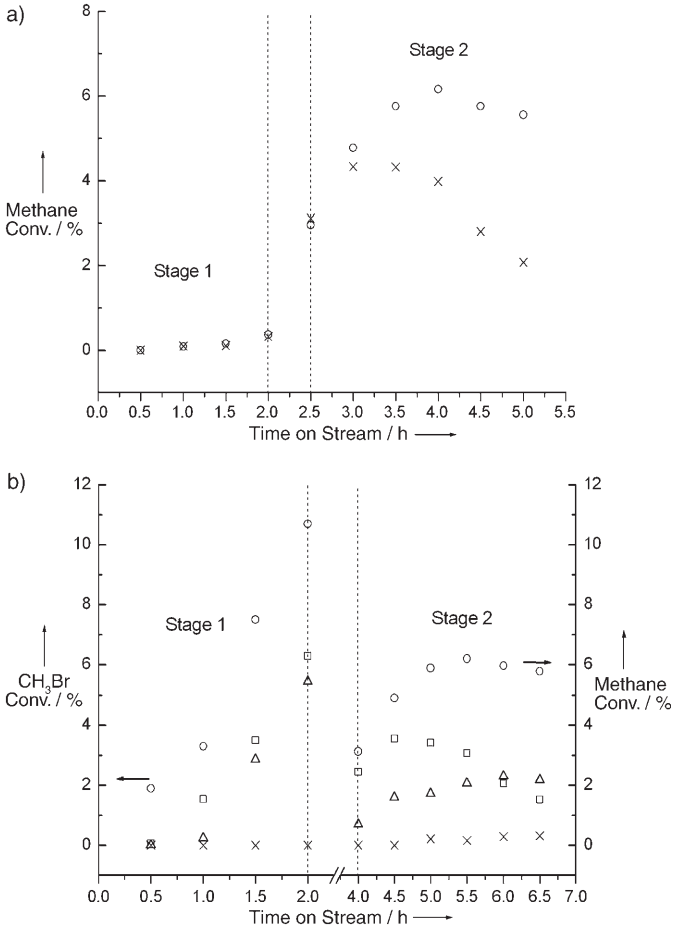

Figure 2. a) Time-on-stream data for MoO_3/Zn-MCM-48-20 (○) and MoO_3/MCM-48 (×), demonstrating the mediator role of bromine in the catalytic cycle. Stage 1: $CH_4/O_2/Ar$ (2:1:7) feed gas; Stage 2: after injection of bromine to the feed gas at 2 h. b) Control experiments on MoO_3/Zn-MCM-48-20 (○), MoO_3/MCM-48 (□), Zn-MCM-48-20 (△), and MCM-48 (×) to determine the bromine-metathesis activity of the catalyst components. Stage 1: $CH_3Br/HBr/Ar$ (1:1:8) feed gas; Stage 2: $CH_4/O_2/Ar$ (2:1:7) feed gas. After 2.0 h, the catalyst was gradually cooled in an argon flow.

 © 2006 Wiley-VCH Verlag GmbH & Co. KGaA, Weinheim

cycle. In Figure 2b, we present data from a control experiment to determine the performance of bromine scavenging from HBr and C–Br bonds by four solid catalysts with different compositions. During Stage 1, the feed gas for the reactor consists of CH_3Br, HBr, and argon. MCM-48 shows no activity for bromine metathesis. MoO_3 supported on Zn-MCM-48 yields some CH_3Br. At 2 h on the reaction stream, the reactor is cooled under an argon flow, and the feed gas is changed to a mixture of methane, oxygen, and argon. Methane conversion is detected for the three samples that show activity for bromine metathesis during Stage 1. The MoO_2Br_2/MoO_3 pairs show high bromine-metathesis activity and the $ZnBr_2/ZnO$ pairs have a high rate of bromine scavenging, but a lower rate of re-oxidation of $ZnBr_2$ to release bromine, which is the main mechanism for holding bromine in the catalytic systems, thus improving catalytic stability.

Based on the above experimental observation, we conclude that the catalytic cycle involves reversible bromine metathesis of two types of metal-bromide/metal-oxide pairs: MoO_2Br_2/MoO_3 pairs and $ZnBr_2/ZnO$ pairs, which show different bromine-metathesis activity. An X-ray photoelectron spectroscopy (XPS) spectrum of $MoO_2Br_2(H_2O)_2$ on Zn-MCM-48-20 was taken after 3 h on a stream of methane, oxygen, and argon (Figure 3a); fitting the Mo 3d envelope identifies two chemical states of molybdenum, in MoO_3 ($3d_{5/2}$ 232.28 eV) and the MoO_2Br_2 core ($3d_{5/2}$ 233.65 eV). The full width at half maximum (FWHM) ratio of MoO_3/MoO_2Br_2 is 1.1:1 and the peak-area ratio is 0.876:1, which evidences MoO_2Br_2/MoO_3 pairs in the catalytic cycle. Fitting of Mo 3d envelope of the XPS spectrum of MoO_3/Zn-MCM-48-20 taken after 2 h on a stream of CH_3Br, HBr, and argon under the given reaction conditions (Figure 3b) also demonstrates the presence of two chemical states of molybdenum, in MoO_3 ($3d_{5/2}$ 232.5 eV) and the MoO_2Br_2 core ($3d_{5/2}$ 233.3 eV). The FWHM ratio of MoO_3/MoO_2Br_2 is 1.13:1 and the peak area ratio is 3.01:1. These results confirm that the key step in bromine metathesis of the MoO_2Br_2/MoO_3 pair is the scavenging of bromine from HBr and a C–Br bond to yield the oxidized products and regenerate dibromodioxomolybdenum. Figure 3c shows XPS survey spectra of Zn-MCM-48-20 and MCM-48 after 2 h on the reaction stream of CH_3Br, HBr, and argon. The presence of the Br^- peak (69.6 eV) in the spectrum of Zn-MCM-48-20 suggests that ZnO can scavenge bromine from HBr and a C–Br bond to yield the oxidized products and form $ZnBr_2$. This result confirms the involvement of $ZnBr_2/ZnO$ pairs in the bromine metathesis.

In summary, we have demonstrated that $MoO_2Br_2(H_2O)_2$ supported on Zn-MCM-48 readily converts methane into oxygenated products (methanol and dimethyl ether) with high selectivity at low reaction temperatures. The catalytic cycle proceeds by the reversible bromine metathesis of MoO_2Br_2/MoO_3 pairs and $ZnBr_2/ZnO$ pairs. Bromine acts as the oxidation mediator, and oxygen is the oxidant. However, many issues require further investigation, such as the bromine-metathesis efficiency of the metal-bromide/metal-oxide pairs and the product control provided by the catalyst components.

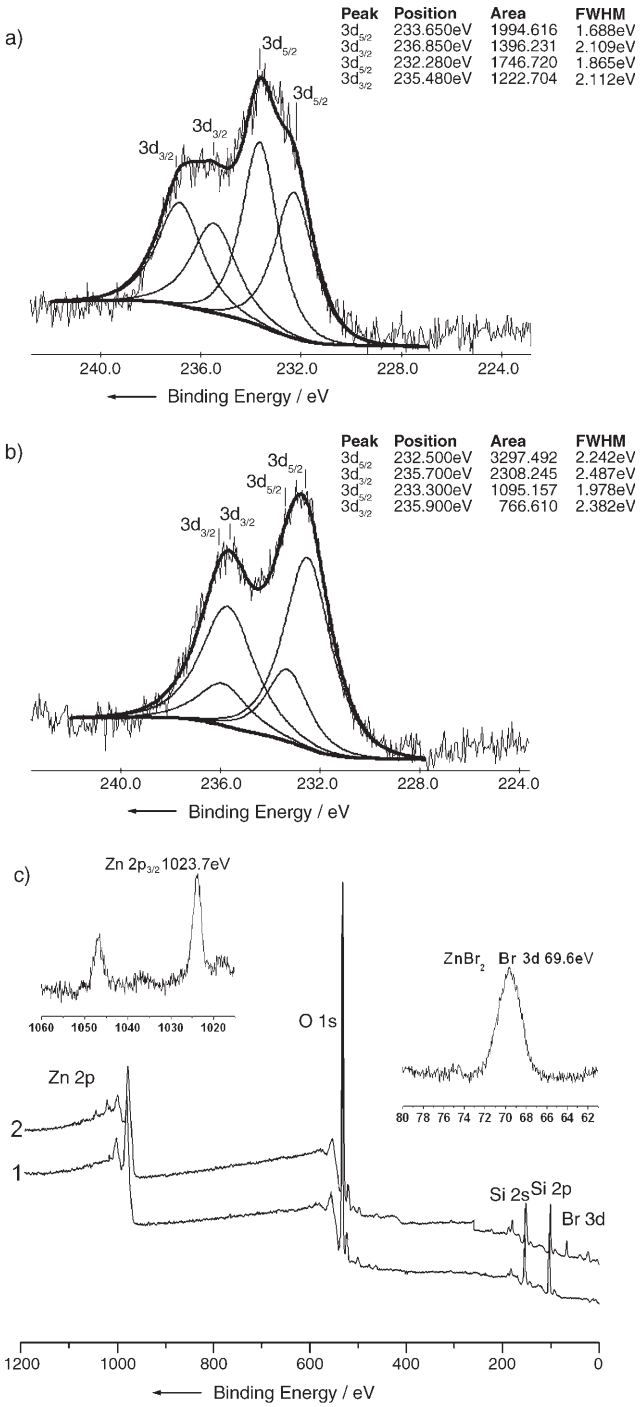

Figure 3. a) Mo 3d envelope in the XPS spectrum of $MoO_2Br_2(H_2O)_2$/Zn-MCM-48-20 after 3 h on a reaction stream of $CH_4/O_2/Ar$; peak fitting is indicated. b) Mo 3d envelope in the XPS spectrum of MoO_3/Zn-MCM-48-20 after 2 h on a reaction stream of $CH_3Br/HBr/Ar$; peak fitting is indicated. c) XPS survey spectra of MCM-48 (1) and Zn-MCM-48-20 (2) after 2 h on a reaction stream of $CH_3Br/HBr/Ar$; insets are enlargements of the Zn 2p and Br 3d envelopes.

Experimental Section

The Zn-MCM-48 materials were synthesized as follows. The required amount of silica (tetraethyl orthosilicate) and zinc precursors (zinc hydroxide) was added to a stirred solution of cetyltrimethylammo-

 © 2006 Wiley-VCH Verlag GmbH & Co. KGaA, Weinheim

nium hydroxide (CTAOH). The molar ratio of the incipient gel was $SiO_2/x\,Zn(OH)_2/0.28\,CTAOH/42\,H_2O$ (for which $x = 0.017$, 0.025, 0.05, 0.1, 0.2). After aging in a sealed autoclave at 150 °C for 24 h, the resulting solid was collected by filtration, washed with a copious amount of deionized water, and then calcinated at 550 °C for 6 h to yield Zn-MCM-48. Pure silica MCM-48 was prepared by using the synthesis gel with a ratio of $SiO_2/0.28\,CTAOH/42\,H_2O$.

A solution of $MoO_2Br_2(H_2O)_2$ in diethyl ether was synthesized by an established method.[15] $MoO_2Br_2(H_2O)_2$/Zn-MCM-48 catalysts were prepared by impregnating Zn-MCM-48 materials (dried at 300 °C under vacuum before use) in a solution of $MoO_2Br_2(H_2O)_2$ in diethyl ether, then drying the materials at room temperature under high vacuum for several hours. The load of $MoO_2Br_2(H_2O)_2$ was 8 wt %. MoO_3/Zn-MCM-48 and MoO_3/MCM-48 were prepared by decomposing $MoO_2Br_2(H_2O)_2$/Zn-MCM-48 and $MoO_2Br_2(H_2O)_2$/MCM-48 in air at 150 °C. The catalytic activity was measured in a conventional fixed-bed reactor at 220 °C with a feed gas consisting of methane, oxygen, and argon (1.6 g of catalyst, $P_{total} = 1.0$ MPa, $P_{Ar}/P_{CH_4}/P_{O_2} = 7{:}2{:}1$, $W/F = 0.3\ g\,min\,cm^{-3}$; P is pressure, W is the weight of catalyst, and F is the reactant flow rate). Product analysis was performed on a DB5 column (30 m × 0.25 mm) by using a VG Trio 200 spectrometer, with a thermal conductivity detector (TCD) or an MS detector. Conversion and selectivity are defined as (% conversion) = $[([CH_4]_{inlet} - [CH_4]_{outlet})/[CH_4]_{inlet}]\,100$ and (% selectivity to X) = $[[X]/([CH_4]_{inlet} - [CH_4]_{outlet})]\,100$.

The Zn-MCM-48 materials and the samples loaded with $MoO_2Br_2(H_2O)_2$ were characterized by powder X-ray diffraction, N_2 adsorption, and XPS. Detailed characterization data are presented in the Supporting Information.

Received: March 3, 2006
Revised: July 6, 2006
Published online: September 5, 2006

Keywords: heterogeneous catalysis · mesoporous materials · metathesis · molybdenum · oxidation

[1] a) R. H. Crabtree, *Chem. Rev.* **1995**, *95*, 987; b) J. H. Lunsford, *Catal. Today* **2000**, *63*, 165.
[2] Z.-P. Liu, P. Hu, *J. Am. Chem. Soc.* **2002**, *124*, 11568.
[3] a) D. Wolf, *Angew. Chem.* **1998**, *110*, 3545; *Angew. Chem. Int. Ed.* **1998**, *37*, 3351; b) X. Gang, H. Birch, Y. Zhu, H. A. Hjuler, N. J. Bjerrum, *J. Catal.* **2000**, *196*, 287.
[4] a) N. Basiches, T. E. Hogan, A. Sen, *J. Am. Chem. Soc.* **1996**, *118*, 13111; b) S. Mukhopadhyay, A. T. Bell, *J. Am. Chem. Soc.* **2003**, *125*, 4406.
[5] S. Mukhopadhyay, M. Zerella, A. T. Bell, V. Srinivas, *Chem. Commun.* **2004**, 472.
[6] a) R. A. Periana, D. J. Taube, S. Gamble, H. Taube, T. Satoh, H. Fuji, *Science* **1998**, *280*, 560; b) R. A. Periana, O. Mirinov, D. J. Taube, S. Gamble, *Chem. Commun.* **2002**, 2376.
[7] a) M. Lin, A. Sen, *Nature* **1994**, *368*, 613; b) M. Zerella, S. Mukhopadhyay, A. T. Bell, *Org. Lett.* **2003**, *5*, 3193; c) Y Taniguchi, T. Hayashida, H. Shibasaki, D. Piao, T. Kitamura, T. Yamaji, Y. Fujiwara, *Org. Lett.* **1999**, *1*, 557; d) R. A. Periana, O. Mirinov, D. Taube, G. Bhalla, C. J. Jones, *Science* **2003**, *301*, 814.
[8] a) W. Cui, X. P. Zhang, B. B. Wayland, *J. Am. Chem. Soc.* **2003**, *125*, 4994; b) I. Bar-Nahum, A. M. Khenkin, R. Neumann, *J. Am. Chem. Soc.* **2004**, *126*, 10236.
[9] M.-H. Baik, M. Newcomb, R. A. Friesner, S. J. Lippard, *Chem. Rev.* **2003**, *103*, 2385.
[10] F. Li, G. Yuan, *Chem. Commun.* **2005**, 2238.
[11] G. A. Olah, B. Gupta, M. Farina, J. D. Felberg, W. M. Ip, A. Husain, R. Karpeles, K. Lammertsma, A. K. Melhotra, N. J. Trivedi, *J. Am. Chem. Soc.* **1985**, *107*, 7097.
[12] X. P. Zhou, A. Yilmaz, G. A. Yilmaz, I. V. Lorkovic, L. E. Laverman, M. Weiss, J. H. Sherman, E. W. McFarland, G. D. Stucky, P. C. Ford, *Chem. Commun.* **2003**, 2294.
[13] H. K. Lee, Y. L. Wong, Z. Y. Zhou, Z. Y. Zhang, D. K. P. Ng, T. C. W. Mak, *J. Chem. Soc. Dalton Trans.* **2000**, 539.
[14] a) P. Ferreira, I. S. Gonçalves, F. E. Kühn, A. D. Lopes, M. A. Martins, M. Pillinger, A. Pina, J. Rocha, C. C. Romão, A. M. Santos, T. M. Santos, A. A. Valente, *Eur. J. Inorg. Chem.* **2000**, 2263; b) M. Jia, A. Seifert, W. R. Thiel, *Chem. Mater.* **2003**, *15*, 2174.
[15] F. J. Arnaiz, M. R. Pedrosa, R. Aguado, *Inorg. Synth.* **2004**, *34*, 49.
[16] J. H. Clark, J. C. Ross, D. J. Macquarrie, S. T. Barlow, T. W. Bastock, *Chem. Commun.* **1997**, 1203.

 © 2006 Wiley-VCH Verlag GmbH & Co. KGaA, Weinheim

Corroles

DOI: 10.1002/anie.200601399

Iron and Manganese Corroles Are Potent Catalysts for the Decomposition of Peroxynitrite**

*Atif Mahammed and Zeev Gross**

Peroxynitrite, which is formed in vivo by the reaction of NO and O_2^-, is more toxic than all other isolable reactive oxygen species because there are no specific enzymes for preventing its spontaneous decay to radical-decomposition products that damage cellular molecules such as DNA, peptides, proteins, sugars, and lipids.[1–4] Strong evidence points toward peroxy nitrite as being heavily involved in many biological malfunctions initiated by oxidative stress,[5] and the same holds for neurodegenerative disorders that (among many others) include Alzheimer's, Parkinson's, and Huntington's diseases.[6–10] The damage-inducing properties of peroxynitrite are known to derive from the homolytic bond cleavage of its protonated form (HOONO, dominant at physiological pH) to $^{\bullet}OH$ and $^{\bullet}NO_2$ [Eq. (1)].[3–5] These strong oxidizing and

$$HOONO \rightarrow {}^{\bullet}OH + {}^{\bullet}NO_2 \quad (1)$$

nitrating species cause irreversible damage and/or chemical modification to almost any biomolecule,[11] thus highlighting the urgent need to develop effective bioavailable compounds that will catalyze the transformation of peroxynitrite into

[*] Dr. A. Mahammed, Prof. Dr. Z. Gross
Department of Chemistry
Technion—Israel Institute of Technology
Haifa 32000 (Israel)
Fax: (+972) 4-8295703
E-mail: chr10zg@tx.technion.ac.il

[**] This work was supported by the ISF under grant 330/04.

WILEY InterScience DISCOVER SOMETHING GREAT
© 2006 Wiley-VCH Verlag GmbH & Co. KGaA, Weinheim

benign products [Eqs. (2) and (3)].

$$HOONO \rightarrow H^+ + NO_3^- \quad (2)$$

$$2\,HOONO \rightarrow 2\,H^+ + 2\,NO_2^- + O_2 \quad (3)$$

The seminal findings that initiated much research in this field were the stoichiometric and catalytic decomposition of peroxynitrite by water-soluble manganese(III) and iron(III) porphyrins, reported by Groves and Marla in 1995 and Stern et al. in 1996, respectively.[12] Metalloenzymes were also explored for the same purpose and some encouraging results were obtained in several in vivo investigations.[13] Another ongoing emphasis is on resolving the mechanism of action, mainly through determination of the rate constants of elementary steps relevant to the overall catalytic process.[14] It is now clear that there are two distinct pathways for detoxification of peroxynitrite: isomerization to nitrate [Eq. (2)] and disproportionation to nitrite and molecular oxygen [Eq. (3)].[15]

Many details regarding the mechanism of catalysis by metalloporphyrins are now resolved, with most indications pointing toward elementary steps that involve only one-electron redox processes (M^{III} and M^{IV}; M = Fe, Mn).[14–17] The (oxo)iron(IV) intermediates react further with the decomposition products of peroxynitrite and thus complete a catalytic cycle. Although (oxo)manganese(IV) porphyrins are formed very fast, by either homolytic O–O scission or by the reduction of (oxo)manganese(V) intermediates by NO_2^-,[12a] they do not react further with either peroxynitrite or any of its products and are hence limited to single-turnover reactions.[13] Catalytic decomposition of peroxynitrite by manganese(III) porphyrins is only achievable in the presence of stoichiometric amounts of sacrificial antioxidants.[17]

The recent disclosures of facile methods for the synthesis of corroles paved the way to research that revealed the great potential of the corresponding metal complexes as catalysts for quite a variety of reactions.[18–20] Of particular relevance to this study are the amphiphilic corrole **1** and its metal complexes (Scheme 1).[21] They associate very strongly to proteins,[22] and the noncovalently conjugated iron(III) and manganese(III) corroles (**1**-Fe and **1**-Mn, respectively) catalyze the peroxidase-like enantioselective oxidation of sulfides and the catalase-like decomposition of hydrogen peroxide to water and molecular oxygen.[23a] The last phenomenon triggered our interest in the reactions of metallocorroles

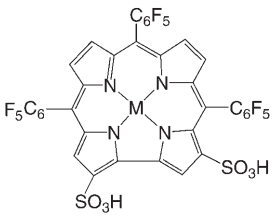

1: M = 3H
1-Fe: M = Fe^{III}
1-Mn: M = Mn^{III}

Scheme 1. Amphiphilic corrole **1** and its metal complexes.

with other reactive oxygen species, of which peroxynitrite was selected as the highest priority target for the reasons outlined above. Herein, we show that the catalytic rate for decomposition of peroxynitrite by **1**-Fe is significantly larger than that of analogous porphyrins and second only to the most-optimized positively charged iron porphyrin. The more important result is that **1**-Mn also displayed catalytic activity, contrary to all other manganese complexes. The results further illustrate that catalysis by **1**-Mn is a genuine disproportionation process [Eq. (3)], which proceeds through reactions that do not create any radical species.

The investigations started by examining the decay of peroxynitrite at pH 7.4 and 25 °C in the presence and absence of various amounts of catalyst. The results shown in Figure 1

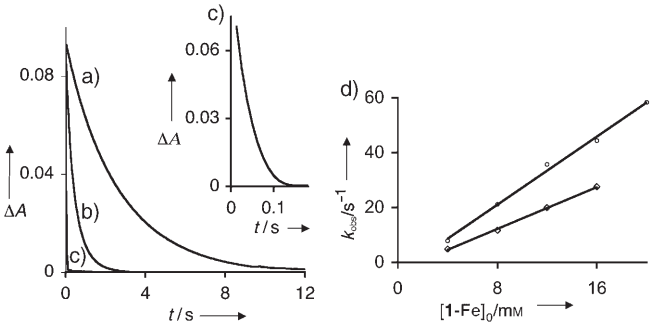

Figure 1. a–c) Decomposition of 385 μM peroxynitrite at pH 7.4 and 25 °C monitored at $\lambda = 302$ nm, the λ_{max} of peroxynitrite, without catalyst (a), or in the presence of 16 μM (4 mol%) **1**-Mn (b) or **1**-Fe (c; shown at two timescales). d) Observed decomposition rates of peroxynitrite (385 μM, pH 7.4) as a function of **1**-Fe concentration at 25 °C (lower trace) and 37 °C (upper trace).

(curves a–c) are representative of the first-order decays that were obtained in all cases. The results obtained without catalyst, that is, spontaneous decay of peroxynitrite with an apparent first-order rate constant of 0.38 s^{-1}, are practically identical to those of previous reports under comparable conditions.[12–17] In the presence of the catalysts the half-life of peroxynitrite was dramatically shortened from 1.8 to 0.31 and 0.025 s with **1**-Mn and **1**-Fe, respectively. Plots of rate constants at various catalyst concentrations revealed linear relationships (Figure 1, right) and the thus-elucidated k_{cat} values were 4.0×10^4 (**1**-Mn, 25 °C), 8.6×10^4 (**1**-Mn, 37 °C), 2.0×10^6 (**1**-Fe, 25 °C), and 3.1×10^6 $M^{-1}s^{-1}$ (**1**-Fe, 37 °C). The catalytic rate of **1**-Fe is two to ten times higher than values reported for the most-active iron porphyrins ($k_{cat} = 0.3$ to 1.6×10^6 $M^{-1}s^{-1}$ at 37 °C),[24] except for the one reported by Szabó et al. ($k_{cat} = 6.25 \times 10^6$ $M^{-1}s^{-1}$ at 25 °C).[13b] The catalytic performance of **1**-Mn (almost 1900 turnovers, see below) is most novel, when considering that all other manganese complexes (including complexes with porphyrins) reported to date do not catalyze the reaction without the aid of sacrificial agents.[13,17]

The amount of nitrite formed was monitored to distinguish between the possible modes for the decomposition of peroxynitrite [Eqs. (1)–(3)]. The yield was almost quantitative (95% NO_2^- relative to $^-OON{=}O$) with **1**-Mn as the

 © 2006 Wiley-VCH Verlag GmbH & Co. KGaA, Weinheim

catalyst, whereas that obtained under catalysis by **1**-Fe (25% NO_2^-) was even less than the yield from the spontaneous decay of peroxynitrite (30% NO_2^-). These results clearly suggest that the main modes of catalytic action are different: isomerization [Eq. (2)] for **1**-Fe and disproportionation [Eq. (3)] for **1**-Mn. The latter conclusion gains further support from the very efficient disproportionation of hydrogen peroxide by **1**-Mn,[23a] considering that both reactions share the same essential requirements. The substrate (H_2O_2 or HOONO) must be able to act as a two-electron oxidant of manganese(III) to (oxo)manganese(V), as well as a two-electron reductant of the latter. These two elementary steps are outlined in Equations (4) and (5) for peroxynitrite, and

$$\text{HOONO} + \textbf{1}\text{-Mn}^{\text{III}} \rightarrow \text{H}^+ + \text{NO}_2^- + \textbf{1}\text{-Mn}^{\text{V}}(\text{O}) \quad (4)$$

$$\text{HOONO} + \textbf{1}\text{-Mn}^{\text{V}}(\text{O}) \rightarrow \text{H}^+ + \text{NO}_2^- + \text{O}_2 + \textbf{1}\text{-Mn}^{\text{III}} \quad (5)$$

the corresponding catalytic cycle [consistent with the stoichiometry of Eq. (3)] is drawn in Scheme 2.

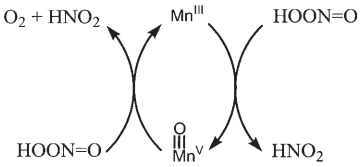

Scheme 2. Proposed catalytic cycle for disproportionation of peroxynitrite catalyzed by manganese(III) corrole.

The above proposal was tested by simultaneously recording spectral changes in the UV (peroxynitrite decomposition) and visible parts of the electronic spectrum (possible time-dependent changes in the structure of the catalyst). At pH 7.4, the decay at 302 nm was not accompanied by any changes in the visible spectrum of **1**-Mn (Figure 2a). This rules out the accumulation of reaction intermediates with lifetimes that would allow detection at the 3-ms intervals that were used. Nevertheless, strong evidence for the involvement of the (oxo)manganese(V) intermediate **1**-Mn(O) (accessible by oxidation of **1**-Mn by iodosylbenzene)[23a] was obtained in separate experiments. The decay of independently prepared **1**-Mn(O) was found to be quite slow in aqueous solutions of pH 7.4 (Figure 2b), but addition of peroxynitrite at any time caused its immediate reduction to **1**-Mn. Secondly, **1**-Mn(O) was the steady-state intermediate when the reaction between peroxynitrite and **1**-Mn was carried out at high pH value (Figure 2c), conditions under which (oxo)manganese(V) complexes are much less reactive.[23b,c] These results add significant confidence to the proposed elementary steps described in Equations (4) and (5) and the catalytic cycle drawn in Scheme 2. Apparently, the reactions of peroxynitrite with both **1**-Mn [Eq. (4)] and the (oxo)manganese(V) intermediate [Eq. (5)] are very fast at physiologically relevant pH values. The results shown in Figure 2a and c also highlight the stability of the catalyst, which is neither bleached nor irreversibly modified, as is the case with iron enzymes.[25] The most critical test was performed by quantifying the

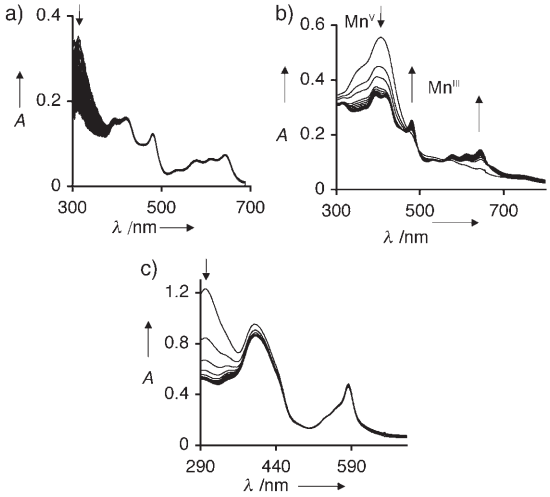

Figure 2. Time-resolved diode-array absorption spectra (25 °C) recorded at a) 3-ms intervals (0–0.3 s) during the reaction of **1**-Mn (40 μM) with peroxynitrite (1400 μM) at pH 7.4; b) at 20-s intervals (0–200 s) during the slow transformation of the (oxo)manganese(V) complex **1**-Mn(O) to **1**-Mn at pH 7.4; and c) at 10-s intervals (0–110 s) during the reaction of **1**-Mn (36 μM) with peroxynitrite (720 μM) at pH 12.7. Note: the spectrum of independently prepared **1**-Mn(O) is identical to that obtained by the reaction of **1**-Mn with peroxynitrite at the same pH value.

amount of molecular oxygen released in a relatively large-scale reaction,[26] which corresponded to a chemical yield of 98% O_2 and 1875 catalytic turnovers of **1**-Mn.

Examination of the **1**-Fe-catalyzed reaction by similar means revealed much more complicated phenomena. Decomposition of peroxynitrite (385 μM, 11 μM catalyst, 302 nm) displayed a first-order decay with a half lifetime of 38 ms (reaction is 94% complete within 0.15 s), while changes in the visible part of the spectrum were clearly inconsistent with one major species in a steady-state concentration. For example, there was an intensity increase at 432 nm in the first 2 ms that was followed by a nonexponential decay extending to 0.3 s. This result is reminiscent of the iron porphyrin system, where multiple pathways contribute to the overall catalytic cycle and its efficiency.[16] Accordingly, the complicated task of elucidating which particular elementary steps are responsible for the fast catalysis by iron corroles was postponed to future studies.

The complexes introduced in this work catalyze the decomposition of peroxynitrite very efficiently. The iron corrole is among the fastest-performing catalysts reported to date and approaches the speed of the most-active positively charged porphyrin.[13b] All results are consistent with disproportionation, by the mechanism shown in Scheme 2, as the dominant mechanism for catalysis by the manganese complex. The striking contrast between the results obtained with manganese(III) complexes of porphyrins and the corrole serves to emphasize the main advantage of the new catalyst. The less-reducing porphyrin-chelated manganese(III) complexes are oxidized by peroxynitrite to (oxo)manganese(IV) porphyrins, which are not reactive enough toward peroxynitrite and/or its decomposition products. However, two-

 © 2006 Wiley-VCH Verlag GmbH & Co. KGaA, Weinheim

electron oxidation of manganese(III) corroles is a facile process,[27] and the (oxo)manganese(V) corroles obtained are of sufficient reactivity for oxidizing peroxynitrite and thus completing the catalytic cycle.

This difference is of fundamental importance as regards the possible utilization of such catalysts in medicinal applications. While catalytic systems that rely on one-electron redox processes may be very useful for synthetic purposes,[28] the radical species that are involved are clearly prohibitive in biochemical environments. Recent demonstrations of the low cytotoxicity of these corroles and their facile, noncovalent conjugation to targeting proteins[29] further highlight the great potential of these compounds as catalysts for the prevention of peroxynitrite-induced damage to biological molecules. We assume that these findings will have a profound impact on the possible use of metallocorroles in preventive therapeutic treatments. One focus in forthcoming research is on increasing the catalytic rate to reach that obtained by the combination of metalloporphyrins and sacrificial reducing agents.[17]

Experimental Section

1-Fe and **1**-Mn were prepared by reported procedures.[21–23] Peroxynitrite was prepared from the reaction of sodium nitrite with acidified hydrogen peroxide according to reported procedures, which included a treatment for destroying excess H_2O_2.[30] Nitrite was quantified by the Griese reagent.[16] Time-resolved visible spectra were recorded on an Applied Photophysics PiStar-180 spectrometer in the photodiode-array fast-scan mode. Reaction kinetics were collected in the photomultiplier mode on the PiStar-180 spectrometer, using a single mixing mode. One syringe contained peroxynitrite (770 μM) in NaOH (50 mM), and the other contained phosphate buffer with or without the catalysts. Equal volumes were injected into a stopped-flow cell, and the pH value of the reaction mixture was measured at the outlet. The configuration of the instrument permitted continuous flow of water from a thermostated bath over the flow path and firing syringes containing the reagents. Peroxynitrite decay was monitored at 302 nm. First-order decay rates (k_{obs}) were fitted by standard techniques with software provided by the instrument manufacturer.

Received: April 9, 2006
Revised: June 20, 2006
Published online: September 8, 2006

Keywords: corroles · homogeneous catalysis · iron · manganese · peroxynitrite

[1] C. Szabo, *Toxicol. Lett.* **2003**, *140–141*, 105.
[2] R. Bryk, P. Griffin, C. Nathan, *Nature* **2000**, *407*, 211.
[3] G. Merenyl, J. Lind, S. Goldstein, G. Czapski, *Chem. Res. Toxicol.* **1998**, *11*, 712.
[4] J. S. Beckman, *Chem. Res. Toxicol.* **1996**, *9*, 836.
[5] J. S. Beckman, T. W. Beckman, J. Chen, P. A. Marshall, B. A. Freeman, *Proc. Natl. Acad. Sci. USA* **1990**, *87*, 1620.
[6] S. A. Lipton, Y.-B. Choi, Z.-H. Pan, S. Z. Lei, H.-S. Vincent Chen, N. J. Sucher, J. Loscalzo, D. J. Singel, J. S. Stamler, *Nature* **1993**, *364*, 626.
[7] J. Zhang, V. L. Dawson, T. M. Dawson, S. H. Snyder, *Science* **1994**, *263*, 687.
[8] J. S. Beckman, M. Carson, C. D. Smith, W. H. Koppenol, *Nature* **1993**, *364*, 584.
[9] M. Wiedau-Pazos, J. J. Goto, S. Rabizadeh, E. B. Gralla, J. A. Roe, M. K. Lee, J. S. Valentine, D. E. Bredsen, *Science* **1996**, *271*, 515.
[10] W. R. Markesbery, *Free Radical Biol. Med.* **1997**, *23*, 134.
[11] R. E. Huie, S. Padmaja, *Free Radical Res. Commun.* **1993**, *18*, 195.
[12] a) J. T. Groves, S. S. Marla, *J. Am. Chem. Soc.* **1995**, *117*, 9578; b) M. K. Stern, M. P. Jensen, K. Kramer, *J. Am. Chem. Soc.* **1996**, *118*, 8735.
[13] a) G. Ferrer-Sueta, C. Quijano, B. Alvarez, R. Radi, *Methods Enzymol.* **2002**, *349*, 23; b) C. Szabó, J. G. Mabley, S. M. Moeller, R. Shimanovich, P. Pacher, L. Virág, F. G. Soriano, J. H. Van Duzer, W. Williams, A. L. Salzman, J. T. Groves, *Mol. Med.* **2002**, *8*, 571.
[14] J. L. Julianne, A. Hunt, J. T. Groves, *J. Am. Chem. Soc.* **1998**, *120*, 7493.
[15] J. W. Coddington, J. K. Hurst, S. V. Lymar, *J. Am. Chem. Soc.* **1999**, *121*, 2438.
[16] R. Shimanovich, J. T. Groves, *Arch. Biochem. Biophys.* **2001**, *387*, 307.
[17] J. Lee, J. A. Hunt, J. T. Groves, *J. Am. Chem. Soc.* **1998**, *120*, 6053.
[18] Z. Gross, H. B. Gray, *Adv. Synth. Catal.* **2004**, *346*, 165.
[19] L. Simkovich, A. Mahammed, I. Goldberg, Z. Gross, *Chem. Eur. J.* **2001**, *7*, 1041.
[20] L. Simkhovich, Z. Gross, *Tetrahedron Lett.* **2001**, *42*, 8089.
[21] A. Mahammed, I. Goldberg, Z. Gross, *Org. Lett.* **2001**, *3*, 3443.
[22] A. Mahammed, H. B. Gray, J. J. Weaver, K. Sorasaene, Z. Gross, *Biconj. Chem.* **2004**, *15*, 738.
[23] a) A. Mahammed, Z. Gross, *J. Am. Chem. Soc.* **2005**, *127*, 2883; b) F. Chen, S.-H. Cheng, C.-H. Yu, M.-H. Liu, Y. O. Su, *J. Electroanal. Chem.* **1999**, *474*, 52; c) N. Jin, J. L. Bourassa, S. C. Tizio, J. T. Groves, *Angew. Chem.* **2000**, *112*, 4007; *Angew. Chem. Int. Ed.* **2000**, *39*, 3849.
[24] M. P. Jensen, D. P. Riley, *Inorg. Chem.* **2002**, *41*, 4788.
[25] J. L. Bourassa, E. P. Ives, A. L. Marqueling, R. Shimanovich, J. T. Groves, *J. Am. Chem. Soc.* **2001**, *123*, 5142.
[26] A peroxynitrite solution (0.15 M, 2 mL) was added to a phosphate buffer solution of **1**-Mn (2.66×10^{-5} M, 6 mL, final pH of 7.4) at 25 °C and the amount of O_2(g) was quantified volumetrically as 3.6 mL. This result translates to 49% relative to peroxynitrite, which corresponds to a chemical yield of 98% with respect to Equation (3) and 1875 catalytic turnovers.
[27] Z. Gross, G. Golubkov, L. Simkhovich, *Angew. Chem.* **2000**, *112*, 4211; *Angew. Chem. Int. Ed.* **2000**, *39*, 4045.
[28] M. W. Grinstaff, M. G. Hill, J. A. Labinger, H. B. Gray, *Science* **1994**, *264*, 1311.
[29] H. Agadjanian, J. J. Weaver, A. Mahammed, A. Rentsenorj, S. Bass, J. Kim, I. J. Dmochowski, R. Margalit, H. B. Gray, Z. Gross, L. K. Medina-Kauwe, *Pharm. Res.* **2006**, *23*, 367.
[30] J. A. Hunt, J. Lee, J. T. Groves, *Chem. Biol.* **1997**, *4*, 845.

 © 2006 Wiley-VCH Verlag GmbH & Co. KGaA, Weinheim

Metalation

DOI: 10.1002/anie.200602288

Alkali-Metal-Mediated Zincation of Polycyclic Aromatic Hydrocarbons: Synthesis and Structures of Mono- and Dizincated Naphthalenes**

William Clegg, Sophie H. Dale, Eva Hevia, Lorna M. Hogg, Gordon W. Honeyman, Robert E. Mulvey, and Charles T. O'Hara*

Since the pioneering work of Schlenk nearly a century ago, alkali-metal–organic compounds (organolithium reagents, in particular) have served as frontline reagents in the battle to advance chemical synthesis. Metal–hydrogen exchange (metalation) in which a relatively inert carbon–hydrogen bond is transformed into a more labile carbon–alkali-metal bond, thus opening up a myriad of bond-forming possibilities at the carbon center, represents one of the oldest and still most important general uses of these centurial reagents.[1,2] Recently, however, new variations of these fundamental synthetic strategies have started to emerge in which the alkali metal, though still actively involved in the exchange reaction, takes on more of a secondary, supporting role, as the vanguard metals attacking the carbon centers are now either magnesium, zinc, or aluminum. On their own, these less electropositive metals generally form slow-reacting, ineffectual metalating agents, but combining them with an alkali-metal component appears to activate a special synergy that greatly enhances the power of the magnesiation, zincation, or alumination. Kondo et al. emphasized the importance of the "precomplexation of lithium TMP and tBu$_2$Zn" (TMP = 2,2,6,6-tetramethylpiperidine) in the zincate reagent "[Li$^+${tBu$_2$Zn(tmp)}]$^-$", which acts as a highly chemoselective base towards a series of functionalized aromatic and heteroaromatic compounds.[3] We recently extended this idea of alkali-metal-mediated zincation (AMMZ) to sodium through the *N*,*N*,*N*′,*N*′-tetramethyl-1,2-ethanediamine (TMEDA)-chelated zincate [(tmeda)Na(μ-tmp)(μ-tBu)Zn(tBu)] (**1**),[4] which can effect the directed *ortho*-zincation of *N*,*N*-diisopropylbenzamide,[5] directed *meta*-zincation of *N*,*N*-dimethylanilines,[6] and the selective delivery of a tBu$^-$ nucleophile to the 6-position of benzophenone.[7] Herein, we report the first study in which AMMZ with **1** has been applied to a fused-ring aromatic hydrocarbon, using the simplest and most important compound of this type, naphthalene, as a case study. This investigation breaks new ground in establishing that AMMZ can provide 1) access to new zincated naphthalene molecules not directly accessible by mainstream organozinc reagents; 2) an improved method for metalation of naphthalene; 3) a degree of stoichiometric control, which enables di- and monometalation applications; and 4) an unprecedented set of crystalline 2-monometalated and 2,6-dimetalated naphthalene products from which the first crystal structures of zincated (or any metalated in the 2,6-case) naphthalene compounds have been obtained.

Scheme 1 summarizes the reactions between **1** and naphthalene that yielded crystalline products. Carried out under mild conditions (room temperature, stirring for 2 h), the equimolar experiment (pathway a) produced yellow [(tmeda)Na(μ-tmp)(μ-2-C$_{10}$H$_7$)Zn(tBu)] (**2**) in yields of typically 50% of the isolated product. ^{1}H and ^{13}C NMR spectra of a solution of an isolated sample **2** in C$_6$D$_6$ reveal a pattern of seven and ten distinct resonances, respectively, in the aromatic region consistent with monometalation/monodeprotonation of naphthalene at the 2-position (NMR spectra of the remaining filtrates showed only the starting material naphthalene and no other metalated isomers). This regioselectivity was confirmed by X-ray crystallography (see below). The reasonable yield of this pure 2-naphthalenide compares favorably with previous metalation studies that used, for example, BuLi[8] or superbasic LICKOR,[9] both of which are nonselective in affording mixtures of the isomers 1- and 2-naphthalene after quenching protocols (yields of the combined products, 20 and 28%, respectively). In contrast, when a solution of an isolated sample of **2** in THF was quenched with I$_2$, the yield of 2-iodonaphthalene was found to be (83 ± 5)% from quantitative NMR spectroscopic studies with ferrocene as the internal standard.

The molecular structure of **2** (Figure 1)[10] reveals that the zinc center is located at the deprotonated 2-position (Zn–C(1): 2.076(4) Å) and lies in the naphthyl-ring plane (deviation from mean plane: 0.007 Å); whereas, the sodium center engages in a long η^2-interaction at the 1- and 2-positions (Na–C(2): 2.857(4) Å; Na–C(1): 2.828(4) Å) and lies 2.490 Å from this plane. These distinctions confirm that the metalation process that leads to **2** was AMMZ as opposed to sodiation. A comparison of the structure of **2** with that of its precursor **1**[4] reveals that, aside from substitution of a tBu$^-$ by a C$_{10}$H$_7^-$ ion, there is retention of connectivity within the remainder of the molecule. Thus, linked by a TMP N bridge (Zn–N(1): 2.020(3) Å; Na–N(1): 2.427(3) Å), the Zn and Na atoms also carry terminal tBu (C-attached) and TMEDA (*N*,*N*′-attached) ligands, respectively. As **2** represents the first authenticated zinc–naphthalenide structure, there is no precedent available for comparison. Moreover, there is only one previous structure containing both a Na center and naphthalene ligands, although only remotely related to **2**: In the lutetium complex [{[(C$_5$Me$_5$Lu)$_3$(C$_{10}$H$_8$)(C$_{10}$H$_7$)(H)][Na(thf)$_3$]}$_2$C$_{10}$H$_8$],[11] Na interacts in a η^3-mode (Na–C: 2.686,

[*] Dr. E. Hevia, L. M. Hogg, Dr. G. W. Honeyman, Prof. R. E. Mulvey, Dr. C. T. O'Hara
WestCHEM
Department of Pure and Applied Chemistry
University of Strathclyde, Glasgow, G1 1XL (UK)
Fax: (+44) 141-552-0876
E-mail: r.e.mulvey@strath.ac.uk
Prof. W. Clegg, Dr. S. H. Dale
School of Natural Sciences (Chemistry)
University of Newcastle
Newcastle upon Tyne, NE1 7RU (UK)

[**] This study was supported by the UK Engineering and Physical Science Research Council through grant award no. GR/T27228/01.

Supporting information for this article is available on the WWW under http://www.angewandte.org or from the author.

InterScience
© 2006 Wiley-VCH Verlag GmbH & Co. KGaA, Weinheim

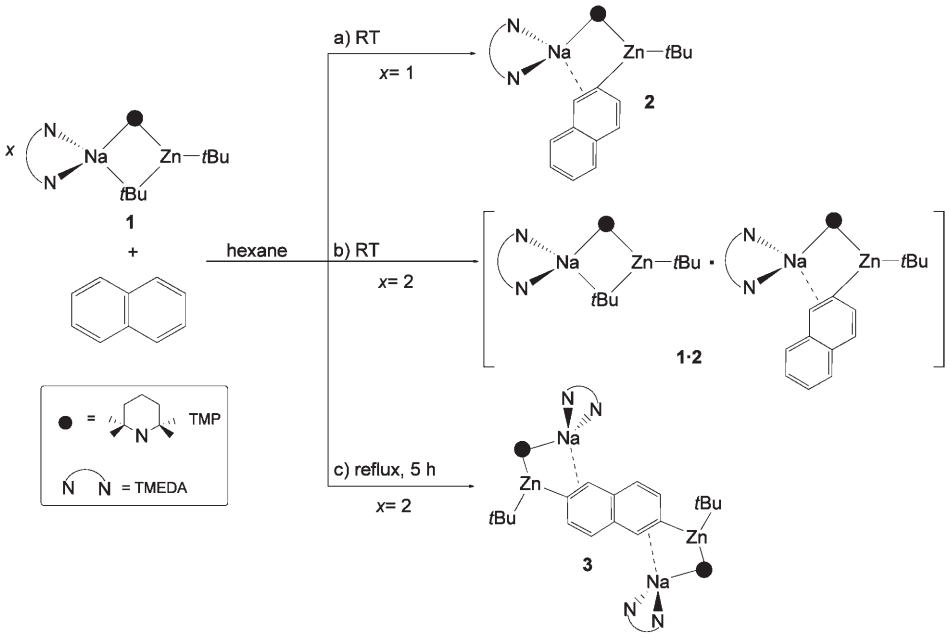

Scheme 1. Stoichiometry- and temperature-dependent reactions of naphthalene with the synergic zincate base **1**.

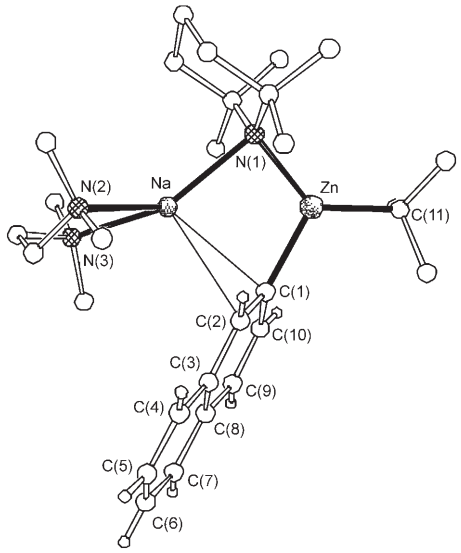

Figure 1. Molecular structure of **2** with selective atom labels indicated and Na–π(arene) interactions shown as thin lines. Hydrogen atoms, except for those of the naphthalenide ring and minor disorder components, are omitted for clarity.

2.852, and 2.912 Å), with a nonplanar (but planar in **2**) $C_{10}H_7$ ligand.

Hitherto, applications of **1** have been confined to monozincation reactions. It was therefore of interest to investigate the effect of subjecting naphthalene to an excess of **1**. Polymetalation of naphthalene by superbasic LICKOR is an unsatisfactory, messy operation: with a threefold excess of the base in hexane, a mixture of mono- and disubstituted naphthalenes is obtained in yields of 28 and 25%, respectively, with the latter containing all 10 disubstituted isomers, although some only at trace level.[9] Intriguingly, the first attempt to use **1**, carried out at room temperature with two equivalents of base (pathway b), produced crystals of [{(tmeda)Na(μ-tmp)(μ-*t*Bu)Zn-(*t*Bu)}·{(tmeda)Na(μ-tmp)(μ-2-$C_{10}H_7$)Zn(*t*Bu)}] (**1·2**), in which molecules of "unreacted" base **1** and monozincated naphthalene **2** sit side by side in 1:1 ratio in the crystal structure.[12] This stand-off can be largely overcome by applying more forceful reaction conditions. Following a reflux for 5 h, the same reaction solution yielded a mixture of the dizincated 2,6-naphthalenediide [$(tmeda)_2Na_2(\mu\text{-}tmp)_2(\mu\text{-}2,6\text{-}C_{10}H_6)Zn_2(t\text{Bu})_2$] (**3**; pathway c), the monozincated product **1** and starting material naphthalene in 7:1:1 ratio, as confirmed by NMR spectroscopic analysis of the isolated solid (NMR spectra of the remaining filtrate revealed only the starting material naphthalene). Longer reflux times did not appear to improve this ratio further. Complex **3** was characterized by ^1H and ^{13}C NMR spectroscopic analysis; the aromatic region of the former was especially diagnostic and showed the expected singlet and two distinct doublets of a symmetrical 2,6-dideprotonated naphthalene.

The centrosymmetric molecular structure of **3** (Figure 2)[10] closely resembles that of **2** but with an additional {(tmeda)Na(μ-tmp)Zn(*t*Bu)} cationic unit grafted onto the 6-position, thus replacing the second cleaved proton. As a

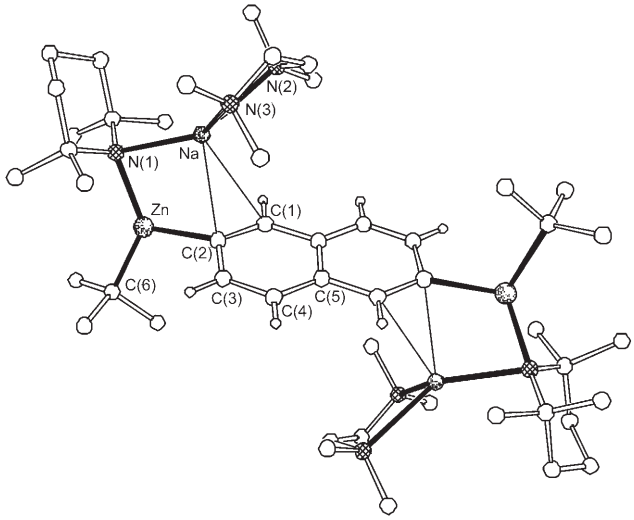

Figure 2. Molecular structure of **3** with selective atom labels indicated and Na–π(arene) interactions shown as thin lines. Hydrogen atoms, except for those of the naphthalenide ring, are omitted for clarity.

 © 2006 Wiley-VCH Verlag GmbH & Co. KGaA, Weinheim

consequence of the centrosymmetry, the cationic-base residues occupy sterically minimizing transoid positions either side of the naphthalene-ring plane. The zinc center is located at the deprotonated 2- and 6-positions (Zn–C(2): 2.062(6) Å), only slightly out of the naphthyl-ring plane (deviation: 0.299 Å), whereas the sodium center engages in a long η^2-interaction at the 1- and 2-positions more asymmetrically than that in **2** (that is, Na–C(1): 2.957(6) Å; Na–C(2): 2.706(6) Å) and lies 2.443 Å out of this plane.

In summary, this case study of naphthalene establishes that AMMZ can effect dimetalation as well as monometalation of polycyclic aromatic hydrocarbons, thus resulting in access to new zincated naphthalenes inaccessible directly through mainstream organozinc reagents.

Experimental Section

Synthesis of **2**: A solution of tBu$_2$Zn (0.358 g, 2 mmol) in hexane (10 mL) was transferred through a cannula to a suspension of NaTMP in hexane (prepared in situ by reaction of BuNa[13] (0.16 g, 2 mmol) with TMP(H) (0.34 mL, 2 mmol)), followed by the addition of a molar equivalent of TMEDA (0.30 mL, 2 mmol). The resultant suspension was heated gently to form a yellow solution. At this stage, one molar equivalent of naphthalene (0.26 g, 2 mmol) was added through a solids addition tube, and the reaction mixture was allowed to stir at room temperature for 2 h. The resulting yellow solution was transferred to the freezer to aid crystallization. A crop of transparent yellow crystals (0.52 g, 50 %) formed in solution which were suitable for X-ray crystallographic analysis.

Synthesis of **3**: Following a similar procedure as described above, [(tmeda)Na(μ-tmp)(μ-tBu)Zn(tBu)] was prepared in situ by reaction of tBu$_2$Zn (0.358 g, 2 mmol), NaTMP (2 mmol), and TMEDA (0.30 mL, 2 mmol). Naphthalene (0.13 g, 1 mmol) was then introduced to the reaction mixture, which was heated to reflux for 5 h before being cooled to ambient temperature and moved to the freezer to aid crystallization. A crop of pale-yellow crystals (0.60 g) was formed in solution. Though this sample was contaminated with small amounts of **2** and free naphthalene, on the basis of NMR integrals the product equates to an absolute yield of **3** of (50 ± 5) %.

Received: June 7, 2006
Published online: September 4, 2006

Keywords: alkali metals · crystal structures · metalation · polycyclic aromatic hydrocarbons · zinc

[1] M. Schlosser, *Organometallics in Synthesis*, Wiley, Chichester, 2nd ed., **2002**, chap. 1.
[2] The classical "LICKOR" (Li–C + KOR) superbases are heterobimetallic examples, see: a) M. Schlosser, *Mod. Synth. Methods* **1992**, *6*, 227; b) L. Lochmann, *Eur. J. Inorg. Chem.* **2000**, 115.
[3] a) Y. Kondo, M. Shilai, M. Uchiyama, T. Sakamoto, *J. Am. Chem. Soc.* **1999**, *121*, 3539; b) T. Imahori, M. Uchiyama, T. Sakamoto, Y. Kondo, *Chem. Commun.* **2001**, 2450; c) M. Uchiyama, T. Miyoshi, Y. Kajihara, T. Sakamoto, Y. Otani, T. Ohwada, Y, Kondo, *J. Am. Chem. Soc.* **2002**, *124*, 8514.
[4] P. C. Andrikopoulos, D. R. Armstrong, H. R. L. Barley, W. Clegg, S. H. Dale, E. Hevia, G. W. Honeyman, A. R. Kennedy, R. E. Mulvey, *J. Am. Chem. Soc.* **2005**, *127*, 6184.
[5] a) W. Clegg, S. H. Dale, E. Hevia, G. W. Honeyman, R. E. Mulvey, *Angew. Chem.* **2006**, *118*, 2430; *Angew. Chem. Int. Ed.* **2006**, *45*, 2370; b) W. Clegg, S. H. Dale, R. W. Harrington, E. Hevia, G. W. Honeyman, R. E. Mulvey, *Angew. Chem.* **2006**, *118*, 2434; *Angew. Chem. Int. Ed.* **2006**, *45*, 2374.
[6] D. R. Armstrong, W. Clegg, S. H. Dale, E. Hevia, L. M. Hogg, G. W. Honeyman, R. E. Mulvey, *Angew. Chem.* **2006**, *118*, 3859; *Angew. Chem. Int. Ed.* **2006**, *45*, 3775.
[7] E. Hevia, G. W. Honeyman, A. R. Kennedy, R. E. Mulvey, *J. Am. Chem. Soc.* **2005**, *127*, 13106.
[8] H. Gilman, R. L. Bebb, *J. Am. Chem. Soc.* **1939**, *61*, 109.
[9] M. Schlosser, J. H. Choi, S. Takagishi, *Tetrahedron* **1990**, *46*, 5633.
[10] Crystal data for **2**: $C_{29}H_{50}N_3NaZn$, $M_r = 529.1$, orthorhombic, space group $Pca2_1$, $a = 18.169(4)$, $b = 10.9855(19)$, $c = 15.500(3)$ Å, $V = 3093.7(10)$ Å^3, $Z = 4$, $\rho_{calcd} = 1.136$ g cm^{-3}, μ($Mo_{K\alpha}$) = 0.83 mm^{-1}, $T = 150$ K, $R = 0.058$ ($F^2 > 2\sigma$), $R_w = 0.100$ (for all F^2 values) for 7046 data and 344 refined parameters; final difference synthesis within ± 0.41 e Å^{-3}. The tBu group is disordered over two orientations with a common central C atom. All H atoms were constrained with a riding model. Crystal data for **3**: $C_{48}H_{92}N_6Na_2Zn_2$, $M_r = 930.0$, monoclinic, space group $P2_1/c$, $a = 9.9246(16)$, $b = 18.848(8)$, $c = 15.716(3)$ Å, $\beta = 108.364(11)°$, $V = 2790.1(14)$ Å^3, $Z = 2$, $\rho_{calcd} = 1.107$ g cm^{-3}, μ($Mo_{K\alpha}$) = 0.91 mm^{-1}, $T = 150$ K, $R = 0.062$ ($F^2 > 2\sigma$), $R_w = 0.138$ (for all F^2 values) for 3398 data and 273 refined parameters; final difference synthesis within ± 0.52 e Å^{-3}. The molecule is ordered on a crystallographic inversion center. CCDC-609230 (**2**) and 609228 (**3**) contain the supplementary crystallographic data. These data can be obtained free of charge from The Cambridge Crystallographic Data Centre via www.ccdc.cam.ac.uk/data_request/cif.
[11] A. V. Protchenko, O. G. Almazova, L. N. Zakharov, G. K. Fukin, Y. T. Struchkov, M. N. Bochkarev, *J. Organomet. Chem.* **1997**, *536–537*, 457.
[12] As there are only minor geometrical differences between this composite structure and its separate components, **1·2** is not discussed further herein; see Supporting Information for the experimental details and crystal data.
[13] C. Schade, W. Bauer, P. v. R. Schleyer, *J. Organomet. Chem.* **1985**, *295*, C25.

 © 2006 Wiley-VCH Verlag GmbH & Co. KGaA, Weinheim

Organocatalysis

DOI: 10.1002/anie.200602275

Organocatalytic Enantioselective Nucleophilic Vinylic Substitution**

*Thomas B. Poulsen, Luca Bernardi, Mark Bell, and Karl Anker Jørgensen**

Many fundamental reactions in organic synthesis rely upon the use of enolates derived from carbonyl compounds as nucleophilic reaction partners. For this reason, the development of catalytic reaction protocols that result in the formation of enolates in chiral settings—thus enabling enantioselective transformations—must be considered a fundamental task for contemporary organic chemistry.[1]

Organocatalysis[2] has recently provided many fascinating examples of exquisite stereocontrol in C–C bond-forming reactions involving enolates. However, the majority of these lead to the formation of a bond between two sp^3-hybridized carbon atoms. Traditionally, the coupling of sp^3- and sp^2-hybridized carbon atoms has been a challenge and task for transition-metal-based catalytic systems,[3] and recently, examples of asymmetric α-arylations of carbonyl compounds have emerged.[4] However, despite the synthetic potential, there exist only a few reports that describe the coupling of vinylic compounds.[5] Furthermore, examples of such asymmetric reactions with electron-deficient alkenes [Eq. (1); EWG = electron-withdrawing group] have, to the best of our knowledge, been absent until now. Herein, we attempt to address this transformation by presenting the first catalytic enantioselective vinylic substitution reaction.

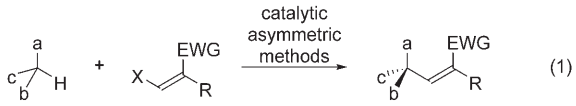

(1)

We envisioned that nucleophiles derived from 1,3-dicarbonyl compounds, such as β-ketoesters, could substitute a vinylic halide from activated β-haloalkenes through an addition–elimination (Ad_N–E) mechanism,[6] thereby forming a new C–C bond and an attractive vinyl-substituted all-carbon quaternary stereocenter. The complexation of the enolate with a chiral phase-transfer catalyst (PTC),[7] **1** or **1′**, derived from a cinchona alkaloid was anticipated to confer asymmetric induction to the reaction (Scheme 1). A major advantage of this protocol is the fact that vinylic substitutions on compounds such as **3**—readily prepared as the *Z* isomer from the corresponding alkyne[8]—often take place with complete retention of configuration of the C–C double bond.[9]

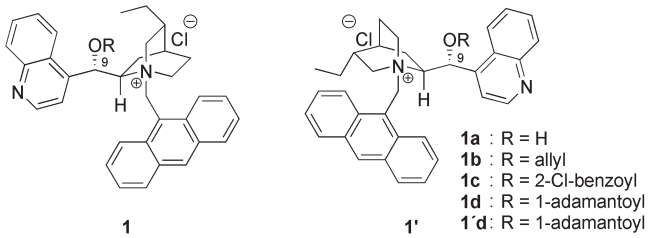

Scheme 1. Structures of phase-transfer catalysts derived from cinchonine (**1**) and from cinchonidine (**1′**).

Therefore, we set forward to identify suitable conditions for the reaction between (*Z*)-β-chloro-1-phenylpropenone ((*Z*)-**3a**) with alkyl cyclopentanone-2-carboxylates (e.g., **2a**), thus leading to **4a** [Eq. (2)]. A successful implementation of the strategy mentioned above would allow access to both geometric double-bond isomers, as the *Z*-configured products are readily isomerized to the more stable *E* configuration (see below). Initial screening (see the Supporting Information for the screening of ester groups, catalysts, and reaction conditions) revealed that the reaction did in fact proceed with virtually complete retention of the double-bond configuration. Furthermore, it was found that the combination of a PTC with a 9-anthracenylmethyl group[10] attached to the quinuclidine nitrogen atom and cyclopentanone 2-carboxylates **2** with bulky ester groups, such as *tert*-butyl, afforded promising levels of asymmetric induction. Table 1 shows further screening results. Catalysts **1b–d** (from dihydrocinchonine), substituted at 9-OH (Table 1, entries 2–4), performed better than the unsubstituted parent compound **1a** (Table 1, entry 1) both in terms of conversion and enantioselectivity.

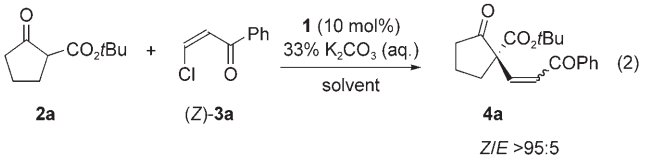

(2)

The presence of a bulky 1-adamantoyl group in the catalyst (**1d**, obtained from **1a** under Schotten–Baumann conditions; see Supporting Information) proved to be optimal, and with this catalyst the reaction was readily carried out at −20 °C, thus affording the product (*Z*)-**4a** with 88 % *ee* (Table 1, entry 4). An exchange of the leaving group from chloride to bromide (Table 1, entry 5) afforded (*Z*)-**4a** with unchanged enantioselectivity, albeit at a slower rate.

[*] T. B. Poulsen, Dr. L. Bernardi, Dr. M. Bell, Prof. Dr. K. A. Jørgensen
The Danish National Research Foundation
Center for Catalysis Department of Chemistry
Aarhus University, 8000 Aarhus C (Denmark)
Fax: (+45) 8919-6199
E-mail: kaj@chem.au.dk

[**] This work was made possible by a grant from The Danish National Research Foundation. Thanks are given to Dr. Jacob Overgaard for performing the X-ray analysis.

Supporting information for this article is available on the WWW under http://www.angewandte.org or from the author.

© 2006 Wiley-VCH Verlag GmbH & Co. KGaA, Weinheim

Table 1: Enantioselective vinylic substitution: Screening of catalysts and reaction conditions.[a]

Entry	Cat.	Solvent	T [°C]	t [h]	Conv. [%][b]	*ee* [%][c]
1	**1a**	toluene/$CHCl_3$ (7:1)	0	4.3	25	57
2	**1b**	toluene/$CHCl_3$ (7:1)	0	4.5	87	74
3	**1c**	toluene/$CHCl_3$ (7:1)	0	4.0	61	82
4	**1d**	toluene/$CHCl_3$ (7:1)	−20	5.0	>95	88
5[d]	**1d**	toluene/$CHCl_3$ (7:1)	−20	5.5	50	88
6	**1d**	*o*-xylene	−20	6.0	88	89
7	**1d**	*o*-xylene/$CHCl_3$ (7:1)	−20	5.5	>95	91
8	**1d**[e]	*o*-xylene/$CHCl_3$ (7:1)	−20	13.5	>95	94

[a] Performed with (*Z*)-**3a** (0.12 mmol, 0.15 M) and **2a** (1.3 equiv). [b] Determined by ^{1}H NMR spectroscopic analysis. [c] The *ee* value of the *Z* isomer was determined by chiral stationary phase (CSP) HPLC. [d] Br as the leaving group instead of Cl. [e] Catalyst loading: 2.5 mol%.

Finally, it was found that high enantioselectivity—up to 94% *ee*—was obtained when changing the principal component of the reaction solvent to *o*-xylene instead of toluene (Table 1, entries 6 and 7), and most gratifyingly when the catalytic loading was decreased to 2.5 mol% (Table 1, entry 8).

Having established an optimal reaction protocol, we then explored the scope of the transformation with respect to both reaction partners. Various aromatic, heteroaromatic, and aliphatic β-halopropenones are suitable substrates for the catalytic reaction (Table 2, entries 1 and 3–9) and the products **4a**–**h** were obtained in good yields with enantioselectivities exceeding 90% *ee*. In all cases, the stereospecificity of the transformation was nearly complete—maintaining the *Z*-configured double bond (Table 2, entries 1 and 3–10). In a similar manner, the *E* product was obtained using (*E*)-**3a** as the substrate; however, the enantioselectivity was slightly decreased (Table 2, entry 2).

Table 2: Enantioselective vinylic substitution: Scope of disubstituted β-haloalkenes.[a]

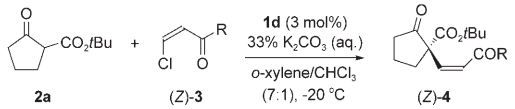

2a (*Z*)-**3** (*Z*)-**4**

Entry	Substrate	R	Product	Yield [%][b]	Z/E[c]	*ee* [%][d]
1	**3a**	C_6H_5	**4a**	89 (92)	>95:5	94 (84)
2[e]	**3a**	C_6H_5	**4a**	85	<5:95	75
3	**3b**	4-$CF_3C_6H_4$	**4b**	89	>95:5	93
4	**3c**	4-$MeOC_6H_4$	**4c**	71	>95:5	93
5	**3d**	2-thienyl	**4d**	87	>95:5	91 (*S*)[f]
6	**3e**	1-naphthyl	**4e**	86	>95:5	94
7[g]	**3f**	Me[h]	**4f**	87	95:5	91 (*S*)[i]
8[j]	**3g**	$(CH_2)_2Ph$	**4g**	78	>95:5	93
9[j]	**3h**	*t*Bu	**4h**	90	>95:5	96
10[g]	**3i**	OEt	**4i**	77 (84)	>95:5	91 (81)

[a] Performed with **2a** (0.20 mmol, 0.15 M) and (*Z*)-**3** (1.1 equiv); the values in parenthesis were obtained with the catalyst derived from dihydrocinchonidine **1′d**. [b] Yield of the isolated product for both diastereomers. [c] Determined by ^{1}H NMR spectroscopic and HPLC analysis. [d] The *ee* value of the *Z* isomer was determined by CSP-HPLC. [e] (*E*)-**3a** was used. [f] The configuration was determined by X-ray analysis. [g] Method B was used (see Table 3). [h] Br as the leaving group. [i] The configuration was determined by chemical correlation. [j] Catalyst loading: 6 mol%.

Of special interest is the use of (*Z*)-**3f**, which is derived from 3-butyn-2-one, as the electrophilic reaction partner (Table 2, entry 7). The presence of both a *Z*-configured double bond and an enolizable methyl ketone in product (*Z*)-**4f**—formed in 87% yield with 91% *ee*—provides versatile functional handles for further synthetic manipulations.[11] Although less reactive, (*Z*)-**3i**, with an ester as the activating group, also undergoes the transformation to afford (*Z*)-**4i** with satisfactory results (Table 2, entry 10; 77% yield, 91% *ee*).

Further investigation of the reaction scope is presented in Table 3. Various cyclic β-ketoesters (Table 3, entries 1–3 and 5–7) undergo the vinylation with excellent selectivity. For example, a 1-indanone-derived β-ketoester with the ubiquitous 6,7-dimethoxy motif afforded product (*Z*)-**4l** in 95% yield with 95% *ee* (Table 3, entry 3). A similar result was also obtained for an *E*-alkene (Table 3, entry 4), thus giving (*E*)-**4l** in high yields, in good *E*/*Z* ratio, and with 97% *ee*; furthermore, this result shows that also the nucleophilic vinylic substitution for the *E*-alkenes (see also Table 2) maintains the configuration at the double bond. When the ring size is increased, slightly modified conditions (Table 3, method B, entries 5–7) are necessary as a result of the lower reactivity of the parent β-ketoesters. Interestingly, a slight drop in diastereoselectivity was also observed (compare Table 2, entry 1 with Table 3, entries 5 and 7), the possible origin of which is discussed below. Note, however, that in the case of product **4o** (entry 7) the *Z* and *E* isomers were easily separable by flash chromatography, thus allowing access to diastereomerically pure material.

An attempt to perform the reaction using noncyclic β-ketoesters revealed a limitation of the catalyst system described herein, as the products were obtained with less than 40% *ee*. Reactions were also carried out using the quasi-enantiomeric catalyst **1′d** (see Tables 2 and 3, values in parentheses) with consistent, although in some cases slightly lower, selectivities.

In the case of disubstituted alkenes, the vinylic substitution reaction can be regarded as a synthetic equivalent of the addition to electron-deficient triple bonds,[12] but with the advantages of yielding a wider range of compounds and being able to control the double-bond geometry of the products. The two reactions, however, being mechanistically distinct, imply that only the vinylic substitution affords the possibility of forming trisubstituted alkenes, for example, (*E*)-**4p**. As can be seen in entry 8 (Table 3), the α-iodine atom is easily tolerated in the catalytic reaction, affording the product with $E/Z > 95:5$[13] and 91% *ee*. In conjunction with cross-coupling methodology,[14] this reaction may provide a versatile platform for the synthesis of complex molecular structures. In this respect, it is important to note that **4p** was also prepared on a gram scale (81% yield, 1.67 g of **4p**, $E/Z > 95:5$, 91% *ee*).

As mentioned above, easy access to both double-bond isomers of **4** can be gained through isomerization of the *Z*-configured double bond. For example, a catalytic amount of tri-*n*-butyl phosphine smoothly converts (*Z*)-**4a** into (*E*)-**4a** as

 © 2006 Wiley-VCH Verlag GmbH & Co. KGaA, Weinheim

Table 3: Enantioselective vinylic substitution: Scope of nucleophiles and trisubstituted electrophiles.

Entry	Product	Y/Ph	Product	Yield [%][a]	Z/E[b]	*ee* [%][c]
1[d]	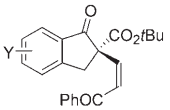	H	**4j**	90 (85)	>95:5 (>95:5)	90 (89)
2[d]		6-Cl	**4k**	96	>95:5	79
3[d]		6,7-$(MeO)_2$	**4l**	95	>95:5	95
4[d,e]	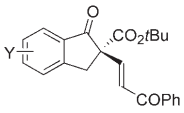	6,7-$(MeO)_2$	**4l**	94	<5:95	97[f]
5[g]	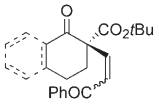	–	**4m**	77	90:10	89
6[g]		Ph	**4n**	96 (95)	95:5 (92:8)	95 (94)
7[h]	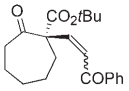	–	**4o**	81	86:14	75
8[g]	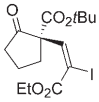	–	**4p**	74	<5:95	91[f]

[a] Yield of the isolated product for both diastereomers. [b] Determined by ^{1}H NMR spectroscopic and HPLC analysis. [c] The *ee* value of the *Z* isomers (except **4p**) was determined by CSP-HPLC. [d] Method A: β-ketoester (0.20 mmol, 0.15 M) and **3** (1.1 equiv), K_2CO_3 (33% aq.), *o*-xylene/$CHCl_3$ (7:1), and **1d** (3 mol%); the values in parentheses were obtained with the catalyst derived from **1′d**. [e] (*E*)-**3a** was used. [f] *E* isomer. [g] Method B: β-ketoester (0.20 mmol, 0.30 M), **3** (2.0 equiv), Cs_2CO_3 (66% aq.), *o*-xylene/$CHCl_3$ (7:1), and **1d** (6 mol%). [h] Method B, but with solid Cs_2CO_3.

shown in Equation (3). Alternatively, the *E* isomer of the products can be prepared directly by the catalytic reaction from (*E*)-**3** with moderate to excellent enantioselectivities (Table 2, entry 2 and Table 3, entry 4).

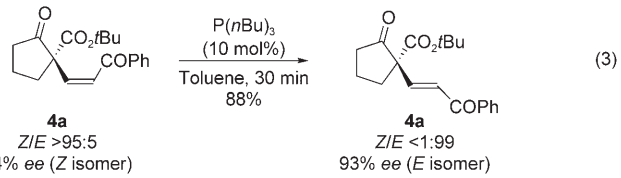

(3)

The overall substitution of the halide with retention of configuration can be rationalized through an Ad_N–E mechanism (Scheme 2).[15] Complexation of the enolate and the chiral PTC allows for the stereoselective addition to the α,β-unsaturated carbonyl compound in an initial rate-determining step. This addition results in the formation of a mixture of diastereomeric intermediates **5**, the composition of which cannot be ascertained as a result of their transient nature. Intermediates **5**, β-halo-substituted enolates, undergo rapid elimination of the leaving group to reform the C=C double bond. However, stereoelectronic effects demand the periplanar alignment of the enolate π orbital and the C–X σ* orbital for the elimination to be feasible. Such conformations can be achieved through either a short bond rotation (ca. 60°; indicated in Scheme 2) or a longer rotation (ca. 120°; not indicated). The preference for the short rotation (resulting in retention of configuration of the double bond) may be explained by the avoidance of destabilizing eclipsing interactions during the bond rotation[9a] and hyperconjugation between the electron-rich π system of the enolate and the σ* orbital of the C–X group.[9c]

Both diastereomeric intermediates in Scheme 2 eventually collapse to the same product, but the likely influence of the stereogenic center present at C2 in the elimination step is not considered in this preliminary model. The slight drop in diastereoselectivity (not as a result of product isomerization) observed for products **4m–o** may be trivially attributed to an overall (namely, in both diastereomeric intermediates) destabilization of the preferred rotational pathway. However, it may also originate from a difference among the two intermediates in the tendency to form products with retention of configuration. In the latter case, the key to obtaining very high diastereoselectivities for these more demanding substrates might be exquisite diastereocontrol of the initial addition reaction. This hypothesis is currently being tested in our laboratories.

In summary, we have presented the first example of a catalytic enantioselective vinylic substitution reaction. The reaction proceeds with high diastereoselectivity for both di- and trisubstituted alkenes and is carried out under experimentally simple conditions. Furthermore, we have presented new bulky phase-transfer catalysts that enable a highly enantioselective procedure.

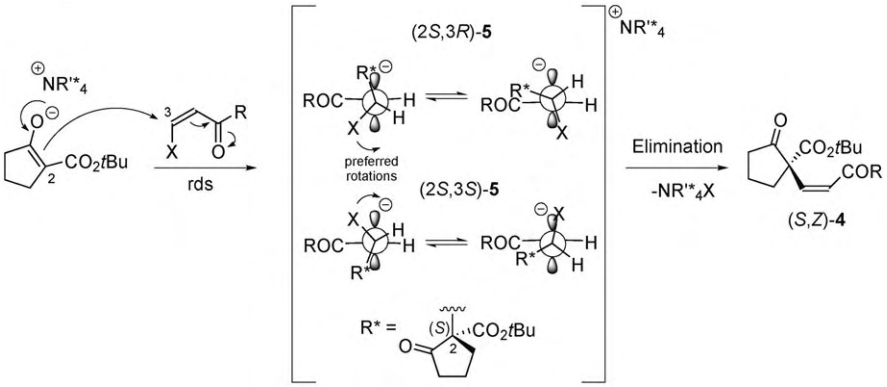

Scheme 2. Proposed mechanism of the vinylic substitution reaction (rds = rate-determining step).

 © 2006 Wiley-VCH Verlag GmbH & Co. KGaA, Weinheim

Experimental Section

Representative experimental procedure: **2a** (36.8 mg, 0.20 mmol), *o*-xylene/$CHCl_3$ (7:1, 1.3 mL), **3a** (36.7 mg, 0.22 mmol), and catalyst **1d** (3 mol%, 0.006 mmol, 4.1 mg) were added to a sample vial equipped with a magnetic stirring bar. The mixture was stirred for a short time at ambient temperature and then placed at −20 °C. When the mixture had cooled, a cold (−20 °C) solution of K_2CO_3 (33% aq., 0.6 mL) was added, and the biphasic mixture was vigorously stirred for 21 h, at which time the reaction was judged to be complete by TLC analysis. The organic phase was collected and the aqueous layer extracted with toluene (2 × 1 mL). The combined organic fractions were loaded onto SiO_2, and **4a** (55.2 mg, 0.176 mmol, 89% yield, *Z*/*E* > 95:5) was obtained by flash chromatography with Et_2O/CH_2Cl_2 (0:100–3:97) as the eluent.

Received: June 7, 2006
Published online: September 5, 2006

Keywords: addition–elimination · asymmetric synthesis · organocatalysis · phase-transfer catalysis · vinylation

[1] *Comprehensive Asymmetric Catalysis*, *Vol. 3* (Eds.: E. N. Jacobsen, A. Pfaltz, H. Yamamoto), Springer, Berlin, **1999**.
[2] a) P. I. Dalko, L. Moisan, *Angew. Chem.* **2001**, *113*, 3840; *Angew. Chem. Int. Ed.* **2001**, *40*, 3726; b) P. I. Dalko, L. Moisan, *Angew. Chem.* **2004**, *116*, 5248; *Angew. Chem. Int. Ed.* **2004**, *43*, 5138.
[3] See, for example: J. Tsuji, in *Palladium Reagents and Catalysts—New Perspectives for the 21st Century*, 2nd ed., Wiley, New York, **2004**.
[4] See, for example: a) T. Hamada, A. Chieffi, J. Åhman, S. L. Buchwald, *J. Am. Chem. Soc.* **2002**, *124*, 1261; b) D. J. Spielvogel, S. L. Buchwald, *J. Am. Chem. Soc.* **2002**, *124*, 3500; c) S. Lee, J. F. Hartwig, *J. Org. Chem.* **2001**, *66*, 3402; through nucleophilic aromatic substitution, see: d) M. Bella, S. Kobbelgaard, K. A. Jørgensen, *J. Am. Chem. Soc.* **2005**, *127*, 3670; e) S. Kobbelgaard, M. Bella, K. A. Jørgensen, *J. Org. Chem.* **2006**, *71*, 4980.
[5] a) A. Chieffi, K. Kamikawa, J. Åhman, J. Fox, S. L. Buchwald, *Org. Lett.* **2001**, *3*, 1897; b) T. Hamada, S. L. Buchwald, *Org. Lett.* **2002**, *4*, 999; see also c) B. K. Corkey, F. D. Toste, *J. Am. Chem. Soc.* **2005**, *127*, 17168.
[6] a) N. K. Kochetkov, L. J. Kudryashov, B. P. Gottich, *Tetrahedron* **1961**, 63; for an example of allylation through an addition–elimination mechanism, see: b) P. V. Ramachandran, S. Madhi, L. Bland-Berry, M. V. R. Reddy, M. J. O'Donnell, *J. Am. Chem. Soc.* **2005**, *127*, 13450.
[7] For a review, see, for example: a) M. J. O'Donnell in *Catalytic Asymmetric Synthesis*, 2nd ed (Ed.: I. Ojima), Wiley-VCH, Weinheim, **2000**, p. 727; for recent examples of phase-transfer-catalyzed asymmetric reactions, see, for example: b) T. Ooi, Y. Uematsu, K. Maruoka, *J. Am. Chem. Soc.* **2006**, *128*, 2548; c) F. Fini, V. Sgarzani, D. Pettersen, R. P. Herrera, L. Bernardi, A. Ricci, *Angew. Chem.* **2005**, *117*, 8189; *Angew. Chem. Int. Ed.* **2005**, *44*, 7975; d) A. Okada, T. Shibuguchi, T. Ohshima, H. Masu, K. Yamaguchi, M. Shibasaki, *Angew. Chem.* **2005**, *117*, 4640; *Angew. Chem. Int. Ed.* **2005**, *44*, 4564; e) T. Ooi, M. Kameda, K. Maruoka, *J. Am. Chem. Soc.* **2003**, *125*, 5139; f) T. Ooi, T. Miki, M. Taniguchi, M. Shiraishi, M. Takeuchi, K. Maruoka, *Angew. Chem.* **2003**, *115*, 3926; *Angew. Chem. Int. Ed.* **2003**, *42*, 3981; g) H.-g. Park, B.-S. Jeong, M.-S. Yoo, J.-H. Lee, M.-k. Park, Y.-J. Lee, M.-J. Kim, S.-s. Jew, *Angew. Chem.* **2002**, *114*, 3162; *Angew. Chem. Int. Ed.* **2002**, *41*, 3036; h) T. Kita, A. Georgieva, Y. Hashimoto, T. Nakata, K. Nagasawa, *Angew. Chem.* **2002**, *114*, 2956; *Angew. Chem. Int. Ed.* **2002**, *41*, 2832.
[8] S. Ma, X. Lu, Z. Li, *J. Org. Chem.* **1992**, *57*, 709.
[9] a) G. Modena, *Acc. Chem. Res*, **1971**, *4*, 73; b) S. I. Miller, *Tetrahedron* **1977**, *33*, 1211; c) Y. Apeloig, Z. Rappoport, *J. Am. Chem. Soc.* **1979**, *101*, 5095.
[10] a) B. Lygo, P. G. Wainwright, *Tetrahedron Lett.* **1997**, *38*, 8595; b) E. J. Corey, F. Xu, M. C. Noe, *J. Am. Chem. Soc.* **1997**, *119*, 12414.
[11] M. Miesch, G. Mislin, M. Franck-Neumann, *Tetrahedron Lett.* **1998**, *39*, 6873.
[12] M. Bella, K. A. Jørgensen, *J. Am. Chem. Soc.* **2004**, *126*, 5672.
[13] Note that the change of *Z* to *E* selectivity is due to the iodine having a higher priority than the ester group according to the CIP system.
[14] A. B. Lemay, K. S. Vulic, W. W. Ogilvie, *J. Org. Chem.* **2006**, *71*, 3615.
[15] As noted by a referee, formation of alkynone intermediates in situ by dehydrohalogenation of **3** might also be a possible reaction pathway. Subjecting (*Z*)-**3b** to the reaction conditions resulted in the formation of trace amounts (< 5%) of the alkynone, only after prolonged reaction times (> 70 h). Furthermore, the reaction was carried out (with **2a**) using the corresponding alkynone under otherwise identical conditions. The result obtained (**4b**, *Z*/*E* = 4:1, 66/40% *ee*; compare with Table 2, entry 3) again suggests that alkynone intermediates are not involved.

 © 2006 Wiley-VCH Verlag GmbH & Co. KGaA, Weinheim

Nanostructures

DOI: 10.1002/anie.200602383

Oxygen-Deficiency-Induced Superlattice Structures of Chromia Nanobelts**

Wei-Qiang Han, Lijun Wu, Aaron Stein, Yimei Zhu, James Misewich, and John Warren*

Nanostructures have attracted wide attention in recent years, because of their fascinating properties and promising technological applications. While nanowires can be used as elements for miniaturized electrical, fluidic, and optical devices, nanobelts can provide engineers with new building

[*] Dr. W.-Q. Han, Dr. L. J. Wu, Dr. Y. M. Zhu
Center for Functional Nanomaterials
Brookhaven National Laboratory
Upton, NY 11973 (USA)
Fax: (+1) 631-344-7370
E-mail: whan@bnl.gov
Dr. A. Stein, Dr. J. Warren
Instrumentation Division
Brookhaven National Laboratory
Upton, NY 11973 (USA)
Dr. J. Misewich
Condensed Matter Physics and Materials Science Department
Brookhaven National Laboratory
Upton, NY 11973 (USA)

[**] This work is supported by the U.S. DOE under contract DE-AC02-98CH10886.

WILEY InterScience DISCOVER SOMETHING GREAT
© 2006 Wiley-VCH Verlag GmbH & Co. KGaA, Weinheim

materials for creating nanoscale sensors, waveguides, and lasers.[1–7] ZnO nanobelts with a rigid helical conformation were recently found to have a superlattice structure, which forms to reduce the electrostatic energy of the polar nanobelt surface.[7] Modulation structures have also been reported in other one-dimensional nano-objects, such as ZnSe nanowires,[8] ZnO:In nanowires,[9] and CdSe nanoribbons.[10]

The physical and chemical properties of transition-metal oxides can be changed dramatically by altering the oxidation state of the transition metal. In its different valence states, chromium forms various chromium oxides, such as CrO_3, Cr_2O_5, CrO_2, and Cr_2O_3. Chromium dioxide (CrO_2) is a half-metallic ferromagnet and, thus, has potential applications in magnetic-tunneling and spin-injection devices.[11,12] Chromia (Cr_2O_3) has been widely used as a green pigment, as a coating material for thermal protection and wear resistance, as a refractory material, and as a heterogeneous catalyst. Chromia is also an important insulating antiferromagnet, with a Néel temperature of 307 K, and is a suitable material for tunnel-junction barriers, both below and above the Néel temperature.[13] For antiferromagnetic nanomaterials, the number of surface spins increases as the particle size decreases. The uncompensated spins on the nanostructure surfaces may significantly affect the magnetic properties of the materials. Néel suggested that very fine particles of an antiferromagnetic material should exhibit particular magnetic properties, such as superparamagnetism or weak ferromagnetism.[14] Size and shape are two important factors affecting the properties of nanostructures.

Chromia nanoparticles and nanopores have been prepared by several methods, including sol–gel processes, microwave-plasma processes, sonochemical reactions, gas condensation, laser-induced pyrolysis, hydrazine reduction followed by thermal treatment, mechanochemical processing, urea-assisted homogeneous precipitation, and precipitation–gelation reactions.[15,16] Chromia whiskers with diameters of 2–10 μm were synthesized by heating a mixture of Cr_2O_3, Al_2O_3, SiO_2, and carbon powders in an electric furnace at 1400 °C.[17] Herein, we use a simple and efficient route to synthesize chromia nanobelts and nanorods: a piece of chromium is heated at 800 °C under an ethanol vapor flow. To our knowledge, this is the first report of chromia nanobelts and nanorods. Two new types of superlattice structures related to oxygen deficiency are also reported.

The synthesis of the chromia nanobelts and nanorods is as follows. First, we insert a chromium piece into a quartz tube inside a horizontal furnace. Argon is used as a protective gas during the heating stage. Once the temperature reaches 800 °C, ethanol vapor is introduced, while the temperature is kept at 800 °C for 1 hour. Next, we stop the heating and the flow of ethanol vapor, but maintain the flow of argon until the sample cools.

We first examined the shape and structure of the nanoparticles in the product by using scanning electron microscopy (SEM) and X-ray diffraction (XRD). To prepare the sample for transmission electron microscopy (TEM), we separated the nanobelts and nanorods from the substrate by supersonication in an alcohol solution, and then dispersed the solution containing the nanoparticles onto copper grids coated with lacy carbon. The TEM experiments were carried out with a high-resolution JEOL 3000F microscope equipped with a field-emission gun, at an accelerating voltage of 300 kV. Electron energy-loss spectroscopy (EELS) was performed using a Gatan energy-filter system.

In Figure 1, SEM images of the as-produced sample are shown. The sample consists mainly of nanobelts, but also contains some nanorods. The nanobelts have lengths of several micrometers, widths ranging from tens to hundreds of nanometers, and thicknesses ranging from a few nanometers to tens of nanometers. In general, the width and thickness of an individual nanobelt are quite uniform. Interestingly, nanobelts with thick bases and a fold along the belt axis are also observed in SEM images (Figure 1c), and confirmed by TEM images (Figure 1d). In the XRD patterns of the nanobelts and nanorods, most peaks can be indexed to rhombohedral Cr_2O_3 (JCPDS 38-1479: space group $R\bar{3}c$, $a = 0.495876$, $c = 1.35942$ nm), while the remaining peaks arise from the chromium substrate.

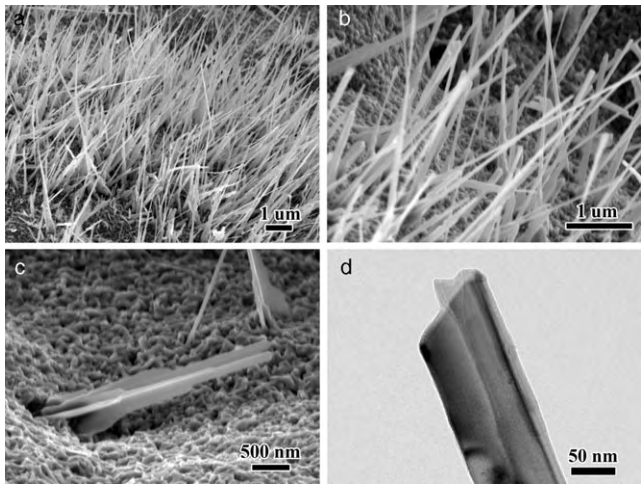

Figure 1. a), b) SEM images (at different magnifications) showing the growth of Cr_2O_{3-x} nanobelts and nanorods on the Cr substrate. c) SEM image and d) TEM image of nanobelts with a fold along the belt axis.

In Figure 2, a high-resolution TEM image along the [001] direction of a nanobelt and the corresponding selected-area electron diffraction (SAED) pattern are shown. Tilting experiments confirmed that the average structure of the nanobelts is rhombohedral with $a \approx 0.496$ and $c \approx 1.359$ nm. Actually, we found that many nanobelts are single-crystalline, with the surface normal of the largest faces being $\langle 001 \rangle$.

Figure 3a is a high-resolution TEM image along the $[\bar{1}11]$ direction of another nanobelt. The top-left part of the image shows the basic lattice fringes of the rhombohedral Cr_2O_3 structure, whereas the bottom-right part exhibits additional modulation fringes, as indicated by the arrows. Moiré effects can be ruled out, since no slightly mismatched or misorientated lattices are evident in the TEM image (Figure 3a), nor in the SAED pattern (Figure 3b). The diffraction pattern of the nanobelt exhibits satellite reflections indicating a structure modulation along the [110] direction (Figure 3b). The modulation wave vector is $q_1 = 1/3\,(a^* + b^*)$, and the perio-

 © 2006 Wiley-VCH Verlag GmbH & Co. KGaA, Weinheim

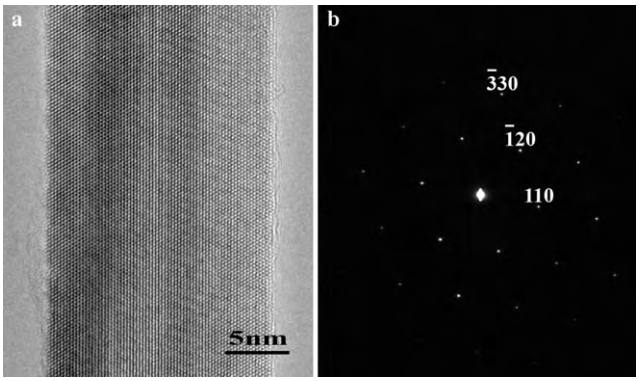

Figure 2. a) High-resolution TEM image and b) SAED pattern (along the [001] direction) of a Cr_2O_{3-x} nanobelt. Indexing refers to the cell of rhombohedral Cr_2O_3.

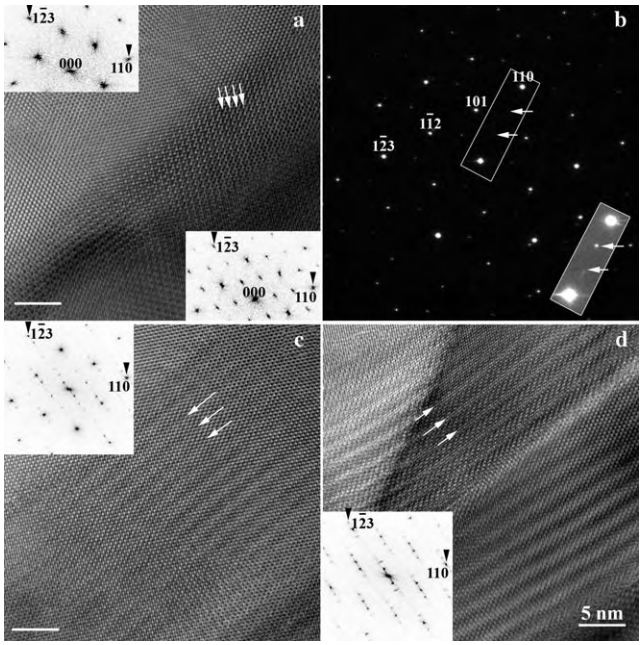

Figure 3. a) High-resolution TEM image (along the [$\bar{1}$11] direction) of a Cr_2O_{3-x} nanobelt with modulation I. No modulation of the basic rhombohedral Cr_2O_3 structure is observed in the top-left part of the image or in the corresponding Fourier transform (top-left inset). However, modulation I (arrows) is observed in the bottom-right part of the image and in the corresponding Fourier transform (bottom-right inset). b) SAED pattern (along the [$\bar{1}$11] direction) of the same nanobelt (from an area containing both unmodulated and modulated parts). Superlattice reflections (arrows) are enhanced in the inset. c) High-resolution TEM image (along the [$\bar{1}$11] direction) and corresponding Fourier transform (inset) of a nanobelt with modulation II at a periodicity of 1.64 nm (arrows). d) High-resolution TEM image (along the [$\bar{1}$11] direction) and corresponding Fourier transform (inset) of a nanobelt with modulation II at a periodicity of 1.84 nm (arrows). Indexing refers to the cell of rhombohedral Cr_2O_3. Scale bars = 5 nm.

dicity of the modulation in real space is 0.74 nm (hereafter, referred to as modulation I). Besides this commensurate modulation along the [110] direction, there is another incommensurate modulation approximately along the [$1\bar{2}3$]* (or [$0\bar{5}1$]) direction (hereafter, referred to as modulation II). The wave vector of the type-II modulation in Figure 3c is $q_2 \approx 0.133\,a^* - 0.267\,b^* + 0.401\,c^*$, and the periodicity in real space is 1.64 nm. The type-II modulation in Figure 3d is similar, but with a slightly longer periodicity of 1.84 nm in real space. Most of the nanobelts have structures with modulation II, but the periodicity of the modulation varies.

Electron energy-loss spectroscopy (EELS) can be used to analyze the chemical composition of TEM specimens, with a lateral resolution down to approximately 1 nm. To determine the origin of the modulation, we performed EELS analysis on the different types of nanobelts. In Figure 4a–c, EEL spectra

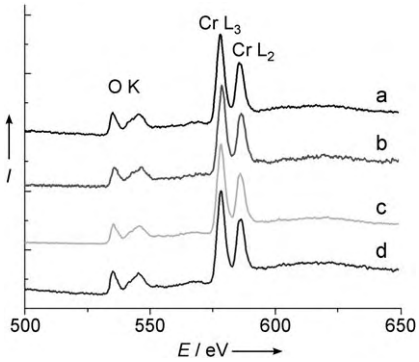

Figure 4. EEL spectra of Cr_2O_{3-x} nanobelts a) without modulation, b) with modulation I, and c) with modulation II, and of d) micron-sized Cr_2O_3 particles.

of chromia nanobelts without modulation, with modulation I, and with modulation II, respectively, are shown. For comparison, we also acquired a reference EEL spectrum (Figure 4d) of micron-sized Cr_2O_3 particles (Alfa–Aesar). The spectra were normalized to equalize the maximum intensities of the Cr L_3 peaks. Quantitative calculations show that the atomic ratio of oxygen to chromium in the nanobelts without modulation is $r_{O/Cr} = 1.47$ (Figure 4a), close to that of $r_{O/Cr} \approx 1.5$ in the micron-sized Cr_2O_3 particles. The $r_{O/Cr}$ of the nanobelts with modulations, however, is significantly lower: for those with modulation I, $r_{O/Cr} = 1.18$ (Figure 4b); for those with modulation II, $r_{O/Cr} = 1.22$ (Figure 4c). These ratios indicate an oxygen deficiency in the nanobelts with modulated structures. According to a series of EELS analyses, the composition of the nanobelts with modulations is Cr_2O_{3-x} with $x \approx 0.25$–0.70. Interestingly, many of the nanobelts with modulations have a composition near $Cr_2O_{2.4}$. No other elements were detected in the nanobelts by EELS (we examined the energy range of the C K edge in particular). TEM studies indicate that approximately 80% of the nanobelts have modulated structures.

The preparation of oxygen-deficient chromia, Cr_2O_{3-x}, as a powder was reported by Pop et al.[18] They first synthesized chromium hydroxide ($Cr(OH)_3$) gel by using CrO_3 and ethanol, and then heated the gel 1250 K in a hydrogen atmosphere. The XRD pattern of the product revealed that the nonstoichiometric product Cr_2O_{3-x} adopts the same structure as stoichiometric rhombohedral Cr_2O_3; only a slight difference in the peak positions and relative peak intensities was observed. Studies of X-ray K edge spectra by

 © 2006 Wiley-VCH Verlag GmbH & Co. KGaA, Weinheim

Pop et al. further demonstrated that the composition of the nonstoichiometric Cr_2O_{3-x} is $Cr_2O_{2.4}$. As mentioned above, many of the nanobelts with modulations prepared by us also have a composition near $Cr_2O_{2.4}$, although their synthesis, morphology, and microstructure are completely different from those of the powder prepared by Pop et al. The oxygen vacancies in the nanobelts with modulations are ordered and are, thus, responsible for the observed superstructures.

The chemical reaction for the formation of the chromia nanobelts can be explained as: $4\,Cr + (3-x)\,O_2 \rightarrow 2\,Cr_2O_{3-x}$. The oxygen reactant mainly comes from the decomposition of ethanol at high temperatures (although we used argon (99.999%) to purge the reaction tube prior to heating, it may still have contained some remnant oxygen). The decomposition of ethanol not only supplies oxygen, but also carbon and hydrogen. Small amounts of carbon soot were found in the product by TEM. At high temperatures, chromium, like some other transition metals, such as tungsten,[19] is very easily oxidized, even at low oxygen concentrations. The presence of ethanol vapor ensures that chromium can be oxidized, but under oxygen-deficient conditions. To understand the role of ethanol in the synthesis, we tried replacing the ethanol vapor by water vapor or air, but in these cases, no nanobelts or nanorods were formed. Thus, ethanol plays an important role in the formation of the nanostructures. Further investigation of the formation mechanism will be carried out.

The Cr_2O_{3-x} nanobelts grow in an oxygen-deficient environment, which results in most of the nanobelts having an oxygen deficiency, as confirmed by the EELS measurements. The superstructures occur in the nanobelts containing oxygen defects (or vacancies), but not in those without oxygen defects. Thus, the modulations found in the oxygen-deficient nanobelts are due to the ordering of the oxygen vacancies. This hypothesis is also consistent with the XRD results, since X-ray scattering is not very sensitive to the light oxygen atoms.

The folded shape observed for some Cr_2O_{3-x} nanobelts is related to their crystal structure (Figure 1c,d). The structure of rhombohedral Cr_2O_3 is generally described by a hexagonal lattice with $a_H = 0.495876$ and $c_H = 1.35942$ nm (JCPDS 38-1479). However, it can be also described by a face-centered rhombohedral (fcr) lattice with $a_C = 0.7302$ nm and $\alpha = 85.546°$ according to Equations (1)–(3). The fcr lattice of

$$a_H = -1/2\,a_C + 1/2\,b_C \quad (1)$$

$$b_H = -1/2\,b_C + 1/2\,c_C \quad (2)$$

$$c_H = a_C + b_C + c_C \quad (3)$$

Cr_2O_3 deviates only slightly from a face-centered cubic (fcc) lattice ($\alpha = 90°$). In the fcc lattice, there are four equivalent axes with threefold symmetry ([111], $[\bar{1}11]$, $[1\bar{1}1]$, and $[11\bar{1}]$). For the fcr lattice, however, there is only one axis ($[001]_H$ or $[111]_C$) with true threefold symmetry. The other three ($[\bar{1}11]_C$, $[1\bar{1}1]_C$, and $[11\bar{1}]_C$) are pseudo-threefold axes. Since the deviation of the fcr lattice of Cr_2O_3 from an ideal fcc lattice is very small (4.454°), the differences between the true and the pseudo-threefold axes are also small. This situation often results in twin formation during crystal growth (for example, in $PrCo_2C_x$[20] and $YBa_2Cu_3O_{7-x}$ (YBCO)[21]). In Figure 5a, growth occurs along the $[111]_C$ direction in the left domain of a bulk crystal, but along the $[\bar{1}11]_C$ direction in the right domain. The twin domains are related by the $(100)_C$ plane. As mentioned above, the Cr_2O_{3-x} nanobelts have the tendency to grow with their surface normals parallel to the $[001]_H$ (or $[111]_C$) direction. Thus, twinning across the $(100)_C$ plane results in the nanobelt folding shown in Figure 5b.

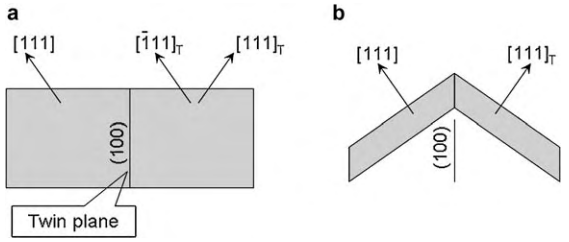

Figure 5. a) Formation of a (100) twin during bulk crystal growth. b) Formation of a folded nanobelt. Indexing refers to the fcr lattice; T subscripts refer to the second twin domain.

The oxygen-deficient chromia nanobelts with modulation structures and folded shapes described herein are expected to have distinct antiferromagnetic and catalytic properties.

Received: June 14, 2006
Revised: July 18, 2006
Published online: September 8, 2006

Keywords: chromium · nanostructures · oxides · superlattices · twinning

[1] Z. W. Pan, Z. R. Dai, Z. L. Wang, *Science* **2001**, *291*, 1647–1655.
[2] Z. L. Wang, *Annu. Rev. Phys. Chem.* **2004**, *55*, 159–196.
[3] M. Law, D. J. Sirbuly, J. C. Johnson, J. Goldberg, R. J. Saykally, P. D. Yang, *Science* **2004**, *305*, 1269–1273.
[4] H. Q. Yan, J. Johnson, M. Law, R. He, K. Knutsen, J. R. McKinney, J. Pham, R. Saykally, P. D. Yang, *Adv. Mater.* **2003**, *15*, 1907–1911.
[5] E. Comini, G. Faglia, G. Sberveglieri, Z. W. Pan, Z. L. Wang, *Appl. Phys. Lett.* **2002**, *81*, 1869–1871.
[6] W. Q. Han, L. J. Wu, Y. M. Zhu, M. Strongin, *Nano Lett.* **2005**, *5*, 1419–1422.
[7] P. X. Gao, Y. Ding, W. J. Mai, W. L. Hughes, C. S. Lao, Z. L. Wang, *Science* **2005**, *309*, 1700–1704.
[8] Q. Li, X. Gong, C. Wang, J. Wang, K. Ip, S. Hark, *Adv. Mater.* **2004**, *16*, 1436–1440.
[9] J. Jie, G. Wang, X. Han, J. G. Hou, *J. Phys. Chem. B* **2004**, *108*, 17027–17031.
[10] J. Joo, J. S. Son, S. G. Kwon, J. H. Yu, T. Hyeon, *J. Am. Chem. Soc.* **2006**, *128*, 5632–5633.
[11] K. P. Kamper, W. Schmitt, G. Guntherodt, R. J. Gambino, R. Ruf, *Phys. Rev. Lett.* **1987**, *59*, 2788–2791.
[12] G. A. Prinz, *Phys. Today* **1995**, *48*, 58–63.
[13] T. P. Kobylins, B. W. Taylors, *J. Catal.* **1973**, *31*, 450–458.
[14] L. Néel, *IEEE Trans. Magn.* **1981**, *17*, 2516.
[15] A. Kawabata, M. Yoshinaka, K. Hirota, O. Yamaguchi, *J. Am. Ceram. Soc.* **1995**, *78*, 2271–2273, and references therein.

 © 2006 Wiley-VCH Verlag GmbH & Co. KGaA, Weinheim

[16] D. W. Kim, S. Shin, J. D. Lee, S. G. Oh, *Mater. Lett.* **2004**, *58*, 1894 – 1898.
[17] S. Hashimoto, A. Yamaguchi, *J. Mater. Sci.* **1996**, *31*, 317 – 322.
[18] I. Pop, M. Andrecut, I. Burda, C. Andrecut, O. Pop, I. Ivan, I. Nazarenco, C. Oprea, *Mater. Chem. Phys.* **1997**, *47*, 85 – 89.
[19] G. Gu, B. Zhang, W. Q. Han, S. Roth, J. Liu, *Nano Lett.* **2005**, *5*, 849 – 851.
[20] L. Wu, Y. Zhang, *Philos. Mag. A* **1997**, *76*, 481 – 492.
[21] Y. Zhu, M. Suenaga, J. Tafto, D. O. Welch, *Phys. Rev. B* **1991**, *44*, 2871 – 2874.

 © 2006 Wiley-VCH Verlag GmbH & Co. KGaA, Weinheim

Polyquinane Synthesis

DOI: 10.1002/anie.200602553

One-Step Synthesis of Benzotetra- and Benzopentacyclic Compounds through Intramolecular [2+3] Photocycloaddition of Alkenes to Naphthalene**

*Hirofumi Mukae, Hajime Maeda, and Kazuhiko Mizuno**

Photocycloaddition of unsaturated compounds to aromatic rings is a useful and convenient method for the construction of polycyclic compounds in organic synthesis.[1–7] In particular, the inter- and intramolecular metaphotocycloaddition of alkenes to benzene rings has been extensively developed from the synthetic and mechanistic points of view in recent decades.[1,2] Wender et al. first reported the synthesis of natural products by using an intramolecular *meta*-photocycloaddition as a key step.[2] However, little is known about the [2+3] photocycloaddition of alkenes to naphthalene at the 1,3-positions, except the relatively inefficient intermolecular photocycloaddition of cyclooctene to naphthalene.[6] We now report a novel intramolecular [2+3] photocycloaddition of 1-cyano-2-(4-pentenyl)naphthalene derivatives to give benzo-tetra- and benzopentacyclic compounds with tri- and tetraquinane skeletons in a highly selective manner.[7,8]

Irradiation of an acetonitrile solution containing **1a** (0.03 M) with a high-pressure mercury lamp through a Pyrex filter (> 280 nm) and under an argon atmosphere exclusively gave a benzotetracyclic product (**3a**) in 70% yield (Scheme 1). The ^{1}H NMR spectrum of **3a** showed four

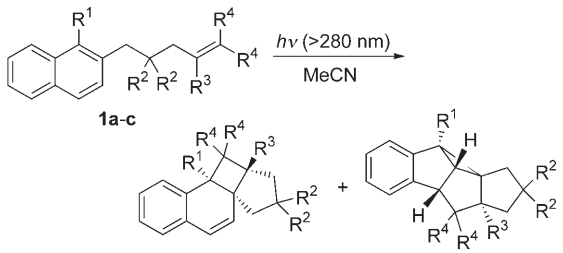

	R^1	R^2	R^3	R^4
1a-3a	CN	CN	H	H
1b-3b	CN	CN	H	Me
1c-3c	CN	CO_2Me	Me	Me

Scheme 1. Intramolecular photocycloadditions of **1a–c**.

aromatic and nine aliphatic protons, but no olefinic protons; the ^{13}C NMR spectrum showed nine nonequivalent unsaturated carbon signals in the $\delta = 100$–150 ppm region and nine nonequivalent aliphatic carbon signals. The IR, UV, and mass spectra clearly showed the existence of a cyano group, the lack of a styrene chromophore, and the identical molecular weight to **1a**, respectively. Since these data are not sufficient to establish the structure of **3a**, the structure was determined by X-ray crystallography analysis. Similar irradiation of **1b** and **1c** afforded the corresponding products **3b** and **3c** in good yields (Table 1).

In the initial stages (less than 20% conversion) of these photoreactions, intramolecular [2+2] photocycloadducts **2a–c**, formed by reaction at the 1,2-positions, were obtained as the major products. For example, the rate for the formation of **2b** is 10 times faster than that for **3b**. However, prolonged irradiation afforded **3b** as the sole product in a highly

Table 1: Intramolecular photocycloadditions of **1a–c**, **4a,b**, and **6a–e** in acetonitrile.

Compound	t[a] [h]	Yield of 1,2-adduct[b] [%]	Yield of 2,4-adduct[b] [%]
1a	20	0	70
1b	10	0	74
1b[c]	3	10	41
1c	160	0	64
4a	25	0	74
4b	10	0	85
6a	40	0	84
6b	40	0	60
6c[c]	20	39	52
6d[c]	100	trace	33
6e	160	6[d]	18[d]

[a] Irradiation time. [b] Yields of isolated products. [c] Reaction performed in benzene. [d] Yields were determined by GC analysis.

[*] H. Mukae, Dr. H. Maeda, Dr. K. Mizuno
Department of Applied Chemistry
Graduate School of Engineering
Osaka Prefecture University
1-1 Gakuen-cho, Naka-ku, Sakai, Osaka 599-8531 (Japan)
Fax: (+81) 72-254-9289
E-mail: mizuno@chem.osakafu-u.ac.jp

[**] The authors thank Prof. H. Roth (The State University of New Jersey) for helpful discussions. The authors also thank Akihito Yamano and Motoo Shiro (Rigaku Corporation) for analysis of the X-ray crystallography data. This work was partially supported by Grants-in-Aid for Scientific Research on Priority Areas "Advanced Molecular Transformations of Carbon Resources" (18037063 to K.M.), Exploratory Research (16655018 to K.M.), and Young Scientists (B) (16750039 to H.M.) from the Ministry of Education, Culture, Sports, Science, and Technology of Japan.

© 2006 Wiley-VCH Verlag GmbH & Co. KGaA, Weinheim

regioselective manner. Irradiation of isolated **2b** quickly gave **1b**; clearly, the [2+2] cycloaddition in this system is reversible. Therefore, the selective formation of **3a–c** can be reasonably explained by efficient cycloreversion of **2a–c** to **1a–c** and gradual accumulation of **3a–c**.

This photoreaction was applied to the synthesis of benzopentacyclic compounds **5a,b** from **4a,b** (Scheme 2). Irradiation of **4a,b** in acetonitrile gave exclusively **5a,b** in good yields (Table 1). The structures of **5a,b** were confirmed by X-ray crystallography analyses (Figure 1).[9]

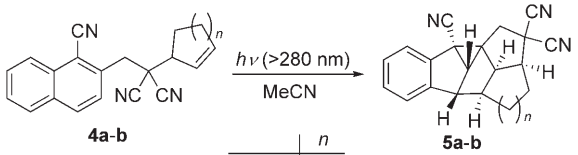

	n
4a, 5a	1
4b, 5b	2

Scheme 2. Intramolecular photocycloadditions of **4a,b**.

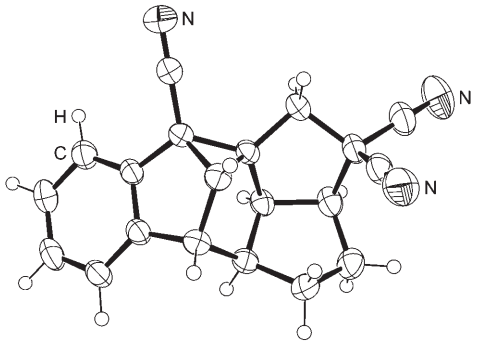

Figure 1. ORTEP drawing of **5a**.

The related intramolecular photocycloaddition of **6c** was reported by McCullough et al. to give two types of [2+2] photocycloadducts, **7c** and **8c**, with **7c** as the major product (Scheme 3).[4] We had previously studied the related reactions of **6a–e** and obtained products to which we originally assigned structures **7a–e** and **8a–e**, by analogy with the assignment of McCullough et al.[5] We have found recently that the product ratios of both product types in the photoreactions of **6a–e** are dependent on additives and solvents. In addition, the major products **7a–e** gradually reverted to the starting compounds **6a–e**, but the minor products were stable under the reaction conditions.

Based on our finding that [2+3] cycloadducts were formed from **1a–c**, we reinvestigated the structures of the cycloadducts that had been assigned structures of type **8**. The X-ray crystallography analyses of these adducts showed unambiguously that the second type of adduct has the benzotetracyclic structure of type **9** (Table 1). All spectral properties of these adducts support the newly assigned structure type.

The formation of the benzotetracyclic compound **3b** was not sensitized by triplet sensitizers, such as benzophenone and Michler's ketone, and was not quenched by 2-methyl-1,3-butadiene. The monomer fluorescence typically observed for 1-cyanonaphthalene chromophores such as **1b** was replaced by a weak exciplex emission at longer wavelengths than that of the monomer emission, a result indicating intramolecular quenching by the alkenyl group. Based on these results, we propose an exciplex mechanism for the formation of the benzotetra- and benzopentacyclic compounds by intramolecular [2+3] photocycloaddition of **1**, **4**, and **6**, in competition with the formation of intramolecular [2+2] photocycloadducts (Scheme 4). Both cycloadducts seem to be controlled by Hirayama's $n=3$ rule.[10] The position of the cyano or ester group on the naphthalene skeleton seems to be important for the excellent regioselectivity.[11] In general, the nature of an exciplex is represented by both charge-transfer and exciton resonance forms. In the series of photoreactions reported here, an intramolecular charge-transfer interaction between naphthalene derivatives bearing electron-withdrawing groups and electron-donating alkenes in their excited singlet states is quite important for [2+3] photocycloaddition; however, polar intermediates are not observed at this stage.[12] In fact, the photoreaction of 2-(2-oxa-4-pentenyl)naphthalene did not give any isolable cycloadducts at all.

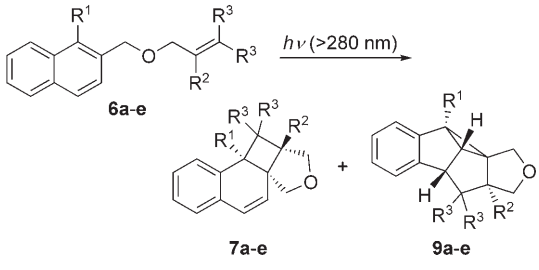

	R¹	R²	R³
6a-9a	CN	H	H
6b-9b	CN	H	Me
6c-9c	CN	Me	Me
6d-9d	CO_2Me	H	Me
6e-9e	CO_2Me	Me	Me

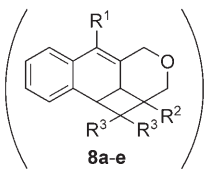

Scheme 3. Intramolecular photocycloadditions of **6a–e**.

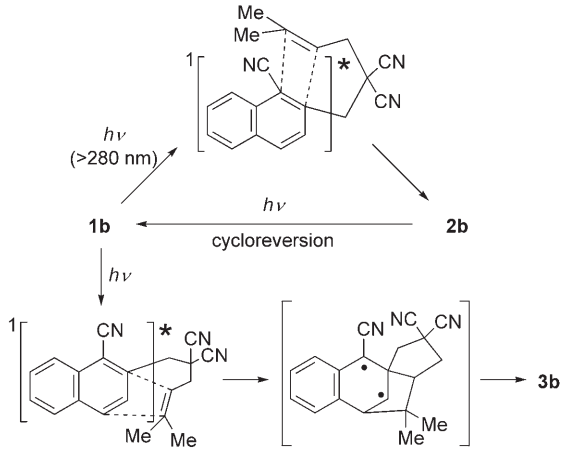

Scheme 4. Proposed mechanism for the intramolecular photocycloaddition of **1b**.

 © 2006 Wiley-VCH Verlag GmbH & Co. KGaA, Weinheim

In conclusion, we have obtained intramolecular [3+2] photocycloadducts in a highly selective manner. The scope and limitations of these photocycloadditions are now under investigation.

Received: June 26, 2006
Published online: September 5, 2006

Keywords: cycloaddition · exciplexes · photochemistry · polycycles · triquinanes

[1] J. Mattay, *Tetrahedron* **1985**, *41*, 2405 – 2417; J. Mattay, *Tetrahedron* **1985**, *41*, 2393 – 2404; J. J. McCullough, *Chem. Rev.* **1987**, *87*, 811 – 860; J. Cornelisse, *Chem. Rev.* **1993**, *93*, 615 – 669; D. Döpp in *Molecular and Supramolecular Photochemistry*, *Vol. 6* (Eds.: V. Ramamurthy, K. S. Schanze), Marcel Dekker, New York, **2000**, pp. 101 – 148; K. Mizuno, H. Maeda, A. Sugimoto, K. Chiyonobu in *Molecular and Supramolecular Photochemistry*, *Vol. 8* (Eds.: V. Ramamurthy, K. S. Schanze), Marcel Dekker, New York, **2001**, pp. 127 – 241; N. Hoffmann in *Molecular and Supramolecular Photochemistry*, *Vol. 12* (Eds.: A. G. Griesbeck, J. Mattay), Marcel Dekker, New York, **2005**, pp. 529 – 552.

[2] P. A. Wender, J. J. Howbert, *J. Am. Chem. Soc.* **1981**, *103*, 688 – 690; P. A. Wender, R. Ternansky, M. deLong, S. Singh, A. Olivero, K. Rice, *Pure Appl. Chem.* **1990**, *62*, 1597 – 1602, and references therein.

[3] K. Mizuno, H. Maeda, Y. Inoue, A. Sugimoto, L. P. Vo, R. A. Caldwell, *Tetrahedron Lett.* **2000**, *41*, 4913 – 4916; H. Maeda, S. Waseda, K. Mizuno, *Chem. Lett.* **2000**, 1238 – 1239; H. Maeda, A. Sugimoto, K. Mizuno, *Org. Lett.* **2000**, *2*, 3305 – 3308; A. Yokoyama, K. Mizuno, *Org. Lett.* **2000**, *2*, 3457 – 3459.

[4] J. J. McCullough, W. K. MacInnis, C. J. L. Lock, R. Faggiani, *J. Am. Chem. Soc.* **1980**, *102*, 7780 – 7782; J. J. McCullough, W. K. MacInnis, C. J. L. Lock, R. Faggiani, *J. Am. Chem. Soc.* **1982**, *104*, 4644 – 4658.

[5] K. Mizuno, S. Konishi, T. Takata, H. Inoue, *Tetrahedron Lett.* **1996**, *37*, 7775 – 7778; K. Mizuno, S. Konishi, Y. Yoshimi, A. Sugimoto, *Chem. Commun.* **1998**, 1659 – 1660; Y. Yoshimi, S. Konishi, H. Maeda, K. Mizuno, *Tetrahedron Lett.* **2001**, *42*, 3475 – 3477; Y. Yoshimi, S. Konishi, H. Maeda, K. Mizuno, *Synthesis* **2001**, 1197 – 1202; H. Maeda, H. Mukae, K. Mizuno, *Chem. Lett.* **2005**, *34*, 66 – 67.

[6] D. Bryce-Smith, A. Gilbert, B. H. Orger, *J. Chem. Soc. Chem. Commun.* **1966**, 512 – 514; Y. Inoue, K. Nishida, K. Ishibe, T. Hakushi, N. J. Turro, *Chem. Lett.* **1982**, 471 – 474; N. Zupančič, B. Šket, *J. Chem. Soc. Perkin Trans. 1* **1992**, 179 – 180.

[7] Related benzotricyclic compounds were obtained by di-π-methane rearrangement of [4+2] cycloadducts: D. Döpp, H. R. Memarian, *Chem. Ber.* **1990**, *123*, 315 – 319.

[8] For other examples of [3+2] photocycloaddition, see: I. Saito, K. Shimozono, T. Matsuura, *Tetrahedron Lett.* **1982**, *23*, 5439 – 5442; T. Miyashi, Y. Takahashi, T. Mukai, H. D. Roth, M. L. M. Schilling, *J. Am. Chem. Soc.* **1985**, *107*, 1079 – 1080; P. H. Mazzocchi, C. Somich, M. Edwards, T. Morgan, H. L. Ammon, *J. Am. Chem. Soc.* **1986**, *108*, 6828 – 6829; H. Tomioka, D. Kobayashi, A. Hashimoto, S. Murata, *Tetrahedron Lett.* **1989**, *30*, 4685 – 4688; K. Mizuno, K. Nire, H. Sugita, Y. Otsuji, *Tetrahedron Lett.* **1993**, *34*, 6563 – 6566; H. Suginome, K. Kobayashi, A. Konishi, H. Minakawa, H. Sakurai, *J. Chem. Soc. Chem. Commun.* **1993**, 807 – 809; F. Müller, J. Mattay, S. Steenken, *J. Org. Chem.* **1993**, *58*, 4462 – 4464; Y. Kubo, K. Kiuchi, I. Inamura, *Bull. Chem. Soc. Jpn.* **1999**, *72*, 1101 – 1108; K. Mizuno, N. Ichinose, Y. Yoshimi, *J. Photochem. Photobiol. C* **2000**, *1*, 167 – 193; K. Mizuno, H. Sugita, T. Hirai, H. Maeda, Y. Otsuji, M. Yasuda, M. Hashiguchi, K. Shima, *Tetrahedron Lett.* **2001**, *42*, 3363 – 3366; H. Maeda, Y. Miyata, K. Mizuno, *Tetrahedron Lett.* **2002**, *43*, 1481 – 1486.

[9] A colorless block crystal of $C_{20}H_{15}N_3$ with approximate dimensions of $0.70 \times 0.50 \times 0.30\ mm^3$ was mounted on a glass fiber. All measurements were made on a Rigaku Raxis Rapid imaging plate area detector with graphite monochromated $Mo_{K\alpha}$ radiation. The data were collected at a temperature of 23 ± 1 °C to a maximum 2θ value of 55.0°. Cell constants and an orientation matrix for data collection corresponded to a primitive triclinic cell with dimensions: $a = 6.803(4)$, $b = 10.585(6)$, $c = 11.665(9)$ Å; $\alpha = 67.57(3)$, $\beta = 74.27(3)$, $\gamma = 85.95(2)$°; $V = 746.8(8)$ Å^3. The space group was determined to be $P\bar{1}$ (no. 2). $\rho_{calcd} = 1.322\ g\,cm^{-3}$. The structure was solved by direct methods (SIR88) and expanded by using Fourier techniques. The non-hydrogen atoms were refined anisotropically. Hydrogen atoms were refined by using the riding model. The final cycle of full-matrix least-squares refinement on F was based on 2590 observed reflections ($I > 5.00\sigma(I)$) and 224 variable parameters and was converged with unweighted and weighted agreement factors of $R = 0.0383$ and $R_w = 0.0421$.

[10] F. Hirayama, *J. Chem. Phys.* **1965**, *42*, 3163 – 3171.

[11] Intramolecular photocycloaddition of 1-cyano-2-(4-pentenyl)-benzene also proceeds by the 2,4-addition, 1,3-closure mode: H. A. Neijenesch, R. J. P. J. de Ruiter, E. J. Ridderikhoff, J. O. van den Ende, L. J. Laarhoven, L. J. W. van Putten, J. Cornelisse, *J. Photochem. Photobiol. A* **1991**, *60*, 325 – 343.

[12] The addition of methanol in the photoreaction of **1b** did not afford any methanol-incorporated products via the dipolar intermediate.

 © 2006 Wiley-VCH Verlag GmbH & Co. KGaA, Weinheim

Total Synthesis

DOI: 10.1002/anie.200602569

Total Synthesis of (+)-Phyllantidine**

*Cheryl A. Carson and Michael A. Kerr**

Dedicated to Professor K. C. Nicolaou on the occasion of his 60th birthday

There exists a small group of alkaloids isolated from the *Euporbiaceae* family of plants known as the securinega alkaloids (Figure 1).[1] These compounds have an indolizidine

[*] C. A. Carson, Dr. M. A. Kerr
Department of Chemistry
The University of Western Ontario
London, ON, N6A5B7 (Canada)
Fax: (+1) 519-661-3022
E-mail: makerr@uwo.ca

[**] We thank the Natural Sciences and Engineering Research Council (NSERC) of Canada and Boehringer Ingelheim Canada for funding. We are grateful to D. Hairsine for performing MS analyses. C.A.C. is the recipient of an NSERC CGSM postgraduate scholarship.

Supporting information for this article is available on the WWW under http://www.angewandte.org or from the author.

WILEY InterScience DISCOVER SOMETHING GREAT
© 2006 Wiley-VCH Verlag GmbH & Co. KGaA, Weinheim

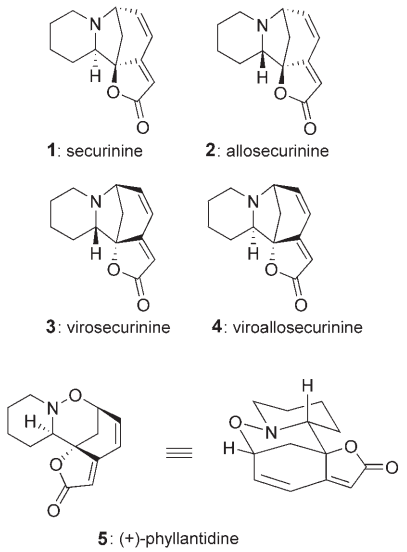

Figure 1. The securinega alkaloids including (+)-phyllantidine (**5**).

core imbedded within an azabicyclo [3.2.1] ring system. This is fused to a butenolide moiety forming a rather interesting and structurally complex molecular framework. Securinine (**1**) and its C2 epimer allosecurinine (**2**) are constituents of *Securinega suffruticosa*,[2] and the antipodal compounds virosecurinine (**3**) and viroallosecurinine (**4**) are found in *Securinega virosa*.[3] While these compounds show interesting activity in the central nervous system (CNS) in the form of antagonism of the γ-aminobutyric acid (GABA) receptor,[4] the synthetic chemist is drawn to the compact and complex architecture of the compounds. Indeed several syntheses of the securinine series of compounds have been reported.[5] Of interest to us are not the indolizidines **1**–**4** but a related and much rarer alkaloid phyllantidine **5** (isolated from *Phyllanthus discoides* and *Seurinega suffruticosa*)[6] and its enantiomer (from *Breynia coronata*).[7]

To date, no syntheses of phyllantidine (or *ent*-phyllantidine) have been reported, although phyllantidine is available through the peroxide (or peracid) oxidation of virosecurinine.[8] This proceeds via the *N*-oxide which undergoes a Meisenheimer rearrangement yielding phyllantidine. Since the synthetic routes to the securinine alkaloids are quite complex and lengthy, this route to phyllantidine is less than appealing. Herein, we present a convenient and direct synthesis of (+)-phyllantidine.

Perhaps the most significant structural feature of phyllantidine is the tetrahydro-1,2-oxazine ring. This heterocyclic motif is uncommon in natural products and is found in FR-900482 (and a few related compounds)[9]. This structural feature also makes phyllantidine an elusive target since there are few ways to directly prepare tetrahydro-1,2-oxazines. Recently, however, we reported that nitrones (either as isolated compounds or generated in situ) react smoothly with 1,1-cyclopropane diesters under the influence of Lewis acids to form tetrahydro-1,2-oxazines in what we have termed a "homo-1,3-dipolar cycloaddition".[10] The reactions are diastereoselective and yield only 3,6-*cis* adducts. Both the substitution pattern and relative stereochemistry of the adducts from this cycloaddition would fulfill the requirements of a practical synthetic route to phyllantidine (Scheme 1).

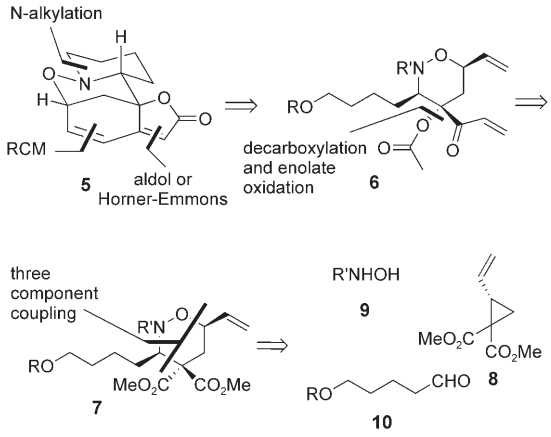

Scheme 1. Retrosynthesis of phyllantidine. RCM = ring-closing olefin metathesis.

Initially, we envisioned a cycloaddition between a cyclic nitrone **11** and cyclopropane **8** as a rapid access to an advanced bicyclic intermediate such as **12** [Eq. (1)]. However, we have not been able to obtain adducts from the cyclo-

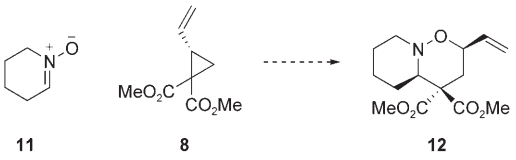

(1)

addition reaction using nitrones such as **11** as the substrate.

Our synthesis of phyllantidine commenced with the three-component coupling of hydroxylamine **13**, aldehyde **14**, and cyclopropane **8**[11] under the influence of catalytic ytterbium triflate hydrate to give the tetrahydro-1,2-oxazine **15** in 86% yield as a 12:1 mixture of diastereomers, in which the major product bore the required *cis* relationship between the oxazine vinyl substituent and the alkyl chain (Scheme 2). Interestingly, we occasionally saw this slight loss of diastereochemical integrity when the cycloaddition reaction mixture was heated to reflux. However, perhaps more interesting and surprising is that there was approximately 10% erosion of the absolute stereochemistry, with the *cis* adduct isolated as a 90:10 mixture of enantiomers. This has mechanistic implications and a detailed study of the stereochemistry of these cycloadditions is underway. Krapcho decarboxylation proceeded smoothly to produce **16** as a 1:1 mixture of diastereomers in 85% yield. Treatment of **16** (mixture of epimers) with KHMDS to generate the potassium enolate followed by treatment with the Davis oxaziridine[12] gave the hydroxy esters **17** and **18** as an inseparable mixture of diastereomers (1:3 in favor of the desired isomer; Scheme 2).

We were delighted to find that our expectations of a diastereoselective hydroxylation were born out, since this

 © 2006 Wiley-VCH Verlag GmbH & Co. KGaA, Weinheim

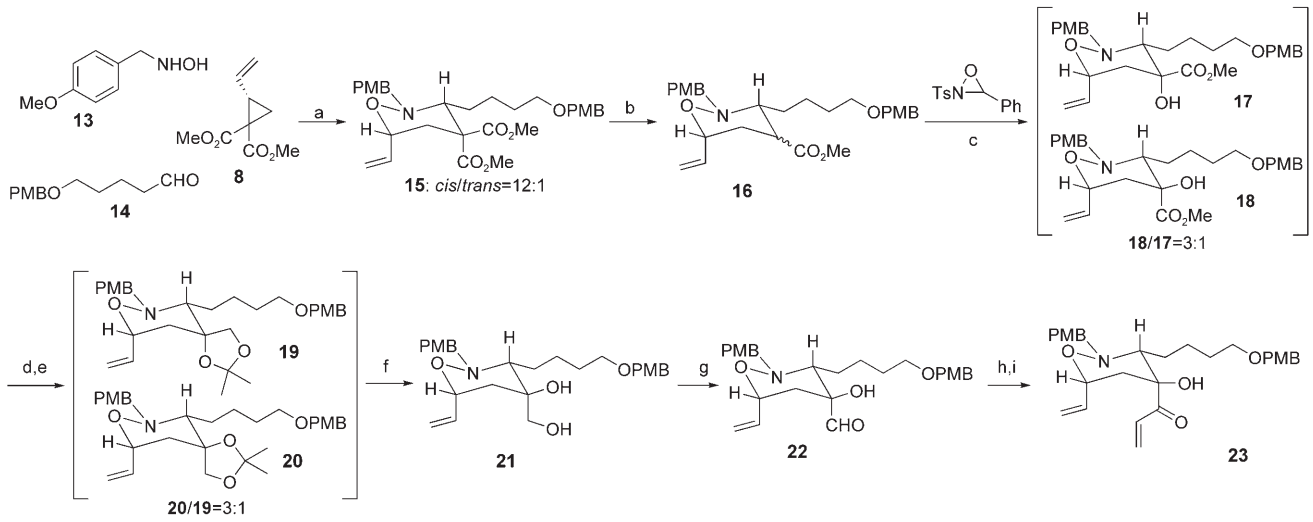

Scheme 2. Synthesis of advanced intermediate **23**. a) Ytterbium(III) trifluoromethanesulfonate hydrate (5 mol%), MS (4 Å), toluene, heated at reflux (86%); b) LiCl (5 equiv), DMSO, H_2O, 160°C (85%); c) KHMDS, Davis oxaziridine, THF, −78°C (80% as a 3:1 diastereomeric mixture of **18** and **17**); d) LAH, THF, 0°C (97%); e) 2,2-dimethoxypropane, *p*-toluenesulfonic acid, DMSO (74%); f) 6 N HCl, THF (93% based on **20**); g) IBX, DMSO (64%); h) CH_2=CHMgBr, THF, (76%); i) IBX, DMSO (79%). PMB = *p*-methoxybenzyl, Ts = toluene-4-sulfonyl, LAH = lithium aluminum hydride, KHMDS = potassium bis(trimethylsilyl)amide, IBX = *o*-iodoxybenzoic acid.

transformation was the greatest concern to us at the outset of the project. Our rationale for the predicted selectivity is shown in Scheme 3. The enolate derived from **16** may be envisaged as the chair conformers **A** or **B**. Whether one invokes **A** or **B**, approach of the electrophilic oxidant should be from the top face (bold arrow in Scheme 3) to avoid either a 1,3-diaxial interaction with the vinyl group in **A** or a 1,2-interaction with the alkyl chain in **B**. It is worth noting that in a simpler model system, in which both the substituents on the nitrogen atom and the alkyl chain were replaced by phenyl moieties, there was complete selectivity for the desired isomer.

Reduction of this mixture with LAH afforded the diols (in 97% yield), which upon derivatization gave the acetonides **19** and **20** as a 1:3 mixture as expected (Scheme 3). This mixture was amenable to simple separation by flash column chromatography giving, after acetonide removal (in 93% yield), **21** as a single isomer. Oxidation of the primary hydroxy group gave an aldehyde **22** (in 64% yield), which was treated with vinylmagnesium bromide to give a diastereomeric mixture of the allylic alcohols in 76% yield. Oxidation gave the enone **23**, which we anticipated would be an appropriate substrate for RCM.

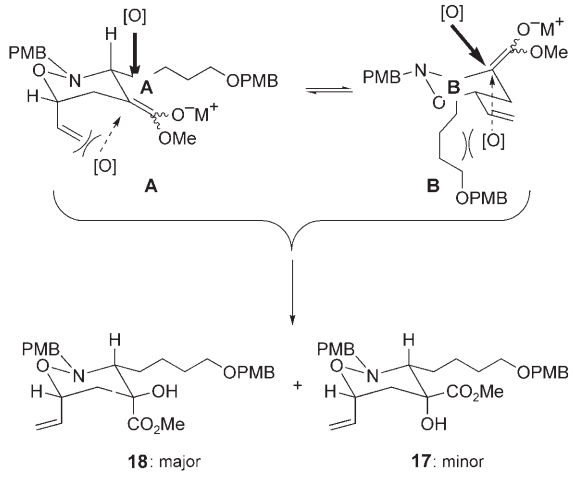

Scheme 3. Model for selective hydroxylation showing steric interactions between oxidant and vinyl group in **A** and between oxidant and alkyl chain in **B**.

While the sequence of reactions in Scheme 2 certainly produced **23** in a relatively efficient way, this sequence of protection through formation of acetonides, separation, and deprotection seemed rather clumsy. This procedure was necessary at the time to better understand the reaction sequence. In addition, separation of the diols resulting from the reduction of mixture **17**/**18** was not possible in a preparative manner.

In order to circumvent the tedious protection/deprotection sequence, the diastereomeric mixture of **17**/**18** (ratio 1:3) was subjected to a sequence of four reactions (Scheme 4), namely, reduction using LAH, oxidation of the primary alcohol to an aldehyde using IBX, addition of vinylmagnesium bromide, and finally oxidation of the allylic alcohol to give the vinyl ketone **23**. At this juncture, the unwanted diastereomer was readily removed by flash column chromatography. Enone **23** proved to be a suitable substrate for RCM with Grubbs second-generation catalyst. In the event, ring closure to give enone **24** proceeded in 74% yield. The O-acetyl derivative of **24** was explored as a substrate for aldol-type ring closure to form the butenolide, yet all attempts to affect this cyclization failed. Fortunately, an alternative acylation[13] using diethylphosphonoacetic acid afforded substrate **25** (in 71% yield), which after an intramolecular Horner–Emmons reaction, was converted into the desired **26** in quantitative yield.[14] The natural product **5** was ultimately

 © 2006 Wiley-VCH Verlag GmbH & Co. KGaA, Weinheim

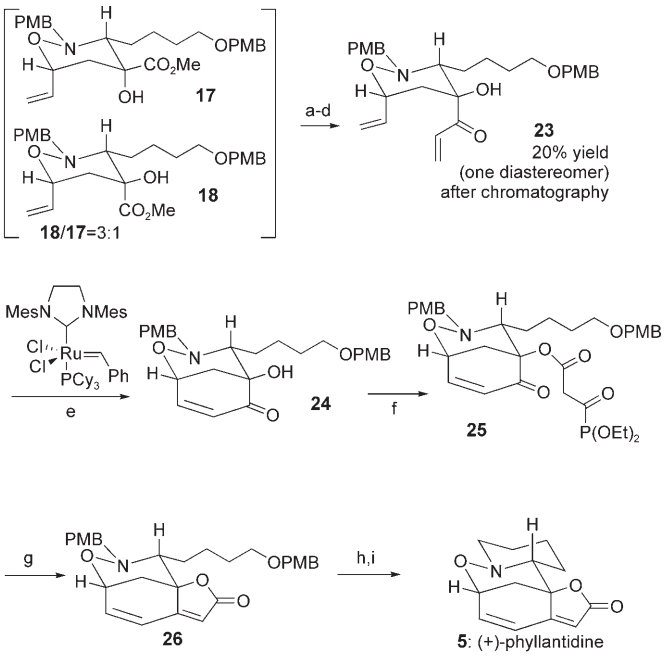

Scheme 4. Synthesis of (+)-phyllantidine. a) LAH, THF, 0°C; b) IBX, DMSO; c) CH_2=CHMgBr, THF; d) IBX, DMSO (20% overall yield of one diastereomer from a mixture of **17** and **18**); e) second-generation Grubbs catalyst (20 mol%), CH_2Cl_2, heated at reflux (74%); f) diethylphosphonoacetic acid, DCC, CH_2Cl_2 (71%); g) K_2CO_3, [18]crown-6, toluene (quant.); h) DDQ/CH_2Cl_2, H_2O (98%); i) Ph_3P, DIAD, toluene (98%). Mes = mesityl = 2,4,6-trimethylphenyl, DCC = 1,3-dicyclohexylcarbodiimide, DDQ = 2,3-dichloro-4,6-dicyano-1,4-benzoquinone, DIAD = diisopropylazodicarboxylate.

secured through oxidative removal of both the *p*-methoxybenzyl groups and ring closure under Mitsunobu conditions. This method of piperidine formation is unusual for C–N bond formation, and we were pleasantly surprised at its efficiency. However, there is ample precedent for such transformations.[15] The spectral data for synthetic (+)-phyllantidine correspond to those reported in the literature, including the sign of optical rotation. Analysis by HPLC on a chiral stationary phase indicated no trace of the (−) isomer.

In summary, we have succeeded in preparing for the first time the structurally unusual and demanding alkaloid phyllantidine using a homo [3+2] dipolar cycloaddition. The overall yield of the natural product is around 6% over 12 synthetic operations from the cycloaddition. Efforts to adapt this protocol (through N–O bond reduction and ring closure to form a pyrrolidine) to other *securinega* alkaloids are in progress.

Received: June 27, 2006
Published online: September 13, 2006

Keywords: alkaloids · cycloaddition · nitrone · oxazine · total synthesis

[1] V. Snieckus, *The Alkaloids*, *Vol. 14*, Academic Press, New York, **1973**, p. 425–506.

[2] For information on original isolation, see: a) V. I. Murav'eva, A. I. Ban'kovskii, *Dokl. Acad. Nauk SSSR* **1956**, *110*, 998–1000; b) V. I. Murav'eva, A. I. Ban'kovskii, *Med. Prom-st. SSSR* **1956**, *10*, 27–28; for structure determination of securinine and isolation of allosecurinine, see: c) I. Satoda, M. Murayama, J. Tsuji, E. Yoshii, *Tetrahedron Lett.* **1962**, 1199–1206.

[3] a) For isolation of virosecurinine, see: T. Nakano, T. H. Yang, S. Terao, *Tetrahedron* **1963**, 609–619; b) for isolation of viroallosecurinine, see: S. Saito, T. Iwamoto, T. Tanaka, C. Matsumura, N. Sugimoto, Z. Horii, Y. Tamura, *Chem. Ind.* **1964**, *28*, 1263–1264.

[4] I. A. Beutler, E. W. Karbon, A. N. Brubaker, R. Malik, D. R. Curtis, S. J. Enna, *Brain Res.* **1985**, *330*, 135–140.

[5] a) T. Honda, H. Namiki, M. Watanabe, H. Mizutani, *Tetrahedron Lett.* **2004**, *45*, 5211–5213; b) R. Alibes, M. Ballbe, F. Busque, P. de March, L. Elias, M. Figueredo, J. Font, *Org. Lett.* **2004**, *6*, 1813–1816; c) T. Honda, H. Namiki, K. Kaneda, H. Mizutani, *Org. Lett.* **2004**, *6*, 87–89; d) T. Honda, H. Namiki, M. Kudoh, H. Nagase, H. Mizutani, *Heterocycles* **2003**, *59*, 169–187; e) T. Honda, H. Namiki, M. Kudoh, N. Watanabe, H. Nagase, H. Mizutani, *Tetrahedron Lett.* **2000**, *41*, 5927–5930; f) Z. Horii, M. Hanaoka, Y. Yamawaki, Y. Tamura, S. Saito, N. Shigematsu, K. Kotera, H. Yoshikawa, Y. Sato, H. Nakai, N. Sugimoto, *Tetrahedron* **1967**, *23*, 1165–1174; g) S. Saito, H. Yoshikawa, Y. Sato, H. Nakai, N. Sugimoto, Z. Horii, N. Hanaoka, Y. Tamura, *Chem. Pharm. Bull.* **1966**, *14*, 313–314.

[6] a) Z. Horii, T. Imanishi, M. Yamauchi, M. Hanaoka, J. Parello, S. Munavalli, *Tetrahedron Lett.* **1972**, 1877–1880; b) J. Parello, S. Munavalli, *C. R. Hebd. Seances Acad. Sci.* **1965**, *260*, 337–340.

[7] N. H. Lajis, O. B. Guan, M. V. Sargent, B. W. Skelton, A. H. White, *Aust. J. Chem.* **1992**, *45*, 1893–1897.

[8] T. Nakano, S. Terao, K. H. Lee, Y. Saeki, L. J. Durham, *J. Org. Chem.* **1966**, *31*, 2274–2799.

[9] I. Uchida, S. Takase, H. Kayakiri, S. Kiyoto, M. Hashimoto, T. Tada, S. Koda, Y. Morimoto, *J. Am. Chem. Soc.* **1987**, *109*, 4108–4109.

[10] a) M. D. Ganton, M. A. Kerr, *J. Org. Chem.* **2004**, *69*, 8554–8557; b) I. S. Young, M. A. Kerr, *Org. Lett.* **2004**, *6*, 139–141; I. S. Young, M. A. Kerr, *Angew. Chem.* **2003**, *115*, 3131–3134; *Angew. Chem. Int. Ed.* **2003**, *42*, 3023–3026.

[11] These compounds are all readily prepared in short sequences from commercial materials. Their preparation is included in the Supporting Information.

[12] a) F. A. Davis, J. Lamendola, U. Nadir, E. W. Lluger, T. C. Sedergran, T. W. Panunto, R. Billmers, R. Jenkins, Jr., I. J. Turchi, W. H. Watson, J. S. Chen, M. Kimura, *J. Am. Chem. Soc.* **1980**, *102*, 2000–2005; b) F. A. Davis, L. C. Vishwakarma, J. M. Billmers, J. Finn, *J. Org. Chem.* **1984**, *49*, 3243–3244.

[13] M. Nahmany, A. Melman, *Org. Lett.* **2001**, *3*, 3733–3735.

[14] This method was used in a similar butenolide formation for the synthesis of related alkaloids norsecurinine and phyllanthine. See: a) G. Han, M. G. LaPorte, J. J. Folmer, K. M. Werner, S. M. Weinreb, *Angew. Chem.* **2000**, *112*, 243–246; *Angew. Chem. Int. Ed.* **2000**, *39*, 237–240; b) G. Han, M. G. LaPorte, J. J. Folmer, K. M. Werner, S. M. Weinreb, *J. Org. Chem.* **2000**, *65*, 6293–6306.

[15] For examples of piperidine formation through Mitsunobu cyclization, see: a) T. Tsunoda, F. Ozaki, N. Shirakata, Y. Tamaoka, H. Yamamoto, S. Ito, *Tetrahedron Lett.* **1996**, *37*, 2463–2466; b) G. E. Keck, A. Palani, *Tetrahedron Lett.* **1993**, *34*, 3223–3224.

 © 2006 Wiley-VCH Verlag GmbH & Co. KGaA, Weinheim

Perovskite Nanoparticles

DOI: 10.1002/anie.200602571

Template-Free, Low-Temperature Synthesis of Crystalline Barium Titanate Nanoparticles under Bio-Inspired Conditions**

*Richard L. Brutchey and Daniel E. Morse**

Perovskite materials are of interest because they have a wide range of useful applications, for example, in ferroelectric random access memory (FeRAM), piezoelectric transducers, solid-oxide fuel cells, high-temperature superconductors, thermoelectrics, ferromagnets, capacitors, pyroelectric detectors, and colossal magnetoresistors.[1] Perovskites are traditionally prepared by high-temperature solid-state reactions; specifically, $BaTiO_3$ is prepared by the reaction of TiO_2 and $BaCO_3$ at temperatures above 1100 °C, which yields a wide range of grain sizes (0.5–3 μm) and provides very little control over the shape of the particles.[2] Consequently, lower-temperature solution-based synthetic routes (for example, sol–gel and hydrothermal methods) are being explored to better control the nanostructure of the $BaTiO_3$ product. O'Brien et al. first reported the synthesis of $BaTiO_3$ nanoparticles of 6–12 nm by a sol–gel reaction at 100–140 °C, in the presence of oleic acid as a stabilizing agent.[3a] Niederberger et al. described a nonhydrolytic synthesis of 6-nm $BaTiO_3$ nanoparticles at 200–220 °C.[3b] Additionally, Wang et al. recently reported the hydrothermal synthesis of well-defined 17-nm $BaTiO_3$ nanoparticles at 180 °C under highly alkaline conditions.[3c] The low-temperature synthesis of perovskite nanocrystals is inherently difficult; an accurate control over stoichiometry, a close matching of the reaction rates of the precursors, and the identification of specific conditions for crystallization (that is, temperature, pressure, and pH) are all critically important.[4] While several examples of successful controlled syntheses of $BaTiO_3$ nanostructures now exist, they rely on elevated reaction temperatures (> 140 °C) and/or strongly alkaline conditions for crystallization.

Techniques that mimic biomineralization have received much attention because of nature's ability to produce crystalline biominerals with exquisite nanostructures under inherently benign conditions (low temperature, ambient pressure, and near-neutral pH).[5] We recently developed an entirely new low-temperature bio-inspired method for the nanofabrication of metal hydroxides, oxides, and phosphates, which is based on the "re-engineering" of the mechanisms responsible for the enzyme-mediated generation of silica in marine sponges.[6] We have translated the fundamental mechanisms underlying enzyme-mediated biomineralization to an approach wholly controlled by chemical physics, which uses vapor diffusion to establish temporal and vectorial catalyst gradients for the slow growth of nanocrystals at room temperature and ambient pressure. Herein, we report a vapor-diffusion sol–gel route to well-defined crystalline 6-nm $BaTiO_3$ nanoparticles at low temperatures, in the absence of a structure-directing template.

Nanoparticles of $BaTiO_3$ were readily prepared by the kinetically controlled vapor diffusion of $H_2O_{(g)}/HCl_{(g)}$ into a non-aqueous solution of the single-source bimetallic alkoxide $BaTi[OCH_2CH(CH_3)OCH_3]_6$ at 16 °C [Eq. (1)]. Powder X-ray diffraction (XRD) analysis of the as-prepared material revealed that the nanoparticles consist of crystalline $BaTiO_3$ with the cubic perovskite structure (space group $Pm3m$; Figure 1). The thermodynamically stable polymorph of bulk $BaTiO_3$, on the other hand, is the noncentrosymmetric tetragonal phase (space group $P4mm$), which is a room-temperature ferroelectric material.[1] The lattice constant of $a = 4.052(\pm 0.016)$ Å calculated for the nanoparticles is in excellent agreement with the literature value of $a = 4.058$ Å for cubic $BaTiO_3$ (JCPDS no. 75-0215). Crystalline impurities, such as TiO_2 or $BaCO_3$, were not detected by XRD. In situ heating of the nanoparticles to 750 and 1000 °C causes an incremental increase in particle size to 14 and 32 nm, as a result of the coalescence and agglomeration of the nano-

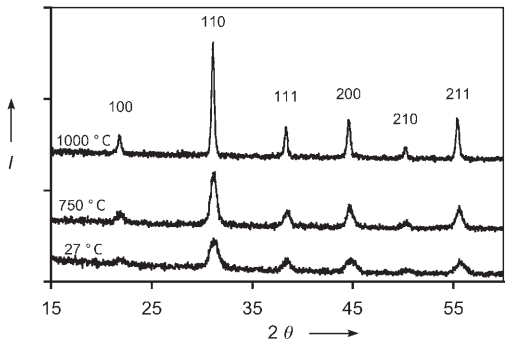

Figure 1. Powder XRD patterns of the $BaTiO_3$ nanoparticles heated in situ to the indicated temperatures.

[*] Dr. R. L. Brutchey, Prof. Dr. D. E. Morse
Institute for Collaborative Biotechnologies
California Nanosystems Institute, Materials Research Laboratory
University of California, Santa Barbara
Santa Barbara, CA 93106-9610 (USA)
Fax: (+1) 805-893-8062
E-mail: d_morse@lifesci.ucsb.edu
Prof. Dr. D. E. Morse
Department of Molecular, Cellular and Developmental Biology
University of California, Santa Barbara
Santa Barbara, CA 93106 (USA)

[**] We thank E. Yoo for his help, as well as Dr. T. Mates and Dr. J. Löfvander for their assistance with the characterization. This work was supported in part by grants from the U.S. Department of Energy (DE-FG03-02ER46006), DARPA (HR0011-04-1-0059), the U.S. Army Research Office (DAAD19-03-D-0004 to the Institute for Collaborative Biotechnologies, and W911NF-05-1-0072), the Biologically Inspired Materials Institute of NASA (NCC-1-02037 and NAG1-01-003), the NOAA National Sea Grant College Program of the U.S. Department of Commerce through the California Sea Grant College System (NA36RG0537, Project R/MP-92), and the MRSEC Program of the National Science Foundation (DMR05-20415 to the UCSB Materials Research Laboratory). The U.S. Government is authorized to reproduce and distribute copies of this Communication for governmental purposes.

Supporting information for this article is available on the WWW under http://www.angewandte.org or from the author.

InterScience
© 2006 Wiley-VCH Verlag GmbH & Co. KGaA, Weinheim

particles (Figure 1). Similarly, O'Brien et al. obtained 40-nm $BaTiO_3$ nanoparticles after heating 6-nm particles to 700 °C.[3a]

$$BaTi[OCH_2CH(CH_3)OCH_3]_6 + 3\,H_2O_{(g)} \xrightarrow[16\,^\circ C]{HCl_{(g)}\ cat.} BaTiO_3 + 6\,HOCH_2CH(CH_3)OCH_3 \quad (1)$$

Further structural characterization was performed by transmission electron microscopy (TEM). An assembly of quasispherical $BaTiO_3$ nanoparticles, which are partially agglomerated owing to the absence of surface-stabilizing ligands, is shown in Figure 2a,c. The nanoparticles have a

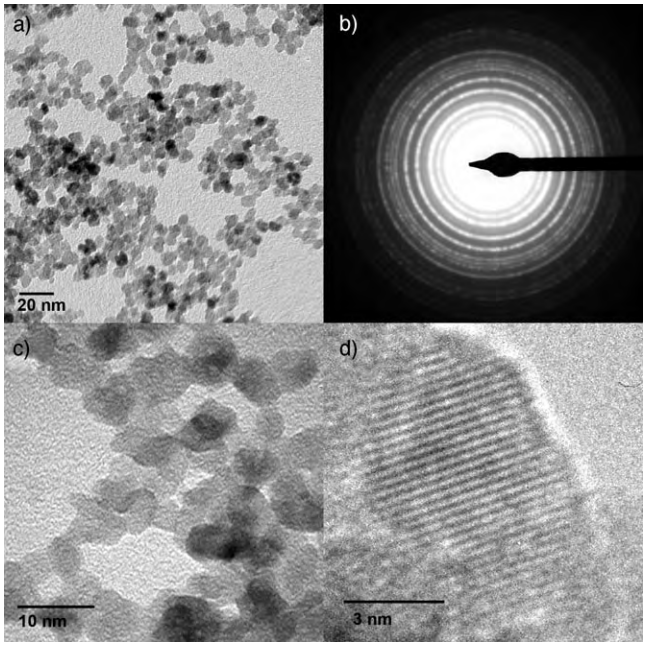

Figure 2. a), c), and d) TEM images of the $BaTiO_3$ nanoparticles at different resolutions. b) SAED pattern of the $BaTiO_3$ nanoparticles.

mean diameter of 5.9 ± 0.1 nm, as measured by TEM, which is in good agreement with the particle size determined by Scherrer analysis of the XRD pattern. A representative selected area electron diffraction (SAED) pattern for the cubic $BaTiO_3$ nanoparticles is presented in Figure 2b. The lattice constant ($a = 4.038(\pm 0.047)$ Å) calculated from randomly selected SAED patterns is in agreement with that determined by XRD. A TEM image of an apparent single-crystalline nanoparticle (oriented along the [110] direction), showing the lattice fringes, is displayed in Figure 2d.

Whereas XRD provides information on long-range order, Raman spectroscopy is a useful technique for probing the structure of the $BaTiO_3$ nanoparticles at the atomic scale, on the basis of vibrational symmetry. Cubic $BaTiO_3$ inherently has no Raman active modes; however, Raman active modes are expected for the noncentrosymmetric tetragonal structure.[7] The spectrum of the as-prepared nanoparticles displays bands at 712 [A_1, E(LO)] and 523 cm^{-1} [E, A_1(TO)], in addition to an intense non-Gaussian band with a maximum at 303 cm^{-1} [B_1, E(TO)], all of which suggest local tetragonal distortion (Figure 3).[7] Even though XRD analysis indicates a cubic perovskite structure, the observed Raman active modes imply a certain degree of tetragonality on the atomic scale.

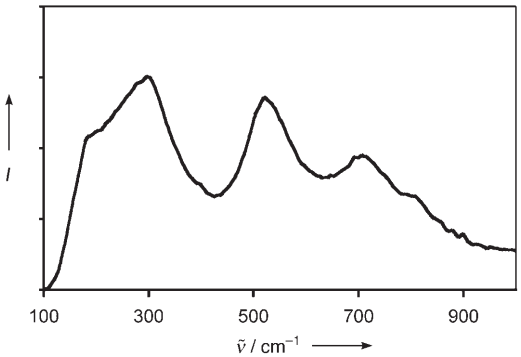

Figure 3. Raman spectrum of the $BaTiO_3$ nanoparticles.

X-ray photoelectron spectroscopy (XPS) was used to confirm the Ba^{2+} and Ti^{4+} oxidation states and coordination environments, as well as to verify the composition of the nanoparticles. The Ba $3d_{5/2}$ and Ti $2p_{3/2}$ binding energies measured for the nanoparticles were 778.3 and 457.8 eV, respectively, which are in excellent agreement with reported values of 778.9 and 458.2 eV.[8] The average surface ratio of Ba:Ti was determined to be 1.3:1, and the XPS spectra did not reveal any contamination by elements other than carbon and chlorine (0.2 wt %). Combustion analysis confirmed a residual carbon content of 3.4 wt %, which presumably results from unhydrolyzed alkoxide ligands. This hypothesis is supported by the observation of Raman bands at 2880 and 2938 cm^{-1} that are indicative of C–H stretches. Moreover, no CO_3^{2-} impurity was detected by Raman spectroscopy.

In bimetallic single-source molecular precursors, two metals A and B are present in a pre-existing geometric relationship. Such precursors have been demonstrated to produce a higher abundance of A–O–B bonds upon conversion to the bimetallic oxide by conventional high-temperature methods (for example, pyrolysis or metal–organic chemical vapor deposition (MOCVD)).[4,9] Utilizing a single-source bimetallic alkoxide in our vapor-diffusion approach yields highly crystalline $BaTiO_3$ nanoparticles at 16 °C, whereas utilizing two separate barium and titanium 2-propoxides as precursors yields an amorphous material under identical conditions. Furthermore, simply adding water (2–100 equiv) to the bimetallic alkoxide yields an amorphous material at 16 °C, a result which is similar to that reported by Hubert-Pfalzgraf et al.[10] Thus, it is the marriage of the single-source bimetallic alkoxide and its temporally controlled catalytic hydrolysis/polycondensation that provides the necessary conditions for the facile crystallization and growth of small, well-defined $BaTiO_3$ nanoparticles at a very low temperature. To our knowledge, similar results have not been achieved to date. Previous syntheses at very low temperatures have produced larger (ca. 50 nm), ill-defined particles.[11]

 © 2006 Wiley-VCH Verlag GmbH & Co. KGaA, Weinheim

In summary, we have presented a novel vapor-diffusion sol–gel method that, for the first time, offers a pathway to small, well-defined $BaTiO_3$ nanoparticles at very low temperatures. The synthesis is based on the delivery of water and catalyst in a spatial and temporal gradient to promote the slow, kinetically controlled growth of highly crystalline 6-nm nanoparticles, which are among the smallest reported for $BaTiO_3$. By varying the single-source bimetallic precursor, this methodology may be extended to the synthesis of other perovskite nanoparticles. The ability to rationally synthesize a wide range of technologically interesting perovskite nanoparticles in a controlled manner represents a significant step toward the miniaturization and development of next-generation devices, such as FeRAM.[12]

Experimental Section

All manipulations were performed under an inert atmosphere, and solutions were degassed prior to use. An aqueous solution of HCl (0.75 M, 2 mL) and a separate solution of $BaTi[OCH_2CH(CH_3)OCH_3]_6$ (0.42 M; Gelest, Inc.) in *n*-butanol (0.45 mL) and 2-methoxypropanol (0.75 mL) were placed in an enclosed chamber under argon. The solution containing the bimetallic alkoxide was then exposed to the H_2O/HCl vapor over 15 h at 16 °C to produce the $BaTiO_3$ nanoparticles. The gel product was collected, rinsed with *n*-butanol (3×2 mL), and dried in vacuo. The as-prepared powder was off-white in appearance and could be dispersed in several common organic solvents (for example, THF, hexane, and toluene) with sonication.

XRD was performed on a Bruker D8 Advance X-ray diffractometer with an Anton Parr HTK 16 high-temperature stage, using $Cu_{K\alpha}$ radiation. TEM was done on an FEI Tecnai G^2 Sphera microscope at an operating voltage of 200 kV. SAED patterns were collected at a camera distance of 100 cm for areas selected at random (15 areas on independently prepared samples). The average lattice parameters were determined from the 200 reflection of XRD patterns and from the 320 reflection of SAED patterns. XPS was done on a Kratos Axis Ultra system with a monochromated aluminum anode. The binding energy of C 1s in all spectra was standardized to 285 eV. Raman spectra were obtained on a Nicolet Magna 850 IR/Raman spectrometer. Combustion analyses were performed at the MSI Analytical Lab at UCSB.

Received: June 27, 2006
Published online: September 5, 2006

Keywords: barium titanate · nanostructures · perovskite phases · sol–gel processes

[1] a) M. E. Lines, A. M. Glass, *Principles and Applications of Ferroelectrics and Related Materials*, Clarendon Press, Oxford, **1977**; b) A. S. Bhalla, R. Guo, R. Roy, *Mater. Res. Innovations* **2000**, *4*, 3; c) R. E. Newnham, L. E. Cross, *MRS Bull.* **2005**, *30*, 845.
[2] I. Maclaren, C. B. Ponton, *J. Eur. Ceram. Soc.* **2000**, *20*, 1267.
[3] a) S. O'Brien, L. Brus, C. B. Murray, *J. Am. Chem. Soc.* **2001**, *123*, 12085; b) M. Niederberger, N. Pinna, J. Polleux, M. Antonietti, *Angew. Chem.* **2004**, *116*, 2320; *Angew. Chem. Int. Ed.* **2004**, *43*, 2270; c) X. Wang, J. Zhuang, Q. Peng, Y. Li, *Nature* **2005**, *437*, 121.
[4] K. G. Caulton, L. G. Hubert-Pfalzgraf, *Chem. Rev.* **1990**, *90*, 969.
[5] S. Mann, *Biomineralization Principles and Concepts in Bioinorganic Materials Chemistry*, Oxford University Press, Oxford, **2001**.
[6] a) R. L. Brutchey, E. S. Yoo, D. E. Morse, *J. Am. Chem. Soc.* **2006**, *128*, 10288; b) D. Kisailus, B. Schwenzer, J. Gomm, J. C. Weaver, D. E. Morse, *J. Am. Chem. Soc.* **2006**, *128*, 10276; c) B. Schwenzer, K. M. Roth, J. R. Gomm, M. Murr, D. E. Morse, *J. Mater. Chem.* **2006**, *16*, 401; d) D. E. Morse, *Trends Biotechnol.* **1999**, *17*, 230.
[7] a) M. El Marssi, F. Le Marrec, I. A. Lukyanchuk, M. G. Karkut, *J. Appl. Phys.* **2003**, *94*, 3307; b) G. Busca, G. Ramis, J. M. Gallardo Amores, V. Sanchez Escribano, P. Piaggio, *J. Chem. Soc. Faraday Trans.* **1994**, *90*, 3181.
[8] M. del Carmen Blanco López, G. Fourlaris, B. Rand, F. L. Riley, *J. Am. Ceram. Soc.* **1999**, *82*, 1777.
[9] K. L. Fujdala, R. L. Brutchey, T. D. Tilley in *Topics in Organometallic Chemistry, Vol. 16* (Eds.: C. Copéret, B. Chaudret), Springer, New York, **2005**, pp. 69–116.
[10] L. G. Hubert-Pfalzgraf, S. Daniele, J. M. Decams, J. Vaissermann, *J. Sol-Gel Sci. Technol.* **1997**, *8*, 49.
[11] H. Shimooka, M. Kuwabara, *J. Am. Ceram. Soc.* **1995**, *78*, 2849.
[12] a) R. Waser, A. Rüdiger, *Nat. Mater.* **2004**, *3*, 81; b) N. A. Spaldin, *Science* **2004**, *304*, 1606.

 © 2006 Wiley-VCH Verlag GmbH & Co. KGaA, Weinheim

Asymmetric Catalysis

DOI: 10.1002/anie.200600379

Lipase/Aluminum-Catalyzed Dynamic Kinetic Resolution of Secondary Alcohols**

Albrecht Berkessel, M. Luisa Sebastian-Ibarz, and Thomas N. Müller*

The combination of enzymatic kinetic resolution with a metal-catalyzed racemization by reversible hydrogen transfer was reported by Williams and co-workers for the preparation of enantiomerically pure secondary alcohols. In this early work, the rhodium catalyst $[Rh_2(OAc)_4]$ and a lipase effected dynamic kinetic resolution (DKR) with 60% conversion and 98% *ee*.[1] The research groups of Bäckvall,[2–5] Kim, and Park[6–8] have devised related protocols using ruthenium-based racemization catalysts originally developed by Shvo and Menashe[9] in combination with an immobilized lipase from *Candida antarctica* (CALB, commercially available as Novozym 435). In general, high yields and enantiomeric excesses were obtained. As shown by Jacobs et al., the DKR of secondary benzylic alcohols can also be achieved by combining an acidic zeolite as the racemization catalyst with a lipase in a biphasic system.[10,11]

We considered using aluminum-based catalysts, which are easily obtainable and inexpensive. The Meerwein–Ponndorf–Verley–Oppenauer (MPVO) reaction can be exploited for the racemization of alcohols:[1,12–14] Oppenauer oxidation of the alcohol is followed by nonstereoselective reduction of the resulting ketone by the Meerwein–Pondorf–Verley reaction. In general, preformed aluminum alkoxide catalysts such as commercially available $Al(i\text{PrO})_3$ are less active than Ru-based systems.[1] As a consequence, relatively high temperatures and prolonged reaction times are usually required. However, much higher reactivities for MPV reductions have recently been reported for dinuclear Al^{III} complexes[15–17] and for Al^{III} alkoxides generated in situ.[18] With this in mind, we set out to investigate the activity of aluminum alkoxides prepared in situ for the racemization of chiral secondary alcohols and in particular their utility for the DKR of these substrates in the presence of lipases and acylating agents.

We first generated several aluminum species by reaction of $ClAlMe_2$ or $AlMe_3$ with the bidentate ligands (*R*)- and (*S*)-1,1′-bi-2-naphthol (binol), in different ratios, and examined their ability to racemize (*S*)-1-phenylethanol ((*S*)-**1**). Acetophenone (**2**, 0.5 equiv) was employed as a hydrogen acceptor (Scheme 1).

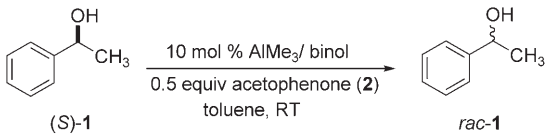

Scheme 1. Racemization of (*S*)-1-phenylethanol ((*S*)-**1**).

$AlMe_3$/binol (1:1) proved to be a very effective catalyst: At room temperature, 10 mol% of the Al catalyst sufficed to racemize the substrate completely within three hours. The aluminum catalysts generated from (*R*)- and (*S*)-binol showed virtually identical activity. On the basis of these findings, we developed a method for the DKR of 1-phenylethanol (*rac*-**1**). We chose 1-phenylvinyl acetate (**3**) as the acylating agent. The commonly used 2-propenyl acetate (**4**) gives acetone as the by-product, which acts as a hydrogen acceptor and oxidizes 1-phenylethanol (**1**) to acetophenone (**2**). 1-Phenylvinyl acetate (**3**) is easily synthesized (Scheme 2; see the Supporting Information for experimental details) from the corresponding ketone, acetophenone (**2**). During the acylation of 1-phenylethanol (**1**) by the enol ester **3**, 1 equivalent of acetophenone (**2**) is released; it does not need to be removed, as it acts as a hydrogen acceptor in the racemization.

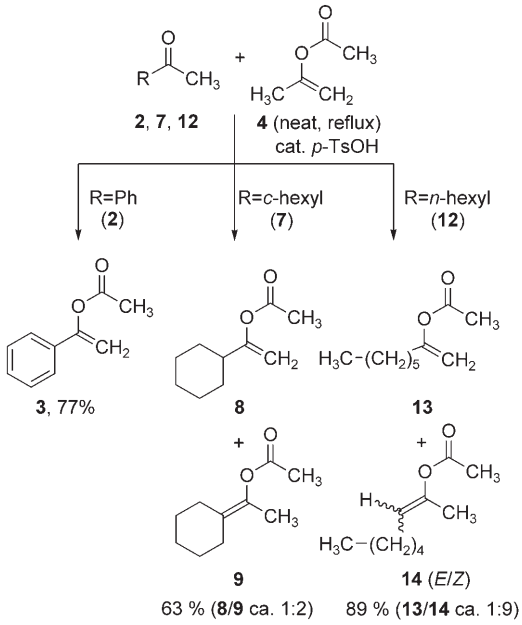

Scheme 2. Synthesis of 1-phenylvinyl acetate (**3**), 1-cyclohexylvinyl acetate (**8**) and (1-cyclohexylidene ethyl) acetate (**9**), and 2-(1-octenyl) acetate (**13**) and (*E*/*Z*)-2-(2-octenyl) acetate (**14**). Ts = toluenesulfonyl.

Table 1 summarizes the results of the DKR of 1-phenylethanol (*rac*-**1**) under a range of conditions with Novozym 435 as the lipase. The best results were obtained with binol as the ligand (Table 1, entries 1 and 2). 2,2′-Biphenol showed almost the same activity (entry 3): acetate **5** was obtained in up to 96% yield and 96% *ee*. When phenol was used as the ligand (Table 1, entry 4), significantly lower catalyst activity and lower enantioselectivity resulted. Similarly, the use of the

[*] Prof. Dr. A. Berkessel, M. L. Sebastian-Ibarz, Dr. T. N. Müller
Institut für Organische Chemie
Universität zu Köln
Greinstrasse 4, 50939 Köln (Germany)
Fax: (+49) 221-470-5102
E-mail: berkessel@uni-koeln.de

[**] This work was supported by the Fonds der Chemischen Industrie.

Supporting information for this article is available on the WWW under http://www.angewandte.org or from the author.

© 2006 Wiley-VCH Verlag GmbH & Co. KGaA, Weinheim

Table 1: DKR of 1-phenylethanol (*rac*-**1**).[a]

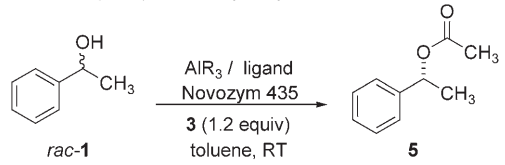

rac-**1** → **5**

Entry	Ligand (equiv)	AlR_3 (equiv)	*t* [h]	Yield of **5** [%]	*ee* [%]
1	(*R*)-binol (0.1)	$AlMe_3$ (0.1)	3	93	95
2	binol (0.1)	$AlMe_3$ (0.1)	3	96	96
3	2,2′-biphenol (0.1)	$AlMe_3$ (0.1)	3	96	94
4	phenol (0.2)	$AlMe_3$ (0.1)	25	82	85
5	2,5-dimethylhexane-2,5-diol (0.1)	$AlMe_3$ (0.1)	3	51	78
6	binol (0.2)	$AlMe_3$ (0.1)	3	60	95
7	binol (0.05)	$AlMe_3$ (0.1)	3	89	92
8	–	$AlMe_3$ (0.1)	18	84	55
9	–	$AlMe_3$ (0.05)	20	64	74
10[b]	binol (0.1)	$Al(iPrO)_3$ (0.1)	70	94	95

[a] Unless otherwise noted, reactions were run on a 2.5-mmol scale at RT under Ar atmosphere with **3** (1.2 equiv) as the acylating agent and with 12 mg of Novozym per mmol of alcohol. Yields and *ee* values were determined by chiral GC. The configuration of the product ester **5** was assigned by conversion of enantiomerically pure (*S*)-1-phenylethanol ((*S*)-**1**) to the acetate and GC co-injection. [b] Reaction conducted at 60 °C.

aliphatic diol 2,5-dimethylhexane-2,5-diol as the ligand led to unsatisfactory yields and enantiomeric excesses of product **5** (Table 1, entry 5). Apparently, the ligand on Al must be bidentate and of the bisphenol type. When the amount of aromatic bidentate ligand exceeded 1 equivalent relative to aluminum, the activity of the catalyst decreased significantly (Table 1, entry 6). Similarly, when the amount of aluminum exceeded that of the aromatic bidentate ligand, the results obtained were again below optimum (Table 1, entry 7). When the phenolic ligand was omitted completely, the yields and enantiomeric excesses decreased considerably (Table 1, entries 8 and 9). It was interesting to note that even the low activity of commercial $Al(iPrO)_3$ increased upon combination with binol (Table 1, entry 10). Nevertheless, the reaction times were considerably longer and the temperatures higher than those required with the $AlMe_3$-derived catalyst system.

To demonstrate the scope of the DKR process, we tested the aliphatic alcohols 1-cyclohexylethanol (*rac*-**6**) and 2-octanol (*rac*-**11**) as substrates. In both cases, we used "specific" acylating agents that were synthesized from the corresponding ketones cyclohexyl methyl ketone (**7**), and 2-octanone (**12**), respectively (Scheme 2). The racemization of 1-cyclohexylethanol (**6**) turned out to be slower than that of 1-phenylethanol (**1**). However, when longer reaction times and higher amounts of the aluminum catalyst (usually 20 mol %) were applied in the DKR, excellent yields and enantioselectivities were obtained (Table 2). For example, in the presence of 20 mol % of $AlMe_3$/binol (or 2,2′-biphenol), acetate **10** was obtained in virtually quantitative yields and 99 % *ee* (Table 2, entries 1, 2, and 4). Comparable results could be achieved after shorter reaction times when the temperature was increased to 60 °C (Table 2, entry 3).

Table 2: DKR of 1-cyclohexylethanol (*rac*-**6**).[a]

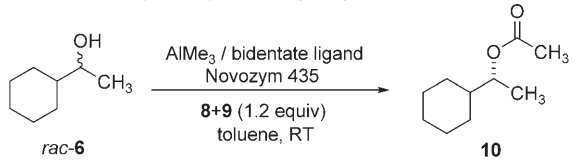

rac-**6** → **10**

Entry	Ligand	$AlMe_3$ [equiv]	*t* [h]	Conv. [%]	Yield of **10** [%]	*ee* [%]
1	(*R*)-binol	0.2	19	98	98	99
2	binol	0.2	19	97	97	99
3[b,c]	2,2′-biphenol	0.2	9	98	98	99
4	2,2′-biphenol	0.2	14	97	97	99

[a] Unless otherwise noted, reactions were run on a 0.625-mmol scale at RT under Ar atmosphere with **8**/**9** (ca. 1:2, 1.2 equiv) as the acylating agent and with 4 mg of Novozym per mmol of alcohol. Yields and *ee* values were determined by chiral GC. The bidentate ligand and $AlMe_3$ were added in a 1:1 ratio. The configuration of the product **10** was assigned by comparison with data in Ref. [4]. [b] Reaction conducted on a 2.5-mmol scale. [c] Reaction conducted at 60 °C.

In the case of 2-octanol (*rac*-**11**), we again observed that the racemization of the alcohol was slower than that of 1-phenylethanol (*rac*-**1**). In addition, the selectivity of Novozym as the lipase was not optimal as evidenced in the KR of *rac*-**11**: Although the initial values obtained in the KR were satisfactory (48 % yield, and 96 % *ee* of the ester **15** after 20 min), the enantioselectivity dropped considerably upon increasing conversion of *rac*-**11**, reaching values as low as 64 % *ee* (63 % conversion) after 18 h. This decrease results from acylation of the "wrong" enantiomer, (*S*)-2-octanol ((*S*)-**11**), once most of (*R*)-2-octanol ((*R*)-**11**) had been consumed. However, when the racemization of the alcohol **11** was accelerated by addition of more of the Al catalyst, satisfactory results were obtained in the DKR of 2-octanol (*rac*-**11**) as well (Table 3). In the presence of 20 mol % of the $AlMe_3$/2,2′-

Table 3: DKR of 2-octanol (*rac*-**11**).[a]

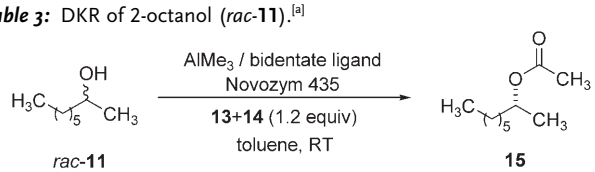

rac-**11** → **15**

Entry	Ligand	$AlMe_3$ [equiv]	*t* [h]	Conv. [%]	Yield of **15** [%]	*ee* [%]
1[b,c]	2,2′-biphenol	0.2	24	95	95	92
2[b–d]	2,2′-biphenol	0.2	6	98	98	90
3	2,2′-biphenol	0.2	18	92	92	86
4	(*R*)-binol	0.2	18	91	91	77
5[e]	binol	0.2	18	93	93	80

[a] Unless otherwise noted, reactions were run on a 0.625-mmol scale at RT under Ar atmosphere with **13**/**14** (ca. 1:9, 1.2 equiv) as the acylating agent and with 2 mg of Novozym per mmol of alcohol. Yields and *ee* values were determined by chiral GC. Bidentate ligand and $AlMe_3$ were added in a 1:1 ratio. The configuration of the product **15** was assigned by conversion of enantiomerically pure (*S*)-2-octanol to the acetate, and GC co-injection. [b] 1.1 equiv of acylating agent (**13**/**14** ca. 1:9). [c] Reaction conducted on a 2.5-mmol scale. [d] Reaction conducted at 60 °C. [e] Reaction conducted with 4 mg of Novozym per mmol of alcohol.

 © 2006 Wiley-VCH Verlag GmbH & Co. KGaA, Weinheim

biphenol catalyst and 1.1 equivalents of the acylating agent (**13**/**14**), ester **15** was obtained in up to 95% yield and 92% *ee* on a 2.5-mmol scale at room temperature (Table 3, entry 1). Comparable results but after shorter reaction times were achieved when the reaction temperature was increased to 60°C (Table 3, entry 2). Reactions run on smaller scale were found to afford slightly lower yields and enantiomeric excesses (Table 3, entry 3). In the case of 2-octanol (*rac*-**11**), binol appeared to be less effective than 2,2′-biphenol as a bidentate ligand (Table 3).

We then extended our study to the DKR of the 1-propanol derivatives 1-phenyl-1-propanol (*rac*-**16**) and 3-octanol (*rac*-**19**). Once again, we used "specific" acylating agents that were synthesized from the corresponding ketones propiophenone (**17**) and 3-octanone (**20**). In these cases, the lipase-catalyzed acylation, though highly enantioselective, was rather slow. However, increasing the amount of lipase resulted in almost quantitative yields and high enantioselectivities after 18 h. The DKR of the substrates *rac*-**16** and *rac*-**19** gave excellent results (up to 99% yield and 98% *ee*) with either binol or 2,2′-biphenol as ligands (Table 4).

We postulate that the bisphenol-type ligands play a dual role in the DKR. First, they increase the activity of the aluminum catalyst by impeding aggregation. Second, the bisphenol aluminum complexes maintain their activity toward racemization of the alcohol in the presence of the lipase. In contrast, $Al(OtBu)_3$, prepared in situ from $AlMe_3$ and *t*BuOH, is a highly active racemization catalyst, but it loses its activity almost completely when combined with the lipase. By the application of bisphenolic ligands, the two processes, racemization effected by the aluminum catalyst and acylation mediated by the lipase, become compatible.

Another remarkable feature of the bisphenol-type ligands is that they increase the activity of the aluminum catalyst towards racemization but not acylation. When $Al(OtBu)_3$ prepared in situ was used as the catalyst for the DKR of 1-phenylethanol (*rac*-**1**), we observed nonenantiospecific chemical esterification at a rate comparable to the racemization of the alcohol. On the other hand, the Al/binol catalyst, although it is a Lewis acid, was shown in control experiments to only weakly promote the direct chemical esterification of 1-phenylethanol (*rac*-**1**). Under these conditions, the substantially higher activity of the lipase towards acylation ensures high product enantiopurity (Table 1). We also deduce from the results obtained in the DKR of the other substrates that such direct "chemical" esterification of the alcohol is not promoted considerably by the Al/2,2′-biphenol catalyst either.

In summary, we have demonstrated that chemoenzymatic DKR of secondary alcohols is possible in high yields and high enantioselectivity through the use of an inexpensive and readily available aluminum catalyst generated in situ in combination with a lipase. We expect that this procedure, owing to the mild conditions and the simplicity of operation, will prove useful for the preparation of a variety of optically pure secondary alcohols, also on larger scale.

Table 4: DKR of *rac*-**16** and rac-**19**.[a]

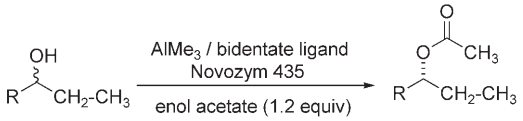

rac-**16**: R = Ph
rac-**19**: R = *n*-pentyl

18: R = Ph
21: R = *n*-pentyl

Entry	Alcohol	Ligand	$AlMe_3$ [equiv]	Prod.	Yield [%]	*ee* [%]
1	*rac*-16	binol	0.1	(*R*)-**18**	99	98
2	*rac*-16	2,2′-biphenol	0.1	(*R*)-**18**	97	97
3[b]	*rac*-19	binol	0.2	(*R*)-**21**	95	95
4[b]	*rac*-19	2,2′-biphenol	0.2	(*R*)-**21**	95	94

[a] Unless otherwise noted, reactions were run on a 0.5-mmol scale over 18 h at RT under Ar atmosphere with 1.2 equiv of the acylating agents (prepared from propiophenone (**17**) and 3-octanone (**20**), respectively; see the Supporting Information for experimental details) and with 80 mg of Novozym per mmol of alcohol. Yields and *ee* values were determined by chiral GC. Bidentate ligand and $AlMe_3$ were added in a 1:1 ratio. The configuration of the product **18** was assigned by comparison with data in Ref. [4]. The configuration of the product **21** was assigned in analogy to the DKR of 2-octanol (*rac*-**11**). [b] The reaction was conducted with 40 mg of Novozym per mmol of alcohol.

Experimental Section

All reactions were performed under argon atmosphere in oven-dried glassware. Toluene was dried over sodium and distilled under argon atmosphere. All commercially available chemicals were used without further purification. GC analysis was performed using a CP-Chirasil-Dex CB phase column.

DKR of *rac*-**1**: A Schlenk tube was charged with binol (72 mg, 0.25 mmol, 0.1 equiv), 4 mL of a stock solution of trimethylaluminum in absolute toluene (62.5 mM, 0.25 mmol, 0.1 equiv) was added, and the resulting solution was stirred for 15 min at RT. *rac*-**1** (0.302 mL, 305 mg, 2.5 mmol, 1 equiv) was added, and the resulting solution was stirred for a further 5 min. Subsequently, Novozym 435 (30 mg), diphenyl ether (internal standard) (0.397 mL, 2.5 mmol, 1 equiv), and **3** (3 mmol, 1.2 equiv) were added. Argon atmosphere was maintained throughout the reaction. Yields were determined by GC. Samples of 20 μL were withdrawn from the reaction mixture by means of a syringe, diluted to 1 mL with CH_2Cl_2/MeOH (1:1), and filtered through a pad of cotton.

DKR of *rac*-**6** on preparative scale: A 50-mL flask was charged with 2,2′-biphenol (0.29 g, 1.56 mmol, 0.2 equiv), 12.5 mL of a stock solution of trimethylaluminum in toluene (0.125 M, 1.56 mmol, 0.2 equiv) was added, and the resulting solution was stirred for 15 min at RT. *rac*-**6** (1.075 mL, 1.00 g, 7.8 mmol, 1 equiv) was added, and the resulting solution was stirred for a further 5 min. Subsequently, Novozym 435 (31 mg), dodecane (internal standard) (1.774 mL, 7.8 mmol, 1 equiv), and 1.34 mL (7.8 mmol, 1 equiv) of the acylating agent (**8**/**9** ca. 1:2) were added. The resulting mixture was allowed to stir at RT for 24 h. Argon atmosphere was assured throughout the reaction. The solution was filtered through a pad of celite, washed with CH_2Cl_2, and the solvent was evaporated in vacuo. The residue was purified by column chromatography on silica gel with *n*-hexane/EtOAc (95:5). The product ester **10** ($R_f = 0.27$) was obtained as a colorless oil (1.18 g, 90%, 99% *ee*). The ^1H and ^{13}C NMR spectroscopic data obtained from this material were identical to those in the literature.[4]

Supplementary Information contains all experimental details for the synthesis and characterization of the racemic acetates used for the calibrations (*rac*-**5**, *rac*-**10**, *rac*-**15**, *rac*-**18**, and *rac*-**21**), and acylating agents (enol acetates of the ketones **2**, **7**, **12**, **17**, and **20**). Furthermore, the procedures for the DKR of the alcohols (*rac*-**1**, *rac*-**6**, *rac*-**11**, *rac*-

 © 2006 Wiley-VCH Verlag GmbH & Co. KGaA, Weinheim

16, and *rac*-**19**), methods used for GC analysis, and retention times of substrates, products, and internal standards are given.

Received: January 29, 2006
Revised: June 9, 2006
Published online: September 4, 2006

Keywords: aluminum · kinetic resolution · lipases · metal catalysis · secondary alcohols

[1] P. M. Dinh, J. A. Howarth, A. R. Hudnott, J. M. J. Williams, W. Harris, *Tetrahedron Lett.* **1996**, *37*, 7623 – 7626.
[2] A. L. E. Larsson, B. A. Persson, J. E. Bäckvall, *Angew. Chem.* **1997**, *109*, 1256 – 1258; *Angew. Chem. Int. Ed. Engl.* **1997**, *36*, 1211 – 1212.
[3] B. Martin-Matute, M. Edin, K. Bogar, J. E. Bäckvall, *Angew. Chem.* **2004**, *116*, 6697 – 6701; *Angew. Chem. Int. Ed.* **2004**, *43*, 6535 – 6539.
[4] B. Martin-Matute, M. Edin, K. Bogar, F. B. Kaynak, J. E. Bäckvall, *J. Am. Chem. Soc.* **2005**, *127*, 8817 – 8825.
[5] B. A. Persson, A. L. E. Larsson, M. Le Ray, J. E. Bäckvall, *J. Am. Chem. Soc.* **1999**, *121*, 1645 – 1650.
[6] J. H. Choi, Y. H. Kim, S. H. Nam, S. T. Shin, M. J. Kim, J. Park, *Angew. Chem.* **2002**, *114*, 2479 – 2482; *Angew. Chem. Int. Ed.* **2002**, *41*, 2373 – 2376.
[7] J. H. Choi, Y. K. Choi, Y. H. Kim, E. S. Park, E. J. Kim, M. J. Kim, J. W. Park, *J. Org. Chem.* **2004**, *69*, 1972 – 1977.
[8] N. Kim, S. B. Ko, M. S. Kwon, M. J. Kim, J. Park, *Org. Lett.* **2005**, *7*, 4523 – 4526.
[9] N. Menashe, Y. Shvo, *Organometallics* **1991**, *10*, 3885 – 3891.
[10] S. Wuyts, K. De Temmerman, D. De Vos, P. Jacobs, *Chem. Commun.* **2003**, 1928 – 1929.
[11] S. Wuyts, K. De Temmerman, D. E. De Vos, P. A. Jacobs, *Chem. Eur. J.* **2005**, *11*, 386 – 397.
[12] "Process for the preparation of enantiomerically enriched esters and alcohols": G. K. M. Verzijl, J. G. De Vries, Q. B. Broxterman, WO 0190396A1, November 29, **2001**.
[13] D. Klomp, T. Maschmeyer, U. Hanefeld, J. A. Peters, *Chem. Eur. J.* **2004**, *10*, 2088 – 2093.
[14] D. Klomp, K. Djanashvili, N. C. Svennum, N. Chantapariyavat, C. S. Wong, F. Vilela, T. Maschmeyer, J. A. Peters, U. Hanefeld, *Org. Biomol. Chem.* **2005**, *3*, 483 – 489.
[15] E. J. Campbell, H. Zhou, S. T. Nguyen, *Angew. Chem.* **2002**, *114*, 1062 – 1064; *Angew. Chem. Int. Ed.* **2002**, *41*, 1020 – 1022.
[16] T. Ooi, T. Miura, Y. Itagaki, H. Ichikawa, K. Maruoka, *Synthesis* **2002**, *2*, 279 – 291.
[17] T. Ooi, H. Ichikawa, K. Maruoka, *Angew. Chem.* **2001**, *113*, 3722 – 3724; *Angew. Chem. Int. Ed.* **2001**, *40*, 3610 – 3612.
[18] E. J. Campbell, H. Zhou, S. T. Nguyen, *Org. Lett.* **2001**, *3*, 2391 – 2393.

 © 2006 Wiley-VCH Verlag GmbH & Co. KGaA, Weinheim

Tumor Therapeutics

DOI: 10.1002/anie.200600935

Investigation of Reactivity and Selectivity of DNA-Alkylating Duocarmycin Analogues by High-Resolution Mass Spectrometry**

Lutz F. Tietze, Birgit Krewer, Holm Frauendorf, Felix Major, and Ingrid Schuberth*

Dedicated to Professor Dieter Enders on the occasion of his 60th birthday

The treatment of malignant tumors with currently available chemotherapeutic agents is generally associated with extensive side effects owing to an inadequate differentiation between malignant and healthy tissue. As described in the preceeding communication,[1] in the context of antibody-directed enzyme prodrug therapy (ADEPT),[2,3] we have developed the new prodrug (+)-**2** based upon duocarmycin antibiotics. Prodrug (+)-**2** is characterized by an excellent QIC_{50} value of 4800 ($QIC_{50} = IC_{50}$[***] (prodrug)/IC_{50}(prodrug in the presence of the enzyme β-D-galactosidase)) in combination with a high cytotoxicity of the corresponding seco drug (+)-**3**, which has an IC_{50} value of 0.75 nM (Scheme 1). Seco drug (+)-**3**, formed from (+)-**2** by an enzymatic transformation, cyclizes rapidly to yield the highly reactive drug (+)-**4** containing a spirocyclopropylcyclohexadienone moiety in situ.

Herein we describe investigations on the DNA-alkylating efficiency of the new cytotoxic (+)-**3** and compare its reactivity with that of the less toxic compounds (+)-**2** and (−)-**3**. The alkylation of a double- and a single-stranded oligodeoxynucleotide was analyzed by high-resolution electrospray mass spectrometry. The electrospray ionization Fourier transform ion cyclotron resonance mass spectrometry (ESI-FTICRMS) measurements were carried out directly with the reaction solution (diluted with methanol), without chromatographic purification and enrichment of the alkylated DNA that was applied in similar MS investigations.[4] The simultaneous detection of substrates, intermediates, and

[*] Prof. Dr. L. F. Tietze, Dipl.-Chem. B. Krewer, Dr. H. Frauendorf, Dipl.-Chem. F. Major, Dr. I. Schuberth
Institut für Organische und Biomolekulare Chemie
Georg-August-Universität Göttingen
Tammannstrasse 2, 37077 Göttingen (Germany)
Fax: (+49) 551-39-9476
E-mail: ltietze@gwdg.de

[**] This research was supported by the Deutsche Forschungsgemeinschaft (SFB 416) and the Fonds der chemischen Industrie. F.M. would like to thank the Studienstiftung des deutschen Volkes for a PhD scholarship.

Supporting information for this article, including experimental methods and selected mass spectra, may be found in the Supporting Information available on the WWW under http://www.angewandte.com or from the author.

[***] IC_{50}: Toxin concentration at which cell growth is inhibited by 50 %.

WILEY InterScience DISCOVER SOMETHING GREAT

© 2006 Wiley-VCH Verlag GmbH & Co. KGaA, Weinheim

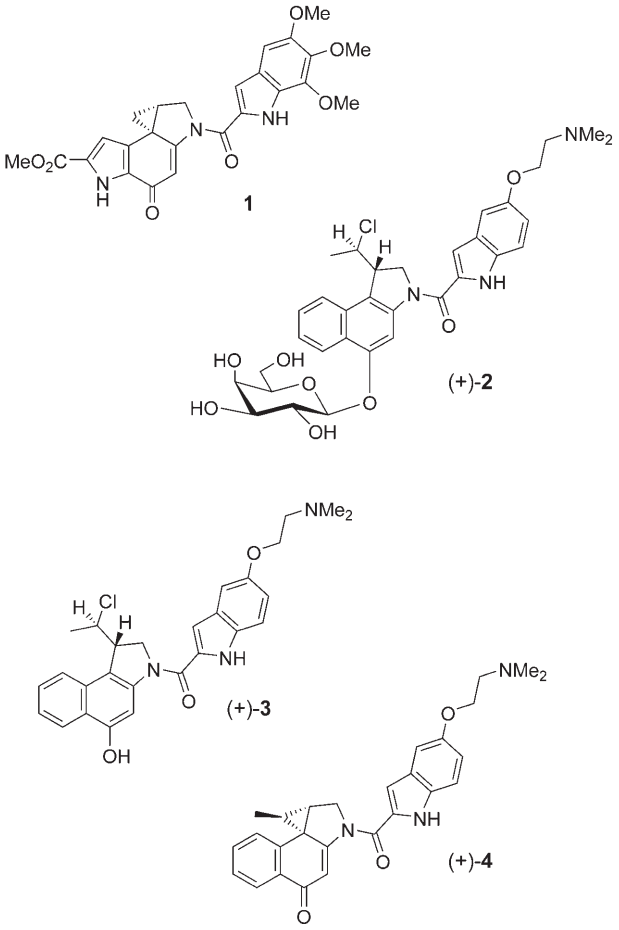

Scheme 1. (+)-Duocarmycin SA (**1**), prodrug (+)-**2**, seco drug (+)-**3**, and drug (+)-**4**.

alkylated oligonucleotide products is of considerable advantage as it allows direct conclusions concerning the efficiency and the selectivity of the alkylation as well as the nature and amount of the compounds present in the reaction solution. Moreover, fragmentation of the adducts in the region of the alkylation site can be induced by variation of the measurement conditions, which allows precise localization of the binding site.[5]

Unlike other methods for the structure analysis of DNA–drug complexes, such as NMR spectroscopy[6] and X-ray crystal structure analysis,[7] the procedure developed has some clear advantages as it allows a direct measurement, is significantly faster, needs only low concentrations, and no crystalline adducts are necessary as is required for X-ray crystal structure determination. Other methods for the determination of sequence selectivity, such as PCR-stop assay, DNAseI footprinting, and PAGE after thermally induced strand cleavage, are significantly less convenient than the method described herein.[8]

The high cytotoxicity of duocarmycin SA (**1**) and related compounds is presumably based on an alkylation of adenine at the N3 atom located within AT-rich binding sites in the minor groove of double-stranded DNA.[9] The duplex DNA **5** with 15 base pairs (Figure 1) was chosen for the binding

5'-d(CGG TC A ATT A GT CGC)-3' (ON-1)
3'-d(GCC AG T TAA T CA GCG)-5' (ON-2) } **5**

Figure 1. Sequence of the selected duplex DNA **5**.

studies with (+)-**3**, (−)-**3**, and (+)-**2**. This double-stranded oligonucleotide contains a high-affinity binding site, is able to form a minor grove, and in addition to adenine, the bases cytosine, guanine, and thymine border on the AT-rich sequence.

A solution of the double-stranded oligonucleotide **5** in water was treated with a solution of the compound under investigation in DMSO/water in the molar ratios of active compound/**5** of 1:1 and 5:1. ESI-FTICRMS measurements in the negative-ion mode were carried out immediately after mixing the components and after incubation for 24 h at 25 °C. The reaction solutions were diluted with methanol in the ratio 1:1. As expected, at the time point $t = 0$ h (Figure 2), only

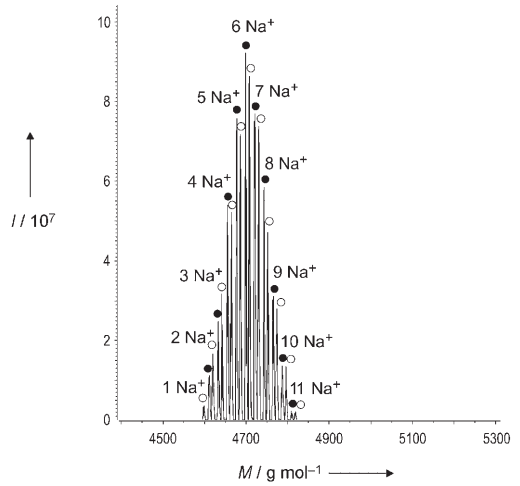

Figure 2. Deconvoluted ESI-HRMS (negative-ion mode) spectrum: (+)-**3**/**5** = 1:1, $t = 0$ h; Na^+ adducts of ON-1 (●) and ON-2 (○); I = intensity.

isotope-resolved signals of the sodium adducts of the two single-stranded DNA oligonucleotides (ON-1 and ON-2) as well as seco drug (+)-**3** and drug (+)-**4** were detected for a 1:1 mixture of (+)-**3** and **5**; after incubation for 24 h (Figure 3), the peaks of ON-1 covalently bonded with the drug (ON-1*), ON-1 after cleavage of the base adenine (ON-1−A), adenine alkylated by the drug (**6**), and the unchanged ON-2 were detected.[*][10]

The formation of alkylated adenine (**6**) may be explained by a weakening of the *N*-glycosidic bond between the nucleobase and the desoxyribose in ON-1*. As a result of this, thermal cleavage to form **6** and ON-1−A becomes possible (Scheme 2).[5] By changing the CapExit voltage from −100 to −150 V, fragmentation of ON-1−A could be induced by capillary-skimmer dissociation, and thus, on the basis of the w_5(ON-1) and a_{10}–B_{10}(ON-1) fragments (Figure 4), the alkylation position on ON-1 could be unambiguously identi-

[*] For further spectra, see the Supporting Information.

 © 2006 Wiley-VCH Verlag GmbH & Co. KGaA, Weinheim

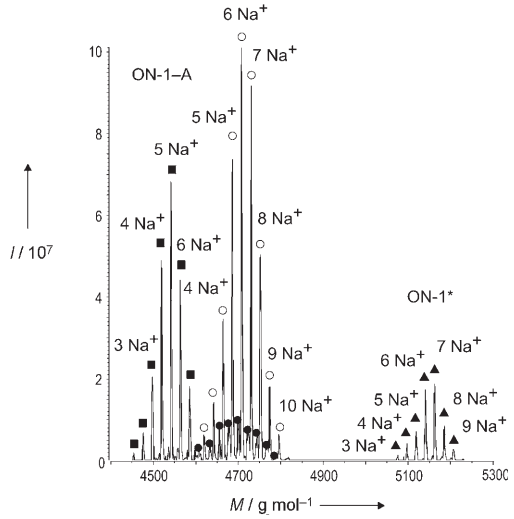

Figure 3. Deconvoluted ESI-HRMS (negative-ion mode) spectrum: (+)-**3**/**5** = 1:1, t = 24 h; Na^+ adducts of ON-1 (●), ON-2 (○), ON-1* (▲) and ON-1−A (■); A = adenine.

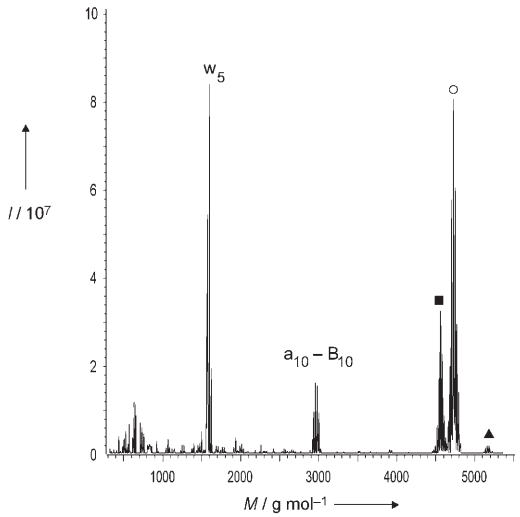

Figure 4. Deconvoluted ESI-HRMS (negative-ion mode) spectrum (fragmentation conditions): (+)-**3**/**5** = 1:1, t = 24 h; Na^+ adducts of ON-2 (○), ON-1* (▲), ON-1−A (■), w_5(ON-1), and a_{10}–B_{10}(ON-1).

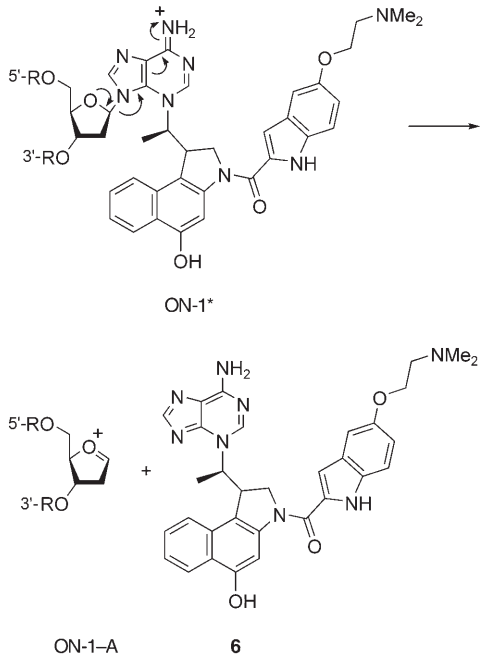

Scheme 2. Cleavage of the glycosidic bond in ON-1* resulting in the formation of ON-1−A and **6**.

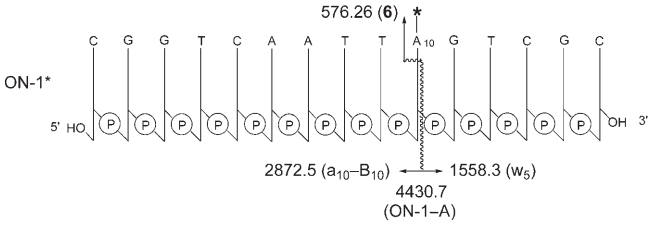

Figure 5. ON-1* and the ensuing fragmentations. ⋆ = Drug.

fied (Figure 5). The fragmentation of ON-1−A into w_5 und a_{10}–B_{10} was confirmed by collision-induced dissociation (CID)-MS–MS. By using a 1:1 mixture of (+)-**3**/duplex DNA **5**, ON-1 was exclusively and almost quantitatively alkylated at adenine A10. With the use of a higher (+)-**3**/**5** ratio, an additional minor alkylation at guanine could be determined. This corresponds to the results of investigations on duocarmycin SA (**1**).[4,6,11]

In the reaction of prodrug (+)-**2** with duplex DNA **5** in a (+)-**2**/**5** ratio of 1:1, almost no alkylation was found (Figure 6), and at a ratio of 5:1, only about 10% alkylation was observed

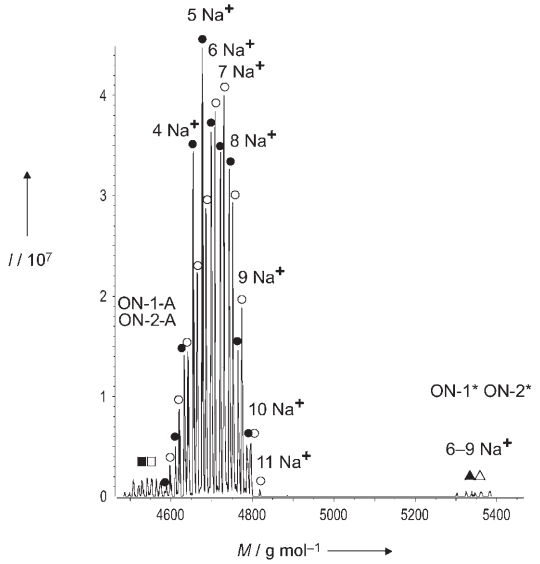

Figure 6. Deconvoluted ESI-HRMS (negative-ion mode) spectrum: (+)-**2**/**5** = 1:1, t = 24 h; Na^+ adducts of ON-1 (●), ON-2 (○), ON-1−A (■), ON-2−A (□), ON-1* (▲), and ON-2* (△). ⋆ = alkylated by (+)-**2**.

(see the Supporting Information). This result correlates very well with the cytotoxicity of prodrug (+)-**2** (determined on human bronchial carcinoma cells (A549)), which is signifi-

 © 2006 Wiley-VCH Verlag GmbH & Co. KGaA, Weinheim

cantly lower than that of the seco drug (+)-**3**.[3] In contrast to the selective alkylation of **5** by (+)-**3**, the reaction of (+)-**2** with **5** takes place at the adenines A10 in ON-1 and A7 in ON-2 (Figure 7). This indicates that (+)-**2** binds noncovalently to

5'-d(CGG TC A ATT A GT CGC)-3' (ON-1)
3'-d(GCC AG T TAA T CA GCG)-5' (ON-2)

Figure 7. Alkylation positions of the prodrug (+)-**2**.

the DNA analogously to (+)-**4**, which was formed in situ from (+)-**3**. However, owing to the greater flexibility of the alkylating chloroethyl unit of the seco prodrug (+)-**2**, both oligonucleotides can act as nucleophiles. This clearly confirms that the alkylation of DNA by (+)-**3** takes place after conversion into (+)-**4**.

Investigations with the enantiomeric seco drug (−)-**3** showed that this compound has a far lower alkylation tendency than (+)-**3** (Figure 8); this result is again consistent with the results from the cytotoxicity tests.[3]

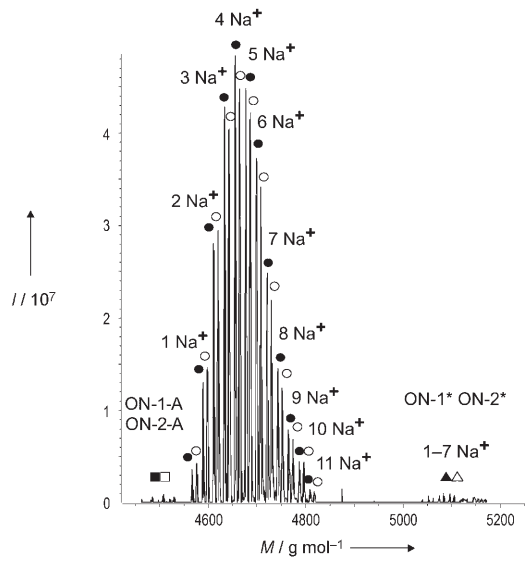

Figure 8. Deconvoluted ESI-HRMS (negative-ion mode) spectrum: (−)-**3**/**5** = 1:1, t = 24 h; Na^+ adducts of ON-1 (●), ON-2 (○), ON-1−A (■), ON-2−A (□), ON-1* (▲) and ON-2* (△). * = alkylated by (−)-**4**.

In addition to the measurements on double-stranded DNA **5**, investigations of the reaction of (+)-**2**, (+)-**3**, and (−)-**3** with single-stranded ON-1 were carried out. After incubation for 24 h, and even with an excess of active compound, only a comparably weak alkylation could be observed, and both guanine as well as adenine were alkylated. These results clearly show that selectivity and reactivity decrease significantly when switching from a double-stranded to a single-stranded oligonucleotide. This is in agreement with the observation that duocarmycin SA (**1**) and analogous compounds exhibit unusually poor reactivity with conventional nucleophiles but react very rapidly with double-stranded DNA.[11a,12]

The ESI-HRMS measurements described herein allow direct conclusions to be drawn concerning the reactivity and selectivity of DNA-alkylating duocarmycin analogues. Thus, it could be shown that the cytotoxic (+)-**3** developed by us exhibits a high alkylation tendency and selectivity towards double-stranded DNA but is only slightly alkylating towards single-stranded oligonucleotides. The comparably low alkylation tendency of the prodrug (+)-**2** and the enantiomeric seco drug (−)-**3**, which correlates very well with the low cytotoxicity of these compounds in cell culture investigations, is notable. The method described with the example of the duocarmycin analogues (+)-**3**, (+)-**2**, and (−)-**3** should also be suitable for the estimation of the reactivity and the selectivity of other DNA-alkylating compounds.

Received: March 9, 2006
Published online: September 8, 2006

Keywords: alkylation · DNA · duocarmycin · mass spectrometry

[1] L. F. Tietze, F. Major, I. Schuberth, *Angew. Chem.* **2006**, *118*, 6724–6727; *Angew. Chem. Int. Ed.* **2006**, *45*, 6574–6577.
[2] a) W. A. Denny, *Cancer Invest.* **2004**, *22*, 604–619; b) G. Xu, H. L. McLeod, *Clin. Cancer Res.* **2001**, *7*, 3314–3324; c) M. P. Napier, S. K. Sharma, C. J. Springer, K. D. Bagshawe, A. J. Green, J. Martin, S. M. Stribbling, N. Cushen, D. O'Malley, R. H. J. Begent, *Clin. Cancer Res.* **2000**, *6*, 765–772; d) K. D. Bagshawe, *Br. J. Cancer* **1987**, *56*, 531–532.
[3] a) L. F. Tietze, T. Feuerstein, *Aust. J. Chem.* **2003**, *56*, 841–854; b) L. F. Tietze, T. Feuerstein, *Curr. Pharm. Des.* **2003**, *9*, 2155–2175; c) L. F. Tietze, T. Feuerstein, A. Fecher, F. Haunert, O. Panknin, U. Borchers, I. Schuberth, F. Alves, *Angew. Chem.* **2002**, *114*, 785–787; *Angew. Chem. Int. Ed.* **2002**, *41*, 759–761; d) L. F. Tietze, M. Lieb, T. Herzig, F. Haunert, I. Schuberth, *Bioorg. Med. Chem.* **2001**, *9*, 1929–1939; e) L. F. Tietze, R. Hannemann, W. Buhr, M. Lögers, P. Menningen, M. Lieb, D. Starck, T. Grote, A. Döring, I. Schuberth, *Angew. Chem.* **1996**, *108*, 2840–2842; *Angew. Chem. Int. Ed. Engl.* **1996**, *35*, 2674–2677.
[4] a) M. L. Colgrave, P. Iannitti-Tito, G. Wickham, M. M. Sheil, *Aust. J. Chem.* **2003**, *56*, 401–413; b) J. L. Beck, M. L. Colgrave, S. F. Ralph, M. M. Sheil, *Mass Spectrom. Rev.* **2001**, *20*, 61–87; c) P. Iannitti-Tito, A. Weimann, G. Wickham, M. M. Sheil, *Analyst* **2000**, *125*, 627–634; d) L. A. Marzilli, D. Wang, W. R. Kobertz, J. M. Essigmann, P. Vouros, *J. Am. Soc. Mass Spectrom.* **1998**, *9*, 676–682; e) P. Iannitti, M. M. Sheil, G. Wickham, *J. Am. Chem. Soc.* **1997**, *119*, 1490–1491.
[5] a) J. H. Banoub, R. P. Newton, E. Esmans, D. F. Ewing, G. Mackenzie, *Chem. Rev.* **2005**, *105*, 1869–1915; b) E. Nordhoff, F. Kirpekar, P. Roepstorff, *Mass Spectrom. Rev.* **1996**, *15*, 67–138; c) S. A. McLuckey, S. Habibi-Goudarzi, *J. Am. Chem. Soc.* **1993**, *115*, 12085–12095.
[6] a) J. A. Smith, G. Bifulco, D. A. Case, D. L. Boger, L. Gomez-Paloma, W. J. Chazin, *J. Mol. Biol.* **2000**, *300*, 1195–1204; b) P. S. Eis, J. A. Smith, J. M. Rydzewski, D. A. Case, D. L. Boger, W. J. Chazin, *J. Mol. Biol.* **1997**, *272*, 237–252.
[7] O. Kennard, W. N. Hunter, *Angew. Chem.* **1991**, *103*, 1280–1304; *Angew. Chem. Int. Ed. Engl.* **1991**, *30*, 1254–1277.
[8] a) T. Bando, A. Narita, S. Sasaki, H. Sugiyama, *J. Am. Chem. Soc.* **2005**, *127*, 13890–13895; b) S. Kupchinsky, S. Centioni, T. Howard, J. Trzupek, S. Roller, V. Carnahan, H. Townes, B. Purnell, C. Price, H. Handl, K. Summerville, K. Johnson, J. Toth, S. Hudson, K. Kiakos, J. A. Hartley, M. Lee, *Bioorg. Med. Chem.* **2004**, *12*, 6221–6236; c) D. L. Boger, H. W. Schmitt, B. E. Fink,

 © 2006 Wiley-VCH Verlag GmbH & Co. KGaA, Weinheim

M. P. Hedrick, *J. Org. Chem.* **2001**, *66*, 6654 – 6661; d) Z. Zhang, M. C. Poirier, *Chem. Res. Toxicol.* **1997**, *10*, 971 – 977; e) Y. Pommier, G. Kohlhagen, C. Bailly, M. Waring, A. Mazumder, K. W. Kohn, *Biochemistry* **1996**, *35*, 13303 – 13309.

[9] a) D. L. Boger, B. Bollinger, D. L. Hertzog, D. S. Johnson, H. Cai, P. Mésini, R. M. Garbaccio, Q. Jin, P. A. Kitos, *J. Am. Chem. Soc.* **1997**, *119*, 4987 – 4998; b) D. L. Boger, D. S. Johnson, *Angew. Chem.* **1996**, *108*, 1542 – 1580; *Angew. Chem. Int. Ed. Engl.* **1996**, *35*, 1438 – 1474; c) L. H. Hurley, D. R. Needham-VanDevanter, *Acc. Chem. Res.* **1986**, *19*, 230 – 237.

[10] To simplify the evaluation, the spectra were deconvoluted, that is, a computer-assisted conversion of the signals of the multiply charged ions into the signals of the respective neutral species was carried out. All spectra discussed in the following are deconvoluted spectra.

[11] a) A. Asai, S. Nagamura, H. Saito, *J. Am. Chem. Soc.* **1994**, *116*, 4171 – 4177; b) H. Sugiyama, K. Ohmori, K. L. Chan, M. Hosoda, A. Asai, H. Saito, I. Saito, *Tetrahedron Lett.* **1993**, *34*, 2179 – 2182; c) K. Yamamoto, H. Sugiyama, S. Kawanishi, *Biochemistry* **1993**, *32*, 1059 – 1066.

[12] a) K. N. Kirschner, M. Lee, R. C. Stanley, J. P. Bowen, *Bioorg. Med. Chem.* **2000**, *8*, 329 – 335; b) D. L. Boger, R. M. Garbaccio, *Acc. Chem. Res.* **1999**, *32*, 1043 – 1052.

 © 2006 Wiley-VCH Verlag GmbH & Co. KGaA, Weinheim

Prodrugs

DOI: 10.1002/anie.200600936

Antitumor Agents: Development of Highly Potent Glycosidic Duocarmycin Analogues for Selective Cancer Therapy**

Lutz F. Tietze, Felix Major, and Ingrid Schuberth*

Dedicated to Professor Gerhard Erker on the occasion of his 60th birthday

Effective chemotherapy of malignant tumors is one of the great challenges of modern medicine. Chemotherapy is generally connected with severe side effects as the selectivity of traditional cytostatic agents is mainly based on the difference in the proliferation rate between malignant and normal cells. In comparison with cells particularly from the hematopoietic system, intestinal tract, and hair follicles, this difference is very small. The aim of modern cancer therapy, therefore, should be the targeted removal of malignant cells without impairment of normal cell populations. The approach that we have adopted for selective cancer treatment is "antibody-directed enzyme prodrug therapy" (ADEPT). With this method, nontoxic compounds (prodrugs) are enzymatically transformed into highly cytotoxic agents in cancerous tissue in a targeted manner.[1,2] In this binary approach, selectivity is achieved through the use of monoclonal antibodies that bind to tumor-associated antigens and are covalently bound to the required enzyme. Other approaches for selective cancer therapy depend on the application of immunoconjugates,[3] angiogenesis inhibitors,[4] antitumor vaccines,[5] kinase inhibitors,[6] and conjugates between a neuropeptide and an antitumor agent.[7]

Based on our previous work, which dates back to 1985, we have defined the main criterion for the ADEPT concept to be that the cytotoxic agent derived from the prodrug should achieve an IC_{50}[***] value of < 10 nM. Furthermore, the comparative toxicity ratio between the prodrug and drug, which we define as the QIC_{50} ($QIC_{50} = IC_{50}$(prodrug)/IC_{50}(prodrug+enzyme)),[8] should exceed 1000.

Herein we describe a new prodrug, (+)-**2a**, which we have developed for selective cancer therapy. The compound is based on the cytotoxic duocarmycin antibiotics, which for example, include duocarmycin SA (**1**). Not only does this compound fulfill the outlined criteria, but owing to its excellent QIC_{50} value, its good water solubility, and its easy synthesis, it exceeds all prodrugs prepared to date by us[1b,c,9] and others.[1,10]

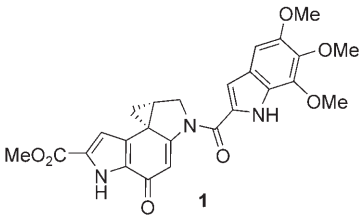

1

Duocarmycin SA was isolated from *Streptomyces* DO-113 and has an IC_{50} value of 10 pM in the L1210 tumor cell line.[11] The spirocyclopropylcyclohexadienone moiety, which is necessary for biological activity, can be formed in situ from the corresponding seco compound with a free phenolic hydroxy group.[12] In prodrug (+)-**2a**, the phenolic hydroxy group is protected as a galactoside so that spirocyclization cannot occur. The prodrug can, however, be easily converted to give the required seco compound, (+)-**3**, which further reacts to give the cytotoxic agent (+)-**4** (Scheme 1). The *N*,*N*-dimethylaminoethoxyindole carboxylic acid component[13] not only facilitates intercalation in the minor DNA groove, but also increases water solubility owing to its salification.

The racemic benzyl ether **5**, which was easily obtained by using published methods,[9c,14] was used to synthesize prodrug **2** and seco compound **3**. To synthesize the diastereomerically pure glycosidic prodrugs as well as the enantiomerically pure

[*] Prof. Dr. L. F. Tietze, Dipl.-Chem. F. Major, Dr. I. Schuberth
Institut für Organische und Biomolekulare Chemie
Georg-August-Universität Göttingen
Tammannstrasse 2, 37077 Göttingen (Germany)
Fax: (+49) 551-39-9476
E-mail: ltietze@gwdg.de

[**] This research was supported by the Deutschen Forschungsgemeinschaft (SFB 416) and the Fonds der Chemischen Industrie. F.M. would like to thank the Studienstiftung des deutschen Volkes for a PhD scholarship.

[***] IC_{50}: drug concentration at which 50% of cell growth is inhibited.

WILEY InterScience DISCOVER SOMETHING GREAT
© 2006 Wiley-VCH Verlag GmbH & Co. KGaA, Weinheim

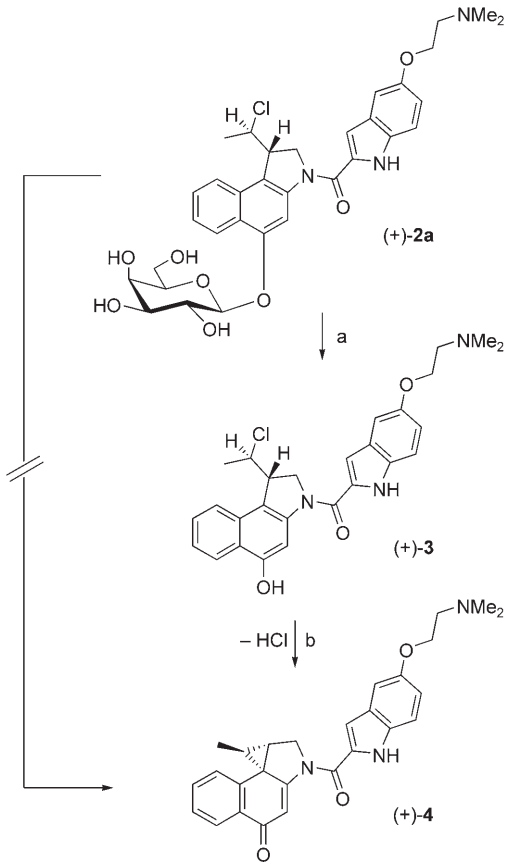

Scheme 1. Enzymatic toxification of the glycosidic prodrug (+)-**2a**: a) Transformation into the seco compound (+)-**3** and b) Winstein cyclization in situ to give the drug (+)-**4**, which is an analogue of the antibiotic (+)-duocarmycin SA (**1**).

toxins, it was necessary to maintain **5** in an enantiomerically pure form. Owing to the sensitivity of the free amine of **5**, it was not possible to use classical resolution methods, such as formation of diastereomeric salts or derivatives with enantiomerically pure reagents. However, efficient preparative HPLC separation was carried out by using a column with a chiral stationary phase (Chiralpak IA).[15] The absolute configuration of (+)-**5** was determined after derivatization with 3,5-dibromobenzoic acid by using X-ray crystal structure analysis.[16]

The galactosides **2** were prepared from **5** after removal of the benzyl protecting group with palladium on activated carbon and ammonium formate as the hydrogen source.[17] Glycosylation was carried out with **6** by using the trichloroacetimidate method developed by Schmidt.[18] Subsequently, $BF_3{\cdot}OEt_2$ was employed for *N*-*tert*-butoxycarbonyl (*N*-Boc) deprotection and the obtained secondary free amines were coupled with the indolecarboxylic acid hydrochloride **7**.[13] Finally, base-catalyzed solvolysis of the acetyl groups resulted in the desired galactosides **2** in very good final yields of 37–43% in four steps (Scheme 2). The free toxins **3**, which were required as control compounds for the in vitro experiments, were obtained from **5** by *N*-Boc deprotection, followed by coupling with **7** and final debenzylation to give **3** in yields of 51–65%. Direct glycosylation of **3** with **6** was not successful.

The cytotoxic effects of the newly synthesized compounds were tested on human tumor cells by using a colony-forming assay carried out in triplicate (Table 1). This test reflects the proliferation capacity of single cells and is based on the HTCFA assay (human tumor colony forming ability test)[9d]. In experiments using human bronchial carcinoma cell line A549, a QIC_{50} of 6600 was achieved with the mixture of diastereomeric prodrugs **2a**/**2b**, and for the diastereomerically pure prodrug (+)-(1*S*,10*R*)-**2a**, a QIC_{50} value of 4800 was observed. The cytotoxicity of seco compound (+)-(1*S*,10*R*)-**3** was determined as $IC_{50} = 0.75$ nM. It was not possible to assign the QIC_{50} value of prodrug (−)-(1*R*,10*S*)-**2b** owing to its low cytotoxicity. Thus, a higher quantity of this prodrug had to be used, which then led to solubility problems. Interestingly, the underlying seco compound (−)-(1*R*,10*S*)-**3**, with an IC_{50} value of 560 nM, showed an almost 1000-fold lower cytotoxicity than its enantiomer, (+)-(1*S*,10*R*)-**3**. The results of the cytotoxicity assays are in good agreement with MS data obtained from alkylation of duplex DNA with (+)-(1*S*,10*R*)-**2a**, (+)-(1*S*,10*R*)-**3**, and (−)-(1*R*,10*S*)-**3**.[19] As a further important finding from the cytotoxicity assays in vitro, it should be emphasized that after treatment of prodrug (+)-(1*S*,10*R*)-**2a** with β-D-galactosidase, the observed cytotoxicity was identical to that determined for seco compound (+)-(1*S*,10*R*)-**3**.

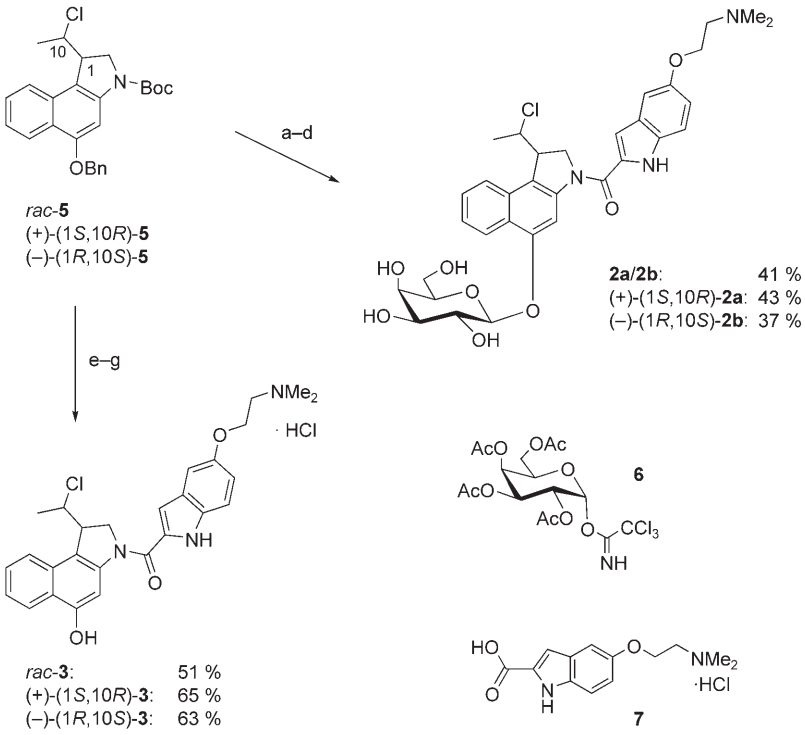

Scheme 2. Synthesis of prodrugs **2** and seco compounds **3**: a) $Pd/C/NH_4HCO_2$, THF, 40°C, 15 min; b) **6**, $BF_3{\cdot}OEt_2$, CH_2Cl_2, molecular sieves (4 Å), −10°C, 3.5 h, then $BF_3{\cdot}OEt_2$, RT, 5 h; c) **7**, EDC·HCl, DMF, RT, 20 h; d) NaOMe/MeOH, RT, 2 h; e) 4 M HCl/EtOAc, RT, 2 h; f) **7**, EDC·HCl, DMF, RT, 19 h; g) 4 M HCl/EtOAc, RT, 2 h, followed by $Pd/C/NH_4HCO_2$, THF, 40°C, 2 h. Bn = Benzyl, DMF = *N*,*N*-dimethylformamide ,EDC = 3-(3-dimethylaminopropyl)-1-ethylcarbodiimide.

 © 2006 Wiley-VCH Verlag GmbH & Co. KGaA, Weinheim

This confirms the principle of reversible detoxification, the stability of the prodrugs under test conditions, and the nondisruptive effects of the enzyme activity.

Table 1: Results of the HTCFA assay for the in vitro analysis of the cytotoxicity of **2** and **3** against human bronchial carcinoma cells of line A549.[a]

Compound	β-D-gal.[b]	IC_{50} [nM]	QIC_{50}
2a/**2b**	−	7.9×10^{3}	6600
2a/**2b**	+	1.2	
(+)-(1*S*,10*R*)-**2a**	−	3.6×10^{3}	4800
(+)-(1*S*,10*R*)-**2a**	+	0.75	
(−)-(1*R*,10*S*)-**2b**	−	$>7.8\times10^{4}$	>140
(−)-(1*R*,10*S*)-**2b**	+	5.5×10^{2}	
rac-**3**	−	1.5	
(+)-(1*S*,10*R*)-**3**	−	0.75	
(−)-(1*R*,10*S*)-**3**	−	5.6×10^{2}	

[a] Cells were incubated with the corresponding compounds for 24 h at 37 °C; after 12 days incubation, the clone formation rates were determined in comparison with untreated control cells (β-D-galactosidase: *Escherichia coli*, 4 U mL^{-1}). [b] Presence or absence of β-D-galactosidase.

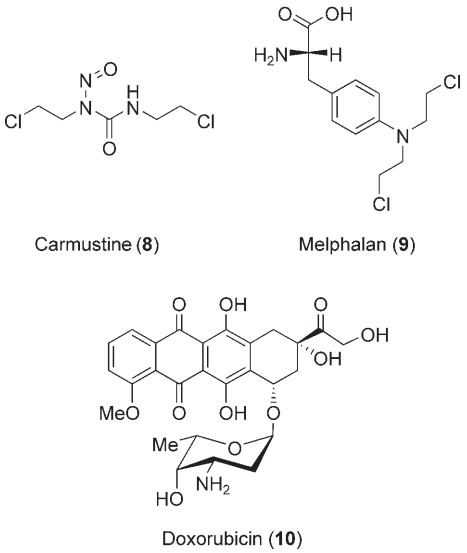

Scheme 3. The antitumor agents carmustine (**8**), melphalan (**9**), and doxorubicin (**10**).

To compare the compounds **2** and **3** that we have developed with other cytotoxic drugs, HTCFA assays were performed on the A549 cell line with carmustine (**8**), melphalan (**9**) and doxorubicin (**10**), which are currently used as anticancer agents (Scheme 3 and Figure 1). The results confirm that in the presence of the enzyme β-D-galactosidase, the new prodrug (+)-(1*S*,10*R*)-**2a** has a higher biological activity than compounds **8**–**10**. Consequently, the new compound has considerable benefits for use within the framework of the ADEPT concept.

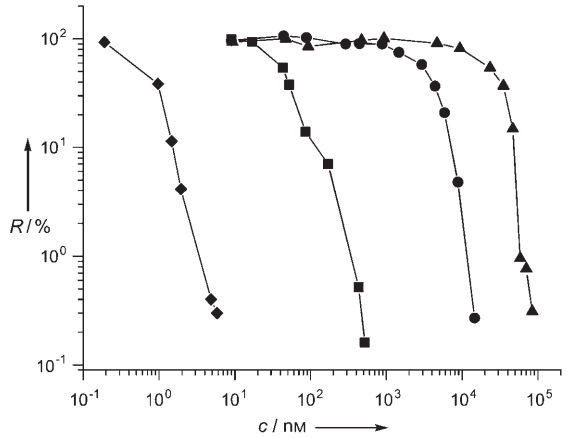

Figure 1. Comparison of the cytotoxicities in vitro of various antitumor agents against human bronchial carcinoma cells of line A549. (◆) (+)-(1*S*,10*R*)-**2a** in the presence of β-D-galactosidase (4 U mL^{-1}): IC_{50} = 0.75 nM; (▲) carmustine (**8**): $IC_{50}=2.6\times10^{4}$ nM; (●) melphalan (**9**): $IC_{50}=3.4\times10^{3}$ nM; (■) doxorubicin (**10**): IC_{50} = 45 nM. *R* = relative clone-formation rate.

Received: March 9, 2006
Published online: September 8, 2006

Keywords: antitumor agents · cytostatic agents · duocarmycin · glycosides · prodrugs

[1] Reviews: a) W. A. Denny, *Cancer Invest.* **2004**, *22*, 604–619; b) L. F. Tietze, T. Feuerstein, *Curr. Pharm. Des.* **2003**, *9*, 2155–2175; c) L. F. Tietze, T. Feuerstein, *Aust. J. Chem.* **2003**, *56*, 841–854; d) W. A. Denny, *Eur. J. Med. Chem.* **2001**, *36*, 577–595; e) M. Jung, *Mini-Rev. Med. Chem.* **2001**, *1*, 399–407; f) G. Xu, H. L. McLeod, *Clin. Cancer Res.* **2001**, *7*, 3314–3324; g) K. N. Syrigos, A. A. Epenetos, *Anticancer Res.* **1999**, *19*, 605–614; h) G. M. Dubowchik, M. A. Walker, *Pharmacol. Ther.* **1999**, *83*, 67–123; i) C. J. Springer, I. Niculescu-Duvaz, *Adv. Drug Delivery Rev.* **1997**, *26*, 151–172; j) L. N. Jungheim, T. A. Shepherd, *Chem. Rev.* **1994**, *94*, 1553–1566.
[2] K. D. Bagshawe, *Br. J. Cancer* **1987**, *56*, 531–532.
[3] A. M. Wu, P. D. Senter, *Nat. Biotechnol.* **2005**, *23*, 1137–1146.
[4] a) T. Arndt, U. Arndt, U. Reuning, H. Kessler in *Cancer Therapy: Molecular Targets in Tumor–Host Interactions* (Ed.: G. F. Weber), Horizon Bioscience, Norfolk, **2005**, 93–141; b) D. Ribatti, A. Vacca, F. Merchionne, M. Presta, *Mini-Rev. Med. Chem.* **2005**, *5*, 313–317; c) K. A. El Sayed, *Mini-Rev. Med. Chem.* **2005**, *5*, 971–993.
[5] a) S. Dziadek, D. Kowalczyk, H. Kunz, *Angew. Chem.* **2005**, *117*, 7798–7803; *Angew. Chem. Int. Ed.* **2005**, *44*, 7624–7630; b) S. Dziadek, A. Hobel, E. Schmitt, H. Kunz, *Angew. Chem.* **2005**, *117*, 7803–7808; *Angew. Chem. Int. Ed.* **2005**, *44*, 7630–7635.
[6] a) M. E. M. Noble, J. A. Endicott, L. N. Johnson, *Science* **2004**, *303*, 1800–1805; b) C. Garcia-Echeverria, D. Fabbro, *Mini-Rev. Med. Chem.* **2004**, *4*, 273–283.
[7] a) M. Langer, F. Kratz, B. Rothen-Rutishauser, H. Wunderli-Allenspach, A. G. Beck-Sickinger, *J. Med. Chem.* **2001**, *44*, 1341–1348; b) M. Langer, A. G. Beck-Sickinger, *Curr. Med. Chem.: Anti-Cancer Agents* **2001**, *1*, 71–93.
[8] L. F. Tietze, T. Herzig, T. Feuerstein, I. Schuberth, *Eur. J. Org. Chem.* **2002**, 1634–1645.
[9] a) L. F. Tietze, T. Feuerstein, A. Fecher, F. Haunert, O. Panknin, U. Borchers, I. Schuberth, F. Alves, *Angew. Chem.* **2002**, *114*,

 © 2006 Wiley-VCH Verlag GmbH & Co. KGaA, Weinheim

785 – 787; *Angew. Chem. Int. Ed.* **2002**, *41*, 759 – 761; b) L. F. Tietze, M. Lieb, T. Herzig, F. Haunert, I. Schuberth, *Bioorg. Med. Chem.* **2001**, *9*, 1929 – 1939; c) L. F. Tietze, T. Herzig, A. Fecher, F. Haunert, I. Schuberth, *ChemBioChem* **2001**, *2*, 758 – 765; d) L. F. Tietze, R. Hannemann, W. Buhr, M. Lögers, P. Menningen, M. Lieb, D. Starck, T. Grote, A. Döring, I. Schuberth, *Angew. Chem.* **1996**, *108*, 2840 – 2842; *Angew. Chem. Int. Ed. Engl.* **1996**, *35*, 2674 – 2677.

[10] a) G. Wei, N. A. Loktionova, A. E. Pegg, R. C. Moschel, *J. Med. Chem.* **2005**, *48*, 256 – 261; b) H. Cheng, X. Cao, M. Xian, L. Fang, T. B. Cai, J. J. Ji, J. B. Tunac, D. Sun, P. G. Wang, *J. Med. Chem.* **2005**, *48*, 645 – 652; c) M. Y. Torgov, S. C. Alley, C. G. Cerveny, D. Farquhar, P. D. Senter, *Bioconjugate Chem.* **2005**, *16*, 717 – 721; d) E. Bouvier, S. Thirot, F. Schmidt, C. Monneret, *Bioorg. Med. Chem.* **2004**, *12*, 969 – 977; e) T. Kline, M. Y. Torgov, B. A. Mendelsohn, C. G. Cerveny, P. D. Senter, *Mol. Pharm.* **2004**, *1*, 9 – 22; f) E. Bouvier, S. Thirot, F. Schmidt, C. Monneret, *Org. Biomol. Chem.* **2003**, *1*, 3343 – 3352; g) H. Townes, K. Summerville, B. Purnell, M. Hooker, E. Madsen, S. Hudson, M. Lee, *Med. Chem. Res.* **2002**, *12*, 248 – 253; h) N. Amishiro, S. Nagamura, C. Murakata, A. Okamoto, E. Kobayashi, M. Asada, K. Gomi, T. Tamaoki, M. Okabe, N. Yamaguchi, K. Yamaguchi, H. Saito, *Bioorg. Med. Chem.* **2000**, *8*, 381 – 391.

[11] a) M. Ichimura, T. Ogawa, K. Takahashi, E. Kobayashi, I. Kawamoto, T. Yasuzawa, I. Takahashi, H. Nakano, *J. Antibiot.* **1990**, *43*, 1037 – 1038; b) M. Ichimura, T. Ogawa, S. Katsumata, K. Takahashi, I. Takahashi, H. Nakano, *J. Antibiot.* **1991**, *44*, 1045 – 1053; c) D. L. Boger, D. S. Johnson, *Angew. Chem.* **1996**, *108*, 1542 – 1580; *Angew. Chem. Int. Ed. Engl.* **1996**, *35*, 1438 – 1474.

[12] a) L. F. Tietze, F. Haunert, T. Feuerstein, T. Herzig, *Eur. J. Org. Chem.* **2003**, 562 – 566; b) R. Baird, S. Winstein, *J. Am. Chem. Soc.* **1963**, *85*, 567 – 578.

[13] J. B. J. Milbank, M. Tercel, G. J. Atwell, W. R. Wilson, A. Hogg, W. A. Denny, *J. Med. Chem.* **1999**, *42*, 649 – 658.

[14] For the synthesis of **5**, the toxic nBu$_3$SnH, which was formerly used, was replaced by tris(trimethylsilyl)silane.

[15] Preparative HPLC separation: Chiralpak IA column (250 × 20 mm, particle size: 5 μm), mobile phase: *n*-heptane/dichloromethane (4:1), flow rate: 18 mL min^{-1}, $\alpha = 2.05$, (+)-**5**: 99.9 % *ee*, (−)-**5**: 99.9 % *ee*.

[16] L. F. Tietze, F. Major, J. Magull, unpublished results.

[17] a) S. Ram, L. D. Spicer, *Tetrahedron Lett.* **1987**, *28*, 515 – 516; b) T. Bieg, W. Szeja, *Synthesis* **1985**, 76 – 77.

[18] a) R. R. Schmidt, *Angew. Chem.* **1986**, *98*, 213 – 236; *Angew. Chem. Int. Ed. Engl.* **1986**, *25*, 212 – 235; b) W. Dullenkopf, J. C. Castro-Palomino, L. Manzoni, R. R. Schmidt, *Carbohydr. Res.* **1996**, *296*, 135 – 147.

[19] L. F. Tietze, B. Krewer, H. Frauendorf, F. Major, I. Schuberth, *Angew. Chem.* **2006**, *118*, 6720 – 6724; *Angew. Chem. Int. Ed.* **2006**, *45*, 6570 – 6574.

 © 2006 Wiley-VCH Verlag GmbH & Co. KGaA, Weinheim

Nanomaterials

DOI: 10.1002/anie.200602209

Tailor-Made Ligands for Biocompatible Nanoparticles**

*Marija S. Nikolic, Maren Krack, Vesna Aleksandrovic, Andreas Kornowski, Stephan Förster, and Horst Weller**

Nanobiotechnology is one of the most exciting fields of nanotechnology.[1,2] A few years ago semiconductor nanocrystals were recognized as materials perfectly suited to replace organic dyes currently used in experiments involving fluorescent labeling. In addition to their better photostability, nanoparticles are superior to organic dyes in other aspects, such as broader excitation and narrower emission spectra, which can be easily tuned. As far as magnetic materials used in biomedicine are concerned the use of nanoparticles of high monodispersity with sizes in the range of those of the biological entities under investigation offers attractive possibilities.[3] Magnetic materials currently used in magnetic resonance imaging (MRI) techniques are obtained in a water-based synthesis and suffer from poor size distribution resulting in only a low enhancement of the magnetic resonance signal.

The drawback concerning further biological applications of nanoparticles with superior properties is that synthetic approaches used yield nanoparticles that are insoluble in aqueous media. However, the first step in making the nanoparticles useful for any bioapplication is efficient phase transfer to water. A great deal of effort has been put into this task and all the developed methods belong to one of two strategies:[4] ligand exchange,[5,6] or encapsulation of the original nanocrystals into a thick and cross-linked polymer coating.[7–9]

Herein, a ligand-exchange method for the transfer of nanoparticles into an aqueous solution using amino-modified poly(ethylene oxide)s (PEOs) is presented. Poly(ethylene oxide) is a water-soluble polymer suitable for biological application since surfaces covered with PEO have proven to be non-immunogenic, non-antigenic, and protein resistant.[10] Recently, it was also shown that the use of PEO in the hitherto developed nanoparticle bioconjugates reduced nonspecific binding.[11]

[*] M. S. Nikolic, Dr. M. Krack, V. Aleksandrovic, Dipl.-Ing. A. Kornowski, Prof. Dr. S. Förster, Prof. Dr. H. Weller
Institute of Physical Chemistry
University of Hamburg
Grindelallee 117, 20146 Hamburg (Germany)
Fax: (+49) 40-42838-3452
E-mail: weller@chemie.uni-hamburg.de

[**] This work was funded by the German Research Foundation (SFB508, GK611)and FCI.

Supporting information for this article is available on the WWW under http://www.angewandte.org or from the author.

© 2006 Wiley-VCH Verlag GmbH & Co. KGaA, Weinheim

The end groups of PEOs were modified to obtain amino functionalities at one end of the polymer chain. Amino functionalities are anchor groups which can bind to the metal sites of nanoparticles and, in some cases, improve the luminescent properties of semiconductor nanocrystals.[12]

The diisocyanate coupling reaction was used to obtain amino-functionalized PEOs. This reaction has already shown itself to be suitable for coupling PEOs to high-molecular-weight poly(ethylene imine)s (PEI).[13] In the first step, PEOs terminated with OH groups were treated with hexamethylene diisocyanate to obtain PEOs with NCO end groups. In the second step, the NCO end groups were treated with a large excess of diethylenetriamine (DETA) to obtain PEOs with two amino groups at one end of the polymer chains (Scheme 1). The NCO-activated PEOs were also treated with a branched PEI of low molecular weight (Scheme 1). The ratio of the reactants was chosen to produce molecules carrying two PEO chains of the desired molecular weight.

Direct extraction, a very frequently used method for phase transfer of nanoparticles, did not yield nanoparticles soluble in water. An alternative approach consisting of the precipitation of the nanoparticles using a nonsolvent for the new capping ligands (hexane or cyclohexane) was applied. The precipitate obtained was readily soluble in water as well as in other protic solvents, such as methanol. A control test carried out with unmodified PEOs of different molecular weights resulted in precipitation of the polymer only, while the nanoparticles remained well dispersed in the hexane/chloroform mixture. This result indicated a successful binding of the amino groups of the modified PEO to the metal sites of nanoparticles and excluded any possible agglomeration of the nanoparticles by poly(ethylene oxide) itself.

Amino-functionalized PEOs are excellent universal ligands because various nanoparticles can be easily transferred into water using a similar simple procedure (Figure 1).

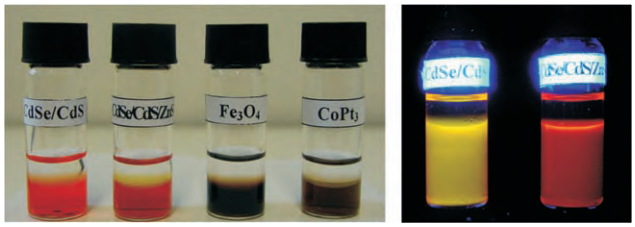

Figure 1. Different nanoparticles dispersed in the aqueous phase below a hexane phase. The quantum dots retain their fluorescence properties in water (right).

After transfer into a protic solvent, luminescent nanoparticles retained their original optical properties; although the emitting efficiency was lower (quantum yield (QY) 20%) as has been observed before for nanoparticles which were brought into the aqueous environment.[14–17]

The best quantum efficiencies for CdSe/CdS nanoparticles were observed when PEO of $M_w = 2000\ g\,mol^{-1}$ (PEO2000) modified with linear DETA was used (Figure 2). This result could indicate a higher grafting density than when PEO modified with branched PEI was used, which is expected from steric considerations (Scheme 2). Because of the steric disadvantages, lower grafting density is also to be expected for higher-molecular-weight PEOs. The lower grafting densities in all these cases might result in an incomplete passivation of the surface states and the formation of looser barriers to water penetration, all these factors give rise to the lower quantum efficiencies (Figure 2).

The advantage of PEO–PEI-branched polymers is that this structure enables an easier approach to the inner binding NH_2-rich shell for any molecule of interest. Currently, the possibility of this inner shell to be used in cross-linking reactions, which should further stabilize the organic coating of nanoparticles, is under investigation.

The results obtained in dynamic light-scattering (DLS) measurements (Figure 3.) show the expected trends for both the PEO–PEI- and the PEO–DETA-based series. With the increase of the polymer-chain length the hydrodynamic radii increase. However, in the PEO–DETA series the values obtained in DLS measurements are con-

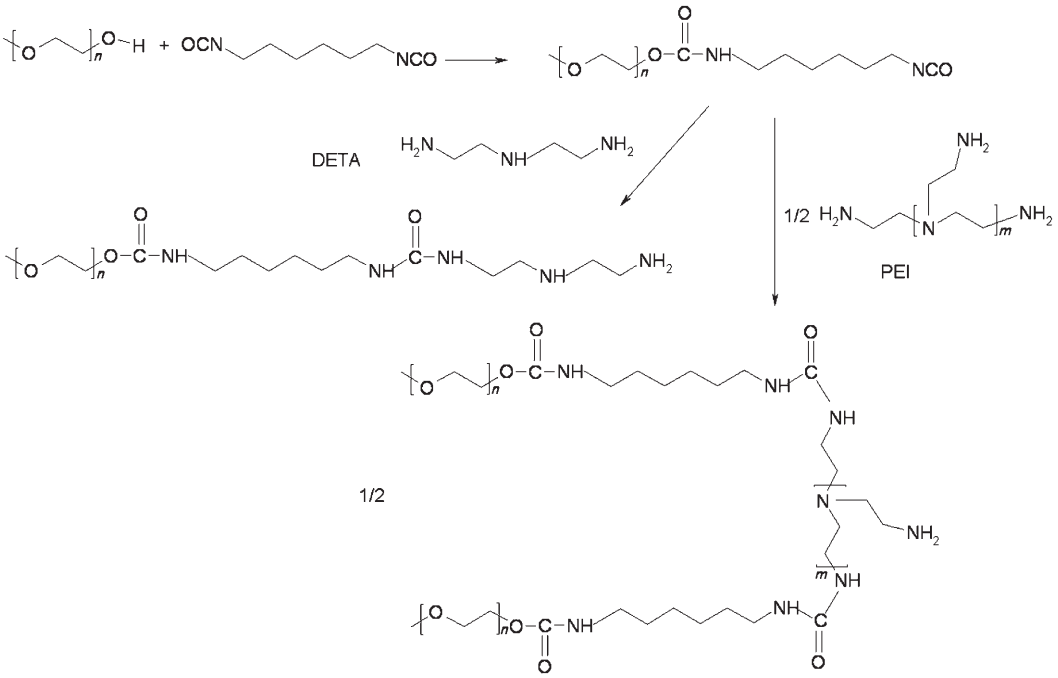

Scheme 1. Synthesis of amino-functionalized PEOs; $n = 45$ or 144, $m \approx 4$ (M_w(PEI) = 423 g mol^{-1}).

 © 2006 Wiley-VCH Verlag GmbH & Co. KGaA, Weinheim

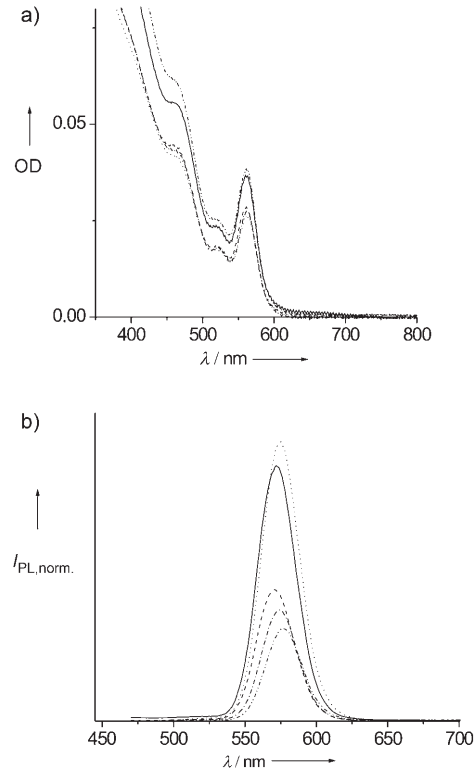

Figure 2. a) Absorption and b) luminescence spectra of CdSe/CdS nanoparticles in chloroform (——) and in water with PEO2000–PEI-branched (-----), PEO2000–DETA (•••••), PEO5000–PEI-branched (–•–•), and PEO5000–DETA (–···–).

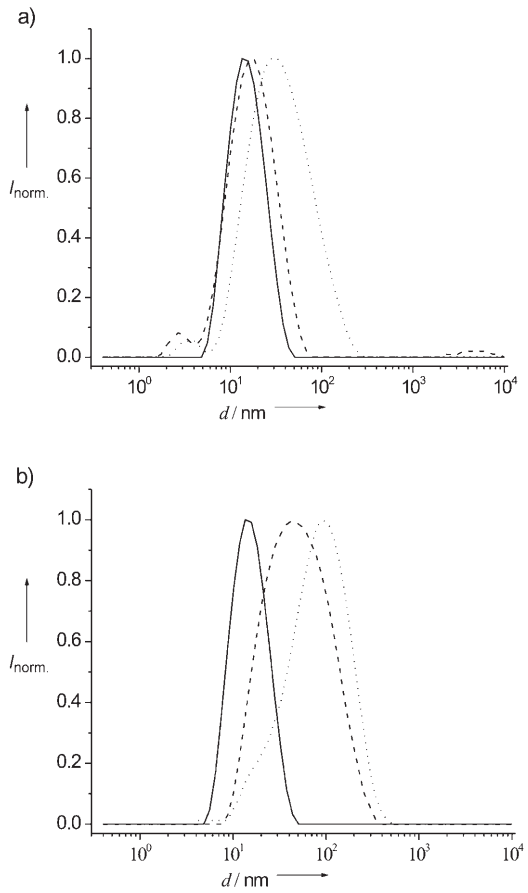

Figure 3. Diameter of the CdSe/CdS nanoparticles in chloroform (——), and in water with different polymer shells: a) PEO–PEI series, b) PEO–DETA series (----- PEO2000, ••••• PEO5000).

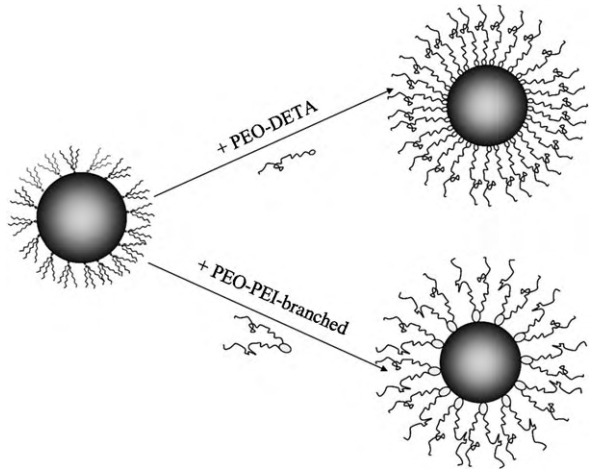

Scheme 2. Ligand exchange with two different types of amino-functionalized PEOs.

siderably higher than the corresponding values in PEO–PEI series.

This unexpected behavior is clarified after investigation of the water-soluble nanoparticle/polymer conjugates with TEM. Figure 4 shows that in PEO–PEI series only single, well separated particles are present, whereas in the PEO–DETA series wormlike agglomerates are observed (Figure 4c, d), which give rise to the larger hydrodynamic radii in the DLS measurements. This type of organization only appears in water, in the TEM images obtained from chloroform solutions after ligand exchange only single particles were observed without any wormlike agglomerates present.

The packing density and the distance between individual nanoparticles are also influenced by the sizes of nanoparticles/polymer conjugates. TEM images obtained after evaporation of a chloroform solution of $CoPt_3$ nanoparticles before and after ligand exchange with two polymers of different molecular weight are presented in Figure 5. In a control experiment (Figure 5b), TEM images were taken after evaporation of the chloroform from the solution of nanoparticles and unmodified poly(ethylene oxide).

The arrangement of nanoparticles was the same as that of nanoparticles without the addition of polymer (Figure 5a). However, after ligand exchange, not only was the arrangement, but also the distance between the nanoparticles changed. The separation increases with the increasing size of the polymer chain, that is, the hydrodynamic radius. This feature can be also seen in the TEM images of CdSe/CdS nanoparticles obtained from water solution (Figure 4a and b).

In conclusion, a series of polymeric ligands which enable the phase transfer of nanoparticles has been designed. The method used to change solubility properties is simple and can be applied to a variety of nanoparticles that were originally

 © 2006 Wiley-VCH Verlag GmbH & Co. KGaA, Weinheim

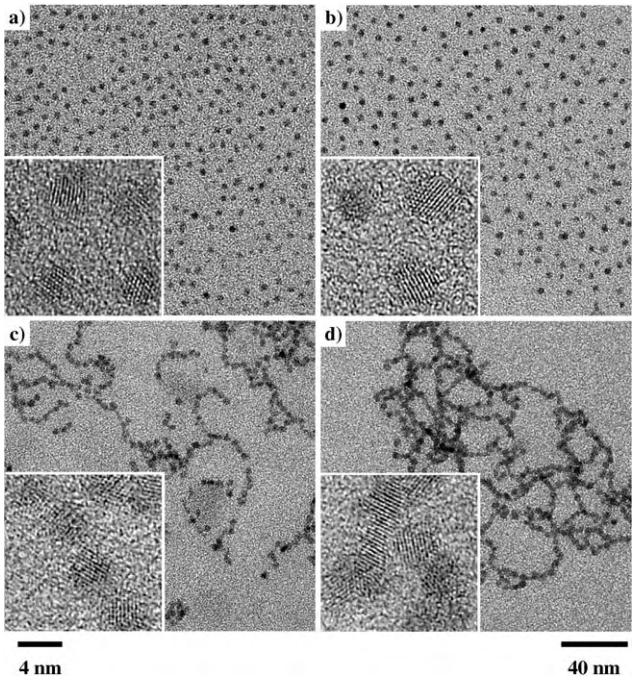

Figure 4. TEM image of water soluble CdSe/CdS nanoparticles modified with a) PEO2000–PEI-branched, b) PEO5000–PEI-branched, c) PEO2000–DETA, and d) PEO5000-DETA. Insets show enlargements. 40-nm and 4-nm scale bars apply to all main images and insets, respectively.

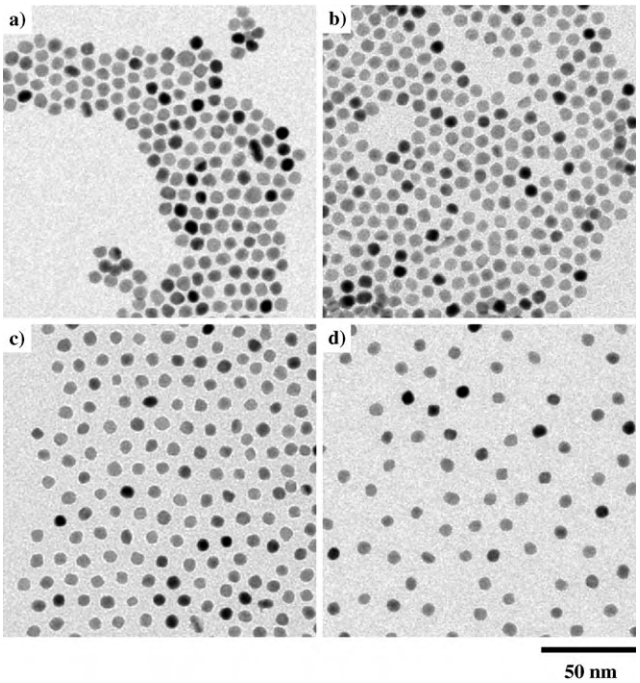

Figure 5. TEM images of $CoPt_3$ nanoparticles with a) ligand shell from the synthesis, b) after mixing with unmodified PEO5000, and after ligand exchange with c) PEO2000–PEI-branched and d) PEO5000–PEI-branched. 50-nm scale bar applies to all images.

only soluble in organic solvents. As a result, modified PEO-coated nanoparticles suitable for biological applications were obtained. The number of functional-anchor groups in the new ligands can be tailored, leaving sufficient space for further functionalization of the nanoparticle/polymer conjugates.

Received: June 2, 2006
Revised: July 3, 2006
Published online: September 12, 2006

Keywords: bioapplications · colloids · ligand design · nanotechnology · poly(ethylene oxide)

[1] J. Parak, D. Gerion, T. Pellegrino, D. Zanchet, C. Micheel, S. C. Williams, R. Boudreau, M. A. Le Gros, C. A. Larabel, P. A. Alivisatos, *Nanotechnology* **2003**, *14*, 15–27.
[2] R. E. Bailey, A. M. Smith, S. Nie, *Phys. E* **2004**, *25*, 1–12.
[3] Q. A. Pankhurst, J. Connolly, S. K. Jones, J. Dobson, *J. Phys. D* **2003**, *36*, 167–181.
[4] I. L. Medintz, H. T. Uyeda, E. R. Goldman, H. Mattoussi, *Nat. Mater.* **2005**, *4*, 435–446.
[5] C. W. Warren, S. Nie, *Science* **1998**, *281*, 2016–2018.
[6] G. P. Mitchell, C. A. Mirkin, R. L. Letsinger, *J. Am. Chem. Soc.* **1999**, *121*, 8122–8123.
[7] B. Dubertret, P. Skourides, D. J. Norris, V. Noireaux, A. H. Brivanlou, A. Libchaber, *Science* **2002**, *298*, 1759–1762.
[8] X. Wu, H. Liu, J. Liu, K. N. Haley, J. A. Treadway, J. P. Larson, N. Ge, F. Peale, M. P. Bruchez, *Nat. Biotechnol.* **2003**, *21*, 41–46.
[9] T. Pellegrino, L. Manna, S. Kudera, T. Liedl, D. Koktysh, A. L. Rogach, S. Keller, J. Radler, G. Natile, W. J. Parak, *Nano Lett.* **2004**, *4*, 703–707.
[10] C. G. Golander, J. N. Herron, K. Lim, P. Claesson, J. D. Andrade in *Polyethylene Glycol Chemistry, Biotechnical and Biomedical Applications* (Ed.: J. M. Harris), Plenum, New York, **1992**, pp. 221–245.
[11] E. L. Bentyen, I. D. Tomlinson, J. Mason, P. Gresch, M. R. Warnement, D. Wright, E. Sanders-Bush, R. Blakely, S. J. Rosenthal, *Bioconjugate Chem.* **2005**, *16*, 1488–1494.
[12] D. V. Talapin, A. L. Rogach, I. Mekis, S. Haubold, A. Kornowski, M. Haase, H. Weller, *Colloids Surf. A* **2002**, *202*, 145–154.
[13] H. Petersen, P. M. Fechner, D. Fischer, T. Kissel, *Macromolecules* **2002**, *35*, 6867–6874.
[14] S. Kim, M. G. Bawendi, *J. Am. Chem. Soc.* **2003**, *125*, 14652–14653.
[15] S.-W. Kim, S. Kim, J. B. Tracy, A. Jasanoff, M. G. Bawendi, *J. Am. Chem. Soc.* **2005**, *127*, 4556–4557.
[16] T. Nann, *Chem. Commun.* **2005**, *13*, 1735–1736.
[17] H. T. Uyeda, I. L. Medinty, J. K. Jaiswal, S. M. Simon, H. Mattoussi, *J. Am. Chem. Soc.* **2005**, *127*, 3870–3878.

 © 2006 Wiley-VCH Verlag GmbH & Co. KGaA, Weinheim

Pathogen Detection

DOI: 10.1002/anie.200602048

Anti-Carbohydrate Antibodies for the Detection of Anthrax Spores**

*Marco Tamborrini, Daniel B. Werz, Joachim Frey, Gerd Pluschke, and Peter H. Seeberger**

Spores of *Bacillus anthracis* have been used as biowarfare agents to terrorize civilian populations. Once this durable form of the pathogen has been inhaled it will kill most victims if treatment does not commence within 24–48 h.[1] After uptake into the body, the spores germinate and vegetative cells multiply and produce toxins, leading to the development of lesions from which the infection may disseminate, which is frequently fatal. It is assumed that an effective anthrax-subunit vaccine should contain multiple antigens. A surface antigen of the spores eliciting antibodies that suppress germination and enhance phagocytosis of spores by macrophages would be a suitable component for such a vaccine.

Several detection systems have been developed to identify *B. anthracis*[2–4] and process the large number of samples that have to be tested each year. PCR-based assays or traditional phenotyping of bacteria are the most accurate but are also complex, expensive, and slow. Antibody binding to spore-surface peptide and protein antigens is less complicated, although it is plagued by higher false-positive and false-negative readouts. The similarity of spore-cell-surface antigens of the opportunistic human pathogen *B. cereus* and other bacteria of this group makes it difficult to create selective, reliable, antibody-based detection systems.

On the surface of *B. anthracis* spores, a unique tetrasaccharide **1** (Scheme 1) containing an entirely novel monosaccharide, named anthrose, was discovered recently.[5] Access to usable quantities of pure cell surface oligosaccharides by isolation is often difficult and leaves synthetic chemistry as a last resort to procure carbohydrate antigens. We envisioned the detection of *B. anthracis* spores based on antibodies against carbohydrate antigen **1**, which is not present on related strains of bacteria.

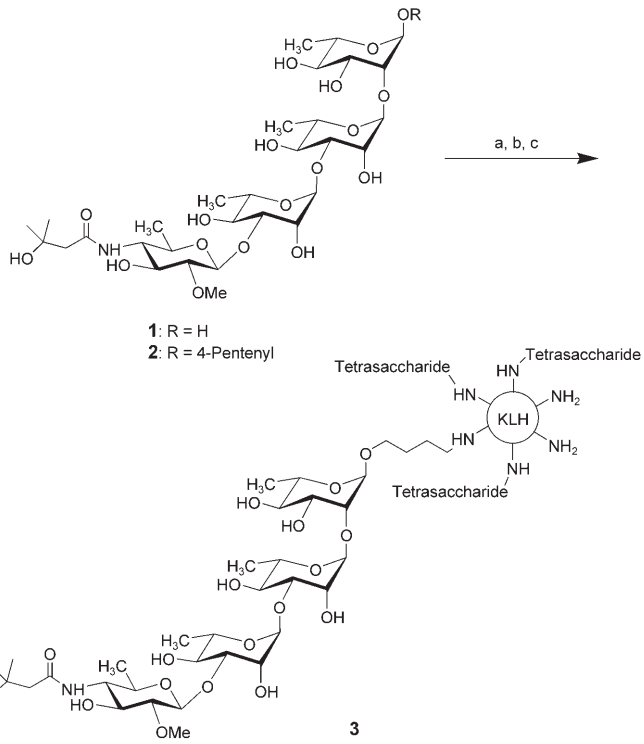

Scheme 1. Structure of the tetrasaccharide **1** found on the surface of *B. anthracis* spores and its synthetic analogue **2**. Attachment through a pentenyl handle to the KLH carrier protein afforded the conjugate **3**: a) O_3, MeOH, −78 °C, 10 min; b) Me_2S, MeOH, RT, 2 h; c) KLH carrier protein, PBS buffer solution (pH 7.2), $NaBH_3CN$, 37 °C, 48 h. PBS = phosphate-buffered saline.

The tetrasaccharide was chemically synthesized[6,7] in the form of the *n*-pentenyl glycoside **2**.[6] The chemical handle on the reducing end was utilized to introduce a reactive terminal aldehyde moiety through ozonolysis. Covalent attachment[8,9] of synthetic **2** to the keyhole-limpet-hemocyanine (KLH) carrier protein by reductive amination produced a carbohydrate–protein conjugate **3** that was immunogenic in mice (Scheme 1). The conjugation to protein carriers is an efficient way to improve the immunogenicity of oligosaccharide antigens. The proteins provide peptide units that can be recognized by carrier-specific T cells, thus converting a T-cell-independent response against an unconjugated oligosaccharide into a more efficient T-cell-dependent response.

Tetrasaccharide–KLH conjugates formulated in Immun-Easy adjuvant (QIAGEN) elicited tetrasaccharide binding immunoglobulin G (IgG) antibodies after the third immunization in mice. Three B cell hybridoma lines producing tetrasaccharide specific monoclonal IgG antibodies (mAbs) were generated from spleen cells of one of the immunized mice. In an indirect immunofluorescence assay, all three mAbs bound specifically to native *B. anthracis* endospores. No binding was found to endospores of *B. cereus, B. subtilis*,

[*] Dr. D. B. Werz, Prof. Dr. P. H. Seeberger
Laboratory for Organic Chemistry
Swiss Federal Institute of Technology (ETH) Zürich
ETH Hönggerberg, HCI F 315
Wolfgang-Pauli-Str. 10, 8093 Zürich (Switzerland)
Fax: (+41) 44-633-1235
E-mail: seeberger@org.chem.ethz.ch
M. Tamborrini, Prof. Dr. G. Pluschke
Swiss Tropical Institute
Socinstr. 57, 4002 Basel (Switzerland)
Prof. Dr. J. Frey
Institute of Veterinary Bacteriology
University of Bern
Länggassstr. 122
3012 Bern (Switzerland)

[**] This research was supported by ETH Zürich, by a Feodor Lynen Research Fellowship of the Alexander von Humboldt Foundation, and by an Emmy Noether Fellowship of the Deutsche Forschungsgemeinschaft (to D.B.W.).

Supporting information for this article is available on the WWW under http://www.angewandte.org or from the author.

© 2006 Wiley-VCH Verlag GmbH & Co. KGaA, Weinheim

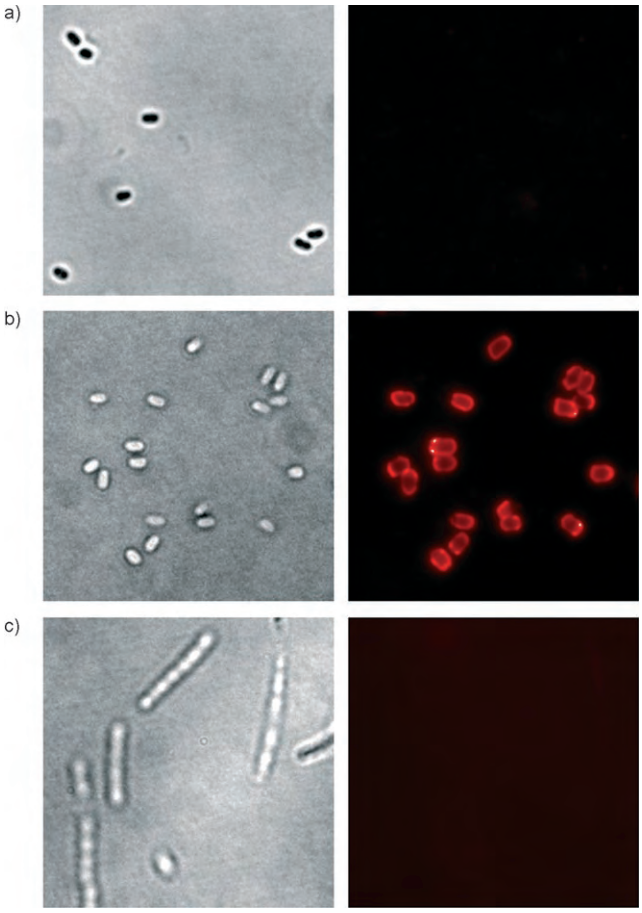

Figure 1. Indirect immunofluorescent staining of *B. anthracis* and *B. cereus* endospores by a mAb that was generated against the synthetic tetrasaccharide **2**. Left column: bright-field microscopy; right column: Cy3-specific immunofluorescence staining of a) *B. anthracis* spores with an isotype-matched control mAb, b) *B. anthracis* spores with a **2**-specific mAb, and c) *B. cereus* spores with a **2**-specific mAb.

and *B. thuringiensis*, which are close relatives of *B. anthracis* (Figure 1).

These results demonstrate that distinct differences in cell-surface carbohydrate antigens can provide the basis for the generation of specific immunological reagents. This was demonstrated herein for the synthetic tetrasaccharide antigen **2** of *B. anthracis*. The tetrasaccharide-specific mAbs may be suitable to develop a highly sensitive and specific detection system for *B. anthracis* endospores and contribute to the development of novel therapeutic or preventive approaches.

Received: May 23, 2006
Published online: August 17, 2006

Keywords: anthrax · carbohydrates · monoclonal antibodies · oligosaccharides · pathogen detection

[1] R. M. Atlas, *Annu. Rev. Microbiol.* **2002**, *56*, 167 – 185.
[2] D. King, V. Luna, A. Cannons, J. Cattani, P. Amuso, *J. Clin. Microbiol.* **2003**, *41*, 3454 – 3455.
[3] A. Fasanella, S. Losito, R. Adone, F. Ciuchini, T. Trotta, S. A. Altamura, D. Chiocco, G. Ippolito, *J. Clin. Microbiol.* **2003**, *41*, 896 – 899.
[4] X. Zhang, M. A. Young, O. Lyandres, R. P. van Duyne, *J. Am. Chem. Soc.* **2005**, *127*, 4484 – 4489.
[5] J. M. Daubenspeck, H. Zeng, P. Chen, S. Dong, C. T. Steichen, N. R. Krishna, D. G. Pritchard, C. L. Turnbough, Jr., *J. Biol. Chem.* **2004**, *279*, 30945 – 30953.
[6] D. B. Werz, P. H. Seeberger, *Angew. Chem.* **2005**, *117*, 6474 – 6476; *Angew. Chem. Int. Ed.* **2005**, *44*, 4315 – 4318.
[7] a) R. Adamo, R. Saksena, P. Kováč, *Carbohydr. Res.* **2005**, *340*, 2579 – 2582; b) R. Adamo, R. Saksena, P. Kováč, *Helv. Chim. Acta* **2006**, *89*, 1075 – 1089.
[8] G. Raguputhi, R. R. Koganty, D. Qiu, K. O. Lloyd, P. O. Livingston, *Glycoconjugate J.* **1998**, *15*, 217 – 221.
[9] Z.-G. Wang, L. J. Williams, X.-F. Zhang, A. Zatorski, V. Kudryashov. G. Ragupathi, M. Spassova, W. Bornmann, S. F. Slovin, H. I. Scher, P. O. Livingston, K. O. Lloyd, S. J. Danishefsky, *Proc. Natl. Acad. Sci. USA* **2000**, *97*, 2719 – 2724.

 © 2006 Wiley-VCH Verlag GmbH & Co. KGaA, Weinheim

Neurochemistry

DOI: 10.1002/anie.200601579

Glycomimetic Cyclic Peptides Stimulate Neurite Outgrowth**

*Dirk Bächle, Gabriele Loers, Eckhart W. Guthöhrlein, Melitta Schachner, and Norbert Sewald**

Carbohydrates are involved in a broad spectrum of physiological and pathological processes, many of which rely on molecular recognition.[1] Oligosaccharides that are exposed on the surface of, for example, tumor cells or pathogens can be regarded as potential therapeutic targets, either for direct application or for vaccination.[2] Despite the tremendous methodological advances in oligosaccharide synthesis,[3,4] carbohydrate-based therapeutics or vaccines require non-

[*] Dr. D. Bächle, Dr. E. W. Guthöhrlein, Prof. Dr. N. Sewald
Department of Chemistry, Organic and Bioorganic Chemistry
University of Bielefeld
Universitätsstrasse 25, 33615 Bielefeld (Germany)
Fax: (+49) 521-106-8094
E-mail: norbert.sewald@uni-bielefeld.de
Dr. G. Loers, Prof. Dr. M. Schachner
Zentrum für Molekulare Neurobiologie
Universität Hamburg
Martinistrasse 52, 20246 Hamburg (Germany)

[**] Support from the Erika und Conrad W. Schnyder-Stiftung, NRW Graduate School in Bioinformatics and Genome Research at Bielefeld University (PhD grant to E.W.G.), the Deutsche Forschungsgemeinschaft (SFB 613), and the Fonds der Chemischen Industrie is gratefully acknowledged.

Supporting information for this article is available on the WWW under http://www.angewandte.org or from the author.

WILEY InterScience DISCOVER SOMETHING GREAT
© 2006 Wiley-VCH Verlag GmbH & Co. KGaA, Weinheim

routine multistep syntheses. Moreover, oligosaccharides mostly display unfavorable ADME (absorption, distribution metabolism, excretion) parameters.[5]

Peptides that functionally and/or structurally mimic oligosaccharides provide a straightforward and elegant alternative for interfering with the interaction between complex carbohydrates and their receptors;[6] cyclic peptides are especially privileged because of their increased metabolic stability.

Phage display techniques either use an oligosaccharide receptor or monoclonal antibodies specific for an oligosaccharide antigen for retrieval of glycomimetic peptides. We chose the human natural killer cell glycan HNK-1[7,8] as a target for our investigations (Figure 1). Its consensus epitope

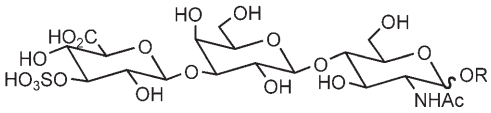

Figure 1. The HNK-1 trisaccharide consensus epitope.

consists of a 3′-sulfated glucuronic acid attached to *N*-acetyl lactosamine and is found on glycolipids and glycoproteins. HNK-1 and its binding partners are involved in many developmental processes in the nervous system.[9] Neurite outgrowth from motor neurons in culture is enhanced in the presence of a substrate that contains HNK-1, while neurite outgrowth from sensory neurons remains unaffected.[8] HNK-1 is indeed expressed along the routes that motor axons follow as they regrow after peripheral nerve damage.[10] Hence, HNK-1 and its mimetics have the potential to promote motor-neuron-specific reinnervation. As HNK-1 is difficult to isolate from natural sources and is equally difficult to synthesize chemically, the isolation and structural optimization of glycomimetics, for example, peptides imitating the HNK-1 oligosaccharide are viable and intriguing possibilities for potential clinical applications.

A library comprising 26 cyclic hexapeptides (see Figure 2 and the Supporting Information) was synthesized on the basis of the linear sequences TFKLSETTLEYY and TFQLSTRTLPFS, which were discovered by randomized peptide phage display against the monoclonal antibody 412.[11] The parent sequences were divided virtually into sets of overlapping hexapeptides, providing a total of six hexapeptide sequences. Each of these was taken as the basis for the synthesis of cyclic hexapeptide sublibraries, and a D-amino acid scan was performed with the cyclic hexapeptides derived from the six linear basis peptide epitopes. In each discrete member of these cyclic hexapeptide sublibraries, one amino acid was incorporated as its D enantiomer,[12] providing diastereomeric cyclic peptides. While a cyclic hexapeptide displays several interconverting conformations, the presence of a building block with conformational bias (e.g. proline, D-amino acids) locks the overall conformation of the peptide. D-Amino acids are predominantly found in position $i+1$ of a βII′ turn. Consequently, the peptide presents the functionalities of putative recognition elements in predictable three-

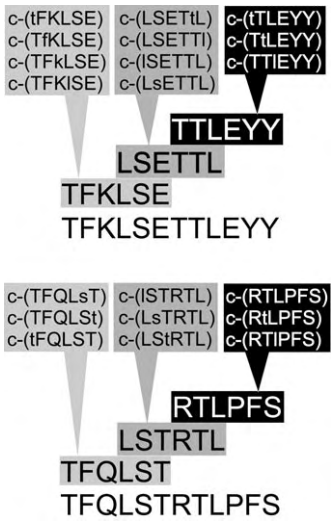

Figure 2. Cyclic-peptide scan and D-amino acid scan provide different series of linear and cyclic hexapeptides derived from the peptide sequences TFKLSETTLEYY and TFQLSTRTLPFS. Cyclic hexapeptides can be regarded as pairwise pseudosymmetric with respect to the geometry of the two complementary β turns. Therefore, in many cases only three of six peptides were examined.

dimensional arrays, determined by the relative position of the D-amino acid (spatial screening[13]). A cyclic peptide has less conformational flexibility than its linear parent and, hence, fewer degrees of freedom. If binding to a receptor is still possible for the cyclic peptide, the loss of entropy in the binding event is smaller than in the binding of the linear peptide.

The peptides were functionally characterized by surface plasmon resonance with respect to binding to the immobilized 412 antibody. Striking effects were observed in the TFKLSETTLEYY series (Figure 3). Clear sequence- and conformation-dependent effects occurred in the middle epitope LSETTL (Figure 3a). The D-Leu-containing cyclic peptide c-(LSETTl) binds to the antibody with $K_D = 67\ \mu M$, which is 12 times stronger than the binding of the linear dodecapeptide and four times stronger than that of the linear LSETTL.

An alanine scan revealed the importance of the ETTl sequence. Peptide c-(lSETTL), where the D-amino acid is shifted by one position relative to c-(LSETTl), represents the mismatch case with an improper display of the side chains and entropically disfavored interaction. Interestingly, the two cyclic hexapeptides c-(LSETtL) and c-(LsETTL), which can be regarded as pseudo-symmetric with respect to the geometry of the two complementary β turns, display similar affinities to the antibody (Figure 3a). Another affine peptide, c-(RTLPFS) ($K_D = 73\ \mu M$), was discovered in the TFQLSTRTLPFS series (Figure 3b). It does not require the incorporation of a D-amino acid for turn stabilization because proline also induces turns. The cyclic derivatives of the C-terminal hexapeptide RTLPFS all display considerably higher affinity to the antibody than the linear hexapeptide (64-fold) and the linear dodecapeptide (sixfold) do.

 © 2006 Wiley-VCH Verlag GmbH & Co. KGaA, Weinheim

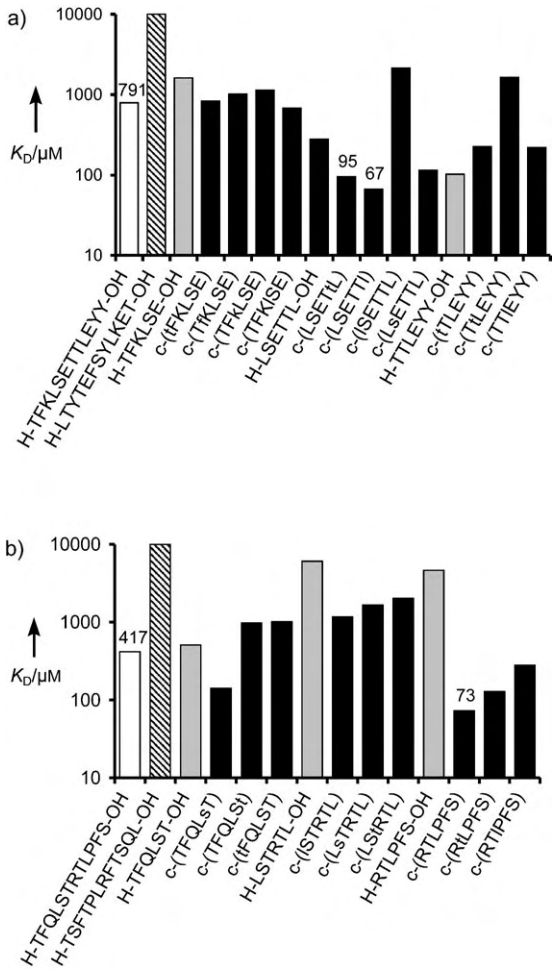

Figure 3. K_D values of the peptides derived from the basis sequences for binding to the antibody 412 as determined by surface plasmon resonance. White bars: basis sequence; hatched bars: randomized sequence; gray bars: linear hexapeptides; black bars: cyclic hexapeptides. In exceptional cases, the K_D values are given on top of the bars. For bars reaching the maximum displayed value (10000 μM), no binding was detected at all. Error bars are not visible because of the logarithmic scale. a) TFKLSETTLEYY; b) TFQLSTRTLPFS.

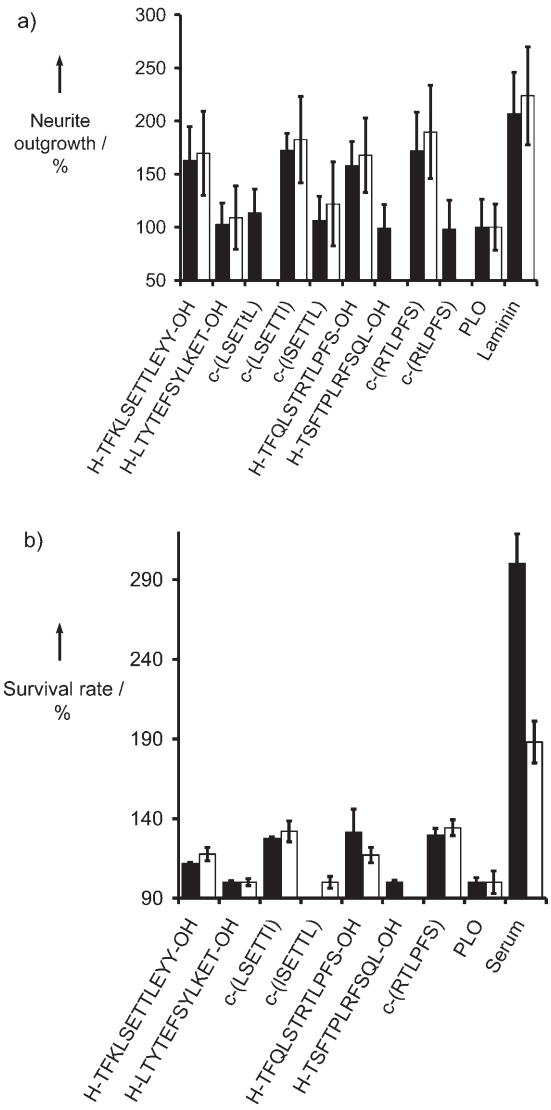

Figure 4. Neurite outgrowth (Figure 4a; mean values ± standard error of the mean (SEM)) and survival rates (Figure 4b; mean values ± SEM) of murine (black bars) and human (white bars) motor neurons plated onto substrate-coated poly-L-ornithine (PLO) in the presence of glycomimetic peptides, laminin, and serum, respectively. Neurite outgrowth and survival are quoted relative to the negative control PLO (=100%). The experiments were performed three times for neuritogenesis and twice for neuronal survival.

Selected peptides were investigated with respect to their ability to stimulate neurite outgrowth of murine and human motor neurons (Figure 4a). For this purpose enriched motor neuron preparations were isolated from embryos and cultured on glass coverslips coated with poly-L-ornithine (PLO) alone, which served as a negative control, or with PLO and the HNK-1 mimetics. Laminin is known to stimulate outgrowth of neurites[14,15] and was used as a positive control. Neurite outgrowth of both murine and human motor neurons (Figure 4a) was stimulated by the glycomimetic cyclic peptides c-(LSETTl) and c-(RTLPFS). The two cyclic hexapeptides also increased survival of motor neurons by approximately 30% after eight days in vitro when compared to experiments with PLO alone (Figure 4b). Both effects, stimulation of neurite outgrowth and increase of survival, were not only much stronger than with the linear dodecapeptide sequences but also significantly depended on the conformation. Peptide c-(lSETTL), which can be assumed to adopt a different turn geometry than that of c-(LSETTl) because of the different position of the D-amino acid, did not display any significant functional activity. Preincubation of the 412 antibody with the HNK-1 presenting murine glycoprotein L1 led to a significant decrease in binding to c-(LSETTl) and c-(RTLPFS), which suggests that the two peptides represent functional mimics of the HNK-1 oligosaccharide.

The solution conformations of c-(LSETTl) and c-(RTLPFS) were determined by NMR spectroscopy in combination with molecular dynamics simulations. Peptide c-(LSETTl) populates a single conformer cluster characterized by a βII′ turn with D-Leu in position $i+1$ and a comple-

 © 2006 Wiley-VCH Verlag GmbH & Co. KGaA, Weinheim

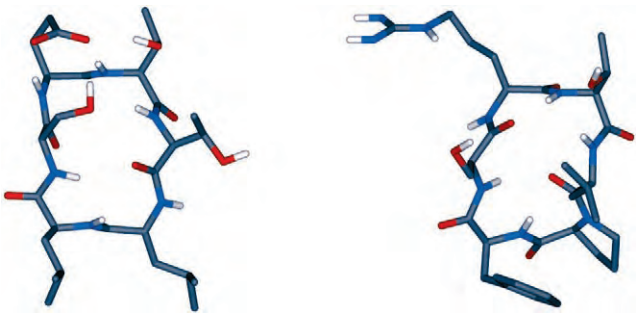

Figure 5. Left: Solution conformation of c-(LSETTl) in [D_6]DMSO. Right: Solution conformation of c-(RTLPFS) in [D_6]DMSO, major conformer. Blue N, red O, white H, gray C.

mentary βI-like turn around -Ser-Glu-Thr-Thr- (Figure 5). The βII′ turn is supported by strong NOEs between H^{α}(D-Leu) and H^{N}(Leu), as well as between H^{N}(Leu) and H^{N}(Ser), while strong NOEs between H^{N}(Glu) and H^{N}(Thr^{4}) as well as between H^{N}(Thr^{4})and H^{N}(Thr^{5}) support classification of the complementary turn as βI-like.

Peptide c-(RTLPFS) exists as a 2:1 mixture of conformers with *trans* and *cis* configurations at the Leu–Pro peptide bond. The major conformer contains only *trans* peptide bonds and adopts a structure comprising a γ turn with Arg in position $i+1$, which is stabilized by a hydrogen bond between H^{N}(Thr) and CO(Ser). This γ turn is nested during the trajectory with a β turn containing Arg in the $i+1$ position. This is supported by a strong NOE between H^{N}(Thr) and H^{N}(Leu). Proline occupies position $i+1$ of a γ turn which is nested with a β-turn-like conformation that cannot be classified as one of the ideal turn types (Figure 5). The minor conformer comprises a *cis* peptide bond at Leu–Pro and is much more flexible than its all-*trans* configured correlate.

As expected for carbohydrate mimetics, both peptides contain several amino acids with hydroxylated side chains (Ser, Thr). Additionally, the backbone amide groups of the peptide may act as intermolecular hydrogen-bond donors and acceptors. Unpolar amino acids are present in both peptides to establish hydrophobic interactions with the receptor(s). c-(LSETTl) essentially requires the Glu residue for affinity to the antibody 412, which presumably imitates a negatively charged residue of the HNK-1 epitope. Interestingly, c-(RTLPFS) does not contain an acidic side chain but a basic Arg residue instead.

Compounds able to enhance neurite regeneration after damage may hold promise, for example, in the treatment of paraplegic patients. The results obtained by transformation of the basis linear peptide sequences TFKLSETTLEYY and TFQLSTRTLPFS as mimetics of the HNK-1 trisaccharide into subsets of cyclic hexapeptides in a spatial screening approach clearly show that it is possible to increase the biological activity of glycomimetic peptides by backbone cyclization.

Received: April 21, 2006
Published online: September 8, 2006

Keywords: bioorganic chemistry · glycomimetics · neuroactive substances · neurochemistry · peptides

[1] G. Reuter, H.-J. Gabius, *Cell. Mol. Life Sci.* **1999**, *55*, 368–422.
[2] G. B. Lesinski, S. L. Smithson, N. Srivastava, D. Chen, G. Widera, M. A. J. Westerink, *Vaccine* **2001**, *19*, 1717–1726.
[3] H. Herzner, T. Reipen, M. Schultz, H. Kunz, *Chem. Rev.* **2000**, *100*, 4495–4537.
[4] K. M. Koeller, C.-H. Wong, *Chem. Rev.* **2000**, *100*, 4465–4493.
[5] P. Sears, C.-H. Wong, *Angew. Chem.* **1999**, *111*, 2446–2471; *Angew. Chem. Int. Ed.* **1999**, *38*, 2300–2324.
[6] M. A. Johnson, B. M. Pinto, *Aust. J. Chem.* **2002**, *55*, 13–25.
[7] M. Simon-Haldi, N. Mantei, J. Franke, H. Voshol, M. Schachner, *J. Neurochem.* **2002**, *83*, 1380–1388.
[8] R. Kleene, M. Schachner, *Nat. Rev. Neurosci.* **2004**, *5*, 195–208.
[9] D. K. Chou, S. Tobet, F. B. Jungalwala, *J. Neurosci. Res.* **2000**, *59*, 188–201.
[10] R. Martini, M. Schachner, T. M. Brushart, *J. Neurosci.* **1994**, *14*, 7180–7191.
[11] A. B. Noronha, A. Ilyas, H. Antonicek, M. Schachner, R. H. Quarles, *Brain Res.* **1986**, *385*, 237–244.
[12] The one-letter codes are used for the amino acid abbreviations; D-amino acids are symbolized by the corresponding lowercase letter.
[13] R. Haubner, D. Finsinger, H. Kessler, *Angew. Chem.* **1997**, *109*, 1440–1456; *Angew. Chem. Int. Ed. Engl.* **1997**, *36*, 1374–1389.
[14] D. Edgar, R. Timpl, H. Thoenen, *EMBO J.* **1984**, *3*, 1463–1468.
[15] G. C. Sephel, K. I. Tashiro, M. Sasaki, D. Greatorex, G. R. Martin, Y. Yamada, H. K. Kleinman, *Biochem. Biophys. Res. Commun.* **1989**, *162*, 821–829.

 © 2006 Wiley-VCH Verlag GmbH & Co. KGaA, Weinheim